DICTYOSTELIUM: A TRACTABLE CELL AND DEVELOPMENTAL MODEL IN BIOMEDICAL RESEARCH

EDITED BY: Robert J. Huber, Robin S. B. Williams and Annette Müller-Taubenberger
PUBLISHED IN: Frontiers in Cell and Developmental Biology

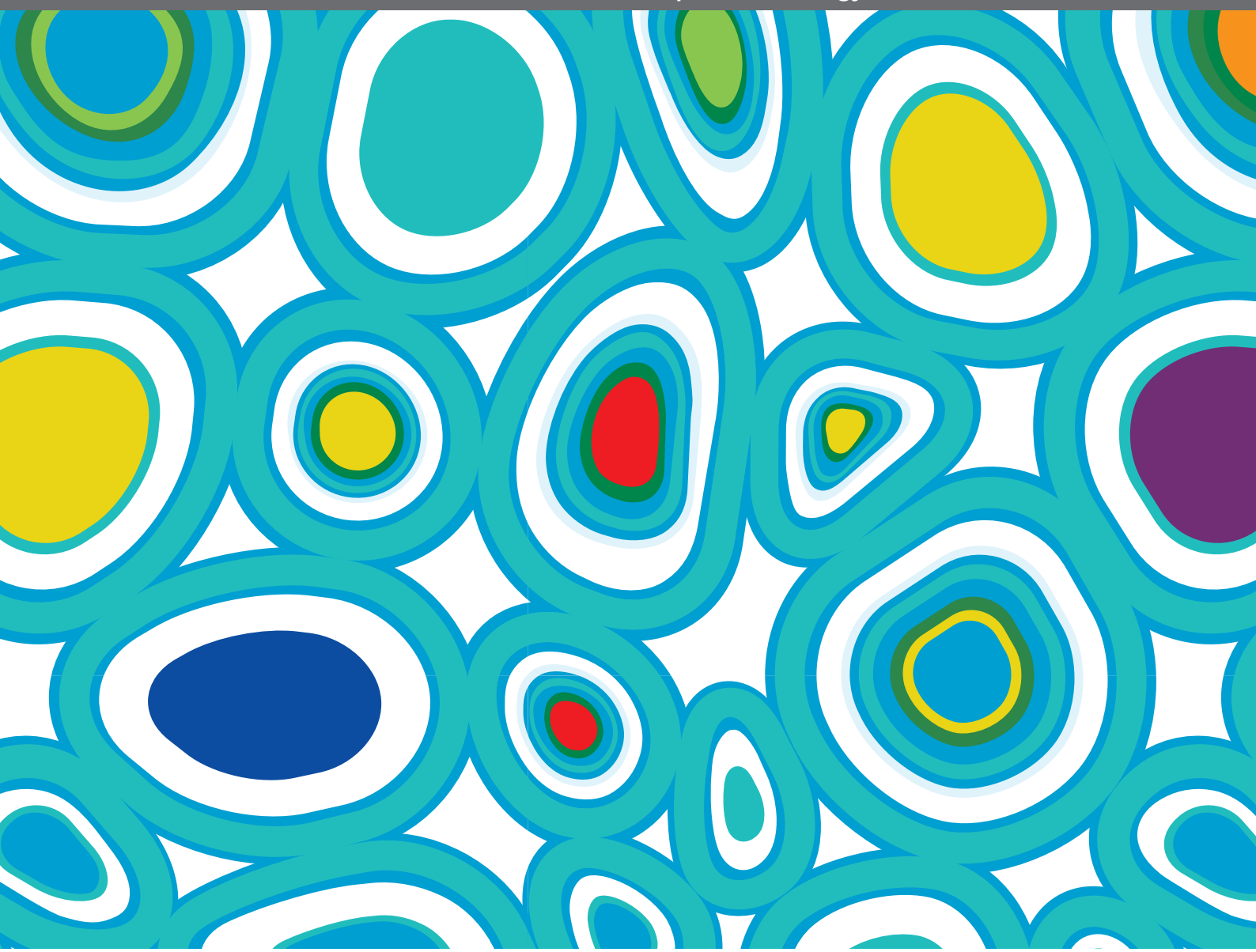

frontiers Research Topics

frontiers

Frontiers eBook Copyright Statement

The copyright in the text of individual articles in this eBook is the property of their respective authors or their respective institutions or funders. The copyright in graphics and images within each article may be subject to copyright of other parties. In both cases this is subject to a license granted to Frontiers.

The compilation of articles constituting this eBook is the property of Frontiers.

Each article within this eBook, and the eBook itself, are published under the most recent version of the Creative Commons CC-BY licence. The version current at the date of publication of this eBook is CC-BY 4.0. If the CC-BY licence is updated, the licence granted by Frontiers is automatically updated to the new version.

When exercising any right under the CC-BY licence, Frontiers must be attributed as the original publisher of the article or eBook, as applicable.

Authors have the responsibility of ensuring that any graphics or other materials which are the property of others may be included in the CC-BY licence, but this should be checked before relying on the CC-BY licence to reproduce those materials. Any copyright notices relating to those materials must be complied with.

Copyright and source acknowledgement notices may not be removed and must be displayed in any copy, derivative work or partial copy which includes the elements in question.

All copyright, and all rights therein, are protected by national and international copyright laws. The above represents a summary only. For further information please read Frontiers' Conditions for Website Use and Copyright Statement, and the applicable CC-BY licence.

ISSN 1664-8714
ISBN 978-2-88976-181-4
DOI 10.3389/978-2-88976-181-4

About Frontiers

Frontiers is more than just an open-access publisher of scholarly articles: it is a pioneering approach to the world of academia, radically improving the way scholarly research is managed. The grand vision of Frontiers is a world where all people have an equal opportunity to seek, share and generate knowledge. Frontiers provides immediate and permanent online open access to all its publications, but this alone is not enough to realize our grand goals.

Frontiers Journal Series

The Frontiers Journal Series is a multi-tier and interdisciplinary set of open-access, online journals, promising a paradigm shift from the current review, selection and dissemination processes in academic publishing. All Frontiers journals are driven by researchers for researchers; therefore, they constitute a service to the scholarly community. At the same time, the Frontiers Journal Series operates on a revolutionary invention, the tiered publishing system, initially addressing specific communities of scholars, and gradually climbing up to broader public understanding, thus serving the interests of the lay society, too.

Dedication to Quality

Each Frontiers article is a landmark of the highest quality, thanks to genuinely collaborative interactions between authors and review editors, who include some of the world's best academicians. Research must be certified by peers before entering a stream of knowledge that may eventually reach the public - and shape society; therefore, Frontiers only applies the most rigorous and unbiased reviews.
Frontiers revolutionizes research publishing by freely delivering the most outstanding research, evaluated with no bias from both the academic and social point of view. By applying the most advanced information technologies, Frontiers is catapulting scholarly publishing into a new generation.

What are Frontiers Research Topics?

Frontiers Research Topics are very popular trademarks of the Frontiers Journals Series: they are collections of at least ten articles, all centered on a particular subject. With their unique mix of varied contributions from Original Research to Review Articles, Frontiers Research Topics unify the most influential researchers, the latest key findings and historical advances in a hot research area! Find out more on how to host your own Frontiers Research Topic or contribute to one as an author by contacting the Frontiers Editorial Office: frontiersin.org/about/contact

DICTYOSTELIUM: A TRACTABLE CELL AND DEVELOPMENTAL MODEL IN BIOMEDICAL RESEARCH

Topic Editors:
Robert J. Huber, Trent University, Canada
Robin S. B. Williams, University of London, United Kingdom
Annette Müller-Taubenberger, Ludwig Maximilian University of Munich, Germany

Citation: Huber, R. J., Williams, R. S. B., Müller-Taubenberger, A., eds. (2022). Dictyostelium: A Tractable Cell and Developmental Model in Biomedical Research. Lausanne: Frontiers Media SA. doi: 10.3389/978-2-88976-181-4

Table of Contents

05 ***Editorial:* Dictyostelium*: A Tractable Cell and Developmental Model in Biomedical Research***
Robert J. Huber, Robin SB Williams and Annette Müller-Taubenberger

09 ***Role of LrrkA in the Control of Phagocytosis and Cell Motility in* Dictyostelium discoideum**
Romain Bodinier, Ayman Sabra, Jade Leiba, Anna Marchetti, Otmane Lamrabet, Imen Ayadi, Vedrana Filić, Takefumi Kawata, Igor Weber and Pierre Cosson

20 ***Aberrant Autophagy Impacts Growth and Multicellular Development in a* Dictyostelium *Knockout Model of CLN5 Disease***
Meagan D. McLaren, Sabateeshan Mathavarajah, William D. Kim, Shyong Q. Yap and Robert J. Huber

40 ***Using* Dictyostelium *to Develop Therapeutics for Acute Respiratory Distress Syndrome***
Sara A. Kirolos, Ramesh Rijal, Kristen M. Consalvo and Richard H. Gomer

51 ***Membrane Targeting of C2GAP1 Enables* Dictyostelium discoideum *to Sense Chemoattractant Gradient at a Higher Concentration Range***
Xuehua Xu, Smit Bhimani, Henderikus Pots, Xi Wen, Taeck J. Jeon, Arjan Kortholt and Tian Jin

61 ***Different Heterotrimeric G Protein Dynamics for Wide-Range Chemotaxis in Eukaryotic Cells***
Yoichiro Kamimura and Masahiro Ueda

69 ***Development of a Positive Selection High Throughput Genetic Screen in* Dictyostelium discoideum**
Felicia N. Williams, Yumei Wu and K. Matthew Scaglione

77 ***Differential Roles of Actin Crosslinking Proteins Filamin and* α*-Actinin in Shear Flow-Induced Migration of* Dictyostelium discoideum**
Aaron Cole, Sarah Buckler, Jack Marcucci and Yulia Artemenko

90 ***CRISPR Toolbox for Genome Editing in* Dictyostelium**
Kensuke Yamashita, Hoshie Iriki, Yoichiro Kamimura and Tetsuya Muramoto

106 ***How Phagocytes Acquired the Capability of Hunting and Removing Pathogens From a Human Body: Lessons Learned From Chemotaxis and Phagocytosis of* Dictyostelium discoideum *(Review)***
Xuehua Xu, Miao Pan and Tian Jin

119 ***The* WIPI *Gene Family and Neurodegenerative Diseases: Insights From Yeast and* Dictyostelium *Models***
Olivier Vincent, Laura Antón-Esteban, Miranda Bueno-Arribas, Alba Tornero-Écija, María-Ángeles Navas and Ricardo Escalante

132 ***Interactions and Cytotoxicity of Human Neurodegeneration-Associated Proteins Tau and* α*-Synuclein in the Simple Model* Dictyostelium discoideum**
Katelyn Mroczek, Sanjanie Fernando, Paul R. Fisher and Sarah J. Annesley

158 ***A Conserved Role for LRRK2 and Roco Proteins in the Regulation of Mitochondrial Activity***
Katharina E. Rosenbusch, Asmaa Oun, Oana Sanislav, Sui T. Lay, Ineke Keizer-Gunnink, Sarah J. Annesley, Paul R. Fisher, Amalia M. Dolga and Arjan Kortholt

172 ***Using* Dictyostelium *to Advance Our Understanding of the Role of Medium Chain Fatty Acids in Health and Disease***
Erwann Pain, Sonia Shinhmar and Robin S. B. Williams

180 ***Local Membrane Curvature Pins and Guides Excitable Membrane Waves in Chemotactic and Macropinocytic Cells - Biomedical Insights From an Innovative Simple Model***
Marcel Hörning, Torsten Bullmann and Tatsuo Shibata

194 ***Domain Organization of the UBX Domain Containing Protein 9 and Analysis of Its Interactions With the Homohexameric AAA + ATPase p97 (Valosin-Containing Protein)***
Jana Riehl, Ramesh Rijal, Leonie Nitz, Christoph S. Clemen, Andreas Hofmann and Ludwig Eichinger

211 ***Using Live-Cell Imaging and Synthetic Biology to Probe Directed Migration in* Dictyostelium**
Jonathan Kuhn, Yiyan Lin and Peter N. Devreotes

230 **Dictyostelium discoideum *as a Model to Assess Genome Stability Through DNA Repair***
Catherine J. Pears, Julien Brustel and Nicholas D. Lakin

243 **Dictyostelium *Dynamin Superfamily GTPases Implicated in Vesicle Trafficking and Host-Pathogen Interactions***
Ana Katic, Dario Hüsler, François Letourneur and Hubert Hilbi

256 ***Possible Involvement of the Nutrient and Energy Sensors mTORC1 and AMPK in Cell Fate Diversification in a Non-Metazoan Organism***
Julian D. Gross and Catherine J. Pears

265 ***Formation of Cytoplasmic Actin-Cofilin Rods is Triggered by Metabolic Stress and Changes in Cellular pH***
Hellen C. Ishikawa-Ankerhold, Sophie Kurzbach, Arzu S. Kinali and Annette Müller-Taubenberger

277 ***The Dynamics of Aerotaxis in a Simple Eukaryotic Model***
Marta Biondo, Cristina Panuzzo, Shahzad M. Ali, Salvatore Bozzaro, Matteo Osella, Enrico Bracco and Barbara Pergolizzi

291 ***The* Dictyostelium *Model for Mucolipidosis Type IV***
Claire Y. Allan and Paul R. Fisher

311 ***The Polarized Redistribution of the Contractile Vacuole to the Rear of the Cell is Critical for Streaming and is Regulated by PI(4,5)P2-Mediated Exocytosis***
Sana A. Fadil and Chris Janetopoulos

frontiers | Frontiers in Cell and Developmental Biology

EDITORIAL
published: 26 April 2022
doi: 10.3389/fcell.2022.909619

Editorial: *Dictyostelium*: A Tractable Cell and Developmental Model in Biomedical Research

Robert J. Huber[1]*, *Robin SB Williams*[2]* and *Annette Müller-Taubenberger*[3]*

[1]Department of Biology, Trent University, Peterborough, ON, Canada, [2]Centre for Biomedical Sciences, School of Biological Sciences, Royal Holloway University of London, Egham, United Kingdom, [3]Department of Cell Biology (Anatomy III), Biomedical Center (BMC), LMU Munich, Munich, Germany

Keywords: cancer, cell biology, cell motility and chemotaxis, cell signalling, development, model system, neurological disease, pharmacogenetics screens

Editorial on the Research Topic

Dictyostelium: A Tractable Cell and Developmental Model in Biomedical Research

For almost a century, the social amoeba *Dictyostelium discoideum* has been used as an inexpensive and high-throughput model system for studying a variety of fundamental cellular and developmental processes including cell movement, chemotaxis, differentiation, and autophagy (Müller-Taubenberger et al., 2013; Mathavarajah et al., 2017). The life cycle of *Dictyostelium* is comprised of a unicellular growth phase and a 24-h multicellular developmental phase with distinct stages (**Figure 1A**). *Dictyostelium* development shares many common features with metazoan development but occurs in a much shorter time frame, which allows for the rapid detection of developmental phenotypes. The fully sequenced, low redundancy genome of *Dictyostelium* provides a less complex system to work with, whilst still maintaining many genes and related signalling pathways found in more complex eukaryotes (Eichinger et al., 2005). The *Dictyostelium* genome is haploid, which allows researchers to introduce one or multiple gene disruptions with relative ease, and gene function can be studied in a true multicellular organism with measurable phenotypic outcomes (Kuspa, 2006; Faix et al., 2013; Friedrich et al., 2015; Sekine et al., 2018). In addition, insertional mutant libraries facilitate pharmacogenetics screens that have enhanced our understanding of the function of bioactive compounds at a cellular level (Damstra Oddy et al., 2021; Warren et al., 2020). Finally, a variety of expression constructs are available that enable studies on protein localization and function in *Dictyostelium* (Levi et al., 2000; Veltman et al., 2009; Müller-Taubenberger and Ishikawa-Ankerhold, 2013).

More recently, *Dictyostelium* has emerged as a valuable biomedical model system for studying several human diseases. The genome encodes orthologs of genes associated with human disease and the signalling pathways that regulate the behaviour of *Dictyostelium* cells are remarkably similar to those observed in mammalian cells, which has allowed findings from *Dictyostelium* to be successfully translated to mammalian systems (Alexander and Alexander, 2011; Chang et al., 2012). As a result, *Dictyostelium* has, and will continue to offer, excellent opportunities to advance biomedical research.

This Research Topic contains 23 articles that showcase the use of *Dictyostelium* as a tractable cell, molecular, and developmental model system in biomedical research, and includes two methods articles that enhance the biomedical applications of this valuable model organism (**Figure 1B**). Yamashita et al. describe the application of CRISPR-based gene disruption in *Dictyostelium*, while Williams et al. report the development of a new positive selection high throughput genetic screen.

The use of *Dictyostelium* as a model system for studying fundamental cellular and developmental processes is well established and this Research Topic contains several articles describing new findings on conserved processes in *Dictyostelium* with biomedical relevance (**Figure 1B**). In their original

OPEN ACCESS

Edited and reviewed by:
Ramani Ramchandran, Medical College of Wisconsin, United States

***Correspondence:**
Robert J. Huber
roberthuber@trentu.ca
Robin SB Williams
robin.williams@rhul.ac.uk
Annette Müller-Taubenberger
amueller@bmc.med.lmu.de

Specialty section:
This article was submitted to Molecular and Cellular Pathology, a section of the journal Frontiers in Cell and Developmental Biology

Received: *31 March 2022*
Accepted: *07 April 2022*
Published: *26 April 2022*

Citation:
Huber RJ, Williams RSB and Müller-Taubenberger A (2022) Editorial: Dictyostelium: A Tractable Cell and Developmental Model in Biomedical Research. Front. Cell Dev. Biol. 10:909619. doi: 10.3389/fcell.2022.909619

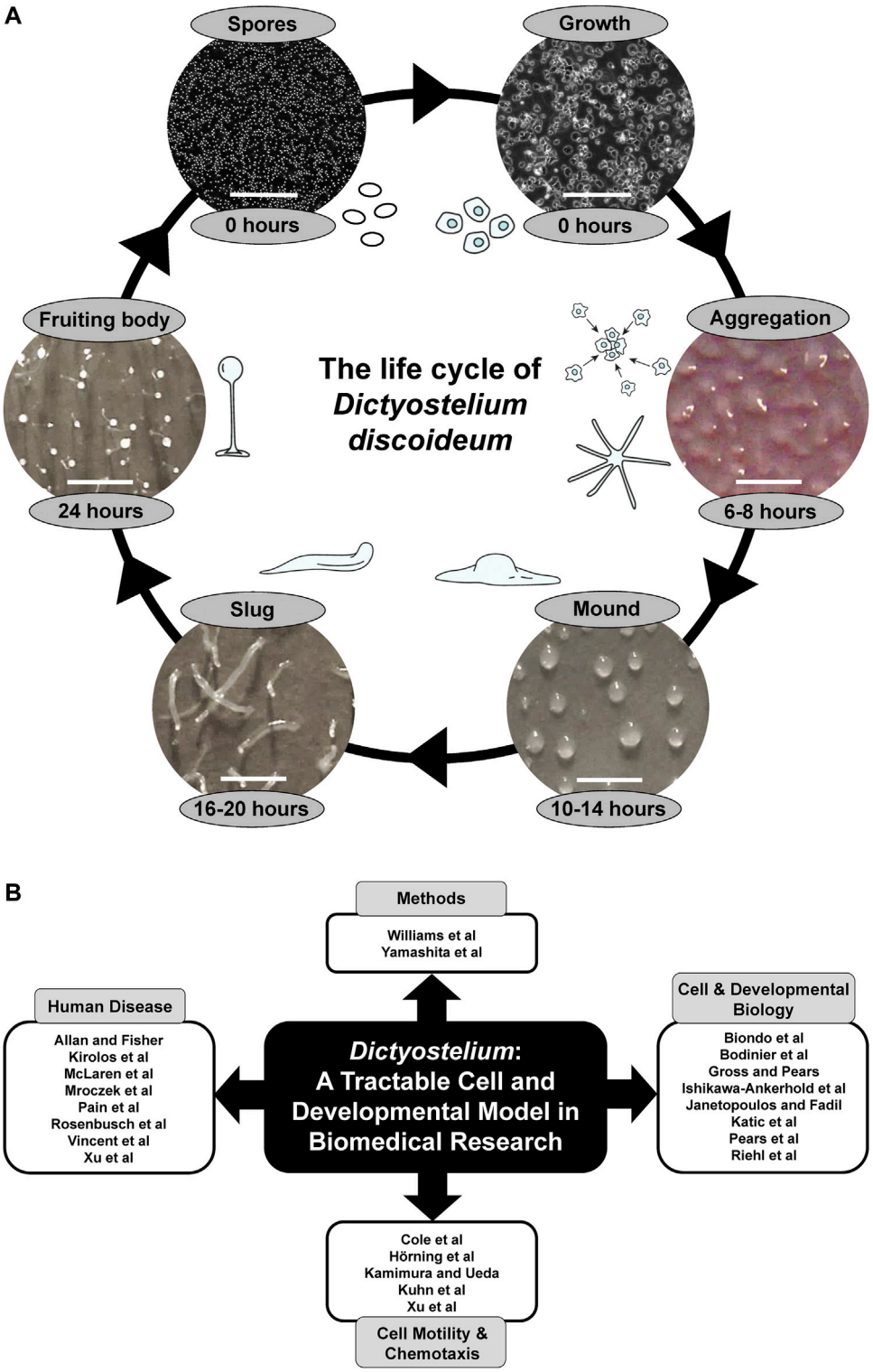

FIGURE 1 | (A) The life cycle of *Dictyostelium discoideum*. During the growth phase, haploid amoebae consume nutrients and divide mitotically. Starvation initiates a 24-h developmental program that begins with the chemotactic aggregation of cells to form multicellular mounds, which is followed by a series of morphological events that generate motile slugs. The final phase of development involves terminal differentiation of cells and the formation of fruiting bodies composed of a mass of viable spores that rest atop a slender stalk. When nutrients become available, the spores germinate to restart the life cycle. White scale bars: 0.2 mm (spores and growth), 1 mm (aggregation, mound, slug, fruiting body). Some of the illustrations and microscopy images depicting the different life cycle stages were previously published in Huber, 2021 (permission provided by CC-BY license). **(B)** Themes of this Research Topic. Articles within this Research Topic are grouped into four main categories: Methods, Cell and Developmental Biology, Cell Motility and Chemotaxis, and Human Disease.

research article, Bodinier et al. reveal a mechanism regulated by the leucine-rich repeat kinase LrrkA that facilitates the sensing, phagocytosis, and killing of bacteria by *Dictyostelium* amoebae. In addition, Biondo et al. describe how *Dictyostelium* can be used as a model system for studying aerotaxis, Riehl et al. propose a role for UBX domain-containing protein nine in protein homeostasis in *Dictyostelium*, and Ishikawa-Ankerhold et al. reveal the role of pH in cytoplasmic rod formation in *Dictyostelium*, which has implications for human diseases caused by actin-cofilin rod formation. In review articles, Katic et al. summarize the roles of dynamin superfamily proteins in regulating vesicular trafficking and host-pathogen interactions in *Dictyostelium*, Janetopoulos and Fadil review the role of PIP_2 in regulating the localization and exocytosis of the contractile vacuole system in migrating *Dictyostelium* amoebae, and Pears et al. describe DNA repair mechanisms in *Dictyostelium*, and how further study of DNA repair in *Dictyostelium* can help us better understand how this process is dysregulated in cancer. Finally, in their Hypothesis and Theory article, Gross and Pears discuss how *Dictyostelium* can be used to study the roles of the nutrient and energy sensors, mTORC1 and AMPK, which are linked to several human diseases including Alzheimer's disease, cancer, obesity, and type 2 diabetes.

Historically, *Dictyostelium* has been used as a model system to elucidate the signalling pathways regulating eukaryotic cell motility and chemotaxis, which has furthered our understanding of the mechanisms regulating cancer cell movement. This Research Topic includes several exciting articles highlighting recent advancements in this area (**Figure 1B**). For example, in their original research article, Hörning et al. describe the dynamics of actin polymerization and PIP_3 activity in amoeboid cells. In addition, Xu et al. reveal the molecular mechanism and biological function of C2GAP1 membrane targeting for chemotaxis, and Cole et al. show the roles of actin-binding proteins in sensing and transmitting mechanical stimuli that drive directed cell migration. To supplement these original research articles, Kamimura and Ueda review studies in *Dictyostelium* that have helped elucidate the role of G protein-coupled receptor signalling in regulating eurkaryotic chemotaxis, and Kuhn et al. summarize recent advances in imaging, synthetic biology, and computational analysis that have allowed researchers to tune the activity of individual molecules in cells and precisely measure the effects on cellular motility and signalling.

A central theme that emerges from this Research Topic is the use of *Dictyostelium* as a model system for studying specific human diseases (**Figure 1B**). In their original research article, McLaren et al. knock out the *Dictyostelium* ortholog of human ceroid lipofuscinosis neuronal 5 (*CLN5*) and show that loss of the gene impacts growth and multicellular development by affecting autophagy. In humans, mutations in *CLN5* cause a subtype of Batten disease, the most common form of childhood neurodegeneration. This Research Topic also reports the ability of *Dictyostelium* to further our understanding of Parkinson's disease. For example, in their original research article, Rosenbusch et al. report findings from *Dictyostelium* that link mutations in Parkinson's disease-associated genes to aberrant mitochondrial activity. In addition, Mroczek et al. present data that improve our understanding of the interactions and cytotoxicity of tau and alpha-synuclein, both of which are linked to Parkinson's disease. Further supporting the use of *Dictyostelium* as a model system for studying neurological disease, Vincent et al. review work in *Dictyostelium* and yeast that has provided insight into the roles of WIPI proteins in neurodegeneration, and Allan and Fisher characterize a new *Dictyostelium* model for the lysosomal storage disease, mucolipidosis type IV. This Research Topic also contains articles related to other human diseases. In their review, Pain et al. describe work in *Dictyostelium* that studied the role of decanoic acid in ketogenic diets, which have been used in the treatment of epilepsy, bipolar disorder, cancer, and diabetes. In addition, Kirolos et al. review work in *Dictyostelium* that has enhanced our understanding of the pathology underlying acute respiratory distress syndrome, and Xu et al. summarize studies in *Dictyostelium* that have provided insight into how phagocytes use chemotaxis and phagocytosis to detect and kill pathogens.

In total, this Research Topic showcases exciting new research in *Dictyostelium* biology that strengthen its position as a tractable cellular and developmental model system in biomedical research. However, we offer here only a sample of the many facets of medically relevant research currently performed using *Dictyostelium*. Therefore, we encourage readers to seek out additional literature from the field that has used *Dictyostelium* as a biomedical model system to learn more about its valuable contributions to human disease research.

AUTHOR CONTRIBUTIONS

RH: writing—original draft, review and editing, **Figure 1A** and **Figure 1B** preparation. RW and AM-T, writing—review and editing. All authors approved the final draft of this Editorial.

ACKNOWLEDGMENTS

The Editors would like to thank all the authors who contributed articles to this Research Topic and the reviewers who evaluated the submitted manuscripts. They would also like to thank the dictyBase team (dictybase.org) for their continuing support of *Dictyostelium* researchers worldwide.

REFERENCES

Alexander, S., and Alexander, H. (2011). Lead Genetic Studies in *Dictyostelium discoideum* and Translational Studies in Human Cells Demonstrate that Sphingolipids Are Key Regulators of Sensitivity to Cisplatin and Other Anticancer Drugs. *Semin. Cel Dev. Biol.* 22, 97–104. doi:10.1016/j.semcdb.2010.10.005

Chang, P., Orabi, B., Deranieh, R. M., Dham, M., Hoeller, O., Shimshoni, J. A., et al. (2012). The Antiepileptic Drug Valproic Acid and Other Medium-

Chain Fatty Acids Acutely Reduce Phosphoinositide Levels Independently of Inositol in *Dictyostelium*. *Dis. Model. Mech.* 5 (1), 115–124. doi:10.1242/dmm.008029

Damstra-Oddy, J. L., Warren, E. C., Perry, C. J., Desfougères, Y., Fitzpatrick, J. K., Schaf, J., et al. (2021). Phytocannabinoid-dependent mTORC1 Regulation Is Dependent upon Inositol Polyphosphate Multikinase Activity. *Br. J. Pharmacol.* 178, 1149–1163. doi:10.1111/bph.15351

Eichinger, L., Pachebat, J. A., Glöckner, G., Rajandream, M. A., Sucgang, R., Berriman, M., et al. (2005). The Genome of the Social Amoeba *Dictyostelium discoideum*. *Nature* 435, 43–57. doi:10.1038/nature03481

Faix, J., Linkner, J., Nordholz, B., Platt, J. L., Liao, X.-H., and Kimmel, A. R. (2013). The Application of the Cre-loxP System for Generating Multiple Knock-Out and Knock-In Targeted Loci. *Methods Mol. Biol.* 983, 249–267. doi:10.1007/978-1-62703-302-2_13

Friedrich, M., Meier, D., Schuster, I., and Nellen, W. (2015). A Simple Retroelement Based Knock-Down System in *Dictyostelium*: Further Insights into RNA Interference Mechanisms. *PLoS One* 10, e0131271. doi:10.1371/journal.pone.0131271

Huber, R. J. (2021). Altered Protein Secretion in Batten Disease. *Dis. Model. Mech.* 14, dmm049152. doi:10.1242/dmm.049152

Kuspa, A. (2006). Restriction Enzyme-Mediated Integration (REMI) Mutagenesis. *Methods Mol. Biol.* 346, 201–209. doi:10.1385/1-59745-144-4:201

Levi, S., Polyakov, M., and Egelhoff, T. T. (2000). Green Fluorescent Protein and Epitope Tag Fusion Vectors for *Dictyostelium discoideum*. *Plasmid* 44, 231–238. doi:10.1006/plas.2000.1487

Mathavarajah, S., Flores, A., and Huber, R. J. (2017). *Dictyostelium discoideum*: a Model System for Cell and Developmental Biology. *Curr. Protoc. Essent. Lab. Tech.* 15, 14. doi:10.1002/cpet.15

Müller-Taubenberger, A., and Ishikawa-Ankerhold, H. C. (2013). Fluorescent Reporters and Methods to Analyze Fluorescent Signals. *Methods Mol. Biol.* 983, 93–112.

Müller-Taubenberger, A., Kortholt, A., and Eichinger, L. (2013). Simple System - Substantial Share: the Use of *Dictyostelium* in Cell Biology and Molecular Medicine. *Eur. J. Cel Biol.* 92, 45–53.

Sekine, R., Kawata, T., and Muramoto, T. (2018). CRISPR/Cas9 Mediated Targeting of Multiple Genes in *Dictyostelium*. *Sci Rep.* 8 (1), 8471.

Veltman, D. M., Akar, G., Bosgraaf, L., and Van Haastert, P. J. M. (2009). A New Set of Small, Extrachromosomal Expression Vectors for *Dictyostelium discoideum*. *Plasmid* 61, 110–118. doi:10.1016/j.plasmid.2008.11.003

Warren, E. C., Dooves, S., Lugarà, E., Damstra-Oddy, J., Schaf, J., Heine, V. M., et al. (2020). Decanoic Acid Inhibits mTORC1 Activity Independent of Glucose and Insulin Signaling. *Proc. Natl. Acad. Sci. U S A.* 117, 23617–23625. doi:10.1073/pnas.2008980117

Conflict of Interest: The authors declare that the research was conducted in the absence of any commercial or financial relationships that could be construed as a potential conflict of interest.

Publisher's Note: All claims expressed in this article are solely those of the authors and do not necessarily represent those of their affiliated organizations, or those of the publisher, the editors and the reviewers. Any product that may be evaluated in this article, or claim that may be made by its manufacturer, is not guaranteed or endorsed by the publisher.

Copyright © 2022 Huber, Williams and Müller-Taubenberger. This is an open-access article distributed under the terms of the Creative Commons Attribution License (CC BY). The use, distribution or reproduction in other forums is permitted, provided the original author(s) and the copyright owner(s) are credited and that the original publication in this journal is cited, in accordance with accepted academic practice. No use, distribution or reproduction is permitted which does not comply with these terms.

frontiers in Cell and Developmental Biology

ORIGINAL RESEARCH
published: 08 March 2021
doi: 10.3389/fcell.2021.629200

Role of LrrkA in the Control of Phagocytosis and Cell Motility in *Dictyostelium discoideum*

Romain Bodinier[1†], Ayman Sabra[1†], Jade Leiba[1†], Anna Marchetti[1], Otmane Lamrabet[1], Imen Ayadi[1], Vedrana Filić[2], Takefumi Kawata[3], Igor Weber[2] and Pierre Cosson[1]*

[1] Department of Cell Physiology and Metabolism, Faculty of Medicine, University of Geneva, Geneva, Switzerland, [2] Division of Molecular Biology, Ruder Boskovic Institute, Zagreb, Croatia, [3] Department of Biology, Faculty of Science, Toho University, Tokyo, Japan

OPEN ACCESS

Edited by:
Annette Müller-Taubenberger, Ludwig Maximilian University of Munich, Germany

Reviewed by:
Sol Sotillos, Andalusian Center for Development Biology (CABD), Spain
Jason King, The University of Sheffield, United Kingdom

***Correspondence:**
Pierre Cosson
pierre.cosson@unige.ch

[†] *These authors have contributed equally to this work*

Specialty section:
This article was submitted to Molecular Medicine, a section of the journal Frontiers in Cell and Developmental Biology

Received: *13 November 2020*
Accepted: *15 February 2021*
Published: *08 March 2021*

Citation:
Bodinier R, Sabra A, Leiba J, Marchetti A, Lamrabet O, Ayadi I, Filić V, Kawata T, Weber I and Cosson P (2021) Role of LrrkA in the Control of Phagocytosis and Cell Motility in Dictyostelium discoideum. Front. Cell Dev. Biol. 9:629200. doi: 10.3389/fcell.2021.629200

LrrkA is a *Dictyostelium discoideum* kinase with leucine-rich repeats. LrrkA stimulates Kil2 and intra-phagosomal killing of ingested bacteria in response to folate. In this study, we show that genetic inactivation of *lrrkA* also causes a previously unnoticed phenotype: *lrrkA* KO cells exhibit enhanced phagocytosis and cell motility compared to parental cells. This phenotype is cell autonomous, is reversible upon re-expression of LrrkA, and is not due to an abnormal response to inhibitory quorum-sensing factors secreted by *D. discoideum* in its medium. In addition, folate increases motility in parental *D. discoideum* cells, but not in *lrrkA* KO cells, suggesting that LrrkA plays a pivotal role in the cellular response to folate. On the contrary, *lrrkA* KO cells regulate gene transcription in response to folate in a manner indistinguishable from parental cells. Overall, based on analysis of mutant phenotypes, we identify gene products that participate in the control of intracellular killing, cell motility, and gene transcription in response to folate. These observations reveal a mechanism by which *D. discoideum* encountering bacterially-secreted folate can migrate, engulf, and kill bacteria more efficiently.

Keywords: LrrkA, folate, phagocytosis, motility, *Dictyostelium discoideum*

INTRODUCTION

The initial contact between a cell and its substrate is a key element that determines the ability of the cell to adhere and spread on the substrate, and depending on its size to ingest it by phagocytosis (if it is small enough), or to move on its surface (Cougoule et al., 2004). Phagocytosis as well as cell adhesion, spreading, and motility involve massive changes in cell shape, which are carried out by a dynamic reorganization of the actin cytoskeleton. Actin-driven changes in cell shape can also lead to the enclosure of a large volume of extracellular medium, and its capture within an intracellular macropinosome, although in this situation the process of reshaping and ingestion is not driven by adhesion to a substrate (Buckley and King, 2017).

Phagocytosis is the process by which specialized mammalian cells (e.g., neutrophils and macrophages) and environmental amoebae ingest microorganisms, in particular bacteria (Bozzaro et al., 2008; Cosson and Soldati, 2008). Ingested bacteria are transferred from early phagosomes to

acidic phago-lysosomes, where they are killed and digested. In mammals, one of the main functions of phagocytic cells is to destroy invading microorganisms and to protect the body against infections. Amoebae rather use phagocytosis to feed upon other microorganisms.

Dictyostelium discoideum has been an instrumental model to study the molecular mechanisms controlling the dynamics of the actin cytoskeleton, the phagocytic and endocytic pathway, and intracellular killing of bacteria (Cosson and Soldati, 2008; Mori et al., 2018; Stuelten et al., 2018). Due to the relative ease with which these haploid cells can be grown, observed, and genetically altered, they have proven instrumental to discover and analyze the role of multiple gene products in various facets of these cellular processes (Bretschneider et al., 2016; Buckley and King, 2017). *D. discoideum* has also proven useful to better understand human genetic diseases (McLaren et al., 2019) or to determine the mechanism of action of therapeutic drugs targeting a range of cellular mechanisms (Schaf et al., 2019).

Characterization of adhesion-defective *D. discoideum* mutant cells led to the discovery that SibA, a protein with integrin features, is a surface adhesion molecule necessary for efficient phagocytosis of certain substrates (Cornillon et al., 2006). Talin and myosin VII form a cytosolic complex (Tuxworth et al., 2005) that interacts with the cytosolic domain of SibA (Cornillon et al., 2006) and of several other cell surface adhesion molecules and is thus also necessary for efficient phagocytosis (Titus, 2005). Similarly, characterization of a mutant defective for intracellular killing of Klebsiella *pneumoniae* bacteria showed that Kil2, a putative magnesium pump in the phagosomal membrane, plays a key role in intraphagosomal killing of bacteria (Lelong et al., 2011). To the best of our current knowledge, molecular mechanisms involved in ingestion and killing of bacteria appear to be largely similar in *D. discoideum* and mammalian cells (Cosson and Soldati, 2008). *D. discoideum* has been used as a model system to isolate new bacteriolytic proteins (Dhakshinamoorthy et al., 2018) or anti-infective molecules of potential biomedical interest (Hanna et al., 2020).

Phagocytosis, phagosome maturation, and intracellular bacterial killing and digestion are complex processes involving multiple gene products (Pluddemann et al., 2011; Rosales and Uribe-Querol, 2017). Our understanding of the role of individual gene products in these processes is still largely incomplete. In addition, today, there is no unified model that would account for the diverse facets of phagocytosis and link it to other cellular functions that make use of similar mechanisms and gene products, notably macropinocytosis, cell motility, and intracellular signaling (Thomas et al., 2018; Pal et al., 2019; Vines and King, 2019).

In a recent study, we characterized a new *D. discoideum* mutant which kills ingested *K. pneumoniae* bacteria inefficiently (Bodinier et al., 2020). The *lrrkA* gene, inactivated in this mutant, encodes a kinase with leucine-rich repeats. Detailed analysis revealed that a putative signaling pathway implicating Far1 (the cell surface folate receptor), LrrkA, and Kil2 stimulates intracellular killing in response to extracellular folate.

In this study, we show that in addition to its role in killing, LrrkA also controls phagocytosis and cell motility. LrrkA is thus endowed with the ability to regulate coordinately cell motility, phagocytosis, and intracellular killing when *D. discoideum* cells are exposed to bacterially secreted folate.

RESULTS

lrrkA KO Cells Phagocytose Particles More Efficiently Than WT Cells

LrrkA KO cells were initially shown to kill inefficiently ingested *K. pneumoniae* bacteria (Bodinier et al., 2020). Beyond this defect, *lrrkA* KO cells did not exhibit any major alteration of the organization of the endocytic pathway: the overall structure of endocytic compartments appeared unchanged, as well as the acidic pH of lysosomes and phagolysosomes (Bodinier et al., 2020). Staining of the actin cytoskeleton also failed to reveal any gross anomaly of the actin cytoskeleton in *lrrkA* KO cells (**Supplementary Figure S1**). These observations left open, however, the possibility that kinetic parameters such as rates of endocytosis or of phagocytosis were modified in *lrrkA* KO cells. In order to measure the ability of *lrrkA* KO cells to perform phagocytosis, wild-type (WT) and *lrrkA* KO cells were incubated in the presence of fluorescent beads for 20 min in HL5 medium, and the number of internalized beads was then determined by flow cytometry (**Figure 1A**). *LrrkA* KO cells phagocytosed beads more efficiently than WT cells (171 $\pm$ 12% of WT). On the contrary, *lrrkA* KO cells did not ingest a fluid phase marker (fluorescent dextran) more efficiently than WT cells (93 $\pm$ 6% of WT). We also assessed phagocytosis of beads over a period of 2 h, and observed that *lrrkA* KO cells ingested beads more efficiently than WT cells at all times, even after 5 min of internalization (**Figure 1B**). The fact that phagocytosis was increased upon genetic inactivation of *lrrkA* while macropinocytosis was not, suggested that an increase in cell size was not responsible for the increased phagocytosis. We verified this by measuring directly cell size using two different techniques: image-based analysis (Tali cytometer) and electric current exclusion (CASY analyzer). Both techniques revealed that the size of *lrrkA* KO cells was essentially identical to that of WT cells: 100 $\pm$ 0.2% (average $\pm$ SEM; $N = 3$ independent experiments) for image analysis and 97.6 $\pm$ 0.2% ($N = 3$) for electric current exclusion.

The Increased Phagocytosis of *lrrkA* KO Cells Is Cell Autonomous

Phagocytosis is a highly regulated process in *D. discoideum*. In particular, previous studies have shown that accumulation of (unidentified) quorum-sensing factors in the cell culture medium can inhibit significantly cell adhesion, phagocytosis, and cell motility in *D. discoideum* (Cornillon et al., 2008; Gole et al., 2011). A modification in the secretion of quorum-sensing factors could thus in principle result in a modification of phagocytosis rates.

We first studied whether the medium in which *lrrkA* KO cells grew contained less phagocytosis-inhibiting quorum-sensing factors than the medium in which WT cells grew. For this, we grew *lrrkA* KO or WT cells to the same density and collected the cell supernatants. WT cells were then exposed for 4 h to

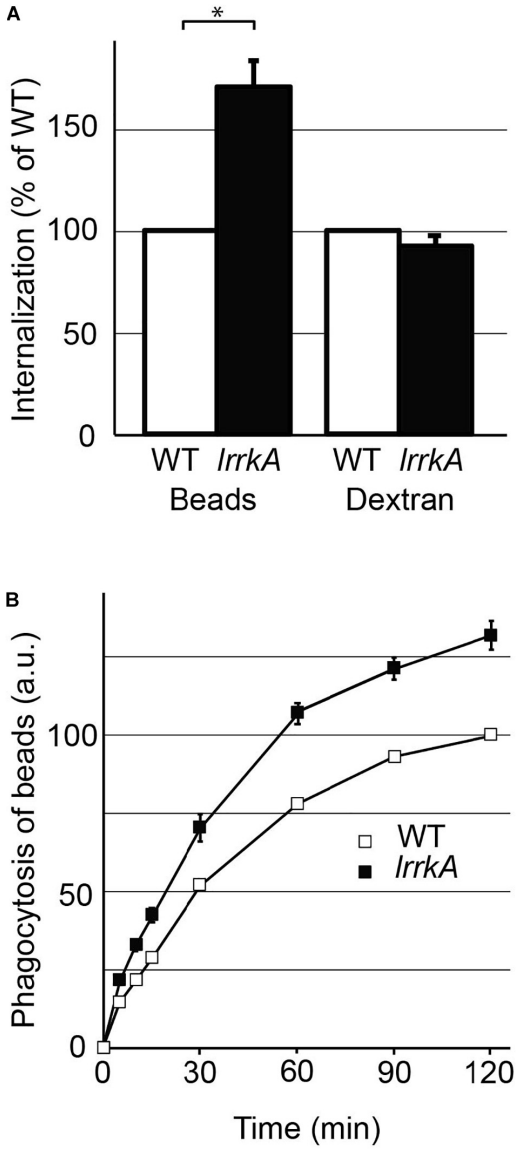

FIGURE 1 | Genetic inactivation of *lrrkA* stimulates phagocytosis. **(A)** *D. discoideum* cells (WT or *lrrkA* KO) were incubated for 20 min in HL5 medium containing either fluorescent polystyrene beads, or a fluorescent dextran. Internalization of beads or of dextran was measured by flow cytometry in seven independent experiments and averaged. Internalization by *lrrkA* KO cells was expressed as the percentage of internalization by WT cells in the same experiment (mean ± SEM, $*p < 0.01$, Mann–Whitney test, $N = 7$ independent experiments). **(B)** *D. discoideum* cells (WT or *lrrkA* KO) were incubated for the indicated time in HL5 medium containing fluorescent polystyrene beads. The average and SEM at each time are indicated. *LrrkA* KO cells phagocytosed beads significantly more than WT cells at all times ($p < 0.01$, $N = 9$, Mann–Whitney test).

increasing concentrations of these two supernatants, and their rate of phagocytosis was measured. The rates of phagocytosis were identical for cells exposed to supernatants from *lrrkA* KO or from WT cells (**Supplementary Figure S2**), indicating that both supernatants contained the same amounts of phagocytosis-inhibiting quorum-sensing factors.

We further tested whether the phenotype of *lrrkA* KO cells is cell-autonomous. For this, we mixed and co-cultured WT cells expressing GFP and *lrrkA* KO cells for 6 days. We then incubated the mixed population with rhodamine-labeled polystyrene beads, and analyzed uptake of beads by flow cytometry. Since GFP-expressing WT cells can readily be distinguished from *lrrkA* KO cells based on the fluorescence of GFP (**Figure 2A**), the phagocytosis of beads was analyzed for the two populations of cells (**Figure 2B**). The single experiment shown in **Figures 2A,B** was repeated and quantified: *lrrkA* KO cells mixed with GFP-expressing WT cells exhibited a higher level of phagocytosis (150 ± 4% of WT) (**Figure 2C**). This result indicates that the phenotype of *lrrkA* KO cells is cell-autonomous and does not reflect differences in the conditions (medium, cell density, contact with other cells. . .) in which the cells are grown.

A modification in the cellular response to quorum-sensing factors could also in principle result in a cell-autonomous modification of phagocytosis rates. To test this possibility, we exposed *lrrkA* KO and WT cells for 4 h to an increasing concentration of quorum-sensing factors secreted by WT cells; then we measured their ability to perform phagocytosis. At all concentrations of quorum-sensing factors tested, including in the absence of quorum-sensing factors, *lrrkA* KO cells phagocytosed more efficiently than WT cells (**Figure 3A**). Moreover, when the rates of phagocytosis were compared between *lrrkA* KO and WT cells incubated in the same conditions, the phenotype was quantitatively virtually identical in all conditions, with *lrrkA* KO cells ingesting approximately 1.7 times more beads than WT cells (**Figure 3B**). These observations indicate that *lrrkA* KO cells respond normally to secreted quorum-sensing factors.

Finally, in order to verify that the increased phagocytosis observed in *lrrkA* KO cells resulted from the genetic inactivation of *lrrkA*, we introduced in these cells a plasmid producing GFP-tagged LrrkA. Approximately 75% of the transfected cells expressed detectable levels of GFP-LrrkA (**Figure 4A**). The fusion protein was localized mostly in the nucleus and cytosol, with no clear accumulation at the level of cellular membranes (**Supplementary Figure S3**). Phagocytosis in cells expressing GFP-LrrkA was compared to phagocytosis in non-expressing cells (**Figure 4B**). We observed that expression of GFP-LrrkA in *lrrkA* KO cells decreased phagocytosis (**Figure 4C**), which demonstrates that the increased phagocytosis in *lrrkA* KO cells was indeed caused by the loss of LrrkA in these cells.

LrrkA Controls Interaction of *D. discoideum* With Its Substrate

The phagocytosis experiments described above take place in HL5 medium. In these conditions, SibA is the phagocytic receptor responsible for phagocytosis of beads, while it is dispensable in phosphate buffer where other (unidentified) receptors are engaged (Benghezal et al., 2003). We compared by western blot the amount of SibA found in *lrrkA* KO and WT cells, and did not detect any significant difference (**Supplementary Figure S4**).

We then measured phagocytosis in phosphate buffer for WT and *lrrkA* KO cells. *LrrkA* KO cells phagocytosed more efficiently than WT cells both in HL5 medium (164 ± 16% of WT) and

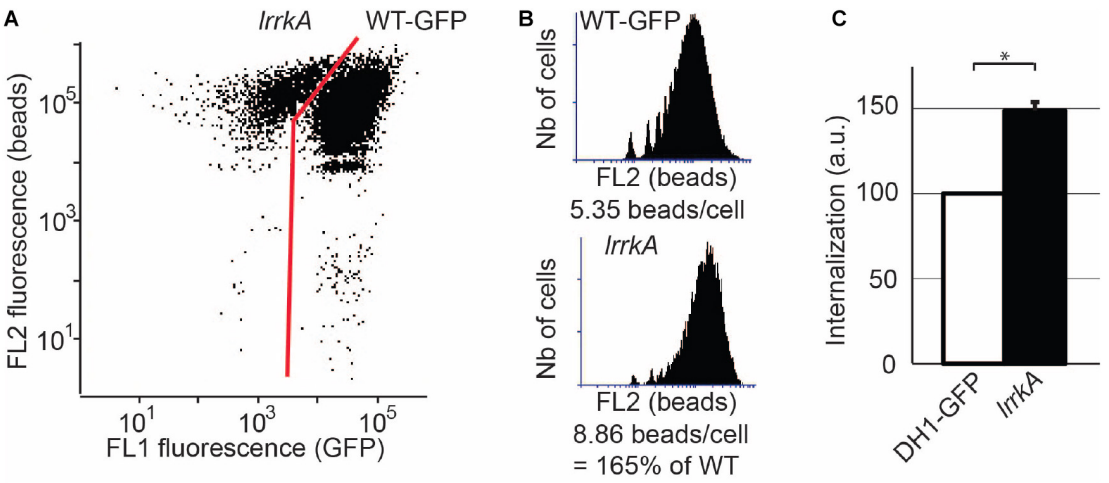

FIGURE 2 | The phenotype of *lrrkA* KO cells is cell-autonomous. WT cells expressing GFP were mixed with *lrrkA* KO cells and co-cultured for 6 days. The mixed population of cells was then incubated with rhodamine-labeled polystyrene beads for 20 min, washed, and analyzed by flow cytometry. **(A)** Based on the GFP fluorescence, WT cells were easily distinguished from *lrrkA* KO cells. **(B)** Phagocytosis of beads was determined for WT and *lrrkA* KO cells. Even when mixed with WT cells, *lrrkA* KO cells exhibited more phagocytic activity than WT cells. In the experiment shown, *lrrkA* KO cells ingested 1.65 times more beads than WT cells. **(C)** The single experiment shown in **A** and **B** was repeated and quantified (*$p < 0.01$, Mann–Whitney test; $N = 6$ independent experiments).

in phosphate buffer (PB) (160 ± 8% of WT) (**Figure 5A**). As expected, genetic inactivation of Talin A (*talA*) and Myosin VII (*myoVII*) also inhibited phagocytosis in both HL5 medium and PB, while genetic inactivation of SibA inhibited phagocytosis only in HL5 (**Figure 5A**). Thus, phagocytosis of beads is increased in *lrrkA* KO cells in PB, i.e., in conditions where SibA does not play a role in phagocytosis. In summary, the increased phagocytosis of *lrrkA* KO cells is not caused by an increase in the amount or activity of SibA.

In many mutants, changes in the phagocytic process result from alterations in the interaction between the phagocytosed particle and the phagocytic cell, for example, an alteration in the ability of cells to adhere to a particle or to spread on its surface. However, the phagocytic event is transient and difficult to visualize, and it is much easier to characterize the interaction of *D. discoideum* with a flat surface. In order to measure the ability of *lrrkA* KO cells to interact with a substrate, we visualized and measured their zone of tight contact with a glass surface by interference reflection microscopy (**Figure 5B**). Quantitative analysis revealed that *lrrkA* KO cells spread more efficiently than WT cells on the substrate, both in HL5 and in phosphate buffer (**Figure 5C**). As expected, *talA* and *myoVII* KO cells exhibited defective spreading in both HL5 and phosphate buffer, while *sibA* KO cells spread less efficiently than WT cells in HL5, but normally in phosphate buffer (**Figure 5C**).

Together these results suggest that LrrkA negatively regulates the cytosolic machinery engaged in cellular adhesion and phagocytosis.

LrrkA Plays a Role in the Control of Cell Motility

To characterize in a more kinetic manner the interaction between cells and their substrate, we measured the ability of cells to move on their substrate. We first determined the random motility of WT and *lrrkA* KO cells on a glass substrate in HL5 by taking pictures every 10 seconds. This revealed a significant increase in motility of *lrrkA* KO cells compared to WT cells (**Figure 6A**). We also observed a major increase in motility of *lrrkA* KO cells compared to WT cells when analyzed in phosphate buffer (**Figure 6B**).

Our recent results suggested that LrrkA participates in a putative signaling pathway linking the Far1 folate receptor to Kil2 and allowing folate to stimulate intracellular killing (Bodinier et al., 2020). We thus tested similarly the ability of various mutant cells to modify their motility in response to folate. For this, we measured random cell motility in phosphate buffer supplemented or not with 1 mM folate. As previously described (Lima et al., 2014), folate stimulated motility of WT and of *kil2* KO cells (**Figure 6C**). Unstimulated *lrrkA* KO cells were more mobile than WT cells, but their motility did not increase further upon addition of folate (**Figure 6C**). Unstimulated *far1* KO cells, devoid of folate receptor, exhibited normal motility but did not respond to the addition of folate (**Figure 6C**). In *talA* or *myoVII* KO cells, the unstimulated motility was reduced, and the cells failed to respond to folate (**Figure 6C**). As discussed below, the fact that motility is higher in *lrrkA* KO cells and that it is unchanged upon addition of folate indicates that LrrkA plays a role in the control of cell motility in *D. discoideum* cells.

LrrkA Is Dispensable for the Transcriptional Response to Folate

We recently studied by RNA sequencing the transcription profiles of *D. discoideum* cells exposed to various stimuli, in particular folate (Lamrabet et al., 2020). This allowed us to define a set of ten genes whose expression varies specifically upon exposure to folate (**Supplementary Figure S5A**). We first validated these

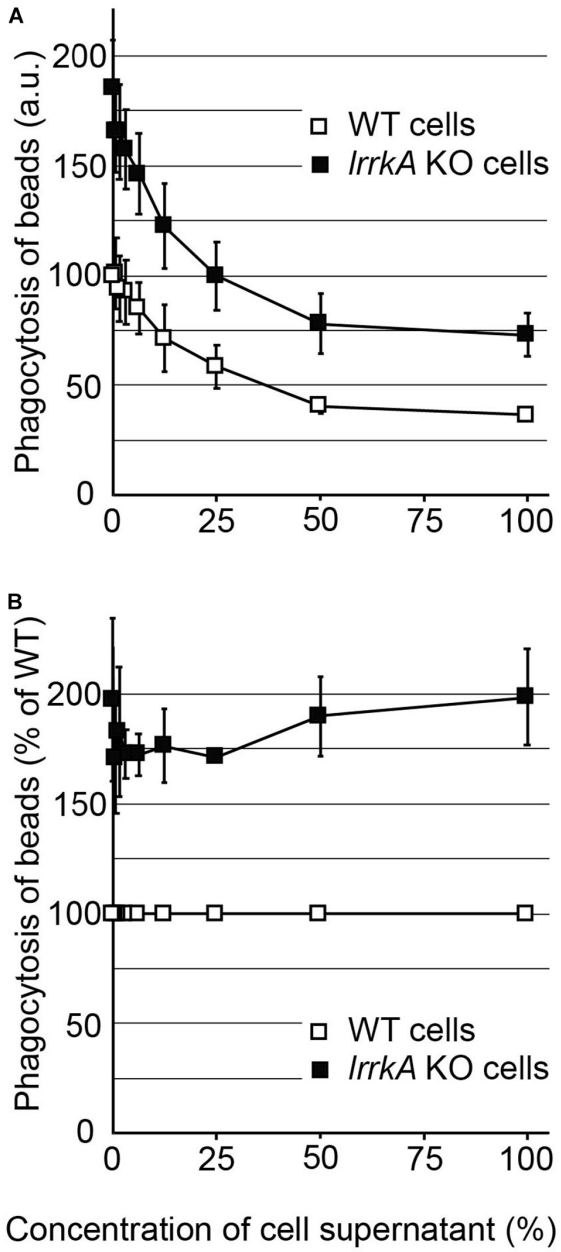

FIGURE 3 | Response of *lrrkA* KO cells to secreted quorum-sensing factors. **(A)** WT or *lrrkA* KO cells were incubated for 4 h with a cellular supernatant of WT cells diluted in fresh medium as indicated. The ability of the cells to ingest polystyrene beads was then measured as described in the legend to **Figure 1**. At all concentrations of quorum-sensing factors, *lrrkA* KO cells phagocytosed beads more efficiently than WT cells (average ± SEM, $N = 3$ independent experiments). **(B)** For each condition, phagocytosis by *lrrkA* KO cells was represented as a percentage of WT phagocytosis in the same condition. In all conditions, *lrrkA* KO cells phagocytosed 1.5–2 times more beads than WT cells.

results by preparing RNA from WT *D. discoideum* cells exposed to folate or not. This experiment confirmed that the expression of the selected set of genes is regulated by folate (**Supplementary Figure S5B**). We then measured the expression of these genes in WT, *far1*, or *lrrkA* KO cells (**Figure 7**). In *far1* KO cells, gene expression was not modified by exposure to folate, confirming that folate sensing relies critically on the Far1 receptor. On the contrary, *lrrkA* KO cells responded to folate in a manner indistinguishable from WT cells (**Figure 7**), indicating that LrrkA does not play a critical role in gene regulation upon folate exposure.

DISCUSSION

In this study, we describe a new role for LrrkA as a negative regulator of cell motility and phagocytosis. Based on these observations and on the previously published role of LrrkA in activation of intracellular killing (Bodinier et al., 2020), we propose a model where LrrkA functions in two modes, as schematized in **Figure 8**. In the absence of folate (**Figure 8A**), LrrkA does not stimulate killing. It inhibits motility and phagocytosis, as evidenced by the fact that genetic inactivation of *lrrkA* leads to an increase in phagocytosis and motility in these conditions. In the presence of a high concentration of folate (**Figure 8B**), which in the environment is secreted by bacteria, Far1 activates LrrkA which in turn stimulates intracellular killing via activation of Kil2, as previously reported (Bodinier et al., 2020). In the same conditions, the inhibitory effect of LrrkA on motility is lost, as evidenced by the fact that *lrrkA* KO cells are as motile as parental cells. According to this model, the ability of folate to increase cell motility would at least partly be due to the fact that it relieves the inhibition of cell motility by LrrkA. This rapid LrrkA-dependent adaptation of cellular physiology to changes in the environment should be distinguished from slower adaption involving changes in gene transcription which, according to our observations, does not rely on the function of LrrkA. Our study does not provide biochemical evidence demonstrating direct physical interaction of LrrkA with other proteins, or identifying the proteins that are phosphorylated by LrrkA. The proposed model is the simplest model compatible with the observed phenotype of mutant cells, but many alternative models could be proposed. Whatever the molecular organization of these signaling pathways, our results suggest that LrrkA plays an important role in allowing *D. discoideum* cells to increase coordinately motility, phagocytosis, and intracellular killing when they sense the presence of bacterial folate, thus favoring both an efficient capture and intracellular killing of bacteria. We are aware that intracellular signaling pathways are often more branched and complex than the simple scheme proposed in this study. More detailed studies will certainly be necessary to determine the exact role of LrrkA in the hierarchy of intracellular signaling pathways controlling cell motility, phagocytosis, and intracellular killing.

Dictyostelium discoideum has been used as a simple model system to analyze the mode of action of bioactive compounds like lithium and valproic acid (two mood-stabilizing drugs), or to discover new compounds with similar modes of action (Schaf et al., 2019). Similarly, *D. discoideum* has proven valuable to study the molecular basis for lysosomal diseases like the neuronal ceroid lipofuscinoses (McLaren et al., 2019). In these two

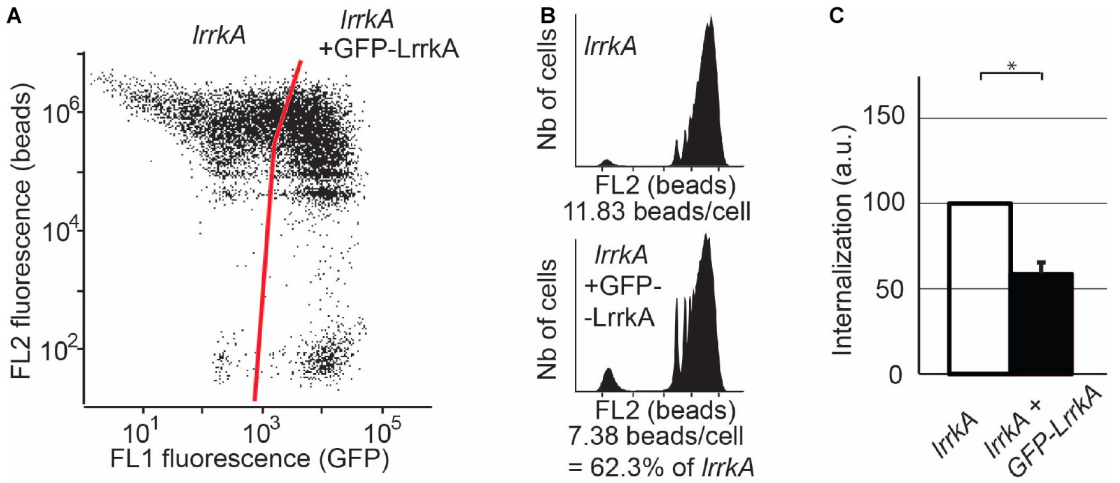

FIGURE 4 | Reexpression of LrrkA decreases phagocytosis in *lrrkA* KO cells. **(A)** Expression of GFP-LrrkA in *lrrkA* KO cells was assessed by flow cytometry. After 5 days of culture with no G418 selection, approximately 75% of transfected cells exhibited detectable GFP-LrrkA, while 25% did not produce the protein. **(B)** Phagocytosis was assessed by flow cytometry in *lrrkA* KO cells expressing GFP-LrrkA and in non-expressing cells. **(C)** Phagocytosis in *lrrkA* KO cells expressing GFP-LrrkA was measured in five independent experiments and expressed as a percentage of phagocytosis in cells that did not express GFP-LrrkA (mean ± SEM, $*p < 0.05$, Mann–Whitney test, $N = 5$ independent experiments).

instances, a detailed understanding of the underlying molecular mechanisms was an essential prerequisite to allow extrapolation of the results from *D. discoideum* to human. Human LRRK2 kinase has been linked to the function of the endocytic pathway, but its function is still incompletely understood, as well as its presumptive role in the etiology of sporadic Parkinson's disease (Bodinier et al., 2020). It is difficult at this stage to establish a parallel between the molecular function(s) of Lrr kinases in human and in *D. discoideum*, since the family of Lrr kinases is much less diverse in human than in *D. discoideum* (Bodinier et al., 2020). However, our results suggest that LrrkA, like LRRK2, is linked to the regulation of the endocytic pathway in *D. discoideum*. Hopefully, these observations will contribute to the development of *D. discoideum* as a tractable model system for biomedical research.

MATERIALS AND METHODS

Strains and Cell Culture

Dictyostelium discoideum cells were grown at 21°C in HL5 medium (Froquet et al., 2009). *D. discoideum* cells were all derived from the DH1-10 parental strain (Cornillon et al., 2000), referred to in this study as WT. *lrrk*A KO, *far*1 KO, *kil*2 KO, *sib*A KO, *tal*A KO, and *myo*VII KO cells were described previously (Gebbie et al., 2004; Tsujioka et al., 2008; Lelong et al., 2011; Froquet et al., 2012; Pan et al., 2016; Bodinier et al., 2020). In order to re-express GFP-LrrkA in *lrrkA* KO cells, we cloned the coding sequence of LrrkA in the pDM351 expression vector (Veltman et al., 2009), which drives the production of LrrkA fused at its N-terminal end to the GFP protein. The transfected cells were selected in the presence of G418 (12.5 μg/mL). They were transferred to HL5 without G418 5 days before testing their ability to perform phagocytosis.

Phagocytosis and Macropinocytosis

To measure efficiency of phagocytosis, 3×10^5 *D. discoideum* cells were washed once, resuspended in either 1 mL of HL5 or 1 mL of phosphate buffer (PB: 2 mM Na_2HPO_4, 14.7 mM KH_2PO_4, pH 6.5) containing 1 μl of FITC polystyrene beads (Fluoresbrite plain YG 1 micron, Polysciences), and incubated for 30 min in a shaken suspension. To assess macropinocytosis, cells were incubated in either HL5 or PB containing 10 μg/mL Alexa-647 Dextran (Life Technologies) for 30 min. Then, cells were washed in ice cold HL5 supplemented with 0.1% NaN_3 and internalized fluorescence was measured by flow cytometry. Ingested fluorescence was determined for each strain and normalized to internalization in WT cells.

For phagocytosis kinetic measurements, cells were incubated in 1 mL of HL5 containing 1 μL FITC polystyrene beads, and a 100 μL aliquot of the suspension was taken at each indicated time point. Cells were then washed, and phagocytosis was analyzed as described above.

When mixed populations containing GFP-expressing cells (FL1 channel) were used, they were allowed to ingest red fluorescent beads (Fluoresbrite Polychromatic Red, Polysciences, FL2 channel). The fluorescence values were corrected to compensate for leakage of fluorescence between the FL1 and FL2 channels. To ascertain that the cells were adequately identified as GFP-positive or -negative, control populations were analyzed. When *lrrkA* KO cells were mixed with WT-GFP cells (**Figure 2**), *lrrkA* KO and WT-GFP cells were analyzed separately in parallel, and each cell type was present almost exclusively in the assigned window (99.9 and 99.5%, respectively).

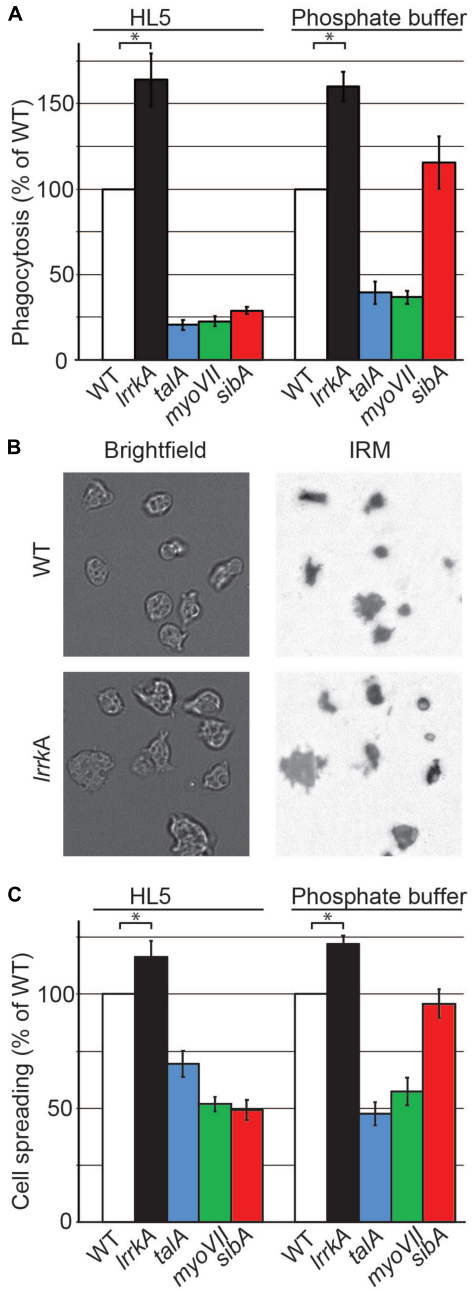

FIGURE 5 | Genetic inactivation of *lrrkA* increases interaction with substrates in HL5 and in phosphate buffer. **(A)** Phagocytosis of polystyrene beads was measured for the indicated mutant cells as described in the legend to **Figure 1**. *LrrkA* KO cells phagocytosed more efficiently than WT cells both in HL5 and in phosphate buffer (PB) (average ± SEM; $*p < 0.01$, Mann–Whitney test; $N = 19$ independent experiments). **(B)** Brightfield and interference reflection pictures of WT and *lrrkA* KO cells (here in HL5) allow to visualize the contact area between cells and their substratum. **(C)** Spreading of WT and mutant cells on their substrate in HL5 and in PB reflects their ability to phagocytose particles. The contact surface between WT cells and the glass substrate was 62 and 87 μm^2 in HL5 and SB, respectively. Spreading of all mutants analyzed was significantly different from WT, except for *sibA* KO cells in phosphate buffer (average ± SEM; $*p < 0.01$, Student's *t*-test, number of cells analyzed in HL5/SB: WT 197/162; *lrrkA* 199/85; *talA* 173/125; *myoVII* 242/79; *sibA* 202/121; $N = 2$ independent experiments).

Similarly, when *lrrkA* KO cells were transfected with a GFP-LrrkA expressing plasmid, untransfected cells were analyzed in parallel and were almost exclusively (99.8%) found in the GFP-negative window. In the transfected population, GFP-negative cells represented 24% of the total in a control sample (no beads phagocytosed), and 23.6% in the sample of cells having ingested beads, indicating that no significant number of cells were assigned to the wrong population. In all measures of phagocytosis, median values were used, ensuring that a small percentage of cells improperly identified as GFP-negative or GFP-positive would not significantly affect the results.

To produce conditioned cellular supernatant, *D. discoideum* cells were grown to a density of 4×10^6 cells in a shaken suspension in HL5 medium. The cell supernatant was recovered by centrifuging cells at 1,500 *g* for 10 min. To assess the effect of conditioned medium on phagocytosis, cells were incubated for 4 h in fresh or conditioned medium in six-well plates (450,000 cells per well in 1.5 mL), then resuspended, and allowed to phagocytose beads for 5 min in fresh HL5 medium.

Cell Volume Measurement

Cell size was determined based on electric current exclusion (CASY technology), using a CASY 1 cell counter as previously described (Dias et al., 2016). The Tali image-based cytometer (ThermoFischer Scientific) was also used to automatically measure the size of cells based on pictures of cell suspension.

Cellular Motility

To assess the motility of *D. discoideum* cells, 10^5 cells were washed once and resuspended in 1 mL of PB/Sorbitol (PB + 100 mM Sorbitol). 100 µL of the cell suspension was deposited in 96-well plates (Greiner Bio one; Ref 655090), and the cells allowed to settle for 30 min. Then 100 µL of PB/Sorbitol supplemented or not with 1 mM folate was added to each well. Cells were imaged every 15 s for 30 min with a Nikon Eclipse T*i*2 equipped with a DS-Qi2 camera. The resulting movies were analyzed with the software MetaMorph (Molecular Devices) using the "Track points" function.

Cell Spreading

To measure the spreading of *D. discoideum* cells on a surface, 5×10^5 cells were washed once and resuspended in either 1 mL HL5 or 1 mL PB. A 50 µL drop was deposited on a glass-bottom fluorodish (WPI, Inc.; ref: FD35-100), and the cells allowed to attach for 30 min. A Zeiss Axio Observer Z1 equipped with a Neofluar 63x/1.25 Oil Ph3 Antiflex objective for RICM measurement was used for imaging. Quantification of the cell speading surface was done using FiJi (v1.52j).

To visualize the actin cytoskeleton, 10^6 *D. discoideum* cells were let to adhere to a glass coverslip for 30 min in HL5 medium. Cells were then fixed with 4% paraformaldehyde for 30 min, washed, permeabilized with methanol at −20°C for 2 min, and labeled with 1 µg/mL tetramethylrhodamine B isothiocyanate (TRITC)-coupled phalloidin in PBS containing 0.2% bovine serum albumin (PBS-BSA) for 1 h. The coverslips were washed twice in PBS-BSA, once in PBS, then mounted, and observed by laser scanning confocal microscopy (Zeiss LSM 800).

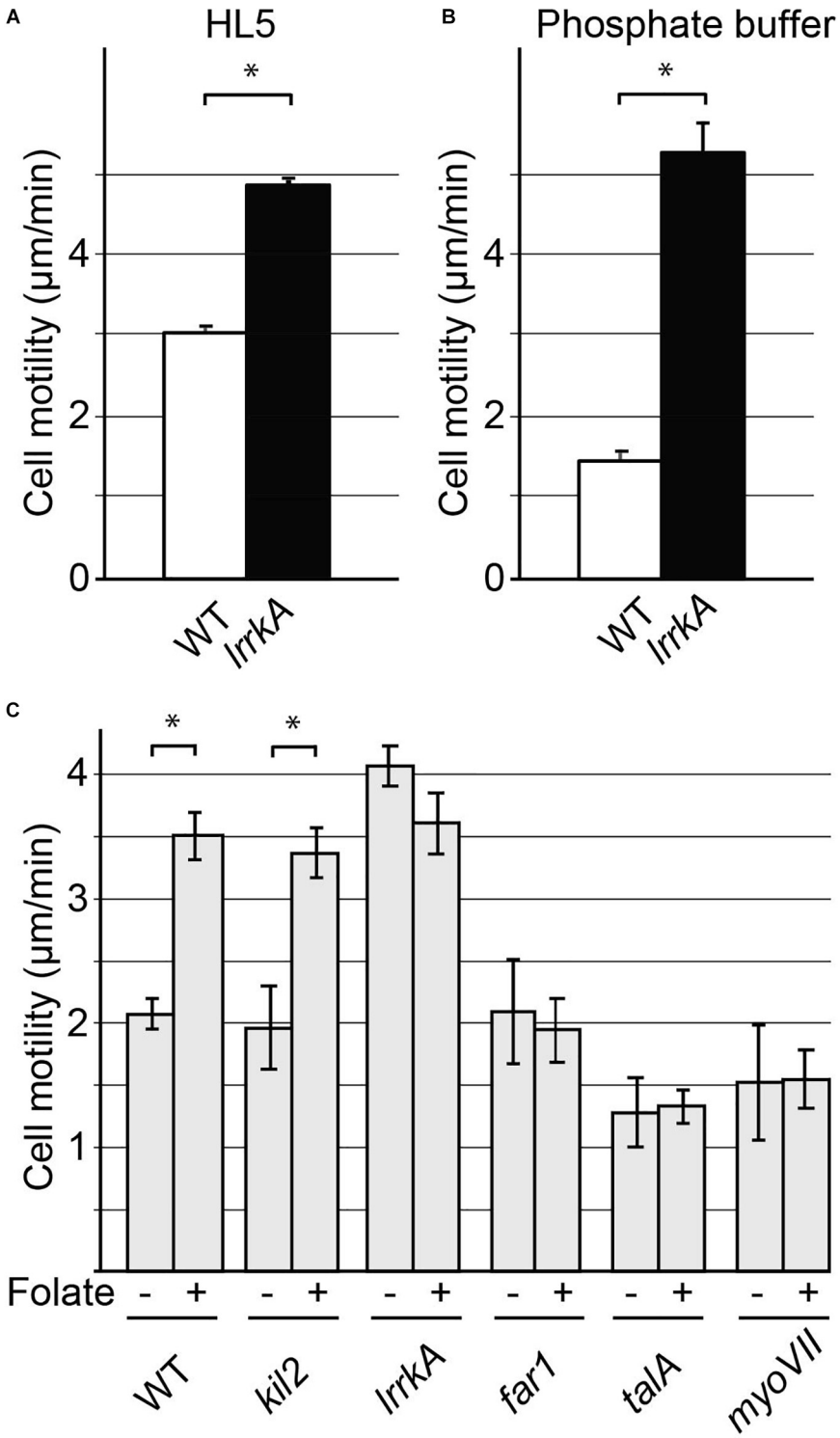

FIGURE 6 | Cell motility is increased by genetic inactivation of *lrrkA*. Random motility of WT or *lrrkA* KO cells on a substrate was measured in HL5 **(A)** and phosphate buffer **(B)**. Motility was significantly higher in *lrrkA* KO cells than in WT cells (average ± SEM; $*p < 0.01$, Student's *t*-test, number of cells analyzed in HL5/SB: WT 110/195; *lrrkA* 363/225; *N* = 3 independent experiments). Random motility of WT or mutant cells was also measured in phosphate buffer in the presence or absence of folate **(C)**. Motility increased significantly in WT cells or in *kil2* KO cells upon exposure to folate. In *lrrkA* KO cells, cell motility was high even in the absence of folate, and was not further stimulated upon folate addition. In *far1*, *talA*, and *myoVII* KO cells, folate failed to stimulate cell motility (average ± SEM; $*p < 0.01$, Student's *t*-test, number of cells analyzed in SB/SB + folate: WT 225/90; *lrrkA* 315/150; *kil2*, far1, *talA, myoVII* 45/45; *N* = 3 independent experiments). Distinct experiments are reported in **(B)** and **(C)**.

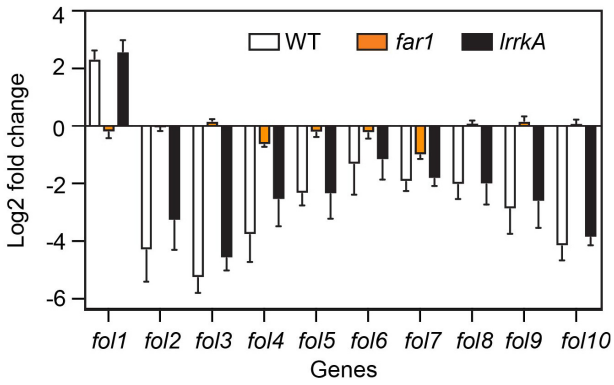

FIGURE 7 | Folate control of gene transcription is independent of LrrkA. We measured by qPCR the levels of various RNAs in cells exposed or not to folate. The average and SEM of three independent experiments are shown. As previously observed, the transcription of genes *fol1-fol10* is altered when cells are exposed to folate (increased for *fol1*, decreased for *fol2-10*). This regulation is essentially lost in *far1* KO cells. On the contrary, in *lrrkA* KO cells, transcriptional response to folate is indistinguishable from that observed in WT cells.

Western Blot

To determine the levels of cellular proteins, 10^6 cells were resuspended in 10 µL of sample buffer (0.103 g/mL sucrose, 50 mM Tris, pH 6.8, 10 mM EDTA, 0.5 mg/mL bromophenol blue, 2% SDS), and proteins were separated by electrophoresis on an SDS-polyacrylamide gel. Proteins were then transferred to a nitrocellulose membrane before immunodetection with anti-SibA (Cornillon et al., 2006), anti-TalinA (Benghezal et al., 2006), or anti-protein disulfide isomerase (PDI) (Lelong et al., 2011) primary antibodies. Horseradish-peroxidase-coupled anti-mouse (for anti-TalinA and anti-PDI) and anti-rabbit (for anti-SibA) antibodies were used as secondary antibodies. The signal was revealed by enhanced chemiluminescence (ECL) (Amersham Biosciences) using a PXi-4 gel imaging systems (Syngene).

Reverse-Transcription Quantitative PCR (RT-PCR)

Reverse-transcription (RT)-PCR experiments were performed essentially as previously described (Lamrabet et al., 2020). *D. discoideum* cells (4×10^6 cells/mL) were incubated for 4 h in HL5 supplemented or not with 1 mM folate. The total RNAs from *D. discoideum* or mutant cells exposed or not to 1 mM folate were purified with a Qiagen RNeasy kit following manufacturer's instructions. cDNA was synthesized from 1 µg of total RNA using random hexamers and Superscript II reverse transcriptase (Invitrogen).

For each gene analyzed, oligonucleotide sequences were aligned against the *D. discoideum* coding sequence database by BLAST to ensure that they were specific for the gene tested. PCR reactions (10 µL) contained SYBR Green Master Mix (Applied Biosystems), diluted cDNA (150 ng), and 500 nM of forward and reverse oligonucleotides, and were analyzed in a StepOnePlus cycler (Invitrogen) with the following parameters: 95°C for 1 min, 40 cycles of 95°C/10 s, and 60°C/1 min. Twofold changes were calculated as Δ(ΔCT), with the *rnlA* and *gpdA* genes used as a standard for normalization. Data were collected from three biological replicates.

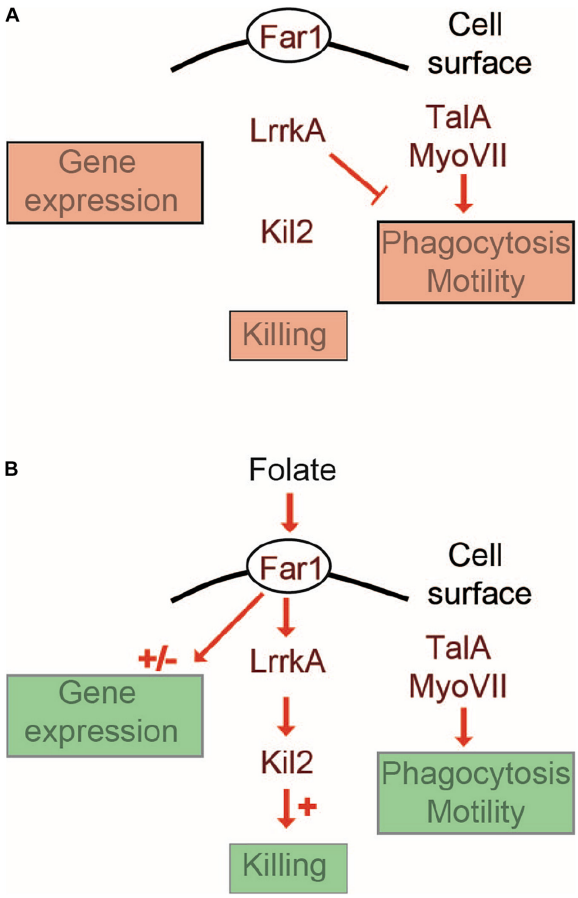

FIGURE 8 | Cellular response to folate: a working model. This schematic overview proposes a minimalist interpretation of the results presented in this manuscript and in previous publications. Far1, the cell surface receptor for folate is essential for all cellular responses to folate. A Far1-LrrkA-Kil2 pathway stimulates intracellular killing in response to folate. LrrkA inhibits cell motility in the absence of folate **(A)**, and the inhibition is relieved upon stimulation by folate **(B)**. The transcriptional response to folate operates in an LrrkA-independent manner.

DATA AVAILABILITY STATEMENT

The raw data supporting the conclusions of this article will be made available by the authors, without undue reservation.

AUTHOR CONTRIBUTIONS

RB, AS, JL, AM, OL, IA, and VF designed and performed the experiments and interpreted the data. RB and PC wrote the manuscript. TK, IW, and PC supervised the project. All authors reviewed the manuscript.

FUNDING

This work was supported by the Swiss National Science Foundation (grant 31003A_172951 to PC) and financed within the Croatian-Swiss Research Program of the Croatian Science Foundation and the Swiss National Science Foundation with funds obtained from the Swiss-Croatian Cooperation Program (IZHRZ0_180584 to IW and PC).

SUPPLEMENTARY MATERIAL

The Supplementary Material for this article can be found online at: https://www.frontiersin.org/articles/10.3389/fcell.2021.629200/full#supplementary-material

Supplementary Figure S1 | Morphology of the actin cytoskeleton in WT and *lrrkA* KO cells. WT and *lrrkA* KO were allowed to adhere to a glass coverslip, then fixed, permeabilized, and stained with fluorescent phalloidin to reveal the structure of the actin cytoskeleton. Three pictures are shown for WT and for *lrrkA* KO cells. The morphology of the actin cytoskeleton appeared highly similar in WT and *lrrkA* KO cells. Bar: 10 μm.

Supplementary Figure S2 | Secretion of quorum-sensing factors by *lrrkA* KO cells. WT cells were incubated for 4 h with cell supernatants from WT or *lrrkA* KO cells diluted as indicated with fresh HL5. The cells were then incubated with polystyrene beads and phagocytosis measured as described in the legend to **Figure 1**. Phagocytosis was expressed as the percentage of internalization by WT cells in fresh medium in the same experiment (average ± SEM, *N* = 3 independent experiments). Cells incubated in fresh medium (0% cell supernatant) phagocytosed beads approximately four times more efficiently than cells incubated in pure cell supernatants (100% cell supernatant) containing concentrated quorum-sensing factors. Cell supernatants diluted with fresh medium were also assessed to evaluate more precisely the quorum-sensing activity. The supernatant of *lrrkA* KO cells exhibited exactly the same inhibitory effect on phagocytosis as the supernatant of WT cells.

Supplementary Figure S3 | GFP-LrrkA is localized in the nucleus and the cytosol. *LrrkA* KO cells expressing GFP-LrrkA were fixed with 2% formaldehyde and visualized by confocal microscopy. GFP fluorescence was visible in the nucleus (arrowheads) and in the cytosol. Untransfected *lrrkA* KO cells were used in parallel as negative controls and did not show any GFP fluorescence. Bar: 5 μm.

Supplementary Figure S4 | Cellular levels of SibA, PDI, and Talin A are similar in WT and *lrrkA* KO cells. **(A)** Cellular proteins were separated on an SDS-polyacrylamide gel, transferred to nitrocellulose, and the indicated proteins were detected with specific antibodies. **(B)** The intensity of the signal was determined in several independent experiments, and is indicated as a ratio of the signal in *lrrkA* KO and WT cells. The quantification of the experiment shown in **A** is indicated in red. The amount of SibA, Talin, and PDI (used as a control) was indistinguishable in *lrrkA* KO and WT cells.

Supplementary Figure S5 | Regulation of gene expression by folate. *D. discoideum* WT cells grown in HL5 were exposed or not to 1 mM folate for 4 h. RNA-seq analysis allowed the identification of 10 genes for which transcription was significantly altered by exposure to folate. **(A)** For each gene considered (*fol1* to *fol10*), the gene identity and name are indicated, as well as the pair of primers used for RT-PCR and the size of the amplicon. **(B)** For the 10 genes analyzed, RT-PCR analysis confirmed the results obtained by RNA-seq.

REFERENCES

Benghezal, M., Cornillon, S., Gebbie, L., Alibaud, L., Bruckert, F., Letourneur, F., et al. (2003). Synergistic control of cellular adhesion by transmembrane 9 proteins. *Mol. Biol. Cell* 14, 2890–2899. doi: 10.1091/mbc.e02-11-0724

Benghezal, M., Fauvarque, M. O., Tournebize, R., Froquet, R., Marchetti, A., Bergeret, E., et al. (2006). Specific host genes required for the killing of Klebsiella bacteria by phagocytes. *Cell Microbiol.* 8, 139–148. doi: 10.1111/j.1462-5822.2005.00607.x

Bodinier, R., Leiba, J., Sabra, A., Jauslin, T. N., Lamrabet, O., Guilhen, C., et al. (2020). LrrkA, a kinase with leucine-rich repeats, links folate sensing with Kil2 activity and intracellular killing. *Cell Microbiol.* 22:e13129.

Bozzaro, S., Bucci, C., and Steinert, M. (2008). Phagocytosis and host-pathogen interactions in *Dictyostelium* with a look at macrophages. *Int. Rev. Cell Mol. Biol.* 271, 253–300. doi: 10.1016/s1937-6448(08)01206-9

Bretschneider, T., Othmer, H. G., and Weijer, C. J. (2016). Progress and perspectives in signal transduction, actin dynamics, and movement at the cell and tissue level: lessons from *Dictyostelium*. *Interface Focus* 6:20160047. doi: 10.1098/rsfs.2016.0047

Buckley, C. M., and King, J. S. (2017). Drinking problems: mechanisms of macropinosome formation and maturation. *FEBS J.* 284, 3778–3790. doi: 10.1111/febs.14115

Cornillon, S., Froquet, R., and Cosson, P. (2008). Involvement of sib proteins in the regulation of cellular adhesion in *Dictyostelium discoideum*. *Eukaryot Cell* 7, 1600–1605. doi: 10.1128/ec.00155-08

Cornillon, S., Gebbie, L., Benghezal, M., Nair, P., Keller, S., Wehrle-Haller, B., et al. (2006). An adhesion molecule in free-living *Dictyostelium* amoebae with integrin beta features. *EMBO Rep.* 7, 617–621. doi: 10.1038/sj.embor.7400701

Cornillon, S., Pech, E., Benghezal, M., Ravanel, K., Gaynor, E., Letourneur, F., et al. (2000). Phg1p is a nine-transmembrane protein superfamily member involved in *Dictyostelium* adhesion and phagocytosis. *J. Biol. Chem.* 275, 34287–34292. doi: 10.1074/jbc.m006725200

Cosson, P., and Soldati, T. (2008). Eat, kill or die: when amoeba meets bacteria. *Curr. Opin. Microbiol.* 11, 271–276. doi: 10.1016/j.mib.2008.05.005

Cougoule, C., Wiedemann, A., Lim, J., and Caron, E. (2004). Phagocytosis, an alternative model system for the study of cell adhesion. *Semin. Cell Dev. Biol.* 15, 679–689. doi: 10.1016/s1084-9521(04)00087-4

Dhakshinamoorthy, R., Bitzhenner, M., Cosson, P., Soldati, T., and Leippe, M. (2018). The saposin-like protein AplD displays pore-forming activity and participates in defense against bacterial infection during a multicellular stage of *Dictyostelium discoideum*. *Front. Cell Infect. Microbiol.* 8:73.

Dias, M., Brochetta, C., Marchetti, A., Bodinier, R., Bruckert, F., and Cosson, P. (2016). Role of SpdA in cell spreading and phagocytosis in *Dictyostelium*. *PLoS One* 11:e0160376. doi: 10.1371/journal.pone.0160376

Froquet, R., le Coadic, M., Perrin, J., Cherix, N., Cornillon, S., and Cosson, P. (2012). TM9/Phg1 and SadA proteins control surface expression and stability of SibA adhesion molecules in *Dictyostelium*. *Mol. Biol. Cell* 23, 679–686. doi: 10.1091/mbc.e11-04-0338

Froquet, R., Lelong, E., Marchetti, A., and Cosson, P. (2009). *Dictyostelium discoideum*: a model host to measure bacterial virulence. *Nat. Protoc.* 4, 25–30. doi: 10.1038/nprot.2008.212

Gebbie, L., Benghezal, M., Cornillon, S., Froquet, R., Cherix, N., Malbouyres, M., et al. (2004). Phg2, a kinase involved in adhesion and focal site modeling in *Dictyostelium*. *Mol. Biol. Cell* 15, 3915–3925. doi: 10.1091/mbc.e03-12-0908

Gole, L., Riviere, C., Hayakawa, Y., and Rieu, J. P. (2011). A quorum-sensing factor in vegetative *Dictyostelium discoideum* cells revealed by quantitative migration analysis. *PLoS One* 6:e26901. doi: 10.1371/journal.pone.0026901

Hanna, N., Kicka, S., Chiriano, G., Harrison, C., Sakouhi, H. O., Trofimov, V., et al. (2020). Identification of anti-mycobacterium and anti-legionella compounds with potential distinctive structural scaffolds from an HD-PBL using phenotypic screens in amoebae host models. *Front. Microbiol.* 11:266.

Lamrabet, O., Melotti, A., Burdet, F., Hanna, N., Perrin, J., Nitschke, J., et al. (2020). Transcriptional responses of *Dictyostelium discoideum* exposed to different classes of bacteria. *Front. Microbiol.* 11:410.

Lelong, E., Marchetti, A., Gueho, A., Lima, W. C., Sattler, N., Molmeret, M., et al. (2011). Role of magnesium and a phagosomal P-type ATPase in intracellular bacterial killing. *Cell Microbiol.* 13, 246–258. doi: 10.1111/j.1462-5822.2010.01532.x

Lima, W. C., Balestrino, D., Forestier, C., and Cosson, P. (2014). Two distinct sensing pathways allow recognition of *Klebsiella pneumoniae* by *Dictyostelium* amoebae. *Cell Microbiol.* 16, 311–323. doi: 10.1111/cmi.12226

McLaren, M. D., Mathavarajah, S., and Huber, R. J. (2019). Recent insights into NCL protein function using the model organism *Dictyostelium discoideum*. *Cells* 8:115. doi: 10.3390/cells8020115

Mori, M., Mode, R., and Pieters, J. (2018). From phagocytes to immune defense: roles for coronin proteins in *Dictyostelium* and mammalian immunity. *Front. Cell Infect. Microbiol.* 8:77.

Pal, D. S., Li, X., Banerjee, T., Miao, Y., and Devreotes, P. N. (2019). The excitable signal transduction networks: movers and shapers of eukaryotic cell migration. *Int. J. Dev. Biol.* 63, 407–416. doi: 10.1387/ijdb.190265pd

Pan, M., Xu, X., Chen, Y., and Jin, T. (2016). Identification of a chemoattractant G-Protein-coupled receptor for folic acid that controls both chemotaxis and phagocytosis. *Dev. Cell* 36, 428–439. doi: 10.1016/j.devcel.2016.01.012

Pluddemann, A., Mukhopadhyay, S., and Gordon, S. (2011). Innate immunity to intracellular pathogens: macrophage receptors and responses to microbial entry. *Immunol. Rev.* 240, 11–24. doi: 10.1111/j.1600-065x.2010.00989.x

Rosales, C., and Uribe-Querol, E. (2017). Phagocytosis: a fundamental process in immunity. *Biomed. Res. Int.* 2017:9042851.

Schaf, J., Damstra-Oddy, J., and Williams, R. S. B. (2019). *Dictyostelium discoideum* as a pharmacological model system to study the mechanisms of medicinal drugs and natural products. *Int. J. Dev. Biol.* 63, 541–550. doi: 10.1387/ijdb.190228rw

Stuelten, C. H., Parent, C. A., and Montell, D. J. (2018). Cell motility in cancer invasion and metastasis: insights from simple model organisms. *Nat. Rev. Cancer* 18, 296–312. doi: 10.1038/nrc.2018.15

Thomas, M. A., Kleist, A. B., and Volkman, B. F. (2018). Decoding the chemotactic signal. *J. Leukoc. Biol.* 104, 359–374. doi: 10.1002/jlb.1mr0218-044

Titus, M. A. (2005). A conserved role for myosin VII in adhesion. *Novart. Found Symp.* 269, 16–24; discussion 24–34, 223–230.

Tsujioka, M., Yoshida, K., Nagasaki, A., Yonemura, S., Muller-Taubenberger, A., and Uyeda, T. Q. (2008). Overlapping functions of the two talin homologues in *Dictyostelium*. *Eukaryot. Cell* 7, 906–916. doi: 10.1128/ec.00464-07

Tuxworth, R. I., Stephens, S., Ryan, Z. C., and Titus, M. A. (2005). Identification of a myosin VII-talin complex. *J. Biol. Chem.* 280, 26557–26564. doi: 10.1074/jbc.m503699200

Veltman, D. M., Akar, G., Bosgraaf, L., and Van Haastert, P. J. (2009). A new set of small, extrachromosomal expression vectors for *Dictyostelium discoideum*. *Plasmid* 61, 110–118. doi: 10.1016/j.plasmid.2008.11.003

Vines, J. H., and King, J. S. (2019). The endocytic pathways of *Dictyostelium discoideum*. *Int. J. Dev. Biol.* 63, 461–471. doi: 10.1387/ijdb.190236jk

Conflict of Interest: The authors declare that the research was conducted in the absence of any commercial or financial relationships that could be construed as a potential conflict of interest.

Copyright © 2021 Bodinier, Sabra, Leiba, Marchetti, Lamrabet, Ayadi, Filić, Kawata, Weber and Cosson. This is an open-access article distributed under the terms of the Creative Commons Attribution License (CC BY). The use, distribution or reproduction in other forums is permitted, provided the original author(s) and the copyright owner(s) are credited and that the original publication in this journal is cited, in accordance with accepted academic practice. No use, distribution or reproduction is permitted which does not comply with these terms.

frontiers in Cell and Developmental Biology

ORIGINAL RESEARCH
published: 05 July 2021
doi: 10.3389/fcell.2021.657406

Aberrant Autophagy Impacts Growth and Multicellular Development in a *Dictyostelium* Knockout Model of CLN5 Disease

Meagan D. McLaren[1†], Sabateeshan Mathavarajah[2†], William D. Kim[1], Shyong Q. Yap[1] and Robert J. Huber[2†]*

[1] Environmental and Life Sciences Graduate Program, Trent University, Peterborough, ON, Canada, [2] Department of Biology, Trent University, Peterborough, ON, Canada

OPEN ACCESS

Edited by:
Mario Antonio Bianchet, Johns Hopkins University, United States

Reviewed by:
Ancuta Jurj, Iuliu Hatieganu University of Medicine and Pharmacy, Romania
Shweta Saran, Jawaharlal Nehru University, India
Jonathan D. Cooper, Washington University in St. Louis, United States

***Correspondence:**
Robert J. Huber
roberthuber@trentu.ca

[†] These authors have contributed equally to this work

Specialty section:
This article was submitted to Molecular Medicine, a section of the journal Frontiers in Cell and Developmental Biology

Received: 22 January 2021
Accepted: 28 May 2021
Published: 05 July 2021

Citation:
McLaren MD, Mathavarajah S, Kim WD, Yap SQ and Huber RJ (2021) Aberrant Autophagy Impacts Growth and Multicellular Development in a Dictyostelium Knockout Model of CLN5 Disease. Front. Cell Dev. Biol. 9:657406. doi: 10.3389/fcell.2021.657406

Mutations in *CLN5* cause a subtype of neuronal ceroid lipofuscinosis (NCL) called CLN5 disease. While the precise role of CLN5 in NCL pathogenesis is not known, recent work revealed that the protein has glycoside hydrolase activity. Previous work on the *Dictyostelium discoideum* homolog of human CLN5, Cln5, revealed its secretion during the early stages of development and its role in regulating cell adhesion and cAMP-mediated chemotaxis. Here, we used *Dictyostelium* to examine the effect of *cln5*-deficiency on various growth and developmental processes during the life cycle. During growth, *cln5*$^-$ cells displayed reduced cell proliferation, cytokinesis, viability, and folic acid-mediated chemotaxis. In addition, the growth of *cln5*$^-$ cells was severely impaired in nutrient-limiting media. Based on these findings, we assessed autophagic flux in growth-phase cells and observed that loss of *cln5* increased the number of autophagosomes suggesting that the basal level of autophagy was increased in *cln5*$^-$ cells. Similarly, loss of *cln5* increased the amounts of ubiquitin-positive proteins. During the early stages of multicellular development, the aggregation of *cln5*$^-$ cells was delayed and loss of the autophagy genes, *atg1* and *atg9*, reduced the extracellular amount of Cln5. We also observed an increased amount of intracellular Cln5 in cells lacking the *Dictyostelium* homolog of the human glycoside hydrolase, hexosaminidase A (HEXA), further supporting the glycoside hydrolase activity of Cln5. This observation was also supported by our finding that *CLN5* and *HEXA* expression are highly correlated in human tissues. Following mound formation, *cln5*$^-$ development was precocious and loss of *cln5* affected spore morphology, germination, and viability. When *cln5*$^-$ cells were developed in the presence of the autophagy inhibitor ammonium chloride, the formation of multicellular structures was impaired, and the size of *cln5*$^-$ slugs was reduced relative to WT slugs. These results, coupled with the aberrant autophagic flux observed in *cln5*$^-$ cells during growth, support a role for Cln5 in autophagy during the *Dictyostelium* life cycle. In total, this study highlights the multifaceted role of Cln5 in *Dictyostelium* and provides insight into the pathological mechanisms that may underlie CLN5 disease.

Keywords: autophagy, Batten disease, CLN5, development, *Dictyostelium discoideum*, glycoside hydrolase, growth, neuronal ceroid lipofuscinosis

INTRODUCTION

The neuronal ceroid lipofuscinoses (NCLs), commonly known as Batten disease, comprise a family of rare neurodegenerative disorders that affect all ages and ethnicities (Dolisca et al., 2013). Batten disease is defined by two characteristics; (1) the accumulation of autofluorescent storage deposits in virtually every cell type and (2) the progressive loss of neurons in the cerebral cortex, cerebellum, and retina (Radke et al., 2015). The combination of storage body accumulation and neurodegeneration causes vision loss, seizures, loss of cognitive and motor function, and premature death (Radke et al., 2015). The cellular and molecular mechanisms underlying the NCLs are still unknown, largely because the normal functions of the 13 proteins associated with the disease (CLN1-8, CLN10-14) are not fully understood (Cárcel-Trullols et al., 2015). As a result, there is no curative therapy for any of the Batten disease subtypes. Mutations in ceroid neuronal lipofuscinosis protein 5 (*CLN5*) cause a late-infantile onset form of NCL known as CLN5 disease. Juvenile and adult cases have also been reported (Cannelli et al., 2007; Xin et al., 2010). CLN5 is a soluble lysosomal glycoside hydrolase that is secreted (Isosomppi et al., 2002; Moharir et al., 2013; Hughes et al., 2014; Huber and Mathavarajah, 2018a,b). Research has speculated that CLN5 may function in sphingolipid transport, lipid metabolism, lysosome receptor sorting, adhesion, endosomal retromer recruitment, mitophagy, and autophagy (Haddad et al., 2012; Mamo et al., 2012; Schmiedt et al., 2012; Leinonen et al., 2017; Huber and Mathavarajah, 2018a,b; Adams et al., 2019; Doccini et al., 2020).

The localizations and functions of NCL proteins have been studied in a variety of mammalian and non-mammalian systems (Huber et al., 2020a). One of these model systems is *Dictyostelium discoideum*, which is a soil-living eukaryotic microbe that is an exceptional organism for studying a variety of fundamental cellular and developmental processes (Huber, 2016, 2020; Mathavarajah et al., 2017; McLaren et al., 2019). The *Dictyostelium* genome encodes homologs of 11 of the 13 human NCL proteins, including a homolog of the TBC domain-containing protein kinase-like (TBCK) protein, which has been linked to a new possible subtype of NCL (CLN15 disease) (Huber, 2016; Beck-Wödl et al., 2018). In addition, *Dictyostelium* is the only lower eukaryotic model system that contains homologs of human tripeptidyl peptidase (TPP1, also known as CLN2) and CLN5 (Huber, 2016). Homologs of human TPP1/CLN2, CLN3, CLN5, and major facilitator superfamily domain-containing protein 8 (MFSD8, also known as CLN7) have been previously studied in *Dictyostelium*, which has contributed to our understanding of the localizations and functions of these proteins in human cells (Huber et al., 2014, 2017, 2020b; Phillips and Gomer, 2015; Huber, 2017, 2020; Stumpf et al., 2017; Huber and Mathavarajah, 2018a,b, 2019; Mathavarajah et al., 2018; Smith et al., 2019). Like human CLN5, *Dictyostelium*, Cln5 is secreted and has glycoside hydrolase activity (Huber and Mathavarajah, 2018a,b). Previous work revealed the Cln5 interactome in *Dictyostelium* and showed that Cln5 plays a role in regulating adhesion and cAMP-mediated chemotaxis (Huber and Mathavarajah, 2018a,b).

In nutrient-rich conditions, *Dictyostelium* amoebae grow as single cells, multiply by mitosis, and obtain nutrients by endocytosis (Mathavarajah et al., 2017). In nature (and in the laboratory), *Dictyostelium* cells find their food source by chemotactically responding to folic acid that is secreted by bacteria. Removal of nutrients places cells in a starved state and prompts a 24-h multicellular developmental program that relies on autophagy to generate energy and facilitate cell death during terminal differentiation. Cells first undergo chemotactic aggregation toward cyclic adenosine monophosphate (cAMP) to form multicellular mounds. Mounds develop into finger-like projections that rise above the surface only to fall back to the surface as motile pseudoplasmodia, or slugs. Cell populations within each slug terminally differentiate to form a fruiting body composed of a stalk of vacuolized cells that supports a mass of spores. When nutrients become available, the spores germinate to restart the life cycle. Owing to its dynamic life cycle, research in *Dictyostelium* has contributed to our understanding of conserved eukaryotic processes including chemotaxis, morphogenesis, differentiation, and autophagy, among others (Jeon et al., 2009; Uchikawa et al., 2011; Loomis, 2014; Mesquita et al., 2017).

Under basal conditions, and when nutrients are limited, cells undergo autophagy to break down and recycle their own reserves as a source of energy (e.g., organelles) (Mizushima, 2009). Autophagy has been thoroughly studied in *Dictyostelium* and many assays have been developed to study the process in detail (Domínguez-Martín et al., 2017). When autophagy is activated, an elongating double membrane known as the phagophore engulfs intracellular cargo (protein aggregates, misfolded proteins, and defective organelles) and then closes to become an autophagosome. The outer membrane of the autophagosome then fuses with the lysosome to form an autolysosome, leading to autophagic degradation of the autophagosomal inner membrane and cargo by lysosomal hydrolases. The rate of turnover of autophagosomes and the efficiency of autophagic degradation is known as autophagic flux (Mizushima et al., 2010). Autophagy occurs throughout the *Dictyostelium* life cycle. As a result, *Dictyostelium* serves as a powerful model for exploring autophagic processes at the single cell and multicellular levels.

In this study, we examined the role of Cln5 in regulating growth and multicellular development in *Dictyostelium*. During growth, we assessed the effect of *cln5*-deficiency on cell proliferation, cytokinesis, pinocytosis, viability, and folic acid-mediated chemotaxis. We then linked these growth-phase defects to aberrant autophagy in *cln5*$^{-}$ cells. We also examined the development of *cln5*$^{-}$ cells to determine the effects of *cln5*-deficiency on aggregation and the timing of development, which we also linked to aberrant autophagy in *cln5*$^{-}$ cells. Finally, we provide additional evidence supporting the glycoside hydrolase

Abbreviations: cAMP, cyclic adenosine monophosphate; CadA, calcium-dependent cell adhesion molecule A; CLN, ceroid lipofuscinosis neuronal; CtnA, countin; CtsD, cathepsin D; FM, minimal media; HEXA, hexosaminidase A; HL5, nutrient-rich media; NagA, *N*-acetylglucosaminidase A; NCL, neuronal ceroid lipofuscinosis; NGT, N-acetylglucosamine thiazoline; TPP1, tripeptidyl peptidase 1; WT, wild type.

activity of Cln5 in *Dictyostelium*. In total, our findings are consistent with a role for Cln5 in regulating autophagy during *Dictyostelium* growth and multicellular development.

MATERIALS AND METHODS

Cell Lines, Media, and Buffers

AX3 cells, hereafter referred to as wild type (WT), were the parental line for *cln5*$^-$ cells (Huber and Mathavarajah, 2018b). The *cln5*$^-$ cell line expressing Cln5 in pDM323 (*cln5*$^-$ + Cln5-GFP) was generated and validated in a previous study (Huber and Mathavarajah, 2018b). WT and *cln5*$^-$ cells expressing either pA15/GFP-Atg8a or pA15/RFP-GFP-Atg8a (constructs purchased from the Dicty Stock Center) were generated using a transformation protocol described elsewhere (Otto et al., 2004; Fey et al., 2007, 2013; Calvo-Garrido et al., 2011). *atg1*$^-$ (DBS0236346), *atg9*$^-$ (DBS0305977), and *nagA*$^-$ (DBS0235654) cells were purchased from the Dicty Stock Center (Dimond et al., 1973; Otto et al., 2004; Tung et al., 2010; Fey et al., 2013). The parental lines for these cells were also purchased from the Dicty Stock Center and are referred to as WT for the experiments where they were used (KAX3 for *atg1*$^-$, DBS0236345; AX2 for *atg9*$^-$, DBS0235525; AX3 for *nagA*$^-$, DBS0235542). Cells were maintained on SM/2 agar with *Klebsiella aerogenes* at 22°C (Fey et al., 2007). Cells used for experiments were grown axenically in nutrient-rich medium (HL5) at 22°C with shaking at 150 rpm. HL5, minimal medium (FM), FM lacking amino acids (FM-aa), and low-fluorescence HL5 were purchased from Formedium (Hunstanton, Norfolk, United Kingdom). Cultures were supplemented with ampicillin (100 μg/ml) and streptomycin sulfate (300 μg/ml) to prevent bacterial growth (Bioshop Canada Incorporated, Burlington, ON, Canada). *cln5*$^-$ cells required the addition of blasticidin S hydrochloride (10 μg/ml) for selection and cell lines carrying extrachromosomal vectors (e.g., pA15/GFP-Atg8a) required the addition of Geneticin (G418) (10 μg/ml) (Bioshop Canada Incorporated, Burlington, ON, Canada) (Levi et al., 2000; Veltman et al., 2009; Faix et al., 2013). KK2 buffer was composed of 2.2 g/l KH_2PO_4 and 0.7 g/l K_2HPO_4, pH 6.5.

Antibodies and Chemicals

Mouse monoclonal anti-GFP and mouse monoclonal anti-beta-actin were purchased from Santa Cruz Biotechnology Incorporated (Dallas, TX, United States). Mouse monoclonal P4D1 anti-ubiquitin was purchased from New England Biolabs Canada (Whitby, ON, Canada). Mouse monoclonal anti-alpha-actinin (47-62-17) and mouse monoclonal anti-alpha-tubulin (12G10) were purchased from the Developmental Studies Hybridoma Bank (University of Iowa, Iowa City, IA, United States). The generation and validation of anti-Cln5 and anti-CtsD were described elsewhere (Huber and Mathavarajah, 2018b; Huber et al., 2020b). Anti-countin (CtnA) was provided as a gift by Dr. Richard Gomer (Brock and Gomer, 1999). A polyclonal antibody was raised in rabbits against a synthetic peptide corresponding to the epitope ^{187}KDETFPKNMTVTQD^{200} in the C-terminal region of *Dictyostelium* calcium-dependent cell adhesion molecule A (CadA) (Genscript, Piscataway, NJ, United States). The antibody was affinity purified and validated using a peptide competition assay (Huber et al., 2020b; **Supplementary Figure 1**). Briefly, a 1:67 dilution of anti-CadA was prepared in 1 ml of western blotting washing buffer (TBST) ± the peptide epitope (500 μg). The solutions were then incubated overnight at 4°C with head over tail rotation, after which time the tubes were spun at 14000 rpm for 5 min. The supernatants were then added to 2% milk/TBST solution for western blotting. Goat anti-rabbit and horse anti-mouse IgG linked to HRP were purchased from New England Biolabs Canada (Whitby, ON, Canada). Alexa-488 Fluor-conjugated secondary antibodies were purchased from Fisher Scientific Company (Ottawa, ON, Canada). FITC-dextran and folic acid were purchased from Sigma-Aldrich Canada (Oakville, ON, Canada). Ammonium chloride was purchased from Bioshop Canada Incorporated (Burlington, ON, Canada). Prolong Gold Anti-Fade Reagent with DAPI was purchased from Fisher Scientific Company (Ottawa, ON, Canada).

Cell Proliferation, Cytokinesis, Pinocytosis, and Viability Assays

Growth assays were performed using a method described elsewhere (Huber et al., 2014). Briefly, cells in the mid-log phase of growth (1–5 × 106 cells/ml) were diluted to 1 × 105 cells/ml in fresh HL5, FM, or FM-aa at 22°C with shaking at 150 rpm. Every 24 h for 4–5 days, the densities of cell suspensions were measured (in triplicate aliquots) using a hemocytometer. For the cytokinesis assay, cells (2×10^5 total) in the mid-log phase of growth (1–5 × 10^6 cells/ml) were deposited onto coverslips placed inside separate wells of a 12-well dish. Coverslips were then submerged in low-fluorescence HL5 (to reduce background fluorescence) and incubated overnight at 22°C. Cells were fixed in −80°C methanol for 45 min (Hagedorn et al., 2006) and mounted on slides with Prolong Gold Anti-Fade Reagent with DAPI. Cells were imaged using a Nikon Ts2R-FL inverted microscope equipped with a Nikon Digital Sight Qi2 monochrome camera (Nikon Canada Incorporated Instruments Division, Mississauga, ON, Canada). The number of nuclei within each cell was scored. For each experiment, 10 random images were obtained from each coverslip and each image contained at least 10 cells. The pinocytosis assay was conducted using a method described elsewhere (Rivero and Maniak, 2006; Huber et al., 2014). Briefly, cells in the mid-log phase of growth (1–5 × 10^6 cells/ml) were placed in fresh HL5 at a density of 5.0×10^6 cells/ml. After 15 min, 100 μl of a 20 mg/ml FITC-dextran (70,000 M_r) stock solution was added to the suspension generating a final concentration of 400 μg/ml, respectively. Every 15 min over a 90-min period, 500 μl of cells were collected, washed twice with 500 μl of ice-cold Sorenson's buffer (2 mM Na_2HPO_4, 14.6 mM KH_2PO_4, pH 6.0) and lysed with 1 ml of pinocytosis lysis buffer (50 mM Na_2HPO_4, pH 9.3, 0.2% Triton-X). Lysates (100 μl) were added to separate wells of a black 96-well plate and fluorescence was measured using a BioTek Synergy HTX plate reader (excitation 470 nm, emission 515 nm) (BioTek Instruments Incorporated, Winooski, VT, United States). To

assess cell viability, cells were grown in FM and FM-aa according to the growth assay protocol described above. The CellTiter-Glo Luminescent Cell Viability Assay was then used according to the manufacturer's instructions (Promega Corporation, Madison, WI, United States). Aliquots of 50 μl were taken from each culture at the indicated time points. These aliquots were then quickly added to separate wells of a black 96-well plate each containing 50 μl of CellTiter-Glo reagent. The solution was incubated at 22°C for 20 min after which time luminescence was measured using a BioTek Synergy HTX microplate reader.

Radial Bioassay of Chemotaxis Toward Folic Acid

Chemotaxis toward folic acid was assessed using a radial bioassay (O'Day, 1979). Briefly, cells in the mid-log phase of growth (1–5 × 10^6 cells/ml) were grown in HL5 overnight to confluency in Petri dishes. The following day, cells were harvested, washed two times with KK2 buffer, and plated (1 × 10^8 cells/ml) in 0.6 μl volumes on 0.5% agar/KK2 buffer ± folic acid (50 μM). Cell spots were imaged at 0 and 5 h using a Nikon Ts2R-FL inverted microscope equipped with a Nikon Digital Sight Qi2 monochrome camera. Images were viewed using NIS Elements Basic Research and analyzed using Fiji/ImageJ (Schneider et al., 2012).

Autophagic Flux Assay

Wild type and *cln5*$^-$ cells expressing GFP-Atg8a in the mid-log phase of growth (1–5 × 10^5 cells/ml) were grown in HL5 overnight to confluency in Petri dishes. The following day, cells were washed twice with KK2 buffer and then submerged in fresh HL5 ± ammonium chloride (150 mM) for 4 h. Treatment with ammonium chloride elevates the pH of the lysosome, thereby inhibiting autophagy (Calvo-Garrido et al., 2011). An additional pulse of ammonium chloride (150 mM) was added halfway through the treatment (after 2 h). After 4 h, cells were harvested, lysed with NP40 lysis buffer (150 mM NaCl, 50 mM Tris, 0.5% NP-40, pH 8.3) containing a protease cocktail inhibitor tablet (Fisher Scientific Company, Ottawa, ON, Canada), and analyzed for GFP-Atg8a cleavage by western blotting. WT and *cln5*$^-$ cells expressing RFP-GFP-Atg8a in the mid-log phase of growth (1–5 × 10^5 cells/mL) were deposited onto coverslips (5.0 × 10^5 total) submerged in low fluorescence HL5 (in separate wells of a 12-well dish) and incubated overnight at 22°C. The following day, cells were incubated in fresh low-fluorescence HL5 ± ammonium chloride (150 mM) for 4 h. An additional pulse of ammonium chloride (150 mM) was added halfway through the treatment (after 2 h) (Domínguez-Martín et al., 2017). Cells were fixed in −80°C methanol for 45 min (Hagedorn et al., 2006) and mounted on slides with Prolong Gold Anti-Fade Reagent with DAPI so that they could be viewed by epifluorescence microscopy. Cells were imaged using a Leica DM6000B microscope equipped with a Leica DFC350FX digital camera (Leica Microsystems Canada Incorporated, Richmond Hill, ON, Canada). Images were viewed and merged using Fiji/ImageJ. To assess the effect of *cln5*-deficiency on the levels of ubiquitin-positive proteins, WT and *cln5*$^-$ cells in the mid-log phase of growth (1–5 × 10^5 cells/ml) were grown in HL5 overnight to confluency in Petri dishes. The following day, cells were washed twice with KK2 buffer and then submerged in fresh HL5 ± ammonium chloride (100 mM) for 2 h. Cells were then harvested, lysed with NP40 lysis buffer, and analyzed by western blotting to assess the levels of ubiquitin-positive proteins in WT and *cln5*$^-$ cells.

Aggregation Assay

Cells in the mid-log phase of growth (1−5 × 10^6 cells/ml) were grown in HL5 overnight to confluency in Petri dishes. The following day, cells were washed twice with KK2 buffer and then submerged in fresh KK2 buffer. Starving cells were imaged using a Nikon Ts2R-FL inverted microscope equipped with a Nikon Digital Sight Qi2 monochrome camera. Cells were also harvested after 4 h of starvation, lysed with NP40 lysis buffer, and analyzed by western blotting to assess the effect of *cln5*-deficiency on the intracellular and extracellular amounts of CadA, CtnA, and CtsD, as well as the intracellular and extracellular amounts of Cln5 in *atg1*$^-$ and *atg9*$^-$ cells. In separate experiments, 5 × 10^6 cells were deposited into 6 well dishes and allowed to adhere for 30 min. Cells were then washed twice with FM-aa and incubated in fresh FM-aa for 24 h. Mounds were imaged after 24 h using a Nikon Ts2R-FL inverted microscope equipped with a Nikon Digital Sight Qi2 monochrome camera.

Multicellular Development Assay

Multicellular development was assessed on two substrates using previously described methods: (1) black, gridded, nitrocellulose filters (0.45 mm pore size) (Fisher Scientific Company, Ottawa, ON, Canada) and (2) 0.5% agar/distilled water ± ammonium chloride (60 mM) (Huber et al., 2014). For development on nitrocellulose filters, developmental chambers were prepared in 60 mm × 15 mm Petri dishes. In each chamber, a black gridded nitrocellulose filter was placed on top of four Whatman #3 cellulose filters (Fisher Scientific Company, Ottawa, ON, Canada) pre-soaked in KK2 buffer. For development on 0.5% agar/distilled water ± ammonium chloride (60 mM), 5 ml of agar was poured into 60 mm × 15 mm Petri dishes. For both substrates, confluent cells grown in HL5 overnight on Petri dishes were washed twice with KK2 buffer. Washed cells (3 × 10^7 cells/ml) were deposited in 25 μl droplets (750,000 cells total) on nitrocellulose filters or 0.5% agar/distilled water ± ammonium chloride (60 mM). During multicellular development, cells were maintained in a dark humidity chamber at 22°C. Developmental structures were imaged using a Leica EZ4W stereomicroscope equipped with an internal 5MP CMOS camera (Leica Microsystems Canada Incorporated, Richmond Hill, ON, Canada). For development on nitrocellulose filters, the percentage of respective morphological structures in each cell droplet was quantified at specific developmental time points. Slug size on 0.5% agar/distilled water ± ammonium chloride (60 mM) was quantified using Fiji/ImageJ.

Spore Morphology, Germination, and Viability

To assess spore morphology, spores were collected from fresh fruiting bodies (24–48 h after development) and suspended

in KK2 buffer (1×10^6 spores/ml). Suspensions were then deposited in 60 mm × 15 mm Petri dishes and imaged using a Nikon Ts2R-FL inverted microscope equipped with a Nikon Digital Sight Qi2 monochrome camera. The area and roundedness of spores were analyzed using Fiji/ImageJ. For roundedness, a value of 1.0 indicated a completely circular spore. Statistical significance was determined using the Kruskal–Wallis test followed by Dunn's multiple comparisons test. To examine germination, spores were collected and deposited in Petri dishes containing HL5. Spores within a specific field-of-view were examined every 10 min using a Nikon Ts2R-FL inverted microscope equipped with a Nikon Digital Sight Qi2 monochrome camera. When spores appeared to swell, marking the beginning of germination, the time was noted (Cotter and Raper, 1966). Statistical significance was determined using one-way ANOVA followed by Bonferroni's multiple comparisons test. Finally, spore viability was assessed using a previously described method (Myre et al., 2011). Briefly, 50 spores were collected and spread with a fixed amount of *K. aerogenes* on SM/2 agar. After 4 days, the number of plaques formed on the bacterial lawn were counted to assess how many of the initial 50 spores were viable (i.e., how many germinated). Statistical significance was determined using the Kruskal–Wallis test followed by Dunn's multiple comparisons test.

SDS-PAGE and Western Blotting

Proteins in whole cell lysates and samples of conditioned buffer were quantified using a Qubit 2.0 Fluorometer (Fisher Scientific Company, Ottawa, ON, Canada). SDS-PAGE and western blotting were performed using standard methods (2-h incubation at 22°C for primary and secondary antibodies in 5% milk/TBST). The following antibody dilutions were used; anti-GFP (1:1000); anti-beta-actin (1:1000); anti-ubiquitin (1:1000); anti-alpha-actinin (1:1000); anti-alpha-tubulin (1:1000); anti-Cln5 (1:500); anti-CtsD (1:500); anti-CtnA (1:1000); anti-CadA (1:1000); anti-rabbit and anti-mouse IgG linked to HRP (1:5000). Protein bands were imaged using the enhanced chemiluminescence clarity max substrate and the ChemiDoc Imaging System (Bio-Rad Laboratories Limited, Mississauga, ON, Canada). Protein bands were quantified using Fiji/ImageJ.

Statistical Analyses

All statistical analyses were performed using GraphPad Prism 8 (GraphPad Software Incorporated, La Jolla, CA, United States). A p-value < 0.05 was considered significant for all analyses and n represents the number of biological replicates analyzed. Details on the specific statistical analyses that were performed are found in the individual figure captions.

RESULTS

cln5-Deficiency Inhibits Cell Proliferation and Cytokinesis in Nutrient-Rich Media but Has No Effect on Pinocytosis

To examine the role of Cln5 during *Dictyostelium* growth, we assessed the effect of *cln5*-deficiency on cell proliferation in nutrient-rich media (HL5). *cln5*$^-$ cell proliferation was significantly reduced after 72 and 96 h of growth, causing *cln5*$^-$ cells to reach a lower maximum cell density (**Figure 1A**). During

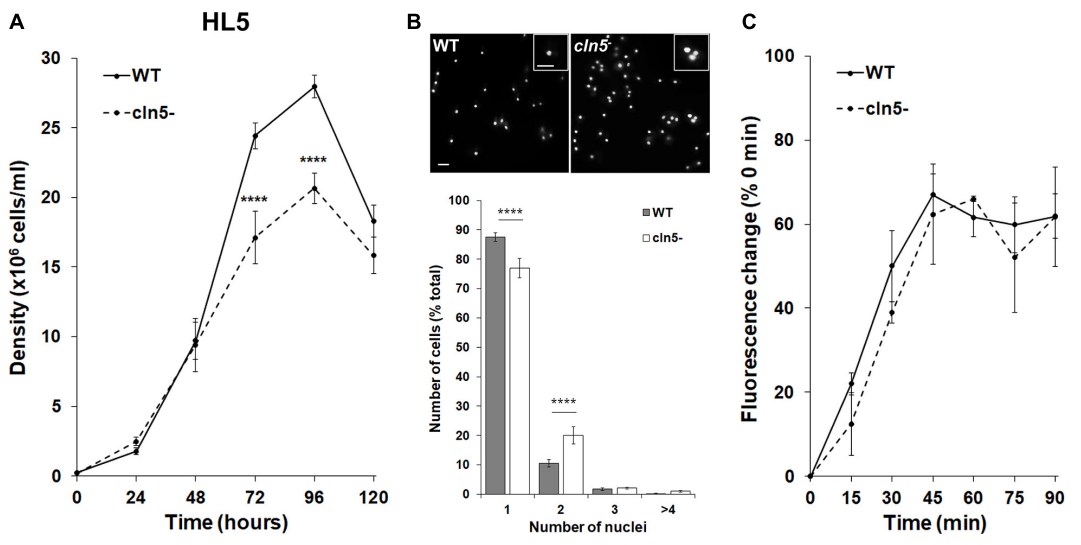

FIGURE 1 | Effect of *cln5*-deficiency on cell proliferation, cytokinesis, and pinocytosis in HL5. **(A)** WT and *cln5*$^-$ cells were placed in HL5 at 1.0×10^5 cells/ml. Cell densities were measured every 24 h for 120 h. Data presented as mean density ± SEM (n = 11). Statistical significance was assessed using two-way ANOVA followed by Bonferroni's multiple comparisons test. ****p-value < 0.0001 at the indicated time points vs. WT. **(B)** Growth-phase WT and *cln5*$^-$ cells were fixed on coverslips and stained with DAPI to reveal nuclei. The percentage of cells in the population containing 1, 2, 3, or ≥4 nuclei was measured. Data presented as mean number of cells (% total) ± SEM (n = 6). Statistical significance was determined using the Student's t-test. ****p-value < 0.0001 vs. WT. Scale bar = 10 μm. **(C)** WT and *cln5*$^-$ cells (5.0×10^6 cells/ml) were incubated in HL5 containing FITC-dextran (400 μg/ml). Starting at 0 min, and every 15 min thereafter, cells were collected, washed with ice-cold Sorenson's buffer, and lysed. The fluorescence of the lysates was then measured. Data presented as mean fluorescence change (% 0 min) ± SEM (n = 3).

the assay, we observed that *cln5*$^-$ cultures had comparatively more multinucleated cells compared to WT. To confirm this observation, *cln5*$^-$ cells grown in suspension were fixed and stained with DAPI to reveal nuclei and assess the effect of *cln5*-deficiency on cytokinesis. The number of mono-nucleated, di-nucleated, tri-nucleated, and poly-nucleated (>3) cells were then scored. In *cln5*$^-$ cell populations, 77 ± 3% of the cells had one nucleus compared to 88 ± 2% of WT cell populations (**Figure 1B**). Conversely, *cln5*$^-$ cell populations had a greater number of di-nucleated cells compared to WT cell populations (20 ± 3% compared to 11 ± 1%, respectively) (**Figure 1B**). Next, we reasoned that the reduced proliferation of *cln5*$^-$ cells could have potentially been due to a decreased rate of extracellular nutrient uptake known as pinocytosis. Therefore, we assessed the rate of pinocytosis of FITC-dextran by WT and *cln5*$^-$ cells. In this assay, cells were incubated with FITC-dextran and intracellular FITC-dextran fluorescence was measured every 15 min over a 90-min period (**Figure 1C**). Two-way ANOVA did not reveal statistically significant differences between the cell lines indicating that the reduced proliferation of *cln5*$^-$ cells was not due to aberrant pinocytosis. Combined, these data indicate that Cln5 plays a role in regulating cell proliferation and cytokinesis during *Dictyostelium* growth.

Nutrient Limitation Severely Impacts the Proliferation and Viability of *cln5*$^-$ Cells

In nutrient-deprived states, *Dictyostelium* cells maintain their viability by generating nutrients through autophagy (Marin, 1976; Mesquita et al., 2017). Since the impaired proliferation of *cln5*$^-$ cells in nutrient-rich media could not be explained by reduced pinocytosis, we were interested in assessing the effect of *cln5*-deficiency on cell proliferation in minimal media (FM) and minimal media lacking amino acids (FM-aa). FM is an alternate culturing media that has the minimal amounts of resources required for *Dictyostelium* growth (Franke and Kessin, 1977). FM-aa places cells in an environment where their survival is dependent on autophagy. WT and *cln5*$^-$ cell densities were significantly reduced in both FM and FM-aa compared to their densities in HL5 (**Figures 1A**, **2A**). In FM, *cln5*$^-$ cell densities were significantly reduced after 48, 72, and 96 h compared to WT (**Figure 2A**). In contrast, the growth of WT cultures increased until 72 h, after which time they began to decrease (**Figure 2A**). In FM-aa, *cln5*$^-$ cell densities were significantly reduced over the entire 96-h experimental period compared to WT cultures. The aberrant proliferation of *cln5*$^-$ cells in both FM and FM-aa was restored by introducing Cln5-GFP into *cln5*$^-$ cells (**Figure 2A**). Loss of *cln5* also significantly reduced the viability of cells cultured in FM and FM-aa, as determined by a commercially available kit that measures relative ATP levels (i.e., indicator of cell viability) (**Figure 2B**). Finally, we allowed WT, *cln5*$^-$, and *cln5*$^-$ + Cln5-GFP cells to adhere to the bottom of Petri dishes while submerged in FM-aa. After 24 h, WT and *cln5*$^-$ + Cln5-GFP cells formed large circular mounds composed of tightly adhered cells (**Figure 2C**). In contrast, *cln5*$^-$ cells were more dispersed, which was consistent with a previous study that reported an effect of *cln5*-deficiency on cell adhesion (**Figure 2C**; Huber and Mathavarajah, 2018b). Together, these findings indicated that Cln5 may play a role in autophagy during *Dictyostelium* growth.

cln5-Deficiency Reduces Folic Acid-Mediated Chemotaxis

Based on the previous results, we examined the effect of *cln5*-deficiency on folic acid-mediated chemotaxis since work in human cells lines (HEK-293 and U87 glioblastoma cells) supports a link between chemotaxis and autophagy, specifically autophagosome biogenesis (Coly et al., 2016). In addition, previous work showed that loss of *cln5* reduces cAMP-mediated chemotaxis during the early stages of *Dictyostelium* development (Huber and Mathavarajah, 2018b). For this assay, a droplet of cells was deposited on agar containing folic acid. After 5 h, the population of cells migrated outward forming a halo around the original deposition spot (**Figure 3**). The spot diameters were then quantified to determine the mean distance migrated by the cell population. Loss of *cln5* reduced folic acid-mediated chemotaxis by 27 ± 6% and introduction of Cln5-GFP into *cln5*$^-$ cells restored the reduced chemotaxis (**Figure 3**). Together, these results link the function of Cln5 to folic acid-mediated chemotaxis.

Autophagic Flux Is Increased in *cln5*-Deficient Cells During Growth

Since the previous experiments suggested that Cln5 may play a role in regulating autophagy during growth, we performed two autophagic flux assays; (1) a GFP-Atg8a assay, which provides insight into the number of autophagosomes per cell and (2) an RFP-GFP-Atg8a assay, which measures the number of autophagic puncta per cell and the efficiency of autophagic cargo turnover (Mizushima et al., 2010; Calvo-Garrido et al., 2011; Domínguez-Martín et al., 2017). GFP-Atg8a associates with the inner autophagosomal membrane. When the autophagosome fuses with the lysosome, GFP-Atg8a is cleaved and degraded by lysosomal enzymes. In many organisms, GFP is resistant to autophagic degradation. However, in *Dictyostelium*, GFP is rapidly degraded since *Dictyostelium* cells contain extremely acidic lysosomes (Marchetti et al., 2009; Calvo-Garrido et al., 2011; Domínguez-Martín et al., 2017). Treatment of cells with a non-saturating concentration of ammonium chloride elevates the pH of the lysosome, thereby inhibiting autophagy. This causes free, cleaved GFP to accumulate, which can be visualized by western blotting (Calvo-Garrido et al., 2011; Domínguez-Martín et al., 2017). When WT and *cln5*$^-$ cells expressing GFP-Atg8a were incubated in HL5 containing ammonium chloride, *cln5*$^-$ cells consistently had higher amounts of free, cleaved GFP suggesting that *cln5*$^-$ cells may have had more autophagosomes than WT cells (**Figure 4A**). This observation could indicate one of two things, that (1) autophagy is induced, or that (2) autophagy is blocked, meaning that autophagosome-lysosome fusion is impaired (Mizushima et al., 2010; Domínguez-Martín et al., 2017). Therefore, to further investigate the autophagic defect in *cln5*$^-$ cells, an RFP-GFP-Atg8a autophagic flux assay was

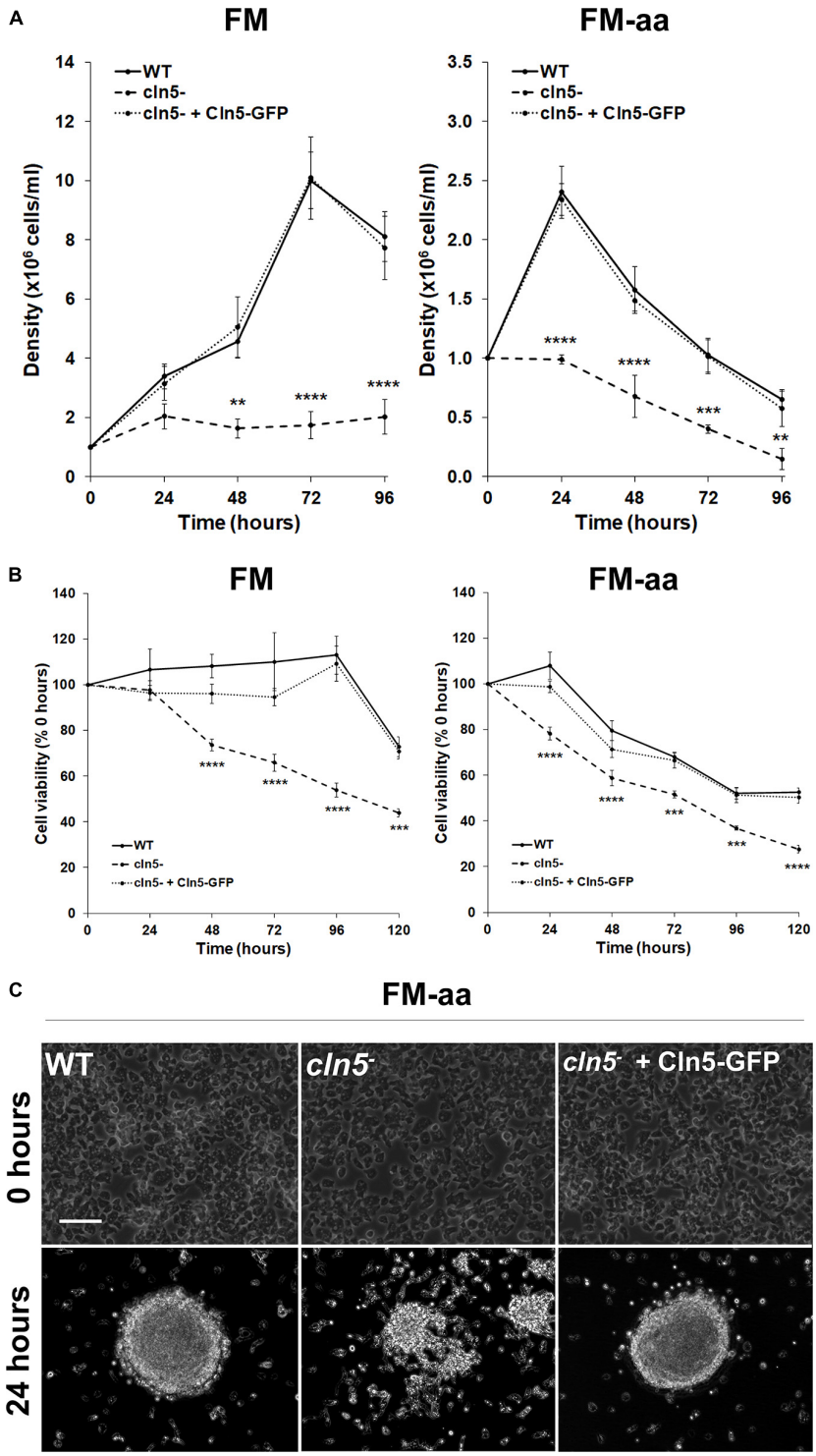

FIGURE 2 | Effect of *cln5*-deficiency on cell proliferation and viability in FM and FM-aa. **(A)** WT, *cln5*$^{-}$, and *cln5*$^{-}$ + Cln5-GFP cells were placed in FM or FM-aa at a density of 1.0 × 10^5 cells/ml. Cell densities were measured every 24 h for 96 h. Data presented as mean density ± SEM ($n \geq 4$). Statistical significance was assessed using two-way ANOVA followed by Bonferroni's multiple comparisons test. ***p*-value < 0.01, ****p*-value < 0.001, and *****p*-value < 0.0001 at the indicated time points vs. WT. **(B)** Cells were grown in FM and FM-aa as described in panel **(A)**. The CellTiter-Glo Luminescent Cell Viability Assay was used to quantify cell viability at the indicated time points. Statistical significance was determined using two-way ANOVA followed by Bonferroni's multiple comparisons test. ****p*-value < 0.001 and *****p*-value < 0.0001 at the indicated time points vs. WT. **(C)** Cells (20 × 10^6 total) were harvested from HL5 suspension and placed in a 100 × 15 mm Petri dish containing HL5. After 1 h, the HL5 was removed and replaced with FM-aa. Images were taken after 24 h and are representative of four independent experiments. Scale bar = 50 μm.

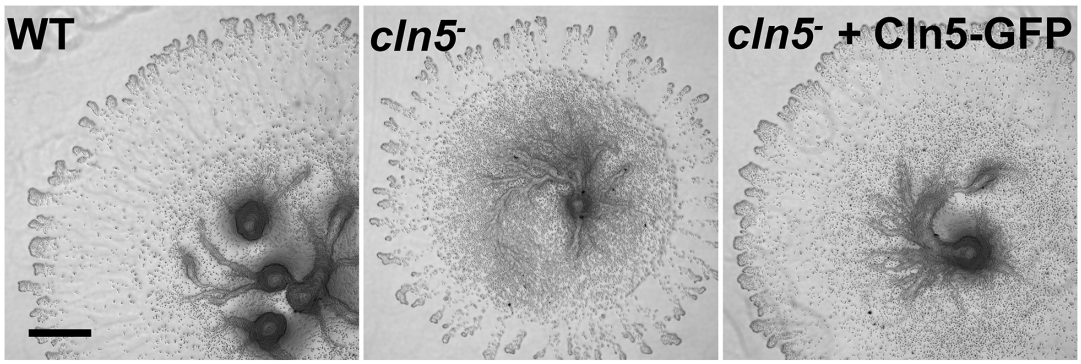

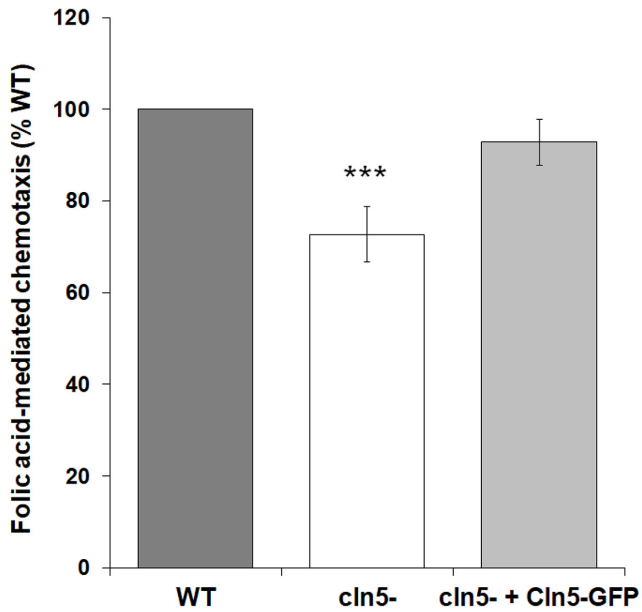

FIGURE 3 | Effect of *cln5*-deficiency on folic acid-mediated chemotaxis. WT, *cln5*$^{-}$, and *cln5*$^{-}$ + Cln5-GFP cells were deposited onto 0.5% agar/KK2 buffer + folic acid (50 μM). Images were taken once cells were deposited and after 5 h. Scale bar = 500 μm. The amount of migration of each cell line was quantified and the raw values were then expressed as a percentage of the migration of WT cells. Data presented as mean folic acid-mediated chemotaxis (% WT) ± SEM ($n \geq 5$). Statistical significance was assessed using the one sample *t*-test. ***$p < 0.001$ vs. WT.

performed using WT and *cln5*$^{-}$ cells expressing RFP-GFP-Atg8a. RFP-GFP-Atg8a is incorporated on the inner autophagosomal membrane. When autophagosomes fuse with lysosomes, GFP fluorescence is quenched due to the acidic environment of the lysosome. Thus, lysosomes appear red and autophagosomes appear yellow (overlap of RFP and GFP fluorescence) (Calvo-Garrido et al., 2011; Domínguez-Martín et al., 2017). In this assay, it was observed that *cln5*$^{-}$ cells had more autophagic puncta than WT cells (autophagosomes and lysosomes) (**Figure 4B**). More specifically, *cln5*$^{-}$ cells had approximately 3 autophagosomes and 6 lysosomes per cell, compared to approximately 2 autophagosomes and 5 lysosomes in WT cells. As in the GFP-Atg8a assay, the increased number of autophagic puncta in *cln5*$^{-}$ cells could mean autophagy is induced or there is a block between the fusion of the autophagosome and lysosome. To further investigate this, WT and *cln5*$^{-}$ cells were treated with ammonium chloride which increases lysosomal pH, thereby suppressing autophagy. This treatment should decrease the number of red puncta (lysosomes) in cells. If the number of red puncta does not decrease after ammonium chloride treatment, then the cells have a block in autophagy, meaning a block in the fusion between the autophagosome and lysosome. In this study, we observed that ammonium chloride reduced the number of red puncta in *cln5*$^{-}$ cells compared to WT cells (**Figure 4B**). Together, the two autophagic flux assays provide evidence that the basal level of autophagy in *cln5*$^{-}$ cells is higher than in WT cells.

cln5-Deficiency Increases the Amounts of Ubiquitinated Proteins During Growth

In *Dictyostelium*, ubiquitination regulates several processes and co-localizes with the autophagosomal markers Atg8a and Atg8b (Welchman et al., 2005; Pankiv et al., 2007; Kirkin et al., 2009; Matthias et al., 2016). Since autophagy was dysregulated in *cln5*$^{-}$ cells, we used western blotting to assess the effect of *cln5*-deficiency on the amounts of ubiquitinated proteins in growth-phase cells. *cln5*-deficiency increased the amounts of ubiquitin-positive proteins by 10 ± 3% during growth (**Figure 5**).

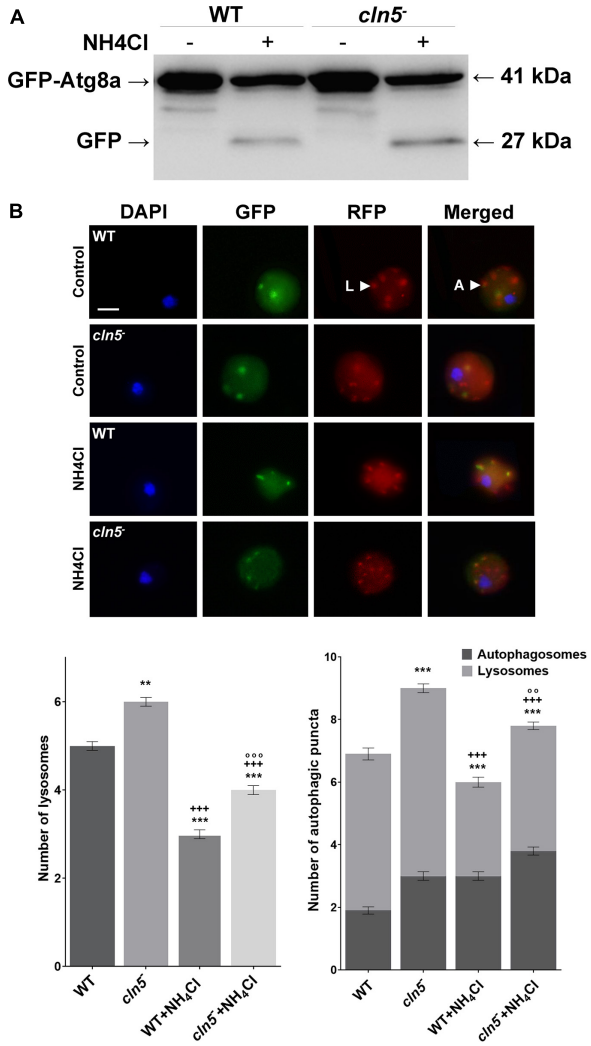

FIGURE 4 | GFP-Atg8a and RFP-GFP-Atg8a autophagic flux assays. **(A)** WT and *cln5*$^{-}$ cells expressing GFP-Atg8a were submerged in HL5 ± ammonium chloride (150 mM) for 4 h. A pulse of ammonium chloride (150 mM) was added halfway through the incubation (after 2 h). Whole cell lysates (30 μg) were separated by SDS-PAGE and analyzed by western blotting using anti-GFP. Molecular weight markers (in kDa) are shown to the right of the blot. Western blot is representative of three independent experiments. **(B)** WT and *cln5*$^{-}$ cells were submerged in low fluorescence HL5 ± ammonium chloride (150 mM) for 4 h, with a pulse of ammonium chloride (150 mM) added halfway through the incubation (after 2 h). Cells were fixed and stained with DAPI to reveal nuclei (blue). Scale bar = 2.5 μm. The average number of autophagosomes and lysosomes was quantified. Data presented as mean number of lysosomes ± SEM (n = 3, at least 60 in total were analyzed) and mean total number of autophagic puncta ± SEM (n = 3, at least 60 in total were analyzed). Statistical significance was assessed using the non-parametric Kruskal–Wallis test followed by Dunn's multiple comparisons test. $^{**}p < 0.01$, $^{***}p < 0.001$ vs. WT/$^{+++}p < 0.001$ vs. *cln5*$^{-}$/$^{\circ\circ\circ}p < 0.01$, $^{\circ\circ\circ}p < 0.001$ vs. WT + ammonium chloride.

When cells were incubated in HL5 containing ammonium chloride for 2 h, the amounts of ubiquitin-positive proteins in both WT and *cln5*$^{-}$ cells increased, which was expected since ammonium chloride inhibits autophagy (**Figure 5**). Under these conditions, the amounts of ubiquitin-positive proteins were again increased in *cln5*$^{-}$ cells relative to WT cells (**Figure 5**). These findings support the increased level of basal autophagy in *cln5*$^{-}$ cells and suggest that proteins are being tagged in *cln5*$^{-}$ cells but they are not being broken down effectively.

Cln5 Plays a Role in Aggregation but Has No Effect on Mound Size

As nutrients are not readily available during multicellular development, *Dictyostelium* cells use autophagy to meet the energy demands required for the transition to multicellularity (Mesquita et al., 2017). Previous work showed that *cln5*$^{-}$ cells display reduced adhesion and cAMP-mediated chemotaxis during the early stages of development (Huber and Mathavarajah, 2018b). In human cells, defects in adhesion and chemotaxis have been associated with aberrant autophagy (Coly et al., 2016; Ligon et al., 2020). Since Cln5 was shown to regulate autophagy during growth, and multicellular development relies on autophagic mechanisms, the effect of *cln5*-deficiency during multicellular development was assessed (Otto et al., 2003, 2004). WT, *cln5*$^{-}$, and *cln5*$^{-}$ + Cln5-GFP cells were deposited into Petri dishes and then starved in KK2 buffer. Under these conditions, loss of *cln5* delayed aggregation by ∼2 h (**Figure 6**). We then explored the effect of *cln5*-deficiency on the intracellular and extracellular amounts of two proteins linked to cell adhesion and aggregation, CadA and CtnA (Brar and Siu, 1993; Brock and Gomer, 1999). Loss of *cln5* decreased the extracellular amount of CadA after 4 h of starvation but had no effect on the amount of extracellular CtnA or the intracellular amounts of either protein (**Figure 7A**). Since autophagy relies on the activity of lysosomal enzymes, we also examined the effect of *cln5*-deficiency on the intracellular and extracellular amounts of the lysosomal aspartyl protease, cathepsin D (CtsD) (Journet et al., 1999). In humans, mutations in *CTSD* cause a subtype of NCL called CLN10 disease (Tyynelä et al., 2000). Loss of *cln5* significantly decreased the intracellular amount of CtsD but had no effect on the extracellular amount of the protein (**Figure 7A**). Combined, these data suggest that Cln5 regulates the trafficking of CadA and the intracellular amount of CtsD during the early stages of multicellular development. Previous work showed that pharmacological inhibition of autophagy with ammonium chloride or chloroquine reduces the extracellular amount of Cln5 during starvation (Huber and Mathavarajah, 2018b). To further examine the role of Cln5 in autophagy, we assessed the secretion of Cln5 in cells lacking either *atg1* or *atg9*. Atg1 is a protein kinase that co-localizes with Atg8 and is required for macroautophagy and multicellular development (Otto et al., 2004; Tekinay et al., 2006). Atg9 is a transmembrane protein that localizes to small vesicles and is predicted to play a role in membrane trafficking to autophagosomes (Calvo-Garrido et al., 2010; Tung et al., 2010). Loss of *atg9* disrupts growth, phagocytosis, and morphogenesis during development (Tung et al., 2010; Yamada and Schaap, 2019). Consistent with our previous findings, we observed reduced extracellular amounts of Cln5 in *atg1*$^{-}$ and *atg9*$^{-}$ cells (**Figure 7B**). To complete our analysis of the effect of *cln5*-deficiency on the early stages of

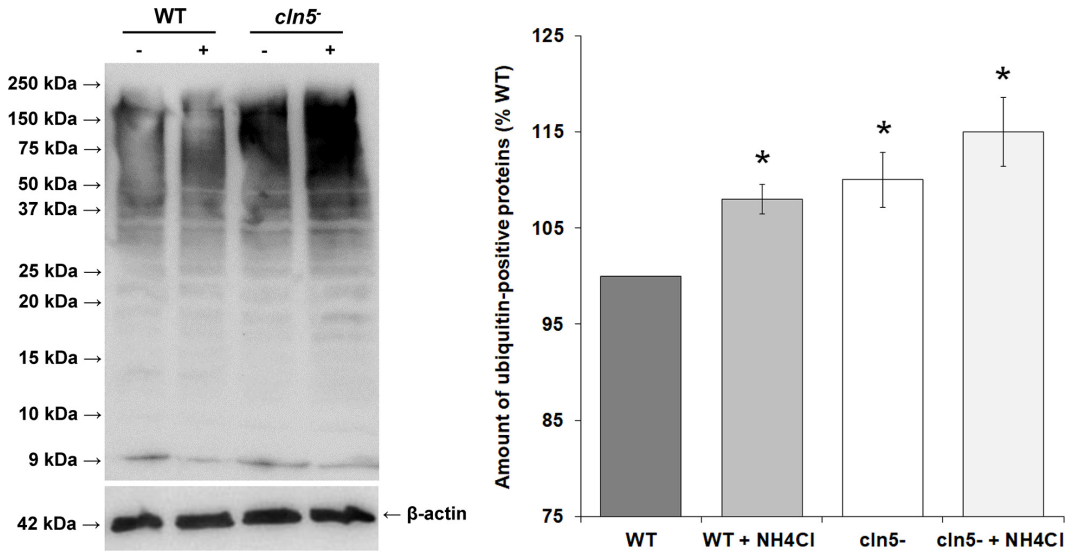

FIGURE 5 | Effect of *cln5*-deficiency on the amounts of ubiquitin-positive proteins. WT and *cln5*$^{-}$ cells were submerged in HL5 ± ammonium chloride (100 mM) for 2 h. Whole cell lysates (25 μg) were separated by SDS-PAGE and analyzed by western blotting with anti-ubiquitin and anti-beta-actin (loading control). Molecular weight markers (in kDa) are shown to the left of the blot. The amounts of ubiquitin-positive proteins were quantified, normalized to beta-actin, and plotted. Raw values were then expressed as a percentage of the amounts of ubiquitin-positive proteins in WT cells. Data presented as the mean amounts of ubiquitin-positive proteins (% WT) ± SEM (n = 3). Statistical significance was assessed using the one-sample t-test. *p-value < 0.05 vs. WT.

development, we observed no significant effect of *cln5* loss on mound number or size (**Supplementary Figure 2**). Together, these results show that *cln5*-deficiency delays aggregation by affecting the trafficking of CadA. The role of Cln5 in autophagy is further supported by the impact of *cln5*-deficiency on the intracellular amount of CtsD and the reduced secretion of Cln5 in *atg1*$^{-}$ and *atg9*$^{-}$ cells.

Cln5 and NagA May Participate in the Same Biological Pathway to Regulate Autophagy

To further explore the role of Cln5 in autophagy during the early stages of development, we referenced our previous work that identified a putative N-acetylglucosamine thiazoline (NGT)-binding site in human CLN5 (Huber and Mathavarajah, 2018a). In humans, a well-established NGT-binding protein is the lysosomal enzyme hexosaminidase A (HEXA). HEXA activity is linked to autophagy and mutations in *HEXA* cause the lysosomal storage disorder Tay-Sachs disease (Okada and O'Brien, 1969; Urbanelli et al., 2014; Matsushita et al., 2019). HEXA, CLN5, and *Dictyostelium* Cln5 all have glycoside hydrolase activity (Okada and O'Brien, 1969; Huber and Mathavarajah, 2018a). Based on these findings, we were interested in further exploring the relationship between CLN5 and HEXA. Using the GEPIA database[1], we found that the expression profiles of *CLN5* and *HEXA* are highly correlated in human tissues (8,587 samples from a collective overview of 53 non-diseased tissue sites) (Tang et al., 2019; **Figure 8A**). Expression is also highly correlated in brain tissues where *CLN5* is highly expressed and most affected by CLN5 disease (cortex, cerebellum, and hippocampus) (Heinonen et al., 2000; Holmberg et al., 2004; **Figure 8A**). These observations, coupled with the glycoside hydrolase activity of CLN5 and HEXA, suggested that the two proteins may participate in the same biological pathway and that there may be a potential overlap in how autophagy is disrupted in Tay-Sachs disease and the NCLs. To examine this possibility in *Dictyostelium*, we assessed the amounts of intracellular and extracellular Cln5 in cells lacking *N*-acetylglucosaminidase (*nagA*), the *Dictyostelium* homolog of human HEXA (Dimond et al., 1973). Loss of *nagA* increased the intracellular amount of Cln5 by over 500% in cells starved for 4 h but had no effect on the amount of extracellular Cln5 suggesting that *nagA*-deficient cells upregulate *cln5*, potentially as a compensatory mechanism to increase glycoside hydrolase activity (**Figure 8B**). In total, these results suggest that CLN5/Cln5 and HEXA/NagA may participate in the same pathway to regulate autophagy, which is consistent with their shared function as glycoside hydrolases.

Loss of *cln5* Accelerates Tipped Mound, Slug, and Fruiting Body Formation

CLN5 has been linked to brain development in mice and humans (Heinonen et al., 2000; Holmberg et al., 2004; Fabritius et al., 2014; Singh et al., 2019). In addition, recent work in *Cln5*-deficient mice speculated that CLN5 function is linked to neurogenesis (Savchenko et al., 2017). We were therefore interested in using *Dictyostelium* to further study the role of CLN5 in developmental processes. Following aggregation, *cln5*$^{-}$ cells formed tipped mounds prior to WT cells (39 ± 2% of *cln5*$^{-}$ mounds were tipped after 12 h of development compared to 19 ± 2% of WT mounds) (**Figure 9A**). We then observed that

[1]http://gepia.cancer-pku.cn/index.html

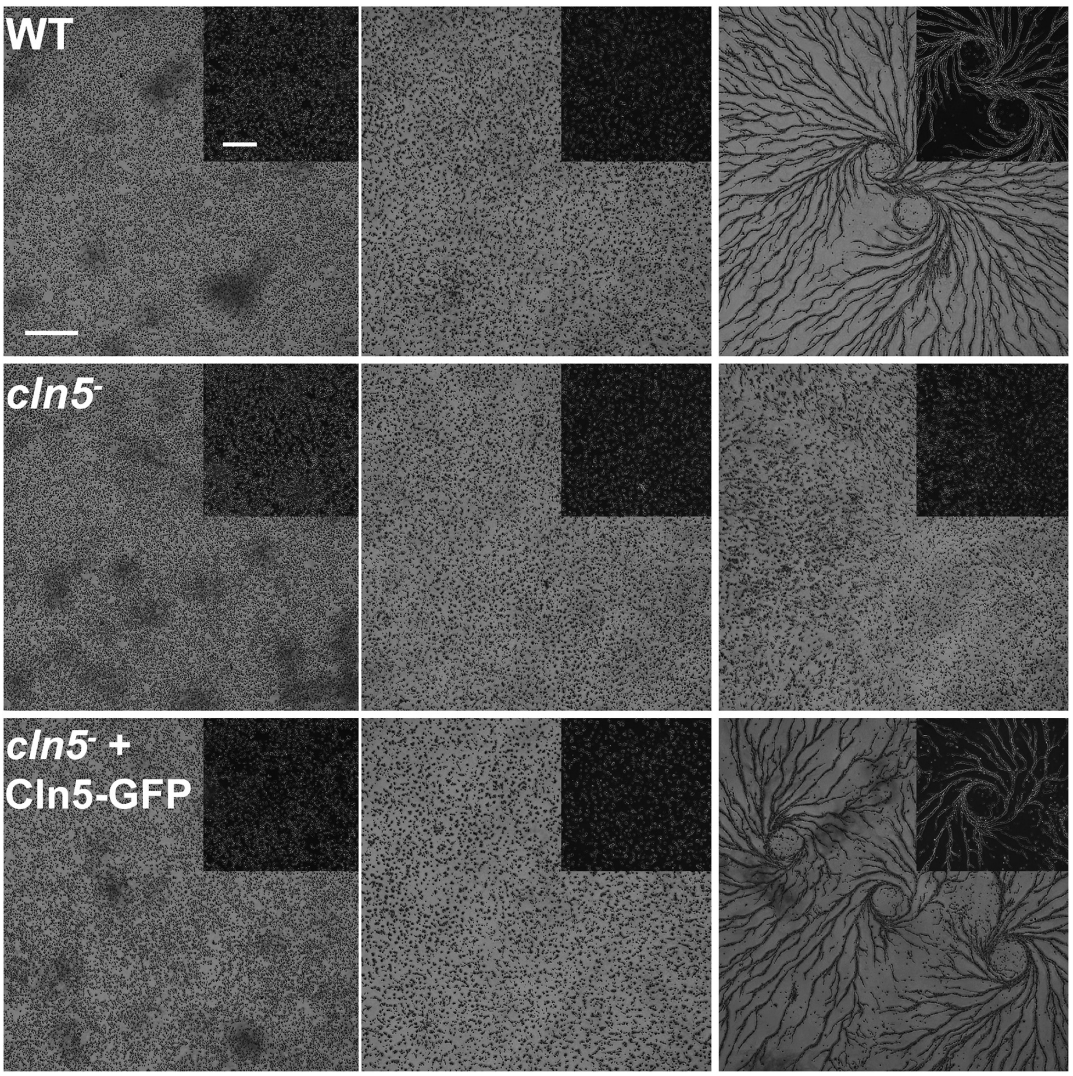

FIGURE 6 | Effect of *cln5*-deficiency on aggregation. WT, *cln5*$^{-}$, and *cln5*$^{-}$ + Cln5-GFP cells were submerged in KK2 buffer and imaged at the indicated times. Scale bar = 500 μm. Insert scale bar = 250 μm.

development of *cln5*$^{-}$ cells into fingers, slugs, and fruiting bodies was also precocious. More specifically, after 16 h of development, 38 ± 2% of *cln5*$^{-}$ multicellular structures were fingers and slugs compared to 21 ± 2% of WT multicellular structures (**Figure 9B**). After 22 h of development, 55 ± 2% of *cln5*$^{-}$ multicellular structures developed into fruiting bodies compared to 32 ± 2% of WT multicellular structures (**Figure 9C**). Introducing Cln5-GFP into *cln5*$^{-}$ cells suppressed the precocious development of *cln5*$^{-}$ cells into fruiting bodies providing evidence that the accelerated development of *cln5*$^{-}$ cells was due to the absence of the Cln5 protein in mutant cells (**Figure 9C**). Intriguingly, these findings are consistent with observations in *Dictyostelium* knockout models of CLN2 and CLN3 disease suggesting that a similar pathway may be perturbed in the three knockout models (*tpp1A*$^{-}$, *cln3*$^{-}$, and *cln5*$^{-}$) (Huber et al., 2014; Phillips and Gomer, 2015). Together, these results show that *cln5*-deficiency affects developmental timing in *Dictyostelium*.

Loss of *cln5* Affects Spore Morphology, Germination, and Viability

Autophagy is known to regulate terminal differentiation in *Dictyostelium* (Kin et al., 2018; Yamada and Schaap, 2019, 2020). This knowledge, combined with the precocious development of *cln5*$^{-}$ cells, led us to investigate the effects of *cln5*-deficiency on spore morphology, germination, and viability. Loss of *cln5* had no effect on spore area (**Table 1**). However, *cln5*$^{-}$ spores were more rounded compared to WT spores (**Table 1**). We also assessed the effect of *cln5*-deficiency on the timing of spore germination and observed that the time required for *cln5*$^{-}$ spores to germinate

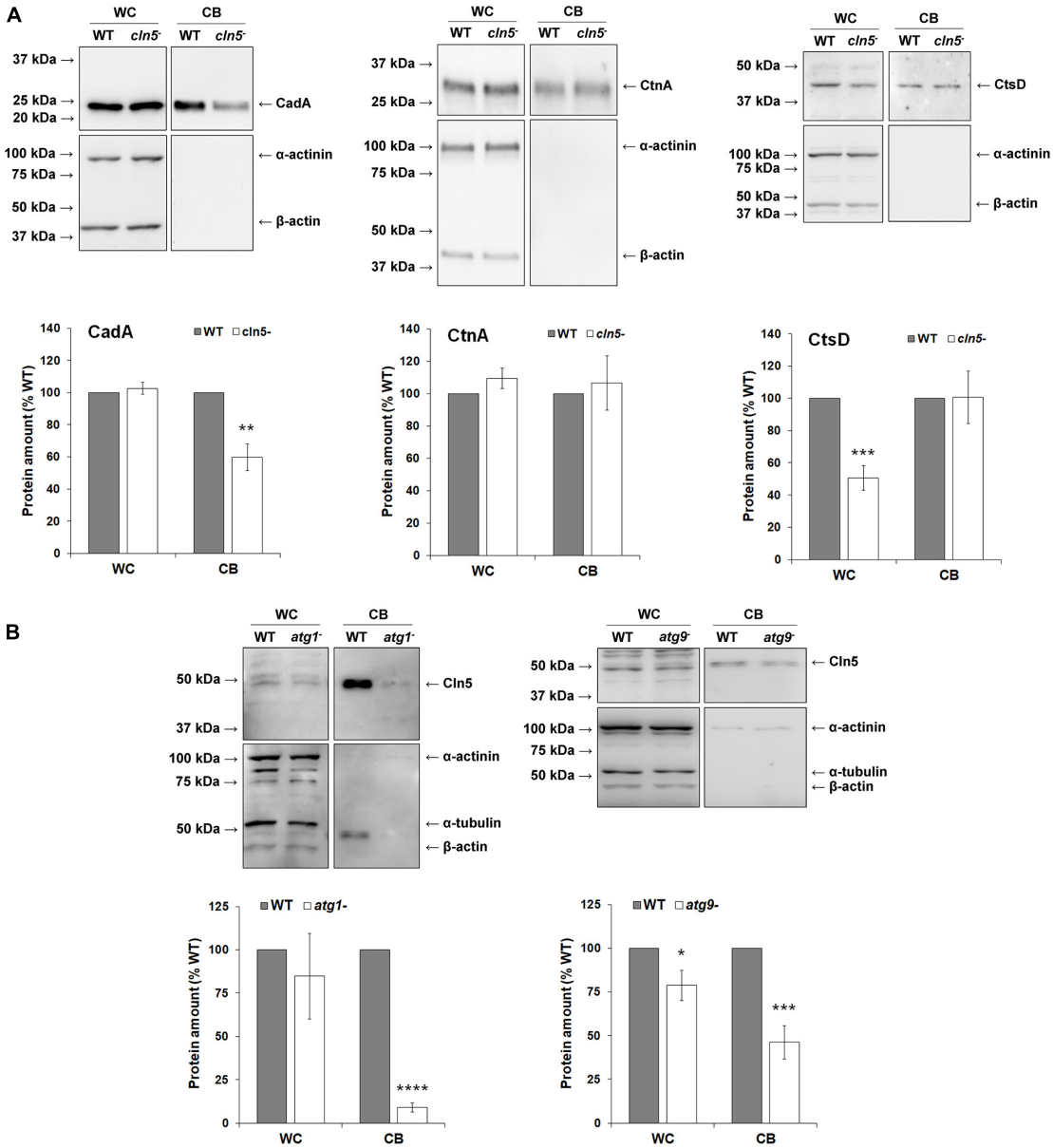

FIGURE 7 | Examining the role and secretion of Cln5 during aggregation. **(A)** Effect of *cln5*-deficiency on the intracellular and extracellular amounts of CadA, CtnA, and CtsD during starvation. WT and *cln5*$^{-}$ cells were starved for 4 h in KK2 buffer after which time the cells were lysed. Whole cell (WC) lysates (25 μg) and conditioned buffer (CB, 0.25 μg) were separated by SDS-PAGE and analyzed by western blotting with anti-CadA, anti-CtnA, anti-CtsD, anti-alpha-actinin (loading control), and anti-beta-actin (loading control). Molecular weight markers (in kDa) are shown to the left of each blot. Protein bands were quantified and standardized to the levels of alpha-actinin and beta-actin. Raw values were then expressed as a percentage of the protein amounts in WT WC lysates and CB. Data presented as mean amount of protein (% WT) ± SEM ($n \geq 7$). Statistical significance was determined using the one sample *t*-test. $^{**}p < 0.01$ and $^{***}p < 0.001$ vs. WT. **(B)** Assessing the role of Atg proteins in Cln5 secretion. WT, *atg1*$^{-}$, and *atg9*$^{-}$ cells were starved for 4 h in KK2 buffer after which time the cells were lysed. WC lysates (20 μg) and CB (0.2 μg) were separated by SDS-PAGE and analyzed by western blotting with anti-Cln5, anti-alpha-actinin (loading control), anti-alpha-tubulin (loading control), and anti-beta-actin (loading control). Molecular weight markers (in kDa) are shown to the left of each blot. Protein bands were quantified and standardized to the levels of alpha-actinin, alpha-tubulin, and beta-actin. Raw values were then expressed as a percentage of the amount of Cln5 in WT WC lysates and CB. Data presented as mean amount of protein (% WT) ± SEM ($n \geq 4$). Statistical significance was determined using the one sample *t*-test. $^{***}p < 0.001$ and $^{****}p < 0.0001$ vs. WT.

was increased by ∼30 min compared to WT spores (**Table 1**). Finally, we used a plaque assay to assess spore viability. When WT spores were plated with bacteria on SM/2 agar, 70 ± 4% of the spores formed plaques, compared to only 49 ± 2% of *cln5*$^{-}$ spores (**Table 1**). Expression of Cln5-GFP in *cln5*$^{-}$ cells rescued the defects in spore roundedness, germination, and viability suggesting that Cln5 regulates these processes in *Dictyostelium* possibly via its role in autophagy.

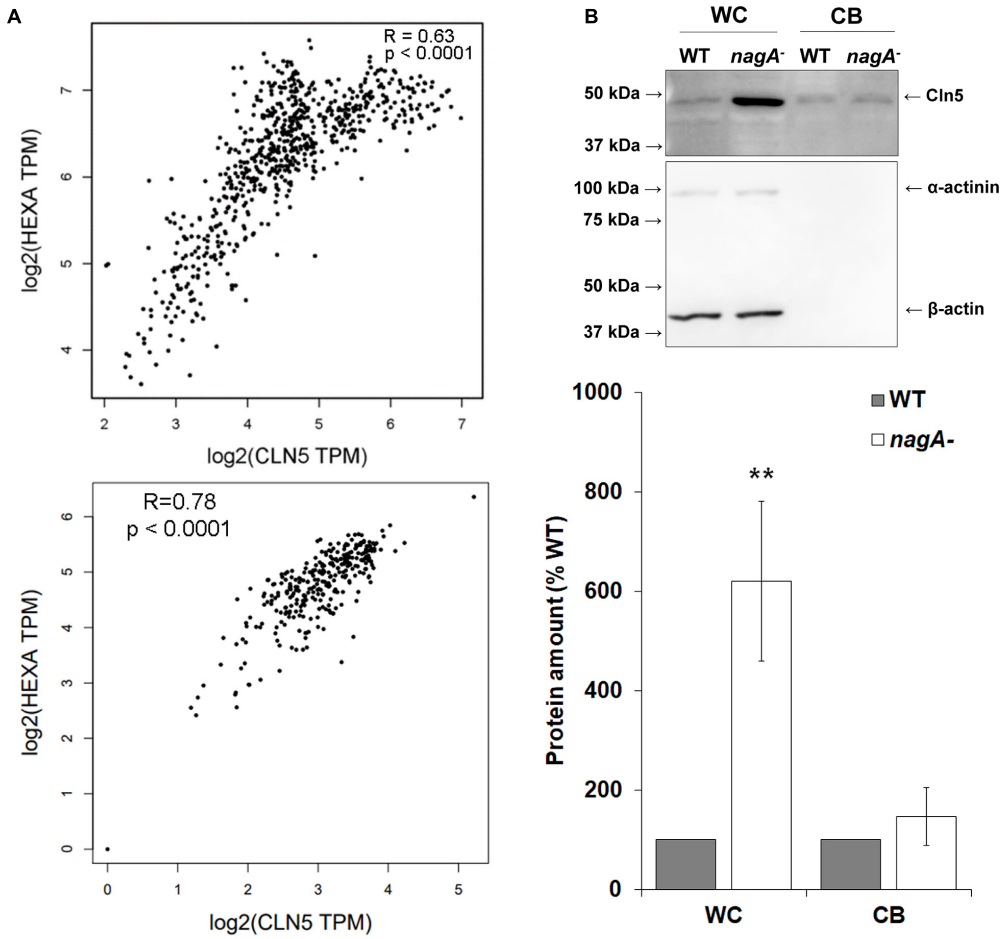

FIGURE 8 | Examining the link between CLN5/Cln5 and HEXA/NagA. **(A)** Co-expression of *CLN5* and *HEXA* in human tissues. RNA sequencing data across 53 non-diseased tissue sites (8,587 samples) were collected from the GTEx Project, which is available on the GEPIA2 database (http://gepia.cancer-pku.cn/index.html). The correlation analysis tool on the GEPIA2 database was used to analyze the expression of *CLN5* and *HEXA* in these samples (top). The correlation analysis tool was also used to analyze the expression of *CLN5* and *HEXA* in a subset of samples from brain tissue (cerebellum, cortex, and hippocampus) (bottom). Pearson correlation statistics were calculated for each plot and the statistical significance for the correlations were determined. Transcripts per million (TPM). **(B)** Effect of *nagA*-deficiency on the intracellular and extracellular amounts of Cln5. Cells were starved for 4 h in KK2 buffer after which time the cells were lysed. Whole cell (WC) lysates (20 μg) and samples of conditioned buffer (CB, 0.2 μg) were separated by SDS-PAGE and analyzed by western blotting with anti-Cln5, anti-alpha-actinin (loading control), and anti-beta-actin (loading control). Molecular weight markers (in kDa) are shown to the left of the blot. Protein bands were quantified and standardized to the levels of alpha-actinin and beta-actin. Raw values were then expressed as a percentage of the amount of Cln5 in WT WC lysates and CB. Data presented as mean amount of protein (% WT) ± SEM ($n = 7$). Statistical significance was determined using the one sample *t*-test. $^{**}p$-value < 0.01 vs. WT.

Aberrant Autophagy Underlies the Development of *cln5*$^{-}$ Cells

Dictyostelium autophagy mutants display a variety of abnormal developmental phenotypes (Otto et al., 2004). These defects are more prominent during development on agar as opposed to nitrocellulose filters, and even more pronounced when autophagy is inhibited (Otto et al., 2003, 2004; Kosta et al., 2004). Therefore, we monitored the development of WT and *cln5*$^{-}$ cells on distilled water agar containing ammonium chloride. *cln5*$^{-}$ development was more impaired compared to WT in the presence of ammonium chloride. *cln5*$^{-}$ mounds appeared smaller and flatter than WT mounds (**Figure 10A**). Slugs formed by *cln5*$^{-}$ cells were smaller and translucent, making them difficult to see with the unaided eye (**Figure 10B**). Slug size was reduced by 15 ± 4% on distilled water agar and by 68 ± 2% on distilled water agar containing ammonium chloride, demonstrating that the phenotype was exaggerated when autophagy was inhibited (**Figure 10B**). Lastly, fruiting body stalks appeared shorter and delicate, while sori appeared smaller (**Figure 10A**). The impaired development of *cln5*$^{-}$ cells in autophagy-inhibiting conditions provides additional evidence linking Cln5 to autophagy during *Dictyostelium* development.

DISCUSSION

The aim of this study was to better understand the function of Cln5 in *Dictyostelium*. During growth, *cln5*-deficiency inhibited cell proliferation and cytokinesis but had no effect on pinocytosis.

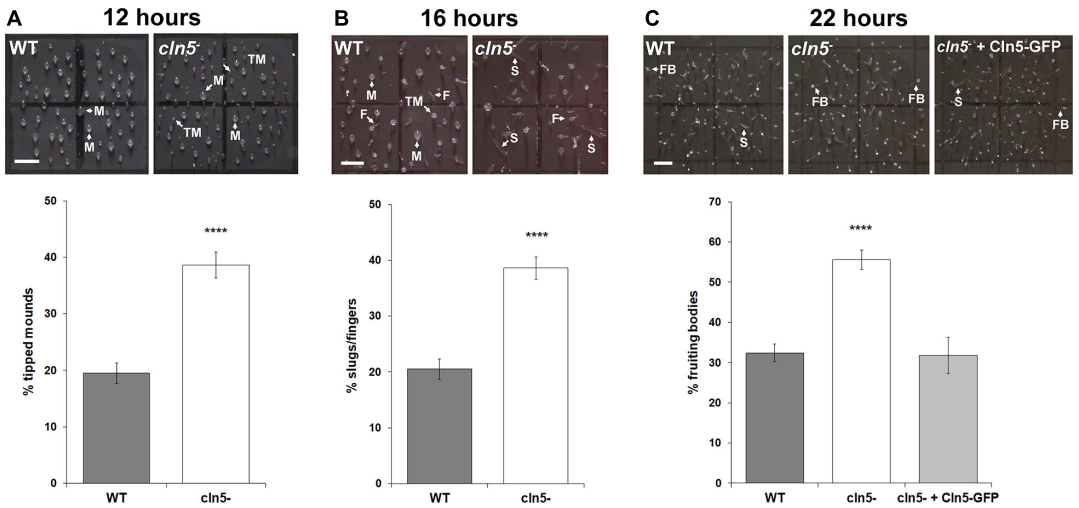

FIGURE 9 | Effect of *cln5*-deficiency on the mid-to-late stages of development. **(A)** Effect of *cln5*-deficiency on tipped mound formation after 12 h of development. Data presented as mean percentage of tipped mounds ± SEM ($n > 84$). **(B)** Effect of *cln5*-deficiency on finger and slug formation after 16 h of development. Data presented as mean percentage of fingers/slugs ± SEM ($n > 88$). **(C)** Effect of *cln5*-deficiency on fruiting body formation after 22 h of development. Data presented as mean percentage of fruiting bodies ± SEM ($n > 32$). Arrows (white) indicate mounds (M), tipped mounds (TM), slugs (S), fingers (F), and fruiting bodies (FB). Scale bar = 1 mm. Statistical significance for panels **(A,B)** was determined using the Student's *t*-test. Statistical significance for panel **(C)** was determined using one-way ANOVA followed by Tukey's multiple comparisons test. ****p-value < 0.0001 vs. WT.

Loss of *cln5* also compromised proliferation and viability in nutrient-limiting media and inhibited folic acid-mediated chemotaxis. GFP-Atg8a and RFP-GFP-Atg8a autophagic flux assays revealed that *cln5*-deficiency increased the numbers of autophagic puncta (autophagosomes and lysosomes) within cells, suggesting that loss of *cln5* increases the basal level of autophagy during growth. *cln5*-deficiency also increased the amounts of ubiquitin-positive proteins. During multicellular development, *cln5*-deficiency delayed aggregation. However, following mound formation, the development of *cln5*$^-$ cells was precocious. *cln5*$^-$ spores displayed aberrant morphology, germination, and viability. The involvement of Cln5 in many of these processes was validated by expressing Cln5-GFP in *cln5*$^-$ cells to rescue the gene-deficiency phenotypes.

Loss of *cln5* reduced the rate of cell proliferation in nutrient-rich media and the maximum titer of cultures. In addition, the proliferation and viability of *cln5*$^-$ cells was severely compromised in nutrient-limiting media. These observations are consistent with work that examined CLN5 function in mammalian cells. For example, silencing *CLN5* (via RNAi) causes G0/1 arrest in *HeLa* cells, reduces cell number in clear cell renal cell carcinoma, and reduces the viability of HEK293 and primary endothelial cells (Kittler et al., 2007; Gerlinger et al., 2012; Warner et al., 2014; de Rojas-P et al., 2020). However, there may be a cell type-dependent role for CLN5 in regulating cell proliferation since neural progenitor cells derived from a *Cln5*$^{-/-}$ mouse display increased cell proliferation (Savchenko et al., 2017). Therefore, future work is required to clarify the precise role of CLN5 in regulating cell proliferation.

Consistent with the reduced proliferation of *cln5*$^-$ cells, we also observed a mild defect in cytokinesis. Interestingly, Cln3 regulates the secretion of Cln5 in *Dictyostelium*, and we observed similar cytokinesis defects in *cln3*$^-$ cells (Huber and Mathavarajah, 2018b; Mathavarajah et al., 2018). In addition, our previous work revealed that Cln5 has glycoside hydrolase activity (Huber and Mathavarajah, 2018a). Together, these findings suggest that Cln5 may promote cytokinesis in *Dictyostelium* by cleaving glycosides outside the cell to alter the polysaccharide content in the extracellular space. This is supported by work in *Caenorhabditis elegans* showing that secreted proteins can influence cytokinesis by altering the polysaccharide composition of the extracellular matrix (Vogel et al., 2011; Xu and Vogel, 2011).

In this study, we showed that the reduced proliferation of *cln5*$^-$ cells was not due to decreased intake of nutrients via pinocytosis. This finding suggests that while *cln5*$^-$ cells can internalize nutrients normally, the ability of cells to process those nutrients may be compromised. This was supported by

TABLE 1 | Effect of *cln5*-deficiency on spore area, morphology, germination, and viability.

	WT	*cln5*$^-$	*cln5*$^-$ + Cln5-GFP
Normalized spore area	0.048 ± 0.002	0.048 ± 0.002	0.047 ± 0.003
Spore roundedness	0.63 ± 0.010	0.70 ± 0.003*	0.65 ± 0.005
Timing of spore germination (min)	358 ± 3	390 ± 6****	351 ± 3
Spore viability (% initial spores plated)	70 ± 4	49 ± 1****	69 ± 8

All data presented as mean ± SEM (n = 3–4). At least 300 spores were analyzed for each biological replicate. Details on the methods and statistical analyses performed are found in section "Spore Morphology, Germination, and Viability."
**p-value < 0.05 and ****p-value < 0.0001 vs. WT.*

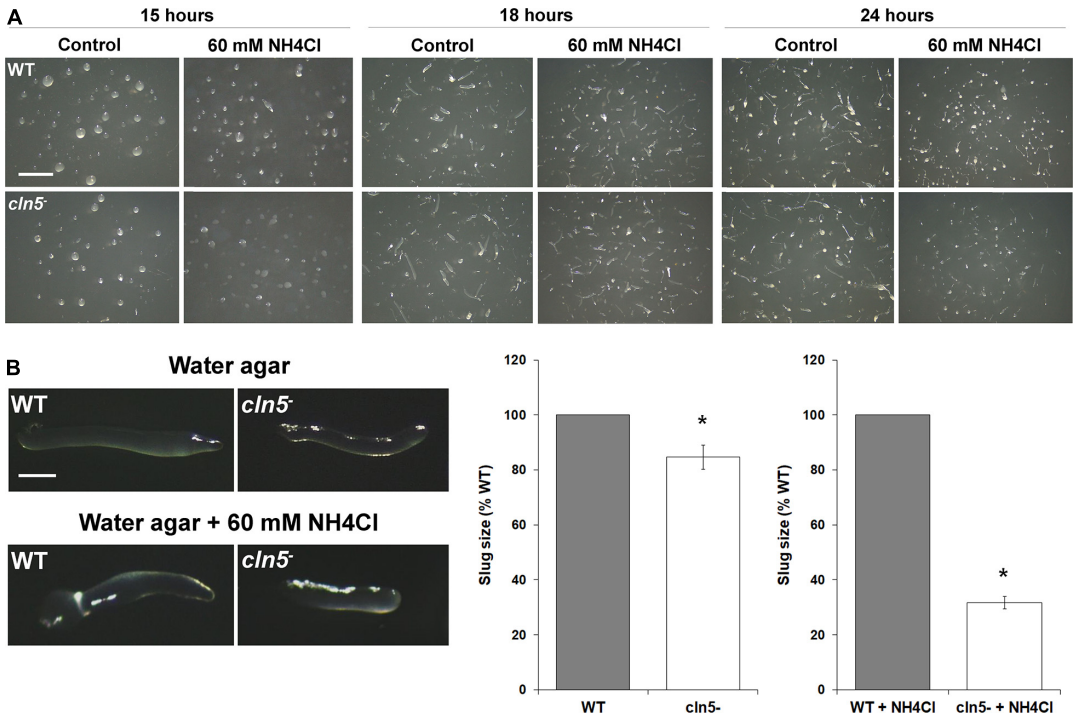

FIGURE 10 | Effect of *cln5*-deficiency on multicellular development when autophagy is inhibited. **(A)** WT and *cln5*$^{-}$ cells were deposited on 0.5% agar/distilled water ± ammonium chloride (60 mM). Images were taken at the mound/tipped mound (15 h), finger/slug (18 h), and fruiting body (24 h) stages of development. Images are representative of three independent experiments. Scale bar = 2.5 mm. **(B)** Effect of *cln5*-deficiency on slug size ± ammonium chloride (60 mM). Scale bar = 50 μm. Raw values were then expressed as a percentage of WT slug size. Data presented as mean slug size (% WT) ± SEM (n = 3, at least eight slugs were quantified for each biological replicate). Statistical significance was determined using the one-sample t-test. *p-value < 0.05 vs. WT.

our findings that loss of *cln5* increases the basal level of autophagy during growth, which may reflect a cellular approach to compensate for the reduced degradation of internal resources in *cln5*$^{-}$ cells. CLN5 has also been linked to autophagy in mammalian systems. Retinal extracts from *Cln5*-deficient mice have increased amounts of LC3-II and other proteins involved in autophagosome formation (Leinonen et al., 2017). CLN5 disease patient fibroblasts and *CLN5*-deficient *HeLa* cells have increased LC3-II and an increased number of basal autophagic puncta, specifically lysosomes, suggesting autophagy is induced in those experimental systems, which is consistent with our findings in *Dictyostelium* (Adams et al., 2019). Finally, work in cellular and murine models of CLN5 disease suggests that CLN5 may play a role in activating mitophagy (Doccini et al., 2020).

Upon activation of the autophagy pathway, polyubiquitinated proteins and inclusion bodies are delivered to the autophagosome for degradation. When autophagy is disrupted, so is the clearance of proteins tagged by ubiquitin (Hara et al., 2006; Komatsu et al., 2006; Nezis et al., 2008; Kocaturk and Gozuacik, 2018). In *Dictyostelium* and other cell models, aberrant autophagic flux is coupled with the accumulation of ubiquitin-positive protein aggregates, which could explain why we observed increased amounts of ubiquitinated proteins in *cln5*$^{-}$ cells (Calvo-Garrido et al., 2010; Tung et al., 2010; Arhzaouy et al., 2012; Muñoz-Braceras et al., 2015; Xiong et al., 2015; Meßling et al., 2017). Since we observed an increased level of basal autophagy in *cln5*$^{-}$ cells, it is also possible that the increased amounts of ubiquitinated proteins could reflect an attempt by *cln5*$^{-}$ cells to generate more nutrients. However, future work will be required to determine why ubiquitin-positive proteins are increased in *cln5*$^{-}$ cells.

In addition to aberrant proliferation and cytokinesis, *cln5*$^{-}$ cells also displayed reduced folic acid-mediated chemotaxis, which allows amoebae to detect and internalize their food source during the growth phase of the life cycle. In *Dictyostelium*, the G protein-coupled folic acid receptor mediates both chemotaxis toward folic acid and the phagocytosis of bacteria (Pan et al., 2016). In HEK-293 and U87 glioblastoma cells, chemotactic G protein-coupled receptors have been shown to control cell migration by repressing autophagosome biogenesis (Coly et al., 2016). Therefore, these findings suggest that the reduced chemotaxis of *cln5*$^{-}$ cells toward folic acid may have been due to alterations in the autophagy pathway.

In this study, we revealed that loss of *cln5* delays aggregation, which could be explained by the previously reported effects of *cln5*-deficiency on cAMP-mediated chemotaxis and adhesion (Huber and Mathavarajah, 2018b). Interestingly, these phenotypes have also been reported in *cln3*$^{-}$ cells (Huber et al., 2017). Consistent with these findings, we revealed that loss of *cln5* altered the extracellular amount of the calcium-dependent cell adhesion protein CadA. We also observed no effect of *cln5*-deficiency on the intracellular and extracellular levels of CtnA. Since CtnA regulates aggregate size, it was not

surprising that loss of *cln5* had no effect on aggregate number or size (Brock and Gomer, 1999). Like growth, the delayed aggregation of *cln5*$^-$ cells could also be explained by aberrant autophagy. This is supported by our observation that loss of *cln5* reduced the intracellular amount of the lysosomal enzyme CtsD. In addition, we revealed reduced secretion of Cln5 in *atg1*$^-$ and *atg9*$^-$ cells suggesting that the trafficking of Cln5 is dependent on the activities of these two autophagy proteins. Atg1 is a protein kinase that is required for macroautophagy and co-localizes with Atg8a, which was used as a marker of autophagic flux in this study (Otto et al., 2004; Tekinay et al., 2006). Atg9 localizes to small vesicles and is predicted to play a role in membrane trafficking to autophagosomes (Calvo-Garrido et al., 2010; Tung et al., 2010). Importantly, these findings adhere to previous work that reported reduced secretion of Cln5 when WT cells were treated with ammonium chloride or chloroquine, two inhibitors of autophagy (Huber and Mathavarajah, 2018b).

Loss of *cln5* accelerated the mid-to-late stages of *Dictyostelium* development, which has also been reported for *tpp1A*$^-$ and *cln3*$^-$ cells (Huber et al., 2014; Phillips and Gomer, 2015). Precocious development is a common phenotype of *Dictyostelium* autophagy mutants and can be explained by the inability of cells to either sense nutrients in their environment or process nutrients that have been internalized (Mesquita et al., 2017). This prematurely places cells in a starved state and causes them to progress through the developmental program faster. *cln5*$^-$ development was also impaired when cells were placed on distilled water agar containing ammonium chloride, an inhibitor of autophagy. Since ammonium chloride treatment suppressed the precocious development of *cln5*$^-$ cells, this finding aligns with the increased basal level of autophagy observed in *cln5*$^-$ cells. In addition, *cln5*-deficient slugs were smaller than WT slugs when developed on distilled water agar. This phenotype was exaggerated on distilled water agar containing ammonium chloride further supporting the role of Cln5 in autophagy. Previous work showed that *tpp1A*$^-$ and *cln3*$^-$ cells are also sensitive to ammonium chloride during development (Phillips and Gomer, 2015; Mathavarajah et al., 2018). In addition, *tpp1A*$^-$ development was impaired by chloroquine, another autophagy-inhibiting chemical (Phillips and Gomer, 2015). These findings support mounting evidence that aberrant autophagy may be a common phenotype underlying all forms of NCL (Huber, 2020). It is important to note that while ammonium chloride is routinely used to inhibit autophagy in *Dictyostelium*, it has also been shown to affect cAMP signaling during *Dictyostelium* development (Williams et al., 1984). Therefore, at this time, we cannot discount the possibility that the observed effects of ammonium chloride on development may have been due to altered cAMP signaling. Nonetheless, our observations show clear differences between WT and *cln5*$^-$ development in the presence of ammonium chloride. Finally, while there are significant differences between *Dictyostelium* and mammalian development, the impact of *cln5*-deficiency on multicellular development in *Dictyostelium* mirrors observations in mammalian systems that have linked CLN5 to brain development and neurogenesis (Heinonen et al., 2000; Holmberg et al., 2004; Fabritius et al., 2014; Savchenko et al., 2017; Singh et al., 2019).

Autophagy regulates terminal differentiation in *Dictyostelium* (Kin et al., 2018; Yamada and Schaap, 2019, 2020). Not surprisingly, we observed that loss of *cln5* impacted spore shape, viability, and the timing of germination. Previous work showed that acyl coenzyme A (CoA) binding protein (AcbA), an essential protein in spore formation, is trafficked via autophagosomes and secreted unconventionally, after which it is processed into spore differentiation factor 2 (SDF-2) (Duran et al., 2010). The defects in the shape of *cln5*$^-$ spores may possibly be explained by defects in the autophagy-mediated trafficking of key proteins required for spore formation, thus contributing to altered spore shape and reduced viability. In addition, ultrastructural images taken during spore germination suggest that autophagic vacuoles play an important role in *Dictyostelium* spore germination (Cotter et al., 1969). Therefore, the autophagy defects in *cln5*$^-$ cells may have contributed to the reduced germination of spores.

Previous work showed that *Dictyostelium* Cln5 and human CLN5 have glycoside hydrolase activity (Huber and Mathavarajah, 2018a). A well-characterized glycoside hydrolase in humans is HEXA, which localizes to the lysosome and is associated with Tay-Sachs disease (Okada and O'Brien, 1969). Not surprisingly, HEXA has also been linked to autophagy (Urbanelli et al., 2014; Matsushita et al., 2019). In this study, we showed that the expression profiles of *HEXA* and *CLN5* are highly correlated in human tissues, particularly in brain tissue most affected by CLN5 disease. We then showed that loss of *nagA*, the *Dictyostelium* homolog of *HEXA*, dramatically increases the intracellular amount of Cln5 during starvation. Since the extracellular amount of Cln5 was unaffected by the loss of nagA these findings suggest that *nagA*$^-$ cells increase the expression of *cln5* to compensate for the reduced glycoside hydrolase activity in *nagA*-deficient cells. These observations not only provide additional evidence supporting the glycoside hydrolase activity of Cln5, but they also suggest that Cln5 and NagA may participate in the same biological pathway. This is further supported by previous work that identified NagA as a Cln5-interactor (Huber and Mathavarajah, 2018a). In addition, like *cln5*-deficiency, loss of *nagA*, also reduces slug size in *Dictyostelium* (Dimond et al., 1973). Together, these important findings provide additional insight into the molecular function of CLN5 and the pathological mechanisms that may underlie CLN5 disease.

The online bioinformatics resource for the *Dictyostelium* research community, dictyBase, maintains a database listing the phenotypes of knockout mutants that have been generated by the community. For the purposes of this study, we identified those mutants that were characterized as displaying aberrant autophagy, increased autophagy, or an increased number of autophagosomes (**Supplementary Table 1**). We then compared the additional phenotypes revealed in those mutants to the growth and developmental phenotypes of *cln5*$^-$ cells to gain insight into the pathways that may mediate the function of Cln5 in *Dictyostelium*. Not surprisingly, this analysis revealed many autophagy genes (e.g., *atg1*$^-$, *atg5*$^-$, *atg6*$^-$, *atg7*$^-$, *atg8*$^-$, *atg9*$^-$, and *atg13*$^-$), providing additional evidence linking Cln5 to the autophagy pathway. Common phenotypes displayed by autophagy mutants include decreased or abolished growth

and aberrant fruiting body development, which were both observed in *cln5*$^{-}$ cells. Of the mutants identified, *ino1*$^{-}$ cells share several common phenotypes with *cln5*$^{-}$ cells, including an increased number of autophagosomes, abolished growth, aberrant cytokinesis, decreased cell-substrate adhesion, and aberrant fruiting body morphology (Frej et al., 2016). *ino1* encodes inositol-3-phosphate synthase, which is involved in inositol phosphate metabolism and is linked to many human diseases including diabetes, bipolar disorder, and Alzheimer's disease (McLaurin et al., 1998; Silverstone et al., 2005; Fischbach et al., 2006; Scioscia et al., 2007). Altered inositol levels have also been reported in CLN2 disease patients and a CLN3 disease mouse model (Seitz et al., 1998; Pears et al., 2005). Combined, these findings suggest that Cln5 may play a role in maintaining inositol homeostasis within cells.

In summary, this study reports several growth and developmental phenotypes in *cln5*$^{-}$ cells that are associated with aberrant autophagy, which supports mounting evidence in other systems linking the NCLs to the autophagy pathway. However, it is important to note that some of our observations of *cln5*$^{-}$ cells, including aberrant cytokinesis, chemotaxis, and aggregation, could be due to defects in cytoskeletal components. Therefore, while the sum of our data suggest that autophagy is compromised in *cln5*$^{-}$ cells, the impact of *cln5*-deficiency on the cytoskeleton should be examined in future studies. We previously showed that *Dictyostelium* Cln5 and human CLN5 have glycoside hydrolase activity (Huber and Mathavarajah, 2018a). Since both proteins are secreted, another possible explanation for *cln5*-deficient phenotypes is that Cln5 generates a signaling molecule required for *Dictyostelium* growth and development. This is consistent with observations that secreted proteins can influence developmental timing (Chubb et al., 2006). However, additional work is required to confirm this hypothesis. Since the molecular function of CLN5 is conserved between humans and *Dictyostelium*, studying the multifaceted role of Cln5 during *Dictyostelium* growth and development could provide valuable new insight into the function of CLN5 in human cells. As the pathological mechanism of CLN5 disease is unknown, this work provides exciting new insight into the cellular mechanisms that may contribute to CLN5 disease, and on a larger scale, all subtypes of NCL.

DATA AVAILABILITY STATEMENT

The original contributions presented in the study are included in the article/**Supplementary Material**, further inquiries can be directed to the corresponding author/s.

AUTHOR CONTRIBUTIONS

RH: conceptualization, writing–review and editing, funding acquisition, and supervision. MM, SM, WK, SY, and RH: experimentation and data analysis. MM, SM, and RH: writing–original draft. All authors read and approved the final draft of the manuscript.

FUNDING

This work was supported by a Project Grant from the Canadian Institutes of Health Research (PJT165873 to RH). WK was supported by a Canada Graduate Scholarship from the Natural Sciences and Engineering Council of Canada and a Queen Elizabeth II Graduate Scholarship in Science and Technology. SY was supported by an Ontario Graduate Scholarship.

ACKNOWLEDGMENTS

The authors would like to thank Dr. Richard Gomer (Texas A&M University) for generously providing the anti-CtnA antibody.

SUPPLEMENTARY MATERIAL

The Supplementary Material for this article can be found online at: https://www.frontiersin.org/articles/10.3389/fcell.2021.657406/full#supplementary-material

REFERENCES

Adams, J., Feuerborn, M., Molina, J. A., Wilden, A. R., Adhikari, B., Budden, T., et al. (2019). Autophagy – lysosome pathway alterations and alpha-synuclein up-regulation in the subtype of neuronal ceroid lipofuscinosis, CLN5 disease. *Sci. Rep.* 9:151.

Arhzaouy, K., Strucksberg, K. H., Tung, S. M., Tangavelou, K., Stumpf, M., Faix, J., et al. (2012). Heteromeric p97/p97R155C complexes induce dominant negative changes in wild-type and autophagy 9-deficient *Dictyostelium* strains. *PLoS One* 7:e0199548. doi: 10.1371/journal.pone.0046879

Beck-Wödl, S., Harzer, K., Sturm, M., Buchert, R., Rieß, O., Mennel, H. D., et al. (2018). Homozygous TBC1 domain-containing kinase (TBCK) mutation causes a novel lysosomal storage disease - a new type of neuronal ceroid lipofuscinosis (CLN15)? *Acta Neuropathol. Commun.* 6:145.

Brar, S. K., and Siu, C. H. (1993). Characterization of the cell adhesion molecule gp24 in *Dictyostelium discoideum*. Mediation of cell-cell adhesion via a Ca(2+)-dependent mechanism. *J. Biol. Chem.* 268, 24902–24909. doi: 10.1016/s0021-9258(19)74550-5

Brock, D. A., and Gomer, R. H. (1999). A cell-counting factor regulating structure size in *Dictyostelium*. *Genes Dev.* 13, 1960–1969. doi: 10.1101/gad.13.15.1960

Calvo-Garrido, J., Carilla-Latorre, S., Kubohara, Y., Santos-Rodrigo, N., Mesquita, A., Soldati, T., et al. (2010). Autophagy in *Dictyostelium*: genes and pathways, cell death and infection. *Autophagy* 6, 686–701. doi: 10.4161/auto.6.6.12513

Calvo-Garrido, J., Carilla-Latorre, S., Mesquita, A., and Escalante, R. (2011). A proteolytic cleavage assay to monitor autophagy in *Dictyostelium discoideum*. *Autophagy* 7, 1063–1068. doi: 10.4161/auto.7.9.16629

Cannelli, N., Nardocci, N., Cassandrini, D., Morbin, M., Aiello, C., Bugiani, M., et al. (2007). Revelation of a novel CLN5 mutation in early juvenile neuronal ceroid lipofuscinosis. *Neuropediatrics* 38, 46–49. doi: 10.1055/s-2007-981449

Cárcel-Trullols, J., Kovács, A. D., and Pearce, D. A. (2015). Cell biology of the NCL proteins: What they do and don't do. *BBA Mol. Basis Dis.* 1852, 2242–2255. doi: 10.1016/j.bbadis.2015.04.027

Chubb, J. R., Bloomfield, G., Xu, Q., Kaller, M., Ivens, A., Skelton, J., et al. (2006). Developmental timing in *Dictyostelium* is regulated by the Set1 histone methyltransferase. *Dev. Biol.* 292, 519–532. doi: 10.1016/j.ydbio.2005.12.054

Coly, P. M., Perzo, N., Le Joncour, V., Lecointre, C., Schouft, M. T., Desrues, L., et al. (2016). Chemotactic G protein-coupled receptors control cell migration

by repressing autophagosome biogenesis. *Autophagy* 12, 2344–2362. doi: 10.1080/15548627.2016.1235125

Cotter, D. A., Miura-Santo, L. Y., and Hohl, H. R. (1969). Ultrastructural changes during germination of *Dictyostelium discoideum* spores. *J. Bacteriol.* 100, 1020–1026. doi: 10.1128/jb.100.2.1020-1026.1969

Cotter, D. A., and Raper, K. B. (1966). Spore germination in *Dictyostelium discoideum*. *Proc. Natl. Acad. Sci. U.S.A.* 56, 880–887.

de Rojas-P, I., Albiñana, V., Recio-Poveda, L., Rodriguez-Rufián, A., Cuesta, ÁM., and Botella, L. M. (2020). CLN5 in heterozygosis may protect against the development of tumors in a VHL patient. *Orphanet. J. Rare Dis.* 15:132.

Dimond, R. L., Brenner, M., and Loomis, W. F. (1973). Mutations affecting N-acetylglucosaminidase in *Dictyostelium discoideum*. *Proc. Natl. Acad. Sci. U.S.A.* 70, 3356–3360. doi: 10.1073/pnas.70.12.3356

Doccini, S., Morani, F., Nesti, C., Pezzini, F., Calza, G., Soliymani, R., et al. (2020). Proteomic and functional analyses in disease models reveal CLN5 protein involvement in mitochondrial dysfunction. *Cell Death Discov.* 6:18.

Dolisca, S., Mehta, M., Pearce, D., Mink, J., and Maria, B. (2013). Batten disease: clinical aspects, molecular mechanisms, translational science, and future directions. *J. Child Neurol.* 28, 1074–1100. doi: 10.1177/0883073813493665

Domínguez-Martín, E., Cardenal-Muñoz, E., King, J., Soldati, T., Coria, R., and Escalante, R. (2017). Methods to monitor and quantify autophagy in the social amoeba *Dictyostelium discoideum*. *Cells* 6:18. doi: 10.3390/cells6030018

Duran, J. M., Anjard, C., Stefan, C., Loomis, W. F., and Malhotra, V. (2010). Unconventional secretion of Acb1 is mediated by autophagosomes. *J. Cell Biol.* 188, 527–536. doi: 10.1083/jcb.200911154

Fabritius, A.-L., Vesa, J., Minye, H. M., Nakano, I., Kornblum, H., and Peltonen, L. (2014). Neuronal ceroid lipofuscinosis genes, CLN2, CLN3 and CLN5 are spatially and temporally co-expressed in a developing mouse brain. *Exp. Mol. Pathol.* 97, 484–491. doi: 10.1016/j.yexmp.2014.10.003

Faix, J., Linkner, J., Nordholz, B., Platt, J. L., Liao, X. H., and Kimmel, A. R. (2013). The application of the Cre-loxP system for generating multiple knock-out and knock-in targeted loci. *Methods Mol. Biol.* 983, 249–267. doi: 10.1007/978-1-62703-302-2_13

Fey, P., Dodson, R., Basu, S., and Chrisholm, R. L. (2013). One stop shop for everything *Dictyostelium*: dictybase and the Dicty Stock Center. *Methods Mol. Biol.* 983, 59–92. doi: 10.1007/978-1-62703-302-2_4

Fey, P., Kowal, A. S., Gaudet, P., Pilcher, K. E., and Chisholm, R. L. (2007). Protocols for growth and development of *Dictyostelium discoideum*. *Nat. Protoc.* 2, 1307–1316. doi: 10.1038/nprot.2007.178

Fischbach, A., Adelt, S., Müller, A., and Vogel, G. (2006). Disruption of inositol biosynthesis through targeted mutagenesis in *Dictyostelium discoideum*: generation and characterization of inositol-auxotrophic mutants. *Biochem. J.* 397, 509–518. doi: 10.1042/bj20060277

Franke, J., and Kessin, R. A. (1977). Defined minimal medium for axenic strains of *Dictyostelium discoideum*. *Proc. Natl. Acad. Sci. U S A.* 74, 2157–2161. doi: 10.1073/pnas.74.5.2157

Frej, A. D., Clark, J., Le Roy, C. I., Lilla, S., Thomason, P. A., Otto, G. P., et al. (2016). The inositol-3-phosphate synthase biosynthetic enzyme has distinct catalytic and metabolic roles. *Mol. Cell. Biol.* 36, 1464–1479. doi: 10.1128/mcb.00039-16

Gerlinger, M., Santos, C. R., Spencer-Dene, B., Martinez, P., Endesfelder, D., Burrell, R. A., et al. (2012). Genome-wide RNA interference analysis of renal carcinoma survival regulators identifies MCT4 as a Warburg effect metabolic target. *J. Pathol.* 227, 146–156. doi: 10.1002/path.4006

Haddad, S. E., Khoury, M., Daoud, M., Kantar, R., Harati, H., Mousallem, T., et al. (2012). CLN5 and CLN8 protein association with ceramide synthase: biochemical and proteomic approaches. *Electrophoresis* 33, 3798–3809. doi: 10.1002/elps.201200472

Hagedorn, M., Neuhaus, E., and Soldati, T. (2006). Optimized fixation and immunofluorescence staining methods for *Dictyostelium* cells. *Methods Mol. Biol.* 346, 327–338. doi: 10.1385/1-59745-144-4:327

Hara, T., Nakamura, K., Matsui, M., Yamamoto, A., Nakahara, Y., Suzuki-Migishima, R., et al. (2006). Suppression of basal autophagy in neural cells causes neurodegenerative disease in mice. *Nature* 441, 885–889. doi: 10.1038/nature04724

Heinonen, O., Salonen, T., Jalanko, A., Peltonen, L., and Copp, A. (2000). CLN-1 and CLN-5, genes for infantile and variant late infantile neuronal ceroid lipofuscinoses, are expressed in the embryonic human brain. *J. Comp. Neurol.* 426, 406–412. doi: 10.1002/1096-9861(20001023)426:3<406::aid-cne5>3.0.co;2-5

Holmberg, V., Jalanko, A., Isosomppi, J., Fabritius, A. L., Peltonen, L., and Kopra, O. (2004). The mouse ortholog of the neuronal ceroid lipofuscinosis CLN5 gene encodes a soluble lysosomal glycoprotein expressed in the developing brain. *Neurobiol. Dis.* 16, 29–40. doi: 10.1016/j.nbd.2003.12.019

Huber, R. J. (2016). Using the social amoeba *Dictyostelium* to study the functions of proteins linked to neuronal ceroid lipofuscinosis. *J. Biomed. Sci.* 23:83.

Huber, R. J. (2017). Loss of Cln3 impacts protein secretion in *Dictyostelium*. *Cell. Signal.* 35, 61–72. doi: 10.1016/j.cellsig.2017.03.022

Huber, R. J. (2020). Molecular networking in the neuronal ceroid lipofuscinoses: insights from mammalian models and the social amoeba *Dictyostelium discoideum*. *J. Biomed. Sci.* 27:64.

Huber, R. J., Hughes, S. M., Liu, W., Morgan, A., Tuxworth, R. I., and Russell, C. (2020a). The contribution of multicellular model organisms to neuronal ceroid lipofuscinosis research. *BBA Mol. Basis Dis.* 1866:165614. doi: 10.1016/j.bbadis.2019.165614

Huber, R. J., and Mathavarajah, S. (2018a). Cln5 is secreted and functions as a glycoside hydrolase in *Dictyostelium*. *Cell. Signal.* 42, 236–248. doi: 10.1016/j.cellsig.2017.11.001

Huber, R. J., and Mathavarajah, S. (2018b). Secretion and function of Cln5 during the early stages of *Dictyostelium* development. *BBA Mol. Cell Res.* 1865, 1437–1450. doi: 10.1016/j.bbamcr.2018.07.017

Huber, R. J., and Mathavarajah, S. (2019). Comparative transcriptomics reveals mechanisms underlying cln3-deficiency phenotypes in *Dictyostelium*. *Cell. Signal.* 58, 79–90. doi: 10.1016/j.cellsig.2019.02.004

Huber, R. J., Mathavarajah, S., and Yap, S. Q. (2020b). Mfsd8 localizes to endocytic compartments and influences the secretion of Cln5 and cathepsin D in *Dictyostelium*. *Cell. Signal.* 70:109572. doi: 10.1016/j.cellsig.2020.109572

Huber, R. J., Myre, M. A., and Cotman, S. L. (2014). Loss of Cln3 function in the social amoeba *Dictyostelium discoideum* causes pleiotropic effects that are rescued by human CLN3. *PLoS One* 9:e110544. doi: 10.1371/journal.pone.0110544

Huber, R. J., Myre, M. A., and Cottman, S. L. (2017). Aberrant adhesion impacts early development in a *Dictyostelium* model for juvenile neuronal ceroid lipofuscinosis. *Cell Adh. Migr.* 11, 399–418. doi: 10.1080/19336918.2016.1236179

Hughes, S. M., Hope, K. M., Xu, J. B., Mitchell, N. L., and Palmer, D. N. (2014). Inhibition of storage pathology in prenatal CLN5-deficient sheep neural cultures by lentiviral gene therapy. *Neurobiol. Dis.* 62, 543–550. doi: 10.1016/j.nbd.2013.11.011

Isosomppi, J., Vesa, J., Jalanko, A., and Peltonen, L. (2002). Lysosomal localization of the neuronal ceroid lipofuscinosis CLN5 protein. *Hum. Mol. Genet.* 11, 885–891. doi: 10.1093/hmg/11.8.885

Jeon, T. J., Lee, S., Weeks, G., and Firtel, R. A. (2009). Regulation of *Dictyostelium morphogenesis* by RapGAP3. *Dev. Biol.* 328, 210–220. doi: 10.1016/j.ydbio.2009.01.016

Journet, A., Chapel, A., Jehan, S., Adessi, C., Freeze, H., Klein, G., et al. (1999). Characterization of *Dictyostelium discoideum* cathepsin D. *J. Cell Sci.* 112, 3833–3843. doi: 10.1242/jcs.112.21.3833

Kin, K., Forbes, G., Cassidy, A., and Schaap, P. (2018). Cell-type specific RNA-Seq reveals novel roles and regulatory programs for terminally differentiated *Dictyostelium* cells. *BMC Genomics* 19:764. doi: 10.1186/s12864-018-5146-3

Kirkin, V., McEwan, D. G., Novak, I., and Dikic, I. (2009). A role for ubiquitin in selective autophagy. *Mol. Cell.* 34, 259–269. doi: 10.1016/j.molcel.2009.04.026

Kittler, R., Pelletier, L., Heninger, A.-K., Slabicki, M., Theis, M., Miroslaw, L., et al. (2007). Genome-scale RNAi profiling of cell division in human tissue culture cells. *Nat. Cell Biol.* 9, 1401–1412. doi: 10.1038/ncb1659

Kocaturk, N. M., and Gozuacik, D. (2018). Crosstalk between mammalian autophagy and the ubiquitin proteasome system. *Front. Cell Dev. Biol.* 6:128. doi: 10.3389/fcell.2018.00128

Komatsu, M., Waguri, S., Chiba, T., Murata, S., Iwata, J. I., Tanida, I., et al. (2006). Loss of autophagy in the central nervous system causes neurodegeneration in mice. *Nature* 441, 880–884. doi: 10.1038/nature04723

Kosta, A., Roisin-Bouffay, C., Luciani, M.-F., Otto, G. P., Kessin, R. H., and Golstein, P. (2004). Autophagy gene disruption reveals a non-vacuolar cell death pathway in *Dictyostelium*. *J. Biol. Chem.* 279, 48404–48409. doi: 10.1074/jbc.m408924200

Leinonen, H., Keksa-Goldsteine, V., Ragauskas, S., Kohlmann, P., Singh, Y., Savchenko, E., et al. (2017). Retinal Degeneration in a mouse model of CLN5 disease is associated with compromised autophagy. *Sci. Rep.* 7:1597.

Levi, S., Polyakov, M., and Egelhoff, T. T. (2000). Green fluorescent protein and epitope tag fusion vectors for *Dictyostelium discoideum*. *Plasmid* 44, 231–238. doi: 10.1006/plas.2000.1487

Ligon, C., Seong, E., Schroeder, E. J., DeKorver, N. W., Yuan, L., Chaudoin, T. R., et al. (2020). δ-Catenin engages the autophagy pathway to sculpt the developing dendritic arbor. *J. Biol. Chem.* 295, 10988–11001. doi: 10.1074/jbc.ra120.013058

Loomis, W. F. (2014). Cell signaling during development of *Dictyostelium*. *Dev. Biol.* 391, 1–16. doi: 10.1016/j.ydbio.2014.04.001

Mamo, A., Jules, F., Dumaresq-Doiron, K., Costantino, S., and Lefrancois, S. (2012). The role of ceroid lipofuscinosis neuronal protein 5 (CLN5) in endosomal sorting. *Mol. Cell. Biol.* 32, 1855–1866. doi: 10.1128/mcb.06726-11

Marchetti, A., Lelong, E., and Cosson, P. (2009). A measure of endosomal pH by flow cytometry in *Dictyostelium*. *BMC Res. Notes* 2:7. doi: 10.1186/1756-0500-2-7

Marin, F. T. (1976). Regulation of development in *Dictyostelium discoideum*: I. Initiation of the growth to development transition by amino acid starvation. *Dev. Biol.* 48, 110–117.

Mathavarajah, S., Flores, A., and Huber, R. J. (2017). Dictyostelium discoideum: a model system for cell and developmental biology. *Curr. Protoc. Essent. Lab. Tech.* doi: 10.1002/cpet.15

Mathavarajah, S., McLaren, M. D., and Huber, R. J. (2018). Cln3 function is linked to osmoregulation in a *Dictyostelium* model of Batten disease. *Biochim. Biophys. Acta* 1864, 3559–3573. doi: 10.1016/j.bbadis.2018.08.013

Matsushita, K., Numakawa, T., Odaka, H., Kajihara, R., Soga, M., Ozasa, S., et al. (2019). Presynaptic dysfunction in neurons derived from Tay-Sachs iPSCs. *Neuroscience* 414, 128–140. doi: 10.1016/j.neuroscience.2019.06.026

Matthias, J., Meßling, S., and Eichinger, L. (2016). The two *Dictyostelium* autophagy eight proteins, ATG8a and ATG8b, associate with the autophagosome in succession. *Eur. J. Cell Biol.* 95, 15–25. doi: 10.1016/j.ejcb.2015.10.007

McLaren, M. D., Mathavarajah, S., and Huber, R.J. (2019). Recent insights into NCL protein function using the model organism dictyostelium Discoideum. *Cells* 8:115. doi: 10.3390/cells8020115

McLaurin, J., Franklin, T., Chakrabartty, A., and Fraser, P. E. (1998). Phosphatidylinositol and inositol involvement in Alzheimer amyloid-beta fibril growth and arrest. *J. Mol. Biol.* 278, 183–194. doi: 10.1006/jmbi.1998.1677

Mesquita, A., Cardenal-Muñoz, E., Dominguez, E., Muñoz-Braceras, S., Nuñez-Corcuera, B., Phillips, B. A., et al. (2017). Autophagy in *Dictyostelium*: mechanisms, regulation and disease in a simple biomedical model. *Autophagy* 13, 24–40. doi: 10.1080/15548627.2016.1226737

Meßling, S., Matthias, J., Xiong, Q., Fischer, S., and Eichinger, L. (2017). The two *Dictyostelium discoideum* autophagy 8 proteins have distinct autophagic functions. *Eur. J. Cell Biol.* 96, 312–324. doi: 10.1016/j.ejcb.2017.03.014

Mizushima, N. (2009). Physiological functions of autophagy. *Curr. Top. Microbiol. Immunol.* 335, 71–84. doi: 10.1007/978-3-642-00302-8_3

Mizushima, N., Yoshimori, T., and Levine, B. (2010). Methods in mammalian autophagy research. *Cell* 140, 313–326. doi: 10.1016/j.cell.2010.01.028

Moharir, A., Peck, S. H., Budden, T., and Lee, S. Y. (2013). The role of N-glycosylation in folding, trafficking, and functionality of lysosomal protein CLN5. *PLoS One* 8:e74299. doi: 10.1371/journal.pone.0074299

Muñoz-Braceras, S., Calvo, R., and Escalante, R. (2015). TipC and the chorea-acanthocytosis protein VPS13A regulate autophagy in *Dictyostelium* and human HeLa cells. *Autophagy* 11, 918–927. doi: 10.1080/15548627.2015.1034413

Myre, M. A., Lumsden, A. L., Thompson, M. N., Wasco, W., MacDonald, M. E., and Gusella, J. F. (2011). Deficiency of huntingtin has pleiotropic effects in the social amoeba *Dictyostelium discoideum*. *PLoS Genet.* 7:e1002052. doi: 10.1371/journal.pgen.1002052

Nezis, I. P., Simonsen, A., Sagona, A. P., Finley, K., Gaumer, S., Contamine, D., et al. (2008). Ref(2)P, the Drosophila melanogaster homologue of mammalian p62, is required for the formation of protein aggregates in adult brain. *J. Cell Biol.* 180, 1065–1071. doi: 10.1083/jcb.200711108

O'Day, D. H. (1979). Aggregation during sexual development in *Dictyostelium discoideum*. *Can. J. Microbiol.* 25, 1416–1426. doi: 10.1139/m79-221

Okada, S., and O'Brien, J. S. (1969). Tay-Sachs disease: generalized absence of a beta-D-N-acetylhexosaminidase component. *Science* 165, 698–700. doi: 10.1126/science.165.3894.698

Otto, G. P., Wu, M. Y., Kazgan, N., Anderson, O. R., and Kessin, R. H. (2003). Macroautophagy is required for multicellular development of the social amoeba *Dictyostelium discoideum*. *J. Biol. Chem.* 278, 17636–17645. doi: 10.1074/jbc.m212467200

Otto, G. P., Wu, M. Y., Kazgan, N., Anderson, O. R., and Kessin, R. H. (2004). *Dictyostelium* macroautophagy mutants vary in the severity of their developmental defects. *J. Biol. Chem.* 279, 15621–15629. doi: 10.1074/jbc.m311139200

Pan, M., Xu, X., Chen, Y., and Jin, T. (2016). Identification of a chemoattractant G-protein-coupled receptor for folic acid that controls both chemotaxis and phagocytosis. *Dev. Cell* 36, 428–439. doi: 10.1016/j.devcel.2016.01.012

Pankiv, S., Clausen, T. H., Lamark, T., Brech, A., Bruun, J.-A., Outzen, H., et al. (2007). p62/SQSTM1 binds directly to Atg8/LC3 to facilitate degradation of ubiquitinated protein aggregates. *J. Biol. Chem.* 282, 24131–24145. doi: 10.1074/jbc.m702824200

Pears, M. R., Cooper, J. D., Mitchison, H. M., Mortishire-Smith, R. J., Pearce, D. A., and Griffin, J. L. (2005). High resolution 1H NMR-based metabolomics indicates a neurotransmitter cycling deficit in cerebral tissue from a mouse model of Batten disease. *J. Biol. Chem.* 280, 42508–42514. doi: 10.1074/jbc.m507380200

Phillips, J. E., and Gomer, R. H. (2015). Partial genetic suppression of a loss-of-function mutant of the neuronal ceroid lipofuscinosis-associated protease TPP1 in *Dictyostelium discoideum*. *Dis. Model Mech.* 8, 147–156.

Radke, J., Stenzel, W., and Goebel, H. H. (2015). Human NCL neuropathology. *Biochim. Biophys. Acta* 1852, 2262–2266. doi: 10.1016/j.bbadis.2015.05.007

Rivero, F., and Maniak, M. (2006). Quantitative and microscopic methods for studying the endocytic pathway. *Methods Mol. Biol.* 346, 423–438. doi: 10.1385/1-59745-144-4:423

Savchenko, E., Singh, Y., Konttinen, H., Lejavova, K., Santos, L. M., Grubman, A., et al. (2017). Loss of Cln5 causes altered neurogenesis in a mouse model of a childhood neurodegenerative disorder. *Dis. Model Mech.* 10, 1089–1100.

Schmiedt, M.-L., Blom, T., Blom, T., Kopra, O., Wong, A., von Schantz-Fant, C., et al. (2012). Cln5-deficiency in mice leads to microglial activation, defective myelination and changes in lipid metabolism. *Neurobiol. Dis.* 46, 19–29. doi: 10.1016/j.nbd.2011.12.009

Schneider, C. A., Rasband, W. S., and Eliceiri, K. W. (2012). NIH Image to ImageJ: 25 years of image analysis. *Nat. Methods* 9, 671–675. doi: 10.1038/nmeth.2089

Scioscia, M., Kunjara, S., Gumaa, K., McLean, P., Rodeck, C. H., and Rademacher, T. W. (2007). Urinary excretion of inositol phosphoglycan P-type in gestational diabetes mellitus. *Diabet Med.* 24, 1300–1304. doi: 10.1111/j.1464-5491.2007.02267.x

Seitz, D., Grodd, W., Schwab, A., Seeger, U., Klose, U., and Nägele, T. (1998). MR imaging and localized proton MR spectroscopy in late infantile neuronal ceroid lipofuscinosis. *AJNR Am. J. Neuroradiol.* 19, 1373–1377.

Silverstone, P. H., McGrath, B. M., and Kim, H. (2005). Bipolar disorder and myo-inositol: a review of the magnetic resonance spectroscopy findings. *Bipolar Disord.* 7, 1–10. doi: 10.1111/j.1399-5618.2004.00174.x

Singh, Y., Leinonen, H., Fazaludeen, F., Jaronen, M., Guest, D., Buckley, N., et al. (2019). Loss of Cln5 leads to altered Gad1 expression and deficits in interneuron development in mice. *Hum. Mol. Genet.* 28, 3309–3322. doi: 10.1093/hmg/ddz165

Smith, P. K., Sen, M. G., Fisher, P. R., and Annesley, S. J. (2019). Modelling of neuronal ceroid lipofuscinosis type 2 in *Dictyostelium discoideum* suggests that cytopathological outcomes result from altered TOR signalling. *Cells* 8;469. doi: 10.3390/cells8050469

Stumpf, M., Müller, R., Gaßen, B., Wehrstedt, R., Fey, P., Karow, M. A., et al. (2017). A tripeptidyl peptidase 1 is a binding partner of the Golgi pH regulator (GPHR) in *Dictyostelium*. *Dis. Model Mech.* 10, 897–907.

Tang, Z., Kang, B., Li, C., Chen, T., and Zhang, Z. (2019). GEPIA2: an enhanced web server for large-scale expression profiling and interactive analysis. *Nucleic Acids Res.* 47, W556–W560.

Tekinay, T., Wu, M. Y., Otto, G. P., Anderson, O. R., and Kessin, R. H. (2006). Function of the *Dictyostelium discoideum* Atg1 kinase during autophagy and development. *Eukaryot. Cell* 5, 1797–17806. doi: 10.1128/ec.00342-05

Tung, S. M., Ünal, C., Ley, A., Peña, C., Tunggal, B., Noegel, A. A., et al. (2010). Loss of *Dictyostelium* ATG9 results in a pleiotropic phenotype affecting growth, development, phagocytosis and clearance and replication of *Legionella pneumophila*. *Cell Microbiol.* 12, 765–780. doi: 10.1111/j.1462-5822.2010.01432.x

Tyynelä, J., Sohar, I., Sleat, D. E., Gin, R. M., Donnelly, R. J., Baumann, M., et al. (2000). A mutation in the ovine cathepsin D gene causes a congenital lysosomal

storage disease with profound neurodegeneration. *EMBO J.* 19, 2786–2792. doi: 10.1093/emboj/19.12.2786

Uchikawa, T., Yamamoto, A., and Inouye, K. (2011). Origin and function of the stalk-cell vacuole in *Dictyostelium*. *Dev. Biol.* 352, 48–57. doi: 10.1016/j.ydbio.2011.01.014

Urbanelli, L., Magini, A., Ercolani, L., Sagini, K., Polchi, A., Tancini, B., et al. (2014). Oncogenic H-Ras up-regulates acid β-hexosaminidase by a mechanism dependent on the autophagy regulator TFEB. *PLoS One* 9:e89485. doi: 10.1371/journal.pone.0089485

Veltman, D. M., Akar, G., Bosgraaf, L., and Van Haastert, P. J. M. (2009). A new set of small, extrachromosomal expression vectors for *Dictyostelium discoideum*. *Plasmid* 61, 110–118. doi: 10.1016/j.plasmid.2008.11.003

Vogel, B. E., Wagner, C., Paterson, J. M., Xu, X., and Yanowitz, J. L. (2011). An extracellular matrix protein prevents cytokinesis failure and aneuploidy in the *C. elegans* germline. *Cell Cycle* 10, 1916–1920. doi: 10.4161/cc.10.12.15896

Warner, N., Burberry, A., Pliakas, M., McDonald, C., and Núñez, G. (2014). A genome-wide small interfering RNA (siRNA) screen reveals nuclear factor-κB (NF-κB)-independent regulators of NOD2-induced interleukin-8 (IL-8) secretion. *J. Biol. Chem.* 289, 28213–28224. doi: 10.1074/jbc.m114.574756

Welchman, R. L., Gordon, C., and Mayer, R. J. (2005). Ubiquitin and ubiquitin-like proteins as multifunctional signals. *Nat. Rev. Mol. Cell Biol.* 6, 599–609. doi: 10.1038/nrm1700

Williams, G. B., Elder, E. M., and Sussman, M. (1984). Modulation of the cAMP relay in *Dictyostelium discoideum* by ammonia and other metabolites: possible morphogenetic consequences. *Dev. Biol.* 105, 377–388. doi: 10.1016/0012-1606(84)90294-x

Xin, W., Mullen, T. E., Kiely, R., Min, J., Feng, X., Cao, Y., et al. (2010). CLN5 mutations are frequent in juvenile and late-onset non-Finnish patients with NCL. *Neurology* 74, 565–571. doi: 10.1212/wnl.0b013e3181cff70d

Xiong, Q., Ûnal, C., Matthias, J., Steinert, M., and Eichinger, L. (2015). The phenotypes of ATG9, ATG16 and ATG9/16 knock-out mutants imply functions. *Open Biol.* 5:150008. doi: 10.1098/rsob.150008

Xu, X., and Vogel, B. E. (2011). A secreted protein promotes cleavage furrow maturation during cytokinesis. *Curr. Biol.* 21, 114–119. doi: 10.1016/j.cub.2010.12.006

Yamada, Y., and Schaap, P. (2019). Cyclic AMP induction of *Dictyostelium* prespore gene expression requires autophagy. *Dev. Biol.* 452, 114–126. doi: 10.1016/j.ydbio.2019.04.017

Yamada, Y., and Schaap, P. (2020). The proppin Bcas3 and its interactor KinkyA localize to the early phagophore and regulate autophagy. *Autophagy* 17, 640–655. doi: 10.1080/15548627.2020.1725403

Conflict of Interest: The authors declare that the research was conducted in the absence of any commercial or financial relationships that could be construed as a potential conflict of interest.

Copyright © 2021 McLaren, Mathavarajah, Kim, Yap and Huber. This is an open-access article distributed under the terms of the Creative Commons Attribution License (CC BY). The use, distribution or reproduction in other forums is permitted, provided the original author(s) and the copyright owner(s) are credited and that the original publication in this journal is cited, in accordance with accepted academic practice. No use, distribution or reproduction is permitted which does not comply with these terms.

frontiers in Cell and Developmental Biology

REVIEW
published: 19 July 2021
doi: 10.3389/fcell.2021.710005

Using *Dictyostelium* to Develop Therapeutics for Acute Respiratory Distress Syndrome

*Sara A. Kirolos, Ramesh Rijal, Kristen M. Consalvo and Richard H. Gomer**

Department of Biology, Texas A&M University, College Station, TX, United States

Acute respiratory distress syndrome (ARDS) involves damage to lungs causing an influx of neutrophils from the blood into the lung airspaces, and the neutrophils causing further damage, which attracts more neutrophils in a vicious cycle. There are ∼190,000 cases of ARDS per year in the US, and because of the lack of therapeutics, the mortality rate is ∼40%. Repelling neutrophils out of the lung airspaces, or simply preventing neutrophil entry, is a potential therapeutic. In this minireview, we discuss how our lab noticed that a protein called AprA secreted by growing *Dictyostelium* cells functions as a repellent for *Dictyostelium* cells, causing cells to move away from a source of AprA. We then found that AprA has structural similarity to a human secreted protein called dipeptidyl peptidase IV (DPPIV), and that DPPIV is a repellent for human neutrophils. In animal models of ARDS, inhalation of DPPIV or DPPIV mimetics blocks neutrophil influx into the lungs. To move DPPIV or DPPIV mimetics into the clinic, we need to know how this repulsion works to understand possible drug interactions and side effects. Combining biochemistry and genetics in *Dictyostelium* to elucidate the AprA signal transduction pathway, followed by drug studies in human neutrophils to determine similarities and differences between neutrophil and *Dictyostelium* chemorepulsion, will hopefully lead to the safe use of DPPIV or DPPIV mimetics in the clinic.

Keywords: *Dictyostelium discoideum*, chemorepulsion, acute respiratory disease syndrome, neutrophil (PMN), DPPIV, PAR2

OPEN ACCESS

Edited by:
Annette Müller-Taubenberger, Ludwig Maximilian University of Munich, Germany

Reviewed by:
Salvatore Bozzaro, University of Turin, Italy
Jeffrey Hadiwger, Oklahoma State University, United States
Shigehiko Yumura, Yamaguchi University, Japan

***Correspondence:**
Richard H. Gomer
rgomer@tamu.edu

Specialty section:
This article was submitted to Molecular Medicine, a section of the journal Frontiers in Cell and Developmental Biology

Received: *14 May 2021*
Accepted: *22 June 2021*
Published: *19 July 2021*

Citation:
Kirolos SA, Rijal R, Consalvo KM and Gomer RH (2021) Using Dictyostelium to Develop Therapeutics for Acute Respiratory Distress Syndrome. Front. Cell Dev. Biol. 9:710005. doi: 10.3389/fcell.2021.710005

ACUTE RESPIRATORY DISTRESS SYNDROME (ARDS)

Acute respiratory distress syndrome (ARDS) is an acute onset of low blood oxygen levels due to abnormal accumulation of multiple cell types in the lungs, including immune cells (Ashbaugh et al., 1967). The cells can damage the lungs, as well as clog airspaces, leading to lung dysfunction and thus low blood oxygen levels. The abnormal accumulation of cells is caused by either direct or indirect lung injury; direct lung injury can be from pneumonia caused by viruses, bacteria, or fungi, trauma from mechanical ventilation, or injury caused by inhaling harmful substances, while indirect lung injury is primarily from inflammation or trauma to other organ systems (Shaver and Bastarache, 2014; Cochi et al., 2016; Lynn et al., 2019). There are approximately 190,000 cases of ARDS in the United States each year (Rubenfeld et al., 2005). ARDS can have a rapid progression, with patients advancing from breathing normally despite lung damage (mild ARDS) to requiring a ventilator

(moderate or severe ARDS) within a week (Ranieri et al., 2012). The mortality rate for ARDS is 27% for mild, 32% for moderate, and 45% for severe ARDS (Ranieri et al., 2012) and the 3-year mortality rate is 44, 47, and 71% respectively (Parhar et al., 2019).

In ARDS patients, neutrophils migrate from the blood into the airspaces of the lungs (Steinberg et al., 1994; Zemans et al., 2009) in response to increased levels of inflammatory mediators, chemokines, and cell damage (**Figures 1A–C**; Thompson et al., 2017; Lin and Fessler, 2021). Once in the lungs, the neutrophils target pathogens for phagocytosis and release proteases, reactive oxidants, and neutrophil extracellular traps (Zemans et al., 2009). In ARDS, some neutrophils in the lungs release proteases and reactive oxygen species even if there is no pathogen present, causing lung damage, and this then recruits more neutrophils in a vicious cycle (**Figures 1D,E**; Weiss, 1989). The inflammation and damage reduce gas exchange, promotes vascular permeability, and increases fluid in the lung tissues and air spaces (Matthay et al., 2012; Kao et al., 2015; Lynn et al., 2019). The only effective management for ARDS is protection of the lungs, putting the patient on oxygen and a ventilator with low tidal volume ventilation to reduce stretching of the lung tissue (Acute Respiratory Distress Syndrome Network et al., 2000). There are currently no therapeutics for ARDS (Chen et al., 2020).

As described above, neutrophils entering the lungs appear to cause most of the damage in ARDS. An intriguing possible therapy for ARDS is to prevent neutrophils from entering the lungs, or to repel neutrophils that have entered the lungs back out of the lungs (**Figure 1F**). Some prokaryotes can sense repellent chemicals (chemorepellents) and move away from the source of the chemorepellent, and this process is fairly well understood (Pandey and Jain, 2002; Anderson et al., 2015). As described below, there are a few examples of chemorepellents in eukaryotic cells, including neutrophils, but how these affect cells is poorly understood. To move a neutrophil chemorepellent into the clinic, we need to know how this repulsion works to understand possible drug interactions and side effects.

CHEMOREPULSION CAN CAUSE CELLS TO MOVE AWAY FROM A SIGNAL

Chemotaxis allows migratory cells to either move toward (chemoattract) or move away (chemorepel) from an external chemotactic stimulus (**Figure 2**; Vianello et al., 2005). In eukaryotes, chemoattraction plays important roles during development and morphogenesis, and in immune responses (Sadik and Luster, 2012; Kolaczkowska and Kubes, 2013; Theveneau and Mayor, 2013). Directed migration of a cell toward a chemoattractant involves chemoattractant gradient sensing through a receptor-mediated signal transduction processes to induce rearrangement of cytoskeletal proteins at the front and rear of a cell, a conserved mechanism used by migrating cells (Dandekar et al., 2013; Fukujin et al., 2016). Similar to chemoattraction, chemorepulsion also plays an important role in

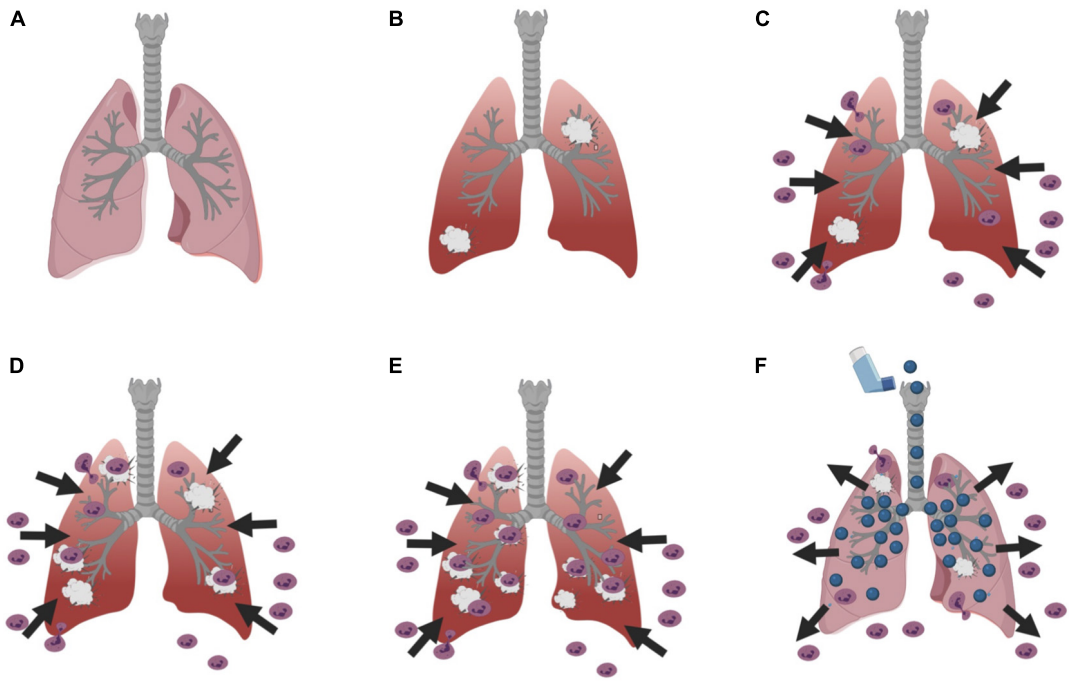

FIGURE 1 | Diagram of the basic process of ARDS and a potential therapeutic mechanism. **(A)** A cartoon of a normal lung, and **(B)** a lung with damage. **(C)** Neutrophils leave the blood and enter the lung tissue and airspaces in response to the damage. **(D)** In ARDS, this can result in further lung damage, which **(E)** results in even more neutrophils attracted to the lungs causing more damage in a vicious cycle. **(F)** An intriguing possibility is that inhalation of a nebulized neutrophil chemorepellent could drive neutrophils out of the lungs and/or prevent neutrophils from entering the lungs, and thus break the vicious cycle and reduce neutrophil-induced lung damage. Figures were created using BioRender.com.

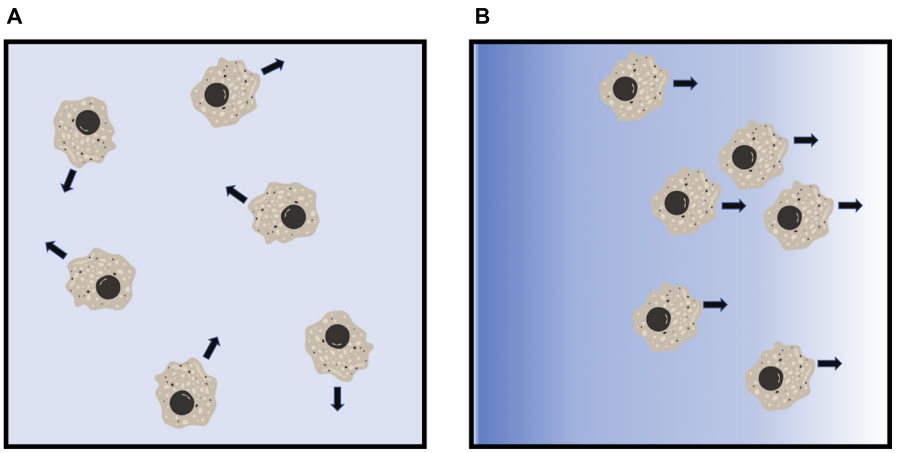

FIGURE 2 | Diagram of eukaryotic chemorepulsion. **(A)** In the absence of a gradient, cells extend pseudopods, and move, in random directions. **(B)** In a gradient of a chemorepellent (blue shading), cells move away from the higher concentration of the chemorepellent. Figures were created using BioRender.com.

development and immune responses (Mark et al., 1997; Vianello et al., 2005; Levine et al., 2006; Clark et al., 2014a; Guidobaldi et al., 2017; Tang, 2017). However, the mechanisms of eukaryotic chemorepulsion is still being elucidated.

The bacterium *Escherichia coli* (*E. coli*) responds to both chemoattractants and chemorepellents (Adler and Templeton, 1967; Berg and Brown, 1972; Berg and Tedesco, 1975). *E. coli* cells that sense decreasing concentrations of an attractant, or increasing concentrations of a repellent, causes the cells to tumble induced by clockwise flagellar rotation instead of smooth swimming induced by counter clockwise flagellar rotation, and the cells thus change direction to increase the probability that they will be moving in the right direction (Larsen et al., 1974). In *Helicobacter pylori*, chemorepulsion from the autocrine quorum sensing signal autoinducer-2 determines spatial organization and dispersal of biofilms (Anderson et al., 2015). The unicellular eukaryote *Trichomonas vaginalis* chemorepels from toxic agents such as metronidazole, ketoconazole, and miconazole (Sugarman and Mummaw, 1988). In the presence of a chemorepellent, such as conditioned supernatant factor (CSF), unicellular eukaryotes such as *Tetrahymena* and *Paramecium* swim backward (Rodgers et al., 2008; Plattner, 2015; Zou and Hennessey, 2017). In fungi, chemorepulsion can direct filament growth and mat formation (Karunanithi et al., 2012).

SEVERAL PROTEINS ACT AS NEURONAL CHEMOREPELLENTS

In higher eukaryotes, during neuronal development, neurons extend axons to reach specific targets (Kalil et al., 2011; Santos et al., 2020). For axons to correctly navigate to their targets, attractive and repulsive factors guide neuronal growth, regeneration, and collapse (Cregg et al., 2014; Thiede-Stan and Schwab, 2015). Many of the repulsive factors inhibit growth cone outgrowth and promote their collapse (Liu et al., 2006). Some of these repulsive molecules are proteins such as Nogo, Ephrins, Semaphorins, Draxin and Netrins. Nogo-A (the active form is called Nogo-66) is expressed by many projection neurons in the central and peripheral nervous systems (Nash et al., 2009; Schwab, 2010). Ephrins are negative guidance molecules for axons (Kolpak et al., 2009; Chatzizacharias et al., 2014; Savino et al., 2015). Ephrins signal through neuronal Eph receptors including EphA5 (Wahl et al., 2000). Other repulsive molecules such as the semaphorins Sema3A and 3F bind to plexin and neuropilin co-receptors to induce the repulsion of axons (Liu et al., 2006; Andrews et al., 2013; Vo et al., 2013).

Draxin is an axon guidance cue that is vital for the development of the thick bundle of nerve fibers, called the corpus collosum, between the two hemispheres of the brain (Islam et al., 2009) and signals through the "deleted in colorectal cancer (DCC)" receptor (Islam et al., 2009; Meli et al., 2015). Although DCC is vital for axonal repulsive behavior, the binding of Netrin-1 to neuronal DCC induces attraction (Guijarro et al., 2006). Netrin-1 has both chemoattractive and chemorepulsive effects on many migratory axons during development and injury repair (Colamarino and Tessierlavigne, 1995; Furne et al., 2008). The binding of Netrin-1 to uncoordinated family member 5 (UNC-5) (Bashaw and Goodman, 1999; Hong et al., 1999) induces chemorepulsion in axons and immune cells (Hedgecock et al., 1990; Tadagavadi et al., 2010).

In mammals, multiple pathways are required for chemorepulsion (Riches et al., 2013; Holt et al., 2021). The Wnt signaling pathway is a highly conserved pathway involved in multiple cell processes such as fate determination, polarity, migration, and neural patterning (Komiya and Habas, 2008). Wnt5a activation of the non- canonical Wnt receptor RYK on specific neurons induces chemorepulsion (Clark et al., 2014b). Secreted Wnt protein also bind to Frizzled receptors, a family of integral membrane protein receptors, to repel axon growth (Huang and Klein, 2004; Freese et al., 2010). Slit guidance ligand 2 (Slit2), a chemoattractant or chemorepellent dependent on the isoform, and activation of Roundabout receptor (Robo1),

a coreceptor of Slit2, induces chemorepulsion of axons as well as neutrophils (Hu, 1999; Nguyen Ba-Charvet et al., 1999; Park et al., 2016). Slit1 and Slit3 also induce chemorepulsion of olfactory tract and spinal motor axons during development (Patel et al., 2001).

SEVERAL PROTEINS ACT AS IMMUNE CELL CHEMOREPELLENTS

In addition to Slit2, protein signals such as eotaxin-3, CXCL10, IL-8 and stromal cell derived factor-1 induce dendritic cell, monocyte, leukocyte, and/or neutrophil chemorepulsion (Ogilvie et al., 2003; Kohrgruber et al., 2004; Tharp et al., 2006). The chemokine stromal derived factor-1/CXCL12 is involved in tumor growth, metastasis and promotion of tumor immunity (Chen et al., 1994; Jager et al., 1996), possibly because CXCL12 secreted by tumors decreases T-cell infiltration (Vianello et al., 2006; d'Onofrio, 2012). In neutrophils, Slit2 plays a role in neutrophil migration toward and away from regions of inflammation (Tole et al., 2009; Ye B. Q. et al., 2010; Pilling et al., 2019). A ∼110- kDa N-terminal fragment of Slit2 induces chemorepulsion in neutrophils, and inhibiting Slit2 receptors Robo1 and syndecan-4 diminishes neutrophil chemorepulsion (Pilling et al., 2019).

EUKARYOTIC CHEMOREPULSION INVOLVES REGULATION OF THE CYTOSKELETON

Downstream of their receptors, many axon growth chemorepellents induce axonal repulsion by activating Rho GTPases, small signaling G protein molecular switches that play a role in cytoskeletal organization, cell movement, and cell polarity (Hall, 1998; Bustelo et al., 2007; Ridley, 2015). The activation of Rho GTPases in turn activates Rho-associated protein kinases (ROCKs), effector molecules downstream of Rho GTPases that play a role in cell shape and movement by regulating cytoskeletal elements (Leung et al., 1996; Maekawa et al., 1999). The signal transduction pathways then diverge to rearrange essential cytoskeletal proteins necessary for directed cell migration (Schmandke et al., 2007; Gelfand et al., 2009; Schwab, 2010).

Dictyostelium discoideum SECRETES AN ENDOGENOUS CHEMOREPELLENT CALLED AprA

The simple eukaryote *Dictyostelium discoideum* is an excellent model system to study chemotaxis. In a nutrient-rich environment, *D. discoideum* cells grow and proliferate as single cells. When the nutrients become depleted, *D. discoideum* cells aggregate and form multicellular structures bearing spores that can survive harsh conditions (Bonner and Scharf, 1978; Kessin, 2001). The aggregation is mediated by cells secreting, and moving toward, relayed pulses of 3′, 5′-cyclic adenosine monophosphate (cAMP) (Bonner, 1970; Tomchik and Devreotes, 1981).

During their growth phase, *D. discoideum* cells secrete a protein called autocrine proliferation repressor A (AprA). AprA acts as a signal that partially inhibits cell division without inhibiting cell growth (the increase in accumulated mass) (Brock and Gomer, 2005). AprA is a 60 kDa protein which forms a ∼150 kDa complex with a protein called CfaD (Brock and Gomer, 2005; Bakthavatsalam et al., 2008).

How cells regulate the accumulation of AprA is not fully understood. Eukaryotic initiation factor 2 (eIF2) (Dever, 2002; Ye J. et al., 2010), initiation factor kinases, IfkA, IfkB, and IfkC (Fang et al., 2003; Rai et al., 2006), and Ceroid lipofuscinosis neuronal 3 (Cln3) and Cln5 that are associated with a childhood onset neurological disorder called Batten disease or neuronal ceroid lipofuscinosis (NCL) (Santavuori, 1988), are important for extracellular accumulation of AprA and CfaD (Bowman et al., 2011; Huber et al., 2014; Huber and Mathavarajah, 2018; **Figure 3**).

Dictyostelium discoideum cells lacking AprA are able to aggregate, but form abnormal structures with fewer and less viable spores, suggesting that cells lacking AprA can still migrate toward cAMP and aggregate (Brock and Gomer, 2005). In colonies of growing cells, wild type cells show directed movement away from the edge of the colony while cells lacking AprA do not move away from the edge of the colony (Phillips and Gomer, 2010). This suggested that AprA acts as a chemorepellent (Phillips and Gomer, 2010). In artificial gradients, *D. discoideum* cells move away from physiological concentrations of AprA, indicating that AprA is indeed a chemorepellent (Phillips and Gomer, 2010).

AprA ACTIVATES A COMPLEX SIGNAL TRANSDUCTION PATHWAY TO INDUCE CHEMOREPULSION

Dictyostelium discoideum cells migrating toward cAMP and folic acid (a waste product released by bacteria, which *D. discoideum* cells uses as a chemoattractant to find and eat bacteria) require G protein-coupled receptors (GPCRs) and multiple conserved signal transduction pathways (De Wit and Bulgakov, 1985; Hadwiger et al., 1994; Ma et al., 1997; Lim et al., 2005; Kortholt et al., 2011; Yan et al., 2012). AprA activates G-proteins Gα8 and Gβ through the GPCR glutamate receptor-like H (GrlH) to induce chemorepulsion (Bakthavatsalam et al., 2009; Phillips and Gomer, 2012; Tang et al., 2018; Rijal et al., 2019; **Figure 3**). To decrease cell proliferation and induce chemorepulsion, AprA requires QkgA, a ROCO family kinase (Gotthardt et al., 2008; Phillips and Gomer, 2010), PakD, a member of a conserved family of p-21 activated kinases (PAKs) (Bokoch, 2003), CnrN, a phosphatase and tensin homolog (PTEN)-like phosphatase (Tang and Gomer, 2008), RblA, a homolog of a human Retinoblastoma (Rb) protein (MacWilliams et al., 2006), protein kinase A, components of the target of rapamycin (TOR) complex 2, phospholipase A, extracellular signal-regulated protein kinase (Erk1), and the Ras proteins

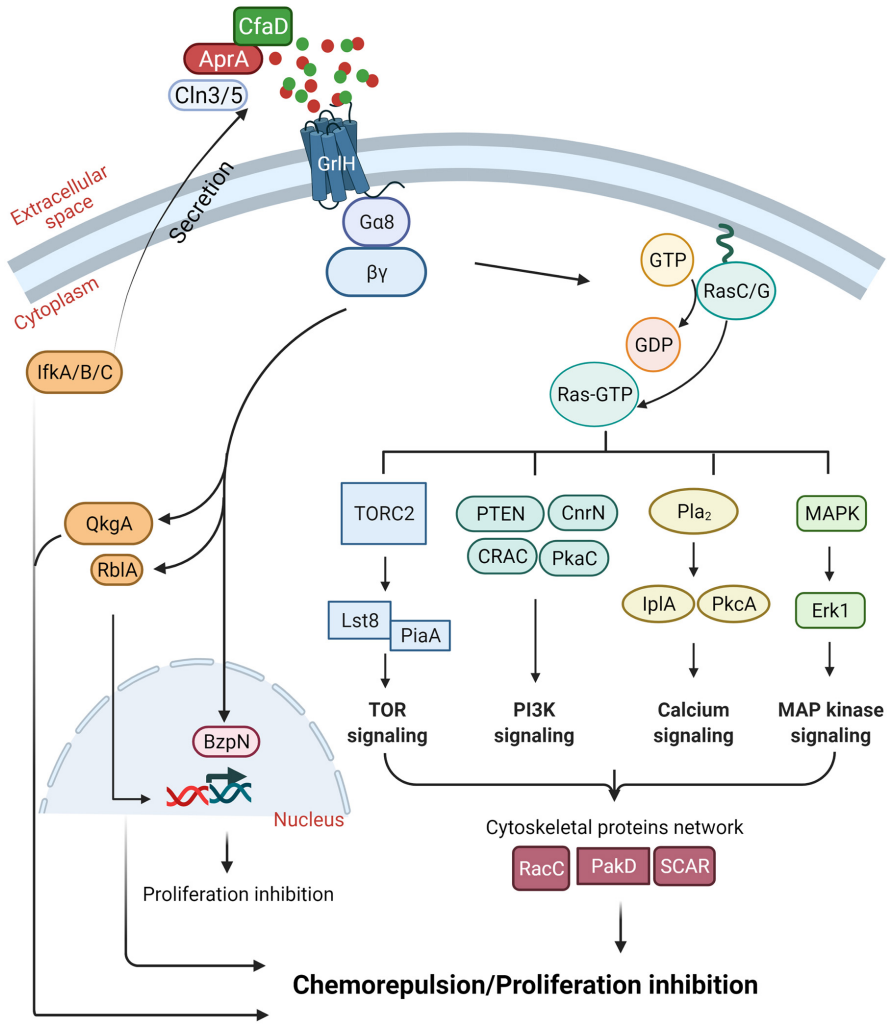

FIGURE 3 | Summary of our current understanding of the AprA signal transduction pathway. See text for details. Figure created with BioRender.com.

RasC and RasG (Bakthavatsalam et al., 2009; Garcia et al., 2014; Phillips and Gomer, 2014; Tang et al., 2018; Rijal et al., 2019). In addition, AprA requires the putative bZIP transcription factor BzpN for its proliferation-inhibiting activity but not for chemorepulsion activity (Phillips et al., 2011), suggesting that AprA uses partially overlapping pathways to mediate proliferation inhibition and chemorepulsion.

THE AprA CHEMOREPULSION MECHANISM HAS A PARTIAL BUT NOT COMPLETE OVERLAP WITH THE cAMP CHEMOATTRACTION MECHANISM

For chemorepulsion, in addition to the components mentioned above, AprA also uses some but not all components of the cAMP chemoattraction signal transduction pathway (Rijal et al., 2019). Similar to chemoattraction to cAMP, cells in a rAprA gradient show actin-rich protrusions at the leading edge of the cell and myosin II mediated contraction at the trailing edge of the cell, allowing the cells to move in a biased direction away from the chemorepellent (Phillips and Gomer, 2012). Although phospholipase C (PLC) and PI3 kinases 1 and 2 are important for chemorepulsion of starved *D. discoideum* cells by the synthetic cAMP analog 8-CPT-cAMP, and for cAMP chemoattraction (Keizer-Gunnink et al., 2007), PLC and PI3 kinases are not necessary for AprA chemorepulsion (Phillips and Gomer, 2012). In addition, unlike chemoattraction toward cAMP, AprA does not require Akt and PKB, guanylyl cyclases, and the cytosolic regulator of adenylate cyclase (CRAC) (Parent et al., 1998; Rijal et al., 2019).

Some of the key regulators of the AprA-induced chemorepulsion pathway are Ras GTPases. AprA induces translocation of RBDRaf1-GFP, an active Ras binding protein that when translocated to the cell cortex indicates Ras activation (Rijal et al., 2019). Although PakD is necessary for AprA mediated chemorepulsion, PakD is not necessary for AprA

induced translocation of RBDRaf1-GFP to the cell cortex (Rijal et al., 2019). While PakD localizes at the rear of a migrating cell (Phillips and Gomer, 2014), PakD may negatively regulate Ras activation at the side of the cells facing away from AprA during chemorepulsion (Rijal et al., 2019). Several other proteins can negatively regulate Ras local activity at the membrane including Rho GTPases and ERK1/2 (Wang et al., 2013; Lake et al., 2016). AprA does not cause translocation of RBDRaf1-GFP in cells lacking a WASP-related cytoskeletal protein suppressor of cAR (SCAR), suggesting that AprA requires cytoskeletal proteins to activate Ras (Rijal et al., 2019).

AprA INDUCES CHEMOREPULSION BY INHIBITING PSEUDOPOD FORMATION AT THE SIDE OF THE CELL CLOSEST TO THE SOURCE OF AprA

When cells such as *D. discoideum* and neutrophils move, they induce a localized polymerization of actin to form a pseudopod that protrudes from the cell, and when this attaches to a substrate, the cells can then move following their pseudopod (King and Insall, 2009). In the absence of a chemoattractant or chemorepellent gradient, cells form pseudopods at random locations, and thus move in random directions (Sasaki et al., 2004; Rijal et al., 2019). During chemoattraction, cells polymerize actin and extend a pseudopod toward the source of the attractant (Sasaki et al., 2004). During chemorepulsion, AprA inhibits filamentous actin (F-actin) polymerization at the region of the cell closest to the source of AprA, inhibiting pseudopod formation in the sector of the cell closest to the source of AprA (Rijal et al., 2019). This then allows the cells to move in any direction except the direction toward the source of AprA, resulting in chemorepulsion. This then indicates a fundamental difference between chemoattraction and chemorepulsion in *D. discoideum*: if a chemoattractant is coming from the West, a cell will tend to extend a pseudopod and move toward the West; to a first approximation, if a chemorepellent is coming from the West, cells will extend pseudopods randomly, and move toward, the East, North, or South.

THE IDENTIFICATION OF AprA LED TO THE IDENTIFICATION OF A HUMAN NEUTROPHIL CHEMOREPELLENT

Dictyostelium discoideum and neutrophils share chemotaxis properties (Wang, 2009; Wang et al., 2011). Although AprA has little similarity to mammalian proteins, a predicted tertiary structure of AprA showed similarity to the structure of human dipeptidyl peptidase IV (DPPIV) (Zhang, 2008; Roy et al., 2010, 2012; Herlihy et al., 2013). DPPIV is a 110 kDa serine protease that localizes on the extracellular surface of some lymphocytes, endothelial cells, and is also present in plasma, serum, cerebrospinal fluid, synovial fluid, semen, and urine in a soluble form, and cleaves peptides with a proline or alanine in the second position at the N-terminus end (Walborg et al., 1985; Thoma et al., 2003; Cordero et al., 2009; Kotacková et al., 2009; Nauck et al., 2011; Pan et al., 2021). In addition to the predicted structural similarity, AprA has a DPPIV -like protease activity (Herlihy et al., 2013, 2017). Although AprA is not able to repel human neutrophils, DPPIV induces chemorepulsion of *D. discoideum* cells, suggesting a conserved mechanism of action (Herlihy et al., 2017). In a range of concentrations encompassing its concentration in human plasma, DPPIV acts as a chemorepellent for human and mouse neutrophils, but does not affect the motility of macrophages and lymphocytes (Herlihy et al., 2013). In the presence of the DPPIV inhibitors Diprotin A and DPPP 1c hydrochloride, the chemorepellent activity of DPPIV was significantly reduced, and suggesting that the protease activity of DPPIV mediates its ability to induce neutrophil chemorepulsion (Herlihy et al., 2013).

DPPIV, THE AprA-LIKE THE NEUTROPHIL CHEMOREPELLENT, SHOWS EFFICACY IN A MOUSE MODEL OF ARDS AS WELL AS A MOUSE MODEL OF RHEUMATOID ARTHRITIS

A standard mouse model of ARDS is to damage the lungs with aspiration of a drug called bleomycin (Walters and Kleeberger, 2008). The mouse is lightly anesthetized, and 50 μl of saline with bleomycin is quickly pipetted through the mouth into the trachea as the mouse is inhaling. A gentle tailward shake of the mouse then disperses the bleomycin into the lungs. One day later, activated neutrophils start accumulating in the lungs (Walters and Kleeberger, 2008). Using this model, recombinant DPPIV or an equal volume of saline was introduced into the airspaces of the lungs of bleomycin-treated mice on day 1 and day 2 after bleomycin treatment by a similar aspiration procedure (Herlihy et al., 2013). Three days after bleomycin treatment, mice were euthanized. Phosphate buffered saline was put into the lungs through the trachea and then removed along with cells and other material in the airspaces in a procedure called bronchoalveolar lavage (BAL) (Herlihy et al., 2013). At day 3, the DPPIV treatments reduced both neutrophils in the BAL fluid as well as neutrophils remaining in the lungs (as determined by immunostaining of sections of the post-BAL lungs), but did not affect the numbers of macrophages and lymphocytes, suggesting that the effect of DPPIV is specific to neutrophils (Herlihy et al., 2013). Inhalation of DPPIV thus showed efficacy in a mouse model of ARDS.

Inflammatory arthritis, also known as rheumatoid arthritis (RA), is an autoimmune disorder with characteristic chronic inflammation due to neutrophil accumulation in the joints causing destruction of the joints (Kaplan, 2013). RA patients have lower level of DPPIV in plasma compared to non-inflammatory osteoarthritis (Busso et al., 2005). Injection of DPPIV directly into the joint in a mouse model of arthritis reduced the accumulation of neutrophils in the joint, and reduced the severity of arthritis and synovial inflammation (Herlihy et al., 2015).

Together with the ARDS model results, this suggests that DPPIV can reduce inflammation by causing neutrophils to move away from a site of accumulation.

AGONISTS OF THE DPPIV RECEPTOR PAR2 INDUCE NEUTROPHIL CHEMOREPULSION AND SHOW EFFICACY IN A MOUSE MODEL OF ARDS

As mentioned above, soluble DPPIV acts as a human and mouse neutrophil chemorepellent (Herlihy et al., 2013; White et al., 2018) via the activation of protease activated receptor 2 (PAR2) (White et al., 2018). PAR2 is a member of the PAR family of GPCRs, which consists of PAR1/2/3/4 (Ossovskaya and Bunnett, 2004). PAR2 is activated by the proteolytic cleavage of the extracellular N-terminus domain causing the remaining tethered N-terminus to act as a ligand that binds to extracellular loop 2 of the receptor thereby activating it (Vu et al., 1991; Gardell et al., 2008) DPPIV requires protease activated receptor (PAR2) to induce chemorepulsion of human neutrophils (White et al., 2018). Similar to DPPIV, the PAR2 agonists 2f-LIGRL-amide (a small peptide with modifications at the N and C termini), SLIGKVNH2 (a small peptide with a modifications at the C terminus), and AC55541 (a small molecule) induce chemorepulsion of human and mouse neutrophils (White et al., 2018). Although DPPIV induces stronger chemorepulsion of male neutrophils than female neutrophils, PAR2 agonists induce chemorepulsion of neutrophils from both male and female mice (White et al., 2018). In the mouse ARDS model described above, aspiration of SLIGKVNH2, starting 24 h after oropharyngeal aspiration of bleomycin, reduced neutrophil accumulation in lungs at day 3, similar to the effects of DPPIV described above (White et al., 2018), suggesting that aspiration of PAR2 agonists could be used to treat ARDS in human patients (Herlihy et al., 2013; White et al., 2018). Since DPPIV is a protease that cleaves many target molecules in addition to PAR2 (Zhu et al., 2003; Mulvihill and Drucker, 2014; Wronkowitz et al., 2014; White et al., 2018; Deacon, 2019; Trzaskalski et al., 2020), in terms of potential therapeutics, exogenous delivery of PAR2 agonists may have fewer side effects than exogenous delivery of DPPIV.

CONCLUSION

Chemorepulsion is an essential process for development, morphogenesis, and immune responses in eukaryotes. The identification of AprA, an endogenous chemorepellent in *D. discoideum* led to the identification of DPPIV, a chemorepellent that acts on human (and mouse) neutrophils. This in turn led to the identification of small-molecule PAR2 agonists as neutrophil chemorepellents. Given by aspiration into the lungs, both DPPIV and a PAR2 agonist showed efficacy in a mouse model of ARDS. Although the activation of PAR2 can reduce damage caused by arthritis, ARDS, and ischemia (McLean et al., 2002; McCulloch et al., 2018; White et al., 2018), the activation of PAR2 can lead to unwanted effects such as fetal injury, fibrosis, and inflammatory, metabolic and cardiovascular disorders (Cicala, 2002; Redecha et al., 2008; Grimsey et al., 2011; Kagota et al., 2016; Shearer et al., 2016; Heuberger and Schuepbach, 2019). Although intriguing possibilities are that inhalation of a nebulized mist containing DPPIV and/or PAR2 agonists might be useful as therapeutics for ARDS, and localized delivery of these neutrophil chemorepellents might be useful in other neutrophil-driven diseases, caution will be needed to limit dosing to prevent systemic toxicity.

AUTHOR CONTRIBUTIONS

All authors listed have made a substantial, direct and intellectual contribution to the work, and approved it for publication.

FUNDING

This work was supported by NIH grants GM118355 and GM139486 to RG. The figures were created using BioRender.com.

REFERENCES

Acute Respiratory Distress Syndrome Network, Brower, R. G., Matthay, M. A., Morris, A., Schoenfeld, D., Thompson, B. T., et al. (2000). Ventilation with lower tidal volumes as compared with traditional tidal volumes for acute lung injury and the acute respiratory distress syndrome. *N. Engl. J. Med.* 342, 1301–1308. doi: 10.1056/nejm200005043421801

Adler, J., and Templeton, B. (1967). The effect of environmental conditions on the motility of *Escherichia coli*. *J. Gen. Microbiol.* 46, 175–184. doi: 10.1099/00221287-46-2-175

Anderson, J. K., Huang, J. Y., Wreden, C., Sweeney, E. G., Goers, J., Remington, S. J., et al. (2015). Chemorepulsion from the quorum signal autoinducer-2 promotes *Helicobacter* pylori biofilm dispersal. *mBio* 6:e00379.

Andrews, W. D., Zito, A., Memi, F., Jones, G., Tamamaki, N., and Parnavelas, J. G. (2013). Limk2 mediates semaphorin signalling in cortical interneurons migrating through the subpallium. *Biol. Open* 2, 277–282. doi: 10.1242/bio.20133202

Ashbaugh, D. G., Bigelow, D. B., Petty, T. L., and Levine, B. E. (1967). Acute respiratory distress in adults. *Lancet* 290, 319–323.

Bakthavatsalam, D., Brock, D. A., Nikravan, N. N., Houston, K. D., Hatton, R. D., and Gomer, R. H. (2008). The secreted *Dictyostelium* protein CfaD is a chalone. *J. Cell Sci.* 121, 2473–2480. doi: 10.1242/jcs.026682

Bakthavatsalam, D., Choe, J. M., Hanson, N. E., and Gomer, R. H. (2009). A *Dictyostelium* chalone uses G proteins to regulate proliferation. *BMC Biol.* 7:44. doi: 10.1186/1741-7007-7-44

Bashaw, G. J., and Goodman, C. S. (1999). Chimeric axon guidance receptors: the cytoplasmic domains of slit and netrin receptors specify attraction versus repulsion. *Cell* 97, 917–926. doi: 10.1016/s0092-8674(00)80803-x

Berg, H. C., and Brown, D. A. (1972). Chemotaxis in *Escherichia coli* analysed by three-dimensional tracking. *Nature* 239, 500–504. doi: 10.1038/239500a0

Berg, H. C., and Tedesco, P. M. (1975). Transient response to chemotactic stimuli in *Escherichia coli*. *Proc. Natl. Acad. Sci. U.S.A.* 72, 3235–3239. doi: 10.1073/pnas.72.8.3235

Bokoch, G. M. (2003). Biology of the p21-activated kinases. *Annu. Rev. Biochem.* 72, 743–781. doi: 10.1146/annurev.biochem.72.121801.161742

Bonner, J. T. (1970). Induction of stalk cell differentiation by cyclic AMP in the cellular slime mold *Dictyostelium discoideum*. *Proc. Natl. Acad. Sci. U.S.A.* 65, 110–113. doi: 10.1073/pnas.65.1.110

Bonner, J. T., and Scharf, D. (1978). Life-cycle of cellular slime-molds. *Nat. Hist.* 87, 70–79.

Bowman, R. L., Xiong, Y., Kirsten, J. H., and Singleton, C. K. (2011). eIF2α kinases control chalone production in *Dictyostelium discoideum*. *Eukaryot. Cell* 10, 494–501. doi: 10.1128/ec.00270-10

Brock, D. A., and Gomer, R. H. (2005). A secreted factor represses cell proliferation in *Dictyostelium*. *Development* 132, 4553–4562. doi: 10.1242/dev.02032

Busso, N., Wagtmann, N., Herling, C., Chobaz-Péclat, V., Bischof-Delaloye, A., So, A., et al. (2005). Circulating CD26 is negatively associated with inflammation in human and experimental arthritis. *Am. J. Pathol.* 166, 433–442. doi: 10.1016/s0002-9440(10)62266-3

Bustelo, X. R., Sauzeau, V., and Berenjeno, I. M. (2007). GTP-binding proteins of the Rho/Rac family: regulation, effectors and functions in vivo. *BioEssays* 29, 356–370. doi: 10.1002/bies.20558

Chatzizacharias, N. A., Giaginis, C. T., Agapitos, E., and Theocharis, S. E. (2014). The role of ephrins' receptors and ephrins' ligands in normal placental development and disease. *Expert. Opin. Ther. Targets* 18, 269–275. doi: 10.1517/14728222.2014.864638

Chen, C. M., Lu, H. C., Tung, Y. T., and Chen, W. (2020). Antiplatelet therapy for acute respiratory distress syndrome. *Biomedicines* 8:230. doi: 10.3390/biomedicines8070230

Chen, L., McGowan, P., Ashe, S., Johnston, J., Li, Y., Hellstrom, I., et al. (1994). Tumor immunogenicity determines the effect of B7 costimulation on T cell-mediated tumor immunity. *J. Exp. Med.* 179, 523–532. doi: 10.1084/jem.179.2.523

Cicala, C. (2002). Protease activated receptor 2 and the cardiovascular system. *Br. J. Pharmacol.* 135, 14–20. doi: 10.1038/sj.bjp.0704438

Clark, C. E., Liu, Y., and Cooper, H. M. (2014a). The Yin and Yang of Wnt/Ryk axon guidance in development and regeneration. *Sci. China Life Sci.* 57, 366–371. doi: 10.1007/s11427-014-4640-3

Clark, C. E., Richards, L. J., Stacker, S. A., and Cooper, H. M. (2014b). Wnt5a induces Ryk-dependent and -independent effects on callosal axon and dendrite growth. *Growth Factors* 32, 11–17. doi: 10.3109/08977194.2013.875544

Cochi, S. E., Kempker, J. A., Annangi, S., Kramer, M. R., and Martin, G. S. (2016). Mortality trends of acute respiratory distress syndrome in the United States from 1999 to 2013. *Ann. Am. Thorac. Soc.* 13, 1742–1751.

Colamarino, S. A., and Tessierlavigne, M. (1995). The axonal chemoattractant netrin-1 is also a chemorepellent for trochlear motor axons. *Cell* 81, 621–629. doi: 10.1016/0092-8674(95)90083-7

Cordero, O. J., Salgado, F. J., and Nogueira, M. (2009). On the origin of serum CD26 and its altered concentration in cancer patients. *Cancer Immunol. Immunother.* 58, 1723–1747. doi: 10.1007/s00262-009-0728-1

Cregg, J. M., DePaul, M. A., Filous, A. R., Lang, B. T., Tran, A., and Silver, J. (2014). Functional regeneration beyond the glial scar. *Exp. Neurol.* 253, 197–207. doi: 10.1016/j.expneurol.2013.12.024

Dandekar, S. N., Park, J. S., Peng, G. E., Onuffer, J. J., Lim, W. A., and Weiner, O. D. (2013). Actin dynamics rapidly reset chemoattractant receptor sensitivity following adaptation in neutrophils. *Philos. Trans. R. Soc. Lond. B Biol. Sci.* 368:20130008. doi: 10.1098/rstb.2013.0008

De Wit, R. J., and Bulgakov, R. (1985). Guanine nucleotides modulate the ligand binding properties of cell surface folate receptors in *Dictyostelium discoideum*. *FEBS Lett.* 179, 257–261. doi: 10.1016/0014-5793(85)80530-5

Deacon, C. F. (2019). Physiology and pharmacology of DPP-4 in glucose homeostasis and the treatment of type 2 diabetes. *Front. Endocrinol.* 10:80. doi: 10.3389/fendo.2019.00080

Dever, T. E. (2002). Gene-specific regulation by general translation factors. *Cell* 108, 545–556. doi: 10.1016/s0092-8674(02)00642-6

d'Onofrio, A. (2012). Spatiotemporal effects of a possible chemorepulsion of tumor cells by immune system effectors. *J. Theor. Biol.* 296, 41–48. doi: 10.1016/j.jtbi.2011.11.013

Fang, R., Xiong, Y., and Singleton, C. K. (2003). IfkA, a presumptive eIF2 alpha kinase of *Dictyostelium*, is required for proper timing of aggregation and regulation of mound size. *BMC Dev. Biol.* 3:3. doi: 10.1186/1471-213x-3-3

Freese, J. L., Pino, D., and Pleasure, S. J. (2010). Wnt signaling in development and disease. *Neurobiol. Dis.* 38, 148–153.

Fukujin, F., Nakajima, A., Shimada, N., and Sawai, S. (2016). Self-organization of chemoattractant waves in *dictyostelium* depends on F-actin and cell-substrate adhesion. *J. R. Soc. Interface* 13:20160233. doi: 10.1098/rsif.2016.0233

Furne, C., Rama, N., Corset, V., Chedotal, A., and Mehlen, P. (2008). Netrin-1 is a survival factor during commissural neuron navigation. *Proc. Natl. Acad. Sci. U.S.A.* 105, 14465–14470. doi: 10.1073/pnas.0803645105

Garcia, M., Ray, S., Brown, I., Irom, J., and Brazill, D. (2014). PakD, a putative p21-activated protein kinase in *Dictyostelium discoideum*, regulates actin. *Eukaryot. Cell* 13, 119–126. doi: 10.1128/ec.00216-13

Gardell, L. R., Ma, J. N., Seitzberg, J. G., Knapp, A. E., Schiffer, H. H., Tabatabaei, A., et al. (2008). Identification and characterization of novel small-molecule protease-activated receptor 2 agonists. *J. Pharmacol. Exp. Ther.* 327, 799–808. doi: 10.1124/jpet.108.142570

Gelfand, M. V., Hong, S., and Gu, C. (2009). Guidance from above: common cues direct distinct signaling outcomes in vascular and neural patterning. *Trends Cell Biol.* 19, 99–110. doi: 10.1016/j.tcb.2009.01.001

Gotthardt, K., Weyand, M., Kortholt, A., Van Haastert, P. J., and Wittinghofer, A. (2008). Structure of the Roc-COR domain tandem of C. tepidum. a prokaryotic homologue of the human LRRK2 Parkinson kinase. *Embo J.* 27, 2239–2249. doi: 10.1038/emboj.2008.150

Grimsey, N., Soto, A. G., and Trejo, J. (2011). Regulation of protease-activated receptor signaling by post-translational modifications. *IUBMB Life* 63, 403–411. doi: 10.1002/iub.442

Guidobaldi, H. A., Cubilla, M., Moreno, A., Molino, M. V., Bahamondes, L., and Giojalas, L. C. (2017). Sperm chemorepulsion, a supplementary mechanism to regulate fertilization. *Hum. Reprod.* 32, 1560–1573. doi: 10.1093/humrep/dex232

Guijarro, P., Simo, S., Pascual, M., Abasolo, I., Del Rio, J. A., and Soriano, E. (2006). Netrin1 exerts a chemorepulsive effect on migrating cerebellar interneurons in a Dcc-independent way. *Mol. Cell Neurosci.* 33, 389–400. doi: 10.1016/j.mcn.2006.08.010

Hadwiger, J. A., Lee, S., and Firtel, R. A. (1994). The G alpha subunit G alpha 4 couples to pterin receptors and identifies a signaling pathway that is essential for multicellular development in *Dictyostelium*. *Proc. Natl. Acad. Sci. U.S.A.* 91:10566. doi: 10.1073/pnas.91.22.10566

Hall, A. (1998). Rho GTPases and the actin cytoskeleton. *Science* 279, 509–514. doi: 10.1126/science.279.5350.509

Hedgecock, E. M., Culotti, J. G., and Hall, D. H. (1990). The unc-5, unc-6, and unc-40 genes guide circumferential migrations of pioneer axons and mesodermal cells on the epidermis in C. elegans. *Neuron* 4, 61–85. doi: 10.1016/0896-6273(90)90444-k

Herlihy, S. E., Brown, M. L., Pilling, D., Weeks, B. R., Myers, L. K., and Gomer, R. H. (2015). Role of the neutrophil chemorepellent soluble dipeptidyl peptidase IV in decreasing inflammation in a murine model of arthritis. *Arthritis Rheumatol.* 67, 2634–2638. doi: 10.1002/art.39250

Herlihy, S. E., Pilling, D., Maharjan, A. S., and Gomer, R. H. (2013). Dipeptidyl peptidase IV is a human and murine neutrophil chemorepellent. *J. immunol.* 190, 6468–6477. doi: 10.4049/jimmunol.1202583

Herlihy, S. E., Tang, Y., Phillips, J. E., and Gomer, R. H. (2017). Functional similarities between the *Dictyostelium* protein AprA and the human protein dipeptidyl-peptidase IV. *Protein Sci.* 26, 578–585. doi: 10.1002/pro.3107

Heuberger, D. M., and Schuepbach, R. A. (2019). Protease-activated receptors (PARs): mechanisms of action and potential therapeutic modulators in PAR-driven inflammatory diseases. *Thromb. J.* 17:4.

Holt, E., Stanton-Turcotte, D., and Iulianella, A. (2021). Development of the vertebrate trunk sensory system: origins, specification, axon guidance, and central connectivity. *Neuroscience* 458, 229–243. doi: 10.1016/j.neuroscience.2020.12.037

Hong, K. S., Hinck, L., Nishiyama, M., Poo, M. M., Tessier-Lavigne, M., and Stein, E. (1999). A ligand-gated association between cytoplasmic domains of UNC5 and DCC family receptors converts netrin-induced growth cone attraction to repulsion. *Cell* 97, 927–941. doi: 10.1016/s0092-8674(00)80804-1

Hu, H. (1999). Chemorepulsion of neuronal migration by Slit2 in the developing mammalian forebrain. *Neuron* 23, 703–711. doi: 10.1016/s0896-6273(01)80029-5

Huang, H. C., and Klein, P. S. (2004). The Frizzled family: receptors for multiple signal transduction pathways. *Genome Biol.* 5:234.

Huber, R. J., and Mathavarajah, S. (2018). Cln5 is secreted and functions as a glycoside hydrolase in *Dictyostelium*. *Cell Signal* 42, 236–248. doi: 10.1016/j.cellsig.2017.11.001

Huber, R. J., Myre, M. A., and Cotman, S. L. (2014). Loss of Cln3 function in the social amoeba *Dictyostelium discoideum* causes pleiotropic effects that are rescued by human CLN3. *PLoS One* 9:e110544. doi: 10.1371/journal.pone.0110544

Islam, S. M., Shinmyo, Y., Okafuji, T., Su, Y., Naser, I. B., Ahmed, G., et al. (2009). Draxin, a repulsive guidance protein for spinal cord and forebrain commissures. *Science* 323, 388–393. doi: 10.1126/science.1165187

Jager, E., Ringhoffer, M., Karbach, J., Arand, M., Oesch, F., and Knuth, A. (1996). Inverse relationship of melanocyte differentiation antigen expression in melanoma tissues and CD8+ cytotoxic-T-cell responses: evidence for immunoselection of antigen-loss variants in vivo. *Int. J. Cancer* 66, 470–476. doi: 10.1002/(sici)1097-0215(19960516)66:4<470::aid-ijc10>3.0.co;2-c

Kagota, S., Maruyama, K., and McGuire, J. J. (2016). Characterization and functions of protease-activated receptor 2 in obesity, diabetes, and metabolic syndrome: a systematic review. *Biomed. Res. Int.* 2016:3130496.

Kalil, K., Li, L., and Hutchins, B. I. (2011). Signaling mechanisms in cortical axon growth, guidance, and branching. *Front. Neuroanat.* 5:62. doi: 10.3389/fnana.2011.00062

Kao, K. C., Hu, H. C., Chang, C. H., Hung, C. Y., Chiu, L. C., Li, S. H., et al. (2015). Diffuse alveolar damage associated mortality in selected acute respiratory distress syndrome patients with open lung biopsy. *Crit. Care* 19:228.

Kaplan, M. J. (2013). Role of neutrophils in systemic autoimmune diseases. *Arthritis Res. Ther.* 15:219. doi: 10.1186/ar4325

Karunanithi, S., Joshi, J., Chavel, C., Birkaya, B., Grell, L., and Cullen, P. J. (2012). Regulation of mat responses by a differentiation MAPK pathway in Saccharomyces cerevisiae. *PLoS One* 7:e32294. doi: 10.1371/journal.pone.0032294

Keizer-Gunnink, I., Kortholt, A., and Van Haastert, P. J. (2007). Chemoattractants and chemorepellents act by inducing opposite polarity in phospholipase C and PI3-kinase signaling. *J. Cell Biol.* 177, 579–585. doi: 10.1083/jcb.200611046

Kessin, R. H. (2001). *Dictyostelium: Evolution, Cell Biology, and the Development of Multicellularity*. Cambridge: Cambridge University Press.

King, J. S., and Insall, R. H. (2009). Chemotaxis: finding the way forward with *Dictyostelium*. *Trends Cell Biol.* 19, 523–530. doi: 10.1016/j.tcb.2009.07.004

Kohrgruber, N., Groger, M., Meraner, P., Kriehuber, E., Petzelbauer, P., Brandt, S., et al. (2004). Plasmacytoid dendritic cell recruitment by immobilized CXCR3 ligands. *J. Immunol.* 173, 6592–6602. doi: 10.4049/jimmunol.173.11.6592

Kolaczkowska, E., and Kubes, P. (2013). Neutrophil recruitment and function in health and inflammation. *Nat. Rev. Immunol.* 13, 159–175. doi: 10.1038/nri3399

Kolpak, A. L., Jiang, J., Guo, D., Standley, C., Bellve, K., Fogarty, K., et al. (2009). Negative guidance factor-induced macropinocytosis in the growth cone plays a critical role in repulsive axon turning. *J. Neurosci.* 29, 10488–10498. doi: 10.1523/jneurosci.2355-09.2009

Komiya, Y., and Habas, R. (2008). Wnt signal transduction pathways. *Organogenesis* 4, 68–75. doi: 10.4161/org.4.2.5851

Kortholt, A., Kataria, R., Keizer-Gunnink, I., Van Egmond, W. N., Khanna, A., and Van Haastert, P. J. (2011). *Dictyostelium* chemotaxis: essential Ras activation and accessory signalling pathways for amplification. *EMBO Rep.* 12, 1273–1279. doi: 10.1038/embor.2011.210

Kotacková, L., Baláziová, E., and Sedo, A. (2009). Expression pattern of dipeptidyl peptidase IV activity and/or structure homologues in cancer. *Folia Biol.* 55, 77–84.

Lake, D., Correa, S. A., and Muller, J. (2016). Negative feedback regulation of the ERK1/2 MAPK pathway. *Cell Mol. Life Sci.* 73, 4397–4413. doi: 10.1007/s00018-016-2297-8

Larsen, S. H., Reader, R. W., Kort, E. N., Tso, W. W., and Adler, J. (1974). Change in direction of flagellar rotation is the basis of the chemotactic response in *Escherichia coli*. *Nature* 249, 74–77. doi: 10.1038/249074a0

Leung, T., Chen, X. Q., Manser, E., and Lim, L. (1996). The p160 RhoA-binding kinase ROK alpha is a member of a kinase family and is involved in the reorganization of the cytoskeleton. *Mol. Cell. Biol.* 16, 5313–5327. doi: 10.1128/mcb.16.10.5313

Levine, H., Kessler, D. A., and Rappel, W. J. (2006). Directional sensing in eukaryotic chemotaxis: a balanced inactivation model. *Proc. Natl. Acad. Sci. U.S.A.* 103, 9761–9766. doi: 10.1073/pnas.0601302103

Lim, C. J., Zawadzki, K. A., Khosla, M., Secko, D. M., Spiegelman, G. B., and Weeks, G. (2005). Loss of the *Dictyostelium* RasC protein alters vegetative cell size, motility and endocytosis. *Exp. Cell Res.* 306, 47–55. doi: 10.1016/j.yexcr.2005.02.002

Lin, W. C., and Fessler, M. B. (2021). Regulatory mechanisms of neutrophil migration from the circulation to the airspace. *Cell Mol. Life Sci.* 78, 4095–4124. doi: 10.1007/s00018-021-03768-z

Liu, B. P., Cafferty, W. B., Budel, S. O., and Strittmatter, S. M. (2006). Extracellular regulators of axonal growth in the adult central nervous system. *Philos. Trans. R. Soc. Lond. B Biol. Sci.* 361, 1593–1610. doi: 10.1098/rstb.2006.1891

Lynn, H., Sun, X., Casanova, N., Gonzales-Garay, M., Bime, C., and Garcia, J. G. N. (2019). Genomic and genetic approaches to deciphering acute respiratory distress syndrome risk and mortality. *Antioxid. Redox Signal.* 31, 1027–1052. doi: 10.1089/ars.2018.7701

Ma, H., Gamper, M., Parent, C., and Firtel, R. A. (1997). The *Dictyostelium* MAP kinase kinase DdMEK1 regulates chemotaxis and is essential for chemoattractant-mediated activation of guanylyl cyclase. *Embo. J.* 16, 4317–4332. doi: 10.1093/emboj/16.14.4317

MacWilliams, H., Doquang, K., Pedrola, R., Dollman, G., Grassi, D., Peis, T., et al. (2006). A retinoblastoma ortholog controls stalk/spore preference in *Dictyostelium*. *Development* 133, 1287–1297. doi: 10.1242/dev.02287

Maekawa, M., Ishizaki, T., Boku, S., Watanabe, N., Fujita, A., Iwamatsu, A., et al. (1999). Signaling from Rho to the actin cytoskeleton through protein kinases ROCK and LIM-kinase. *Science* 285, 895–898. doi: 10.1126/science.285.5429.895

Mark, M. D., Lohrum, M., and Puschel, A. W. (1997). Patterning neuronal connections by chemorepulsion: the semaphorins. *Cell Tissue Res.* 290, 299–306. doi: 10.1007/978-3-642-60905-3_15

Matthay, M. A., Ware, L. B., and Zimmerman, G. A. (2012). The acute respiratory distress syndrome. *J. Clin. Invest.* 122, 2731–2740.

McCulloch, K., McGrath, S., Huesa, C., Dunning, L., Litherland, G., Crilly, A., et al. (2018). Rheumatic disease: protease-activated receptor-2 in synovial joint pathobiology. *Front. Endocrinol.* 9:257. doi: 10.3389/fendo.2018.00257

McLean, P. G., Aston, D., Sarkar, D., and Ahluwalia, A. (2002). Protease-activated receptor-2 activation causes EDHF-like coronary vasodilation: selective preservation in ischemia/reperfusion injury: involvement of lipoxygenase products, VR1 receptors, and C-fibers. *Circ Res.* 90, 465–472. doi: 10.1161/hh0402.105372

Meli, R., Weisova, P., and Propst, F. (2015). Repulsive axon guidance by Draxin is mediated by protein Kinase B (Akt), glycogen synthase kinase-3beta (GSK-3beta) and microtubule-associated protein 1B. *PLoS One* 10:e0119524. doi: 10.1371/journal.pone.0119524

Mulvihill, E. E., and Drucker, D. J. (2014). Pharmacology, physiology, and mechanisms of action of dipeptidyl peptidase-4 inhibitors. *Endocr. Rev.* 35, 992–1019. doi: 10.1210/er.2014-1035

Nash, M., Pribiag, H., Fournier, A. E., and Jacobson, C. (2009). Central nervous system regeneration inhibitors and their intracellular substrates. *Mol. Neurobiol.* 40, 224–235. doi: 10.1007/s12035-009-8083-y

Nauck, M. A., Vardarli, I., Deacon, C. F., Holst, J. J., and Meier, J. J. (2011). Secretion of glucagon-like peptide-1 (GLP-1) in type 2 diabetes: what is up, what is down? *Diabetologia* 54, 10–18. doi: 10.1007/s00125-010-1896-4

Nguyen Ba-Charvet, K. T., Brose, K., Marillat, V., Kidd, T., Goodman, C. S., Tessier-Lavigne, M., et al. (1999). Slit2-Mediated chemorepulsion and collapse of developing forebrain axons. *Neuron* 22, 463–473. doi: 10.1016/s0896-6273(00)80702-3

Ogilvie, P., Paoletti, S., Clark-Lewis, I., and Uguccioni, M. (2003). Eotaxin-3 is a natural antagonist for CCR2 and exerts a repulsive effect on human monocytes. *Blood* 102, 789–794. doi: 10.1182/blood-2002-09-2773

Ossovskaya, V. S., and Bunnett, N. W. (2004). Protease-activated receptors: contribution to physiology and disease. *Physiol Rev.* 84, 579–621. doi: 10.1152/physrev.00028.2003

Pan, K., Ohnuma, K., Morimoto, C., and Dang, N. H. (2021). CD26/Dipeptidyl peptidase IV and its multiple biological functions. *Cureus* 13, e13495.

Pandey, G., and Jain, R. K. (2002). Bacterial chemotaxis toward environmental pollutants: role in bioremediation. *Appl. Environ. Microbiol.* 68, 5789–5795. doi: 10.1128/aem.68.12.5789-5795.2002

Parent, C. A., Blacklock, B. J., Froehlich, W. M., Murphy, D. B., and Devreotes, P. N. (1998). G protein signaling events are activated at the leading edge of chemotactic cells. *Cell* 95, 81–91. doi: 10.1016/s0092-8674(00)81784-5

Parhar, K. K. S., Zjadewicz, K., Soo, A., Sutton, A., Zjadewicz, M., Doig, L., et al. (2019). Epidemiology, mechanical power, and 3-Year outcomes in acute respiratory distress syndrome patients using standardized screening. An observational cohort study. *Ann. Am. Thorac. Soc.* 16, 1263–1272. doi: 10.1513/annalsats.201812-910oc

Park, J. H., Pak, H. J., Riew, T. R., Shin, Y. J., and Lee, M. Y. (2016). Increased expression of Slit2 and its receptors Robo1 and Robo4 in reactive astrocytes of the rat hippocampus after transient forebrain ischemia. *Brain Res.* 1634, 45–56. doi: 10.1016/j.brainres.2015.12.056

Patel, K., Nash, J. A., Itoh, A., Liu, Z., Sundaresan, V., and Pini, A. (2001). Slit proteins are not dominant chemorepellents for olfactory tract and spinal motor axons. *Development* 128, 5031–5037. doi: 10.1242/dev.128.24.5031

Phillips, J. E., and Gomer, R. H. (2010). The ROCO kinase QkgA is necessary for proliferation inhibition by autocrine signals in *Dictyostelium discoideum*. *Eukaryot. Cell* 9, 1557–1565. doi: 10.1128/ec.00121-10

Phillips, J. E., and Gomer, R. H. (2012). A secreted protein is an endogenous chemorepellant in *Dictyostelium discoideum*. *Proc. Natl. Acad. Sci. U.S .A.* 109, 10990–10995. doi: 10.1073/pnas.1206350109

Phillips, J. E., and Gomer, R. H. (2014). The p21-activated kinase (PAK) family member PakD is required for chemorepulsion and proliferation inhibition by autocrine signals in *Dictyostelium discoideum*. *PLoS One* 9:e96633. doi: 10.1371/journal.pone.0096633

Phillips, J. E., Huang, E., Shaulsky, G., and Gomer, R. H. (2011). The putative bZIP transcription factor BzpN slows proliferation and functions in the regulation of cell density by autocrine signals in *Dictyostelium*. *PLoS One* 6:e21765. doi: 10.1371/journal.pone.0021765

Pilling, D., Chinea, L. E., Consalvo, K. M., and Gomer, R. H. (2019). Different isoforms of the neuronal guidance molecule Slit2 directly cause chemoattraction or chemorepulsion of human neutrophils. *J. Immunol.* 202, 239–248. doi: 10.4049/jimmunol.1800681

Plattner, H. (2015). Molecular aspects of calcium signalling at the crossroads of unikont and bikont eukaryote evolution–the ciliated protozoan Paramecium in focus. *Cell Calcium* 57, 174–185. doi: 10.1016/j.ceca.2014.12.002

Rai, M., Xiong, Y., and Singleton, C. K. (2006). Disruption of the ifkA and ifkB genes results in altered cell adhesion, morphological defects and a propensity to form pre-stalk O cells during development of *Dictyostelium*. *Differentiation* 74, 583–595. doi: 10.1111/j.1432-0436.2006.00085.x

Ranieri, V. M., Rubenfeld, G. D., Thompson, B. T., Ferguson, N. D., Caldwell, E., Fan, E., et al. (2012). Acute respiratory distress syndrome: the Berlin Definition. *JAMA* 307, 2526–2533.

Redecha, P., Franzke, C. W., Ruf, W., Mackman, N., and Girardi, G. (2008). Neutrophil activation by the tissue factor/Factor VIIa/PAR2 axis mediates fetal death in a mouse model of antiphospholipid syndrome. *J. Clin. Invest.* 118, 3453–3461.

Riches, K., Franklin, L., Maqbool, A., Peckham, M., Adams, M., Bond, J., et al. (2013). Apolipoprotein(a) acts as a chemorepellent to human vascular smooth muscle cells via integrin alphaVbeta3 and RhoA/ROCK-mediated mechanisms. *Int. J. Biochem. Cell Biol.* 45, 1776–1783. doi: 10.1016/j.biocel.2013.05.021

Ridley, A. J. (2015). Rho GTPase signalling in cell migration. *Curr. Opin. Cell Biol.* 36, 103–112. doi: 10.1016/j.ceb.2015.08.005

Rijal, R., Consalvo, K. M., Lindsey, C. K., and Gomer, R. H. (2019). An endogenous chemorepellent directs cell movement by inhibiting pseudopods at one side of cells. *Mol. Biol. Cell* 30, 242–255. doi: 10.1091/mbc.e18-09-0562

Rodgers, L. F., Markle, K. L., and Hennessey, T. M. (2008). Responses of the ciliates tetrahymena and paramecium to vertebrate odorants and tastants. *J. Eukaryot. Microbiol.* 55, 27–33. doi: 10.1111/j.1550-7408.2007.00300.x

Roy, A., Kucukural, A., and Zhang, Y. (2010). I-TASSER: a unified platform for automated protein structure and function prediction. *Nat. Protoc.* 5, 725–738. doi: 10.1038/nprot.2010.5

Roy, A., Yang, J., and Zhang, Y. (2012). COFACTOR: an accurate comparative algorithm for structure-based protein function annotation. *Nucleic Acids Res.* 40, W471–W477.

Rubenfeld, G. D., Caldwell, E., Peabody, E., Weaver, J., Martin, D. P., Neff, M., et al. (2005). Incidence and outcomes of acute lung injury. *N. Engl. J. Med.* 353, 1685–1693.

Sadik, C. D., and Luster, A. D. (2012). Lipid-cytokine-chemokine cascades orchestrate leukocyte recruitment in inflammation. *J. Leukoc. Biol.* 91, 207–215. doi: 10.1189/jlb.0811402

Santavuori, P. (1988). Neuronal ceroid-lipofuscinoses in childhood. *Brain Dev.* 10, 80–83. doi: 10.1016/s0387-7604(88)80075-5

Santos, T. E., Schaffran, B., Broguiere, N., Meyn, L., Zenobi-Wong, M., and Bradke, F. (2020). Axon growth of CNS neurons in three dimensions is amoeboid and independent of adhesions. *Cell Rep.* 32:107907. doi: 10.1016/j.celrep.2020.107907

Sasaki, A. T., Chun, C., Takeda, K., and Firtel, R. A. (2004). Localized Ras signaling at the leading edge regulates PI3K, cell polarity, and directional cell movement. *J. Cell Biol.* 167, 505–518. doi: 10.1083/jcb.200406177

Savino, W., Mendes-da-Cruz, D. A., Golbert, D. C., Riederer, I., and Cotta-de-Almeida, V. (2015). Laminin-mediated interactions in thymocyte migration and development. *Front. Immunol.* 6:579. doi: 10.3389/fimmu.2015.00579

Schmandke, A., Schmandke, A., and Strittmatter, S. M. (2007). ROCK and Rho: biochemistry and neuronal functions of Rho-associated protein kinases. *Neuroscientist* 13, 454–469. doi: 10.1177/1073858407303611

Schwab, M. E. (2010). Functions of Nogo proteins and their receptors in the nervous system. *Nat. Rev. Neurosci.* 11, 799–811. doi: 10.1038/nrn2936

Shaver, C. M., and Bastarache, J. A. (2014). Clinical and biological heterogeneity in acute respiratory distress syndrome: direct versus indirect lung injury. *Clin. Chest Med.* 35, 639–653.

Shearer, A. M., Rana, R., Austin, K., Baleja, J. D., Nguyen, N., Bohm, A., et al. (2016). Targeting liver fibrosis with a cell-penetrating protease-activated receptor-2 (PAR2) pepducin. *J. Biol. Chem.* 291, 23188–23198. doi: 10.1074/jbc.m116.732743

Steinberg, K. P., Milberg, J. A., Martin, T. R., Maunder, R. J., Cockrill, B. A., and Hudson, L. D. (1994). Evolution of bronchoalveolar cell populations in the adult respiratory distress syndrome. *Am. J. Respir. Crit. Care Med.* 150, 113–122. doi: 10.1164/ajrccm.150.1.8025736

Sugarman, B., and Mummaw, N. (1988). Effects of antimicrobial agents on growth and chemotaxis of Trichomonas vaginalis. *Antimicrob. Agents Chemother.* 32, 1323–1326. doi: 10.1128/aac.32.9.1323

Tadagavadi, R. K., Wang, W., and Ramesh, G. (2010). Netrin-1 regulates Th1/Th2/Th17 cytokine production and inflammation through UNC5B receptor and protects kidney against ischemia-reperfusion injury. *J. Immunol.* 185, 3750–3758. doi: 10.4049/jimmunol.1000435

Tang, V. (2017). Cell-cell adhesion interface: rise of the lateral membrane. *F1000Res.* 6:276. doi: 10.12688/f1000research.10680.1

Tang, Y., and Gomer, R. H. (2008). A protein with similarity to PTEN regulates aggregation territory size by decreasing cyclic AMP pulse size during *Dictyostelium discoideum* development. *Eukaryot. Cell* 7, 1758–1770. doi: 10.1128/ec.00210-08

Tang, Y., Wu, Y., Herlihy, S. E., Brito-Aleman, F. J., Ting, J. H., Janetopoulos, C., et al. (2018). An autocrine proliferation repressor regulates *Dictyostelium discoideum* proliferation and chemorepulsion using the G protein-coupled receptor GrlH. *mBio* 9:e2443-17.

Tharp, W. G., Yadav, R., Irimia, D., Upadhyaya, A., Samadani, A., Hurtado, O., et al. (2006). Neutrophil chemorepulsion in defined interleukin-8 gradients in vitro and in vivo. *J. Leukoc. Biol.* 79, 539–554. doi: 10.1189/jlb.0905516

Theveneau, E., and Mayor, R. (2013). Collective cell migration of epithelial and mesenchymal cells. *Cell Mol. Life Sci.* 70, 3481–3492. doi: 10.1007/s00018-012-1251-7

Thiede-Stan, N. K., and Schwab, M. E. (2015). Attractive and repulsive factors act through multi-subunit receptor complexes to regulate nerve fiber growth. *J. Cell Sci.* 128, 2403–2414.

Thoma, R., Löffler, B., Stihle, M., Huber, W., Ruf, A., and Hennig, M. (2003). Structural basis of proline-specific exopeptidase activity as observed in human dipeptidyl peptidase-IV. *Structure* 11, 947–959. doi: 10.1016/s0969-2126(03)00160-6

Thompson, B. T., Chambers, R. C., and Liu, K. D. (2017). Acute respiratory distress syndrome. *N. Engl. J. Med.* 377, 562–572.

Tole, S., Mukovozov, I. M., Huang, Y. W., Magalhaes, M. A., Yan, M., Crow, M. R., et al. (2009). The axonal repellent, Slit2, inhibits directional migration of circulating neutrophils. *J. Leukoc. Biol.* 86, 1403–1415. doi: 10.1189/jlb.0609391

Tomchik, K. J., and Devreotes, P. N. (1981). Adenosine 3.5′-monophosphate waves in *Dictyostelium discoideum*: a demonstration by isotope dilution–fluorography. *Science* 212, 443–446. doi: 10.1126/science.6259734

Trzaskalski, N. A., Fadzeyeva, E., and Mulvihill, E. E. (2020). Dipeptidyl Peptidase-4 at the Interface Between Inflammation and Metabolism. *Clin. Med. Insights Endocrinol. Diabetes* 13:1179551420912972.

Vianello, F., Olszak, I. T., and Poznansky, M. C. (2005). Fugetaxis: active movement of leukocytes away from a chemokinetic agent. *J. Mol. Med.* 83, 752–763. doi: 10.1007/s00109-005-0675-z

Vianello, F., Papeta, N., Chen, T., Kraft, P., White, N., Hart, W. K., et al. (2006). Murine B16 melanomas expressing high levels of the chemokine stromal-derived factor-1/CXCL12 induce tumor-specific T cell chemorepulsion and escape from immune control. *J. Immunol.* 176, 2902–2914. doi: 10.4049/jimmunol.176.5.2902

Vo, T., Carulli, D., Ehlert, E. M., Kwok, J. C., Dick, G., Mecollari, V., et al. (2013). The chemorepulsive axon guidance protein semaphorin3A is a constituent of perineuronal nets in the adult rodent brain. *Mol. Cell Neurosci.* 56, 186–200. doi: 10.1016/j.mcn.2013.04.009

Vu, T. K., Hung, D. T., Wheaton, V. I., and Coughlin, S. R. (1991). Molecular cloning of a functional thrombin receptor reveals a novel proteolytic mechanism of receptor activation. *Cell* 64, 1057–1068. doi: 10.1016/0092-8674(91)90261-v

Wahl, S., Barth, H., Ciossek, T., Aktories, K., and Mueller, B. K. (2000). Ephrin-A5 induces collapse of growth cones by activating Rho and Rho kinase. *J. Cell Biol.* 149, 263–270. doi: 10.1083/jcb.149.2.263

Walborg, E. F. Jr., Tsuchida, S., Weeden, D. S., Thomas, M. W., Barrick, A., McEntire, K. D., et al. (1985). Identification of dipeptidyl peptidase IV as a protein shared by the plasma membrane of hepatocytes and liver biomatrix. *Exp. Cell Res.* 158, 509–518. doi: 10.1016/0014-4827(85)90474-4

Walters, D. M., and Kleeberger, S. R. (2008). Mouse models of bleomycin-induced pulmonary fibrosis. *Curr. Protoc. Pharmacol.* 40, 5.46.1–5.46.17.

Wang, F. (2009). The signaling mechanisms underlying cell polarity and chemotaxis. *Cold Spring Harb. Perspect Biol.* 1:a002980. doi: 10.1101/cshperspect.a002980

Wang, Y., Chen, C. L., and Iijima, M. (2011). Signaling mechanisms for chemotaxis. *Dev. Growth Differ.* 53, 495–502. doi: 10.1111/j.1440-169x.2011.01265.x

Wang, Y., Senoo, H., Sesaki, H., and Iijima, M. (2013). Rho GTPases orient directional sensing in chemotaxis. *Proc. Natl. Acad. Sci. U.S.A.* 110, E4723–E4732.

Weiss, S. J. (1989). Tissue destruction by neutrophils. *N. Engl. J. Med.* 320, 365–376. doi: 10.1056/nejm198902093200606

White, M. J. V., Chinea, L. E., Pilling, D., and Gomer, R. H. (2018). Protease activated-receptor 2 is necessary for neutrophil chemorepulsion induced by trypsin, tryptase, or dipeptidyl peptidase IV. *J. Leukoc. Biol.* 103, 119–128. doi: 10.1002/jlb.3a0717-308r

Wronkowitz, N., Görgens, S. W., Romacho, T., Villalobos, L. A., Sánchez-Ferrer, C. F., Peiró, C., et al. (2014). Soluble DPP4 induces inflammation and proliferation of human smooth muscle cells via protease-activated receptor 2. *Biochim. Biophys. Acta* 1842, 1613–1621. doi: 10.1016/j.bbadis.2014.06.004

Yan, J., Mihaylov, V., Xu, X., Brzostowski, J. A., Li, H., and Liu, L. (2012). A Gβγ Effector, ElmoE, transduces GPCR signaling to the actin network during chemotaxis. *Dev. Cell* 22, 92–103. doi: 10.1016/j.devcel.2011.11.007

Ye, B. Q., Geng, Z. H., Ma, L., and Geng, J. G. (2010). Slit2 regulates attractive eosinophil and repulsive neutrophil chemotaxis through differential srGAP1 expression during lung inflammation. *J. Immunol.* 185, 6294–6305. doi: 10.4049/jimmunol.1001648

Ye, J., Kumanova, M., Hart, L. S., Sloane, K., Zhang, H., De Panis, D. N., et al. (2010). The GCN2-ATF4 pathway is critical for tumour cell survival and proliferation in response to nutrient deprivation. *Embo J.* 29, 2082–2096. doi: 10.1038/emboj.2010.81

Zemans, R. L., Colgan, S. P., and Downey, G. P. (2009). Transepithelial migration of neutrophils: mechanisms and implications for acute lung injury. *Am. J. Respir. Cell Mol. Biol.* 40, 519–535. doi: 10.1165/rcmb.2008-0348tr

Zhang, Y. (2008). I-TASSER server for protein 3D structure prediction. *BMC Bioinformatics* 9:40. doi: 10.1186/1471-2105-9-40

Zhu, L., Tamvakopoulos, C., Xie, D., Dragovic, J., Shen, X., Fenyk-Melody, J. E., et al. (2003). The role of dipeptidyl peptidase IV in the cleavage of glucagon family peptides: in vivo metabolism of pituitary adenylate cyclase activating polypeptide-(1-38). *J. Biol. Chem.* 278, 22418–22423.

Zou, D., and Hennessey, T. M. (2017). Behavioral effects of a chemorepellent receptor knockout mutation in Tetrahymena thermophila. *mSphere* 2:e182-17.

Conflict of Interest: The authors declare that the research was conducted in the absence of any commercial or financial relationships that could be construed as a potential conflict of interest.

Copyright © 2021 Kirolos, Rijal, Consalvo and Gomer. This is an open-access article distributed under the terms of the Creative Commons Attribution License (CC BY). The use, distribution or reproduction in other forums is permitted, provided the original author(s) and the copyright owner(s) are credited and that the original publication in this journal is cited, in accordance with accepted academic practice. No use, distribution or reproduction is permitted which does not comply with these terms.

frontiers in Cell and Developmental Biology

ORIGINAL RESEARCH
published: 30 July 2021
doi: 10.3389/fcell.2021.725073

Membrane Targeting of C2GAP1 Enables *Dictyostelium discoideum* to Sense Chemoattractant Gradient at a Higher Concentration Range

Xuehua Xu[1], Smit Bhimani[1], Henderikus Pots[2], Xi Wen[1], Taeck J. Jeon[3], Arjan Kortholt[2] and Tian Jin[1]*

[1] *Chemotaxis Signaling Section, Laboratory of Immunogenetics, National Institute of Allergy and Infectious Diseases, National Institutes of Health, Rockville, MD, United States,* [2] *Department of Cell Biochemistry, Univeristy of Groningen, Groningen, Netherlands,* [3] *Department of Biology and BK21-Plus Research Team for Bioactive Control Technology, College of Natural Sciences, Chosun University, Gwangju, South Korea*

OPEN ACCESS

Edited by:
Robin S. B. Williams, Royal Holloway, University of London, United Kingdom

Reviewed by:
Shashi Prakash Singh, University of Glasgow, United Kingdom
Yoichiro Kamimura, RIKEN Center for Biosystems Dynamics Research (BDR), Japan

***Correspondence:**
Xuehua Xu
xxu@niaid.nih.gov

Specialty section:
This article was submitted to Molecular and Cellular Pathology, a section of the journal Frontiers in Cell and Developmental Biology

Received: *14 June 2021*
Accepted: *12 July 2021*
Published: *30 July 2021*

Citation:
Xu X, Bhimani S, Pots H, Wen X, Jeon TJ, Kortholt A and Jin T (2021) Membrane Targeting of C2GAP1 Enables Dictyostelium discoideum to Sense Chemoattractant Gradient at a Higher Concentration Range. Front. Cell Dev. Biol. 9:725073. doi: 10.3389/fcell.2021.725073

Chemotaxis, which is G protein-coupled receptor (GPCR)-mediated directional cell migration, plays pivotal roles in diverse human diseases, including recruitment of leukocytes to inflammation sites and metastasis of cancer. It is still not fully understood how eukaryotes sense and chemotax in response to chemoattractants with an enormous concentration range. A genetically traceable model organism, *Dictyostelium discoideum*, is the best-studied organism for GPCR-mediated chemotaxis. Recently, we have shown that C2GAP1 controls G protein coupled receptor-mediated Ras adaptation and chemotaxis. Here, we investigated the molecular mechanism and the biological function of C2GAP1 membrane targeting for chemotaxis. We show that calcium and phospholipids on the plasma membrane play critical roles in membrane targeting of C2GAP1. Cells lacking C2GAP1 (*c2gapA*$^{-}$) displayed an improved chemotaxis in response to chemoattractant gradients at subsensitive or low concentrations ($<$100 nM), while exhibiting impaired chemotaxis in response to gradients at high concentrations ($>$1 μM). Taken together, our results demonstrate that the membrane targeting of C2GAP1 enables *Dictyostelium* to sense chemoattractant gradients at a higher concentration range. This mechanism is likely an evolutionarily conserved molecular mechanism of Ras regulation in the adaptation and chemotaxis of eukaryotes.

Keywords: chemotaxis, C2GAP1, adaptation, sensitivity, G protein coupled receptor, gradient sensing

INTRODUCTION

Chemotaxis, which is G protein-coupled receptor (GPCR)-mediated directional cell migration, plays pivotal roles in diverse physiological and pathological processes, such as embryo development, angiogenesis, recruitment of neutrophils to inflammation sites, and metastasis of cancer. *Dictyostelium* is a genetically traceable model organism that is the best-studied organism for GPCR-mediated chemotaxis. Chemotaxis is crucial for detecting, moving toward, and eventually

engulfing bacteria as food source, as well as development of *Dictyostelium*. A key feature of chemotaxis in eukaryotic cells is that cells sense a large concentration range of chemoattractants (10^{-9}–10^{-5} M cAMP in *Dictyostelium* and 10^{-9}–10^{-5} M fMLP in neutrophils). To accurately navigate through an enormous concentration-range gradient of various chemoattractants, both *Dictyostelium* and neutrophils employ a mechanism called adaptation, in which they no longer respond to present stimuli but remain sensitive to stronger stimuli. Homogeneous, sustained chemoattractant stimuli trigger transient, adaptive responses in many steps of the GPCR-mediated signaling pathway downstream of heterotrimeric G proteins (Janetopoulos et al., 2001; Hoeller et al., 2014). Adaptation provides a fundamental strategy for eukaryotic cell chemotaxis through large concentration-range gradients of chemoattractants. However, little connection has been made between GPCR-mediated adaptation and the basal activity of a cell.

The small GTPase Ras mediates multiple signaling pathways that control directional cell migration in both neutrophils and *Dictyostelium* (Zheng et al., 1997; Sasaki et al., 2004; Zhang et al., 2008; Suire et al., 2012; Wang et al., 2014; van Haastert et al., 2017). In *Dictyostelium*, the activation of Ras is the first signaling event that displays adaptation behavior in GPCR-mediated signaling pathways (Sasaki et al., 2004). Ras signaling is activated through guanine nucleotide exchange factors (GEFs) and deactivated by GTPase-activating proteins (GAPs). Several RasGEFs and RasGAPs have been found to activate and deactivate Ras signaling, respectively (Insall et al., 1996; Zhang et al., 2008; Xu et al., 2017). Recently, we identified a locally recruited RasGAP protein, C2GAP1, that is essential for F-actin-independent Ras adaptation and long-range chemotaxis in *Dictyostelium* (Xu et al., 2017). However, the molecular mechanism of membrane targeting of C2GAP1 is not fully understood. Here, we show that calcium and phospholipids on the plasma membrane, but not GAP activity, play critical roles in membrane targeting of C2GAP1. More importantly, C2GAP1 controls both the basal activity and the GPCR-mediated adaptation in *Dictyostelium* cells and thereby enables cells to sense chemoattractant gradients at a higher concentration range.

RESULTS

Calcium Negatively Mediates Membrane Targeting of C2GAP1

C2GAP1 possesses a C2 domain, which is a calcium-binding motif and is often involved in membrane targeting of host proteins (Nalefski and Falke, 1996; Corbalan-Garcia and Gomez-Fernandez, 2014). Thus, we first examined whether calcium affects the interaction between C2GAP1 and Ras by immunoprecipitation and found an interesting effect of $[Ca^{2+}]$ on the interaction between C2GAP1 and Ras (**Figure 1A**). The presence of high $[Ca^{2+}]$ (> 100 nM) decreased the C2GAP1/Ras interaction. Interestingly, the highest interaction of C2GAP1 and Ras was detected with the presence of 1 nM calcium, while lower $[Ca^{2+}]$ to none again decreased the interaction (**Figure 1B**). The effect of $[Ca^{2+}]$ on the interaction between C2GAP1 and Ras might be due to its effect on C2GAP1 membrane targeting. To understand the effect of $[Ca^{2+}]$, we first monitored the cAMP-induced calcium response by an ultrasensitive $[Ca^{2+}]$ indicator, Nano15, using fluorescence resonance energy transfer (FRET) microscopy in live cells (Horikawa et al., 2010; Xu et al., 2016). Consistent with a previous report (Horikawa et al., 2010), 1 μM cAMP stimulation induced a transient increase in the FRET efficiency of Nano15, indicating a clear $[Ca^{2+}]$ increase peaking around 40 s after stimulation in wild-type (WT) cells (**Figure 1C**). In *iplA*$^-$ cells, which lack the IP_3 receptor, cAMP stimulation triggered no $[Ca^{2+}]$ increase, as previously reported (Traynor et al., 2000). Calcium-binding protein 7 (CbpG) has the highest calcium-binding capacity among 14 *Dictyostelium* calcium-binding proteins (Cbps) and is highly expressed during early development (Sakamoto et al., 2003). Cells lacking Cbp7 (*cbpG*$^-$) have a slightly higher level of $[Ca^{2+}]$ in the resting state, indicating that Cbp7 functions as a Ca^{2+}-binding protein (Wilczynska et al., 2005; Park et al., 2018). In response to 1 μM cAMP stimulation, *cbpG*$^-$ cells showed a much more rapid $[Ca^{2+}]$ increase with the peak at about 20 s. This $[Ca^{2+}]$ dynamics is typically observed in *Dictyostelium* mutants that lack calcium-binding proteins: earlier onset, earlier peak, and faster fall rate (Wilczynska et al., 2005).

We next monitored membrane translocation of C2GAP1-YFP in WT and mutant cells (**Figure 1D** and **Supplementary Video 1**). We found that 1 μM cAMP induced a robust membrane translocation of C2GAP1-YFP in WT cells (**Supplementary Video 1**, top left). The same cAMP stimulation induced a prolonged membrane translocation of C2GAP1 in *iplA*$^-$ cells (**Supplementary Video 1**, middle left). In the resting *cbpG*$^-$ cells, membrane localization of C2GAP1-YFP was notably increased. cAMP stimulation triggered little membrane translocation in *cbpG*$^-$ cells (**Supplementary Video 1**, bottom left). We also monitored C2GAP1-YFP in WT, *iplA*$^-$, and *cbpG*$^-$ cells treated with 5 μM Latrunculin B (+ LatB), an actin polymerization inhibitor, to eliminate cell migration for quantitative measurement of membrane translocation of C2GAP1-YFP. Interestingly, there was notably more membrane localization of C2GAP1 in resting *iplA*$^-$ and *cbpG*$^-$ cells (**Supplementary Figure 1**). In WT cells, cAMP stimulation induced membrane translocation of C2GAP1-YFP that was similar in both immobile cells and motile cells (**Supplementary Video 1**, top right). cAMP stimulation triggered a significantly prolonged membrane translocation of C2GAP1 in *iplA*$^-$ cells (**Supplementary Video 1**, middle right), while the same cAMP stimulation induced little membrane translocation of C2GAP1, instead, further reduced membrane localization of C2GAP1 in *cbpG*$^-$ cells (**Supplementary Video 1**, bottom right). Quantitative measurement of the precise membrane translocation dynamics of C2GAP1 in these cells confirmed what we observed in motile cells (**Figure 1E**). In contrast to WT cells, cAMP stimulation triggered a significant prolonged membrane translocation of C2GAP1 in *iplA*$^-$ cells and little membrane translocation in *cbpG*$^-$ cells. Taken together, the above results indicate that calcium dynamically regulates membrane targeting of C2GAP1.

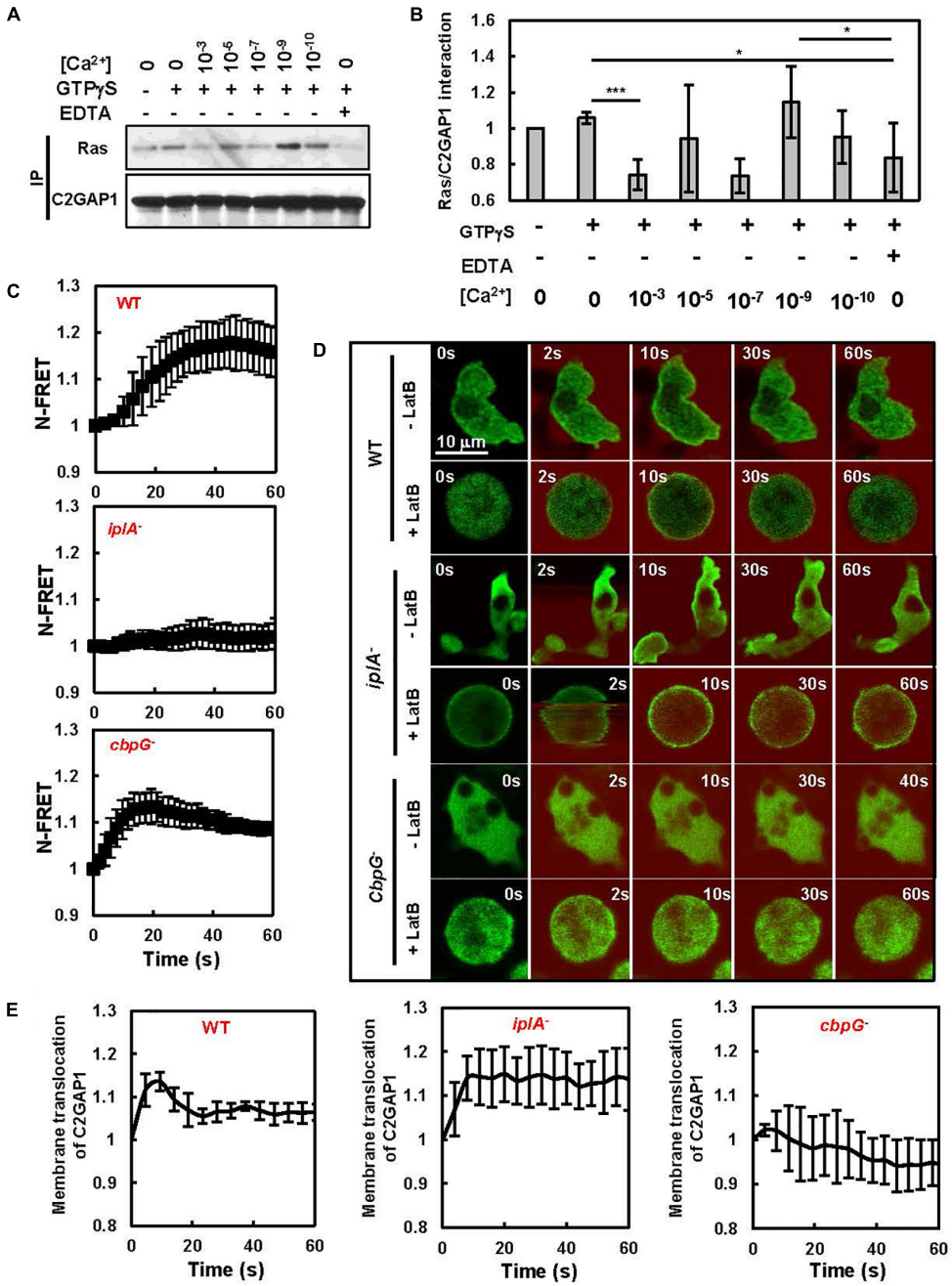

FIGURE 1 | [Ca^{2+}] is dynamically involved in the membrane targeting of C2GAP1. **(A)** High [Ca^{2+}] decreases the association of C2GAP1-YFP and Ras determined by co-immunoprecipitation (co-IP). Cells expressing C2GAP1-YFP were lysed in the presence or absence of GTPγS (10 μM), $CaCl_2$ at the indicated concentrations, or 2 mM EDTA and then subjected to IP assay and western blot detection of the indicated protein with their specific antibodies. **(B)** Quantitative measurement of C2GAP1 and Ras association presented in **(A)**. The ratio of Ras and C2GAP1 at time 0 s was normalized to 1. Mean ± SD from three independent experiments is shown. The *p*-values of Student's *t*-test are indicated as * ($p < 0.1$) and *** ($p < 0.001$). **(C)** cAMP-induced calcium response in WT, *iplA*$^-$, or *cbpG*$^-$ cells using calcium FRET sensor YC-Nano15. Cells expressing YC-nano15 were stimulated with 1 μM cAMP at 0 s. To eliminate cell migration for quantitative measurement, cells were treated with 5 μM Lat B for 10 min prior to the experiment. Calcium response was measured by sensitized emission FRET using a Zeiss 780 fluorescent microscope, analyzed using Zen software, and then graphed with Microsoft Excel. The FRET signal (N-FRET) at time 0 s was normalized to 1. Mean ± SD is shown; $n = 7$, 8, or 8 in WT, *iplA*$^-$, or *cbpG*$^-$ group, respectively. **(D)** Montage shows cAMP-induced membrane translocation of C2GAP1-YFP (green) in WT, *iplA*$^-$, or *cbpG*$^-$ cells in response to homogeneously applied 10 μM cAMP stimulation (red). cAMP-chemotactic cells expressing C2GAP-YFP (green) were stimulated with cAMP at time 0 s. To visualize the stimuli, cAMP was mixed with fluorescent dye Alexa 594 (red). Also see **Supplementary Video 1**. **(E)** Quantitative measurement of membrane-bound C2GAP1-YFP upon exposure to a cAMP gradient is shown. The quantitative measurement of membrane translocation was measured from the cells treated with 5 μM Lat B shown in **(D)** Membrane translocation of C2GAP1 was quantified by the decreased in the cytosolic intensity of C2GAP1. The cytosolic intensity at time 0 s was normalized to 1. Mean ± SD is shown; $n = 5$, 6, or 8 for the groups of WT, *iplA*$^-$, or *cbpG*$^-$ cells, respectively.

C2GAP1 Binds to Phospholipids on the Plasma Membrane

Proteins and phospholipids on the plasma membrane play critical roles in membrane targeting of C2 domain-containing RasGAPs (Corbalan-Garcia and Gomez-Fernandez, 2014; Xu et al., 2017). In order to understand whether GAP activity plays a crucial role in the interaction between Ras and RasGAP1, we generated a GFP-tagged GAP-inactive mutant of C2GAP1 (R616A) and expressed it in *c2gapA*$^-$ cells (*c2gapA*$^-$/R616A). We then examined the chemotaxis behavior of *c2gapA*$^-$/R616A cells and compared it with that of WT and *c2gapA*$^-$ cells (**Figure 2A**). We found that *c2gapA*$^-$/R616A cells displayed similar chemotaxis defect to *c2gapA*$^-$ cells in a 10 μM cAMP gradient in contrast to WT cells, as previously reported (**Figure 2B**). The above result indicates that R616A does not rescue the chemotaxis defect of *c2gapA*$^-$ cells. Using immunoprecipitation, we found that the R616A mutant showed a binding with Ras similar to that of the WT C2GAP1 (**Figure 2C**). The above results indicate that GAP activity is not required for the interaction between C2GAP1 and Ras.

Phospholipids on the plasma membrane play critical roles in the membrane targeting of C2 domain-containing proteins (Corbalan-Garcia and Gomez-Fernandez, 2014). We found that cAMP stimulation also triggered clear membrane translocation of R616A (**Figure 2D** and **Supplementary Video 2**). Therefore, we used a PIP strip assay to determine the species of phospholipids that bind to C2GAP1. We incubated PIP strips with cell lysates collected from the cells expressing GFP-tagged PH_{Crac} (PH_{Crac}-GFP), WT, or R616 of C2GAP1. PH_{Crac}-GFP was used as a control. The phospholipid-binding specificity of PHCrac-GFP is consistent with the previous report (Zhang et al., 2010). We found that both WT and R616A of C2GAP1 bound to multiple phospholipids (**Figure 2E**), including the products of PI3K, such as PI(3)P, PI(3,4)P2, and PI(3,4,5)P3, and the substrates of PI3K. Interestingly, R616A showed a preference for PI(4,5)P2, while the WT showed a better affinity to PI(3,4,5)P3.

Sensitivity of *c2gapA*$^-$ Cells Is Increased in Response to Chemoattractant Stimulus

Little connection has been made between GPCR-mediated adaptation and the sensitivity of a cell. We noticed that C2GAP1 localized on the membrane of resting cells, suggesting its potential role in inhibiting the basal Ras activity of resting cells (Xu et al., 2017). It has also been previously shown that depletion of multiple PIP2 species, such as phosphatidylinositol-4,5-bisphosphate [PI(4,5)P2)] or phosphatidylinositol-3,4-bisphosphate [PI(3,4)P2)] increases Ras/Rap-related activities and excitability in a cell (Miao et al., 2017; Li et al., 2018). C2GAP1 binds to both PI(3,4)P2 and PI(4,5)P (**Figure 2E**). More importantly, cAMP-induced membrane translocation of C2GAP1 is F-actin independent (Xu et al., 2017). We speculated that the higher basal Ras activity in *c2gapA*$^-$ cells might enhance their sensitivity to chemoattractant stimulation in an F-actin-independent fashion. Therefore, we next determined the sensitivity of both WT and *c2gapA*$^-$ cells without the actin cytoskeleton (**Figure 3A**). Cells expressing the PIP_3 biosensor PH_{Crac}-GFP were treated with 5 μM Latrunculin B for 10 min prior to the experiment to diminish the existing cytoskeleton. In response to 10 μM Sp-cAMP stimulation, F-actin-free immobile WT cells displayed a transient membrane translocation of PH_{Crac}-GFP (**Supplementary Video 3**, left), an adaptive behavior of WT cells. However, *c2gapA*$^-$ cells displayed a secondary, persistent accumulation of PH_{Crac}-GFP on the plasma membrane after its initial, transient membrane translocation, a non-adaptive behavior as previously shown (**Supplementary Video 3**, right) (Xu et al., 2017). In response to 0.1 nM Sp-cAMP stimulation, few WT cells (<15%) responded (**Supplementary Video 4**, left), while most of the *c2gapA*$^-$ cells (>85%) showed clear membrane translocation of PH_{Crac}-GFP (**Supplementary Video 4**, right). Quantitative measurement of the responsiveness and adaptation behavior of WT and *c2gapA*$^-$ cells confirmed the above observation (**Figures 3C,D**). These results together demonstrate that *c2gapA*$^-$ cells, lacking Ras inhibitor, are more sensitive to chemoattractant stimuli independent of the actin-based cytoskeleton.

The Concentration Range of cAMP Gradients in Which Cells Chemotax Efficiently Is Upshifted in *c2gapA*$^-$ Cells

The basal activity of Ras is essential for the regulation of actin dynamics and, more importantly, promotes chemotaxis of *Dictyostelium* cells in a shallow chemoattractant gradient (van Haastert et al., 2017). We observed the localization of C2GAP1 not only on the protrusion sites but also on the plasma membrane of resting cells, indicating a role of C2GAP1 in regulating both basal and chemoattractant-stimulated Ras signaling (Xu et al., 2017). Consistent with the above, *c2gapA*$^-$ cells displayed an enhanced basal Ras activity and sensitivity in response to chemoattractant stimulation (**Figure 3**). To precisely determine the function of C2GAP1 in chemotaxis in response to gradients at different concentrations, we monitored the chemotaxis behavior of WT and *c2gapA*$^-$ cells in the gradients with a wide concentration range (**Figure 4A**). For the experiments, we used *EZ-TAXIScan* to apply a well-controlled linear gradient (Wen et al., 2016). Without a gradient, *c2gapA*$^-$ cells displayed a bigger random walk than WT cells. In the gradients generated from a source concentration greater than 1 μM, *c2gapA*$^-$ cells, in clear contrast to WT cells, displayed a significant decrease in the four parameters of chemotaxis: migration speed, directionality, total path length, and polarity (**Figures 4A,B** and **Supplementary Video 5**). When exposed to a gradient at a lower concentration (100 nM), WT and *c2gapA*$^-$ cells displayed similar directionality. The above results are consistent with the previous report (Xu et al., 2017). Next, we monitored chemotaxis behaviors of both WT and *c2gapA*$^-$ cells in response to gradients at low or subsensitive concentrations. We found that in the gradients generated from 1 and 10 nM cAMP sources, *c2gapA*$^-$ cells displayed significantly improved chemotaxing behavior, especially in

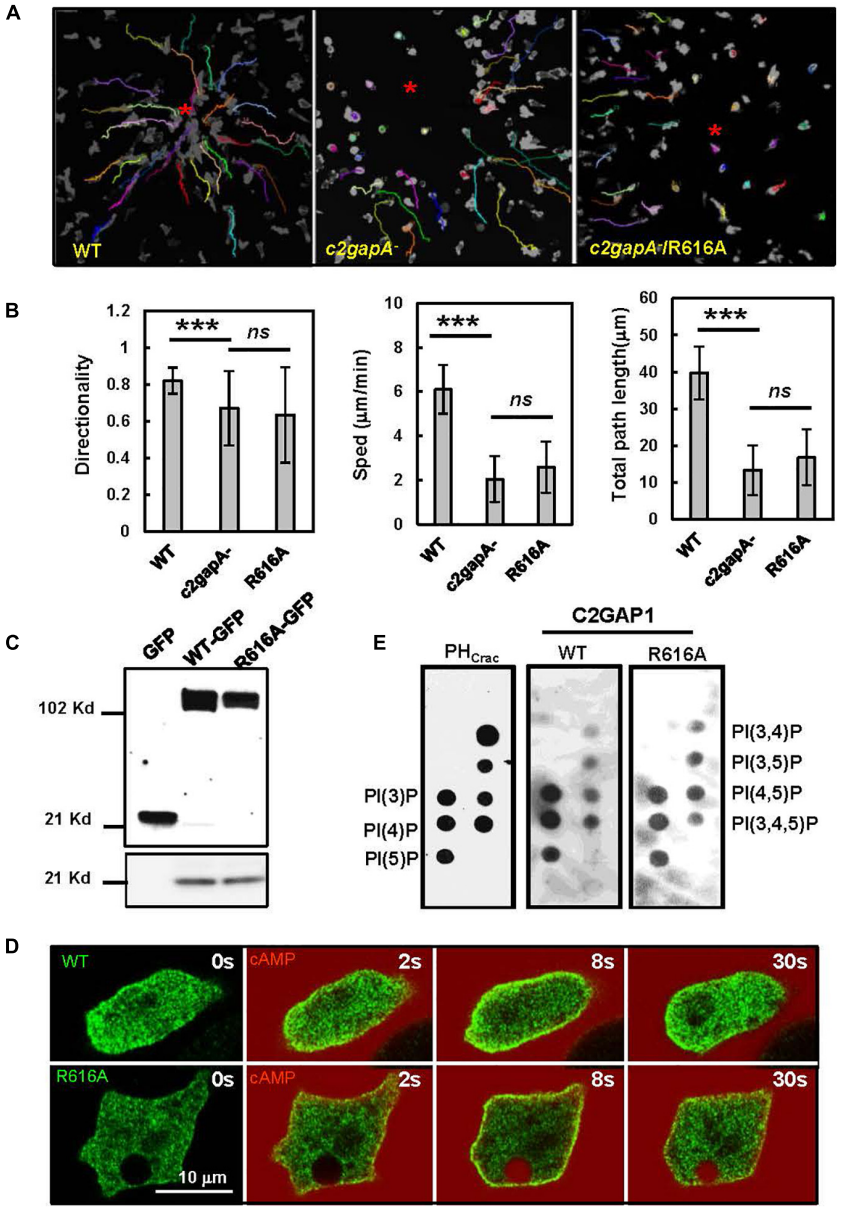

FIGURE 2 | GAP activity is not required for the binding of C2GAP1 and phospholipids on the plasma membrane. **(A)** Montage show the tracing paths of chemotaxing cells of WT or *c2gapA*$^-$ cells expressing empty vector (*c2gapA*$^-$), or R616R (*c2gapA*/R616A) mutant of C2GAP1. Red dots indicate the source of the cAMP gradients (10 μM). **(B)** Quantitative measurements of chemotaxis parameters such as directionality, speed, and total path length using FIJI(NIH) with the MTrackJ plugin. Directionality, where 0 represents random movement and 1 represents straight movement toward the source of a gradient; speed, defined as the distance that the centroid of the cell moves as a function of time; total path length, the total distance the cell has traveled. 30 cells were traced in each group were measured for 5 min in each group. Mean ± SD is shown. The *p*-values of Student's *t*-test are indicated as *ns* (not significant, $p > 0.05$) and *** ($p < 0.001$). **(C)** Interaction between WT or R616A mutant of C2GAP1 and Ras determined by co-IP. Lysates of cells expressing GFP or GFP-tagged WT (WT-GFP) or R616A (R616A-GFP) of C2GAP1 were incubated with agarose beads conjugated with anti-GFP antibodies and then subjected to immunoprecipitation and western blot detection of GFP and Ras using their specific antibodies. **(D)** cAMP stimulation triggers membrane translocation of WT or R616A mutant of C2GAP1 in the cells. Cells expressing GFP-tagged WT or R616A (green) were stimulated with 10 μM cAMP. The application of cAMP was visualized by mixing cAMP with a fluorescent dye, Alexa 594 (red). Also see **Supplementary Video 2**. **(E)** Phospholipid binding of WT or R616A mutant of C2GAP1. Lysates of cells expressing either PH_{Crac}-GFP, WT-GFP, or R616A-GFP were incubated with PIP strips and then subjected to western blot detection by anti-GFP. The western blotting of three PIP-strip membranes were performed using the same procedures.

migration speed, directionality, and polarity, in comparison with CTL cells. In a subsensitive, 0.1 nM cAMP gradient, most WT cells (more than 70%) displayed random migration, while the majority of *c2gapA*$^-$ cells displayed directional cell migration with improved directionality and migration speed. Taken together, these data indicate that *c2gapA*$^-$ cells

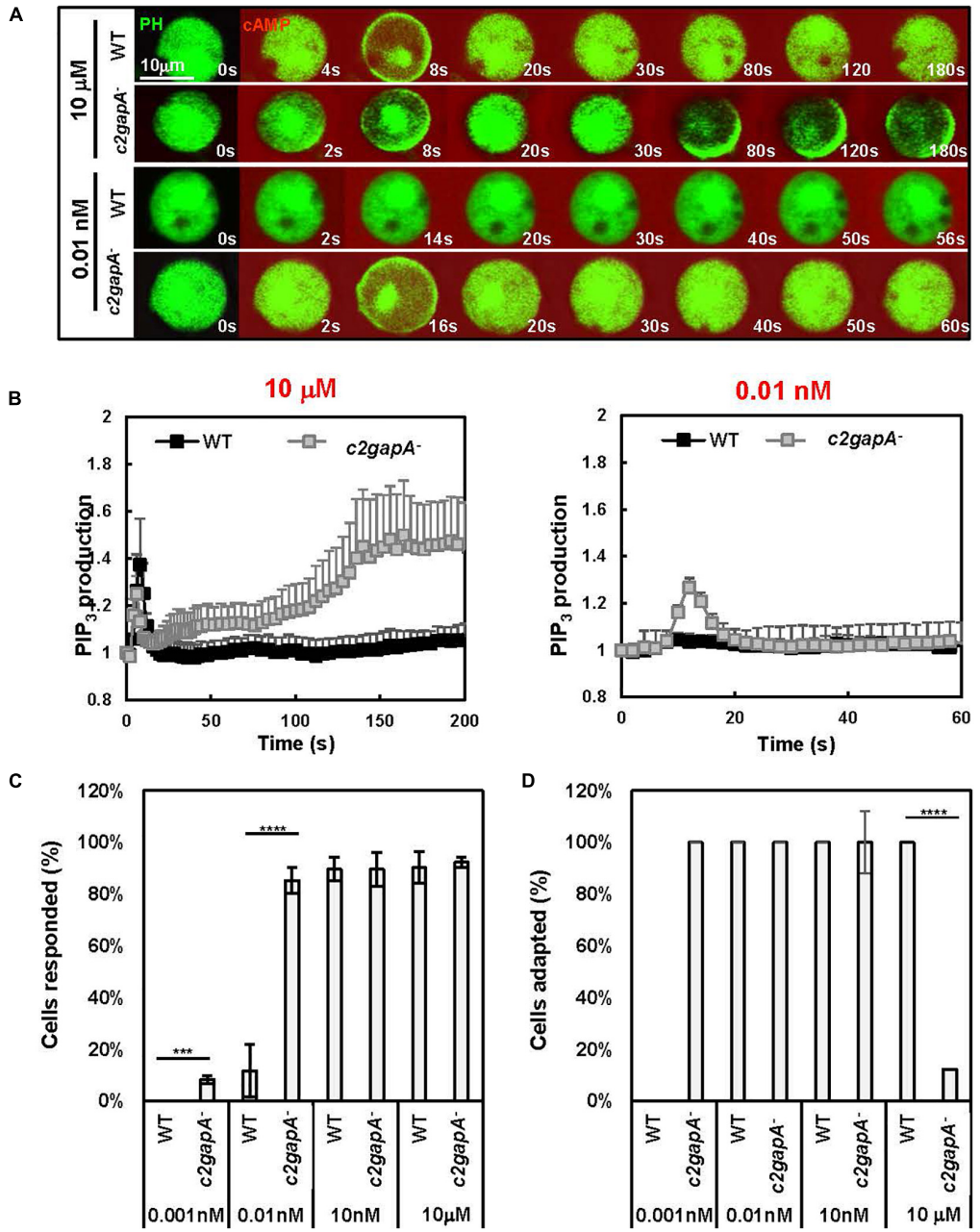

FIGURE 3 | *c2gapA*$^{-}$ cells are more sensitive to the stimuli at low concentrations and fail to adapt to the stimuli at high concentrations. **(A)** Montage shows cell response as PIP_3 production monitored through the membrane translocation of the PIP_3 probe PH_{Crac}-GFP, in WT or *c2gapA*$^{-}$ cells. Cells were stimulated with either 0.01 nM or 10 μM Sp-cAMPS, respectively. Also see **Supplementary Videos 3, 4** for cell response to 10 μM or 0.01 nM Sp-cAMPS stimulation, respectively. **(B)** Quantitative measurement of PIP3 production in WT and *c2gapA*$^{-}$ in response to 10 μM or 0.01 nM Sp-cAMP stimulation shown in **(C)**. PIP3 production was quantified by the decrease in the cytosolic intensity of PH_{Crac}-GFP. The cytosolic intensity at time 0 s was normalized to 1. Mean ± SD is shown; n = 8 and 12, or 8 and 11 for WT, *c2gapA*$^{-}$ cells in response to 10 μM or 0.01 nM Sp-cAMPS stimulation, respectively. **(C)** Percentage (%) of cells displaying response to 0.001 nM,0.01 nM, 10 nM, and 10 μM Sp-cAMPS stimulation in WT and *c2gapA*$^{-}$ cells, respectively. The same three independent experiments were used to calculate for **(C,D)**. Student's t-test was used to calculate the p-value, which is indicated as *** ($p < 0.001$) and **** ($p < 0.0001$). **(D)** Percentage (%) of cells failing to display adaptation to 0.001, 0.01, 10 nM, and 10 μM cAMP stimulation in WT and *c2gapA*$^{-}$ cells.

display defective chemotaxis in high-concentration gradients but improved chemotaxis in low- or subsensitive-concentration gradients. The above result indicates that WT cells chemotaxed efficiently through gradients of various chemoattractants ranging from 10^{-9} to 10^{-6} M, while *c2gapA*$^{-}$ cells did so from 10^{-10} to 10^{-7} M. In other words, the concentration range of cAMP gradients in which cells chemotax efficiently is upshifted in *c2gapA*$^{-}$ cells.

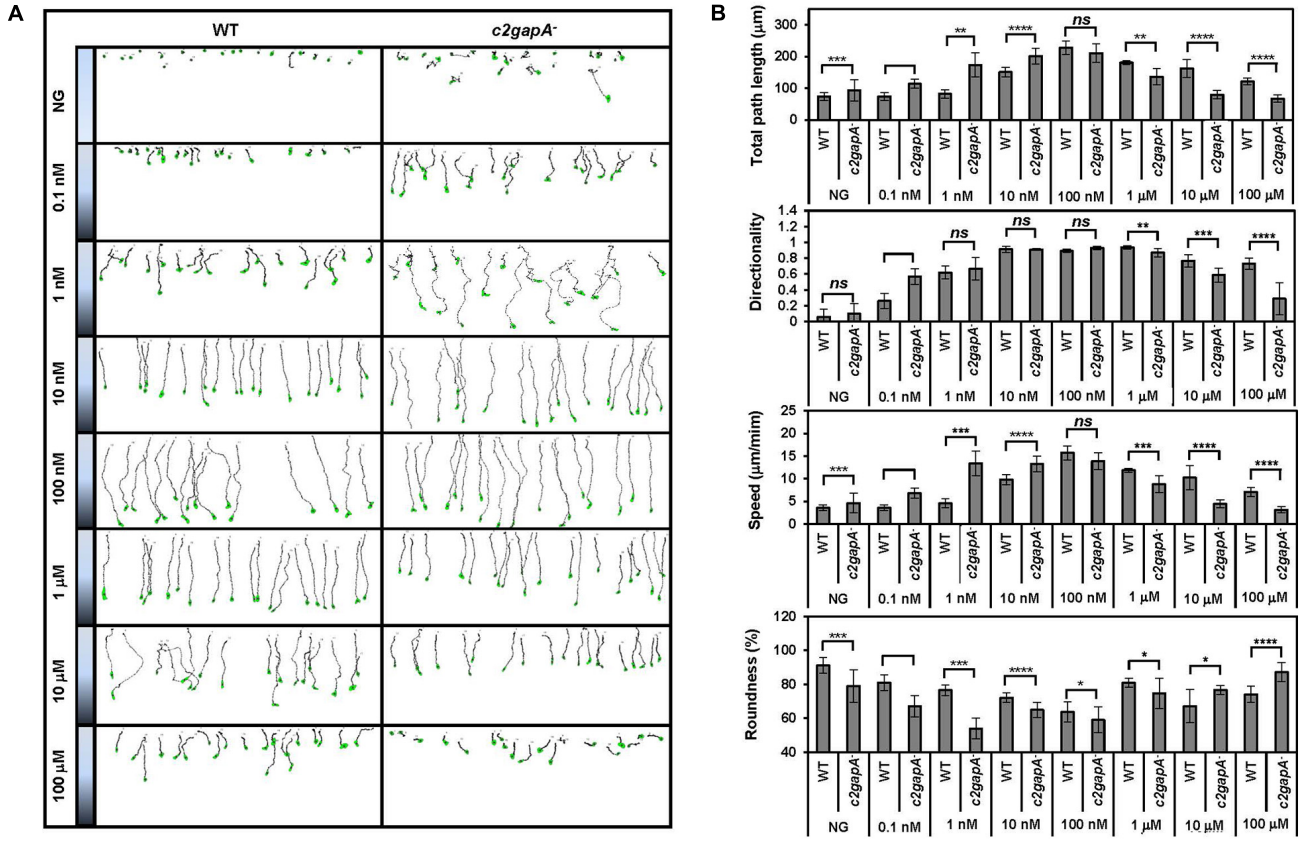

FIGURE 4 | The concentration range of cAMP gradients in which cells chemotax efficiently is upshifted in *c2gapA*$^{-}$ cells. **(A)** Montages show the traveling path of chemotaxing WT or *c2gapA*$^{-}$ cells in response to gradients generated from a cAMP source at wide-range concentrations. Also see **Supplementary Video 5**. **(B)** Chemotaxis behaviors measured from **(A)** are described by four parameters: directionality, specifically "upward" directionality, where 0 represents random movement and 1 represents straight movement toward the gradient; speed, defined as the distance that the centroid of the cell moves as a function of time; total path length, the total distance the cell has traveled; and roundness (%) for polarization, which is calculated as the ratio of the width to the length of the cell. Thus, a circle (no polarization) is 1 and a line (perfect polarization) is 0. Twenty-five cells in each group were measured for 6.25 min. The mean ± SD is shown. The *p*-values of Student's *t*-test are indicated as *ns* (not significant, $p > 0.1$), * ($p < 0.1$), ** ($p < 0.01$), *** ($p < 0.001$), or **** ($p < 0.0001$).

DISCUSSION

An amazing feature of eukaryotic cells is that they sense chemoattractants over an enormous concentration range. We have previously shown that C2GAP1 mediates cAMP receptor cAR1-mediated adaptation. Here, we reveal the molecular mechanism of C2GAP1 membrane targeting by which C2GAP1 controls both GPCR-mediated adaptation and the sensitivity of a cell. More importantly, we show that C2GAP1 allows *Dictyostelium* cells to sense chemoattractant at a higher concentration range through membrane targeting by lowering cell sensitivity and GPCR-mediated adaptation.

Calcium is involved in C2GAP1 membrane targeting. C2GAP1 has a calcium binding domain (C2 domain) that is often required for membrane targeting of the host proteins. In contrast to several other C2 domains, which require calcium binding for their membrane translocation (Damer and Creutz, 1994; Ilacqua et al., 2018), we found a decreased membrane localization of C2GAP1 in the presence of high [Ca^{2+}] (**Figure 1A**). Consistent with the above result, *iplA*$^{-}$ cells without [Ca^{2+}] increase in response to cAMP stimulation, displayed an increased, prolonged membrane translocation of C2GAP1-YFP, while *cbpG*$^{-}$ cells with higher basal [Ca^{2+}] and stronger, quicker peaking [Ca^{2+}] upon cAMP stimulation exhibited little membrane translocation of C2GAP1, instead, more further withdrawal of C2GAP1 from the plasma membrane to the cytoplasm in response to cAMP stimulation (**Figures 1C–E**; Wilczynska et al., 2005; Fisher and Wilczynska, 2006). An intracellular calcium gradient that was higher at the trailing edge of chemotaxing cells has been previously reported (Yumura et al., 1996). This spatial distribution of [Ca^{2+}] might reinforce the leading-front targeting of C2GAP1 in the chemotaxing cells. However, the role of calcium in chemotaxis has been under debate for the past two decades. Initially, chemoattractant-induced calcium influx was thought to play no role in chemotaxis. This conclusion comes from the following two facts: firstly, mouse *plcb2*$^{-/-}$*b3*$^{-/-}$ neutrophils without two major PLC isoforms, PLCβ2/β3, display impaired calcium influx yet show normal chemotaxis (Li et al., 2000); secondly, *Dictyostelium* cells lacking the IP_3 receptor (*iplA*$^{-}$) show no chemoattractant-induced Ca^{2+} response and

chemotax just like WT cells do (Traynor et al., 2000). Recent studies demonstrate the essential role of chemoattractant-induced PLCβ/γ activation and subsequent Ca^{2+} response in neutrophil chemotaxis (Tang et al., 2011; Xu et al., 2015). More importantly, the chemotaxis assays in both studies in *Dictyostelium* gradients generated from 100 nM cAMP sources, in which we observed little difference in chemotaxis behavior between WT and *c2gapA*$^-$ cells (**Figure 3**). Importantly, we observed more membrane localization of C2GAP1-YFP in resting *cbpG*$^-$ cells that might be resulted from a higher basal [Ca^{2+}] in the cells. Agreeing with the increased localization of C2GAP1 and subsequent downregulation of Ras/Rap1 function, *cbpG*$^-$ cells display decreased adhesion and cell migration (Park et al., 2018). It is important to investigate the chemotaxis behavior of cells lacking mediators of calcium signaling, such as *iplA*$^-$ and *cbpG*$^-$ cells, in response to gradients of different concentrations.

Little connection has been made between GPCR-mediated adaptation and the basal activity of a cell. Interestingly, *Dictyostelium* cells lacking RasGAPs often display higher basal Ras activity (Zhang et al., 2008; Bloomfield et al., 2015; Xu et al., 2017), indicating that the regulation of basal Ras activity through RasGAPs might be a common mechanism in *Dictyostelium*. Recently, it has been shown that active Ras plays a role in cell locomotion and in chemotaxis through very shallow gradients (van Haastert et al., 2017). Thus, we examined the chemotaxis behavior of WT and *c2gapA*$^-$ cells in response to a cAMP gradient over a large concentration range (10^{-10}–10^{-4} M) (**Figure 3**) and found that in WT cells chemotaxed better than *c2gapA*$^-$ cells did in gradients at high concentrations (>100 nM), while they displayed chemotaxis capability similar to that of *c2gapA*$^-$ cells gradients at mid-concentration range (10 nM of cAMP). In gradients at low concentrations (<1 nM), *c2gapA*$^-$ cells chemotaxed better than WT cells did, indicating a higher sensitivity of *c2gapA*$^-$ cells. We further confirmed that the increased sensitivity of *c2gapA*$^-$ cells is independent of F-actin (**Figure 4**). Importantly, human neutrophils lacking CAPRI, a RasGAP protein that controls Ras adaptation in GPCR-mediated chemotaxis, are more sensitive to chemoattractant gradients and sense gradients with a lower concentration range (Xuehua et al., 2020). In conclusion, membrane targeting of Ras inhibitors allows both human neutrophils and *D. discoideum* to sense chemoattractant gradients at a higher concentration range. These findings suggest that locally recruiting a Ras inhibitor of gradient sensing and chemotaxis for sensing an enormous concentration range of chemoattractants is an evolutionarily conserved mechanism.

MATERIALS AND METHODS

Cell Lines, Cell Growth, and Differentiation

AX2 cells are the parent, WT cell line for *c2gapA*$^-$ cells. *iplA*$^-$ cells were from *Dictybase.org*. *cbpG*$^-$ cells were from Park et al. (2018). Cells expressing the protein of interest were selected by growth in the presence of 20 μg/ml geneticin (Sigma, Steinheim, Germany) or 10 μg/ml blasticidin S, and/or hygromycin (Sigma, Steinheim, Germany) with the requirement of double selection. For differentiation, log-phase vegetative cells were harvested from shaking culture (5×10^6 cells/ml) and washed twice with developmental buffer (DB: 5 mM Na_2HPO_4, 5 mM KH_2PO_4, 2 mM $MgSO_4$, and 0.2 mM $CaCl_2$). Cells were resuspended at 2×10^7 cells/ml in shaking flask at 100 rpm, and allowed to differentiate with 75 nM adenosine 3′:5′-cyclic monophosphate (cAMP) (Sigma Aldrich, St. Louis, MO) pulses at 6 min intervals for 5–7 h or longer to obtain chemotactic cells. Differentiated cells were diluted to 1×10^7 cells/ml in DB buffer with 2.5 mM caffeine and shaken at 200 rpm for 15 min.

Plasmids

The YC-nano15 vector was obtained from Catherine Pears (Horikawa et al., 2010). PH_{Crac}-RFP and C2GAP1-R616A-GFP were from AK, University of Groningen, Netherlands.

Imaging and Data Processing

Differentiated cells (5×10^4) in DB buffer with 2.5 mM caffeine were plated and allowed to adhere to the cover glass of a 4-well or a 1-well chamber (Nalge Nunc International, Naperville, IL) for 10 min, and then covered with DB buffer for the live cell imaging experiment. If necessary, cells were treated with 5.0 μM Latrunculin B (Molecular Probes, Eugene, OR) for 10 min prior to the experiments. Cells were imaged using a Carl Zeiss Laser Scanning Microscope Zen 780 (Carl Zeiss, Thornwood, NY) with a 40x/NA 1.4 Oil DIC Plan-Apochromatic objective. Images were processed and analyzed by Zen 780 software. Images were further processed in Adobe Photoshop (Adobe Systems, San Jose, CA), and the intensity of the ROI (region of interest) was explored and analyzed with Microsoft Office Excel (Redmond, WA). To measure the membrane translocation of the indicated protein, we first measured the intensity change of the cytoplasm in response to uniformly applied stimuli over time. To obtain the relative intensity change of each individual cell during the time lapse, we divided the cytosolic intensity at time 0 (I_0) by its intensity at given time (I_t); consequently, the relative intensity of any cells at time 0 became 1. To compensate for significant photobleaching that might occur with long-time acquisition, we also normalized the intensity relative to the photobleaching of the cells. Lastly, we calculated and presented the mean and standard deviation (Mean ± SD) of membrane translocation from more than five independent cells. To measure calcium response using the calcium sensor YC-nano15 with *D. discoideum cells* (Horikawa et al., 2010), we monitored FRET change by sensitized emission FRET measurement, a process previously reported in detail (Xu et al., 2016). The FRET signal change (Rt/R_0) is presented as a function of [Ca^{2+}] using Zen Software provided by Carl Zeiss Zen 780 software.

Immunoprecipitation Assay

Cells were differentiated, washed with PM buffer (5 mM Na2PO4, 5 mM KH2PO4, and 2 mM MgSO4) with 2.5 mM caffeine, resuspended to 8×10^7 cells per ml in same PM buffer, and kept on ice before assay. If necessary, the cells were stimulated with 10 μM cAMP. 0.5 ml aliquots of cells at indicated time points were lysed with 10 ml immunoprecipitation buffer (IB,

20 mM Tris, pH8.0, 20 mM $MgCl_2$, 10% glycerol, 2 mM Na_3VO_4, 0.25% NP40, and complete 1 × EDTA-free proteinase inhibitor) for 30 min on ice. Cell extracts were centrifuged at 16,000 × *g* for 10 min at 4°C. Supernatant fractions were collected and incubated with 25 μl anti-GFP agarose beads at 4°C for 2 h. Beads were washed four times with immunoprecipitation buffer and proteins were eluted by boiling the beads in 50 μl SDS sample buffer. A second set of aliquots of the cells at each time point was taken for the assessment of total Ras protein in the sample. The indicated proteins were detected by Western blotting using specific antibodies.

PIP Strip Assay

Cells were suspended with PM buffer and run through a filter system with 5 μm pores. The lysed cells were centrifuged at 16,000 rpm for one min. The supernatants were immediately mixed with immunoprecipitation buffer (IB, 20 mM Tris, pH8.0, 20 mM $MgCl_2$, 10% glycerol, 2 mM Na_3VO_4, 0.25% NP40, and complete 1 × EDTA-free proteinase inhibitor) pre-cooled on ice. PIP-strip membranes were incubated with the mixtures obtained from the above at 4°C for 2 h and washed using IB buffer and then subject to western blot detection of the indicated proteins.

EZ-TAXIScan Chemotaxis Assay and Data Analysis

The procedure was as previously reported (Wen et al., 2016). Briefly, differentiated cells were loaded onto one side of a 4-μm EZ-TAXIScan chamber. The chemoattractants at the indicated concentrations were added to the other side of the well across the terrace to generate a linear gradient which the cells chemotax through. The traveled distance is the traveled length (μm). The length of the terrace is the total length of the gradient generated (260 μm). The chemoattractant concentration of gradient (C) a cell experienced at each given position depends on both the concentration of the fMLP source (C_{source}) and the ratio of the distance the cell traveled from no gradient (the traveled length) to the total distance to the cAMP source (the total length). In other words, $C = C_{source} \times$ ratio of the traveled length to the total length). The cells migrated for 30 min at room temperature. Images were taken for 30 min at 15 s intervals. For chemotaxis parameter measurements, 25 cells in each group were analyzed with DIAS software (Wessels et al., 1998). Chemotaxis behaviors are measured as four parameters: directionality, specifically "upward" directionality, where 0 represents random movement and 1 represents straight movement toward the gradient; speed, defined as the distance that the centroid of the cell moves as a function of time; total path length, which is the total distance the cell has traveled; and roundness (%) for polarization, which is calculated as the ratio of the width to the length of the cell. Thus, a circle (no polarization) is 1 and a line (perfect polarization) is 0. Student's *t*-test was used to calculate the *p*-values. The bar graphs of chemotaxis parameters in mean ± SD were plotted with Microsoft Office Excel (Redmond, WA) or shown directly in the table.

DATA AVAILABILITY STATEMENT

The original contributions presented in the study are included in the article/**Supplementary Material**, further inquiries can be directed to the corresponding author/s.

AUTHOR CONTRIBUTIONS

XX designed the research. XX, SB, HP, and XW performed the research and analyzed the data. XX, AK, TJe, and TJi wrote the manuscript. All authors contributed to the article and approved the submitted version.

FUNDING

This work was supported by the intramural fund of the National Institute of Allergy and Infectious Diseases, National Institutes of Health.

SUPPLEMENTARY MATERIAL

The Supplementary Material for this article can be found online at: https://www.frontiersin.org/articles/10.3389/fcell.2021.725073/full#supplementary-material

REFERENCES

Bloomfield, G., Traynor, D., Sander, S. P., Veltman, D. M., Pachebat, J. A., and Kay, R. R. (2015). Neurofibromin controls macropinocytosis and phagocytosis in *Dictyostelium*. *eLife* 4:e04940. doi: 10.7554/eLife.04940

Corbalan-Garcia, S., and Gomez-Fernandez, J. C. (2014). Signaling through C2 domains: more than one lipid target. *Biochim. Biophys. Acta* 1838, 1536–1547. doi: 10.1016/j.bbamem.2014.01.008

Damer, C. K., and Creutz, C. E. (1994). Synergistic membrane interactions of the two C2 domains of synaptotagmin. *J. Biol. Chem.* 269, 31115–31123.

Fisher, P. R., and Wilczynska, Z. (2006). Contribution of endoplasmic reticulum to Ca(2+) signals in *Dictyostelium* depends on extracellular Ca(2+). *FEMS Microbiol. Lett.* 257, 268–277. doi: 10.1111/j.1574-6968.2006.00180.x

Hoeller, O., Gong, D., and Weiner, O. D. (2014). How to understand and outwit adaptation. *Dev. Cell* 28, 607–616. doi: 10.1016/j.devcel.2014.03.009

Horikawa, K., Yamada, Y., Matsuda, T., Kobayashi, K., Hashimoto, M., Matsuura, T., et al. (2010). Spontaneous network activity visualized by ultrasensitive Ca(2+) indicators, yellow Cameleon-Nano. *Nat. Methods* 7, 729–732. doi: 10.1038/nmeth.1488

Ilacqua, A. N., Price, J. E., Graham, B. N., Buccilli, M. J., McKellar, D. R., and Damer, C. K. (2018). Cyclic AMP signaling in *Dictyostelium* promotes the translocation of the copine family of calcium-binding proteins to the plasma membrane. *BMC Cell Biol.* 19:13. doi: 10.1186/s12860-018-0160-5

Insall, R. H., Borleis, J., and Devreotes, P. N. (1996). The aimless RasGEF is required for processing of chemotactic signals through G-protein-coupled receptors in *Dictyostelium*. *Curr. Biol.* 6, 719–729.

Janetopoulos, C., Jin, T., and Devreotes, P. (2001). Receptor-mediated activation of heterotrimeric G-proteins in living cells. *Science* 291, 2408–2411. doi: 10.1126/science.1055835

Li, X., Edwards, M., Swaney, K. F., Singh, N., Bhattacharya, S., Borleis, J., et al. (2018). Mutually inhibitory Ras-PI(3,4)P2 feedback loops mediate cell

migration. *Proc. Natl. Acad. Sci. U.S.A.* 115, E9125–E9134. doi: 10.1073/pnas.1809039115

Li, Z., Jiang, H., Xie, W., Zhang, Z., Smrcka, A. V., and Wu, D. (2000). Roles of PLC-beta2 and -beta3 and PI3Kgamma in chemoattractant-mediated signal transduction. *Science* 287, 1046–1049.

Miao, Y., Bhattacharya, S., Edwards, M., Cai, H., Inoue, T., Iglesias, P. A., et al. (2017). Altering the threshold of an excitable signal transduction network changes cell migratory modes. *Nat. Cell Biol.* 19, 329–340. doi: 10.1038/ncb3495

Nalefski, E. A., and Falke, J. J. (1996). The C2 domain calcium-binding motif: structural and functional diversity. *Protein Sci.* 5, 2375–2390. doi: 10.1002/pro.5560051201

Park, B., Shin, D. Y., and Jeon, T. J. (2018). CBP7 interferes with the multicellular development of *Dictyostelium* cells by inhibiting chemoattractant-mediated cell aggregation. *Mol. Cells* 41, 103–109. doi: 10.14348/molcells.2018.2170

Sakamoto, H., Nishio, K., Tomisako, M., Kuwayama, H., Tanaka, Y., Suetake, I., et al. (2003). Identification and characterization of novel calcium-binding proteins of *Dictyostelium* and their spatial expression patterns during development. *Dev. Growth Differ.* 45, 507–514. doi: 10.1111/j.1440-169x.2003.00718.x

Sasaki, A. T., Chun, C., Takeda, K., and Firtel, R. A. (2004). Localized Ras signaling at the leading edge regulates PI3K, cell polarity, and directional cell movement. *J. Cell Biol.* 167, 505–518. doi: 10.1083/jcb.200406177

Suire, S., Lecureuil, C., Anderson, K. E., Damoulakis, G., Niewczas, I., Davidson, K., et al. (2012). GPCR activation of Ras and PI3Kc in neutrophils depends on PLCb2/b3 and the RasGEF RasGRP4. *EMBO J.* 31, 3118–3129. doi: 10.1038/emboj.2012.167

Tang, W., Zhang, Y., Xu, W., Harden, T. K., Sotraveled length tndek, J., Sun, L., et al. (2011). A PLCbeta/PI3Kgamma-GSK3 signaling pathway regulates cofilin phosphatase slingshot2 and neutrophil polarization and chemotaxis. *Dev. Cell* 21, 1038–1050. doi: 10.1016/j.devcel.2011.10.023

Traynor, D., Milne, J. L., Insall, R. H., and Kay, R. R. (2000). Ca(2+) signalling is not required for chemotaxis in *Dictyostelium*. *EMBO J.* 19, 4846–4854. doi: 10.1093/emboj/19.17.4846

van Haastert, P. J., Keizer-Gunnink, I., and Kortholt, A. (2017). Coupled excitable Ras and F-actin activation mediates spontaneous pseudopod formation and directed cell movement. *Mol. Biol. Cell* 28, 922–934. doi: 10.1091/mbc.E16-10-0733

Wang, M. J., Artemenko, Y., Cai, W. J., Iglesias, P., and Devreotes, A. P. N. (2014). The directional response of chemotactic cells depends on a balance between cytoskeletal architecture and the external gradient. *Cell Rep.* 9, 1110–1121. doi: 10.1016/j.celrep.2014.09.047

Wen, X., Jin, T., and Xu, X. (2016). Imaging G protein-coupled receptor-mediated chemotaxis and its signaling events in neutrophil-like HL60 Cells. *J. Vis. Exp.* 115:54511. doi: 10.3791/54511

Wessels, D., Voss, E., Von Bergen, N., Burns, R., Stites, J., and Soll, D. R. (1998). A computer-assisted system for reconstructing and interpreting the dynamic three-dimensional relationships of the outer surface, nucleus and pseudopods of crawling cells. *Cell. Motil. Cytoskeleton* 41, 225–246.

Wilczynska, Z., Happle, K., Müller-Taubenberger, A., Schlatterer, C., Malchow, D., and Fisher, P. R. (2005). Release of Ca^{2+} from the endoplasmic reticulum contributes to Ca^{2+} signaling in *Dictyostelium discoideum*. *Eukaryot. Cell* 4, 1513–1525. doi: 10.1128/ec.4.9.1513-1525.2005

Xu, X., Gera, N., Li, H., Yun, M., Zhang, L., Wang, Y., et al. (2015). GPCR-mediated PLCbetagamma/PKCbeta/PKD signaling pathway regulates the cofilin phosphatase slingshot 2 in neutrophil chemotaxis. *Mol. Biol. Cell* 26, 874–886. doi: 10.1091/mbc.E14-05-0982

Xu, X., Wen, X., Veltman, D. M., Keizer-Gunnink, I., Pots, H., Kortholt, A., et al. (2017). GPCR-controlled membrane recruitment of negative regulator C2GAP1 locally inhibits Ras signaling for adaptation and long-range chemotaxis. *Proc. Natl. Acad. Sci. U.S.A.* 114, E10092–E10101. doi: 10.1073/pnas.1703208114

Xu, X., Yun, M., Wen, X., Brzostowski, J., Quan, W., Wang, Q. J., et al. (2016). Quantitative monitoring spatiotemporal activation of Ras and PKD1 using confocal fluorescent microscopy. *Methods Mol. Biol.* 1407, 307–323. doi: 10.1007/978-1-4939-3480-5_22

Xuehua, X., Wen, X., Moosa, A., Bhimani, S., and Jin, T. (2020). Inhibitor CAPRI enables neutrophils to chemotax through a higher-concentration range of gradients. *bioRxiv* [Preprint]. doi: 10.1101/2020.04.23.058131

Yumura, S., Furuya, K., and Takeuchi, I. (1996). Intracellular free calcium responses during chemotaxis of *Dictyostelium* cells. *J. Cell Sci.* 109(Pt 11), 2673–2678.

Zhang, P., Wang, Y., Sesaki, H., and Iijima, M. (2010). Proteomic identification of phosphatidylinositol (3,4,5) triphosphate-binding proteins in *Dictyostelium discoideum*. *Proc. Natl. Acad. Sci. U.S.A.* 107, 11829–11834. doi: 10.1073/pnas.1006153107

Zhang, S., Charest, P., and Firtel, G. R. A. (2008). Spatiotemporal regulation of Ras activity provides directional sensing. *Curr. Biol.* 18, 1587–1593. doi: 10.1016/j.cub.2008.08.069

Zheng, L., Eckerdal, J., Dimitrijevic, I., and Andersson, T. (1997). Chemotactic peptide-induced activation of Ras in human neutrophils is associated with inhibition of p120-GAP activity. *J. Biol. Chem.* 272, 23448–23454.

Conflict of Interest: The authors declare that the research was conducted in the absence of any commercial or financial relationships that could be construed as a potential conflict of interest.

Publisher's Note: All claims expressed in this article are solely those of the authors and do not necessarily represent those of their affiliated organizations, or those of the publisher, the editors and the reviewers. Any product that may be evaluated in this article, or claim that may be made by its manufacturer, is not guaranteed or endorsed by the publisher.

Copyright © 2021 Xu, Bhimani, Pots, Wen, Jeon, Kortholt and Jin. This is an open-access article distributed under the terms of the Creative Commons Attribution License (CC BY). The use, distribution or reproduction in other forums is permitted, provided the original author(s) and the copyright owner(s) are credited and that the original publication in this journal is cited, in accordance with accepted academic practice. No use, distribution or reproduction is permitted which does not comply with these terms.

frontiers in Cell and Developmental Biology

REVIEW
published: 03 August 2021
doi: 10.3389/fcell.2021.724797

Different Heterotrimeric G Protein Dynamics for Wide-Range Chemotaxis in Eukaryotic Cells

Yoichiro Kamimura[1,2]* *and Masahiro Ueda*[1,2]*

[1] *Laboratory for Cell Signaling Dynamics, RIKEN, Center for Biosystems Dynamics Research (BDR), Suita, Japan,*
[2] *Laboratory of Single Molecule Biology, Graduate School of Frontier Biosciences, Osaka University, Suita, Japan*

Chemotaxis describes directional motility along ambient chemical gradients and has important roles in human physiology and pathology. Typical chemotactic cells, such as neutrophils and *Dictyostelium* cells, can detect spatial differences in chemical gradients over a background concentration of a 10^5 scale. Studies of *Dictyostelium* cells have elucidated the molecular mechanisms of gradient sensing involving G protein coupled receptor (GPCR) signaling. GPCR transduces spatial information through its cognate heterotrimeric G protein as a guanine nucleotide change factor (GEF). More recently, studies have revealed unconventional regulation of heterotrimeric G protein in the gradient sensing. In this review, we explain how multiple mechanisms of GPCR signaling ensure the broad range sensing of chemical gradients in *Dictyostelium* cells as a model for eukaryotic chemotaxis.

Keywords: chemotaxis, GPCR signaling, heterotrimeric G protein, gradient sensing, dynamic range

OPEN ACCESS

Edited by:
Robert Joseph Huber,
Trent University, Canada

Reviewed by:
Xuehua Xu,
National Institute of Allergy and Infectious Diseases, National Institutes of Health (NIH), United States
Carole Parent,
University of Michigan, United States

***Correspondence:**
Yoichiro Kamimura
ykamimur@riken.jp
Masahiro Ueda
masahiroueda@fbs.osaka-u.ac.jp

Specialty section:
This article was submitted to Molecular and Cellular Pathology, a section of the journal Frontiers in Cell and Developmental Biology

Received: *14 June 2021*
Accepted: *13 July 2021*
Published: *03 August 2021*

Citation:
Kamimura Y and Ueda M (2021) Different Heterotrimeric G Protein Dynamics for Wide-Range Chemotaxis in Eukaryotic Cells. Front. Cell Dev. Biol. 9:724797. doi: 10.3389/fcell.2021.724797

INTRODUCTION

Chemotaxis describes the directional migration of cells in response to chemical gradients. It is required for many essential physiological processes including early embryogenesis, wound healing, immune responses (Sonnemann and Bement, 2011; Trepat et al., 2012; Nourshargh and Alon, 2014; de Oliveira et al., 2016; Shellard and Mayor, 2016; Norden and Lecaudey, 2019) and more. Conversely, aberrations of chemotaxis result in various pathological conditions, such as autoimmune diseases and cancer metastasis (Stuelten et al., 2018). *Dictyostelium discoideum* cells as well as their evolutionally distant cells, mammalian neutrophils, are common model systems for the study of chemotaxis mechanisms (Artemenko et al., 2014; Thomas et al., 2018). These cells move fast, a phenomenon known as amoeboid movement. The movement is propelled by the protrusion of plasma membrane filled with filamentous actin (f-actin), which leads to the structure known as the pseudopod. Cells spontaneously form pseudopods during random motility. However, chemical cues bias pseudopod formation to the front of the cells, which is defined as the membrane portion facing the higher concentration. The back of the cells ensures the directional motility by producing contractile forces from the action of myosin II on cortical f-actin. Therefore, cells have morphological anisotropy or polarity during chemotaxis. Eukaryotic chemotactic cells can decipher ambient chemical gradients by spatial sensing, whereas bacteria use temporal sensing (Parent and Devreotes, 1999; Tu and Rappel, 2018). Indeed, *D. discoideum* cells treated with latrunculin, an inhibitor of actin polymerization, only activate signaling molecules at their front side (Parent et al., 1998).

D. discoideum cells use chemotaxis in their lifecycle; for example, folate chemotaxis is used to forage for bacteria and chemotaxis to 3′,5′-cyclic adenosine monophosphate (cAMP), which

D. discoideum cells secrete upon starvation to make multicellular structures that finally reach fruiting bodies (Artemenko et al., 2014). Mammalian neutrophils are recruited to a wide range of signals including N-formyl peptides, CXC-chemokine ligand 8 (CXCL8), leukotriene B_4, and others (Nourshargh and Alon, 2014; de Oliveira et al., 2016). Furthermore, chemotaxis functions in very shallow gradients within broad ranges of background chemical concentrations. For example, *D. discoideum* cells can move in response to 2% cAMP gradients along their cellular length in a sub-μM to mM background concentration range (Mato et al., 1975; Fisher et al., 1989; Song et al., 2006; Ohtsuka et al., 2021). Similar quantitative properties have been observed in leukocyte chemotaxis (Zigmond, 1977). Chemical attractants associate with cognate receptors on the plasma membrane, triggering intracellular signal transduction, and the association simultaneously gives rise to receptor modifications (Hoeller et al., 2014; Tu and Rappel, 2018). Thereby, the receptors return to the pre-stimulated state in a process known as adaptation (Hoeller et al., 2014; Tu and Rappel, 2018). However, while true for bacteria, recent studies have shown chemotaxis mechanisms besides receptor adaptation are used by eukaryotic cells.

Studies on *D. discoideum* cells and neutrophils have formed a molecular framework for eukaryotic chemotaxis that is evolutionally conserved. G protein-coupled receptor (GPCR) signaling serves as a sensor of chemical gradients (Artemenko et al., 2014). The cAMP chemotactic signaling pathway of *D. discoideum* cells has been well-characterized and provides a general concept for how gradient information is processed to initiate directional motility (Swaney et al., 2010; Artemenko et al., 2014; Tang et al., 2014; Nichols et al., 2015). cAMP binds to cAMP receptor 1 (cAR1), a member of the GPCR family, to activate its cognate heterotrimeric G protein (G protein), making cAR1 a guanine exchange factor (GEF). The activation is transmitted to several redundant downstream pathways including phosphatidylinositol-3,4,5-trisphophate (PIP3), TorC2-PDK-PKB, 3',5'-cyclic guanosine monophosphate (cGMP), and phospholipase A2 (Pla2) signaling. PIP3 production and TorC2-PDK-PKB activity are mediated by the localized activation of RasG and RasC, respectively, at the front of the cells, resulting in pseudopod formation. The cGMP pathway regulates myosin II to generate contractile force at the back (Bosgraaf et al., 2005; Veltman and Van Haastert, 2007), while one recent report suggested an additional negative role of the cGMP pathway in the depolymerization of f-actin at the front (Tanabe et al., 2018). Importantly, each signaling pathway displays an intrinsic excitable property with the all-or-none response to a suprathreshold stimulus (Arai et al., 2010; Nishikawa et al., 2014; Fukushima et al., 2019; Li et al., 2020). In addition to excitability, PIP3 is produced in a bistable manner (Matsuoka and Ueda, 2018). Thus, shallow gradient signals can be amplified for a cell to output and sustain the constant activity of each signaling molecule at the front.

However, recent research on *D. discoideum* cells has indicated that additional G protein dynamics in response to cAR1 activation occur in chemotaxis. Here we describe these new dynamics after reviewing classical chemotaxis G protein signaling in *D. discoideum* cells as a model for eukaryotes.

Overview of cAMP Chemotactic GPCR Signaling

cAMP-induced chemotaxis is one of the most common experimental settings for studying chemotaxis and is a framework of the eukaryotic chemotaxis mechanism (Swaney et al., 2010; **Figure 1**; the major factors are summarized in **Table 1**). When environmental nutrients are depleted, solitary *D. discoideum* cells start the developmental process to make a multicellular structure. In early development, some cells produce cAMP, which is relayed to other cells through a process known as cAMP signal relay to make periodic cAMP propagating waves. The waves can guide about a hundred thousand cells into an aggregate via chemotaxis. During this aggregation, cells form migration streams in which they align their morphological directionality and attach to each other side by side. cAMP binds to a series of receptors, cAR1 – cAR4, with different affinities (Kim et al., 1996). cAR1 is the major receptor for cAMP chemotaxis in early development. It binds to cAMP with two different affinities: a high affinity of 3.5∼30 nM and a low affinity of 200∼500 nM (Van Haastert, 1984). It is known that cAR1 transduces signals in G protein-dependent and -independent manners. GPCR-independent events include extracellular calcium influx and Extracellular signal-regulated kinase 2 (Erk2) activation (Milne and Devreotes, 1993; Milne et al., 1995; Brzostowski and Kimmel, 2006). Erk2 has been associated with cAMP chemotaxis because of its role in folate chemotaxis (Nichols et al., 2019). The role of G protein, which is comprised of the subunits Gα2 and Gβγ, in cAMP chemotaxis is less controversial. There are twelve Gα subunits in *D. discoideum* cells, whereas Gβγ is encoded by a single gene. Gα2 is myristoylated at the N terminus, and Gγ is geranylgeranylated at the C terminus (Miyagawa et al., 2018). These lipid modifications ensure the localization of G proteins to the plasma membrane. cAR1 catalyzes a guanine exchange reaction of the α subunit of the Gα2-Gβγ complex. The GTP bound form of Gα2 forces the dissociation of Gβγ. The *Dictyostelium* homolog of Resistance to inhibitors of cholinesterase 8 (Ric8) was isolated as a binding protein to Gα and shown to facilitate a GEF-reaction of Gα independently of cAR1 (Kataria et al., 2013). Ric8-mediated G protein activation is especially required for chemotaxis at lower cAMP concentrations. The dissociated subunits transmit information of an ambient chemical gradient on the plasma membrane. Another Gα2 binding protein, GEF like protein B (GflB), serves as an effector of Gα2 to regulate the cytoskeleton through Ras and Rap1 (Liu et al., 2016). GflB is also a RacE-binding protein (Senoo et al., 2016). Furthermore, GflB coordinates the activities of Ras and Rho for proper gradient sensing. ElmoE binds to Gβγ and serves as a GEF for RacB with Dock-like proteins to form f-actin (Yan et al., 2012).

cAR1 undergoes multiple phosphorylations in the C terminus cytoplasmic region upon cAMP stimulation, although the corresponding kinase is still unknown (Hereld et al., 1994). The phosphorylation shifts the low cAMP binding affinity from ∼300 to 800 nM, suggesting that the chemotactic dynamic range moves toward lower concentrations (Caterina et al., 1995). This hypothesis was tested using a non-phosphorylatable mutant of cAR1. The mutant still showed chemotaxis even

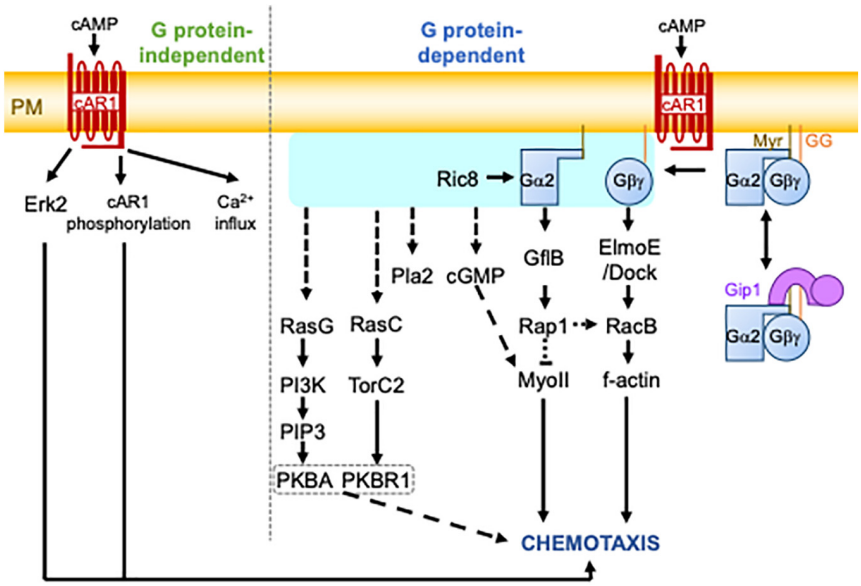

FIGURE 1 | The cAMP chemotactic signaling pathway in *D. discoideum* cells. Upon cAMP binding, the cAR1 receptor triggers heterotrimeric G protein-independent and -dependent pathways. The G protein-independent pathway involves Erk2 activation, cAR1 phosphorylation, and calcium (Ca^{2+}) influx. The G protein-dependent pathway involves the activation or dissociation of G proteins catalyzed by the GEF activity of cAR1. The activation of G proteins is shown by the light blue box. This is followed by the activation of several signaling molecules, finally leading to chemotaxis. It is still unknown how G protein activity is transmitted to some signaling molecules, including RasG, RasC, Pla2, and cGMP. G proteins are comprised of Gα2 and Gγ subunits, which are myristoylated (Myr) and geranylgeranylated (GG), respectively, for their plasma membrane localization. They undergo complex formation with Gip1 in the cytoplasm, which allows for the spatial regulation of G proteins. The dashed lines represent several or unknown steps.

TABLE 1 | GPCR signaling and its related factors in the cAMP chemotactic signaling pathway.

Gene (protein)	Gene ID (DDB number)	Molecular feature	Mammalian homolog
cARA (cAR1)	DDB_G0273397	GPCR	No cAR1 homologs but various GPCR serve for chemotaxis, e.g., formyl-peptide receptor and CXCL8 receptor
gpaB (Gα2)	DDB_G0276267	Heterotrimeric G protein α subunit	Gαi
gpbA (Gβ)	DDB_G0277143	Heterotrimeric G protein βγ subunit	Gβ
gpgA (Gγ)	DDB_G0274125	Heterotrimeric G protein βγ subunit	Gγ
adcB (AdcB)	DDB_G0274395	Arrestin	β-arrestin
adcC (AdcC)	DDB_G0271022	Arrestin	β-arrestin
ric8 (Ric8)	DDB_G0292036	Non-receptor GEF	Ric8
gipA (Gip1)	DDB_G0271086	G protein shuttling factor	TNFAIP8 family proteins
gflB (GflB)	DDB_G0286773	Gα2 binding factor, RapGEF, RasGEF, RhoGAP	
elmoE (ElmoE)	DDB_G0279657	Gβγ binding factor, RacGEF as the Elmo/Dock complex	ELMO1

in higher concentration ranges, though the efficiency was reduced (Kim et al., 1997). Thus, phosphorylation could be required for attenuating the cAMP signal pathway, such as adenylyl cyclase and Erk2 activities, and for secondary actin polymerization (Brzostowski et al., 2013). In mammalian cells, phosphorylated cytoplasmic residues of GPCR recruit Arrestin, which competes with G protein dependent signaling, leading to internalization. *D. discoideum* has six genes, *adcA-F*, which encode arrestin domain-containing protein. AdcB and AdcC have redundant functions in the early development (Cao et al., 2014). AdcC associates with cAR1, the phosphorylation of which increases the efficiency of the association. AdcB and AdcC are required for cAR1 internalization under high cAMP concentrations and longer times than in the effective ranges for chemotaxis at early development. Consistently, cells lacking AdcB and AdcC show normal chemotaxis. These results suggest that receptor internalization does not extend the chemotactic dynamic range.

D. discoideum cells can sense spatial information in cAMP gradients. Cells treated with latrunculin become round because of f-actin depletion. When such immotile cells are stimulated by cAMP gradients, downstream signaling, such as PIP3 production and Ras activation, are transiently activated along the entire membrane (Parent et al., 1998; Xu et al., 2005;

Kamimura et al., 2016). Subsequently, the activation is biased at the higher concentration side of the gradient. In the whole process, G proteins are persistently activated at different levels at the front and back of the cells (Xu et al., 2005). Therefore, G protein activity reflects the local concentration along the gradient.

cAR1 Activates Heterotrimeric G Protein Gα2-Gβγ

As described above, cAR1 activates heterotrimeric G protein through its GEF activity, in which Gα2 changes GDP to GTP and simultaneously dissociates from Gβγ. The activation has been visualized *in vivo* by fluorescence resonance energy transfer (FRET) experiments in which Gα2 and Gβ are fused to cyan and yellow fluorescent proteins, respectively (Janetopoulos et al., 2001). Before cAMP stimulation, the heterotrimeric form of Gα2-Gβγ showed FRET signals, but after the stimulation the FRET was lost, reflecting the dissociation into Gα2 and Gβγ. We recapitulated these results using a combination of Gα2-Cerulean and Gβ-Venus, the activation of which had an EC_{50} = 2.3 nM, finding G protein activation is saturated at a lower concentration than at which *D. discoideum* cells show chemotaxis (Miyanaga et al., 2018). The full activation of G proteins at lower cAMP concentrations was explained by a model in which ligand-bound receptors continuously activate G proteins (Xu et al., 2010).

Gip1-Mediated G Protein Translocation

G protein interacting protein 1 (Gip1) was identified as a binding protein of Gβγ by a biochemical tandem affinity purification experiment in *D. discoideum* cells (Kamimura et al., 2016). It has an N-terminal Pleckstrin-homology (PH) domain and C terminus that is weakly similar to mammalian tumor necrosis factor α induced protein 8 (TNFIP8). A deletion analysis showed that its C terminus is sufficient for binding to G proteins. However, its full-length, which includes the PH domain, is required for its physiological function based on rescue experiments of the early developmental phenotype. *gip1*Δ cells show small aggregates at early development upon starvation, whereas wild-type cells make streams by chemotaxis. Interestingly, *gip1*Δ cells lose chemotactic ability, especially at higher cAMP concentrations. G proteins localize in the cytosol as well as the plasma membrane in wild-type cells. In contrast, *gip1*Δ cells lose cytosolic G proteins but not membrane ones. These results indicate that G proteins shuttle between the plasma membrane and the cytosol, consistent with previous observations (Elzie et al., 2009). Cytosolic G proteins bind to Gip1. Moreover, cytosolic G proteins translocate to the plasma membrane upon cAMP stimulation in a Gip1-dependent manner, with an EC_{50} from the cytosol of 10 nM. The translocation still occurs without Ras activation, PIP3 production, or f-actin, suggesting unknown upstream signaling. The dynamic spatial regulation ensures the redistribution of G proteins at the plasma membrane along ambient cAMP gradients. This redistribution is required for gradient sensing at higher concentration ranges.

The crystal structure of the C terminus of Gip1 can help clarify the mechanism underlying its complex formation with G proteins (Miyagawa et al., 2018). The G protein binding region of Gip1 is composed of six α-helices which fold into a cylinder-like structure with a central hydrophobic cavity. The cavity is 22 Å in depth and 10 Å in diameter and includes glycerophospholipids derived from bacteria for Gip1 overproduction. Experiments on the binding site of G proteins have also been performed. Biochemical and genetic analyses revealed that the geranylgeranyl modification on Gγ is essential for the complex formation. This result suggests that the hydrophobic cavity of Gip1 accommodates the lipid modification of Gγ in the cytosol. Consistently, when steric hindrance is introduced into the cavity by replacing the amino acid residues making the cavity with tryptophan, the binding to G proteins deteriorates. Collectively, a model for G protein shuttling has been proposed. In the resting state, G proteins are not permanently anchored on the plasma membrane. Therefore, some detach from the membrane, resulting in cytosolic sequestration by interacting with Gip1. This interaction involves the hydrophobic cavity of Gip1 and the lipid modification of G proteins, stabilizing the complex in the hydrophilic environment of the cytosol. Chemoattractant signaling causes G proteins to dissociate from Gip1 by a plausible conformational change of the hydrophobic cavity. The N-terminal PH domain of Gip1 may regulate the configuration of the cavity upon cAMP stimulation.

Stable Complex Formation Between Activated Gα2 and cAR1 Receptor

We established a single molecular imaging technique to analyze the binding of fluorescently labeled cAMP to *D. discoideum* cells in chemotaxis (Ueda et al., 2001). This technique has since been applied to cAR1, Gα2, and Gγ to show their molecular dynamics upon cAMP stimulation (Miyanaga et al., 2018). These molecules were fluorescently labeled by tetramethylrhodamine (TMR) via HaloTag. TMR is a small organic fluorescent dye and shows a stronger signal and longer fluorescence longevity than fluorescent proteins, thus providing better data (Miyanaga et al., 2009). All molecules showed free diffusion despite their distinct diffusion coefficients. While cAR1-TMR has a single diffusion coefficient of 0.017 $\mu m^2/s$ in the absence of cAMP, Gα2-TMR and Gγ-TMR have two diffusion coefficients of 0.016 and 0.20 $\mu m^2/s$ and of 0.029 and 0.21 $\mu m^2/s$, respectively. When cells are stimulated with saturating cAMP concentration (10 μM), neither cAR1-TMR nor Gγ-TMR changed their motility, but the slower fraction of Gα2-TMR increased from 20 to 53%. A dose-dependent study revealed that the shift to the slower fraction had an EC_{50} of 270 nM. There are two points we want to highlight from these studies. First, the diffusion coefficients of cAR1-TMR and the slower fraction of Gα2-TMR are similar; and second, the EC_{50} of 270 nM matches the lower affinity of cAR1 receptors for cAMP. These findings indicate that activated Gα2 interacts with low-affinity cAR1 to make a stable complex and slows down in the plasma membrane.

To test this hypothesis, Gα2-TMR mobility was observed upon the external modulation of cAR1. Benomyl, an inhibitor of tubulin polymerization, is known to reduce cAR1 motility (de Keijzer et al., 2011). When cells were treated with benomyl, Gα2-TMR showed slowed cAMP-stimulated motility based on the

diffusion coefficient changing from 0.015 to 0.005 $\mu m^2/s$, which was concomitant with the decrease in the cAR1-TMR diffusion coefficient. In these experiments, cAR1 is tethered to a glass surface through biotin and avidin. Thus, cAMP stimulation slows the slower mobile fraction of Gα2-TMR such that the diffusion coefficient is almost the same as that of tethered cAR1, supporting the hypothesis. Additionally, experiments using a constitutively active form of Gα2 with a Q208L mutation revealed that the cAMP-stimulated slow mobile fraction includes the activated, or GTP-bound, form of Gα2, since this mutant also showed the shift to the slow mobile fraction.

The stable complex formation provides a mechanism for gradient sensing at higher concentration ranges (Miyanaga et al., 2018). Furthermore, single molecular analysis techniques can measure membrane binding lifetimes. The lifetime of Gα2-TMR prolongs after cAMP stimulation, but the lifetime of Gγ-TMR does not. When a cell is exposed to a steep gradient, the side facing the higher cAMP concentration has a longer lifetime with slower mobility than the side facing the lower concentration. This feature relates to the stable complex formation between low-affinity cAR1 receptors and activated Gα2, which has an extended lifetime. Thus, cAMP concentrations are affected by the generation of intracellular G protein gradients along cAMP gradients at higher concentration ranges.

Three Different G Protein Dynamics for Broad Range Chemotaxis

The quantitative characterization of chemotaxis has shown that *D. discoideum* cells detect a chemical gradient over broad ranges of average concentrations (Mato et al., 1975; Fisher et al., 1989; Song et al., 2006; Ohtsuka et al., 2021). Cells can move up cAMP gradients as small as sub-nM to as large as μM. How cAMP gradient information is converted into intracellular gradients for G protein signals is unknown, however. cAR1 receptors activate G proteins as GEF in cAMP gradients but saturate at a lower concentration than at which cells show chemotaxis (Janetopoulos et al., 2001; Miyanaga et al., 2018). Therefore, *D. discoideum* cells must rely on another mechanism to produce an intracellular gradient of G protein activity. High-affinity cAR1 can likely activate G proteins, as it has an EC_{50} that is comparable to high-affinity cAR1 for cAMP. However, the fraction of high-affinity cAR1 is estimated to be about 10% (Milne et al., 1997), meaning we still lack understanding for the other 90% of cAR1, which is low-affinity. Three distinct G-protein dynamics offer an explanation for wide-range chemotaxis (**Figure 2**). In the first, cAR1-catalyzed G protein activation occurs at an EC_{50} of 2.3 nM (Miyanaga et al., 2018). In this concentration range, high-affinity cAR1 produces biased G protein activity along the cAMP gradient. In the second, in increasing cAMP concentrations, Gip1-mediated G protein translocates with an EC_{50} of about 10 nM to recruit G proteins from the cytosol to the membrane (Kamimura et al., 2016; Miyanaga et al., 2018). The spatial regulation of G proteins facilitates their distribution along the cAMP gradient. If this distribution does not occur, which is the case in *gip1*Δ cells, chemotactic cells cannot discern the proper direction because the G protein activity is already saturated. In the third, further increases in cAMP concentration trigger the stable complex formation of activated Gα2 and cAR1 with an EC_{50} of 270 nM, which is similar to the Kd for low-affinity receptors (Van Haastert, 1984; Miyanaga et al., 2018). Therefore, at higher concentration ranges, low-affinity receptors provide cAMP gradient information to G proteins through physical interactions. Collectively, these three G protein dynamics mechanisms cover the whole chemotactic dynamic range, from the sub-nanomolar to several micromolar, of cAMP.

CONCLUSION AND FUTURE PERSPECTIVES

Broad range chemotaxis is important for the physiology of *Dictyostelium* cells and human cells; for example, starved *Dictyostelium* cells and mammalian neutrophils are efficiently recruited to the center of aggregates and to tissue damage or infection sites from the blood circulation, respectively. Although it was shown more than 30 years ago that chemotactic cells show directional movement over broad ranges, the mechanism has only been revealed in the past several years using *D. discoideum* cells as a model organism. Key findings include distinct G protein dynamics in response to distinct chemoattractant concentrations. How GPCR generally activates G protein by its GEF activity is well characterized (Weis and Kobilka, 2018). However, the intracellular spatial regulation of G proteins has received less attention. The identification of Gip1 in *D. discoideum* cells provides the molecular basis of the spatial regulation, but many questions remain (Kamimura et al., 2016; Miyagawa et al., 2018). How does Gip1 bind to the trimeric form of G proteins? Does the spontaneous dissociation of G proteins require any factors? What is the signaling molecule target for the PH domain of Gip1 to break the complex formation with G proteins? And, how are G proteins stabilized on the plasma membrane upon cAMP stimulation? Furthermore, it is unknown if the mechanisms for G protein dynamics is conserved in mammalian cells. Some evidence supports conservation. For example, G proteins shuttle between the plasma membrane and organelles in mammalian cells (Saini et al., 2009). Also, the binding region of Gip1 has homology with the mammalian TNFAIP8 family. TNFAIP8 proteins have a hydrophobic cavity like Gip1 and have been reported to participate in immunity and various diseases (Goldsmith et al., 2017; Niture et al., 2018; Zhang et al., 2018). Collectively, TNFAIP8 may regulate the spatial regulation of G proteins for the broad range chemotaxis of neutrophils. Another G protein dynamics found in *D. discoideum* cells by single molecular analysis is the stable complex formation mechanism (Miyanaga et al., 2018). Activated Gα2 but not the trimeric form of G proteins is responsible for this formation. The result indicates that the stable complex is formed by yet unidentified binding sites of Gα2 and cAR1. This mechanism has a unique feature in that the low-affinity fraction of cAR1 receptors provides the binding site for activated G proteins to make intracellular gradients. Given that GPCR signaling is conserved in eukaryotes, the same mechanism may serve in mammalian cells.

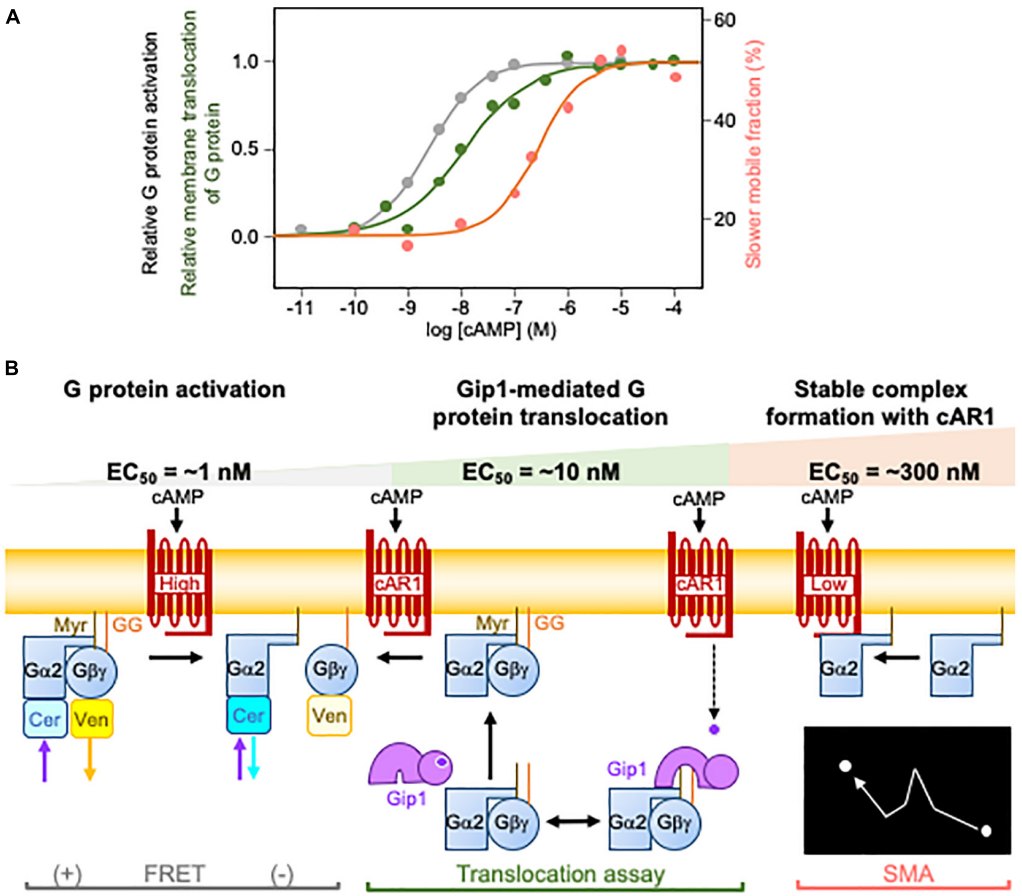

FIGURE 2 | Three different G protein dynamics for cAMP wide-range chemotaxis. **(A)** The three different G protein dynamics include G protein activation, Gip1-mediated G protein translocation, and a slower mobile fraction caused by the stable complex formation with cAR1. Each has a distinct EC_{50} shown in black, green, and red, respectively. **(B)** Schematic illustration of the three different G protein dynamics. G protein activation, Gip1-mediated G protein translocation, and the slower mobile fraction caused by the stable complex formation. Experimentally, they are assessed by fluorescence resonance energy transfer (FRET) between Gα2 with Cerulean (Cer) and Gβ with Venus (Ven), the translocation of G proteins upon cAMP stimulation, and single molecular imaging analysis (SMA), respectively.

Chemotaxis is comprised of many factors operating in a complex network for stable directional motility in fluctuating environments. To understand how this network conducts gradient sensing, several mathematical models have been proposed in *D. discoideum* cells, including Local Excitation and Global Inhibition (LEGI) (Parent and Devreotes, 1999; Iglesias and Devreotes, 2008). The three types of G protein dynamics described here have still not been incorporated into such models, however. For that, more quantitative parameters of G protein dynamics are needed. In addition to such G protein dynamics, cAR1 phosphorylation influences the chemotactic dynamic range (Kim et al., 1997), and the RasGAP C2GAP1 regulates the chemotactic range (Xu et al., 2017). These reactions should be included in models for the complete understanding of broad range chemotaxis.

Finally, studies on eukaryotic chemotaxis using *D. discoideum* cells as a model system have provided insights into the mechanism of not only broad dynamic range chemotaxis but also GPCR signaling. Especially, the spatial and temporal regulation of G proteins has been found in *D. discoideum* cells as a novel mechanism of GPCR signaling. However, more structural and biochemical analyses are required for complete understanding of the mechanism and its physiological significance. Such analyses could give way to new therapeutic targets for human diseases derived from compromised chemotaxis and more broadly advance GPCR-related biology.

AUTHOR CONTRIBUTIONS

YK and MU conceptualized the contents, revised the manuscript, and approved the submitted version. YK wrote the initial draft of the manuscript and prepared the figures. Both authors contributed to the article and approved the submitted version.

FUNDING

This study was partly supported by JSPS KAKENHI to YK (grant no. 20K06631) and MU (grant no. 19H00982).

REFERENCES

Arai, Y., Shibata, T., Matsuoka, S., Sato, M. J., Yanagida, T., and Ueda, M. (2010). Self-organization of the phosphatidylinositol lipids signaling for random cell migration. *Proc. Natl. Acad. Sci. U.S.A.* 107, 12399–12404. doi: 10.1073/pnas.0908278107

Artemenko, Y., Lampert, T. J., and Devreotes, P. N. (2014). Moving towards a paradigm: common mechanisms of chemotactic signaling in *Dictyostelium* and mammalian leukocytes. *Cell. Mol. Life Sci.* 71, 3711–3747. doi: 10.1007/s00018-014-1638-8

Bosgraaf, L., Waijer, A., Engel, R., Visser, A. J. W. G., Wessels, D., Soll, D., et al. (2005). RasGEF-containing proteins GbpC and GbpD have differential effects on cell polarity and chemotaxis in *Dictyostelium*. *J. Cell Sci.* 118, 1899–1910. doi: 10.1242/jcs.02317

Brzostowski, J. A., and Kimmel, A. R. (2006). Nonadaptive regulation of ERK2 in *Dictyostelium*: implications for mechanisms of cAMP relay. *Mol. Biol. Cell* 17, 4220–4227. doi: 10.1091/mbc.e06-05-0376

Brzostowski, J. A., Sawai, S., Rozov, O., Liao, X. H., Imoto, D., Parent, C. A., et al. (2013). Phosphorylation of chemoattractant receptors regulates chemotaxis, actin reorganization and signal relay. *J. Cell Sci.* 126, 4614–4626. doi: 10.1242/jcs.122952

Cao, X., Yan, J., Shu, S., Brzostowski, J. A., and Jin, T. (2014). Arrestins function in cAR1 GPCR-mediated signaling and cAR1 internalization in the development of *Dictyostelium discoideum*. *Mol. Biol. Cell* 25, 3210–3221. doi: 10.1091/mbc.E14-03-0834

Caterina, M. J., Devreotes, P. N., Borleis, J., and Hereld, D. (1995). Agonist-induced loss of ligand binding is correlated with phosphorylation of cAR1, a G protein-coupled chemoattractant receptor from *Dictyostelium*. *J. Biol. Chem.* 270, 8667–8672. doi: 10.1074/jbc.270.15.8667

de Keijzer, S., Galloway, J., Harms, G. S., Devreotes, P. N., and Iglesias, P. A. (2011). Disrupting microtubule network immobilizes amoeboid chemotactic receptor in the plasma membrane. *Biochim. Biophys. Acta* 1808, 1701–1708. doi: 10.1016/j.bbamem.2011.02.009

de Oliveira, S., Rosowski, E. E., and Huttenlocher, A. (2016). Neutrophil migration in infection and wound repair: going forward in reverse. *Nat. Rev. Immunol.* 16, 378–391. doi: 10.1038/nri.2016.49

Elzie, C. A., Colby, J., Sammons, M. A., and Janetopoulos, C. (2009). Dynamic localization of G proteins in *Dictyostelium discoideum*. *J. Cell Sci.* 122, 2597–2603. doi: 10.1242/jcs.046300

Fisher, P. R., Merkl, R., and Gerisch, G. (1989). Quantitative analysis of cell motility and chemotaxis in *Dictyostelium discoideum* by using an image processing system and a novel chemotaxis chamber providing stationary chemical gradients. *J. Cell Biol.* 108, 973–984. doi: 10.1083/jcb.108.3.973

Fukushima, S., Matsuoka, S., and Ueda, M. (2019). Excitable dynamics of Ras triggers spontaneous symmetry breaking of PIP3 signaling in motile cells. *J. Cell. Sci.* 132:jcs.224121. doi: 10.1242/jcs.224121

Goldsmith, J. R., Fayngerts, S., and Chen, Y. H. (2017). Regulation of inflammation and tumorigenesis by the TIPE family of phospholipid transfer proteins. *Cell. Mol. Immunol.* 14, 482–487. doi: 10.1038/cmi.2017.4

Hereld, D., Vaughan, R., Kim, J. Y., Borleis, J., and Devreotes, P. (1994). Localization of ligand-induced phosphorylation sites to serine clusters in the C-terminal domain of the *Dictyostelium* cAMP receptor, cAR1. *J. Biol. Chem.* 269, 7036–7044. doi: 10.1016/s0021-9258(17)37479-3

Hoeller, O., Gong, D., and Weiner, O. D. (2014). How to understand and outwit adaptation. *Dev. Cell* 28, 607–616. doi: 10.1016/j.devcel.2014.03.009

Iglesias, P. A., and Devreotes, P. N. (2008). Navigating through models of chemotaxis. *Curr. Opin. Cell Biol.* 20, 35–40. doi: 10.1016/j.ceb.2007.11.011

Janetopoulos, C., Jin, T., and Devreotes, P. (2001). Receptor-mediated activation of heterotrimeric G-proteins in living cells. *Science* 291, 2408–2411. doi: 10.1126/science.1055835

Kamimura, Y., Miyanaga, Y., and Ueda, M. (2016). Heterotrimeric G-protein shuttling via Gip1 extends the dynamic range of eukaryotic chemotaxis. *Proc. Natl. Acad. Sci. U.S.A.* 113, 4356–4361. doi: 10.1073/pnas.1516767113

Kataria, R., Xu, X., Fusetti, F., Keizer-Gunnink, I., Jin, T., van Haastert, P. J., et al. (2013). *Dictyostelium* Ric8 is a nonreceptor guanine exchange factor for heterotrimeric G proteins and is important for development and chemotaxis. *Proc. Natl. Acad. Sci. U.S.A.* 110, 6424–6429. doi: 10.1073/pnas.1301851110

Kim, J. Y., Haastert, P. V., and Devreotes, P. N. (1996). Social senses: G-protein-coupled receptor signaling pathways in *Dictyostelium discoideum*. *Chem. Biol.* 3, 239–243. doi: 10.1016/s1074-5521(96)90103-9

Kim, J. Y., Soede, R. D., Schaap, P., Valkema, R., Borleis, J. A., Van Haastert, P. J., et al. (1997). Phosphorylation of chemoattractant receptors is not essential for chemotaxis or termination of G-protein-mediated responses. *J. Biol. Chem.* 272, 7313–7318. doi: 10.1074/jbc.272.43.27313

Li, X., Miao, Y., Pal, D. S., and Devreotes, P. N. (2020). Excitable networks controlling cell migration during development and disease. *Semin. Cell Dev. Biol.* 100, 133–142. doi: 10.1016/j.semcdb.2019.11.001

Liu, Y., Lacal, J., Veltman, D. M., Fusetti, F., van Haastert, P. J., Firtel, R. A., et al. (2016). A Gα-Stimulated RapGEF is a receptor-proximal regulator of *Dictyostelium* chemotaxis. *Dev. Cell* 37, 458–472. doi: 10.1016/j.devcel.2016.05.001

Mato, J. M., Losada, A., Nanjundiah, V., and Konijn, T. M. (1975). Signal input for a chemotactic response in the cellular slime mold *Dictyostelium discoideum*. *Proc. Natl. Acad. Sci. U.S.A.* 72, 4991–4993. doi: 10.1073/pnas.72.12.4991

Matsuoka, S., and Ueda, M. (2018). Mutual inhibition between PTEN and PIP3 generates bistability for polarity in motile cells. *Nat. Commun.* 9:4481. doi: 10.1038/s41467-018-06856-0

Milne, J. L., Caterina, M. J., and Devreotes, P. N. (1997). Random mutagenesis of the cAMP chemoattractant receptor, cAR1, of *Dictyostelium*. Evidence for multiple states of activation. *J. Biol. Chem.* 272, 2069–2076. doi: 10.1074/jbc.272.4.2069

Milne, J. L., and Devreotes, P. N. (1993). The surface cyclic AMP receptors, cAR1, cAR2, and cAR3, promote Ca2+ influx in *Dictyostelium discoideum* by a G alpha 2-independent mechanism. *Mol. Biol. Cell* 4, 283–292. doi: 10.1091/mbc.4.3.283

Milne, J. L., Wu, L., Caterina, M. J., and Devreotes, P. N. (1995). Seven helix cAMP receptors stimulate Ca2+ entry in the absence of functional G proteins in *Dictyostelium*. *J. Biol. Chem.* 270, 5926–5931. doi: 10.1074/jbc.270.11.5926

Miyagawa, T., Koteishi, H., Kamimura, Y., Miyanaga, Y., Takeshita, K., Nakagawa, A., et al. (2018). Structural basis of Gip1 for cytosolic sequestration of G protein in wide-range chemotaxis. *Nat. Commun.* 9:4635. doi: 10.1038/s41467-018-07035-x

Miyanaga, Y., Kamimura, Y., Kuwayama, H., Devreotes, P. N., and Ueda, M. (2018). Chemoattractant receptors activate, recruit and capture G proteins for wide range chemotaxis. *Biochem. Biophys. Res. Commun.* 507, 304–310. doi: 10.1016/j.bbrc.2018.11.029

Miyanaga, Y., Matsuoka, S., and Ueda, M. (2009). Single-molecule imaging techniques to visualize chemotactic signaling events on the membrane of living *Dictyostelium* cells. *Methods Mol. Biol.* 571, 417–435. doi: 10.1007/978-1-60761-198-1_28

Nichols, J. M., Veltman, D., and Kay, R. R. (2015). Chemotaxis of a model organism: progress with *Dictyostelium*. *Curr. Opin. Cell Biol.* 36, 7–12. doi: 10.1016/j.ceb.2015.06.005

Nichols, J. M. E., Paschke, P., Peak-Chew, S., Williams, T. D., Tweedy, L., Skehel, M., et al. (2019). The Atypical MAP Kinase ErkB transmits distinct chemotactic signals through a core signaling module. *Dev. Cell* 48, 491–505.e9. doi: 10.1016/j.devcel.2018.12.001

Nishikawa, M., Hörning, M., Ueda, M., and Shibata, T. (2014). Excitable signal transduction induces both spontaneous and directional cell asymmetries in the phosphatidylinositol lipid signaling system for eukaryotic chemotaxis. *Biophys. J.* 106, 723–734. doi: 10.1016/j.bpj.2013.12.023

Niture, S., Dong, X., Arthur, E., Chimeh, U., Niture, S. S., Zheng, W., et al. (2018). Oncogenic role of tumor necrosis factor α-induced protein 8 (TNFAIP8). *Cells* 8:9. doi: 10.3390/cells8010009

Norden, C., and Lecaudey, V. (2019). Collective cell migration: general themes and new paradigms. *Curr. Opin. Genet. Dev.* 57, 54–60. doi: 10.1016/j.gde.2019.06.013

Nourshargh, S., and Alon, R. (2014). Leukocyte migration into inflamed tissues. *Immunity* 41, 694–707. doi: 10.1016/j.immuni.2014.10.008

Ohtsuka, D., Ota, N., Amaya, S., Matsuoka, S., Tanaka, Y., and Ueda, M. (2021). A sub-population of *Dictyostelium discoideum* cells shows extremely high sensitivity to cAMP for directional migration. *Biochem. Biophys. Res. Commun.* 554, 131–137. doi: 10.1016/j.bbrc.2021.03.095

Parent, C. A., Blacklock, B. J., Froehlich, W. M., Murphy, D. B., and Devreotes, P. N. (1998). G protein signaling events are activated at the leading edge of chemotactic cells. *Cell* 95, 81–91. doi: 10.1016/s0092-8674(00)81784-5

Parent, C. A., and Devreotes, P. N. (1999). A cell's sense of direction. *Science* 284, 765–770. doi: 10.1126/science.284.5415.765

Saini, D. K., Chisari, M., and Gautam, N. (2009). Shuttling and translocation of heterotrimeric G proteins and Ras. *Trends Pharmacol. Sci.* 30, 278–286. doi: 10.1016/j.tips.2009.04.001

Senoo, H., Cai, H., Wang, Y., Sesaki, H., and Iijima, M. (2016). The novel RacE-binding protein GflB sharpens Ras activity at the leading edge of migrating cells. *Mol. Biol. Cell* 27, 1596–1605. doi: 10.1091/mbc.E15-11-0796

Shellard, A., and Mayor, R. (2016). Chemotaxis during neural crest migration. *Semin. Cell Dev. Biol.* 55, 111–118. doi: 10.1016/j.semcdb.2016.01.031

Song, L., Nadkarni, S. M., Bödeker, H. U., Beta, C., Bae, A., Franck, C., et al. (2006). *Dictyostelium discoideum* chemotaxis: threshold for directed motion. *Eur. J. Cell Biol.* 85, 981–989. doi: 10.1016/j.ejcb.2006.01.012

Sonnemann, K. J., and Bement, W. M. (2011). Wound repair: toward understanding and integration of single-cell and multicellular wound responses. *Annu. Rev. Cell Dev. Biol.* 27, 237–263. doi: 10.1146/annurev-cellbio-092910-154251

Stuelten, C. H., Parent, C. A., and Montell, D. J. (2018). Cell motility in cancer invasion and metastasis: insights from simple model organisms. *Nat. Rev. Cancer* 18, 296–312. doi: 10.1038/nrc.2018.15

Swaney, K. F., Huang, C. H., and Devreotes, P. N. (2010). Eukaryotic chemotaxis: a network of signaling pathways controls motility, directional sensing, and polarity. *Annu. Rev. Biophys.* 39, 265–289. doi: 10.1146/annurev.biophys.093008.131228

Tanabe, Y., Kamimura, Y., and Ueda, M. (2018). Parallel signaling pathways regulate excitable dynamics differently to mediate pseudopod formation during eukaryotic chemotaxis. *J. Cell. Sci.* 131:jcs214775. doi: 10.1242/jcs.214775

Tang, M., Wang, M., Shi, C., Iglesias, P. A., Devreotes, P. N., and Huang, C. H. (2014). Evolutionarily conserved coupling of adaptive and excitable networks mediates eukaryotic chemotaxis. *Nat. Commun.* 5:5175. doi: 10.1038/ncomms6175

Thomas, M. A., Kleist, A. B., and Volkman, B. F. (2018). Decoding the chemotactic signal. *J. Leukoc. Biol.* 104, 359–374. doi: 10.1002/JLB.1MR0218-044

Trepat, X., Chen, Z., and Jacobson, K. (2012). Cell migration. *Compr. Physiol.* 2, 2369–2392. doi: 10.1002/cphy.c110012

Tu, Y., and Rappel, W. J. (2018). Adaptation of living systems. *Annu. Rev. Condens. Matter Phys.* 9, 183–205. doi: 10.1146/annurev-conmatphys-033117-054046

Ueda, M., Sako, Y., Tanaka, T., Devreotes, P., and Yanagida, T. (2001). Single-molecule analysis of chemotactic signaling in *Dictyostelium* cells. *Science* 294, 864–867. doi: 10.1126/science.1063951

Van Haastert, P. J. (1984). Guanine nucleotides modulate cell surface cAMP-binding sites in membranes from *Dictyostelium discoideum*. *Biochem. Biophys. Res. Commun.* 124, 597–604. doi: 10.1016/0006-291x(84)91596-1

Veltman, D. M., and Van Haastert, P. J. M. (2007). The role of cGMP and the rear of the cell in *Dictyostelium* chemotaxis and cell streaming. *J. Cell Sci.* 121, 120–127. doi: 10.1242/jcs.015602

Weis, W. I., and Kobilka, B. K. (2018). The molecular basis of G protein-coupled receptor activation. *Annu. Rev. Biochem.* 87, 897–919. doi: 10.1146/annurev-biochem-060614-033910

Xu, X., Meckel, T., Brzostowski, J. A., Yan, J., Meier-Schellersheim, M., and Jin, T. (2010). Coupling mechanism of a GPCR and a heterotrimeric G protein during chemoattractant gradient sensing in *Dictyostelium*. *Sci. Signal.* 3:ra71. doi: 10.1126/scisignal.2000980

Xu, X., Meier-Schellersheim, M., Jiao, X., Nelson, L. E., and Jin, T. (2005). Quantitative imaging of single live cells reveals spatiotemporal dynamics of multistep signaling events of chemoattractant gradient sensing in *Dictyostelium*. *Mol. Biol. Cell* 16, 676–688. doi: 10.1091/mbc.e04-07-0544

Xu, X., Wen, X., Veltman, D. M., Keizer-Gunnink, I., Pots, H., Kortholt, A., et al. (2017). GPCR-controlled membrane recruitment of negative regulator C2GAP1 locally inhibits Ras signaling for adaptation and long-range chemotaxis. *Proc. Natl. Acad. Sci. U.S.A.* 114, E10092–E10101. doi: 10.1073/pnas.1703208114

Yan, J., Mihaylov, V., Xu, X., Brzostowski, J. A., Li, H., Liu, L., et al. (2012). Gβγ effector, ElmoE, transduces GPCR signaling to the actin network during chemotaxis. *Dev. Cell* 22, 92–103. doi: 10.1016/j.devcel.2011.11.007

Zhang, L., Liu, R., Luan, Y. Y., and Yao, Y. M. (2018). Tumor necrosis factor-α Induced Protein 8: pathophysiology, clinical significance, and regulatory mechanism. *Int. J Biol. Sci.* 14, 398–405. doi: 10.7150/ijbs.23268

Zigmond, S. H. (1977). Ability of polymorphonuclear leukocytes to orient in gradients of chemotactic factors. *J. Cell Biol.* 75, 606–616. doi: 10.1083/jcb.75.2.606

Conflict of Interest: The authors declare that the research was conducted in the absence of any commercial or financial relationships that could be construed as a potential conflict of interest.

Publisher's Note: All claims expressed in this article are solely those of the authors and do not necessarily represent those of their affiliated organizations, or those of the publisher, the editors and the reviewers. Any product that may be evaluated in this article, or claim that may be made by its manufacturer, is not guaranteed or endorsed by the publisher.

Copyright © 2021 Kamimura and Ueda. This is an open-access article distributed under the terms of the Creative Commons Attribution License (CC BY). The use, distribution or reproduction in other forums is permitted, provided the original author(s) and the copyright owner(s) are credited and that the original publication in this journal is cited, in accordance with accepted academic practice. No use, distribution or reproduction is permitted which does not comply with these terms.

frontiers in Cell and Developmental Biology

METHODS
published: 13 August 2021
doi: 10.3389/fcell.2021.725678

Development of a Positive Selection High Throughput Genetic Screen in *Dictyostelium discoideum*

*Felicia N. Williams[1], Yumei Wu[1] and K. Matthew Scaglione[1,2,3]**

[1] Department of Molecular Genetics and Microbiology, Duke University, Durham, NC, United States, [2] Department of Neurology, Duke University, Durham, NC, United States, [3] Duke Center for Neurodegeneration and Neurotherapeutics, Duke University, Durham, NC, United States

The cellular slime mold *Dictyostelium discoideum* is a powerful model organism that can be utilized to investigate human health and disease. One particular strength of *Dictyostelium* is that it can be utilized for high throughput genetic screens. For many phenotypes, one limitation of utilizing *Dictyostelium* is that screening can be an arduous and time-consuming process, limiting the genomic depth one can cover. Previously, we utilized a restriction enzyme-mediated integration screen to identify suppressors of polyglutamine aggregation in *Dictyostelium*. However, due to the time required to perform the screen, we only obtained ∼4% genome coverage. Here we have developed an efficient screening pipeline that couples chemical mutagenesis with the 5-fluoroorotic acid counterselection system to enrich for mutations in genes of interest. Here we describe this new screening methodology and highlight how it can be utilized for other biological systems.

Keywords: *Dictyostelium discoideum*, 5-FOA, polyglutamine, protein aggregation, genetic screen

OPEN ACCESS

Edited by:
Robert Joseph Huber, Trent University, Canada

Reviewed by:
Gad Shaulsky, Baylor College of Medicine, United States
Ricardo Escalante, Consejo Superior de Investigaciones Científicas (CSIC), Spain

***Correspondence:**
K. Matthew Scaglione
matt.scaglione@duke.edu

Specialty section:
This article was submitted to Molecular and Cellular Pathology, a section of the journal Frontiers in Cell and Developmental Biology

Received: *15 June 2021*
Accepted: *21 July 2021*
Published: *13 August 2021*

Citation:
Williams FN, Wu Y and Scaglione KM (2021) Development of a Positive Selection High Throughput Genetic Screen in Dictyostelium discoideum. Front. Cell Dev. Biol. 9:725678. doi: 10.3389/fcell.2021.725678

INTRODUCTION

Model organisms like *Dictyostelium discoideum* (*Dictyostelium*) offer numerous advantages for identifying key components of cellular systems. *Dictyostelium* is particularly useful for these types of studies because a number of different genetic screening technologies have been developed for *Dictyostelium* biology (Bozzaro, 2019). For example, restriction enzyme-mediated integration (REMI) enables screens that rely on disrupting gene function *via* integration of plasmid into the *Dictyostelium* genome (Guerin and Larochelle, 2002). Affected genes can be identified by extracting the plasmid from the genome with restriction enzymes and sequencing retained pieces of genomic DNA to identify disrupted genes (Guerin and Larochelle, 2002). Alternatively, mutagenesis using a chemical mutagen such as *N*-methyl-*N*′-nitro-*N*-nitroguanidine (NTG) can also introduce mutations into the *Dictyostelium* genome that can later be identified by whole-genome sequencing (Li et al., 2016). With these assays, one can rapidly generate mutations at near genome saturation. However, screening randomly mutated cells to identify phenotypes of interest can be a limitation that prevents analysis at near genome wide saturation. Therefore, developing methods to positively select for phenotypes of interest is a powerful way to increase the depth of genomic coverage.

In addition to REMI and NTG mutagenesis, other powerful molecular techniques have been established for *Dictyostelium*. These include the 5-fluoroorotic acid (5-FOA)/*pyr56* counterselection, a method that has supported genetic investigations in *Dictyostelium*

(Kalpaxis et al., 1991; Kuspa and Loomis, 1992; Insall et al., 1994; Gaudet et al., 2007). In this system, the prodrug 5-FOA is processed to the toxic form 5-fluorouracil by a uridine monophosphate (UMP) synthase enzyme (Kalpaxis et al., 1991). This allows for selection against cells with an active UMP synthase (Pyr56 in *Dictyostelium)* in the presence of 5-FOA. Alternatively, one can use the same system to select for cells with active Pyr56. In this case, cells are grown in the absence of uracil, a downstream product of Pyr56. In the absence of uracil, cells that do not have a functional copy of *pyr56* are selected against (Kalpaxis et al., 1991). 5-FOA screening can also be modified for monitoring specific phenomena. For example, in yeast attachment of aggregation prone regions such as amyloid-β (Aβ) can tune this system to measure the effect of protein phase separation on cellular fitness (Sanchez de Groot et al., 2019). Overall, this powerful counterselection system is highly useful in *Dictyostelium* research.

Having access to highly effective screening methodologies is vital to efficient genetic investigation. Previous work from our group and others identified that *Dictyostelium* was a proteostatic outlier that is highly resistant to polyglutamine aggregation (Malinovska et al., 2015; Santarriaga et al., 2015). To determine mechanisms that *Dictyostelium* utilize to resist polyglutamine aggregation, we performed a REMI screen to identify suppressors of polyglutamine aggregation in *Dictyostelium* (Santarriaga et al., 2018). While successful in identifying one suppressor of polyglutamine aggregation, the screen was limited in scope and did not approach genome wide coverage. This was largely due to the lack of a simple readout that required little labor coupled with the lack of any positive selection for hits of interest. Development of more efficient screening pipelines is therefore warranted to enable near genome wide saturation in reasonable time frames. Here we describe a novel screening pipeline that couples NTG mutagenesis with 5-FOA counterselection to robustly enrich for genes that suppress polyglutamine aggregation. We further discuss how this system can be modified to answer other biological questions.

MATERIALS AND EQUIPMENT

Streptomycin (Gold Biotechnology, Cat. #S-150).
Carbenicillin (Gold Biotechnology, Cat. #SC-103).
Uracil (Alfa Aesar, Cat. #ch-0238).
CellTiter-Glo Luminescent Cell Viability Assay (Promega, Cat. #G7572).
DMSO (Gold Biotechnology, Cat. #SD-361).
5-FOA (Gold Biotechnology, Cat. #F-440).
NTG (Pfaltz & Bauer, Cat. #M23230).
Dictyostelium discoideum AX4 (Dictybase).
Dictyostelium discoideum pyr56-KO (developed here, available through Dictybase).
Klebsiella aerogenes (Dictybase).
pTX-GFP (Dictybase).
^{Pyr56}mHtt^{Q103,GFP} plasmid (developed here, available through Dictybase).
α-GFP antibody (ThermoFisher Scientific, cat. # A-11122).
α-β-actin antibody [Iowa Developmental Studies Hybridoma Bank (DSHB)].
Enhanced chemiluminescence (ECL) buffer (GE Healthcare 28980926).
Tecan Spark M20 plate reader.
EVOS fluorescence microscope.
ChemiDoc imaging system (BioRad).

Methods

General Culture

Dictyostelium cells were cultured at 22°C in HL5 medium supplemented with 300 μg/mL streptomycin (GoldBio cat. #S-150-100) and 100 μg/mL carbenicillin (GoldBio cat. #C-103-50). *pyr56*-KO cells were additionally supplemented with 20 μg/mL uracil (Alfa Aesar cat. #A15570). Where applicable, 5-fluoroorotic acid (GoldBio cat. #F-230-25) was added to the specified concentration. Cells were split regularly to maintain a density between $1 - 4 \times 10^6$.

HL5 medium: 17.8 g proteose peptone (Millipore cat. #107229), 7.2 g yeast extract (BD cat. # 212720), 0.54 g Na_2HPO_4 (J. T. Baker cat. #3824-01), 0.4 g KH_2PO_4 (Sigma cat. #P9791-1KG), 130 μL B12/folic acid mix. Bring to 1 L with deionized water and adjust pH to 6.5 ± 0.1. Autoclave and add 20 mL of filter sterilized 50% glucose prior to use (Eichinger and Rivero-Crespo, 2006). B12/folic acid mix: 5 mg B_{12} (Sigma cat. #V2876-1G), 200 mg folic acid (Sigma cat. #F7876-10G). Add 95 mL deionized water and adjust pH to 6.5. Adjust volume to 100 mL, filter sterilize, and store at −20°C (Eichinger and Rivero-Crespo, 2006). FM minimal medium: 19.3 g premixed FM minimal medium (Formedium cat. #FMM0102). Add 1 L deionized water and filter sterilize.

Knockout Generation by CRISPR-Cas9

CRISPR-Cas9 knockout generation was completed as previously described for *Dictyostelium* (Sekine et al., 2018). Axenic *Dictyostelium* strain AX4 served as the wild-type starting strain for this gene knockout. Guide RNAs (gRNAs) against the *Dictyostelium pyr56* gene were developed using the CRISPR RGEN Tools Cas-Designer (Park et al., 2015) (Fwd: 5′ AGCATATCAAAAGGTTTATAAATC 3′; Rev: 5′ AAACGATTTATAAACCTTTTGATA 3′). These gRNAs were checked for off-target sites using the CRISPR RGEN Tools Cas-OFFinder (Bae et al., 2014).

Plasmid Construction

To develop the PTX(act15/pyr56-mHtt-GFP) plasmid, Htt exon 1 with 103 glutamines (sourced from Addgene plasmid #1385, the pYES2/103Q plasmid deposited by Michael Sherman) was first cloned into pTxGFP using *Kpn*I and *Xba*I (Levi et al., 2000; Santarriaga et al., 2015). The *pyr56* gene was PCR-amplified from AX4 genomic DNA and cloned into this construct using *Kpn*I. The *Kpn*I site within the *pyr56* gene was mutated using the QuikChange Lightning Site-Directed Mutagenesis Kit (Agilent Cat.# 210518), resulting in a synonymous t306c single nucleotide mutation that is silent at the amino acid level and removal of the internal restriction site. The Pyr56^{GFP} plasmid was constructed by cloning the t306c *pyr56* gene into pTxGFP using *Kpn*I.

Analysis of Viability

Cell viability was measured using the CellTiter-Glo Luminescent Cell Viability Assay from Promega (Cat. #G7572). To assess the sensitivity of wild-type *Dictyostelium* to 5-FOA, AX4 cells were washed and then resuspended in FM minimal media containing 0 μg/mL (DMSO) to 500 μg/mL 5-FOA. These cells were incubated in a stationary incubator at 22°C for 48 h. Cells were then mixed with the Cell-Titer Glo reagent according to manufacturer's protocol, and luminescence was measured using a Tecan Spark M20 plate reader. Similarly, to confirm resistance to 5-FOA in the *pyr56*-KO strain, knockout cells in FM minimal media containing 20 μg/mL uracil were exposed to 0–500 μg/mL 5-FOA and incubated for 48 h at 22°C, followed by measurement with the CellTiter-Glo assay. To assess rescue of 5-FOA sensitivity, *pyr56*-KO cells were electroporated with the PTX(act15/pyr56-mHtt-GFP) plasmid. Following isolation of a clonal line from a bacterial lawn, *pyr56*-KO cells expressing ^{Pyr56}mHtt^{Q103,GFP}, AX4 wild-type, and *pyr56*-KO cells were exposed to either DMSO or 500 μg/mL 5-FOA. After 48 h, viability was measured using the CellTiter-Glo assay. Each of these viability experiments were performed in triplicate. Statistical analysis was performed using GraphPad Prism.

NTG Mutagenesis, 5-FOA Selection, Isolation of Clonal Populations

Chemical mutagenesis by NTG was performed as previously described (Li et al., 2016). Approximately 10^8 *pyr56*-KO cells expressing ^{Pyr56}mHtt^{Q103,GFP} were treated with 500 μg/mL NTG for 12 min in a shaking 22°C incubator. Following removal of NTG, cells were left to recover for 24 h. Cells were then treated with either DMSO or 1 mg/mL 5-FOA. Media was refreshed on days two and four following 5-FOA addition. Images taken after 5 days of culturing using an EVOS fluorescence microscope and quantification was performed using the ImageJ Cell Counter plugin to determine the number of cells with blinded, manual counting of the number of puncta.

5-FOA selected cells were collected for clonal isolation 5-days post 5-FOA addition. Clonal populations of mutagenized *Dictyostelium* were isolated from *Klebsiella aerogenes* bacterial lawns on SM agar plates. Isolated cells were then grown for 48 h before protein aggregation phenotype was recorded. Protein aggregation was observed as punctate GFP using an EVOS fluorescence microscope. Isolates with approximately five percent or more cells containing puncta were considered mutant for the protein aggregation phenotype.

SDS-PAGE and Western Blot Analysis

Lysates from *pyr56*-KO cells expressing empty vector (pTxGFP), Pyr56-GFP, and Pyr56-mHtt^{Q103}-GFP were collected in boiling 1X Laemmli buffer followed by sonication for completion of cell lysis. Lysates were then run on a 4–20% gradient SDS-PAGE gel and transferred to polyvinylidene difluoride (PVDF) membrane for analysis by western blot. Membranes were blocked for 30 min with 5% milk in TBST, followed by overnight incubation with primary antibody at 4°C. Green fluorescent protein (GFP) expression was probed using polyclonal rabbit anti-GFP antibody at a 1:1,000 dilution in milk (ThermoFisher Scientific, cat. # A-11122) and beta actin expression was probed using a *Dictyostelium* specific monoclonal mouse anti-beta actin antibody at a 1:100 dilution (DSHB Hybridoma

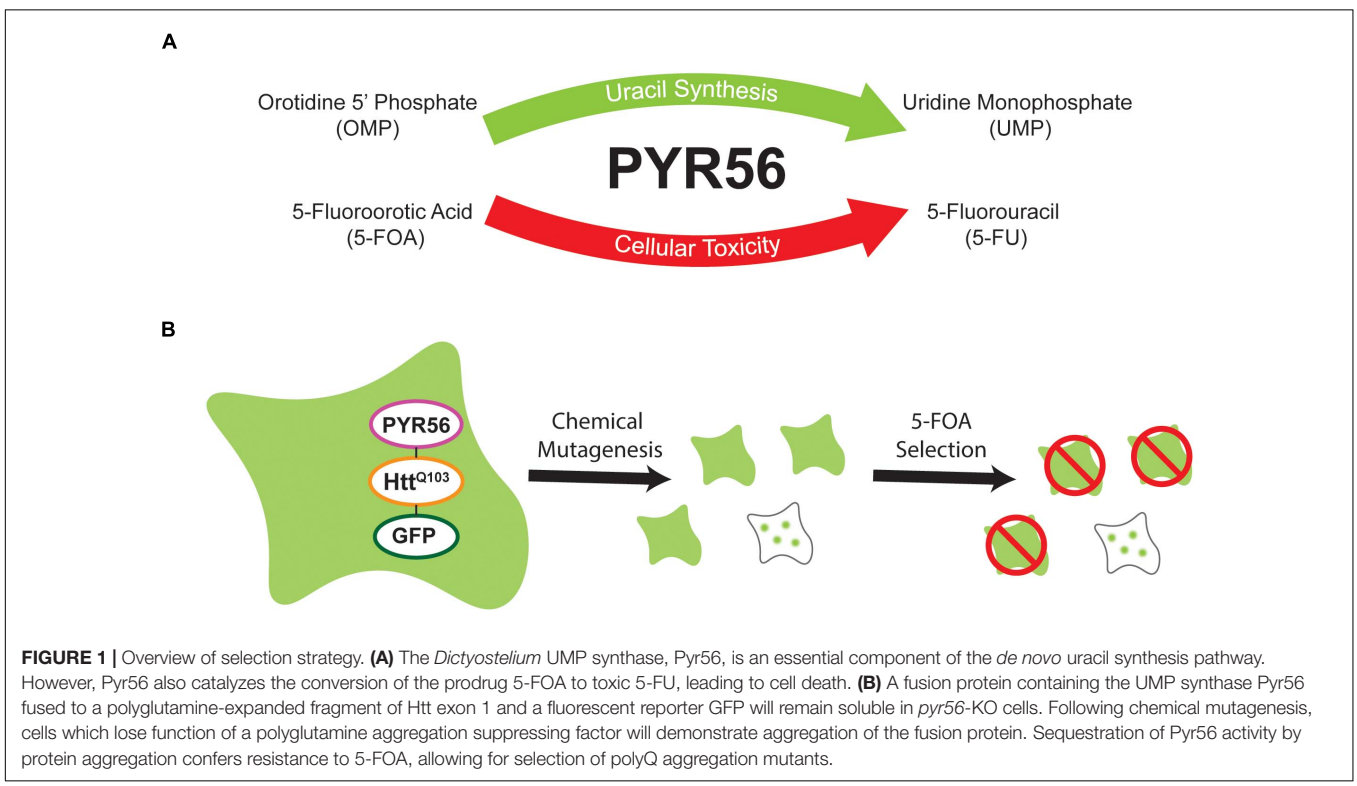

FIGURE 1 | Overview of selection strategy. **(A)** The *Dictyostelium* UMP synthase, Pyr56, is an essential component of the *de novo* uracil synthesis pathway. However, Pyr56 also catalyzes the conversion of the prodrug 5-FOA to toxic 5-FU, leading to cell death. **(B)** A fusion protein containing the UMP synthase Pyr56 fused to a polyglutamine-expanded fragment of Htt exon 1 and a fluorescent reporter GFP will remain soluble in *pyr56*-KO cells. Following chemical mutagenesis, cells which lose function of a polyglutamine aggregation suppressing factor will demonstrate aggregation of the fusion protein. Sequestration of Pyr56 activity by protein aggregation confers resistance to 5-FOA, allowing for selection of polyQ aggregation mutants.

Product 224-236-1, deposited to the DSHB by Gerisch, G.). Membranes were washed with TBST three times for 10 min at room temperature before and after incubation with secondary antibody for 1 h. For development, membranes were incubated in enhanced chemiluminescence (ECL) buffer for 2 min at room temperature then imaged using a ChemiDoc imaging system.

RESULTS

Dictyostelium is a tractable model system that can be utilized to gain insight into processes that regulate human health and disease. One advantage of *Dictyostelium* is that genetic tools exist to allow near genome saturation screens, allowing one to identify genes that participate in pathways of interest. While creating libraries of mutated *Dictyostelium* is rapid and efficient, downstream processes like clonal cell isolation can be time consuming, leading to constraints on the depth of genome coverage obtained. This is largely because a low percentage of cells will be positive for a given phenotype and the fact that clonal isolation is tedious. This is exacerbated in screens that rely on readouts like fluorescence which require isolation of clones, removal of bacteria, clonal outgrowth, and imaging. To overcome these issues, we sought to develop a selection system that would enhance for phenotypes of interest, in our case the presence of aggregated GFP puncta, thus eliminating the majority of cells lacking the desired phenotype and subsequently increasing throughput (**Figure 1**).

To accomplish this, we utilized the 5-FOA counterselection system (Kalpaxis et al., 1991). This system is ideal in *Dictyostelium* as the genome encodes a single copy of the uridine monophosphate (UMP) synthase enzyme, Pyr56. To enable 5-FOA screening, we generated a *pyr56* knockout strain (*pyr56*-KO) using CRISPR-Cas9. In this strain, there is an 8 bp insertion after amino acid residue 58, resulting in a frame shift and introduction of a premature stop codon after residue 71 (**Figures 2A,B**). Importantly, the *pyr56*-KO strain was viable and resistant to 5-FOA toxicity (**Figure 2C**). It is worth mentioning that cells may escape selection when grown in monolayer culture, as noted in the original characterization of the *pyr56*/5-FOA selection system (Kalpaxis et al., 1991). Thus, one may want to consider culturing conditions when determining the required strength of selection.

In our initial screen to identify suppressors of polyglutamine aggregation, we isolated clonal populations of *Dictyostelium* and screened *via* high content imaging. This required screening large numbers of colonies as the number of hits was low. To greatly enhance the number of hits, we next wanted to develop a system that positively select for *Dictyostelium* cells that contained polyglutamine aggregates. To accomplish this, we cloned the Pyr56 protein as a fusion with a fragment of mutant huntingtin protein containing a homopolymeric repeat of 103 glutamines and GFP [pTX(act15/pyr56-mHtt-GFP)] to express the Pyr56-mHtt^{Q103}-GFP protein (**Figure 3A**). This construct was introduced into *Dictyostelium* cells using pTX-GFP, an extrachromosomal multi-copy plasmid. This is important because resistance to 5-FOA could arise from mutations in

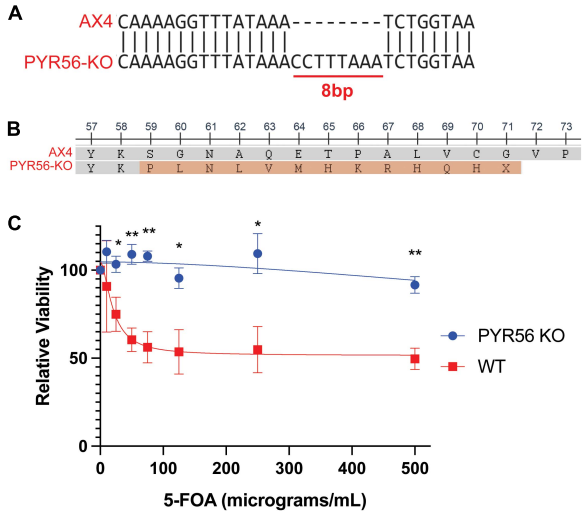

FIGURE 2 | Deletion of *pyr56* confers resistance to 5-FOA toxicity. **(A)** The *pyr56*-KO generated by CRISPR-Cas9 contains an 8 bp insertion in the Pyr56 gene. **(B)** The 8 bp insertion in the Pyr56 gene results in a frameshift after amino acid residue 58 and a premature stop after residue 71. **(C)** Deletion of *pyr56* results in survival when cells are grown in media containing 5-FOA. Either wild-type or *pyr56*-KO *Dictyostelium* at a starting concentration of 5×10^3 cells/mL were grown in presence of increasing concentrations of 5-FOA. Viability was measured by luminescence using the CellTiter-Glo Viability Assay at 48 h ($n = 3$). Samples were analyzed for statistical significance using an unpaired *t*-test, $^*p < 0.05$. $^{**}p < 0.001$.

the exogenous *pyr56* gene rather than sequestration of Pyr56 activity by protein aggregation. However, even if this were to occur, it is unlikely that it would result in false positives as it would likely accumulate as soluble protein rather than aggregated protein and therefore not be identified as a hit in our screen. Using this construct, we confirmed that Pyr56-mHtt^{Q103}-GFP is expressed and soluble in *Dictyostelium* and migrates at the expected molecular weight when analyzed by western blot (**Figures 3B,C**). Importantly, Pyr56-mHtt^{Q103}-GFP expressed by the PTX(act15/pyr56-mHtt-GFP) plasmid is active and is capable of restoring toxicity in the presence of 5-FOA (**Figure 3D**).

We next wanted to utilize the PTX(act15/pyr56-mHtt-GFP) construct to develop a screen that positively selects for *Dictyostelium* cells containing mutations in genes that suppress polyglutamine aggregation. To accomplish this, we performed NTG mutagenesis as previously described on *pyr56*-KO *Dictyostelium* expressing Pyr56-mHtt^{Q103}-GFP (Li et al., 2016). These cells were grown for 24 h prior to addition of either DMSO or 1 mg/mL 5-FOA for 5 days. At the end of 5 days, we observed a clear enrichment of *Dictyostelium* that contain Pyr56-mHtt^{Q103}-GFP aggregates (**Figure 4A**). To determine the percentage of *Dictyostelium* cells positive for the protein aggregation phenotype, we analyzed 3 populations of mutagenized cells that had been treated with either DMSO or 1 mg/mL 5-FOA using fluorescence microscopy and found a significant increase in the number of cells with Pyr56-mHtt^{Q103}-GFP aggregates (**Figure 4B**). To isolate clonal populations of mutant *Dictyostelium*, we plated 5-FOA selected

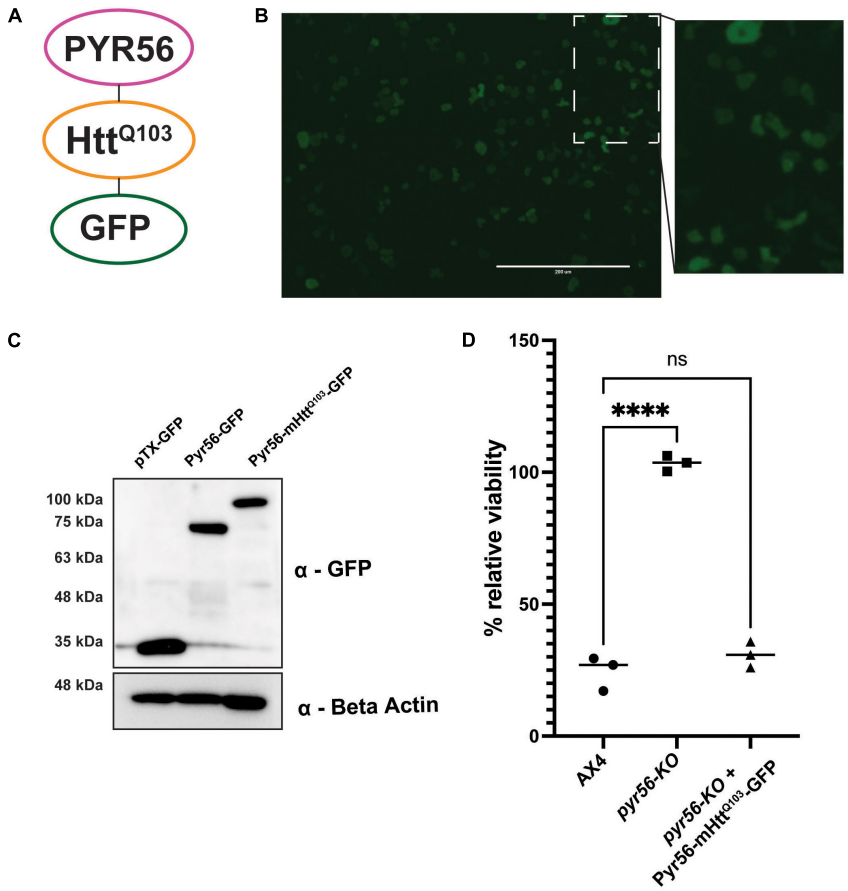

FIGURE 3 | The Pyr56-mHtt^{Q103}-GFP fusion protein is soluble and active in *Dictyostelium*. **(A)** The Pyr56-mHtt^{Q103}-GFP fusion protein is composed of the UMP synthase Pyr56, Htt exon 1 containing a tract of 103 glutamines, and a GFP reporter express by the PTX(act15/pyr56-mHtt-GFP) plasmid. **(B)** Pyr56-mHtt^{Q103}-GFP remains soluble in *Dictyostelium*. *pyr56*-KO cells expressing Pyr56-mHtt^{Q103}-GFP were imaged for GFP localization using an EVOS microscope. Scale bar represents 200 μm. **(C)** Pyr56-mHtt^{Q103}-GFP is expressed in *Dictyostelium*. *pyr56*-KO cells expressing either empty vector (pTxGFP), Pyr56^{GFP} or Pyr56-mHtt^{Q103}-GFP were lysed, and lysates were run on a gradient SDS-PAGE gel. Gels were analyzed by western blot analysis to probe for GFP expression, indicating that Pyr56-mHtt^{Q103}-GFP is expressed in *Dictyostelium* and runs at the expected size. **(D)** Expression of Pyr56-mHtt^{Q103}-GFP in the *pyr56*-KO strain rescues sensitivity to 5-FOA. 2×10^3 cells/mL of either wild-type, *pyr56*-KO, or *pyr56*-KO expressing Pyr56-mHtt^{Q103}-GFP were treated with 500 μg/mL 5-FOA and viability was measured at $t = 48$ h by luminescence using the CellTiter-Glo Viability Assay ($n = 3$). Samples were analyzed by one-way ANOVA with multiple comparisons, **** indicates $p < 0.0001$.

Dictyostelium cells on bacterial lawns and picked individual colonies following plaque formation. Representative images of mutant isolates of cells with polyglutamine aggregates are shown (**Figure 5**). With this system, screening just 500 colonies is expected to yield hundreds of desired mutants. Following isolation of desired mutants, these strains can be subjected to whole genome sequencing and variant analysis to identify potential causative mutations for further investigation (Li et al., 2016).

DISCUSSION

Summary of Findings

Here we have developed a highly efficient genetic screening workflow for *Dictyostelium* that allows for positive or negative selection of hits (**Figure 1**). We utilized CRISPR-Cas9 to develop a *Dictyostelium* strain that lacks *pyr56*, the gene that encodes for *Dictyostelium's* UMP synthase gene and demonstrated that the *pyr56*-KO strain is resistant to 5-FOA induced toxicity (**Figure 2**). We also constructed a vector for overexpression of Pyr56-mHtt^{Q103}-GFP and demonstrated that this protein was soluble and induced toxicity in the presence of 5-FOA (**Figure 3**). We further demonstrated that sequestration of Pyr56 activity by protein aggregation coupled with selection by 5-FOA resulted in an increase in *Dictyostelium* cells that have Pyr56-mHtt^{Q103}-GFP puncta (**Figures 4,5**). Together these experiments outline high throughput screening strategies that offer negative selection to greatly enrich hit rate and reduce the number of clones that must be screened.

Utilization of This Platform for Assessing Other Biological Systems

In addition to being useful for screening for proteins that suppress polyglutamine aggregation this screening modality can

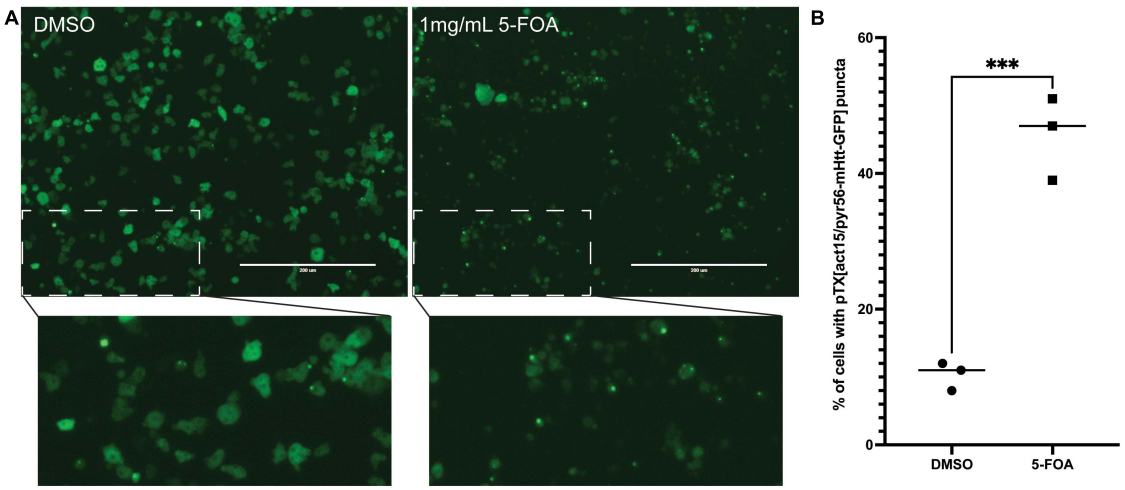

FIGURE 4 | Selection of NTG mutagenized cells with 5-FOA enriches for protein aggregation mutants. **(A)** Mutagenized cells treated with 5-FOA are enriched for punctate GFP. *pyr56*-KO cells expressing ^{Pyr56}mHtt^{Q103,GFP} were treated with NTG and allowed to recover for 24 h following mutagenesis. After recovery, cells were treated with either DMSO control (left) or 1 mg/ml 5-FOA (right). Five days after 5-FOA addition, there is clear enrichment for cells containing GFP puncta in the 5-FOA treated cells when compared to the DMSO control which contains a majority of cells with diffuse GFP. This indicates enrichment of polyQ aggregation mutants in the population of 5-FOA selected cells. Scale bar represents 200 μm. **(B)** Average number of cells containing puncta. Cell number and percentage of cells containing Pyr56-mHtt^{Q103}-GFP were quantified using the ImageJ Cell Counter (n = 3). Samples were analyzed by an unpaired t-test, *** indicates p = 0.0007.

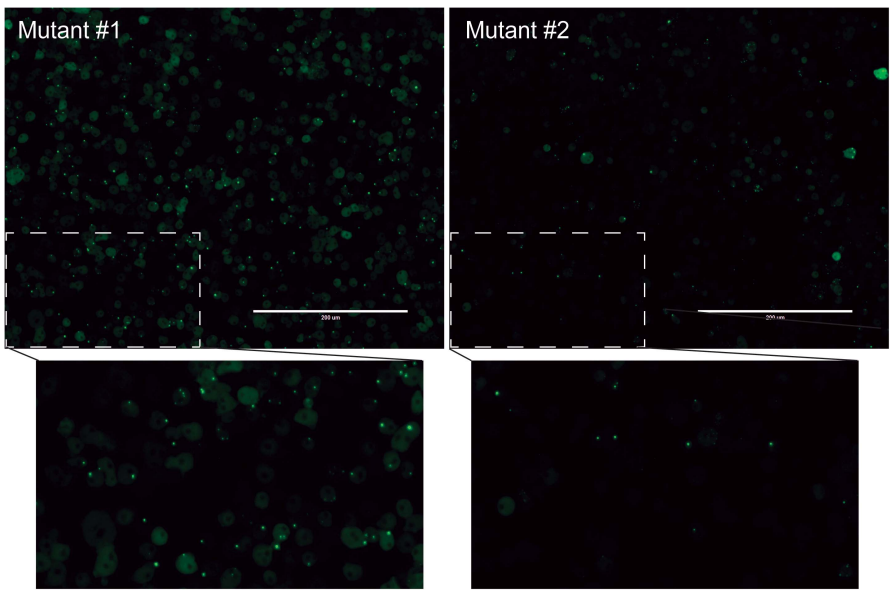

FIGURE 5 | Two protein aggregation mutants obtained using this selection technique. Mutagenized and 5-FOA selected cells were plated on SM agar plates containing bacterial lawns. Colonies were isolated following plaque formation. After 48 hours of growth, cells were analyzed for GFP puncta using an EVOS microscope.

be modified for use in other systems. For example, *Dictyostelium* has been reported to have a proteome extremely rich in prion-like proteins (Eichinger et al., 2005); however, virtually nothing is known about factors that regulate prion-like proteins in *Dictyostelium*. Using this screening workflow, one could both identify factors that promote and suppress aggregation of prion-like proteins. Similarly, one could use this system to investigate regulators which interact with structurally distinct protein domains that present similar aggregation phenotypes. These regulators include various categories of RNA which are becoming increasingly studied in the context of phase separation (Guo et al., 2021). For example, this screening methodology could also be used for investigating the role of long non-coding RNAs (lncRNAs) in phase separation. lncRNAs can sequester proteins into foci to inhibit their function and little is known about factors that regulate lncRNA function (Luo et al., 2021). Genetic screens

to identify factors that modulate lncRNA function could provide new insight into lncRNA biology.

While many proteins are known or believed to phase separate, the exact behavior of these proteins within the cell can be difficult to observe. However, certain characteristics of the selection system we have presented here may be adapted to improve the techniques available to investigate this phenomenon. For instance, given that aggregation of URA3-GFP-Aβ is linked to cellular fitness for yeast in 5-FOA enriched media (Sanchez de Groot et al., 2019), one can extrapolate that sequestration of essential Pyr56 activity into a phase-separated compartment is directly related to cellular growth in *Dictyostelium*. Thus, given that protein aggregation is correlated with cellular growth in these conditions, the techniques described here could be adapted to quantitatively estimate relative amounts of phase separated protein *in vivo* using *Dictyostelium*.

Selection by 5-FOA has recently been applied to human cell lines (Wiebking et al., 2020). While this selection system has not yet been widely investigated in human cells, one can envision how our screening methodology could be applied to investigate factors which influence protein aggregation and phase separation in human cells. Thus, beyond translational relevance from model organisms, our technique has great potential for understanding human health in aspects such as neurodegeneration, aging, and many more.

Uracil Auxotrophy Can Be Utilized for Selection

In addition to negatively selecting against Pyr56 activity, this system could also be altered to positively select for soluble, active Pyr56. In this case, one would exploit the fact that the *pyr56*-KO strain is a uracil auxotroph that requires the presence of uracil to grow. Here, a lack of uracil in the media would positively select for clones that have soluble, active Pyr56 protein. Coupled with NTG mutagenesis or REMI screening, this could be useful for identifying genes that negatively regulate cellular processes where proteins reversibly form puncta. Such a screen could be useful for proteins that prevent processes like liquid-liquid phase separation (LLPS) or promote the resolution of biomolecular condensates. This would be a useful screen as LLPS has recently been identified in *Dictyostelium* (Santarriaga et al., 2019). More recent work has also demonstrated that one type of biomolecular condensate, stress granules, are dynamically modulated and that different stressors alter which factors are needed to resolve the stress granules once the stressor has been removed (Gwon et al., 2021; Maxwell et al., 2021). Furthermore, LLPS has also been investigated recently in yeast as a tunable mechanism of responding to environmental changes, thus conferring a fitness benefit under certain stressful conditions (Riback et al., 2017; Franzmann et al., 2018; Franzmann and Alberti, 2019; Lau et al., 2020). This suggests that genetic screens in *Dictyostelium* may serve as one mechanism to identify genes that regulate stress granule dynamics and cellular responses to environmental stressors.

DATA AVAILABILITY STATEMENT

The raw data supporting the conclusions of this article will be made available by the authors, without undue reservation.

AUTHOR CONTRIBUTIONS

FW and KS developed and planned the project, interpreted the results, and wrote the manuscript. FW and YW performed the experiments. KS supervised the research. All authors reviewed and edited the manuscript.

FUNDING

This work was supported by National Institutes of Health grants NS112191 and GM119544 to KS and the Diverse Scientists in Ataxia Predoctoral Fellowship from the National Ataxia Foundation to FW.

REFERENCES

Bae, S., Park, J., and Kim, J.-S. (2014). Cas-OFFinder: a fast and versatile algorithm that searches for potential off-target sites of Cas9 RNA-guided endonucleases. *Bioinformatics* 30, 1473–1475. doi: 10.1093/bioinformatics/btu048

Bozzaro, S. (2019). The past, present and future of Dictyostelium as a model system. *Int. J. Dev. Biol.* 63, 321–331. doi: 10.1387/ijdb.190128sb

Eichinger, L., and Rivero-Crespo, F. (2006). *Dictyostelium Discoideum Protocols*. Totowa: Humana Press.

Eichinger, L., Pachebat, J. A., Glöckner, G., Rajandream, M. A., Sucgang, R., Berriman, M., et al. (2005). The genome of the social amoeba Dictyostelium discoideum. *Nature* 435, 43–57.

Franzmann, T. M., and Alberti, S. (2019). Protein Phase Separation as a Stress Survival Strategy. *Cold Spring Harb. Perspect. Biol.* 11:a034058. doi: 10.1101/cshperspect.a034058

Franzmann, T. M., Jahnel, M., Pozniakovsky, A., Mahamid, J., and Holehouse, A. S. (2018). Phase separation of a yeast prion protein promotes cellular fitness. *Science* 359:eaao5654. doi: 10.1126/science.aao5654

Gaudet, P., Pilcher, K. E., Fey, P., and Chisholm, R. L. (2007). Transformation of Dictyostelium discoideum with plasmid DNA. *Nat. Protoc.* 2, 1317–1324. doi: 10.1038/nprot.2007.179

Guerin, N. A., and Larochelle, D. A. (2002). A user's guide to restriction enzyme-mediated integration in Dictyostelium. *J. Muscle Res. Cell Motil.* 23, 597–604.

Guo, Q., Shi, X., and Wang, X. (2021). RNA and liquid-liquid phase separation. *Noncoding RNA Res.* 6, 92–99. doi: 10.1016/j.ncrna.2021.04.003

Gwon, Y., Maxwell, B. A., Kolaitis, R.-M., Zhang, P., Kim, H. J., and Taylor, J. P. (2021). Ubiquitination of G3BP1 mediates stress granule disassembly in a stress-specific manner. *bioRxiv* [Preprint]. doi: 10.1101/2021.04.22.440930

Insall, R. H., Soede, R. D., Schaap, P., and Devreotes, P. N. (1994). Two cAMP receptors activate common signaling pathways in Dictyostelium. *Mol. Biol. Cell* 5, 703–711. doi: 10.1091/mbc.5.6.703

Kalpaxis, D., Zündorf, I., Werner, H., Reindl, N., Boy-Marcotte, E., Jacquet, M., et al. (1991). Positive selection for Dictyostelium discoideum mutants lacking UMP synthase activity based on resistance to 5-fluoroorotic acid. *Mol. Gen. Genet.* 225, 492–500. doi: 10.1007/bf00261692

Kuspa, A., and Loomis, W. F. (1992). Tagging developmental genes in Dictyostelium by restriction enzyme-mediated integration of plasmid DNA. *Proc. Natl. Acad. Sci. U. S. A.* 89, 8803–8807. doi: 10.1073/pnas.89.18.8803

Lau, Y., Oamen, H. P., and Caudron, F. (2020). Protein Phase Separation during Stress Adaptation and Cellular Memory. *Cells* 9:1302. doi: 10.3390/cells9051302

Levi, S., Polyakov, M., and Egelhoff, T. T. (2000). Green Fluorescent Protein and Epitope Tag Fusion Vectors for Dictyostelium discoideum. *Plasmid* 44, 231–238. doi: 10.1006/plas.2000.1487

Li, C.-L., Santhanam, B., Webb, A. N., Zupan, B., and Shaulsky, G. (2016). Gene discovery by chemical mutagenesis and whole-genome sequencing in Dictyostelium. *Genome Res.* 26, 1268–1276. doi: 10.1101/gr.205682.116

Luo, J., Qu, L., Gao, F., Lin, J., Liu, J., and Lin, A. (2021). LncRNAs: architectural Scaffolds or More Potential Roles in Phase Separation. *Front. Genet.* 12:626234. doi: 10.3389/fgene.2021.626234

Malinovska, L., Palm, S., Gibson, K., Verbavatz, J.-C., and Alberti, S. (2015). Dictyostelium discoideum has a highly Q/N-rich proteome and shows an unusual resilience to protein aggregation. *Proc. Natl. Acad. Sci. U. S. A.* 112, E2620–E2629.

Maxwell, B. A., Gwon, Y., Mishra, A., Peng, J., Zhang, K., Kim, H. J., et al. (2021). Ubiquitination is essential for recovery of cellular activities following heat shock. *bioRxiv* [Preprint]. doi: 10.1101/2021.04.22.440934

Park, J., Bae, S., and Kim, J.-S. (2015). Cas-Designer: a web-based tool for choice of CRISPR-Cas9 target sites. *Bioinformatics* 31, 4014–4016.

Riback, J. A., Katanski, C. D., Kear-Scott, J. L., Pilipenko, E. V., Rojek, A. E., Sosnick, T. R., et al. (2017). Stress-Triggered Phase Separation Is an Adaptive, Evolutionarily Tuned Response. *Cell* 168, 1028–1040.e19.

Sanchez de Groot, N., Torrent Burgas, M., Ravarani, C. N., Trusina, A., Ventura, S., and Babu, M. M. (2019). The fitness cost and benefit of phase-separated protein deposits. *Mol. Syst. Biol.* 15:e8075.

Santarriaga, S., Fikejs, A., Scaglione, J., and Scaglione, K. M. (2019). A Heat Shock Protein 48 (HSP48) Biomolecular Condensate Is Induced during Dictyostelium discoideum Development. *mSphere* 4, e00314–19.

Santarriaga, S., Haver, H. N., Kanack, A. J., Fikejs, A. S., Sison, S. L., Egner, J. M., et al. (2018). SRCP1 Conveys Resistance to Polyglutamine Aggregation. *Mol. Cell* 71, 216–228.e7.

Santarriaga, S., Petersen, A., Ndukwe, K., Brandt, A., Gerges, N., Bruns Scaglione, J., et al. (2015). The Social Amoeba Dictyostelium discoideum Is Highly Resistant to Polyglutamine Aggregation. *J. Biol. Chem.* 290, 25571–25578. doi: 10.1074/jbc.m115.676247

Sekine, R., Kawata, T., and Muramoto, T. (2018). CRISPR/Cas9 mediated targeting of multiple genes in Dictyostelium. *Sci. Rep.* 8:8471.

Wiebking, V., Patterson, J. O., Martin, R., Chanda, M. K., Lee, C. M., Srifa, W., et al. (2020). Metabolic engineering generates a transgene-free safety switch for cell therapy. *Nat. Biotechnol.* 38, 1441–1450. doi: 10.1038/s41587-020-0580-6

Conflict of Interest: The authors declare that the research was conducted in the absence of any commercial or financial relationships that could be construed as a potential conflict of interest.

Publisher's Note: All claims expressed in this article are solely those of the authors and do not necessarily represent those of their affiliated organizations, or those of the publisher, the editors and the reviewers. Any product that may be evaluated in this article, or claim that may be made by its manufacturer, is not guaranteed or endorsed by the publisher.

Copyright © 2021 Williams, Wu and Scaglione. This is an open-access article distributed under the terms of the Creative Commons Attribution License (CC BY). The use, distribution or reproduction in other forums is permitted, provided the original author(s) and the copyright owner(s) are credited and that the original publication in this journal is cited, in accordance with accepted academic practice. No use, distribution or reproduction is permitted which does not comply with these terms.

frontiers in Cell and Developmental Biology

ORIGINAL RESEARCH
published: 16 August 2021
doi: 10.3389/fcell.2021.743011

Differential Roles of Actin Crosslinking Proteins Filamin and α-Actinin in Shear Flow-Induced Migration of *Dictyostelium discoideum*

*Aaron Cole, Sarah Buckler, Jack Marcucci and Yulia Artemenko**

Department of Biological Sciences, State University of New York Oswego, Oswego, NY, United States

OPEN ACCESS

Edited by:
Robert J. Huber, Trent University, Canada

Reviewed by:
Douglas N. Robinson, Johns Hopkins Medicine, United States
Pascale G. Charest, University of Arizona, United States

***Correspondence:**
Yulia Artemenko
yulia.artemenko@oswego.edu

Specialty section:
This article was submitted to Molecular and Cellular Pathology, a section of the journal Frontiers in Cell and Developmental Biology

Received: *17 July 2021*
Accepted: *28 July 2021*
Published: *16 August 2021*

Citation:
Cole A, Buckler S, Marcucci J and Artemenko Y (2021) Differential Roles of Actin Crosslinking Proteins Filamin and α-Actinin in Shear Flow-Induced Migration of Dictyostelium discoideum. Front. Cell Dev. Biol. 9:743011. doi: 10.3389/fcell.2021.743011

Shear flow-induced migration is an important physiological phenomenon experienced by multiple cell types, including leukocytes and cancer cells. However, molecular mechanisms by which cells sense and directionally migrate in response to mechanical perturbation are not well understood. *Dictyostelium discoideum* social amoeba, a well-established model for studying amoeboid-type migration, also exhibits directional motility when exposed to shear flow, and this behavior is preceded by rapid and transient activation of the same signal transduction network that is activated by chemoattractants. The initial response, which can also be observed following brief 2 s stimulation with shear flow, requires an intact actin cytoskeleton; however, what aspect of the cytoskeletal network is responsible for sensing and/or transmitting the signal is unclear. We investigated the role of actin crosslinkers filamin and α-actinin by analyzing initial shear flow-stimulated responses in cells with or without these proteins. Both filamin and α-actinin showed rapid and transient relocalization from the cytosol to the cortex following shear flow stimulation. Using spatiotemporal analysis of Ras GTPase activation as a readout of signal transduction network activity, we demonstrated that lack of α-actinin did not reduce, and, in fact, slightly improved the response to acute mechanical stimulation compared to cells expressing α-actinin. In contrast, shear flow-induced Ras activation was significantly more robust in filamin-null cells rescued with filamin compared to cells expressing empty vector. Reduced responsiveness appeared to be specific to mechanical stimuli and was not due to a change in the basal activity since response to global stimulation with a chemoattractant and random migration was comparable between cells with or without filamin. Finally, while filamin-null cells rescued with filamin efficiently migrated upstream when presented with continuous flow, cells lacking filamin were defective in directional migration. Overall, our study suggests that filamin, but not α-actinin, is involved in sensing and/or transmitting mechanical stimuli that drive directed migration; however, other components of the actin cytoskeleton likely

also contribute to the initial response since filamin-null cells were still able to activate the signal transduction network. These findings could have implications for our fundamental understanding of shear flow-induced migration of leukocytes, cancer cells and other amoeboid-type cells.

Keywords: directed migration, mechanotransduction, signal transduction network, mechanical perturbation, shear stress, cell cortex

INTRODUCTION

Directed migration of cells to cues from their environment plays an important role in diverse physiological and pathophysiological processes, including embryo development, inflammation and cancer metastasis (Barriga and Theveneau, 2020; SenGupta et al., 2021). The best understood mode of directed cell migration is chemotaxis, where cells detect a chemical gradient in the environment and migrate relative to that gradient. However, other environmental conditions, such as substrate stiffness (durotaxis), electric fields (galvanotaxis), and physical forces, such as shear flow, can also guide migration, although the molecular mechanisms of these types of directed migration are not well understood (Shellard and Mayor, 2020).

In vivo cells experience a variety of shear forces depending on the anatomical location. In addition to the shear forces experienced by cells within blood and lymphatic vessels, ranging from < 1 to 12 dyn/cm^2 in the lymphatic system, up to 6 dyn/cm^2 in the veins, and 10–70 dyn/cm^2 in the arteries, most cells are also subject to interstitial fluid flow caused by plasma that leaks out of the capillaries and drains through the tissue to the lymphatic system (Malek et al., 1999; Wiig and Swartz, 2012). Although shear stress values generated by interstitial fluid flow are small under physiological conditions (<0.1 dyn/cm^2), lymphatic and interstitial flow is increased in the stroma of most tumors because of the leaky vasculature, and this can influence multiple processes in the tumor microenvironment, including adhesion and migration of fibroblasts and tumor cells (Swartz and Lund, 2012). Recent studies have shown that shear flow promotes migration of various cancer cell lines and can even induce changes from mesenchymal to amoeboid-type migration of breast cancer cells in a 3D matrix (Qazi et al., 2013; Huang et al., 2015). Shear flow is also critical for migration of leukocytes following arrest within the blood vessel, as well as for transmigration (Valignat et al., 2013; Fine et al., 2016). Somewhat surprisingly, the direction of cell migration in response to shear flow appears to be dependent on a variety of factors and migration can occur either upstream or downstream of the flow depending on the type of cells, the types of adhesion molecules they express, and the strength of the shear stress (Fache et al., 2005; Valignat et al., 2013; Dominguez et al., 2015; Artemenko et al., 2016; Buffone et al., 2018, 2019).

Social amoeba *Dictyostelium discoideum* has been instrumental in understanding the biochemical and molecular pathways that control directional cell movement (Devreotes et al., 2017; Stuelten et al., 2018; Bozzaro, 2019). The amoeboid-type migration of single *D. discoideum* cells, characterized by fast speed and weak interaction with the substrate, is remarkably similar to the migration of mammalian cells, including neutrophils, stem cells and metastatic cancer cells (Paluch et al., 2016). Importantly, both the overall organization of the regulatory networks, as well as individual signal transduction pathways, are conserved between *D. discoideum* and mammalian cells, such as leukocytes (Artemenko et al., 2014). *D. discoideum* relies on directed migration to chemoattractants throughout its unique life cycle (Bozzaro, 2019). During the single-cell growth (vegetative) stage, *D. discoideum* sense chemoattractants to locate food sources. When food becomes scarce, cells initiate a developmental program that allows thousands of cells to chemotax toward each other, eventually forming multicellular aggregates that differentiate to produce a fruiting body with spores. However, given the diverse environment of the forest floor, where *D. discoideum* is naturally found, it is not surprising that these cells are also able to respond and directionally migrate to other stimuli, including shear flow, making this organism an excellent model system for investigating the molecular mechanisms of this process.

Unlike chemotaxis, where the process is initiated by binding of a chemoattractant to a receptor, how mechanical stimuli are detected and converted to a biochemical response that leads to directed migration is less clear. Mechanical perturbation could cause physical changes in the interaction between the cell and the substrate, induce ion channel opening, affect the linkage between the membrane and the cytoskeleton, and/or perturb the cytoskeleton itself. In particular, integrins and mechanosensitive ion channels have been implicated as important mechanotransducers in a variety of cell types, although relatively few studies examined the mechanism of mechanotransduction in shear flow-induced migration (Ranade et al., 2015; Han and de Rooij, 2016). In *Dictyostelium* and some mammalian cells, Ca^{2+} appears to be an important regulator of shear flow-induced motility (Fache et al., 2005; Zhu et al., 2014; Gao et al., 2019). Consistent with the role of calcium in this type of directed migration, Lima et al. (2014) demonstrated that PKD2, a homolog of human polycystin-2 component of the mechanosensitive cation channel PKD, is required for migration of vegetative *Dictyostelium* cells in response to shear flow, although another mechanosensitive channel MclN might also play a minor role (Lima et al., 2014). Interestingly, studies in T lymphocytes, whose direction of migration depends on whether they express integrins that can bind to ICAM or LFA-1, might not have specific mechanosensors and their shear flow-induced migration appears to be determined by passive steering by the non-adherent part of the cell (Valignat et al., 2013, 2014; Hornung et al., 2020).

Although the initial steps in sensing mechanical cues are not clear, previous research has shown that shear flow activates the same signal transduction network that is activated by chemoattractants (Artemenko et al., 2016). This excitable signal transduction network consists of multiple parallel and interconnected pathways that ultimately feed into the actin cytoskeletal network, biasing actin polymerization and pseudopod protrusion in the direction of the guidance cue (Devreotes et al., 2017). The polarized distribution of signal transduction network components defines the leading and lagging edges of the cell, with similar distribution seen at the tip and bases of individual protrusions. Importantly, uniform stimulation with a chemoattractant or brief stimulation with shear flow leads to a transient global response of the signal transduction and cytoskeletal networks, which can be observed by accumulation and/or activation of leading edge markers, such as Ras, phosphatidylinositol 3-kinase (PI3K) and actin polymerization, at the cell cortex. Concomitantly, back markers, such as PTEN and myosin II, relocalize from the cortex to the cytosol. When cells are first introduced to a gradient of a chemoattractant or to shear flow, biased signal transduction and cytoskeletal network activity is observed only after the initial global response (Artemenko et al., 2016). Thus, measurement of the initial response allows us to gain insight into the ability of the cell to sense and respond to the stimulus.

One clear distinction between chemical and mechanical stimulus sensing is that cells treated with latrunculin A, which disrupts the actin cytoskeleton, are unable to activate their signal transduction network in response to shear flow, but can do so in response to a chemoattractant (Parent et al., 1998; Artemenko et al., 2016; Pal et al., 2019). This suggests that an intact actin cytoskeleton is required for sensing or transmitting mechanical stimuli; however, what aspect of the cytoskeleton is involved in this process is unclear. The importance of the actin cytoskeleton in this system suggests that actin-associated proteins may bridge the gap between mechanical stimulation and a biochemical response.

Several actin crosslinkers, including filamin and α-actinin, have been implicated in mechanosensation downstream of integrins in mammalian cells, as well as in cortical mechanosensing independent of adhesion (Han and de Rooij, 2016; Schiffhauer and Robinson, 2017). Both filamin and α-actinin possess an actin-binding domain (ABD) as well as a dimerization domain responsible for mediating formation of Y-shaped or anti-parallel dimers, respectively. While α-actinin bundles actin filaments tightly and crosslinks them in a parallel orientation, filamin crosslinks actin filaments together orthogonally (Razinia et al., 2012; Murphy and Young, 2015). Mechanical stress applied to filamin or α-actinin reveals cryptic binding sites that provide alternate binding locations, for example for integrin or vinculin, while under mechanical stress (Razinia et al., 2012; Le et al., 2017). Importantly, filamin and α-actinin accumulate at different zones of stress in response to mechanical stimuli delivered by micropipette aspiration (Luo et al., 2013), suggesting they likely have divergent functions in sensing or transmitting mechanical stimuli.

Unlike multiple isoforms of filamin and α-actinin found in mammalian cells, *D. discoideum* has a single isoform of each crosslinker. Mutant strains lacking *D. discoideum* filamin (ddFLN, ABP120, gelation factor) or α-actinin (ddACTN) did not have strong phenotypes on overall behavior at the single cell stage, including growth, development, random motility and chemotaxis, although more severe defects were observed when ddFLN was deleted in a different genetic background (Schleicher et al., 1988; Brink et al., 1990; Cox et al., 1992; Rivero et al., 1996). This could be due to functional redundancy of the crosslinkers, since mutants lacking both ddFLN and ddACTN had severe defects in growth, development, and migration (Witke et al., 1992; Rivero et al., 1996). Despite the minor differences in behavior in the original null strains, absence of individual crosslinkers led to changes in the viscoelastic properties of the cells (Eichinger et al., 1996). Increased levels of actin crosslinkers likely also have effects on cortical stiffness and could explain why overexpression of ddFLN adversely affects cell migration, particularly in a 3D environment (Roth et al., 2015).

Although both filamin and α-actinin have been implicated in mechanosensation, their role in regulating shear flow-induced migration has remained largely unexplored. Thus, in this study we investigated the role of filamin and α-actinin in the initial response of *D. discoideum* cells to brief stimulation with shear flow and demonstrated that only filamin appears to participate in sensing and/or transmitting the mechanical stimulus in this system. Consistent with the requirement of the initial response for shear-flow induced migration under continuous flow, cells lacking filamin had aberrant directed migration against the flow direction compared to cells with filamin, further implicating this actin crosslinker as an important player in this mechanically-driven form of directed migration.

MATERIALS AND METHODS

Cell Culture and Generation of *D. discoideum* Strains

D. discoideum cells were maintained under standard conditions on plates or in shaking culture in HL-5 media (Artemenko et al., 2011). Wild-type (Ax2) cells were generously provided by R. Kay (MRC Laboratory of Molecular Biology, Cambridge, United Kingdom). α-actinin-null (*abpA*$^-$; strain ID DBS0235459) and filamin-null (*abpC*$^-$; strain ID DBS0236077) cell lines used in this study were obtained from the Dicty Stock Center (Chicago, IL, United States). Note that for clarity, *abpA*$^-$ and *abpC*$^-$ will be referred to as *actn*$^-$ and *fln*$^-$, respectively.

Ax2, *actn*$^-$, or *fln*$^-$ cells were transformed with RBD-GFP and/or mCherry-ddFLN, mCherry-ddFLN$_{\Delta ABD}$, mCherry-ddACTN or pDRH by electroporation according to the standard electroporation protocol (Gaudet et al., 2007). Transformed cells were selected with 20 μg/ml G418 and/or 50 μg/ml hygromycin B for at least 2 weeks prior to analysis.

pDRH, mCherry-ddFLN in pDRH, and ddACTN-GFP in pDN plasmids were generously provided by D. Robinson (Johns Hopkins University). RBD-GFP construct in pDM323 was generously provided by P. Devreotes (Johns Hopkins University).

mCherry-ddFLN$_{\Delta ABD}$ and mCherry-ddACTN were generated in this study as described below.

Plasmid Construction

To generate mCherry-ddACTN in the pDRH vector, the ddACTN gene was amplified from a pDN-ddACTN-GFP template by PCR utilizing Phusion High-Fidelity PCR Master Mix (Thermo Scientific). The forward and reverse primers used were 5′-GGCGTCGACTCAGAAGAACCAACCCCAG-3′ and 5′-ACTACAATTCATTTGCTGGCGGCCGCCC-3′, which incorporated *Sal*I and *Not*I restriction sites, respectively. pDRH-mCherry-ddFLN plasmid was digested with *Sal*I and *Not*I restriction enzymes (Thermo Scientific) to remove the ddFLN gene without the mCherry tag, dephosphorylated with FastAP thermosensitive alkaline phosphatase (Thermo Scientific), and purified with the GeneJET^{TM} gel extraction kit (Thermo Scientific). Following digestion with *Sal*I and *Not*I, ddACTN gene was ligated into the digested pDRH-mCherry fragment using T4 DNA ligase (Thermo Scientific). Ligation products were transformed into NEB® 5-alpha competent *Escherichia coli* (high efficiency) cells (New England Biolabs) and selected on LB agar plates with 150 μg/mL ampicillin. Plasmids were isolated using the GeneJET^{TM} Plasmid Miniprep Kit (Thermo Scientific) and digested with *Sal*I and *Not*I to confirm successful ligation. Successful clones were verified by sequencing (Genewiz).

mCherry-ddFLN$_{\Delta ABD}$ was generated by amplifying ddFLN starting at position 745 (corresponding to amino acid 249) based on the study by Washington and Knecht using 5′-GGCGTCGACGATGCCAGCAAGGTTGAAGTTTATGG-3′ and 5′-GGCGCGGCCGCTTAATTGGCAGTACGAGTAGTAG TG-3′ primers, which incorporated *Sal*I and *Not*I sites, respectively (Washington and Knecht, 2008). Following amplification, the insert was ligated into pDRH-mCherry as described above for the ddACTN construct.

Preparation of Vegetative *D. discoideum* Cells

D. discoideum cells were grown in the presence of *Klebsiella aerogenes* on SM plates as described in Artemenko and Devreotes (2017). Briefly, *K. aerogenes* was grown in an antibiotic-free HL-5 medium overnight (16–18 h). 6×10^5–1.2×10^6 *D. discoideum* cells were added onto SM plates with 260 μL of the *K. aerogenes* suspension. The plates were incubated at room temperature for 2 days. To collect the cells, the lawn containing *K. aerogenes* and *D. discoideum* was scraped with a sterile spreader into DB buffer (1x phosphate buffer supplemented with 2 mM MgSO4 and 0.2 mM CaCl2), collected in a 50 mL polypropylene centrifuge tube, and centrifuged at 500 *g* for 3–4 min. Following several washes with DB, the pellet was resuspended to $\sim 5 \times 10^6$ cells/mL.

Mechanical Stimulation of *D. discoideum*

Vegetative cells collected from *K. aerogenes* lawn were diluted to $\sim 1 \times 10^6$ cells/mL in DB, plated on a μ-Slide III^{3in1} fluidic chamber (Ibidi) and allowed to attach for 10 min. The fluidic slide was attached to the Ibidi pump system and the cells were briefly washed with DB buffer as previously described (Artemenko and Devreotes, 2017). Cells were imaged with epifluorescence with a GFP or an RFP filter on a Zeiss LSM 700 microscope equipped with a 63 × /1.3 oil objective lens and a Zeiss MRc AxioCam camera. Images were taken at 3 s intervals for 60 s. Immediately after the fifth frame, the cells were mechanically stimulated using the Ibidi pump at the indicated pressure for 2 s. The highest pressure applied was 50 mbar, which corresponded to ∼45 dyn/cm^2 shear stress. We also used flow driven by gravity alone and varied the pressure by changing the height of the pump, which allowed us to generate shear stress values of ∼23, ∼17, ∼12 and ∼6 dyn/cm^2. Shear stress values were calculated by measuring the volume of fluid collected in the drain over time and converting it to shear stress values using the formula provided by the manufacturer (Ibidi) for the 3 mm channel in the μ-Slide III^{3in1} fluidic chamber: $\tau = \eta \times 227.4 \times \Phi$, where τ is shear stress, η is the dynamic viscosity of the medium, which is the viscosity of water at 20°C (0.01 dyn·s/cm^2), and Φ is the flow rate in mL/min. It should be noted that shear stress values are approximated, rather than exact, because there was slight variation (maximum of ∼4 dyn/cm^2) between shear stress values depending on the volume of buffer in the reservoir; however, for the assays the fluctuation in the volume of buffer in the reservoir was kept to a minimum. In all of the images produced, flow was applied from right to left.

Chemical Stimulation of *D. discoideum*

Vegetative cells were grown and collected from *K. aerogenes* lawn as described above. 1×10^5 cells were plated in 450 μl of DB in 8-well Nunc^{TM} Lab–Tek^{TM} II chambered coverglass. Cells were imaged every 3 s for 20 frames with epifluorescence with a GFP or RFP filter set on a Zeiss LSM 700 microscope equipped with a 63 × /1.3 oil objective lens and a Zeiss MRc AxioCam camera. After frame 5, 50 μl of 1 mM folic acid was introduced to the cells.

Image Analysis for Mechanical and Chemical Stimulation

Images were analyzed using Fiji (ImageJ 1.53c) software (Schindelin et al., 2012; Artemenko and Devreotes, 2017). Every cell image that was in focus was quantified, except for analysis of RBD-GFP signal in rescue cells, where only cells expressing mCherry-ddFLN, mCherry-ddFLN$_{\Delta ABD}$ or mCherry-ddACTN were quantified. The background was subtracted, and a box was drawn within the cytoplasm of a given cell. The mean intensity inside this box was quantified for every frame produced. Care was taken to avoid areas within the cell with a visible nucleus or a concentration of vesicles as this would provide false drops in levels of cytoplasmic intensity. The quantified levels of cytosolic intensity were normalized for time 0 and inverted to provide values of cortical accumulation. Note that due to slight transient shift in the focal plane that was occasionally observed for the frame immediately following the stimulation, the 3 s time point was omitted from the analysis.

Migration Assay

To measure cell movement, both randomly and in response to shear flow, vegetative cells grown with *K. aerogenes* were collected, washed, and plated as described above for mechanical stimulation experiments. Cells were imaged with brightfield illumination using a Zeiss LSM 700 confocal microscope equipped with a 20X objective lens and a Zeiss MRc AxioCam camera. Time lapse images were taken every 10 s. To quantify random migration, cells were imaged for 60 frames in the absence of flow. To measure directed migration, cells were subjected to continuous flow for 120 frames using the Ibidi pump with an open reservoir. For this assay 6, 12, or 17 dyn/cm^2 shear stress value was used.

50 randomly selected cells were tracked for each experiment with the Tracking Tool^{TM} PRO v2.1 software (Gradientech). For random migration, analysis was started 2 min after the beginning of the assay and proceeded for 5 min. For directed migration, analysis was started 2 min after shear flow was introduced and proceeded for 18 min. Velocity, directness, and forward migration index were calculated using TrackingTool Pro, which reports average values for the 50 cells analyzed. Velocity measures the overall cell displacement over time in μm/min. Directness is calculated as a ratio of the shortest distance between the start and end points of the path traveled to the total accumulated distance traveled by a cell. Forward migration index refers to the directness in the direction of the applied stimulus and is calculated using the end point in the x direction divided by accumulated distance. In this case flow was applied from right to left, so a forward migration index value of 1 would indicate migration directly against the flow and −1 would indicate migration with the flow.

Statistical Analysis

An unpaired two-tailed, two-sample equal variance student's t-test was used to analyze differences between cell lines at every time point of mechanical or chemical stimulation assays. A paired student's t-test was used to test for differences between two cell lines for migration analysis. $P < 0.05$ was considered statistically significant.

RESULTS

Filamin and α-Actinin Transiently Accumulate at the Cortex in Response to Mechanical Stimulation

To determine whether actin crosslinking proteins ddFLN and ddACTN are involved in regulating the response of cells to shear flow, we first examined the behavior of these proteins following stimulation with shear flow. Both mCherry-tagged ddFLN and ddACTN transiently localized to the cell cortex of wild-type cells following 2 s stimulation with shear flow at 45 dyn/cm^2 (**Figure 1** and **Supplementary Video 1**). Cortical accumulation peaked at 6–9 s after shear flow stimulation, consistent with the timing of the peak response of other leading edge markers and actin polymerization at the cortex (Artemenko et al., 2016).

Filamin Is Required for Optimal Response to Acute Mechanical Stimulation

To test if filamin is required for the response to mechanical perturbation, we assessed spatiotemporal activation of Ras using the Ras-binding domain (RBD) biosensor, which has been previously shown to detect transient activation of Ras on the cortex following brief stimulation with shear flow (Artemenko et al., 2016). We used cells that lack filamin and express either empty vector (*fln*$^-$) or mCherry-ddFLN (rescue), as well as GFP-tagged RBD. Following 2 s stimulation with shear flow at 45 dyn/cm^2, rescue cells showed the expected peak of RBD accumulation at the cortex at around 6 s (**Figure 2A**). Although *fln*$^-$ cells expressing an empty vector also showed a robust transient RBD response following stimulation, the peak response was significantly reduced compared to rescue cells by 32% (0.16 ± 0.02 vs. 0.23 ± 0.03 response over basal for *fln*$^-$ vs. rescue cells, respectively; mean ± SE; $P < 0.05$; **Figure 2D**).

Since 45 dyn/cm^2 is a strong stimulus that might mask the reduced sensitivity of *fln*$^-$ cells, we also tested RBD-GFP response in *fln*$^-$ and rescue cells following exposure to weaker shear forces, although the time of stimulation remained brief (2 s). At 23 dyn/cm^2, the response of rescue cells was still very robust, although the peak shifted to 9 s (**Figure 2B**). The response of *fln*$^-$ cells was even further reduced and was significantly different from the rescue both at 6 and 9 s, with a decrease of 50% for the 6 s peak (0.11 ± 0.02 vs. 0.23 ± 0.03 response over basal for *fln*$^-$ vs. rescue cells, respectively; mean ± SE; $P < 0.001$; **Figures 2B, D**). Finally, at 12 dyn/cm^2 the difference in the response was even more pronounced at 6 s with a 68% reduction in the response for *fln*$^-$ vs. rescue cells (0.06 ± 0.02 vs. 0.20 ± 0.03 response over basal for *fln*$^-$ vs. rescue cells, respectively; mean ± SE; $P < 0.001$; **Figures 2C, D** and **Supplementary Video 2**). A somewhat surprising observation was that while the response of *fln*$^-$ cells was reduced at subsequently lower shear stress values, the response of rescue cells remained relatively constant, suggesting rescue cells might have increased sensitivity to mechanical stimulation. Overall, this suggests that ddFLN plays a role in the cell's ability to respond to brief mechanical perturbation.

Reduced Response of Cells Lacking ddFLN to Mechanical Stimulation Is Not Due to Overall Disruption of the Signal Transduction Network

We noticed that *fln*$^-$ cells tended to have increased cortical RBD localization following the shut-off after the initial response to shear flow stimulation, suggesting that, perhaps, these cells generate more protrusions and/or become more motile compared to cells rescued with mCherry-ddFLN following stimulation. To check if *fln*$^-$ and rescue cells might have differences in their basal activity, which would explain their differential responsiveness to stimulation, we examined random motility of both cell lines (**Figure 3A, Table 1,** and **Supplementary Video 3**). However, the two cell lines had comparable random migration speeds of 10.6 ± 1.6 and

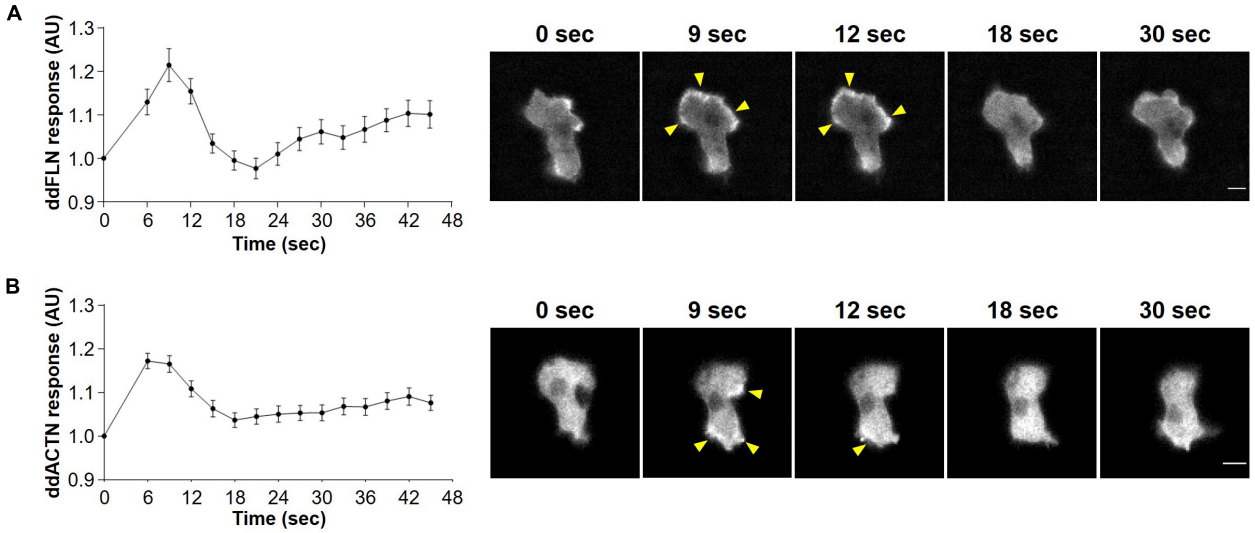

FIGURE 1 | Localization of filamin and α-actinin in response to acute treatment with shear flow. Wild-type cells expressing mCherry-tagged ddFLN **(A)** or mCherry-tagged ddACTN **(B)** were imaged every 3 s by epifluorescence microscopy with an RFP filter set under 630X magnification with oil immersion. Shear flow at 45 dyn/cm^2 was applied at time 0 for 2 s. Response was measured as protein relocalization from the cytosol to the cell cortex. Data is displayed as mean ± SE of 45 **(A)** or 85 **(B)** cells pooled from three independent experiments. A representative cell is shown to the right of the graph. Arrowheads point to mCherry-tagged protein accumulation at the cortex. Scale bar, 5 μm.

8.2 ± 1.3 μm/min for *fln*$^-$ and rescue cells, respectively (mean ± SE; $n = 4$; $P > 0.05$). It should be noted that there was a very small, but statistically significant, difference in the directness of the two cell lines (0.54 ± 0.03 vs. 0.50 ± 0.03 for *fln*$^-$ vs. rescue cells, respectively; mean ± SE; $n = 4$; $P < 0.01$).

We also tested the response of these cells to a chemoattractant; however, global stimulation with folic acid resulted in the same magnitude of the RBD response in both rescue and *fln*$^-$ cells (**Figure 3B** and **Supplementary Video 4**). This suggests that the reduced responsiveness of cells lacking ddFLN to mechanical cues is not due to a general decrease in the ability to activate the signal transduction network.

Filamin Overexpression Slightly Improves the Response of the Signal Transduction Network to Mechanical Stimulation

It is possible that expression of ddFLN in *fln*$^-$ cells improved the response because of increased levels of ddFLN compared to endogenous levels in wild-type cells. To address this, we expressed mCherry-tagged ddFLN in wild-type cells and assessed their responsiveness to acute shear flow stimulation. Following application of the strong 45 dyn/cm^2 shear stress stimulus, the initial response was comparable between wild-type cells expressing empty vector and mCherry-tagged ddFLN (**Figures 4A,C**). However, at the lower shear stress of 23 dyn/cm^2 the initial response of overexpressors at 6 s post-stimulation was slightly stronger compared to cells with endogenous levels of ddFLN, although this difference did not quite reach statistical significance (0.10 ± 0.02 vs. 0.15 ± 0.02 response over basal for wild-type vs. overexpressor cells, respectively; mean ± SE; $P = 0.05$; **Figures 4B,C**). Interestingly, similarly to the observations in rescue cells in **Figures 2A–C**, overexpression of ddFLN in wild-type cells also appeared to reduce the secondary cortical RBD accumulation after the initial shut-off with significant differences found for most time points between 15 and 45 s following stimulation (**Figure 4A**). This was not likely due to differences in the overall basal activation state of the cells since random motility was comparable between the two cell lines (**Figure 4D, Table 1,** and **Supplementary Video 5**).

Filamin's Actin-Binding Domain Is Required for Its Role in Shear Flow-Induced Response

To begin understanding how ddFLN is able to regulate cell response to shear flow, we generated mCherry-tagged ddFLN that lacks its actin-binding domain (ddFLN$_{\Delta ABD}$). Surprisingly, ddFLN$_{\Delta ABD}$ was still transiently recruited to the cortex of wild-type cells following 2 s stimulation with shear flow at 45 dyn/cm^2 (**Figure 5A** and **Supplementary Video 6**). Since this relocalization could be mediated by dimerization of ddFLN$_{\Delta ABD}$ with endogenous ddFLN, we also tested ddFLN$_{\Delta ABD}$ response in *fln*$^-$ cells. In the absence of endogenous ddFLN, there was no change in localization of ddFLN$_{\Delta ABD}$ following shear flow stimulation (**Figure 5B** and **Supplementary Video 6**). Since overall signal transduction network response to shear flow is reduced in *fln*$^-$ cells, we observed the behavior of ddFLN$_{\Delta ABD}$ concomitantly with RBD-GFP; however, even when RBD-GFP translocation was clearly observed, ddFLN$_{\Delta ABD}$ failed to relocalize in response to acute shear flow stimulation (**Figure 5C**).

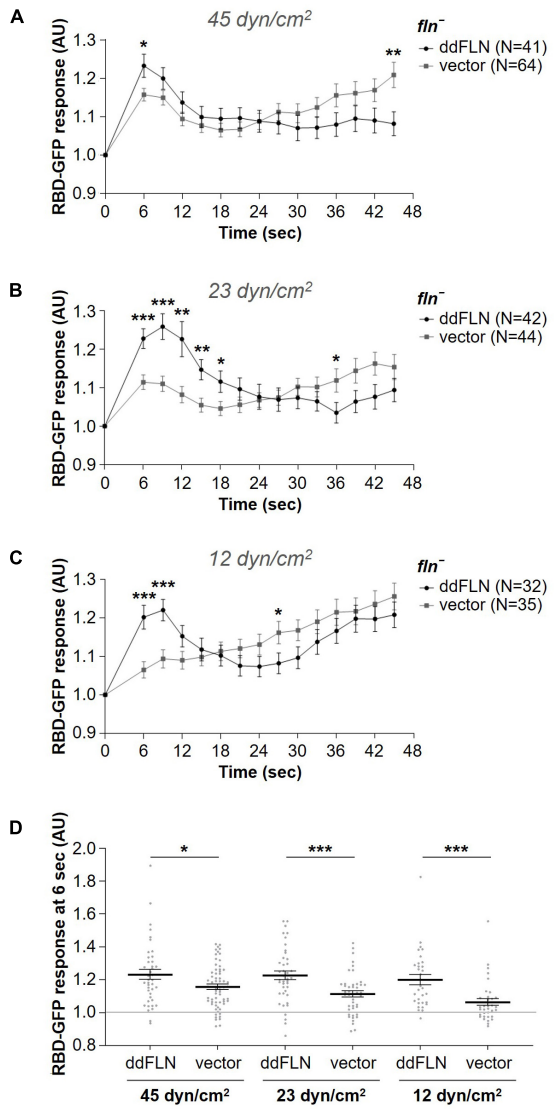

FIGURE 2 | Filamin is required for optimal activation of the signal transduction network in response to acute stimulation with shear flow. **(A–C)** Activation of Ras, which reflects activation of the signal transduction network, was measured by the relocalization of RBD-GFP from the cytosol to the cell cortex. *fln*⁻ cells expressing RBD-GFP and either mCherry-tagged ddFLN or empty vector were imaged every 3 s by epifluorescence microscopy with a GFP filter set under 630X magnification with oil immersion. Shear flow was applied at time 0 for 2 s. The shear stress delivered to the cells was 45 dyn/cm^2 **(A)**, 23 dyn/cm^2 **(B)**, or 12 dyn/cm^2 **(C)**. Data is displayed as mean ± SE. Number of cells analyzed is provided in the key and was pooled from four **(A)** or three **(B, C)** independent experiments. **(D)** RBD-GFP response values for individual cells from panels **(A–C)** at the 6 s time point. Horizontal lines with error bars correspond to mean ± SE. A line at the RBD-GFP response value of 1.0 is shown as a reference to indicate basal levels at time 0. *$P < 0.05$, **$P < 0.01$, and ***$P < 0.001$.

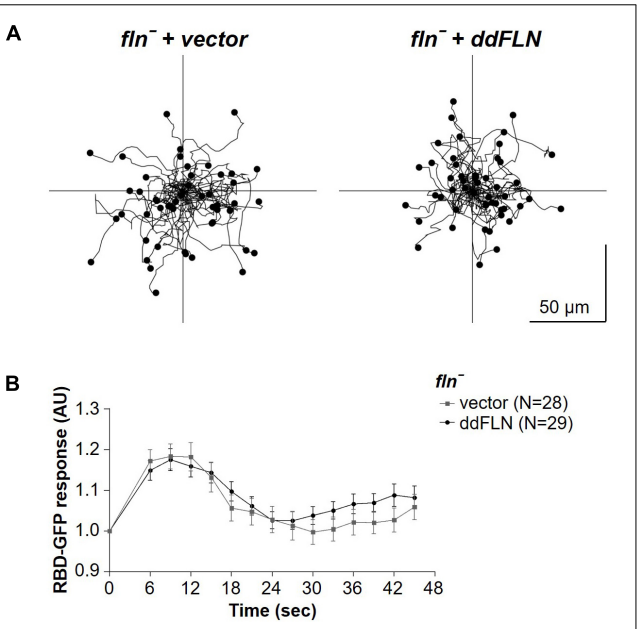

FIGURE 3 | Response to chemical stimulation and random motility is not affected by lack of filamin. **(A)** *fln*⁻ cells expressing RBD-GFP and either mCherry-tagged ddFLN or empty vector were imaged using brightfield illumination under 200X magnification every 10 s as they were migrating without any stimulation. Tracks of 50 individual cells for each condition from one representative experiment are shown. Average data from four separate experiments is shown in **Table 1**. **(B)** The same cells as in panel **(A)** were stimulated with 100 µM folic acid at time 0. Response was measured as an inverse of drop in cytosolic intensity of RBD-GFP. Data is shown as mean ± SE. Number of cells analyzed is provided in the key and was pooled from four (ddFLN) or three (vector) separate stimulations.

TABLE 1 | Random migration of *fln*− and wild-type cells expressing mCherry-tagged ddFLN or empty vector.

Strain	Velocity (µm/min)	Directness
fln− + ddFLN	8.2 ± 1.3[a]	0.50 ± 0.03
fln− + vector	10.6 ± 1.6	0.54 ± 0.03**
WT + ddFLN	16.6 ± 1.1	0.489 ± 0.007
WT + vector	17.5 ± 1.1	0.477 ± 0.003

[a]*Values are mean ± SE of three experiments with 50 cells analyzed and averaged for each experiment. Images were acquired every 10 s for 7 min and cells were tracked for the last 5 min.*

***P < 0.01 compared to fln− + ddFLN cells.*

Thus, ddFLN accumulation at the cortex is likely mediated *via* its interaction with the actin cytoskeleton.

Next, we examined whether ddFLN$_{\Delta ABD}$ can rescue the impaired response of *fln*− cells to acute mechanical stimulation by examining localization of active Ras using the RBD-GFP biosensor (**Figure 5D**). As expected, *fln*− cells expressing ddFLN$_{\Delta ABD}$ had a similar response to cells expressing empty vector, confirming that ddFLN requires its ability to interact with the actin cytoskeleton for its role in sensing or transmitting mechanical stimuli.

Lack of ddFLN Leads to Impaired Shear Flow-Induced Migration

Since ddFLN appears to be important for the activation of the signal transduction network in response to shear flow, we next

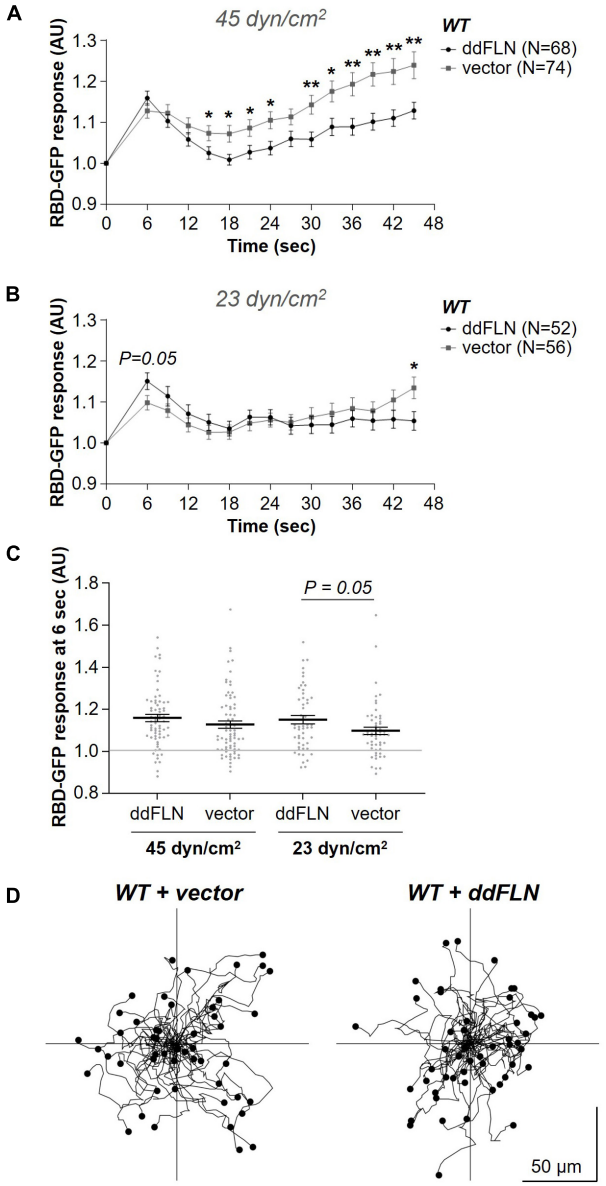

FIGURE 4 | Overexpression of filamin slightly improves activation of the signal transduction network in response to shear flow without affecting the basal activity of the cells. **(A–C)** Activation of Ras, which reflects activation of the signal transduction network, was measured by the relocalization of RBD-GFP from the cytosol to the cell cortex. Vegetative wild-type (WT) cells expressing RBD-GFP and either mCherry-ddFLN or empty vector were imaged every 3 s by epifluorescence microscopy with a GFP filter set under 630X magnification with oil immersion. The shear stress delivered to the cells was 45 dyn/cm^2 **(A)** or 23 dyn/cm^2 **(B)**. Data is displayed as mean ± SE. Number of cells analyzed is provided in the key and was pooled from four **(A)** or three **(B)** independent experiments. **(C)** RBD-GFP response values for individual cells from panels **(A,B)** at the 6 s time point. Horizontal lines with error bars correspond to mean ± SE. A line at the RBD-GFP response value of 1.0 is shown as a reference to indicate basal levels at time 0. *$P < 0.05$, **$P < 0.01$. **(D)** The same cells as in panels **(A–C)** were imaged as they were migrating without any stimulation using brightfield illumination under 200X magnification every 10 s. Tracks of 50 individual cells for each condition from one representative experiment are shown. Average data from three separate experiments is shown in **Table 1**.

wanted to test if it is required for shear flow-induced migration. We first subjected wild-type cells to a variety of shear forces to determine the optimal conditions for examining shear flow-induced migration. As can be seen in **Supplementary Video 7**, wild-type cells migrated upstream at shear stress values of 6 and 12 dyn/cm^2, but began losing direction and started detaching by 17 dyn/cm^2. We chose to perform subsequent migration analysis at 6 dyn/cm^2 since this condition resulted in robust migration against the flow without loss of cells by detachment. Similarly to wild-type cells, *fln*$^-$ cells transformed with mCherry-tagged ddFLN showed a clear preference for migration against shear flow (**Figure 6, Table 2,** and **Supplementary Video 8**). On the other hand, *fln*$^-$ cells appeared to be migrating more randomly, which was reflected in a significant reduction in the forward migration index compared to the rescue cells (0.1 ± 0.2 vs. 0.5 ± 0.1 for *fln*$^-$ vs. rescue, respectively; $n = 3$; $P < 0.05$). Interestingly, the velocity of the two cell lines was comparable under continuous flow, although somewhat lower than when cells were migrating randomly (**Table 1**), suggesting the ddFLN plays a specific role in determining the direction of migration in response to a mechanical stimulus rather than affecting overall motility.

α-Actinin Is Not Required for Optimal Response to Acute Mechanical Stimulation

Since *fln*$^-$ cells were still able to mount a response to acute mechanical stimulation, it is likely that other actin crosslinking proteins might be involved in sensing and/or transmitting the mechanical stimulus to downstream activation of the signal transduction network. Since α-actinin is a known mechanosensor in other systems (Luo et al., 2013; Schiffhauer et al., 2016; Le et al., 2017) and is recruited to the cortex following exposure to a brief shear flow stimulus (**Figure 1B**), we tested whether this actin-binding protein is necessary for the activation of the signal transduction network in response to shear flow similarly to ddFLN. Cells lacking ddACTN (*actn*$^-$) with RBD-GFP and mCherry-tagged ddACTN or empty vector were subjected to a 2 s shear flow stimulation; however, both *actn*$^-$ and rescue cells showed similar levels of Ras activation at 45 dyn/cm^2 shear stress (**Figures 7A, C**). Notably, despite a similar initial response, *actn*$^-$ cells appeared to have increased cortical RBD signal compared to rescue cells at later time points after the stimulation ($P < 0.05$ at all time points between 24 and 45 s), although the significance of this finding is unclear. Surprisingly, at the lower 23 dyn/cm^2 shear stress level, *actn*$^-$ cells had a slightly better response than rescue cells (0.13 ± 0.02 vs. 0.08 ± 0.02 response over basal at 6 s post-stimulation for *actn*$^-$ vs. rescue cells, respectively; mean ± SE; $P < 0.05$; **Figures 7B, C**). This could mean that ddACTN is a negative regulator of the response. However, when we overexpressed ddACTN in wild-type cells, the RBD response was similar to cells with endogenous levels of ddACTN at both 45 and 23 dyn/cm^2 (**Figures 7D, E**). Thus, ddACTN is likely not required for the cell's ability to respond to acute mechanical stimulation.

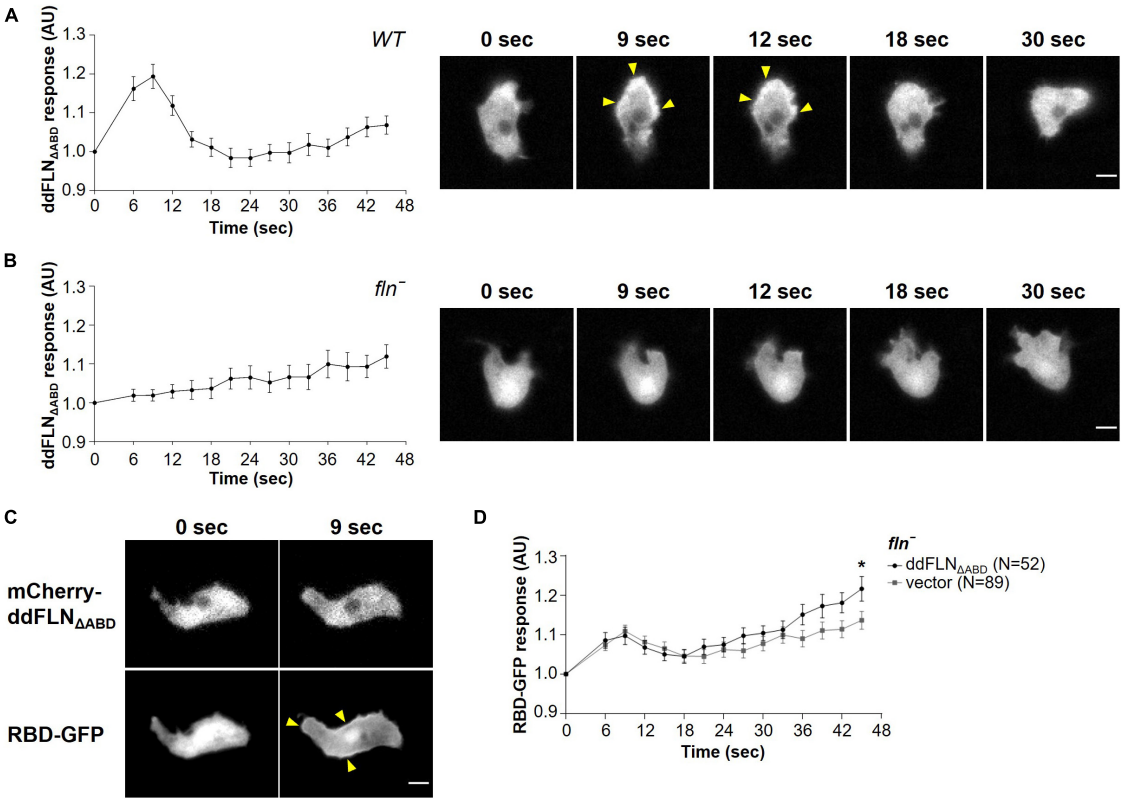

FIGURE 5 | Filamin's actin-binding domain is required for its role in shear flow-induced response. **(A–C)** Wild-type (WT) **(A)** or *fln*⁻ **(B)** cells expressing RBD-GFP and mCherry-tagged ddFLN$_{\Delta ABD}$ were imaged every 3 s by epifluorescence microscopy with an RFP filter set under 630X magnification with oil immersion. Shear flow (45 dyn/cm^2) was applied at time 0 for 2 s. Response was measured as protein relocalization from the cytosol to the cell cortex. Data is displayed as mean ± SE of 42 **(A)** or 30 **(B)** cells pooled from two independent experiments. A representative cell is shown to the right of the graph. **(C)** A representative *fln*⁻ cell expressing RBD-GFP and mCherry-tagged ddFLN$_{\Delta ABD}$ is shown to demonstrate the lack of ddFLN $_{\Delta ABD}$ translocation even in cells that have robust RBD-GFP recruitment to the cortex. Arrowheads point to biosensor accumulation at the cortex. Scale bar, 5 μm. **(D)** Activation of Ras, which reflects activation of the signal transduction network, was measured by the relocalization of RBD-GFP from the cytosol to the cell cortex in *fln*⁻ cells expressing RBD-GFP and either mCherry-tagged ddFLN$_{\Delta ABD}$ or empty vector. Cells were imaged as above with a GFP filter set every 3 s and stimulated with 2 s of shear flow (45 dyn/cm^2) at time 0. Data is displayed as mean ± SE. Number of cells analyzed is provided in the key and was pooled from three independent experiments. *$P < 0.05$.

DISCUSSION

Our study demonstrated that actin crosslinkers filamin and α-actinin play differential roles in the cell's ability to respond to mechanical stimulation delivered by shear flow. Although both of these crosslinkers have direct mechanosensitive properties, only filamin appeared to be involved in the context of shear flow-induced activation of the signal transduction network and subsequent migration against the direction of flow. Not surprisingly, this function of filamin depended on its ability to bind to actin as evidenced by the lack of rescue of the reduced response in *fln*⁻ cells by ddFLN without ABD. The residual ability of cells without ddFLN to respond to shear flow suggests that other actin-binding proteins likely contribute to sensing and/or transmitting the response.

Both filamin and α-actinin were rapidly and transiently recruited to the cortex following mechanical stimulation with the same dynamics as recruitment of other leading edge markers, such as Ras or PI3K (Artemenko et al., 2016). This is consistent with the recruitment of these proteins to the pseudopods (Washington and Knecht, 2008) and is likely driven by their association with the newly polymerizing actin at the cortex. This is supported by the finding that ddFLN without ABD is not recruited except in wild-type cells, where it can presumably dimerize with the endogenous ddFLN that is recruited to the actin cortex. It would be interesting to determine whether ddFLN function in mechanotransduction observed here depends on the newly recruited ddFLN or on ddFLN that is basally present at the cortex. Given that the peak recruitment is observed at 6–9 s, it is likely that the initial sensing or transmission of the stimulus would occur prior to the bulk accumulation of ddFLN, which likely just follows actin polymerization, although it is possible that the stabilization of the actin network by newly recruited ddFLN is what is required to efficiently transmit the stimulus.

It is unclear whether filamin is directly involved in sensing or transmitting the mechanical stimulus in this system or if it simply affects the overall cortical tension, which in turn alters the ability of a cell to sense and/or respond to the mechanical stimulus. However, it seems unlikely that reduced cortical tension overall is responsible for the decreased initial response of cells

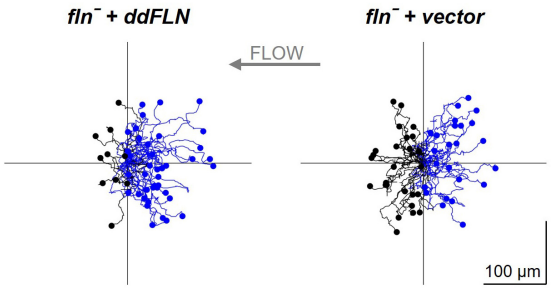

FIGURE 6 | Filamin is required for shear flow-induced migration. *fln*⁻ cells expressing RBD-GFP and either mCherry-tagged ddFLN or empty vector were subjected to continuous flow at 6 dyn/cm^2 and were imaged using brightfield illumination under 200X magnification every 10 s for 20 min. Individual cells were tracked starting 2 min after initiation of flow for the remaining 18 min. Tracks of 50 individual cells for each condition from one representative experiment are shown. Cells that showed displacement in the direction opposite of the flow are shown in blue; the rest are in black. Average data for cell speed and directionality from three separate experiments is shown in **Table 2**.

TABLE 2 | Shear flow-induced directed migration of *fln*$^-$ cells expressing mCherry-tagged ddFLN or empty vector.

Strain	Velocity (µm/min)	Directness	Forward migration index
fln$^-$ + ddFLN	7.4 ± 0.4[a]	0.51 ± 0.02	0.5 ± 0.1
fln$^-$ + vector	6.1 ± 1.2	0.48 ± 0.01	0.1 ± 0.2*

[a]*Values are mean ± SE of three experiments with 50 cells analyzed and averaged for each experiment. Images were acquired every 10 s for 20 min while cells were continuously exposed to 6 dyn/cm^2 shear stress. Cells were tracked for the last 18 min for analysis.*

*$P < 0.05$ *compared to fln*$^-$ *+ ddFLN cells.*

lacking ddFLN since cortical tension is comparable or even slightly lower in cells lacking ddACTN (Luo et al., 2013), yet α-actinin-null cells had the same or even slightly improved response to shear flow stimulation. It should be noted that in the Luo et al. (2013) study, cortical tension was measured on cells in suspension, and it is possible that cells lacking ddFLN or ddACTN have differences in their cortical properties when they are adhered to a substrate. Both filamin and α-actinin participate in the formation of adhesion complexes and their linkage to the actin cytoskeleton in mammalian cells (Han and de Rooij, 2016). Although *D. discoideum* cells do not form focal adhesions similarly to other cells undergoing amoeboid-type migration, they nonetheless have specific adhesion molecules, such as SibA (Cornillon et al., 2006), that could potentially engage with ddFLN and/or ddACTN and contribute to cortical stiffness. This possibility needs to be further explored.

Although ddACTN did not appear to be required for the initial response of the signal transduction network to the shear flow stimulus, it may still play a role in the response since cells lacking ddACTN had improved Ras activation at the cortex. Although it is possible that ddACTN somehow negatively regulates the system, this is unlikely since addition of ddACTN did not adversely affect the initial response of wild-type cells. A more likely possibility is that cells without ddACTN might have a compensatory increase in ddFLN, or other crosslinkers, which could improve the response as was shown in this study for ddFLN. Other studies have suggested functional redundancy between ddFLN and ddACTN, since only knockout of both of these actin crosslinkers leads to severe defects in cell behavior and these defects can be rescued by the addition of one or the other protein (Witke et al., 1992; Rivero et al., 1996, 1999). However, since only *fln*$^-$ cells had a clear defect in the response to shear flow stimulation in our study, it seems likely that ddFLN and ddACTN have non-redundant roles in mechanosensation and/or mechanotransduction that leads to shear flow-induced migration.

An interesting observation was that cells expressing ddFLN, either in the *fln*$^-$ or wild-type background, appeared to remain less active, as judged by Ras activation at the cortex, for the duration of the assay following the initial response. This finding was somewhat surprising since we did not notice an overt reduction in cell activity by visual inspection of the videos, nor did we see a change in the basal activity of the cells based on random migration. However, it is possible that since ddFLN improved the initial response of the cells to the shear flow stimulus, this resulted in more efficient activation of the delayed negative feedback loop that turns off the network as is proposed by the STEN-CEN model (Pal et al., 2019). Alternatively, reduced Ras activity of ddFLN-expressing cells after the initial peak could be due to a general increase in cortical tension in these cells. This is supported by the observation that *actn*$^-$ cells expressing ddACTN also showed significantly reduced RBD accumulation at the cortex between 24 and 45 s after stimulation, despite having no or inhibitory effects on the initial response. It would be interesting to examine whether cortical tension plays a role in a cell's ability to resume its activity following global stimulation with a mechanical cue. Finally, accumulation of actin crosslinkers could also lead to increased bearing of the load from shear force, which would reduce further responsiveness, and might be especially relevant in cases of continuous stimulation with shear flow.

Cells expressing ddFLN responded strongly regardless of the stimulus strength, which ranged between 12 and 45 dyn/cm^2, even though we previously showed that wild-type cells are able to distinguish between these shear stress levels and respond progressively better (Artemenko et al., 2016). Indeed, in this study, wild-type, ddFLN-null, and ddACTN-null cells showed a stronger response at higher shear stress levels. In contrast, cells expressing mCherry-ddFLN appeared to have a lower threshold for activation and responded equally strongly at all shear levels tested. Such improved sensitivity would give cells an advantage during continuous shear flow application that leads to directed migration. As the side of the cell facing the flow gets stimulated, the activation of the signal transduction network would bias actin polymerization in the direction of the gradient. Although this may suggest that the observed defect in the response of *fln*$^-$ cells only appears as a defect because it is compared to the improved response of cells overexpressing ddFLN, this is unlikely since *fln*$^-$ cells failed to sense direction during continuous shear flow application under conditions when wild-type cells efficiently migrate against the flow.

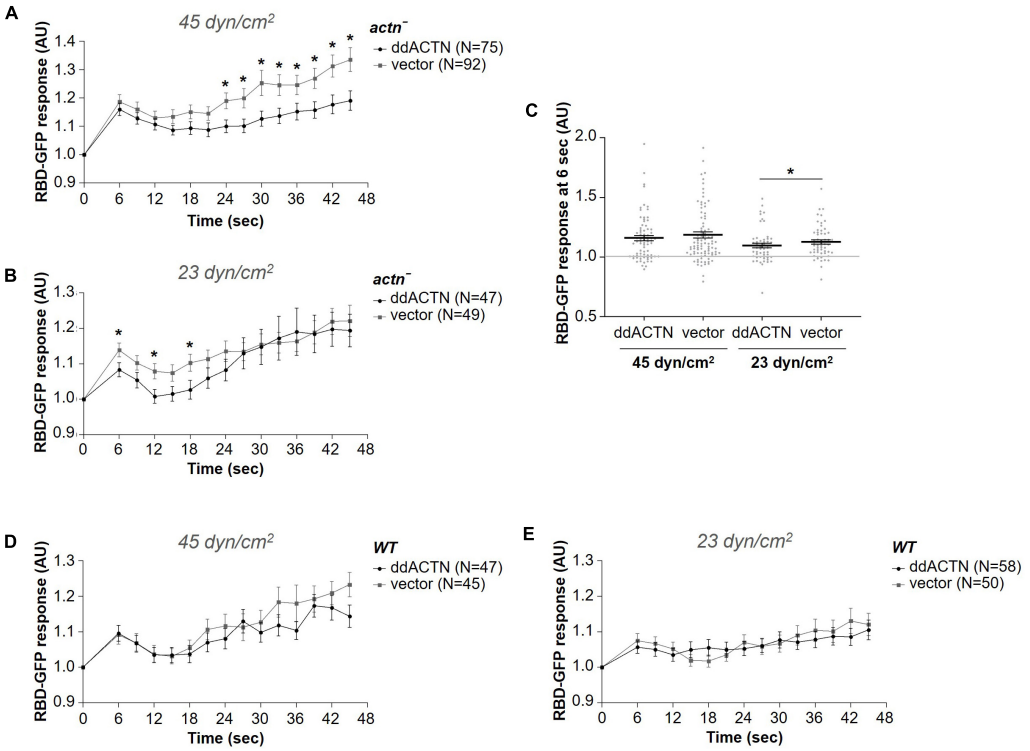

FIGURE 7 | α-actinin is not required for the activation of the signal transduction network in response to shear flow. Activation of Ras, which reflects activation of the signal transduction network, was measured by the relocalization of RBD-GFP from the cytosol to the cell cortex. *actn*⁻ **(A–C)** or wild-type (WT) **(D,E)** cells expressing RBD-GFP and either mCherry-tagged ddACTN or empty vector were imaged every 3 s by epifluorescence microscopy with a GFP filter set under 630X magnification with oil immersion. Shear flow was applied at time 0 for 2 s. The shear stress delivered to the cells was 45 dyn/cm^2 **(A,D)** or 23 dyn/cm2 **(B,E)**. Data is displayed as mean ± SE. Number of cells analyzed is provided in the key and was pooled from seven **(A)** or three **(B,D,E)** independent experiments. **(C)** RBD-GFP response values for individual cells from panels **(A,B)** at the 6 s time point. Horizontal lines with error bars correspond to mean ± SE. A line at the RBD-GFP response value of 1.0 is shown as a reference to indicate basal levels at time 0. *$P < 0.05$, **$P < 0.01$.

The upstream migration of cells in this study is consistent with our previous observations of vegetative wild-type cells grown in association with bacteria, which migrated against the flow at 10 dyn/cm^2 but switched their direction at 25 dyn/cm^2 (Artemenko et al., 2016). A study by Fache et al. (2005) also noted that *D. discoideum* cells migrate against the flow at lower shear stresses, although in that study cells switched to migration with the flow at shear stresses > 0.6 Pa (6 dyn/cm^2). The discrepancy in the shear stress values that the cells can withstand and actively migrate toward is likely due to differences between cells grown axenically or in association with bacteria. Regardless of the specific shear stress values that induce directed migration in different cell types, it would be interesting to examine whether the underlying mechanisms that allow the cells to sense and orient themselves to face the flow are conserved and if filamin plays a similar role in shear flow-induced migration of *D. discoideum* at other stages of development or in other cell types.

It remains unclear whether filamin is a primary sensor of the mechanical stimulus or is an intermediate link between the sensor and signal transduction network activation. Physical force that transiently deforms the actin network could lead to a conformational change in filamin and expose cryptic binding sites for molecules that could transmit the stimulus to activate Ras or another component of the signal transduction or cytoskeletal machinery, causing firing of the entire network due to the presence of multiple feedback loops. Many candidate molecules have been identified as binding partners for filamin in mammalian cells, including R-Ras, Rac1 and RhoA (Lamsoul et al., 2020), although this remains to be examined in *D. discoideum* specifically in response to shear flow stimulation. The ability of filamin to accumulate in zones of high shear stress (Luo et al., 2013), makes filamin a good candidate for being the primary sensor in this system. Indeed, the differential involvement of filamin and α-actinin in mediating shear flow-induced cell migration is consistent with the differences in the mechanical properties of the two actin crosslinkers, and, more specifically, with how they directly respond to mechanical forces. Luo et al. (2013) demonstrated that while ddACTN accumulates in response to dilational stress generated by micropipette aspiration, ddFLN is observed at the neck of the micropipette, where it responds to shear deformation. Intriguingly, mammalian filamin B, but not filamin A, shows accumulation in response to shear deformation (Schiffhauer et al., 2016), suggesting that if filamin plays a conserved role in shear flow-induced migration in mammalian cells, it may do so in an isoform-specific manner.

An alternative scenario would be that another primary sensor, such as an adhesion molecule or a mechanosensitive ion channel, recruits filamin, which then transmits the signal downstream. Savinko et al. (2018) demonstrated that filamin is important for shear force-mediated increase in adhesion *via* integrins during shear flow-induced migration of T lymphocytes. However, it remains unclear whether filamin plays a similar role in *D. discoideum* cells, which do not rely on integrin-dependent adhesion (Sebe-Pedros et al., 2010; Loomis et al., 2012; Kamprad et al., 2018). Additionally, a cation channel PKD2 has been implicated in shear flow motility in *Dictyostelium* (Lima et al., 2014) and filamin has been shown to associate with PKD2 homolog polycystin-2 in mammalian cells (Wang et al., 2015). Although PKD2 did not appear to be involved in the initial response of cells to acute stimulation with shear flow (Artemenko et al., 2016), it is possible that under more stringent conditions, such as reduced shear stress levels, cells lacking PKD2 would show defects in their ability to respond to mechanical cues. Future studies should focus on determining whether ddFLN associates with unique partners following stimulation with shear flow to figure out how it is able to alter cell response to this type of stimulus.

DATA AVAILABILITY STATEMENT

The raw data supporting the conclusions of this article will be made available by the authors, without undue reservation.

AUTHOR CONTRIBUTIONS

AC contributed to experimental design, performed experiments and data analysis, and wrote sections of the manuscript. SB performed experiments and data analysis. JM acquired and analyzed preliminary data and contributed to experimental design. YA conceived the study and experimental design, supervised the project, and wrote the manuscript. All authors read and approved the submitted manuscript.

FUNDING

This work was supported by NSF-RUI grant no. 1817378 (to YA) and Faculty-Student Challenge Grants from SUNY Oswego (to JM and YA).

ACKNOWLEDGMENTS

The authors would like to thank Peter Devreotes and Douglas Robinson for generously sharing constructs used in this study.

SUPPLEMENTARY MATERIAL

The Supplementary Material for this article can be found online at: https://www.frontiersin.org/articles/10.3389/fcell.2021.743011/full#supplementary-material

REFERENCES

Artemenko, Y., Axiotakis, L. Jr., Borleis, J., Iglesias, P. A., and Devreotes, P. N. (2016). Chemical and mechanical stimuli act on common signal transduction and cytoskeletal networks. *Proc. Natl. Acad. Sci. U.S.A.* 113, E7500–E7509. doi: 10.1073/pnas.1608767113

Artemenko, Y., and Devreotes, P. N. (2017). Assessment of dictyostelium discoideum response to acute mechanical stimulation. *J. Vis. Exp.* 129:56411. doi: 10.3791/56411

Artemenko, Y., Lampert, T. J., and Devreotes, P. N. (2014). Moving towards a paradigm: common mechanisms of chemotactic signaling in Dictyostelium and mammalian leukocytes. *Cell. Mol. Life Sci.* 71, 3711–3747. doi: 10.1007/s00018-014-1638-8

Artemenko, Y., Swaney, K. F., and Devreotes, P. N. (2011). Assessment of development and chemotaxis in Dictyostelium discoideum mutants. *Methods Mol. Biol.* 769, 287–309. doi: 10.1007/978-1-61779-207-6_20

Barriga, E. H., and Theveneau, E. (2020). In vivo neural crest cell migration is controlled by "Mixotaxis.". *Front. Physiol.* 11:586432. doi: 10.3389/fphys.2020.586432

Bozzaro, S. (2019). The past, present and future of Dictyostelium as a model system. *Int. J. Dev. Biol.* 63, 321–331. doi: 10.1387/ijdb.190128sb

Brink, M., Gerisch, G., Isenberg, G., Noegel, A. A., Segall, J. E., Wallraff, E., et al. (1990). A Dictyostelium mutant lacking an F-actin cross-linking protein, the 120-kD gelation factor. *J. Cell Biol.* 111, 1477–1489. doi: 10.1083/jcb.111.4.1477

Buffone, A., Anderson, N. R., and Hammer, D. A. (2018). Migration against the direction of flow is LFA-1 dependent in human hematopoietic stem and progenitor cells. *J. Cell Sci.* 131:jcs.205575. doi: 10.1242/jcs.205575

Buffone, A., Anderson, N. R., and Hammer, D. A. (2019). Human neutrophils will crawl upstream on ICAM-1 If Mac-1 is blocked. *Biophys. J.* 117, 1393–1404. doi: 10.1016/j.bpj.2019.08.044

Cornillon, S., Gebbie, L., Benghezal, M., Nair, P., Keller, S., Wehrle-Haller, B., et al. (2006). An adhesion molecule in free-living *Dictyostelium* amoebae with integrin β features. *EMBO Rep.* 7, 617–621. doi: 10.1038/sj.embor.7400701

Cox, D., Condeelis, J., Wessels, D., Soll, D., Kern, H., and Knecht, D. A. (1992). Targeted disruption of the ABP-120 gene leads to cells with altered motility. *J. Cell Biol.* 116, 943–955. doi: 10.1083/jcb.116.4.943

Devreotes, P. N., Bhattacharya, S., Edwards, M., Iglesias, P. A., Lampert, T., and Miao, Y. (2017). Excitable signal transduction networks in directed cell migration. *Annu. Rev. Cell Dev. Biol.* 33, 103–125. doi: 10.1146/annurev-cellbio-100616-060739

Dominguez, G. A., Anderson, N. R., and Hammer, D. A. (2015). The direction of migration of T-lymphocytes under flow depends upon which adhesion receptors are engaged. *Integr. Biol.* 7, 345–355. doi: 10.1039/C4IB00201F

Eichinger, L., Köppel, B., Noegel, A. A., Schleicher, M., Schliwa, M., Weijer, K., et al. (1996). Mechanical perturbation elicits a phenotypic difference between Dictyostelium wild-type cells and cytoskeletal mutants. *Biophys. J.* 70, 1054–1060. doi: 10.1016/S0006-3495(96)79651-0

Fache, S., Dalous, J., Engelund, M., Hansen, C., Chamaraux, F., Fourcade, B., et al. (2005). Calcium mobilization stimulates Dictyostelium discoideum shear-flow-induced cell motility. *J. Cell Sci.* 118, 3445–3458. doi: 10.1242/jcs.02461

Fine, N., Dimitriou, I. D., Rullo, J., Sandí, M. J., Petri, B., Haitsma, J., et al. (2016). GEF-H1 is necessary for neutrophil shear stress–induced migration during inflammation. *J. Cell Biol.* 215, 107–119. doi: 10.1083/jcb.201603109

Gao, Y., Li, T., Sun, Q., and Huo, B. (2019). Gradient fluid shear stress regulates migration of osteoclast precursors. *Cell Adhes. Migr.* 13, 183–191. doi: 10.1080/19336918.2019.1619433

Gaudet, P., Pilcher, K. E., Fey, P., and Chisholm, R. L. (2007). Transformation of Dictyostelium discoideum with plasmid DNA. *Nat. Protoc.* 2, 1317–1324. doi: 10.1038/nprot.2007.179

Han, M. K. L., and de Rooij, J. (2016). Converging and unique mechanisms of mechanotransduction at adhesion sites. *Trends Cell Biol.* 26, 612–623. doi: 10.1016/j.tcb.2016.03.005

Hornung, A., Sbarrato, T., Garcia-Seyda, N., Aoun, L., Luo, X., Biarnes-Pelicot, M., et al. (2020). A bistable mechanism mediated by integrins controls mechanotaxis of leukocytes. *Biophys. J.* 118, 565–577. doi: 10.1016/j.bpj.2019.12.013

Huang, Y. L., Tung, C., Zheng, A., Kim, B. J., and Wu, M. (2015). Interstitial flows promote amoeboid over mesenchymal motility of breast cancer cells revealed by a three dimensional microfluidic model. *Integr. Biol.* 7, 1402–1411. doi: 10.1039/C5IB00115C

Kamprad, N., Witt, H., Schröder, M., Kreis, C. T., Bäumchen, O., Janshoff, A., et al. (2018). Adhesion strategies of *Dictyostelium discoideum* – a force spectroscopy study. *Nanoscale* 10, 22504–22519. doi: 10.1039/C8NR07107A

Lamsoul, I., Dupré, L., and Lutz, P. G. (2020). Molecular tuning of filamin a activities in the context of adhesion and migration. *Front. Cell Dev. Biol.* 8:591323. doi: 10.3389/fcell.2020.591323

Le, S., Hu, X., Yao, M., Chen, H., Yu, M., Xu, X., et al. (2017). Mechanotransmission and mechanosensing of human alpha-Actinin 1. *Cell Rep.* 21, 2714–2723. doi: 10.1016/j.celrep.2017.11.040

Lima, W. C., Vinet, A., Pieters, J., and Cosson, P. (2014). Role of PKD2 in Rheotaxis in Dictyostelium. *PLoS One* 9:e88682. doi: 10.1371/journal.pone.0088682

Loomis, W. F., Fuller, D., Gutierrez, E., Groisman, A., and Rappel, W.-J. (2012). Innate non-specific cell substratum adhesion. *PLoS One* 7:e42033. doi: 10.1371/journal.pone.0042033

Luo, T., Mohan, K., Iglesias, P. A., and Robinson, D. N. (2013). Molecular mechanisms of cellular mechanosensing. *Nat. Mater.* 12, 1064–1071. doi: 10.1038/nmat3772

Malek, A. M., Alper, S. L., and Izumo, S. (1999). Hemodynamic shear stress and its role in atherosclerosis. *JAMA* 282:2035. doi: 10.1001/jama.282.21.2035

Murphy, A. C. H., and Young, P. W. (2015). The actinin family of actin cross-linking proteins – a genetic perspective. *Cell Biosci.* 5:49. doi: 10.1186/s13578-015-0029-7

Pal, D. S., Li, X., Banerjee, T., Miao, Y., and Devreotes, P. N. (2019). The excitable signal transduction networks: movers and shapers of eukaryotic cell migration. *Int. J. Dev. Biol.* 63, 407–416. doi: 10.1387/ijdb.190265pd

Paluch, E. K., Aspalter, I. M., and Sixt, M. (2016). Focal adhesion–independent cell migration. *Annu. Rev. Cell Dev. Biol.* 32, 469–490. doi: 10.1146/annurev-cellbio-111315-125341

Parent, C. A., Blacklock, B. J., Froehlich, W. M., Murphy, D. B., and Devreotes, P. N. (1998). G Protein signaling events are activated at the leading edge of chemotactic cells. *Cell* 95, 81–91. doi: 10.1016/S0092-8674(00)81784-5

Qazi, H., Palomino, R., Shi, Z.-D., Munn, L. L., and Tarbell, J. M. (2013). Cancer cell glycocalyx mediates mechanotransduction and flow-regulated invasion. *Integr. Biol.* 5, 1334–1343. doi: 10.1039/c3ib40057c

Ranade, S. S., Syeda, R., and Patapoutian, A. (2015). Mechanically activated ion channels. *Neuron* 87, 1162–1179. doi: 10.1016/j.neuron.2015.08.032

Razinia, Z., Mäkelä, T., Ylänne, J., and Calderwood, D. A. (2012). Filamins in mechanosensing and signaling. *Annu. Rev. Biophys.* 41, 227–246. doi: 10.1146/annurev-biophys-050511-102252

Rivero, F., Furukawa, R., Fechheimer, M., and Noegel, A. A. (1999). Three actin cross-linking proteins, the 34 kDa actin-bundling protein, alpha-actinin and gelation factor (ABP-120), have both unique and redundant roles in the growth and development of Dictyostelium. *J. Cell Sci.* 112, 2737–2751. doi: 10.1242/jcs.112.16.2737

Rivero, F., Koppel, B., Peracino, B., Bozzaro, S., Siegert, F., Weijer, C. J., et al. (1996). The role of the cortical cytoskeleton: f-actin crosslinking proteins protect against osmotic stress, ensure cell size, cell shape and motility, and contribute to phagocytosis and development. *J. Cell Sci.* 109, 2679–2691. doi: 10.1242/jcs.109.11.2679

Roth, H., Samereier, M., Trommler, G., Noegel, A. A., Schleicher, M., and Müller-Taubenberger, A. (2015). Balanced cortical stiffness is important for efficient migration of Dictyostelium cells in confined environments. *Biochem. Biophys. Res. Commun.* 467, 730–735. doi: 10.1016/j.bbrc.2015.10.073

Savinko, T., Guenther, C., Uotila, L. M., Llort Asens, M., Yao, S., Tojkander, S., et al. (2018). Filamin a is required for optimal T cell integrin-mediated force transmission, flow adhesion, and T cell trafficking. *J. Immunol.* 200, 3109–3116. doi: 10.4049/jimmunol.1700913

Schiffhauer, E. S., Luo, T., Mohan, K., Srivastava, V., Qian, X., Griffis, E. R., et al. (2016). Mechanoaccumulative elements of the mammalian actin cytoskeleton. *Curr. Biol.* 26, 1473–1479. doi: 10.1016/j.cub.2016.04.007

Schiffhauer, E. S., and Robinson, D. N. (2017). Mechanochemical signaling directs cell-shape change. *Biophys. J.* 112, 207–214. doi: 10.1016/j.bpj.2016.12.015

Schindelin, J., Arganda-Carreras, I., Frise, E., Kaynig, V., Longair, M., Pietzsch, T., et al. (2012). Fiji: an open-source platform for biological-image analysis. *Nat. Methods* 9, 676–682. doi: 10.1038/nmeth.2019

Schleicher, M., Noegel, A., Schwarz, T., Wallraff, E., Brink, M., Faix, J., et al. (1988). A Dictyostelium mutant with severe defects in alpha-actinin: its characterization using cDNA probes and monoclonal antibodies. *J. Cell Sci.* 90, 59–71. doi: 10.1242/jcs.90.1.59

Sebe-Pedros, A., Roger, A. J., Lang, F. B., King, N., and Ruiz-Trillo, I. (2010). Ancient origin of the integrin-mediated adhesion and signaling machinery. *Proc. Natl. Acad. Sci. U.S.A.* 107, 10142–10147. doi: 10.1073/pnas.1002257107

SenGupta, S., Parent, C. A., and Bear, J. E. (2021). The principles of directed cell migration. *Nat. Rev. Mol. Cell Biol.* 22, 529–547. doi: 10.1038/s41580-021-00366-6

Shellard, A., and Mayor, R. (2020). All roads lead to directional cell migration. *Trends Cell Biol.* 30, 852–868. doi: 10.1016/j.tcb.2020.08.002

Stuelten, C. H., Parent, C. A., and Montell, D. J. (2018). Cell motility in cancer invasion and metastasis: insights from simple model organisms. *Nat. Rev. Cancer* 18, 296–312. doi: 10.1038/nrc.2018.15

Swartz, M. A., and Lund, A. W. (2012). Lymphatic and interstitial flow in the tumour microenvironment: linking mechanobiology with immunity. *Nat. Rev. Cancer* 12, 210–219. doi: 10.1038/nrc3186

Valignat, M.-P., Nègre, P., Cadra, S., Lellouch, A. C., Gallet, F., Hénon, S., et al. (2014). Lymphocytes can self-steer passively with wind vane uropods. *Nat. Commun.* 5:5213. doi: 10.1038/ncomms6213

Valignat, M.-P., Theodoly, O., Gucciardi, A., Hogg, N., and Lellouch, A. C. (2013). T Lymphocytes orient against the direction of fluid flow during LFA-1-mediated migration. *Biophys. J.* 104, 322–331. doi: 10.1016/j.bpj.2012.12.007

Wang, Q., Zheng, W., Wang, Z., Yang, J., Hussein, S., Tang, J., et al. (2015). Filamin-A increases the stability and plasma membrane expression of polycystin-2. *PLoS One* 10:e0123018. doi: 10.1371/journal.pone.0123018

Washington, R. W., and Knecht, D. A. (2008). Actin binding domains direct actin-binding proteins to different cytoskeletal locations. *BMC Cell Biol.* 9:10. doi: 10.1186/1471-2121-9-10

Wiig, H., and Swartz, M. A. (2012). Interstitial fluid and lymph formation and transport: physiological regulation and roles in inflammation and cancer. *Physiol. Rev.* 92, 1005–1060. doi: 10.1152/physrev.00037.2011

Witke, W., Schleicher, M., and Noegel, A. A. (1992). Redundancy in the microfilament system: abnormal development of dictyostelium cells lacking two F-actin cross-linking proteins. *Cell* 68, 53–62. doi: 10.1016/0092-8674(92)90205-Q

Zhu, X., Bouffanais, R., and Yue, D. K. P. (2014). Persistent cellular motion control and trapping using mechanotactic signaling. *PLoS One* 9:e105406. doi: 10.1371/journal.pone.0105406

Conflict of Interest: The authors declare that the research was conducted in the absence of any commercial or financial relationships that could be construed as a potential conflict of interest.

Publisher's Note: All claims expressed in this article are solely those of the authors and do not necessarily represent those of their affiliated organizations, or those of the publisher, the editors and the reviewers. Any product that may be evaluated in this article, or claim that may be made by its manufacturer, is not guaranteed or endorsed by the publisher.

Copyright © 2021 Cole, Buckler, Marcucci and Artemenko. This is an open-access article distributed under the terms of the Creative Commons Attribution License (CC BY). The use, distribution or reproduction in other forums is permitted, provided the original author(s) and the copyright owner(s) are credited and that the original publication in this journal is cited, in accordance with accepted academic practice. No use, distribution or reproduction is permitted which does not comply with these terms.

frontiers in Cell and Developmental Biology

METHODS
published: 18 August 2021
doi: 10.3389/fcell.2021.721630

CRISPR Toolbox for Genome Editing in *Dictyostelium*

Kensuke Yamashita[1†], Hoshie Iriki[1†], Yoichiro Kamimura[2] and Tetsuya Muramoto[1]*

[1] Department of Biology, Faculty of Science, Toho University, Funabashi, Japan, [2] Laboratory for Cell Signaling Dynamics, RIKEN, Center for Biosystems Dynamics Research (BDR), Osaka, Japan

The development of new techniques to create gene knockouts and knock-ins is essential for successful investigation of gene functions and elucidation of the causes of diseases and their associated fundamental cellular processes. In the biomedical model organism *Dictyostelium discoideum*, the methodology for gene targeting with homologous recombination to generate mutants is well-established. Recently, we have applied CRISPR/Cas9-mediated approaches in *Dictyostelium*, allowing the rapid generation of mutants by transiently expressing sgRNA and Cas9 using an all-in-one vector. CRISPR/Cas9 techniques not only provide an alternative to homologous recombination-based gene knockouts but also enable the creation of mutants that were technically unfeasible previously. Herein, we provide a detailed protocol for the CRISPR/Cas9-based method in *Dictyostelium*. We also describe new tools, including double knockouts using a single CRISPR vector, drug-inducible knockouts, and gene knockdown using CRISPR interference (CRISPRi). We demonstrate the use of these tools for some candidate genes. Our data indicate that more suitable mutants can be rapidly generated using CRISPR/Cas9-based techniques to study gene function in *Dictyostelium*.

Keywords: *Dictyostelium*, biomedical model, CRISPR/Cas9, Cas9-NG, SpRY, gene manipulation, CRISPRi, drug-inducible knockout

OPEN ACCESS

Edited by:
Robin S. B. Williams, University of London, United Kingdom

Reviewed by:
Tian Jin, National Institute of Allergy and Infectious Diseases, National Institutes of Health (NIH), United States
Jason King, The University of Sheffield, United Kingdom

***Correspondence:**
Tetsuya Muramoto
tetsuya.muramoto@sci.toho-u.ac.jp

[†] These authors have contributed equally to this work

Specialty section:
This article was submitted to Molecular and Cellular Pathology, a section of the journal Frontiers in Cell and Developmental Biology

Received: *07 June 2021*
Accepted: *21 July 2021*
Published: *18 August 2021*

Citation:
Yamashita K, Iriki H, Kamimura Y and Muramoto T (2021) CRISPR Toolbox for Genome Editing in Dictyostelium. Front. Cell Dev. Biol. 9:721630. doi: 10.3389/fcell.2021.721630

INTRODUCTION

Many human diseases, such as cancer, heart disease, and diabetes, are characterized by multifactorial genetic inheritance (Khera et al., 2018; Ishigaki et al., 2020). Therefore, manipulating the genome is crucial for elucidating the causes of disease and systematically studying the many genes that underlie intracellular processes. To understand gene function, many researchers edit specific DNA sequences in the genome. For instance, homologous recombination in ES cells introduces mutations in tumor suppressor genes and oncogenes involved in the onset and progression of the multiple diseases (Thomas et al., 1986; Mansour et al., 1988; Di Cristofano et al., 1998; Capecchi, 2005). Various methods to generate mutations, including knockouts, knock-ins, large deletions and point mutations, have been developed using homologous recombination; however, the techniques are limited by their inefficiency and time requirements (Gerlai, 2016). Recent advances in the development of CRISPR/Cas9 have made it possible to program specific DNA cleavage in eukaryotic cells precisely and efficiently. By simply expressing Cas9 with a sgRNA that is complementary to a target sequence, it is possible to introduce any genetic modification effectively at nearly any position within the genome and minimize off-target effects

(Jinek et al., 2012; Cong et al., 2013). In the last decade, this useful genetic tool has greatly improved our understanding of the onset and progression of human genetic diseases.

Research on genes associated with human diseases have also been conducted using the biomedical model organism *Dictyostelium* (Williams et al., 2006; Martin-Gonzalez et al., 2021). This organism lacks the complexity of the metazoan models *Caenorhabditis elegans* and *Drosophila melanogaster*, but it shares many fundamental biological processes related to human diseases such as mitochondrial dysfunction, lysosomal dysregulation, and autophagy dysfunction. In particular, biological processes including cell motility and cytoskeletal rearrangement, cell shape regulation, cell cycle control, DNA repair mechanisms, phagocytosis, and pinocytosis are actively studied (Kessin, 2001; Eichinger et al., 2005). Genome sequence data revealed that many genes related to human disease are present in *Dictyostelium* and various orthologs have already been characterized to elucidate their functional similarity (Pears and Lakin, 2014; Mesquita et al., 2017; Huber and Mathavarajah, 2019; Vogel et al., 2019). Because this organism is haploid, it is easy to generate genetic mutants, and phenotypes can be directly determined in the clone without further manipulation. A wide range of genetic techniques are available including homologous recombination–based methods (knockout, knock-in, and point mutation generation) and protein overexpression and expression of fusion-tagged proteins using various expression vectors (Gaudet et al., 2007; Veltman et al., 2009a). Genome editing using CRISPR/Cas9 has also been added to the toolbox for functional analysis in *Dictyostelium*, making it possible to modify genomes with higher efficiency than methods based on homologous recombination (Sekine et al., 2018; Iriki et al., 2019; Asano et al., 2021).

Since the first demonstrations of programmed DNA cleavage by Cas9 nuclease from *Streptococcus pyogenes* (SpCas9) (Jinek et al., 2012), the discovery and engineering of CRISPR/Cas9 systems as tools for genome manipulation has progressed rapidly. In this paper, we focus on CRISPR/Cas9-based technologies to create knockouts, knock-ins, point mutations and deletion mutants. CRISPR applications such as epigenetic modification, chromatin manipulation, and live cell chromatin imaging are expanding and valuable for functional analyses (Adli, 2018; Knight et al., 2018; Pickar-Oliver and Gersbach, 2019; Anzalone et al., 2020), but will not be dealt with in this article. The Cas9 nuclease is guided by a sgRNA for target-site recognition and then generates a DNA double-strand break (DSB) using two nuclease domains (RuvC and HNH) (Cong et al., 2013; Mali et al., 2013; Ran et al., 2013). A blunt-ended DSB typically occurs at the site preceding the three nucleotides upstream of a protospacer adjacent motif (PAM), followed by DSB repair through an end-joining DNA repair pathway. Uncontrollable, but considered predictable, insertion/deletion (indel) mutations can typically be achieved through non-homologous end joining (NHEJ) or microhomology-mediated end joining (MMEJ); hence, most knockout mutants have been generated by frameshift mutations through this process. If the targeted gene is essential, mutants carry only non-frameshift mutations (You et al., 2020). In the presence of a donor DNA template, homology directed repair (HDR) occurs and the large tagged DNA sequence is knocked-in. By contrast, in the presence of single-stranded DNA oligonucleotide (ssODN) donors, precise point mutations or single nucleotide substitutions are introduced into a target site in the genome. Recently, newly engineered SpCas9 and Cas9 orthologs have been discovered, resulting in an expansion in the targeting scope of the genome (Ran et al., 2015; Kim et al., 2017; Chatterjee et al., 2018). SpCas9 recognizes the PAM "NGG", which is located 3′-end of the target sequence. Different versions of Cas9, such as xCas9, SpCas9-NG and SpRY, recognize a broader variety of PAM recognition sequences with less stringent motif requirements (Hu et al., 2018; Nishimasu et al., 2018; Walton et al., 2020).

Using these various types of Cas9, a wide range of genome editing applications, including knockouts, inducible knockouts, knockdowns, knock-ins, point mutations and deletions, have been established in *Dictyostelium* (**Table 1**; Muramoto et al., 2019; Asano et al., 2021). SpCas9 is commonly used to create knockouts and has the highest efficiency among the available vectors, but the system is limited to applications in which genome editing does not need to be controlled temporally. In this study, we developed a doxycycline-inducible CRISPR/Cas9 system that allows for temporal control of genome editing activity. SpCas9 is capable of editing the target sequence in the presence of canonical "NGG" PAMs; however, due to the presence of AT-enriched regions in *Dictyostelium* genome, design of appropriate targets is elusive. To overcome this limitation, the newly engineered SpCas9 variants SpCas9-NG and SpRY were developed and are able to recognize a wider range of PAM sequences (Asano et al., 2021). This system provides valuable tools that will significantly expand the number of targetable gene loci available to generate mutants, even in AT-rich regions, with sufficient efficiency. Cas9 nuclease sometimes cleaves off-target sites that possesses high sequence homology to the target sites. To reduce the probability of off-target effects and increase specificity for DSB, a pair of sgRNAs for a Cas9 nickase were used. Inactivation of either of the nuclease domains generates a Cas9 nickase, which creates a nick on one strand of DNA, and precise gene knockouts and long deletions were achieved (Iriki et al., 2019). Moreover, a mutation in both nuclease domains generates a catalytically inactive Cas9 (dCas9), which is still able to bind to specific DNA sequences. dCas9 is a useful tool for knockdown (CRISPRi) (Gilbert et al., 2013; Qi et al., 2013). In this study, we developed a straightforward CRISPRi system to reduce mRNA and protein levels in the cells.

In this methodological paper, we summarize these applications and focus on detailing the selection of appropriate CRISPR/Cas9 vectors and procedures for each technology to manipulate the *Dictyostelium* genome for the study of human disease-related genes.

MATERIALS AND EQUIPMENT

Reagents for Cell Culture

(1) *D. discoideum* cells (e.g., AX2, AX3 or any other cell line of interest, available from the Dicty Stock Center or NBRP Nenkin).

TABLE 1 | Comparison of various Cas9 nucleases and applications in genome editing.

Cas9 nucleases	PAM	Key features	Applications
SpCas9	NGG	Double-strand break Commonly used in genome editing	Knockout
SpCas9 (Dox-On)	NGG	Controllable genome editing Possibility of minimizing off-targets	Inducible knockout
SpCas9-NG	NG	Genome editing at NG PAM sequences Majority of genomic region editable	Knockout Knock-in (with donor DNA) Point mutation (with a ssODN)
SpRY	NR	Genome editing at NR PAM sequences (R = A and G) Majority of genomic region editable	Knockout Knock-in (with donor DNA) Point mutation (with a ssODN)
Cas9 nickase	NGG	Single-strand break Lower off-targets than Cas9	Large deletion Knock-in (with donor DNA) Point mutation (with a ssODN)
SpCas9-NG nickase	NG	Single-strand break at NG PAM sequences Lower off-targets than Cas9	Large deletion
dCas9	NGG	Lack of endonuclease activity Inhibition of gene expression	Knockdown (CRISPRi)
dCas9 (Dox-On)	NGG	Controllable inhibition of gene expression	Knockdown (CRISPRi)

(2) *Klebsiella pneumoniae* KpGe strain (Lima et al., 2018) (Genome was sequenced and non-pathogenic strain, available from the Dicty Stock Center or NBRP Nenkin).
(3) HL5 medium including glucose (Formedium, HLG0102). Autoclave and store at RT.
(4) SM agar (Formedium, SMA0102). Sterilized by autoclaving and approximately 35 mL are poured into the 10 cm petri dishes. Store at 4°C.
(5) KK2 buffer: 16.5 mM KH_2PO_4 and 3.8 mM K_2HPO_4. Autoclave and store at RT.
(6) H50 buffer: 50 mM KCl, 20mM HEPES pH 7.0, 10 mM NaCl, 5 mM $NaHCO_3$, 1mM NaH_2PO_4, 1 mM $MgSO_4$. Sterilize and store at 4°C.
(7) Streptomycin stock solution: 50 mg/mL in distillated water, sterile filtered. Store at 4°C or freeze in aliquots.
(8) Blasticidin S stock solution (1,000×): 10 mg/mL in KK2, sterile filtered. Store at 4°C or freeze in aliquots.
(9) G418 stock solution: 20 mg/mL in KK2, sterile filtered. Store at 4°C or freeze in aliquots.
(10) Hygromycin B stock solution: 50 mg/mL in distillated water, sterile filtered. Store at 4°C or freeze in aliquots.
(11) Doxycycline stock solution: 10 mg/mL in distillated water, sterile filtered. Store at 4°C or freeze in aliquots.

Reagents for Molecular Cloning

(1) Competent *E. coli* cells (e.g., TOP10 or any other suitable strain).
(2) LB broth Lennox (Formedium, LBX0102). Autoclave and store at RT.
(3) Ampicillin stock solution (1,000×): 100 mg/mL in distillated water, sterile filtered. Store at 4°C or freeze in aliquots.
(4) LB plates: 15.0 g of Agar, 20.0 g of LB broth Lennox, bring to 1 L and autoclave, cool to approximately 50°C, and add 1 ml of ampicillin stock solution.
(5) CRISPR/Cas9 all-in-one vectors. List of vectors is available in **Table 2**. (Available from NBRP Nenkin).
(6) Oligonucleotides for sgRNA construction. Detailed of construction methods are available in Procedure section.
(7) Annealing buffer (10×): 400 mM Tris-HCl pH 8.0, 200 mM $MgCl_2$, 500 mM NaCl. Store at −20°C.
(8) T4 Polynucleotide kinase, 10 U/μL (Takara Bio, 2021A).
(9) T4 DNA ligase, 400 U/μL (NEB, M0202S).
(10) 10 × T4 DNA ligase buffer (NEB, B0202S).
(11) BpiI, 10 U/μL (Thermo Scientific, ER1011).
(12) 10 × Buffer G (Thermo Scientific, BG5).
(13) Esp3I, 10 U/μL (NEB, R0734S).
(14) 10 × CutSmart Buffer (NEB, B7204S).
(15) OneTaq or other equivalent Taq DNA polymerase (NEB, M0480S).
(16) Agarose (No particular preference).
(17) Plasmid DNA mini kit (No particular preference, we used FastGene Plasmid Mini Kit.).
(18) Plasmid DNA midi kit (No particular preference, we used NucleoBond Xtra Midi Kit.).
(19) Primer for PCR screening (**Supplementary Table 1**). Detailed of primer design is available in Procedure section.
(20) Primer for sequencing (**Supplementary Table 1**).

Reagents for Mutation Detection Protocol

(1) DNA extraction buffer: 0.5 × Ex Taq buffer, 0.5% NP40, 50 ng/μL of Proteinase K. The buffer must be prepared fresh and kept on ice while using.
(2) KOD -Plus- Neo, 1 U/μL (TOYOBO, KOD-401).
(3) Ex Taq, 5 U/μL (Takara Bio, RR001A).
(4) Primer for PCR screening and sequencing (**Supplementary Table 1**).

Equipment

(1) Cell culture incubator (set at 22°C).
(2) Sterile 10 cm culture dishes.
(3) Electroporator Xcell (BIO-RAD).
(4) Electroporation cuvettes: 1-mm gap.
(5) Thermal cycler.
(6) Microcentrifuge.

TABLE 2 | CRISPR/Cas9 vectors.

CRISPR vector	Cas9 (* GFP fusion)	Inducible Expression	Number of tRNA–sgRNA	GG enzyme	Drug resistance	Transient/ Stable	References
pTM1285	Cas9 *	–	1	BpiI	Neo	Transient	Sekine et al., 2018
pTM1599	Cas9	–	1	BpiI	Neo	Transient	Asano et al., 2021
pTM1416	Cas9 *	–	1	Esp3I	Neo	Transient	Asano et al., 2021
pTM1644	Cas9	–	1	Esp3I	Neo	Transient	Asano et al., 2021
pTM1756	Cas9	–	1	Esp3I	Hyg	Transient	This study
pTM1725	Cas9 *	–	2	BpiI	Neo	Transient	This study
pTM1859	Cas9	–	2	Esp3I	Neo	Transient	This study
pTM1860	Cas9	–	2	Esp3I	Hyg	Transient	This study
pTM1676	Cas9	Tet-On	1	Esp3I	Blast	Stable	This study
pTM1670	Cas9	Tet-On	1	Esp3I	Neo	Stable	This study
pTM1544	Cas9 nickase *	–	2	BpiI	Neo	Transient	Iriki et al., 2019
pTM1866	Cas9 nickase *	–	2	BpiI	Hyg	Transient	This study
pTM1702	dCas9	–	1	Esp3I	Neo	Stable	This study
pTM1869	dCas9	–	1	Esp3I	Hyg	Stable	This study
pTM1765	dCas9	–	2	Esp3I	Neo	Stable	This study
pTM1870	dCas9	–	2	Esp3I	Hyg	Stable	This study
pTM1826	dCas9	Tet-On	1	Esp3I	Blast	Stable	This study
pTM1827	dCas9	Tet-On	1	Esp3I	Neo	Stable	This study
pTM1718	Cas9-NG	–	1	BpiI	Neo	Transient	Asano et al., 2021
pTM1719	Cas9-NG	–	1	Esp3I	Neo	Transient	Asano et al., 2021
pTM1631	Cas9-NG	–	2	BpiI	Neo	Transient	This study
pTM1726	Cas9-NG nickase	–	2	BpiI	Neo	Transient	This study
pTM1668	SpRY	–	1	Esp3I	Neo	Transient	Asano et al., 2021
pTM1825	SpRY	–	1	Esp3I	Hyg	Transient	This study
pTM1748	SpRY	–	2	Esp3I	Neo	Transient	This study
pTM1865	SpRY	–	2	Esp3I	Hyg	Transient	This study

(7) DNA electrophoresis apparatus.
(8) Nanodrop (ThermoFisher).

Software and Bioinformatic Tools

(1) Cas-Designer[1] (Park et al., 2015).
(2) Cas-OFFinder[2] (Bae et al., 2014).
(3) Standalone edition of Cas9-Designer to search with various PAM types.
(4) CRISPOR[3] (Concordet and Haeussler, 2018).

STEPWISE PROCEDURES

Overview

Protocols described herein are an optimized version of the CRISPR/Cas9 system that uses co-expression of vectors for Cas9 and tRNA-flanked sgRNAs in *Dictyostelium*. These protocols include: selection of appropriate CRISPR/Cas9 vectors, identification of appropriate target sites in the genome, design of oligonucleotide-flanking overhang sequences for target cloning, Golden Gate cloning into a suitable CRISPR/Cas9 vector, transformation of the *Dictyostelium* cells, and screening and validation of mutants. A scheme for each of these protocols, from design of sgRNA to isolation of mutants, is shown in **Figure 1**.

Selection of Appropriate CRISPR/Cas9 Vectors

Choosing the appropriate CRISPR/Cas9 vector is critical to the success of genome editing. The all-in-one vectors are easy-to-use genome-editing tools and consist of three modules: Cas9, tRNA–sgRNA, and a drug resistance gene (**Table 2**). The first module, Cas9 nuclease, has many options (**Table 1**); hence, we can select the appropriate vector according to the application in genome editing. Some of the vectors contain a GFP sequence followed by the Cas9 nuclease; however, genome editing can be induced with high efficiency regardless of the presence or absence of GFP. For temporal control of genome editing, doxycycline-inducible Cas9 vectors are available. The second module, tRNA–sgRNA, is an isoleucine tRNA and sgRNA cassette. A high level of sgRNA transcription is induced by an RNA polymerase III–dependent promoter for an isoleucine tRNA instead of the commonly used U6 promoter in various organisms. High levels of sgRNA readily form a ribonucleoprotein (RNP) complex with Cas9 and target specific genomic sequences. The number of tRNA–sgRNA cassettes required depends on the application in

[1]http://www.rgenome.net/cas-designer/
[2]http://www.rgenome.net/cas-offinder/
[3]http://crispor.tefor.net/

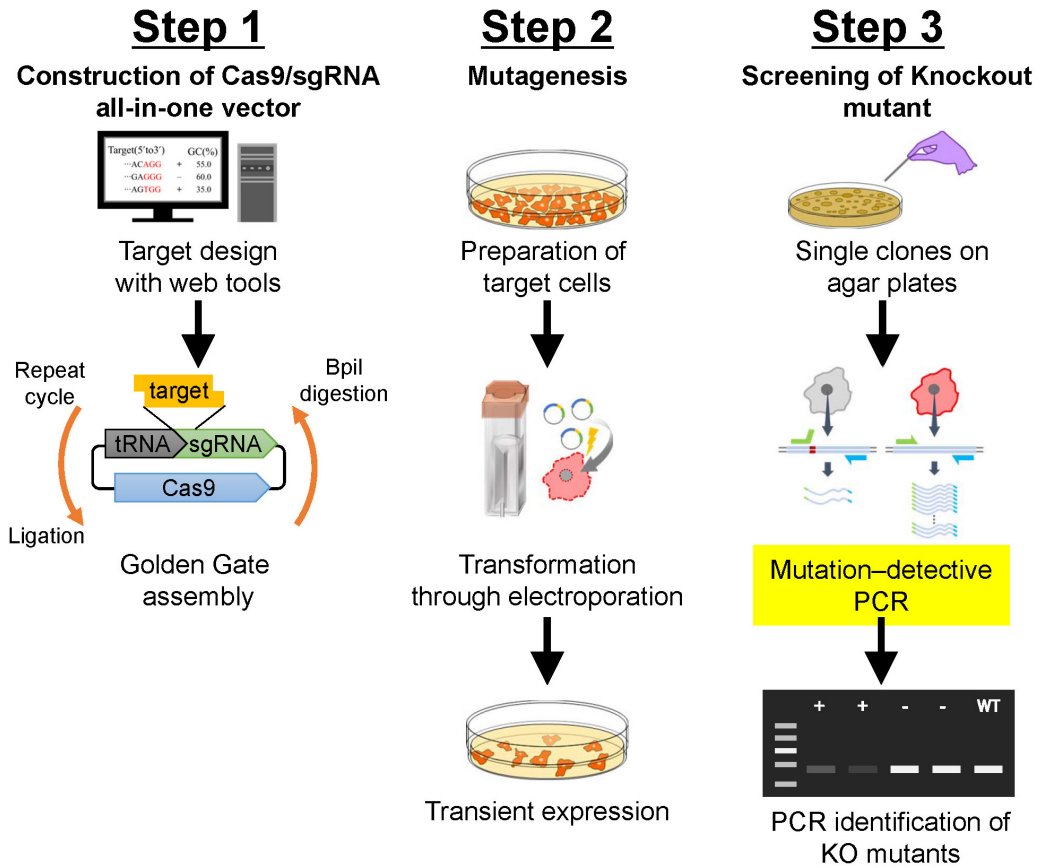

FIGURE 1 | Schematic description of gene manipulation in *Dictyostelium* using CRISPR/Cas9. **Step 1**: Construction of CRISPR/Cas9 vector using Golden Gate assembly. Correctly integrated clones are selected using colony PCR followed by Sanger sequencing. **Step 2**: Transformation of *Dictyostelium* cells. Electroporation is used to transform *Dictyostelium*. Transient expression of CRISPR/Cas9 vector is induced via the addition of a small amount of antibiotics. **Step 3**: Screening of knock-out mutants. After isolation of individual colonies, mutation–detective PCR is conducted to identify positive knock-out mutants. For further validation of the mutation, genomic sequencing of the mutated region is analyzed.

genome editing. When disrupting two genes at the same time, generating a deletion with a nickase, or inducing repression of gene expression are desired, a vector with two tRNA–sgRNA cassettes is useful. The cassette contains the Type IIS restriction enzyme site BpiI or Esp3I, which is used to insert the target sequence between the tRNA and sgRNA sequences via Golden Gate assembly. For the third module, the drug resistance gene, three antibiotic choices are available: neomycin, hygromycin, and blasticidin.

The three modules were cloned into pBlueScript II or pDM304-derived vectors to obtain transient or stable expression, respectively. Because pBlueScript II does not contain an element for extra-chromosomal replication in *Dictyostelium*, Cas9 nuclease is only expressed for a short period of time after electroporation, which minimizes off-target effects. Each vector contains one of the drug resistance genes used in *Dictyostelium*, and transient expression is induced when a low volume of the appropriate antibiotics is added. Moreover, it is better to select a vector with a hygromycin-resistance cassette than a vector with a G418-resistance cassette when genome editing of G418-resistant cells is desired. For the dCas9 or doxycycline-controlled inducible Cas9 system, pDM304-derived vectors (Veltman et al., 2009a) were used to obtain stable expression cell lines. These vectors have no or extremely low levels of off-target effects because of expression of dCas9, which lacks nuclease activity, or temporal expression of Cas9 nuclease, respectively. All of the plasmids and predicted sequences are available from the National BioResource Project "Cellular Slime Molds" (NBRP Nenkin, https://nenkin.nbrp.jp/locale/change?lang=en), which collects and distributes bioresources of *Dictyostelium* and other cellular slime molds that mainly originate in Japan.

Design of Guide RNA for Gene Knockouts, Knockdowns, Knock-ins and Point Mutations

(1) Identify a gene or region of interest to introduce mutations.
Note: For knockouts, targets can be selected within the gene. The gene function can be completely disrupted by designing target sequences in the first half of the gene or in a functional domain, if possible. By contrast, the range of knock-ins and point mutations available is limited

because the target can only be designed around the narrow genomic region of interest. Cas9 variants with relaxed PAM sequences, such as Cas9-NG and SpRY, are useful for generation of knock-ins and point mutations because they increase the number of places where targets can be designed. In knockdowns, the target is designed inside and upstream of the gene including the transcriptional initiation site.

(2) Find candidate target sequences in the region of interest using web tools such as Cas-Designer.
Note: 5′-NGG-3′ is a canonical PAM sequence that is recognized by SpCas9. The output is 23 nucleotides, which includes 20 nucleotides for the target and 3 nucleotides for the PAM. PAM sequences appear in either DNA strand (the upper strand or complementary lower strand). Four-thymidine repeats should be avoided because they are a termination signal for RNA polymerase III. More than 20% of GC content without the PAM sequence is recommended. An out-of-frame score of 66 or higher returned by Cas-designer is recommended, but even if the score is lower than 66, it is possible to edit a gene of interest. It is more important to select a target with a mismatch score of zero to prevent off-target cleavage. The potential for genome wide off-target effects remains undetermined in *Dictyostelium*, but a non-specific mutation was rarely observed when a target sequence with single-nucleotide mismatch in the 20-nucleotide target sequence was selected. Indeed, a single-nucleotide mismatch at the 3rd nucleotide from the NGG PAM prevented a non-specific mutation, while a target sequence with a mismatch at the 19th nucleotide from the PAM sometimes showed off-target effects. Because sequences with a single-nucleotide mismatch are not selected as targets, we expect the non-specific mutation rate to be low.
Further consideration is needed to design the target. Designing targets around AT-rich regions or regions containing repeat sequences should be avoided to allow the design of good primers that amplify the locus to detect the mutation via DNA sequencing. Although the commonly used U6 promoter prefers a G at the 5′ end for effective expression, no extra G is necessary in our CRISPR/Cas9 vectors because of the tRNA-based expression system. In addition to Cas-Designer, the program CRISPOR is also available (Concordet and Haeussler, 2018).

(3) Synthesize two complementary oligonucleotides corresponding to the target sequence. Appropriate overhang sequences should be added for Golden Gate cloning.
Note: The 20 bp target is included in the oligonucleotides but the PAM sequence should not be added. Add 5′-AGCA-3′ to the 5′ end of the sense oligonucleotide and 5′-AAAC-3′ to the 5′ end of the antisense oligonucleotide for the Golden Gate digestion/ligation reaction. These overhangs are common to both BpiI and Esp3I mediated Golden Gate reactions. When cloning two sgRNAs into a vector to generate a double knockout, different overhangs are added to the oligonucleotides (**Table 3**). Two target sequences can be integrated into a CRISPR vector with a single tube reaction. Schematic illustration of the overhangs is shown in **Figure 2**.

Design of Guide RNA for Generation of Gene Deletions and Point Mutations Using Cas9 Nickase

(1) Identify a gene of interest to generate a deletion or point mutation.

(2) Find a pair of target sequences in the region using a web tool.
Note: A combination of sgRNAs with PAM sites flanking the opposite DNA strand should be selected in order to induce double-nicking (**Figure 3**). If the target sequence cannot be designed in the appropriate position, consider using Cas9-NG nickase, where NG is the PAM sequence.

(3) Synthesize sgRNA sequences as a pair of forward and reverse oligonucleotides. Each pair of oligonucleotides contains unique overhangs for Golden Gate assembly.
Note: The unique overhangs are the same as the ones used in double gene knockouts shown in **Table 3**. Details are also shown in **Figure 2**.

Design of a HDR Template for a Tag Knock-in or Precise Point Mutation

By combining the CRISPR/Cas9 vector with ssODN or donor DNA, a tag knock-in or single nucleotide substitution can be efficiently achieved, respectively.

Design of ssODN for Precise Point Mutations

(1) The ssODN consists of substituted nucleotides flanked by homology arms on both left and right sides. The base substitutions are designed to be placed near the center of the ssODN and the targeting sgRNA region is located near the mutation. Homology arms are designed to include 30–80 perfectly matched nucleotides on both sides.

(2) Synthesize an ∼120 nucleotide ssODN as a template for HDR. Use 2.5 μl of 10 μM ssODN per electroporation.

Design of Donor DNA for Tag Knock-in

(1) To knock-in relatively longer sequences such as GFP, HDR template with the tag sequence is amplified using PCR with primers containing the homologous sequence of the target

TABLE 3 | Appropriate overhang sequences for sgRNA oligonucleotides.

	Sequence (5′ to 3′)
First sgRNA site	
Sense oligonucleotide	AGCA-N_{20}
Antisense oligonucleotide	AAAC-N_{20}
Second sgRNA site	
Sense oligonucleotide	GAGCA-N_{20}-G
Antisense oligonucleotide	TAAAC-N_{20}-T

N_{20} = 20 nucleotides genomic target.

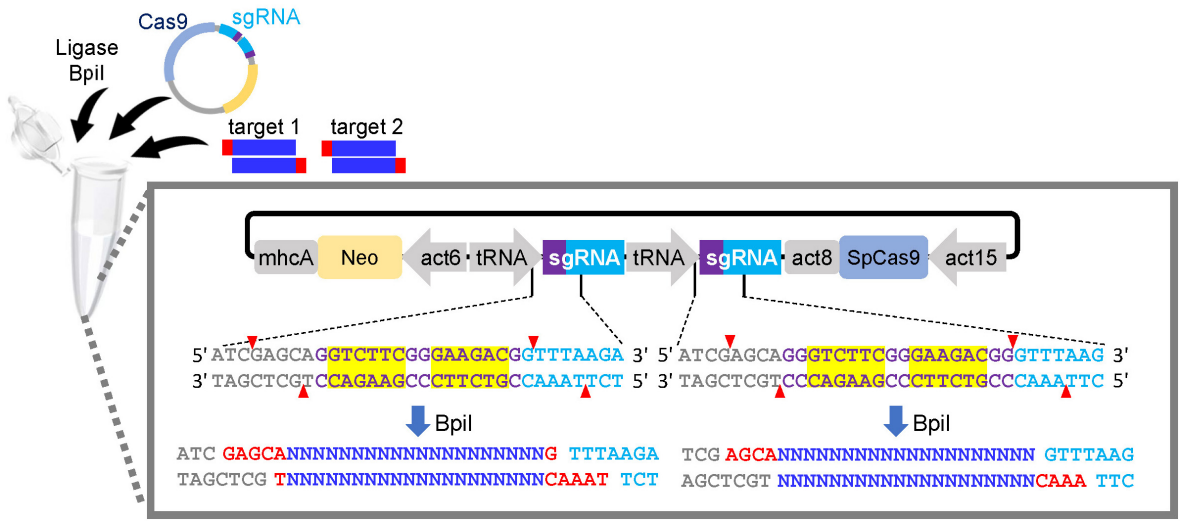

FIGURE 2 | Single cloning step of a dual sgRNA expression vector. Annealed oligonucleotides are ligated to the tRNA–sgRNA junctions via Golden Gate reaction. DNA sequences of BpiI sites are indicated in yellow box. As the BpiI site is non-palindromic, re-digestion/ligation is not possible. Red and blue letters show the overhangs for cloning and target sequences of sgRNAs, respectively. CRISPR vector, T4 DNA ligase and annealed oligonucleotides for the first and second targets are mixed in a single tube to integrate two targets.

gene. The homologous sequences at both ends are designed to be 30–90 nucleotides in length, with 60 nucleotides generally being sufficient to achieve high efficiency. Shortening or extending the length of the homologous sequence alters knock-in efficiency (Asano et al., 2021).

(2) Amplify the tag sequence containing the homologous sequence using PCR with a high-fidelity DNA polymerase. Prepare ∼2 μg of donor DNA per electroporation.

Molecular Cloning of CRISPR/Cas9 Constructs

Preparation of Annealed Oligonucleotides for the Target Gene

(1) Dissolve oligonucleotides to a concentration of 10 μM with distilled water.

(2) Prepare the following annealing mixture (10 μL):
10 μM sense oligo for target 4.5 μL
10 μM antisense oligo for target 4.5 μL
10 × annealing buffer 1.0 μL

(3) Anneal the mixture in a thermal cycler under the following conditions:
95°C for 5 min, followed by slowly cooling to 25°C (1°C/min).

Cloning of Annealed Oligonucleotides Into the tRNA–sgRNA Junction Using Golden Gate Assembly

(4) Set up a Golden Gate reaction under the following conditions.
<single tRNA–sgRNA expression vector (4.0 μL)>
CRISPR/Cas9 vector (25 ng/μL) 0.8 μL
10 × T4 DNA ligase buffer 0.4 μL
T4 DNA ligase 0.2 μL
Annealed oligo 0.3 μL
BpiI* 0.2 μL
Autoclaved milli-Q water 2.1 μL
<dual tRNA–sgRNA expression vector (8.0 μL)>
CRISPR/Cas9 vector (25 ng/μL) 1.6 μL
10 × T4 DNA ligase buffer 0.8 μL
T4 DNA ligase 0.4 μL
Annealed oligo first target 0.3 μL
Annealed oligo second target 0.3 μL
BpiI* 0.4 μL
Autoclaved milli-Q water 4.2 μL
Note: *If there is an Esp3I site between tRNA and sgRNA, Esp3I is used instead of BpiI. When using Esp3I, adding CutSmart buffer to the reaction mixture may increase the efficiency of the Golden Gate reaction.

(5) Digestion/ligation reaction is conducted under the following thermocycling conditions:
37°C for 5 min
16°C for 15 min
Repeat 5–8 times

(6) Prepare complete digestion reaction to prevent contamination of the non-integrated vector by combining:
<single tRNA–sgRNA expression vector (4.0 μL)>
Golden Gate product 4.0 μL
10 × Buffer G* 0.4 μL
BpiI 0.2 μL
<dual tRNA–sgRNA expression vector (8.0 μL)>
Golden Gate product 8.0 μL
10 × Buffer G* 0.9 μL
BpiI 0.2 μL
Note: *When Esp3I is used in the Golden Gate reaction, Esp3I and 10 × CutSmart buffer are used instead.

(7) Incubate the mixture at 37°C for 60 min, followed by 80°C for 5 min.

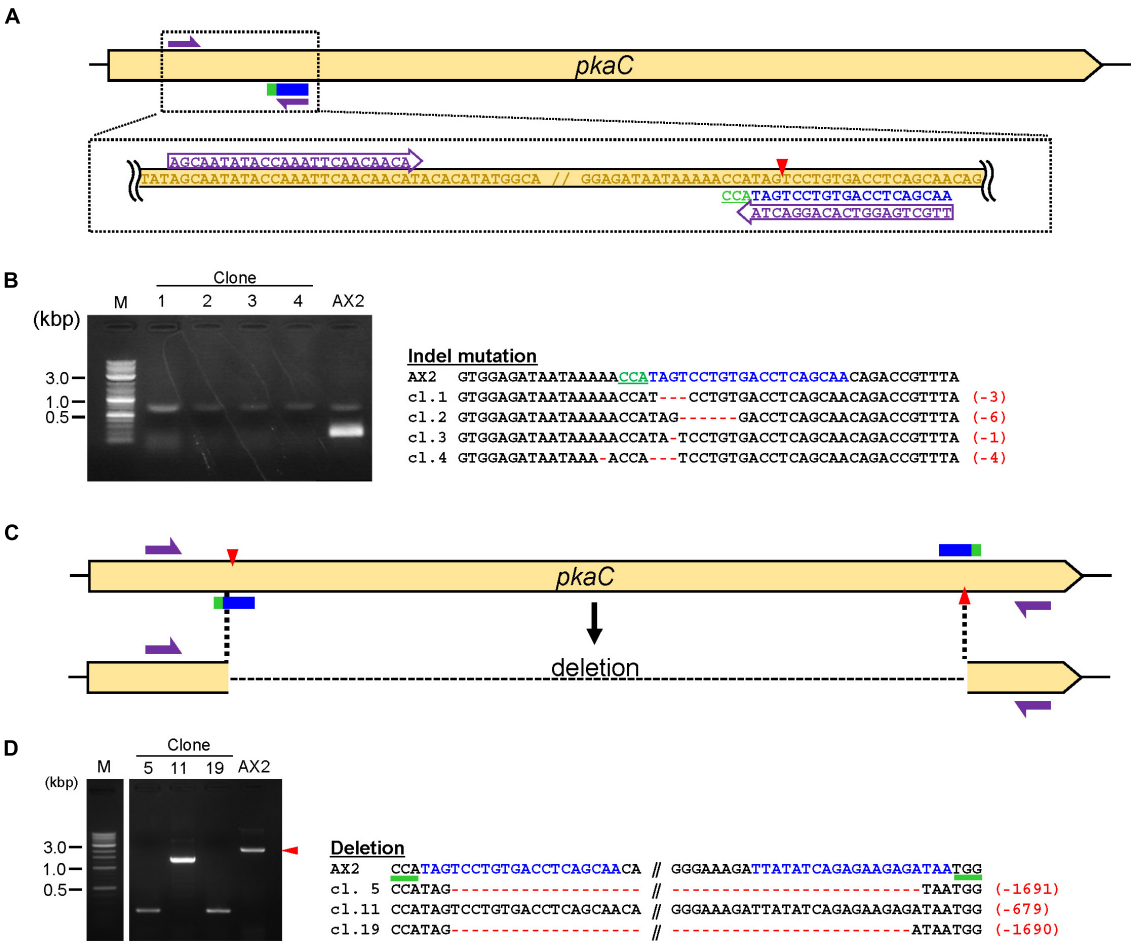

FIGURE 3 | Validation of knock-out and deletion mediated by CRISPR/Cas9. **(A)** Schematic diagram of the target site for knock-out. Target sequences in *pkaC* and primers for mutation–detective PCR are shown. **(B)** Results of mutation–detective PCR and sequencing of the target regions are shown. The PCR products that revealed low amplification compared to the control were candidate mutants. The target sequence is in blue and mutations are in red. Numbers in parentheses indicate the number of modified nucleotides. **(C)** Schematic illustration of target sites for deletion mediated by Cas9-nickase. **(D)** PCR and Sequencing results of deletion mutants.The PCR fragments that were different in size compared to the control were deletion mutants.

(8) For transforming the products into chemically competent cells using a standard protocol, spread the transformation mix on an LB agar plate containing ampicillin.

Confirmation of Successful Cloning by Using Colony PCR

(9) Pick a single colony and dissolve in 10 μL of autoclaved milli-Q water. A total of 4–12 colonies are selected to test cloning.
Note: The correct clones are picked and inoculated into LB medium for DNA preparation.

(10) Heat the solution at 95°C for 5 min and use 2 μL of this solution as template DNA for the following PCR.

(11) Prepare the following PCR mixture (10 μL).
5 × One Taq Standard Reaction buffer 2.0 μL
2.5 mM dNTPs 0.8 μL
10 μM sense oligo for target 0.3 μL
10 μM tracr-Rv primer 0.3 μL
Template DNA 2.0 μL
One Taq DNA Polymerase 0.05 μL
Autoclaved milli-Q water 4.55 μL
Note: Primer sequence of tracr-Rv is shown in **Supplementary Table 1**. The correct assembly of the dual tRNA–sgRNA vector is confirmed using the following primers: sense oligo for second target and antisense oligo for the first target.

(12) Perform PCR under the following conditions:

(1) 94°C, 30 s
(2) 94°C, 12 s
(3) 55°C, 30 s
(4) 68°C, 20 s
Repeat steps (2)– (4), 30 times

(13) Run the amplified DNA on 2% agarose gel to check cloning. A band of ∼120 bp implies successful cloning.

Note: For the dual tRNA–sgRNA vector, a ∼250 bp band is observed.

(14) For further validation of the insertion, analyze the sequence via Sanger sequencing using a NeoUp primer.
Note: For vectors that use a cassette other than the neomycin resistance gene, use primers for the appropriate drug resistance gene (**Supplementary Table 1**). blasticidin; BsrUp, hygromycin; HygUp. For doxycycline-inducible vector, use the following primer: blasticidin; BsrDown, neomycin; NeoDown.

Transformation of *Dictyostelium* Cells

Preparation of Plasmid DNA and *Dictyostelium* Cells

(1) Prepare a high-quality CRISPR/Cas9 plasmid DNA using a commercially available plasmid purification kit. The standard amount of DNA for a transient expression vector is 10 μg per transformation. Whereas, for a stable expression vector, 3 μg of DNA is sufficient.

(2) Culture *Dictyostelium* cells (e.g. AX2, AX3 or any other cell line of interest) in HL5 medium at 22°C to a density of 1.5–4.0 × 10^6 cells/mL. Healthy cells should be used for further experiments and cultured cells older than 2 weeks should be avoided.

Transformation of *Dictyostelium* Cells Through Electroporation

(3) Place 1 mm electroporation cuvettes, 1.5 mL tubes containing an appropriate amount of DNA and H50 buffer on ice. The total volume of DNA should be less than 10 μL.
Note: For the transformation of tag knock-in and precise point mutation, HDR templates should be added.

(4) Transfer the growing cells into 50 mL tubes and incubate on ice for 10 min.

(5) Pellet the cells by centrifugation at 500*g* for 2 min.

(6) Discard the supernatant and wash the cells with 10 mL of ice-cold H50 buffer. Pellet again the cells by centrifugation at 500*g* for 2 min.

(7) Resuspend the pellet in ice-cold H50 buffer at a density of 5 × 10^7 cells/mL.

(8) Transfer 100 μL of the cell suspension to a 1.5 mL tube containing CRISPR/Cas9 vector.

(9) Transfer the mixture to the electroporation cuvette and electroporate the cells at 0.75 kV, 25 μF, 2 pulses and 5 s pulse interval.

(10) Place the cuvette on ice for 5 min.

(11) To mix the cells, pipette the cells gently up and down and plate the cells in a petri dish containing 10 mL of HL5. Transfer a few hundred microliters of HL5 from the dish to the cuvette, and collect the cell mixture and return to the petri dish.

Selection of Transformants

(12) Allow the cells to recover for 8–16 h after electroporation.

(13) Aspirate HL5 medium and replace it with 10 mL of fresh HL5 medium containing appropriate antibiotics. G418; 10 μg/mL, blasticidin; 10 μg/mL and hygromycin; 30 μg/mL.

(14) To induce the transient expression of CRISPR/Cas9 vector, incubate the cells for another 1–3 days before the cells turn round in shape. To select stable transformants, replace HL5 medium few times a week until the transformants become visible. In this process, the antibiotic concentration is increased to G418 20 μg/mL or hygromycin 50 μg/mL.
Note: A crucial part of transient expression is the selection of appropriate transformants. The duration of antibiotic selection needs to be adjusted according to the condition of cells and the quantity and/or quality of DNA added to the electroporation cuvette. If it is difficult to determine the optimal duration, we recommend that some of the cells from the selection on day 1 be transferred to an SM agar plate as described below and the remainder be maintained on HL5 medium for further antibiotic selection. The resulting transformants can be used directly for the isolation of single clones on SM plates, or the cells can be recovered after a few days of incubation in HL5 medium without antibiotic selection because they contain dead cells.

Validation of Genome Editing

To identify the desired mutants, perform PCR to amplify the mutated region and sequencing analysis to further validate the desired mutants.

Isolation of Single Clones

(1) Collect cells from the transformation plate, count them using a hemocytometer, and the density adjust to 1.5 × 10^4 cells/mL in KK2.

(2) Plate 100, 35, 15 and 5 μL of the cell mixture containing 1,500, 525, 225 and 75 cells on SM agar plate containing 200 μL of pre-cultured *K. pneumoniae* KpGe strain. Spread the cells over the entire SM plate.
Note: When cells are plated immediately after transient selection, 75–1,500 cells are inoculated on the plate because they contain dead cells. If rescued cells cultured in HL5 medium for a few days are used, 50–300 cells are transferred to the plate. Certain mutants grow poorly on bacteria, in which case single clones can also be isolated by limiting dilution into 96-well plates containing HL5 medium.

(3) Allow the plates to dry and incubate them at 22°C for ∼4 days. Well-isolated plaque forming colonies will appear on the bacterial lawn of the SM plate containing either diluted cells.

Isolation of Genomic DNA for PCR

(4) After individual colonies attain a size of 2 mm, pick single clones with sterile pipette tips and transfer them to PCR tubes containing 20 μL of DNA extraction buffer.
Note: To save colonies for later culture, label the colonies that were picked from the bacterial plate. The correct clones are picked and inoculated into a 24-well plate or bacterial lawn.

(5) Incubate the mixture at 56°C for 45 min, followed by 95°C for 10 min to inactivate the ProK. This mixture is used as a template for PCR.

Genomic PCR for Validation of Genome Editing

(6) Prepare the following PCR mix (10 μL).
10 × PCR Buffer for KOD -Plus- Neo 1.0 μL
2 mM dNTPs 1.0 μL
10 μM sense oligo for target 0.3 μL
10 μM screening primer Rv 0.3 μL
Extracted genomic DNA 2.0 μL
KOD -Plus- Neo 0.2 μL
Autoclaved milli-Q water 5.2 μL
Note: A screening primer is designed to amplify the editing region and is used in combination with a sense oligo for target (**Figure 3A**).

(7) Perform PCR under the following conditions:

(1) 94°C, 30 s
(2) 94°C, 12 s
(3) 58–65°C, 30 s
(4) 68°C, 20 s
Repeat steps (2)– (4), 30 times
Note: For successful mutation–detective PCR, an appropriate annealing temperature should be optimized using the wild-type genome. Because one of the primers, sense oligo for target, is designed to span the mutated nucleotides (**Figure 3A**), no or weak genome amplification is observed in most of the mutants on performing PCR. PCR of a wild-type genome should be performed as a control. To minimize false-positive amplification, use of a high-fidelity DNA polymerase is recommended.

(8) Validate the mutation using agarose gel electrophoresis. Clones with no or weak amplification are selected as candidates for mutants.

Validation of the Mutation Using Sequencing Analysis

Genomic sequencing of the mutated region should be performed for any mutants used for further phenotypic analysis.

(9) Prepare a set of primers to amplify the mutated region.
(10) Perform PCR to amplify the region using the standard protocol.
(11) Run the amplified DNA on agarose gel and purify the desired product using a gel purification kit according to the manufacturer's instructions.
(12) Validate the mutation using Sanger sequencing.
Note: For knock-out, indel mutation is observed around three nucleotides upstream of the PAM sequence. In insertions or deletions of three or six nucleotides, no frameshift has occurred and the gene is not entirely disrupted. Mutants with a frameshift are used for further phenotypic analysis. For knock-in and point mutation, ensure that there are no unexpected frameshifts around the target sgRNA or homology arm. For gene deletion, sequencing analysis is unessential if long deletion is observed via PCR. For knock-down, no sequencing analysis is required because dCas9 that lacks nuclease activity is used.

EXPECTED RESULTS

We used the above procedures to generate a CRISPR/Cas9-mediated gene manipulation system in *Dictyostelium*. An all-in-one vector containing Cas9 and sgRNA was transiently expressed, and several thousands of cells were obtained, of which a portion were used for further screening. The mutants with indel mutations were generated with high efficiency, generally >50% but this ratio differs depending on the target genes. Most of our CRISPR vectors contain a G418-resistant gene. Genome editing within G418-resistant mutants requires vectors with different drug resistance genes. We tested a CRISPR vector with a hygromycin-resistance gene and observed a highly efficient loss of fluorescence resulting from genome editing within the gene encoding for tdTomato (**Supplementary Figure 1**). The most common method to detect indel mutations is PCR amplification of the targeting region (**Figure 3A**). Data presented here are a representative result, demonstrating that no PCR band was observed in most of the CRISPR mutants because one of the PCR primers was designed to span the cleavage site (**Figure 3B**). Even if the mutation was predicted by mutation–detective PCR, it sometimes contained false-positive clones or mutated clones in which multiples of three nucleotides were inserted or deleted. Hence, indel mutations were verified through Sanger sequencing and frameshift mutants were used for further functional analysis (**Figure 3B**). One of the disadvantages of this method is false-positive clones, where no PCR band is detected, even in non-mutated clones. Hence, long deletions mediated by Cas9 nickase are a straightforward method to detect the mutations effectively because PCR products of the wild-type and mutant genes differ in size (**Figures 3C,D**). All of the PCR-positive clones exhibited long deletion of the target (**Figure 3D**). Efficiency of the knockout mutation method was slightly lower (10–30%) than the conventional Cas9 method (>50%), but it was efficient enough to obtain knockout mutants via deletion.

We constructed a CRISPR/Cas9 vector that disrupts multiple genes simultaneously and successfully modified five PI3K genes (Sekine et al., 2018). However, three steps of Golden Gate cloning were required to produce the targeting vector, which was time consuming. In general, even when analyzing several genes simultaneously, a few genes are often disrupted at the same time. We therefore constructed CRISPR/Cas9 vectors containing two tRNA–sgRNA cassettes to be able to generate a targeting vector for two genes in a single cloning step. We designed a target sequence for both the *pkaC* and *tdTomato* genes, and two pairs of sgRNAs containing different overhangs at the 5′ end of the oligonucleotides were assembled into a CRISPR vector, pTM1725 (**Figure 4A**). Colony PCR confirmed that the colonies analyzed contained both sgRNA sequences (**Figure 4B**). The CRISPR vectors were introduced into tdTomato–knock-in cells to determine the ratio of cells in which the two genes were simultaneously disrupted, which would result in loss of red

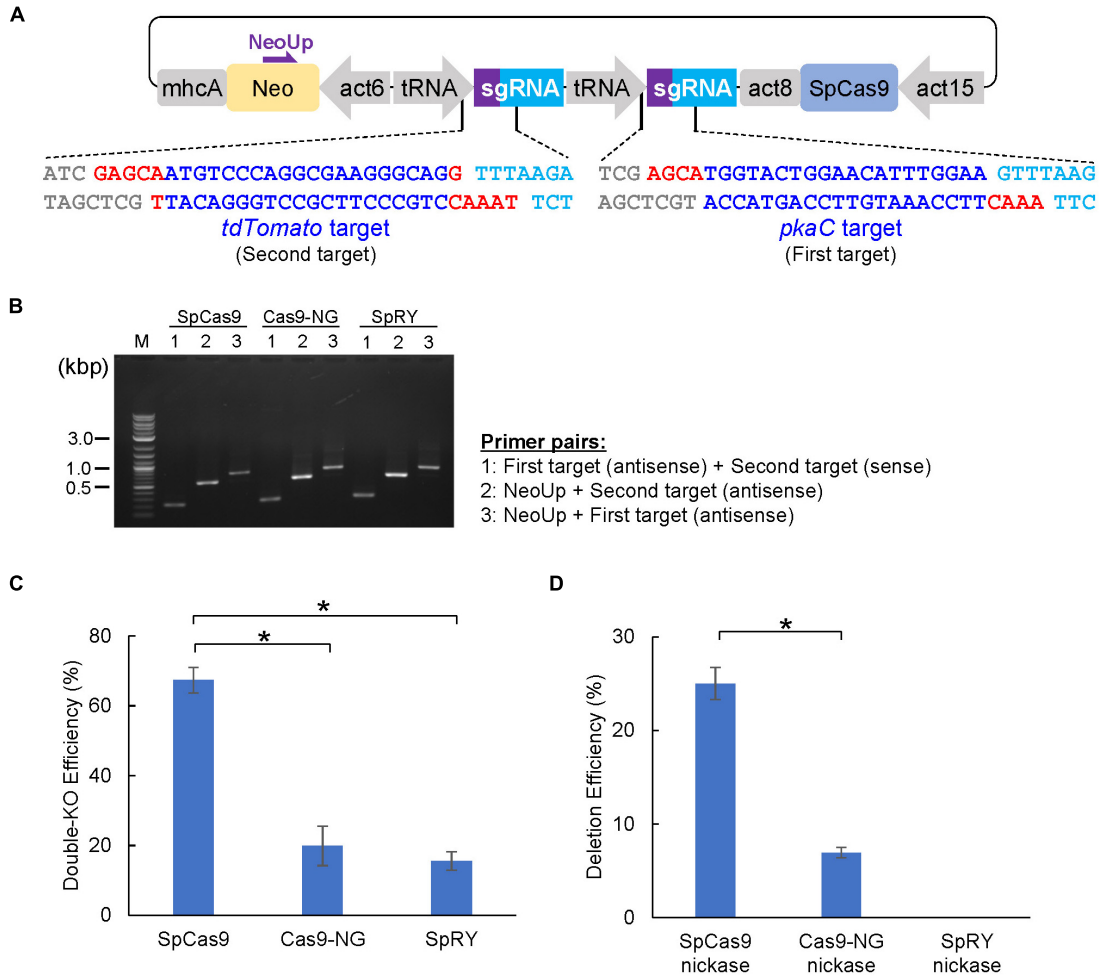

FIGURE 4 | CRISPR/Cas9-mediated double-knockout and genomic deletion. **(A)** Schematic of the dual sgRNA expression vector designed for single cloning step. Red and blue letters represent overhands for the cloning and 20-nt of target sequences, respectively. **(B)** Correct insertion of the first and second targets was confirmed via colony PCR. **(C)** Summary of double knock-out efficiencies by various Cas9 and sgRNA that target *pkaC* and *tdTomato* gene. **(D)** Summary of deletion efficiency in *pkaC* gene by various Cas9 nickase. Data shown are mean ± SEM ($n = 3$ biological replication). *$P<0.05$.

fluorescence and aggregation defects. As a result, both genes were disrupted in over 60% of the mutants with the SpCas9 vector. By contrast, knockouts of both genes using SpCas9-NG or SpRY were less efficient than what we observed for SpCas9 (**Figure 4C**). Therefore, the use of SpCas9 is preferred unless a NGG PAM cannot be identified in the genes of interest. Furthermore, a nickase (D10A mutant) was generated based on SpCas9-NG and SpRY, and we found that using SpCas9 nickase was the most effective method to generate long deletions (**Figure 4D**). Hence, CRISPR vectors targeting two genes can be constructed using one cloning step, and the genes of interest are disrupted with high efficiency.

Tagging a protein of interest with an epitope tag or fluorescent protein is one of the most popular methods used to study protein function. Overexpression of the fusion protein enables observation of the protein in cells, but overproduction may lead to artifacts such as ectopic expression or dominant-negative effects. Recent methods based on CRISPR/Cas9-mediated HDR allow for the knock-in of endogenous genes to achieve expression levels close to those observed endogenously. To knock-in GFP immediately after the start codon, we generated a SpRY-based CRISPR vector and donor DNA containing the GFP sequence and homology arms (**Figure 5A**). About half of the transformed cells exhibited bands ∼700 bp larger than the parental strain when analyzed using mutation–detective PCR (**Figure 5B**), indicating that knock-in efficiency was high enough. However, when we tried to generate knock-in strains by combining the same donor DNA with other neighboring target sequence, we found that knock-in frequencies were less than 1%. Therefore, trying several target sequences is essential for the successful generation of knock-in strains. CRISPR/Cas9-mediated HDR allows not only for knock-in of tag sequences but also the introduction of precise point mutations in the genome. When we transformed a CRISPR vector with ssODN, which contains substituted nucleotides in the middle of the sequence and 30–80 bp homology arms on each side (**Figure 5C**), PCR-positive

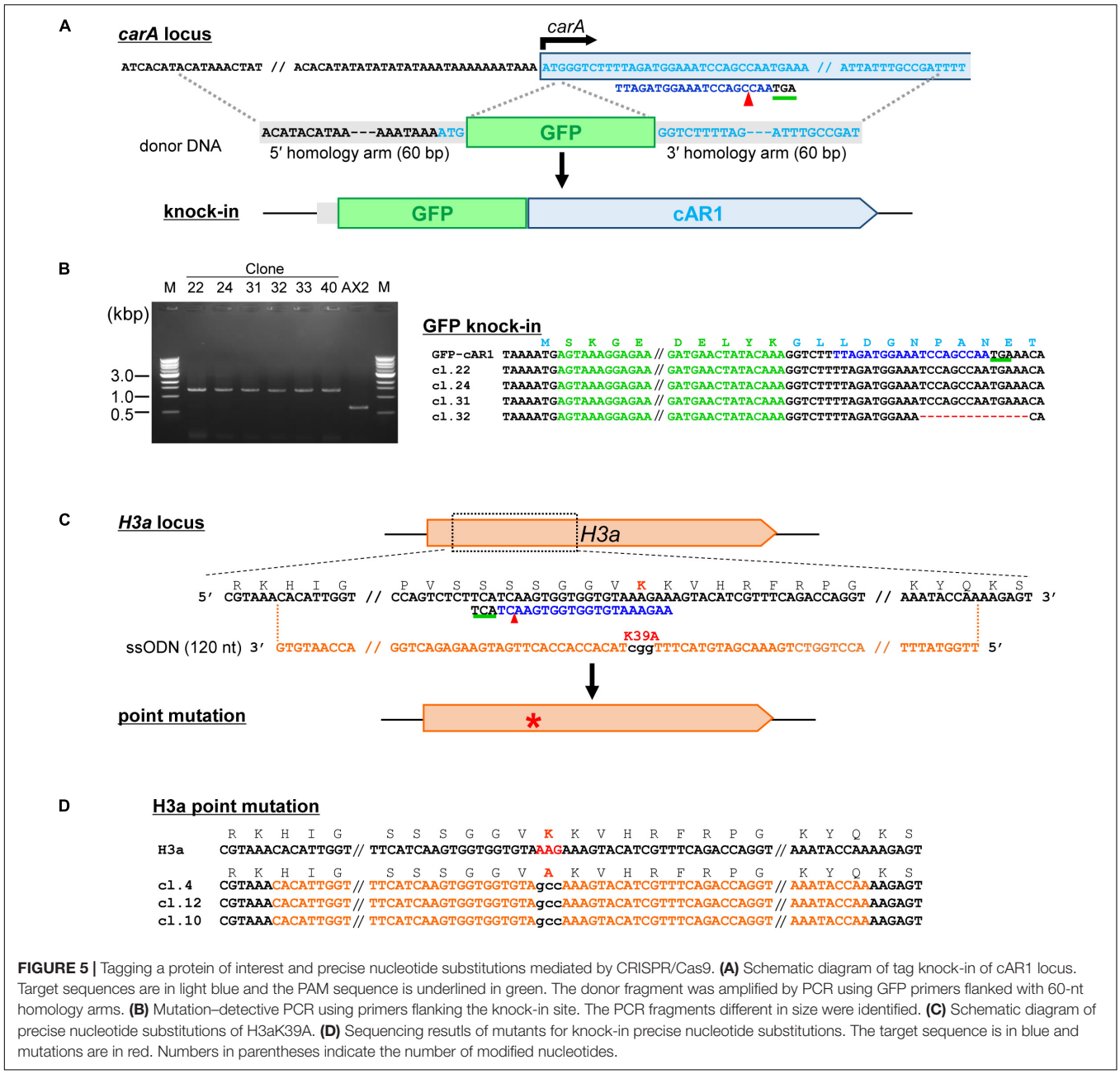

FIGURE 5 | Tagging a protein of interest and precise nucleotide substitutions mediated by CRISPR/Cas9. **(A)** Schematic diagram of tag knock-in of cAR1 locus. Target sequences are in light blue and the PAM sequence is underlined in green. The donor fragment was amplified by PCR using GFP primers flanked with 60-nt homology arms. **(B)** Mutation–detective PCR using primers flanking the knock-in site. The PCR fragments different in size were identified. **(C)** Schematic diagram of precise nucleotide substitutions of H3aK39A. **(D)** Sequencing resutls of mutants for knock-in precise nucleotide substitutions. The target sequence is in blue and mutations are in red. Numbers in parentheses indicate the number of modified nucleotides.

nucleotide substitutions were observed in 6.8–97.7% of the clones. All clones were analyzed by sequencing to confirm correct knock-in and point mutation generation (**Figures 5B,D**). The use of several target sequences was also effective for obtaining the mutants, because efficiency depended on the position of the target sequence.

Genome editing using CRISPR/Cas9 relies on the nuclease activity of Cas9. This limits its use in applications in which genetic perturbation needs to be controlled temporally; i.e., when it is desired to edit genes that induce strong side effects on growth or development. A drug-inducible CRISPR/Cas9 system allows for temporal control of genome editing. A doxycycline-inducible expression vector was constructed and high efficiency of expression induction was demonstrated in *Dictyostelium* (Veltman et al., 2009b). Therefore, we designed a CRISPR/Cas9 system that enables temporal control of the Cas9 nuclease through drug-treatment. We integrated the target sequence of *tdTomato* into a tRNA–sgRNA cassette of the CRISPR vector to obtain stable expression strains. The loss of fluorescence was then determined with/without doxycycline-treatment (**Figure 6A**). As a result, loss of fluorescence was observed in more than 60% of cells after 3 days of drug-treatment, whereas no change in fluorescence was observed in cells without doxycycline-treatment (**Figures 6B,C**). We then selected *pkaC* as a target gene because the knockout mutant exhibits a defect in cell aggregation. Upon treatment with doxycycline for 2 days,

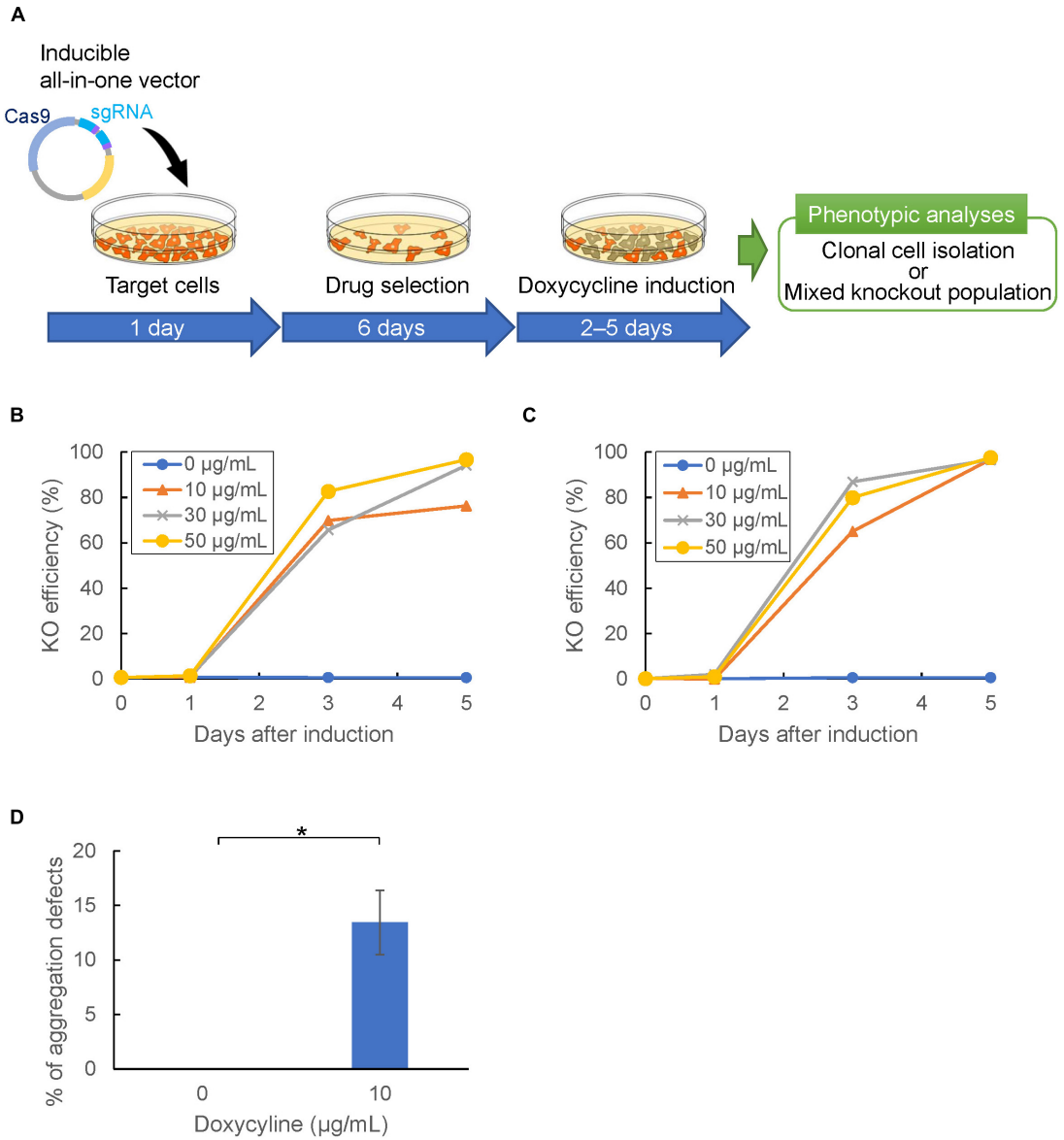

FIGURE 6 | Temporal control of CRISPR/Cas9-mediated gene knockout. **(A)** Gene knockout workflow using inducible all-in-one vector. Target cells were transformed with the inducible vector and selected with Blasticidin or G418 in doxycycline-free HL5 for 6 days. Cas9-stable cells were then incubated in HL5 with doxycycline to induce Cas9. **(B,C)** Temporal control of genome editing via inducible Cas9 vector containing neomycin **(B)** or blasticidin **(C)** resistance cassette, respectively. The mean of knock-out efficiency at different doxycycline concentrations (0, 10, 30, 50 μg/mL) was represented. **(D)** Frequency of aggregation defect mutants targeting *pkaC* gene at different doxycycline concentrations. The error bar shows the standard deviation based on four independent biological replicates. *$P<0.001$.

approximately 15% of the independent clones were aggregation-negative, whereas all the clones exhibited normal aggregation in the mock controls (**Figure 6D**). Hence, we developed a drug-inducible CRISPR/Cas9 system that exhibits high knockout efficiency upon induction of Cas9 activity.

In general, it is difficult to analyze the functions of essential genes because their knockout is lethal. Gene silencing that inhibits expression of the target gene is an alternate method to investigate their functions. Although RNA interference (RNAi) has been used for this purpose, CRISPR/Cas9-based gene silencing methods have been developed in various organisms. Catalytically inactive Cas9 (dCas9) lacks endonuclease activity, and it remains bound to specific target DNA sequences, which allows for silencing of gene expression without altering DNA sequences. We designed target sequences for the *tdTomato* gene and co-expressed dCas9 and tRNA–sgRNAs within the tdTomato–knock-in cells. We selected 10 different pairs of target sequences (**Supplementary Table 2**) and found loss of fluorescence in most of the CRISPRi cell lines. The fluorescence intensity was reduced by about half when the targets were located

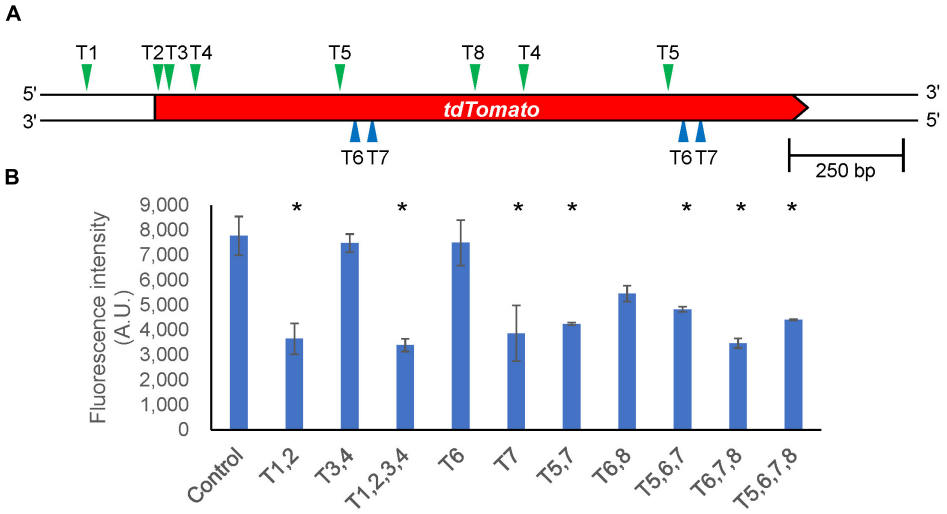

FIGURE 7 | Silencing gene expression by CRISPRi. **(A)** Schematic illustration of target sites in the *tdTomato* knock-in region. The position of each target site on the upper strand and complementary lower strand is indicated by green and blue arrowheads, respectively. **(B)** Intracellular fluorescence intensity in different target combinations. Data shown are mean ± SEM ($n = 3$ biological replication). *$P<0.05$; ANOVA folloed by Tukey's *post hoc* test.

around the transcription start site (T1,2,3,4) of the gene, but the efficiency of gene silencing varied depending on the targets (**Figure 7**). We also investigated RNA levels in the CRISPRi cells expressing T1, 2, 3, and 4 sgRNA and found that RNA levels were less than 10% of what was observed for controls. We also investigated whether drug-induced CRISPRi resulted in suppression of fluorescence levels. However, cells in which dCas9 was induced by doxycycline treatment for 4 days exhibited no major repression of either fluorescence or RNA levels. Therefore, constitutive expression of a CRISPRi vector is an effective tool for functional analysis of genes whose knockout produces strong defects in cell growth.

DISCUSSION

Gene knockout was performed by introducing a linearized DNA construct containing a drug-resistance gene flanked by homology arms complementary to the target gene locus. This method is still widely used in *Dictyostelium*, but CRISPR/Cas9-mediated gene manipulation is just now emerging. The development and improvement of the CRISPR toolbox provides straightforward procedures to generate knockouts, inducible knockouts, knockdowns, knock-ins, point mutations and deletions without integrating a drug-resistance gene. Therefore, the CRISPR toolbox developed in our study increases the robustness of functional analysis in the biomedical model organism *Dictyostelium*.

In the case of knockout using homologous recombination, it is not possible to obtain knockout mutants for essential genes. By contrast, using our CRISPR/Cas9 method, mutants with insertions or deletions of multiples of three nucleotides are generated even if the gene is essential. Indeed, this method was used to identify essential genes (You et al., 2020). Simultaneous editing of multiple genes is achieved by expressing Cas9 and multiple sgRNAs from a single CRISPR vector (Sekine et al., 2018). This is a huge advantage of the CRISPR-mediated knockout method because Cre-loxP–mediated multiple gene disruption is much more time-consuming. The multiplex CRISPR vector is able to carry up to 20 sgRNAs in a single vector with 4-step cloning, but practically, it is unlikely that it is necessary to disrupt more than five genes at the same time. The new CRISPR vectors presented in this study are able to integrate two target sequences in a single cloning step in a single tube reaction. By changing the overhangs of oligonucleotides at the end of the target, it is possible to create vectors containing three or four sgRNAs in one or two Golden-Gate cloning steps, respectively. This reduces the time required to clone and manipulate multiple genes quickly.

This cloning method, which uses multiplex sgRNAs, is useful for CRISPRi-mediated gene repression targeting multiple positions within a single gene. By varying the number of target sequences, the degree of gene repression can be controlled. For repression of gene expression, RNAi has been the most common method of choice since the early 2000s (Martens et al., 2002; Muramoto et al., 2003). The RNAi usually targets gene regions avoiding the UTRs of an mRNA, whereas CRISPRi targets multiple positions in a promoter or a sequence inside a gene, which enables more efficient and fine tuning of gene repression by adjusting the number of targets. In the future, the doxycycline-inducible CRISPR/Cas9 and CRISPRi systems will help us to analyze genes that exhibit strong defects in growth and development.

The CRISPR/Cas9 system can also be adapted to many applications. Genes can be disrupted upon conditional expression of Cas9 during development. Many promoters that control the expression of specific cell types are known in *Dictyostelium* (Williams, 2006; Zhukovskaya et al., 2006; Yamada et al., 2008;

Chen et al., 2017). Hence, it should be possible to study the effects of knockout at specific developmental stages. We replaced the *act15* promoter with an *ecmA* promoter that is expressed in pstA cells and then induced a cell-type specific knockout in the gene encoding for a fluorescent protein. However, no distinct loss of fluorescence was observed in either growing cells or cells in the pstA region of the slug. The presence of fluorescence may be due to the stability of the fluorescent protein, which is stable for at least several hours (Deichsel et al., 1999). Genome-wide knockout libraries are also an attractive application of the CRISPR/Cas9 system (Shalem et al., 2014). Unlike the well-established forward genetic approach of restriction enzyme-mediated integration (REMI) mutagenesis (Kuspa, 2006), CRISPR-mediated screening can be designed genome-wide or for sub-pooled targets such as kinases or transcription factors. Hence, further refinement of related methods could lead to a breakthrough in the understanding of *Dictyostelium* genetics.

The versatile CRISPR/Cas9 toolboxes presented herein expand the number of genes available for manipulation in the biomedical model organism *Dictyostelium*. The rapid pace of improvement makes it an important leap in a new era of gene manipulation. We conclude that our established protocols pave the way for efficient and simple genetic manipulation.

DATA AVAILABILITY STATEMENT

The original contributions presented in the study are included in the article/**Supplementary Material**, further inquiries can be directed to the corresponding author/s.

AUTHOR CONTRIBUTIONS

TM conceived the original idea and supervised the project and wrote the initial draft of the manuscript. KY and HI performed experiments presented in this manuscript. KY, HI, and TM worked closely to analyze and interpret data. YK co-conceptualized and provided materials of NBRP Nenkin. All authors revised the manuscript, and read and approved the submitted version.

FUNDING

This study was partly supported by JSPS KAKENHI to TM (grant number: 20K06659), to YK (grant number: 20K06631) and Sasakawa Scientific Research Grant to KY.

ACKNOWLEDGMENTS

We would like to thank Yuu Asano and Takanori Ogasawara, and other former members of the Muramoto lab (Toho University) for their contributions to establishing the system and protocol described here.

SUPPLEMENTARY MATERIAL

The Supplementary Material for this article can be found online at: https://www.frontiersin.org/articles/10.3389/fcell.2021.721630/full#supplementary-material

REFERENCES

Adli, M. (2018). The CRISPR tool kit for genome editing and beyond. *Nat. Commun.* 9:1911. doi: 10.1038/s41467-018-04252-2

Anzalone, A. V., Koblan, L. W., and Liu, D. R. (2020). Genome editing with CRISPR-Cas nucleases, base editors, transposases and prime editors. *Nat. Biotechnol.* 38, 824–844. doi: 10.1038/s41587-020-0561-9

Asano, Y., Yamashita, K., Hasegawa, A., Ogasawara, T., Iriki, H., and Muramoto, T. (2021). Knock-in and precise nucleotide substitution using near-PAMless engineered Cas9 variants in *Dictyostelium discoideum*. *Sci. Rep.* 11:11163. doi: 10.1038/s41598-021-89546-0

Bae, S., Park, J., and Kim, J. S. (2014). Cas-OFFinder: a fast and versatile algorithm that searches for potential off-target sites of Cas9 RNA-guided endonucleases. *Bioinformatics* 30, 1473–1475. doi: 10.1093/bioinformatics/btu048

Capecchi, M. R. (2005). Gene targeting in mice: functional analysis of the mammalian genome for the twenty-first century. *Nat. Rev. Genet.* 6, 507–512. doi: 10.1038/nrg1619

Chatterjee, P., Jakimo, N., and Jacobson, J. M. (2018). Minimal PAM specificity of a highly similar SpCas9 ortholog. *Sci. Adv.* 4:eaau0766. doi: 10.1126/sciadv.aau0766

Chen, Z. H., Singh, R., Cole, C., Lawal, H. M., Schilde, C., Febrer, M., et al. (2017). Adenylate cyclase A acting on PKA mediates induction of stalk formation by cyclic diguanylate at the *Dictyostelium* organizer. *Proc. Natl. Acad. Sci. U.S.A.* 114, 516–521. doi: 10.1073/pnas.1608393114

Concordet, J. P., and Haeussler, M. (2018). CRISPOR: intuitive guide selection for CRISPR/Cas9 genome editing experiments and screens. *Nucleic Acids Res.* 46, W242–W245. doi: 10.1093/nar/gky354

Cong, L., Ran, F. A., Cox, D., Lin, S., Barretto, R., Habib, N., et al. (2013). Multiplex genome engineering using CRISPR/Cas systems. *Science* 339, 819–823. doi: 10.1126/science.1231143

Deichsel, H., Friedel, S., Detterbeck, A., Coyne, C., Hamker, U., and MacWilliams, H. K. (1999). Green fluorescent proteins with short half-lives as reporters in *Dictyostelium discoideum*. *Dev. Genes Evol.* 209, 63–68. doi: 10.1007/s004270050228

Di Cristofano, A., Pesce, B., Cordon-Cardo, C., and Pandolfi, P. P. (1998). Pten is essential for embryonic development and tumour suppression. *Nat. Genet.* 19, 348–355. doi: 10.1038/1235

Eichinger, L., Pachebat, J. A., Glockner, G., Rajandream, M. A., Sucgang, R., Berriman, M., et al. (2005). The genome of the social amoeba *Dictyostelium discoideum*. *Nature* 435, 43–57. doi: 10.1038/nature03481

Gaudet, P., Pilcher, K. E., Fey, P., and Chisholm, R. L. (2007). Transformation of *Dictyostelium discoideum* with plasmid DNA. *Nat. Protoc.* 2, 1317–1324. doi: 10.1038/nprot.2007.179

Gerlai, R. (2016). Gene targeting using homologous recombination in embryonic stem cells: the future for behavior genetics? *Front. Genet.* 7:43. doi: 10.3389/fgene.2016.00043

Gilbert, L. A., Larson, M. H., Morsut, L., Liu, Z., Brar, G. A., Torres, S. E., et al. (2013). CRISPR-mediated modular RNA-guided regulation of transcription in eukaryotes. *Cell* 154, 442–451. doi: 10.1016/j.cell.2013.06.044

Hu, J. H., Miller, S. M., Geurts, M. H., Tang, W., Chen, L., Sun, N., et al. (2018). Evolved Cas9 variants with broad PAM compatibility and high DNA specificity. *Nature* 556, 57–63. doi: 10.1038/nature26155

Huber, R. J., and Mathavarajah, S. (2019). Comparative transcriptomics reveals mechanisms underlying cln3-deficiency phenotypes in *Dictyostelium*. *Cell. Signal.* 58, 79–90. doi: 10.1016/j.cellsig.2019.02.004

Iriki, H., Kawata, T., and Muramoto, T. (2019). Generation of deletions and precise point mutations in *Dictyostelium discoideum* using the CRISPR nickase. *PLoS One* 14:e0224128. doi: 10.1371/journal.pone.0224128

Ishigaki, K., Akiyama, M., Kanai, M., Takahashi, A., Kawakami, E., Sugishita, H., et al. (2020). Large-scale genome-wide association study in a Japanese population identifies novel susceptibility loci across different diseases. *Nat. Genet.* 52, 669–679. doi: 10.1038/s41588-020-0640-3

Jinek, M., Chylinski, K., Fonfara, I., Hauer, M., Doudna, J. A., and Charpentier, E. (2012). A programmable dual-RNA-guided DNA endonuclease in adaptive bacterial immunity. *Science* 337, 816–821. doi: 10.1126/science.1225829

Kessin, R. H. (2001). *Dictyostelium–Evolution, Cell Biology, and the Development of Multicellularity*. Cambridge, UK: Cambridge Univ. Press.

Khera, A. V., Chaffin, M., Aragam, K. G., Haas, M. E., Roselli, C., Choi, S. H., et al. (2018). Genome-wide polygenic scores for common diseases identify individuals with risk equivalent to monogenic mutations. *Nat. Genet.* 50, 1219–1224. doi: 10.1038/s41588-018-0183-z

Kim, E., Koo, T., Park, S. W., Kim, D., Kim, K., Cho, H. Y., et al. (2017). In vivo genome editing with a small Cas9 orthologue derived from *Campylobacter jejuni*. *Nat. Commun.* 8:14500. doi: 10.1038/ncomms14500

Knight, S. C., Tjian, R., and Doudna, J. A. (2018). Genomes in focus: development and applications of CRISPR-Cas9 imaging technologies. *Angew. Chem. Int. Ed. Engl.* 57, 4329–4337. doi: 10.1002/anie.201709201

Kuspa, A. (2006). Restriction enzyme-mediated integration (REMI) mutagenesis. *Methods Mol. Biol.* 346, 201–209. doi: 10.1385/1-59745-144-4:201

Lima, W. C., Pillonel, T., Bertelli, C., Ifrid, E., Greub, G., and Cosson, P. (2018). Genome sequencing and functional characterization of the non-pathogenic *Klebsiella pneumoniae* KpGe bacteria. *Microbes Infect.* 20, 293–301. doi: 10.1016/j.micinf.2018.04.001

Mali, P., Aach, J., Stranges, P. B., Esvelt, K. M., Moosburner, M., Kosuri, S., et al. (2013). CAS9 transcriptional activators for target specificity screening and paired nickases for cooperative genome engineering. *Nat. Biotechnol.* 31, 833–838. doi: 10.1038/nbt.2675

Mansour, S. L., Thomas, K. R., and Capecchi, M. R. (1988). Disruption of the proto-oncogene int-2 in mouse embryo-derived stem cells: a general strategy for targeting mutations to non-selectable genes. *Nature* 336, 348–352. doi: 10.1038/336348a0

Martens, H., Novotny, J., Oberstrass, J., Steck, T. L., Postlethwait, P., and Nellen, W. (2002). RNAi in *Dictyostelium*: the role of RNA-directed RNA polymerases and double-stranded RNase. *Mol. Biol. Cell* 13, 445–453. doi: 10.1091/mbc.01-04-0211

Martin-Gonzalez, J., Montero-Bullon, J. F., and Lacal, J. (2021). *Dictyostelium discoideum* as a non-mammalian biomedical model. *Microb. Biotechnol.* 14, 111–125. doi: 10.1111/1751-7915.13692

Mesquita, A., Cardenal-Munoz, E., Dominguez, E., Munoz-Braceras, S., Nunez-Corcuera, B., Phillips, B. A., et al. (2017). Autophagy in *Dictyostelium*: mechanisms, regulation and disease in a simple biomedical model. *Autophagy* 13, 24–40. doi: 10.1080/15548627.2016.1226737

Muramoto, T., Iriki, H., Watanabe, J., and Kawata, T. (2019). Recent advances in CRISPR/Cas9-mediated genome editing in *Dictyostelium*. *Cells* 8:46. doi: 10.3390/cells8010046

Muramoto, T., Suzuki, K., Shimizu, H., Kohara, Y., Kohriki, E., Obara, S., et al. (2003). Construction of a gamete-enriched gene pool and RNAi-mediated functional analysis in *Dictyostelium discoideum*. *Mech. Dev.* 120, 965–975. doi: 10.1016/s0925-4773(03)00136-9

Nishimasu, H., Shi, X., Ishiguro, S., Gao, L., Hirano, S., Okazaki, S., et al. (2018). Engineered CRISPR-Cas9 nuclease with expanded targeting space. *Science* 361, 1259–1262. doi: 10.1126/science.aas9129

Park, J., Bae, S., and Kim, J. S. (2015). Cas-Designer: a web-based tool for choice of CRISPR-Cas9 target sites. *Bioinformatics* 31, 4014–4016. doi: 10.1093/bioinformatics/btv537

Pears, C. J., and Lakin, N. D. (2014). Emerging models for DNA repair: *Dictyostelium discoideum* as a model for nonhomologous end-joining. *DNA Repair (Amst.)* 17, 121–131. doi: 10.1016/j.dnarep.2014.01.008

Pickar-Oliver, A., and Gersbach, C. A. (2019). The next generation of CRISPR-Cas technologies and applications. *Nat. Rev. Mol. Cell Biol.* 20, 490–507. doi: 10.1038/s41580-019-0131-5

Qi, L. S., Larson, M. H., Gilbert, L. A., Doudna, J. A., Weissman, J. S., Arkin, A. P., et al. (2013). Repurposing CRISPR as an RNA-guided platform for sequence-specific control of gene expression. *Cell* 152, 1173–1183. doi: 10.1016/j.cell.2013.02.022

Ran, F. A., Cong, L., Yan, W. X., Scott, D. A., Gootenberg, J. S., Kriz, A. J., et al. (2015). In vivo genome editing using *Staphylococcus aureus* Cas9. *Nature* 520, 186–191. doi: 10.1038/nature14299

Ran, F. A., Hsu, P. D., Lin, C. Y., Gootenberg, J. S., Konermann, S., Trevino, A. E., et al. (2013). Double nicking by RNA-guided CRISPR Cas9 for enhanced genome editing specificity. *Cell* 154, 1380–1389. doi: 10.1016/j.cell.2013.08.021

Sekine, R., Kawata, T., and Muramoto, T. (2018). CRISPR/Cas9 mediated targeting of multiple genes in *Dictyostelium*. *Sci. Rep.* 8:8471. doi: 10.1038/s41598-018-26756-z

Shalem, O., Sanjana, N. E., Hartenian, E., Shi, X., Scott, D. A., Mikkelson, T., et al. (2014). Genome-scale CRISPR-Cas9 knockout screening in human cells. *Science* 343, 84–87. doi: 10.1126/science.1247005

Thomas, K. R., Folger, K. R., and Capecchi, M. R. (1986). High frequency targeting of genes to specific sites in the mammalian genome. *Cell* 44, 419–428. doi: 10.1016/0092-8674(86)90463-0

Veltman, D. M., Akar, G., Bosgraaf, L., and Van Haastert, P. J. (2009a). A new set of small, extrachromosomal expression vectors for *Dictyostelium discoideum*. *Plasmid* 61, 110–118. doi: 10.1016/j.plasmid.2008.11.003

Veltman, D. M., Keizer-Gunnink, I., and Haastert, P. J. (2009b). An extrachromosomal, inducible expression system for *Dictyostelium discoideum*. *Plasmid* 61, 119–125. doi: 10.1016/j.plasmid.2008.11.002

Vogel, E., Pittman, P. B., and Naylor, K. (2019). The FtsZ Homolog, FszB, inhibits mitochondrial dynamics in *Dictyostelium discoideum*. *Cells* 9:64. doi: 10.3390/cells9010064

Walton, R. T., Christie, K. A., Whittaker, M. N., and Kleinstiver, B. P. (2020). Unconstrained genome targeting with near-PAMless engineered CRISPR-Cas9 variants. *Science* 368, 290–296. doi: 10.1126/science.aba8853

Williams, J. G. (2006). Transcriptional regulation of *Dictyostelium* pattern formation. *EMBO Rep.* 7, 694–698. doi: 10.1038/sj.embor.7400714

Williams, R. S., Boeckeler, K., Graf, R., Muller-Taubenberger, A., Li, Z., Isberg, R. R., et al. (2006). Towards a molecular understanding of human diseases using *Dictyostelium discoideum*. *Trends Mol. Med.* 12, 415–424. doi: 10.1016/j.molmed.2006.07.003

Yamada, Y., Wang, H. Y., Fukuzawa, M., Barton, G. J., and Williams, J. G. (2008). A new family of transcription factors. *Development* 135, 3093–3101. doi: 10.1242/dev.026377

You, Y., Ramachandra, S. G., and Jin, T. (2020). A CRISPR-based method for testing the essentiality of a gene. *Sci. Rep.* 10:14779. doi: 10.1038/s41598-020-71690-8

Zhukovskaya, N. V., Fukuzawa, M., Yamada, Y., Araki, T., and Williams, J. G. (2006). The *Dictyostelium* bZIP transcription factor DimB regulates prestalk-specific gene expression. *Development* 133, 439–448. doi: 10.1242/dev.02190

Conflict of Interest: The authors declare that the research was conducted in the absence of any commercial or financial relationships that could be construed as a potential conflict of interest.

Publisher's Note: All claims expressed in this article are solely those of the authors and do not necessarily represent those of their affiliated organizations, or those of the publisher, the editors and the reviewers. Any product that may be evaluated in this article, or claim that may be made by its manufacturer, is not guaranteed or endorsed by the publisher.

Copyright © 2021 Yamashita, Iriki, Kamimura and Muramoto. This is an open-access article distributed under the terms of the Creative Commons Attribution License (CC BY). The use, distribution or reproduction in other forums is permitted, provided the original author(s) and the copyright owner(s) are credited and that the original publication in this journal is cited, in accordance with accepted academic practice. No use, distribution or reproduction is permitted which does not comply with these terms.

frontiers in Cell and Developmental Biology

REVIEW
published: 20 August 2021
doi: 10.3389/fcell.2021.724940

How Phagocytes Acquired the Capability of Hunting and Removing Pathogens From a Human Body: Lessons Learned From Chemotaxis and Phagocytosis of *Dictyostelium discoideum* (Review)

*Xuehua Xu, Miao Pan and Tian Jin**

Chemotaxis Signal Section, Laboratory of Immunogenetics, NIAID, NIH, Rockville, MD, United States

OPEN ACCESS

Edited by:
Robin S. B. Williams, University of London, United Kingdom

Reviewed by:
Thierry Soldati, Université de Genève, Switzerland
Pascale G. Charest, University of Arizona, United States

***Correspondence:**
Tian Jin
Tjin@niaid.nih.gov

Specialty section:
This article was submitted to Molecular and Cellular Pathology, a section of the journal Frontiers in Cell and Developmental Biology

Received: *14 June 2021*
Accepted: *15 July 2021*
Published: *20 August 2021*

Citation:
Xu X, Pan M and Jin T (2021) How Phagocytes Acquired the Capability of Hunting and Removing Pathogens From a Human Body: Lessons Learned From Chemotaxis and Phagocytosis of Dictyostelium discoideum (Review). Front. Cell Dev. Biol. 9:724940. doi: 10.3389/fcell.2021.724940

How phagocytes find invading microorganisms and eliminate pathogenic ones from human bodies is a fundamental question in the study of infectious diseases. About 2.5 billion years ago, eukaryotic unicellular organisms–protozoans–appeared and started to interact with various bacteria. Less than 1 billion years ago, multicellular animals–metazoans–appeared and acquired the ability to distinguish self from non-self and to remove harmful organisms from their bodies. Since then, animals have developed innate immunity in which specialized white-blood cells phagocytes- patrol the body to kill pathogenic bacteria. The social amoebae *Dictyostelium discoideum* are prototypical phagocytes that chase various bacteria via chemotaxis and consume them as food via phagocytosis. Studies of this genetically amendable organism have revealed evolutionarily conserved mechanisms underlying chemotaxis and phagocytosis and shed light on studies of phagocytes in mammals. In this review, we briefly summarize important studies that contribute to our current understanding of how phagocytes effectively find and kill pathogens via chemotaxis and phagocytosis.

Keywords: chemotaxis, phagocytosis, innate immunity, *D. discoideum*, phagocyte

INTRODUCTION

How eukaryotic cells interact with bacteria and viruses is a fundamental question in biology. Eukaryotic cells and their interactions with other life forms began when single-cell organisms such as protozoa appeared about 2.5 billion years ago. Since then, multicellular organisms with increasingly complex genomes have developed innate immune systems in which specialized phagocytic cells, such as neutrophils and macrophages in humans, patrol the body to detect, recognize and eliminate invading pathogens. Specialized eukaryotic cells that can recognize foreign objects by migrating toward them and engulfing them were discovered by Elie Metchnikoff in 1882 (Beck and Habicht, 1996). One day, he pierced the larva of a starfish with a rose thorn.

When he examined the transparent larva the next day, he saw many cells covering the thorn and trying to engulf it. He imagined that these cells migrated from afar toward foreign invaders, a cellular process known as chemotaxis, and attempted to engulf the invaders, a cellular process known as phagocytosis. Both processes were also described in some specialized cells by others at the time. Engelmann T. W. (1881) and Pfeffer W. F. (1884) described chemotaxis of bacteria (Mc, 1946; Drews, 2005), and Leber T. (1888) discovered that leukocytes migrated in straight paths to sites of rabbit corneal irritation (Mc, 1946). Those observations gave rise to the hypothesis that diffusible substances guide the migration (chemotaxis) of those cells. Many reports of phagocytosis described the uptake of microorganisms, red cells, or various particles by cells in different animal systems. For example, Hayem (1870) and Klebs (1872) observed bacteria in white blood cells; Waldeyer (1876) found bacteria in peritoneal pus cells, Koch (1876) found anthrax bacilli in spleen and lymph node cells, and Osler (1875) reported that human alveolar cells engulfed coal dust particles (Ambrose, 2006). Metchnikoff proposed that recognizing foreign substances and engulfing them represents a fundamental mechanism by which organisms in the animal kingdom defend themselves against infections. Therefore, he created the discipline of cellular immunology, which is now called innate immunity.

It was generally believed that human phagocytes use at least two different types of receptors for defense against bacteria pathogens: one for detecting and chasing pathogens via chemotaxis and another for recognizing and engulfing them via phagocytosis. Detection and chasing are facilitated by chemoattractant G-protein-coupled-receptors (GPCRs) (Jin et al., 2008; Metzemaekers et al., 2020), whereas recognition and engulfing employ pattern-recognition receptors (PRRs), such as Toll-like receptors (TLRs), scavenger receptors, and C-type lectin receptors, as well as phagocytic receptors that include complement receptors and Fcγ receptors (Flannagan et al., 2012; Amarante-Mendes et al., 2018).

The social amoebae *Dictyostelium discoideum* inhabit soil and feed on diverse bacterial species, including gram-positive and gram-negative bacteria (Vogel et al., 1980; Gerisch, 1982; Devreotes and Zigmond, 1988; Soldati and Cardenal-Munoz, 2019). The amoebae locate bacteria by detecting metabolites, such as folic acid; move toward the bacteria via chemotaxis; then engulf the bacteria by recognizing their surface molecules and consume them through phagocytosis. Over the years, many molecular components involved in eukaryotic chemotaxis and phagocytosis have been discovered. Studies in *D. discoideum* have helped us to uncover molecular components and pathways and to develop new techniques. Importantly, molecular mechanisms are evolutionarily conserved allowing us to apply knowledge gained from the model organism to the study of chemotaxis and phagocytosis in human phagocytes. In this review, we will summarize landmark discoveries in phagocytic cells that shape our knowledge of innate immunity and highlight important studies in *D. discoideum* that provide novel insights to our current understanding of chemotaxis and phagocytosis.

CHEMOATTRACTANTS AND CHEMOKINES

The idea that eukaryotic cells can migrate in a gradient of diffusible substances and move toward their sources took root before 1900 (Mc, 1946). In 1882, Metchnikoff first noted that cells migrated from afar and covered a rose thorn inserted into the larva of a starfish (Beck and Habicht, 1996), and Leber (1888) discovered that leukocytes migrated in straight paths to sites of rabbit corneal irritation (Mc, 1946). Those observations gave rise to the hypothesis that diffusible substances generated by a foreign object or at the site of injury establish chemical gradients that guide cell migration.

It had been known for many years that some motile cells, including mammalian leukocytes and metazoan cells, move toward the sources of diffusible chemicals, but the chemical nature of the substances was not known and could be not be properly analyzed because experimental techniques did not yet exist. In 1962, Boyden reported a technique, now known as the Boyden chamber assay, to test for chemotactic activity of diffusible substances (Boyden, 1962). The first chemoattractant to be reported for eukaryotic cells was 3′5′-cyclic adenosine monophosphate (cAMP) for *Dictyostelium discoideum* (**Table 1**). In 1947, Bonner reported that the eukaryotic social amoebae, *D. discoideum*, migrate robustly toward the source of diffusible chemicals (Bonner, 1947). In 1969, it was discovered that cAMP is a chemoattractant for the social amoeba (Konijn et al., 1969). A couple of years later, the Bonner group found that the folic acid released from bacteria serves as another chemotactic substance used by *D. discoideum* cells to hunt their bacterial food (Pan et al., 1972). A chemotactic factor for leukocytes was found in the complement system of serum in 1968, later known as C5a (Snyderman et al., 1968). In 1975, N-formyl peptides, which are released from bacteria, were identified as chemoattractants for leukocytes (Schiffmann et al., 1975). By the early 1980s, the "classical" chemoattractants, including N-formyl peptides, C5a, and the lipid mediator leukotriene B4 (LTB4) (Borgeat et al., 1976; Fernandez et al., 1978), had been identified, and the cytokine-like-chemoattractants, chemokines, would be discovered in the coming years.

TABLE 1 | Chemoattractants, chemokines, and their receptors are listed in the table.

Chemoattractants	Receptors	Organisms
cAMP	cAR1-cAR4	*D. discoideum*
Folate	fARl	*D. discoideum*
C5a	C5aR	Human
N-formyl peptides (fMLP)	FPRl and FPR2	Human
LTB4	BLTl and BLT2	Human
CXCL8 (IL-8)	CXCRl and CXCR2	Human
CCL2 (MCP-1)	CCR2	Human
CXCL10 (IP-10)	CXCR3A and CXCR3B	Human
CCL3L1 (LD78)	CCRl, CCR3, and CCRS	Human
CCL1 (I-309)	CCR8	Human

The chemokine field started with the cloning of the human gene encoding IL-8, also known as CXCL8 (Baggiolini, 2015). Several groups independently cloned the human gene encoding CXCL8 (Walz et al., 1987; Yoshimura et al., 1987). The amino acid sequences of CXCL8 and monocyte chemoattractant protein-1 (MCP-1, also known as CCL2) contained either CXC or CC, which led to the identification of the protein family of chemokines with at least two CXC or CC subgroups (Matsushima et al., 1989; Yoshimura et al., 1989). Interestingly, chemokine-like proteins, such as IP-10 (CXCL10) (Luster et al., 1985), LD78 (CCL3L1) (Obaru et al., 1986), and the mouse ortholog of human I-309 (CCL1) (Miller et al., 1989), had been identified several years before CXCL8. However, their chemoattractant activity remained unclear until the discovery of CXCL8.

By the early 1990s, the new field of chemokines took off. Today, we can easily identify genes encoding typical chemokines in genome sequences due to their size (about 70–90 amino acids) and conserved N-terminal, cysteine motifs (Murphy et al., 2000). Based on the number and spacing of cysteines in these motifs, chemokines have been classified into C, CC, CXC, and CX3C subfamilies. There are more than fifty chemokines that are produced by leukocytes and tissue cells. Some chemokines are involved in normal housekeeping functions, such as the maturation of leukocytes in the bone marrow, the trafficking and homing of lymphocytes, and the regeneration of circulating leukocytes, while others orchestrate inflammatory responses for the recruitment of immune cells to the inflamed regions. Interestingly, some chemokines have been shown to also play significant roles in cancer metastasis (Jin et al., 2008; Li et al., 2013).

CHEMOATTRACTANT- AND CHEMOKINE-RECEPTORS

The molecular identities of chemoattractant receptors for eukaryotic cells began to be revealed in the late 1980s when DNA cloning techniques became widely available for laboratories. The first breakthrough was the discovery of a cAMP chemoattractant receptor cAR1 in *D. discoideum* and the realization that it belongs to the family of G protein-coupled receptors (GPCRs) (**Table 1**), which contains seven transmembrane domains and (Klein et al., 1988). A couple of years later, the receptors for classical chemoattractants, such as fMLP and C5a, had been cloned and were found to be GPCRs (Boulay et al., 1990; Gerard and Gerard, 1991). Before the identification of the IL-8 (CXCL8) receptor, evidence suggested that the putative receptor would be a GPCR since activation of neutrophils by IL-8 (CXCL8) was shown to be inhibited by pertussis toxin, a drug blocking GPCR/Gi signaling. However, single transmembrane tyrosine kinase receptors, such as the receptor for platelet-derived growth factor (Williams, 1989), can mediate chemotaxis, therefore it was speculated that tyrosine kinase receptors could also detect other protein-ligands, such as chemokines, at the time.

In 1991, two back-to-back papers reported the discoveries of two GPCRs as IL-8 receptors (Holmes et al., 1991; Murphy and Tiffany, 1991). The two receptors are similar but not identical, sharing 77% amino acid identity. Each of them triggered transient Ca^{2+} responses upon IL-8 stimulation and had a high affinity for IL-8 (Kd = 2 nM). They were named IL-8RA and IL-8RB at the time and are now known as CXCR1 and CXCR2. Currently, about twenty chemokine GPCRs mediate signal events induced by more than 50 chemokines (Murphy et al., 2000). Interestingly, chemokines and their receptors, unlike other types of GPCRs, have overlapping specificities for each other, and many chemokine-receptor-mediated signals appear to be redundant. It became a paradigm that phagocytes use GPCRs to detect diffusible chemicals (both classical chemoattractants and chemokines) and to mediate signaling pathways that control the reorganization of the actin cytoskeleton for cell migration toward the sites of infection and pathogens via chemotaxis. Once reaching the pathogens, these phagocytes employ pattern-recognition receptors (PRRs) to recognize surface molecules of the pathogens and to mediate signaling pathways that regulate the reorganization of the actin cytoskeleton for the engulfment of particles via phagocytosis (Greenberg, 1995; Flannagan et al., 2012; Kaufmann and Dorhoi, 2016).

PHAGOCYTOSIS AND OPSONIC- AND NON-OPSONIC RECEPTORS

Phagocytosis was observed by Oster in 1875 and others, and later was studied and named by Metchnikoff in 1883 (Ambrose, 2006). Phagocytosis is a process of sensing and engulfing particles larger than 0.5 μm. The particle is internalized into an organelle, called a phagosome. The phagosome fuses with lysosomes to become a phagolysosome, which contains enzymes that can degrade the particle (Flannagan et al., 2012; Kaufmann and Dorhoi, 2016). Phagocytosis is a basic process for obtaining nutrition in unicellular organisms, such as free-living amoebae of *D. discoideum* (Dunn et al., 2017; King and Kay, 2019), and for the elimination of foreign microorganisms in multicellular organisms by a group of cells, such as neutrophils and macrophages in mammals.

Detection of the target particles is the first step of phagocytosis. In 1903, Wright and Douglas discovered that the uptake of staphylococci by human leukocytes is enhanced by serum (Wright et al., 1989). They concluded that blood fluids have an opsonic power that modifies bacteria to be ingested by the leukocytes. The idea that phagocytosis begins with pathogenic bacteria being labeled with opsonins–host-derived proteins that bind specific receptors on phagocytes–was widely accepted. Nowadays it is well known that the major opsonins promoting efficient phagocytosis by leukocytes are complement components and immunoglobulin G (IgG) antibodies (Uribe-Querol and Rosales, 2020). These opsonins and their receptors are the best studied.

Complement is a system of more than 30 proteins in the plasma and on the cell surface, and it constitutes more than 15 of the globular fractions of plasma (Dunkelberger and Song, 2010). The complement system comprises vital components of innate immunity and influences T- and B-cell biology and adaptive responses. A major role of complement in innate

immunity is providing complement opsonins, such as C4b, C3b, and C3bi, to decorate the surface of microorganisms, and phagocytes recognize these marked microorganisms via the complement receptors (CRs), including CR1, CR2, CR3, and CR4, and then eliminate them via phagocytosis (Walport, 2001a,b; Dunkelberger and Song, 2010). IgG antibodies are another family of opsonins that bind to the surface of pathogenic microorganisms, and on human cells, IgG receptors are Fcγ receptors, such as FcγRI, FcγRII, and FcγRIII (Uribe-Querol and Rosales, 2020). Fcγ receptors specifically bind to the Fc part of IgG molecules to form clusters on the surface of phagocytes, and these clusters then trigger phagocytosis and other cellular responses.

JanewayJr. (1989) proposed that innate immune cells must express receptors that recognize specific molecules on foreign microorganisms. Since then, receptors directly recognizing pathogen-associated-molecular-patterns (PAMPs) have been discovered, and these so-called pattern recognition receptors (PRRs) are proteins capable of binding to molecules associated with pathogens (Walsh et al., 2013; Amarante-Mendes et al., 2018). PRRs are found associated with different subcellular compartments, such as on cellular and endosomal membranes, in the cytosol, and the bloodstream as the secreted forms. Four main classes of PRRs are recognized, including the Toll-like receptors (TLRs), the nucleotide-binding oligomerization domain (NOD)-leucine-rich-repeats (LRRs)-containing receptors (NLRs), the retinoic acid-inducible gene 1 (RIG-1)-like receptors (RLRs), and the C-type lectin receptors (CLRs). Some of them, such as TLRs, can bind to PAMPs but cannot induce phagocytosis, while others, such as some CLRs (Dectin-1, Dectin-3, and DC-SIGN) can induce phagocytosis; the latter type is called non-opsonic receptors.

When a particle is recognized by either opsonic- or non-opsonic receptors, many signaling pathways in phagocytic cells are activated, resulting in reorganization of the actin cytoskeleton and the formation of a phagocytic cup around the particle for engulfment. Opsonic- and non-opsonic receptors, unlike chemoattractant GPCRs that have seven transmembrane domains, are single transmembrane proteins with extracellular ligand-binding domains and intracellular signaling domains (Greenberg, 1995; Greenberg and Grinstein, 2002; Flannagan et al., 2012). Activation of these receptors mediates phosphorylation of tyrosine residues on the intracellular domain that induces signaling events that lead to the rearrangement of the actin cytoskeleton for the engulfment of particles. It appeared that chemotaxis and phagocytosis are two distinct cellular processes that are sequentially connected by phagocytes during the fight against pathogens. Studies of *D. discoideum* suggest that chemotaxis and phagocytosis may be originated from one cellular process in ancient phagocytes.

CHEMOTAXIS OF *D. discoideum* AND LEUKOCYTES

Before 1900, it was known that leukocytes migrated in straight paths to inflamed sites of rabbit corneal irritation (Mc, 1946). Leukocytes are amoeboid cells, and their movement closely resembles that of the amoebae of *D. discoideum* (Devreotes and Zigmond, 1988). In the 1970s, Gerisch used time-lapse microscopy to directly observe the behaviors of *D. discoideum* cells in response to cAMP stimuli (Gerisch et al., 1975). In response to a uniform cAMP increase, the cells became elongated and polarized, with clear leading fronts and trailing ends, and their random motility increased, a behavior termed chemokinesis. When placed in a cAMP gradient, the cells instantly migrated toward the source of cAMP by extending pseudopods (leading fronts) followed by retraction of the trailing ends (Gerisch et al., 1975; Gerisch, 1982; Swanson and Taylor, 1982). Zigmond observed movements of individual leukocytes in response to chemical gradients using time-lapse microscopy (Zigmond, 1974, 1978). Together, the studies of *D. discoideum* and leukocytes showed that these amoeboid cells can initiate locomotion by extending pseudopods in the direction of a higher concentration of chemoattractant (Devreotes and Zigmond, 1988).

Based on the observations, two different models have been proposed to explain how cells measure gradients (Parent and Devreotes, 1999; Rappel et al., 2002). In the first model, a cell detects changes in chemical concentration over time only and adjusts its movement in the chemical gradient based on the change in concentration it detects as it moves (Berg, 1975). Bacteria employ this temporal mechanism of chemotaxis (Berg, 1975). In the second model, a cell simultaneously compares differences in chemoattractant concentration around its perimeter, detecting spatial changes (Parent and Devreotes, 1999). Using this spatial mechanism, a cell does not need to move before judging the direction of a gradient. Zigmond proposed that amoeboid cells, unlike bacteria, utilize a spatial sensing mechanism to detect a chemical gradient and to guide their movement (Zigmond, 1974). Since then, the model system *D. discoideum* has been used to raise fundamental questions in eukaryotic chemotaxis, propose hypotheses of gradient sensing, discover essential components involved in chemotaxis, and develop techniques to study chemotaxis.

A GPCR-MEDIATED SIGNALING NETWORK FOR EUKARYOTIC CHEMOTAXIS

The receptor for chemoattractant cAMP in *D. discoideum* was discovered as a GPCR in 1988 (Klein et al., 1988). In the ensuing years, receptors for fMLP, C5a, and IL-8 (CXCL8) in human leukocytes were also found to be members of the GPCR family (Boulay et al., 1990; Gerard and Gerard, 1991; Holmes et al., 1991; Murphy and Tiffany, 1991). These findings established the paradigm that chemoattractants of eukaryotic cells are detected by GPCRs. Many components involved in chemotaxis were discovered in *D. discoideum*, and their homologs were then found to play similar roles in the chemotaxis of leukocytes.

Over the years, pathways involved in the cAMP receptor (cAR1)-mediated cell migration have been identified in *D. discoideum* (**Figure 1**). The binding of cAMP to cAR1 induces

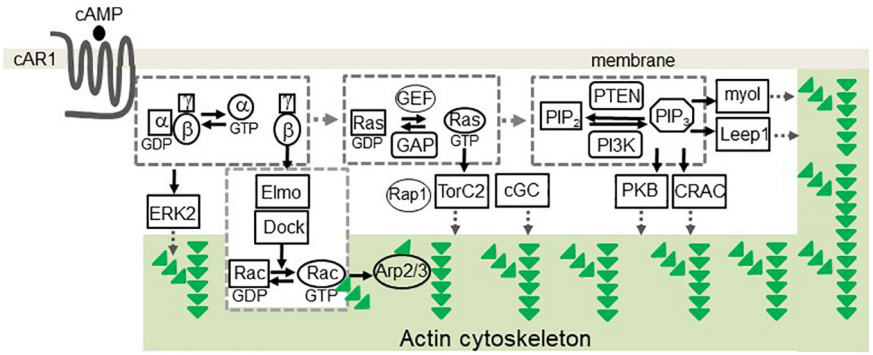

FIGURE 1 | cAR1-mediated signaling pathways involved in chemotaxis in *Dictyostelium discoideum*. The binding of cAMP to cAR1 triggered signaling events leading to the reorganization of the actin cytoskeleton. The events include the dissociation of heterotrimeric G protein into Gα and Gβγ subunits, the activation of Ras, PIP3 production. PIP3 recruits signaling components, including PKB, CRAC, myol, and Leep1, to transduce signals. Activation of heterotrimeric G-proteins activates Erk2 signaling to mediate chemotaxis and phagocytosis. Free Gβγs associate with the Elmo/Dock complex to activate Rac. Ras-GTP activates Rap1, TorC2 complex, and cGC. These signaling events regulate the actin cytoskeleton for cell migration. Green triangles represent G-actin molecules.

dissociation (activation) of heterotrimeric G proteins into Gα2 and Gβγ subunits (Firtel et al., 1989; Janetopoulos et al., 2001; Ueda et al., 2001), which, in turn, activate downstream signaling components to control the reorganization of the actin cytoskeleton for chemotaxis (Gerisch et al., 1993). Free Gβγ subunits activate small G protein Ras proteins (Sasaki et al., 2004; Charest et al., 2010; Kortholt et al., 2011; van Haastert et al., 2017), which activate PI3K to convert PIP_2 to PIP_3 (Sasaki et al., 2004). Activation of cAR1 also induces a transient membrane dissociation of PTEN and then a reassociation of PTEN to the trailing back of the cell (Funamoto et al., 2002; Iijima and Devreotes, 2002). PTEN dephosphorylates PIP_3 and converts it to PIP_2, and local PIP_3 levels on the membrane provide an intracellular cue to recruit proteins containing pleckstrin homology (PH) domains from the cytosol to the membrane (Funamoto et al., 2002; Iijima and Devreotes, 2002; Matsuoka and Ueda, 2018). The recruited proteins include cytosolic regulator of adenylyl cyclase (CRAC) (Insall et al., 1994; Parent et al., 1998), Akt/PKB (Meili et al., 1999), myosin I (Chen et al., 2012), and Leep1 (Yang et al., 2021), each of which plays a role in regulating the reorganization of the actin cytoskeleton. It is still not clear how CRAC and Akt/PKB binding to PIP_3 regulate the actin cytoskeleton. PIP_3 binding proteins of myosin I, an actin-based motor protein, and Leep1 promote actin polymerization at the leading front of a migrating cell. Three myosin-I proteins, myosin ID, IE, and IF, bind to PIP_3 and therefore are recruited to the leading edge of a cell to promote actin-polymerization for chemotaxis (Chen et al., 2012). Recently, it was found that Leep1 interacts with PIP_3 and the Scar/WAVE complex to control the actin cytoskeleton at the leading edge of a migrating cell (Yang et al., 2021). In addition, several PIP_3-independent pathways have been implicated in the chemotaxis of *D. discoideum*. One pathway is that the activation of G proteins mediates cGMP signaling that controls myosin phosphorylation and chemotaxis (Bosgraaf and Van Haastert, 2002; Kortholt et al., 2011). The second one is a GPCR-mediated mTORC2 and AKT signaling (Charest et al., 2010). Upon the activation of cAR1, the small G-protein Ras is activated and becomes Ras-GTP, and the small G-protein RacE is phosphorylated by GSK3. Ras-GTP, RacE-P, and mTORC2 form a signaling complex to promote AKT phosphorylation, which regulates cell migration (Senoo et al., 2019). In addition, activation of the small G-proteins RasC/G and Rap1 transduces signals to mTOR2 for chemotaxis (Khanna et al., 2016; Tariqul Islam et al., 2019). The fourth pathway is that the free Gβγ subunit associates with an ELMO/Dock complex to activate Rac leading to actin polymerization for cell migration (Yan et al., 2012). Finally, activation of cAR1 induces the phosphorylation of Erk2 that mediates signaling for both chemotaxis and phagocytosis (Hadwiger and Nguyen, 2011; Schwebs et al., 2018; Nichols et al., 2019; Tariqul Islam et al., 2019).

Chemoattractant GPCR-mediated signaling mechanisms for the regulation of chemotaxis have also been studied in leukocytes. Many molecular mechanisms involved in GPCR-mediated chemotaxis are evolutionarily conserved in *D. discoideum* and mammalian cells. Activation of GPCRs by chemoattractants triggers dissociation (activation) of heterotrimeric Gi proteins into Gαi and Gβγ subunits (Neptune and Bourne, 1997), which control several signaling pathways. Activation of Gi-proteins produces free Gβγ that activates PI3Ks to generate PIP_3, regulates mTORC2, and produces active forms of small G-proteins (Servant et al., 2000; Suire et al., 2006; Liu et al., 2010), including Ras and Rac, to regulate the reorganization of the actin cytoskeleton. Leukocytes express several PIP_3 phosphatases, such as PTEN and SHIP, that are involved in the regulation of chemotaxis (Nishio et al., 2007; Heit et al., 2008). In addition, a pathway consisting of CXCR4/Gi, ELMO1/Dock180, and Rac appears to play a role in CXCL12-mediated chemotaxis and metastasis of breast cancer cells (Li et al., 2013). Another GPCR-mediated pathway of PLC, PKC, and PKD is involved in the regulation of chemotaxis of neutrophils (Xu et al., 2015).

Chemotaxing cells, including *D. discoideum* and neutrophils, are morphologically polarized with leading pseudopods and trailing ends (Devreotes and Zigmond, 1988). Many components

involved in chemotaxis are asymmetrically distributed in these polarized amoebae (Parent and Weiner, 2013). Eukaryotic chemotaxis is a complicated cell behavior that conceptually consists of three interconnected cellular processes: gradient sensing, cell polarization, and cell motility. Advances in fluorescence microscopy have allowed us to visualize subcellular localization of cAR1 and other signaling components in live *D. discoideum* cells since the 1990s. These studies shed new light on the question of how eukaryotic cells generate directional biochemical responses in response to a chemical gradient.

GRADIENT SENSING

Over the years, researchers have proposed different models, which involve either a temporal-sensing or a spatial-sensing mechanism (Zigmond, 1974; Parent and Devreotes, 1999; Rappel et al., 2002), to explain how eukaryotic cells detect and respond to chemical gradients. Many concepts have been developed and tested in the studies of *D. discoideum* chemotaxis. For example, one early hypothesis was that the accumulation of chemokine receptors at the front of a cell is essential for chemotaxis (Nieto et al., 1997). In 1997, cAR1 receptors were shown to be uniformly distributed on the membrane of chemotaxing *D. discoideum* cells (Xiao et al., 1997), and later, chemokine receptors were found to be the same on the surface of migrating neutrophils (Servant et al., 2000). In the ensuing years, studies showed that the *D. discoideum* cells can detect cAMP gradients to generate polarized responses even when cAR1 and its G-proteins are uninformedly distributed on the membrane (Parent et al., 1998; Jin et al., 2000). With the development of live-cell fluorescence microscopy, the spatiotemporal dynamics of key signaling events could be visualized (Gerisch and Muller-Taubenberger, 2003; Miyanaga et al., 2018). One breakthrough was the discovery that the chemoattractant sensing machinery works in cells without polarity and mobility (Parent et al., 1998). Specifically, *D. discoideum cells* become non-polar and immobile upon treatment with latrunculin, an inhibitor of actin polymerization. In latrunculin-treated cells, cAR1 and G proteins are uniformly distributed around the cell surface and PHcrac-GFP, a fluorescent probe for PIP_3, is uniformly distributed in the cytosol (Parent et al., 1998; Jin et al., 2000; Matsuoka et al., 2006). When suddenly exposed to a cAMP gradient, a cell responds by initially inducing a transient PIP_3 increase followed by a decrease around the membrane (a temporal adaptation) and producing a highly polarized distribution of PIP_3 (a spatial amplification) in less than 2 min (Xu et al., 2005). During the application process, the membrane-bound PTENs gradually translocate from the front to the back (Iijima and Devreotes, 2002; Xu et al., 2007). The cAR1/G protein-controlled PIP_3 responses display the key features of a spatial mechanism of gradient sensing. To truly understand gradient sensing mechanisms in chemotaxis, it is necessary to identify all regulatory components and to connect molecular mechanisms in a signaling network with a complexity that reflects that of chemotactic cells.

Over the last 20 years, many models have been proposed to explain GPCR-mediated gradient sensing and chemotaxis of eukaryotic cells (Parent and Devreotes, 1999; Postma and Van Haastert, 2001; Rappel et al., 2002; Van Haastert and Devreotes, 2004; Levine et al., 2006; Meier-Schellersheim et al., 2006; Iglesias and Devreotes, 2012; Takeda et al., 2012; Nakajima et al., 2014; Cheng and Othmer, 2016; Li et al., 2020). Most models were constructed by writing mathematical equations "by hand," which is defining each reaction for molecule complex formation, association/de-association, or enzymatic transformation separately, and the tasks are time-consuming and very difficult due to a large number of reaction equations. It is almost impossible for experimental biologists to complete the tasks by themselves. The computer software packages have been developed and improved to allow researchers to construct signaling networks and to run simulations without dealing with mathematical equations. We hope that the software will be widely used by biologists to develop and analyze computational models that parallel live-cell experiments without writing reaction equations themselves, so more researchers can construct, examine, and validate their models. Future studies are needed to identify missing links and to understand how these components interact in a signaling network in time and space in a cell to achieve gradient sensing and chemotaxis.

SIGNAL RELAY AND SELF-GENERATED GRADIENTS

How eukaryotic cells migrate over long distances toward the source of chemoattractants is an interesting question. Eukaryotic cells guide their movement by spatially detecting chemical gradients. Because diffusible gradients diminish quickly over a distance, eukaryotic cells have developed systems to generate signals and move collectively as a group of cells. This process has been studied in *D. discoideum*. *D. discoideum* amoebae ingest bacteria as food in the soil. When food is depleted, *D. discoideum* cells stop dividing and enter a developmental process during which individual cells aggregate and form multi-cellular structures (Devreotes, 1994). Within a few hours following starvation, a few cells spontaneously secrete cAMP. cAMP acts as a chemoattractant binding to cAR1 that leads to the dissociation of the heterotrimeric G-protein into Gα2 and Gβγ and the activation of the adenylyl cyclase A(ACA) that converts ATP into cAMP, most of which is secreted to relay chemotactic signals to neighboring cells. These cells respond to cAMP stimuli by moving toward the center (chemotaxis) and secreting additional cAMP (signal relay). The net result is that cAMP waves spread outward through a population of 10^6 cells as the cells moving toward the center. The cells migrate collectively toward secreted cAMPs in a head-to-tail fashion (streaming) and form an aggregation territory of about 0.5–1 cm in radius. It was found that ACA is not required for chemotaxis of individual cells, but ACA, specifically its asymmetric localization, is essential for cells to align head-to-tail in a stream and to migrate together as a group into aggregates (Kriebel et al., 2003).

A molecular system to relay chemotactic signals was discovered in neutrophils. Neutrophils are recruited to the site of an infection by primary chemoattractants, such as fMLP and

C5a (Kolaczkowska and Kubes, 2013). After reaching the site, neutrophils respond to primary chemoattractants to produce and secrete secondary chemoattractants and recruit additional leukocytes to fight infection. A study showed that in response to an fMLP gradient, some neutrophils become polarized and migrate directionally, and they also release the secondary chemoattractant LTB4 (Afonso et al., 2012). All neutrophils, including those that have not yet responded to fMLP, respond to LTB4 and migrate toward the source of fMLP, indicating that LTB4 acts as a signal-relay molecule for neutrophils migrating collectively toward infection sites (Afonso et al., 2012; Lammermann et al., 2013). Interestingly, a recent study reported that *D. discoideum* cells can create chemoattractant gradients by degrading cAMP molecules and can achieve long-range chemotaxis by following these self-generated gradients (Tweedy et al., 2020). Mammalian cells may have systems to degrade attractants and make gradients for long-range migration toward the target sites.

SIGNALING EVENTS IN PHAGOCYTOSIS

Once they reach the infection sites, leukocytes catch and eliminate pathogenic bacteria via phagocytosis. Phagocytosis consists of several phases. (1) *Detection of the particles to be ingested*. Phagocytic receptors recognize specific molecules on the surface of bacteria. (2) *Activation of internalization*. Ligands binding to the receptors induce the reorganization of the actin cytoskeleton, which mediates the formation of a phagocytic cup to engulf the bacteria. (3) *Formation of the phagosome, a specialized vacuole*. The membrane protrusions of a phagocytic cup cover the particle and fuse at the distal ends creating a new vacuole containing the engulfed particle that then separates from the plasma membrane. (4) *Maturation of the phagosome into a phagolysosome*. The new phagosomes fuse with early endosomes and late endosomes that have accumulated V-ATPase and lysosomal-associated proteins on the membrane and luminal proteases; and then fuse with lysosomes to become phagolysosomes, where the ingested bacteria are degraded (Amulic et al., 2012; Flannagan et al., 2012; Buckley et al., 2019). This review will focus mostly on phases 1 and 2, which share similarities with chemotaxis, and will not cover phases 3 and 4 and instead recommend two excellent reviews (Boulais et al., 2010; Dunn et al., 2017).

Phagocytosis begins when a particle interacts with phagocytic receptors. The activation of these receptors initiates intracellular signaling pathways that lead to the reorganization of the actin cytoskeleton, the extension of pseudopods, and the engulfment of the particles. In leukocytes, phagocytic receptor-mediated signaling events include activation of tyrosine kinases and PI3K that regulate the actin cytoskeleton (Greenberg, 1995; Underhill and Ozinsky, 2002; Uribe-Querol and Rosales, 2020). For Fcγ receptors, the initial intracellular signaling event is phosphorylation of tyrosine residuals of the receptors and association of the receptors containing immunoreceptor tyrosine-based activating motifs (ITAMs) with members of the Src family. The phosphorylated receptors and ITAMs serve as docking sites for tyrosine kinases, such as Syk, to activate downstream components leading to the reorganization of actin cytoskeleton for the engulfment of the particles. Activation of the Fcγ receptor also promotes PI3K activities that contribute to the engulfment. As mentioned earlier, PI3Ks may regulate actin cytoskeleton for pseudopod extensions for both cell migration and particle ingestion. For a long time, it was generally thought that phagocytes use GPCRs to detect soluble chemoattractants derived from infection sites and to migrate toward bacteria, and then switch to phagocytic receptors to bind the bacteria for phagocytosis. The social amoebae *D. discoideum*, which detect folic acid released from bacteria and pursue them via chemotaxis and consume them through phagocytosis, have a simpler solution.

Dictyostelium discoideum cells do not encode orthologs of any known phagocytic receptors (non-opsonic- or opsonic-receptors) or tyrosine kinases (Goldberg et al., 2006), yet they are highly evolved as professional phagocytes (Dunn et al., 2017; King and Kay, 2019). In the 1990s, one study showed that a heterotrimeric G protein β subunit is required for both chemotaxis and phagocytosis (Peracino et al., 1998). Two other studies reported that either diffusible cAMPs or one yeast particle induced the accumulation of coronin, an actin-associated protein, in a leading pseudopod for either cell migration or the formation of a phagocytic cup to engulf the yeast (Gerisch et al., 1995; Maniak et al., 1995). These studies suggested heterotrimeric G-proteins are involved in signal transduction for the reorganization of actin cytoskeleton for both chemotaxis and phagocytosis. More than two decades later, it was discovered that *D. discoideum* cells utilize a GPCR (fAR1) linking to heterotrimeric G proteins to detect both diffusible folic acids released from bacteria and lipopolysaccharide (LPS) on the surface of the bacteria (Pan et al., 2016, 2018). Thus, this simple organism uses one GPCR/G protein machinery to regulate a signaling network for both "chemoattractant-mediated cell migration" to chase bacteria and "microbe-associated molecular pattern (MAMP)-mediated engulfment" to ingest bacteria. Interestingly, recent studies have suggested that neutrophils can utilize the chemoattractant GPCR/Gi signaling to mediate (Dunn et al., 2017) not only cell migration but also particle ingestion to fight against invading bacteria, indicating that mammalian phagocytes retain this mechanism to chase and interact with bacteria through the evolution (WoodJr., Smith and Watson, 1946; Osei-Owusu et al., 2019; Wen et al., 2019).

A CLASS C GPCR IS A NEW MEMBERS OF PATTERN RECOGNITION RECEPTORS

Dictyostelium discoideum amoebae utilize fAR1 and cognate G-proteins to detect folate for chasing bacteria and the immobile LPS on the bacterial surface for engulfing them (**Figure 2**). fAR1 contains a Venus-Flytrap (VFT) extracellular domain and belongs to the class C GPCR family (Pan et al., 2018). More than 800 human GPCRs have been identified so far and are classified into five main families: class A, which includes chemokine

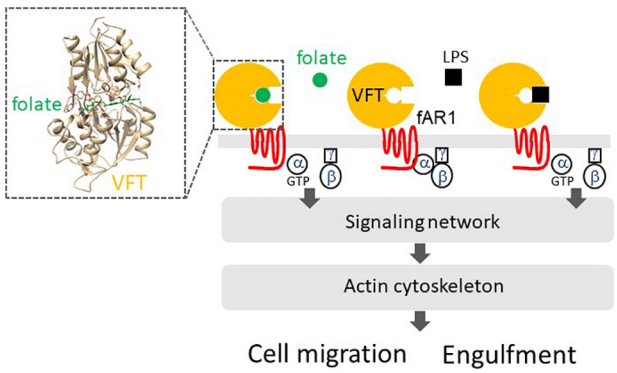

FIGURE 2 | fAR1 binds to folate or LPS to activate heterotrimeric G-proteins that mediate a signaling network, which regulates the actin cytoskeleton for cell migration or particle engulfment. fAR1 contains a Venus-flytrap domain (VFT) for ligand binding. On the right box, Structural modeling and computational docking predict the extracellular domain of fAR1 folding into a VFT structure as the binding site for folate (green).

receptors, class B1, class B2, class C, and class F (Fredriksson et al., 2003; Foord et al., 2005). Based on phylogenetic sequence analysis and structure similarity, cAMP receptors (cAR1-cAR4) in *D. discoideum* constitute their own class (SaxeIII, Johnson et al., 1991; Ginsburg et al., 1995; Moran et al., 2016), while fAR1 is a member of the class C family.

Class C GPCRs have a common structure consisting of an N-terminal extracellular Venus-flytrap (VFT) domain for ligand recognition and binding (Cao et al., 2009). VFT architecture is a typical structure of bacterial periplasmic binding proteins (PBPs) that sense small molecules and transport them into the cytoplasm (Borrok et al., 2009). A PBP consists of two globular domains connected by a small hinge region and exists in an open form in the absence of a ligand. The binding of a ligand induces a dramatic conformational change from an open to a close form, in which the ligand is clamped between the two lobes just like the carnivorous plant Venus-flytrap closing itself when a bug moving into the trap (Borrok et al., 2009). The class C GPCRs in humans are mainly composed of metabotropic glutamate receptors (mGluRs), gamma aminobutyric acid type B receptors ($GABA_BRs$), Ca^{2+}-sensing receptors (CaSRs), taste receptors (T1Rs), pheromone receptors, and olfactory receptors (Cao et al., 2009). *D. discoideum* genome encodes 14 class C GPCRs, including fAR1 (Prabhu and Eichinger, 2006; Fey et al., 2013). The VFT domains of class C GPCRs in *D. discoideum* are closers to bacterial PBPs than those of human class C GPCRs (Cao et al., 2009). Interestingly, a bacterial PBP binds multiple ligands, while most human class C GPCRs expressed in the central nerve system bind only one natural ligand (Cao et al., 2009). However, the VFT in fAR1 retains the ability to recognize different molecules: folate released by bacteria and the sugar part of LPS (**Figure 2**), which is a major microbe-associated-molecular-pattern (MAMP) on the gram-negative bacteria (Pan et al., 2018). It appears is that the fusion of a PBP and an ancestral rhodopsin-like receptor (a class A GPCR) formed the common ancestor of the class C GPCRs, and fAR1 represents a prototype of class C GPCRs and is a new member of PRRs. Future studies will reveal the receptors of *D. discoideum* that recognize gram-positive bacteria and commune them as food.

HUMAN LEUKOCYTES ACQUIRED FEATURES FOR FIGHTING FOREIGN PATHOGENS

Chemotaxis and phagocytosis can be observed in amoeboid cells from many eukaryotic organisms, including *D. discoideum*, *Caenorhabditis elegans*, fruit fly, sea urchin, zebrafish, frog, chicken, mouse, and human. Some molecular components involved in these two processes are found in the early life forms, such as protozoans that go back about 2.5 billion years. Other components are unique to higher vertebrates but bear similarities to those of invertebrates (**Figure 3**). Collectively, these links represent compelling evidence that human leukocytes evolved from ancient life forms and acquired new features over a billion years.

The major components involved in GPCR-mediated chemotaxis are evolutionarily conserved from *D. discoideum* to human cells. Earlier we have briefly mentioned the molecular components involved in a GPCR-mediated signaling network of eukaryotic chemotaxis. We know that the molecular components of the actin cytoskeleton and their regulators are evolutionarily conserved from amoebae of simple organisms to human leukocytes. We will not review these components and regulators of the actin cytoskeleton and instead recommend several outstanding reviews (Pollard and Borisy, 2003; Insall and Machesky, 2009; Devreotes and Horwitz, 2015).

Dictyostelium discoideum phagocytosis is not very different from humans (Dunn et al., 2017; King and Kay, 2019). After binding to a particle, amoebae of *D. discoideum* perform the internalization, formation of the phagosome, and maturation of the phagosome into phagolysosome. The *D. discoideum* genome encodes evolutionarily conserved components required for these processes, including particle internalization, phagosome formation, and maturation. For example, the *D. discoideum* genome encodes catalytic NOX (NADPH oxidase) subunits, which are homologs of NOX2 in humans. NOX2 generates superoxide by transferring an electron from cytosolic NADPH to O_2 in the lumen of the phagosome. Reactions convert superoxide into reactive oxygen species (ROS), which contribute to the killing of internalized bacteria. *D. discoideum* and mammalian phagocytes use conserved strategies to kill bacteria. They both have V-ATPase for phagosome acidification. In addition, their phagosome acquires a series of proteases, hydrolases, and lysozymes to break down bacterial components. Interestingly, *D. discoideum* has a primitive innate immune system. In the multicellular slug stage, specialized phagocytic cells, sentinel (S) cells, circulate within the slug to trap, engulf, and kill bacteria. Recent studies revealed that S cells use Toll/interleukin-1 receptor (TIR) domain protein, TirA, to recognize bacteria, produce extracellular traps (ETs) and reactive oxygen species to

	D. discoideum	*C. elegans*	Fruit fly	Sea urchin	Zebrafish	Frog	Chicken	Mouse	Human
Phagocytes	Yes	Yes	Yes	Yes	Yes	Yes	Yes	Yes	Yes
GPCR/G-protein	Yes	Yes	Yes	Yes	Yes	Yes	Yes	Yes	Yes
NADPH Oxidase	Yes	Yes	Yes	Yes	Yes	Yes	Yes	Yes	Yes
Tyrosine Kinase Receptors	No	Yes	Yes	Yes	Yes	Yes	Yes	Yes	Yes
Complements	No	No	No/Yes	Yes	Yes	Yes	Yes	Yes	Yes
Adaptive Immunity	No	No	No	No	Yes	Yes	Yes	Yes	Yes

FIGURE 3 | Summary of various phagocytosis components that have been acquired by phagocytes from simple organisms to humans.

kill bacteria in the slug of *D. discoideum* (Chen et al., 2007; Zhang et al., 2016).

Several features found in leukocytes for pathogen recognition are missing from the primitive phagocytes of *D. discoideum*. The *D. discoideum* genome does not encode complements, IgGs, or phagocytic receptors, such as tyrosine kinases/tyrosine kinase receptors (Goldberg et al., 2006; Cosson and Soldati, 2008). *D. discoideum* amoebae utilize a GPCR/G-protein machinery and signaling pathways for recognizing both the chemoattractant folic acid and a phagocytic cue LPS for chasing and ingesting *Klebsiella aerogenes* (Pan et al., 2016, 2018). Recent reports suggested that *D. discoideum* encodes lectins and the scavenger receptor, LmpB (Dinh et al., 2018; Sattler et al., 2018), but it is not clear how (or whether) they form a functional signaling pathway to mediate phagocytosis. *Caenorhabditis elegans* does not encode complements or adaptive immune system but expresses tyrosine kinases that have the potential to associate with scavenger receptors for phagocytosis (Stuart and Ezekowitz, 2008). Animals ranging from sea urchins to humans have a version of the complement system, and vertebrates from fish to humans have both a complement system and adaptive immunity. Since phagocytes from all organisms have chemoattractant GPCR/G-protein machinery, we propose that the GPCR-mediated signaling network is an ancient system for regulating the actin cytoskeleton for both chemotaxis and the engulfment of particles during phagocytosis. The molecular machinery required for phagosome formation and maturation also existed in ancient phagocytes. Although having the ability to distinguish of self from non-self, the simpler machinery of an ancient phagocyte might not work sufficiently when multicellular organisms encounter more complicated situations. New features were acquired by phagocytes of multicellular organisms to fight against various foreign microorganisms during the evolution. A receptor system that links to tyrosine kinases was added in *C. elegans*, a complement system was added in sea urchins and retained in animals with a fluid-filled body cavity or a circulatory system, and adaptive immunity was then acquired by vertebrates as the latest feature. Human phagocytes have evolved by retaining early features and acquiring new ones that have gradually increased the complexity of their machinery and enhanced their ability to fight foreign pathogens in different situations.

PATHOGENS HIJACK RECEPTORS ON IMMUNE CELLS

Throughout their long co-evolution with their eukaryotic hosts, infectious pathogens, such as bacteria and viruses, have developed strategies for evading and (or) invading the immune system (Alcami, 2003). For example, *Yersinia pestis*, the bacterial agent of plague, selectively kills immune cells, enabling its multiplication and systemic spread (Osei-Owusu et al., 2019). The plague receptor on human immune cells is FPR1, a chemoattractant GPCR of N-formyl peptides released from the bacteria. Once it has attracted immune cells, *Y. pestis* uses its cap protein in the type III secretion system (T3SS) to bind FPR1 and then delivers effector proteins to the host immune cells. The injected effector proteins inhibit host cell signaling and activate apoptosis of these host cells.

Many viruses have also exploited chemokine receptor systems for their entry and replication in the host cells (Alcami, 2003; Lisco et al., 2007). For example, the binding of the HIV envelope proteins to CXCR4 or CCR5 triggers membrane fusion and signal transduction and promotes the entry of HIV into T cells or macrophages (Berger et al., 1999). A previous study showed that HIV-mediated CXCR4/Gi signaling activates cofilin, which regulates actin dynamics and is known to be involved in cell migration, to facilitate remodeling of the actin cytoskeleton for viral entry (Yoder et al., 2008). Therefore, HIV hijacks chemokine receptor systems to actively promote its entry and its nuclear localization to infect and multiply in host cells. Large DNA viruses, such as herpesvirus, encode a set of proteins that mimic chemokines and chemokine receptors, or secreted proteins that bind chemokines. These viral proteins have various functions to modulate immune systems for viral spread and replication (Alcami, 2003).

Chemokines and their receptors are indispensable for time- and site-dependent trafficking of human phagocytes to fight pathogens in the human body. On the other hand, pathogens have exploited chemokines and their receptors by hijacking and reprogramming chemokine signaling systems for their entry and replication in human cells. One challenge in fighting infectious diseases is to develop therapies that efficiently stop replication and the spread of pathogens without compromising

the effectiveness of the human immune system or hyper-activating the system.

CONCLUDING REMARKS

In this review, we have highlighted some important findings in the research on chemotaxis and phagocytosis of *D. discoideum* and human phagocytes. We believe that the intricacies of human innate immune response can only be fully understood by analyzing simpler organisms. The discoveries made over the last 100 years on the social amoebae and human phagocytes have shed a light on our understanding of not only the basic evolution of the innate immune system but also problems of human disease. Future research on *D. discoideum* and new findings from this simple organism will further enrich our knowledge of innate immunity and human health.

AUTHOR CONTRIBUTIONS

All authors listed have made a substantial, direct and intellectual contribution to the work, and approved it for publication.

FUNDING

This work was supported by an intramural fund from NIAID, NIH.

REFERENCES

Afonso, P. V., Janka-Junttila, M., Lee, Y. J., McCann, C. P., Oliver, C. M., Aamer, K. A., et al. (2012). LTB4 is a signal-relay molecule during neutrophil chemotaxis. *Dev. Cell* 22, 1079–1091. doi: 10.1016/j.devcel.2012.02.003

Alcami, A. (2003). Viral mimicry of cytokines, chemokines and their receptors. *Nat. Rev. Immunol.* 3, 36–50. doi: 10.1038/nri980

Amarante-Mendes, G. P., Adjemian, S., Branco, L. M., Zanetti, L. C., Weinlich, R., and Bortoluci, K. R. (2018). Pattern Recognition Receptors and the Host Cell Death Molecular Machinery. *Front. Immunol.* 9:2379. doi: 10.3389/fimmu.2018.02379

Ambrose, C. T. (2006). The Osler slide, a demonstration of phagocytosis from 1876 Reports of phagocytosis before Metchnikoff's 1880 paper. *Cell Immunol.* 240, 1–4. doi: 10.1016/j.cellimm.2006.05.008

Amulic, B., Cazalet, C., Hayes, G. L., Metzler, K. D., and Zychlinsky, A. (2012). Neutrophil function: from mechanisms to disease. *Annu. Rev. Immunol.* 30, 459–489. doi: 10.1146/annurev-immunol-020711-074942

Baggiolini, M. (2015). CXCL8 - The First Chemokine. *Front. Immunol.* 6:285. doi: 10.3389/fimmu.2015.00285

Beck, G., and Habicht, G. S. (1996). Immunity and the invertebrates. *Sci. Am.* 275, 60–63.

Berg, H. C. (1975). Chemotaxis in bacteria. *Annu. Rev. Biophys. Bioeng.* 4, 119–136.

Berger, E. A., Murphy, P. M., and Farber, J. M. (1999). Chemokine receptors as HIV-1 coreceptors: roles in viral entry, tropism, and disease. *Annu. Rev. Immunol.* 17, 657–700. doi: 10.1146/annurev.immunol.17.1.657

Bonner, J. T. (1947). Evidence for the formation of cell aggregates by chemotaxis in the development of the slime mold Dictyostelium discoideum. *J. Exp. Zool.* 106, 1–26. doi: 10.1002/jez.1401060102

Borgeat, P., Hamberg, M., and Samuelsson, B. (1976). Transformation of arachidonic acid and homo-gamma-linolenic acid by rabbit polymorphonuclear leukocytes. Monohydroxy acids from novel lipoxygenases. *J. Biol. Chem.* 251, 7816–7820. doi: 10.1016/s0021-9258(19)57008-9

Borrok, M. J., Zhu, Y., Forest, K. T., and Kiessling, L. L. (2009). Structure-based design of a periplasmic binding protein antagonist that prevents domain closure. *ACS Chem. Biol.* 4, 447–456. doi: 10.1021/cb900021q

Bosgraaf, L., and Van Haastert, P. J. (2002). A model for cGMP signal transduction in Dictyostelium in perspective of 25 years of cGMP research. *J. Muscle Res. Cell Motil.* 23, 781–791.

Boulais, J., Trost, M., Landry, C. R., Dieckmann, R., Levy, E. D., Soldati, T., et al. (2010). Molecular characterization of the evolution of phagosomes. *Mol. Syst. Biol.* 6:423. doi: 10.1038/msb.2010.80

Boulay, F., Tardif, M., Brouchon, L., and Vignais, P. (1990). Synthesis and use of a novel N-formyl peptide derivative to isolate a human N-formyl peptide receptor cDNA. *Biochem. Biophys. Res. Commun.* 168, 1103–1109. doi: 10.1016/0006-291x(90)91143-g

Boyden, S. (1962). The chemotactic effect of mixtures of antibody and antigen on polymorphonuclear leucocytes. *J. Exp. Med.* 115, 453–466. doi: 10.1084/jem.115.3.453

Buckley, C. M., Heath, V. L., Gueho, A., Bosmani, C., Knobloch, P., Sikakana, P., et al. (2019). PIKfyve/Fab1 is required for efficient V-ATPase and hydrolase delivery to phagosomes, phagosomal killing, and restriction of Legionella infection. *PLoS Pathog.* 15:e1007551. doi: 10.1371/journal.ppat.1007551

Cao, J., Huang, S., Qian, J., Huang, J., Jin, L., Su, Z., et al. (2009). Evolution of the class C GPCR Venus flytrap modules involved positive selected functional divergence. *BMC Evol. Biol.* 9:67. doi: 10.1186/1471-2148-9-67

Charest, P. G., Shen, Z., Lakoduk, A., Sasaki, A. T., Briggs, S. P., and Firtel, R. A. (2010). A Ras signaling complex controls the RasC-TORC2 pathway and directed cell migration. *Dev. Cell* 18, 737–749. doi: 10.1016/j.devcel.2010.03.017

Chen, C. L., Wang, Y., Sesaki, H., and Iijima, M. (2012). Myosin I links PIP3 signaling to remodeling of the actin cytoskeleton in chemotaxis. *Sci. Signal* 5:ra10. doi: 10.1126/scisignal.2002446

Chen, G., Zhuchenko, O., and Kuspa, A. (2007). Immune-like phagocyte activity in the social amoeba. *Science* 317, 678–681. doi: 10.1126/science.1143991

Cheng, Y., and Othmer, H. (2016). A Model for Direction Sensing in Dictyostelium discoideum: Ras Activity and Symmetry Breaking Driven by a Gbetagamma-Mediated, Galpha2-Ric8 – Dependent Signal Transduction Network. *PLoS Comput. Biol.* 12:e1004900. doi: 10.1371/journal.pcbi.1004900

Cosson, P., and Soldati, T. (2008). Eat, kill or die: when amoeba meets bacteria. *Curr. Opin. Microbiol.* 11, 271–276. doi: 10.1016/j.mib.2008.05.005

Devreotes, P. N. (1994). G protein-linked signaling pathways control the developmental program of Dictyostelium. *Neuron* 12, 235–241. doi: 10.1016/0896-6273(94)90267-4

Devreotes, P. N., and Zigmond, S. H. (1988). Chemotaxis in eukaryotic cells: a focus on leukocytes and Dictyostelium. *Annu. Rev. Cell Biol.* 4, 649–686. doi: 10.1146/annurev.cb.04.110188.003245

Devreotes, P., and Horwitz, A. R. (2015). Signaling networks that regulate cell migration. *Cold Spring Harb. Perspect. Biol.* 7:a005959. doi: 10.1101/cshperspect.a005959

Dinh, C., Farinholt, T., Hirose, S., Zhuchenko, O., and Kuspa, A. (2018). Lectins modulate the microbiota of social amoebae. *Science* 361, 402–406. doi: 10.1126/science.aat2058

Drews, G. (2005). Contributions of Theodor Wilhelm Engelmann on phototaxis, chemotaxis, and photosynthesis. *Photosynth. Res.* 83, 25–34. doi: 10.1007/s11120-004-6313-8

Dunkelberger, J. R., and Song, W. C. (2010). Complement and its role in innate and adaptive immune responses. *Cell Res.* 20, 34–50. doi: 10.1038/cr.2009.139

Dunn, J. D., Bosmani, C., Barisch, C., Raykov, L., Lefrancois, L. H., Cardenal-Munoz, E., et al. (2017). Eat Prey, Live: Dictyostelium discoideum As a Model for Cell-Autonomous Defenses. *Front. Immunol.* 8:1906. doi: 10.3389/fimmu.2017.01906

Fernandez, H. N., Henson, P. M., Otani, A., and Hugli, T. E. (1978). Chemotactic response to human C3a and C5a anaphylatoxins. I. Evaluation of C3a and C5a leukotaxis in vitro and under stimulated in vivo conditions. *J. Immunol.* 120, 109–115.

Fey, P., Dodson, R. J., Basu, S., and Chisholm, R. L. (2013). One stop shop for everything Dictyostelium: dictyBase and the Dicty Stock Center in 2012. *Methods Mol. Biol.* 983, 59–92. doi: 10.1007/978-1-62703-302-2_4

Firtel, R. A., van Haastert, P. J., Kimmel, A. R., and Devreotes, P. N. (1989). G protein linked signal transduction pathways in development: dictyostelium as an experimental system. *Cell* 58, 235–239. doi: 10.1016/0092-8674(89)90837-4

Flannagan, R. S., Jaumouille, V., and Grinstein, S. (2012). The cell biology of phagocytosis. *Annu. Rev. Pathol.* 7, 61–98.

Foord, S. M., Bonner, T. I., Neubig, R. R., Rosser, E. M., Pin, J. P., Davenport, A. P., et al. (2005). International Union of Pharmacology. XLVI. G protein-coupled receptor list. *Pharmacol. Rev.* 57, 279–288. doi: 10.1124/pr.57.2.5

Fredriksson, R., Lagerstrom, M. C., Lundin, L. G., and Schioth, H. B. (2003). The G-protein-coupled receptors in the human genome form five main families. Phylogenetic analysis, paralogon groups, and fingerprints. *Mol. Pharmacol.* 63, 1256–1272. doi: 10.1124/mol.63.6.1256

Funamoto, S., Meili, R., Lee, S., Parry, L., and Firtel, R. A. (2002). Spatial and temporal regulation of 3-phosphoinositides by PI 3-kinase and PTEN mediates chemotaxis. *Cell* 109, 611–623. doi: 10.1016/s0092-8674(02)00755-9

Gerard, N. P., and Gerard, C. (1991). The chemotactic receptor for human C5a anaphylatoxin. *Nature* 349, 614–617. doi: 10.1038/349614a0

Gerisch, G. (1982). Chemotaxis in Dictyostelium. *Annu. Rev. Physiol.* 44, 535–552.

Gerisch, G., Albrecht, R., De Hostos, E., Wallraff, E., Heizer, C., Kreitmeier, M., et al. (1993). Actin-associated proteins in motility and chemotaxis of Dictyostelium cells. *Symp. Soc. Exp. Biol.* 47, 297–315.

Gerisch, G., Albrecht, R., Heizer, C., Hodgkinson, S., and Maniak, M. (1995). Chemoattractant-controlled accumulation of coronin at the leading edge of Dictyostelium cells monitored using a green fluorescent protein-coronin fusion protein. *Curr. Biol.* 5, 1280–1285. doi: 10.1016/s0960-9822(95)00254-5

Gerisch, G., and Muller-Taubenberger, A. (2003). GFP-fusion proteins as fluorescent reporters to study organelle and cytoskeleton dynamics in chemotaxis and phagocytosis. *Methods Enzymol.* 361, 320–337. doi: 10.1016/s0076-6879(03)61017-7

Gerisch, G., Hulser, D., Malchow, D., and Wick, U. (1975). Cell communication by periodic cyclic-AMP pulses. *Philos. Trans. R. Soc. Lond. B Biol. Sci.* 272, 181–192. doi: 10.1098/rstb.1975.0080

Ginsburg, G. T., Gollop, R., Yu, Y., Louis, J. M., Saxe, C. L., and Kimmel, A. R. (1995). The regulation of Dictyostelium development by transmembrane signalling. *J. Eukaryot. Microbiol.* 42, 200–205. doi: 10.1111/j.1550-7408.1995.tb01565.x

Goldberg, J. M., Manning, G., Liu, A., Fey, P., Pilcher, K. E., Xu, Y., et al. (2006). The dictyostelium kinome–analysis of the protein kinases from a simple model organism. *PLoS Genet.* 2:e38. doi: 10.1371/journal.pgen.0020038

Greenberg, S. (1995). Signal transduction of phagocytosis. *Trends Cell Biol.* 5, 93–99. doi: 10.1016/s0962-8924(00)88957-6

Greenberg, S., and Grinstein, S. (2002). Phagocytosis and innate immunity. *Curr. Opin. Immunol.* 14, 136–145. doi: 10.1016/s0952-7915(01)00309-0

Hadwiger, J. A., and Nguyen, H. N. (2011). MAPKs in development: insights from Dictyostelium signaling pathways. *Biomol. Concepts* 2, 39–46. doi: 10.1515/bmc.2011.004

Heit, B., Robbins, S. M., Downey, C. M., Guan, Z., Colarusso, P., Miller, B. J., et al. (2008). PTEN functions to 'prioritize' chemotactic cues and prevent 'distraction' in migrating neutrophils. *Nat. Immunol.* 9, 743–752. doi: 10.1038/ni.1623

Holmes, W. E., Lee, J., Kuang, W. J., Rice, G. C., and Wood, W. I. (1991). Structure and functional expression of a human interleukin-8 receptor. *Science* 253, 1278–1280. doi: 10.1126/science.1840701

Iglesias, P. A., and Devreotes, P. N. (2012). Biased excitable networks: how cells direct motion in response to gradients. *Curr. Opin. Cell Biol.* 24, 245–253. doi: 10.1016/j.ceb.2011.11.009

Iijima, M., and Devreotes, P. (2002). Tumor suppressor PTEN mediates sensing of chemoattractant gradients. *Cell* 109, 599–610.

Insall, R. H., and Machesky, L. M. (2009). Actin dynamics at the leading edge: from simple machinery to complex networks. *Dev. Cell* 17, 310–322. doi: 10.1016/j.devcel.2009.08.012

Insall, R., Kuspa, A., Lilly, P. J., Shaulsky, G., Levin, L. R., Loomis, W. F., et al. (1994). CRAC, a cytosolic protein containing a pleckstrin homology domain, is required for receptor and G protein-mediated activation of adenylyl cyclase in Dictyostelium. *J. Cell Biol.* 126, 1537–1545. doi: 10.1083/jcb.126.6.1537

Janetopoulos, C., Jin, T., and Devreotes, P. (2001). Receptor-mediated activation of heterotrimeric G-proteins in living cells. *Science* 291, 2408–2411. doi: 10.1126/science.1055835

Janeway, C. A. Jr. (1989). Approaching the asymptote? Evolution and revolution in immunology. *Cold Spring Harb. Symp. Quant. Biol.* 54(Pt 1), 1–13. doi: 10.1101/sqb.1989.054.01.003

Jin, T., Xu, X., and Hereld, D. (2008). Chemotaxis, chemokine receptors and human disease. *Cytokine* 44, 1–8. doi: 10.1016/j.cyto.2008.06.017

Jin, T., Zhang, N., Long, Y., Parent, C. A., and Devreotes, P. N. (2000). Localization of the G protein betagamma complex in living cells during chemotaxis. *Science* 287, 1034–1036. doi: 10.1126/science.287.5455.1034

Kaufmann, S. H. E., and Dorhoi, A. (2016). Molecular Determinants in Phagocyte-Bacteria Interactions. *Immunity* 44, 476–491. doi: 10.1016/j.immuni.2016.02.014

Khanna, A., Lotfi, P., Chavan, A. J., Montano, N. M., Bolourani, P., Weeks, G., et al. (2016). The small GTPases Ras and Rap1 bind to and control TORC2 activity. *Sci. Rep.* 6:25823.

King, J. S., and Kay, R. R. (2019). The origins and evolution of macropinocytosis. *Philos. Trans. R. Soc. Lond. B Biol. Sci.* 374:20180158. doi: 10.1098/rstb.2018.0158

Klein, P. S., Sun, T. J., Saxe, C. L. III, Kimmel, A. R., Johnson, R. L., and Devreotes, P. N. (1988). A chemoattractant receptor controls development in Dictyostelium discoideum. *Science* 241, 1467–1472. doi: 10.1126/science.3047871

Kolaczkowska, E., and Kubes, P. (2013). Neutrophil recruitment and function in health and inflammation. *Nat. Rev. Immunol.* 13, 159–175. doi: 10.1038/nri3399

Konijn, T. M., van de Meene, J. G., Chang, Y. Y., Barkley, D. S., and Bonner, J. T. (1969). Identification of adenosine-3′,5′-monophosphate as the bacterial attractant for myxamoebae of *Dictyostelium discoideum*. *J. Bacteriol.* 99, 510–512. doi: 10.1128/jb.99.2.510-512.1969

Kortholt, A., Kataria, R., Keizer-Gunnink, I., Van Egmond, W. N., Khanna, A., and Van Haastert, P. J. (2011). Dictyostelium chemotaxis: essential Ras activation and accessory signalling pathways for amplification. *EMBO Rep.* 12, 1273–1279. doi: 10.1038/embor.2011.210

Kriebel, P. W., Barr, V. A., and Parent, C. A. (2003). Adenylyl cyclase localization regulates streaming during chemotaxis. *Cell* 112, 549–560. doi: 10.1016/s0092-8674(03)00081-3

Lammermann, T., Afonso, P. V., Angermann, B. R., Wang, J. M., Kastenmuller, W., Parent, C. A., et al. (2013). Neutrophil swarms require LTB4 and integrins at sites of cell death in vivo. *Nature* 498, 371–375. doi: 10.1038/nature12175

Levine, H., Kessler, D. A., and Rappel, W. J. (2006). Directional sensing in eukaryotic chemotaxis: a balanced inactivation model. *Proc. Natl. Acad. Sci. U S A.* 103, 9761–9766. doi: 10.1073/pnas.0601302103

Li, H., Yang, L., Fu, H., Yan, J., Wang, Y., Guo, H., et al. (2013). Association between Galphai2 and ELMO1/Dock180 connects chemokine signalling with Rac activation and metastasis. *Nat. Commun.* 4, 1706.

Li, X., Miao, Y., Pal, D. S., and Devreotes, P. N. (2020). Excitable networks controlling cell migration during development and disease. *Semin. Cell Dev. Biol.* 100, 133–142. doi: 10.1016/j.semcdb.2019.11.001

Lisco, A., Grivel, J. C., Biancotto, A., Vanpouille, C., Origgi, F., Malnati, M. S., et al. (2007). Viral interactions in human lymphoid tissue: Human herpesvirus 7 suppresses the replication of CCR5-tropic human immunodeficiency virus type 1 via CD4 modulation. *J. Virol.* 81, 708–717. doi: 10.1128/jvi.01367-06

Liu, L., Das, S., Losert, W., and Parent, C. A. (2010). mTORC2 regulates neutrophil chemotaxis in a cAMP- and RhoA-dependent fashion. *Dev. Cell* 19, 845–857. doi: 10.1016/j.devcel.2010.11.004

Luster, A. D., Unkeless, J. C., and Ravetch, J. V. (1985). Gamma-interferon transcriptionally regulates an early-response gene containing homology to platelet proteins. *Nature* 315, 672–676. doi: 10.1038/315672a0

Maniak, M., Rauchenberger, R., Albrecht, R., Murphy, J., and Gerisch, G. (1995). Coronin involved in phagocytosis: dynamics of particle-induced relocalization visualized by a green fluorescent protein Tag. *Cell* 83, 915–924. doi: 10.1016/0092-8674(95)90207-4

Matsuoka, S., and Ueda, M. (2018). Mutual inhibition between PTEN and PIP3 generates bistability for polarity in motile cells. *Nat. Commun.* 9:4481.

Matsuoka, S., Iijima, M., Watanabe, T. M., Kuwayama, H., Yanagida, T., Devreotes, P. N., et al. (2006). Single-molecule analysis of chemoattractant-stimulated

membrane recruitment of a PH-domain-containing protein. *J. Cell Sci.* 119(Pt 6), 1071–1079. doi: 10.1242/jcs.02824

Matsushima, K., Larsen, C. G., DuBois, G. C., and Oppenheim, J. J. (1989). Purification and characterization of a novel monocyte chemotactic and activating factor produced by a human myelomonocytic cell line. *J. Exp. Med.* 169, 1485–1490. doi: 10.1084/jem.169.4.1485

Mc, C. M. (1946). Chemotaxis in leukocytes. *Physiol. Rev.* 26, 319–336. doi: 10.1152/physrev.1946.26.3.319

Meier-Schellersheim, M., Xu, X., Angermann, B., Kunkel, E. J., Jin, T., and Germain, R. N. (2006). Key role of local regulation in chemosensing revealed by a new molecular interaction-based modeling method. *PLoS Comput. Biol.* 2:e82. doi: 10.1371/journal.pcbi.0020082

Meili, R., Ellsworth, C., Lee, S., Reddy, T. B., Ma, H., and Firtel, R. A. (1999). Chemoattractant-mediated transient activation and membrane localization of Akt/PKB is required for efficient chemotaxis to cAMP in Dictyostelium. *EMBO J.* 18, 2092–2105. doi: 10.1093/emboj/18.8.2092

Metzemaekers, M., Gouwy, M., and Proost, P. (2020). Neutrophil chemoattractant receptors in health and disease: double-edged swords. *Cell Mol. Immunol.* 17, 433–450. doi: 10.1038/s41423-020-0412-0

Miller, M. D., Hata, S., De Waal Malefyt, R., and Krangel, M. S. (1989). A novel polypeptide secreted by activated human T lymphocytes. *J. Immunol.* 143, 2907–2916.

Miyanaga, Y., Kamimura, Y., Kuwayama, H., Devreotes, P. N., and Ueda, M. (2018). Chemoattractant receptors activate, recruit and capture G proteins for wide range chemotaxis. *Biochem. Biophys. Res. Commun.* 507, 304–310. doi: 10.1016/j.bbrc.2018.11.029

Moran, B. M., Flatt, P. R., and McKillop, A. M. (2016). G protein-coupled receptors: signalling and regulation by lipid agonists for improved glucose homoeostasis. *Acta Diabetol.* 53, 177–188. doi: 10.1007/s00592-015-0826-9

Murphy, P. M., and Tiffany, H. L. (1991). Cloning of complementary DNA encoding a functional human interleukin-8 receptor. *Science* 253, 1280–1283. doi: 10.1126/science.1891716

Murphy, P. M., Baggiolini, M., Charo, I. F., Hebert, C. A., Horuk, R., Matsushima, K., et al. (2000). International union of pharmacology. XXII. Nomenclature for chemokine receptors. *Pharmacol. Rev.* 52, 145–176.

Nakajima, A., Ishihara, S., Imoto, D., and Sawai, S. (2014). Rectified directional sensing in long-range cell migration. *Nat. Commun.* 5:5367.

Neptune, E. R., and Bourne, H. R. (1997). Receptors induce chemotaxis by releasing the betagamma subunit of Gi, not by activating Gq or Gs. *Proc. Natl. Acad. Sci. U S A.* 94, 14489–14494. doi: 10.1073/pnas.94.26.14489

Nichols, J. M. E., Paschke, P., Peak-Chew, S., Williams, T. D., Tweedy, L., Skehel, M., et al. (2019). The Atypical MAP Kinase ErkB Transmits Distinct Chemotactic Signals through a Core Signaling Module. *Dev. Cell* 48, 491–505e499.

Nieto, M., Frade, J. M., Sancho, D., Mellado, M., Martinez, A. C., and Sanchez-Madrid, F. (1997). Polarization of chemokine receptors to the leading edge during lymphocyte chemotaxis. *J. Exp. Med.* 186, 153–158. doi: 10.1084/jem.186.1.153

Nishio, M., Watanabe, K., Sasaki, J., Taya, C., Takasuga, S., Iizuka, R., et al. (2007). Control of cell polarity and motility by the PtdIns(3,4,5)P3 phosphatase SHIP1. *Nat. Cell Biol.* 9, 36–44. doi: 10.1038/ncb1515

Obaru, K., Fukuda, M., Maeda, S., and Shimada, K. (1986). A cDNA clone used to study mRNA inducible in human tonsillar lymphocytes by a tumor promoter. *J. Biochem.* 99, 885–894. doi: 10.1093/oxfordjournals.jbchem.a135549

Osei-Owusu, P., Charlton, T. M., Kim, H. K., Missiakas, D., and Schneewind, O. (2019). FPR1 is the plague receptor on host immune cells. *Nature* 574, 57–62. doi: 10.1038/s41586-019-1570-z

Pan, M., Neilson, M. P., Grunfeld, A. M., Cruz, P., Wen, X., Insall, R. H., et al. (2018). A G-protein-coupled chemoattractant receptor recognizes lipopolysaccharide for bacterial phagocytosis. *PLoS Biol.* 16:e2005754. doi: 10.1371/journal.pbio.2005754

Pan, M., Xu, X., Chen, Y., and Jin, T. (2016). Identification of a Chemoattractant G-Protein-Coupled Receptor for Folic Acid that Controls Both Chemotaxis and Phagocytosis. *Dev. Cell* 36, 428–439. doi: 10.1016/j.devcel.2016.01.012

Pan, P., Hall, E. M., and Bonner, J. T. (1972). Folic acid as second chemotactic substance in the cellular slime moulds. *Nat. New Biol.* 237, 181–182. doi: 10.1038/newbio237181a0

Parent, C. A., and Devreotes, P. N. (1999). A cell's sense of direction. *Science* 284, 765–770.

Parent, C. A., and Weiner, O. D. (2013). The symphony of cell movement: how cells orchestrate diverse signals and forces to control migration. *Curr. Opin. Cell Biol.* 25, 523–525. doi: 10.1016/j.ceb.2013.07.011

Parent, C. A., Blacklock, B. J., Froehlich, W. M., Murphy, D. B., and Devreotes, P. N. (1998). G protein signaling events are activated at the leading edge of chemotactic cells. *Cell* 95, 81–91. doi: 10.1016/s0092-8674(00)81784-5

Peracino, B., Borleis, J., Jin, T., Westphal, M., Schwartz, J. M., Wu, L., et al. (1998). G protein beta subunit-null mutants are impaired in phagocytosis and chemotaxis due to inappropriate regulation of the actin cytoskeleton. *J. Cell Biol.* 141, 1529–1537. doi: 10.1083/jcb.141.7.1529

Pollard, T. D., and Borisy, G. G. (2003). Cellular motility driven by assembly and disassembly of actin filaments. *Cell* 112, 453–465. doi: 10.1016/s0092-8674(03)00120-x

Postma, M., and Van Haastert, P. J. (2001). A diffusion-translocation model for gradient sensing by chemotactic cells. *Biophys. J.* 81, 1314–1323. doi: 10.1016/s0006-3495(01)75788-8

Prabhu, Y., and Eichinger, L. (2006). The Dictyostelium repertoire of seven transmembrane domain receptors. *Eur. J. Cell Biol.* 85, 937–946. doi: 10.1016/j.ejcb.2006.04.003

Rappel, W. J., Thomas, P. J., Levine, H., and Loomis, W. F. (2002). Establishing direction during chemotaxis in eukaryotic cells. *Biophys. J.* 83, 1361–1367. doi: 10.1016/s0006-3495(02)73906-4

Sasaki, A. T., Chun, C., Takeda, K., and Firtel, R. A. (2004). Localized Ras signaling at the leading edge regulates PI3K, cell polarity, and directional cell movement. *J. Cell Biol.* 167, 505–518. doi: 10.1083/jcb.200406177

Sattler, N., Bosmani, C., Barisch, C., Gueho, A., Gopaldass, N., Dias, M., et al. (2018). Functions of the Dictyostelium LIMP-2 and CD36 homologues in bacteria uptake, phagolysosome biogenesis and host cell defence. *J. Cell Sci.* 131:17.

Saxe, C. L. III, Johnson, R., Devreotes, P. N., and Kimmel, A. R. (1991). Multiple genes for cell surface cAMP receptors in Dictyostelium discoideum. *Dev. Genet.* 12, 6–13. doi: 10.1002/dvg.1020120104

Schiffmann, E., Corcoran, B. A., and Wahl, S. M. (1975). N-formylmethionyl peptides as chemoattractants for leucocytes. *Proc. Natl. Acad. Sci. U S A.* 72, 1059–1062. doi: 10.1073/pnas.72.3.1059

Schwebs, D. J., Pan, M., Adhikari, N., Kuburich, N. A., Jin, T., and Hadwiger, J. A. (2018). Dictyostelium Erk2 is an atypical MAPK required for chemotaxis. *Cell Signal* 46, 154–165. doi: 10.1016/j.cellsig.2018.03.006

Senoo, H., Kamimura, Y., Kimura, R., Nakajima, A., Sawai, S., Sesaki, H., et al. (2019). Phosphorylated Rho-GDP directly activates mTORC2 kinase towards AKT through dimerization with Ras-GTP to regulate cell migration. *Nat. Cell Biol.* 21, 867–878. doi: 10.1038/s41556-019-0348-8

Servant, G., Weiner, O. D., Herzmark, P., Balla, T., Sedat, J. W., and Bourne, H. R. (2000). Polarization of chemoattractant receptor signaling during neutrophil chemotaxis. *Science* 287, 1037–1040. doi: 10.1126/science.287.5455.1037

Snyderman, R., Gewurz, H., and Mergenhagen, S. E. (1968). Interactions of the complement system with endotoxic lipopolysaccharide. Generation of a factor chemotactic for polymorphonuclear leukocytes. *J. Exp. Med.* 128, 259–275. doi: 10.1084/jem.128.2.259

Soldati, T., and Cardenal-Munoz, E. (2019). A brief historical and evolutionary perspective on the origin of cellular microbiology research. *Cell Microbiol.* 21:e13083.

Stuart, L. M., and Ezekowitz, R. A. (2008). Phagocytosis and comparative innate immunity: learning on the fly. *Nat. Rev. Immunol.* 8, 131–141. doi: 10.1038/nri2240

Suire, S., Condliffe, A. M., Ferguson, G. J., Ellson, C. D., Guillou, H., Davidson, K., et al. (2006). Gbetagammas and the Ras binding domain of p110gamma are both important regulators of PI(3)Kgamma signalling in neutrophils. *Nat. Cell Biol.* 8, 1303–1309. doi: 10.1038/ncb1494

Swanson, J. A., and Taylor, D. L. (1982). Local and spatially coordinated movements in Dictyostelium discoideum amoebae during chemotaxis. *Cell* 28, 225–232. doi: 10.1016/0092-8674(82)90340-3

Takeda, K., Shao, D., Adler, M., Charest, P. G., Loomis, W. F., Levine, H., et al. (2012). Incoherent feedforward control governs adaptation of activated ras in a eukaryotic chemotaxis pathway. *Sci. Signal* 5:ra2. doi: 10.1126/scisignal.2002413

Tariqul Islam, A. F. M., Scavello, M., Lotfi, P., Daniel, D., Haldeman, P., and Charest, P. G. (2019). Caffeine inhibits PI3K and mTORC2 in Dictyostelium and differentially affects multiple other cAMP chemoattractant signaling effectors. *Mol. Cell Biochem.* 457, 157–168. doi: 10.1007/s11010-019-03520-z

Tweedy, L., Thomason, P. A., Paschke, P. I., Martin, K., Machesky, L. M., Zagnoni, M., et al. (2020). Seeing around corners: Cells solve mazes and respond at a distance using attractant breakdown. *Science* 369:6507.

Ueda, M., Sako, Y., Tanaka, T., Devreotes, P., and Yanagida, T. (2001). Single-molecule analysis of chemotactic signaling in Dictyostelium cells. *Science* 294, 864–867. doi: 10.1126/science.1063951

Underhill, D. M., and Ozinsky, A. (2002). Phagocytosis of microbes: complexity in action. *Annu. Rev. Immunol.* 20, 825–852. doi: 10.1146/annurev.immunol.20.103001.114744

Uribe-Querol, E., and Rosales, C. (2020). Phagocytosis: Our Current Understanding of a Universal Biological Process. *Front. Immunol.* 11:1066. doi: 10.3389/fimmu.2020.01066

Van Haastert, P. J., and Devreotes, P. N. (2004). Chemotaxis: signalling the way forward. *Nat. Rev. Mol. Cell Biol.* 5, 626–634. doi: 10.1038/nrm1435

van Haastert, P. J., Keizer-Gunnink, I., and Kortholt, A. (2017). Coupled excitable Ras and F-actin activation mediates spontaneous pseudopod formation and directed cell movement. *Mol. Biol. Cell* 28, 922–934. doi: 10.1091/mbc.e16-10-0733

Vogel, G., Thilo, L., Schwarz, H., and Steinhart, R. (1980). Mechanism of phagocytosis in Dictyostelium discoideum: phagocytosis is mediated by different recognition sites as disclosed by mutants with altered phagocytotic properties. *J. Cell Biol.* 86, 456–465. doi: 10.1083/jcb.86.2.456

Walport, M. J. (2001a). Complement. Second of two parts. *N. Engl. J. Med.* 344, 1140–1144.

Walport, M. J. (2001b). Complement. First of two parts. *N. Engl. J. Med.* 344, 1058–1066.

Walsh, D., McCarthy, J., O'Driscoll, C., and Melgar, S. (2013). Pattern recognition receptors–molecular orchestrators of inflammation in inflammatory bowel disease. *Cytokine Growth Factor Rev.* 24, 91–104. doi: 10.1016/j.cytogfr.2012.09.003

Walz, A., Peveri, P., Aschauer, H., and Baggiolini, M. (1987). Purification and amino acid sequencing of NAF, a novel neutrophil-activating factor produced by monocytes. *Biochem. Biophys. Res. Commun.* 149, 755–761. doi: 10.1016/0006-291x(87)90432-3

Wen, X., Xu, X., Sun, W., Chen, K., Pan, M., Wang, J. M., et al. (2019). G-protein-coupled formyl peptide receptors play a dual role in neutrophil chemotaxis and bacterial phagocytosis. *Mol. Biol. Cell* 30, 346–356. doi: 10.1091/mbc.e18-06-0358

Williams, L. T. (1989). Signal transduction by the platelet-derived growth factor receptor. *Science* 243, 1564–1570. doi: 10.1126/science.2538922

Wood, W. B. Jr., Smith, M. R., and Watson, B. (1946). Surface phagocytosis; its relation to the mechanism of recovery in pneumococcal pneumonia. *Science* 104:28.

Wright, A. E., Douglas, S. R., and Sanderson, J. B. (1989). An experimental investigation of the role of the blood fluids in connection with phagocytosis. 1903. *Rev. Infect. Dis.* 11, 827–834. doi: 10.1093/clinids/11.5.827

Xiao, Z., Zhang, N., Murphy, D. B., and Devreotes, P. N. (1997). Dynamic distribution of chemoattractant receptors in living cells during chemotaxis and persistent stimulation. *J. Cell Biol.* 139, 365–374. doi: 10.1083/jcb.139.2.365

Xu, X., Gera, N., Li, H., Yun, M., Zhang, L., Wang, Y., et al. (2015). GPCR-mediated PLCbetagamma/PKCbeta/PKD signaling pathway regulates the cofilin phosphatase slingshot 2 in neutrophil chemotaxis. *Mol. Biol. Cell* 26, 874–886. doi: 10.1091/mbc.e14-05-0982

Xu, X., Meier-Schellersheim, M., Jiao, X., Nelson, L. E., and Jin, T. (2005). Quantitative imaging of single live cells reveals spatiotemporal dynamics of multistep signaling events of chemoattractant gradient sensing in Dictyostelium. *Mol. Biol. Cell* 16, 676–688. doi: 10.1091/mbc.e04-07-0544

Xu, X., Meier-Schellersheim, M., Yan, J., and Jin, T. (2007). Locally controlled inhibitory mechanisms are involved in eukaryotic GPCR-mediated chemosensing. *J. Cell Biol.* 178, 141–153. doi: 10.1083/jcb.200611096

Yan, J., Mihaylov, V., Xu, X., Brzostowski, J. A., Li, H., Liu, L., et al. (2012). A Gbetagamma effector, ElmoE, transduces GPCR signaling to the actin network during chemotaxis. *Dev. Cell* 22, 92–103. doi: 10.1016/j.devcel.2011.11.007

Yang, Y., Li, D., Chao, X., Singh, S. P., Thomason, P., Yan, Y., et al. (2021). Leep1 interacts with PIP3 and the Scar/WAVE complex to regulate cell migration and macropinocytosis. *J. Cell Biol.* 220:7.

Yoder, A., Yu, D., Dong, L., Iyer, S. R., Xu, X., Kelly, J., et al. (2008). HIV envelope-CXCR4 signaling activates cofilin to overcome cortical actin restriction in resting CD4 T cells. *Cell* 134, 782–792. doi: 10.1016/j.cell.2008.06.036

Yoshimura, T., Matsushima, K., Tanaka, S., Robinson, E. A., Appella, E., Oppenheim, J. J., et al. (1987). Purification of a human monocyte-derived neutrophil chemotactic factor that has peptide sequence similarity to other host defense cytokines. *Proc. Natl. Acad. Sci. U S A.* 84, 9233–9237. doi: 10.1073/pnas.84.24.9233

Yoshimura, T., Robinson, E. A., Tanaka, S., Appella, E., Kuratsu, J., and Leonard, E. J. (1989). Purification and amino acid analysis of two human glioma-derived monocyte chemoattractants. *J. Exp. Med.* 169, 1449–1459. doi: 10.1084/jem.169.4.1449

Zhang, X., Zhuchenko, O., Kuspa, A., and Soldati, T. (2016). Social amoebae trap and kill bacteria by casting DNA nets. *Nat. Commun.* 7:10938.

Zigmond, S. H. (1974). Mechanisms of sensing chemical gradients by polymorphonuclear leukocytes. *Nature* 249, 450–452. doi: 10.1038/249450a0

Zigmond, S. H. (1978). Chemotaxis by polymorphonuclear leukocytes. *J. Cell Biol.* 77, 269–287. doi: 10.1083/jcb.77.2.269

Conflict of Interest: The authors declare that the research was conducted in the absence of any commercial or financial relationships that could be construed as a potential conflict of interest.

Publisher's Note: All claims expressed in this article are solely those of the authors and do not necessarily represent those of their affiliated organizations, or those of the publisher, the editors and the reviewers. Any product that may be evaluated in this article, or claim that may be made by its manufacturer, is not guaranteed or endorsed by the publisher.

Copyright © 2021 Xu, Pan and Jin. This is an open-access article distributed under the terms of the Creative Commons Attribution License (CC BY). The use, distribution or reproduction in other forums is permitted, provided the original author(s) and the copyright owner(s) are credited and that the original publication in this journal is cited, in accordance with accepted academic practice. No use, distribution or reproduction is permitted which does not comply with these terms.

frontiers in Cell and Developmental Biology

REVIEW
published: 01 September 2021
doi: 10.3389/fcell.2021.737071

The *WIPI* Gene Family and Neurodegenerative Diseases: Insights From Yeast and *Dictyostelium* Models

*Olivier Vincent[1], Laura Antón-Esteban[1], Miranda Bueno-Arribas[1], Alba Tornero-Écija[1], María-Ángeles Navas[2] and Ricardo Escalante[1]**

[1] Instituto de Investigaciones Biomédicas Alberto Sols CSIC/UAM, Madrid, Spain, [2] Departamento de Bioquímica y Biología Molecular, Facultad de Medicina, Universidad Complutense de Madrid, Madrid, Spain

WIPIs are a conserved family of proteins with a characteristic 7-bladed β-propeller structure. They play a prominent role in autophagy, but also in other membrane trafficking processes. Mutations in human *WIPI4* cause several neurodegenerative diseases. One of them is BPAN, a rare disease characterized by developmental delay, motor disorders, and seizures. Autophagy dysfunction is thought to play an important role in this disease but the precise pathological consequences of the mutations are not well established. The use of simple models such as the yeast *Saccharomyces cerevisiae* and the social amoeba *Dictyostelium discoideum* provides valuable information on the molecular and cellular function of these proteins, but also sheds light on possible pathways that may be relevant in the search for potential therapies. Here, we review the function of WIPIs as well as disease-causing mutations with a special focus on the information provided by these simple models.

Keywords: autophagy, BPAN, *Dictyostelium discoideum*, *Saccharomyces cerevisiae*, PROPPIN, Vmp1, WDR45, *WIPI*

OPEN ACCESS

Edited by:
Annette Müller-Taubenberger, Ludwig Maximilian University of Munich, Germany

Reviewed by:
Ludwig Eichinger, University of Cologne, Germany
Matt Scaglione, Duke University, United States

****Correspondence:***
Ricardo Escalante
r.escalante@csic.es

Specialty section:
This article was submitted to Molecular and Cellular Pathology, a section of the journal Frontiers in Cell and Developmental Biology

Received: *06 July 2021*
Accepted: *12 August 2021*
Published: *01 September 2021*

Citation:
Vincent O, Antón-Esteban L, Bueno-Arribas M, Tornero-Écija A, Navas M-Á and Escalante R (2021) The WIPI Gene Family and Neurodegenerative Diseases: Insights From Yeast and Dictyostelium Models. Front. Cell Dev. Biol. 9:737071. doi: 10.3389/fcell.2021.737071

INTRODUCTION

Degradation and recycling of cellular components are essential for cell homeostasis. Autophagy (from the Greek, "self-eating") includes several pathways that deliver different types of cargos to lysosomes for degradation. Macroautophagy (referred to as autophagy hereafter) is characterized by the formation of double-membrane vesicles, known as autophagosomes, which can engulf non-specific cellular material (bulk autophagy) or specific cargoes, such as protein aggregates or defective organelles (selective autophagy). After the fusion of autophagosomes with the lysosomes, the simple biochemical compounds generated during the degradation process are transported to the cytosol and reused for energy production or recycling (see recent reviews Lahiri et al., 2019; Melia et al., 2020; Gubas and Dikic, 2021). Autophagosome biogenesis is a highly regulated process involving different stages: induction, lipidation, and elongation of the autophagosome membrane (also known as the isolation membrane or phagophore), vesicle closure, and fusion with lysosomes. These steps are controlled by protein complexes formed mainly by the so-called Atg proteins. **Figure 1** summarizes schematically the essential components of the autophagy machinery and their function in the different steps of autophagosome formation.

The nutritional and energetic status of cells regulates autophagy through two master regulators, TORC1 and AMPK (Hindupur et al., 2015). These kinases oppositely control autophagy

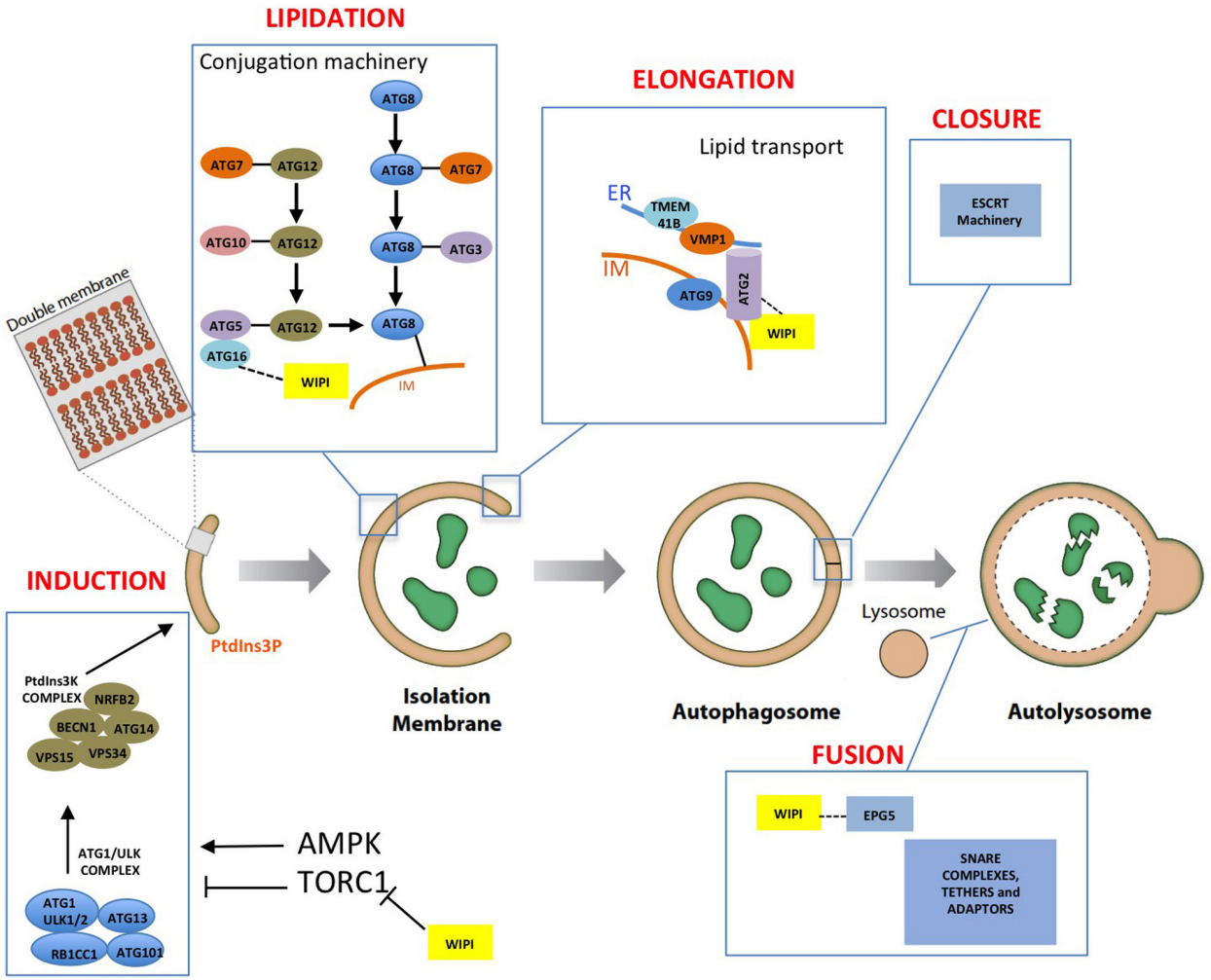

FIGURE 1 | Autophagosome formation and the autophagic machinery. The different steps of autophagosome formation are shown together with the proteins and protein complexes involved in autophagy regulation. WIPIs (yellow boxes) are involved in different steps of autophagosome formation (see the text for a detailed explanation of the specific WIPIs involved in each step).

through phosphorylation of key subunits of two essential complexes, Atg1/ULK and PI3KC3. Atg1/ULK kinase complex composed of Atg1, Atg13, Atg17, Atg29, and Atg31 in *Saccharomyces cerevisiae* (yeast hereafter), and by ULK1/2, ATG13, ATG101, and FIP200 in mammalian cells (Hurley and Young, 2017). Atg1, Atg13, and Atg101 have also been identified in *Dictyostelium discoideum* (Otto et al., 2004; Mesquita et al., 2015). During nucleation the Atg1/ULK complex is activated and recruited to specialized regions of the endoplasmic reticulum (ER) through interaction with VAMP-associated proteins (VAPs) (Zhao et al., 2018). The Atg1/ULK complex subsequently activates the PI3KC3 complex composed of Vps34, Vps15, Atg6, and Atg14 in yeast and VPS34, VPS15, BECN1, NRFB2, and ATG14 in mammals (Hurley and Young, 2017). The homologues of all these components can also be recognized in *Dictyostelium* (Calvo-Garrido et al., 2010; Fischer and Eichinger, 2019). The phosphoinositide 3-kinase Vps34/VPS34 generates PtdIns3P by phosphorylation of phosphatidylinositol in the nascent autophagosome membrane and in the specialized ER-derived structure known as omegasome (Axe et al., 2008; Nishimura et al., 2017). The incorporation of Atg9 containing vesicles, which seed the initial autophagosome membrane, is also under the control of the Atg1/ULK complex (Papinski et al., 2014; Karanasios et al., 2016; Nishimura et al., 2017; Sawa-Makarska et al., 2020).

The PtdIns3P generated at the autophagosome assembly site recruits a family of proteins called WIPIs (WD-repeat protein Interacting with phosphoinositides), also known as PROPPINs (beta-propellers that bind polyphosphoinositides), which are necessary for the subsequent recruitment of other autophagic proteins. Their structure, function and role in disease are the focus of this review. One of the proteins recruited by WIPIs is Atg2 in yeast (ATG2A/ATG2B in mammalian cells), a lipid transport protein that appears to be responsible for

autophagosome membrane elongation through lipid transport from the ER (Maeda et al., 2019; Osawa et al., 2019, 2020; Valverde et al., 2019). Autophagosome membrane elongation also requires the function of several transmembrane proteins, ATG9 in the phagophore membrane, and VMP1 and TMEM41B in the ER membrane, which have recently been reported to have scramblase activity *in vitro* (Valverde et al., 2019; Matoba et al., 2020; Li et al., 2021). Since lipids are extracted by Atg2 from the outer leaflet of the ER membrane and delivered to the outer leaflet of the autophagosome membrane, lipid transport from one leaflet to the other that is accomplished by these scramblases is necessary to equilibrate the lipid composition on both sides of the bilayer of the donor and acceptor membranes.

Atg8 lipidation, a ubiquitin-like mechanism that covalently attaches the protein Atg8 to the autophagosome membrane, is also required for elongation and closure of the autophagosome membrane. In mammalian cells, Atg8 proteins are classified into three groups: LC3, GABARAP, and GABARAPL (Slobodkin and Elazar, 2013). In this process, the Atg12 protein is first conjugated to Atg5 and this complex interacts non-covalently with Atg16. The WIPI-mediated recruitment of the Atg12-Atg5/Atg16 complex to the autophagosome membrane promotes the conjugation of Atg8 to phosphatidyl-ethanolamine (PE) in a process that also involves the E1-like and E2-like enzymes Atg7 and Atg3 (Geng and Klionsky, 2008). The proteins involved in this ubiquitin-like mechanism are highly conserved in all eukaryotes, including *Dictyostelium* (Calvo-Garrido et al., 2010; Mesquita et al., 2017; Fischer and Eichinger, 2019). Closure of the autophagosome membrane and fusion with lysosomes requires the function of the ESCRT machinery and SNARE complexes, respectively (Lőrincz and Juhász, 2019).

Autophagy influences virtually all cellular processes, as it regulates the cellular response to the immediate metabolic demands and also plays a direct role in the quality control of protein and organelles. Consequently, autophagy has a major impact at the organismal level and regulates many physiological functions in mammalian cells, including differentiation and development, tissue and organ homeostasis, immunity and aging. Mutations in autophagy-related genes have been associated with different diseases (see a recent review for an overview; Mizushima and Levine, 2020). Mutations in *WIPI* genes lead to severe neurological disorders, including neurodegeneration, intellectual disability, epilepsy, developmental abnormalities, etc. Specifically, mutations in the *WIPI4/WDR45* gene lead to BPAN (beta propeller-associated neurodegeneration), an ultra-rare disease with no cure that affects children. The use of simple model organisms such as Yeast and *Dictyostelium* can help to understand the molecular basis of these diseases.

THE YEAST AND *DICTYOSTELIUM* MODELS IN AUTOPHAGY AND DISEASE

Yeast has been the pioneer model in which most of the components of the autophagic machinery have been discovered and characterized. The lack of autophagy in this organism leads to reduced survival under conditions of nitrogen starvation. Nobel laureate Yoshinory Ohsumi took advantage of the powerful genetics and manipulability of yeast to screen for genes required for autophagy, whose encoded proteins were named Atg proteins (Tsukada and Ohsumi, 1993; Scott et al., 1996; Matsuura et al., 1997). Although the simplicity of the yeast model has allowed the fundamental leap of identifying the key components of the autophagic machinery, this model lacks the complexity of phenotypes usually associated with autophagy dysfunction in multicellular organisms. *Dictyostelium* can therefore complement the use of yeast, primarily for certain genes or pathways that are not found in yeast, while conserved between *Dictyostelium* and animal cells.

The species *Dictyostelium discoideum* was discovered in 1935 by Kenneth Raper in Western North Carolina (United States) (Raper, 1935), and the potential of this organism as an experimental model became apparent very early on. *Dictyostelium* belongs to the amoebozoa group, and although this group of organisms diverged before the opistokonta (fungi and animals), it retains many features of animal cells that have been lost during the evolution of fungi. Cell motility and chemotaxis, phagocytosis and macropynocytosis are very similar to those observed in animal cells and *Dictyostelium* presents a multicellular stage that allows the study of cell differentiation and morphogenesis (see this series of reviews collected in a special issue dedicated to *Dictyostelium* in *IJDB* (Araki and Saito, 2019; Batsios et al., 2019; Bloomfield, 2019; Bozzaro, 2019; Consalvo et al., 2019; Escalante and Cardenal-Muñoz, 2019; Farinholt et al., 2019; Fey et al., 2019; Fischer and Eichinger, 2019; Ishikawa-Ankerhold and Müller-Taubenberger, 2019; Jaiswal et al., 2019; Kawabe et al., 2019; Kay et al., 2019; Knecht et al., 2019; Kundert and Shaulsky, 2019; Kuspa and Shaulsky, 2019; Medina et al., 2019; Nanjundiah, 2019; Pal et al., 2019; Pearce et al., 2019; Pergolizzi et al., 2019; Schaf et al., 2019; Vines and King, 2019). Individual *Dictyostelium* cells ingest bacteria and yeasts in soil and the transition to a multicellular state, triggered when the food source is depleted, is accomplished by aggregation of preexisting cells. This developmental program culminates in the formation of a fruiting body containing spores (**Figure 2**). As this process takes place in the absence of nutrients, autophagy is essential to sustain the energy-demanding processes of chemotaxis, morphogenesis and cell differentiation. Therefore, autophagy dysfunction results in distinct phenotypes that vary in severity from the complete absence of development to the formation of aberrant, multi-tipped mounds that may eventually form abnormal fruiting bodies containing non-viable spores (Otto et al., 2003, 2004; Calvo-Garrido and Escalante, 2010; Tung et al., 2010; Mesquita et al., 2015; Muñoz-Braceras et al., 2015; Xiong et al., 2015, 2018; Fischer et al., 2019; Sharma et al., 2019; Yamada and Schaap, 2019, 2020; Karow et al., 2020; **Figure 2**). *Dictyostelium* has become a useful model for studying autophagy. The function of many autophagy genes have been analyzed in this organism and diverse techniques have been fine-tuned to precisely study this process (Calvo-Garrido et al., 2010; Mesquita et al., 2017; Fischer and Eichinger, 2019).

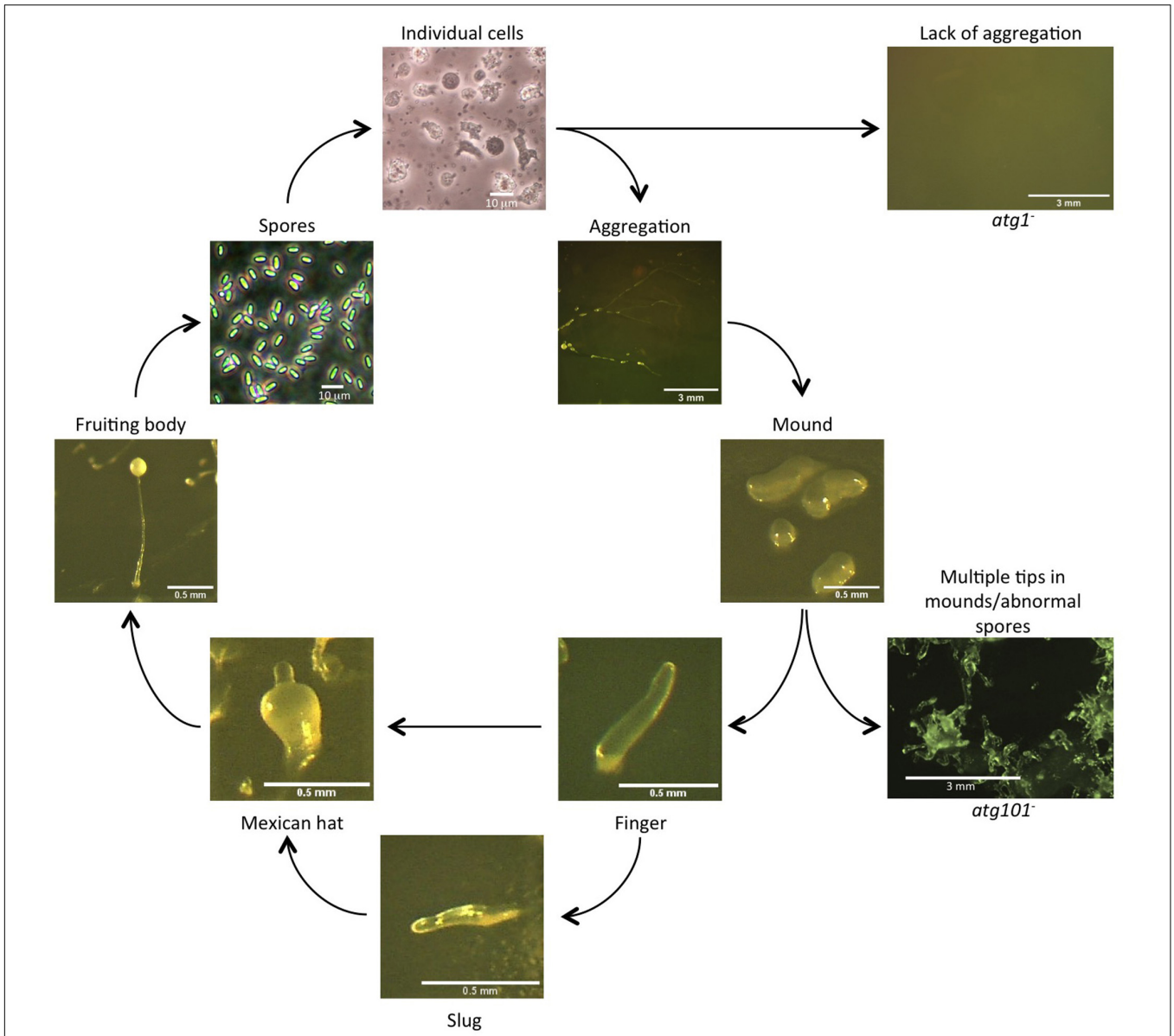

FIGURE 2 | Autophagy is required for *Dictyostelium* development. Representative pictures of the *Dictyostelium* life cycle are shown. Strains defective in autophagy (right panels) show distinct phenotypes, such as lack of aggregation (Atg1 mutant is shown as an example) or abnormal development with a lack of spores (Atg101 mutant is shown as an example). Scale bars are shown in each photograph.

In addition, *Dictyostelium* expresses some key autophagic proteins absent in yeast but present in animal cells. Notable examples are the Atg1/ULK complex protein Atg101 (Mesquita et al., 2015), the ER protein Vmp1 (Calvo-Garrido et al., 2008, 2014; Calvo-Garrido and Escalante, 2010), the Atg16 protein containing a C-terminal WD-repeat domain also present in mammalian ATG16L (Xiong et al., 2018) but absent in the yeast homolog, the autophagy regulators KinkyA and Bcas3 (Yamada and Schaap, 2020), and orthologues of the Gamma-secretase PSEN1 (psenA and psenB), NCSTN (nicastrin), and APH1 (gamma-secretase subunit Aph-1) (Sharma et al., 2019).

The use of simple model organisms, such as yeast and *Dictyostelium*, has allowed fundamental advances to be made in the basic principles of many diseases, contributing to the 3R principle (replacing, reducing and refining the use of animals in research, directive 2010/63/EU). The high conservation of protein and signaling pathways during evolution makes it possible to study diseases at different levels: (i) At the molecular level, for example by analyzing the biochemical function, structure and interactions of proteins involved in the disease; (ii) At the cellular and organism level, by analyzing cell physiology, affected pathways, differentiation and development of diseased models; and (iii) At the pharmacological levels

by studying the mechanism of action of drugs or even the search for new therapeutic compounds for well-conserved pathways (see some recent works as examples of point iii; Cocorocchio et al., 2017; Schaf et al., 2019; Perry et al., 2020; Warren et al., 2020).

THE FUNCTION OF WIPIs IN THE DIFFERENT STEPS OF AUTOPHAGOSOME FORMATION

The number of members of this protein family varies among organisms. In mammalian cells there are four members (WIPI1, WIPI2, WDR45B/WIPI3, and WDR45/WIPI4), three in yeast (Atg18, Atg21, and Hsv2) and two in *Dictyostelium* (Atg18 and Wdr45l). A phylogenetic analysis based on sequence similarity clusters WIPI sequences into two groups (**Figure 3**). One contains the highly similar WIPI1 and WIPI2 along with *Dictyostelium* Atg18 and yeast Atg18 and Atg21. In the other branch, human WIPI3 and WIPI4 are found together with *Dictyostelium* Wdr45l and yeast Hsv2 (**Figure 3**). Despite the apparent clarity in their distribution, the functions attributed to each member do not always correspond to this position based on sequence similarity. The most striking example is that of Hsv2, which is the closest sequence homologue in yeast of human WIPI3/4 and *Dictyostelium* Wdr45l, proteins that play a prominent role in autophagy, whereas Hsv2 does not appear to play a role in bulk autophagy in yeast (Krick et al., 2008). Next, we will describe in detail and in a comparative way the functions attributed to the human, yeast and *Dictyostelium* WIPI proteins in the different steps of autophagosome formation (**Figure 1** shows the WIPIs in their proposed functions throughout the different steps of autophagosome formation).

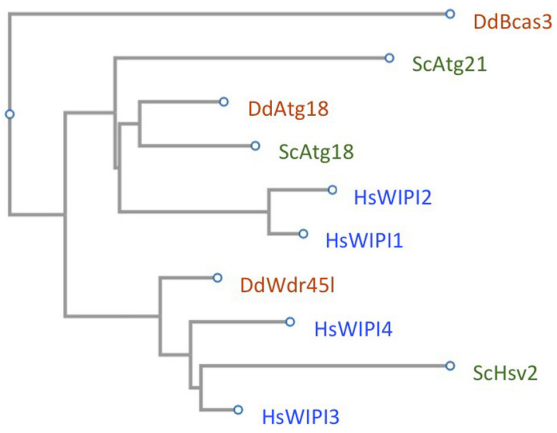

FIGURE 3 | The WIPI family in yeast, *Dictyostelium* and human. The amino acid sequences of yeast Atg18, Atg21, and Hsv2 (UniProt entry: P43601; Q02887; P50079), *Dictyostelium* Atg18 and Wdr45l (UniProt entry: Q54NA2; Q54SA0), and the human WIPI1, WIPI2, WDR45B/WIPI3, and WDR45/WIPI4 (UniProt entry: Q5MNZ9; Q9Y4P8; Q5MNZ6; Q9Y484), were used for a phylogenetic analysis using Fast Tree (https://www.genome.jp/tools-bin/clustalw). The *Dictyostelium* proppin Bcas3 (UniProt entry: Q559F5) was used as an outgroup.

Induction Step

The induction of autophagy is regulated by the interplay between AMPK and TORC1. AMPK activates and TORC1 inhibits autophagy. TORC1 is activated by growth factor through RHEB, and aminoacids through RRAG/Rag GTPases that activate TORC1 on the surface of lysosomes, leading to phosphorylation of the ATG1/ULK complex and inhibition of autophagy. AMPK activates autophagy through phosphorylation and activation of the TORC1 inhibitor TSC1/2. In addition, AMPK activates autophagy directly through phosphorylation and inhibition of TORC1, and also through activation by phosphorylation of the ATG1/ULK complex. Analysis of the WIPI3 interactome suggests a regulatory role of this protein in TORC1 inhibition through the TSC1/2 complex. Specifically, WIPI3 interacts with TSC1 when the latter is phosphorylated by AMPK. The complex formed by WIPI3/TSC1/2/FIP200 localizes to the lysosome when TORC1 is absent, suggesting a role in inhibiting and releasing TORC1 from lysosomes to activate autophagy (Bakula et al., 2017). Upon starvation, WIPI3 also translocates to the nascent autophagosome colocalizing with FIP200 and other ATG proteins (Bakula et al., 2017). This possible role of human WIPI3 in the initiation step contrasts with the phenotype associated to human WIPI3 or WIPI4 knock-down (KD) (Bakula et al., 2017) and to Wdr45l knock-out (KO) in *Dictyostelium* (Tornero-Écija et al., 2021), as autophagy is blocked at a later step, following recruitment of the conjugation machinery and lipidation of Atg8/LC3.

Elongation and Atg8/LC3 Lipidation

WIPI proteins play an essential role in the recruitment of the conjugation machinery responsible for the lipidation of Atg8/LC3 protein at the phagophore membrane. In particular, the interaction of human WIPI2 with ATG16L1 mediates the recruitment of the ATG12-ATG5/ATG16L1 complex (Dooley et al., 2014; Fracchiolla et al., 2020). Accordingly, WIPI2 KD results in a large reduction in LC3 lipidation and autophagosome formation (Polson et al., 2010; Dooley et al., 2014; Bakula et al., 2017). There is also an accumulation of PtdIns3P and DFCP1 (double FYVE-domain containing protein 1) positive structures in WIPI2-depleted HEK293A cells, suggesting a defect in the omegasome structure (Polson et al., 2010).

WIPI1 has been proposed to assist WIPI2 in the recruitment of the conjugation machinery although its role is not essential (Bakula et al., 2017, 2018). Accordingly, WIPI1 KD in G361 cells does not prevent the formation of autophagosomes although a slight decrease in the number of autophagosomal structures is observed (Bakula et al., 2017). However, there is no detectable effect on LC3 lipidation (Proikas-Cezanne et al., 2015), indicating that WIPI1 is partially dispensable for the recruitment of the conjugation machinery.

In yeast, Atg21, like WIPI2 in humans, interacts with Atg16 and is essential for effective recruitment and lipidation of Atg8 (Juris et al., 2015; Krick and Thumm, 2016; Sawa-Makarska et al., 2020). Interestingly, the closest sequence homolog of Atg21 and

WIPI2 in *Dictyostelium*, termed Atg18, is largely dispensable for autophagy, as Atg8-containing autophagosomes are formed in Atg18 KO cells, although a slight reduction in autophagy flux can be detected (Tornero-Écija et al., 2021). The other WIPI protein in *Dictyostelium*, Wdr45l, does not appear to be required for lipidation despite the complete block in autophagy, as abnormal Atg8-containing structures are detected in the Wdr45l KO strain (Tornero-Écija et al., 2021). This raises the possibility that in *Dictyostelium*, recruitment of the conjugation machinery is largely independent of WIPI proteins. The existence of alternative mechanisms to WIPIs in this process is consistent with the observation that LC3 lipidation is not completely blocked in mammalian cells depleted of WIPI1 or WIPI2 (Polson et al., 2010), and that a C-terminal region of ATG16L1 can bind to membranes on its own and sustain LC3 lipidation in the absence of WIPI2 (Lystad et al., 2019). Interestingly, this C-terminal extension is absent in yeast Atg16 but present in the *Dictyostelium* Atg16 homolog (Xiong et al., 2018), which could explain the apparently minor role of WIPIs in the conjugation process in this organism, although no direct study has been performed on the ability of this protein region in *Dictyostelium* to bind to the autophagosome membrane.

Elongation and Lipid Transport Mediated by ATG2

Phagophore elongation requires lipid transport from the ER by the lipid transfer protein ATG2, which forms a complex with WIPI4 in mammalian cells (Bakula et al., 2017, 2018; Chowdhury et al., 2018; Maeda et al., 2019; Osawa et al., 2020; Sawa-Makarska et al., 2020) and Atg18 in yeast (Obara et al., 2008; Gómez-Sánchez et al., 2018; Kotani et al., 2018). A proteomic analysis suggests that WIPI4 forms a complex with AMPK and ULK1 under fed conditions and is released upon starvation to localize together with ATG2 at the phagophore (Bakula et al., 2017, 2018).

Functionally, both WIPI3 and WIPI4 are downstream of LC3 lipidation as their depletion in G316 cell lines leads to abnormal accumulation of other autophagic proteins such as WIPI1 and LC3 (Bakula et al., 2017). In addition, mice with double KO of WIPI3 and 4 show a more severe autophagy defect than single KO, suggesting that these two proteins act cooperatively in autophagy (Ji et al., 2020). In *Dictyostelium*, accumulation of Atg18 and Atg8 is also observed in cells lacking Wdr45l, suggesting that this protein is the functional counterpart of WIPI3 and 4 (Tornero-Écija et al., 2021). Thus, mammalian WIPI3 and 4, *Dictyostelium* Wdr45l and yeast Atg18 appear to be functionally equivalent, even though the yeast Atg18 belongs to the other phylogenetic group formed by WIPI1 and 2, *Dictyostelium* Atg18 and yeast Atg21. This is another clear example of the lack of correlation between sequence similarity and functional conservation.

Fusion of Autophagosomes With Lysosomes

Defects in lipid transport during autophagosome formation resulting from lack of ATG2 or WIPI3/4 are expected to cause abnormal small phagophores to accumulate. However, a recent report showed that WIPI3/4 double KO mouse neuroblastome cells (N2a) can form autophagosomes that appear to be closed but are very small (Ji et al., 2021). The small size of these autophagosomes is overcome by overexpression of ATG2A, which is consistent with the involvement of ATG2/WIPI3/4 in lipid transfer and autophagosome membrane growth. Interestingly, WIPI3/4 appears to be required for a later stage of the autophagy pathway, as the fusion of these small autophagosomes with lysosomes is impaired in WIPI3/4 double KO (Ji et al., 2021). In the proposed model, WIPI3 or WIPI4 binds to EPG5, a protein required for the tethering of autophagosomes to lysosomes and the assembly of the SNARE complex necessary for fusion. As previously observed in the mouse model, autophagy defects are observed in WIPI3/4 double KO in N2a cells but not in single KOs of WIPI3 or WIPI4, again suggesting redundancy of function in this neural cell line.

Non-autophagic Functions of WIPIs

The versatility and complexity of WIPI proteins are also evidenced by their function in pathways other than canonical autophagy. Indeed, WIPI1 (also known as WIPI49 for 49 KD) was initially characterized for its function in endosome trafficking. It localizes to the trans-Golgi and endosomes (in COS-7 cells) and siRNA-mediated KD in COS7 leads to impaired CI-MPR (mannose 6-P receptor) trafficking (Jeffries et al., 2004). Inactivation of WIPI1 leads to enlargement of endosomes and accumulation of endosomal membrane tubules. In addition, WIPI1 (but not the other WIPIs) has recently been shown to be required for transferrin receptor recycling to the plasma membrane in HK2 (human kidney) cells (De Leo et al., 2021). It is required for the formation of tubulo-vesicular endosomal transport carriers. The binding of the two phosphatidyl inositol binding sites to PtdIns3P or PI(3, 5)P2 appear to determine WIPI1 function in autophagy or endosomal trafficking. Interestingly, yeast Atg18 (formerly known as Svp1) is required for protein recycling from the vacuole to the Golgi and its inactivation leads to vacuole enlargement and accumulation of PtdIns(3, 5)P2 (Dove et al., 2004). PI(3, 5)P2 recruits Atg18 to the vacuole where it regulates retrograde transport of proteins from the vacuole to Golgi. Its function in autophagy is independent of binding to this lipid (Dove et al., 2004).

Human WIPI3 has been implicated in an alternative form of autophagy known as GOMED (Golgi-membrane-associated degradation) that is independent of the conjugation machinery and generates autophagic structures from Golgi membranes (Yamaguchi et al., 2020).

STRUCTURAL AND FUNCTIONAL FEATURES OF WIPI PROTEINS: INTERACTIONS WITH PHOSPHOINOSITIDES AND THE PROTEINS Atg16 AND Atg2

The crystal structure of Hsv2 from *Kluyveromyces lactis* revealed a characteristic structure shared by the entire WIPI protein family

(Krick et al., 2012), corresponding to a seven-bladed β-propeller, each blade being formed by four antiparallel β-strands. This structure is reminiscent of a barrel-like structure and has a non-velcro closure, whereby the N-terminus is not part of the last C-terminal blade. Interaction with lipids and with proteins such as Atg2 and Atg16 involve different regions of the protein.

WIPIs bind to the membrane through two lipid-binding sites that require the conserved motif L/FRRG, which can be considered a signature of this family of proteins. Each R residue is in opposite directions, located in the two pockets (site1 and site 2) that are involved in phosphoinositide binding. Site 1 is located in blade 5 and is associated with one of the conserved R and the other site is located in blade 6 and is associated with the second R (Baskaran et al., 2012; Krick et al., 2012; Watanabe et al., 2012). *In vitro* analyses showed that WIPI1 (formerly known as WIPI49) binds preferentially to PtdIns3P and to a lesser extent to PtdIns5P and PtdIns(3, 5)P2 (Jeffries et al., 2004), while yeast Atg18 (Svp1) binds to both PtdIns3P and PI(3, 5)P2 (Dove et al., 2004; Strømhaug et al., 2004).

Site-directed mutagenesis analysis of the interaction between yeast Atg2 and Atg18, combined with yeast-two hybrid (Y2H) and co-immunoprecipitation studies, identified blade 2 and the region between blade 2 and 3 (loop 2) as the regions required for the interaction (Watanabe et al., 2012; Rieter et al., 2013). The interaction between mammalian ATG2 and WIPI4 proteins has been investigated by cross-linking mass spectrometry analysis and several lysine residues in blade 1 and blade 3 were found to cross-link to ATG2. In addition, alanine scanning mutagenesis located additional residues important for the interaction in loop 3 (the region between blade 3 and blade 4) (Zheng et al., 2017). These results suggest that the surface of interaction is extensive, which is consistent with results obtained from studies of the interaction between WIPI3 and the WIR (WIPI-interacting region), an ATG2A peptide that interacts with WIPI3. Structural analyses showed that the WIR peptide wraps around WIPI3 and binds to three sites in blades 1, 2, and 3 (Ren et al., 2020). Recently, a different site located on blade 7 has been proposed to be involved in the interaction between yeast Atg18 and Atg2 (Lei et al., 2021).

The interaction of the WIPI protein Atg21 with Atg16 has been characterized by the crystal structure of the yeast Atg16-Atg21 complex (using *K. lactis* Atg21 and *A. gossypii* Atg16). Three consecutive alpha-helical turns in Atg16 form a hydrophobic patch that inserts into a hydrophobic cleft of KIAtg21 between blades 2 and 3 (Munzel et al., 2020).

WIPIs AND DISEASE

Giving the important role of WIPI proteins in autophagy and other membrane-trafficking processes, it is not surprising that they play prominent roles in human health and disease. Indeed, mutations in any of the four WIPI proteins are associated with a variety of diseases affecting the nervous system (**Table 1**). Among these, mutations in WIPI4 have been extensively characterized concerning β-proppeler associated neurodegeneration (BPAN), a disease also referred to as SENDA (static encephalopathy of childhood with neurodegeneration in adulthood) or NBIA5 (neurodegeneration with brain iron accumulation-5). BPAN is an X-linked neurodegenerative disease characterized by developmental delay in early childhood that later progresses to other symptoms such as dystonia, parkinsonism and psychiatric disorders. BPAN is more common in females than in males, who tend to have more severe forms of the disease. The wide spectrum of disease phenotypes associated with WIPI4 mutations probably results from a combination of different factors, including mutation severity, somatic mosaicism and skewed X-chromosome inactivation in females.

TABLE 1 | Missense mutations in WIPI proteins and associated diseases.

	Mutation	Disease*	References
WIPI1	R328Q	ANPH	Wang et al., 2019
	G313R	ANPH	Wang et al., 2019
	T418M	ANPH	Wang et al., 2019
	L406P	ANPH	Wang et al., 2019
WIPI2	V249M	IDDSSA	Jelani et al., 2019
WIPI3	R109Q	IDM	Najmabadi et al., 2011
WIPI4	N61K	BPAN	Haack et al., 2012
	D84G	BPAN	Long et al., 2015
	L98P	BPAN	Haack et al., 2012; Nishioka et al., 2015
	F100S	BPAN	Adang et al., 2020
	N202K	BPAN	Cong et al., 2021
	G205D	BPAN/DEE	Carvill et al., 2018; Chard et al., 2019
	A209D	BPAN	Tschentscher et al., 2015
	S210P	BPAN	Nishioka et al., 2015
	V66E	DEE	Khoury et al., 2019
	R134P	DEE	Chen et al., 2019
	G168E	DEE	Chen et al., 2019
	L160R	EOEE	Russo et al., 2019

BPAN, β-propeller associated neurodegeneration;
DEE, Developmental and epileptic encephalopathy;
EOEE, Early onset epileptic encephalopathies;
ANPH, Anencephaly;
IDDSSA, Intellectual developmental disorder with short stature and variable skeletal anomalies;
IDM, Intellectual disability and microcephaly.
**Nomenclature for WIPI4-related diseases was taken from Cong et al. (2021).*

Most of the mutations reported in WIPI4 are truncations, internal deletions and nonsense mutations that profoundly alter the structure of the protein, probably resulting in loss of function. However, some are missense mutations that result in the substitution of a single amino acid (**Table 1**). These types of mutations can be very informative, as they can point to key residues for the function of specific domains of the protein. This is the case of the BPAN mutations N202K, G205D, A209D, and S210P in WIPI4, which are all located in the PtdIns3P binding domain (Baskaran et al., 2012; Krick et al., 2012; Watanabe et al., 2012), and therefore could potentially alter the correct subcellular localization of the protein (**Figure 4**). In agreement with this hypothesis, the introduction of three of these mutations in the conserved residues of the WIPI4 homolog in *Dictyostelium*, Wdr45l, prevents its localization in autophagic structures. In addition, these mutant proteins do not complement the phenotypic defects of the KO mutant.

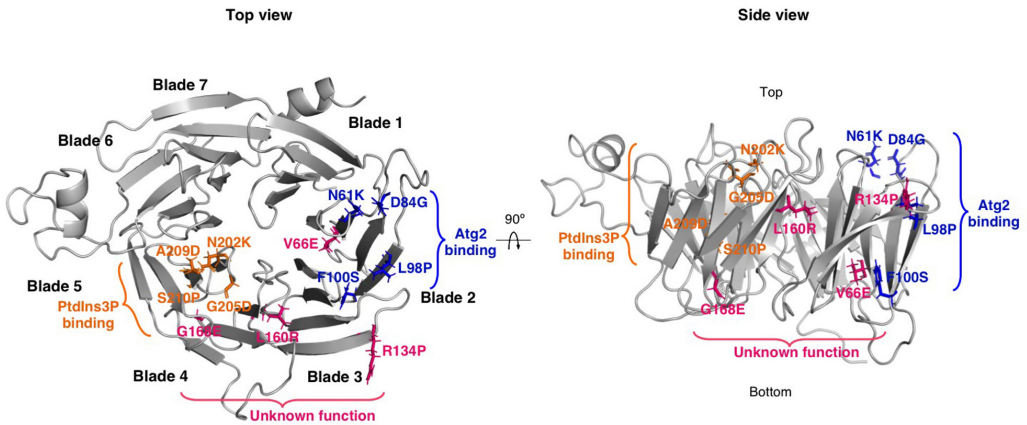

FIGURE 4 | Localization of BPAN missense mutations in the 3D structure of WIPI4. WIPI4 structure was predicted using Robetta (http://robetta.bakerlab.org) based on the structure of WIPI3 (PDB: 6IYY). Top and side views of WIPI4 structure were generated with PyMOL software (The PyMOL Molecular Graphics System, Version 2.4.0 Schrödinger, LLC). Mutated residues localized in the PtdIns3P and ATG2 binding domains are shown as orange and blue sticks, respectively. Other mutated residues are shown as pink sticks.

These findings confirm the effect of these mutations on the localization of the protein during autophagy and the relevance of this localization *in vivo* (Tornero-Écija et al., 2021). Notably, a pathogenic mutation in WIPI2 (V249M) is also located in the PtdIns3P binding domain (Jelani et al., 2019), and is also likely to alter the localization of the protein. In the same line, the pathogenic mutations N61K, D84G, L98P, and F100S are all located in the Atg2 binding region (**Figure 4**) and the introduction of two of these mutations in the conserved residues of WIPI3 prevent binding to the ATG2A WIR sequence (Ren et al., 2020). Consistent with these findings, the introduction of three of these mutations in *Dictyostelium* Wdr45l inactivate the protein but do not alter the normal localization of the protein in autophagosomes (Tornero-Écija et al., 2021). Moreover, a pathogenic mutation in WIPI3 (R109Q) is also located in the ATG2 binding region and this mutation has been shown to impair ATG2A WIR binding (Ren et al., 2020). Finally, in addition to mutations in the PtdIns3P and ATG2A binding domains, other pathogenic missense mutations have been identified in WIPI4 (**Figure 4**). Notably, unlike the mutations described above, these mutations are not associated with BPAN but with other disorders such as developmental and epileptic encephalopathy (DEE) and early onset epileptic encephalopathy (EOEE) (**Table 1**).

The reason for the variety of clinical manifestations associated to WIPI4 mutations (see Cong et al., 2021 for a comprehensive review of the clinical symptoms) is not yet clear and could be due to the influence of genetic and environmental factors.

The severity of the phenotype of the Wdr45l KO in *Dictyostelium* is similar to that observed after expressing Wdr45l with BPAN mutations in the KO strain, suggesting that all these pathogenic mutations greatly affect protein function to the same extent as lack of the protein. This is consistent with the severity of the symptoms of BPAN patients, as no clear difference in severity is observed between missense mutations and those causing truncations or deletions of the protein. One exception is the mutation D84G that has been reported to cause milder symptoms in one patient (Stige et al., 2018). Notably, this mutation, as well as the pathogenic N61K mutation, is located in the ATG2 binding site. However, unlike N61K, D84G leads only to a partial defect in the interaction with ATG2, which could explain the unexpectedly mild phenotype (Bueno-Arribas et al., 2021).

INSIGHTS FROM THE *DICTYOSTELIUM* MODEL IN WIPI4-RELATED DISEASES

KO of Wdr45l, the functional homolog of human WIPI4 in *Dictyostelium*, impairs growth and development in this organism, a phenotype that is remarkably similar to the KO of Vmp1 (Tornero-Écija et al., 2021). Vmp1 is an essential protein in autophagy that is conserved from *Dictyostelium* to humans but is absent in yeast (Calvo-Garrido et al., 2008). Mammalian VMP1 plays an essential role in organellar communication by regulating the function of membrane contact sites (MCS) between the ER and other organelles, including mitochondria, endosomes, peroxisomes and also the phagophore membrane during elongation (Tábara and Escalante, 2016; Zhao et al., 2017). Consistent with this variety of localizations, *Dictyostelium* Vmp1 KO exhibits pleiotropic defects affecting organellar morphology, protein sorting, and autophagy (Calvo-Garrido et al., 2008; Calvo-Garrido and Escalante, 2010). It has been recently proposed that the scramblase activity of VMP1 is essential for lipid trafficking between the ER membrane and the phagophore (Ghanbarpour et al., 2021; Li et al., 2021). The current model predicts that the lack of any of the components involved in lipid trafficking, such as the WIPI-ATG2 complex and the VMP1 and ATG9 scramblases, may lead to similar or related phenotypes. This appears to be the case for *Dictyostelium* Vmp1 and Wdr45l, the absence of which leads to similar phenotypes, including a block in autophagy downstream of Atg8 lipidation and accumulation of PtdIns3P at the autophagosome assembly

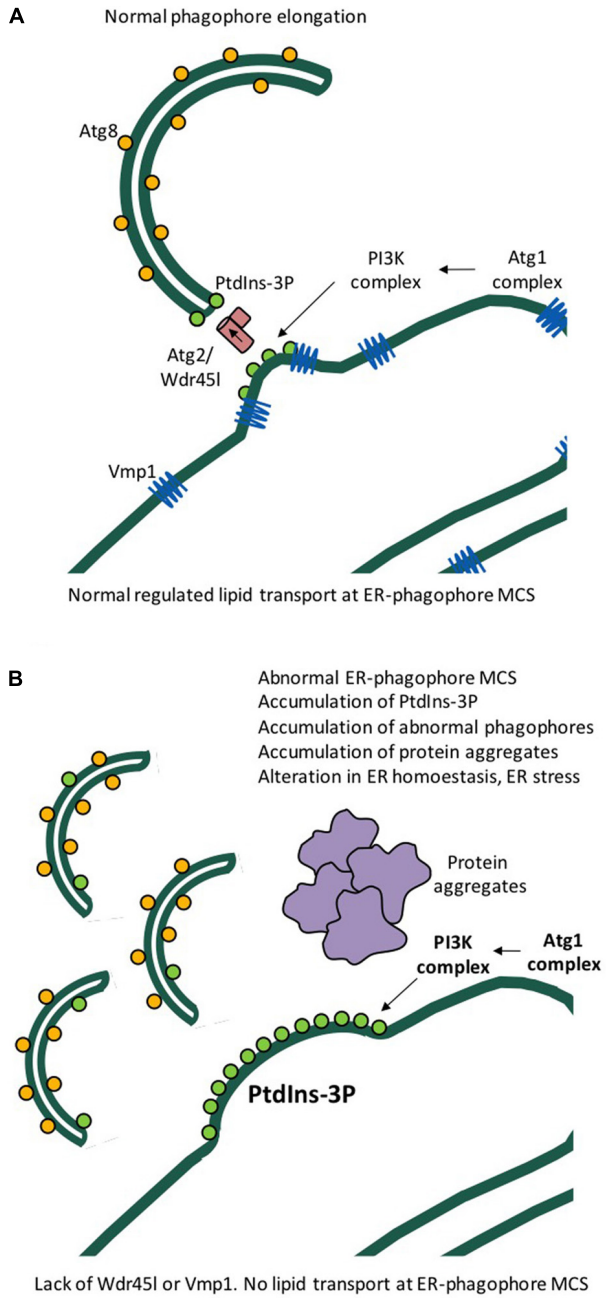

FIGURE 5 | Model of phagophore expansion and the function of *Dictyostelium* Wdr45l and Vmp1. **(A)** Lipid transport and phagophore elongation from the ER occur at membrane contact sites (ER-phagophore MCS) and require Atg2, Wdr45l, and Vmp1. **(B)** Cells deficient in Vmp1 or Wdr45l have similar phenotypes, including the accumulation of PtdIns3P, abnormal autophagic structures, and formation of protein aggregates. Abnormal accumulation of PtdIns3P leads to chronic ER stress and cell growth arrest. These defects are rescued by inhibition of the upstream signaling protein Atg1.

site. This accumulation appears to be responsible for additional phenotypes, including, interestingly, chronic activation of the endoplasmic reticulum (ER) stress response (also known as UPR, unfolded protein response) (**Figure 5**). The UPR is a complex pathway triggered by the accumulation of unfolded proteins that regulates many aspects of cellular physiology and is closely related to neurodegenerative diseases (van Ziel and Scheper, 2020). In *Dictyostelium*, the UPR regulates a gene expression program that inhibits cell growth and global protein synthesis, while activating specific genes encoding proteins that will increase the folding and degradation capacity of cells (Domínguez-Martín et al., 2018a,b). Notably, mutation of the key upstream regulator Atg1 suppresses growth and UPR activation phenotypes by preventing PtdIns3P formation (Tornero-Écija et al., 2021). The possible role of the UPR pathway in BPAN is reinforced by the observation of WIPI4-deficient neurons from a KO mouse showing accumulation of misfolded proteins and activation of the ER-stress response (Wan et al., 2019). If a similar relationship between UPR and abnormal autophagy-associated PtdIns3P occurs in human cells, attenuation of PtdIns3P signaling could be a therapeutic target (**Figure 5**). The *Dictyostelium* model also suggests that mutations in any other component of the lipid transport machinery such as VMP1 and ATG2 could also lead to neurological diseases similar to BPAN.

OPEN QUESTIONS AND FUTURE DIRECTIONS

The function of WIPI proteins is complex and not yet clearly established. Although they are phosphatidylinositol effectors that recognize at least PtdIns3P and PtdIns(3, 5)P2, their interaction with membranes is dictated not only by the presence of the signaling lipid. For example, *Dictyostelium* Atg18 and human WIPI1 are used as autophagic markers because of their localization at autophagic structures, as they seem to preferentially recognize autophagy-associated PtdIns3P despite the abundant presence of PtdIns3P in other cellular locations (Domínguez-Martín et al., 2017; Klionsky et al., 2021). Therefore, it is important to further investigate where and how the different WIPIs localize, and what determinants regulate their localizations. WIPIs interact with many other proteins and it is often unclear whether they act simply to recruit other proteins to particular locations or have a regulatory role as well (Bakula et al., 2017). An example of this second function has been described for WIPI2, which not only recruits but also activates the lipidation machinery (Fracchiolla et al., 2020).

WIPIs appear to have both specific and redundant functions, which further complicates their characterization and the study of their role in disease. Although autophagy appears to play a prominent role in many neurodegenerative diseases, it is unclear whether the cytopathological alterations in WIPI-related diseases are caused by defects in other autophagy-independent processes, such as the ER-stress response pathway. Many basic questions remain to be answered before effective knowledge-based treatments for these incurable diseases are feasible. In this complex scenario, the use of simple models such as yeast and *Dictyostelium* may lead to new avenues of discovery and understanding the function of WIPI proteins in the cell.

AUTHOR CONTRIBUTIONS

OV: bibliographic study and manuscript writing. LA-E, MB-A, and AT-É: revision of the manuscript and figure preparation. M-ÁN: revision of manuscript. RE: coordination, bibliographic study, and manuscript writing. All authors contributed to the article and approved the submitted version.

FUNDING

This work has been supported by the "Ministerio de Ciencia e Innovación," grant no. PGC2018-093604-B-I00 (MCIU/AEI/FEDER,UE). MB-A has been supported by a fellowship from the Spanish "Ministerio de Ciencia, Innovación y Universidades".

REFERENCES

Adang, L. A., Pizzino, A., Malhotra, A., Dubbs, H., Williams, C., Sherbini, O., et al. (2020). Phenotypic and imaging spectrum associated with WDR45. *Pediatric Neurol.* 109, 56–62. doi: 10.1016/j.pediatrneurol.2020.03.005

Araki, T., and Saito, T. (2019). Small molecules and cell differentiation in *Dictyostelium* discoideum. *Int. J. Dev. Biol.* 63, 429–438. doi: 10.1387/ijdb.190192ts

Axe, E. L., Walker, S. A., Manifava, M., Chandra, P., Roderick, H. L., Habermann, A., et al. (2008). Autophagosome formation from membrane compartments enriched in phosphatidylinositol 3-phosphate and dynamically connected to the endoplasmic reticulum. *J. Cell Biol.* 182, 685–701. doi: 10.1083/jcb.200803137

Bakula, D., Mueller, A. J., and Proikas-Cezanne, T. (2018). WIPI β-propellers function as scaffolds for STK11/LKB1-AMPK and AMPK-related kinase signaling in autophagy. *Autophagy* 14, 1082–1083. doi: 10.1080/15548627.2017.1382784

Bakula, D., Müller, A. J., Zuleger, T., Takacs, Z., Franz-Wachtel, M., Thost, A.-K., et al. (2017). WIPI3 and WIPI4 β-propellers are scaffolds for LKB1-AMPK-TSC signalling circuits in the control of autophagy. *Nat. Commun.* 8:15637. doi: 10.1038/ncomms15637

Baskaran, S., Ragusa, M. J., Boura, E., and Hurley, J. H. (2012). Two-site recognition of phosphatidylinositol 3-phosphate by PROPPINs in autophagy. *Mol. Cell* 47, 339–348. doi: 10.1016/j.molcel.2012.05.027

Batsios, P., Gräf, R., Koonce, M. P., Larochelle, D. A., and Meyer, I. (2019). Nuclear envelope organization in Dictyostelium discoideum. *Int. J. Dev. Biol.* 63, 509–519. doi: 10.1387/ijdb.190184rg

Bloomfield, G. (2019). Sex and macrocyst formation in *Dictyostelium*. *Int. J. Dev. Biol.* 63, 439–446. doi: 10.1387/ijdb.190183gb

Bozzaro, S. (2019). The past, present and future of *Dictyostelium* as a model system. *Int. J. Dev. Biol.* 63, 321–331. doi: 10.1387/ijdb.190128sb

Bueno-Arribas, M., Blanca, I., Cruz-Cuevas, C., Escalante, R., Navas, M. A., and Vincent, O. (2021). A conserved ATG2 binding site WIPI4 and yeast Hsv2 is disrupted by mutations causing beta-propeller protein-associated neurodegeneration. *Hum. Mol. Genet.* doi: 10.1093/hmg/ddab227 Epub ahead of print.

Calvo-Garrido, J., Carilla-Latorre, S., Kubohara, Y., Santos-Rodrigo, N., Mesquita, A., Soldati, T., et al. (2010). Autophagy in *Dictyostelium*: genes and pathways, cell death and infection. *Autophagy* 6, 686–701. doi: 10.4161/auto.6.6.12513

Calvo-Garrido, J., Carilla-Latorre, S., Lázaro-Diéguez, F., Egea, G., and Escalante, R. (2008). Vacuole membrane protein 1 is an endoplasmic reticulum protein required for organelle biogenesis, protein secretion, and development. *Mol. Biol. Cell* 19, 3442–3453. doi: 10.1091/mbc.e08-01-0075

Calvo-Garrido, J., and Escalante, R. (2010). Autophagy dysfunction and ubiquitin-positive protein aggregates in *Dictyostelium* cells lacking Vmp1. *Autophagy* 6, 100–109. doi: 10.4161/auto.6.1.10697

Calvo-Garrido, J., King, J. S., Muñoz-Braceras, S., and Escalante, R. (2014). Vmp1 regulates PtdIns3P signaling during autophagosome formation in *Dictyostelium discoideum*. *Traffic* 15, 1235–1246. doi: 10.1111/tra.12210

Carvill, G. L., Liu, A., Mandelstam, S., Schneider, A., Lacroix, A., Zemel, M., et al. (2018). Severe infantile onset developmental and epileptic encephalopathy caused by mutations in autophagy gene WDR45. *Epilepsia* 59, e5–e13. doi: 10.1111/epi.13957

Chard, M., Appendino, J. P., Bello-Espinosa, L. E., Curtis, C., Rho, J. M., Wei, X.-C., et al. (2019). Single-center experience with Beta-propeller protein-associated neurodegeneration (BPAN); expanding the phenotypic spectrum. *Mol. Genet. Metab. Rep.* 20:100483. doi: 10.1016/j.ymgmr.2019.100483

Chen, H., Qian, Y., Yu, S., Xiao, D., Guo, X., Wang, Q., et al. (2019). Early onset developmental delay and epilepsy in pediatric patients with WDR45 variants. *Eur. J. Med. Genet.* 62, 149–160. doi: 10.1016/j.ejmg.2018.07.002

Chowdhury, S., Otomo, C., Leitner, A., Ohashi, K., Aebersold, R., Lander, G. C., et al. (2018). Insights into autophagosome biogenesis from structural and biochemical analyses of the ATG2A-WIPI4 complex. *Proc. Natl. Acad. Sci. U.S.A.* 115, E9792–E9801. doi: 10.1073/pnas.1811874115

Cocorocchio, M., Baldwin, A. J., Stewart, B., Kim, L., Harwood, A. J., Thompson, C. R. L., et al. (2017). Curcumin and derivatives function through protein phosphatase 2A and presenilin orthologues in *Dictyostelium discoideum*. *Dis. Model. Mech.* 11:dmm032375. doi: 10.1242/dmm.032375

Cong, Y., So, V., Tijssen, M. A. J., Verbeek, D. S., Reggiori, F., and Mauthe, M. (2021). WDR45, one gene associated with multiple neurodevelopmental disorders. *Autophagy* 1–16. doi: 10.1080/15548627.2021.1899669 Epub ahead of print.

Consalvo, K. M., Rijal, R., Tang, Y., Kirolos, S. A., Smith, M. R., and Gomer, R. H. (2019). Extracellular signaling in *Dictyostelium*. *Int. J. Dev. Biol.* 63, 395–405. doi: 10.1387/ijdb.190259rg

De Leo, M. G., Berger, P., and Mayer, A. (2021). WIPI1 promotes fission of endosomal transport carriers and formation of autophagosomes through distinct mechanisms. *Autophagy* 1–27. doi: 10.1080/15548627.2021.1886830 Epub ahead of print.

Domínguez-Martín, E., Cardenal-Muñoz, E., King, J., Soldati, T., Coria, R., and Escalante, R. (2017). Methods to monitor and quantify autophagy in the social amoeba *Dictyostelium discoideum*. *Cells* 6:18. doi: 10.3390/cells6030018

Domínguez-Martín, E., Hernández-Elvira, M., Vincent, O., Coria, R., and Escalante, R. (2018a). Unfolding the endoplasmic reticulum of a social amoeba: *dictyostelium discoideum* as a new model for the study of endoplasmic reticulum stress. *Cells* 7:56. doi: 10.3390/cells7060056

Domínguez-Martín, E., Ongay-Larios, L., Kawasaki, L., Vincent, O., Coello, G., Coria, R., et al. (2018b). IreA controls endoplasmic reticulum stress-induced autophagy and survival through homeostasis recovery. *Mol. Cell Biol.* 38, e00054–18. doi: 10.1128/MCB.00054-18

Dooley, H. C., Razi, M., Polson, H. E. J., Girardin, S. E., Wilson, M. I., and Tooze, S. A. (2014). WIPI2 Links LC3 conjugation with PI3P, Autophagosome formation, and pathogen clearance by recruiting Atg12–5-16L1. *Mol. Cell* 55, 238–252. doi: 10.1016/j.molcel.2014.05.021

Dove, S. K., Piper, R. C., McEwen, R. K., Yu, J. W., King, M. C., Hughes, D. C., et al. (2004). Svp1p defines a family of phosphatidylinositol 3,5-bisphosphate effectors. *EMBO J* 23, 1922–1933. doi: 10.1038/sj.emboj.7600203

Escalante, R., and Cardenal-Muñoz, E. (2019). The *Dictyostelium discoideum* model system. *Int. J. Dev. Biol.* 63, 317–320. doi: 10.1387/ijdb.190275re

Farinholt, T., Dinh, C., and Kuspa, A. (2019). Microbiome management in the social amoeba *Dictyostelium discoideum* compared to humans. *Int. J. Dev. Biol.* 63, 447–450. doi: 10.1387/ijdb.190240ak

Fey, P., Dodson, R. J., Basu, S., Hartline, E. C., and Chisholm, R. L. (2019). dictyBase and the dicty stock center (version 2.0) - a progress report. *Int. J. Dev. Biol.* 63, 563–572. doi: 10.1387/ijdb.190226pf

Fischer, S., and Eichinger, L. (2019). *Dictyostelium discoideum* and autophagy – a perfect pair. *Int. J. Dev. Biol.* 63, 485–495. doi: 10.1387/ijdb.190186LE

Fischer, S., Rijal, R., Frommolt, P., Wagle, P., Konertz, R., Faix, J., et al. (2019). Functional characterization of Ubiquitin-like core autophagy protein ATG12 in *Dictyostelium discoideum*. *Cells* 8:72. doi: 10.3390/cells8010072

Fracchiolla, D., Chang, C., Hurley, J. H., and Martens, S. (2020). A PI3K-WIPI2 positive feedback loop allosterically activates LC3 lipidation in autophagy. *J. Cell Biol.* 219:e201912098. doi: 10.1083/jcb.201912098

Geng, J., and Klionsky, D. J. (2008). The Atg8 and Atg12 ubiquitin-like conjugation systems in macroautophagy. *EMBO Rep.* 9, 859–864. doi: 10.1038/embor.2008.163

Ghanbarpour, A., Valverde, D. P., Melia, T. J., and Reinisch, K. M. (2021). A model for a partnership of lipid transfer proteins and scramblases in membrane expansion and organelle biogenesis. *Proc. Natl. Acad. Sci. U.S.A.* 118:e2101562118. doi: 10.1073/pnas.2101562118

Gómez-Sánchez, R., Rose, J., Guimarães, R., Mari, M., Papinski, D., Rieter, E., et al. (2018). Atg9 establishes Atg2-dependent contact sites between the endoplasmic reticulum and phagophores. *J. Cell Biol.* 217, 2743–2763. doi: 10.1083/jcb.201710116

Gubas, A., and Dikic, I. (2021). A guide to the regulation of selective autophagy receptors. *FEBS J.* doi: 10.1111/febs.15824 [Epub ahead of print].

Haack, T. B., Hogarth, P., Kruer, M. C., Gregory, A., Wieland, T., Schwarzmayr, T., et al. (2012). Exome sequencing reveals De Novo WDR45 mutations causing a phenotypically distinct, X-Linked Dominant Form of NBIA. *Am. J. Hum. Genet.* 91, 1144–1149. doi: 10.1016/j.ajhg.2012.10.019

Hindupur, S. K., González, A., and Hall, M. N. (2015). The opposing actions of target of rapamycin and AMP-Activated protein kinase in cell growth control. *Cold Spring Harb. Perspect. Biol.* 7:a019141. doi: 10.1101/cshperspect.a019141

Hurley, J. H., and Young, L. N. (2017). Mechanisms of autophagy initiation. *Annu. Rev. Biochem.* 86, 225–244. doi: 10.1146/annurev-biochem-061516-044820

Ishikawa-Ankerhold, H. C., and Müller-Taubenberger, A. (2019). Actin assembly states in *Dictyostelium discoideum* at different stages of development and during cellular stress. *Int. J. Dev. Biol.* 63, 417–427. doi: 10.1387/ijdb.190256am

Jaiswal, P., Majithia, A. R., Rosel, D., Liao, X.-H., Khurana, T., and Kimmel, A. R. (2019). Integrated actions of mTOR complexes 1 and 2 for growth and development of *Dictyostelium*. *Int. J. Dev. Biol.* 63, 521–527. doi: 10.1387/ijdb.190245ak

Jeffries, T. R., Dove, S. K., Michell, R. H., and Parker, P. J. (2004). PtdIns-specific MPR pathway association of a novel WD40 repeat protein. *WIPI49. MBoC* 15, 2652–2663. doi: 10.1091/mbc.e03-10-0732

Jelani, M., Dooley, H. C., Gubas, A., Mohamoud, H. S. A., Khan, M. T. M., Ali, Z., et al. (2019). A mutation in the major autophagy gene, WIPI2, associated with global developmental abnormalities. *Brain* 142, 1242–1254. doi: 10.1093/brain/awz075

Ji, C., Zhao, H., Chen, D., Zhang, H., and Zhao, Y. G. (2021). β-propeller proteins WDR45 and WDR45B regulate autophagosome maturation into autolysosomes in neural cells. *Curr. Biol.* 31, 1666–1677. doi: 10.1016/j.cub.2021.01.081

Ji, C., Zhao, H., Li, D., Sun, H., Hao, J., Chen, R., et al. (2020). Role of Wdr45b in maintaining neural autophagy and cognitive function. *Autophagy* 16, 615–625. doi: 10.1080/15548627.2019.1632621

Juris, L., Montino, M., Rube, P., Schlotterhose, P., Thumm, M., and Krick, R. (2015). PI3P binding by Atg21 organises Atg8 lipidation. *EMBO J.* 34, 955–973. doi: 10.15252/embj.201488957

Karanasios, E., Walker, S. A., Okkenhaug, H., Manifava, M., Hummel, E., Zimmermann, H., et al. (2016). Autophagy initiation by ULK complex assembly on ER tubulovesicular regions marked by ATG9 vesicles. *Nat. Commun.* 7:12420. doi: 10.1038/ncomms12420

Karow, M., Fischer, S., Meßling, S., Konertz, R., Riehl, J., Xiong, Q., et al. (2020). Functional characterisation of the autophagy ATG12˜5/16 complex in *Dictyostelium discoideum*. *Cells* 9:1179. doi: 10.3390/cells9051179

Kawabe, Y., Du, Q., Schilde, C., and Schaap, P. (2019). Evolution of multicellularity in *Dictyostelia*. *Int. J. Dev. Biol.* 63, 359–369. doi: 10.1387/ijdb.190108ps

Kay, R. R., Williams, T. D., Manton, J. D., Traynor, D., and Paschke, P. (2019). Living on soup: macropinocytic feeding in amoebae. *Int. J. Dev. Biol.* 63, 473–483. doi: 10.1387/ijdb.190220rk

Khoury, J., Kotagal, P., and Moosa, A. N. V. (2019). Epileptic encephalopathy and brain iron accumulation due to WDR45 mutation. *Seizure* 71, 245–246. doi: 10.1016/j.seizure.2019.08.002

Klionsky, D. J., Abdel-Aziz, A. K., Abdelfatah, S., Abdellatif, M., Abdoli, A., Abel, S., et al. (2021). Guidelines for the use and interpretation of assays for monitoring autophagy (4th edition) 1. *Autophagy* 17, 1–382. doi: 10.1080/15548627.2020.1797280

Knecht, D. A., Cooper, K. M., and Moore, J. E. (2019). Teaching a biology laboratory course using *Dictyostelium*. *Int. J. Dev. Biol.* 63, 551–561. doi: 10.1387/ijdb.190249dk

Kotani, T., Kirisako, H., Koizumi, M., Ohsumi, Y., and Nakatogawa, H. (2018). The Atg2-Atg18 complex tethers pre-autophagosomal membranes to the endoplasmic reticulum for autophagosome formation. *Proc. Natl. Acad. Sci. U.S.A.* 115, 10363–10368. doi: 10.1073/pnas.1806727115

Krick, R., Busse, R. A., Scacioc, A., Stephan, M., Janshoff, A., Thumm, M., et al. (2012). Structural and functional characterization of the two phosphoinositide binding sites of PROPPINs, a β-propeller protein family. *Proc. Natl. Acad. Sci. U.S.A.* 109, E2042–E2049. doi: 10.1073/pnas.1205128109

Krick, R., Henke, S., Tolstrup, J., and Thumm, M. (2008). Dissecting the localization and function of Atg18, Atg21 and Ygr223c. *Autophagy* 4, 896–910. doi: 10.4161/auto.6801

Krick, R., and Thumm, M. (2016). Atg8 lipidation is coordinated in a PtdIns3P-dependent manner by the PROPPIN Atg21. *Autophagy* 12, 2260–2261. doi: 10.1080/15548627.2016.1221564

Kundert, P., and Shaulsky, G. (2019). Cellular allorecognition and its roles in Dictyostelium development and social evolution. *Int. J. Dev. Biol.* 63, 383–393. doi: 10.1387/ijdb.190239gs

Kuspa, A., and Shaulsky, G. (2019). (Auto)Biographical reflections on the contributions of William F. Loomis (1940-2016) to Dictyostelium biology. *Int. J. Dev. Biol.* 63, 343–357. doi: 10.1387/ijdb.190224ak

Lahiri, V., Hawkins, W. D., and Klionsky, D. J. (2019). Watch what you (Self-) Eat: autophagic mechanisms that modulate metabolism. *Cell Metab.* 29, 803–826. doi: 10.1016/j.cmet.2019.03.003

Lei, Y., Tang, D., Liao, G., Xu, L., Liu, S., Chen, Q., et al. (2021). The crystal structure of Atg18 reveals a new binding site for Atg2 in Saccharomyces cerevisiae. *Cell. Mol. Life Sci.* 78, 2131–2143. doi: 10.1007/s00018-020-03621-9

Li, Y. E., Wang, Y., Du, X., Zhang, T., Mak, H. Y., Hancock, S. E., et al. (2021). TMEM41B and VMP1 are scramblases and regulate the distribution of cholesterol and phosphatidylserine. *J. Cell Biol.* 220:e202103105. doi: 10.1083/jcb.202103105

Long, M., Abdeen, N., Geraghty, M. T., Hogarth, P., Hayflick, S., and Venkateswaran, S. (2015). Novel WDR45 mutation and pathognomonic BPAN imaging in a young female with mild cognitive delay. *Pediatrics* 136, e714–e717. doi: 10.1542/peds.2015-0750

Lőrincz, P., and Juhász, G. (2019). Autophagosome-Lysosome fusion. *J. Mol. Biol.* 432, 2462–2482. doi: 10.1016/j.jmb.2019.10.028

Lystad, A. H., Carlsson, S. R., de la Ballina, L. R., Kauffman, K. J., Nag, S., Yoshimori, T., et al. (2019). Distinct functions of ATG16L1 isoforms in membrane binding and LC3B lipidation in autophagy-related processes. *Nat. Cell Biol.* 21, 372–383. doi: 10.1038/s41556-019-0274-9

Maeda, S., Otomo, C., and Otomo, T. (2019). The autophagic membrane tether ATG2A transfers lipids between membranes. *Elife* 8:e45777. doi: 10.7554/eLife.45777

Matoba, K., Kotani, T., Tsutsumi, A., Tsuji, T., Mori, T., Noshiro, D., et al. (2020). Atg9 is a lipid scramblase that mediates autophagosomal membrane expansion. *Nat. Struct. Mol. Biol.* 27, 1185–1193. doi: 10.1038/s41594-020-00518-w

Matsuura, A., Tsukada, M., Wada, Y., and Ohsumi, Y. (1997). Apg1p, a novel protein kinase required for the autophagic process in Saccharomyces cerevisiae. *Gene* 192, 245–250. doi: 10.1016/S0378-1119(97)00084-X

Medina, J. M., Shreenidhi, P. M., Larsen, T. J., Queller, D. C., and Strassmann, J. E. (2019). Cooperation and conflict in the social amoeba *Dictyostelium discoideum*. *Int. J. Dev. Biol.* 63, 371–382. doi: 10.1387/ijdb.190158jm

Melia, T. J., Lystad, A. H., and Simonsen, A. (2020). Autophagosome biogenesis: from membrane growth to closure. *J. Cell Biol.* 219:e202002085. doi: 10.1083/jcb.202002085

Mesquita, A., Cardenal-Muñoz, E., Dominguez, E., Muñoz-Braceras, S., Nuñez-Corcuera, B., Phillips, B. A., et al. (2017). Autophagy in *Dictyostelium*?: mechanisms, regulation and disease in a simple biomedical model. *Autophagy* 13, 24–40. doi: 10.1080/15548627.2016.1226737

Mesquita, A., Tábara, L. C., Martinez-Costa, O., Santos-Rodrigo, N., Vincent, O., and Escalante, R. (2015). Dissecting the function of Atg1 complex in *Dictyostelium* autophagy reveals a connection with the pentose phosphate pathway enzyme transketolase. *Open Biol.* 5:150088. doi: 10.1098/rsob.150088

Mizushima, N., and Levine, B. (2020). Autophagy in human diseases. *N. Engl. J. Med.* 383, 1564–1576. doi: 10.1056/NEJMra2022774

Muñoz-Braceras, S., Calvo, R., and Escalante, R. (2015). TipC and the chorea-acanthocytosis protein VPS13A regulate autophagy in *Dictyostelium* and human HeLa cells. *Autophagy* 11, 918–927. doi: 10.1080/15548627.2015.1034413

Munzel, L., Neumann, P., Otto, F. B., Krick, R., Metje-Sprink, J., Kroppen, B., et al. (2020). Atg21 organizes Atg8 lipidation at the contact of the vacuole with the phagophore. *Autophagy* 17, 1458–1478. doi: 10.1080/15548627.2020.1766332

Najmabadi, H., Hu, H., Garshasbi, M., Zemojtel, T., Abedini, S. S., Chen, W., et al. (2011). Deep sequencing reveals 50 novel genes for recessive cognitive disorders. *Nature* 478, 57–63. doi: 10.1038/nature10423

Nanjundiah, V. (2019). Individual and collective behaviour in cellular slime mould development: contributions of John Bonner (1920-2019). *Int. J. Dev. Biol.* 63, 333–342. doi: 10.1387/ijdb.190272vn

Nishimura, T., Tamura, N., Kono, N., Shimanaka, Y., Arai, H., Yamamoto, H., et al. (2017). Autophagosome formation is initiated at phosphatidylinositol synthase-enriched ER subdomains. *EMBO J.* 36, 1719–1735. doi: 10.15252/embj.201695189

Nishioka, K., Oyama, G., Yoshino, H., Li, Y., Matsushima, T., Takeuchi, C., et al. (2015). High frequency of beta-propeller protein-associated neurodegeneration (BPAN) among patients with intellectual disability and young-onset parkinsonism. *Neurobiol. Aging* 36, 2004.e9–e2004.e15. doi: 10.1016/j.neurobiolaging.2015.01.020

Obara, K., Sekito, T., Niimi, K., and Ohsumi, Y. (2008). The Atg18-Atg2 complex is recruited to autophagic membranes via phosphatidylinositol 3-phosphate and exerts an essential function. *J. Biol. Chem.* 283, 23972–23980. doi: 10.1074/jbc.M803180200

Osawa, T., Ishii, Y., and Noda, N. N. (2020). Human ATG2B possesses a lipid transfer activity which is accelerated by negatively charged lipids and WIPI4. *Genes Cells* 25, 65–70. doi: 10.1111/gtc.12733

Osawa, T., Kotani, T., Kawaoka, T., Hirata, E., Suzuki, K., Nakatogawa, H., et al. (2019). Atg2 mediates direct lipid transfer between membranes for autophagosome formation. *Nat. Struct. Mol. Biol.* 26, 281–288. doi: 10.1038/s41594-019-0203-4

Otto, G. P., Wu, M. Y., Kazgan, N., Anderson, O. R., and Kessin, R. H. (2003). Macroautophagy is required for multicellular development of the social amoeba *Dictyostelium discoideum*. *J. Biol. Chem.* 278, 17636–17645. doi: 10.1074/jbc.M212467200

Otto, G. P., Wu, M. Y., Kazgan, N., Anderson, O. R., and Kessin, R. H. (2004). *Dictyostelium* macroautophagy mutants vary in the severity of their developmental defects. *J. Biol. Chem.* 279, 15621–15629. doi: 10.1074/jbc.M311139200

Pal, D. S., Li, X., Banerjee, T., Miao, Y., and Devreotes, P. N. (2019). The excitable signal transduction networks: movers and shapers of eukaryotic cell migration. *Int. J. Dev. Biol.* 63, 407–416. doi: 10.1387/ijdb.190265pd

Papinski, D., Schuschnig, M., Reiter, W., Wilhelm, L., Barnes, C. A., Maiolica, A., et al. (2014). Early steps in autophagy depend on direct phosphorylation of Atg9 by the Atg1 Kinase. *Mol. Cell* 53, 471–483. doi: 10.1016/j.molcel.2013.12.011

Pearce, X. G., Annesley, S. J., and Fisher, P. R. (2019). The Dictyostelium model for mitochondrial biology and disease. *Int. J. Dev. Biol.* 63, 497–508. doi: 10.1387/ijdb.190233pf

Pergolizzi, B., Bozzaro, S., and Bracco, E. (2019). Dictyostelium as model for studying ubiquitination and deubiquitination. *Int. J. Dev. Biol.* 63, 529–539. doi: 10.1387/ijdb.190260eb

Perry, C. J., Finch, P., Müller-Taubenberger, A., Leung, K., Warren, E. C., Damstra-Oddy, J., et al. (2020). A new mechanism for cannabidiol in regulating the one-carbon cycle and methionine levels in DICTYOSTELIUM and in mammalian epilepsy models. *Br. J. Pharmacol.* 177, 912–928. doi: 10.1111/bph.14892

Polson, H. E. J., de Lartigue, J., Rigden, D. J., Reedijk, M., Urbé, S., Clague, M. J., et al. (2010). Mammalian Atg18 (WIPI2) localizes to omegasome-anchored phagophores and positively regulates LC3 lipidation. *Autophagy* 6, 506–522. doi: 10.4161/auto.6.4.11863

Proikas-Cezanne, T., Takacs, Z., Donnes, P., and Kohlbacher, O. (2015). WIPI proteins: essential PtdIns3P effectors at the nascent autophagosome. *J. Cell Sci.* 128, 207–217. doi: 10.1242/jcs.146258

Raper, K. B. (1935). *Dictyostelium discoideum*, a new species of slime mold from decaying forest leaves. *J. Agric. Res.* 50, 135–147.

Ren, J., Liang, R., Wang, W., Zhang, D., Yu, L., and Feng, W. (2020). Multi-site-mediated entwining of the linear WIR-motif around WIPI β-propellers for autophagy. *Nat. Commun.* 11:2702. doi: 10.1038/s41467-020-16523-y

Rieter, E., Vinke, F., Bakula, D., Cebollero, E., Ungermann, C., Proikas-Cezanne, T., et al. (2013). Atg18 function in autophagy is regulated by specific sites within its β-propeller. *J. Cell. Sci.* 126, 593–604. doi: 10.1242/jcs.115725

Russo, C., Ardissone, A., Freri, E., Gasperini, S., Moscatelli, M., Zorzi, G., et al. (2019). Substantia Nigra swelling and dentate nucleus T2 hyperintensity may be early magnetic resonance imaging signs of β-propeller protein-associated neurodegeneration: early MRI Features in 4 Cases of BPAN. *Mov. Disord. Clin. Pract.* 6, 51–56. doi: 10.1002/mdc3.12693

Sawa-Makarska, J., Baumann, V., Coudevylle, N., von Bülow, S., Nogellova, V., Abert, C., et al. (2020). Reconstitution of autophagosome nucleation defines Atg9 vesicles as seeds for membrane formation. *Science* 369:eaaz7714. doi: 10.1126/science.aaz7714

Schaf, J., Damstra-Oddy, J., and Williams, R. S. B. (2019). *Dictyostelium discoideum* as a pharmacological model system to study the mechanisms of medicinal drugs and natural products. *Int. J. Dev. Biol.* 63, 541–550. doi: 10.1387/ijdb.190228rw

Scott, S. V., Hefner-Gravink, A., Morano, K. A., Noda, T., Ohsumi, Y., and Klionsky, D. J. (1996). Cytoplasm-to-vacuole targeting and autophagy employ the same machinery to deliver proteins to the yeast vacuole. *Proc. Natl. Acad. Sci. U.S.A.* 93, 12304–12308. doi: 10.1073/pnas.93.22.12304

Sharma, D., Otto, G., Warren, E. C., Beesley, P., King, J. S., and Williams, R. S. B. (2019). Gamma secretase orthologs are required for lysosomal activity and autophagic degradation in *Dictyostelium discoideum*, independent of PSEN (presenilin) proteolytic function. *Autophagy* 15, 1407–1418. doi: 10.1080/15548627.2019.1586245

Slobodkin, M. R., and Elazar, Z. (2013). The Atg8 family: multifunctional ubiquitin-like key regulators of autophagy. *Essays Biochem.* 55, 51–64. doi: 10.1042/bse0550051

Stige, K. E., Gjerde, I. O., Houge, G., Knappskog, P. M., and Tzoulis, C. (2018). Beta-propeller protein-associated neurodegeneration: a case report and review of the literature. *Clin. Case Rep.* 6, 353–362. doi: 10.1002/ccr3.1358

Strømhaug, P. E., Reggiori, F., Guan, J., Wang, C.-W., and Klionsky, D. J. (2004). Atg21 is a phosphoinositide binding protein required for efficient lipidation and localization of Atg8 during uptake of aminopeptidase I by selective autophagy. *Mol. Biol. Cell* 15, 3553–3566. doi: 10.1091/mbc.e04-02-0147

Tábara, L.-C., and Escalante, R. (2016). VMP1 establishes ER-Microdomains that regulate membrane contact sites and autophagy. *PLoS One* 11:e0166499. doi: 10.1371/journal.pone.0166499

Tornero-Écija, A., Tábara, L., Bueno-Arribas, M., Antón-Esteban, L., Navarro-Gómez, C., Sánchez, I., et al. (2021). A *Dictyostelium* model for BPAN disease reveals a functional relationship between the WDR45/WIPI4 homolog Wdr45l and Vmp1 in the regulation of autophagy-associated PtdIns3P and ER stress. *Autophagy* doi: 10.1080/15548627.2021.1953262 Epub ahead of print.

Tschentscher, A., Dekomien, G., Ross, S., Cremer, K., Kukuk, G. M., Epplen, J. T., et al. (2015). Analysis of the C19orf12 and WDR45 genes in patients with neurodegeneration with brain iron accumulation. *J. Neurol. Sci.* 349, 105–109. doi: 10.1016/j.jns.2014.12.036

Tsukada, M., and Ohsumi, Y. (1993). Isolation and characterization of autophagy-defective mutants of Saccharomyces cerevisiae. *FEBS Lett.* 333, 169–174. doi: 10.1016/0014-5793(93)80398-E

Tung, S. M., Unal, C., Ley, A., Peña, C., Tunggal, B., Noegel, A. A., et al. (2010). Loss of *Dictyostelium* ATG9 results in a pleiotropic phenotype affecting growth, development, phagocytosis and clearance and replication of *Legionella pneumophila*. *Cell. Microbiol.* 12, 765–780. doi: 10.1111/j.1462-5822.2010.01432.x

Valverde, D. P., Yu, S., Boggavarapu, V., Kumar, N., Lees, J. A., Walz, T., et al. (2019). ATG2 transports lipids to promote autophagosome biogenesis. *J. Cell Biol.* 218, 1787–1798. doi: 10.1083/jcb.201811139

van Ziel, A. M., and Scheper, W. (2020). The UPR in neurodegenerative disease: not just an inside job. *Biomolecules* 10:1090. doi: 10.3390/biom10081090

Vines, J. H., and King, J. S. (2019). The endocytic pathways of *Dictyostelium discoideum*. *Int. J. Dev. Biol.* 63, 461–471. doi: 10.1387/ijdb.190236jk

Wan, H., Wang, Q., Chen, X., Zeng, Q., Shao, Y., Fang, H., et al. (2019). WDR45 contributes to neurodegeneration through regulation of ER homeostasis

and neuronal death. *Autophagy* 16, 531–547. doi: 10.1080/15548627.2019.1630224

Wang, L., Ren, A., Tian, T., Li, N., Cao, X., Zhang, P., et al. (2019). Whole-exome sequencing identifies damaging de novo variants in anencephalic cases. *Front. Neurosci.* 13:1285. doi: 10.3389/fnins.2019.01285

Warren, E. C., Dooves, S., Lugarà, E., Damstra-Oddy, J., Schaf, J., Heine, V. M., et al. (2020). Decanoic acid inhibits mTORC1 activity independent of glucose and insulin signaling. *Proc. Natl. Acad. Sci. U.S.A.* 117, 23617–23625. doi: 10.1073/pnas.2008980117

Watanabe, Y., Kobayashi, T., Yamamoto, H., Hoshida, H., Akada, R., Inagaki, F., et al. (2012). Structure-based analyses reveal distinct binding sites for Atg2 and phosphoinositides in Atg18. *J. Biol. Chem.* 287, 31681–31690. doi: 10.1074/jbc.M112.397570

Xiong, Q., Li, W., Li, P., Yang, M., Wu, C., and Eichinger, L. (2018). The role of ATG16 in autophagy and the ubiquitin proteasome system. *Cells* 8:2. doi: 10.3390/cells8010002

Xiong, Q., Ünal, C., Matthias, J., Steinert, M., and Eichinger, L. (2015). The phenotypes of ATG9, ATG16 and ATG9/16 knock-out mutants imply autophagy-dependent and -independent functions. *Open Biol.* 5:150008. doi: 10.1098/rsob.150008

Yamada, Y., and Schaap, P. (2019). Cyclic AMP induction of *Dictyostelium* prespore gene expression requires autophagy. *Dev. Biol.* 452, 114–126. doi: 10.1016/j.ydbio.2019.04.017

Yamada, Y., and Schaap, P. (2020). The proppin Bcas3 and its interactor KinkyA localize to the early phagophore and regulate autophagy. *Autophagy* 17, 640–655. doi: 10.1080/15548627.2020.1725403

Yamaguchi, H., Honda, S., Torii, S., Shimizu, K., Katoh, K., Miyake, K., et al. (2020). Wipi3 is essential for alternative autophagy and its loss causes neurodegeneration. *Nat. Commun.* 11:5311. doi: 10.1038/s41467-020-18892-w

Zhao, Y. G., Chen, Y., Miao, G., Zhao, H., Qu, W., Li, D., et al. (2017). The ER-Localized Transmembrane protein EPG-3/VMP1 regulates SERCA activity to control ER-Isolation membrane contacts for autophagosome formation. *Mol. Cell* 67, 974–989.e6. doi: 10.1016/j.molcel.2017.08.005

Zhao, Y. G., Liu, N., Miao, G., Chen, Y., Zhao, H., and Zhang, H. (2018). The ER contact proteins VAPA/B interact with multiple autophagy proteins to modulate autophagosome biogenesis. *Curr. Biol.* 28, 1234.e–1245.e. doi: 10.1016/j.cub.2018.03.002

Zheng, J.-X., Li, Y., Ding, Y.-H., Liu, J.-J., Zhang, M.-J., Dong, M.-Q., et al. (2017). Architecture of the ATG2B-WDR45 complex and an aromatic Y/HF motif crucial for complex formation. *Autophagy* 13, 1870–1883. doi: 10.1080/15548627.2017.1359381

Conflict of Interest: The authors declare that the research was conducted in the absence of any commercial or financial relationships that could be construed as a potential conflict of interest.

Publisher's Note: All claims expressed in this article are solely those of the authors and do not necessarily represent those of their affiliated organizations, or those of the publisher, the editors and the reviewers. Any product that may be evaluated in this article, or claim that may be made by its manufacturer, is not guaranteed or endorsed by the publisher.

Copyright © 2021 Vincent, Antón-Esteban, Bueno-Arribas, Tornero-Écija, Navas and Escalante. This is an open-access article distributed under the terms of the Creative Commons Attribution License (CC BY). The use, distribution or reproduction in other forums is permitted, provided the original author(s) and the copyright owner(s) are credited and that the original publication in this journal is cited, in accordance with accepted academic practice. No use, distribution or reproduction is permitted which does not comply with these terms.

frontiers in Cell and Developmental Biology

ORIGINAL RESEARCH
published: 06 September 2021
doi: 10.3389/fcell.2021.741662

Interactions and Cytotoxicity of Human Neurodegeneration-Associated Proteins Tau and α-Synuclein in the Simple Model *Dictyostelium discoideum*

Katelyn Mroczek, Sanjanie Fernando, Paul R. Fisher and Sarah J. Annesley*

Department of Physiology, Anatomy and Microbiology, La Trobe University, Bundoora, VIC, Australia

The abnormal accumulation of the tau protein into aggregates is a hallmark in neurodegenerative diseases collectively known as tauopathies. In normal conditions, tau binds off and on microtubules aiding in their assembly and stability dependent on the phosphorylation state of the protein. In disease-affected neurons, hyperphosphorylation leads to the accumulation of the tau protein into aggregates, mainly neurofibrillary tangles (NFT) which have been seen to colocalise with other protein aggregates in neurodegeneration. One such protein is α-synuclein, the main constituent of Lewy bodies (LB), a hallmark of Parkinson's disease (PD). In many neurodegenerative diseases, including PD, the colocalisation of tau and α-synuclein has been observed, suggesting possible interactions between the two proteins. To explore the cytotoxicity and interactions between these two proteins, we expressed full length human tau and α-synuclein in *Dictyostelium discoideum* alone, and in combination. We show that tau is phosphorylated in *D. discoideum* and colocalises closely (within 40 nm) with tubulin throughout the cytoplasm of the cell as well as with α-synuclein at the cortex. Expressing wild type α-synuclein alone caused inhibited growth on bacterial lawns, phagocytosis and intracellular *Legionella* proliferation rates, but activated mitochondrial respiration and non-mitochondrial oxygen consumption. The expression of tau alone impaired multicellular morphogenesis, axenic growth and phototaxis, while enhancing intracellular *Legionella* proliferation. Direct respirometric assays showed that tau impairs mitochondrial ATP synthesis and increased the "proton leak," while having no impact on respiratory complex I or II function. In most cases depending on the phenotype, the coexpression of tau and α-synuclein exacerbated (phototaxis, fruiting body morphology), or reversed (phagocytosis, growth on plates, mitochondrial respiratory function, *Legionella* proliferation) the defects caused by either tau or α-synuclein expressed individually. Proteomics data revealed distinct patterns of dysregulation in strains ectopically expressing tau or α-synuclein or both, but down regulation of expression of cytoskeletal proteins was apparent in all three groups and most evident in the strain expressing both proteins. These results indicate that tau and α-synuclein exhibit different but overlapping patterns of intracellular localisation, that they individually

OPEN ACCESS

Edited by:
Robin S. B. Williams, University of London, United Kingdom

Reviewed by:
Xuehua Xu, National Institute of Allergy and Infectious Diseases, National Institutes of Health (NIH), United States
Richard H. Gomer, Texas A&M University, United States

***Correspondence:**
Sarah J. Annesley
S.Annesley@latrobe.edu.au

Specialty section:
This article was submitted to Molecular and Cellular Pathology, a section of the journal Frontiers in Cell and Developmental Biology

Received: *15 July 2021*
Accepted: *19 August 2021*
Published: *06 September 2021*

Citation:
Mroczek K, Fernando S, Fisher PR and Annesley SJ (2021) Interactions and Cytotoxicity of Human Neurodegeneration-Associated Proteins Tau and α-Synuclein in the Simple Model Dictyostelium discoideum. Front. Cell Dev. Biol. 9:741662. doi: 10.3389/fcell.2021.741662

exert distinct but overlapping patterns of cytotoxic effects and that they interact, probably physically in the cell cortex as well as directly or indirectly in affecting some phenotypes. The results show the efficacy of using *D. discoideum* as a model to study the interaction of proteins involved in neurodegeneration.

Keywords: tau, α-synuclein, *Dictyostelium*, tauopathies, Alzheimer's disease

INTRODUCTION

Neurodegenerative diseases are the leading cause of disability worldwide and as the population ages they are expected to increase in their prevalence. The WHO estimate that collectively neurological disorders will eclipse cancer as the second leading cause of death worldwide by 2040 (Gammon, 2014). The most common neurodegenerative disease is Alzheimer's disease (AD) in which the hallmarks like other neurodegenerative diseases are the accumulation of aggregated proteins. In AD, first described by Alois Alzheimer in 1906, the most abundant aggregated proteins are tau and amyloid beta (Stelzmann et al., 1995). The accumulation of the tau protein is present as the dominant aggregate in a group of neurodegenerative diseases known as tauopathies with AD being the most common tauopathy. However, tau aggregation is also implicated in other diseases including Pick's disease, Cortico-basal degeneration, Progressive supranuclear palsy and Fronto-temporal dementia with Parkinsonism linked to chromosome 17 (Spillantini and Goedert, 1998; Lee et al., 2001; Goedert and Spillantini, 2011).

Tau is a major mammalian microtubule associated protein (MAP), and in humans it is predominantly found in the neurons (Drubin and Kirschner, 1986). The protein binds to tubulin promoting the assembly and stability of microtubules, supporting axonal transport and structure of neurons (Cleveland et al., 1977; Kosik, 1993). Tau is encoded by the MAPT gene, is 100 kb in size containing 16 exons. Alternative splicing of the RNA transcript at exons 2, 3, and 10 produces six isoforms (Andreadis et al., 1992), which range from 352 to 441 amino acids in length containing either 3 or 4 microtubule binding repeat sequences (Goedert et al., 1989a,b; Himmler et al., 1989). The tau protein contains an acidic N terminal region known as the projection domain, thought to maintain space between microtubules as well as interacting with other cytoskeletal proteins (Avila et al., 2004; Mandelkow et al., 2007). The proline rich middle of the protein binds other proteins and the C terminal contains the microtubule binding domain (MTBD), with either 3 or 4 repeats dependent on the presence or absence of exon 10 (Mandelkow et al., 2007). Four-repeat (4R) tau binds with a higher affinity to microtubules than 3R tau. The longest tau isoform (2N4R) contains both exons 2 and 3 in the N terminus and 4 repeats in the MTBD.

In normal conditions tau binds on and off microtubules depending on the phosphorylation state of the protein. On the 2N4R isoform there have been over 80 phosphorylation sites detected with the majority of these implicated in pathological conditions (Buée et al., 2000; Hanger et al., 2007). Dephosphorylation of tau induces the affinity to bind to MT while phosphorylation leads to a disassociation with MT (Cleveland et al., 1977; Lindwall and Cole, 1984). The further hyperphosphorylation of tau stimulates the accumulation of the protein into aggregates. There are many tau aggregate conformations but the most commonly observed is neurofibrillary tangles (NFT) composed of paired helical filaments (Grundke-Iqbal et al., 1986). Tangles of tau have been pathologically implicated in Alzheimer's disease, Parkinson's disease (PD), Down's syndrome, Parkinsonism–dementia complex of Guam, and progressive supranuclear palsy (Joachim et al., 1987).

The toxic aggregation of tau in diseases like AD, PD, and other tauopathies seems to coincide with mitochondrial impairment associated with transport, dynamics and bioenergetics of the mitochondria (reviewed by Gibson et al., 2010; Eckert et al., 2011; Cabezas-Opazo et al., 2015; Pérez et al., 2018a). Mitochondrial abnormalities include impaired oxidative phosphorylation in a mouse model of AD (Rhein et al., 2009) and impaired mitochondrial dynamics by truncated tau in immortalised cortical neurons and primary cortical neurons from tau knockout mice (Pérez et al., 2018b). The overexpression of tau in neuronal cultures decreased ATP production, the ratio of ATP/ADP and inhibited Complex I activity (Li et al., 2016) and it has been suggested that tau impairs mitochondrial function while simultaneously inhibiting the degradation of damaged mitochondria leading to a cycle of mitochondrial dysfunction (Cummins et al., 2019).

Aggregation and mitochondrial dysfunction are hallmarks of many neurodegenerative diseases. Within the large group of tauopathies the accumulation of proteins other than tau is evident. One such protein is α-synuclein. α-synuclein is encoded by the *SNCA* gene, is 140 amino acids in length and like tau is richly expressed in neurons. Aggregation of α-synuclein and its presence as the dominant protein in Lewy bodies (LB) is a hallmark of a group of neurodegenerative diseases classified as the synucleinopathies. PD is the most common synucleinopathy but other diseases include Lewy Body Dementia, multiple system atrophy, and Parkinsonism with dementia (Galpern and Lang, 2006; Savica et al., 2013). α-Synuclein is the most abundant aggregated protein in these disorders although other proteins like tau have been seen to colocalise within these aggregates as well suggesting an overlap of the tau- and synuclein-opathies.

There have been many neurodegenerative diseases in which tau and α-synuclein have been found to coexist, and several lines of evidence suggest an interaction between the two proteins. Colocalisation of tau and α-synuclein has been seen in both NFT and LB (Arima et al., 2000; Ishizawa et al., 2003). α-synuclein containing LB were seen to be present in AD brains over 50% of the time (Hamilton, 2000), in Down's syndrome brains with AD 50% of the time (Lippa et al., 1999) and found with PHF of tau in the same neurons (Iseki et al., 1999). The C-terminus

of α-synuclein has been seen to bind to the MT Binding Domain of tau promoting phosphorylation by protein-kinase A (Jensen et al., 1999). *In vitro* experiments using human cell lines have shown that tau and α-synuclein can promote the aggregation of each other and increase cytotoxicity (Badiola et al., 2011; Castillo-Carranza et al., 2018). The application of models to study the interaction of the proteins has proved useful and support an interaction. A transgenic mouse model of PD overexpressing α-synuclein increased tau phosphorylation and hyperphosphorylation and aggregates similar to LB were formed containing both tau and α-synuclein (Haggerty et al., 2011). In *Drosophila*, neurotoxic symptoms were enhanced with the coexpression of both proteins compared to when tau or α-synuclein were expressed individually (Roy and Jackson, 2014). In yeast models, the coexpression enhanced aggregation of the proteins, increased phosphorylation of tau and produced toxic effects (Zabrocki et al., 2005; Ciaccioli et al., 2013).

There are many models of tauopathies and using simple models to study complex disease mechanisms has its advantages. *Dictyostelium discoideum* is a novel eukaryotic model organism recognised by the National Institute of Health (NIH) in the United States for its importance in biomedical research. It has been used as a biomedical model for studying human diseases including neurodegeneration, lysosomal trafficking disorders and mitochondrial disease (Annesley and Fisher, 2009a; Francione et al., 2011; Maniak, 2011; Martín-González et al., 2021). The complete nuclear (Eichinger et al., 2005) and also mitochondrial (Ogawa et al., 2000) genomes have been sequenced, allowing for orthologues of human genes to be studied. Of interest is the distinctive life cycle of *D. discoideum* in which there are both unicellular and multicellular stages with numerous cell types. This allows diverse, reproducible phenotypic traits to serve as "readouts" of disease gene-related disturbances in cellular processes and the signalling pathways that control them (Annesley and Fisher, 2009a). Additionally, *D. discoideum* is greatly accessible for use in biomedical research, genetically manipulable and easily grown clonally. Mitochondrial disease has been created and well characterised in *D. discoideum*. Through the knockdown of nuclear encoded mitochondrial proteins or disrupting mitochondrial genes, a clear set of phenotypes was exhibited in each case (reviewed by Francione and Fisher, 2011). Among these phenotypes were: decreased growth on bacterial lawns and in axenic medium, aberrant fruiting body with shorter and thicker stalks, defective slug phototaxis and increased susceptibility to *Legionella* proliferation. These mitochondrially diseased *D. discoideum* phenotypes were attributed to the chronic activation of the energy sensing protein AMP-activated protein kinase (AMPK) by Bokko et al. (2007) and Francione et al. (2009) that showed when AMPK was knocked down by antisense inhibition, the defective phenotypes returned to wildtype levels, and chronic activation of AMPK mimicked the disease phenotypes.

Previously we showed that human α-synuclein can be expressed in *D. discoideum* and has effects on plaque expansion rates, phagocytosis, and PD associated mutations impaired phototaxis. These impaired phenotypes were rescued or partially rescued with the coexpression of an AMPK antisense construct. Suggesting that mitochondrial dysfunction may be attributing to at least some of the defective phenotypes. However, when mitochondrial function was directly measured, α-synuclein displayed an increased mitochondrial respiration rather than a dysfunction (Fernando et al., 2020). This was in line with other PD models in which mitochondrial respiration was seen to be increased including α-synuclein fibrils in neuroblastoma cells (Ugalde et al., 2020), lymphoblast cell lines made from idiopathic PD patients (iPD) (Annesley et al., 2016) and fibroblasts from iPD patients (Haylett et al., 2016). Here we expressed the longest human tau isoform to create a *D. discoideum* model of tauopathies. *D. discoideum* has already been used as a model to study elements involved in AD. Orthologues of the presenilin proteins and other γ secretase subunits that cause the cleavage of amyloid precursor protein (APP) to Aβ have been identified in *D. discoideum* and have similar functionality to the mammalian complex (McMains et al., 2010; Ludtmann et al., 2014). Mutations in the presenilin genes have been known to cause early-onset familial AD (De Strooper and Annaert, 2010). In *D. discoideum*, the knockout of the presenilin genes resulted in a developmental block in aggregation, which was restored with the expression of human presenilin 1 (Ludtmann et al., 2014). Also importantly, *D. discoideum* was seen to process ectopically expressed human APP to the amyloid-β peptides $A\beta_{40}$ and $A\beta_{42}$, while in strains that were deficient in γ secretase this APP processing was blocked (McMains et al., 2010). As is the case with APP, there are no homologues of tau in *D. discoideum,* but many of the proteins that interact with tau have been evolutionarily conserved such as the kinases AMPK and glycogen synthase kinase 3 (GSK3) as well as cytoskeletal proteins tubulin and filamin. This allows the study of the cytotoxic effects of tau directly without the complication of the endogenously expressed protein or homologue.

As there is evidence of an interaction of tau and α-synuclein in neurodegeneration, we also coexpressed human tau and human α-synuclein together to compare to the phenotypes displayed by expressing tau and α-synuclein alone. Tau caused phenotypes similar to those of mitochondrially diseased strains and direct measurements of mitochondrial activity showed a decrease in ATP synthesis. We show here that *D. discoideum* is a viable model to study tauopathies as tau is cytotoxic, can be phosphorylated and is readily coexpressed with other neurodegenerative proteins. The coexpression of human tau and human α-synuclein in this work revealed physical and functional interactions between the two proteins that enhance or reverse their individual cytotoxic effects.

MATERIALS AND METHODS

Dictyostelium Strains and Culture Conditions

Wildtype (AX2) and transformed *D. discoideum* strains were grown both axenically and on SM agar plates. Axenically, strains were shaken at 150 rpm at 21°C in HL5 medium containing glucose (Formedium, Hunstanton, Norfolk, United Kingdom),

with the addition of 20 μg mL^{-1} geneticin (G418—Thermo Fisher Scientific, Waltham, MA, United States) for transformed strains. They were also grown on SM agar plates (Formedium, Hunstanton, Norfolk, United Kingdom), with *Enterobacter aerogenes* as a food source and supplemented with G418 for transformants. The transformants expressed either human tau (containing plasmid construct pPROF665), human α-synuclein (containing plasmid pPROF629) or were cotransformants expressing both tau and α-synuclein.

Plasmid Construction

The human tau gene was PCR amplified using a commercially purchased plasmid template tau/pET29b (Addgene plasmid # 16316) containing a cloned copy of the full-length human tau gene (2N4R). Primers Tau2F (CG**A TCG ATA** TGG CTG AGC CCC GC) and Tau2R (CG**C TCG AG**T CAC AAA CCC TGC TTG GC) synthesised by Gene Works Ltd., incorporated *Xho*I (Promega, Madison, WI, United States) and *Cla*I (Promega, Madison, WI, United States) restriction sites and was initially cloned into the *Escherichia coli* vector pCR®2.1-TOPO (Thermo Fisher, Waltham, MA, United States, A32728) to produce pPROF664. Subsequently, the Tau insert was subcloned into a *D. discoideum* expression vector by replacing the existing tetracycline cassette in pPROF267. The resultant clone was called pPROF665. The construction of the α-synuclein construct (pPROF629) has been described previously (Fernando et al., 2020).

Transformation

The transformation of AX2 cells was performed using the calcium phosphate DNA coprecipitation method (Nellen et al., 1984) with 20 μg of construct DNA. Transformants were selected for on SM agar plates containing 20 μg mL^{-1} G418 and a lawn of *Micrococcus luteus* (Wilczynska and Fisher, 1994), the purified transformants were maintained by subculturing in HL5 medium and onto lawns of *E. aerogenes.*

Quantitative PCR

To quantify the construct copy number in the transformants, quantitative PCR was performed using iQ SYBR Green supermix and an iCycler IQ Multicolor Real-Time PCR Detection system according to manufacturer's instructions (Bio-Rad, Hercules, CA, United States). The primers used for amplification of a portion of each gene were RTTauF (AAGAGCACTCCAACAGCGGAAGAT) and RTTauR (GTGTCTCCAATGCCTGCTTCTTCA) for tau, and for the α-synuclein gene RTsynF (GCGCTCTAGAATCGATATGGATGTATTCATGAAAGGACT TTCAAAGGCC) and RTsynR (GCGCTCTAGACTCGAGTT AAGGATCCACAGGCATATCTTCCAGAATTCC). The filamin gene was amplified and used as loading control, as it is a single copy gene, and amplified using the primers Fil443For (CCACAGAGATATTGGAGTTGCGTACC) and Fil552Rev (CAACTCAACCAATGTGCCTGCCAA). Two calibration curves were prepared, one to estimate loading using genomic DNA of the wildtype AX2 and the filamin primers to estimate the total quantity of genomic DNA, and the second using purified plasmids to determine the quantity of inserted plasmid constructs. Copy numbers of the inserted constructs for each strain were calculated based on the quantity of the construct, the quantity of gDNA and the sizes (in base pairs) of the amplified fragment and the *Dictyostelium* genome. The copy numbers were then normalised against the copy number of the control AX2 parental strain.

Western Blotting

An aliquot of 1×10^7 cells of either tau or cotransformant strains as well as the WT were pelleted, supernatant removed and the pellet resuspended in 75 μL of Laemmli 2× sample buffer (4% SDS, 20% glycerol, 0.004% bromophenol blue and 0.125 M Tris-Cl, pH 6.8). Samples were boiled for 10 min and 15 μL loaded to a 10–15% SDS-PAGE gel and transferred to a PVDF membrane (Bio-Rad, Hercules, CA, United States). To detect tau, membranes were incubated with mouse monoclonal anti-tau antibody [Tau-5] (Abcam, Cambridge, United Kingdom, ab80579) (1:2,000), to detect α-synuclein membranes were incubated with mouse monoclonal anti-alpha-synuclein antibody [syn211] (Abcam, Cambridge, United Kingdom, ab80627) (1:2,000) and to detect phosphorylated tau membranes were incubated with rabbit monoclonal recombinant anti-tau (phosphor S404) antibody [EPR2605] (Abcam, Cambridge, United Kingdom, ab92676) (1:500). This was followed by incubation with (goat) anti-mouse or anti-rabbit Cross-Adsorbed Secondary antibody Alexa-Fluor™ 647 (Thermo Fisher Scientific, Waltham, MA, United States, A32728) (1:1,000). Proteins were visualised using the STORM image analyser.

Multicellular Development

Dictyostelium discoideum wildtype and transformant cells were grown on SM plates containing a lawn of *E. aerogenes* at 21°C until multicellular fruiting bodies were observed. The fruiting bodies were examined using an Olympus S761TM dissecting microscope and images were captured using a digital Moticam 2300TM camera. Photographs were taken from above the plates to gain an overall view of the population as well as pictures of singular fruiting bodies. This was obtained by slicing out a thin section of agar and placing it on its side so that the entire fruiting body could be seen.

Growth on Bacterial Lawns

A scraping of wildtype and transformed amoebae were inoculated into the centre of four normal agar [20 g L^{-1} agar (Difco, Detroit, MI, United States); 1 g L^{-1} peptone (Oxoid, Basingstoke, United Kingdom), 1.1 g L^{-1} anhydrous glucose, 1.9972 g L^{-1} KH_2PO_4, and 0.356 g L^{-1} $Na_2HPO_4_2H_2O$, pH 6.0] plates containing a lawn of *E. coli* B2 as previously described (Bokko et al., 2007). Plates were incubated at 21°C, the diameter of plaque expansion was measured in mm twice daily over a period of approximately 100 h. The plaque expansion rates for each strain was calculated using the statistical computing and graphics software program "R" by linear regression.

Growth in Axenic Medium

Dictyostelium discoideum cells were axenically grown in HL5 until exponential phase was reached, then inoculated into 50 mL of HL5 in 150 mL flasks to a final density of 1×10^4 cells mL^{-1}. Cells were incubated at 21°C on an orbital shaker (Ratek, Boronia, VIC, Australia) at 150 rpm over a period of 100 h. Cells were counted twice daily using a haemocytometer (Bright Line, 0.1 mm deep) and the generation times of each strain was calculated in R by log linear regression during exponential growth phase.

Phagocytosis Assay

The *E. coli* strain expressing the fluorescent protein DsRed (Maselli et al., 2002) was used to measure bacterial uptake of wildtype and transformed cells using the previously described method (Bokko et al., 2007). Cells were grown axenically in HL5, 5×10^6 cells were harvested, washed, and resuspended in 1 mL of phosphate buffer. Cells were starved for 30 min at 21°C with shaking at 150 rpm, then 1 mL of *E. coli* DsRed suspension was added to each sample, and 400 μL of cells were taken in duplicate at time points T = 0 min and T = 30 min. Cells were washed by centrifugation to remove surface bound *E. coli* using 5 mM sodium azide (Sigma-Aldrich, St. Louis, MI, United States) and lysed using 2 mL of 0.25% (v/v) Triton-X-100 in 100 mM Na_2HPO_4, pH 9.2. The hourly rate of bacterial consumption was determined by taking fluorescence measurements at both time points using a Special Module (530 nm excitation and 580 nm emission) in a Modulus Fluorometer (Turner Biosystems, Sunnyvale,CA, United States). The increase in fluorescence over 30 min, the amoebal density and the fluorescence signal per million bacteria (separately determined) were used to calculate the rates of bacterial consumption.

Pinocytosis Assay

The Fluorescein Isothiocyanate (FITC)-dextran (Sigma-Aldrich, St. Louis, MI, United States, average mol. mass 70 kDa) method was used for measuring liquid uptake as previously described (Klein and Satre, 1986). Vegetative cells were harvested to a density of 1×10^7 cells, resuspended in 1 mL of HL5 and starved for 30 min at 21° shaking. FITC-dextran was added to a concentration of 2 μg mL^{-1} and incubated for 70 min. Cell samples (200 μL) were taken in duplicate at T = 0 min and T = 70 min, pelleted by centrifugation, washed twice in Sorenson buffer and lysed in 2 mL of 0.25% (v/v) Triton-X-100 in 100 mM Na_2HPO_4, pH 9.2. Fluorescence was measured in the Modulus Fluorometer using the Green Module (525 nm excitation and 580–640 nm emission). The hourly rate of uptake of the medium was calculated using a calibration curve relating to fluorescence signal to volume of fluorescence medium, the cell density and the increase in fluorescence over 70 min.

Legionella Infection Assay

Legionella pneumophila infection and proliferation rates in *D. discoideum* was measured as previously described (Francione et al., 2009) and was adapted from Hagele et al. (2000) and Otto et al. (2004). Wildtype and transformant strains were grown to exponential phase axenically in HL5 at 25°C with shaking. Cells were pelleted, washed twice in Sorensen 1× C buffer (17 mM KH_2PO_4/Na_2PO_4, 50 μM $CaCl_2$, pH 6.0) at 600 × *g* for 3 min and resuspended in modified broth (MB) medium (0.7% yeast extract, 1.4% proteose peptone, 0.062% $Na_2HPO_4.2H_2O$, 0.049% KH_2PO_4, pH 6.9) at 5×10^5 cells mL^{-1}. Each suspension was aliquoted into 5 wells of a 96 well tissue culture plate to a final density of 1×10^5 cells to be used at a series of time points (0, 24, 48, 72, and 96 h) along with a negative control of only MB, and allowed to adhere for 30 min at 21°C.

The *L. pneumophila* strains used were derivatives of the pathogenic Corby strain (Mampel et al., 2006) and grown on buffered charcoal yeast extract (BCYE) agar containing 5 μg mL^{-1} chloramphenicol at 37°C with 5% CO_2 atmosphere for 3 days. After this time, the bacteria were harvested and resuspended in distilled water and used to infect the *D. discoideum* strains at a multiplicity of infection (MOI) of 1:1. This was achieved by reading the OD of the bacterial suspension, assuming that an OD_{600} of 1 equates to 10^9 bacteria mL^{-1}. Initial adherence of the *L. pneumophila* to *D. discoideum* cells was performed by centrifugation at 1,370 × *g* for 10 min. At each time point 50 μg mL^{-1} gentamycin sulphate was added to each well for 30 min to kill the extracellular *L. pneumophila.* Then cells were resuspended and pelleted at 13,000 × *g* for 12 min in a microcentrifuge, washed twice and resuspended in Sorenson 1× C buffer. The cells were lysed with 0.02% (w/v) Saponin and vortexed vigorously to release the intracellular *L. pneumophila*. A 10-fold dilution series of the harvested bacteria was prepared up to 1,000-fold for the first two time points and from 10^{-1} to 10^{-5} for time points 48 h and over. This was plated onto BCYE agar plates and incubated at 25–26°C with 5% CO_2 for 7 days in order to determine the colony-forming units (c.f.u.).

Phototaxis and Thermotaxis Assays

Qualitative phototaxis and quantitative photo-and-thermotaxis were performed as previously described (Annesley and Fisher, 2009b). Qualitative phototaxis involved scraping the edge of *D. discoideum* plaques growing on *E. aerogenes* lawns and inoculating onto the centre of charcoal agar plates [5% activated charcoal (Sigma-Aldrich, St. Louis, MI, United States), 1.0% agar technical (Thermo Fisher, Waltham, MA, United States)].

For quantitative phototaxis and thermotaxis amoebae were harvested from mass plates and repeatedly washed in cold sterile saline, followed by centrifugation (600 × *g* for 5 min) to remove any bacterial cells. Quantitative phototaxis involved creating dilutions of the cell pellet with cell densities ranging from 6×10^4 to 1.5×10^6. Twenty microlitre of each dilution was plated in duplicate onto charcoal agar plates in a 1 cm^2 area in the middle of the plate. Both qualitative and quantitative phototaxis plates were incubated at 21°C for 48 h with a single lateral light source to allow slug trails to form. Cell pellets were diluted to 20% (approximately 3×10^6 cells) for quantitative thermotaxis. A 20 μL aliquot was placed in a 1 cm^2 area onto the centre of water agar plates (1% agar) and incubated in PVC boxes with no light source on a heat bar producing a 0.2°C cm^{-1} temperature gradient at the agar surface. Plates were placed in duplicate at arbitrary temperature points from 1 to 8 with T1

corresponding to 14°C and increasing in 2°C increments to reach 28°C at T8.

All slug trails were transferred to PVC discs and stained with Coomassie blue (Sigma-Aldrich, St. Louis, MI, United States) before being digitised. Qualitative digitising was performed by tracing entire slug trails with a light source at 0°. For quantitative phototaxis and thermotaxis only the beginning and end of the slug trails were digitised and orientation analysed using directional statistics.

Immunofluorescence

Dictyostelium discoideum transformed and wildtype cells were grown axenically to a density of 2×10^6 cells mL^{-1} and then transferred onto sterile coverslips in six-well Costar plates (Nunc™). The cells were allowed to settle for 30 min before the media was replaced with Lo-Flo HL5 (3.85 g L^{-1} glucose, 1.78 g L^{-1} proteose peptone, 0.45 g L^{-1} yeast extract, 0.485 g L^{-1} KH_2PO_4, and 1.2 g L^{-1} $Na_2HPO_4 \cdot 12H_2O$; filter sterilised) for 1 h to equilibrate the cells. The media was aspirated off and the coverslips rinsed in PBS [12 mM Na_2HPO_4, 12 mM NaH_2PO_4 (pH 6.5)] then cells were fixed with the addition of prechilled (-20°C) methanol/acetone solution (1:1) and left at −20°C for 10 min and again rinsed in PBS.

The coverslips were then incubated with mouse monoclonal anti-tau antibody [Tau-5] (Abcam, Cambridge, United Kingdom, ab80579) or a combination of Tau-5 and rabbit monoclonal anti-alpha + beta synuclein antibody [EP1646Y] (Abcam, Cambridge, United Kingdom, ab51252) diluted (1:100) in blocking buffer [1% (w/v) bovine serum albumin (BSA) and 1% (v/v) cold-water fish skin gelatin in PBS] for 1 h. Coverslips were rinsed in PBS with 0.1% (w/v) BSA twice and incubated with secondary antibody [goat anti-mouse Alexa-Fluor594 (Molecular Probes™ Invitrogen™) or a combination of Alexa-Fluor 594 (goat) and anti-rabbit Alexa-Fluor—488 conjugated IgG antibody (Thermo Fisher Scientific, Waltham, MA, United States, A11034) for cotransformants], diluted (1:500) in PBS with 1% (w/v) BSA and incubated for 45 min in the dark. The coverslips were rinsed in PBS, then DAPI diluted (1:1,000) in PBS was added and incubated for 5 min. The cells were rinsed in PBS then MilliQ H_2O drained and mounted onto a microscope slide with Ultramount No. 4 (Fronine Laboratory Supplies) and left to dry for 4 h or overnight before visualisation. The cells were detected on an Olympus (Shinjuku City, Tokyo, Japan) BX61T fluorescent microscope and images were digitally captured with the use of an Olympus DP80 camera.

Duolink®

Dictyostelium discoideum transformed and wildtype cells were axenically grown to a density of 2×10^6 cells mL^{-1}. Coverslips were lined with a Mini PAP pen (Invitrogen™) to create a 1 cm^2 area then cells were adhered and fixed to the coverslips as described in the previous section. To detect protein interactions using IF techniques, the Duolink® system was used as per manufacturer's instructions.

Cells were stained in combinations using mouse monoclonal anti-tau antibody Tau-5, rabbit monoclonal anti-tau antibody (E178) (Abcam, Cambridge, United Kingdom, ab32057), rabbit monoclonal anti-alpha + beta synuclein antibody [EP1646Y] and mouse monoclonal anti-alpha-tubulin antibody [12G10] (developed by Frankel & Nelsen, Developmental Studies Hybridoma Bank, created by the NICHD of the NIH and maintained at The University of Iowa, Department of Biology, Iowa City, IA, United States, 52242). The protein-protein interaction was observed (as red dots) using secondary proximity probes, anti-Rabbit MINUS and anti-Mouse PLUS Duolink™ *in situ* detection kit (Sigma-Aldrich Co. LLC) according to the manufacturer's instructions. An additional Alexa-Fluor 488 conjugated secondary antibody was added in with the proximity probes at times to visualise tubulin.

Seahorse Respirometry

Mitochondrial respiration of *D. discoideum* wildtype and transformed strains were measured using the Seahorse Extracellular Flux Analyser (Seahorse Biosciences, North Billerica, MA, United States) as described previously (Lay et al., 2016). A combination of drugs were used in sequential order to measure the Oxygen Consumption Rate (OCR) of specific elements of mitochondrial respiration [10 μM DCCD (N,N0-dicyclohexylcarbodimide, an ATP synthase inhibitor (Sigma-Aldrich, St. Louis, MI, United States), 10 μM CCCP (carbonyl cyanide 3-chlorophenol hydrazone, a protonophore (Sigma-Aldrich, St. Louis, MI, United States)], 20 μM rotenone [Complex I inhibitor (Sigma-Aldrich, St. Louis, MI, United States)] and either 10 μM antimycin A [Complex III inhibitor (Sigma-Aldrich, St. Louis, MI, United States)] or 1.5 mM BHAM [benzohydroxamic acid, alternative oxidase (AOX) inhibitor (Sigma-Aldrich, St. Louis, MI, United States)]. Axenically grown *D. discoideum* were harvested, washed, then resuspended in SIH medium (Formedium, Hunstanton, Norfolk, United Kingdom) and supplemented with 20 mM sodium pyruvate and 5 mM sodium malate (pH 7.4). Each strain was plated into eight wells of an assay plate precoated in Matrigel, and the cells were left to settle for 30 min. Measurement cycles consisting of 3 min of mixing, 2 min wait and 3 min measurement time were completed before and after each sequentially added drug, at least three cycles per condition. There were eight replicates of a strain for each condition, except for the last in which either BHAM or Antimycin A were added to four replicate wells. The wildtype AX2 was included as a control in every experiment in four replicate wells, and two each for the final condition. From the measurements taken before and after the addition of the pharmacological agents averages of specific components of mitochondrial respiration were able to be calculated.

Whole Cell Proteomics

For proteomic analysis each sample (5×10^6 cells in 100 μL of PBS) was prepared for analysis by the La Trobe University Comprehensive Proteomics Platform according to the following protocol: Cell pellets were dissolved in digestion buffer (8 M urea, 50 mM NH_4HCO_3, 10 mM dithiothreitol) and incubated at 25°C for 5 h. Iodoacetamide (IAA) was added to a final concentration of 55 mM and incubated for 35 min at 20°C in the dark to alkylate thiol groups. The preparation was then diluted to 1 M urea in

25 mM ammonium bicarbonate (pH 8.5) and sequencing-grade trypsin (Promega) was added to a ratio of 1:50 (wt/wt) to the sample and incubated for 16 h at 37°C. The digests were acidified with 1% (v/v) trifluoroacetic acid (TFA), dried in a SpeedVac centrifuge followed by a desalting step on SDB-XC StageTips (Empore, SDB-XC reversed-phase material, 3M, St. Paul, MN, United States). Briefly: digested proteins were resuspended in 100 μL of 1% (v/v) formic acid and centrifuged at 14,000 rpm for 2 min. The solid-phase extraction was performed according to Rappsilber et al. (2007) with the following modifications: the membrane was conditioned with 50 μL of 80% (v/v) acetonitrile, 0.1% (w/v) trifluoroacetic acid, and then washed with 50 μL of 0.1% trifluoroacetic acid before the tryptic peptides were bound to the membrane. The bound peptides were eluted by 50 μL 80% (v/v) acetonitrile, 0.1% (w/v) trifluoroacetic acid, and dried in a SpeedVac centrifuge.

Peptides reconstituted in 0.1% TFA and 2% acetonitrile (ACN) were loaded using a Thermo Fisher Scientific^{TM} UltiMate^{TM} 3000 RSLCnano system onto a trap column (C18 PepMap 300 μm ID × 2 cm trapping column, Thermo Fisher Scientific) at 15 μL min^{-1} for 6 min. The valve was then switched to allow the precolumn to be in line with the analytical column (Vydac MS C18, 3 μm, 300 Å, and 75 μm ID × 25 cm, Grace Pty. Ltd.). The separation of peptides was performed at 300 nL min^{-1} at 45°C using a linear ACN gradient of buffer A (water with 0.1% formic acid, 2% ACN) and buffer B (water with 0.1% formic acid, 80% ACN), starting at 5% buffer B to 45% over 105 min, then 95% B for 5 min followed by an equilibration step of 15 min (water with 0.1% formic acid, 2% ACN). Data were collected on an Orbitrap Elite (Thermo Fisher Scientific) in Data Dependent Acquisition mode using m/z 300–1,500 as MS scan range, CID MS/MS spectra were collected for the 10 most intense ions at performed at a normalised collision energy of 35% and an isolation width of 2.0 m/z. Dynamic exclusion parameters were set as follows: repeat count 1, duration 90 s, the exclusion list size was set at 500 with early expiration disabled. Other instrument parameters for the Orbitrap were the following: MS scan at 120,000 resolution, maximum injection time 150 ms, AGC target 1×10^6 for a maximum injection time of 75 ms with AGT target of 5000.

The spectra obtained from the instrument were used to search against *Dictyostelium* database (February 2018), together with common contaminants using the Mascot search engine (Matrix Science Ltd., London, United Kingdom). Briefly, carbamidomethylation of cysteines was set as a fixed modification, acetylation of protein N-termini, methionine oxidation was included as variable modifications. Precursor mass tolerance was 10 ppm, product ions were searched at 0.5 Da tolerances, minimum peptide length defined at 6, maximum peptide length 144, and peptide spectral matches (PSM) were validated using Percolator based on q-values at a 1% false discovery rate (FDR).

Quantification and Statistical Analysis

Proteomics data was analysed using Scaffold (Proteome Software) before exporting data to Excel for further analysis. Proteins detected in fewer than five samples were excluded from analysis. Intensity-Based Absolute Quantitation abundance values were normalised for each set of transformants to the mean total abundance of the parental strain AX2. Data was exported to Excel in which genes/proteins were assigned to one of either two groups on the basis of whether they were significantly up or significantly down compared to the WT using the *p*-values of a two sample *t*-test. Gene enrichment in biological functions and cellular components associated with these resultant gene lists were determined in FunRich software using hypergeometric analysis and Bonferroni method to gain *p*-values. Lists were also entered into the STRING database for a visual representation and false discovery rates of biological processes.

RESULTS

Human Tau Can Be Expressed in *D. discoideum* Alone and in Combination With Human α-Synuclein and Is Phosphorylated

The longest human tau isoform (2N4R) was expressed in *D. discoideum* singly and in combination with human α-synuclein. The plasmid expression constructs enter the *D. discoideum* genome through rolling circle replication and recombination, this results in strains with a varying number of the construct and therefore different expression levels. Tau phosphorylation plays a major role in the aggregation of the tau protein found in neurodegenerative diseases. In normal circumstances tau binds on and off MT depending on the phosphorylation state of the protein. Phosphorylation causes tau to disassociate from MT while regained affinity to bind to MT occurs with dephosphorylation (Cleveland et al., 1977; Lindwall and Cole, 1984). Further hyperphosphorylation of the protein leads to aggregation and the pathological conformations of tau seen in the tauopathies (Grundke-Iqbal et al., 1986). *D. discoideum* has homologues of many of the kinases that phosphorylate tau in the human brain and as evident in **Figure 1**, human tau is phosphorylated at least at residue S404 in *D. discoideum*.

Tau Is Localised Throughout the Cytoplasm in *D. discoideum* Whereas α-Synuclein Is Localised to the Cortex

To visualise the localisation of tau in *D. discoideum* immunofluorescence microscopy was performed. Tau was detected using an anti-tau antibody coupled with Alexa-Fluor 594-conjugated secondary antibody and was seen throughout the cytoplasm of the cell. α-synuclein had previously been seen to localise to the cortex of the cell in *D. discoideum* (Fernando et al., 2020). To detect α-synuclein and tau in the cotranformants anti-tau and anti-α-synuclein antibodies were coupled with Alexa-Fluor 594 and 488-conjugated secondary antibodies respectively. In the cotransformants tau was again located throughout the cytoplasm and α-synuclein primarily at the cortex. Tau and α-synuclein have been found to colocalise in many neurodegenerative diseases where they may enhance the pathological process of the other protein. To investigate whether

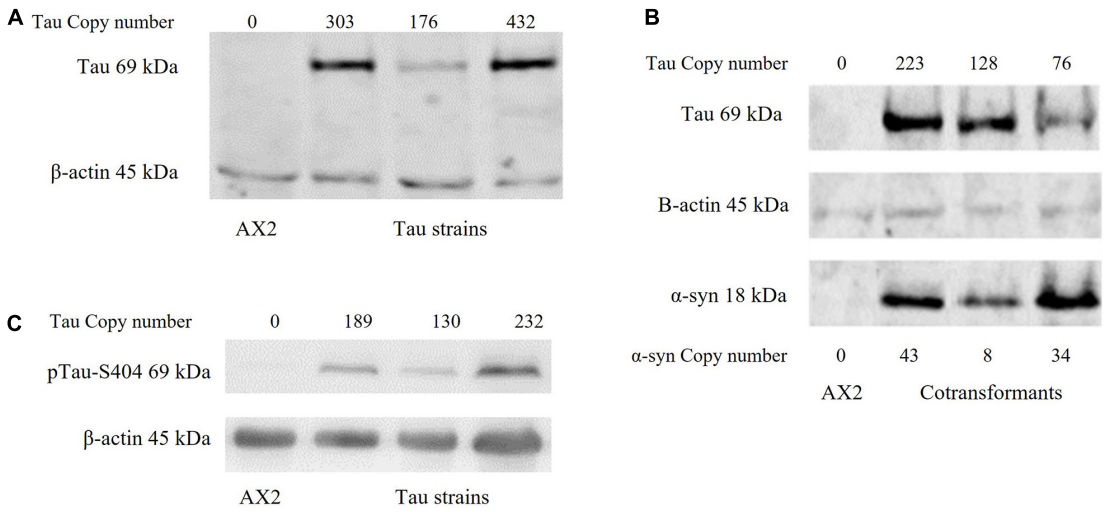

FIGURE 1 | Western blot of strains. **(A)** Human tau can be expressed in *D. discoideum*. A western blot showing the expression of the tau protein in *D. discoideum*. The parental strain AX2 was used as a negative control and β-actin as the loading control. Tau construct copy numbers as estimated by qPCR are indicated at the top of the figure. **(B)** Tau can be expressed in combination with α-synuclein in *D. discoideum*. A western blot showing the expression of both tau and α-synuclein in cotransformant strains. The parental strain AX2 was used as a negative control and β-actin as the loading control. Construct copy numbers are displayed for both tau and α-synuclein. Tau runs at 69 kDa while α-synuclein runs at 18 kDa. **(C)** Tau is phosphorylated in *D. discoideum*. One of the phosphorylation sites implicated in pathological accumulation and aggregation of the tau protein is S404 (Augustinack et al., 2002). An antibody against phosphorylation at this site was used and indicated that tau can be phosphorylated in *D. discoideum*. Construct copy numbers are displayed at the top of each lane. β-actin was used as the loading control and the parental strain AX2 as the negative control.

tau and α-synuclein colocalise within *D. discoideum*, proximity ligation assays (PLA) were performed using the Duolink™ *in situ* protein-protein interaction detection assay. Tau and α-synuclein were found to colocalise at the cortex of the cell where α-synuclein is primarily concentrated (**Figures 2A–C**).

Human Tau and α-Synuclein Can Interact With *D. discoideum* Tubulin

In humans, tau binds to microtubules aiding in their assembly and stability and supporting axonal transport. To determine whether tau interacts with tubulin in *D. discoideum* the Duolink™ detection assay was again used. Tau was seen to localise with tubulin throughout the cytoplasm of the cell (**Figure 2D**). Tubulin and α-synuclein were also seen to colocalise, however, this interaction was seen at the cortex of the cell where α-synuclein is primarily located (**Figure 2E**).

Tau Negatively Affects Fruiting Body Morphology

Loss of a food source induces chemotaxis among unicellular *D. discoideum* leading to aggregation and multicellular development culminating in the development of a fruiting body consisting of a sorus of spores atop a slender stalk. Fruiting body morphology previously seen in α-synuclein expressing strains resembles that of the parental strain AX2 (Fernando et al., 2020). The expression of tau, however, produces an abnormal stalk with enlarged basal disk when compared to the parental strain (**Figure 3A**). Cells in the basal disk have undergone a programmed cell death and the result suggests that expression of tau increases the number of cells entering this pathway. This phenotype was observed in *D. discoideum* strains characterised as mitochondrially diseased. The strains expressing both tau and α-synuclein have a larger sorus and thicker stalk, suggesting that they form larger aggregates (**Figure 3A**).

Tau Causes an Impairment in Phototaxis and Thermotaxis, Which Is Enhanced by the Coexpression With α-Synuclein

Qualitative and quantitative phototaxis experiments were performed with tau strains and cotransformants (**Figures 3B,C**). In agreement with previous studies WT α-synuclein expressing strains exhibited no phototaxis defect when compared with the wildtype (Fernando et al., 2020). The tau strains displayed a mild defect in accuracy of phototaxis which was more severe in the strains expressing both tau and α-synuclein. The increased severity of the phototaxis defect when both tau and α-synuclein were expressed together hints at an interaction between the two proteins. This is consistent with yeast models of a synergistic relationship between the two proteins, with enhanced defects when both proteins are expressed (Zabrocki et al., 2005; Ciaccioli et al., 2013). In *D. discoideum*, phototaxis and thermotaxis pathways share many downstream genes (Darcy et al., 1994), so that when a phototaxis defect is detected, a thermotaxis defect is usually also present. In support of this, strains expressing α-synuclein displayed no defect in thermotaxis with accuracies similar to AX2 and strains expressing tau displayed reduced accuracies of thermotaxis (**Figure 3D**). However, cotransformants expressing

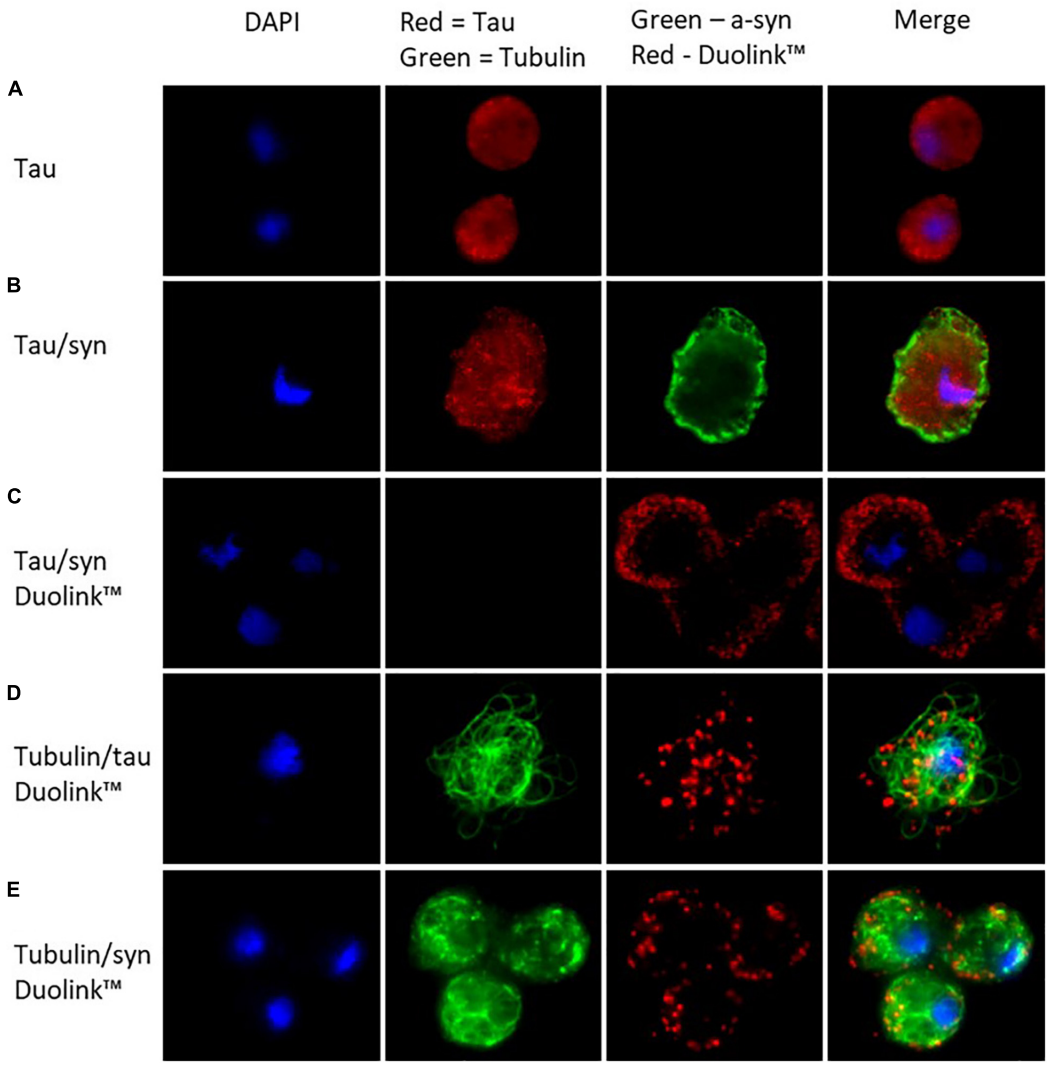

FIGURE 2 | In *D. discoideum* tau localises throughout the cytoplasm of the cell while α-synuclein concentrates at the cortex. The colocalisation of the two proteins takes place at the cortex of the cell where α-synuclein is most concentrated. **(A)** Tau was detected in the tau transformant using an anti-tau primary antibody and observed using Alexa-Fluor 594 conjugated secondary antibody. **(B)** α-synuclein was detected using an anti-α-synuclein antibody and visualised using Alexa Fluor 488 conjugated secondary antibody along with tau in the cotransformant. **(C)** To view colocalisation of tau and α-synuclein the cotransformants were stained with mouse anti-tau antibody and rabbit anti-α-synuclein antibody, the protein–protein interaction was observed (as red dots) using secondary proximity probes, anti-rabbit MINUS and anti-mouse PLUS in the Duolink^{textrmTM} in situ detection kit (Sigma-Aldrich). To visualise colocalisation of tau or α-synuclein with tubulin Duolink^{textrmTM} was again used, this time using a mouse-anti-tubulin primary antibody and rabbit-anti-tau or anti-α-synuclein antibodies. An additional Alexa-Fluor 488 conjugated secondary antibody was added in with the proximity probes in order to visualise tubulin. **(D)** Tau colocalised with tubulin throughout the cytoplasm of the cell. **(E)** The colocalisation of tubulin and α-synuclein occurred at the cortex of the cell where α-synuclein is most abundant.

both tau and α-synuclein showed reduced accuracies of thermotaxis at a similar magnitude to the tau expressing strains suggesting that α-synuclein imparts no additional defect as was seen in phototaxis.

Coexpression of Tau and α-Synuclein Positively Affects Growth on Plates but Negatively Affects Axenic Growth

Dictyostelium discoideum strains expressing tau and α-synuclein alone and in combination were grown on lawns of *E.coli* B2 to measure plaque expansion rates. Previous experiments showed a decrease in plaque expansion rates and no affect on axenic growth by α-synuclein expressing strains (Fernando et al., 2020). Tau strains produced plaque expansion rates similar to AX2, while the cotransformant had slightly faster plaque expansion rates (**Figure 4A**). This could indicate an interaction between tau and α-synuclein that rescues the α-synuclein defect. Axenic growth was slightly impaired in both tau and cotransformant strains with slightly longer generation times (**Figure 4B**). These results differ from those seen with mitochondrially diseased strains which displayed decreased growth on both solid and in liquid media.

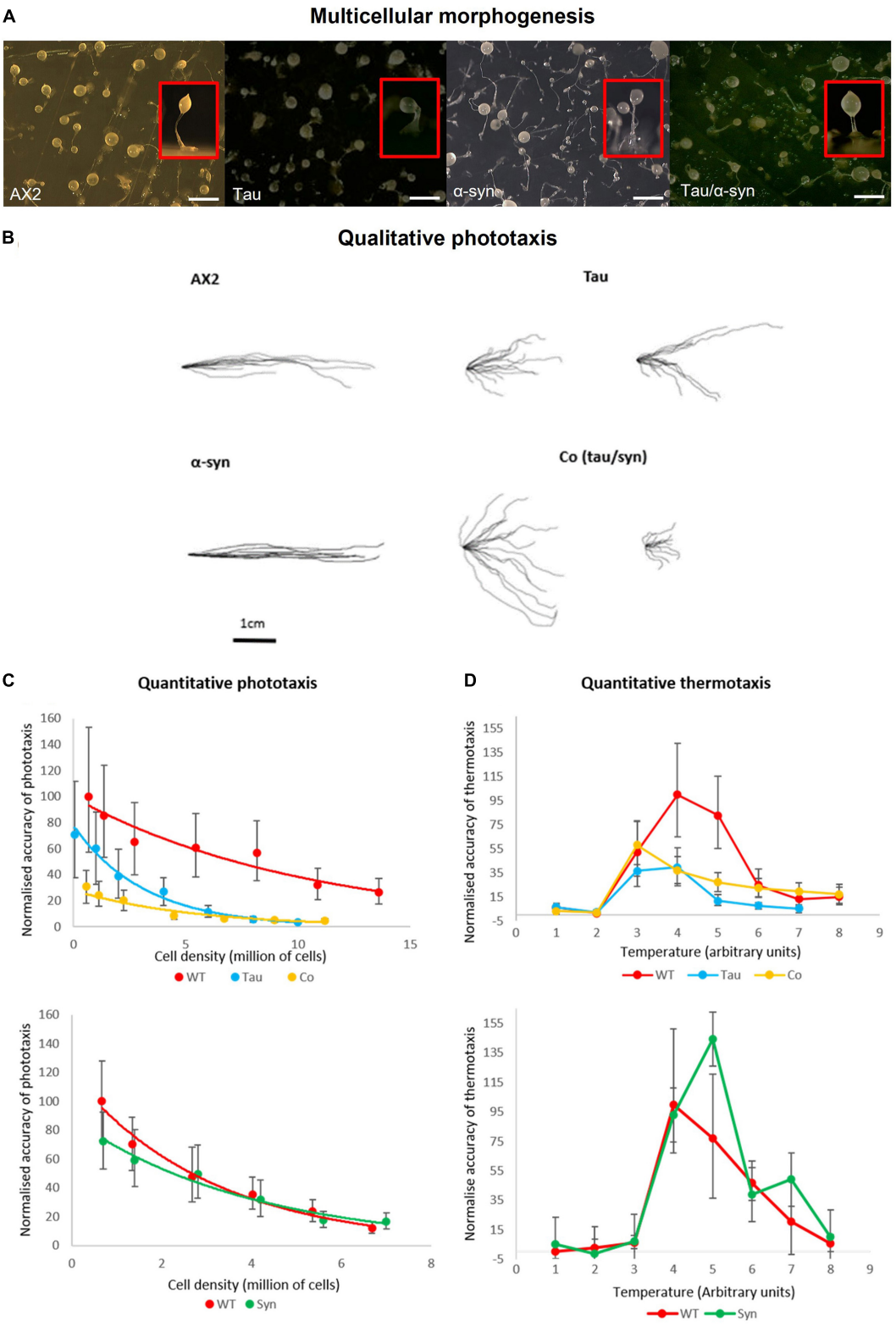

FIGURE 3 | Multicellular morphogenesis, phototaxis and thermotaxis. **(A)** Fruiting body morphology by AX2, strains expressing tau and α-synuclein singularly and coexpression of the two proteins. Tau strains produce an abnormal stalk with enlarged basal disk when compared to the parental strain. The α-synuclein strains resemble that of the parental strain AX2 (Fernando et al., 2020). The strains expressing both tau and α-synuclein have a thicker stalk and larger sorus indicating that these strains produce larger aggregates than AX2. Top view of plates with insets showing the side view of a single representative fruiting body of each strain. Scale

(Continued)

FIGURE 3 | Continued
bar indicates 1 mm. **(B)** Qualitative phototaxis. Slug trails of WT AX2, tau, α-synuclein, and cotransformants were traced and digitised. Strains expressing α-synuclein showed no defect in phototaxis when compared to WT. Tau strains exhibited a reduced accuracy of phototaxis which was enhanced by the coexpression with α-synuclein. **(C)** Quantitative Phototaxis. WT AX2, tau, α-synuclein, and cotransformant strains were statistically analysed to measure the accuracy of phototaxis (κ), normalised, and were plotted againt cell density. Tau expressing strains displayed an impaired accuracy of phototaxis when compared with the WT AX2. This defect was more severe in the strains expressing tau and α-synuclein in combination. Error bars represent standard errors **(D)** Thermotaxis. AX2, tau strain, α-synuclein [HPF885—data taken from previous experiments (Fernando et al., 2020)], and cotransformants were measured for accuracy of thermotaxis (κ), normalised and plotted against temperature. Temperature is expressed in arbitrary units (1–8) corresponding to agar surface temperatures of 14–28°C. α-synuclein caused no thermotaxis defect in comparison to the WT. The tau and cotransformant strains displayed reduced accuracy of thermotaxis, however, there was no significant difference between strains. Error bars represent standard errors.

Combined Expression of Tau and α-Synuclein Positively Affects Phagocytosis Rates While Macropinocytosis Is Not Affected

Dictyostelium discoideum consume nutrients through endocytosis. When feeding on bacterial lawns, bacteria are ingested through phagocytosis, and in liquid media nutrients are taken up through macropinocytosis (pinocytosis). The normalised rates of endocytosis can be seen in **Figures 4C,D**. Tau did not affect phagocytosis or pinocytosis rates, which resembles the phenotypes of mitochondrially diseased cells (Bokko et al., 2007). Phagocytosis but not pinocytosis was affected in α-synuclein strains, indicating the impaired growth on bacterial lawns was due at least partly to a phagocytosis defect. The cotransformants had an increased phagocytosis rate suggesting that the increased growth rate on bacterial lawns was also due to elevated rates of phagocytosis. Pinocytosis was not affected in these strains and therefore not the cause of the impaired axenic growth of the tau and cotransformant strains.

Legionella Proliferation Is Increased in Tau and Cotransformant Strains

Dictyostelium discoideum is naturally found in soil environments where it consumes bacteria as a food source. *Legionella* also reside in moist soil environments where they can infect and proliferate within amoebae by exploiting phagocytosis. In healthy *D. discoideum* cells, *Legionella* is taken up and proliferates, but in mitochondrially diseased cells, *Legionella* proliferation is enhanced by up to two-fold when compared to wildtype (Francione et al., 2009). To measure *Legionella* infection and intracellular proliferation rates, *D. discoideum* amoebae were plated in a monolayer in a tissue culture plate and infected with *L. pneumophila* Corby. Viable counts of *L. pneumophila* were determined over 5 days at time points 0–96 h. Tau strains and cotransformants exhibited increased *L. pneumophila* proliferation compared to the parental strain AX2 (**Figure 5**), which corresponds to previous results seen in mitochondrially diseased cells. *D. discoideum* strains expressing α-synuclein showed a decrease in *L. pneumophila* proliferation.

Phototaxis Defect Is Mediated by AMPK

Some of the phenotypes with tau-expressing stains resemble phenotypes attributed to mitochondrial dysfunction in *D. discoideum.* These phenotypes have previously been attributed to the chronic activation of AMPK, an energy-sensing enzyme important in cellular homeostasis. One of the main phenotypes associated with mitochondrial dysfunction and chronic activation of AMPK is a defective slug phototaxis. This was observed in strains in which Cpn60 had been antisense inhibited (Bokko et al., 2007), the mitochondrial protein MidA was knocked out (Carilla-Latorre et al., 2010) and mitochondrial genes were disrupted in a subset of mitochondrial genomes (Francione and Fisher, 2011; Francione et al., 2011). The phototaxis defect in mitochondrially diseased strains is rescued by antisense inhibition of AMPK. Furthermore AMPK has been shown to interact in a photosensory signalling complex with filamin (Bandala-Sanchez et al., 2006) and other proteins implicated in this pathway including RasD (Wilkins et al., 2000), FIP (Knuth et al., 2004), the protein kinases PKB, and ErkB (Bandala-Sanchez et al., 2006). Knockdown of AMPK has also rescued the defective phototaxis seen in strains expressing PD associated mutations of α-synuclein (Fernando et al., 2020). Because of this, we decided to investigate whether the phototaxis defect caused by the expression of tau and the more severe defect of the cotransformant was mediated by increased AMPK activity. To do this, cotransformants were created expressing tau and an AMPK antisense construct. As the expression of tau and α-synuclein combined yielded a more severe phototaxis defect, strains expressing tau, α-synuclein and AMPK knockdown were also produced. Copy numbers of the tau, AMPK antisense and α-synuclein expression constructs were determined by qPCR. AMPK antisense inhibition rescued the phototaxis defect caused by both the expression of tau and the more severe impairment observed in the α-synuclein/tau cotransformants (**Figure 6**). The slug trails resemble the parental strain in accuracies toward the light source, suggesting that the phototaxis defect in these strains is mediated by chronic AMPK hyperactivity as is known to be the case for mitochondrially diseased strains. It would be of interest in future work to determine if the phenotypes produced by tau that mimic those of mitochondrial disease are also mediated by AMPK. These include the defective fruiting body morphology, axenic growth, thermotaxis, and enhanced *L. pneumophila* proliferation.

Tau Impairs ATP Synthesis While the Coexpression With α-Synuclein Leads to Normally Functioning Mitochondria

The phenotypes caused by ectopic tau expression suggest a possible mitochondrial defect producing at least some AMPK-dependent cytopathological outcomes. Therefore we measured the function of the mitochondria using the Seahorse Extracellular Flux Analyser in combination with a series of inhibiting

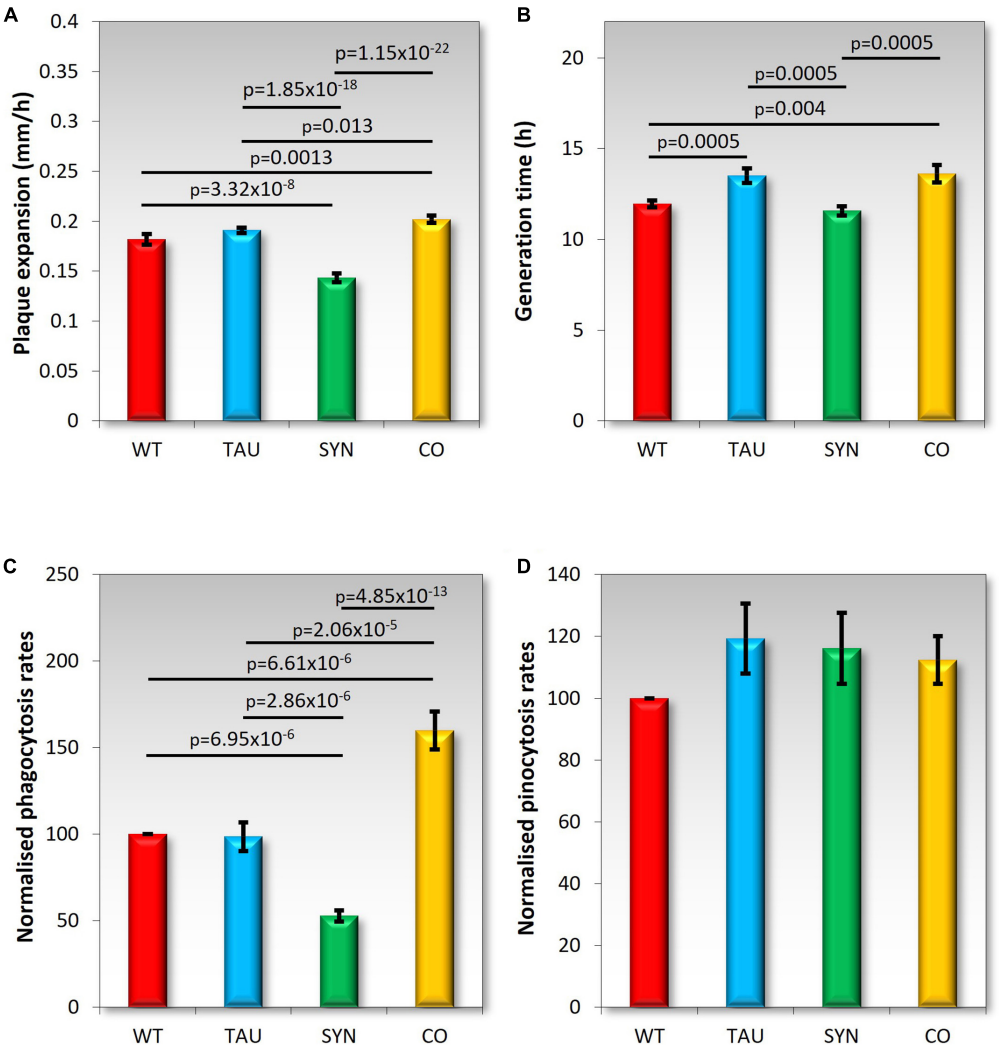

FIGURE 4 | Growth and endocytosis Wild type AX2 (WT) and strains expressing tau (TAU), α-synuclein (SYN), or both tau and α-synuclein (CO) were tested. **(A)** Plaque expansion rates were measured during growth on bacterial lawns of *E. coli* B2. Plaques were measured twice daily over one hundred hours. Experiments were performed in triplicate in four different experiments. As previously seen (Fernando et al., 2020) α-synuclein-expressing strains display slower growth on bacterial lawns when compared to the WT AX2. Tau does not affect growth on plates, but strains expressing both tau and α-synuclein grew slightly but significantly faster. **(B)** Axenic growth rates were measured by determining the generation time of strains (doubling in exponential growth phase). Strains were grown in HL5 liquid medium on a shaker at 21°C for 100 h. Experiments were performed on tau and cotransformant strains over four separate experiments. As previously shown, α-synuclein did not affect axenic growth (Fernando et al., 2020). Strains expressing tau displayed significantly longer generation times during growth in liquid medium. Strains expressing both tau and α-synuclein also showed significantly longer generation times than AX2. Error bars are standard errors of the mean, p-values represent statistically significant values using a two sample *t*-test. **(C)** Phagocytosis rates were measured by feeding *D. discoideum* amoeba *E. coli* DS-Red and taking fluorescent measurements directly after addition of the bacteria, then again after 30 min of incubation at 21°C on a shaker. The uptake rates of bacteria were normalised to the rate of uptake of AX2 (WT). Tau did not affect phagocytosis rates and shows a similar uptake rate to AX2. Previously, α-synuclein expression caused a significant decrease in phagocytosis rates (two-sample *t*-test pictured). The coexpression of tau and α-synuclein significantly increased the rate of phagocytosis (two-sample *t*-test). Cell lines were assayed in at least three separate experiments **(D)** Pinocytosis rates were measured by feeding *D. discoideum* amoeba with HL5 that contained FITC-dextran. Fluorescent measurements were taken directly after the addition of the FITC-dextran and again after an incubation period of 70 min at 21°C on a shaker. Cell lines were assayed in at least three separate experiments. Pinocytosis rates were not significantly affected by the expression of tau, α-synuclein (Fernando et al., 2020), or the combined expression of these two proteins.

drugs added in sequential order. This allows the analysis of various components of mitochondrial respiration using the Oxygen Consumption Rate (OCR) as a readout of mitochondrial activity (**Figure 7**).

Figure 7A shows a typical example of a Seahorse experiment and indicates how each of the components are measured. In agreement with previously conducted experiments, the α-synuclein-expressing strains showed significant increases in mitochondrial respiration and also an increase in the OCR by non-mitochondrial processes. There was no significant difference in the contribution of each component to basal respiration or maximum respiration rates suggesting that all complexes

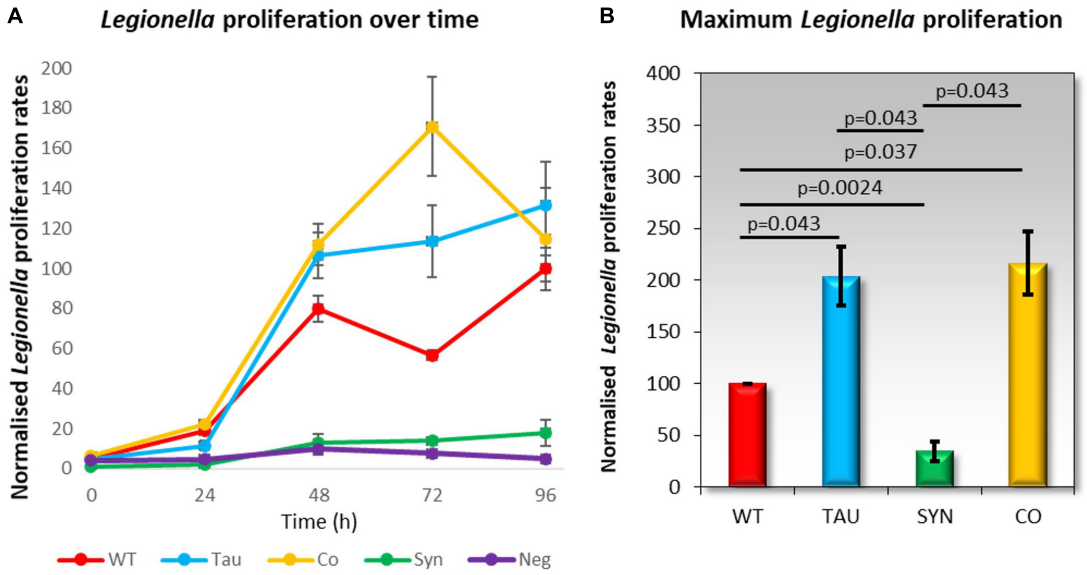

FIGURE 5 | *Legionella* proliferation is increased in tau and cotransformant strains. *Legionella* infection rates were measured by creating a monolayer of *D. discoideum* amoebae in a cell culture plate and infecting these with *L. pneumophila* Corby. The parental strain AX2 (WT), tau expressing strains (TAU), α-synuclein expressing strains (SYN), and cotransformants expressing tau and α-synuclein (CO) were infected with *L. pneumophila* and assayed for viable counts across five days at time periods 0, 24, 48, 72, and 96 h. Extracellular *L. pneumophila* was killed by the addition of Gentamycin sulphate (G418) 30 min before cells were harvested for viable counts. **(A)** The normalised viable counts resulting from the intracellular *L. pneumophila* released by the *D. discoideum* cells were plotted against the corresponding time periods. A negative control was included for comparison and did not contain *D. discoideum* cells. *L. pneumophila* proliferation was increased in tau and co-transformant strains when compared to AX2. The plot values are an average of 3–6 strains per time period and were assayed in at least three individual experiments. The error bars are standard errors of the mean. **(B)** The maximum *L. pneumophila* proliferation rates were normalised to the proliferation in AX2 (WT). *L. pneumophila* proliferation was significantly decreased in α-synuclein expressing strains compared to the WT. There was a significant increase in *L. pneumophila* proliferation in the tau and co-transformant strains in comparison to the parental strain. *p*-Values represent statistical significance using an ANOVA with pairwise comparisons using the Least Squares Difference test. Error bars are the standard errors of the mean.

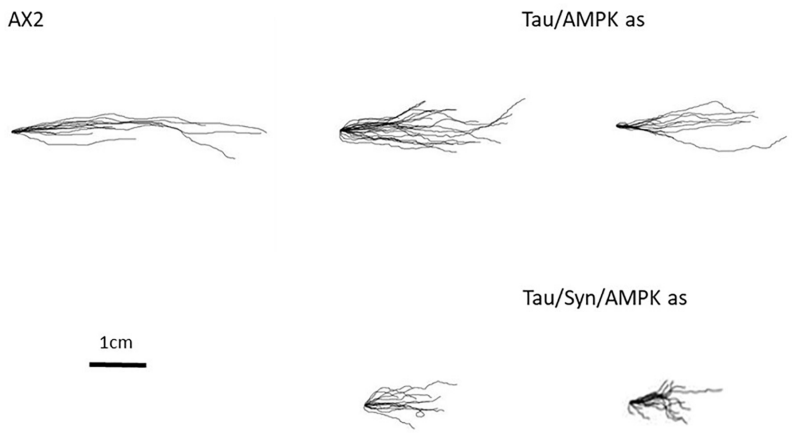

FIGURE 6 | Aberrant phenotypes associated with mitochondrial disease are rescued with antisense inhibition of AMPK. The phototaxis defect is rescued by the knockdown of AMPK. Cotransformants expressing tau and antisense AMPK (Tau/AMPK) rescues the phototaxis defect of tau. The more severe defect that was seen with tau and α-synuclein expression combined was also rescued by antisense inhibition of AMPK (Tau/Syn/AMPK) and strains resemble the WT.

and components are functionally normal but hyperactive, as previously reported. The expression of tau did not affect total mitochondrial respiration but there was a significant decrease in OCR dedicated to ATP synthesis both in absolute terms (pmol min^{-1}) and relative to the basal mitochondrial respiration rate. Tau did not affect the maximum uncoupled O_2 consumption rate, or the contributions to this of Complex I and Complex II. These results suggest a specific defect in Complex V, the mitochondrial ATP synthase. It was accompanied by a significant increase in the O_2 consumption rate attributable to "proton leak," both the absolute rate and the proportion it contributed to basal respiration. This could reflect compensatory

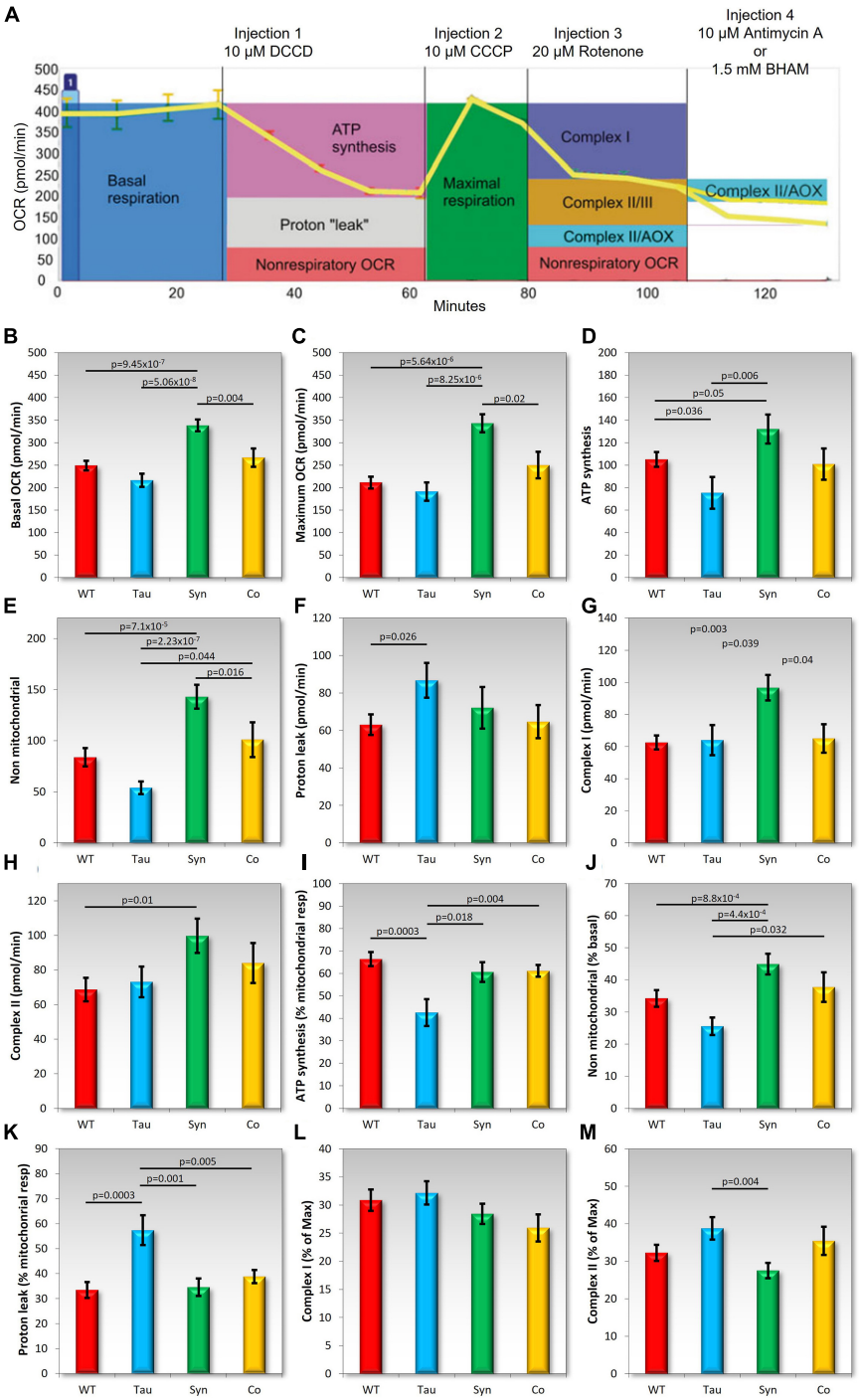

FIGURE 7 | Tau impairs mitochondrial ATP synthesis and coexpression with α-synuclein rescues the defect. In each experiment, cells of the *D. discoideum* parental strain (AX2), and strains expressing tau or α-synuclein alone or in combination were plated in four wells per sample of a Seahorse XFe24 plate. Mitochondrial respiration was measured as the oxygen consumption rate (OCR) using the Seahorse XFe24 Analyzer following the addition of pharmacological agents. The following agents were added sequentially [as seen in panel **(A)** and into all wells: DCCD (dicyclohexylcarbodimide), CCCP (carbonyl cyanide m-chlorophenyl hydrazone), and rotenone]. Then either Antimycin A or BHAM (benzohydroxamic acid) was added to the wells. The coloured boxes in panel **(A)** indicate how each component of the respiratory chain was measured (Lay et al., 2016). Total activity for Complex II was calculated by adding the effects of Antimycin A and BHAM. Panels **(B–H)** represent each component of mitochondrial respiration measured by the OCR. Each strain was assayed as four replicates per experiment across an average of 3–6 experiments. Horizontal bars with *p* values represent statistically significant pairwise comparisons using the *t*-test. All other pairwise differences were not statistically significant. Error bars are a standard error of the mean. The following components were measured: **(B)** Basal OCR, **(C)**, maximum OCR, **(D)** ATP synthesis, **(E)** non-mitochondrial respiration, **(F)** proton leak, **(G)** Complex I activity, and **(H)** Complex II activity. As seen previously, *D. discoideum* expressing

(Continued)

FIGURE 7 | Continued
α-synuclein showed an increase in mitochondrial respiration and also an increase in oxygen consumption rates as a result of non-mitochondrial processes. In contrast tau expressing strains displayed a reduced OCR dedicated to ATP synthesis **(D)** and an increased proton leak **(F)** and the two appeared to balance each other out as basal respiration was unchanged **(A)** The proportion of ATP synthesis and proton leak to basal respiration was also significantly affected suggesting functional defects in Complex V and proton leak. There were significant differences between tau and α-synuclein expressing strains in the basal and maximum OCRs, ATP synthesis, non-mitochondrial respiration and Complex I activity. In all cases α-synuclein displayed higher OCR measurements than tau strains. The effects on either of these strains seemed to be "balanced" out with the combination of the two proteins being expressed together. The cotransformants showed similar results to the parental strain and did not differ significantly in any component when compared to AX2. **(I–M)** The following were plotted as a proportion of either the Basal, maximum, or mitochondrial respiration dedicated OCR in order to determine the contribution of each component to the relative respiration rates. Shown in these panels are the OCR attributed to ATP synthesis as a % of mitochondrial OCR **(I)**, non-mitochondrial OCR as a % of Basal OCR **(J),** the "proton leak" or the mitochondrial OCR rate not contributed to by ATP synthesis; as a % of mitochondrial respiration **(K),** relative contribution of Complex I activity as a % of Maximum OCR **(L)**, and the relative contribution of Complex II activity as a % of Maximum OCR **(M).** Strains expressing α-synuclein increase in non-mitochondrial OCR as a % of basal. Tau expressing strains displayed a decrease in OCR attributed to ATP synthesis relative to mitochondrial OCR but an increase in mitochondrial OCR attributed to by the "proton leak." Once again, the cotransformants expressing both tau and α-synuclein did not differ from the parental strain indicating all complexes were functioning normally, making similar relative contributions to respiration as in the parental strain AX2.

upregulation of mitochondrial transport processes responsible for provisioning the mitochondria with oxidizable substrates and other molecules. The coexpression of tau and α-synuclein rescued all of these defects and these strains displayed normal mitochondrial function resembling the wild type AX2 strain. This again signifies a functional interaction between the two proteins.

Conclusions of Proteomics

To investigate whether any of the phenotypes caused by the expression of tau, α-synuclein or the cotransformant strains were caused by differentially regulated proteins, whole cell proteomics was performed and analysed to compare protein abundances between strains. The number of up- and down-regulated proteins of each strain when compared to AX2 was determined using data exported to Excel from Scaffold and using the *p*-values of two sample *t*-tests. The number of proteins differentially expressed in the tau, α-synuclein, and cotransformant strains can be seen in **Figure 8**. There were more proteins down-regulated (tau $n = 99$, α-synuclein $n = 53$, cotransformants $n = 144$) in all groups compared to proteins that were up-regulated (tau $n = 42$, α-synuclein $n = 27$, cotransformants $n = 59$), and the cotransformants had more proteins differentially expressed than either the tau or α-synuclein alone.

Enrichment analysis using FunRich software (**Figures 9A,B**) revealed that of the proteins up-regulated in the tau strains there were significantly more genes affecting protein catabolism ($p \leq 0.0001$), the proteasome ($p \leq 0.0001$), and translation ($p = 0.0001$) indicating that protein degradation and synthesis i.e., turnover are up-regulated. α-synuclein did not have any effect on these processes while the cotransformants up-regulated fewer proteins involved in protein catabolism but more in the process of protein synthesis (translation, $p = 0.0001$). Thus, the biological processes up-regulated by α-synuclein were unlike those up-regulated by tau. Tau induces protein catabolism, possibly as part of a spectrum of homeostatic compensatory processes that favour energy production by alternative catabolic processes in the face of defective mitochondrial ATP synthesis. By contrast, α-synuclein expression enhances mitochondrial respiration and perhaps in support of this elevated activity, these strains exhibited higher levels of expression of enzymes involved in carbohydrate metabolism. This may provide the energy to support elevated rates of protein biosynthesis.

In α-synuclein-expressing strains, proteins involved in responding to bacteria were up-regulated as well as proteins associated with the pathogen-containing vacuole ($p = 0.0001$). This accords with the *L. pneumophila* infection and proliferation experiments in which α-synuclein was significantly less susceptible to proliferation when compared with the parental strain AX2. These observations suggest that in α-synuclein-expressing strains, *Legionella*-containing vacuoles may be up-regulated increasing the capacity of the cell to directly handle the pathogens through the endolysosomal *Legionella*-destroying pathway.

In accord with their different subcellular localisations, tau up-regulated proteins in the cytosol and cytoplasm where it was localised (as well as the nucleus), while α-synuclein up-regulated proteins in the plasma membrane, extracellular matrix, and phagocytic vesicle which are all associated with the cell cortex (**Figure 9B**). STRING was used as a visual representation of the interacting protein groups up-regulated in the tau and cotransformant strains and the False Discovery Rates of each biological process affected (**Figure 9C**). There were too few up-regulated proteins in the α-synuclein expressing strains for valid comparisons.

More biological process and cellular components were down- than up-regulated in all three strain groups (**Figure 10**). Proteins involved with the cytoskeleton were down-regulated in all strains ($p \leq 0.0001$), with the highest number of proteins down-regulated in strains expressing both tau and α-synuclein. This is another indication of functional interactions between these cytotoxic proteins and is not surprising as the cytoskeleton is involved in many processes that were affected in these strains, including phagocytosis, phototaxis and thermotaxis, differentiation, and development (Noegel and Schleicher, 2000). Of note, the biological processes of cell motility ($p = 0.012$), polarity ($p = 0.018$), morphogenesis ($p = 0.01$), and filopodium assembly ($p = 0.005$) were only significantly down-regulated in the cotransformants. This corresponds with the more severe phototaxis defect in the cotransformants which also displayed a possible motility defect, as the slugs did not travel as far as other strains. It would be of interest to measure single cell motility and chemotaxis in these strains.

Several proteins involved in the response to bacteria are down-regulated in all strain groups, however, this is more significant

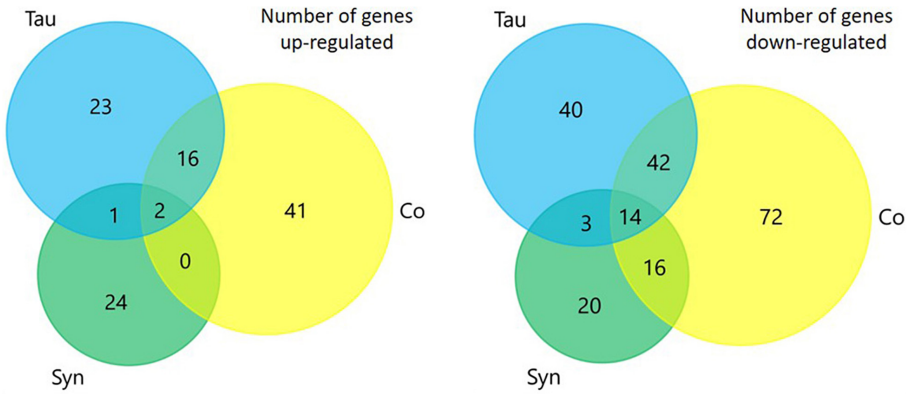

FIGURE 8 | Venn diagrams representing the number of proteins that were differentially expressed in each strain when compared to AX2. There were more proteins down-regulated in each of the sets of strains compared to the number that were up-regulated. The coexpression of tau and α-synuclein lead to the expression of more proteins being up- or down-regulated than either did alone.

and there are more proteins affected in the tau-expressing and cotransformant strains (p = 0.0001) when compared to those expressing α-synuclein alone (p = 0.005). Proteins upregulated in this pathway in the α-synuclein strains were downregulated in the cotransformants. This again relates to the *L. pneumophila* results, wherein the tau and cotransformants both displayed an increased susceptibility to *L. pneumophila* proliferation when compared to the parental strain. Oxidation-reduction processes are significantly down regulated in the tau and cotransformant strains. Most of the proteins involved in these processes are involved in response to oxidative stress and the biosynthetic pathways of amino acid, fatty acid and lipid synthesis.

Lipid metabolism has been found to be dysregulated in association with tau pathology in AD and α-synuclein in PD and synucleinopathies. For reviews see (Bok et al., 2021) and (Alecu and Bennett, 2019). Lewy bodies, the α-synuclein-containing aggregates that are the pathological hallmark of PD, contain high lipid content and lipid membranes (Shahmoradian et al., 2019), while membrane lipids such as those associated with cholesterol have been associated with PHF in AD brains (Gellermann et al., 2006). Here tau and α-synuclein when expressed alone significantly reduced lipid and sterol metabolic pathways, but when coexpressed, the down-regulation was rescued. This resembles the results of mitochondrial respiration where there were effects caused by the single expression of each protein and these were rescued to normal levels with coexpression. Again this signifies a functional interaction between tau and α-synuclein. STRING was used as a visual representation of the protein groups down-regulated in three sets of strains and the False Discovery Rates of each biological process affected (**Figure 11**).

DISCUSSION

Tauopathies are a diverse set of neurodegenerative diseases characterised by the accumulation of the tau protein into aggregates. Tau is important in the stabilisation of MT and axonal transport and binds to microtubules based on the phosphorylation state of the protein. Here we expressed the full-length human tau isoform (2N4R) in *D. discoideum* as a model to study tauopathies. As many neurodegenerative diseases including the tauopathies suggest a synergistic relationship between pathological proteins, we also expressed tau in combination with α-synuclein to investigate the interaction between these two proteins.

Phosphorylation of tau leads to disassociation of tau and MT, and further hyperphosphorylation causes the accumulation of tau into aggregates, while dephosphorylation restores tau/MT binding. Tau is regulated by many different kinases and phosphatases (Avila, 2008). Tau has over 80 different phosphorylation sites on the 2N4R isoform and many of these are involved in pathological conditions (Hanger et al., 1998; Buée et al., 2000). Over 20 kinases have been identified which are able to phosphorylate tau. These can be divided into two main groups—the proline directed protein kinases (PDPKs) and non-PDPKs. The PDPKs phosphorylate tau at Serine/Threonine residues and have been linked to the process of neurodegeneration (Sergeant et al., 2008; De Vos et al., 2011). Some common PDPKs are GSK-3β, mitogen activated protein kinase and cyclin dependent kinases which all have homologues in *D. discoideum* (Goldberg et al., 2006). These kinases phosphorylate tau at multiple Serine/Threonine sites on the 2N4R isoform (Augustinack et al., 2002). Phosphatases of tau have also been defined and include protein phosphatase 1 (PP1), 2A (PP2A), 2B (PP2B), and 5 (PP5), all of which have homologues in *D. discoideum*. Tau was phosphorylated in *D. discoideum* at S404 which is an important residue in the process of aggregation of the tau protein. Mondragón-Rodríguez et al. (2014) found that the double phosphorylation of Ser396 and Ser404 was an early event in AD and Down's syndrome. They saw early pathological tau structures (not yet defined NFT) correlating with phosphorylation at Ser396/404, while other phosphorylation sites corresponded with mature NFT. Pseudophosphorylation of tau (achieved by mutating the serine to glutamic acid to mimic phosphorylation) at this epitope has also been found to be an early event in the

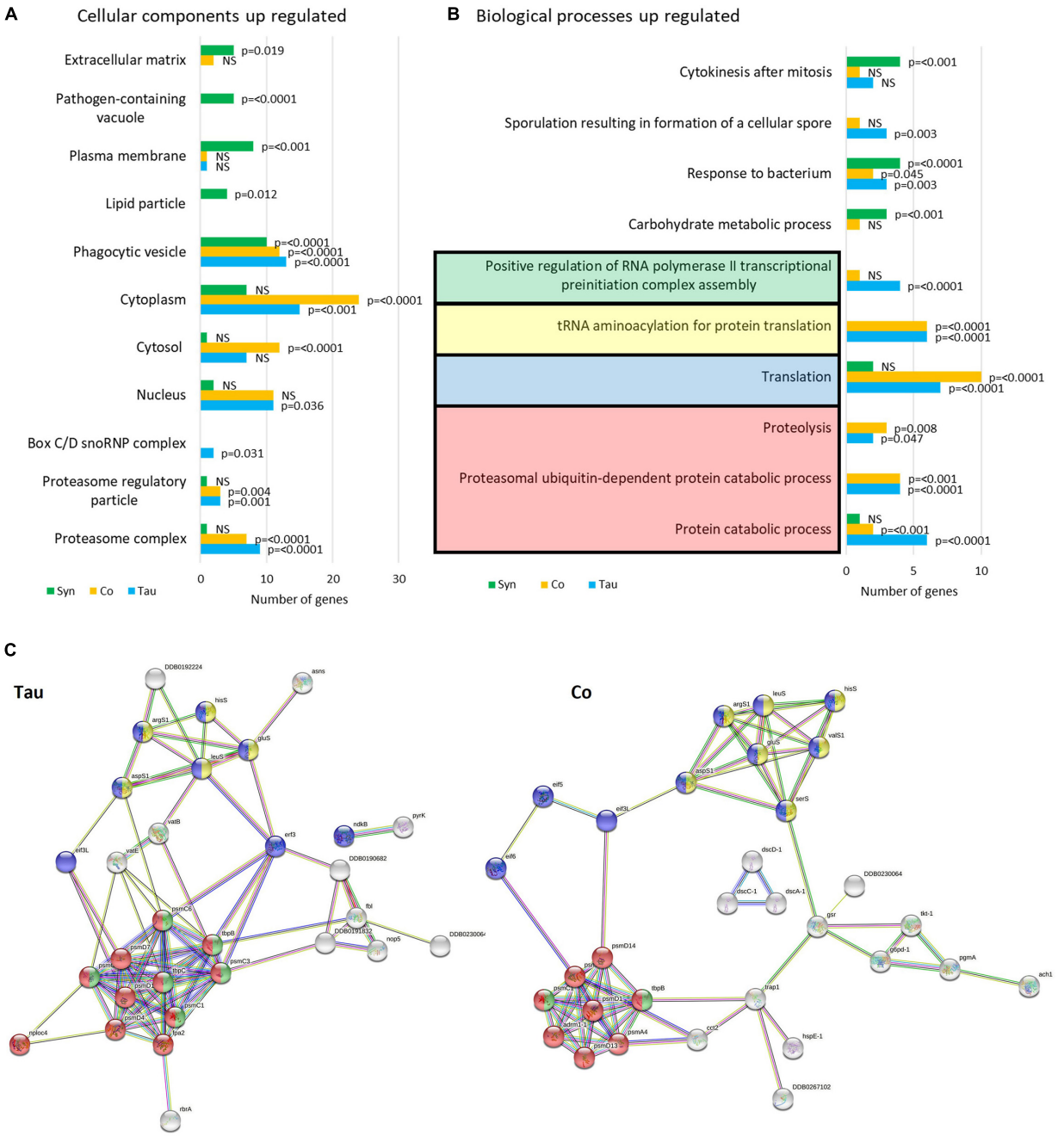

Biological process	Colour	Tau (FDR)	Co (FDR)
Proteolysis	Red	$p=5.89\times10^{-11}$	$p=1.18\times10^{-6}$
Positive regulation of RNA polymerase II transcriptional preinitiation complex	Green	$p=1.15\times10^{-11}$	NS
Translation	Blue	$p=4.09\times10^{-7}$	$p=1.15\times10^{-8}$
tRNA aminoacylation for protein translation	Yellow	$p=5.97\times10^{-7}$	$p=1.18\times10^{-8}$

FIGURE 9 | Cellular components and biological processes up-regulated in strains expressing tau and/or α-synuclein. Funrich enrichment analysis of cellular components **(A)** and biological processes **(B)** indicate that tau affects the proteasome and proteolytic processes as well as translation. The expression of α-synuclein resulted in different biological processes and therefore different cellular components being affected. The cotransformants displayed patterns of up-regulated expression similar to those in strains expressing tau alone. The reported *p*-values are based on hypergeometric tests **(A)** and corrected using the Bonferroni method

(Continued)

FIGURE 9 | Continued
(B) calculated in FunRich software. This is based on the number of genes up-regulated within each strain divided by the total number of genes generated for each process/component using the Gene Ontology database for *D. discoideum.* To give a visual representation of protein groups, STRING was used to view the groups of interacting proteins involved in the major up-regulated processes in the tau-expressing strains and cotransformants and calculate False Discovery Rates (FDR) **(C)** which indicate statistical significance of the overrepresentation of these biological processes in the list of interacting up-regulated proteins. There was insufficient data to provide a network of interacting up-regulated proteins in the α-synuclein expressing strains using STRING (Not pictured). Proteins and STRING protein annotations can be found in **Supplementary Tables 1, 3, 5**.

hyperphosphorylation and aggregation of tau *in vitro* (Abraha et al., 2000; Haase et al., 2004). Phosphorylation specifically at Ser404 has been shown by kinases including GSK-3β and the mitogen activating protein kinase ERK2 (Reynolds et al., 2000). Phosphopeptide mapping and sequencing shows that GSK-3β displays the most pronounced phosphorylation at S404 (Augustinack et al., 2002). Phosphorylation of tau was also seen in other simple models including the yeast model of tauopathy, in which human tau was phosphorylated and dephosphorylated by yeast kinases and phosphatases (De Vos et al., 2011), and site specific phosphorylation resulted in tau aggregates and damage to MT (Vanhelmont et al., 2010). As tau is phosphorylated at S404 in *D. discoideum*, it is likely that it is also phosphorylated at other residues and this could be further investigated. Despite there being no tau orthologue in *D. discoideum*, the presence of homologous kinases that phosphorylate tau and the demonstration that at least one of them does act on tau suggest that the cellular machinery that regulates tau is ancient and could act on it in a similar way in *D. discoideum* as it is in mammals. This is not unlike the case of APP which has no orthologue in *D. discoideum,* but which has been shown to be processed by γ-secretase in *D. discoideum* as in mammalian cells (McMains et al., 2010). As phosphorylation is the first step in the eventual pathological accumulation of tau, the next steps could be to investigate tau aggregation as well as other posttranslational modifications and structural conformations of the protein in *D. discoideum.*

In normal healthy cells, tau binds on and off MT depending on the phosphorylation state of the protein. The longest tau isoform has a high affinity for MT as it has 4 MTBR. Here, tau was localised in the cytoplasm of the cell where it interacted with tubulin, although not necessarily on the MT. As tau was phosphorylated, this could have caused MT disassembly as it does in human neurons. However, as tau is not endogenously expressed in *D. discoideum* it is not necessary for MT stability. In agreement with this, our results provided no evidence of MT disassembly when tau was ectopically expressed in *D. discoideum,* although this was not directly measured.

Ectopic expression of human tau in *Drosophila* revealed that, unlike the endogenous *Drosophila* orthologue, it interacted poorly with *Drosophila* microtubules but was nonetheless cytotoxic (Feuillette et al., 2010). These findings would suggest that tau can exert cytopathological effects that are not related to dysregulated MT assembly/disassembly. What might those processes be? The proteomics results suggested that ectopic tau expression had a major impact on protein turnover with both protein degradation (proteasomal) and protein biosynthesis (transcription and translation) being up-regulated. The phosphorylation state of tau could impact the proteins involved in the proteasome as seen by Ren et al. (2007). Here, tau was expressed in embryonic kidney cells and phosphorylation of tau increased proteasome activity while further hyperphosphorylation decreased activity by the proteasome.

Like tau, α-synuclein has been reported to interact with tubulin heterodimers in the cytosol (Payton et al., 2001) but also with MT, where it altered the cell surface recruitment of the dopamine transporter (Wersinger and Sidhu, 2005). A study by Alim et al. (2002) found that tubulin was a binding partner of α-synuclein and colocalised in LB in a case of PD. However, colocalisation of proteins in the aggregates of Lewy Bodies does not necessarily reflect their normal interactions in the absence of such aggregates. We found that both tubulin and tau colocalise with α-synuclein in *D. discoideum* in the cortex of the cell where α-synuclein is concentrated. It is also here in the cortical regions of the cell that the cytopathological effects of ectopically expressed α-synuclein are exercised—in the inhibition of phagocytosis and *L. pneumophila* proliferation. Furthermore the proteomics revealed significant dysregulation of proteins involved in these processes with α-synuclein-expressing cells having lower levels of proteins involved in phagocytosis, but elevated levels of proteins involved in the response to and uptake of bacteria into pathogen-containing vesicles. The phagocytic vesicle associated proteins that were upregulated were mainly related to membrane fusion and protein transport. While the down regulated proteins were associated mainly with actin binding and the cytoskeleton. In relation to response to bacterium, proteins involved in vesicle transport were upregulated (rab1A, rab5A, rasG, sasA, and vatC). The interaction of tau with α-synuclein in these same cortical regions can explain the ability of tau to reverse the inhibition of phagocytosis by α-synuclein, when tau on its own has no effect on this phenotype, despite also downregulating expression of proteins involved in this pathway.

The colocalisation of tau and α-synuclein at the cortex has been observed in cellular models where tau and α-synuclein have both been found to interact with the plasma membrane (Brandt et al., 1995; Nakamura et al., 2001) and α-synuclein stimulated phosphorylation of tau has been seen to occur here too (Jensen et al., 1999). Esposito et al. (2007) proposed a membrane-bound functional complex with tau and α-synuclein that may involve the actin cytoskeleton. In a Chinese hamster ovary cell line, α-synuclein was found interacting with actin at the plasma membrane and the colocalisation of tau and α-synuclein was highest at the cell periphery. The colocalisation of tau and α-synuclein has been seen in autopsied brain sections of patients with AD (Hamilton, 2000; Arai et al., 2001), cellular

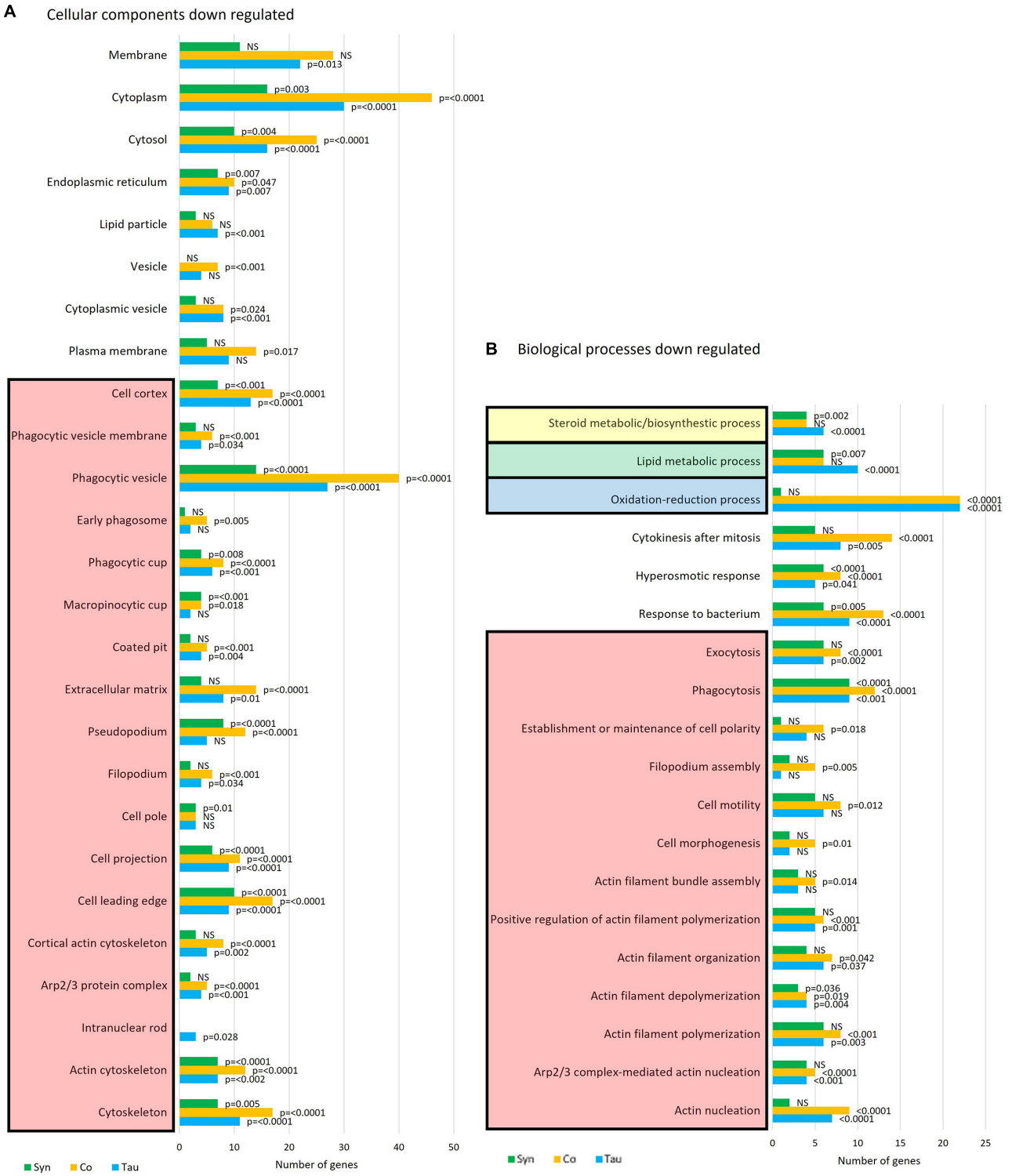

FIGURE 10 | Cellular components and biological processes down-regulated in strains expressing tau and/or α-synuclein. Funrich enrichment analysis of cellular components **(A)** and biological processes **(B)** indicate that the cytoskeleton is significantly down-regulated in all strains. The coexpression of tau and α-synuclein compounded the effect. The reported *p*-values are based on hypergeometric tests using the Bonferroni method of correction calculated in FunRich software. This is based on the number of proteins down-regulated within each strain divided by the total number of proteins generated for each process/component using the Gene Ontology database for *D. discoideum*.

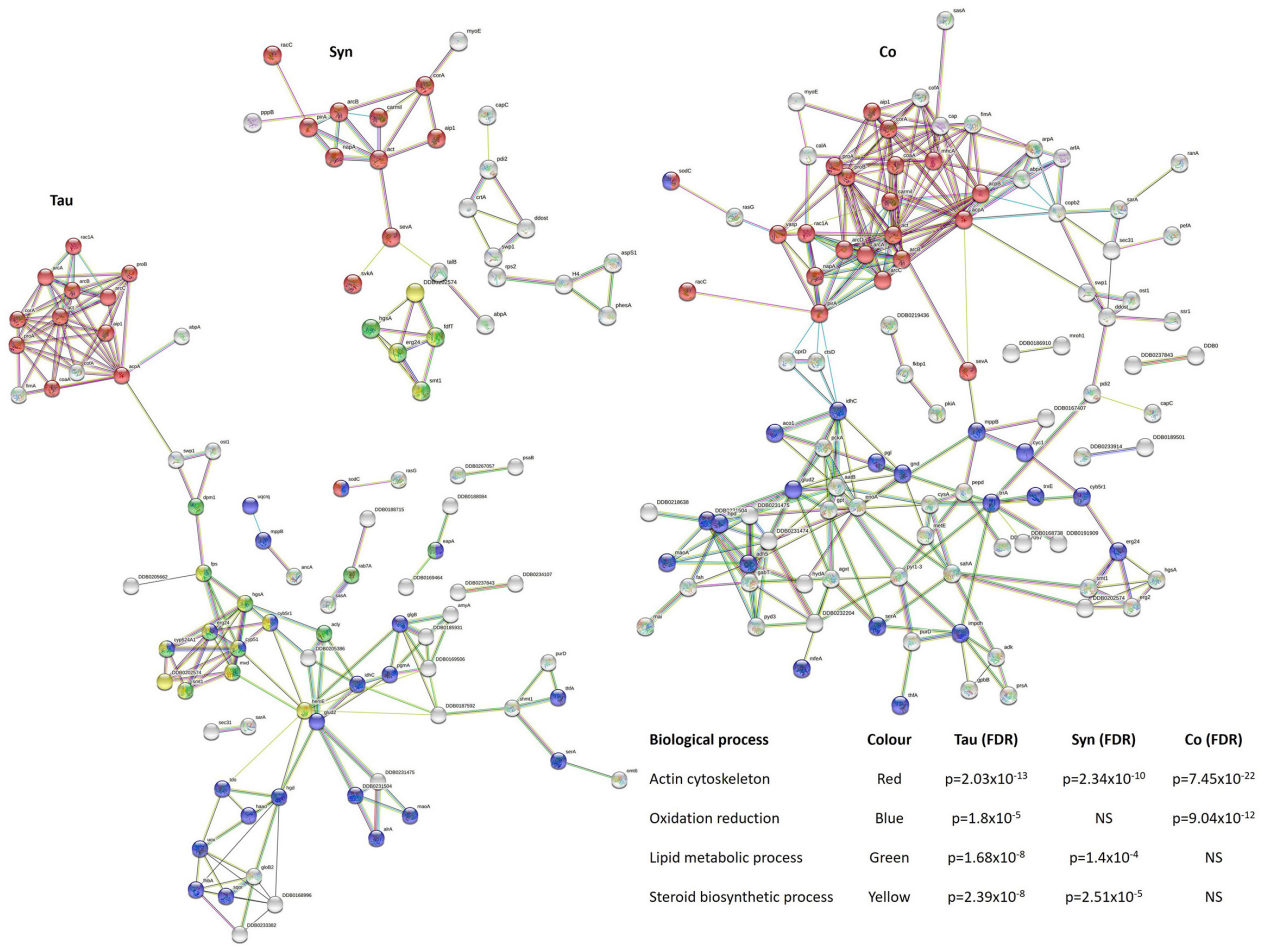

FIGURE 11 | Down-regulated biological processes in strains expressing tau and/or α-synuclein. To give a visual representation of protein groups, STRING was used to view the interacting protein clusters in the main processes down-regulated in the tau, α-synuclein, and cotransformants and calculate False Discovery Rates (FDR) which indicate statistical significance of the overrepresentation of these processes in the list of interacting proteins. Proteins and STRING protein annotations can be found in **Supplementary Tables 2, 4, 6**.

models (Badiola et al., 2011) and in LB from patients with LBD (Ishizawa et al., 2003). *D. discoideum* is an accepted model for investigating microtubule dynamics and interactions with microtubule associated proteins (MAPs) and is the best understood model for actin dynamics and function in eukaryotic cells (Eichinger et al., 1999; Noegel and Schleicher, 2000; Gerisch, 2009). An interaction between actin and MTs at the cell cortex has been established (Hestermann et al., 2002) and *D. discoideum* has many homologues of the mammalian MAPs (Graf et al., 2000; Rehberg and Gräf, 2002; Rehberg et al., 2005; Koch et al., 2006). The results presented here indicate an interaction of tau, tubulin and α-synuclein which could be further investigated in the future exploiting the well-established cytoskeletal genetics and molecular biology of the *D. discoideum* model.

There has been much evidence to suggest that mitochondrial dysfunction is involved in neurodegenerative diseases (Lin and Beal, 2006) and both tau and α-synuclein have been implicated. As *D. discoideum* has been well characterised as a model for mitochondrial disease exhibiting a clear set of phenotypes, we analysed the phenotypes of strains expressing tau or α-synuclein or both to determine which might be shared with mitochondrially diseased strains. The α-synuclein-mediated phenotypes and those caused by mitochondrial dysfunction have been compared previously and shown to be distinct (Fernando et al., 2020). Whereas impaired mitochondrial function caused greater intracellular *L. pneumophila* proliferation as well as defects in phototaxis, thermotaxis, growth and development, but did not impair phagocytosis or pinocytosis. Despite similarities in some of these phenotypes, the expression of wild type α-synuclein differed in that it impaired phagocytosis and *L. pneumophila* proliferation, while having no significant effect on growth in liquid, phototaxis, thermotaxis, or fruiting body morphology. In fact, direct assay of mitochondrial function showed that α-synuclein expression did not impair but enhanced mitochondrial respiration. The overall pattern of phenotypes suggested that α-synuclein cytotoxicity lies not in mitochondrial defects but in its impairment of specific endocytic pathways (Fernando et al., 2020).

In this work we report for the first time that tau expression increases *L. pneumophila* susceptibility, has no significant effect on phagocytosis or pinocytosis, impairs growth in liquid but not on bacterial lawns, and causes moderate phototaxis and thermotaxis defects as well as aberrant fruiting bodies with shorter, thicker stalks. This pattern of phenotypic outcomes is very distinct to those caused by α-synuclein expression and indicates that tau and α-synuclein cause different cytotoxic effects in *D. discoideum*. In fact the phenotypic consequences of tau expression are reminiscent of mitochondrial disease phenotypes, with the exception of the normal plaque expansion rates in tau-expressing strains. When mitochondrial respiratory function was measured using Seahorse respirometry, we found an isolated defect in ATP synthesis by complex V, accompanied by an elevation of the mitochondrial "proton leak" (the use of the mitochondrial proton gradient to drive diverse mitochondrial transport processes other than ATP synthesis). Were it not for the normal growth on bacterial lawns, the cytopathological effects of tau expression in *D. discoideum* could thus be attributed entirely to this mitochondrial defect. This raises the question of what other mechanisms might be involved.

The phenotypic abnormalities caused by tau all involved the cytoskeleton and this corresponds with the downregulation of actin cytoskeletal proteins found in the proteomic analysis. Tau impaired axenic growth with a slower generation time in liquid compared to the WT, but this was not mediated by a pinocytosis defect and there was no significant downregulation of proteins associated with the macropinocytic cup. This suggests that other pathways mediating cell proliferation could be causing the defect. This could be a defect in cytokinesis as proteins involved in this process were down-regulated. *Dictyostelium* cytokinesis during growth in suspension in liquid medium depends entirely on the actomyosin cytoskeleton (Zang et al., 1997; Bosgraaf and van Haastert, 2006), whereas on surfaces it can take place by a different mechanism (De Lozanne and Spudich, 1987; Knecht and Loomis, 1987). In the tau transformant the Rho-related protein racE was downregulated. Larochelle et al. (1996) showed that racE was necessary for cytokinesis as *D. discoideum* mutants that did not express racE did not grow in suspension due to a cytokinesis defect. The same group found that racE cells containing an expression vector for racE were able to produce racE to wildtype levels and had no defect in cytokinesis and growth rates in suspension (Larochelle et al., 1997). A study detailing the effect of an *abiA* null mutant (part of the SCAR/WAVE complex that drives actin polymerisation) in *D. discoideum* showed that the axenic growth defect was due to a defect in cytokinesis (Pollitt and Insall, 2008). Tau-expressing strains also exhibited an increased susceptibility to intracellular *L. pneumophila* proliferation, which again corresponded with proteomics data that indicated proteins responsible for the cellular response to bacteria were down-regulated.

In view of the distinctive and sometimes opposite phenotypic outcomes of expressing tau and α-synuclein in *D. discoideum*, the question arises as to what happens in cotransformants expressing both proteins. We showed here that the cotransformants displayed a third distinct pattern of phenotypes, with the presence of the second protein either exacerbating (phototaxis, fruiting body morphology), reversing (phagocytosis, growth on plates, mitochondrial respiratory function, *L. pneumophila* proliferation), or having no significant impact (growth in liquid) on defects caused by the other. This indicates clear functional interactions of the two proteins in several phenotypic pathways and in some cases a synergistic effect. There is similar evidence to suggest an interaction and synergistic cytotoxicity of these two proteins in other model systems coexpressing tau and α-synuclein. In cellular models Badiola et al. (2011) found that tau and α-synuclein colocalised in primary neuronal cultures and the overexpression of tau lead to enhanced α-synuclein cytotoxicity. In a *Drosophila* model of PD, Roy and Jackson (2014) misexpressed tau and α-synuclein singly and in combination. They found that the expression of α-synuclein produced no phenotype associated with the eye, while the expression of tau caused the rough eye phenotype with smaller eyes and the combined expression of the two proteins resulted in a more severe phenotype. This accords with our finding that α-synuclein exacerbates tau-mediated defects in phototaxis and fruiting body morphology. Similarly in yeast, tau exacerbated the growth defects caused by α-synuclein (tau alone produced no defect) (Ciaccioli et al., 2013).

Although our results support a cytotoxic interaction between the two proteins in some phenotypes, we also found that in relation to other phenotypes the two proteins exerted opposing actions. Thus the significantly impaired growth on bacterial lawns and the phagocytosis defect observed in the α-synuclein strains were reversed in the cotransformants. In the case of intracellular *L. pneumophila* proliferation, tau not only reversed the reduction caused by α-synuclein, but increased the proliferation of the pathogen to the same elevated levels as observed when tau was expressed singly. There is evidence that tau affects neuronal phagocytosis (Xie et al., 2019) and α-synuclein affects synaptic endocytosis (Lautenschläger et al., 2017), but the effect of combined expression on endocytic pathways has not been previously reported.

Another of the phenotypes in which coexpression of tau and α-synuclein had opposing effects was in mitochondrial respiratory function. Previously we showed that α-synuclein did not cause an impairment in mitochondrial function but instead it increased respiratory activity coordinately in all components measured (Fernando et al., 2020). This result was consistent with increases in mitochondrial respiration seen in lymphoblast cell lines made from iPD patients (Annesley et al., 2016), fibroblasts from iPD patients (Haylett et al., 2016) and when neuroblastoma cells were seeded with α-synuclein fibrils (Ugalde et al., 2020). In this work we found that tau expression caused a significant decrease in the OCR dedicated to ATP synthesis thereby revealing a specific defect in Complex V. A decrease in ATP production has been seen in neuronal cultures overexpressing tau (Li et al., 2016) and this was accompanied by decreases in Complex I activity and in the ratio of ATP/ADP. Here we found no Complex I defect caused by tau in *D. discoideum*. The combined expression of tau and α-synuclein returned mitochondrial respiration to normal, reversing the elevated mitochondrial respiration caused by α-synuclein as well as the Complex V defect and elevated proton leak caused by tau. Altered mitochondrial function is associated

with many neurodegenerative diseases and this result highlights that it may occur through different mechanisms and the importance of looking at neuronal protein-protein interactions to advance our understanding of the part played by mitochondria in neurodegeneration. This emphasises the usefulness of using a simple model to study complex interactions and processes.

Many of the defective phenotypes observed in the tau-expressing strains were in line with mitochondrial dysfunction and previously this has been shown to be due to the chronic activation of AMPK (Bokko et al., 2007; Francione et al., 2009). To determine if there was a functional relationship between tau and AMPK in *D. discoideum,* we created cotransformants which expressed tau or tau and α-synuclein and antisense inhibited AMPK. As phototaxis is a signature defect of impaired mitochondrial function we investigated whether this phenotype was mediated by increased AMPK activity. The antisense inhibition of AMPK in tau strains and strains expressing both tau and α-synuclein resulted in a rescue of the phototaxis defect, suggesting that AMPK mediates the phototaxis defect caused by tau and exacerbated by α-synuclein coexpression. This suggests that AMPK may have been upregulated in the transformants, however, we could not measure this directly as AMPK could not be detected in any of the transformants or wild type strains. In neurons containing tau pathology in AD and many other tauopathies, AMPK levels and degree of activation (phosphorylation) are elevated (Vingtdeux et al., 2011). In cell culture a physical interaction between AMPK and tau was established and overexpression of AMPK increased tau toxicity and phosphorylation (Galasso et al., 2017). Interestingly, the inhibition of AMPK might serve as neuronal protection in neurodegenerative diseases (McCullough et al., 2005). Models of motor neuron disease and amylotrophic lateral sclerosis found benefits of downregulating AMPK (Lim et al., 2012). In *Drosophila* expressing tau downregulation of the AMPKα subunit partially rescued the tau rough eye phenotype. In future studies, determining if AMPK knockdown can rescue the other tau-mediated phenotypes would be beneficial, as would investigating whether AMPK phosphorylates tau in *D. discoideum.*

Proteomics analysis revealed that there were a number of proteins up- and down-regulated in these strains. In all strains more proteins were down-regulated than up-regulated, and the combined effect of tau and α-synuclein coexpression dysregulated the expression of more proteins than did expression of either protein on its own. The pattern of dysregulation caused by tau and α-synuclein expression were quite distinct from each other. Tau significantly up-regulated protein degradation and turnover, possibly in response to the defect in ATP synthesis, while α-synuclein up-regulated proteins involved in the response to bacterium corresponding with decreased *Legionella* susceptibility possibly as a result of a more efficient endolysosomal pathway. All strains exhibited a down-regulation of cytoskeletal proteins, which was exacerbated in the cotransformants. Interestingly here, the cotransformants displayed unique downregulation in some aspects of the cytoskeleton relating to cell motility, polarity, morphogenesis, and filopodium assembly corresponding with the more severe phototaxis defect. Both tau and α-synuclein down-regulated proteins involved in lipid and steroid metabolism, which are dysregulated in diseases like AD and PD. However, these pathways were not affected in the cotransformants, again consistent with a functional interaction between these two proteins that is sometimes beneficial rather than cytotoxic.

CONCLUSION

Our results show that *D. discoideum* can be a useful model to study the biological functions of tau and the interactions with other neurodegeneration-associated proteins. Whilst neurodegenerative disease like Alzheimer's and Parkinson's is characterised by death or dysfunction of neurons research is accumulating to suggest that the underlying disease mechanisms are likely to be more systemic occurring in many more cell types and not just isolated to neurons. We believe that by understanding the underlying molecular pathology that is shared by all cell types then we can understand why particular neurons or parts of the brain are selectively affected in these disorders. Here we used an organism which does not contain neurons, or a brain but it does contain many conserved pathways and proteins with humans and has been shown to be a good model for studying mitochondrial function, cell division, growth, endocytosis, autophagy and intracellular signalling all of which have been implicated in neurodegenerative disease. Here we expressed tau alone and in combination with α-synuclein to investigate the cytotoxic effects and interactions between the proteins in this simple model system. The results showed that tau and α-synuclein have different subcellular distributions but they colocalise in the cortical regions of the cell. They affect different pathways and phenotypes when expressed singly and, depending on the pathway and phenotype, these effects can be enhanced or reversed by the expression of both proteins at once. Thus, the *D. discoideum* model has revealed that the α-synuclein/tau interaction is clear but more complex than a simple synergistic cytotoxicity. These complexities are worthy of further investigation in models like *D. discoideum* in which they can be studied without concerns about the possible effects of endogenous orthologues.

DATA AVAILABILITY STATEMENT

The datasets presented in this study can be found in online repositories. The name of the repository and accession number can be found below: MassIVE, https://massive.ucsd.edu/ProteoSAFe/static/massive.jsp, MSV000087848.

AUTHOR CONTRIBUTIONS

KM made the tau construct and tau strains including cotransformants, performed all of the experiments for the

tau and cotransformant strains, analysed the data, and prepared, reviewed, and edited the original manuscript. SF made the α-syn constructs and strains and performed most of the phenotypic experiments with these strains. PF and SA conceptualised the project, supervised KM, advised on data analysis, and reviewed/edited the manuscript. All authors have read and agreed to the published version of the manuscript.

ACKNOWLEDGMENTS

KM was the recipient of a La Trobe University Postgraduate Scholarship and Australian Government Research Training Program Fees Offset.

SUPPLEMENTARY MATERIAL

The Supplementary Material for this article can be found online at: https://www.frontiersin.org/articles/10.3389/fcell.2021.741662/full#supplementary-material

Supplementary Table 1 | Tau up-regulated proteins.

Supplementary Table 2 | Tau down-regulated proteins.

Supplementary Table 3 | α-Synuclein up-regulated proteins.

Supplementary Table 4 | α-Synuclein down-regulated proteins.

Supplementary Table 5 | Cotransformant up-regulated proteins.

Supplementary Table 6 | Cotransformant down-regulated proteins.

REFERENCES

Abraha, A., Ghoshal, N., Gamblin, T. C., Cryns, V., Berry, R. W., Kuret, J., et al. (2000). C-terminal inhibition of tau assembly in vitro and in Alzheimer's disease. *J. Cell Sci.* 113, 3737–3745. doi: 10.1242/jcs.113.21.3737

Alecu, I., and Bennett, S. A. L. (2019). Dysregulated lipid metabolism and its role in α-synucleinopathy in parkinson's disease. *Front. Neurosci.* 13:328. doi: 10.3389/fnins.2019.00328

Alim, M. A., Hossain, M. S., Arima, K., Takeda, K., Izumiyama, Y., Nakamura, M., et al. (2002). Tubulin seeds α-synuclein fibril formation. *J. Biol. Chem.* 277, 2112–2117. doi: 10.1074/jbc.M102981200

Andreadis, A., Brown, W. M., and Kosik, K. S. (1992). Structure and novel exons of the Human-tau Gene. *Biochemistry* 31, 10626–10633. doi: 10.1021/bi00158a027

Annesley, S. J., and Fisher, P. R. (2009a). Dictyostelium discoideum–a model for many reasons. *Mol. Cell. Biochem.* 329, 73–91. doi: 10.1007/s11010-009-0111-8

Annesley, S. J., and Fisher, P. R. (2009b). "Dictyostelium slug phototaxis," in *Chemotaxis: Methods and Protocols*, eds T. Jin and D. Hereld (Totowa, NJ: Humana Press), 67–76. doi: 10.1007/978-1-60761-198-1_4

Annesley, S. J., Lay, S. T., De Piazza, S. W., Sanislav, O., Hammersley, E., Allan, C. Y., et al. (2016). Immortalized Parkinson's disease lymphocytes have enhanced mitochondrial respiratory activity. *Dis. Models Mechan.* 9, 1295–1305. doi: 10.1242/dmm.025684

Arai, Y., Yamazaki, M., Mori, O., Muramatsu, H., Asano, G., and Katayama, Y. (2001). α-Synuclein-positive structures in cases with sporadic Alzheimer's disease: morphology and its relationship to tau aggregation. *Brain Res.* 888, 287–296. doi: 10.1016/S0006-8993(00)03082-1

Arima, K., Mizutani, T., Alim, M. A., Tonozuka-Uehara, H., Izumiyama, Y., Hirai, S., et al. (2000). NACP/α-synuclein and tau constitute two distinctive subsets of filaments in the same neuronal inclusions in brains from a family of parkinsonism and dementia with Lewy bodies: double-immunolabeling fluorescence and electron microscopic studies. *Acta Neuropathol.* 100, 115–121. doi: 10.1007/s004010050002

Augustinack, J., Schneider, A., Mandelkow, E.-M., and Hyman, B. (2002). Specific tau phosphorylation sites correlate with severity of neuronal cytopathology in Alzheimer's disease. *Acta Neuropathol.* 103, 26–35. doi: 10.1007/s004010100423

Avila, J. (2008). Tau kinases and phosphatases. *J. Cell Mol. Med.* 12, 258–259. doi: 10.1111/j.1582-4934.2007.00214.x

Avila, J., Lucas, J. J., Perez, M., and Hernandaz, F. (2004). Role of Tau protein in both physiological and pathological conditions. *Physiol. Rev.* 84, 361–384. doi: 10.1152/physrev.00024.2003

Badiola, N., de Oliveira, R. M., Herrera, F., Guardia-Laguarta, C., Goncalves, S. A., Pera, M., et al. (2011). Tau enhances alpha-synuclein aggregation and toxicity in cellular models of synucleinopathy. *PLoS One* 6:e26609. doi: 10.1371/journal.pone.0026609

Bandala-Sanchez, E., Annesley, S. J., and Fisher, P. R. (2006). A phototaxis signalling complex in *Dictyostelium discoideum*. *Eur. J. Cell Biol.* 85, 1099–1106. doi: 10.1016/j.ejcb.2006.04.005

Bok, E., Leem, E., Lee, B.-R., Lee, J. M., Yoo, C. J., Lee, E. M., et al. (2021). Role of the lipid membrane and membrane proteins in Tau pathology. *Front. Cell Dev. Biol.* 9:2167. doi: 10.3389/fcell.2021.653815

Bokko, P. B., Francione, L., Bandala-Sanchez, E., Ahmed, A. U., Annesley, S. J., Huang, X., et al. (2007). Diverse cytopathologies in mitochondrial disease are caused by AMP-activated protein kinase signaling. *Mol. Biol. Cell.* 18, 1874–1886. doi: 10.1091/mbc.e06-09-0881

Bosgraaf, L., and van Haastert, P. J. M. (2006). The regulation of myosin II in *Dictyostelium*. *Eur. J. Cell Biol.* 85, 969–979. doi: 10.1016/j.ejcb.2006.04.004

Brandt, R., Léger, J., and Lee, G. (1995). Interaction of tau with the neural plasma membrane mediated by tau's amino-terminal projection domain. *J. Cell Biol.* 131, 1327–1340. doi: 10.1083/jcb.131.5.1327

Buée, L., Bussière, T., Buée-Scherrer, V., Delacourte, A., and Hof, P. R. (2000). Tau protein isoforms, phosphorylation and role in neurodegenerative disorders. *Brain Res. Rev.* 33, 95–130. doi: 10.1016/s0165-0173(00)00019-9

Cabezas-Opazo, F. A., Vergara-Pulgar, K., Pérez, M. J., Jara, C., Osorio-Fuentealba, C., and Quintanilla, R. A. (2015). Mitochondrial dysfunction contributes to the pathogenesis of Alzheimer's Disease. *Oxid. Med. Cell Longev.* 2015:509654. doi: 10.1155/2015/509654

Carilla-Latorre, S., Gallardo, M. E., Annesley, S. J., Calvo-Garrido, J., Graña, O., Accari, S. L., et al. (2010). MidA is a putative methyltransferase that is required for mitochondrial complex I function. *J. Cell Sci.* 123, 1674–1683. doi: 10.1242/jcs.066076

Castillo-Carranza, D. L., Guerrero-Muñoz, M. J., Sengupta, U., Gerson, J. E., and Kayed, R. (2018). α-Synuclein oligomers induce a unique toxic Tau strain. *Biol. Psychiatry* 84, 499–508. doi: 10.1016/j.biopsych.2017.12.018

Ciaccioli, G., Martins, A., Rodrigues, C., Vieira, H., and Calado, P. (2013). A powerful yeast model to investigate the synergistic interaction of α-synuclein and Tau in neurodegeneration. *PLoS One* 8:e55848. doi: 10.1371/journal.pone.0055848

Cleveland, D. W., Hwo, S.-Y., and Kirschner, M. W. (1977). Physical and chemical properties of purified tau factor and the role of tau in microtubule assembly. *J. Mol. Biol.* 116, 227–247. doi: 10.1016/0022-2836(77)90214-5

Cummins, N., Tweedie, A., Zuryn, S., Bertran-Gonzalez, J., and Götz, J. (2019). Disease-associated tau impairs mitophagy by inhibiting Parkin translocation to mitochondria. *EMBO J.* 38:e99360. doi: 10.15252/embj.201899360

Darcy, P. K., Wilczynska, Z., and Fisher, P. R. (1994). Genetic analysis of *Dictyostelium* slug phototaxis mutants. *Genetics* 137, 977–985.

De Lozanne, A., and Spudich, J. A. (1987). Disruption of the *Dictyostelium myosin* heavy chain gene by homologous recombination. *Science* 236, 1086–1091. doi: 10.1126/science.3576222

De Strooper, B., and Annaert, W. (2010). Novel research horizons for presenilins and γ-secretases in cell biology and disease. *Annu. Rev. Cell Dev. Biol.* 26, 235–260. doi: 10.1146/annurev-cellbio-100109-104117

De Vos, A., Anandhakumar, J., Van den Brande, J., Verduyckt, M., Franssens, V., Winderickx, J., et al. (2011). Yeast as a model system to study tau biology. *Int. J. Alzheimer's Dis.* 2011, 1–16. doi: 10.4061/2011/428970

Drubin, D. G., and Kirschner, M. W. (1986). Tau protein function in living cells. *J. Cell Biol.* 103, 2739–2746. doi: 10.1083/jcb.103.6.2739

Eckert, A., Schmitt, K., and Götz, J. (2011). Mitochondrial dysfunction - the beginning of the end in Alzheimer's disease? Separate and synergistic modes of tau and amyloid-β toxicity. *Alzheimer's Res. Ther.* 3, 1–11. doi: 10.1186/alzrt74

Eichinger, L., Lee, S. S., and Schleicher, M. (1999). Dictyostelium as model system for studies of the actin cytoskeleton by molecular genetics. *Microsc. Res. Tech.* 47, 124–134. doi: 10.1002/(sici)1097-0029(19991015)47:2<124::aid-jemt5>3.0.co;2-8

Eichinger, L., Pachebat, J. A., Glöckner, G., Rajandream, M. A., Sucgang, R., Berriman, M., et al. (2005). The genome of the social amoeba *Dictyostelium discoideum*. *Nature* 435, 43–57.

Esposito, A., Dohm, C. P., Kermer, P., Bähr, M., and Wouters, F. S. (2007). α-Synuclein and its disease-related mutants interact differentially with the microtubule protein tau and associate with the actin cytoskeleton. *Neurobiol. Dis.* 26, 521–531. doi: 10.1016/j.nbd.2007.01.014

Fernando, S., Allan, C. Y., Mroczek, K., Pearce, X., Sanislav, O., Fisher, P. R., et al. (2020). Cytotoxicity and mitochondrial dysregulation caused by α-synuclein in *Dictyostelium discoideum*. *Cells* 9:2289. doi: 10.3390/cells9102289

Feuillette, S., Miguel, L., Frébourg, T., Campion, D., and Lecourtois, M. (2010). Drosophila models of human tauopathies indicate that Tau protein toxicity in vivo is mediated by soluble cytosolic phosphorylated forms of the protein. *J. Neurochem.* 113, 895–903. doi: 10.1111/j.1471-4159.2010.06663.x

Francione, L. M., and Fisher, P. R. (2011). Heteroplasmic mitochondrial disease in *Dictyostelium discoideum*. *Biochem. Pharmacol.* 82, 1510–1520. doi: 10.1016/j.bcp.2011.07.071

Francione, L. M., Annesley, S. J., Carilla-Latorre, S., Escalante, R., and Fisher, P. R. (2011). The Dictyostelium model for mitochondrial disease. *Semin. Cell Dev. Biol.* 22, 120–130. doi: 10.1016/j.semcdb.2010.11.004

Francione, L., Smith, P. K., Accari, S. L., Taylor, P. E., Bokko, P. B., Bozzaro, S., et al. (2009). *Legionella pneumophila* multiplication is enhanced by chronic AMPK signalling in mitochondrially diseased *Dictyostelium* cells. *Dis. Models Mechan.* 2, 479–489. doi: 10.1242/dmm.003319

Galasso, A., Cameron, C. S., Frenguelli, B. G., and Moffat, K. G. (2017). An AMPK-dependent regulatory pathway in tau-mediated toxicity. *Biol. Open* 6, 1434–1444. doi: 10.1242/bio.022863

Galpern, W. R., and Lang, A. E. (2006). Interface between tauopathies and synucleinopathies: a tale of two proteins. *Ann. Neurol.* 59, 449–458. doi: 10.1002/ana.20819

Gammon, K. (2014). Neurodegenerative disease: brain windfall. *Nature* 515, 299–300. doi: 10.1038/nj7526-299a

Gellermann, G. P., Appel, T. R., Davies, P., and Diekmann, S. (2006). Paired helical filaments contain small amounts of cholesterol, phosphatidylcholine and sphingolipids. *Biol. Chem.* 387, 1267–1274. doi: 10.1515/BC.2006.157

Gerisch, G. (2009). Imaging actin cytoskeleton dynamics in *Dictyostelium chemotaxis*. *Methods Mol. Biol.* 571, 385–400. doi: 10.1007/978-1-60761-198-1_26

Gibson, G. E., Shi, Q., Zhu, X., Beal, M. F., Wang, X., Perry, G., et al. (2010). A mitocentric view of Alzheimer's Disease suggests multi-faceted treatments. *J. Alzheimer's Dis.* 20, S591–S607. doi: 10.3233/JAD-2010-100336

Goedert, M., and Spillantini, M. G. (2011). Pathogenesis of the tauopathies. *J. Mol. Neurosci.* 45, 425–431. doi: 10.1007/s12031-011-9593-4

Goedert, M., Spillantini, M. G., Jakes, R., Rutherford, D., and Crowther, R. A. (1989a). Multiple isoforms of human microtubule-associated protein tau: sequences and localization in neurofibrillary tangles of Alzheimer's disease. *Neuron* 3, 519–526. doi: 10.1016/0896-6273(89)90210-9

Goedert, M., Spillantini, M. G., Potier, M. C., Ulrich, J., and Crowther, R. A. (1989b). Cloning and sequencing of the cDNA encoding an isoform of microtubule-associated protein tau containing four tandem repeats: differential expression of tau protein mRNAs in human brain. *EMBO J.* 8, 393–399. doi: 10.1002/j.1460-2075.1989.tb03390.x

Goldberg, J. M., Manning, G., Liu, A., Fey, P., Pilcher, K. E., Xu, Y., et al. (2006). The dictyostelium kinome—analysis of the protein kinases from a simple model organism. *PLoS Genet.* 2:e38. doi: 10.1371/journal.pgen.0020038

Graf, R., Daunderer, C., and Schliwa, M. (2000). Dictyostelium DdCP224 is a microtubule-associated protein and a permanent centrosomal resident involved in centrosome duplication. *J. Cell Sci.* 113, 1747–1758. doi: 10.1242/jcs.113.10.1747

Grundke-Iqbal, I., Iqbal, K., Quinlan, M., Tung, Y. C., Zaidi, M. S., and Wisniewski, H. M. (1986). Microtubule-associated protein tau. A component of Alzheimer paired helical filaments. *J. Biol. Chem.* 261, 6084–6089.

Haase, C., Stieler, J. T., Arendt, T., and Holzer, M. (2004). Pseudophosphorylation of tau protein alters its ability for self-aggregation. *J. Neurochem.* 88, 1509–1520. doi: 10.1046/j.1471-4159.2003.02287.x

Hagele, S., Kohler, R., Merkert, H., Schleicher, M., Hacker, J., and Steinert, M. (2000). Dictyostelium discoideum: a new host model system for intracellular pathogens of the genus Legionella. *Cell. Microbiol.* 2, 165–171. doi: 10.1046/j.1462-5822.2000.00044.x

Haggerty, T., Credle, J., Rodriguez, O., Wills, J., Oaks, A. W., Masliah, E., et al. (2011). Hyperphosphorylated Tau in an α-synuclein-overexpressing transgenic model of Parkinson's disease. *Eur. J. Neurosci.* 33, 1598–1610. doi: 10.1111/j.1460-9568.2011.07660.x

Hamilton, R. L. (2000). Lewy bodies in alzheimer's disease: a neuropathological review of 145 cases using α−synuclein immunohistochemistry. *Brain Pathol.* 10, 378–384. doi: 10.1111/j.1750-3639.2000.tb00269.x

Hanger, D. P., Betts, J. C., Loviny, T. L. F., Blackstock, W. P., and Anderton, B. H. (1998). New phosphorylation sites identified in hyperphosphorylated tau (paired helical filament-tau) from Alzheimer's Disease brain using nanoelectrospray mass spectrometry. *J. Neurochem.* 71, 2465–2476. doi: 10.1046/j.1471-4159.1998.71062465.x

Hanger, D. P., Byers, H. L., Wray, S., Leung, K.-Y., Saxton, M. J., Seereeram, A., et al. (2007). Novel phosphorylation sites in tau from Alzheimer brain support a role for casein kinase 1 in disease pathogenesis. *J. Biol. Chem.* 282, 23645–23654. doi: 10.1074/jbc.M703269200

Haylett, W., Swart, C., van der Westhuizen, F., van Dyk, H., van der Merwe, L., van der Merwe, C., et al. (2016). Altered mitochondrial respiration and other features of mitochondrial function in parkin-mutant fibroblasts from Parkinson's Disease patients. *Parkinson's Dis.* 2016:1819209. doi: 10.1155/2016/1819209

Hestermann, A., Rehberg, M., and Gräf, R. (2002). Centrosomal microtubule plus end tracking proteins and their role in *Dictyostelium* cell dynamics. *J. Muscle Res. Cell Motility* 23, 621–630. doi: 10.1023/A:1024450922609

Himmler, A., Drechsel, D., Kirschner, M. W., and Martin, D. W. (1989). Tau consists of a set of proteins with repeated C-terminal microtubule-binding domains and variable N-terminal domains. *Mol. Cell. Biol.* 9, 1381–1388. doi: 10.1128/mcb.9.4.1381

Iseki, E., Marui, W., Kosaka, K., and Uéda, K. (1999). Frequent coexistence of Lewy bodies and neurofibrillary tangles in the same neurons of patients with diffuse Lewy body disease. *Neurosci. Lett.* 265, 9–12. doi: 10.1016/S0304-3940(99)00178-0

Ishizawa, T., Mattila, P., Davies, P., Wang, D., and Dickson, D. W. (2003). Colocalization of Tau and alpha-synuclein epitopes in lewy bodies. *J. Neuropathol. Exp. Neurol.* 62, 389–397. doi: 10.1093/jnen/62.4.389

Jensen, P. H., Hager, H., Nielsen, M. S., Højrup, P., Gliemann, J., and Jakes, R. (1999). α-Synuclein binds to tau and stimulates the protein kinase a-catalyzed tau phosphorylation of serine residues 262 and 356. *J. Biol. Chem.* 274, 25481–25489. doi: 10.1074/jbc.274.36.25481

Joachim, C. L., Morris, J. H., Kosik, K. S., and Selkoe, D. J. (1987). Tau antisera recognize neurofibrillary tangles in a range of neurodegenerative disorders. *Ann. Neurol.* 22, 514–520. doi: 10.1002/ana.410220411

Klein, G., and Satre, M. (1986). Kinetics of fluid-phase pinocytosis in *Dictyostelium discoideum* amoebae. *Biochem. Biophys. Res. Commun.* 138, 1146–1152. doi: 10.1016/S0006-291X(86)80402-8

Knecht, D. A., and Loomis, W. F. (1987). Antisense RNA inactivation of myosin heavy chain gene expression in *Dictyostelium discoideum*. *Science* 236, 1081–1086. doi: 10.1126/science.3576221

Knuth, M., Khaire, N., Kuspa, A., Lu, S. J., Schleicher, M., and Noegel, A. A. (2004). A novel partner for *Dictyostelium filamin* is an alpha-helical developmentally regulated protein. *J. Cell Sci.* 117, 5013–5022. doi: 10.1242/jcs.01366

Koch, K. V., Reinders, Y., Ho, T.-H., Sickmann, A., and Gräf, R. (2006). Identification and isolation of *Dictyostelium* microtubule-associated protein interactors by tandem affinity purification. *Eur. J. Cell Biol.* 85, 1079–1090. doi: 10.1016/j.ejcb.2006.05.008

Kosik, K. S. (1993). The molecular and cellular biology of Tau. *Brain Pathol.* 3, 39–43. doi: 10.1111/j.1750-3639.1993.tb00724.x

Larochelle, D. A., Vithalani, K. K., and De Lozanne, A. (1996). A novel member of the rho family of small GTP-binding proteins is specifically required for cytokinesis. *J. Cell Biol.* 133, 1321–1329. doi: 10.1083/jcb.133.6.1321

Larochelle, D. A., Vithalani, K. K., and De Lozanne, A. (1997). Role of *Dictyostelium* racE in cytokinesis: mutational analysis and localization studies by use of green fluorescent protein. *Mol. Biol. Cell* 8, 935–944. doi: 10.1091/mbc.8.5.935

Lautenschläger, J., Kaminski, C. F., and Kaminski Schierle, G. S. (2017). α-Synuclein – regulator of exocytosis, endocytosis, or both? *Trends Cell Biol.* 27, 468–479. doi: 10.1016/j.tcb.2017.02.002

Lay, S. T., Sanislav, O., Annesley, S. J., and Fisher, P. R. (2016). "Mitochondrial stress test using Seahorse respirometry on intact cells," in *Methods in Molecular Biology*, eds D. Herald and T. Jin (Cham: Springer), 41–61. doi: 10.1007/978-1-4939-3480-5_4

Lee, V., Goedert, M., and Trojanowski, J. (2001). Neurodegenerative tauopathies. *Annu. Rev. Neurosci.* 24, 1121–1159.

Li, X. C., Hu, Y., Wang, Z. H., Luo, Y., Zhang, Y., Liu, X. P., et al. (2016). Human wild-type full-length tau accumulation disrupts mitochondrial dynamics and the functions via increasing mitofusins. *Sci. Rep.* 6, 24756–24756. doi: 10.1038/srep24756

Lim, M. A., Selak, M. A., Xiang, Z., Krainc, D., Neve, R. L., Kraemer, B. C., et al. (2012). Reduced activity of AMP-activated protein kinase protects against genetic models of motor neuron disease. *J. Neurosci.* 32, 1123–1141. doi: 10.1523/JNEUROSCI.6554-10.2012

Lin, M. T., and Beal, M. F. (2006). Mitochondrial dysfunction and oxidative stress in neurodegenerative diseases. *Nature* 443, 787–795. doi: 10.1038/nature05292

Lindwall, G., and Cole, R. D. (1984). Phosphorylation affects the ability of tau protein to promote microtubule assembly. *J. Biol. Chem.* 259, 5301–5305. doi: 10.1016/s0021-9258(17)42989-9

Lippa, C. F., Schmidt, M. L., Lee, V. M. Y., and Trojanowski, J. Q. (1999). Antibodies to α−synuclein detect Lewy bodies in many Down's syndrome brains with Alzheimer's disease. *Ann. Neurol.* 45, 353–357. doi: 10.1002/1531-8249(199903)45:3<353::aid-ana11>3.0.co;2-4

Ludtmann, M. H. R., Otto, G. P., Schilde, C., Chen, Z.-H., Allan, C. Y., Brace, S., et al. (2014). An ancestral non-proteolytic role for presenilin proteins in multicellular development of the social amoeba *Dictyostelium discoideum*. *J. Cell Sci.* 127, 1576–1584. doi: 10.1242/jcs.140939

Mandelkow, E., Von Bergen, M., Biernat, J., and Mandelkow, E.-M. (2007). Structural principles of tau and the paired helical filaments of Alzheimer's Disease. *Brain Pathol.* 17, 83–90. doi: 10.1111/j.1750-3639.2007.00053.x

Maniak, M. (2011). Dictyostelium as a model for human lysosomal and trafficking diseases. *Semin. Cell Dev. Biol.* 22, 114–119. doi: 10.1016/j.semcdb.2010.11.001

Mampel, J., Spirig, T., Weber, S. S., Haagensen, J. A. J., Molin, S., and Hilbi, H. (2006). Planktonic replication is essential for biofilm formation by *Legionella pneumophila* in a complex medium under static and dynamic flow conditions. *Appl. Environ. Microbiol.* 72, 2885–2895. doi: 10.1128/AEM.72.4.2885-2895.2006

Martín-González, J., Montero-Bullón, J.-F., and Lacal, J. (2021). Dictyostelium discoideum as a non-mammalian biomedical model. *Microb. Biotechnol.* 14, 111–125. doi: 10.1111/1751-7915.13692

Maselli, A., Laevsky, G., and Knecht, D. A. (2002). Kinetics of binding, uptake and degradation of live fluorescent (DsRed) bacteria by *Dictyostelium discoideum*. *Microbiology* 148, 413–420. doi: 10.1099/00221287-148-2-413

McCullough, L. D., Zeng, Z., Li, H., Landree, L. E., McFadden, J., and Ronnett, G. V. (2005). Pharmacological inhibition of AMP-activated protein kinase provides neuroprotection in stroke. *J. Biol. Chem.* 280, 20493–20502. doi: 10.1074/jbc.M409985200

McMains, V. C., Myre, M., Kreppel, L., and Kimmel, A. R. (2010). Dictyostelium possesses highly diverged presenilin/gamma-secretase that regulates growth and cell-fate specification and can accurately process human APP: a system for functional studies of the presenilin/gamma-secretase complex. *Dis. Model Mech.* 3, 581–594. doi: 10.1242/dmm.004457

Mondragón-Rodríguez, S., Perry, G., Luna-Muñoz, J., Acevedo-Aquino, M. C., and Williams, S. (2014). Phosphorylation of tau protein at sites Ser 396-404 is one of the earliest events in Alzheimer's disease and Down syndrome. *Neuropathol. Appl. Neurobiol.* 40, 121–135. doi: 10.1111/nan.12084

Nakamura, T., Yamashita, H., Takahashi, T., and Nakamura, S. (2001). Activated Fyn phosphorylates α-synuclein at tyrosine residue 125. *Biochem. Biophys. Res. Commun.* 280, 1085–1092. doi: 10.1006/bbrc.2000.4253

Nellen, W., Silan, C., and Firtel, R. A. (1984). DNA-mediated transformation in Dictyostelium discoideum: regulated expression of an actin gene fusion. *Mol. Cell Biol.* 4, 2890–2898. doi: 10.1128/mcb.4.12.2890-2898.1984

Noegel, A. A., and Schleicher, M. (2000). The actin cytoskeleton of *Dictyostelium*: a story told by mutants. *J. Cell Sci.* 113, 759–766.

Ogawa, S., Yoshino, R., Angata, K., Iwamoto, M., Pi, M., Kuroe, K., et al. (2000). The mitochondrial DNA of *Dictyostelium discoideum*: complete sequence, gene content and genome organization. *Mol. Gen. Genet.* 263, 514–519. doi: 10.1007/PL00008685

Otto, G. P., Wu, M. Y., Clarke, M., Lu, H., Anderson, O. R., Hilbi, H., et al. (2004). Macroautophagy is dispensable for intracellular replication of *Legionella pneumophila* in *Dictyostelium discoideum*. *Mol. Microbiol.* 51, 63–72. doi: 10.1046/j.1365-2958.2003.03826.x

Payton, J. E., Perrin, R. J., Clayton, D. F., and George, J. M. (2001). Protein–protein interactions of alpha-synuclein in brain homogenates and transfected cells. *Mol. Brain Res.* 95, 138–145. doi: 10.1016/S0169-328X(01)00257-1

Pérez, M. J., Jara, C., and Quintanilla, R. A. (2018a). Contribution of Tau pathology to mitochondrial impairment in neurodegeneration. *Front. Neurosci.* 12:441. doi: 10.3389/fnins.2018.00441

Pérez, M. J., Vergara-Pulgar, K., Jara, C., Cabezas-Opazo, F., and Quintanilla, R. A. (2018b). Caspase-cleaved tau impairs mitochondrial dynamics in Alzheimer's Disease. *Mol. Neurobiol.* 55, 1004–1018. doi: 10.1007/s12035-017-0385-x

Pollitt, A. Y., and Insall, R. H. (2008). Abi mutants in *Dictyostelium* reveal specific roles for the SCAR/WAVE complex in cytokinesis. *Curr. Biol.* 18, 203–210. doi: 10.1016/j.cub.2008.01.026

Rappsilber, J., Mann, M., and Ishihama, Y. (2007). Protocol for micro-purification, enrichment, pre-fractionation and storage of peptides for proteomics using StageTips. *Nat. Protocols* 2, 1896–1906. doi: 10.1038/nprot.2007.261

Rehberg, M., and Gräf, R. (2002). Dictyostelium EB1 Is a genuine centrosomal component required for proper spindle formation. *Mol. Biol. Cell.* 13, 2301–2310. doi: 10.1091/mbc.e02-01-0054

Rehberg, M., Kleylein-Sohn, J., Faix, J., Ho, T.-H., Schulz, I., and Gräf, R. (2005). *Dictyostelium* LIS1 Is a centrosomal protein required for microtubule/cell cortex interactions, nucleus/centrosome linkage, and actin dynamics. *Mol. Biol. Cell.* 16, 2759–2771. doi: 10.1091/mbc.e05-01-0069

Ren, Q.-G., Liao, X.-M., Chen, X.-Q., Liu, G.-P., and Wang, J.-Z. (2007). Effects of tau phosphorylation on proteasome activity. *FEBS Lett.* 581, 1521–1528. doi: 10.1016/j.febslet.2007.02.065

Reynolds, C. H., Betts, J. C., Blackstock, W. P., Nebreda, A. R., and Anderton, B. H. (2000). Phosphorylation sites on tau identified by nanoelectrospray mass spectrometry. *J. Neurochem.* 74, 1587–1595. doi: 10.1046/j.1471-4159.2000.0741587.x

Rhein, V., Song, X., Wiesner, A., Ittner, L. M., Baysang, G., Meier, F., et al. (2009). Amyloid-beta and tau synergistically impair the oxidative phosphorylation system in triple transgenic Alzheimer's disease mice. *Proc. Natl. Acad. Sci. U.S.A.* 106, 20057–20062. doi: 10.1073/pnas.0905529106

Roy, B., and Jackson, G. R. (2014). Interactions between Tau and α-synuclein augment neurotoxicity in a *Drosophila* model of Parkinson's disease. *Hum. Mol. Genet.* 23, 3008–3023. doi: 10.1093/hmg/ddu011

Savica, R., Grossardt, B. R., Bower, J. H., Ahlskog, J., and Rocca, W. A. (2013). INcidence and pathology of synucleinopathies and tauopathies related to parkinsonism. *JAMA Neurol.* 70, 859–866. doi: 10.1001/jamaneurol.2013.114

Sergeant, N., Bretteville, A., Hamdane, M., Caillet-Boudin, M.-L., Grognet, P., Bombois, S., et al. (2008). Biochemistry of tau in Alzheimer's disease and related neurological disorders. *Expert. Rev. Proteomic* 5, 207–224.

Shahmoradian, S. H., Lewis, A. J., Genoud, C., Hench, J., Moors, T. E., Navarro, P. P., et al. (2019). Lewy pathology in Parkinson's disease consists of crowded organelles and lipid membranes. *Nat. Neurosci.* 22, 1099–1109. doi: 10.1038/s41593-019-0423-2

Spillantini, M. G., and Goedert, M. (1998). Tau protein pathology in neurodegenerative diseases. *Trends Neurosci.* 21, 428–433. doi: 10.1016/s0166-2236(98)01337-x

Stelzmann, R. A., Schnitzlein, N. H., and Murtagh, R. F. (1995). An english translation of alzheimer's 1907 paper, "über eine eigenartige erkankung der hirnrinde". *Clin. Anatomy* 8, 429–431. doi: 10.1002/ca.980080612

Ugalde, C. L., Annesley, S. J., Gordon, S. E., Mroczek, K., Perugini, M. A., Lawson, V. A., et al. (2020). Misfolded α-synuclein causes hyperactive respiration without functional deficit in live neuroblastoma cells. *Dis. Models Mechan.* 13:dmm040899. doi: 10.1242/dmm.040899

Vanhelmont, T., Vandebroek, T., Vos, A. D., Terwel, D., Lamaire, K., Anandhakumar, J., et al. (2010). Serine-409 phosphorylation and oxidative damage define aggregation of human protein tau in yeast. *FEMS Yeast Res.* 10, 992–1005. doi: 10.1111/j.1567-1364.2010.00662.x

Vingtdeux, V., Davies, P., Dickson, D. W., and Marambaud, P. (2011). AMPK is abnormally activated in tangle- and pre-tangle-bearing neurons in Alzheimer's disease and other tauopathies. *Acta Neuropathol.* 121, 337–349. doi: 10.1007/s00401-010-0759-x

Wersinger, C., and Sidhu, A. (2005). Disruption of the interaction of α-synuclein with microtubules enhances cell surface recruitment of the dopamine transporter. *Biochemistry* 44, 13612–13624. doi: 10.1021/bi050402p

Wilczynska, Z., and Fisher, P. R. (1994). Analysis of a complex plasmid insertion in a phototaxis-deficient transformant of *Dictyostelium discoideum* selected on a *Micrococcus luteus* Lawn. *Plasmid* 32, 182–194. doi: 10.1006/plas.1994.1054

Wilkins, A., Khosla, M., Fraser, D. J., Spiegelman, G. B., Fisher, P. R., Weeks, G., et al. (2000). Dictyostelium RasD is required for normal phototaxis, but not differentiation. *Genes Dev.* 14, 1407–1413.

Xie, A. J., Hou, T. Y., Xiong, W., Huang, H. Z., Zheng, J., Li, K., et al. (2019). Tau overexpression impairs neuronal endocytosis by decreasing the GTPase dynamin 1 through the miR-132/MeCP2 pathway. *Aging Cell* 18:e12929. doi: 10.1111/acel.12929

Zabrocki, P., Pellens, K., Vanhelmont, T., Vandebroek, T., Griffioen, G., Wera, S., et al. (2005). Characterization of α-synuclein aggregation and synergistic toxicity with protein tau in yeast. *FEBS J.* 272, 1386–1400. doi: 10.1111/j.1742-4658.2005.04571.x

Zang, J.-H., Cavet, G., Sabry, J. H., Wagner, P., Moores, S. L., and Spudich, J. A. (1997). On the role of myosin-II in cytokinesis: division of dictyostelium cells under adhesive and nonadhesive conditions. *Mol. Biol. Cell* 8, 2617–2629. doi: 10.1091/mbc.8.12.2617

Conflict of Interest: The authors declare that the research was conducted in the absence of any commercial or financial relationships that could be construed as a potential conflict of interest.

Publisher's Note: All claims expressed in this article are solely those of the authors and do not necessarily represent those of their affiliated organizations, or those of the publisher, the editors and the reviewers. Any product that may be evaluated in this article, or claim that may be made by its manufacturer, is not guaranteed or endorsed by the publisher.

Copyright © 2021 Mroczek, Fernando, Fisher and Annesley. This is an open-access article distributed under the terms of the Creative Commons Attribution License (CC BY). The use, distribution or reproduction in other forums is permitted, provided the original author(s) and the copyright owner(s) are credited and that the original publication in this journal is cited, in accordance with accepted academic practice. No use, distribution or reproduction is permitted which does not comply with these terms.

frontiers in Cell and Developmental Biology

ORIGINAL RESEARCH
published: 08 September 2021
doi: 10.3389/fcell.2021.734554

A Conserved Role for LRRK2 and Roco Proteins in the Regulation of Mitochondrial Activity

Katharina E. Rosenbusch[1†], Asmaa Oun[1,2,3†], Oana Sanislav[4], Sui T. Lay[4], Ineke Keizer-Gunnink[4], Sarah J. Annesley[4], Paul R. Fisher[4], Amalia M. Dolga[2] and Arjan Kortholt[1,5*]*

[1] Department of Cell Biochemistry, University of Groningen, Groningen, Netherlands, [2] Groningen Research Institute of Pharmacy (GRIP), Molecular Pharmacology XB10, Groningen, Netherlands, [3] Department of Biotechnology, Institute of Graduate Studies and Research, Alexandria University, Alexandria, Egypt, [4] Department of Physiology Anatomy and Microbiology, La Trobe University, Melbourne, VIC, Australia, [5] Department of Pharmacology, Faculty of Medicine, Suleyman Demirel University, Isparta, Turkey

OPEN ACCESS

Edited by:
Robin S. B. Williams,
University of London, United Kingdom

Reviewed by:
Kari K. Naylor,
University of Central Arkansas, United States
Patrick Lewis,
Royal Veterinary College (RVC), United Kingdom

***Correspondence:**
Amalia M. Dolga
A.M.Dolga@rug.nl
Arjan Kortholt
A.Kortholt@rug.nl

[†] These authors have contributed equally to this work

Specialty section:
This article was submitted to Molecular and Cellular Pathology, a section of the journal Frontiers in Cell and Developmental Biology

Received: 01 July 2021
Accepted: 16 August 2021
Published: 08 September 2021

Citation:
Rosenbusch KE, Oun A, Sanislav O, Lay ST, Keizer-Gunnink I, Annesley SJ, Fisher PR, Dolga AM and Kortholt A (2021) A Conserved Role for LRRK2 and Roco Proteins in the Regulation of Mitochondrial Activity. Front. Cell Dev. Biol. 9:734554. doi: 10.3389/fcell.2021.734554

Parkinson's Disease (PD) is the second most common neurodegenerative disease world-wide. Mutations in the multidomain protein Leucine Rich Repeat Kinase 2 (LRRK2) are the most frequent cause of hereditary PD. Furthermore, recent data suggest that independent of mutations, increased kinase activity of LRRK2 plays an essential role in PD pathogenesis. Isolated mitochondria of tissue samples from PD patients carrying LRRK2 mutations display a significant impairment of mitochondrial function. However, due to the complexity of the mitochondrial signaling network, the role of LRRK2 in mitochondrial metabolism is still not well understood. Previously we have shown that *D. discoideum* Roco4 is a suitable model to study the activation mechanism of LRRK2 *in vivo*. To get more insight in the LRRK2 pathways regulating mitochondrial activity we used this Roco4 model system in combination with murine RAW macrophages. Here we show that both *Dictyostelium roco4* knockout and cells expressing PD-mutants show behavioral and developmental phenotypes that are characteristic for mitochondrial impairment. Mitochondrial activity measured by Seahorse technology revealed that the basal respiration of *D. discoideum roco4-* cells is significantly increased compared to the WT strain, while the basal and maximal respiration values of cells overexpressing Roco4 are reduced compared to the WT strain. Consistently, LRRK2 KO RAW 264.7 cells exhibit higher maximal mitochondrial respiration activity compared to the LRRK2 parental RAW264.7 cells. Measurement on isolated mitochondria from LRRK2 KO and parental RAW 264.7 cells revealed no difference in activity compared to the parental cells. Furthermore, neither *D. discoideum roco4-* nor LRRK2 KO RAW 264.7 showed a difference in either the number or the morphology of mitochondria compared to their respective parental strains. This suggests that the observed effects on the mitochondrial respiratory in cells are indirect and that LRRK2/Roco proteins most likely require other cytosolic cofactors to elicit mitochondrial effects.

Keywords: Parkinson's disease, LRRK2, Roco protein, *Dictyostelium discoideum*, mitochondria

INTRODUCTION

Neurological disorders pose an increasing societal and economic burden within our aging population. Parkinson's Disease (PD) is the second most common neurological disorder affecting 1–2% of the population over 65 years old (Eichinger et al., 2005; Li et al., 2015). PD is characterized by the progressive loss of dopaminergic neurons in the substantia nigra pars compacta and the formation of fibrillar protein aggregates enriched in α-synuclein proteins, called Lewy bodies (Parkinson, 1817; Dauer and Przedborski, 2003). The majority of PD cases are sporadic or idiopathic whereas an increasing amount of familial forms of PD are being identified (Paisán-Ruíz et al., 2004; Zimprich et al., 2004; Karimi-Moghadam et al., 2018). PD-associated mutations have been found in 23 genes or loci, including *SNCA* (α-synuclein), *PARK2* (parkin), *PINK1*, *PARK7* (DJ-1) and *LRRK2* (leucine-rich repeat kinase 2) (Healy et al., 2008). Mutations in *LRRK2* genes cause an autosomal dominant hereditary type of PD and accounts for 5% of the cases among European and North American PD patients (Li et al., 2015). Importantly, it was shown recently that LRRK2 kinase activity was enhanced in post-mortem brain tissue from patients with idiopathic PD (iPD), suggesting that independent of mutations, wild-type LRRK2 plays a role in PD pathology as well (Di Maio et al., 2018).

LRRK2, a large multi-domain protein with a size of 286 kDa, belongs to the Roco protein family (Marín et al., 2008; van Egmond and van Haastert, 2010; Guaitoli et al., 2016). It consists of an N-terminal Armadillo domain, Ankyrin repeats, a LRR (leucine rich repeats) domain, a Roc (Ras of complex protein domain), a COR (C-terminal of Roc) domain, a kinase and a C-terminal WD40 domain (Mata et al., 2006; van Egmond and van Haastert, 2010; Guaitoli et al., 2016). Interestingly, the LRRK2 protein possesses two distinct enzymatic functions; a GTPase activity of the Roc and a kinase activity associated with the kinase domain (Mata et al., 2006; Guaitoli et al., 2016). Several mutations distributed over the *LRRK2* gene are associated with PD, with the G2019S mutation located within the kinase domain, being the most common mutation (Ozelius et al., 2006; Li et al., 2015). On the molecular level, it has been shown that all common LRRK2 PD mutations cause increased LRRK2 kinase activity and/or decreased GTPase activity (West et al., 2005, 2007; Greggio et al., 2006; Jaleel et al., 2007; Luzón-Toro et al., 2007; Aasly et al., 2010; Sheng et al., 2012; Ho et al., 2016). However, the underlying pathways involved in LRRK2- associated signaling with PD pathology are still not completely understood. LRRK2 has been linked to a wide range of biological processes and several LRRK2 kinase substrates have been proposed (Boon et al., 2014; Wallings et al., 2015; Roosen and Cookson, 2016; Rosenbusch and Kortholt, 2016; Tang, 2016). LRRK2 signaling is involved in mitochondrial regulation, autophagy and cell death, actin and microtubule dynamics, synthesis and transport of vesicles as well as neurotransmitter, immune responses, and the activity of the intestinal network (Esteves et al., 2014).

Impaired mitochondrial activity is a common characteristic of both, iPD and familial PD, and several genes linked to PD play an important role in mitochondrial quality control (Narendra et al., 2008; Youle and van der Bliek, 2012; Liu et al., 2017; Toyofuku et al., 2019; Delcambre et al., 2020; Weindel et al., 2020). Even though the mitochondrial morphology was found to be affected e.g., in age mutant Parkinsonian LRRK2(R1441G) mice, mitochondrial shape does not qualify as a biomarker as it is mainly detected in late stages of PD and/or post mortem and inconsistent with the disease pattern (Liu et al., 2020). One theory regarding the underlying trigger of PD involves the presence and accumulation of oxidative stress. Samples of the substantia nigra of PD patients have been found to exhibit increased levels of oxidized DNA, proteins, lipids, and overall ROS levels (Bender et al., 2006; Knoefler et al., 2013; Verma et al., 2014). Further experiments in yeast showed that overexpression of LRRK2 and hence its enzymatic activities triggered the loss of the mitochondrial transmembrane potential, ATP depletion, decreased respiratory capacities, generation of ROS and finally cell death (Aufschnaiter et al., 2018). Consistently, immortalized lymphocytes from individuals with iPD display dramatic elevations of mitochondrial respiratory activities (Annesley et al., 2016). The first indication that LRRK2 plays a role in mitochondrial signaling came from the observations that LRRK2 is localized to mitochondria in transfected HEK-293T cells and in rat brain models (West et al., 2005; Biskup et al., 2006). Subsequently, it was shown that overexpression of WT and PD-associated mutants of LRRK2 in SH- SY5Y cell line and in primary cortical neurons resulted in impaired mitochondrial fission and consequently the accumulation of fragmented mitochondria (Knoefler et al., 2013). This effect on mitochondrial dysfunction is dependent on LRRK2 enzymatic activity and the presence of the fission protein DLP1 (dynamin-like protein 1) (Niu et al., 2012; Wang et al., 2012; Su and Qi, 2013). Moreover, enhanced levels of fragmented mitochondria have also been found in PD patient-derived fibroblast lines with the LRRK2 G2019S mutation (Mortiboys et al., 2010; Smith et al., 2016). Higher levels of mitochondrial fission, CD68 (active microglia maker), Drp1 (mitochondrial fission marker) as well as a shortage of microglial processes were also found in the striatum brain area of LRRK2 G2019S transgenic mice (Ho et al., 2018). Addition of LPS (lipopolysaccharide) triggered enhanced mitochondrial fission and Drp1 levels, an effect which was rescued via the addition of the LRRK2 kinase inhibitor GSK2578215A (Ho et al., 2018). Also the PD associated LRRK2 mutation E193K displayed abnormal scaffold protein activity via an increased binding to Drp1 in primary fibroblasts and thus enhancing mitochondrial fission levels (Carrion et al., 2018). Fibroblasts from LRRK2 mutation G2019S carrier patients in turn demonstrated enhanced autophagy in response to mitochondrial challenging condition, indicating that the exhaustion of mitochondrial bioenergetics and autophagic reverse might contribute to the development of PD phenotypes (Juárez-Flores et al., 2018). Furthermore, brain samples isolated post-mortem from human G2019S PD patients showed increased phosphorylation of peroxiredoxin 3 (PRDX3), antioxidant of thioredoxin peroxidase family, and reduced endogenous peroxidase activity and increased oxidative damage (Angeles et al., 2011). A recent study suggests that LRRK2 also regulates mitochondrial quality control by modulating ER–mitochondrial

tethering by modulating the PERK-dependent ubiquitination pathway under ER stress conditions (Toyofuku et al., 2019). The G2019S mutation induced dissociation of LRRK2 from the E3 ubiquitin ligases MARCH5, MULAN, and Parkin, allowing PERK to phosphorylate and activate these enzymes, resulting in the ubiquitination of their mitochondrial substrates.

From these data it is clear that LRRK2 plays a role in mitochondrial control and/or signaling. However the exact effect LRRK2 mutations have on mitochondrial bioenergetics remains to be identified. Here we used the amoebic model organism *Dictyostelium discoideum* (*D. discoideum*) to further study the effect of Roco/LRRK2 mutations on mitochondrial morphology and activity. *D. discoideum* possesses 11 Roco proteins and has been successfully investigated with regards to gaining insight in the complex activation mechanism of LRRK2/Roco proteins and mitochondrial disease (Barth et al., 2007; van Egmond and van Haastert, 2010; Francione et al., 2011; Gilsbach et al., 2012). Previously, we have shown that Roco4 plays an important role in the late development stage of *D. discoideum* (van Egmond and van Haastert, 2010). Upon starvation cells lacking *roco4* initially undergo the characteristic developmental phases, however, after 12 h of starvation the cells start to display severe developmental defects (see also below). The formation of slugs and subsequent stalks and spore heads is severely delayed and *roco4* knockout (*roco4-*) cells display aberrant fruiting body morphology as the spore heads are located on the agar surface due to instable stalks. Interestingly, replacement of the Roco4 kinase domain with the LRRK2 kinase domain results in the restoration of functional Roco4 protein *in vivo* (Gilsbach et al., 2012). Furthermore, the LRRK2 mutation G2019S is conserved in Roco4, and corresponds to the G1179S mutation resulting likewise in an increased kinase activity (Gilsbach et al., 2012). Here, we showed that both *roco4-* and G1179S-expressing *D. discoideum* cells show behavioral and developmental phenotypes that are characteristic for mitochondrial impairment. Both mutant cell lines show a severe development phenotype and atypical spore morphology. The G1179S strain displayed lower mitochondrial activity, while *roco4-* strain displayed higher mitochondrial activity and ROS production compared to the WT strain although mitochondrial morphology was normal. We have verified these results for LRRK2 in murine macrophages RAW 264.7 cells, highly expressing endogenous LRRK2, and LRRK2 knockout (KO) RAW 264.7 cells. Together, our data show that *D. discoideum* Roco4 and human LRRK2 have a conserved role in the regulation of mitochondrial activity.

RESULTS

Altered *D. discoideum* Roco Protein Activity Results in Mitochondrial Disease-Like Phenotypes *in vivo*

D. discoideum possesses two different life cycles: a vegetative cycle, responsible for cell division, and a developmental cycle initiates upon nutrient depletion that culminates in the formation of dormant spores. During the developmental cycle *D. discoideum* cells aggregate to form a multicellular mobile organism, called a slug, which is able to move in the direction of light and heat, a process called photo-and thermotaxis, respectively, till it settles down to form the spore stalk and head. Roco4 expression is elevated during the later slug phase (> 12 h) and consistently, *roco4-* cells have previously been found to display severe development phenotypes, including delayed development and abnormal spore morphology (**Figures 1A–E**; van Egmond and van Haastert, 2010). The amino acid that is most frequently mutated in PD (G2019S) is conserved in Roco4 and corresponds to G1179S. Previously we have shown that both LRRK2G2019S and Roco4G1179S showed increased kinase activity *in vitro* (Kortholt et al., 2012). Interestingly, expression of Roco4 G1179S *in vivo*, results in a similar phenotype compared to *roco4-* cells (**Figures 1A–C**). Wild-type (WT) cells start forming slugs after 12 h, whereas both *roco4-* and Roco4 G1179S cells still remain in the mound stage after 12 h (**Figure 1A**). The two mutant cell lines remain in the mound stage for an excessive time period followed by multiple attempts to culminate. They eventually generate slugs and form fruiting bodies only after > 50 h (Roco4 G1179S) and > 70 h (*roco4-*) of starvation, respectively (**Figure 1A**). Furthermore, *roco4-* cells hardly make stalks, while Roco4 G1179S make much smaller stalks compared to WT (**Figure 1B**). Consistent with previous studies, we found that re-expression of the Roco4 WT protein (Roco4 rescue) completely restored the developmental defects (**Figures 1A–C**; van Egmond and van Haastert, 2010; Kortholt et al., 2012).

We next addressed whether the impaired development might be accompanied by a defect in phototaxis. Therefore, cells were washed, placed and developed on a non-nutrient agar (NNA) plate with a given light source in front. After 3 days the tracks of the migrated slug were blotted onto a plastic sheet, stained with Coomassie dye and the trails were quantified (**Figures 1D,E**). Wild-type cells showed highly efficient phototaxis toward the light source, with a phototactic index of 0.96 and a track length of 3.64 cm. In contrast both *roco4-* and G1179S cells showed severely impaired phototaxis. The *roco4-* slugs hardly move (**Supplementary Movie 1**) and therefore the accuracy of directional movement is indeterminate. The G1179S slugs do displace although impaired (1.37 cm) and with very poor directional movement toward the light (**Figure 1E**).

Together our results show that both the absence of Roco4 as well as the hyperactivity of the Roco4 kinase lead to impaired *D. discoideum* development and phototaxis. Interestingly, delayed development, impaired stalk formation and dysregulated phototaxis have been strongly linked to impaired mitochondrial function (Francione et al., 2011).

D. discoideum Roco Mutant Cells Have Enhanced ROS Production

To analyze the mitochondrial activity in the Roco4 mutants we determined the accumulation of reactive oxygen species (ROS) levels by analyzing the dye intensity of 2′,7′-Dichlorofluorescin diacetate (DCF-DA). This dye is colorless until it gets oxidized and generates the fluorescent product 2′,7′-dichlorofluorescein (DCF) (Brubacher and Bols, 2001). Accumulation of DCF

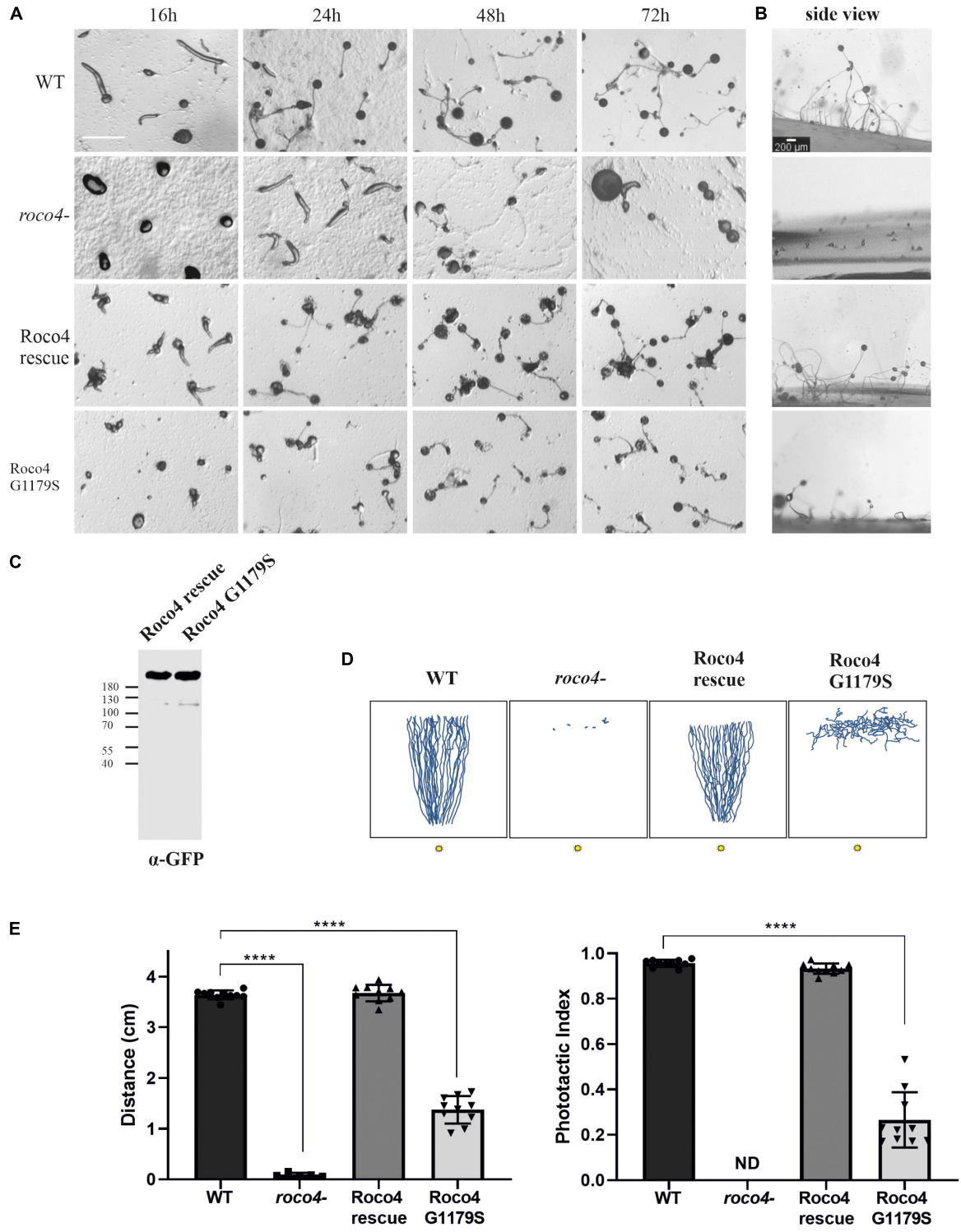

FIGURE 1 | Roco4 mutants have impaired development and phototaxis. **(A)** WT, *roco4-*, Roco4 rescue and Roco4 G1179S cells were plated on NN agar plates and images were taken at the indicated time points. Scale bar indicates 200 µm. **(B)** Side view of fruiting bodies after the completion of the developmental cycle. Scale bar indicates 200 µm. **(C)** Western blot of lysate of cells expressing Roco4-GFP and Roco4 G1179S-GFP cells. **(D)** Representative illustration of slug tracks. The 3 cm wide trench where cells started is positioned horizontally at the top and the 1 mm wide light slit is located at the bottom of the image. Illustrations of the scanned slug tracks have been made via ImageJ. **(E)** Phototactic properties of the indicated strains. Shown are the total distance moved (left panel) and the phototactic index (ratio of the total distance moved and the direct distance moved to the light. The data shown are the means of 20–25 tracks. **** indicates $P < 0.005$ differences from WT in an ANOVA test.

signal thus gives an indication of the amount of redox-active substances produced in the cell. WT and *roco4-* cells were washed with phosphate buffer to limit background noise and subsequently DCF-DA was added in the presence and absence of the Carbonyl cyanide m-chlorophenylhydrazone (CCCP). Mitochondrial uncoupler, CCCP, induces depolarization of the mitochondrial membrane and triggers maximum mitochondrial activity. The fluorescent signal accompanying the oxidation of DCF-DA to DCF has been measured after addition of CCCP. Initially WT and *roco4-* cells have similar low levels of ROS (**Figure 2A**), however, following CCCP addition the ROS production in *roco4-* cells appears to increase more compared to WT. Interestingly, in several *roco4-* cells the DCF fluorescence was so high that the complete cell is fluorescent and no individual patches can be observed (**Figure 2A**). To quantitatively analyze the DCF fluorescence intensity we used a plate reader assay (**Figure 2B**) and the vegetative WT and mutant cells were measured over time in the presence or absence of CCCP (**Figure 2B**). Consistent with the microscopy data, both cell lines display a similarly low level of initial ROS concentrations and *roco4-* cells show a significant increase of ROS levels following 30 min of CCCP challenge (**Figure 2B**).

Roco Proteins and LRRK2 Modulate Mitochondrial Respiration

To determine if the observed increase in ROS production is due to altered mitochondrial functioning, we analyzed the mitochondrial respiration of the WT, *roco4-*, Roco4 G1179S, and Roco4 rescue strains using the Seahorse Bioscience XF24 Extracellular Flux Analyzer (**Figure 3**). Seahorse technique enables kinetic measurement of oxidative metabolism by measuring the rate of oxygen consumption [oxygen consumption rate (OCR)] in real time. This method can provide detailed information on the metabolic phenotype by the addition of mitochondrial substrates and modulators of mitochondrial electron transport chain (Annesley et al., 2016). Cells were added to the Seahorse analyzer and basal OCR levels were determined prior to port injections and represent energetic demand of the cell under baseline conditions (**Figures 3A,E**). The decrease in OCR following the injection of ATP synthase inhibitor (DCCD or oligomycin) indicates the ATP synthesis rate (**Figure 3B**) while the maximum OCR is attained by adding the uncoupler (CCCP or FCCP) (**Figures 3C,F**). Complex I activity can be calculated by the decrease in OCR after rotenone addition (complex I inhibitor) (**Figure 3D**). Our data revealed that the basal mitochondrial respiration, ATP synthesis rate and complex I activity in the *roco4-* strain are significantly increased, while the maximum OCR is slightly increased yet not statistically significant compared to the WT strain (**Figures 3A–D**). In contrast, Roco4 G1179S and the Roco4 rescue cells exhibit a significantly reduced maximal respiration compared to the WT strain, while Roco4 G1179S cells have significantly lower basal respiration as well (**Figures 3E,F**). These data indicate that *D. discoideum* Roco4 mutants have an impact on different steps in the mitochondrial respiratory activity.

LRRK2 is highly expressed in immune cells and several studies have linked LRRK2 signaling to inflammation (Thévenet et al., 2011; Brockmann et al., 2017; Dzamko, 2017; Lee et al., 2017). We therefore used murine LRRK2 parental and LRRK2 KO RAW 264.7 macrophages to analyze whether the absence of LRRK2 (Knocking out) also has an effect on mitochondrial activity. LRRK2 KO RAW 264.7 cells show a higher maximal respiration and increased spare capacity compared to LRRK2 parental RAW 264.7 cells, whereas basal respiration, ATP-production and coupling efficiency [(ATP production/basal respiration)*100] were not significantly altered (**Figures 4A–E**). Previous studies have shown that the majority of LRRK2 is cytosolic and, if at all, only a small fraction of LRRK2 is present in mitochondria (West et al., 2005; Papkovskaia et al., 2012). We used high-resolution respirometry (Oroboros) to measure the activity of isolated mitochondria. Mitochondrial respiration was measured in the presence of the mitochondrial substrates, pyruvate, and malate (state 2). ADP was added in a saturating concentration to determine phosphorylating respiration (state3). Subsequently, oligomycin was applied to inhibit ATP synthase (state 4) and FCCP provided the maximal uncoupled-stimulated respiration (state 3U). Consistent with the proposed cytosolic LRRK2 localization we did not observe any significant differences in any of the mitochondrial respiration states between LRRK2 parental and KO RAW 264.7 cells, and can conclude that the OXPHOS complexes and complex V are functionally normal (**Figure 4F**).

Together our data show that *D. discoideum* Roco4 and LRRK2 mutants affect the mitochondrial respiration activity in a similar way. Furthermore, the differences between the whole cell and mitochondrial fraction measurements, suggest that this effect is indirect and that LRRK2 most likely requires other cytosolic cofactors to elicit mitochondrial effects.

Roco Mutants Do Not Affect Either the Number or the Morphology of Mitochondria

To gain information on the shape and number of mitochondria in the *D. discoideum* cells, we used a specific mitochondrial marker coupled to Alexa-594-conjugated streptavidin (Life Technologies). Alexa-594-streptavidin binds to the heavily biotinylated protein 3-methylcrotonyl-CoA carboxylase α, which is localized in the mitochondrial lumen (Davidson et al., 2013). WT and *roco4-* cells show a similar mitochondrial network both in vegetative cells and in starved cells. In both strains mitochondrial elongation is enhanced upon starvation due to increasing energy demands (**Figure 5A**; Katz, 2002). The fixed cells show very clear elongated and interconnected mitochondria with no visible fragmentation in either WT *or roco4-* cells. Similar observations have been made in living cells using the previously published marker fluorescent marker GFP-gemA (**Supplementary Figure 1**; Vlahou et al., 2011; Davidson et al., 2013). Furthermore, we observed no obvious differences in mitochondrial morphology in LRRK2 parental and KO RAW 264.7 cells (**Figure 5B**). The ratio (percentage) of mitochondria to overall cell size was calculated using area measurements on images with ImageJ software; no differences were observed for

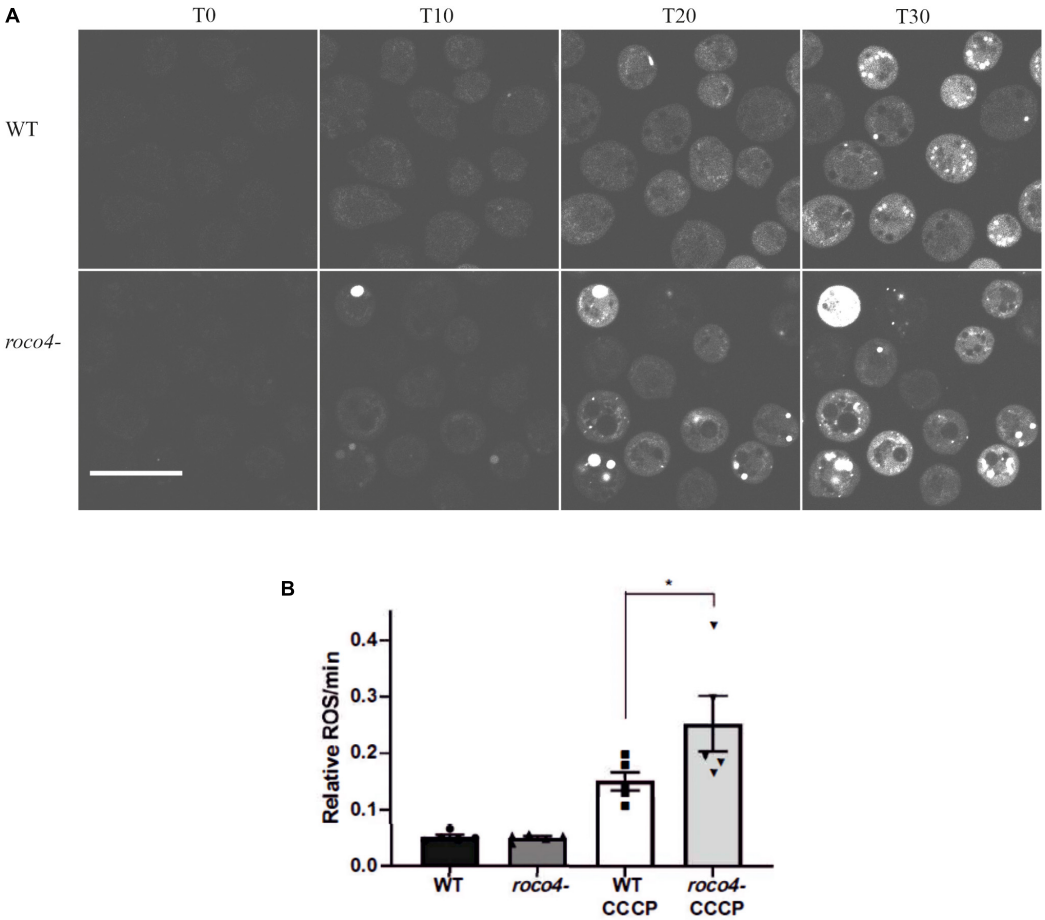

FIGURE 2 | ROS production in *D. discoideum* cells. **(A,B)** Six hours starved WT and *roco4-* cells were incubated with DCF-DA. **(A)** After addition of CCCP images were taken at the indicated time points ("T" minutes). Scale bar indicates 20 μm. **(B)** Total levels of ROS production were determined by measuring the intensity of the DCF signal using a microplate reader (Synergy HTX). Results are displayed as relative values to each other based on the increasing signal intensity. Shown are the means of 5 independent experiments, * indicates $P < 0.05$ difference from the WT control in a paired students *t*-test.

both the *roco4-* and LRRK2 KO RAW 264.7 strains compared to the respective parental strains (**Table 1**). Consistently, manual counting of the mitochondria of the *D. discoideum* cells did not reveal significant differences between WT and *roco4-* cells (**Table 1**). The amount of mitochondria are in accordance with the previous defined number of 50 mitochondria per cell and observer focal lane in healthy WT cells (Gilson et al., 2003).

To visualize qualitative ultrastructural details of the mitochondria within cells, we made use of Electron Microscopy (EM). Due to the high resolution it is possible to visualize the overall mitochondrial shape and organization and also details of the inner lumen with regards to size, folding, and organization of the cristae (**Figures 5C,D** and **Table 1**). *D. discoideum* WT and *roco4-* and RAW 264.7 WT and KO cells were fixed and visualized under the EM. The mitochondria of both *D. discoideum* cell lines are neither aggregated nor clustered in close proximity to a specific organelle (**Figure 5C**). Shape, size and connectivity of the mitochondria are in agreement with previous literature analyzing wild-type-like mitochondrial membranes (Arnoult et al., 2001). In accordance, EM images of LRRK2 parental and KO RAW 264.7 cells do not indicate an abnormal distribution of the mitochondria within the cell or in clusters around an identifiable organelle (**Figure 5D**). The mitochondria appear similar in size, shape, and connectivity compared to the overall cell volume in both cell lines (**Figure 5D** and **Table 1**). The cristae are clearly visible and display proper folding and organization as normal for mitochondria in eukaryotic cells. The differences in mitochondrial physiology as observed between parental and Roco mutants are thus not expressed in their (ultra)structural organization.

DISCUSSION

Although numerous studies have implicated mitochondrial dysfunction in LRRK2 pathogenesis of PD, the role of LRRK2 in mitochondrial bioenergetics is still a central unsettled query (Lin and Beal, 2006). Here we investigated the effect of mutated Roco proteins on mitochondrial functioning in an *in vivo* model system. First of all, we showed that *D. discoideum*

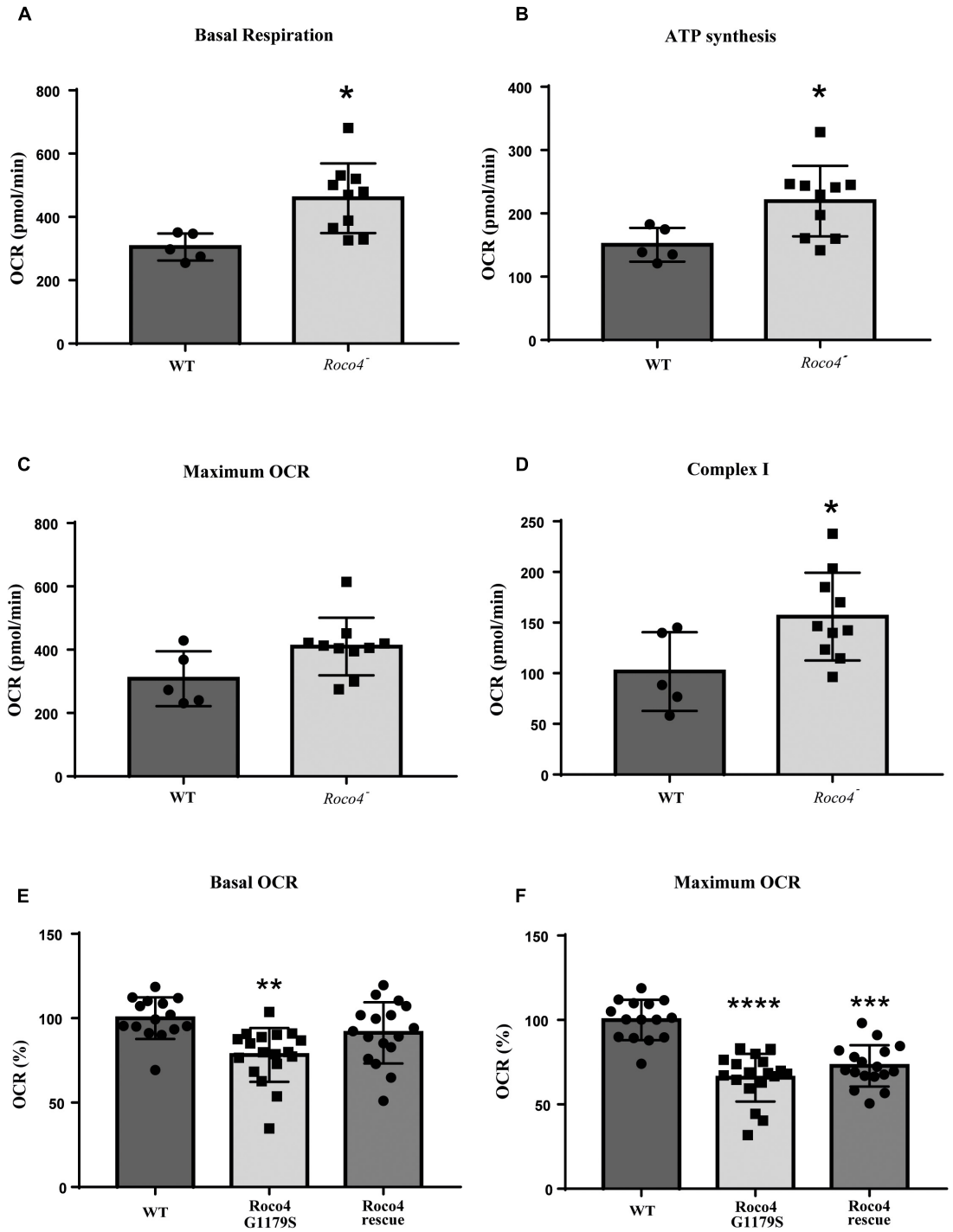

FIGURE 3 | Mitochondrial respirometry measurement in *D. discoideum* cells. The *roco4-* strain has enhanced mitochondrial respiratory activity while the Roco4 G1179S shows decreased mitochondrial respiration compared to the WT strain. Oxygen Consumption Rate (OCR) measurements were obtained over time (min) using an extracellular flux analyzer (Seahorse Bioscience). The mitochondrial stress test was used to obtain bioenergetic parameters. The figure shows the OCR values of the *D. discoideum* strains. **(A–D)** The *roco4-* strain has significantly elevated basal OCR, ATP synthesis rate and complex I activity compared to the WT. **(C)** The maximum OCR is slightly elevated though not significant. **(E,F)** Reduction in the basal and maximum OCR of the Roco4 G1179S strain relative to the WT while the Roco4 rescue cells show reduction only in the maximum OCR compared to the WT cells. All data are represented as mean ± SD. Statistical significance was assessed using unpaired *t*-test for the WT and the *roco4-* strains and one-way ANOVA with Tukey's post-test or Kruskal–Wallis test for the WT, Roco4 G1179S and Roco4 rescue strains. *P*-values indicating statistically significant differences between the mean values compared to the WT control and are defined as follows: $^{*}p < 0.05$, $^{**}p < 0.01$, $^{***}p < 0.001$, and $^{****}p < 0.0001$.

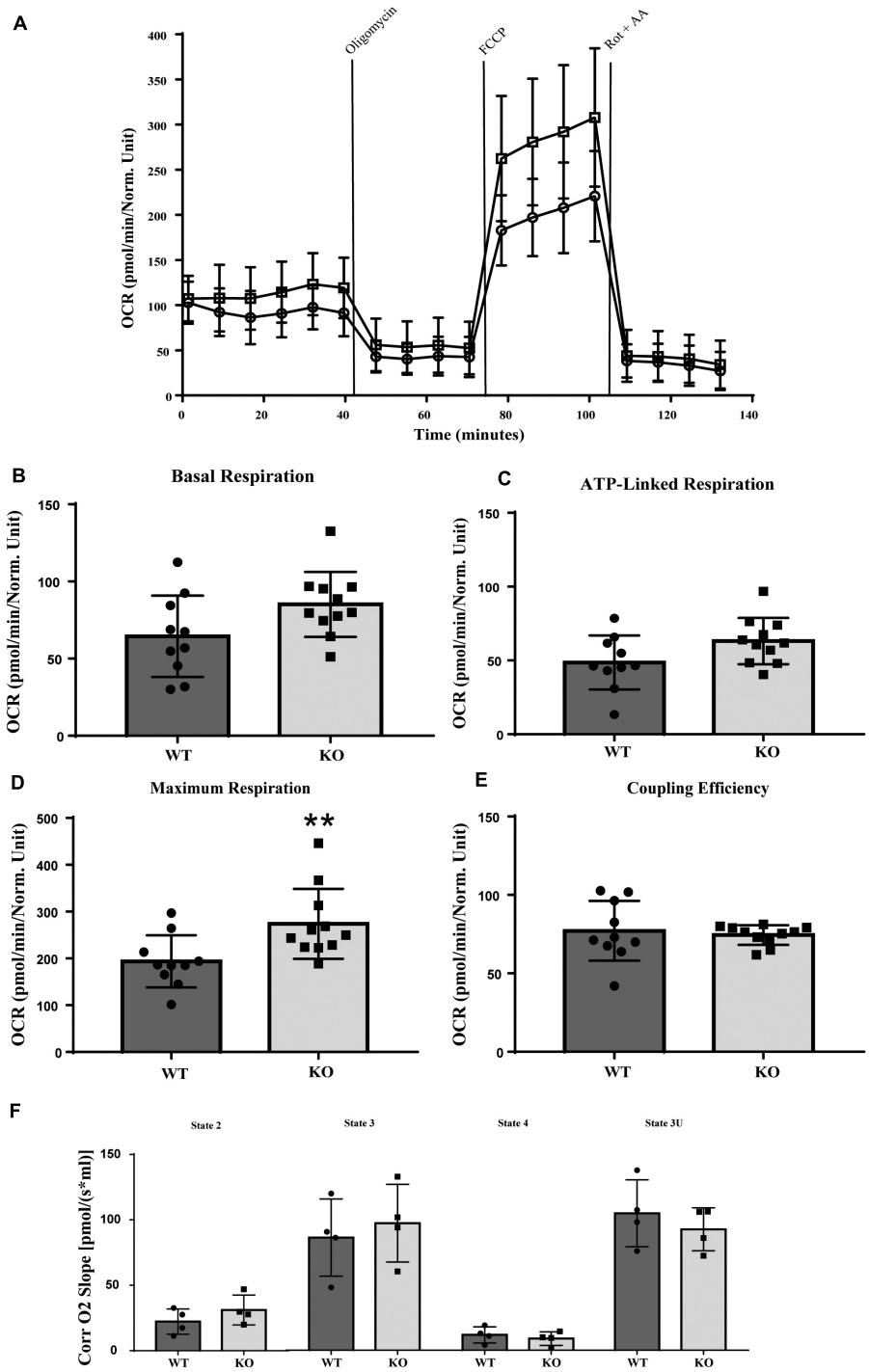

FIGURE 4 | Mitochondrial respirometry measurement in RAW 264.7 cells. LRRK2 KO RAW 264.7 cells have significantly higher maximum OCR in intact cells compared to LRRK2 parental RAW 264.7 cells while in isolated mitochondria the mitochondrial respiration is not altered. **(A)** Line graph of the OCR values of LRRK2 parental (closed circle) and KO RAW 264.7 (open square) cells in a representative seahorse measurement in intact cells. **(B–E)** Bar graphs showing different mitochondrial respiratory parameters for LRRK2 parental (black bar) and KO RAW 264.7 (gray bar) derived from the seahorse analysis. Data are represented as mean ± SD and statistical significance was computed using unpaired *t*-test or Mann-Whitney test. Data shown are representative of 10- 11 different wells/condition and the experiment was repeated at least three times with individual LRRK2 parental RAW 264.7 and LRRK2 KO RAW 264.7 macrophage cells. *P*-values indicating statistically significant differences between the mean values compared to the WT control with $^{**}p < 0.01$. **(F)** Corrected oxygen slope of different mitochondrial respiration states of LRRK2 parental (black bar) and KO RAW 264.7 (gray bar) cells revealing no significant differences in the mitochondrial respiration states in isolated mitochondrial fraction. Four independent experiments were performed and 3–4 measurements/cell line were measured in each experiment. Data are shown as mean ± SD of the average of four experiments.

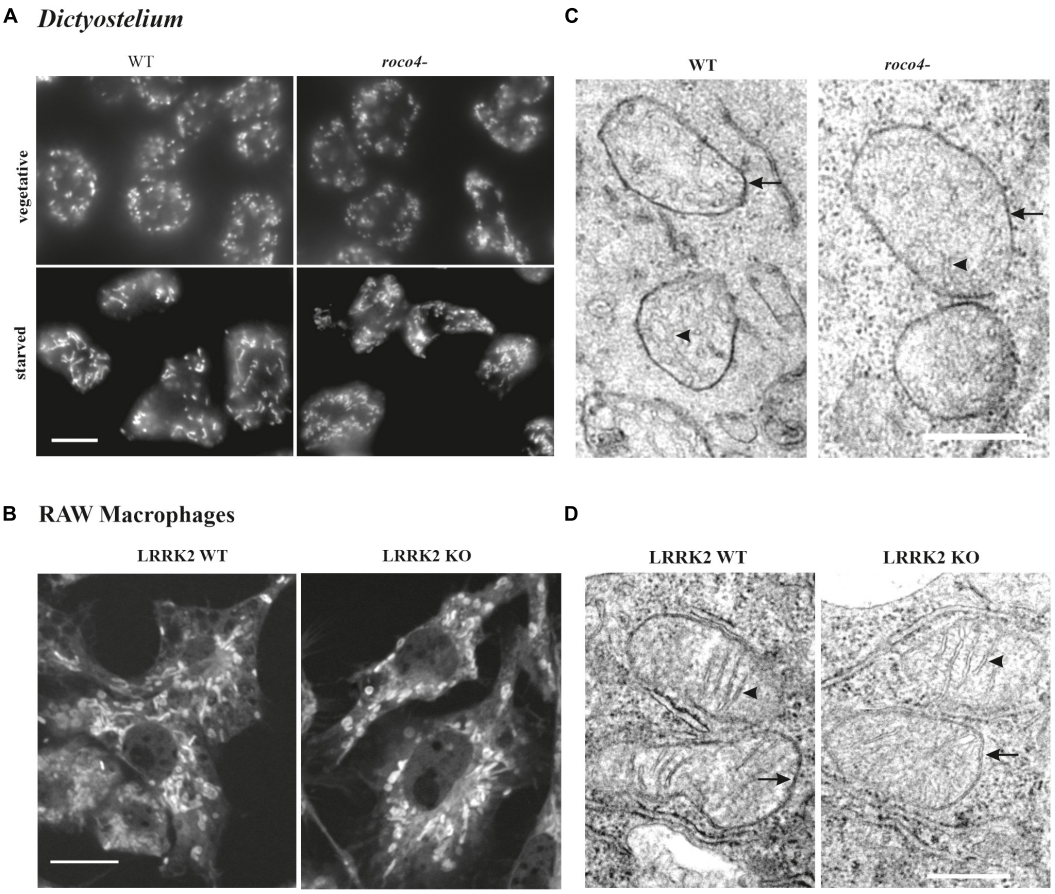

FIGURE 5 | Disruption of Roco4 or LRRK2 does not affect the number and morphology of mitochondria. **(A)** *D. discoideum* WT and *roco4-* cells in vegetative state and after starvation, stained with Alexa-594 conjugated streptavidin. Scale bar indicates 10 μm. **(B)** Macrophages, LRRK2 parental and LRRK2-KO strains, stained with MitoTracker™ Deep Red. Scale bar indicates 10 μm. **(C,D)** TEM images of mitochondria in the respective *D. discoideum* **(C)** and macrophage **(D)** cells. The mitochondrial inner and outer membrane layers are indicated with arrows whereas cristae with arrowheads. Scale bars indicate 1 μm.

cells lacking Roco4 and cells expressing the conserved PD mutation G1179S display strong phenotypes associated with mitochondrial malfunction: a delayed development, affected phototaxis and impaired stalk formation. Secondly, cells lacking Roco4 showed increased ROS production upon mitochondrial stress compared to the WT strain. Thirdly, using the well-established Seahorse XF Technology we showed that Roco4 mutants have altered mitochondrial bioenergetics. Under normal conditions, the cell functions using only a part of its bioenergetic capability, called basal respiration. Upon stress, the demand for extra ATP production increases (Desler et al., 2012). Our data show that *roco4-* cells display overall enhanced mitochondrial respiration compared to WT which is especially evident in the level of basal respiration, ATP synthesis and complex I activity. In contrast, the G1179S mutants cells displayed decreased mitochondrial respiration activities, making the PD-mutation more vulnerable to stress. Consistently, we found that LRRK2 KO RAW 264.7 cells exhibit significant enhanced mitochondrial respiration compared to the parental strain, especially with regards to the maximal respiration as well as spare capacities. So far contradicting effects on mitochondrial activity have been reported for LRRK2 PD mutant strains. Consistent with the Roco4 G1179S data, a previous study reported decreased basal OCRs for iPSC-derived neural cells from individuals carrying the LRRK2 G2019S and R1441C mutations compared to healthy control iPSC-derived neural cells, although the maximum OCR, ATP-synthesis and proton leak were not statistical significant changed (Cooper et al., 2012). Contrarily, the basal and maximal OCRs of fibroblasts from G2019S PD-patients and G2019S unaffected individuals exhibited comparable rates to the control fibroblasts, whereas the proton leak was increased in G2019S carrier fibroblasts independent of the disease status (Grünewald et al., 2013). Furthermore, immortalized PD lymphocytes showed enhanced mitochondrial activities as assessed via Seahorse XF measurements (Annesley et al., 2016), and ROS production was found to be enhanced in fibroblast cells from LRRK2 G2019S patient samples with higher level of oxygen damage (Yakhine-diop et al., 2014; Aufschnaiter et al., 2018; Juárez-Flores et al., 2018). Our data show that LRRK2 KO cells have increased mitochondrial maximum respiration, while LRRK2 mutations exhibit decreased maximum respiration, suggesting that alteration in LRRK2 activity in PD cells leads to

TABLE 1 | Quantification of mitochondria and cristae mitochondria.

Strain	Area mitochondria (% of cell)	Mitochondria (number/cell)	Cristae (number/mitochondrion)
D. d. WT	13.7 ± 1.0	49 ± 2.0	n.d.
D. d. roco4-	13.9 ± 1.1	47 ± 1.5	n.d.
LRRK2 parental	12.6 ± 0.6	n.d.	5.3 ± 0.7
LRRK2 KO	11.8 ± 1.4	n.d.	5.0 ± 0.6

D. discoideum cells were stained with 50 ng/mL Alexa-594 conjugated streptavidin (Life Technologies) for 30 min at 21°C, human RAW 264.7 cells were stained with 200 nM MitoTracker™ Deep Red FM (Invitrogen) for 30 min at 37°C. The number of mitochondria of one focal plane was manually counted in fixed vegetative D. discoideum cells. Shown are the mean and SEM of 25 cells per strain. The surface area [in percent (%)] indicates the ratio of the number of pixels covering the mitochondria with regards to the number of pixels of the overall cell area in the confocal plane. Values are the mean and SEM obtained from 25 cells per strain. The cristae were manually counted from EM pictures of fixed human RAW 264.7 cells of one focal plane. The counted numbers are the mean and SEM obtained from 25 mitochondria per strain. n.d., not determined.

impaired mitochondrial activity, however, the exact cellular effect might differ per cell strain and experimental conditions.

Interestingly, our high-resolution respirometry measurements on isolated mitochondria from LRRK2 KO and parental RAW 264.7 cells revealed no difference in activity compared to the parental cells. Furthermore, neither *D. discoideum roco4-* nor LRRK2 KO RAW 264.7 showed a difference in either the number or the morphology of mitochondria compared to their respective parental strains. This suggests that the observed effects on the mitochondrial respiratory in cells is indirect and that LRRK2/Roco proteins most likely require other cytosolic cofactors to elicit mitochondrial effects. The first evidence that LRRK2 plays a direct role in mitochondrial signaling has come from studies that reported a mitochondrial localization of LRRK2 (West et al., 2005; Biskup et al., 2006), however, others could not reproduce these findings (Greggio et al., 2007). The main reason for this discrepancy is the lack of antibodies and/or markers that convincingly visualize endogenous LRRK2 in cells. Interestingly, a more recent study that used a poly-ADP-ribose assisted protein localization assay (PARAPLAY), that overcomes the need of conventional immunocytochemistry showed that overexpressed LRRK2 does not localize to the mitochondrial matrix (Osuagwu et al., 2019). To confirm these findings for endogenous LRRK2 and understand where and how LRRK2 activation takes place it will be important to develop high-resolution LRRK2 imaging probes and/or GFP-LRRK2 knock-in models. Taken together we conclude that Roco mutant proteins lead to altered mitochondrial respiration *in vivo*, and that this effect is probably indirect. However, the levels of severity vary between the various detection methods, and different cell lines and PD models used.

In this study, we have used the *in vivo* model *D. discoideum* and RAW 264.7 macrophages. LRRK2 is highly expressed in both monocytes and microglia, the residential immune cells or the macrophage cells of the brain, and mutations of LRRK2 also underlie susceptibility to immune diseases, including leprosy and Crohn's disease, highlighting a potential immunologic function. Furthermore, rodent microglia and peripheral blood mononuclear cells display increased expression of LRRK2 and elevated inflammatory response to endotoxin lipopolysaccharide (LPS) and interferon γ (IFN-γ), respectively (Gardet et al., 2010; Moehle et al., 2012). α-synuclein aggregation, a hallmark of PD pathology has also been shown to increase the expression of LRRK2 proteins (Lin et al., 2009). Moreover, *LRRK2*-null rodent microglia have less inflammatory processes and cytokine release in response to the LPS stimulus (Daher et al., 2014). Together these results show that LRRK2 expression and activity are critical in order to achieve a (neuro)inflammatory response. Our data on the RAW 264.7 macrophages show that LRRK2 affects mitochondrial activity. To confirm and further investigate the role of LRRK2 in regulating mitochondrial respiration in immune cells, it will be important to perform high-resolution mitochondrial respirometry measurements in disease-relevant human immune cells, including primary human monocytes and iPSC-derived microglia from PD patients https://pubmed.ncbi.nlm.nih.gov/33540322/.

MATERIALS AND METHODS

Generation of *D. discoideum* Cell Lines

The *D. discoideum* cells were cultured in HL5 (Formedium) media. For starvation the medium was washed away and the cells were incubated in phosphate buffer (PB; 10 mM phosphate buffer, pH 6.5) for 6 h prior to the experiment. Roco4 mutants have been created and described previously. The generation of the *roco4-* cell line (DBS0350095) and the Roco4 constructs (DDB_G0288251)/G1179S (DBS0350100) has been described previously (van Egmond and van Haastert, 2010; Gilsbach et al., 2012). Transformation of the cells has been carried out according to standard protocol and the cells were cultured in the presence of the according selection marker (van Egmond and van Haastert, 2010). Expression of the constructs was verified via Western Blot. For this, vegetative cells were washed in PB and lysed in 1:2 volume ratio in SDS buffer (200 mM Tris, pH 6.8, 400 mM DTT, 8% SDS, 0.05 Bromophenol Blue, 20% Glycerol) at 95°C for 10 min. Cell lysate was loaded on a SDS-PAGE gel, subsequently blotted on a nitrocellulose membrane and incubated with α-GFP according to the standard procedure (Gilsbach et al., 2012) ["GFP Antibody (B-2)" and "m-IgGκ BP-HRP," Santa Cruz Biotechnology].

Origin and Cultivation of Macrophages

The murine cells were obtained from ATCC: parental RAW 264.7 and the LRRK2-KO (knockout) RAW 264.7. The cells were cultured in DMEM (LGC Standards GMBH) supplemented with 10% fetal bovine serum and 1% penicillin–streptomycin at 37°C in 5% CO_2.

Phenotypic Assays of *D. discoideum*

Starvation and onset of the developmental cycle have been induced by washing *D. discoideum* cells with PB. 2×10^7 cells were spread on ϕ5 cm 1.5% non-nutrient agar. Developmental time and stalk formation was monitored and documented using a Stemi SV 11 (Zeiss) microscope. For phototaxis, 5×10^5 cells were washed, resuspended in 10 μL and placed in a trench that

was cut out on the far end of an agar plate. The plate was placed in a dark ϕ6 cm tube with a 1 mm wide open light slit opposite the cells. Cells were allowed to absolve the developmental cycle (24–72 h). Slugs were formed that migrated toward the light source over the agar surface. Slug tracks, consisting of slime and cell debris were blotted to a PVC sheet, stained with Coomassie Blue and scanned via a CanonScan 9000F (Canon). The tracks were digitized and measured via ImageJ and the phototaxis index is expressed as the ratio of the absolute distance traveled to the light divided by the total track length.

Visualization of Mitochondria

For mitochondrial staining, *D. discoideum* cells were settled on glass plates, then fixed with ultracold (–80°C) Ethanol, washed with PB and incubated with 50 ng/mL Alexa-594 conjugated streptavidin (Life Technologies) for 30 min with no subsequent washing steps according to protocol (Davidson et al., 2013). Cell images were taken via a Zeiss Axio Observer microscope. The number of mitochondria was manually counted in 25 cells per cell line. The percentage area of the cell occupied by mitochondria was calculated using ImageJ as the ratio of mitochondrial area to the whole cell area.

Mitochondria in the macrophage cell lines were stained with a mitotracker dye: cells (250,000 cells/well) were grown overnight on coverslips. Then the growth medium was replaced with a fresh medium containing 200 nM MitoTracker^{TM} Deep Red FM (Invitrogen) and incubated for 30 min at 37°C, followed by washing twice with PBS and fixation with 4% PFA for 25 min. After washing with PBS the cover slips were mounted on glass slides using Floroshield^{TM} with DAPI (Sigma) as a mounting medium. To study mitochondrial morphology, images were taken via Zeiss LSM800 confocal microscope and analyzed with ImageJ. The percentage area of the cell occupied by mitochondria was calculated as described above.

For transmission electron microscopy (TEM), *D. discoideum* and macrophage cells were grown to a confluent monolayer on Thermanox coverslips (Thermo Fisher Scientific). The coverslips with cells were fixed by immersion in ice-cold glutaraldehyde (6% in 0.1 M cacodylate-buffer pH 7.2) overnight, washed thoroughly with water and subsequently fixed and contrasted with 1% OsO_4 in 0.1 M cacodylate-buffer pH 7.2 (1 h at RT). For *D. discoideum* $KMnO_4$ (1.5% in double distilled water) was used as additional fixative. After thorough washing with water, the cells were incubated overnight in 1% uranyl-acetate. The coverslips were dehydrated in a rising ethanol series and embedded in Epon with the following steps: infiltration with increasing ratio of Epoxy-resin in ethanol (1:1, 3:1, pure resin, 15 min each step, pure resin overnight). The coverslips were cut into smaller pieces and transferred to beem capsules and covered with fresh resin which was polymerized at 60°C for 48 h. Ultrathin sections were cut and the samples were examined with a transmission electron microscope (Philips CM12) at 80 kV.

Cellular ROS

For the detection of intracellular ROS levels, 5×10^5 vegetative *D. discoideum* cells were settled on glass plates for 30 min. A 10 μM 2′,7′-Dichlorofluorescin diacetate (DCF-DA, Sigma-Aldrich) was added to the cells and allowed to incubate for 30 min. Images (1 frame/min) of cells have been taken with a Zeiss LSM800 microscope with and without the addition of 1 μM Carbonyl cyanide m-chlorophenylhydrazone (CCCP; Sigma- Aldrich) over a time period of 30 min. Alternatively, 5×10^5 vegetative WT and mutant cells, washed and resuspended in PB, were seeded into wells of a black 96-wells-plate. A 10 μM DCF-DA was added to the wells and left to incubate for 30 min. Measurements (every minute) were taken immediately after the addition of 1 μM CCCP to the respective wells for 30 min via the microplate reader Synergy HTX (BioTek). Background measurements were taken of HL5 media with 10 μM DCF-DA and subtracted from the data. Measurements have been conducted five times.

Seahorse Measurements

Oxygen consumption measurements were performed on intact *D. discoideum* cells using the Seahorse XFe24 Flux Analyzer (Seahorse Biosciences) as previously described (Lay et al., 2016). Seahorse measurements were performed in two groups; one for the WT and *roco4-* strains and the other for the WT, Roco4 G1179S and Roco4 rescue. Briefly, *D. discoideum* cells were collected, washed and resuspended in SIH assay medium (SIH0102, ForMedium^{TM}, United Kingdom) supplemented with 20 mM sodium pyruvate and 5 mM sodium malate (pH 7.4). To ensure cell adherence during the assay, cells were seeded in XF24 cell culture plates coated with Matrigel® (growth factor reduced basement membrane matrix; Corning, MA, United States) at 1×10^5 cells/well and allowed to settle for 1–2 h. Bioenergetic profiling was performed by monitoring basal oxygen consumption rate (OCR) for 48 min followed by the sequential injection of the following inhibitors; N,N'-dicyclohexylcarbodiimide (DCCD; 10 μM; Sigma- Aldrich; Port A), carbonyl cyanide 3-chlorophenylhydrazone (CCCP; 10 μM; Sigma- Aldrich; Port B), rotenone (20 μM; Sigma- Aldrich; Port C), and antimycin A (10 μM; Sigma- Aldrich; Port D) at 32 min interval. Mitochondrial responses were monitored every 8 min following a cycle of 3 min mixing/2 min delay/3 min measurement. The following respiratory parameters were utilized to analyze the bioenergetic function: basal OCR, ATP synthesis rate (with DCCD), maximum OCR (with CCCP), complex I activity (with rotenone) and mitochondrial spare capacity (with antimycin A).

For bioenergetics assessment of the effect of LRRK2 on murine macrophage cells, adherent LRRK2 parental RAW 264.7 and LRRK2 KO RAW 264.7 cells were used. Cells were transferred to XF microplates at a seeding density of 75,000 cells/well 24 h before OCR measurement. After replacing the growth medium with 180 μL of assay medium supplemented with 25 mM glucose, 2 mM L-glutamine and 1 mM sodium pyruvate (pH 7.35), cells were preincubated for 1 h in a CO_2 free incubator at 37°C before starting the assay procedure. Following basal respiration measurement, various compounds such as: oligomycin (2.5 μM; Sigma-Aldrich), Carbonyl cyanide-4-(trifluoromethoxy)phenylhydrazone (FCCP; 2.5 μM; Sigma-Aldrich), rotenone (1 μM) and antimycin A (1 μM) were sequentially injected to assess mitochondrial coupling of respiratory chain, maximal and non-mitochondrial oxygen

consumption. OCR values were normalized to protein content in each well, determined with a BCA assay.

High-Resolution Respirometry

The function of the respiratory chain on isolated mitochondria in LRRK2 parental and KO RAW 264.7 cells was assessed via high resolution respirometry at 37°C, Oxygraph 2K (Oroboros systems, Innsbruck, Austria). Mitochondrial isolation was performed using a pump-controlled cell rupture system as formerly described (Schmitt et al., 2013). Isolated mitochondria (200 μg) were injected to an air tight chamber containing Mir05 (0.5 mM EGTA, 3 mM $MgCl_2$, 60 mM lactobionic acid, 20 mM taurine, 10 mM KH_2PO_4, 20 mM HEPES, 110 mM D-Sucrose and 1 mg/mL fatty acid-free BSA). Sequential addition of the following substances were done to measure mitochondrial respiration states; pyruvate (5 mM) and malate (2 mM) to assess non-phosphorylating respiration (mitochondrial state 2), saturating concentration of ADP (500 μM) to quantify the OXPHOS capacity of complex I-linked respiration (state 3), oligomycin (2 μg/mL) to inhibit the ATP-synthase (state 4), and stepwise titration of FCCP (1 μM) to calculate the maximal respiration (state 3U). Oxygen flux were recorded in real-time using the DatLab software and the data was analyzed with DatLab5 (version 5.1.1.91).

DATA AVAILABILITY STATEMENT

The original contributions presented in the study are included in the article/**Supplementary Material**, further inquiries can be directed to the corresponding author/s.

AUTHOR CONTRIBUTIONS

KR, PF, SA, AD, and AK designed the experimental research. KR and IK-G characterized the amoebic mutants and their mitochondrial phenotype. KR, AO, OS, and SL performed mitochondrial measurements. All contributed to writing the manuscript. All authors contributed to the article and approved the submitted version.

FUNDING

AK was the recipient of a TÜBITAK 2232 fellowship. AD was the recipient of a Rosalind Franklin Fellowship co-funded by the European Union and the University of Groningen.

ACKNOWLEDGMENTS

We want to thank P.J.M van Haastert for his scientific input and proofreading of the manuscript and Ahmed Soliman for help with preparation of the graphs.

SUPPLEMENTARY MATERIAL

The Supplementary Material for this article can be found online at: https://www.frontiersin.org/articles/10.3389/fcell.2021.734554/full#supplementary-material

REFERENCES

Aasly, J. O., Vilariño-Güell, C., Dachsel, J. C., Webber, P. J., West, A. B., Haugarvoll, K., et al. (2010). Novel pathogenic LRRK2 p.Asn1437His substitution in familial Parkinson's disease. *Mov. Disord.* 25, 2156–2163. doi: 10.1002/mds.23265

Angeles, D. C., Gan, B.-H., Onstead, L., Zhao, Y., Lim, K.-L., Dachsel, J., et al. (2011). Mutations in LRRK2 increase phosphorylation of peroxiredoxin 3 exacerbating oxidative stress-induced neuronal death. *Hum. Mutat.* 32, 1390–1397. doi: 10.1002/humu.21582

Annesley, S. J., Lay, S. T., De Piazza, S. W., Sanislav, O., Hammersley, E., Allan, C. Y., et al. (2016). Immortalized Parkinson ' s disease lymphocytes have enhanced mitochondrial respiratory activity. *Dis. Models Mech.* 9, 1295–1305. doi: 10.1242/dmm.025684

Arnoult, D., Girard, M., Sureau, F., Tissier, J. P., Grodet, A., Dellinger, M., et al. (2001). On the evolutionary conservation of the cell death pathway?: mitochondrial release of an apoptosis-inducing factor during *Dictyostelium discoideum*. *Cell Death* 12, 3016–3030. doi: 10.1091/mbc.12.10.3016

Aufschnaiter, A., Kohler, V., Walter, C., and Tosal-castano, S. (2018). The enzymatic core of the Parkinson ' s disease-associated protein LRRK2 impairs mitochondrial biogenesis in aging yeast. *Front. Mol. Neurosci.* 11:205. doi: 10.3389/fnmol.2018.00205

Barth, C., Le, P., and Fisher, P. R. (2007). Mitochondrial biology and disease in *Dictyostelium*. *Int. Rev. Cytol.* 263, 207–252. doi: 10.1016/S0074-7696(08)60321-6

Bender, A., Krishnan, K. J., Morris, C. M., Taylor, G. A., Reeve, A. K., Perry, R. H., et al. (2006). High levels of mitochondrial DNA deletions in substantia nigra neurons in aging and Parkinson disease. *Nat. Genet.* 38, 515–517. doi: 10.1038/ng1769

Biskup, S., Moore, D. J., Celsi, F., Higashi, S., West, A. B., Andrabi, S. A., et al. (2006). Localization of LRRK2 to membranous and vesicular structures in mammalian brain. *Ann. Neurol.* 60, 557–569. doi: 10.1002/ana.21019

Boon, J. Y., Dusonchet, J., Trengrove, C., and Wolozin, B. (2014). Interaction of LRRK2 with kinase and GTPase signaling cascades. *Front. Mol. Neurosci.* 7:64. doi: 10.3389/fnmol.2014.00064

Brockmann, K., Schulte, C., Schneiderhan-Marra, N., Apel, A., Pont-Sunyer, C., Vilas, D., et al. (2017). Inflammatory profile discriminates clinical subtypes in LRRK2-associated Parkinson's disease. *Eur. J. Neurol.* 24, 427–e6. doi: 10.1111/ene.13223

Brubacher, J. L., and Bols, N. C. (2001). Chemically de-acetylated 2',7'-dichlorodihydrofluorescein diacetate as a probe of respiratory burst activity in mononuclear phagocytes. *J. Immunol. Methods* 251, 81–91. doi: 10.1016/s0022-1759(01)00308-8

Carrion, M. P., Pischedda, F., Biosa, A., Russo, I., Straniero, L., Civiero, L., et al. (2018). The LRRK2 variant E193K prevents mitochondrial fission upon MPP + treatment by altering LRRK2 binding to DRP1. *Front. Mol. Neurosci.* 11:64. doi: 10.3389/fnmol.2018.00064

Cooper, O., Seo, H., Andrabi, S., Guardia-Laguarta, C., Graziotto, J., Sundberg, M., et al. (2012). Pharmacological rescue of mitochondrial deficits in iPSC-derived neural cells from patients with familial Parkinson's disease. *Sci. Transl. Med.* 4:141ra90. doi: 10.1126/scitranslmed.3003985

Daher, J. P. L., Volpicelli-Daley, L. A., Blackburn, J. P., Moehle, M. S., and West, A. B. (2014). Abrogation of α-synuclein-mediated dopaminergic neurodegeneration in LRRK2-deficient rats. *Proc. Natl. Acad. Sci. U.S.A.* 111, 9289–9294. doi: 10.1073/pnas.1403215111

Dauer, W., and Przedborski, S. (2003). Parkinson's disease: mechanisms and models. *Neuron* 39, 889–909.

Davidson, A. J., King, J. S., and Insall, R. H. (2013). The use of streptavidin conjugates as immunoblot loading controls and mitochondrial markers for use with *Dictyostelium discoideum*. *Biotechniques* 55, 39–41. doi: 10.2144/000114054

Delcambre, S., Ghelfi, J., Ouzren, N., Grandmougin, L., Delbrouck, C., Seibler, P., et al. (2020). Mitochondrial mechanisms of LRRK2 G2019S penetrance. *Front. Neurol.* 11:881. doi: 10.3389/fneur.2020.00881

Desler, C., Hansen, T. L., Frederiksen, J. B., Marcker, M. L., Singh, K. K., and Juel Rasmussen, L. (2012). Is there a link between mitochondrial reserve respiratory capacity and aging? *J. Aging Res.* 2012:192503. doi: 10.1155/2012/192503

Di Maio, R., Hoffman, E. K., Rocha, E. M., Keeney, M. T., Sanders, L. H., De Miranda, B. R., et al. (2018). LRRK2 activation in idiopathic Parkinson's disease. *Sci. Transl. Med.* 10:eaar5429. doi: 10.1126/scitranslmed.aar5429

Dzamko, N. L. (2017). LRRK2 and the immune system. *Adv. Neurobiol.* 14, 123–143. doi: 10.1007/978-3-319-49969-7_7.

Eichinger, L., Pachebat, J. A., Glöckner, G., Rajandream, M., Sucgang, R., Berriman, M., et al. (2005). The genome of the social amoeba *Dictyostelium discoideum*. *Nature* 435, 43–57. doi: 10.1038/nature03481

Esteves, A. R., Swerdlow, R. H., and Cardoso, S. M. (2014). LRRK2, a puzzling protein: insights into Parkinson's disease pathogenesis. *Exp. Neurol.* 261, 206–216. doi: 10.1016/j.expneurol.2014.05.025

Francione, L. M., Annesley, S. J., Carilla-Latorre, S., Escalante, R., and Fisher, P. R. (2011). The Dictyostelium model for mitochondrial disease. *Semin. Cell Dev. Biol.* 22, 120–130. doi: 10.1016/j.semcdb.2010.11.004

Gardet, A., Benita, Y., Li, C., Sands, B. E., Ballester, I., Stevens, C., et al. (2010). LRRK2 is involved in the IFN-gamma response and host response to pathogens. *J. Immunol.* 185, 5577–5585. doi: 10.4049/jimmunol.1000548

Gilsbach, B. K., Ho, F. Y., Vetter, I. R., van Haastert, P. J. M., Wittinghofer, A., and Kortholt, A. (2012). Roco kinase structures give insights into the mechanism of Parkinson disease-related leucine-rich-repeat kinase 2 mutations. *Proc. Natl. Acad. Sci. U.S.A.* 109, 10322–10327. doi: 10.1073/pnas.1203223109

Gilson, P. R., Yu, X., Hereld, D., Barth, C., Savage, A., Kiefel, B. R., et al. (2003). Two *Dictyostelium* orthologs of the prokaryotic cell division protein FtsZ localize to mitochondria and are required for the maintenance of normal mitochondrial morphology. *Eukaryot. Cell* 2, 1315–1326. doi: 10.1128/EC.2.6.1315

Greggio, E., Jain, S., Kingsbury, A., Bandopadhyay, R., Lewis, P., Kaganovich, A., et al. (2006). Kinase activity is required for the toxic effects of mutant LRRK2/dardarin. *Neurobiol. Dis.* 23, 329–341. doi: 10.1016/j.nbd.2006.04.001

Greggio, E., Lewis, P. A., Van Der Brug, M. P., Ahmad, R., Kaganovich, A., Ding, J., et al. (2007). Mutations in LRRK2/dardarin associated with Parkinson disease are more toxic than equivalent mutations in the homologous kinase LRRK1. *J. Neurochem.* 102, 93–102. doi: 10.1111/j.1471-4159.2007.04523.x

Grünewald, A., Arns, B., Meier, B., Brockmann, K., Tadic, V., and Klein, C. (2013). Does uncoupling protein 2 expression qualify as marker of disease status in LRRK2 -associated Parkinson's disease? *Antioxid. Redox Signal.* 20, 1955–1960. doi: 10.1089/ars.2013.5737

Guaitoli, G., Raimondi, F., Gilsbach, B. K., Gómez-Llorente, Y., Deyaert, E., Renzi, F., et al. (2016). Structural model of the dimeric Parkinson's protein LRRK2 reveals a compact architecture involving distant interdomain contacts. *Proc. Natl. Acad. Sci. U.S.A.* 113, E4357–E4366. doi: 10.1073/pnas.1523708113

Healy, D. G., Falchi, M., O'Sullivan, S. S., Bonifati, V., Durr, A., Bressman, S., et al. (2008). Phenotype, genotype, and worldwide genetic penetrance of LRRK2-associated Parkinson's disease: a case-control study. *Lancet Neurol.* 7, 583–590. doi: 10.1016/S1474-4422(08)70117-0

Ho, D. H., Jang, J., Joe, E., Son, I., Seo, H., and Seol, W. (2016). G2385R and I2020T Mutations Increase LRRK2 GTPase Activity. *Biomed Res. Int.* 2016:7917128. doi: 10.1155/2016/7917128

Ho, D. H., Je, A. R., Lee, H., Son, I., Kweon, H.-S., Kim, H.-G., et al. (2018). LRRK2 kinase activity induces mitochondrial fission in microglia via Drp1 and modulates neuroinflammation. *Exp. Neurobiol.* 27:171. doi: 10.5607/en.2018.27.3.171

Jaleel, M., Nichols, R. J., Deak, M., Campbell, D. G., Gillardon, F., Knebel, A., et al. (2007). LRRK2 phosphorylates moesin at threonine-558: characterization of how Parkinson's disease mutants affect kinase activity. *Biochem. J.* 405, 307–317. doi: 10.1042/BJ20070209

Juárez-Flores, D. L., González-Casacuberta, I., Ezquerra, M., Bañó, M., Carmona-Pontaque, F., Catalán-García, M., et al. (2018). Exhaustion of mitochondrial and autophagic reserve may contribute to the development of LRRK2 G2019S -Parkinson's disease. *J. Transl. Med.* 16, 1–13. doi: 10.1186/s12967-018-1526-3

Karimi-Moghadam, A., Charsouei, S., Bell, B., and Jabalameli, M. R. (2018). Parkinson disease from mendelian forms to genetic susceptibility: new molecular insights into the neurodegeneration process. *Cell. Mol. Neurobiol.* 38, 1153–1178. doi: 10.1007/s10571-018-0587-4

Katz, R. H. K. E. R. (2002). *Dictyostelium*: evolution, cell biology, and the development of multicellularity. *Q. Rev. Biol.* 77, 453–454.

Knoefler, D., Tienson, H. L., and Jakob, U. (2013). "Role of oxidative stress in aging," in *Oxidative Stress and Redox Regulation*, eds U. Jakob, and D. Reichmann (Dordrecht: Springer), 389–426. doi: 10.1007/978-94-007-5787-5_14

Kortholt, A., Gilsbach, B., and van Haastert, P. (2012). "Dictyostelium discoideum: a model system to study LRRK2-mediated parkinson disease,"in *Mechanisms in Parkinson's Disease–Models and Treatments*, ed. J. Dushanova, (Croatia: InTech) 293–310. doi: 10.5772/20207

Lay, S., Sanislav, O., Annesley, S. J., and Fisher, P. R. (2016). "Mitochondrial stress tests using seahorse respirometry on intact *Dictyostelium discoideum* cells," in *Methods in Molecular Biology*, eds T. Jin, and D. Hereld (New York, NY: Humana Press) 41–61. doi: 10.1007/978-1-4939-3480-5_4

Lee, H., James, W. S., and Cowley, S. A. (2017). LRRK2 in peripheral and central nervous system innate immunity: its link to Parkinson's disease. *Biochem. Soc. Trans.* 45, 131–139. doi: 10.1042/BST20160262

Li, X. X., Liao, Q., Xia, H., and Yang, X. L. (2015). Association between Parkinson's disease and G2019S and R1441C mutations of the LRRK2 gene. *Exp. Ther. Med.* 10, 1450–1454. doi: 10.3892/etm.2015.2659

Lin, M. T., and Beal, M. F. (2006). Mitochondrial dysfunction and oxidative stress in neurodegenerative diseases. *Nature* 443, 787–795. doi: 10.1038/nature05292

Lin, X., Parisiadou, L., Gu, X.-L., Wang, L., Shim, H., Sun, L., et al. (2009). Leucine-rich repeat kinase 2 regulates the progression of neuropathology induced by Parkinson's-disease-related mutant alpha-synuclein. *Neuron* 64, 807–827. doi: 10.1016/j.neuron.2009.11.006

Liu, H., Ho, P. W., Leung, C., Pang, S. Y., Eun, E., Chang, S., et al. (2020). Aberrant mitochondrial morphology and function associated with impaired mitophagy and DNM1L- MAPK / ERK signaling are found in aged mutant Parkinsonian LRRK2 mice ABSTRACT. *Autophagy* 1–25. doi: 10.1080/15548627.2020.1850008 [Epub ahead of print].

Liu, Z., Bryant, N., Kumaran, R., Beilina, A., Abeliovich, A., Cookson, M. R., et al. (2017). LRRK2 phosphorylates membrane-bound Rabs and is activated by GTP-bound Rab7L1 to promote recruitment to the trans-Golgi network. *Hum. Mol. Genet.* 27, 385–395. doi: 10.1093/hmg/ddx410

Luzón-Toro, B., Rubio de la Torre, E., Delgado, A., Pérez-Tur, J., and Hilfiker, S. (2007). Mechanistic insight into the dominant mode of the Parkinson's disease-associated G2019S LRRK2 mutation. *Hum. Mol. Genet.* 16, 2031–2039. doi: 10.1093/hmg/ddm151

Marín, I., van Egmond, W. N., and van Haastert, P. J. M. (2008). The Roco protein family: a functional perspective. *FASEB J.* 22, 3103–3110. doi: 10.1096/fj.08-111310

Mata, I. F., Wedemeyer, W. J., Farrer, M. J., Taylor, J. P., and Gallo, K. A. (2006). LRRK2 in Parkinson's disease: protein domains and functional insights. *Trends Neurosci.* 29, 286–293. doi: 10.1016/j.tins.2006.03.006

Moehle, M. S., Webber, P. J., Tse, T., Sukar, N., Standaert, D. G., DeSilva, T. M., et al. (2012). LRRK2 inhibition attenuates microglial inflammatory responses. *J. Neurosci.* 32, 1602–1611. doi: 10.1523/JNEUROSCI.5601-11.2012

Mortiboys, H., Johansen, K. K., Aasly, J. O., and Bandmann, O. (2010). Mitochondrial impairment in patients with Parkinson disease with the G2019S mutation in LRRK2. *Neurology* 75, 2017–2020. doi: 10.1212/WNL.0b013e3181ff9685

Narendra, D., Tanaka, A., Suen, D.-F., and Youle, R. J. (2008). Parkin is recruited selectively to impaired mitochondria and promotes their autophagy. *J. Cell Biol.* 183, 795–803. doi: 10.1083/jcb.200809125

Niu, J., Yu, M., Wang, C., and Xu, Z. (2012). Leucine-rich repeat kinase 2 disturbs mitochondrial dynamics via dynamin-like protein. *J. Neurochem.* 122, 650–658. doi: 10.1111/j.1471-4159.2012.07809.x

Osuagwu, N., Dölle, C., and Tzoulis, C. (2019). Poly-ADP-ribose assisted protein localization resolves that DJ-1, but not LRRK2 or α-synuclein, is localized to the mitochondrial matrix. *PLoS One* 14:e0219909. doi: 10.1371/journal.pone.0219909

Ozelius, L. J., Senthil, G., Saunders-Pullman, R., Ohmann, E., Deligtisch, A., Tagliati, M., et al. (2006). LRRK2 G2019S as a cause of Parkinson's disease in Ashkenazi jews. *N. Engl. J. Med.* 354, 424–425. doi: 10.1056/nejmc055509

Paisán-Ruíz, C., Jain, S., Evans, E. W., Gilks, W. P., Simón, J., van der Brug, M., et al. (2004). Cloning of the gene containing mutations that cause PARK8-linked Parkinson's disease. *Neuron* 44, 595–600. doi: 10.1016/j.neuron.2004.10.023

Papkovskaia, T. D., Chau, K.-Y. Y., Inesta-Vaquera, F., Papkovsky, D. B., Healy, D. G., Nishio, K., et al. (2012). G2019s leucine-rich repeat kinase 2 causes uncoupling protein-mediated mitochondrial depolarization. *Hum. Mol. Genet.* 21, 4201–4213. doi: 10.1093/hmg/dds244

Parkinson, J. (1817). *An Essay on the Shaking Palsy*. London: Neely and Jones

Roosen, D. A., and Cookson, M. R. (2016). LRRK2 at the interface of autophagosomes, endosomes and lysosomes. *Mol. Neurodegener.* 11:73. doi: 10.1186/s13024-016-0140-1

Rosenbusch, K. E., and Kortholt, A. (2016). Activation mechanism of LRRK2 and its cellular functions in Parkinson's disease. *Parkinsons Dis.* 2016:7351985. doi: 10.1155/2016/7351985

Schmitt, S., Saathoff, F., Meissner, L., Schropp, E. M., Lichtmannegger, J., Schulz, S., et al. (2013). A semi-automated method for isolating functionally intact mitochondria from cultured cells and tissue biopsies. *Anal. Biochem.* 443, 66–74. doi: 10.1016/j.ab.2013.08.007

Sheng, Z., Zhang, S., Bustos, D., Kleinheinz, T., Le Pichon, C. E., Dominguez, S. L., et al. (2012). Ser1292 autophosphorylation is an indicator of LRRK2 kinase activity and contributes to the cellular effects of PD mutations. *Sci. Transl. Med.* 4:164ra161. doi: 10.1126/scitranslmed.3004485

Smith, G. A., Jansson, J., Rocha, E. M., Osborn, T., Hallett, P. J., and Isacson, O. (2016). Fibroblast biomarkers of sporadic Parkinson's disease and LRRK2 kinase inhibition. *Mol. Neurobiol.* 53, 5161–5177. doi: 10.1007/s12035-015-9435-4

Su, Y. C., and Qi, X. (2013). Inhibition of excessive mitochondrialfissionreduced aberrant autophagy and neuronal damage caused by LRRK2 G2019S mutation. *Hum. Mol. Genet.* 22, 4545–4561. doi: 10.1093/hmg/ddt301

Tang, B. L. (2016). Rabs, membrane dynamics and Parkinson's disease. *J. Cell. Physiol.* 232, 1626–1633. doi: 10.1002/jcp.25713

Thévenet, J., Pescini Gobert, R., Hooft van Huijsduijnen, R., Wiessner, C., Sagot, Y. J., Gobert, R., et al. (2011). Regulation of LRRK2 expression points to a functional role in human monocyte maturation. *PLoS One* 6:e21519. doi: 10.1371/journal.pone.0021519

Toyofuku, T., Okamoto, Y., Ishikawa, T., Sasawatari, S., and Kumanogoh, A. (2019). LRRK 2 regulates endoplasmic reticulum–mitochondrial tethering through the PERK -mediated ubiquitination pathway. *EMBO J.* 39:e100875. doi: 10.15252/embj.2018100875

van Egmond, W. N., and van Haastert, P. J. M. (2010). Characterization of the Roco protein family in *Dictyostelium discoideum*. *Eukaryot. Cell* 9, 751–761. doi: 10.1128/EC.00366-09

Verma, M., Steer, E. K., and Chu, C. T. (2014). ERKed by LRRK2: a cell biological perspective on hereditary and sporadic Parkinson's disease. *Biochim. Biophys. Acta Mol. Basis Dis.* 1842, 1273–1281. doi: 10.1016/j.bbadis.2013.11.005

Vlahou, G., Eliáš, M., von Kleist-Retzow, J. C., Wiesner, R. J., and Rivero, F. (2011). The Ras related GTPase Miro is not required for mitochondrial transport in *Dictyostelium discoideum*. *Eur. J. Cell Biol.* 90, 342–355. doi: 10.1016/j.ejcb.2010.10.012

Wallings, R., Manzoni, C., and Bandopadhyay, R. (2015). Cellular processes associated with LRRK2 function and dysfunction. *FEBS J.* 282, 2806–2826. doi: 10.1111/febs.13305

Wang, X., Yan, M. H., Fujioka, H., Liu, J., Wilson-Delfosse, A., Chen, S. G., et al. (2012). LRRK2 regulates mitochondrial dynamics and function through direct interaction with DLP1. *Hum. Mol. Genet.* 21, 1931–1944. doi: 10.1093/hmg/dds003

Weindel, C. G., Bell, S. L., Vail, K. J., West, K. O., Patrick, K. L., and Watson, R. O. (2020). LRRK2 maintains mitochondrial homeostasis and regulates innate immune responses to *Mycobacterium tuberculosis*. *Elife* 9:e51071. doi: 10.7554/eLife.51071

West, A. B., Moore, D. J., Biskup, S., Bugayenko, A., Smith, W. W., Ross, C. A., et al. (2005). Parkinson's disease-associated mutations in leucine-rich repeat kinase 2 augment kinase activity. *Proc. Natl. Acad. Sci. U.S.A.* 102, 16842–16847. doi: 10.1073/pnas.0507360102

West, A. B., Moore, D. J., Choi, C., Andrabi, S. A., Li, X., Dikeman, D., et al. (2007). Parkinson's disease-associated mutations in LRRK2 link enhanced GTP-binding and kinase activities to neuronal toxicity. *Hum. Mol. Genet.* 16, 223–232. doi: 10.1093/hmg/ddl471

Yakhine-diop, S. M. S., Pedro, J. M. B., Gómez-sánchez, R., Pizarro-estrella, E., Rodríguez-arribas, M., Climent, V., et al. (2014). G2019S LRRK2 mutant fibroblasts from Parkinson ' s disease patients show increased sensitivity to neurotoxin 1-methyl-4-phenylpyridinium dependent of autophagy. *Toxicology* 324, 1–9. doi: 10.1016/j.tox.2014.07.001

Youle, R. J., and van der Bliek, A. M. (2012). Mitochondrial fission, fusion, and stress. *Science* 337, 1062–1065. doi: 10.1126/science.1219855

Zimprich, A., Biskup, S., Leitner, P., Lichtner, P., Farrer, M., Lincoln, S., et al. (2004). Mutations in LRRK2 cause autosomal-dominant parkinsonism with pleomorphic pathology. *Neuron* 44, 601–607. doi: 10.1016/j.neuron.2004.11.005

Conflict of Interest: The authors declare that the research was conducted in the absence of any commercial or financial relationships that could be construed as a potential conflict of interest.

Publisher's Note: All claims expressed in this article are solely those of the authors and do not necessarily represent those of their affiliated organizations, or those of the publisher, the editors and the reviewers. Any product that may be evaluated in this article, or claim that may be made by its manufacturer, is not guaranteed or endorsed by the publisher.

Copyright © 2021 Rosenbusch, Oun, Sanislav, Lay, Keizer-Gunnink, Annesley, Fisher, Dolga and Kortholt. This is an open-access article distributed under the terms of the Creative Commons Attribution License (CC BY). The use, distribution or reproduction in other forums is permitted, provided the original author(s) and the copyright owner(s) are credited and that the original publication in this journal is cited, in accordance with accepted academic practice. No use, distribution or reproduction is permitted which does not comply with these terms.

frontiers in Cell and Developmental Biology

MINI REVIEW
published: 13 September 2021
doi: 10.3389/fcell.2021.722066

Using *Dictyostelium* to Advance Our Understanding of the Role of Medium Chain Fatty Acids in Health and Disease

*Erwann Pain, Sonia Shinhmar and Robin S. B. Williams**

Centre for Biomedical Sciences, School of Biological Sciences, Royal Holloway University of London, Egham, United Kingdom

OPEN ACCESS

Edited by:
Zhihong Yang,
Indiana University, United States

Reviewed by:
Richard H. Gomer,
Texas A& M University, United States
Christopher Janetopoulos,
University of the Sciences,
United States
Fumio Sakane,
Chiba University, Japan

***Correspondence:**
Robin S. B. Williams
robin.williams@rhul.ac.uk

Specialty section:
This article was submitted to Molecular and Cellular Pathology, a section of the journal Frontiers in Cell and Developmental Biology

Received: *08 June 2021*
Accepted: *20 August 2021*
Published: *13 September 2021*

Citation:
Pain E, Shinhmar S and Williams RSB (2021) Using Dictyostelium to Advance Our Understanding of the Role of Medium Chain Fatty Acids in Health and Disease. Front. Cell Dev. Biol. 9:722066. doi: 10.3389/fcell.2021.722066

Ketogenic diets have been utilized for many years to improve health, and as a dietary approach for the treatment of a range of diseases, where the mechanism of these low carbohydrate and high fat diets is widely considered to be through the production of metabolic products of fat breakdown, called ketones. One of these diets, the medium chain triglyceride ketogenic diet, involves high fat dietary intake in the form of medium chain fatty acids (MCFAs), decanoic and octanoic acid, and is commonly used in endurance and high intensity exercises but has also demonstrated beneficial effects in the treatment of numerous pathologies including drug resistant epilepsy, cancer, and diabetes. Recent advances, using *Dictyostelium discoideum* as a model, have controversially proposed several direct molecular mechanisms for decanoic acid in this diet, independent of ketone generation. Studies in this model have identified that decanoic acid reduces phosphoinositide turnover, diacylglycerol kinase (DGK) activity, and also inhibits the mechanistic target of rapamycin complex 1 (mTORC1). These discoveries could potentially impact the treatment of a range of disorders including epilepsy, cancer and bipolar disorder. In this review, we summarize the newly proposed mechanisms for decanoic acid, identified using *D. discoideum,* and highlight potential roles in health and disease treatment.

Keywords: decanoic acid, diacylglycerol kinase, *Dictyostelium*, epilepsy, MCT, mTORC1, phoshoinositides, 4BCCA

INTRODUCTION

In our modern societies, fats are often considered to be damaging to health, with more than half of the European population considered overweight, and with cardiovascular diseases caused by obesity providing the most common cause of death in rich countries (Abdelaal et al., 2017). However, as primary constituents of the cell membrane, in addition to functions in the regulation of numerous signaling pathways, fats are an important group of compounds involved in normal cell physiology and health (Alves-Bezerra and Cohen, 2018;

Kimura et al., 2020). Fatty acids can be classified by carbon chain length, into short chain (up to 6 carbon atoms), medium chain (7–12 carbon atoms), and long chain fatty acids (>14 carbon atoms) (**Figure 1**). These groups can have different physiological roles in a variety of processes including fetal development, cell metabolism, DNA regulation and inflammation (Hamosh and Salem, 1998; Tvrzicka et al., 2011; Kalish et al., 2012; Tan et al., 2014). As part of our dietary intake, fats are mainly consumed as triglycerides (three fatty acids associated with glycerol), that are broken down into fatty acids in the intestine and are then transferred to the liver where they undergo mitochondrial and peroxisomal β-oxidation (Schönfeld and Wojtczak, 2016). Under low carbohydrate conditions, the oxidation of fatty acids results in the formation of acetyl-CoA and three by-products (acetoacetate, β-hydroxybutyrate and acetone) called "ketones" or "ketone bodies," which are circulated around the body in the blood and can cross the blood brain barrier, to be used as an energy source by neurons and astrocytes (Nguyen et al., 2008; Augustin et al., 2018a). This process of ketone body formation is increased in the absence of dietary carbohydrates in a process known as "ketosis" and is considered to offer positive effects on health and disease treatment (Wilhelm et al., 2021; Yurista et al., 2021). However, recent studies using *D. discoideum* as a model have suggested novel direct mechanisms for specific fatty acids.

Ketogenic diets were originally developed to reproduce a state of metabolic starvation (Wheless, 2008), but are currently used by healthy individuals to improve athletic performances or body composition (Paoli et al., 2015; McSwiney et al., 2018), and also in medicine for the treatment of numerous pathologies where they are collectively known as "Foods for Special Medical Purposes." These diets are best known and validated in the treatment of epilepsy (Youngson et al., 2017; D'Andrea Meira et al., 2019), where they are currently used as an alternative to pharmacological treatments, in patients who do not respond to two or more drugs. These dietary approaches have repeatedly shown clinical efficacy in this role (Martin-McGill et al., 2018), providing better seizure control in drug resistant patients than additional pharmaceutical treatments. In addition, ketogenic diets are increasingly being investigated for the treatment of cancers (Klement, 2017), although clinical validation remains to be confirmed (Plotti et al., 2020), and in neurodegenerative disorders like Alzheimer's disease (Augustin et al., 2018a; Rusek et al., 2019; Avgerinos et al., 2020) where they are likely to provide mild improvements in cognition.

The first widely used ketogenic diet, termed the "classical" ketogenic diet, is based upon the consumption of a very high ratio of long chain fatty acids to carbohydrates as a source of energy (90% fats to 10% carbohydrates/proteins) (Hartman and Vining, 2007), which results in ketosis. Interestingly, the mechanisms of action of the diet remain unclear (Rho and Sankar, 2008; Masino and Rho, 2012; Rho and Stafstrom, 2012) and ketones levels do not correlate with seizure control (Bough et al., 1999; Thavendiranathan et al., 2000; Dell et al., 2001; Rho et al., 2002) nor do ketones block seizure activity in various epilepsy model systems (Samoilova et al., 2010). Despite the efficacy of this diet, the high fat: carbohydrate ratio often proves difficult to maintain (Freeman et al., 2006), and numerous variations have been developed with modified fats, and differing ratios of fats to carbohydrates/proteins (Payne et al., 2011).

One variation of the classical ketogenic diet is the medium chain triglyceride (MCT) ketogenic diet that involves the dietary intake of triglycerides containing two MCFAs, decanoic (C10) and octanoic acid (C8), that are found in coconut oil. This diet has been showed to be effective in the treatment of patients with drug resistant epilepsy (Neal et al., 2009) and gives rise to ketosis, but additionally elevate levels of octanoic and decanoic acid. Studies described in this review led to the identification of potent anticonvulsant and neuro-protective effects of decanoic acid and related MCFA (Wlaź et al., 2012; Chang et al., 2013; Augustin et al., 2018a). MCFAs have since been demonstrated to have anti-cancer properties, reducing tumor size and inflammation (Narayanan et al., 2015; Wakana et al., 2019), and are also used in the treatment of metabolic disorders such as diabetes or steatohepatitis (Wang et al., 2017; Sung et al., 2018). Interestingly, several novel MCFAs related to decanoic and octanoic acid also show specific seizure control activity (Chang et al., 2013, 2014b, 2016; Augustin et al., 2018a). Thus, the mechanism of the MCT ketogenic diet in health and disease treatment may be attributed to the effects of both ketone bodies and specific MCFAs. In this review, we highlight the advantages of using *Dictyostelium discoideum* as a biomedical model and specifically outline recent discoveries made in this model leading to the demonstration of seizure control by decanoic acid and other MCFAs, and potentially in other disease treatments, as well as the translation of these studies to preclinical or human models.

The Increasing Use of *Dictyostelium* as a Cell and Developmental Model in Biomedical Research

D. discoideum is increasingly being used as a model in biomedical research to further our understanding of conserved molecular pathways and cellular responses to a wide variety of pharmacological agents and natural products (Waheed et al., 2014; Paschke et al., 2018; Schaf et al., 2019). This interest is due to both a relatively simple genome, compared to animal models, with ∼12,500 genes providing much less redundancy in cellular function (Cocorocchio et al., 2018; Kelly et al., 2018; Paschke et al., 2018), and the simplicity of carrying out a range of experimental approaches that are difficult in mammalian systems. When investigating molecular mechanisms of bioactive compounds, the use of *D. discoideum* enables the production of a library of mutants lacking individual non-essential genes. This method, termed "Restriction Enzyme Mediated Integration" (REMI), involves the insertion of an antibiotic resistance gene (Blasticidin) randomly throughout the genome (Takeda et al., 2003; Kuspa, 2006). This library can be exposed to a compound of interest at a concentration that blocks wild type cell growth, enabling mutants that have lost a potential target protein to show continued growth, and thus allowing the identification of the cellular mechanism of bioactivity (Waheed et al., 2014; Gruenheit et al., 2019; Perry et al., 2020a; Damstra-Oddy et al., 2021). The use of *D. discoideum* also provides a range of useful approaches to define compound resistance, such as monitoring acute changes

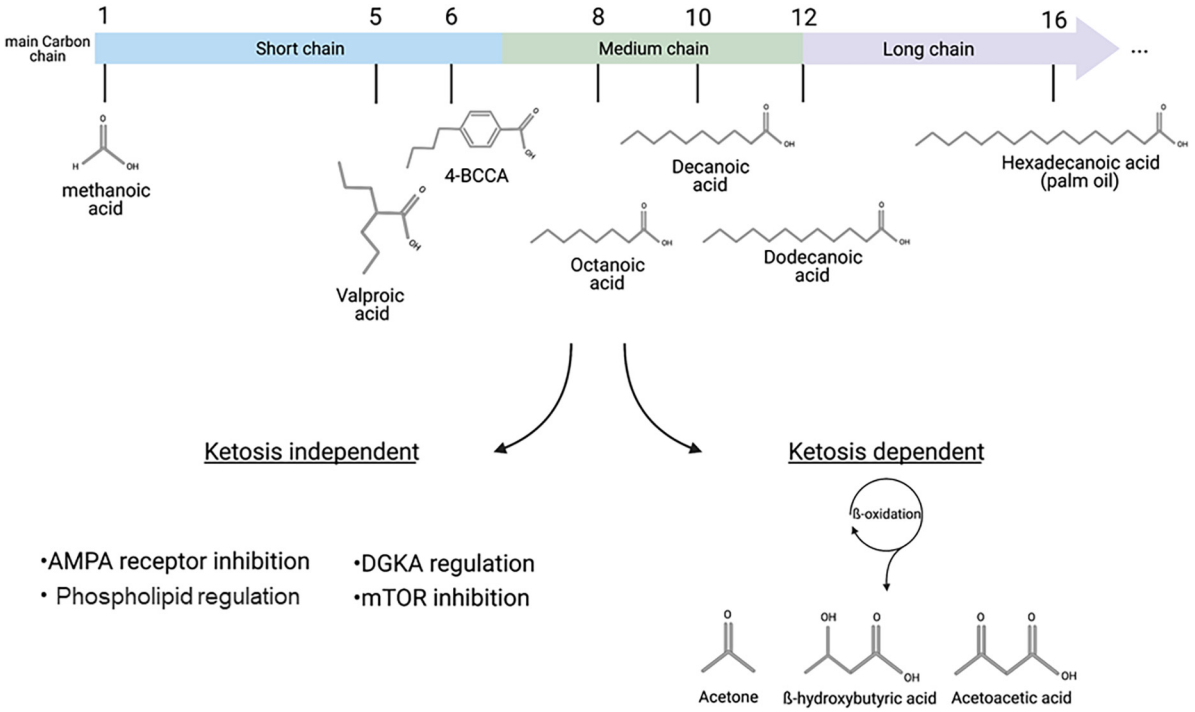

FIGURE 1 | Fatty acids classification and distinct pathways associated with therapeutic mechanisms. Main carbon chain length provides the primary classification of fatty acids, including short chain fatty acid such as valproic acid, MCFAs such as octanoic or decanoic acid, and long chain fatty acids such as hexadecanoic (palmitic) acid. Medium- and long-chain fatty acids can be metabolized in a process called ketosis, where β-oxidation leads to the formation of the three ketone bodies: Acetone, β-hydroxybutyric acid and acetoacetic acid. Recent discoveries, including those based in *D. discoideum*, have identified ketosis-independent mechanisms of some MCFAs, including decanoic acid and a related trans-4-butylcyclohexanecarboxylic acid (4BCCA) acid in a range of therapeutic associated mechanisms. This figure was created with Biorender.com.

in cell shape or movement (Parent, 2004; Cocorocchio et al., 2018; Kelly et al., 2018), inducing autophagy (Mesquita et al., 2017), regulating cell signaling (Perry et al., 2020b; Damstra-Oddy et al., 2021) or phosphoinositide turnover (Xu et al., 2007; Chang et al., 2012). The model allows the use of plasmids to over-express fluorescently tagged proteins in isogenic culture, that define protein cellular location, restore phenotypes in mutants, and enable functional analysis of specific amino acids (Ludtmann et al., 2014). Recent development of the CRISPR-cas9 system for efficiently knocking out genes has also been demonstrated in *D. discoideum* (Sekine et al., 2018). *D. discoideum* also enables a precise and well characterized differentiation between both growth and development, where upon starvation of growing cells, transcriptional events trigger expression of a series of proteins within a defined developmental cycle (Reymond et al., 1995; Singer et al., 2019). This leads to individual cells excreting cyclic AMP (cAMP), resulting in waves of aggregation to form cell mounds, that either mature into a slug enabling phototaxis (Chisholm and Firtel, 2004; Li and Purugganan, 2011) or into a multicellular fruiting body structure (Weijer, 2004). This developmental process can also be used to define the effects of bioactive compounds in both wild type cells and in mutant cells lines lacking potential compound targets or in disease associated processes (Williams et al., 1999; Kelly et al., 2018; Fernando et al., 2020).

Dictyostelium Research to Improve Our Understanding of the Cell and Developmental Mechanisms of MCFAs in Health and Disease Treatment

D. discoideum has played a key role in research focused on identifying and characterizing the pleiotropic effects of MCFAs. This area of research was first initiated through studies on the short, branched chain fatty acid valproic acid (VPA; 2-propylpentanoic acid), commonly used as a medicinal treatment for epilepsy and bipolar disorder (Fontana et al., 2020; Rahim et al., 2021). Surprisingly, the molecular mechanism of this drug has remained largely unclear (Terbach and Williams, 2009). Through the initial analysis of the cellular effects of VPA and other MCFAs in *D. discoideum*, there have been three significant mechanisms of MCFAs identified which have implications on disease treatment, described here.

Attenuating Phosphoinositide Signaling

Initial studies in *D. discoideum* were the first to identify an effect of VPA in attenuating phosphoinositide signaling, through the analysis of VPA-dependent inhibition of cell movement and development in this model (Xu et al., 2007). Further studies in the model characterized the molecular mechanism for this effect (Chang et al., 2012), and ultimately focused on looking

for a replacement to valproic acid that reproduces its cellular mechanism(s), leading to the identification of a range of MCFAs that show enhanced potency in regulating phosphoinositide signaling by reducing PIP and PIP_2 levels (**Figure 2A**). This study provided a pivotal breakthrough in the identification of decanoic acid as reproducing the bioactivity of VPA in a more potent manner (**Figure 1**), that may impact on seizure control since it is a key component of the MCT ketogenic diet (Augustin et al., 2018a), and it is elevated in the plasma of patients on the MCT ketogenic diet (Huttenlocher et al., 1971; Haidukewych et al., 1982; Sills et al., 1986a,b). Other potent compounds identified in this study included the nine-carbon fatty acid, nonanoic acid (C9), and various branched chain derivatives of octanoic acid (C8). Thus, MCFAs were primarily identified to reproduce a cellular effect of VPA in reducing phosphoinositide signaling in *D. discoideum*, with potential implications on seizure control.

Reducing DGK Signaling

Subsequent studies employed *D. discoideum* to demonstrate that both VPA and specific MCFAs reduce the activity of diacylglycerol kinase A (DGK) (Kelly et al., 2018; **Figure 2B**). Mammalian (Human) diacylglycerol kinase (DGK) consists of ten isoenzymes (Mérida et al., 2008), and thus the single isoform of DGK in *D. discoideum* is likely to represent an ancestral progenitor of the various human proteins. This class of enzyme plays a key role in phosphoinositide signaling (Mérida et al., 2008), functioning by phosphorylating diacylglycerol (DAG) to form phosphatidic acid, thereby decreasing DAG levels and regulating essential lipid signaling involved in numerous functions such as membrane trafficking and cell migration (Cutrupi et al., 2000; Fang et al., 2001). Different isoforms of the mammalian DGK are involved in regulating seizure activity (Rodriguez de Turco et al., 2001; Leach et al., 2007; Ishisaka et al., 2013). Three single nucleotide polymorphisms (SNPs) in a specific isoform of DGK in humans have been linked to bipolar disorder (Baum et al., 2008; Squassina et al., 2009), and loss of other isoforms in mammalian models provides bipolar disorder-like behaviors (Kakefuda et al., 2010; Isozaki et al., 2016), including response to lithium, a mainstay in bipolar disorder treatment (McIntyre et al., 2020). In *D. discoideum*, acute VPA treatment triggers loss of cell shape, where this effect was attenuated following loss of DGKA (Kelly et al., 2018). Furthermore, chronic treatment with VPA, or lithium, or specific MCFAs including decanoic acid, blocked multicellular development, and this effect was lost in the $DGKA^-$ mutant. Finally, these compounds triggered an increase in DAG levels in wild type cell, but not in $DGKA^-$ cells (Kelly et al., 2018), where metabolic changes in the mutant were suggested to bypass DGKA and remove sensitivity to pharmacological inhibition of the enzyme by these compounds. Thus, this *D. discoideum*-based research suggests that VPA, lithium and specific MCFAs including decanoic acid may function in the treatment of bipolar disorder through effects on DGK.

Reducing mTORC1 Activity

More recently, *D. discoideum* has been employed to investigate the effect of MCFAs on the evolutionarily conserved mTORC1 complex (Warren et al., 2020; **Figure 2C**). mTORC1 is one of the main cellular nutrient sensors, controlling cell homeostasis by modulating cellular growth, development and autophagy (Laplante and Sabatini, 2012). In the classical ketogenic diet, mTORC1 activity is reduced through a reduction in glucose and insulin signaling (Ostendorf and Wong, 2015; Sweeney et al., 2017; Robert et al., 2018). This inhibitory activity provides a treatment approach for patients with drug-resistant epilepsies, cancers, and neurodegenerative disorders, and also may lead to lifespan extension (Laplante and Sabatini, 2012). Surprisingly, analysis of the mTORC1 complex in *D. discoideum* showed that decanoic acid (but not octanoic acid) down-regulated the activity of mTORC1 under high glucose conditions in the absence of insulin, thus conflicting with the current mechanism proposed for the classical ketogenic diet (Warren et al., 2020). To investigate this mechanism, a *D. discoideum* mutant library was screened to identify insertional mutants showing resistance to the growth inhibitory effect of decanoic acid. This approach led to the identification of a protein, UBXD18 (UBX domain protein 18) to be responsible for decanoic acid-dependent growth sensitivity, and necessary for the decanoic acid-dependent inhibition of mTORC1. These domain proteins represent very highly conserved functions in binding to the endoplasmic reticulum ATPase, p97 (Barthelme and Sauer, 2016). To identify how UBXD18 functioned in this role, both UBXD18-GFP and p97-RFP proteins were expressed together, and immune-precipitation was used to demonstrate direct interaction between these two proteins. It was also found that decanoic acid reduced p97 activity, leading to mTORC1 inhibition. Direct inhibition of p97 using specific inhibitors also reduced mTORC1 activity. Thus, the use of *D. discoideum* as a model to study the effect of decanoic acid on mTOR signaling, provided new insight to the regulation of this evolutionarily conserved complex, and uncovered a potential new target pathway for disease treatment (Warren et al., 2020).

Validating *Dictyostelium*-Based Discoveries in Preclinical and Clinical Models

Innovative research in the fields of health and disease treatment using model systems must be validated in preclinical models to evidence potential clinical relevance. This approach has been demonstrated in *D. discoideum*-based research into short and MCFAs. The reduction of phosphoinositide levels by VPA identified in *D. discoideum* (Chang et al., 2012) was translated to *in vitro* and *in vivo* animal models, where it reduced seizure-induced depletion of a key phosphoinositide PIP_3 in primary neurons during seizure-like activity *in vitro*, and *in vivo* in rodent brains during seizures (Chang et al., 2014a). The identification of a range of MCFAs that were more potent than VPA in *D. discoideum,* suggested that they may also provide more potent seizure control than VPA. The efficacy of these MCFAs was then validated using both *in vitro* and *in vivo* animal seizure models (Chang et al., 2013, 2014b), also providing neuroprotective effects (Chang et al., 2013), and confirming the activity of decanoic acid, 4BCCA (trans-4-butylcyclohexanecarboxylic acid), 4EOA

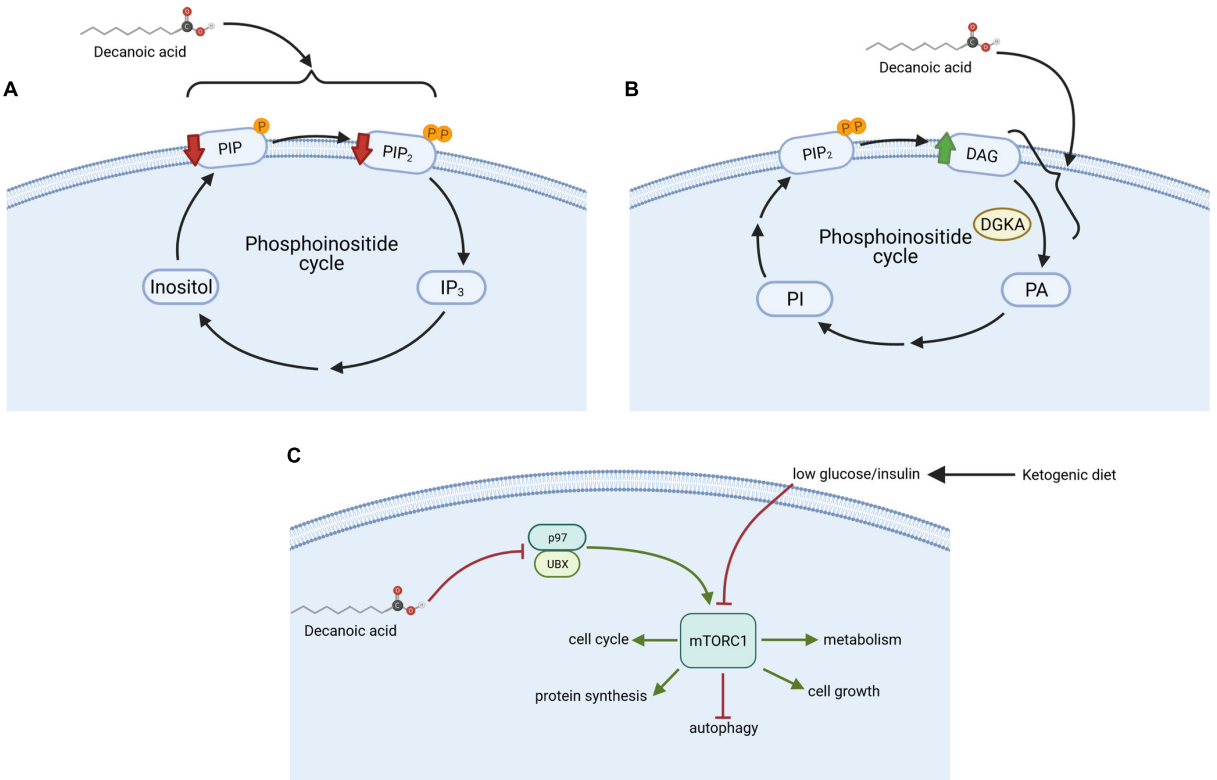

FIGURE 2 | Mechanisms of action of decanoic acid identified in *D. discoideum*. **(A)** Decanoic acid regulates the phosphoinositide pathway by decreasing phosphatidylinositol phosphate (PIP) and phosphatidylinositol diphosphate (PIP_2) concentrations; **(B)** increased diacylglycerol (DAG) levels through the inhibition of diacylglycerol kinase A (DGKA); and **(C)** reduced the activity of the mechanistic target of rapamycin complex 1 (mTORC1) independent from glucose and insulin level through the inhibition of p97, an mTORC1 activator, with a range of downstream effectors including autophagy. This figure was created with Biorender.com.

(4-ethyloctanoic acid) and other compounds to provide strong seizure control in multiple *in vivo* seizure models (**Figure 1**). Finally, decanoic acid but not ketones was also shown to provide strong seizure-control effects in mammalian *in vitro* models, through the direct inhibition of α-amino-3-hydroxy-5-methyl-4-isoxazolepropionic acid (AMPA) receptors, one of the main excitatory neurotransmitter receptors in the brain, through a direct and non-competitive manner (Chang et al., 2016; Yelshanskaya et al., 2020). Specific ratios of MCFAs, with elevated levels of decanoic acid, were then defined to provide enhanced inhibition of AMPA receptors associated with seizure control, and decanoic acid provided synergistic inhibition of AMPA receptors with another epilepsy treatment targeting AMPA receptors, perampanel, in rodent and human models (Augustin et al., 2018b). Thus, in seizure control, specific MCFAs were identified and confirmed to provide potential treatments in epilepsy related disorders.

The glucose- and insulin-independent inhibition of mTORC1 by decanoic acid, identified in *D. discoideum,* was also validated in mammalian and human models (Warren et al., 2020). Initially, the effects of decanoic acid on mTORC1 activity was analyzed using a standard *ex vivo* animal model for epilepsy research, rat hippocampal slices in artificial cerebrospinal fluid. Decanoic acid treatment of these slices (1 h; 100 and 300 μM), and mTORC1 activity analysis by Western blot (Warren et al., 2020), showed that decanoic acid reduced mTORC1 activity without glucose restriction or insulin modification. This mechanism was then analyzed in an *in vitro* human model, using astrocytes from iPSCs cells derived from healthy individuals and people with tuberous sclerosis complex (TSC) mutations. These mutations give rise to elevated mTORC1 activity, and result in tumors, cognitive disabilities and epilepsy (Henske et al., 2016). This approach confirmed that decanoic acid reduced mTORC1 activity in human astrocytes, independent of glucose and insulin levels, validating the results obtained in *D. discoideum*. These translational studies confirm the effect of decanoic acid in inhibiting mTORC1 activity and are also likely to be of clinical significance in disease treatment.

The clinical relevance of decanoic acid in seizure control has recently been demonstrated. This involved the development of a new MCT blend containing elevated levels of decanoic acid, thus maximizing the therapeutic effects of the MCFA treatment. Subsequently, a recent clinical trial has employed a 12 week prospective feasibility study of this new blend, "K.Vita," to evaluate tolerance, acceptability and compliance in children and adults diagnosed with epilepsy (ClinicalTrials.gov Identifier: NCT02825745). The diet increased plasma levels of decanoic

acid by 24–28-fold (in children and adults), and provided a 50% reduction in mean frequency of seizures/events, correlating with decanoic acid levels, despite absent or very low levels of ketosis (Schoeler et al., 2021).

CONCLUSION

Dietary intake of MCFAs through the MCT ketogenic diet provides a range of positive health and disease treatment effects (Neal et al., 2009; Narayanan et al., 2015; Sung et al., 2018). The current view of how this diet functions in these roles has, until recently, been solely based upon ketosis and a shift in metabolism (Wilhelm et al., 2021; Yurista et al., 2021). However, a range of experiments described in this review, initiated in *D. discoideum* and translated to preclinical models and clinical studies, has shed new light on the cellular function of the diet. These studies suggest that decanoic acid may play a direct role in seizure control, independent of ketosis, and identify several compounds (including 4BCCA and 4EOA) that are of potential interest as novel pharmaceutical approaches to replace VPA in epilepsy (and bipolar disorder) treatment. The use of *D. discoideum* as a tractable model (Schaf et al., 2019), with a low redundancy genome and a range of advantageous experimental techniques was essential to identify mechanisms and targets for MCFAs in a range of disease including epilepsy, bipolar disorder and cancer. Validation of these discoveries, through translation to mammalian or human models has confirmed these discoveries are relevant to disease treatment. Thus, *D. discoideum* provides an excellent pre-clinical model for understanding the role of current and potential new therapies, leading to clinically relevant discoveries to build a healthier society.

AUTHOR CONTRIBUTIONS

EP wrote the first draft and subsequent drafts of the article and constructed the figures. SS contributed to the writing. RW proposed the review, structured the sections, drafted text, and reviewed drafts. All authors contributed to the article and approved the submitted version.

FUNDING

SS was funded through a BBSRC DPT award.

REFERENCES

Abdelaal, M., le Roux, C. W., and Docherty, N. G. (2017). Morbidity and Mortality Associated with Obesity. *Ann. Transl. Med.* 5, 1–12. doi: 10.21037/atm.2017.03.107

Alves-Bezerra, M., and Cohen, D. E. (2018). Triglyceride Metabolism in the Liver. *Compr. Physiol.* 8, 1–8. doi: 10.1002/cphy.c170012

Augustin, K., Khabbush, A., Williams, S., Eaton, S., Orford, M., Cross, J. H., et al. (2018a). Mechanisms of Action for the Medium-Chain Triglyceride Ketogenic Diet in Neurological and Metabolic Disorders. *Lancet Neurol.* 17, 84–93. doi: 10.1016/S1474-4422(17)30408-8

Augustin, K., Williams, S., Cunningham, M., Devlin, A. M., Friedrich, M., Jayasekera, A., et al. (2018b). Perampanel and Decanoic Acid Show Synergistic Action against AMPA Receptors and Seizures. *Epilepsia* 59, e172–e178. doi: 10.1111/epi.14578

Avgerinos, K. I., Egan, J. M., Mattson, M. P., and Kapogiannis, D. (2020). Medium Chain Triglycerides induce mild ketosis and may improve cognition in Alzheimer's disease. A systematic review and meta-analysis of human studies. *Ageing Res. Rev.* 58:101001.

Barthelme, D., and Sauer, R. T. (2016). Origin and Functional Evolution of the Cdc48/P97/VCP AAA+ Protein Unfolding and Remodeling Machine. *J. Mol. Biol.* 428, 1861–1869. doi: 10.1016/j.jmb.2015.11.015.Origin

Baum, A. E., Akula, N., Cabanero, M., Cardona, I., Corona, W., Klemens, B., et al. (2008). A Genome-Wide Association Study Implicates Diacylglycerol Kinase Eta (DGKH) and Several Other Genes in the Etiology of Bipolar Disorder. *Mol. Psychiatry* 13, 197–207. doi: 10.1038/sj.mp.4002012

Bough, K. J., Chen, R. S., and Eagles, D. A. (1999). Path Analysis Shows That Increasing Ketogenic Ratio, but Not β-Hydroxybutyrate, Elevates Seizure Threshold in the Rat. *Dev. Neurosci.* 21, 400–406. doi: 10.1159/000017390

Chang, P., Katrin, A., Kim, B., Williams, S., Sun, M., Terschak, J. A., et al. (2016). Seizure Control by Decanoic Acid through Direct AMPA Receptor Inhibition. *Brain* 139, 431–443. doi: 10.1093/brain/awv325

Chang, P., Orabi, B., Deranieh, R. M., Dham, M., Hoeller, O., Shimshoni, J. A., et al. (2012). The Antiepileptic Drug Valproic Acid and Other Medium-Chain Fatty Acids Acutely Reduce Phosphoinositide Levels Independently of Inositol in Dictyostelium. *Dis. Model. Mech.* 5, 115–124. doi: 10.1242/dmm.008029

Chang, P., Terbach, N., Plant, N., Chen, P. E., Walker, M. C., and Williams, R. S. B. (2013). Seizure Control by Ketogenic Diet-Associated Medium Chain Fatty Acids. *Neuropharmacology* 69, 105–114. doi: 10.1016/j.neuropharm.2012.11.004

Chang, P., Walker, M. C., and Williams, R. S. B. (2014a). Seizure-Induced Reduction in PIP3levels Contributes to Seizure-Activity and Is Rescued by Valproic Acid. *Neurobiol. Dis.* 62, 296–306. doi: 10.1016/j.nbd.2013.10.017

Chang, P., Zuckermann, A. M. E., Williams, S., Close, A. J., Cano-Jaimez, M., McEvoy, J. P., et al. (2014b). Seizure Control by Derivatives of Medium Chain Fatty Acids Associated with the Ketogenic Diet Show Novel Branching-Point Structure for Enhanced Potency. *J. Pharmacol. Exp. Ther.* 352, 43–52. doi: 10.1124/jpet.114.218768

Chisholm, R., and Firtel, R. A. (2004). Insights into Morphogenesis from a Simple Developmental System. *Nat. Rev. Mol. Cell Biol.* 5, 531–541. doi: 10.1038/nrm1427

Cocorocchio, M., Baldwin, A. J., Stewart, B., Kim, L., Harwood, A. J., Thompson, C. R. L., et al. (2018). Curcumin and Derivatives Function through Protein Phosphatase 2A and Presenilin Orthologues in Dictyostelium Discoideum. *Dis. Model. Mech.* 11:dmm032375. doi: 10.1242/dmm.032375

Cutrupi, S., Baldanzi, G., Gramaglia, D., Maffè, A., Schaap, D., Giraudo, E., et al. (2000). Src-Mediated Activation of Alpha-Diacylglycerol Kinase Is Required for Hepatocyte Growth Factor-Induced Cell Motility. *EMBO J.* 19, 4614–4622. doi: 10.1093/emboj/19.17.4614

Damstra-Oddy, J., Warren, E. C., Perry, C. J., Desfougères, Y., Fitzpatrick, J. M. K., Schaf, J., et al. (2021). Phytocannabinoid-Dependent MTORC1 Regulation Is Dependent upon Inositol Polyphosphate Multikinase Activity. *Br. J. Pharmacol.* 178, 1149–1163. doi: 10.1111/bph.15351

D'Andrea Meira, I., Romão, T. T., Do Prado, H. J. P., Krüger, L. T., Pires, M. E. P., and Da Conceição, P. O. (2019). Ketogenic Diet and Epilepsy: what We Know so Far. *Front. Neurosci.* 13:5. doi: 10.3389/fnins.2019.00005

Dell, C. A., Likhodii, S. S., Musa, K., Ryan, M. A., Burnham, W. M. I, and Cunnane, S. C. (2001). Lipid and Fatty Acid Profiles in Rats Consuming Different High-Fat Ketogenic Diets. *Lipids* 36, 373–378. doi: 10.1007/s11745-001-0730-8

Fang, Y., Vilella-Bach, M., Bachmann, R., Flanigan, A., and Chen, J. (2001). Phosphatidic Acid-Mediated Mitogenic Activation of MTOR Signaling. *Science* 294, 1942–1945. doi: 10.1126/science.1066015

Fernando, S., Allan, C. Y., Mroczek, K., Pearce, X., Sanislav, O., Fisher, P. R., et al. (2020). Cytotoxicity and Mitochondrial Dysregulation Caused by α-Synuclein in Dictyostelium Discoideum. *Cells* 9:2289. doi: 10.3390/cells9102289

Fontana, E., Mandolini, G. M., Delvecchio, G., Bressi, C., Soares, J. C., and Brambilla, P. (2020). Intravenous Valproate in the Treatment of Acute Manic Episode in Bipolar Disorder: a Review. *J. Affect. Disord.* 260, 738–743. doi: 10.1016/j.jad.2019.08.071

Freeman, J., Veggiotti, P., Lanzi, G., Tagliabue, A., and Perucca, E. (2006). The Ketogenic Diet: from Molecular Mechanisms to Clinical Effects. *Epilepsy Res.* 68, 145–180. doi: 10.1016/j.eplepsyres.2005.10.003

Gruenheit, N., Baldwin, A., Stewart, B., Jaques, S., Keller, T., Parkinson, K., et al. (2019). REMI-Seq: development of Methods and Resources for Functional Genomics in Dictyostelium. *BioRxiv* [Preprint]. doi: 10.1101/582072

Haidukewych, D., Forsythe, W. I., and Sills, M. (1982). Monitoring Octanoic and Decanoic Acids in Plasma from Children with Intractable Epilepsy Treated with Medium-Chain Triglyceride Diet. *Clin. Chem.* 28, 642–645.

Hamosh, M., and Salem, N. (1998). Long-Chain Polyunsaturated Fatty Acid. *Biol. Neonate* 74, 106–120.

Hartman, A. L., and Vining, E. P. G. (2007). Clinical Aspects of the Ketogenic Diet. *Epilepsia* 48, 31–42. doi: 10.1111/j.1528-1167.2007.00914.x

Henske, E. P., Józwiak, S., Kingswood, J. C., Sampson, J. R., and Thiele, E. A. (2016). Tuberous Sclerosis Complex. *Nat. Rev. Dis. Primers* 2:16035. doi: 10.1038/nrdp.2016.35

Huttenlocher, P. R., Wilbourn, A. J., and Signore, J. M. (1971). Medium-Chain Triglycerides as a Therapy for Intractable Childhood Epilepsy. *Neurology* 21, 1097–1103.

Ishisaka, M., Tsuruma, K., Shimazawa, M., Shirai, Y., Saito, N., and Hara, H. (2013). Increased Seizure Susceptibility in a Mouse with Diacylglycerol Kinase β Deficiency. *Neurosci. Med.* 4, 117–122. doi: 10.4236/nm.2013.42019

Isozaki, T., Komenoi, S., Lu, Q., Usuki, T., Tomokata, S., Matsutomo, D., et al. (2016). Deficiency of diacylglycerol kinase eta induces lithium-sensitive mania-like behavior. *J. Neurochem.* 138, 448–456.

Kakefuda, K., Oyagi, A., Ishisaka, M., Tsuruma, K., Shimazawa, M., Yokota, K., et al. (2010). Diacylglycerol kinase beta knockout mice exhibit lithium-sensitive behavioral abnormalities. *PLoS One* 5:e13447. doi: 10.1371/journal.pone.0013447

Kalish, B. T., Fallon, E. M., and Puder, M. (2012). A Tutorial on Fatty Acid Biology. *J. Parenter. Enteral Nutr.* 36, 380–388. doi: 10.1177/0148607112449650

Kelly, E., Sharma, D., Wilkinson, C. J., and Williams, R. S. B. (2018). Diacylglycerol Kinase (DGKA) Regulates the Effect of the Epilepsy and Bipolar Disorder Treatment Valproic Acid in Dictyostelium Discoideum. *Dis. Model. Mech.* 11:dmm035600. doi: 10.1242/dmm.035600

Kimura, I., Ichimura, A., Ohue-Kitano, R., and Igarashi, M. (2020). Free Fatty Acid Receptors in Health and Disease. *Physiol. Rev.* 100, 171–210. doi: 10.1152/physrev.00041.2018

Klement, R. J. (2017). Beneficial Effects of Ketogenic Diets for Cancer Patients: a Realist Review with Focus on Evidence and Confirmation. *Med. Oncol.* 34, 1–15. doi: 10.1007/s12032-017-0991-5

Kuspa, A. (2006). Restriction Enzyme-Mediated Integration (REMI) Mutagenesis. *Methods Mol. Biol.* 346, 201–209. doi: 10.1385/1-59745-144-4:201

Laplante, M., and Sabatini, D. M. (2012). MTOR Signaling in Growth Control and Disease. *Cell* 149, 274–293. doi: 10.1016/j.cell.2012.03.017.mTOR

Leach, N. T., Sun, Y., Michaud, S., Zheng, Y., Ligon, K. L., Ligon, A. H., et al. (2007). Disruption of diacylglycerol kinase delta (DGKD) associated with seizures in humans and mice. *Am. J. Hum. Genet.* 80, 792–799.

Li, S. I., and Purugganan, M. D. (2011). The Cooperative Amoeba: dictyostelium as a model for social evolution. *Trends Genet.* 27, 48–54. doi: 10.1016/j.tig.2010.11.003

Ludtmann, M. H. R., Otto, G. P., Schilde, C., Chen, Z.-H., Allan, C. Y., Brace, S., et al. (2014). An Ancestral Non-Proteolytic Role for Presenilin Proteins in Multicellular Development of the Social Amoeba Dictyostelium Discoideum. *J. Cell Sci.* 127, 1576–1584. doi: 10.1242/jcs.140939

Martin-McGill, K. J., Jackson, C. F., Bresnahan, R., Levy, R. G., and Cooper, P. N. (2018). Ketogenic diets for drug-resistant epilepsy. *Cochrane Database Syst. Rev.* 11:CD001903.

Masino, S. A., and Rho, J. M. (2012). "Mechanisms of Ketogenic Diet Action," in *Jasper's Basic Mechanisms of the Epilepsies 4th Edition*, eds J. L. Noebels, M. Avoli, M. A. Rogawski, and R. W. Olsen (Bethesda: National Center for Biotechnology Information), doi: 10.17116/jnevro201811810272

McIntyre, R. S., Berk, M., Brietzke, E., Goldstein, B. I., López-Jaramillo, C., Kessing, L. V., et al. (2020). Bipolar Disorders. *Lancet* 396, 1841–1856. doi: 10.1016/S0140-6736(20)31544-0

McSwiney, F. T., Wardrop, B., Hyde, P. N., Lafountain, R. A., Volek, J. S., and Doyle, L. (2018). Keto-Adaptation Enhances Exercise Performance and Body Composition Responses to Training in Endurance Athletes. *Metabolism* 81, 25–34. doi: 10.1016/j.metabol.2017.10.010

Mérida, I., Ávila-Flores, A., and Merino, E. (2008). Diacylglycerol Kinases: at the hub of cell signalling. *Biochem. J.* 409, 1–18. doi: 10.1042/BJ20071040

Mesquita, A., Cardenal-Muñoz, E., Dominguez, E., Muñoz-Braceras, S., Nuñez-Corcuera, B., Phillips, B. A., et al. (2017). Autophagy in Dictyostelium: Mechanisms, Regulation and Disease in a Simple Biomedical Model. *Autophagy* 13, 24–40. doi: 10.1080/15548627.2016.1226737

Narayanan, A., Baskaran, S. A., Amalaradjou, M. A. R., and Venkitanarayanan, K. (2015). Anticarcinogenic Properties of Medium Chain Fatty Acids on Human Colorectal, Skin and Breast Cancer Cells in Vitro. *Int. J. Mol. Sci.* 16, 5014–5027. doi: 10.3390/ijms16035014

Neal, E. G., Chaffe, H., Schwartz, R. H., Lawson, M. S., Edwards, N., Fitzsimmons, G., et al. (2009). A Randomized Trial of Classical and Medium-Chain Triglyceride Ketogenic Diets in the Treatment of Childhood Epilepsy. *Epilepsia* 50, 1109–1117. doi: 10.1111/j.1528-1167.2008.01870.x

Nguyen, P., Leray, V., Diez, M., Serisier, S., Le, Bloc' J, Siliart, H. B., et al. (2008). Liver Lipid Metabolism. *J. Anim. Physiol. Anim. Nutr.* 92, 272–283. doi: 10.1111/j.1439-0396.2007.00752.x

Ostendorf, A. P., and Wong, M. (2015). mTOR Inhibition in Epilepsy: rationale and clinical perspectives. *CNS Drugs* 29, 91–99. doi: 10.1007/s40263-014-0223-x.mTOR

Paoli, A., Bianco, A., and Grimaldi, K. A. (2015). The Ketogenic Diet and Sport: a Possible Marriage?. *Exerc. Sport Sci. Rev.* 43, 153–162. doi: 10.1249/JES.0000000000000050

Parent, C. A. (2004). Making all the right moves: chemotaxis in neutrophils and dictyostelium. *Curr. Opin. Cell Biol.* 16, 4–13. doi: 10.1016/j.ceb.2003.11.008

Paschke, P., Knecht, D. A., Silale, A., Traynor, D., Williams, T. D., Thomason, P. A., et al. (2018). Rapid and Efficient Genetic Engineering of Both Wild Type and Axenic Strains of Dictyostelium Discoideum. *PLoS One* 13:e0196809. doi: 10.1371/journal.pone.0196809

Payne, N. E., Cross, J. H., Sander, J. W., and Sisodiya, S. M. (2011).). The Ketogenic and Related Diets in Adolescents and Adults-A Review. *Epilepsia* 52, 1941–1948. doi: 10.1111/j.1528-1167.2011.03287.x

Perry, C. J., Finch, P., Mûller-Taubenberger, A., Leung, K., Warren, E. C., Damstra-Oddy, J., et al. (2020a). A New Mechanism for Cannabidiol in Regulating the One-Carbon Cycle and Methionine Levels in Dictyostelium and in Mammalian Epilepsy Models. *Br. J. Pharmacol.* 177, 912–928. doi: 10.1111/bph.14892

Perry, C. J., Warren, E. C., Damstra-Oddy, J., Storey, C., Francione, L. M., Annesley, S. J., et al. (2020b). A Dictyostelium Discoideum Mitochondrial Fluorescent Tagging Vector That Does Not Affect Respiratory Function. *Biochem. Biophys. Rep.* 22:100751. doi: 10.1016/j.bbrep.2020.100751

Plotti, F., Terranova, C., Luvero, D., Bartolone, M., Messina, G., Feole, L., et al. (2020). Diet and Chemotherapy: the effects of fasting and ketogenic diet on cancer treatment. *Chemotherapy* 65, 77–84.

Rahim, F., Azizimalamiri, R., Sayyah, M., and Malayeri, A. (2021). Experimental Therapeutic Strategies in Epilepsies Using Anti-Seizure Medications. *J. Exp. Pharmacol.* 13, 265–290. doi: 10.2147/JEP.S267029

Reymond, C. D., Schaap, P., Véron, M., and Williams, J. G. (1995). Dual Role of CAMP during Dictyostelium Development. *Experientia* 51, 1166–1174. doi: 10.1007/BF01944734

Rho, J. M., Anderson, G. D., Donevan, S. D., and White, H. S. (2002). Acetoacetate, Acetone, and Dibenzylamine (a Contaminant InL-(+)-B-Hydroxybutyrate) Exhibit Direct Anticonvulsant Actions in Vivo. *Epilepsia* 43, 358–361.

Rho, J. M., and Sankar, R. (2008). The Ketogenic Diet in a Pill: is This Possible?. *Epilepsia* 49, 127–133. doi: 10.1111/j.1528-1167.2008.01857.x.The

Rho, J. M., and Stafstrom, C. E. (2012). The Ketogenic Diet: what Has Science Taught Us?. *Epilepsy Res.* 100, 210–217. doi: 10.1016/j.eplepsyres.2011.05.021

Robert, M. N., Wallace, M. A., Tomilov, A. A., Zhou, Z., and Lopez-Dominguez, J. A. (2018). A Ketogenic Diet Extends Longevity and Healthspan in Adult Mice. *Cell Metabo.* 123, 4757–4763. doi: 10.1016/j.cmet.2017.08.005.A

Rodriguez de Turco, E. B., Tang, W., Topham, M. K., Sakane, F., Marcheselli, V. L., Chen, C., et al. (2001). Diacylglycerol kinase epsilon regulates seizure susceptibility and long-term potentiation through arachidonoyl- inositol lipid signaling. *Proc. Natl. Acad. Sci. U. S. A.* 98, 4740–4745.

Rusek, M., Pluta, R., Ułamek-Kozioł, M., and Czuczwar, S. J. (2019). Ketogenic Diet in Alzheimer's Disease. *Int. J. Mol. Sci.* 20, 1–19. doi: 10.3390/ijms20163892

Samoilova, M., Weisspapir, M., Abdelmalik, P., Velumian, A. A., and Carlen, P. L. (2010). Chronic in Vitro Ketosis Is Neuroprotective but Not Anti-Convulsant. *J. Neurochem.* 113, 826–835. doi: 10.1111/j.1471-4159.2010.06645.x

Schaf, J., Damstra-Oddy, J., and Williams, R. S. B. (2019). Dictyostelium Discoideum as a Pharmacological Model System to Study the Mechanisms of Medicinal Drugs and Natural Products. *Int. J. Dev. Biol.* 63, 541–550. doi: 10.1387/ijdb.190228rw

Schoeler, N., Orford, M., Vivekananda, U., Simpson, Z., Van de Bor, B., Smith, H., et al. (2021). K.Vita® :a feasibility study of a blend of medium chain triglycerides to manage drug-resistant epilepsy. *Brain Commun.* doi: 10.1093/braincomms/fcab160

Schönfeld, P., and Wojtczak, L. (2016). Short- and Medium-Chain Fatty Acids in Energy Metabolism: the cellular perspective. *J. Lipid Res.* 57, 943–954. doi: 10.1194/jlr.R067629

Sekine, R., Kawata, T., and Muramoto, T. (2018). CRISPR/Cas9 Mediated Targeting of Multiple Genes in Dictyostelium. *Sci. Rep.* 8:8471. doi: 10.1038/s41598-018-26756-z

Sills, M. A., Forsythe, W. I., and Haidukewych, D. (1986a). Role of Octanoic and Decanoic Acids in the Control of Seizures. *Arch. Dis. Child.* 61, 1173–1177. doi: 10.1136/adc.61.12.1173

Sills, M. A., Forsythe, W. I., Haidukewych, D., Macdonald, A., and Robinson, M. (1986b). The Medium Chain Triglyceride Diet and Intractable Epilepsy. *Arch. Dis. Child.* 61, 1168–1172. doi: 10.1136/adc.61.12.1168

Singer, G., Araki, T., and Weijer, C. J. (2019). Oscillatory CAMP Cell-Cell Signalling Persists during Multicellular Dictyostelium Development. *Commun. Biol.* 2:139. doi: 10.1038/s42003-019-0371-0

Squassina, A., Manchia, M., Congiu, D., Severino, G., Chillotti, C., Ardau, R., et al. (2009). The Diacylglycerol Kinase Eta Gene and Bipolar Disorder: a Replication Study in a Sardinian Sample. *Mol. Psychiatry* 14, 350–351. doi: 10.1038/mp.2008.93

Sung, M. H., Liao, F. H., and Chien, Y. W. (2018). Medium-Chain Triglycerides Lower Blood Lipids and Body Weight in Streptozotocin-Induced Type 2 Diabetes Rats. *Nutrients* 10:963. doi: 10.3390/nu10080963

Sweeney, P., Park, H., Baumann, M., Dunlop, J., Frydman, J., Kopito, R., et al. (2017). Protein Misfolding in Neurodegenerative Diseases: implications and Strategies. *Transl. Neurodegener.* 6:6. doi: 10.1186/s40035-017-0077-5

Takeda, K., Saito, T., Tanaka, T., Morio, T., Maeda, M., Tanaka, Y., et al. (2003). A Novel Gene Trap Method Using Terminator-REMI and 3' Rapid Amplification of CDNA Ends (RACE) in Dictyostelium. *Gene* 312, 321–333. doi: 10.1016/s0378-1119(03)00558-4

Tan, J., McKenzie, C., Potamitis, M., Thorburn, A. N., Mackay, C. R., and Macia, L. (2014). The Role of Short-Chain Fatty Acids in Health and Disease. *Adv. Immunol.* 121, 91–119. doi: 10.1016/B978-0-12-800100-4.00003-9

Terbach, N., and Williams, R. S. B. (2009). Structure-Function Studies for the Panacea, Valproic Acid. *Biochem. Soc. Trans.* 37, 1126–1132. doi: 10.1042/BST0371126

Thavendiranathan, P., Mendonca, A., Dell, C., Likhodii, S. S., Musa, K., Iracleous, C., et al. (2000). The MCT Ketogenic Diet: effects on Animal Seizure Models. *Exp. Neurol.* 161, 696–703. doi: 10.1006/exnr.1999.7298

Tvrzicka, E., Kremmyda, L. S., Stankova, B., and Zak, A. (2011). Fatty Acids as Biocompounds: their Role in Human Metabolism, Health and Disease - a Review. Part 1: classification, Dietary Sources and Biological Functions. *Biomed. Pap. Med. Fac. Univ. Palacky Olomouc Czech Repub.* 155, 117–130. doi: 10.5507/bp.2011.038

Waheed, A., Ludtmann, M. H. R., Pakes, N., Robery, S., Kuspa, A., Dinh, C., et al. (2014). Naringenin Inhibits the Growth of Dictyostelium and MDCK-Derived Cysts in a TRPP2 (Polycystin-2)-Dependent Manner. *Br. J. Pharmacol.* 171, 2659–2670. doi: 10.1111/bph.12443

Wakana, H., Kono, H., Fukushima, H., Nakata, Y., Akazawa, Y., Maruyama, S., et al. (2019). Effects of Medium-Chain Triglycerides Administration in Chemically-Induced Carcinogenesis in Mice. *Anticancer Res.* 39, 6653–6660. doi: 10.21873/anticanres.13880

Wang, M. E., Singh, B. K., Hsu, M. C., Huang, C., Yen, P. M., Wu, L. S., et al. (2017). Increasing Dietary Medium-Chain Fatty Acid Ratio Mitigates High-Fat Diet-Induced Non-Alcoholic Steatohepatitis by Regulating Autophagy. *Sci. Rep.* 7:13999 . doi: 10.1038/s41598-017-14376-y

Warren, E. C., Dooves, S., Lugara, E., Damstra-Oddy, J., Schaf, J., Heine, V. M., et al. (2020). Decanoic Acid Inhibits MTORC1 Activity Independent of Glucose and Insulin Signalling. *Proc. Natl. Acad. Sci. U. S. A.* 117, 23617–23625. doi: 10.1073/pnas.2008980117

Weijer, C. J. (2004). Dictyostelium morphogenesis. *Curr. Opin. Genet. Dev.* 14, 392–398.

Wheless, J. W. (2008). History of the ketogenic diet. *Epilepsia* 49, 3–5.

Wilhelm, C., Surendar, J., and Karagiannis, F. (2021). Enemy or Ally? Fasting as an Essential Regulator of Immune Responses. *Trends Immunol.* 42, 389–400. doi: 10.1016/j.it.2021.03.007

Williams, R. S. B., Eames, M., Ryves, W. J., Viggars, J., and Harwood, A. J. (1999). Loss of a Prolyl Oligopeptidase Confers Resistance to Lithium by Elevation of Inositol (1,4,5) Trisphosphate. *EMBO J.* 18, 2734–2745. doi: 10.1093/emboj/18.10.2734

Wlaź, P., Socała, K., Nieoczym, D., Łuszczki, J. J., Arnowska, I., Arnowski, T., et al. (2012). Anticonvulsant Profile of Caprylic Acid, a Main Constituent of the Medium-Chain Triglyceride (MCT) Ketogenic Diet, in Mice. *Neuropharmacology* 62, 1882–1889. doi: 10.1016/j.neuropharm.2011.12.015

Xu, E., Müller-Taubenberger, A., Adley, K. E., Pawolleck, N., Lee, V. W. Y., Wiedemann, C., et al. (2007). Attenuation of Phospholipid Signaling Provides a Novel Mechanism for the Action of Valproic Acid. *Eukaryot. Cell* 6, 899–906. doi: 10.1128/EC.00104-06

Yelshanskaya, M. V., Singh, A. K., Narangoda, C., Williams, R. S. B., Kurnikova, M. G., and Sobolevsky, A. I. (2020). Structural Basis of AMPA Receptor Inhibition by Trans-4-Butylcyclohexane Carboxylic Acid. *Br. J. Pharmacol.* doi: 10.1111/bph.15254 [Online ahead of print].

Youngson, N. A., Morris, M. J., and Ballard, B. (2017). The Mechanisms Mediating the Antiepileptic Effects of the Ketogenic Diet, and Potential Opportunities for Improvement with Metabolism-Altering Drugs. *Seizure* 52, 15–19. doi: 10.1016/j.seizure.2017.09.005

Yurista, S. R., Chong, C. R., Badimon, J. J., Kelly, D. P., de Boer, R. A., and Daan Westenbrink, B. (2021). Therapeutic Potential of Ketone Bodies for Patients With Cardiovascular Disease: JACC State-of-the-Art Review. *J. Am. Coll. Cardiol.* 77, 1660–1669. doi: 10.1016/j.jacc.2020.12.065

Conflict of Interest: RW has patents related to MCFAs in therapeutic use (WO2012069790A1, WO2016038379A1, WO2018189113, and WO2019002435A1).

The remaining authors declare that the research was conducted in the absence of any commercial or financial relationships that could be construed as a potential conflict of interest.

Publisher's Note: All claims expressed in this article are solely those of the authors and do not necessarily represent those of their affiliated organizations, or those of the publisher, the editors and the reviewers. Any product that may be evaluated in this article, or claim that may be made by its manufacturer, is not guaranteed or endorsed by the publisher.

Copyright © 2021 Pain, Shinhmar and Williams. This is an open-access article distributed under the terms of the Creative Commons Attribution License (CC BY). The use, distribution or reproduction in other forums is permitted, provided the original author(s) and the copyright owner(s) are credited and that the original publication in this journal is cited, in accordance with accepted academic practice. No use, distribution or reproduction is permitted which does not comply with these terms.

frontiers in Cell and Developmental Biology

ORIGINAL RESEARCH
published: 15 September 2021
doi: 10.3389/fcell.2021.670943

Local Membrane Curvature Pins and Guides Excitable Membrane Waves in Chemotactic and Macropinocytic Cells - Biomedical Insights From an Innovative Simple Model

Marcel Hörning[1,2]*, *Torsten Bullmann*[3] *and Tatsuo Shibata*[2]

[1] *Institute of Biomaterials and Biomolecular Systems, University of Stuttgart, Stuttgart, Germany,* [2] *Laboratory for Physical Biology, RIKEN Center for Biosystems Dynamics Research, Kobe, Japan,* [3] *Carl-Ludwig-Institute for Physiology, University of Leipzig, Leipzig, Germany*

OPEN ACCESS

Edited by:
Robin S. B. Williams, University of London, United Kingdom

Reviewed by:
Robert Roger Kay, Medical Research Council, United Kingdom
Cornelis Weijer, University of Dundee, United Kingdom
Till Bretschneider, University of Warwick, United Kingdom

***Correspondence:**
Marcel Hörning
marcel.hoerning@bio.uni-stuttgart.de

Specialty section:
This article was submitted to Molecular and Cellular Pathology, a section of the journal Frontiers in Cell and Developmental Biology

Received: *22 February 2021*
Accepted: *16 August 2021*
Published: *15 September 2021*

Citation:
Hörning M, Bullmann T and Shibata T (2021) Local Membrane Curvature Pins and Guides Excitable Membrane Waves in Chemotactic and Macropinocytic Cells - Biomedical Insights From an Innovative Simple Model. Front. Cell Dev. Biol. 9:670943. doi: 10.3389/fcell.2021.670943

PIP3 dynamics observed in membranes are responsible for the protruding edge formation in cancer and amoeboid cells. The mechanisms that maintain those PIP3 domains in three-dimensional space remain elusive, due to limitations in observation and analysis techniques. Recently, a strong relation between the cell geometry, the spatial confinement of the membrane, and the excitable signal transduction system has been revealed by Hörning and Shibata (2019) using a novel 3D spatiotemporal analysis methodology that enables the study of membrane signaling on the entire membrane (Hörning and Shibata, 2019). Here, using 3D spatial fluctuation and phase map analysis on actin polymerization inhibited *Dictyostelium* cells, we reveal a spatial asymmetry of PIP3 signaling on the membrane that is mediated by the contact perimeter of the plasma membrane — the spatial boundary around the cell-substrate adhered area on the plasma membrane. We show that the contact perimeter guides PIP3 waves and acts as a pinning site of PIP3 phase singularities, that is, the center point of spiral waves. The contact perimeter serves as a diffusion influencing boundary that is regulated by a cell size- and shape-dependent curvature. Our findings suggest an underlying mechanism that explains how local curvature can favor actin polymerization when PIP3 domains get pinned at the curved protrusive membrane edges in amoeboid cells.

Keywords: dissipative structure, biochemical oscillation, small systems, signal transduction, chemotaxis, PIP3, membrane curvature, macropinocytosis

1. INTRODUCTION

Signal transduction systems exhibit a variety of self-organized pattern formations to control pivotal biological roles. Prominent examples are the oscillations of the Min proteins in *Escherichia coli* (Loose et al., 2011), orientation of cell polarity through regulation of the Cdc42 GTPase (Rho) cycle in yeast (Slaughter et al., 2009), the mechanochemical control of the asymmetric cell division by PAR proteins in *Caenorhabditis elegans* (Goldstein and Macara, 2007; Goehring and Grill, 2013), the directed migration of chemotactic eukaryotic cells (Devreotes et al., 2017), and the organization of macropinocytic cups (Buczynski et al., 1997; Hoeller et al., 2013; Veltman et al., 2016). Whereas,

these dynamics maintain the natural life cycle of cells, there are also undesired miss-functions in biological systems in which signal transduction plays a crucial role. The most prominent examples are the cardiovascular system and cancerous tumors that can lead to life-threatening conditions. In cancer cells, signaling pathways are often altered in a way that results in uncontrolled growth and an increased capability to invade surrounding tissue (Bianco et al., 2006). Therefore, the understanding of the key signal transduction pathways that regulate the production of lipids and their spatiotemporal pattern evolution on the membrane are of crucial importance.

PI3 kinase is a critical regulator of cell survival and proliferation that controls the production of the membrane lipid PIP3 (Whitman et al., 1988), while PTEN, a lipid phosphatase, limits the increase in PIP3 (Sansal and Sellers, 2004). It is still under debate, whether PIP3 pathway play an indispensable role in gradient sensing under shallow chemoattractant gradients (Bosgraaf et al., 2008), or is independently regulated by PI3 kinase and thus pseudopod generation is controlled independently of chemotactic signaling (Andrew and Insall, 2007). However, PIP3 is also proposed to be linked to the formation of macropinocytic cups (Veltman et al., 2016), and therefore is involved in membrane remodeling. The spatiotemporal distribution of PIP3 has been studied extensively in migrating (Sasaki et al., 2007; Xiong et al., 2010) and actin polymerization-inhibited *Dictyostelium* cells (Arai et al., 2010; Shibata et al., 2012; Taniguchi et al., 2013; Nishikawa et al., 2014). The latter offers the advantage of studying the microscopic PIP3 domain dynamics under various perturbations without considering the spatiotemporal displacement and deformation of cells. The chemical inhibition of membrane deformation (change of local curvature) enables an easier identification of PIP3 dynamics that is critically influenced by PI3 kinase in the absence of the actin cytoskeleton (Janetopoulos et al., 2004; Xiong et al., 2010). However, most investigations are limited to a single focal plane and thus capture only a very limited fraction of the PIP3 dynamics (Sasaki et al., 2007; Arai et al., 2010; Xiong et al., 2010; Taniguchi et al., 2013; Nishikawa et al., 2014; Yamazaki et al., 2020), and therefore cannot provide comprehensive links to the influence of membrane curvature that may critically regulate PI3 kinase.

Recently, the PIP3 dynamics on entire cell membrane of *Dictyostelium* cells have been observed and analyzed using a novel automated computational methodology (Hörning and Shibata, 2019). The entire three-dimensional (3D) plasma membrane was localized and the corresponding PIP3 dynamics extracted using Delaunay triangulation and spherical harmonic analysis. It has been found that the dynamics of PIP3-enriched domains are influenced by subtle differences in cell shape (i.e., size and adhesion-mediated membrane distortion). Further, the velocity of the traveling wave depends on the refractory period, that is the time until the membrane becomes again excitable. In spatially extended systems, the refractory properties affect the behavior of traveling domain. In the case of *Dicyostelium* cell, the smaller the size of the cell, the slower the domain speed. This is because the cell membrane is a closed system that leads to the interaction of the domain front and rear. For very small cells the domain movement is suppressed and only localized transient spots can be observed. These self-regulatory effects of domain dynamics, which follow basic principles seen in other excitable media such as cardiac tissue (Campanari et al., 2017; Li et al., 2020) and Belousov-Zhabotinsky reactive medium (Courtemanche et al., 1993; Suematsu et al., 2011), have been confirmed using independent experiments of spatially constrained *Dictyostelium* cells that were embedded in narrow grooves of micro-chambers. The spatial constraint led to dominant domain circulations along the horizontal direction (parallel to the grooves) in contrast to the circulating waves along the periphery of cells that are adhered to flat substrates (Hörning and Shibata, 2019).

In this study, we took advantage of the high 3D spatial resolution that our previously introduced signal mapping routines offers (Hörning and Shibata, 2019). We investigated the local fluctuation of PIP3 signaling on the entire plasma membrane of the same *Dictyostelium* cells using detrended fluctuation analysis (DFA). We payed special attention to the edge of the ventral membrane, as it exhibits the largest membrane curvature on the actin-inhibited plasma membranes. We call this edge the contact perimeter, as it defines the border of the membrane in contact to the substrate and the membrane freely exposed to the culture medium. DFA allows us to quantify the underlying noise and signaling regime by determining the parameter α in the range of $\alpha = [0, 2]$ (Molz et al., 1997). The time series with value of α smaller than unity is a noise dominant process that has no underlying detectable signal. In contrast, when α is larger than unity, the time series is considered to contain an underlying signal (see example signals, **Supplementary Figure 1**). Those processes have been useful for interpreting various physiological or behavioral data (Delignières, 2015), such as heart-beat variability (Wallot et al., 2013), brain activity (Montez et al., 2009) and sensorimotor processes (Gilden et al., 1995). We mapped α over the entire surface of single cells using the local time series of PIP3 signaling measured before using a fluorescent indicator (Hörning and Shibata, 2019). We identified two different modes of the PIP3 domain dynamics in the observed cells, that are seemingly influenced by the contact perimeter. (1) Periodic PIP3 lipid-signaling ($\alpha > 1$) only on the upper membrane with noise dominant signaling ($\alpha \sim 0.5$) on the ventral membrane, and (2) periodic PIP3 lipid-signaling activity ($\alpha > 1$) that are anchored at the contact perimeter. The latter is observed in particular in larger cells that have a larger ventral membrane. We suggest that the contact perimeter serves as an anchor that can pin and guide propagating PIP3 domains, which means that the contact perimeter acts as an interactive boundary. The statistical analysis of the membrane shape and PIP3 domain dynamics showed that the strength of interaction between the domain and the contact perimeter is positively related to the degree of local membrane curvature at the contact perimeter, which might influence the local diffusivity between ventral and non-adherent membrane. That means a larger membrane curvature increases the effect of interaction between the PIP3 domain and the contact perimeter. We visualized those dynamics using high resolution phase analysis without spatial filtering.

2. MATERIALS AND METHODS

Dictyostelium discoideum cells were used to observe spatiotemporal dynamics of $PH_{Akt/PKB}$-EGFP molecules as they either bind to PIP3 on the membrane or move throughout to the cytoplasm. For this study we used the previously introduced signal mapping routines and the same cells that we observed in Hörning and Shibata (2019), as follows.

2.1. Cell Preparation

The GFP-fused pleckstrin-homology domain of Akt/PKB (PHAkt/PKB) was expressed in wild-type AX-2 cells. Cells were cultured at 21°C in HL-5 medium and selected with 20 μg/mL G418 (Watts and Ashworth, 1970). Before observation, the cells were placed in glass bottom dishes (IWAKI, Japan) 27 mm in diameter and starved in development buffer (DB: 5 mM Na phosphate buffer, 2 mM MgSO4, and 0.2 mM CaCl2, pH 6.3) for 4.5 h, leading to chemotactic competency with respect to cAMP (Arai et al., 2010). The glass bottom dishes were used in the presence or the absence of polyethylenimine (PEI) at a concentration of 2.4 μg/mL in DB. The number of cells was maintained at less than 5 ± 10^5 cells to sufficiently separate neighboring cells. After starvation the extracellular fluid was exchanged and the cells were incubated for an additional 20 min incubated before observation with 1 mL DB supplemented with 20 μM latrunculin A (L5163-100UG, Sigma), which inhibits actin polymerization, and 4 mM caffeine, that inhibits the secretion of cAMP (Brenner and Thoms, 1984). A total of 79 cells were observed on glass and 98 cells on PEI-coated glass. The latter increases the adhesion strength of cells and leads therefore to a larger fraction of the plasma membrane adhering to the substrate (ventral membrane) (Hörning and Shibata, 2019).

2.2. Cell Observation

Fluorescence images were obtained using an inverted microscope (IX81-ZDC2; Olympus) equipped with a motorized piezo stage and a spinning disc confocal unit (CSU-X1-A1; Yokogawa) through a 60x oil immersion objective lens (N.A. 1.35; UPLSAPO 60XO). $PH_{Akt/PKB}$-EGFP was excited by 488-nm laser diode (50 mW). The images were passed through an emission filter (YOKO 520/35, Yokogawa) and captured simultaneously by a water-cooled EMCCD camera (Evolve-, Photometrics). Time-lapse movies were acquired at 10-s intervals at a spatial resolution of dx = dy = 0.2666 μm and dz = 0.5 μm using z-streaming (MetaMorph 7.7.5), which enables recording the entire focal volume in about 3s.

2.3. 3D Reconstruction of Membrane Topology and Signals

The recorded spatiotemporal fluorescence signaling of cells was reconstructed considering the entire four-dimensional data set (x, y, z and t). The cell surface was represented by a triangular mesh that was generated using a Delaunay triangulation routine in MATLAB (Mathworks) (Persson and Strang, 2004), and transformed to a volume filling three-dimensional tetrahedral mesh by connecting the surface triangles to the center coordinate of the cell. The sections were evaluated by the time-averaged, radial intensity profile of all pixels within one grid element. The maximum intensity of the time-averaged standard deviation determined the membrane position. Thereafter, the position of nodes is determined, so that the average node area was approximately 0.3 μm^2. Finally, the grid nodes were smoothed among neighboring nodes using a triangular low-gaussian kernel. The PIP3 domain dynamics were quantified by spherical harmonic expansion to the 3rd order (octupole moment), which smoothened the intensity distribution for peak detection of the domains. The domain velocity, v is calculated from the temporal peak displacement on the membrane by approximating the peak-to-peak distance as the shortest distance along a straight line on the membrane. A more detailed methodological description can be found in Hörning and Shibata (2019). The generated data tables used for this study can be found in the **Supplementary Material**.

2.4. Mollweide Projection

The two-dimensional homolographic equal-area Mollweide projection is used to visualize membrane signaling in 2D. The transformation from spherical coordinates (ϕ, θ) to cartesian coordinates (x, y) is performed through the equations

$$x = \frac{2\sqrt{2}}{\pi}\theta \cos\gamma \tag{1}$$

$$y = \sqrt{2}\sin\gamma, \tag{2}$$

with the auxiliary angle γ given as

$$2\gamma + \sin 2\gamma = \pi \sin\phi, \tag{3}$$

which can be solved iteratively by the Newton-Raphson method (Snyder, 1987; Hörning and Shibata, 2019).

2.5. Detrended Fluctuation Analysis

The statistical self-affinity of the extracted PIP3 signaling on the membrane of *Dictyostelium* cells was determined by Detrended Fluctuation Analysis (DFA) of first order (Peng et al., 1994). A previously introduced scheme in Matlab was used to determine the scaling exponent, α from the time series (Habib, 2017; Habib et al., 2017). The cumulated sum $S(t_i)$ of the discrete signal $s(t_i)$ is computed as

$$S_i = \sum_{i=1}^{N} s(t_i) - \hat{s}, \tag{4}$$

where $\hat{s}$ denotes the mean of $s(t_i)$. The variance $F^2(\tau)$ is determined within the time window $T_{\max} = 180$ s by obtaining the best linear fit P of the cumulated sum S, as

$$F^2(\tau) = \frac{1}{\tau}\sum_{i=1}^{\tau}(S_i - P_i)^2\,. \tag{5}$$

Plotting the τ against $F^2(\tau)$ on a log-log graph indicates α as the linear slope, since $F(\tau) \sim \tau^{\alpha}$. The extension of this framework for higher orders (i.e., DFAn) is explained elsewhere (Habib, 2017; Habib et al., 2017). Examples of different numerically generated and analyzed time series are shown in **Supplementary Figure 1**.

2.6. Phase Analysis

Phase information was extracted from the raw signals using the WAVOS toolkit for wavelet analysis and visualization of oscillatory systems in Matlab (Harang et al., 2012). The complex Morlet wave function

$$\psi(t) = \frac{1}{\sqrt{\omega}} \exp(i\omega t) \exp\left(-\frac{t^2}{2}\right) \quad (6)$$

is applied to the PIP3 fluorescence intensity data at each membrane node using $\omega = 2\pi$ in the range of $t_{\min} = 60$ s to $t_{\max} = 330$ s. The dominant frequency in the power spectra was determined as the dominant frequency mode. The phase was calculated from the complex wavelet coefficients of the dominant frequency mode. Finally, all extracted phases were reconstructed and mapped on the membrane mesh.

3. RESULTS

PIP3 domains self-regulate their dynamics on the spatially confined plasma membrane of actin polymerization-inhibited *Dicyostelium* cells. Those dynamics are determined by the geometrical shape of the membrane and the underlying excitability of the signal transduction system (Hörning and Shibata, 2019). While PIP3 domain dynamics were revealed using spherical harmonics analysis on the entire plasma membrane, the role of local signaling differences on the plasma membrane in influencing domain dynamics remains to be understood.

3.1. 3D Quantification of Cell Shape and Signaling

In this study, actin polymerization-inhibited *Dicyostelium* cells were observed and analyzed by taking advantage of the simple and symmetric cell shape. For that cells were treated with 10 mM latrunculin A and 4 mM caffeine to suppress cell motility, formation of membrane protrusions, and cell-cell interactions (Arai et al., 2010). Thus, the cell membrane can be described and mapped using a spherical coordinate system with the polar angle θ and the periodic azimuthal angle ϕ (**Figure 1A**). Further, the cell shape was described by the contact angle Ω and the area of the ventral membrane, i.e., the area of the membrane that adheres to the substrate, A_{adh}.

Due to the simple symmetric shape of the cells, it is also possible to project the three dimensional PIP3 signal activity onto a two dimensional map, as shown in **Figure 1B**. The upper two panels show the front and back side of a cell with irregular complex shaped PIP3 domains, and the lower panel shows the corresponding 2D map (Mollweide projection; see Materials and Methods) of the entire membrane signaling. For that a customized mapping routine was applied, as introduced in detail before by Hörning and Shibata (2019). Briefly, the temporal fluorescence variation of the signaling at each local position was used to specify the membrane position, from which a three-dimensional triangular map was constructed using a Delaunay triangulation routine (Persson and Strang, 2004) with a constant mesh size of approximately 0.3 μm^2. Depending on the cell size, this approach leads to membrane grids with 620–6,632 nodes, i.e., triangles. Additionally, part of the cells were cultured on polyethylenimine (PEI) coated glass bottom dishes to increase the adhesiveness of cells to the glass substrate and therefore having a wider range of different cell shapes. The ventral membrane area increased from $A_{\text{Adh, glass}} = 35.6 \pm 5.6\ \mu\text{m}^2$ to $A_{\text{Adh, PEI}} = 51.9 \pm 4.2\ \mu\text{m}^2$ (mean ± SE). Between the two different substrates no influence on the PIP3 signaling was observed.

Using this methodological approach the three basic PIP3 domain dynamics could be observed. The horizontal waves that propagate parallel to the contact perimeter (**Figure 1C**), vertical waves that periodically cross the contact perimeter (**Figure 1D**), and transient spot waves that are small domains that appear and disappear repeatedly at seemingly random positions at the membrane above the contact perimeter (**Figure 1E**). The corresponding movies can be found in the **Supplementary Material**.

3.2. Contact Perimeter Influences Domain Signaling

Figure 2A shows kymographs of the three PIP3 domain dynamics observed on *Dictyostelium* membranes: horizontal waves, vertical waves, and transient spot waves. While those wave patterns have been analyzed by tracking only the domain center using spherical harmonic analysis (Hörning and Shibata, 2019), the raw PIP3 signaling reveals irregular complex shaped domains (**Figures 1B–E**). Taking advantage of the high spatial resolution of the triangular mesh, it is possible to analyse the PIP3 signal at each triangle individually. **Figures 2B,C** show two typical periodic and non-periodic time series observed at single locations on different cells. Those signals can be independently analyzed by DFA. The resulting slopes enable the quantification of signal- and noise-dominant regimes in the range of $\alpha = [0, 2]$, where $\alpha = 0.5$ corresponds to white noise and $\alpha = 2$ to a signal without noise (see also **Supplementary Figure 1**). PIP3 signaling on *Dictyostelium* membranes was observed in the range of $\alpha \simeq [0.5, 1.5]$ similar to the shown periodic ($\alpha \sim 1.2$) and non-periodic ($\alpha \sim 0.6$) examples in **Figures 2B–D**.

Mapping α on the entire membrane (**Figures 2E–G**) reveals the underlying spatiotemporal pattern formations (**Figure 2A**). The yellow ($\alpha > 1$) and blue ($\alpha < 1$) colors distinguish signal- and noise-dominant spatial locations on the membrane, respectively. The dashed line marks the contact perimeter. The right panels show the probability distribution of α along the vertical cell-symmetry axis from $\theta = -\pi/2$ (cell bottom) to $\theta = +\pi/2$ (top of cell) with the contact perimeter marked as a dashed line. Generally, we observed that smaller cells and those with a small ventral membrane area show more uniform distibutions of constant α (**Figure 2E**). Larger cells with a larger ventral membrane showed dominant periodic activity on the ventral membrane (**Figure 2F**), and smaller cells showed dominant periodic (yellow) activity at the upper plasma membrane with noisy activity below the contact perimeter (**Figure 2G**). The latter can be observed in very sharp transitions of activity above and below the contact perimeter (**Figure 3A**), implying an active role of the contact perimeter in PIP3 domain activity. Contrarily, the cell shown in **Figure 3B** shows constant values of α below the

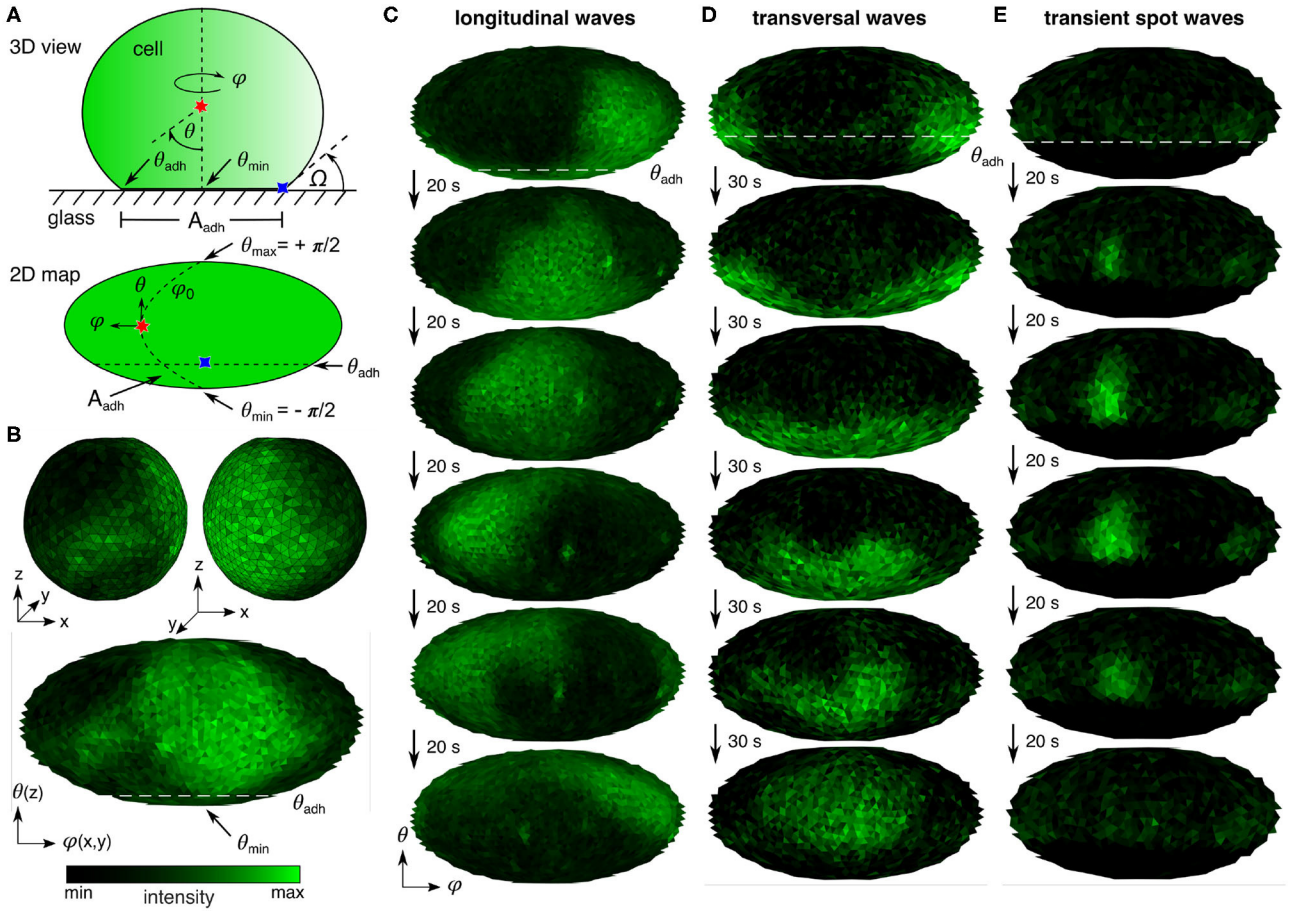

FIGURE 1 | PIP3 domain dynamics on *Dictyostelium* cells. **(A)** Scheme of actin polymerization-inhibited cell attached to glass surface: 3D view and 2D map. Indicated are spherical coordinates, the periodic azimuthal angle ϕ (horizontal) and polar angle θ (vertical), the positions of θ at the center of ventral membrane $\theta_{min} = -\pi/2$ and the contact perimeter θ_{adh}, the contact angle Ω, and the area of the ventral membran A_{adh}. **(B)** 3D visualization of entire membrane PIP3 signaling. The upper two panels show the front and back side of a cell. The lower panel shows the corresponding 2D map (Mollweide projection, see Materials and Methods) of the entire membrane signaling. **(C,D)** Examples of the basic PIP3 domain dynamics. θ_{adh} is indicated at the first map by the white dashed line. **(C)** Horizontal waves that propagate parallel to the contact perimeter. **(D)** Vertical waves that periodically cross the contact perimeter. **(E)** Transient spot waves that appear and disappear repeatedly above the contact perimeter.

contact perimeter, and a gradual decrease of α toward the top of the cells ($\theta = \pi/2$).

Figures 3C,D show time-series snapshots of PIP3 signaling corresponding to the two representative α-distribution maps (**Figures 3A,B**). **Figure 3C** illustrates how the contact perimeter blocks the domain motion toward the ventral membrane of the cell, which leads to domain guidance along the contact perimeter. The difference of domain activity gets more clear when comparing the kymographs above and below the contact perimeter (right panel). The latter shows no domain motion. However, in larger cells (**Figure 3D**), we observed that the domains can pass the contact perimeter and lead to domain motion on the entire membrane.

3.3. Correlation Between Membrane Geometry and Signaling

In order to quantify the role of the contact perimeter in membrane signaling, a total of 178 cells were statistically analyzed with focus on the spatial distribution of α, as shown in **Figures 3A,B** (right panels). The weighted polynomial fits (black solid line) of the α distributions were parameterized by α_{min} and α_{adh}, which define α at the polar angles $\theta_{min}=-\pi/2$ at the bottom of the cell and θ_{adh} at the spatial position of the contact perimeter, respectively (**Figure 4A**). Further, we introduce the scaling parameter $\Delta\alpha = \alpha_{adh} - \alpha_{min}$, which parameterizes the difference in signal activity between the bottom of the cell (θ_{min}) and the contact perimeter (θ_{adh}). A negative $\Delta\alpha$ is associated with a highly periodic or oscillatory signal at the ventral membrane (**Figures 2F**, **4A**, upper black line), while a positive value indicates noise-dominant signaling at the ventral membrane (**Figures 2G**, **4A**, lower black line). **Figure 4B** shows the relation between α_{adh} and α_{min}, where the color scheme indicates cells of different α_{min} (see also **Supplementary Figure 3**). This color scheme provides an additional fingerprint of the membrane signaling independently from the shape of the weighted polynomial fits (**Figure 4C**). Cells that show $\Delta\alpha \simeq 0$ are cells of comparable

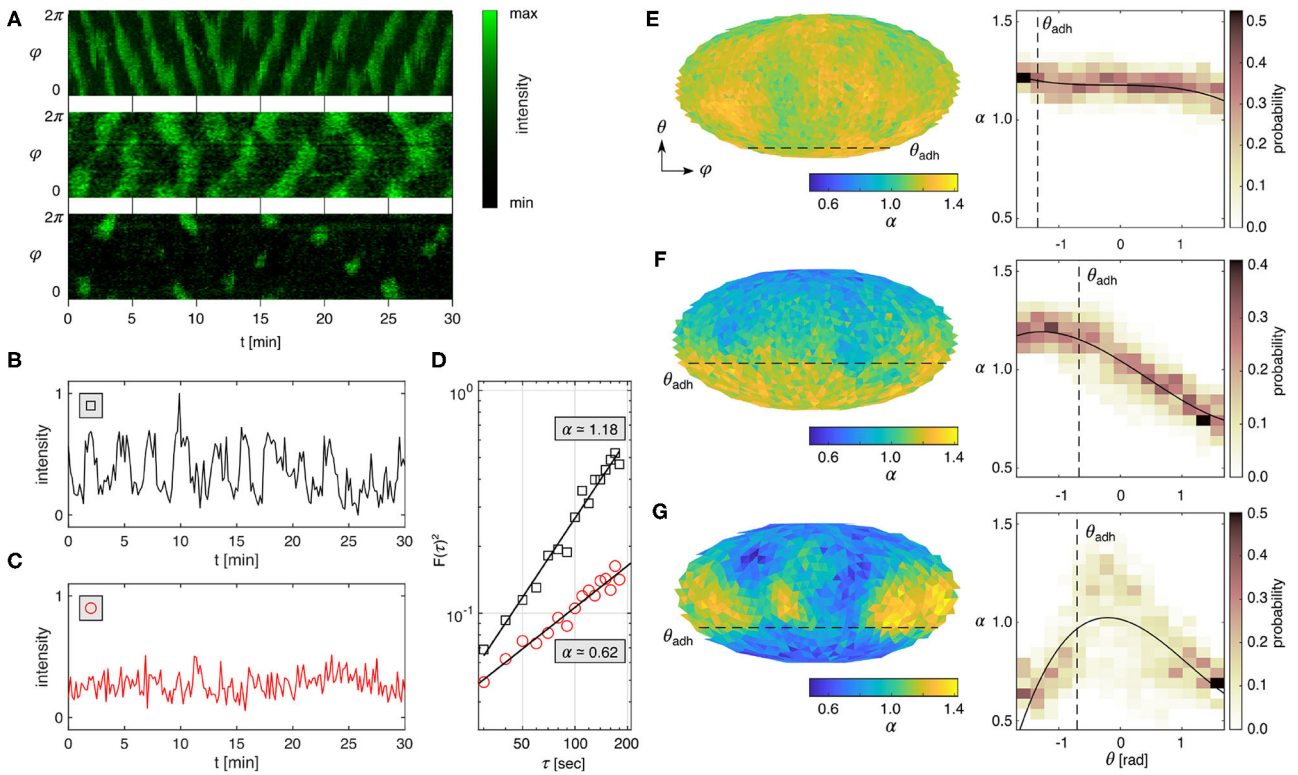

FIGURE 2 | Spatial fluctuation analysis of PIP3 *Dictyostelium* membrane signals. **(A)** PIP3 dynamics recorded on the membrane periphery of *Dictyostelium* cells. Horizontal propagating waves (*top panel*), vertical propagating waves (*middle panel*), transient spot waves (*bottom panel*). Periodic signal **(B)** and noisy signal **(C)** taken at a membrane site that adheres to the substrate that correspond to the examples shown in **(A)** top and bottom panels, respectively. **(D)** Detrended fluctuation analysis of the signals shown in **(B,C)** showing noisy signal ($\alpha \simeq 1.18$) and noise without detectable signal ($\alpha \simeq 0.62$). **(E–G)** Mollweide maps of α for the three different prototypical PIP3 domain dynamics shown in **(A)**. The right panels show the respective histograms along the horizontal direction (θ) and the weighted polynomial fit (black solid line). The black dashed lines indicate the contact perimeter (θ_{adh}) of the *Dictyostelium* membrane.

signaling at the center of ventral membrane and contact perimeter ($\alpha_{\min} \sim \alpha_{\text{adh}}$). Those cells are either dominated by periodic PIP3 signaling or only noise on the membrane. The latter are mainly very small cells that do not even exhibit transient spot dynamics, as shown in **Figure 1E**. Although this is a limitation of the parameter $\Delta\alpha$, as those two types of cells are indistinguishable, they are only a very few cells whose PIP3 signaling is dominated by noise, and therefore statistically negligible (see **Figure 4B**, $\alpha_{\min} \simeq \alpha_{\text{adh}} \simeq 0.6$; **Figure 4C**, $\alpha_{\min} \simeq 0.6$). Despite this limitation using $\Delta\alpha$ as scaling parameter, the major advantage is the normalization of the signaling strength relative to the contact perimeter, since there is a wide distribution of signal activity observed (**Figure 4C**).

Figures 4D–F show the relation between the scaling parameter $\Delta\alpha$ and the membrane geometry. We found that larger cells show an oscillatory signaling activity ($\Delta\alpha < 0$) on the ventral membrane, while smaller cells show a broad distribution of noise dominant signaling activity in the range of $\Delta\alpha > 0$ (**Figure 4D**). Further, smaller cells (cyan color) show a linear correlation between $\Delta\alpha$ and the ventral membrane area A_{adh}, i.e., larger A_{adh} led to larger $\Delta\alpha$, and thus to noise-dominant signaling activity on the ventral membrane (**Figure 4E**). A similar relation was found for cells with negative $\Delta\alpha$, where larger cells (red color) had larger A_{adh} compared to smaller cells $V \sim 0.5$ pL. The presence of two branches implies a pitchfork-like bifurcation in $\Delta\alpha$ at $\Delta\alpha \simeq 0$. This means that different cells with the same A_{adh} can take either a smaller value of $\Delta\alpha$ or larger value. This can be explained by the local membrane curvature at the contact perimeter. Cells of similar ventral membrane area, for example $A_{\text{adh}} \simeq 60\ \mu m^2$, but different volumes (compare small cyan and large red data points) have different contact angles Ω, an indirect measure of the local membrane curvature at the contact perimeter. The inset of **Figure 4E** shows cells with different membrane curvature (see Discussion for more details). This finding suggests that the local membrane curvature at the contact perimeter regulates the diffusibility between the ventral and non-adherent part of the membrane. Considering the dimensionless adhesion area ratio of $r_a = A_{\text{adh}}/A_{\text{mem}}$, a linear relationship between r_a and $\Delta\alpha$ is found (dashed line, **Figure 4F**). Larger r_a lead to larger positive $\Delta\alpha$. The corresponding bifurcation found for A_{adh} at $\Delta\alpha \sim 0$ corresponds to $r_a \simeq 10\%$.

Similar to the geometry of the cells, we have compared the PIP3-enriched domain velocities (see Materials and Methods)

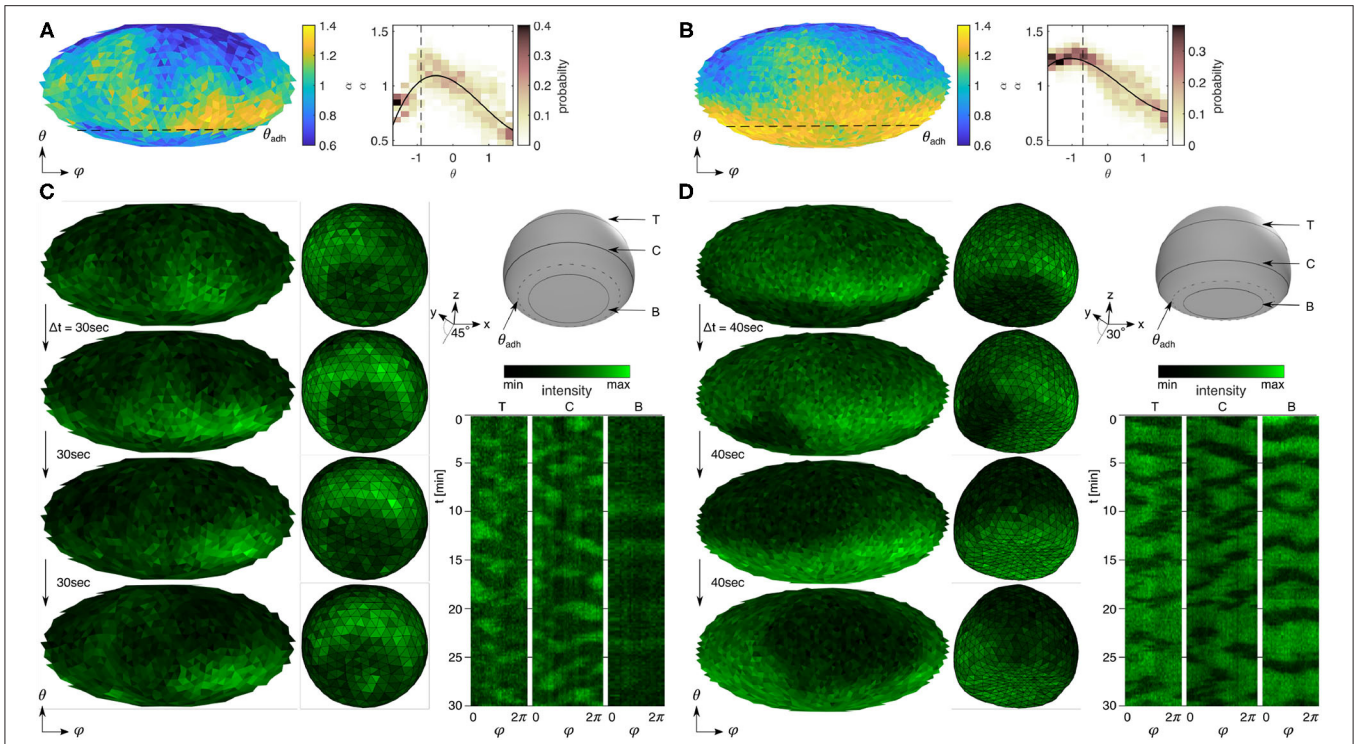

FIGURE 3 | Influence of the contact perimeter on PIP3-enriched domain signaling. **(A,B)** Detrended fluctuation analysis of the cells that show noisy and oscillatory signaling on the ventral membrane sites (below dashed lines). The left panels show the Mollweide maps of α and the right panels show the respective histograms along the horizontal direction (θ) with the weighted polynomial fit (black solid line). See respective fits with confidence intervals in **Supplementary Figure 2**. **(C,D)** Spatiotemporal dynamics of PIP3-enriched domains shown in **(A,B)** indicating the contact perimeter (θ_{adh}) as obstacle **(C)** and pinning site **(D)** of spiraling domains. The left panels are four snapshots—2D map and 3D view—of raw PIP3 signaling. The 3D view shows the ventral membrane from the bottom with a view angle of 45° and 30°. Three spatiotemporal kymographs of a bottom section [B], a center section [C] and a top section [T], as illustrated in the 3D cell scheme above. The dashed section illustrates the contact perimeter (θ_{adh}). The sizes of ventral and entire membrane are **(C)** $A_{adh} = 30\ \mu m^2$ and $A_{mem} = 257\ \mu m^2$, and **(D)** $A_{adh} = 105\ \mu m^2$ and $A_{mem} = 564 \mu m^2$.

to the signal fluctuations. Despite the differences in shape and size of the cell membranes, the average velocity was found to be about $\langle v \rangle \sim 10\ \mu$m/min suggesting comparable diffusion properties among all cells. Therefore, no dependence on membrane geometry was observed (**Figure 4G**). The mean horizontal velocity $\langle v_\varphi \rangle$ shows a similar constant profile, and is the dominant fraction of $\langle v \rangle$ (**Figure 4H**). Contrarily, the mean vertical velocity $\langle v_\theta \rangle$ is by a factor of about two slower than $\langle v_\varphi \rangle$, and linearly correlated with $\Delta\alpha$, i.e., an increase of $\langle v_\varphi \rangle$ is accompanied by an increase in cell size. **Figure 4I** shows $\Delta\alpha$ as a function of the mean velocity ratio $\langle v_a \rangle = \langle v_\varphi / v_\theta \rangle$. A linear relationship is observed similar to the one in **Figure 4F**.

We conclude that the contact perimeter plays an important role for the pattern organization of the PIP3 signaling dynamics on the membrane. Using weighted polynomial fits, two relationships between the cell geometry (**Figure 4F**) and the PIP3 domain speed (**Figure 4I**) were found to be correlated linearly with the introduced contact perimeter dependent parameter $\Delta\alpha$ (**Figure 4E**). While it was shown before that the cell asymmetry induces directed domain propagation along the cell periphery (Hörning and Shibata, 2019), this result identifies the contact perimeter as an additional factor that controls the PIP3 signaling organization.

3.4. Guidance and Pinning of Waves at the Contact Perimeter

Thus, we summarize that not only the adhesion area ratio r_a but also the PIP3 domain velocity ratio v_a is linearly correlated to the scaling parameter $\Delta\alpha$. From those two relationships (dashed lines, **Figures 4F,I**) we can derive the linear relation between r_a and v_a following the general linear equation $v_a = m \times r_a + n_0$, where m defines the slope and n_0 the intersection with the y-axis at $r_a = 0$. Not surprisingly, we get the intersection at $n_0 \sim 1$, since a perfect spherical cell ($r_a = 0$) will lead to a velocity ratio of unity (**Supplementary Figure 4**), as shown in numerical simulations before (Hörning and Shibata, 2019). In order to get a more intuitive view of the contact perimeter influence (**Figures 2A,B**), r_a is transformed to the contact angle Ω from the basic relationship

$$r_a = \frac{A_{adh}}{A_{mem}} = \frac{\pi R^2 \sin^2 \Omega}{4\pi R^2 - \pi R^2 (1 - \cos \Omega)}, \tag{7}$$

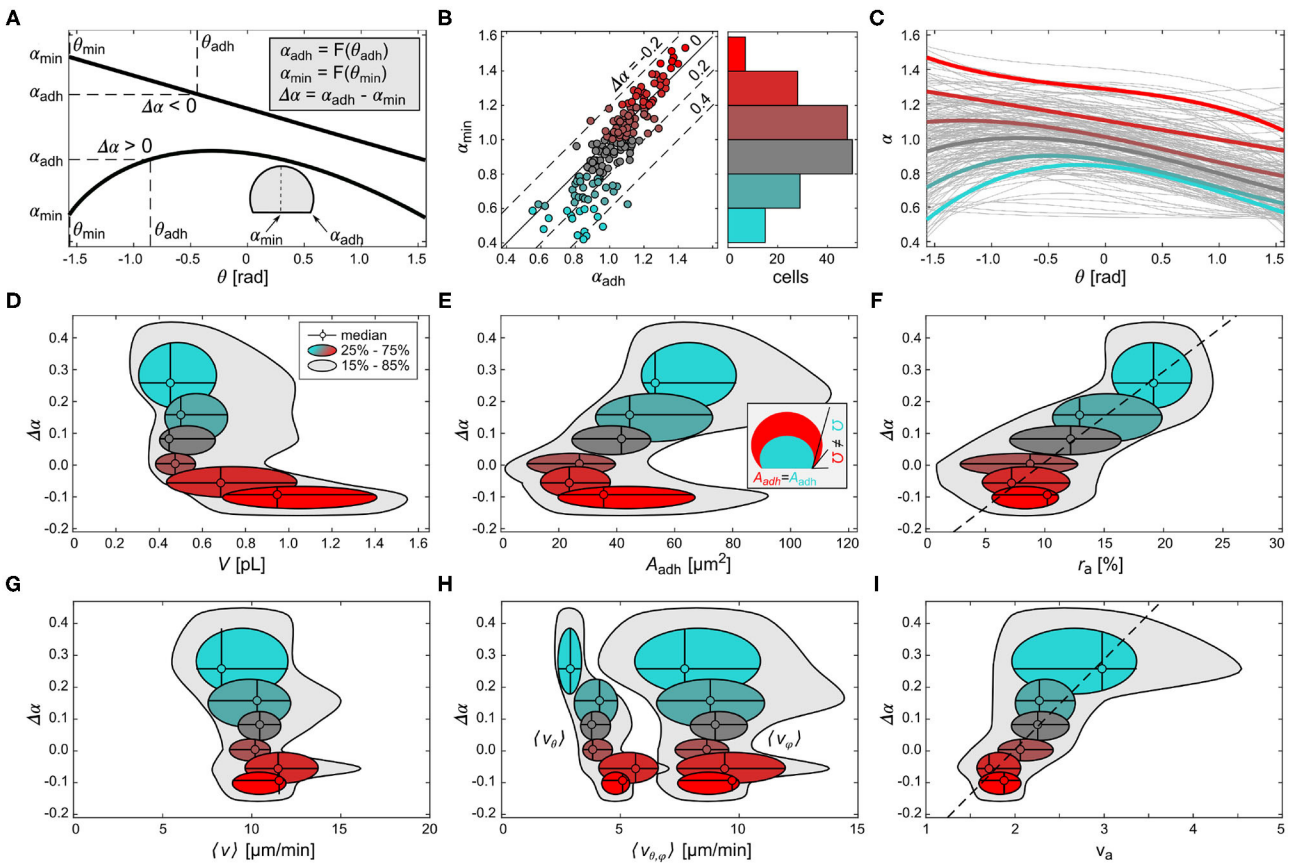

FIGURE 4 | Comparison of fluctuation, geometry and domain dynamics between cells. **(A)** Scheme of two different weighted polynomial fits of α-histogram showing the minimal latitude (θ_{min}) and contact perimeter (θ_{adh}), and the respective levels of α (α_{min}, α_{adh}) that define the difference $\Delta\alpha$. **(B)** The left panel shows the relation between α_{min} and α_{adh}. The color scheme is applied as a function of α_{min}. The right panel shows the number of cells that correspond to each α_{min} level, as a histogram. **(C)** The weighted polynomial fits of all cells (gray lines) and averaged representative fits of the binned α_{min} levels shown in the respective color. **(D–I)** The difference of α, $\Delta\alpha$ plotted as a function of the cell volume V in **(D)**, the ventral membrane area A_{adh} in **(E)**, the ratio between ventral and entire membrane area $r_a = A_{adh}/A_{mem}$ in **(F)**, the mean domain speed $\langle v \rangle$ in **(G)**, average vertical $\langle v_\theta \rangle$ and horizontal $\langle v_\phi \rangle$ wave speed in **(H)**, and the domain speed ratio $v_a = v_\varphi/v_\theta$ **(I)**. The color scheme corresponds to the α_{min} levels shown in **(B)**. The dashed lines in **(F,I)** are the linear fits of the medians. The inset in **(E)** depicts the difference in membrane curvature, representatively shown by the contact angle Ω, for two cells of different volume but equal ventral area A_{adh}.

where R is the radius of the sphere. Equation 7 can be numerically solved as

$$\Omega = 4\tan^{-1}\left(\sqrt{\frac{-2\sqrt{2r_a^2 - 3r_a + 1} - 3r_a + 2}{r_a}}\right). \quad (8)$$

A good approximation for small contact angles ($\Omega \simeq 0$) is $\Omega = -\sin^{-1}(2\sqrt{r_a})$. Here, Ω is obtained purely based on geometric cell features, but does not account for minor membrane variations and possible constraints based on the mechanical properties of the membrane. **Figure 5A** shows the relation between Ω and $\langle v_a \rangle$. The dashed line denotes the weighted polynomial fit derived from **Figures 4F,I**. At $\Omega = 0$ we obtain $v_a \simeq 1$, as the theory predicts when considering isotropic diffusion on membranes. Contrarily the unweighted fit of the data (solid line), where cells with large A_{adh} (cyan) and large cells with comparable A_{adh} (red) are underrepresented (**Figure 4B**, left panel), leads to misleading statistics.

To visualize the influence of the contact perimeter on the signaling dynamics, we utilized the Morlet wavelet transformation (Harang et al., 2012) at all spatially extracted positions on the membrane, as done before only for the ventral membrane of *Dictyostelium* cells (Taniguchi et al., 2013). **Figure 5B** shows a scheme of the phase extraction of the entire membrane from the raw data (left side) to the resulting phase map (right side). The phase is adjusted to the propagation front of the domain, so that the red color ($= 2\pi$) can be considered as wave front. Applied to the entire spatiotemporal raw data, it is also possible to generate kymographs and snapshots of the time-series, as illustrated in **Figures 5C–E**. The example illustrates the dynamics of vertical waves of an almost spherical cell (see **Figure 2E**). The advantage of this visualization method is that the PIP3 wave dynamics and phase singularities can be visualized clearly without application of spatial filters. **Figure 5D** shows the wave directional change from clockwise to anticlockwise rotation during the 10th and 15th min (**Figure 5C**) by rotation

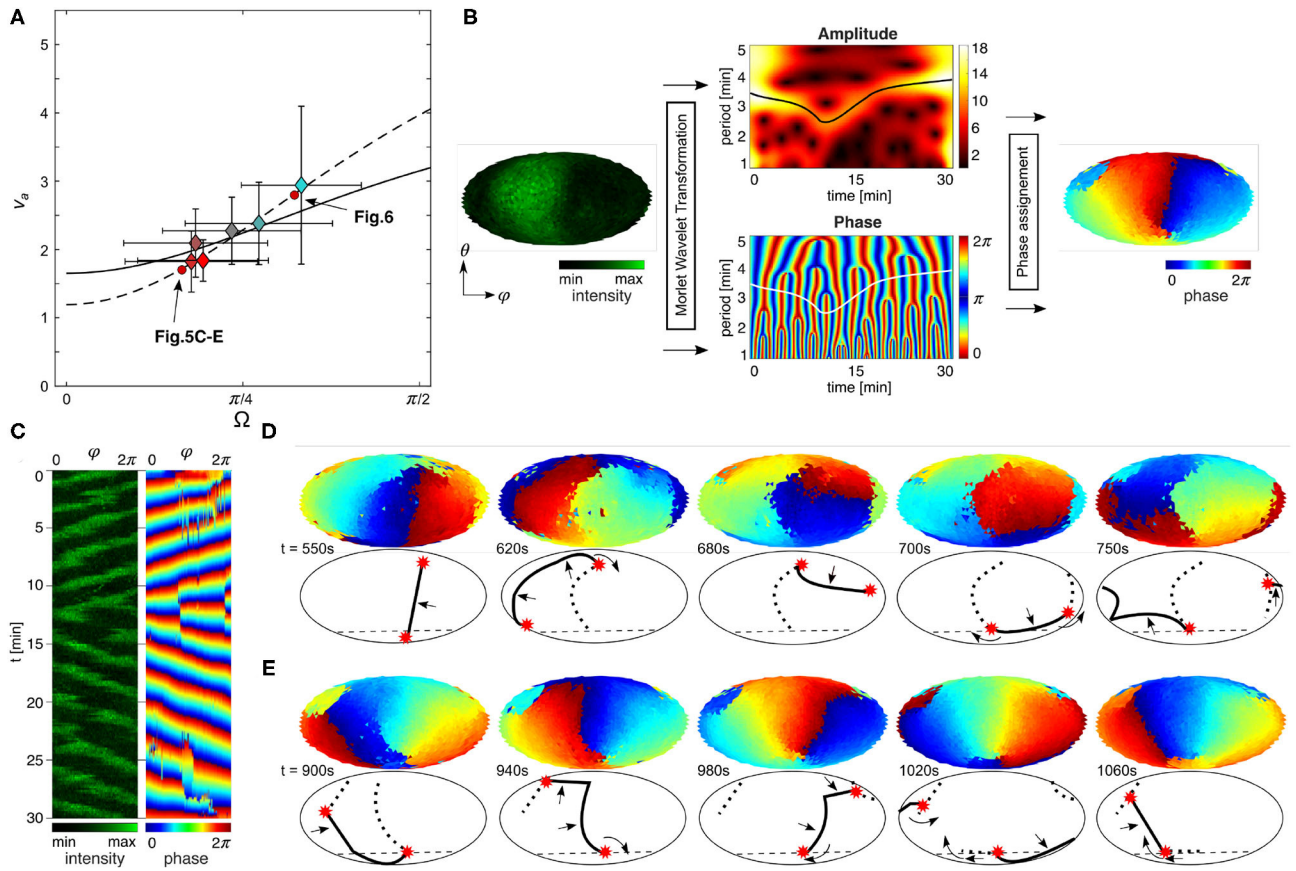

FIGURE 5 | Curvature of contact perimeter acts as pinning site of PIP3 spirals. **(A)** Relation between Ω (contact angle) and v_a (speed ratio). Dashed line is the weighted fit calculated from the linear fits in **Figures 4F,I**. Solid line is the non-weighted fit of all cells without considering $\Delta\alpha$ (see also **Supplementary Figure 4**). Color coding corresponds to α_{min} (see **Figure 4B**). **(B)** Scheme of the phase extraction on entire membrane. Phase of oscillating PIP3 at every spatial point was extracted from fluorescence intensity (left map) by Morlet wavelet transformation [WAVOS] following the approach of Taniguchi et al. (2013). Amplitude and phase of the wavelet transform (center maps). The frequency component having the maximum amplitude at each time point was obtained by ridge extraction (black solid line), and the phase was calculated accordingly (white solid line). Spatially distributed phase is extracted (right map). **(C)** Kymographs of fluorescence intensity and phase maps. **(D,E)** Oscillating waves in nearly spherical cells (see **Figures 1B**, **2E**). Phasemaps (top) and simplified schemes of the dynamics (bottom). **(D)** Change of domain front direction (solid line, 2π) from anticlockwise to clockwise wave direction by vertical phase line (dotted line) with one end pinned to the contact perimeter (dashed line). Phase singularities are denoted by red asterisks, and propagation direction with black arrows. **(E)** Spiral wave of PIP3 pinned to the contact perimeter (see lower red asterisk).

around a phase singularity (red asterisks), which we denote as a pinning site. The PIP3 wave propagates after the turn around the pinning site toward the center of ventral membrane along an elongated phase line. While the pinning site remains spatially anchored at the contact perimeter until $t = 1,020$ s (**Figure 5E**), there is no spatially anchored pinning site at the upper part of the membrane. That means that the PIP3 wave is guided along the contact perimeter, illustrated by the positional change of the phase singularity (red asterisks), because on the upper membrane is no strongly curved membrane as at the contact perimeter. Between $t = 1,020$ s and $t = 1,060$ s the phase singularity moves along the contact perimeter and a new pinning site is formed (last panel). Here, we observe two pinning sites, because of the topology constraints of spiral waves in excitable media (Davidsen et al., 2004). While one pinning site changes its position with time on the upper part of the membrane, the pining site on the contact perimeter does not change its position. This topology constraint together with the refractory behavior of the excitable signaling leads to an $\langle v_a \rangle \sim 1.7$, as marked in **Figure 5A**. Larger cells with large A_{adh} show an even more dominant influence of the contact perimeter on the PIP3 dynamics (**Figure 6**). Pinning sites do not only anchor to the contact perimeter (**Figure 6A**), but can also serve as wave guidance for the wave front (**Figure 6B**). In this case the PIP3 wave edge aligns with the contact perimeter and leads to even larger speed ratios by forcing the PIP3 wave to propagate parallel to the cell perimeter, in this example to almost $\langle v_a \rangle \sim 3$ (**Figure 5A**).

4. DISCUSSION

Self-organization of signals in spatially extended systems are directly and indirectly influenced by the spatial topology. The

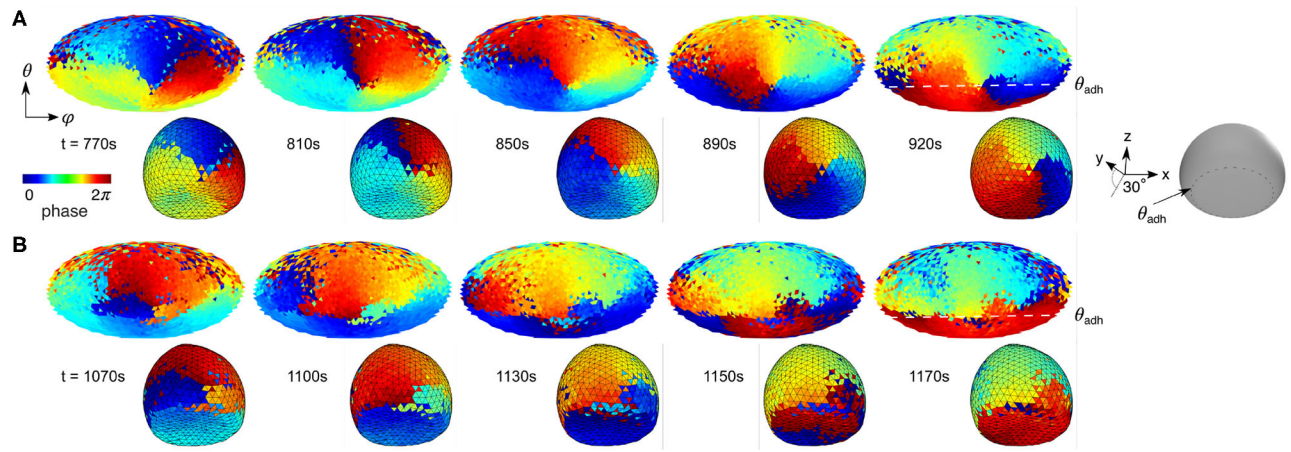

FIGURE 6 | Contact perimeter guides PIP3 waves. **(A)** Contact perimeter serves as pinning site. **(B)** Contact perimeter guides PIP3 waves. Snapshots of phase maps are shown in 2D (top) and 3D (bottom). 3D maps are tilted 30° for showing the ventral membrane too, as shown by the gray 3D illustration where θ_{adh} is illustrated. The cell that is used to show this patterns is shown in **Figures 3B,D**, and its relation between contact angle Ω and speed ratio v_a marked by a red circle in **Figure 5A**.

regulation of reaction in 1D rings (Nishiyama, 1995), 2D rings (Li et al., 2020), and spherical surfaces (Maselko and Showalter, 1989) leads to self-organization of periodic waves, whose length scales are defined by the spatial confinement (Howard et al., 2011) and system size (Campanari et al., 2017). These examples highlight the strong correlation of wave patterning and system topology in confined excitable systems. Most of these systems are artificially formed and do not show large curvatures, such as membrane protrusions in migrating cells. However, recent studies on spatially confined *Dictyostelium* cells indicated the importance of membrane curvature, when observing that excitable dynamics are directly regulated by 3D geometry (i.e., size and shape) on the entire plasma membranes (Hörning and Shibata, 2019). Using the raw data observed on the entire plasma membrane and taking advantage of high-resolution signaling extraction methodology, we were able to statistically analyse and visually proof the importance of larger membrane curvature by using the contact angle Ω, as an indirect measure of the local membrane curvature at the contact perimeter. While the membrane curvature of actin-inhibited cells is not as large as in membrane protrusions, the curvature at the contact perimeter, hereon denoted as κ_{max}, is sufficiently large to pin and guide the PIP3 waves. This leads to a curvature related diffusion change at the contact perimeter, i.e., smaller cells with larger κ_{max} lead to a boundary that restricts diffusion and larger cells with slightly lower κ_{max} lead to lower diffusion properties at the contact perimeter. Therefore, we speculate that the PIP3 waves that propagate to the tips of membrane protrusions (location of largest curvature) get pinned and can promote actin polymerization in *Dictyostelium* cells. Curvature-restricted diffusivity in *Dictyostelium* could be experimentally tested by the use of fluorescence recovery after photobleaching (FRAP). Bleaching the membrane close to the highly curved membrane, such as the edge of ventral membrane, should show a slower recovery than bleaching far from the curved membrane, as the diffusion is restricted by the contact perimeter. This effect should increase with an increase of the contact angle, which can be experimentally controlled by the amount of PEI.

A previous study on *Dictyostelium* cells that were confined between two planar surface reported that a PIP3 wave was formed on either side of the opposing cell surface with switching period of 2–5 min (Helenius et al., 2018). The switching time scale is comparable to the period of PIP3 observed in the present study (see **Figures 2A,B**, **5B**). Such an experimental setup could be used to study the influence of the membrane curvature on the PIP3 domain dynamics in more detail by adjusting the distance between two planar surface.

In the present study, we did not observed the PIP3 domain formation that was confined only in the ventral membrane. This indicated that the entire membrane region (both ventral and non-adhesive membrane regions) have the excitable property. However, we expect that a confined PIP3 wave within either ventral or non-adhesive membrane regions can be formed if the curvature at the boundary between two regions is sufficiently high and due to the inhibition of multiple PIP3 domain formation through cytosol interaction (lateral inhibition) (Gerisch et al., 2012; Taniguchi et al., 2013).

In this study we showed an organizing role of the contact perimeter on the membrane pattern formation. To clarify the mechanism, it is necessary to study how the contact perimeter interacts with the membrane molecules. In particular, PIP3 is known to accumulate on the membrane in a mutually exclusive manner with PTEN. For this sharp transition between the two states, a mutual inhibitory mechanism between PIP3 and PTEN plays an important role (Arai et al., 2010; Gerisch et al., 2012; Matsuoka and Ueda, 2018). In addition to such direct interaction between these molecules, the membrane curvature might play some role on the sharp separation by changing the membrane localization of the regulatory molecules.

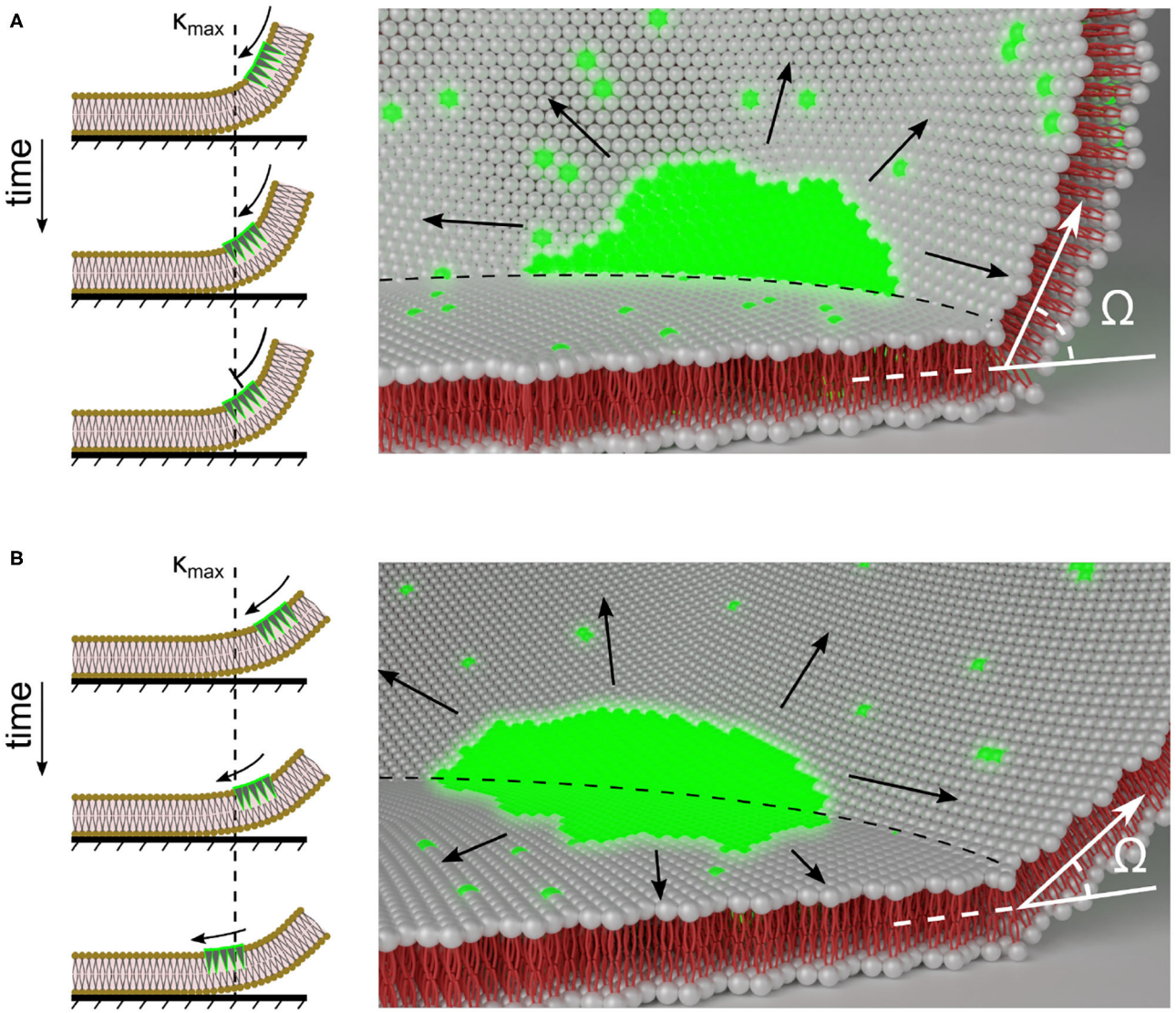

FIGURE 7 | Scheme of membrane curvature regulated PIP3-domain signaling at the contact perimeter. PIP3-domain diffusion across the contact perimeter depends on the degree of local membrane curvature. **(A,B)** show illustrations of differently sized cells that have large and small membrane curvatures, κ at the contact perimeter, and the influence of the contact perimeter on the PIP3-domain (green) propagation. The left panels show the one dimensional view of PIP3-domain propagation. κ_{max} shows the position of the contact perimeter and the membrane location with highest degree of curvature. The black arrows indicate the direction of PIP3-domain propagation. The right panels show the two dimensional view. The black arrows indicate possible directions of PIP3-domain propagation that may also lead to anchored waves at the contact perimeter (dashed line). The contact angle Ω is representatively shown at the contact perimeter.

Following on that, another important aspect of PIP3 dynamics is the macropinocytosis (Buczynski et al., 1997; Hoeller et al., 2013; Veltman et al., 2016), which is a unique pathway of endocytosis to internalize large amounts of extracellular fluid, solutes and membrane (Lin et al., 2020). In non-mammalian cells, such as *Dictyostelium* cells, macropinocytosis requires PIP3 and the persistent activation of Ras Williams et al. (2019) to form patches in macropinosomes Ritter et al. (2021). While this pathway is also observed in diverse range of mammalian cells too, such as immune cells, endothelial and epithelial cells (Lin et al., 2020), they also play an essential role in cancer cells as reviewed in Ha et al. (2016), Recouvreux and Commisso (2017), Zhang and Commisso (2019), and Ritter et al. (2021). It has been identified that macropinocytosis is a mechanism by which cancer cells support their unique metabolic needs (Commisso et al., 2013), and has therefore increased the interest for anticancer therapies (Ritter et al., 2021; Song et al., 2021). The findings presented here open an interesting new aspect to macropinocytosis that suggests relevance to cancer cells too, as PIP3 domain dynamics are observed as self-organizing waves that are prone to be pinned and guided by strongly bended membranes, just as observed

during the formation of macropinocytic cups (Veltman et al., 2016).

Another possible explanation can be given by considering molecular crowding (Liu et al., 2018) and induced changes in lipid composition and their asymmetry (Bigay and Antonny, 2012; McMahon and Boucrot, 2015) at the contact perimeter, which may even lead to local conformational switches (Aisenbrey et al., 2008) and nano-domain clustering, as observed for glycolipid GM3 and PIP2 in molecular simulations of complex lipid bilayers (Koldsø et al., 2014). The large headgroups in PIP3 confers an inverted conical shape to the lipids, thereby favoring the bending of the membrane into a positive curvature (Di Paolo and De Camilli, 2006; McMahon and Boucrot, 2015). As for actin-inhibited *Dictyostelium* cells, the plasma membrane is immobilized and larger curvature is observed at the contact perimeter only. While the membrane area ratio r_a can be comparable for cells of different volumes, κ_{max} depends on the cell volume and ventral membrane size. Thus, larger cells have smaller κ_{max}. Therefore, in larger cells the local diffusivity of PIP3 is reduced at the contact perimeter (**Figure 3B**), while the contact perimeter of smaller cells with larger κ_{max} serves as a diffusion boundary (**Figure 3A**).

One possible explanation of these findings could be the influence of the large polar PIP3 headgroups that may interact and disturb the free diffusibility at the strongly curved contact perimeter and subsequently lead to molecular crowding (see scheme in **Figure 7**). This crowding may affect compartmentalization and other mechanisms in living cells that allow proteins to sense, stabilize or generate a high local membrane curvature (McMahon and Boucrot, 2015), such as PTEN, a cytosolic protein that associates with the plasma membrane. Further experimental investigations on precisely controlled curvatures of artificial cell membrane systems using microfabrication (Komiya et al., 2020) and high-precision 3D printing (Erben et al., 2020) may enhance our understanding of these findings.

DATA AVAILABILITY STATEMENT

The raw data supporting the conclusions of this article will be made available by the authors, without undue reservation. A basic version of the implemented code is available at MATLAB Central File Exchange (Hörning, 2021).

AUTHOR CONTRIBUTIONS

MH, TB, and TS conceptualized and designed research and wrote the manuscript. MH and TS performed data acquisition. MH implemented the analysis routines and analyzed the data. All authors contributed to the article and approved the submitted version.

FUNDING

This study was supported by the core funding at RIKEN Center for Biosystems Dynamics Research (to TS) and the Foreign Postdoctoral Researcher program at RIKEN (to MH).

SUPPLEMENTARY MATERIAL

The Supplementary Material for this article can be found online at: https://www.frontiersin.org/articles/10.3389/fcell.2021.670943/full#supplementary-material

REFERENCES

Aisenbrey, C., Bechinger, B., and Gröbner, G. (2008). Macromolecular crowding at membrane interfaces: adsorption and alignment of membrane peptides. *J. Mol. Biol.* 375, 376–385. doi: 10.1016/j.jmb.2007.10.053

Andrew, N., and Insall, R. H. (2007). Chemotaxis in shallow gradients is mediated independently of PtdIns 3-kinase by biased choices between random protrusions. *Nat. Cell Biol.* 9, 193–200. doi: 10.1038/ncb1536

Arai, Y., Shibata, T., Matsuoka, S., Sato, M. J., Yanagida, T., and Ueda, M. (2010). Self-organization of the phosphatidylinositol lipids signaling system for random cell migration. *Proc. Natl. Acad. Sci. U.S.A.* 107, 12399–12404. doi: 10.1073/pnas.0908278107

Bianco, R., Melisi, D., Ciardiello, F., and Tortora, G. (2006). Key cancer cell signal transduction pathways as therapeutic targets. *Eur. J. Cancer* 42, 290–294. doi: 10.1016/j.ejca.2005.07.034

Bigay, J., and Antonny, B. (2012). Curvature, lipid packing, and electrostatics of membrane organelles: defining cellular territories in determining specificity. *Dev. Cell* 23, 886–895. doi: 10.1016/j.devcel.2012.10.009

Bosgraaf, L., Keizer-Gunnink, I., and Van Haastert, P. J. M. (2008). PI3-kinase signaling contributes to orientation in shallow gradients and enhances speed in steep chemoattractant gradients. *J. Cell Sci.* 121, 3589–3597. doi: 10.1242/jcs.031781

Brenner, M., and Thoms, S. D. (1984). Caffeine blocks activation of cyclic AMP synthesis in *Dictyostelium discoideum*. *Dev. Biol.* 101, 136–146. doi: 10.1016/0012-1606(84)90124-6

Buczynski, G., Grove, B., Nomura, A., Kleve, M., Bush, J., Firtel, R. A., et al. (1997). Inactivation of two *Dictyostelium discoideum* genes, DdPIK1 and DdPIK2, encoding proteins related to mammalian phosphatidylinositide 3-kinases, results in defects in endocytosis, lysosome to postlysosome transport, and actin cytoskeleton organization. *J. Cell Biol.* 136, 1271–1286. doi: 10.1083/jcb.136.6.1271

Campanari, L., You, M. J., Langfield, P., Glass, L., and Shrier, A. (2017). Varieties of reentrant dynamics. *Chaos* 27, 041101. doi: 10.1063/1.4979602

Commisso, C., Davidson, S. M., Soydaner-Azeloglu, R. G., Parker, S. J., Kamphorst, J. J., Hackett, S., et al. (2013). Macropinocytosis of protein is an amino acid supply route in Ras-transformed cells. *Nature* 497, 633–637. doi: 10.1038/nature12138

Courtemanche, M., Glass, L., and Keener, J. P. (1993). Instabilities of a propagating pulse in a ring of excitable media. *Phys. Rev. Lett.* 70, 2182–2185. doi: 10.1103/PhysRevLett.70.2182

Davidsen, J., Glass, L., and Kapral, R. (2004). Topological constraints on spiral wave dynamics in spherical geometries with inhomogeneous excitability. *Phys. Rev. E* 70:056203. doi: 10.1103/PhysRevE.70.056203

Delignières, D. (2015). Correlation properties of (Discrete) fractional gaussian noise and fractional brownian motion. *Math. Prob. Eng.* 2015:e485623. doi: 10.1155/2015/485623

Devreotes, P. N., Bhattacharya, S., Edwards, M., Iglesias, P. A., Lampert, T., and Miao, Y. (2017). Excitable signal transduction networks in directed cell migration. *Annu. Rev. Cell Dev. Biol.* 33, 103–125. doi: 10.1146/annurev-cellbio-100616-060739

Di Paolo, G., and De Camilli, P. (2006). Phosphoinositides in cell regulation and membrane dynamics. *Nature* 443, 651–657. doi: 10.1038/nature05185

Erben, A., Hörning, M., Hartmann, B., Becke, T., Eisler, S. A., Southan, A., et al. (2020). Precision 3D-printed cell scaffolds mimicking native tissue composition and mechanics. *Adv. Healthcare Mater.* 9:2000918. doi: 10.1002/adhm.202000918

Gerisch, G., Schroth-Diez, B., Müller-Taubenberger, A., and Ecke, M. (2012). PIP3 waves and PTEN dynamics in the emergence of cell polarity. *Biophys. J.* 103, 1170–1178. doi: 10.1016/j.bpj.2012.08.004

Gilden, D. L., Thornton, T., and Mallon, M. W. (1995). 1/f noise in human cognition. *Science* 267, 1837–1839. doi: 10.1126/science.7892611

Goehring, N. W., and Grill, S. W. (2013). Cell polarity: mechanochemical patterning. *Trends Cell Biol.* 23, 72–80. doi: 10.1016/j.tcb.2012.10.009

Goldstein, B., and Macara, I. G. (2007). The PAR proteins: fundamental players in animal cell polarization. *Dev. Cell* 13, 609–622. doi: 10.1016/j.devcel.2007.10.007

Ha, K. D., Bidlingmaier, S. M., and Liu, B. (2016). Macropinocytosis exploitation by cancers and cancer therapeutics. *Front. Physiol.* 7:381. doi: 10.3389/fphys.2016.00381

Habib, A. (2017). *R-DFA : Robust Detrended Fluctuation Analysis*. Available online at: https://de.mathworks.com/matlabcentral/fileexchange/60026-r-dfa-robust-detrended-fluctuation-analysis.

Habib, A., Sorensen, J. P. R., Bloomfield, J. P., Muchan, K., Newell, A. J., and Butler, A. P. (2017). Temporal scaling phenomena in groundwater-floodplain systems using robust detrended fluctuation analysis. *J. Hydrol.* 549, 715–730. doi: 10.1016/j.jhydrol.2017.04.034

Harang, R., Bonnet, G., and Petzold, L. R. (2012). WAVOS: A MATLAB toolkit for wavelet analysis and visualization of oscillatory systems. *BMC Res. Notes* 5:163. doi: 10.1186/1756-0500-5-163

Helenius, J., Ecke, M., Müller, D. J., and Gerisch, G. (2018). Oscillatory switches of dorso-ventral polarity in cells confined between two surfaces. *Biophys. J.* 115, 150–162. doi: 10.1016/j.bpj.2018.05.025

Hoeller, O., Bolourani, P., Clark, J., Stephens, L. R., Hawkins, P. T., Weiner, O. D., et al. (2013). Two distinct functions for PI3-kinases in macropinocytosis. *J. Cell Sci.* 126, 4296–4307. doi: 10.1242/jcs.134015

Hörning, M. (2021). 4D Cell Membrane Visualization and Quantification. MATLAB Central File Exchange. Available online at: https://www.mathworks.com/matlabcentral/fileexchange/97802-4d-cell-membrane-visualization-andquantification (retrieved August 24, 2021).

Hörning, M., and Shibata, T. (2019). Three-dimensional cell geometry controls excitable membrane signaling in dictyostelium cells. *Biophys. J.* 116, 372–382. doi: 10.1016/j.bpj.2018.12.012

Howard, J., Grill, S. W., and Bois, J. S. (2011). Turing's next steps: the mechanochemical basis of morphogenesis. *Nat. Rev. Mol. Cell Biol.* 12, 392–398. doi: 10.1038/nrm3120

Janetopoulos, C., Ma, L., Devreotes, P. N., and Iglesias, P. A. (2004). Chemoattractant-induced phosphatidylinositol 3,4,5-trisphosphate accumulation is spatially amplified and adapts, independent of the actin cytoskeleton. *Proc. Natl. Acad. Sci. U.S.A.* 101, 8951–8956. doi: 10.1073/pnas.0402152101

Koldsø, H., Shorthouse, D., Hélie, J., and Sansom, M. S. P. (2014). Lipid clustering correlates with membrane curvature as revealed by molecular simulations of complex lipid bilayers. *PLoS Comput. Biol.* 10:e1003911. doi: 10.1371/journal.pcbi.1003911

Komiya, M., Kato, M., Tadaki, D., Ma, T., Yamamoto, H., Tero, R., et al. (2020). Advances in artificial cell membrane systems as a platform for reconstituting ion channels. *Chem. Record* 20, 730–742. doi: 10.1002/tcr.201900094

Li, J., Zhang, L., Yu, L., Minami, I., Miyagawa, S., Hörning, M., et al. (2020). Circulating re-entrant waves promote maturation of hiPSC-derived cardiomyocytes in self-organized tissue ring. *Commun. Biol.* 3, 1–12. doi: 10.1038/s42003-020-0853-0

Lin, X. P., Mintern, J. D., and Gleeson, P. A. (2020). Macropinocytosis in different Cell Types: similarities and differences. *Membranes* 10:177. doi: 10.3390/membranes10080177

Liu, W., Fu, L., Wang, Z., Sohrabpour, Z., Li, X., Liu, Y., et al. (2018). Two dimensional crowding effects on protein folding at interfaces observed by chiral vibrational sum frequency generation spectroscopy. *Phys. Chem. Chem. Phys.* 20, 22421–22426. doi: 10.1039/C7CP07061F

Loose, M., Kruse, K., and Schwille, P. (2011). Protein self-organization: lessons from the min system. *Annu. Rev. Biophys.* 40, 315–336. doi: 10.1146/annurev-biophys-042910-155332

Maselko, J., and Showalter, K. (1989). Chemical waves on spherical surfaces. *Nature* 339, 609. doi: 10.1038/339609a0

Matsuoka, S., and Ueda, M. (2018). Mutual inhibition between PTEN and PIP3 generates bistability for polarity in motile cells. *Nat. Commun.* 9, 4481. doi: 10.1038/s41467-018-06856-0

McMahon, H. T., and Boucrot, E. (2015). Membrane curvature at a glance. *J. Cell Sci.* 128, 1065–1070. doi: 10.1242/jcs.114454

Molz, F. J., Liu, H. H., and Szulga, J. (1997). Fractional Brownian motion and fractional Gaussian noise in subsurface hydrology: a review, presentation of fundamental properties, and extensions. *Water Resour. Res.* 33, 2273–2286. doi: 10.1029/97WR01982

Montez, T., Poil, S.-S., Jones, B. F., Manshanden, I., Verbunt, J. P. A., van Dijk, B. W., et al. (2009). Altered temporal correlations in parietal alpha and prefrontal theta oscillations in early-stage Alzheimer disease. *Proc. Natl. Acad. Sci. U.S.A.* 106, 1614–1619. doi: 10.1073/pnas.0811699106

Nishikawa, M., Hörning, M., Ueda, M., and Shibata, T. (2014). Excitable signal transduction induces both spontaneous and directional cell asymmetries in the phosphatidylinositol lipid signaling system for eukaryotic chemotaxis. *Biophys. J.* 106, 723–734. doi: 10.1016/j.bpj.2013.12.023

Nishiyama, N. (1995). Experimental observation of dynamical behaviors of four, five and six oscillators in rings and nine oscillators in a branched network. *Phys. D* 80, 181–185. doi: 10.1016/0167-2789(95)90077-2

Peng, C.-K., Buldyrev, S. V., Havlin, S., Simons, M., Stanley, H. E., and Goldberger, A. L. (1994). Mosaic organization of DNA nucleotides. *Phys. Rev. E* 49, 1685–1689. doi: 10.1103/PhysRevE.49.1685

Persson, P.-,o. and Strang, G. (2004). A simple mesh generator in MATLAB. *SIAM Rev.* 46, 2004. doi: 10.1137/S0036144503429121

Recouvreux, M. V., and Commisso, C. (2017). Macropinocytosis: a metabolic adaptation to nutrient stress in cancer. *Front. Endocrinol.* 8:261. doi: 10.3389/fendo.2017.00261

Ritter, M., Bresgen, N., and Kerschbaum, H. H. (2021). From Pinocytosis to methuosis—fluid consumption as a risk factor for cell death. *Front. Cell Dev. Biol.* 9:651982. doi: 10.3389/fcell.2021.651982

Sansal, I., and Sellers, W. R. (2004). The biology and clinical relevance of the PTEN tumor suppressor pathway. *J. Clin. Oncol.* 22, 2954–2963. doi: 10.1200/JCO.2004.02.141

Sasaki, A. T., Janetopoulos, C., Lee, S., Charest, P. G., Takeda, K., Sundheimer, L. W., et al. (2007). G protein–independent Ras/PI3K/F-actin circuit regulates basic cell motility. *J. Cell Biol.* 178, 185–191. doi: 10.1083/jcb.200611138

Shibata, T., Nishikawa, M., Matsuoka, S., and Ueda, M. (2012). Modeling the self-organized phosphatidylinositol lipid signaling system in chemotactic cells using quantitative image analysis. *J. Cell Sci.* 125, 5138–5150. doi: 10.1242/jcs.108373

Slaughter, B. D., Smith, S. E., and Li, R. (2009). Symmetry breaking in the life cycle of the budding yeast. *Cold Spring Harb Perspect Biol.* 1:a003384. doi: 10.1101/cshperspect.a003384

Snyder, J. P. (1987). *Map Projections: A Working Manual*. USGS Numbered Series 1395, U.S. Government Printing Office, Washington, DC.

Song, S., Zhang, Y., Ding, T., Ji, N., and Zhao, H. (2021). The dual role of macropinocytosis in cancers: promoting growth and inducing methuosis to participate in anticancer therapies as targets. *Front. Oncol.* 10:570108. doi: 10.3389/fonc.2020.570108

Suematsu, N. J., Sato, T., Motoike, I. N., Kashima, K., and Nakata, S. (2011). Density wave propagation of a wave train in a closed excitable medium. *Phys. Rev. E Stat. Nonlin Soft. Matter Phys.* 84(4 Pt 2):046203. doi: 10.1103/PhysRevE.84.046203

Taniguchi, D., Ishihara, S., Oonuki, T., Honda-Kitahara, M., Kaneko, K., and Sawai, S. (2013). Phase geometries of two-dimensional excitable waves govern self-organized morphodynamics of amoeboid cells. *Proc. Natl. Acad. Sci. U.S.A.* 110, 5016–5021. doi: 10.1073/pnas.1218025110

Veltman, D. M., Williams, T. D., Bloomfield, G., Chen, B.-C., Betzig, E., Insall, R. H., et al. (2016). A plasma membrane template for macropinocytic cups. *Elife* 5:e20085. doi: 10.7554/eLife.20085

Wallot, S., Fusaroli, R., Tylen, K., and Jegindø, E.-M. (2013). Using complexity metrics with R-R intervals and BPM heart rate measures. *Front. Physiol.* 4:211. doi: 10.3389/fphys.2013.00211

Watts, D. J., and Ashworth, J. M. (1970). Growth of myxamoebae of the cellular slime mould *Dictyostelium discoideum* in axenic culture. *Biochem. J.* 119, 171–174. doi: 10.1042/bj1190171

Whitman, M., Downes, C. P., Keeler, M., Keller, T., and Cantley, L. (1988). Type I phosphatidylinositol kinase makes a novel inositol phospholipid, phosphatidylinositol-3-phosphate. *Nature* 332, 644–646. doi: 10.1038/332644a0

Williams, T. D., Paschke, P. I., and Kay, R. R. (2019). Function of small GTPases in *Dictyostelium macropinocytosis*. *Philos. Trans. R. Soc. B Biol. Sci.* 374, 20180150. doi: 10.1098/rstb.2018.0150

Xiong, Y., Huang, C.-H., Iglesias, P. A., and Devreotes, P. N. (2010). Cells navigate with a local-excitation, global-inhibition-biased excitable network. *Proc. Natl. Acad. Sci. U.S.A.* 107, 17079–17086. doi: 10.1073/pnas.1011271107

Yamazaki, S.-i., Hashimura, H., Morimoto, Y. V., Miyanaga, Y., Matsuoka, S., Kamimura, Y., et al. (2020). Talin B regulates collective cell migration via PI3K signaling in *Dictyostelium discoideum* mounds. *Biochem. Biophys. Res. Commun.* 525, 372–377. doi: 10.1016/j.bbrc.2020.02.060

Zhang, Y., and Commisso, C. (2019). Macropinocytosis in cancer: a complex signaling network. *Trends Cancer* 5, 332–334. doi: 10.1016/j.trecan.2019.04.002

Conflict of Interest: The authors declare that the research was conducted in the absence of any commercial or financial relationships that could be construed as a potential conflict of interest.

Publisher's Note: All claims expressed in this article are solely those of the authors and do not necessarily represent those of their affiliated organizations, or those of the publisher, the editors and the reviewers. Any product that may be evaluated in this article, or claim that may be made by its manufacturer, is not guaranteed or endorsed by the publisher.

Copyright © 2021 Hörning, Bullmann and Shibata. This is an open-access article distributed under the terms of the Creative Commons Attribution License (CC BY). The use, distribution or reproduction in other forums is permitted, provided the original author(s) and the copyright owner(s) are credited and that the original publication in this journal is cited, in accordance with accepted academic practice. No use, distribution or reproduction is permitted which does not comply with these terms.

frontiers in Cell and Developmental Biology

ORIGINAL RESEARCH
published: 23 September 2021
doi: 10.3389/fcell.2021.748860

Domain Organization of the UBX Domain Containing Protein 9 and Analysis of Its Interactions With the Homohexameric AAA + ATPase p97 (Valosin-Containing Protein)

*Jana Riehl[1], Ramesh Rijal[2], Leonie Nitz[1], Christoph S. Clemen[1,3,4], Andreas Hofmann[5] and Ludwig Eichinger[1]**

[1] Medical Faculty, Center for Biochemistry, Institute of Biochemistry I, University of Cologne, Cologne, Germany, [2] Department of Biology, College Station, Texas A&M University, Texas, TX, United States, [3] German Aerospace Center, Institute of Aerospace Medicine, Cologne, Germany, [4] Medical Faculty, Center for Physiology and Pathophysiology, Institute of Vegetative Physiology, University of Cologne, Cologne, Germany, [5] Department of Veterinary Biosciences, Melbourne Veterinary School, The University of Melbourne, Parkville, VIC, Australia

OPEN ACCESS

Edited by:
Annette Müller-Taubenberger, Ludwig Maximilian University of Munich, Germany

Reviewed by:
Pauline Schaap, University of Dundee, United Kingdom
Qianzheng Zhu, The Ohio State University, United States

***Correspondence:**
Ludwig Eichinger
ludwig.eichinger@uni-koeln.de

Specialty section:
This article was submitted to Molecular and Cellular Pathology, a section of the journal Frontiers in Cell and Developmental Biology

Received: 28 July 2021
Accepted: 31 August 2021
Published: 23 September 2021

Citation:
Riehl J, Rijal R, Nitz L, Clemen CS, Hofmann A and Eichinger L (2021) Domain Organization of the UBX Domain Containing Protein 9 and Analysis of Its Interactions With the Homohexameric AAA + ATPase p97 (Valosin-Containing Protein). Front. Cell Dev. Biol. 9:748860. doi: 10.3389/fcell.2021.748860

The abundant homohexameric AAA + ATPase p97 (also known as valosin-containing protein, VCP) is highly conserved from *Dictyostelium discoideum* to human and a pivotal factor of cellular protein homeostasis as it catalyzes the unfolding of proteins. Owing to its fundamental function in protein quality control pathways, it is regulated by more than 30 cofactors, including the UBXD protein family, whose members all carry an Ubiquitin Regulatory X (UBX) domain that enables binding to p97. One member of this latter protein family is the largely uncharacterized UBX domain containing protein 9 (UBXD9). Here, we analyzed protein-protein interactions of *D. discoideum* UBXD9 with p97 using a series of N- and C-terminal truncation constructs and probed the UBXD9 interactome in *D. discoideum*. Pull-down assays revealed that the UBX domain (amino acids 384–466) is necessary and sufficient for p97 interactions and that the N-terminal extension of the UBX domain, which folds into a β_0-α_{-1}-α_0 lariat structure, is required for the dissociation of p97 hexamers. Functionally, this finding is reflected by strongly reduced ATPase activity of p97 upon addition of full length UBXD9 or UBXD9$^{261-573}$. Results from Blue Native PAGE as well as structural model prediction suggest that hexamers of UBXD9 or UBXD9$^{261-573}$ interact with p97 hexamers and disrupt the p97 subunit interactions via insertion of a helical lariat structure, presumably by destabilizing the p97 D1:D1' intermolecular interface. We thus propose that UBXD9 regulates p97 activity *in vivo* by shifting the quaternary structure equilibrium from hexamers to monomers. Using

three independent approaches, we further identified novel interaction partners of UBXD9, including glutamine synthetase type III as well as several actin-binding proteins. These findings suggest a role of UBXD9 in the organization of the actin cytoskeleton, and are in line with the hypothesized oligomerization-dependent mechanism of p97 regulation.

Keywords: p97/VCP/CDC48/TER/VAT ATPase, UBX domain containing protein 9 (UBXD9, TUG, ASPL, PUX1), IBMPFD (Inclusion Body Myopathy associated with Paget disease of bone and Fronto temporal Dementia), ALS (Amyotrophic Lateral Sclerosis), *Dictyostelium discoideum*, hexamer disassembly

INTRODUCTION

The AAA + (ATPase Associated with diverse cellular Activities) ATPase p97, also known as valosin-containing protein (VCP), is a very abundant protein and evolutionarily highly conserved. It was first described in 1982 and has since emerged as a fundamental player in a plethora of cellular processes and signaling pathways (Moir et al., 1982; Madsen et al., 2009; van den Boom and Meyer, 2018). The protein has a tripartite structure comprising a globular N domain followed by the D1 and D2 domains that bind and hydrolyze ATP (**Figure 1A**; Wendler et al., 2012). p97 assembles into a ring shaped hexameric complex of six identical subunits, where the D1 and D2 domains form stacked rings with a "cis" and a "trans" side. The "cis" D1 domain is surrounded by the globular N domain (**Figure 1B**). Depending on nucleotide binding in the D1 domain, the N domain adopts an up- or down conformation (**Figure 1C**; Huyton et al., 2003; Bodnar and Rapoport, 2017; Banchenko et al., 2019).

For a long time, p97 was considered only as a segregase that extracts target proteins from complexes or membranes by ATP hydrolysis, so that they can be degraded by the proteasome (Ye, 2006). However, now it is clear that the fundamental function of p97 is the unfolding of proteins in numerous protein quality control pathways such as chromatin-associated degradation, the ubiquitin-proteasome system (UPS), mitochondria-associated degradation, endo-lysosomal damage response, macroautophagy, and endoplasmic-reticulum associated degradation (ERAD) (Bodnar and Rapoport, 2017; van den Boom and Meyer, 2018; Papadopoulos et al., 2020). The critical importance of p97 for cellular homeostasis is demonstrated by the lethality of knock-out mutations in unicellular and multicellular organisms (Müller et al., 2007). Furthermore, an increasing number of p97 missense mutations have been associated with various human diseases. Prominent examples include the late-onset and slowly progressive multi-system disorder Inclusion Body Myopathy associated with Paget disease of bone and Fronto temporal Dementia (IBMPFD) and Amyotrophic Lateral Sclerosis (ALS) (Watts et al., 2004; Johnson et al., 2010; Clemen et al., 2012; Evangelista et al., 2016). Since cancer cells have a heightened dependence on mechanisms of protein homeostasis, p97 is also a promising target for anti-cancer therapy (Deshaies, 2014).

To exert its locally, functionally and mechanically different tasks, p97 interacts with more than 30 different cofactors, most of which associate with the N domain. The p97 cofactors can be divided into three major classes, (i) substrate-recruiting cofactors, as e.g., the well-studied Ufd1/Npl4 heterodimer, (ii) substrate-processing cofactors as e.g., ubiquitin E3 ligases, and (iii) regulatory cofactors (Hänzelmann and Schindelin, 2017). The largest family of regulatory cofactors is the Ubiquitin Regulatory X (UBX) domain containing protein family, which has thirteen members in human and eleven in *D. discoideum* (Alexandru et al., 2008; Rijal et al., 2016). All members possess the eponymous, highly conserved UBX domain in their C-terminal region, which adopts a ubiquitin-like fold and is critical for the interaction with the N domain of p97 (Rezvani, 2016). Five of the *D. discoideum* UBXD family members, among them UBX domain containing protein 9 (UBXD9), are orthologs of human UBXD proteins (Rijal et al., 2016). Human UBXD9, also known as ASPL (alveolar soft part sarcoma locus) or TUG (tether containing a UBX domain for GLUT4), was originally identified in a genetic screen as part of an oncogenic fusion protein with the transcription factor TFE3 in alveolar soft part sarcoma cells (Ladanyi et al., 2001). The latter name, TUG, reflects its function in the redistribution of the glucose transporter GLUT4 in adipocytes (Bogan et al., 2003). In the basal state, UBXD9 traps GLUT4 storage vesicles (GSVs) at the Golgi apparatus. In response to insulin, UBXD9 is endoproteolytically cleaved by Usp25b, resulting in the release of the GSVs and their transport to the plasma membrane by the kinesin motor protein KIF5B (Habtemichael et al., 2018). Furthermore, it was shown that UBXD9 is required for the efficient re-assembly of the Golgi complex after brefeldin A removal (Orme and Bogan, 2012). A further UBXD9 homolog, PUX1 (plant UBX domain-containing protein 1), has been described in *Arabidopsis thaliana*. PUX1 is only about half the size and lacks the N-terminal half of UBXD9 (Rancour et al., 2004). Among all p97 cofactors described so far, *D. discoideum* UBXD9, human TUG and *A. thaliana* PUX1 are unique as they possess p97 hexamer disassembly activity (Rancour et al., 2004; Orme and Bogan, 2012; Rijal et al., 2016). In the following parts, we will refer to *D. discoideum* UBXD9 mostly just as UBXD9 and specify the orthologouss UBXD9 proteins by adding species names.

Here, we further analyzed UBXD9 by the characterization of the full-length protein and a series of N- and C-terminal truncation constructs with respect to their interactions with p97. Furthermore, to shed light on the UBXD9 interactome and further possible functions of UBXD9, we applied three different approaches to identify new interacting proteins.

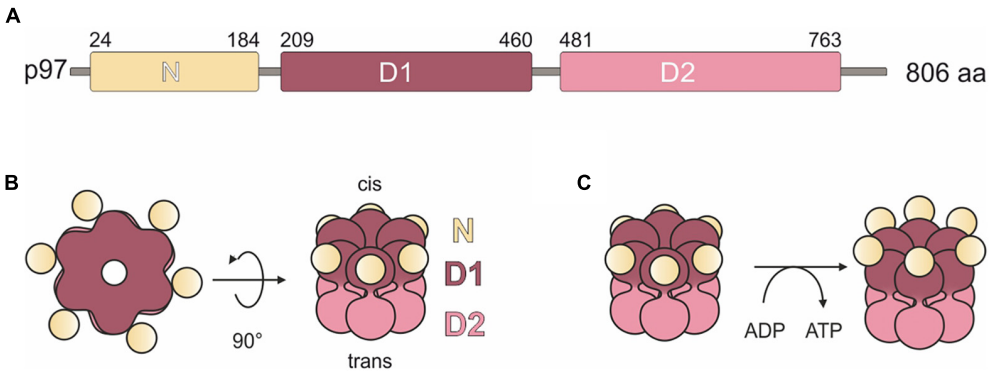

FIGURE 1 | Domain organization and model of *H. sapiens* p97. **(A)** p97 domain organization. N, N domain (yellow); D1, ATPase domain D1 (purple); D2, ATPase domain D2 (pink). Numbers indicate amino acid positions. **(B)** Schematic representation of the structure of the p97 homohexamer. Each monomer comprises a globular N domain (N) depicted in yellow and two ATPase domains, D1 (purple) and D2 (pink), forming two stacked rings. Surrounded by the rings, a central pore forms, which extends from the *cis* side (D1 domain) through the entire protein to the *trans* side (D2 domain). **(C)** Conformational states of the N domains are dependent on the nucleotide bound state of the D1 domains. Left: bound ADP induces down-conformation. Right: bound ATP induces up-conformation.

MATERIALS AND METHODS

Molecular Modeling

A search for *D. discoideum* UBXD9 (Dd-UBXD9) orthologs with known 3D structure using pGenThreader identified human ASPL (alveolar soft part sarcoma locus), also known as TUG (tether containing a UBX domain for GLUT4), UBXD9 and RCC17 (Hs-ASPL; PDB: 5ifs) as the best candidate (score: 86.243; next best score: 54.575). Therefore, a 3D model of Dd-UBXD9 was generated by comparative modeling using the software MODELLER (Sali and Blundell, 1993) and the structure-based amino acid sequence alignment of Dd-UBXD9 and Hs-ASPL (**Supplementary Figure 1**). Twenty different models were computed and the best one selected (lowest value of objective function: 980.54; next lowest value: 1044.5). Next, the modeled structures of *D. discoideum* p97 (VCP) (Rijal et al., 2016) and of *D. discoideum* UBXD9 (residues 320–522, 331–522, and 384–522) were used to generate a complex by aligning the partners to the structure of the human VCP (p97):ASPL complex (PDB: 5ifs) and adding ADP and Mg^{2+}. The helical lariat of Dd-UBXD9 (residues 330–390) was manually adjusted by rigid body movements to remove any clashes with *D. discoideum* p97. The modeled complex was solvated and subjected to a molecular dynamics simulation for ∼5 ns simulation time using Gromacs (Abraham et al., 2015). Analysis of environmental (energy, temperature, pressure) as well as spatial parameters (e.g., distance between centers of gravity) showed that the model was stable throughout the simulation. Structure-based amino acid sequence alignments were generated with SBAL (Wang et al., 2012) based on predictions of secondary structure elements with PSIPRED (Bryson et al., 2005).

Vector Construction

To generate GST-tagged UBXD9 polypeptides, the corresponding UBXD9 sequences were amplified by standard PCR technique from either AX2 cDNA or full-length UBXD9 cloned into the pBsr-C1-GFP vector (Rijal et al., 2016) using UBXD9 specific primers. The PCR products were cloned into the pGEX-6P-1 expression vector (GE Healthcare) and the sequences verified by sequencing. To generate the BirA-UBXD9 expression vector, the full-length UBXD9 coding sequence was amplified from AX2 cDNA and cloned into the previously described *D. discoideum* BirA expression vector (Batsios et al., 2016) via the *Sac*I and *Bam*HI restriction sites. The construct contained a linker encoding YKGGSGGSGGSRLREL between BirA and UBXD9. The insert of the resulting expression plasmid was verified by sequencing.

D. discoideum Culture and Transformation

D. discoideum strains were grown in AX2 medium (for 1 l: 14.3 g bacteriological peptone, 7.15 g yeast extract, 18 g maltose, 0.62 g Na_2HPO_4 $2H_2O$, 0.49 g KH_2PO_4, pH 6.7) at 21°C either on Petri dishes (Ø 100 mm) or in suspension in Erlenmeyer flasks with shaking at 160 rpm (Brink et al., 1990) or on a lawn of *Klebsiella aerogenes* on SM agar plates (Williams and Newell, 1976). Recombinant strains were cultured under selective pressure in the presence of 5 μg/ml blasticidin S. For cell biological and biochemical experiments, log phase cells at 2–4 × 10^6 cells/ml were used. The BirA-UBXD9 expression plasmid was transformed into wild-type AX2 cells by electroporation (Gaudet et al., 2007) and transformants were selected with 5 μg/ml blasticidin S. Stable transformants expressing BirA-UBXD9 were verified by PCR and Western blot analysis. The strains expressing GFP-UBXD9 or UBXD9-GFP have been described previously (Rijal et al., 2016).

Purification of Recombinant Proteins and Immunoblotting

Purification of GST-tagged full-length and truncated UBXD9 proteins and of p97 from either *E. coli* XL1 Blue cells (New England Biolabs) or ArcticExpress cells (Stratagene GmbH)

was performed as described previously (Rijal et al., 2016). For biochemical assays, the purified GST-fusion proteins were either used bound to Glutathione-Agarose 4B beads (MACHEREY-NAGEL GmbH) or the recombinant protein was liberated from the beads by cleavage with 5 U/ml PreScission protease (GE Healthcare GmbH) for 16 h at 4°C on a rotating wheel. Protein concentrations were determined by the Bradford assay (Bradford, 1976). For quality control of purified proteins and GST-fusion protein bound beads, SDS-PAGE (Laemmli, 1970) followed by Coomassie Brilliant Blue staining or Western blotting (Towbin et al., 1979) was performed. Full-length and truncated UBXD9 proteins were detected with rabbit polyclonal UBX23520 antibody at a 1:20,000 dilution (Rijal et al., 2016), p97 was detected with rabbit polyclonal p97_8_6841 antibody at 1:10,000 dilution (Arhzaouy et al., 2012), GFP with mouse monoclonal K3-184-2 antibody at a 1:50 dilution (Noegel et al., 2004), actin with the monoclonal Act1-7 antibody at a 1:40 dilution (Simpson et al., 1984), ubiquitin with mouse monoclonal P4D1 antibody at a 1:1,000 dilution (Cell Signaling Technology), and BirA with a rabbit polyclonal antibody at a 1:5,000 dilution (kindly provided by Dr. Ralph Gräf, University of Potsdam). Secondary antibodies used were anti-rabbit and anti-mouse IgG conjugated with horseradish peroxidase (HRP) at a 1:10,000 dilution (Sigma-Aldrich Corp.). Detection was done by chemiluminescence using the SuperSignal West Pico PLUS chemiluminescent substrate (Thermo Fisher Scientific Inc.) in conjunction with the Intas ECL Chemostar documentation system. The software LabImage 1D L-340 (Intas Science Imaging Instruments GmbH) was used for the determination of molecular masses and the quantification of the detected proteins.

Co-immunoprecipitation

Co-immunoprecipitation experiments for the identification of novel UBXD9 interaction partners were performed with log phase AX2 cells (2–4 $\times$ 10^6 cells/ml) ectopically expressing UBXD9-GFP, GFP-UBXD9, or GFP (negative control). 1 $\times$ 10^8 cells were harvested (500 $\times$ g, 5 min), washed twice with Soerensen phosphate buffer (14.6 mM KH_2PO_4, 2.0 mM KH_2PO_4, pH 6.0) and the cell pellet shock frozen with liquid nitrogen. Pellets were resuspended in 1 ml lysis buffer (20 mM Tris/HCl pH 7.5, 100 mM NaCl, 1 mM DTT, 20 mM $MgCl_2$, 5% glycerol, 1 mM benzamidine, 10 µg/ml aprotinin/leupeptin, 1:50 proteinase inhibitor cocktail (Roche), 1:100 PEFA block) followed by centrifugation at 20,000 $\times$ *g* for 10 min. The supernatant, containing soluble proteins, was incubated with GFP-trap beads (Chromotek) for 2 h at 4°C. Beads were washed four times with wash buffer I (50 mM Tris/HCl pH 7.5, 150 mM NaCl, 1 mM DTT, 0.2% NP-40) and twice with wash buffer II (50 mM Tris/HCl pH 7.5, 150 mM NaCl, 1 mM DTT). Bound proteins were either analyzed by SDS-PAGE and Coomassie Brilliant Blue staining or further processed for mass spectrometry.

Proximity-Dependent Biotin Identification

The BioID method was essentially performed as described (Batsios et al., 2016). Briefly, log phase BirA-UBXD9 expressing AX2 cells were cultured in the presence of 50 µM Biotin for 16 h. 2 $\times$ 10^8 cells were harvested and the cells further processed as for co-immunoprecipitation. Soluble proteins were incubated with streptavidin-coupled sepharose beads (GE Healthcare GmbH) for 2 h at 4°C. After washing of the beads (see procedure for co-immunoprecipitation) bound proteins were either analyzed by Western blot analysis or further processed for mass spectrometry.

Mass Spectrometry

Mass spectrometry was carried out at the CECAD/CMMC Proteomics Facility (University of Cologne). Samples were prepared by the in-solution digestion of proteins and StageTip purification of peptides according to the protocol of the facility[1]. The samples were analyzed using an EASY nLC 1,000 UPLC (Thermo Fisher Scientific) coupled to a Q-Exactive Plus (Thermo Scientific) mass spectrometer. Peptides were loaded with solvent A (0.1% formic acid in water) onto an in-house packed analytical column (50 cm $\times$ 75 µm I.D., packed with 2.7 µm C18 Poroshell beads, Agilent) and were chromatographically separated. The mass spectrometer was operated in data-dependent acquisition mode, where the Orbitrap acquired full MS scans (300–1750 *m/z*) at a resolution of 70,000 with an automated gain control (AGC) target of 3 $\times$ 10^6 ions collected with 20 ms. Precursors were dynamically excluded for 20 s. The ten most intense peaks were subjected to HCD fragmentation. All mass spectrometric raw data were processed with Maxquant (version 1.5.3.8) and its implemented Andromeda search engine (Cox et al., 2011). Two-sample two-tailed Student's *t*-test were performed in Perseus (version 1.6.5) for pairwise comparisons. Proteins with a fold change $>$ 1.4 and a $p < 0.05$ in the experiment versus negative control were considered to represent putative UBXD9 interacting proteins. The mass spectrometry proteomics data have been deposited to the ProteomeXchange Consortium[2] via the PRIDE (Perez-Riverol et al., 2019) partner repository with the dataset identifiers PXD027160 and PXD027162. Four independent biological replicates were performed.

Miscellaneous Methods

Blue Native-PAGE (BN-PAGE) was performed for the analysis of native protein complexes. Purified recombinant proteins in 1 $\times$ PBS, 1 mM DTT, 1 mM ATP were mixed with 4 $\times$ NativePAGE Sample Buffer (Thermo Fisher Scientific Inc.) followed by separation in Invitrogen Novex Native-PAGE 4–16% Bis-Tris Protein-Gels (Thermo Fisher Scientific Inc.). Electrophoresis was performed in the cold-room with pre-chilled buffers (cathode buffer: 50 mM Tricine, 15 mM Bis-Tris pH 7.0, 0.02% Coomassie G-250; anode buffer: 50 mM Bis-Tris pH 7.0) at 150 V for 4 h. Gels were stained with Coomassie Brilliant Blue and protein molecular masses were determined based on the NativeMark protein standard (Invitrogen). The ATPase activity assay for p97 either alone or in the presence of full-length or truncated UBXD9 proteins was carried out in phosphate-free sample buffer (10 mM Tris/HCl pH 7.4, 100 mM NaCl, 1 mM DTT, 1 mM $MgCl_2$) in the presence of 1 mM

[1]http://proteomics.cecad-labs.uni-koeln.de/Protocols.955.0.html

[2]http://www.proteomexchange.org/

ATP according to the instructions of the manufacturer (Enzo Life Sciences, Farmington, NY). The ATPase activity of p97 was calculated based on the amount of the generated free phosphate. Sucrose density gradient sedimentation and pull-down assays were performed as described (Rijal et al., 2016).

RESULTS

Ubiquitin Regulatory X Domain Containing Protein 9 Is Highly Conserved

UBXD9 is a member of the ubiquitin X domain (UBXD) protein family, which makes up the largest subgroup of p97 cofactors. The UBXD9 domain structure is highly conserved across different eukaryotes and is composed of the N-terminal ubiquitin-like (UBL1) and the low homology UBX (LHU) domains followed by a coiled coil domain in the middle part. The C-terminal region harbors the eponymous UBX domain, which is present in and characteristic for all members of the UBXD protein family (**Figure 2**). In addition, we identified in *D. discoideum* UBXD9 a low complexity region (LCR) located between the LHU and coiled coil domains, and a second coiled coil domain in the C-terminal region (**Figure 3A**). The SHP box, a further p97 binding motif, which was identified in human and mouse UBXD9 (Yeung et al., 2008; Orme and Bogan, 2012), is not present in *Drosophila melanogaster*, *Caenorhabditis elegans*, *Saccharomyces cerevisiae,* and *D. discoideum* UBXD9 (not shown). We previously reported the direct interaction of UBXD9 with p97 (Rijal et al., 2016). To analyze the contribution of the different domains of UBXD9 to the interaction with p97 and to narrow down interacting regions, we generated a series of C- and/or N-terminal UBXD9 truncation constructs. The domain structures of full-length *D. discoideum* UBXD9 and of the generated truncation constructs are displayed in **Figure 3A**.

The Ubiquitin Regulatory X Domain Is Necessary and Sufficient for the Interaction With p97

To elucidate the p97 binding region(s) of UBXD9 we performed pull-down experiments with recombinant p97 and full-length UBXD9 and the different UBXD9 truncation constructs tagged with GST (**Figure 3A**). In the presence of full-length UBXD9 most of p97 was found in the pellet fraction of glutathione sepharose beads (**Figure 3B**, left two lanes), while most of p97 remained in the supernatant in the presence of GST (**Figure 3B**, right two lanes). This result confirmed the specific binding of full-length UBXD9 to p97 (Rijal et al., 2016). Deletion of the C-terminal part of UBXD9 in the N-terminal constructs, $UBXD9^{1-336}$ and $UBXD9^{1-164}$, resulted in a loss of p97 binding activity (**Figure 3B**, lanes 3–6 from left). Similarly, the truncation constructs $UBXD9^{467-573}$, $UBXD9^{165-383}$, and $UBXD9^{165-342}$, which all lack the UBX domain, were also not able to bind p97 and almost all p97 remained in the supernatant (**Figure 3B**, lanes 15–16 and 19–22 from left). In contrast, the UBXD9 truncation constructs $UBXD9^{165-573}$, $UBXD9^{261-573}$, $UBXD9^{331-573}$, $UBXD9^{384-573}$, and $UBXD9^{384-466}$, which all

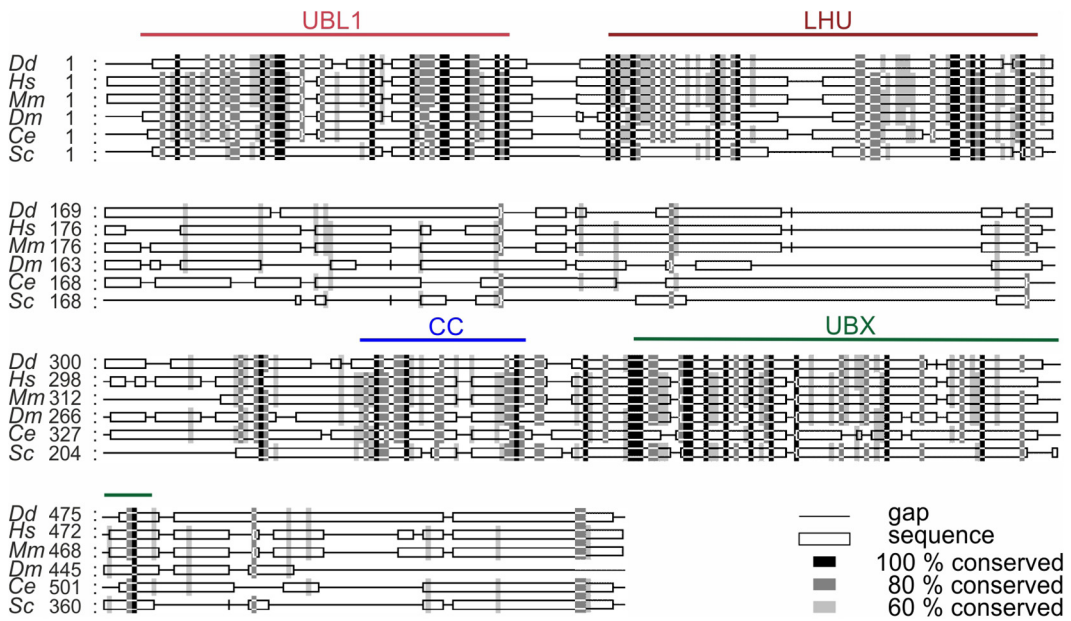

FIGURE 2 | Sequence alignment of UBXD9 proteins from different model organisms. A multiple sequence alignment of UBXD9 protein sequences from *D. discoideum* (*Dd*), *H. sapiens (Hs), Mus musculus (Mm), Drosophila melanogaster (Dm), Caenorhabditis elegans (Ce), and S. cerevisiae (Sc)* was generated with Clustal Omega (Version 1.2.4; Goujon et al., 2010; Sievers et al., 2011) and then edited with Gendoc (v0.7.2). Genbank accession numbers are: (*Dd*) XP_641771, (Hs) NP_076988, (*Mm*) NP_081153, (*Dm*) NP_001027152, (*Ce*) NP_505652, (*Sc*) EWG89362. Shading reflects sequence conservation. The domain organization is homologous in all species and sequence conservation is high in the specified domains. UBL1, Ubiquitin-like domain 1; LHU, Low Homology UBX domain; CC, Coiled coil domain; UBX, Ubiquitin regulatory X domain. Numbers indicate amino acid positions.

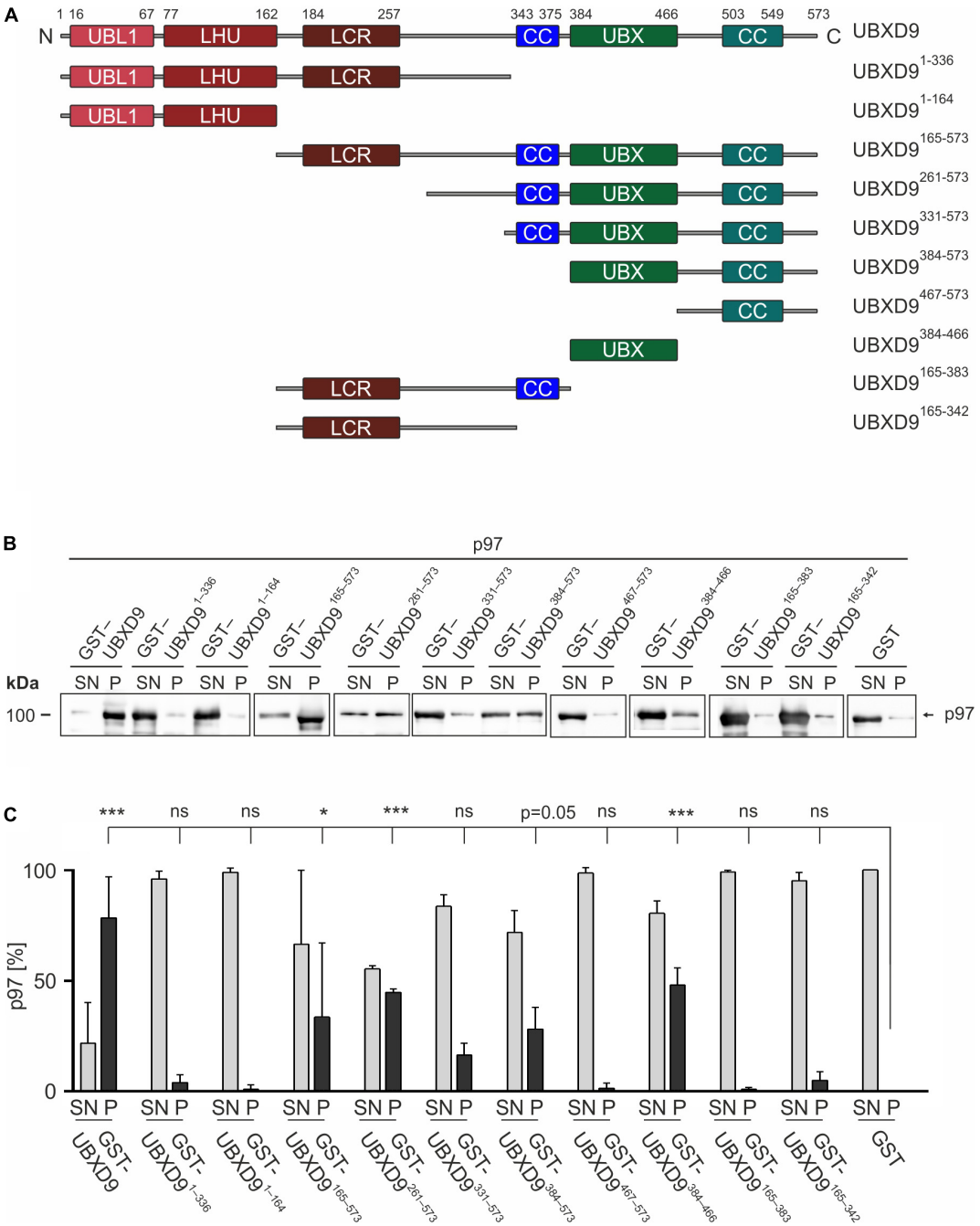

FIGURE 3 | The UBX domain is necessary and sufficient to bind to p97. **(A)** Schematic representation of the *D. discoideum* UBXD9 domain organization and of the analyzed UBXD9 truncation constructs. N, N-terminus; C, C-terminus; LCR, Low complexity region, UBL1, Ubiquitin-like domain 1; LHU, Low Homology UBX domain; CC, Coiled coil domain; UBX, Ubiquitin regulatory X domain. Numbers indicate amino acid positions of UBXD9. **(B)** Pull-down experiments with recombinant p97 and full-length or truncated GST-UBXD9 coupled to glutathione beads. GST coupled to glutathione beads was used as negative control. Representative Western blots with anti p97 antibodies of supernatants (SN) and pellets (P) are shown. The position of p97 is indicated. **(C)** Quantification of p97 in the SN and P fractions. The sum of the values of SN and P for each experiment was taken as 100%. The bar graphs represent mean values and standard deviations (SD) of at least three independent experiments. For statistical analysis, the Dunnett's multiple comparison test, implemented in GraphPad Prism as *post hoc* analysis, was performed. ***$p \leq 0.001$; *$p \leq 0.05$. ns, not significant.

harbor the UBX domain, were all able to bind p97 (**Figure 3B**, lanes 7–14 and 17–18 from left). The shortest construct sufficient to bind p97 was UBXD9$^{384-466}$, which comprises the UBX domain only. SDS-PAGE followed by Coomassie staining showed the presence of GST, GST-tagged full-length UBXD9, and all GST-UBXD9 truncation constructs in the

pellet fraction (**Supplementary Figure 2**). Quantification of p97 in the supernatant and pellet fractions of three independent experiments revealed strongest binding by full length UBXD9, followed by UBXD9$^{261-573}$, UBXD9$^{384-466}$, UBXD9$^{165-573}$, and UBXD9$^{384-573}$ (**Figure 3C**). Quantification also revealed that the interaction of UBXD9$^{331-573}$ with p97 was not significant, although the shorter UBXD9$^{384-573}$ and UBXD9$^{384-466}$ clearly pulled down p97 (**Figure 3C**). We assume that the amino acids 331–383 in this construct somehow interfere with binding of the UBX domain to p97. In summary, these results confirm the interaction of UBXD9 with p97 and show that the UBX domain is necessary and sufficient for binding to p97.

The Presence of a UBX Domain Containing Protein 9 Lariat Structure Is Required for the Disassembly of p97 Hexamers

We used sucrose density gradient centrifugation in combination with SDS-PAGE to monitor the oligomeric status of p97 alone or in the presence of full-length UBXD9 and various UBXD9 truncation constructs. It has previously been shown that full length *D. discoideum* UBXD9, human UBXD9 (also termed TUG, ASPL, RCC17) and *A. thaliana* UBXD9 (termed PUX1, plant UBX domain-containing protein 1) have the ability to disassemble p97 hexamers (Rancour et al., 2004; Orme and Bogan, 2012; Rijal et al., 2016). Analysis of p97 alone showed the presence of most p97 in higher sucrose density fractions, representing p97 hexamers (**Figure 4A** top, fraction 12–14). Only a small amount of p97 was present in lower sucrose density fractions, representing monomers or dimers (**Figure 4A** top, fractions 5–7). A similar result as for p97 alone was obtained when p97 was incubated with either UBXD9$^{1-336}$ (data not shown), UBXD9$^{331-573}$, or UBXD9$^{384-573}$ (**Figure 4A**, four panels from bottom). In contrast, full-length UBXD9 as well as UBXD9$^{261-573}$ were able to disassemble p97 hexamers, as represented by the shift of p97 from high to low molar sucrose fractions (**Figure 4A**, second to fourth panel from top). Quantification of three independent experiments confirmed that the p97 distribution in the presence of UBXD9$^{331-573}$ and UBXD9$^{384-573}$ was comparable to p97 alone and that only full-length UBXD9 and UBXD9$^{261-573}$ were able to disassemble p97 hexamers (**Figure 4B**). Of note, the ATPase activity of p97 is high in the hexameric state and low for p97 monomers (Rijal et al., 2016). In support of the p97 hexamer disassembly activity of UBXD9 and UBXD9$^{261-573}$, we measured in their presence a strong reduction of the p97 ATPase activity (**Supplementary Figure 3**).

As the three UBXD9 truncation constructs UBXD9$^{261-573}$, UBXD9$^{331-573}$, and UBXD9$^{384-573}$ had the ability to bind p97 (**Figures 3B,C**), we next were interested in their structural differences. Recently, the crystal structure of a *H. sapiens* UBXD9 truncation construct encompassing amino acids 317–497 in complex with the N and D1 domains of p97 was solved (Arumughan et al., 2016). The 3D structure of the UBXD9 truncation construct revealed a helical lariat, comprising the α-helices α_{-1}, and α_0 and an unordered region, which embraces the N domain of p97. Upstream of the unordered region a short beta strand (β_0) closes the helical lariat (**Figure 4C**). Only a construct with the extended UBX domain harboring the complete β_0-α_{-1}-α_0 lariat, as present in *H. sapiens* UBXD9$^{317-497}$, had the ability to disassemble p97 hexamers (Arumughan et al., 2016). A structure-based amino acid sequence alignment of *D. discoideum* UBXD9 and *H. sapiens* UBXD9 revealed that the secondary structure elements of the helical lariat are conserved in *D. discoideum* UBXD9 (**Supplementary Figure 1**). We next performed comparative modeling with the *D. discoideum* N and D1 domains of p97 and the UBXD9 truncation constructs UBXD9$^{320-522}$, UBXD9$^{331-522}$, and UBXD9$^{384-522}$, respectively (**Figures 4D–F**). Since our modeling was based on the published *H. sapiens* UBXD9$^{317-497}$ structure, we could not model the regions encompassing amino acids 261–319 and 523–573 of the constructs UBXD9$^{261-573}$, UBXD9$^{331-573}$, and UBXD9$^{384-573}$, which we had analyzed for p97 hexamer disassembling activity. The results showed that only UBXD9$^{261-573}$ carries the complete lariat (**Figure 4D**), whereas UBXD9$^{331-573}$ lacks the closing beta-strand β_0 (**Figure 4E**) and UBXD9$^{384-573}$ the complete lariat (**Figure 4F**). Thus, we conclude that the complete lariat is required for the dissociation of p97 hexamers. The N-terminal β_0 strand appears to be crucial as it mediates the closure of the helical lariat. Its absence likely weakens the lariat structure and results in an inability to disassemble the p97 hexamer.

UBX Domain Containing Protein 9 Forms Oligomers

Since *D. discoideum* UBXD9 contains two coiled coil regions (aa 343–375 and 503–549) and interacts with the hexameric p97, we analyzed by Blue Native PAGE whether UBXD9 forms multimers. We used p97 as positive control and, as expected, we observed a band of about 600 kDa, representing the p97 hexamer. In addition, a band of about 200 kDa was visible, corresponding in size to a p97 dimer (**Figure 5A**, lane 1). Analysis of UBXD9, UBXD9$^{261-573}$, UBXD9$^{331-573}$, and UBXD9$^{384-573}$ (GST-tag cleaved for all) revealed for each protein two major bands. Based on the calculated molecular masses of approximately 65 kDa for UBXD9, 37 kDa for UBXD9$^{261-573}$, 29 kDa for UBXD9$^{331-573}$, and 23 kDa for UBXD9$^{384-573}$, the upper band of each protein corresponds in size to a hexamer and the lower band to either a dimer or trimer (**Figure 5A**, lanes 2 and 4, **Figure 5B**). For UBXD9$^{331-573}$ we detected a third band of approximately 30 kDa, which corresponds in size to a monomer (**Figure 5B**, lane 1). We also analyzed the N-terminal construct UBXD9$^{1-336}$ and detected only a single band of around 120 kDa, corresponding in size to a trimer (**Figure 5A**, lane 3). We do not have an explanation for the possible trimer formation of this construct, as it does not contain the N-terminal coiled coil moiety (aa 343–375) and as the complete N-terminal region of UBXD9 was dispensable for hexamer formation of the other constructs. In summary, our results show, that full-length UBXD9 and the analyzed truncation constructs form dimers or trimers and hexamers. Since all constructs for which multimer formation was observed contained the C-terminal coiled coil domain (aa

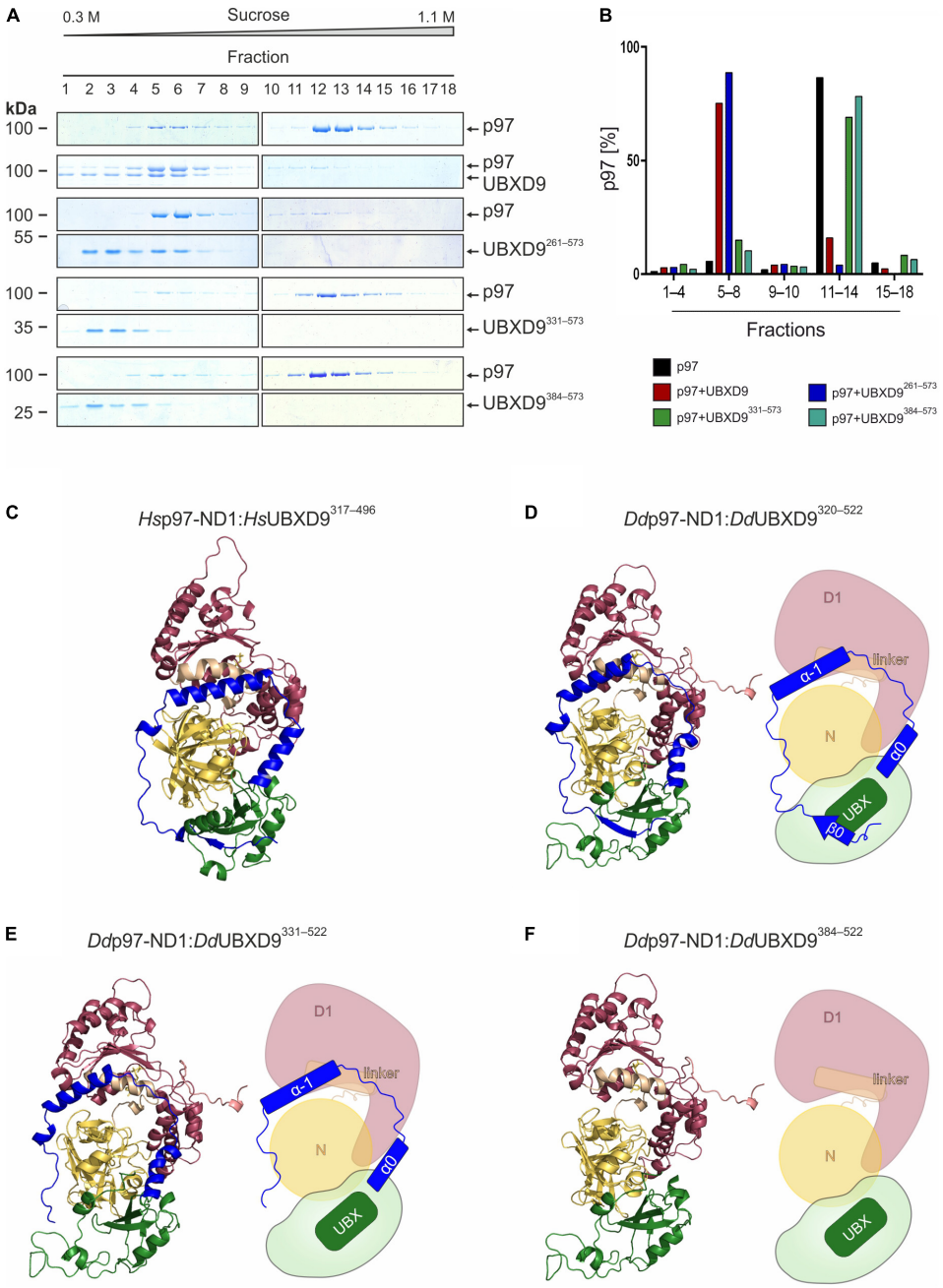

FIGURE 4 | The helical lariat structure of UBXD9 is pivotal for its disassembly activity. **(A)** Sucrose density gradient sedimentation with p97 alone (top panel) or with equimolar amounts of p97 and full-length UBXD9 (2nd panel from top) or p97 and UBXD9$^{261-573}$ (3rd and 4th panels from top), or p97 and UBXD9$^{331-573}$ (5th and 6th panels from top), or p97 and UBXD9$^{384-573}$ (lower two panels). Before loading the samples on the sucrose density gradient (0.3–1.1 M sucrose), they were incubated with 1 mM ATP for 30 min. Fractions were removed consecutively after centrifugation and analyzed by SDS-PAGE and Coomassie Brilliant Blue staining. p97 monomers or dimers are present in fractions 5–8 and p97 hexamers in fractions 11–14. Fractions are numbered, starting with #1 at 0.3 M sucrose. The positions of p97, full-length UBXD9 and UBXD9 truncation constructs are indicated. **(B)** Bar graphs depicting the quantification of p97 in fractions 1–4, 5–8, 9–10, 11–14, and 15–18 of the different experiments. The bar graphs represent mean values of at least three independent experiments. The determined total amount of p97 in all 18 fractions was set to 100%. **(C)** Structural model of the *Hs* p97-ND1:Hs UBXD9$^{317-496}$ (VCP:ASPL; PDB: 5ifs) complex. UBXD9$^{317-496}$ is shown in green and ochre and the ND1 domains of p97 (VCP) are colored yellow and dark pink, respectively. The region N-terminal of the UBX domain forms a loop, which encompasses two α-helices (α_{-1} and α_0; blue), an extended linker (blue) and a β-strand (β_0, blue). The α-helices and the linker embrace the N domain of p97 and the β_0-strand appears to be crucial for the closure of the lariat structure. The helical lariat probably interferes with the D1:D1' inter-monomeric interaction of the p97 hexamer, causing its disassembly (Arumughan et al., 2016; Banchenko et al., 2019). **(D–F)** Homology models and schematic representation of the *D. discoideum* p97-ND1:UBXD9$^{320-522}$ **(D)**, p97-ND1:UBXD9$^{331-522}$ **(E)**, and p97-ND1:UBXD9$^{384-522}$ **(F)** complexes representing our truncation constructs UBXD9$^{261-573}$, UBXD9$^{331-573}$, and UBXD9$^{384-573}$, respectively. Since our modeling was based on the *Hs*-p97-ND1:*Hs*-UBXD9$^{317-496}$ (VCP:ASPL; PDB: 5ifs) complex, the structural models could only be generated from amino acids 320–522 of *D. discoideum* UBXD9.

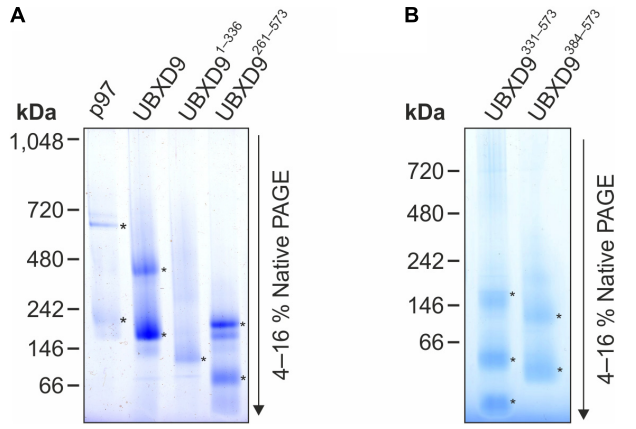

FIGURE 5 | Blue Native PAGE analysis of p97, full-length UBXD9 as well as UBXD9 truncation constructs. Representative Blue Native PAGE gels of purified recombinant non-tagged *D. discoideum* proteins. Specific bands are marked by asterisks. **(A)** p97, UBXD9, UBXD9$^{1-336}$ and UBXD9$^{261-573}$. **(B)** UBXD9$^{331-573}$ and UBXD9$^{384-573}$.

TABLE 1 | Summary of biochemical properties of full length UBXD9 and UBXD9 truncation constructs.

Construct	MM (kDa)	Hexamer formation	p97 binding	p97 Hexamer disassembly
UBXD9	65	Yes	Yes	Yes
UBXD9$^{1-336}$	37	No	No	No*
UBXD9$^{1-164}$	19	nd	No	nd
UBXD9$^{165-573}$	47	nd	Yes	nd
UBXD9$^{261-573}$	37	Yes	Yes	Yes
UBXD9$^{331-573}$	29	Yes	Yes	No
UBXD9$^{384-573}$	23	Yes	Yes	No
UBXD9$^{467-573}$	13	nd	No	nd
UBXD9$^{384-466}$	10	nd	Yes	nd
UBXD9$^{165-383}$	25	nd	No	nd
UBXD9$^{165-342}$	20	nd	No	nd

*MM, molecular mass (rounded); nd, not determined; *, not shown.*

503–549), we conclude that this domain is responsible for the formation of UBXD9 hexamers. The results of our biochemical analyses of full-length UBXD9 and UBXD9 truncation constructs are summarized in **Table 1**.

UBX Domain Containing Protein 9 Interactome Mapping Confirms Interaction With p97 and Identifies Novel Interaction Partners

In order to map the UBXD9 interactome, we employed two experimental approaches. We used AX2 strains that express GFP-UBXD9 or UBXD9-GFP (Rijal et al., 2016) and generated a new BirA-UBXD9 expressing strain for the identification of UBXD9 interacting proteins. The latter strain was used for proximity-dependent biotin identification (BioID), which has become a powerful tool to identify protein-protein interactions (Roux et al., 2012; Batsios et al., 2016). In this assay, the bait protein is fused to the R118G-mutated BirA biotinylase from *E. coli*. Interacting proteins will get biotinylated and can then be isolated through binding to streptavidin-coupled sepharose beads. We first confirmed expression of UBXD9 and the respective fusion proteins in our strains by Western blot analysis of total cell lysates with antibodies against UBXD9, BirA, and GFP. Equal loading was verified by staining with an actin antibody (**Figure 6A**). Next, we performed immune-precipitation (IP) experiments and analyzed the proteins bound to the GFP-trap or streptavidin-sepharose beads by silver staining and Western blotting (**Supplementary Figure 4**). Silver staining revealed weak bands corresponding in size to GFP-UBXD9 and BirA-UBXD9. The identity of these bands was confirmed by immunodetection with the UBXD9 antibody. It also revealed the presence of endogenous UBXD9 in the precipitates via binding to the fusion proteins, supporting the conclusion from Blue Native PAGE that UBXD9 can undergo homo-oligomerization (**Figure 5** and **Supplementary Figure 4**). For mass-spectrometric identification of bound proteins we performed for each approach four independent experiments. To visualize differentially expressed proteins we generated volcano plots of the identified proteins in AX2 versus AX2/BirA-UBXD9, and AX2/GFP versus AX2/UBXD9-GFP and AX2/GFP-UBXD9 (**Figures 6B–D**). Proteins with a fold change $\geq$ 1.4 and a $p \leq 0.05$ were defined as significantly enriched in the BirA-UBXD9, GFP-UBXD9, or UBXD9-GFP expressing strains and are depicted as red, blue or green dots, respectively. Using these criteria we identified 35 putative UBXD9 interacting proteins in the BioID approach, 69 with N-terminally tagged UBXD9 and 120 with C-terminally tagged UBXD9 (**Supplementary Tables 1–3**). We applied Venny to identify common enriched proteins in our three approaches and found 32 common proteins between GFP-UBXD9 and UBXD9-GFP, five between GFP-UBXD9 and BirA-UBXD9, and five between UBXD9-GFP and BirA-UBXD9 expressing strains. Only three proteins, namely p97, UBXD9 and the putative glutamine synthetase type III (GSIII) were found in all three approaches (**Figure 6E** and **Table 2**). The mode of interaction between UBXD9 and GSIII and its cellular function is currently unknown. Those proteins which were identified in at least two of the three approaches are of particular interest as they are strong candidates for further novel UBXD9 interacting proteins (**Figure 6E** and **Table 2**). Among these proteins, we found the ER resident Grp78 (luminal-binding protein 2, Bip), which could link UBXD9 to the ER stress response. To elucidate possible enrichments of biological processes, molecular functions, and cellular components among these proteins, we performed a gene ontology (GO) analysis with PANTHER (Mi et al., 2021). In the biological process category, we found "cytoskeleton" and "actin filament-based organization" significantly enriched (**Figure 7**). This was reflected in the molecular function and cellular component categories by an enrichment of "actin filament binding" and "actin cytoskeleton" as well as "phagocytic vesicle" (**Figure 7**). Thus, GO analysis points to a connection of UBXD9 with the actin cytoskeleton. Indeed, of the 36 proteins that were found enriched in at least two of our approaches seven are classified as cytoskeletal proteins (**Table 2**, bold entries).

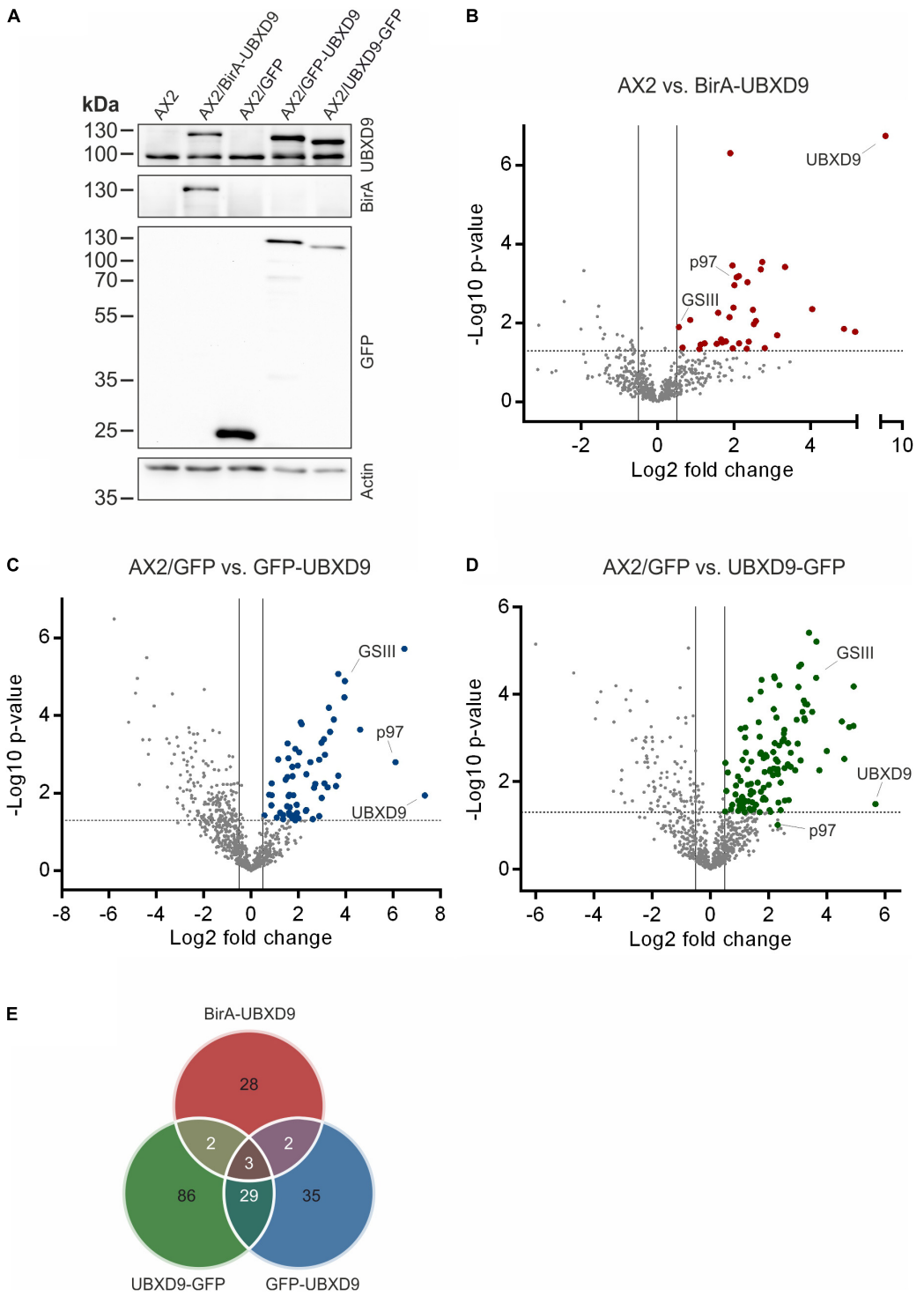

FIGURE 6 | Interaction proteomics. **(A)** Verification of the BirA-UBXD9, GFP, GFP-UBXD9, and UBXD9-GFP expressing strains by western blotting using the polyclonal UBXD9 (top panel), the polyclonal BirA (2nd panel from top), and the monoclonal GFP (3rd panel from top) antibodies. Detection of actin (bottom panel) with the monoclonal actin antibody was used as loading control. **(B–D)** Volcano plots depicting *p*-value versus fold change (FC) for all proteins identified by mass spectrometry in AX2 versus AX2/BirA-UBXD9 expressing cells **(B)**, AX2/GFP versus AX2/GFP-UBXD9 expressing cells **(C)** and AX2/GFP versus AX2/UBXD9-GFP expressing cells **(D)**. Putative UBXD9 interacting proteins with a fold change $\geq$ 1.4 and a $p \leq 0.05$ are depicted as red, blue or green dots, respectively. Dots representing UBXD9, p97, and glutamine synthetase type III (GSIII) are indicated. The plots were done using GraphPad prism. **(E)** Venn diagram of significantly enriched proteins in the pull-down experiments of AX2/BirA-UBXD9 (red), AX2/GFP-UBXD9 (blue), and AX2/UBXD9-GFP (green) cells. The intersections of the circles provide the number of proteins that were identified in two or all three approaches. Only those proteins with a fold change $\geq$ 1.4 and a $p \leq 0.05$ were used as input.

TABLE 2 | List of putative interacting proteins, which were identified in at least two different approaches.

Protein name	DDB_G ID	BirA-UBXD9		UBXD9-GFP		GFP-UBXD9	
		FC	P	FC	P	FC	P
UBXD9	DDB_G0279285	9.23	6.75	5.67	1.49	7.34	1.94
Luminal-binding protein 2	DDB_G0276445	3.12	1.69			3.08	3.39
Uncharacterized protein	DDB_G0272200	2.35	3.04	3.64	5.21		
p97	DDB_G0288065	2.07	3.16	2.31	1.01	6.10	2.80
Hisactophilin-2	**DDB_G0282143**	**1.23**	**1.48**			**2.00**	**1.35**
Eukaryotic peptide chain release factor	DDB_G0288613	1.13	1.45	2.36	2.83		
Putative glutamine synthetase type III	DDB_G0279591	0.56	1.90	3.63	4.38	3.96	4.89
Putative bifunctional amine oxidase	DDB_G0291301			4.91	3.28	2.88	1.41
cAMP-binding protein 1	DDB_G0272560			4.77	3.25	2.98	1.88
Hisactophilin-1	**DDB_G0282141**			**4.00**	**2.70**	**4.61**	**3.64**
Phosphoenolpyruvate carboxykinase	DDB_G0271678			3.23	3.45	3.68	5.07
V-type proton ATPase subunit G	DDB_G0277971			3.17	3.60	3.94	4.47
Myosin-J heavy chain	**DDB_G0272112**			**3.12**	**4.68**	**3.34**	**3.58**
ADP-ribosylation factor 1	DDB_G0289173			3.10	2.49	2.66	2.14
60S ribosomal protein L36	DDB_G0270984			3.05	4.64	2.97	3.30
Probable arginine–tRNA ligase	DDB_G0272867			3.02	4.17	1.33	1.46
Probable replication factor C subunit 3	DDB_G0293702			2.67	2.88	1.87	1.72
Ran binding protein 1 domain-containing protein	DDB_G0287391			2.52	2.98	2.88	2.86
Lysine–tRNA ligase	DDB_G0281437			2.47	2.93	1.86	1.36
Putative rho GDI 1	DDB_G0291077			2.30	2.23	1.74	1.35
Probable aconitate hydratase	DDB_G0278779			2.21	2.88	1.80	1.43
Probable pyridoxal 5-phosphate synthase subunit pdx1	DDB_G0288299			2.07	1.31	3.23	2.15
Vacuolar protein sorting-associated protein 29	DDB_G0288787			2.03	1.35	1.87	1.30
Probable serine/threonine-protein kinase	DDB_G0277449			2.01	1.93	1.61	1.50
Actin-binding protein F	**DDB_G0291229**			**1.90**	**2.61**	**1.64**	**1.64**
Small aggregate formation protein	DDB_G0287587			1.89	2.56	2.50	2.80
Vacuolin-A	DDB_G0289485			1.76	4.33	1.75	2.44
Cysteine proteinase 5	DDB_G0272815			1.74	1.77	2.34	2.49
3-oxoacid CoA-transferase	DDB_G0288105			1.73	4.06	1.54	3.28
Dynamin-A	**DDB_G0277849**			**1.69**	**3.03**	**1.87**	**3.14**
LIM domain-containing protein E	**DDB_G0279415**			**1.63**	**1.98**	**1.23**	**1.50**
Uncharacterized protein	DDB_G0276473			1.44	1.53	1.36	1.44
Uncharacterized protein	DDB_G0288133			1.38	3.88	0.76	1.96
Vacuolar proton translocating ATPase 100 kDa subunit	DDB_G0291858			1.30	1.55	1.58	1.93
Drebrin-like protein	**DDB_G0273447**			**1.20**	**3.24**	**1.15**	**2.87**
Bifunctional purine biosynthesis protein	DDB_G0277087			1.16	1.53	1.78	1.95

Proteins are ordered based on detection in the different experiments and fold change (FC), from largest to smallest. Proteins associated with the cytoskeleton are in bold. DDB_G ID, gene ID (http://dictybase.org). FC, log2 fold change; P, −log10 p-value.

The nature of this observation will have to be investigated in future studies.

DISCUSSION

The ubiquitin X regulatory domain (UBXD) containing protein family is present in all eukaryotes and is the largest subgroup of p97 cofactors (Rijal et al., 2016). In *A. thaliana* fifteen, in human thirteen and in *D. discoideum* eleven largely undescribed UBXD proteins have been identified (Buchberger et al., 2001; Rijal et al., 2016). The UBXD9 subfamily is particularly interesting as its members are so far the only identified p97 interacting proteins, which are able to regulate the oligomeric status of p97. Prominent members are ASPL (TUG) in *H. sapiens*, PUX1 in *A. thaliana*, and UBXD9 in *D. discoideum* (Rancour et al., 2004; Orme and Bogan, 2012; Rijal et al., 2016). UBXD9 orthologs are also present in flies, worms, fungi and other eukaryotes (**Figure 2**). The goal

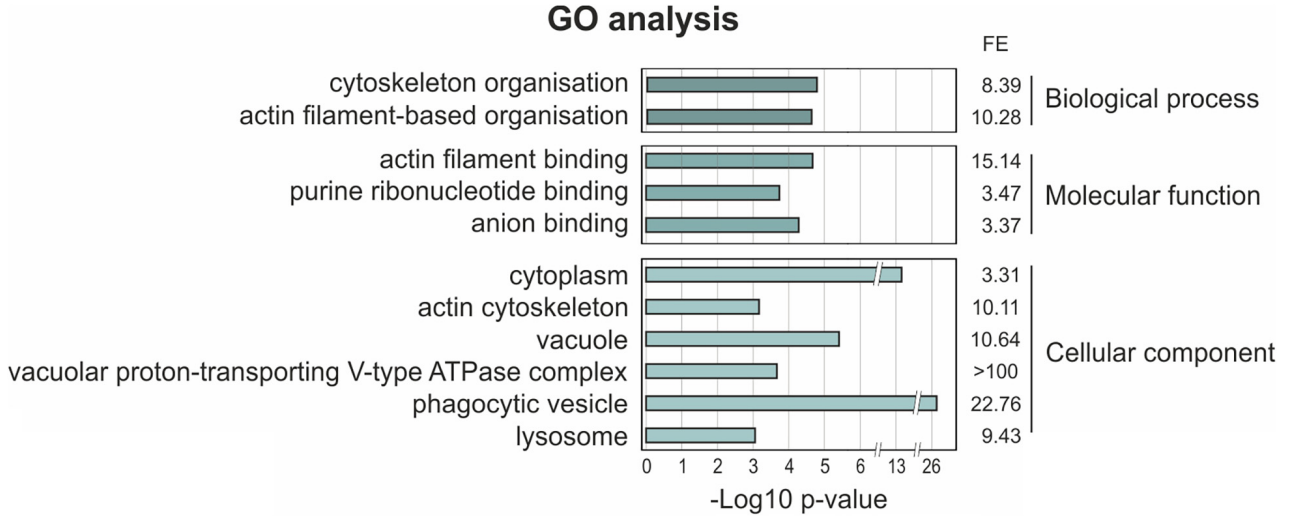

FIGURE 7 | Gene ontology (GO) term enrichment analysis of proteins identified as putative interaction partners of UBXD9 in at least two experimental setups. The proteins, which were identified in at least two experimental approaches (listed in **Table 2**), were used as input for GO analysis. The analysis was performed with PANTHER version 15.0. For the enriched categories –Log10 *p*-value and fold enrichment (FE) are given.

of the present study was the characterization of the functional regions in *D. discoideum* UBXD9 through analysis of full-length and truncated UBXD9 (**Figure 3A**) and the identification of novel UBXD9 interaction partners through IP experiments and proximity labeling proteomics.

The multiple sequence alignment showed significant homology between all UBXD9 members in the N-terminal UBL1 and LHU domains, in the middle coiled coil region and in the C-terminal UBX domain. All regions in between are not well conserved (**Figure 2**). *A. thaliana* UBXD9 was omitted from the alignment, because this protein has only about half the size of the other UBXD9 orthologs and lacks the UBL1 and LHU domains (Rancour et al., 2004). The UBL domain is commonly found in proteins that can interact with the proteasome (Hartmann-Petersen and Gordon, 2004). All UBXD9 proteins harbor the eponymous UBX domain in the C-terminal part, which comprises about 80 amino acids. For *A. thaliana* UBXD9 it was shown that a C-terminal construct harboring the UBX domain and the complete C-terminus (named UBX-C) was able to interact with p97, while the UBX domain alone was not (Rancour et al., 2004). For human UBXD9 two p97 binding regions have been proposed: a region which contains a central SHP box and another region which harbors the conserved central coiled coil domain, the UBX domain and the C-terminal region (Orme and Bogan, 2012). The SHP box is composed of eight amino acid with the sequence (FXGXGQRU, where X is any amino acid and U is a non-polar residue) and was originally identified in the yeast Derlin-1 homolog as p97 binding motif (Yeung et al., 2008). The SHP box was identified in human and mouse UBXD9 but is not detectable in *D. melanogaster*, *C. elegans*, *S. cerevisiae,* and *D. discoideum* UBXD9. The interpretation of the published interactions of human UBXD9 truncation constructs with p97 is complicated, as also an N-terminal construct harboring amino acids 1–237, which neither contained the SHP box nor the UBX domain, was found to bind to p97. On the other hand, a construct equivalent to *A. thaliana* UBX-C (see above) did not interact with p97 (Orme and Bogan, 2012). Recent structural studies suggest that the SHP box is dispensable for binding of human UBXD9 to p97 and confirm the importance of the UBX domain for the interaction of *H. sapiens* and *A. thaliana* UBXD9 with p97 (Arumughan et al., 2016; Banchenko et al., 2019). The UBX domain adopts the common β_1-β_2-α_1-β_3-β_4-α_2-β_5 secondary structure, as originally described for ubiquitin (Buchberger et al., 2001). The structures of the ND1 domains of p97 in complex with truncated human and *A. thaliana* UBXD9 revealed, that the highly conserved β_3/β_4 loop of the UBX domain inserts into a gap between the p97 N_a and N_b subdomains. The loop forms a β-turn containing four residues with two proline residues in position two and three, which are also conserved in *D. discoideum* UBXD9 (**Supplementary Figure 1**). The loop adopts a rare *cis*-Pro touch-turn motif in human and *A. thaliana* UBXD9 which is critical for the interaction with the p97 N domain (Arumughan et al., 2016; Banchenko et al., 2019). We found, that all *D. discoideum* UBXD9 truncation constructs, that contained the UBX domain were able to bind to p97 and that, in contrast to results obtained with human and *A. thaliana* UBXD9, the UBX domain is necessary and sufficient for the interaction of *D. discoideum* UBXD9 with p97 (**Figure 3B** and **Table 1**; Rancour et al., 2004; Orme and Bogan, 2012). Site directed mutagenesis followed by interaction studies will show whether the two proline residues in the β_3/β_4 loop of *D. discoideum* UBXD9 are pivotal for the interaction of this protein with p97.

The 3D structures of human $p97^{ND1}$ with human $UBXD9^{313-500}$ and *A. thaliana* $UBXD9^{39-212}$ were also very informative with respect to the hexamer disassembling activity of these proteins (Arumughan et al., 2016; Banchenko et al., 2019). The structures revealed a helical lariat N-terminal

of the UBX domain, which embraces the N domain and consists of the α-helices α_{-1} and α_0, an unordered region, and the closing beta strand β_0 (**Figure 4C**). It was found, that the extended *H. sapiens* UBX domain with the complete β_0-α_{-1}-α_0 lariat encompassing amino acids 313–500 was sufficient to trigger the disassembly of p97 hexamers (Arumughan et al., 2016). Notably, this construct did not contain the SHP box which was previously suggested to be important for interaction with p97

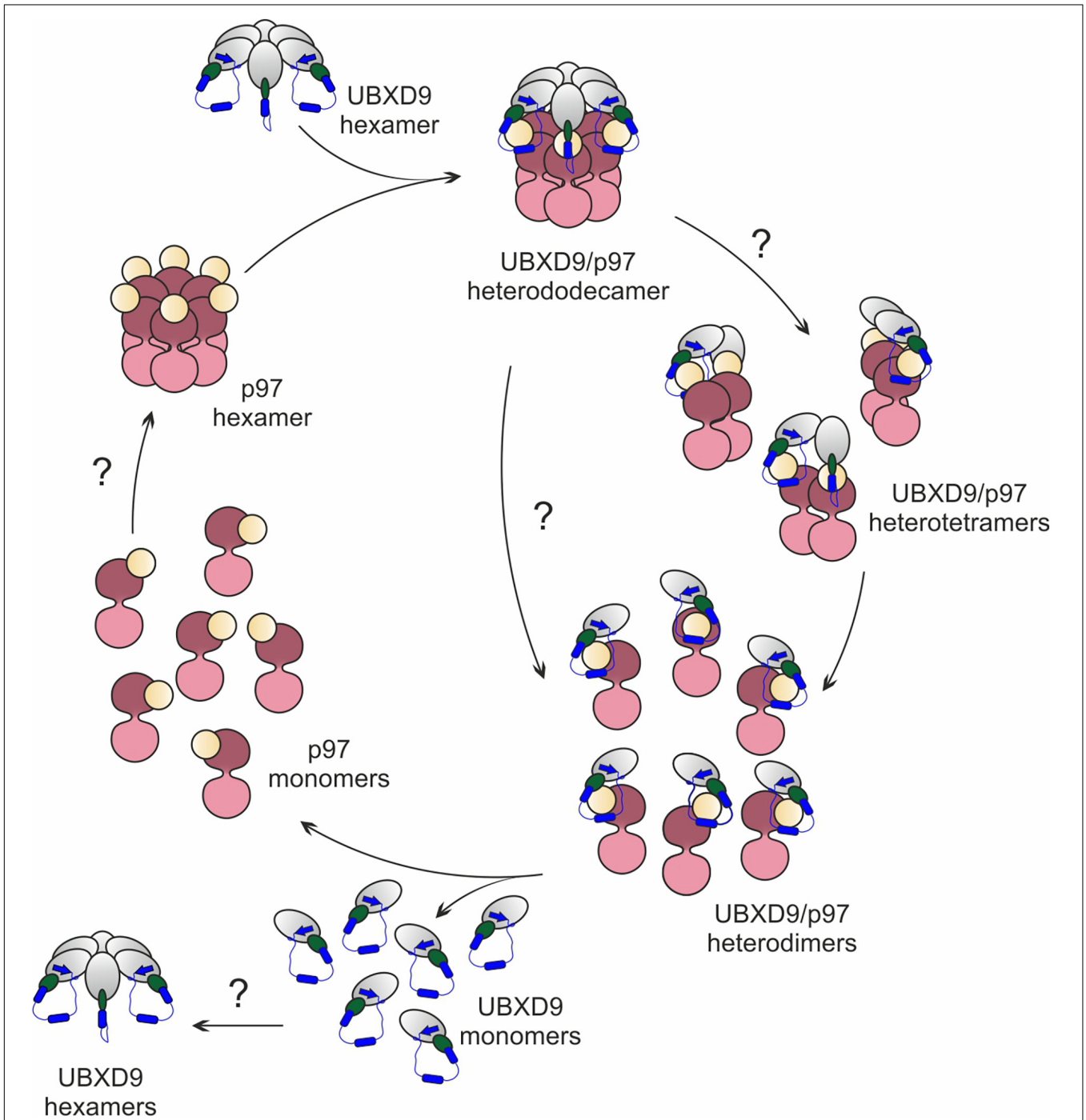

FIGURE 8 | Structure-based model for the disassembly of the p97 hexamer by UBXD9. We propose, that a *D. discoideum* UBXD9 hexamer binds to a p97 hexamer and forms in the first step a hetero-dodecamer. The course of the dissociation of this complex is still unclear and possibly proceeds via intermediate steps. This could result in hetero-tetramers, which then dissociate to heterodimers and finally UBXD9 and p97 monomers are released. These are then free for another round of oligomerization. The p97 D1 and D2 domains are depicted in dark and light pink, respectively, and the N domain in yellow. UBXD9 is shown schematically with the UBX domain in green. The blue cylinders represent the α_0 and α_{-1} helices and the blue arrow the β_0 strand.

(Orme and Bogan, 2012). Our analyses showed that only full-length UBXD9 and UBXD9$^{261-573}$ had p97 hexamer disassembly activity, while UBXD9$^{331-573}$ and UBXD9$^{384-573}$ could bind to but failed to disassemble p97 hexamers (**Figures 3B,C**, **4A,B**). Structure based modeling of *D. discoideum* p97^{ND1} in complex with these three truncation constructs revealed that only UBXD9$^{261-573}$ contains the complete helical lariat, while UBXD9$^{331-573}$ lacks the closing β_0 strand and UBXD9$^{384-573}$ misses the complete β_0-α_{-1}-α_0 lariat (**Figures 4D–F**).

Since UBXD9 family proteins regulate the oligomeric status of p97, it is feasible that they interact with p97 as oligomers. This possibility is still largely unexplored. Based on velocity sedimentation centrifugation *A. thaliana* UBXD9 was reported to be likely monomeric (Rancour et al., 2004). This protein is a short version of UBXD9 family members, it lacks the complete N-terminal half and does not contain the conserved coiled coil domain of other UBXD9 family members (**Figure 2**; Rancour et al., 2004). We found, that full-length *D. discoideum* UBXD9 as well as UBXD9$^{261-573}$, UBXD9$^{331-573}$, and UBXD9$^{384-573}$, the latter harboring only the second, C-terminal coiled coil domain, oligomerize into dimers or trimers and hexamers (**Figure 5**). Oligomerization is often mediated by coiled coil domains (Lupas and Bassler, 2017) and these proteins contain with exception of UBXD9$^{384-573}$ the conserved coiled coil domain in the central part (aa 343–375) and a second coiled coil domain in the C-terminal region (aa 503–549) downstream of the UBX domain (**Figure 3A**). Since the conserved coiled coil domain in the central part is absent in UBXD9$^{384-573}$, we propose that the C-terminal coiled coil domain is responsible for the oligomerization of *D. discoideum* UBXD9. Notably, this domain appears to be absent from the other UBXD9 family members and it is at present not clear whether these other members interact with p97 as monomers, whether they oligomerize via a different region or whether the C-terminal region mediates oligomerization despite the lack of a coiled coil element.

Based on published structures of truncated human and *A. thaliana* UBXD9 in complex with p97^{ND1} (Arumughan et al., 2016; Banchenko et al., 2019), our structural modeling, and biochemical results, we propose a model for the interaction with and the disassembly of p97 by *D. discoideum* UBXD9 (**Figure 8**). The protein has the capacity to oligomerize (**Figure 5**) and likely interacts as a hexamer with the p97 hexamer, leading to the formation of a hetero-dodecamer. Binding is mediated by the UBX domain and the N-terminal extension of the UBX domain, a β_0-α_{-1}-α_0 lariat structure, embraces the N-domain of p97 and presumably destabilizes the D1:D1' intermonomeric interface (**Figures 4C–F**; Arumughan et al., 2016). The course of the dissociation of this complex is still unclear; however, one can speculate that dissociation proceeds via intermediate steps, as it is apparently the case in *H. sapiens* and *A. thaliana*, where hetero-tetramers and hetero-dimers have been observed (Arumughan et al., 2016; Banchenko et al., 2019). Thus, dissociation could result in hetero-hexamers or hetero-tetramers, then hetero-dimers and finally UBXD9 and p97 monomers will be released. These are then free for another round of oligomerization (**Figure 8**). To date, nothing is known about the regulation of UBXD9 in these complex interactions with p97.

Little is also known so far about UBXD9 interacting proteins other than p97. For *A. thaliana* UBXD9 it was even speculated that p97 might be the only interaction partner (Rancour et al., 2004). We applied three different experimental approaches to identify UBXD9 interacting proteins, immune-precipitations with i) UBXD9-GFP and ii) GFP-UBXD9 expressing cells followed by mass spectrometry and iii) proximity labeling proteomics. Our results confirmed the self-association of UBXD9 and its interaction with p97, supporting the functionality, specificity, and efficacy of our approach. In total, we identified 185 potential UBXD9 binding proteins (**Figure 6E** and **Supplementary Tables 1–3**). We detected only three proteins, namely p97, UBXD9 and the putative glutamine synthetase type III (GSIII), in each of the three approaches (**Table 2**). In this context, it has recently been reported that p97 promotes the degradation of glutamine synthetase (GS), a homodecamer, in human cells (Nguyen et al., 2017). We currently do not know which functional consequence direct or indirect binding of *D. discoideum* UBXD9 to GSIII, a homododecamer, may have. An attractive possibility is that it may be involved in its turnover together with p97.

Of particular interest are also the 33 proteins, which we identified in two of our three experimental approaches (**Figure 6E** and **Table 2**). GO analysis revealed a strong enrichment of the actin cytoskeleton, the phagosome and the lysosome (**Figure 7** and **Table 2**). Among these 33 proteins are myosin J heavy chain, a processive F-actin motor protein (Jung et al., 2009), dynamin A, involved in phagosome maturation (Gopaldass et al., 2012), and five additional actin cytoskeletal proteins; thus, UBXD9 appears to be involved in dynamic actin cytoskeletal processes—a notion that is further supported by the involvement of human UBXD9 in dynamic cellular processes, in Golgi reassembly and the redistribution of GLUT4 storage vesicles (Orme and Bogan, 2012; Habtemichael et al., 2018). A further UBXD9 interacting protein of interest was the ER chaperone Grp78 (luminal binding protein 2, BiP) (**Table 2**). Their interaction may be doubtful, as Grp78 localizes to the ER lumen and UBXD9 to the nucleus and cytoplasm (Rijal et al., 2016; Elfiky et al., 2020). However, in response to ER stress a fraction of Grp78 escapes the ER and translocates to the cytoplasm and the plasma membrane, providing an opportunity for the interaction with UBXD9 (Elfiky et al., 2020). Recently, it was shown that *D. discoideum* Grp78 and p97 were up-regulated in response to ER stress (Dominguez-Martin et al., 2018). Thus, it is conceivable that UBXD9 plays a role in the ER stress response together with p97, Grp78 and possible additional factors.

CONCLUSION

p97, an abundant homohexameric AAA + ATPase, is highly conserved from *D. discoideum* to man and plays a central role in cellular protein homeostasis. Its regulation is subject to more than 30 cofactors. The largest family of cofactors is the Ubiquitin Regulatory X (UBX) domain protein family. Members of the

UBXD9 subfamily are so far the only identified p97 interacting proteins, which are able to regulate the oligomeric status of p97. We could show that the UBX domain of *D. discoideum* UBXD9 is necessary and sufficient for the interaction with p97. An N-terminal extension of the UBX domain, which folds into a β_0-α_{-1}-α_0 lariat structure, is required for the dissociation of p97 hexamers. We propose that hexamers of UBXD9 interact with p97 hexamers and disrupt the p97 subunit interactions via destabilization of the p97 D1:D1' intermolecular interface. Immune-precipitations with UBXD9-GFP and GFP-UBXD9 expressing cells as well as proximity labeling proteomics confirmed the self-association of UBXD9 and its interaction with p97. In addition, we identified through this approach 183 novel putative UBXD9 interacting proteins, among them are several cytoskeletal proteins, the glutamine synthetase type III (GSIII) and the ER luminal binding protein 2 (also known as BiP or Grp78).

DATA AVAILABILITY STATEMENT

The datasets presented in this study can be found in online repositories. The names of the repository/repositories and accession number(s) can be found below: https://www.ebi.ac.uk/pride/archive/projects/PXD027160; https://www.ebi.ac.uk/pride/archive/projects/PXD027162.

AUTHOR CONTRIBUTIONS

JR designed and performed experiments, analyzed the data, and drafted the manuscript and figures. RR and LN performed experiments and contributed to reagents. AH performed secondary structure predictions and the molecular modeling. LE and CC designed the experiments. LE analyzed and reviewed all data, and prepared the final version of the manuscript. All authors approved the final version of the manuscript.

FUNDING

Grant support by the German Research Foundation (DFG) within the framework of the multi-location research group FOR1228 (grants EI 399/7–2 to LE and CL 381/3–2 to CC), the Australian Research Council (ARC) (grant LE120100071 to AH), and Köln Fortune (to CC and LE) was gratefully acknowledged.

ACKNOWLEDGMENTS

We thank Ralph Gräf and Irene Meyer, University of Potsdam, Germany, for support with the BioID method and for kindly providing the BirA expression vector and the BirA rabbit polyclonal antibody.

SUPPLEMENTARY MATERIAL

The Supplementary Material for this article can be found online at: https://www.frontiersin.org/articles/10.3389/fcell.2021.748860/full#supplementary-material

Supplementary Figure 1 | Structure-based amino acid sequence alignment of human ASPL (UBXD9) and *D. discoideum* UBXD9. Secondary structure elements are color mapped; (α-helices: green, β-strands: red; cysteine residues: yellow). The UBL domain, the UBX domain, the helical lariat and the coiled coil (CC) regions are indicated by rectangles above and below the sequence alignment. Potential coiled coil motifs were predicted using MultiCoil (Wolf et al., 1997). The conserved aspartate (D) of the helical lariat and the double proline (PP) motif are boxed. Amino acid positions indicated in blue above and below the amino acid sequences denote the limits of various experimental constructs. Genbank accession numbers are XP_641771 for *D. discoideum* and NP_076988 for human UBXD9.

Supplementary Figure 2 | Pull-down experiments with recombinant p97 and full-length or truncated GST-UBXD9 coupled to glutathione beads. GST coupled to glutathione beads was used as negative control. Representative SDS PAGE gels stained with Coomassie Blue. The position of p97 is indicated. *Positions of GST and of full-length UBXD9 and UBXD9 truncation constructs tagged with GST.

Supplementary Figure 3 | UBXD9 and $UBXD9^{261-573}$ reduce the ATPase activity of p97. Data is presented as relative ATPase activity, mean values and SD of three experiments. For statistical analysis, the Dunnett's multiple comparison test, implemented in GraphPad Prism as *post hoc* analysis, was performed. $^{***}p \leq 0.001$.

Supplementary Figure 4 | Analysis of IP experiments and proximity labeling proteomics. **(A)** GFP trap experiments with the soluble proteins from total cell lysates of AX2 cells expressing GFP, UBXD9-GFP, or GFP-UBXD9. Top: SDS-PAGE and silver stain of proteins bound to the beads (Pellet). *Indicates the position of GFP-UBXD9 and # of GFP. +Indicates the position of the absent UBXD9-GFP silver band and of the visible UBXD9-GFP immunoblot band (see Western Blot). Bottom: Western blotting of proteins bound to the beads (Pellet). Endogenous UBXD9 of 95 kDa and GFP-tagged UBXD9 of 120 kDa were detected with the polyclonal UBX23520 antibody. *Indicates the position of GFP-tagged UBXD9 and o of untagged UBXD9. **(B)** BioID experiments with soluble proteins from total cell lysates of AX2 and AX2/BirA-UBXD9 cells. Top: SDS-PAGE and silver stain of soluble proteins before (S^1) and after (S^2) incubation with streptavidin sepharose beads and proteins bound to the beads (Pellet). The position of BirA-UBXD9 is indicated. Bottom: Western blotting of soluble proteins after (S^2) incubation with streptavidin sepharose beads and of proteins bound to the beads (Pellet). Endogenous UBXD9 and BirA-tagged UBXD9 were detected with the polyclonal UBX23520 antibody (top panel) and p97 with the polyclonal p97_8_6842 antibody (lower panel).

REFERENCES

Abraham, M. J., Murtola, T., Schulz, R., Páll, S., Smith, J. C., Hess, B., et al. (2015). GROMACS: high performance molecular simulations through multi-level parallelism from laptops to supercomputers. *SoftwareX* 1-2, 19–25. doi: 10.1016/j.softx.2015.06.001

Alexandru, G., Graumann, J., Smith, G. T., Kolawa, N. J., Fang, R., and Deshaies, R. J. (2008). UBXD7 binds multiple ubiquitin ligases and implicates p97 in HIF1alpha turnover. *Cell* 134, 804–816.

Arhzaouy, K., Strucksberg, K. H., Tung, S. M., Tangavelou, K., Stumpf, M., Faix, J., et al. (2012). Heteromeric p97/$p97^{R155C}$ complexes induce dominant negative changes in wild-type and autophagy 9-deficient *Dictyostelium* strains. *PLoS One* 7:e46879. doi: 10.1371/journal.pone.0046879

Arumughan, A., Roske, Y., Barth, C., Forero, L. L., Bravo-Rodriguez, K., Redel, A., et al. (2016). Quantitative interaction mapping reveals an extended UBX domain in ASPL that disrupts functional p97 hexamers. *Nat. Commun.* 7:13047.

Banchenko, S., Arumughan, A., Petrovic, S., Schwefel, D., Wanker, E. E., Roske, Y., et al. (2019). Common mode of remodeling AAA ATPases p97/CDC48 by their disassembling cofactors ASPL/PUX1. *Structure* 27, 1830–1841.e3.

Batsios, P., Meyer, I., and Graf, R. (2016). Proximity-dependent biotin identification (BioID) in Dictyostelium Amoebae. *Methods Enzymol.* 569, 23–42. doi: 10.1016/bs.mie.2015.09.007

Bodnar, N., and Rapoport, T. (2017). Toward an understanding of the Cdc48/p97 ATPase. *F1000Res.* 6:1318. doi: 10.12688/f1000research.11683.1

Bogan, J. S., Hendon, N., Mckee, A. E., Tsao, T. S., and Lodish, H. F. (2003). Functional cloning of TUG as a regulator of GLUT4 glucose transporter trafficking. *Nature* 425, 727–733. doi: 10.1038/nature01989

Bradford, M. M. (1976). A rapid and sensitive method for the quantitation of microgram quantities of protein utilizing the principle of protein-dye binding. *Anal. Biochem.* 72, 248–254. doi: 10.1016/0003-2697(76)90527-3

Brink, M., Gerisch, G., Isenberg, G., Noegel, A. A., Segall, J. E., Wallraff, E., et al. (1990). A Dictyostelium mutant lacking an F-actin cross-linking protein, the 120-kD gelation factor. *J. Cell Biol.* 111, 1477–1489. doi: 10.1083/jcb.111.4.1477

Bryson, K., Mcguffin, L. J., Marsden, R. L., Ward, J. J., Sodhi, J. S., and Jones, D. T. (2005). Protein structure prediction servers at University College London. *Nucleic Acids Res.* 33, W36–W38.

Buchberger, A., Howard, M. J., Proctor, M., and Bycroft, M. (2001). The UBX domain: a widespread ubiquitin-like module. *J. Mol. Biol.* 307, 17–24. doi: 10.1006/jmbi.2000.4462

Clemen, C. S., Eichinger, L., and Schroder, R. (2012). Reply: hereditary spastic paraplegia caused by a mutation in the VCP gene VCP: A Jack of all trades in neuro- and myodegeneration? *Brain* 135:e224. doi: 10.1093/brain/aws202

Cox, J., Neuhauser, N., Michalski, A., Scheltema, R. A., Olsen, J. V., and Mann, M. (2011). Andromeda: a peptide search engine integrated into the MaxQuant environment. *J. Proteome Res.* 10, 1794–1805. doi: 10.1021/pr101065j

Deshaies, R. J. (2014). Proteotoxic crisis, the ubiquitin-proteasome system, and cancer therapy. *BMC Biol.* 12:94. doi: 10.1186/s12915-014-0094-0

Dominguez-Martin, E., Ongay-Larios, L., Kawasaki, L., Vincent, O., Coello, G., Coria, R., et al. (2018). IreA controls endoplasmic reticulum stress-induced autophagy and survival through homeostasis recovery. *Mol. Cell. Biol.* 38:e00054-18.

Elfiky, A. A., Baghdady, A. M., Ali, S. A., and Ahmed, M. I. (2020). GRP78 targeting: hitting two birds with a stone. *Life Sci.* 260:118317. doi: 10.1016/j.lfs.2020.118317

Evangelista, T., Weihl, C. C., Kimonis, V., Lochmuller, H., and Consortium, V. C. P. R. D. (2016). 215th ENMC International Workshop VCP-related multi-system proteinopathy (IBMPFD) 13-15 November 2015, Heemskerk, The Netherlands. . *Neuromuscul. Disord.* 26, 535–547. doi: 10.1016/j.nmd.2016.05.017

Gaudet, P., Pilcher, K. E., Fey, P., and Chisholm, R. L. (2007). Transformation of Dictyostelium discoideum with plasmid DNA. *Nat. Protoc.* 2, 1317–1324. doi: 10.1038/nprot.2007.179

Gopaldass, N., Patel, D., Kratzke, R., Dieckmann, R., Hausherr, S., Hagedorn, M., et al. (2012). Dynamin A, Myosin IB and Abp1 couple phagosome maturation to F-actin binding. *Traffic* 13, 120–130. doi: 10.1111/j.1600-0854.2011.01296.x

Goujon, M., Mcwilliam, H., Li, W., Valentin, F., Squizzato, S., Paern, J., et al. (2010). A new bioinformatics analysis tools framework at EMBL-EBI. *Nucleic Acids Res.* 38, W695–W699.

Habtemichael, E. N., Li, D. T., Alcazar-Roman, A., Westergaard, X. O., Li, M., Petersen, M. C., et al. (2018). Usp25m protease regulates ubiquitin-like processing of TUG proteins to control GLUT4 glucose transporter translocation in adipocytes. *J. Biol. Chem.* 293, 10466–10486. doi: 10.1074/jbc.ra118.003021

Hänzelmann, P., and Schindelin, H. (2017). The interplay of cofactor interactions and post-translational modifications in the regulation of the AAA+ ATPase p97. *Front. Mol. Biosci.* 4:21. doi: 10.3389/fmolb.2017.00021

Hartmann-Petersen, R., and Gordon, C. (2004). Integral UBL domain proteins: a family of proteasome interacting proteins. *Semin. Cell Dev. Biol.* 15, 247–259. doi: 10.1016/j.semcdb.2003.12.006

Huyton, T., Pye, V. E., Briggs, L. C., Flynn, T. C., Beuron, F., Kondo, H., et al. (2003). The crystal structure of murine p97/VCP at 3.6A. *J. Struct. Biol.* 144, 337–348.

Johnson, J. O., Mandrioli, J., Benatar, M., Abramzon, Y., Van Deerlin, V. M., Trojanowski, J. Q., et al. (2010). Exome sequencing reveals VCP mutations as a cause of familial ALS. *Neuron* 68, 857–864.

Jung, G., Titus, M. A., and Hammer, J. A. III (2009). The Dictyostelium type V myosin MyoJ is responsible for the cortical association and motility of contractile vacuole membranes. *J. Cell Biol.* 186, 555–570.

Ladanyi, M., Lui, M. Y., Antonescu, C. R., Krause-Boehm, A., Meindl, A., Argani, P., et al. (2001). The der(17)t(X;17)(p11;q25) of human alveolar soft part sarcoma fuses the TFE3 transcription factor gene to ASPL, a novel gene at 17q25. *Oncogene* 20, 48–57.

Laemmli, U. K. (1970). Cleavage of structural proteins during the assembly of the head of bacteriophage T4. *Nature* 227, 680–685. doi: 10.1038/227680a0

Lupas, A. N., and Bassler, J. (2017). Coiled coils - a model system for the 21st Century. *Trends Biochem. Sci.* 42, 130–140. doi: 10.1016/j.tibs.2016.10.007

Madsen, L., Seeger, M., Semple, C. A., and Hartmann-Petersen, R. (2009). New ATPase regulators–p97 goes to the PUB. *Int. J. Biochem. Cell Biol.* 41, 2380–2388. doi: 10.1016/j.biocel.2009.05.017

Mi, H., Ebert, D., Muruganujan, A., Mills, C., Albou, L. P., Mushayamaha, T., et al. (2021). PANTHER version 16: a revised family classification, tree-based classification tool, enhancer regions and extensive API. *Nucleic Acids Res.* 49, D394–D403.

Moir, D., Stewart, S. E., Osmond, B. C., and Botstein, D. (1982). Cold-sensitive cell-division-cycle mutants of yeast: isolation, properties, and pseudoreversion studies. *Genetics* 100, 547–563. doi: 10.1093/genetics/100.4.547

Müller, J. M., Deinhardt, K., Rosewell, I., Warren, G., and Shima, D. T. (2007). Targeted deletion of p97 (VCP/CDC48) in mouse results in early embryonic lethality. *Biochem. Biophys. Res. Commun.* 354, 459–465. doi: 10.1016/j.bbrc.2006.12.206

Nguyen, T. V., Li, J., Lu, C. J., Mamrosh, J. L., Lu, G., Cathers, B. E., et al. (2017). p97/VCP promotes degradation of CRBN substrate glutamine synthetase and neosubstrates. *Proc. Natl. Acad. Sci. U.S.A.* 114, 3565–3571. doi: 10.1073/pnas.1700949114

Noegel, A. A., Blau-Wasser, R., Sultana, H., Muller, R., Israel, L., Schleicher, M., et al. (2004). The cyclase-associated protein CAP as regulator of cell polarity and cAMP signaling in *Dictyostelium*. *Mol. Biol. Cell* 15, 934–945. doi: 10.1091/mbc.e03-05-0269

Orme, C. M., and Bogan, J. S. (2012). The ubiquitin regulatory X (UBX) domain-containing protein TUG regulates the p97 ATPase and resides at the endoplasmic reticulum-golgi intermediate compartment. *J. Biol. Chem.* 287, 6679–6692. doi: 10.1074/jbc.m111.284232

Papadopoulos, C., Kravic, B., and Meyer, H. (2020). Repair or lysophagy: dealing with damaged Lysosomes. *J. Mol. Biol.* 432, 231–239. doi: 10.1016/j.jmb.2019.08.010

Perez-Riverol, Y., Csordas, A., Bai, J., Bernal-Llinares, M., Hewapathirana, S., Kundu, D. J., et al. (2019). The PRIDE database and related tools and resources in 2019: improving support for quantification data. *Nucleic Acids Res.* 47, D442–D450.

Rancour, D. M., Park, S., Knight, S. D., and Bednarek, S. Y. (2004). Plant UBX domain-containing protein 1, PUX1, regulates the oligomeric structure and activity of arabidopsis CDC48. *J. Biol. Chem.* 279, 54264–54274. doi: 10.1074/jbc.m405498200

Rezvani, K. (2016). UBXD proteins: a family of proteins with diverse functions in cancer. *Int. J. Mol. Sci.* 17:1724. doi: 10.3390/ijms17101724

Rijal, R., Arhzaouy, K., Strucksberg, K. H., Cross, M., Hofmann, A., Schroder, R., et al. (2016). Mutant p97 exhibits species-specific changes of its ATPase activity and compromises the UBXD9-mediated monomerisation of p97 hexamers. *Eur. J. Cell Biol.* 95, 195–207. doi: 10.1016/j.ejcb.2016.03.004

Roux, K. J., Kim, D. I., Raida, M., and Burke, B. (2012). A promiscuous biotin ligase fusion protein identifies proximal and interacting proteins in mammalian cells. *J. Cell Biol.* 196, 801–810. doi: 10.1083/jcb.201112098

Sali, A., and Blundell, T. L. (1993). Comparative protein modelling by satisfaction of spatial restraints. *J. Mol. Biol.* 234, 779–815. doi: 10.1006/jmbi.1993.1626

Sievers, F., Wilm, A., Dineen, D., Gibson, T. J., Karplus, K., Li, W., et al. (2011). Fast, scalable generation of high-quality protein multiple sequence alignments using Clustal Omega. *Mol. Syst. Biol.* 7:539. doi: 10.1038/msb.2011.75

Simpson, P. A., Spudich, J. A., and Parham, P. (1984). Monoclonal antibodies prepared against *Dictyostelium* actin: characterization and interactions with actin. *J. Cell Biol.* 99, 287–295. doi: 10.1083/jcb.99.1.287

Towbin, H., Staehelin, T., and Gordon, J. (1979). Electrophoretic transfer of proteins from polyacrylamide gels to nitrocellulose sheets: procedure and some applications. *Proc. Natl. Acad. Sci. U.S.A.* 76, 4350–4354. doi: 10.1073/pnas.76.9.4350

van den Boom, J., and Meyer, H. (2018). VCP/p97-mediated unfolding as a principle in protein homeostasis and signaling. *Mol. Cell* 69, 182–194.

Wang, C. K., Broder, U., Weeratunga, S. K., Gasser, R. B., Loukas, A., and Hofmann, A. (2012). SBAL: a practical tool to generate and edit structure-based amino acid sequence alignments. *Bioinformatics* 28, 1026–1027.

Watts, G. D., Wymer, J., Kovach, M. J., Mehta, S. G., Mumm, S., Darvish, D., et al. (2004). Inclusion body myopathy associated with Paget disease of bone and frontotemporal dementia is caused by mutant valosin-containing protein. *Nat. Genet.* 36, 377–381.

Wendler, P., Ciniawsky, S., Kock, M., and Kube, S. (2012). Structure and function of the AAA+ nucleotide binding pocket. *Biochim. Biophys. Acta* 1823, 2–14. doi: 10.1016/j.bbamcr.2011.06.014

Williams, K. L., and Newell, P. C. (1976). A genetic study of aggregation in the cellular slime mould *Dictyostelium discoideum* using complementation analysis. *Genetics* 82, 287–307. doi: 10.1093/genetics/82.2.287

Wolf, E., Kim, P. S., and Berger, B. (1997). MultiCoil: a program for predicting two- and three-stranded coiled coils. *Protein Sci.* 6, 1179–1189. doi: 10.1002/pro.5560060606

Ye, Y. (2006). Diverse functions with a common regulator: ubiquitin takes command of an AAA ATPase. *J. Struct. Biol.* 156, 29–40. doi: 10.1016/j.jsb.2006.01.005

Yeung, H. O., Kloppsteck, P., Niwa, H., Isaacson, R. L., Matthews, S., Zhang, X., et al. (2008). Insights into adaptor binding to the AAA protein p97. *Biochem. Soc. Trans.* 36, 62–67. doi: 10.1042/bst0360062

Conflict of Interest: The authors declare that the research was conducted in the absence of any commercial or financial relationships that could be construed as a potential conflict of interest.

Publisher's Note: All claims expressed in this article are solely those of the authors and do not necessarily represent those of their affiliated organizations, or those of the publisher, the editors and the reviewers. Any product that may be evaluated in this article, or claim that may be made by its manufacturer, is not guaranteed or endorsed by the publisher.

Copyright © 2021 Riehl, Rijal, Nitz, Clemen, Hofmann and Eichinger. This is an open-access article distributed under the terms of the Creative Commons Attribution License (CC BY). The use, distribution or reproduction in other forums is permitted, provided the original author(s) and the copyright owner(s) are credited and that the original publication in this journal is cited, in accordance with accepted academic practice. No use, distribution or reproduction is permitted which does not comply with these terms.

frontiers in Cell and Developmental Biology

REVIEW
published: 05 October 2021
doi: 10.3389/fcell.2021.740205

Using Live-Cell Imaging and Synthetic Biology to Probe Directed Migration in *Dictyostelium*

*Jonathan Kuhn, Yiyan Lin and Peter N. Devreotes**

Department of Cell Biology, School of Medicine, Johns Hopkins University, Baltimore, MA, United States

For decades, the social amoeba *Dictyostelium discoideum* has been an invaluable tool for dissecting the biology of eukaryotic cells. Its short growth cycle and genetic tractability make it ideal for a variety of biochemical, cell biological, and biophysical assays. Dictyostelium have been widely used as a model of eukaryotic cell motility because the signaling and mechanical networks which they use to steer and produce forward motion are highly conserved. Because these migration networks consist of hundreds of interconnected proteins, perturbing individual molecules can have subtle effects or alter cell morphology and signaling in major unpredictable ways. Therefore, to fully understand this network, we must be able to quantitatively assess the consequences of abrupt modifications. This ability will allow us better control cell migration, which is critical for development and disease, *in vivo*. Here, we review recent advances in imaging, synthetic biology, and computational analysis which enable researchers to tune the activity of individual molecules in single living cells and precisely measure the effects on cellular motility and signaling. We also provide practical advice and resources to assist in applying these approaches in *Dictyostelium*.

Keywords: migration, chemotaxis, signaling, imaging, synthetic & systems biology

OPEN ACCESS

Edited by:
Robert J. Huber,
Trent University, Canada

Reviewed by:
Arjan Kortholt,
University of Groningen, Netherlands
Peggy Paschke,
University of Glasgow,
United Kingdom

****Correspondence:***
Peter N. Devreotes
pnd@jhmi.edu

Specialty section:
This article was submitted to Molecular and Cellular Pathology, a section of the journal Frontiers in Cell and Developmental Biology

Received: *12 July 2021*
Accepted: *08 September 2021*
Published: *05 October 2021*

Citation:
Kuhn J, Lin Y and Devreotes PN (2021) Using Live-Cell Imaging and Synthetic Biology to Probe Directed Migration in Dictyostelium. Front. Cell Dev. Biol. 9:740205. doi: 10.3389/fcell.2021.740205

INTRODUCTION

Dictyostelium as a Model Organism for Directed Migration

In order to respond to cues in their environment, cells detect and move toward or away from cues like light, chemical gradients, and mechanical forces. Directed migration is a critical process in all domains of life: unicellular organisms can detect and move toward food and mates, while multicellular organisms use chemical gradients to guide cells during development and immune response (Yamada and Cukierman, 2007; Thomas et al., 2018; Yamada and Sixt, 2019). Understanding how cells sense direction and respond is therefore important both to basic biological questions and for developing new therapies to treat birth defects, immunodeficiencies, and cancers.

Directed migration consists of three processes: directional sensing, motility and polarity. Directional sensing is the orientation of molecules involved in cell migration toward a stimulus. Once cell senses a directional cue, it can use motility proteins to move toward that cue. These two processes are distinct: immobile cells still can align molecules along a chemical gradient and cells with no stimulus can migrate in random directions (Janetopoulos et al., 2004; Song et al., 2006; Swaney et al., 2010). Finally, polarized cells maintain a single "front" and "back" at designated locations in order to move processively. Again, this process is not dependent on the two others:

polarized cells can migrate randomly, unpolarized cells can exhibit chemotactic behavior, and cells can maintain a polarized state without moving (Janetopoulos et al., 2004; Tang et al., 2008; Wang et al., 2014; Park et al., 2017). Because the mechanisms of polarity are less fleshed out than the other two, this review will focus on directional sensing and motility exclusively.

Dictyostelium discoideum undergo directed migration in the presence of chemical, mechanical, and electrical gradients, which makes it an ideal model organism for studying cell migration (Van Haastert and Devreotes, 2004; Annesley and Fisher, 2009; Artemenko et al., 2014; Nichols et al., 2015; Devreotes et al., 2017). Compared to mammalian cells, *Dictyostelium* are easy to maintain, genetically manipulate, and are amenable to large-scale genetic and pharmaceutical screens. Moreover, nearly all the signal molecules are conserved between *Dictyostelium* and mammals. Historically, *Dictyostelium* has been used to identify and study regulators of directional migration. Many of these molecules are now known, but we only have a limited understanding of how they function together as a network. *Dictyostelium* has emerged as a platform for designing and testing tools which can acutely change properties of this network. This approach, in combination with quantitative analysis and computational modeling, has allowed investigators to dissect the structure of the directed migration pathway.

Building a Model of Directed Migration

Directed migration can be broken into three steps: chemical inputs, signal transduction, and cytoskeletal response. Ligands like Cyclic AMP (cAMP) bind to membrane-bound receptors, eliciting downstream signaling transduction events involving Ras GTPases, phosphoinositide lipids, lipid kinases/phosphatases and protein kinases/phosphatases. These molecules then modulate the actomyosin cytoskeleton network that drives cell movement (**Figure 1**; Devreotes et al., 2017).

In order to understand directed migration, several groups have developed computational models of the biochemical networks underlying the process (Zigmond, 1974; Mato et al., 1975; Tranquillo et al., 1988; Meinhardt, 1999; Arrieumerlou and Meyer, 2005; Levine et al., 2006; Hecht et al., 2010; Neilson et al., 2011; Takeda, 2012; Tang et al., 2014). To account for the rapid response to chemoattractant and for directional movement, the Iglesias and Devreotes labs developed a model where chemoattractant stimulation leads to Local Excitation and Global Inhibition (LEGI) (**Figure 2A**; Meinhardt and Gierer, 2000; Xiong et al., 2010; Tang et al., 2014). The LEGI concept explains why cells can respond directionally in shallow gradients and adapt to global concentration changes: chemical stimulation produces both an excitor and an inhibitor. The excitor is fast and localized, while the inhibitor is slow and global, ensuring that excitor is higher than inhibitor only at the high end of a gradient and lower than the inhibitor at the back. The concentration of the excitor then biases the probability of spontaneous signal transduction events such that the cell forms many more protrusions toward a stimulus on average. This LEGI framework helped explain many of the dynamic signaling changes in response to chemoattractants, but it did not detail how these changes helped cells form and control protrusions using the actin cytoskeleton.

In order to explain the coordination between signal transduction and cytoskeletal networks during cell migration,

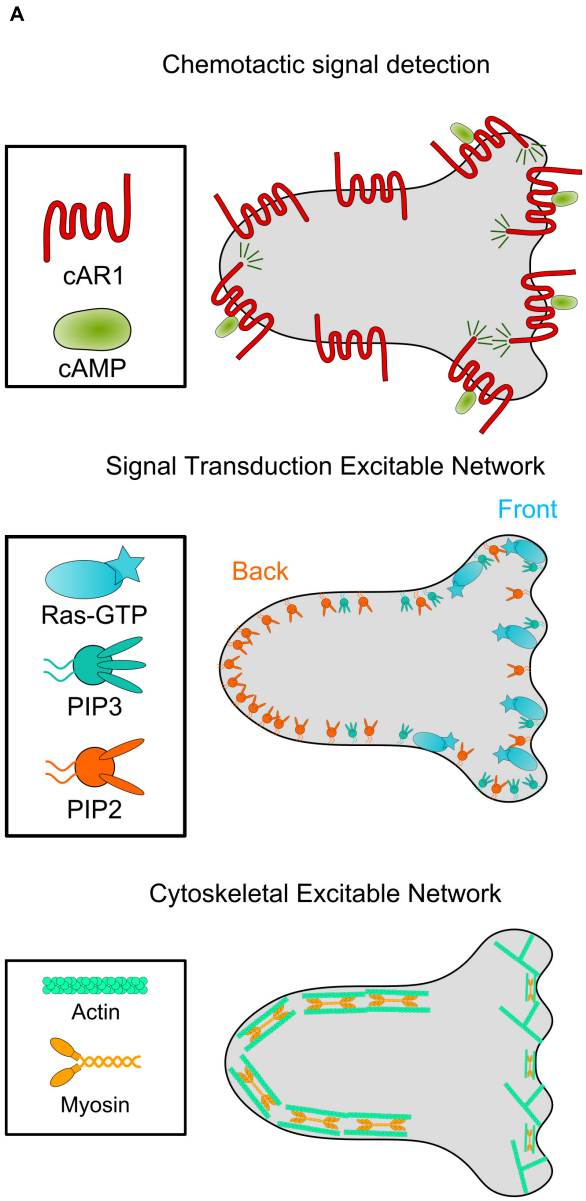

FIGURE 1 | The chemotaxis network in *Dictyostelium*. Diagram of the connected networks controlling *Dictyostelium* cyclic AMP (cAMP) chemotaxis. Top: the uniformly distributed G-Protein Coupled Receptor cAR1 binds to cAMP, leading to motion up the concentration gradient. Middle: cAMP-cAR1 interactions locally increase concentration of activated Ras and membrane lipid PI(3,4,5)P3 (PIP3), among other molecules. These molecules form the cell "front" and are mutually exclusive with localization of cell "back" molecules like PI(4,5)P2 (PIP2). Together, these signaling molecules form the Signal Transduction Excitable Network. Bottom: Active Ras enrichment leads to an increase in actin polymerization at the cell front. Meanwhile, cell back signaling molecules activate the contraction of an actomyosin network. This Cytoskeletal Excitable Network powers motility.

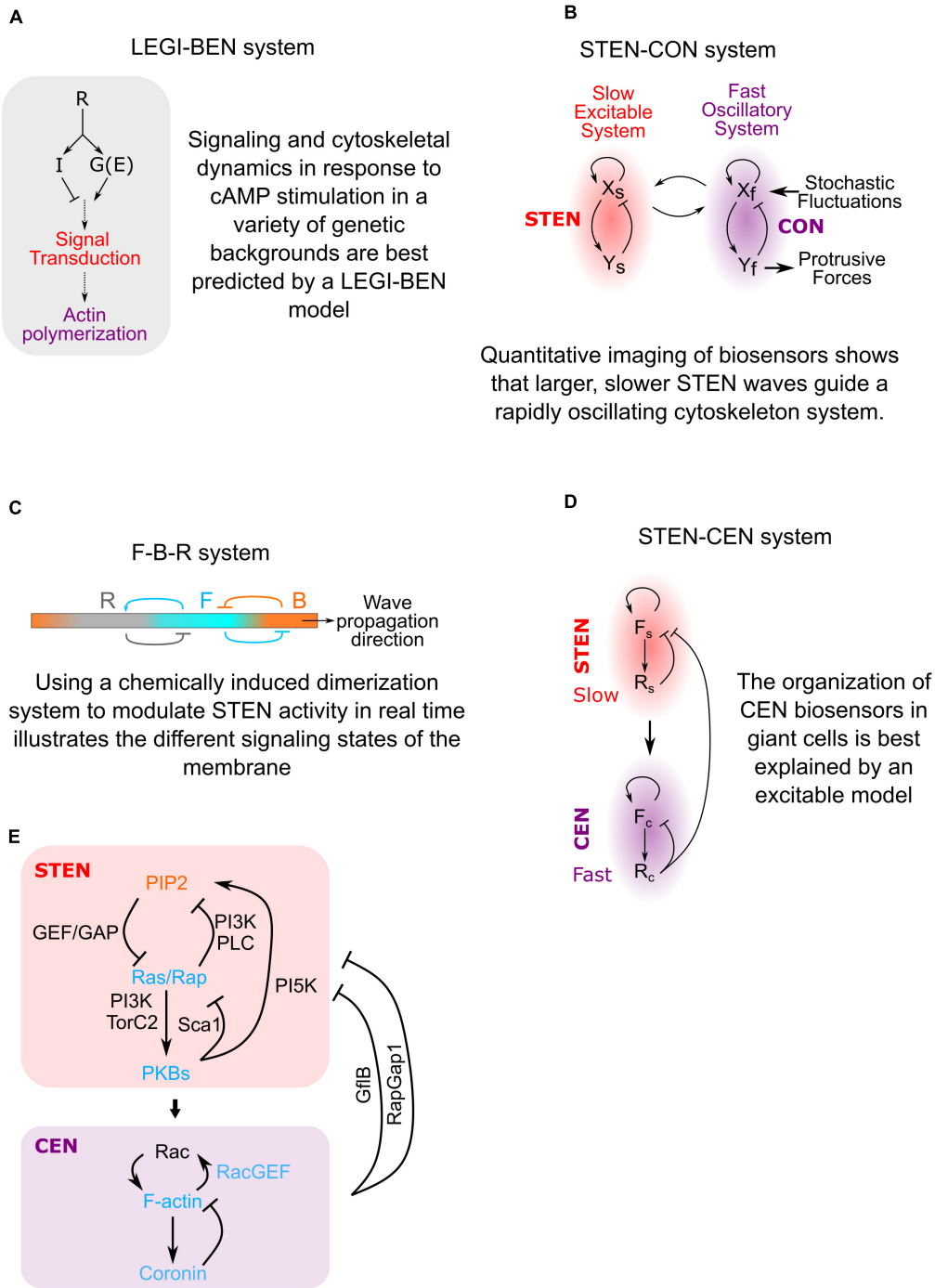

FIGURE 2 | The evolution of directed migration models. **(A)** By monitoring how signaling and cytoskeletal dynamics change during cAMP stimulation in different genetic backgrounds we were able to build a model of gradient-sensing. The cell has two responses to Receptor (R) activation: locally, heterotrimeric G-proteins (G) create an Excitor (E) of signal transduction excitation. Globally, the cell produces an Inhibitor (I) which lowers the probability of excitation. This Local Excitation and Global Inhibition (LEGI) of a Biased Excitable Network (BEN) explains how cells moves in the correct direction even in shallow gradients. **(B)** Imaging of signaling biosensors independent of cytoskeletal proteins revealed excitable behavior. In the absence of signaling activity, cytoskeletal biosensors rapidly oscillate at small membrane patches. The Cytoskeletal Oscillatory Network (CON) is only able to form large, sustained protrusions when driven by the Signal Transduction Excitable Network (STEN). **(C)** Using data from chemically induced dimerization perturbations, a model of how cell front and back activities are segregated was created. The membrane sits in a resting state equivalent to the cell back state (B). STEN excitation converts a patch of the membrane to a front state (F). This F state inhibits the B state but also gradually creates its own inhibitor that converts F-state membrane to a refractory state (R). This explains how activities like Ras activation and actin polymerization propagates across cell membranes but is transient at any single location. **(D)** Biosensor dynamics show that the cytoskeletal network also has excitable properties. The Cytoskeletal Excitable Network (CEN) is coupled to the STEN but works on a faster timescale, explaining the structure of STEN-CEN waves on the bottom membrane of giant cells. **(E)** Diagram of the STEN-CEN network sketched out in panel **(D)** with specific molecules added.

it has been proposed that these systems are directly coupled (**Figures 2B-D**; Vicker, 2002; Gerisch et al., 2012; Huang et al., 2013; Van Haastert et al., 2017). Measurements of signaling protein dynamics in *Dictyostelium* suggested that the signal transduction network had excitable properties similar to an action potential (Nishikawa et al., 2014; Tang et al., 2014). This **S**ignal **T**ransduction **E**xcitable **N**etwork (STEN) exhibits classic characteristics of excitability, including wave propagation, refractoriness and maximal response to suprathreshold stimuli (Xiong et al., 2010; Nishikawa et al., 2014; Tang et al., 2014). This led to the discovery that STEN organizes the activity of a rapidly oscillating cytoskeletal network to localize and shape cell protrusions (**Figure 2B**).

Using chemically induced dimerization to acutely change STEN activity in migrating cells, it was shown how the STEN segregates the front and back of cells: At rest, the cell membrane is dominated by phosphatidylinositol 3,4-bisphosphate[PI(3,4)P2] and phosphatidylinositol 4,5-bisphosphate[PI(4,5)P2], representing an inactive B ("Back") state (Miao et al., 2017). These signaling molecules discourage actin polymerization and activate actomyosin contraction (Weiner et al., 2002; Wong et al., 2005; Papakonstanti et al., 2007). When extracellular signals or internal noise raise STEN activity above a threshold, it converts the local membrane to a F ("Front") state by activating Ras/Rap proteins (Kae et al., 2004; Sasaki et al., 2004; Bolourani et al., 2006; Cai et al., 2010; Gerisch et al., 2011; Kortholt et al., 2011, 2013). These signaling proteins activate actin polymerization, a hallmark of cell fronts. The excitable behavior of STEN relies on feedback loops within the network: Ras/Rap positive feedback loops on short timescales lead to rapid activation and propagation of the F state. Longer-term negative feedback generated by front molecules places recently activated parts of the membrane into a refractory (R) state which cannot immediately fire again (Miao et al., 2017; **Figure 2C**).

Finally, observing the shape and kinetics of cytoskeletal activity markers after altering various regulators of signaling and cytoskeletal activity demonstrated that the cytoskeletal network displayed many of the same hallmarks of excitability as the STEN (**Figure 2D**; Miao et al., 2019). The **C**ytoskeletal **E**xcitable **N**etwork (CEN) model explains the organization of cytoskeletal activity biosensors relative to STEN waves on the bottom membrane of cells. The STEN-CEN model can predict signal transduction and cytoskeletal behavior in other cells, such as mammalian breast cancer cells (Xiong et al., 2016; Zhan et al., 2020).

To develop an understanding of the directed migration network, it was vital to image quantitative changes in activation and localization of dozens of molecules inside cells (**Figure 2**). While biochemical approaches to studying cell migration can be incredibly revealing, they nearly always eliminate spatial information and average differences across a heterogenous cell population. Comparing two fixed cell populations using immunofluorescence also has downsides: because many of the activities discussed here are variable between cells, it can be difficult to distinguish between real biological differences and noise. Imaging cellular processes in living cells circumvents these drawbacks and likely provides the most physiologically relevant information. However, studying activity changes in individual cells over time has many experimental hurdles: how can we measure changes in protein activity without damaging cells? How can we display and measure changes over time reliably? And most importantly, how can we make chemical perturbations to living cells in real time? By reviewing methods and best practices to measure and change the activity of molecules involved in cell migration, this review will provide a resource for others endeavoring to dissect complex and dynamic biological processes.

MONITORING AND ALTERING MIGRATION ACTIVITIES

Reporting Activities in Living Cells in Real-Time

The dynamic localization of proteins within the cell contains important information about the organization and dynamics of the STEN and CEN networks. Many proteins localize toward a stimulus in the cell front or away from a stimulus in the cell back (Li et al., 2020). Using fluorescent fusion proteins that characterize the front or back (**Table 1**), we can determine the signaling state of the cell in response to a variety of perturbations. It is important to understand that while fluorescent fusion proteins indicate where a protein is, they do not report on the catalytic activity of the protein itself. For proteins that do not change activity by relocating, other types of sensors must be developed.

Using Biosensors to Measure Signal Transduction Excitable Network-Cytoskeletal Excitable Network Activity

To understand changes in directed migration network dynamics, it is important to measure activities, not just localizations. This is because there is often not a direct correlation between activity and localization: for example, Ras GTPase localizes to the entire cell periphery, but activated Ras (Ras-GTP) only localizes to the front of cells (Sasaki et al., 2004). Many genetically encoded fluorescent or bioluminescent sensors have been developed to observe the spatial and temporal dynamics of signaling molecules in cells. Biosensors consists of two parts: one that recognizes the analyte (signal molecules) and a reporter (fluorescent or bioluminescent proteins) (Okumoto et al., 2012). For example, the biosensor RBD (Ras Binding Domain) (**Table 2**) uses a protein domain that binds Ras-GTP conjugated to a fluorescent protein in order to detect activated Ras *in vivo* (Taylor et al., 2001). Biosensors can also be used to localize molecules that cannot be detected by standard fluorescence techniques. For example, the PH domain of the protein Crac (**Table 1**) binds to the membrane lipid PI(3,4,5)P3 and can be used to monitor PIP3 localization in the cell (Dormann et al., 2002).

One important note of caution is that biosensor localization does not linearly correlate with activity. Depending on expression level and affinity, only a fraction of the biosensor is bound to the analyte. For example, there are two main populations of RBD

TABLE 1 | Examples of endogenous proteins which can serve as fluorescent biomarkers of the cell front and back due to their well-characterized localization.

Components	Location	References
FRONT		
CRAC (cytosolic regulator of adenylyl cyclase)	Leading edge of migrating cell	Parent et al., 1998
Phg2	Enriched at the membrane of cell front in migrating cells, but also present in cytosol	Gebbie et al., 2004
PKBA/PKBR1	Leading edge of the migrating cells. At rest, PKBR1 is found on membrane by myristoylation, while PKBA is in cytosol	Meili et al., 1999, 2000
RacGEF1	Localized to F-actin polymerization region, mainly along the anterior cortical area and at the posterior of chemotaxing cell	Park et al., 2004
BACK		
PTEN	Membrane and cytosolic distribution, localized at the rear of the migrating cells. Precent on membrane in Latrunculin A treated cells	Iijima and Devreotes, 2002
ACA (adenylyl cyclase)	Back of chemotaxing cells	Kriebel et al., 2003
PAKa	The posterior cell body	Chung and Firtel, 1999
Cortexillin I	The trailing edge of migrating cells	Cha and Jeon, 2011

TABLE 2 | Examples of well-characterized biosensors for important activities in the celll migration network.

Binding targets	Biosensor	*In vivo* location	Protein domain	References
Actin filament (F-actin)	LimE△coil	Protrusions of cell front	A LIM-domain containing protein DdLimE deleted c-terminal coiled-coil domain	Bretschneider et al., 2004
	Lifeact	filamentous actin in whole cell	A 17-amino-acid peptide	Riedl et al., 2008
Ras-GTP	RBD (Ras binding domain)	Active patches on protrusions and macropinocytic cups	Ras binding domain (RBD) of c-Raf-1 (amino acids 51–131)	Chiu et al., 2002
Rap1-GTP	RBDRalGDS	Protrusions of cell fronts	Ras binding domain (RBD) of RalGDS	Bivona et al., 2004
PI(3,4)P2	CynA	Trailing edge and macropinocytic cups	PH domain-containing proteins PH21 that binds PI(3,4)P2	Swaney et al., 2015
PI(4,5)P2	PH-PLCδ1	lamellipodium, base of the endocytic invagination	PH domain of PLCδ1that bind PI45P2. But binds to IP3 ∼ 20 fold more tightly than PI(4,5)P2	Wills et al., 2018
PIP3	PHcrac	Protrusions of cell front, macropinocytic cups	PH (pleckstrin homology) domain of cytosolic regulator of adenylyl cyclase (CRAC)	Huang et al., 2003
Rac-GDP	Coronin CRIB motif	Protrusions of cell fronts, colocalized with polymerizing F-actin	Cdc42- and Rac-interactive binding motif (CRIB) of coronin	Swaminathan et al., 2014
Rac1-GTP	PAK-PBD	Rac1-GTP is throughout the phagocytic cup	The Rac/Cdc42 (p21) binding domain (PBD) of the human p21 activated kinase 1 protein (PAK)	Benard et al., 1999

within a *Dictyostelium* cell: localized to the front region of the membrane and in the cytoplasm. The cytoplasmic pool of RBD contains unbound biosensor and does not indicate Ras activation. Therefore, the specific biology of the analyte must be considered when interpreting data from biosensor experiments.

Using Electrofused Cells to Image Signal Transduction Excitable Network-Cytoskeletal Excitable Network Waves on the Bottom Membrane

In single cells, it is hard to dissect the temporal order of signals in same network because signaling events seems to all initiate spontaneously and stochastically. One reason for this is the small dimensions of a cell: protrusions formed on the cell periphery can quickly travel vertically out of the imaging plane (**Figure 3**). Meanwhile, signaling events starting on the center of the bottom membrane can quickly reach the periphery and go out of view. To gain insight in the spatiotemporal regulation of the chemotactic network, Gerisch and colleagues fused multiple *Dictyostelium* cells using electric pulses and described the generation and propagation of self-organized actin waves on the substrate-attached surface (Gerisch et al., 2013; Gerhardt et al., 2014). Subsequently, giant cells generated by electropulse-induced cell fusion have become a tool for studying the spatial organization of STEN and CEN molecules (**Figure 3**). The giant surface is an ideal platform for observing the propagation of signaling events: Ras, PIP3 and actin polymerization propagate along the surface in coordinated waves (Schroth-Diez et al., 2009; Arai et al., 2010; Shibata et al., 2012; Taniguchi et al., 2013; Gerhardt et al., 2014). Usually, active F state molecules like Ras-GTP, PIP3 form waves that appear to be surrounded by CEN waves (actin) (Miao et al., 2019). Outside the waves are B state molecules such as PTEN. The spatial "phase shift" between waves of the various sensors reveal the organization and kinetics of STEN and CEN. STEN biosensors show a one-peak wave with Rap activity leading Ras activity, in front of PIP3, and followed by PKB. CEN waves span the STEN region but also have an initial peak and a weaker trailing peak. This two peak structure is best explained by a model where the timescale

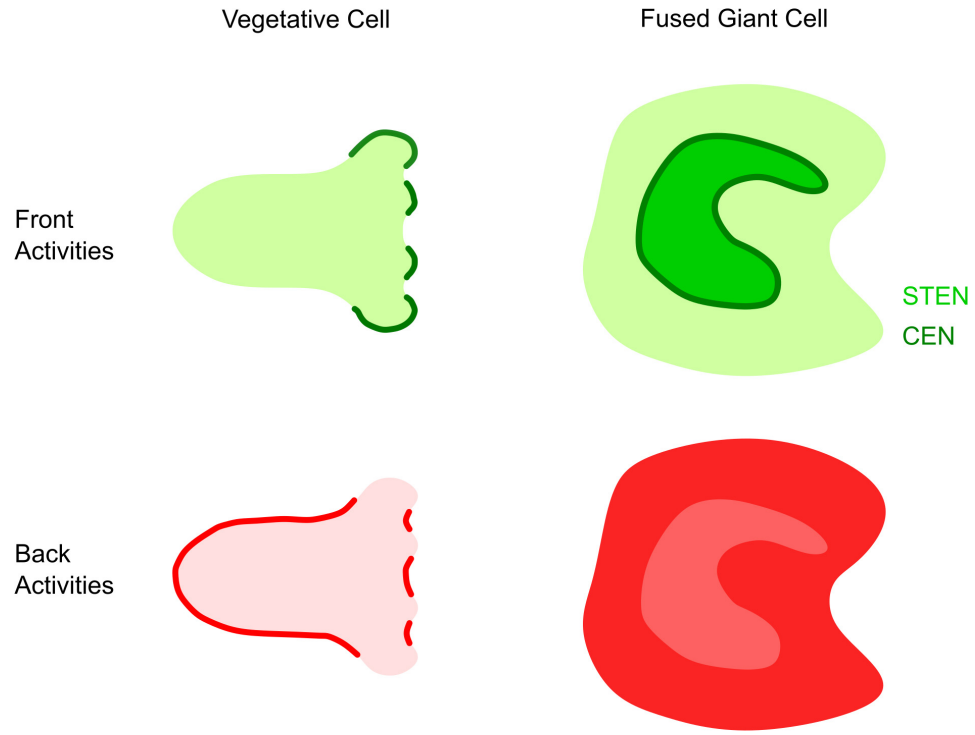

FIGURE 3 | Front and back organization in *Dictyostelium*. Illustration of "front" and "back" activities in the middle focal plane of a single vegetative cells and the bottom membrane of giant cells. Left: in single cells, front (green) activities occur at protrusions or macropinocytic cups, while back (red) activities display complementary patterns at the trailing edge of macropinocytic cups or the cell. Right: in giant cells, front activities (green) propagate as cortical waves. STEN (light green) activities are enclosed by CEN (dark green). Back activities (dark red) are excluded from the area of front activity, creating "shadow waves" of low intensity when imaging back biosensors (light red).

of CEN activation and inhibition is much faster than STEN (Miao et al., 2019).

Altering Protein Activity in Living Cells

The directed migration network contains hundreds of molecules which are linked in an intricate series of feedback loops. Because of this, assessing the role of one individual molecule is difficult: adaptive changes in the level or activity of other proteins can compensate for individual deletions, leading to unexpected phenotypes. Because of this, it is critical to observe how changes in protein activity affect the network immediately. For example, transiently raising Ras activity has different effects on cell morphology than expressing constitutively activated Ras (Miao et al., 2017; Edwards et al., 2018). While this section will focus on newer synthetic methods to alter cell chemistry, some older tools which remain in use today will be briefly noted.

Stimulation of the Directed Migration Network

For decades, researchers have been using the natural response of *Dictyostelium* to chemical signals to alter the directed migration pathway in real time. Cyclic AMP (cAMP) activates a chemotactic response in *Dictyostelium* by binding the GPCR cAR1, leading to elevated Ras activation and actin polymerization at the high end of the gradient. The localization and dynamics of a molecule during cAMP stimulation contain important information about that molecule's position in the directed migration pathway (Devreotes et al., 2017). While representing the true chemotactic response, this approach has a few disadvantages for unraveling network architecture: it alters the activity of many proteins at once, making specific studies more difficult. Cells developed to respond to cAMP are also more polarized complicating direct comparison to the undeveloped cells. However, cAMP activation is fast (2-3 s), robust over many mutant lines, tunable at low concentrations, and does not require any genetic perturbations. This flexibility and accessibility make it a useful tool to place individual molecules within the chemotaxis pathway. Because it requires no molecular biology tools, cAR1 stimulation can even be combined with other techniques like chemical dimerization (Miao et al., 2017) to measure how acute changes in other molecules affect the pathway's response to stimuli. Finally, if cAMP is not feasible, many orthogonal methods to activate the directed migration pathway exist: chemicals like folic acid which act on a different receptor, mechanical forces like shear flow, and electrical fields (Zhao et al., 2002; Décave et al., 2003; Artemenko et al., 2016).

Pharmacological Perturbations

Many *Dictyostelium* proteins involved in directed migration can be controlled with the use of small molecule inhibitors. Commonly used inhibitors like the actin depolymerizing agent latrunculin the PI3K inhibitor LY294002, the Myosin inhibitor

blebbistatin, and the TORC2 inhibitor PP242 are effective in altering STEN and CEN activities in *Dictyostelium* (Gerisch et al., 2004; Shu et al., 2005; Loovers et al., 2006; Cai et al., 2010). There are significant advantages to pharmacological approaches: they are fast, potentially address only a single node in the network, and do not require genetic manipulations. The main drawback to these techniques is availability: most newly developed small molecule inhibitors are optimized to function in human cells for medical applications and may not function well in *Dictyostelium*. Additionally, inhibitors may have significant off-target effects which confound results.

Chemically Induced Dimerization

Chemically **I**nduced **D**imerization (CID) is a flexible method for recruiting proteins to specific locations in the cell. In CID, a protein of interest (an "actuator") is fused to a protein domain which, upon the addition of a chemical agent, will dimerize with another protein domain fused to an organelle (an "anchor") (**Figure 4**). While there a few different versions of this system (Fegan et al., 2010), this section will focus on the well-established FKBP-FRB system. The FKBP-FRB system takes advantage of the ability of **FK**506 **B**inding **P**rotein (FKBP) to heterodimerize with a domain of the signaling protein mTOR (the helpfully named **F**KBP-**R**apamycin **B**inding domain, or FRB) in the presence of the small molecule Rapamycin (Derose et al., 2013). CID is capable of targeting protein activity to certain intracellular regions and is specific to the protein of interest. The FKBP-FRB system also acts within seconds of rapamycin addition and does not require any specialized equipment. These properties make CID an ideal tool to study a complex, dynamic network like the chemotaxis pathway.

The CID system allows researchers to separate how changes in different parts of the directed migration network affect cell function. For example, a truncated, membrane-recruitable RacGEF1 can be used to increase actin polymerization across the cell membrane (**Figure 4C** and **Supplementary Movie 1**). While cAMP stimulation leads to actin polymerization through a signaling cascade, this perturbation directly activates the actin nucleator WASP. Similar to cAMP stimulation and STEN activation, RacGEF1 membrane recruitment causes cells to flatten out as actin polymerizes in all directions (**Figure 4C** and **Supplementary Movie 1**) (Miao et al., 2019). However, unlike upstream perturbations, direct upregulation of actin polymerization leads to a large decrease in Ras activation (Miao et al., 2019). This negative feedback from CEN to STEN was only uncovered by choosing a specific downstream entry point into the chemotaxis pathway. When designing FKBP-FRB experiments in *Dictyostelium* like this one, there are many important considerations in design and execution, which will be discussed below. For a summary of these considerations, see Quick Start Guide 1.

Organelle Anchor Design

The anchor fusion protein determines where a protein of interest localizes within a cell once rapamycin is added. In order to function correctly, it must be stable, highly expressed, and uniformly distributed at the organelle of choice. Because most regulation of directed migration occurs at the membrane or close to it at the cortex, this guide will focus on anchors to recruit proteins to the inner side of the plasma membrane. For a list of other organelle localization strategies, see Derose et al. (2013). Designing a plasma membrane anchor is simple: the targeting sequence or protein must localize uniformly at the plasma membrane and not interfere with cell function. To ensure that the actuator localizes to the membrane instead of the reverse, the anchor must also have slow turnover rate within the plasma membrane. For specific details of recommended anchors, see the **Supplementary Methods**.

Actuator Design

The design of actuators is more involved and varied than anchors. When adapting a protein for use in a CID system, it is important to take its specific biology into account. To illustrate, consider a system designed to transiently raise Ras activity. Because Ras targets involved in cell migration are primarily at the membrane, a constitutively active FRB-tagged RasC mutant ($RasC_{Q62L}$) which could be recruited to the membrane was created. To prevent actuator expression from affecting the cell prior to rapamycin addition, the membrane localization domain (a C-terminal CAAX) was deleted (Miao et al., 2017). When this FRB-$RasC_{Q62L\Delta CAAX}$ was expressed along with a Myr-2XFKBP anchor, robust membrane localization of the actuator was observed only after rapamycin addition. FRB-$RasC_{Q62L\Delta CAAX}$ membrane localization coincided with large increases in PIP3 levels, actin polymerization, and protrusion size. A similar approach can be taken to many classes of molecules, including kinases, phosphatases, and GEFs (Miao et al., 2019). As a general guideline, actuators must be catalytic (as opposed to structural), specific to a process of interest, and have low activity when not localized to the correct region of the cell.

Expression Guidelines – Vectors and Fluorescent Proteins

The primary consideration for expressing CID components is actuator abundance. In previous experiments, transforming the actuator in a high copy number vector was required to observe a phenotype after recruitment (Miao et al., 2017, 2019). When imaging cells in a CID experiment, it is critical to confirm that the actuator is expressed at high levels and localizes to the membrane after rapamycin addition. Therefore, the actuator should always be fused to a bright fluorescent protein. While imaging the membrane anchor is helpful for confirming expression, it is often more useful to leave the anchor unlabeled and also express a fluorescent biosensor. For example, by imaging GFP-conjugated PIP3 and actin polymerization biosensors before and after recruitment of mCherry-FRB-$RasC_{Q62L\Delta CAAX}$, the Devreotes Lab showed that transient increases in Ras activation led to larger fronts of Actin and PIP3 (Miao et al., 2017). Refer to the **Supplementary Methods** for more information.

Experimental Practice and Controls

To confirm that a CID system is working as intended, it is important to show that phenotypic changes are due to the activity of the localized protein rather than some effect of rapamycin addition or an off-target effect. Repeat the CID experiment with an inactive version of the activator, like a catalytic domain

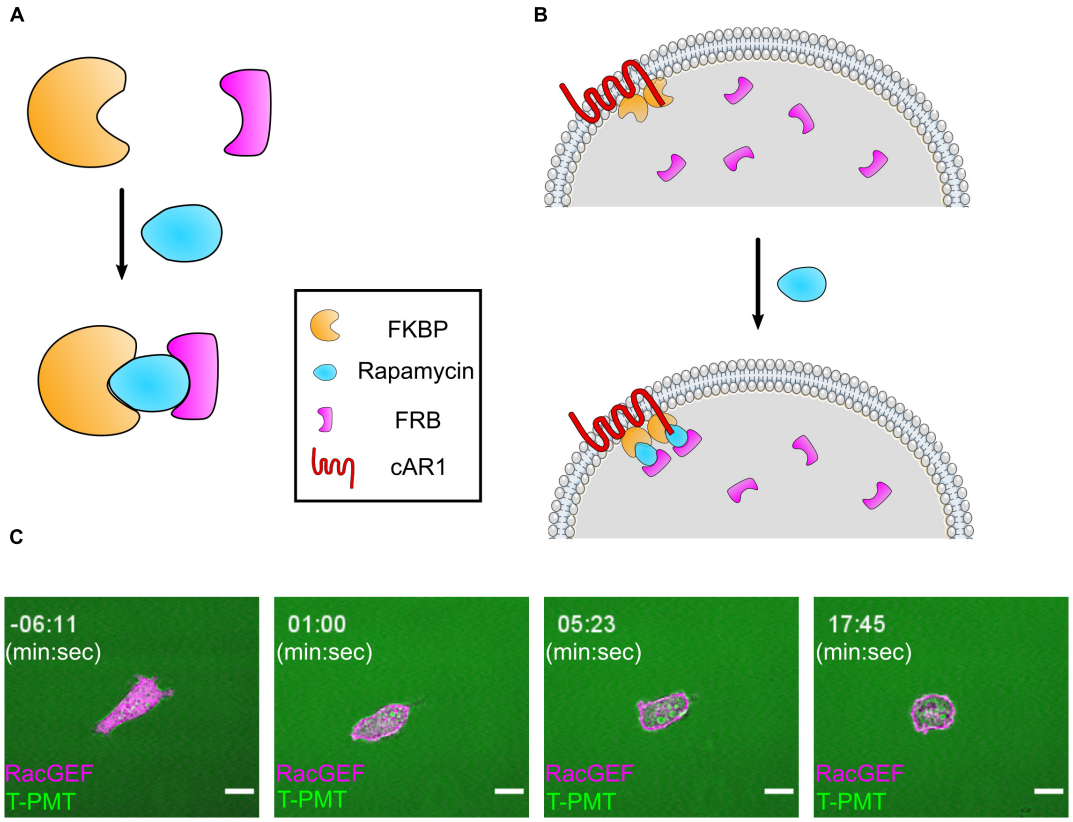

FIGURE 4 | The FKBP/FRB system and its application in cells. **(A)** Diagram of FKBP/FRB system. FKBP and FRB form a heterodimer in the presence of rapamycin. **(B)** Illustration of an experimental setup for recruiting a protein to the membrane with the FKBP/FRB system in *Dictyostelium*. 2 FKBP domains (FX2) are anchored to membrane by cAR1, and the actuator attached to an FRB domain is diffusing in the cytosol. When rapamycin is added, the actuator is recruited to membrane by binding to FKBP. **(C)** Scanning confocal imaging of an AX3 *Dictyostelium* cell expressing a CID system designed to increase RacB and Rac1A activity. The cell is expressing cAR1-FKBP-FKBP (unlabeled) and mCherry-FRB-RacGEF1$_{\Delta N}$, an activator of Rac1 fused to an FRB domain. After rapamycin addition, RacGEF1$_{\Delta N}$ is recruited to the membrane. Consistent with previous reports, the cell became very round with small, short-lived protrusions. Scale bars = 10 μm. *t* = 00:00 indicates rapamycin addition.

mutant. Additionally, confirm that the actuator is acting on its target: For example, membrane localization of a PI(4,5)P2 biosensor should drop after recruiting a PI(4,5) phosphatase (Miao et al., 2017). This can also be done by measuring bulk differences in the levels of a target protein using western blot. However heterogeneous expression of the CID system makes it difficult to observe population-level changes. Finally, confirm that the actuator is affecting the desired pathway by repeating the CID experiment in a knockout or knockdown strain of the intended target protein. For specific guidelines for setting up and performing a CID experiment, see the **Supplementary Methods**.

Optogenetic Control of Cell Activity

In cell biology, optogenetics is a tool for controlling the location and activity of proteins within living cells (**Figure 5**; Toettcher et al., 2011). Optogenetics takes advantage of protein domains that change conformation when exposed to a specific wavelength of light. This conformational change exposes a binding domain or separates protein domains (Kennedy et al., 2010; Strickland et al., 2012; Wang et al., 2016; Van Haren et al., 2018). In conjunction with a patterned illumination system like a Digital Micromirror Device (DMD) or a scanning confocal, optogenetic systems allow for temporal control of protein activity at the subcellular level. This review will focus two separate optogenetic systems which are relatively user-friendly: Cry2$_{PHR}$-CIBN and iLID-SSBP (Kennedy et al., 2010; Guntas et al., 2015). Like CID, these systems can be used to recruit cell migration regulators to the cell membrane by attaching one domain to a uniform membrane protein and one to a catalytic domain. This has some distinct advantages over CID experiments, including subcellular control, reversibility, and the ability to perform many sequential experiments on one dish. However, optogenetics requires more specialized equipment than CID experiments and both systems are activated by 488 nm light (maximally at 440 nm), making it impossible to image green fluorescent proteins. For a summary of optogenetics instructions, see Quick Start Guide 2.

Cry2-CIBN vs. iLID-SSBP

The Cry2$_{PHR}$ domain, based on a plant cryptochrome, binds to CIBN domains in the presence of 450 nm light (Kennedy et al., 2010). Similarly, iLID is a modified LOV domain from *Avena sativa* that binds to a small, engineered peptide – SSBP – when

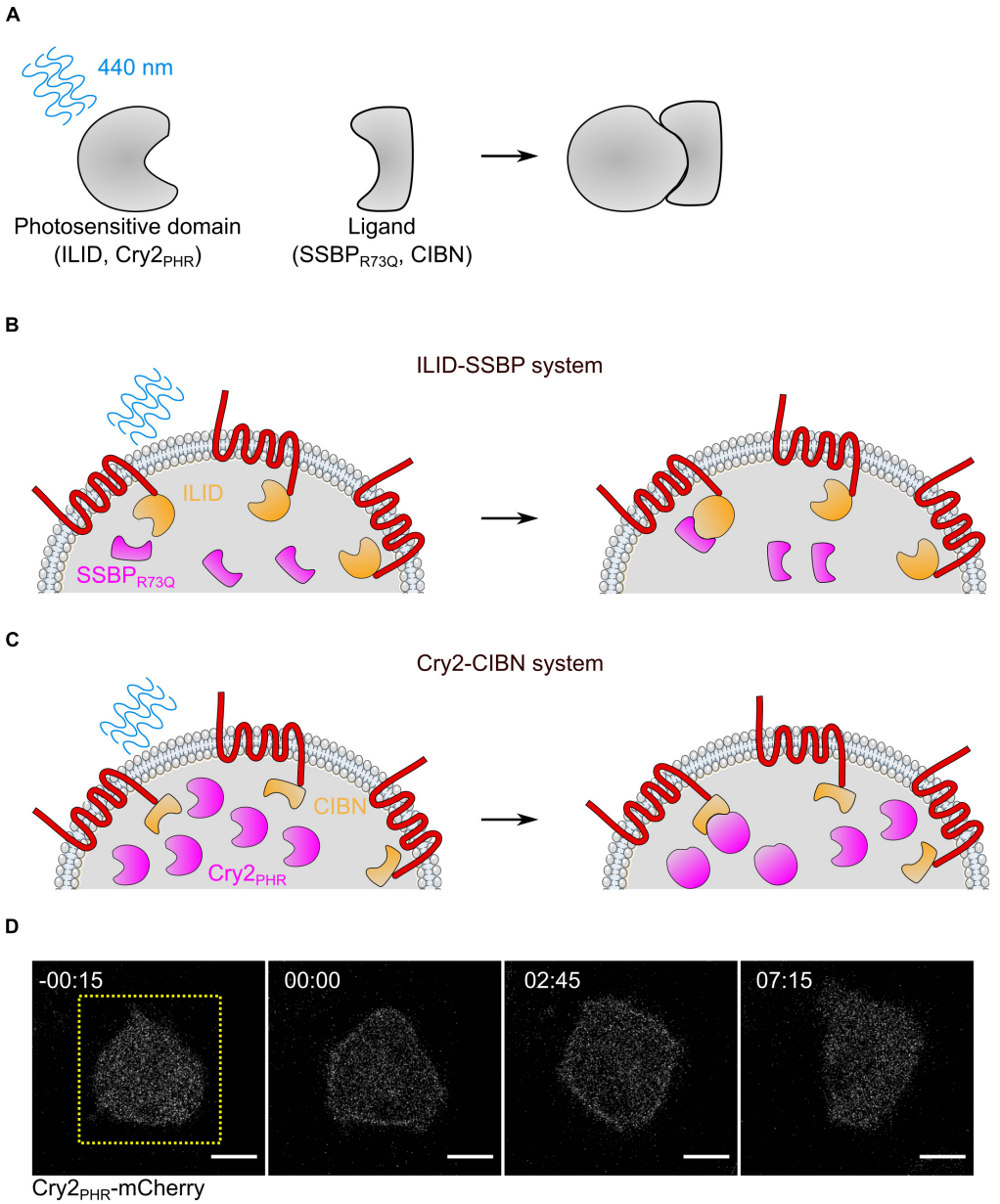

FIGURE 5 | Optogenetic systems for controlling protein localization in *Dictyostelium*. **(A)** Diagram of blue light dimerization systems. In the dark, a photosensitive protein (iLID or Cry2$_{PHR}$) has low affinity for its ligand (SSBP$_{R73Q}$ or CIBN, respectively). When exposed to 450 nm light, a conformational change in the photosensitive domain allows it to bind to the ligand with affinity. **(B,C)** Diagram of iLID-based (B) and Cry2-based (C) systems for recruiting proteins to the membrane in *Dictyostelium*. The actuator (magenta) is recruited to the uniformly distributed membrane anchor (orange) only at the area exposed to blue light. Note that in the iLID system, the photosensitive protein is attached to the membrane anchor, while in the Cry2 system, it is attached to the cytosolic actuator. **(D)** Scanning confocal imaging of Cry2$_{PHR}$ membrane recruitment in AX3 *Dictyostelium* cells. Cells are also expressing an unlabeled membrane anchor, cAR1-CIBN. Yellow dashed square indicates region illuminated with 488 nm light. Scale bars = 5 μm. *t* = 00:00 indicates blue light stimulation.

exposed to blue light (Guntas et al., 2015). The primary difference is turnover time: the Cry2-CIBN interaction has a half-life of 6 min while iLID-SSBP has a half-life of 30 seconds. The short half-life of iLID makes it ideal for subcellular localization because stimulated protein cannot diffuse far from the excitation site. In Cry2 systems, the activated protein can diffuse far away from the light source while remaining active. However, Cry2 requires less periodic reactivation to maintain recruitment, making it easier to work with for whole-cell experiments. In *Dictyostelium*, Cry2 rapidly localizes to the plasma membrane of cells expressing a CIBN membrane anchor, and remains localized minutes later (**Figure 5D** and **Supplementary Movie 2**). Which protein is more suitable for an experiment depends on the specific biology of the system to be perturbed. For more information about designing

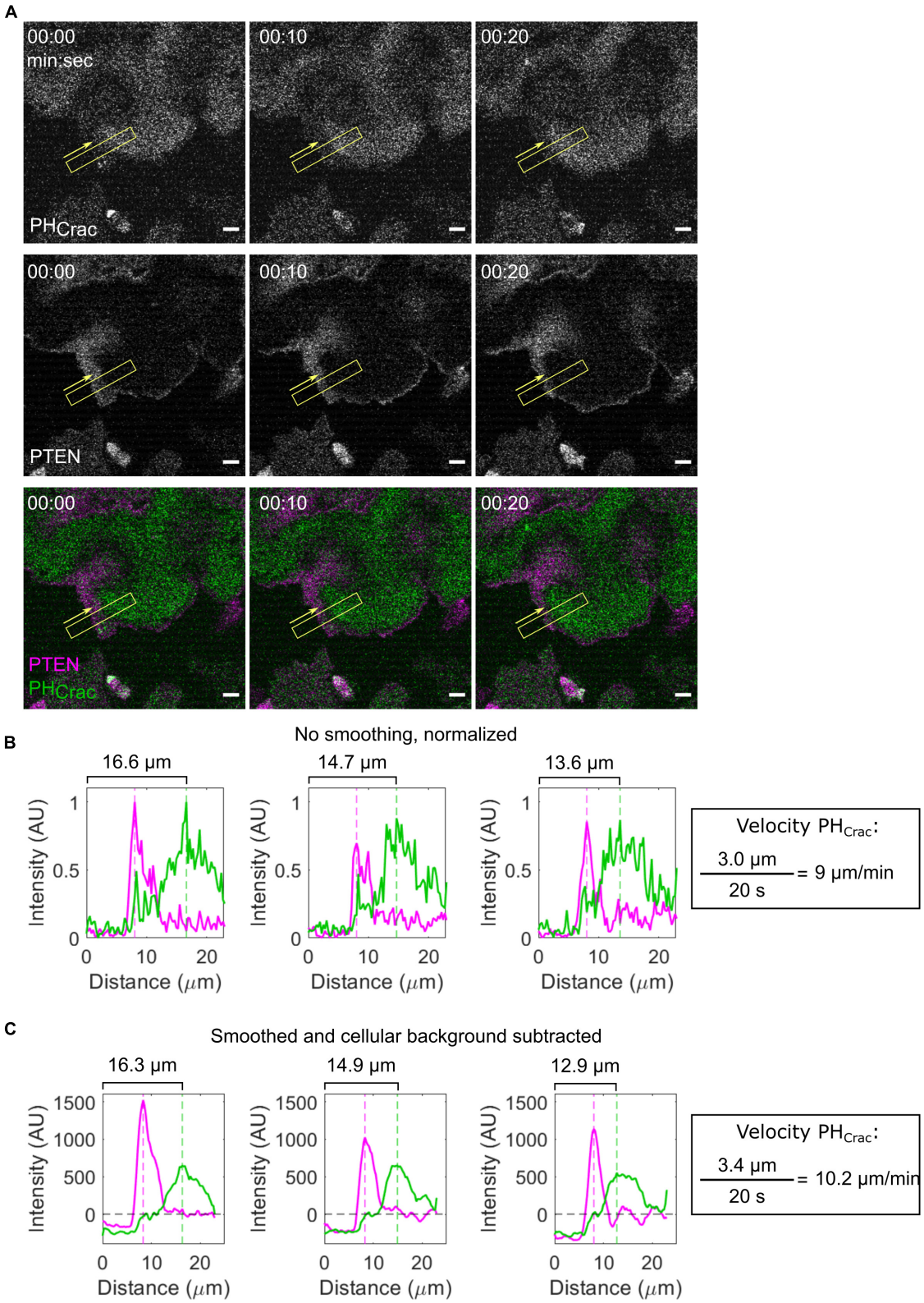

FIGURE 6 | Measuring STEN wave properties. **(A)** Scanning confocal imaging of PIP3 (PH_{Crac}) and a back protein (PTEN) in a giant AX2 *Dictyostelium* cell. Yellow boxes indicate the location and width of the intensity line scan across a membrane wave. Yellow arrows indicate the direction of the line scan. **(B,C)** Raw (B) and smoothed and background-corrected (C) Intensity line scans corresponding to the timepoints in panel **(A)**. The position of the linescan area does not change, while the peak position of PH_{CRAC} decreases. This change can be used to calculate the velocity of the front wave.

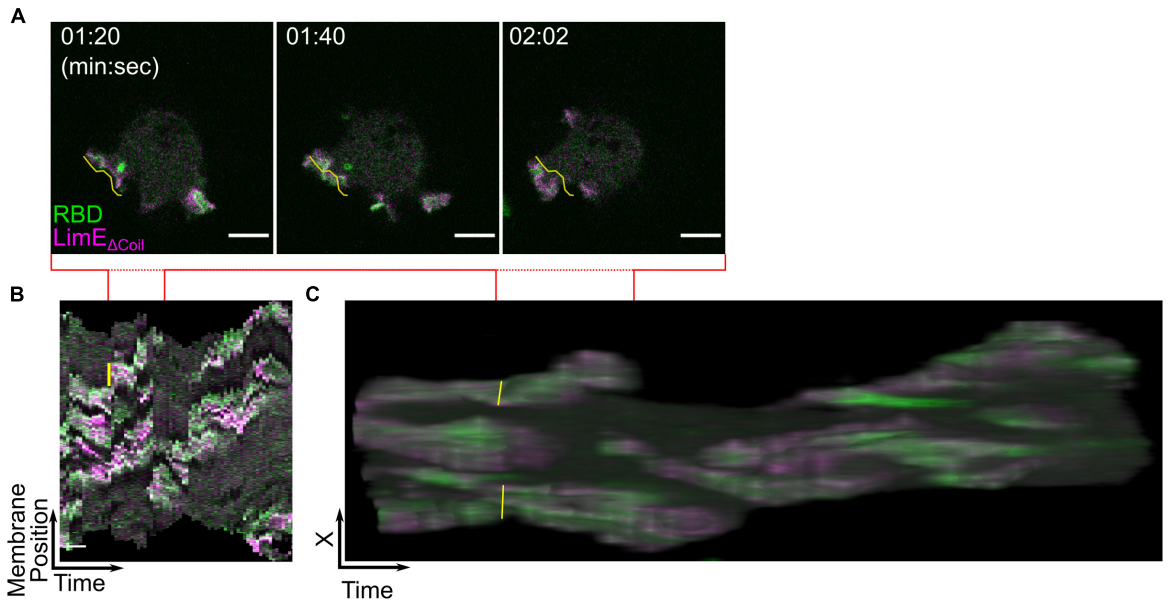

FIGURE 7 | Displaying biosensors on cell protrusions. **(A–C)** Scanning confocal imaging **(A)**, membrane kymograph **(B)**, and t-stack **(C)** of Ras activation (RBD) and actin polymerization (LimE$_{\Delta Coil}$) in AX3 *Dictyostelium* cells. The yellow line highlights the same protrusion in all three images. Scale bars in panels **(A)** = 5 μm and **(B)** = 30 s. *t* = 00:00 indicates the start of acquisition. Red lines indicate the span of time covered by the still images in panel **(A)**.

optogenetic constructs and performing optogenetic experiments, see the **Supplementary Methods**.

ANALYZING SIGNALING CHANGES

There are two primary experimental readouts to quantify after altering cell behavior: cell morphology and biosensor organization. Both properties provide important context that the other does not. For example, it has recently been observed that there are at least two mechanisms which lead to an increase in cell area: increased actin polymerization and increased cell adhesion (Thomas Lampert et al., 2017). Without imaging biosensors of actin polymerization, it would be difficult to determine why a particular actuator leads to cell flattening. The section below will describe how to quantify and display changes in cell morphology and biosensors before and after altering protein activities.

Experimental Guidelines for Analyzing Cells Quantitatively

One of the most important parts of an image analysis pipeline is the initial design of the imaging experiment. There are many problems that are very difficult and time-consuming to fix when processing images which can be avoided when acquiring the data. For example, if two cells touch each other, simple segmentation algorithms often join them into one object, altering the cell area and shape. There are solutions to this problem (e.g., watershed algorithms, Gamarra et al., 2019), but they often need to be tuned dynamically between time points and cells. It is much simpler to plate cells at a low enough density to make two labeled cells touching unlikely. For specific recommendations for plating and imaging cells, see the **Supplementary Methods** and Quick Start Guide 3.

Analyzing Cell Behavior and Morphology

Changing the activity or levels of cell migration regulators can effect cell size, shape, and speed (Devreotes et al., 2017). These properties can be quantified without specialized labels and contain important information about underlying biological changes. Cell shape and motion can be measured manually using a program like ImageJ (Schindelin et al., 2012) or automatically with ImageJ scripting or a coding platform like Matlab or Python's OpenCV library. There are tradeoffs to both methods: identifying cells by hand can be slow and subject to bias. However, writing code that can consistently find and track cells across many different datasets can potentially be more time-consuming than simply tracing the outline of cells frame-by-frame. Some important guidelines for each approach are discussed below.

Manual Quantification

In a CID or optogenetic experiment, either the actuator or the anchor can be used to track cells. Transmitted light techniques like DIC or phase contrast can also be used, though it may produce slightly different results than fluorescence depending on the imaging modality. Manual tracking can quickly uncover changes in cell behavior after perturbing directed migration machinery. For example, in 2017 the Devreotes lab analyzed the motion of cells after lowering the STEN threshold by reducing PI(4,5)P2 levels. These cells exhibited one of three distinct migratory modes: amoeboid cells moved small distances and changed directions, fan-shaped cells moved large distances in a single direction, and oscillators intermittently stopped before

Quick Start Guide 1: CID

- For membrane localization of cell migration regulators, use a uniformly distributed membrane protein like cAR1 with two FKBP domains on the cytoplasmic side.
- Attach catalytic proteins to a FRB domain to create an actuator. Remove any localization domains in the protein. Attach a NES if the actuator localizes to the nucleus.
- When imaging a CID pair alone, express the actuator using pCV5 or pB18 and the anchor using pDM358. When also imaging a biosensor, transform the anchor and actuator in separate pCV5 vectors and the biosensor in a pDM358 background.
- Express proteins using standard protocols for electroporation and K*lebsiella aerogenes* inoculation.
- It is important to always visualize the actuator in order to confirm membrane localization. Fuse the actuator to mCherry or another bright and stable red protein. If using a biosensor in the green channel, attach the anchor to a blue fluorescent protein like CFP or leave it unlabeled and use actuator localization as a proxy for anchor expression.
- To document baseline behavior, image cells for at least 10 minutes before adding rapamycin.
- Add rapamycin to a final concentration of 5 μM.To properly mix the rapamycin with the media, do at most a 1:10 dilution into the imaging chamber. Add dropwise but quickly.
- Allow sufficient time (1-10 minutes) after membrane recruitment to observe a phenotype. This varies between actuators.
- As controls, repeat the CID experiment with an inactive actuator, use a biosensor or a western blot to confirm actuator activity, and redo the experiment in a genetic background that lacks the actuator target.

QUICK START GUIDE 1 | Instructions for designing and carrying out a chemically induced dimerization experiment in *Dictyostelium*.

moving in a new random direction. While these populations could be segregated based on motion alone, they also had different morphologies: amoeboid cells had consistently low areas, fan-shaped cells had larger areas and a clear long axis, and oscillators showed periodic changes in area over a movement cycle (Miao et al., 2017). The observation that altering STEN properties dramatically alters the morphology of a migrating cell suggests that varying STEN and CEN activity could be partially responsible for the diversity of migratory behavior in nature. For more information on how to measure cell shape and track cells, refer to the **Supplementary Methods** and Quick Start Guide 4.

Automatic Quantification

There are many pre-written programs designed to identify and track cells in motion (Emami et al., 2021), although they are not optimized for *Dictyostelium*. For tracking hundreds of cells adapting one of these approaches may be effective. For smaller sample sizes, manually tracking the cells in ImageJ using the Manual Tracking plugin is a simple way to skip a computationally difficult step. Then, with ImageJ, Matlab, or another analysis platform, use the actuator or anchor fluorescence to identify the shape of the cell. Refer to **Supplementary Materials**. Quick Start Guide 5 summarizes this segmentation protocol.

Quick Start Guide 2: Optogenetics

- Cry2-CIBN's slow turnover time makes it convenient for long-term whole-cell experiments because it requires fewer excitations.
- iLID-SSBP's fast turnover rate helps subcellular localization experiments because it prevents proteins from diffusing away for the excitation site in their active form.
- For membrane localization of cell migration regulators, use a uniformly distributed membrane protein like cAR1 or a myristoylation membrane localization domain with an iLid or a CIBN domain on the cytoplasmic side.
- Attach catalytic proteins to a $SSBP_{R73Q}$ or a $Cry2_{PHR}$ domain to create an actuator. Remove any localization domains in the protein. If the actuator localizes to the nucleus, attach a NES.
- When only imaging an optogenetic pair, express the actuator using pCV5 and the anchor using pDM358. To also image biosensors, set up a dual expression system.
- Express proteins using standard protocols for electroporation and K*lebsiella aerogenes* inoculation.
- Always visualize the actuator in order to confirm membrane localization after activation. Fuse the actuator to mCherry or another stable, bright red protein. Do not image any protein in the green channel if possible because it will activate the optogenetic protein. If imaging a biosensor, use the red channel and move the actuator to a far-red channel.
- To document baseline behavior, image cells for at least 10 minutes before stimulation.
- For localized recruitment, shine 450 or 488 nm light in a small (3-5 μm) region 1-2 μm outside of the cell. This prevents activation in other parts of the cell.
- For global recruitment, acquire a full-field image using a 488 or 450 nm laser.
- Allow sufficient time (1-10 minutes) after membrane recruitment to observe a phenotype. This varies between actuators.
- Re-stimulate the cell at about half of a half-life (every 15-20 seconds for iLid, 3-4 minutes for Cry2) to maintain recruitment.
- It is useful to show that the phenotype is reversible by removing stimulation and observing the cell after membrane localization goes away. This may not be possible if the cell has been photodamaged.
- As controls, repeat the experiment with an inactive actuator, use a biosensor or a western blot to confirm actuator activity, and redo the experiment in a genetic background that lacks the actuator target.

QUICK START GUIDE 2 | Instructions for designing and carrying out an optogenetic experiment with Cry2-CIBN or an iLID system in *Dictyostelium*.

Quick Start Guide 3: Ideal experimental practice for analysis

- Plate cells at 2 x 10^5 cells/cm^2 at first and then adjust the density based on experimental needs.
- Starve cells by suspending them in DB buffer at 2 * 10^7 cells/ml for 1-2 hours before imaging to help prevent photodamage.
- Image cells with a 1.45-1.49 NA oil immersion lens.
- An image pixel size of 110 nm is ideal for resolution and contrast.
- Acquire at the highest exposure possible and the fastest speed possible which does not harm the cell over the imaging period.

QUICK START GUIDE 3 | Guidelines for optimizing *Dictyostelium* imaging conditions, with the goal of quantitatively analyzing the output.

Quick Start Guide 4: Manual Analysis of Cell Properties

- To identify and track cells, use transmitted light or markers like a CID actuator or anchor.
- Use ImageJ to manually analyze cell properties.
- Use the ImageJ Manual Tracking plugin to track cell motion and calculate speeds
- Use the Freehand Drawing Tool or the Polygon Selection Tool to identify the outline of the cell.
- Save progress when identifying cells using the ROI Manager.

QUICK START GUIDE 4 | Instructions for manually analyzing cell shape and motion in migrating *Dictyostelium* cells.

Quantifying Fluorescent Biosensors

Fluorescent biosensors report on the level and location, and activity of specific molecules within the cell. In the context of directed cell migration, STEN and CEN biosensors localize along the cell periphery in patches to shape protrusions and travel along the bottom membrane as waves. The properties of these patches and waves (size, brightness, speed, location) contain important information about the properties of the directed migration network. How to quantify changes in STEN and CEN by monitoring bottom membrane waves and protrusions will be discussed here below.

Quantifying Signal Transduction Excitable Network-Cytoskeletal Excitable Network Wave Properties

Signal transduction excitable network and CEN biosensors travel in waves of front activity and complementary waves of back activity on the cell bottom (**Figure 6A** and **Supplementary Movie 3**). Previously, it has been shown that the peak-to-peak distance of STEN and CEN biosensors reports on their order in the directed migration pathway (Miao et al., 2019). Additionally, their speed, size, and propagation distance correspond to the timescale, activity, and threshold of STEN and CEN. Many of these properties can be measured by hand in ImageJ: using the line tool, draw a line in the direction of wave propagation which includes the wave and cellular background on both sides. Then, the Plot Profile tool can be used to obtain the intensity of all pixels along that line for each biosensor. Increasing the width of the line causes the tool to average over more pixels, decreasing measurement noise. After subtracting cellular background, the distance between two biosensors can be calculated by the difference between the maxima of each biosensor. This intensity profile can be also used to calculate the speed of the wave between frames and the integrated intensity of the biosensor (**Figures 6B,C**). For example, PI(3,4,5)P3 biosensor PH_{CRAC} travels along the bottom membrane as a part of a front STEN wave (**Figure 6A** and **Supplementary Movie 3**). Back proteins, like PI(3,4,5)P3 phosphatase PTEN, are excluded from this same area. The speed of the STEN wave can be obtained by measuring the location of the PH_{Crac} maxima over time (**Figures 6B,C**). This speed is directly influenced by STEN and CEN activity and can be increased by lowering the STEN

Quick Start Guide 5: Sample Segmentation Protocol of Whole Cells

- Using the tracking coordinates in an analysis platform of choice, isolate the cell and a small amount of background from the larger image.
- Apply an intensity threshold using Otsu's method or by removing all pixels less than 1 standard deviation above the mean brightness.
- Use a morphological closing operation to fill cracks in binary masks and remove small dots.
- Fill holes in the remaining objects.
- Set a size threshold to remove small objects.
- Use software (eg RegionProps in Matlab) to retrieve information on the size and shape of the remaining objects.
- Monitor the output of the segmentation protocol to ensure that it is functioning correctly between time points and cells.

QUICK START GUIDE 5 | Sample protocol for the automated identification of a *Dictyostelium* cell from microscopy images.

Quick Start Guide 6: Displaying and analyzing biosensor localization

- Use the Line profile Tool in ImageJ to create intensity profiles of STEN-CEN biosensors in waves. These profiles can be used to calculate the intensity, speed, and distance between biosensors
- STEN-CEN waves can also be identified automatically in Matlab, ImageJ, or Python.
- Using Matlab, generate membrane kymographs of biosensors to measure the width, intensity, duration, and speed of STEN-CEN events on the periphery.
- Use ImageJ 3D Projection plugins to create 3D images where the third dimension is time. These T-stacks can be used to visualize the width, length, and duration of signaling and cytoskeletal events on the edge of the cell.

QUICK START GUIDE 6 | Guidelines for displaying and analyzing fluorescent biosensor dynamics on the cell membrane.

threshold (Miao et al., 2019). Because these waves are bright and large structures, the previously described segmentation protocols can also be used for automated identification and analysis.

Quantifying Signal Transduction Excitable Network-Cytoskeletal Excitable Network Events on the Cell Periphery

Like the bottom membrane, the size and shape of STEN-CEN events that create protrusions on the cell periphery contain important information about network properties (Miao et al., 2017). It is possible to measure the size of cell protrusions by hand using ImageJ. However, the number of measurements required per cell may be prohibitive. For example, actin polymerization biosensor $\text{LimE}_{\Delta Coil}$ and Ras activity biosensor RBD colocalize at multiple protrusions along the *Dictyostelium* cell perimeter (**Figure 7A** and **Supplementary Movie 4**). Each of these protrusions undergoes dramatic shape changes between frames, making the assessment of a protrusion's behavior over longer times difficult. To measure signaling events on cell perimeter, creating membrane kymographs and t-stacks is recommended. The basic concept of a membrane kymograph is simple: trace the cell membrane at each frame, divide the traced line into equidistant points, and then display the biosensor intensity at each point as a vertical line. Finally, stack each timepoint's vertical line horizontally to create a single image which reports on changes in biosensor intensity on the membrane across an entire movie. A single protrusion in the original image (**Figure 7A**, yellow line) is simplified to small region of the kymograph

(**Figure 7B**, yellow line) where the height indicates the arc length on the membrane and the width indicates the duration. These quantities can be obtained with single measurements in ImageJ. The code to generate such a kymograph is flexible and available upon request. T-stacks are made by taking a timelapse movie of a migrating cell and creating a 3D projection where the third axis is time (**Figure 7C**). When viewed in the X-T plane (e.g., looking at the edge of the cell over time), the duration, movement, and width, and length of protrusions can be seen and measured. Quick Start Guide 6 details these options.

CONCLUSION

Future Applications of Chemically Induced Dimerization and Optogenetic Techniques to Study Cell Migration

In conjunction with other emerging technologies, CID and optogenetic techniques can help deepen our understanding of how cells move toward signals through difficult environments. For example, micropatterning and microfluidic techniques can subject cells to geometrical and mechanical challenges like they may encounter in a dynamic tissue (Reversat et al., 2020). Acutely altering the activity of individual molecules in a cell in this situation can teach us what is and is not sufficient for robust migration. Additionally, it is possible to use modern imaging technologies like Lattice Lightsheet Microscopy (LLSM) to get dynamic three-dimensional images of cellular structures at high resolution (Gao et al., 2012; Fritz-Laylin et al., 2017). LLSM could allow us to measure how the true structure of a protrusion or STEN-CEN wave changes in response to changes in network regulators. Finally, machine learning algorithms capable of automatically identifying cells and subcellular structures (Al-Kofahi et al., 2018) could help identify subtle changes to cell shape and activity which are not apparent in small datasets. Together, these approaches will help to develop and refine the current working model of directed migration in eukaryotes.

Using Live Cell Perturbations to Study Other Problems in *Dictyostelium*

Many of the same techniques described here for studying cell migration can also be applied to other biological problems. For example, *Dictyostelium* are commonly used to study mechanotransduction and cytokinesis (Liu and Robinson, 2018). Recruiting a Myosin regulator to the cortex or an Aurora Kinase effector to the midzone during cytokinesis may give important quantitative insight about the network that localizes and contracts the cytokinetic ring. Additionally, the formation of multicellular slugs and fruiting bodies during the *Dictyostelium* life cycle is a popular model for multicellular organization (Williams, 2010). Changing the activity of specific molecules at particular times during development many have large effects on body shape which would not be apparent from longer-term genetic manipulations. Finally, *Dictyostelium* is an excellent model for studying micropinocytosis and phagocytosis (Vogel et al., 1980; Bloomfield et al., 2015; Dunn et al., 2018). Macropinocytosis and phagocytosis are tightly regulated in time and share many regulators with directed migration. This similarity makes them an excellent candidate for study using the tools described above. Emerging techniques in synthetic and computational biology will allow us to study old problems in *Dictyostelium* with new levels of detail and insight.

Applying Insights From *Dictyostelium* to Other Organisms

As a model organism, *Dictyostelium* has expanded our understanding of chemotaxis. Importantly, lessons learned in *Dictyostelium* can be applied to other systems. For example, in *Dictyostelium* chemotaxis: gradient sensing, signal transduction and cell motility. These processes all require interactions with receptors on the cell surface which trigger polarized distribution of downstream effectors located at front and back. This distribution rearranges the cytoskeleton in order to move toward a gradient. The signaling network discovered in *Dictyostelium* is also highly conserved in eukaryotic cells (Artemenko et al., 2014). Because of this, and because *Dictyostelium* is easy to culture, manipulate, and image, it is a good platform for designing and testing CID and optogenetic tools for use in other cell migration models. For example, an actuator which lowers PIP2 levels was recently adapted for use in mammalian breast epithelial cells (Zhan et al., 2020). We propose using *Dictyostelium* as a system to rapidly generate hypotheses and build models which can then be broadly applied.

AUTHOR CONTRIBUTIONS

JK and YL wrote the manuscript, acquired the data, and made figures. PD provided conceptual guidance and edited the manuscript. All authors contributed to the article and approved the submitted version.

FUNDING

NIGMS GM118177 was an R35 MIRA grant. The AFOSR MURI grant was an interdisciplinary award shared with the University of Maryland. All funders are responsible for all aspects of the research.

ACKNOWLEDGMENTS

We thank members of the Devreotes lab for feedback and help in preparing the manuscript.

SUPPLEMENTARY MATERIAL

The Supplementary Material for this article can be found online at: https://www.frontiersin.org/articles/10.3389/fcell.2021.740205/full#supplementary-material

Supplementary Movie 1 | Increasing RacB and Rac1A activity using a CID system. Scanning confocal imaging of an AX3 *Dictyostelium* cell (transmitted light, green) expressing a CID system designed to increase RacB and Rac1A activity. The cell is expressing cAR1-FKBP-FKBP (unlabeled) and mCherry-FRB-RacGEF1$_{\Delta\ N}$ (magenta), an activator of Rac1 fused to an FRB domain. After rapamycin addition, RacGEF1$_{\Delta\ N}$ is recruited to the membrane. Consistent with previous reports, the cell became very round with small, short-lived protrusions. *t* = 00:00 indicates rapamycin addition. Playback is 18 frames per second.

Supplementary Movie 2 | The Cry2$_{PHR}$-CIBN system in *Dictyostelium*. Scanning confocal imaging of Cry2$_{PHR}$ membrane recruitment in AX3 *Dictyostelium* cells. Cells are also expressing an unlabeled membrane anchor, cAR1-CIBN. Yellow square indicates region illuminated with 488 nm light. *t* = 00:00 indicates blue light stimulation. Playback is 22 frames per second.

Supplementary Movie 3 | Traveling STEN waves on the bottom of a giant cell. Scanning confocal imaging of PIP3 (PH$_{Crac}$, green) and a back protein (PTEN, magenta) in a giant AX2 *Dictyostelium* cell. Playback is 2 frames per second.

Supplementary Movie 4 | Signal transduction excitable network-CEN protrusions on the cell periphery. Scanning confocal imaging of Ras activation (RBD, green) and actin polymerization (LimE$_{\Delta\ Coil}$, magenta) in AX3 *Dictyostelium* cells. Playback is 15 frames per second.

REFERENCES

Al-Kofahi, Y., Zaltsman, A., Graves, R., Marshall, W., and Rusu, M. (2018). A deep learning-based algorithm for 2-D cell segmentation in microscopy images. *BMC Bioinformatics* 19:365. doi: 10.1186/s12859-018-2375-z

Annesley, S. J., and Fisher, P. R. (2009). Dictyostelium discoideum-a model for many reasons. *Mol. Cell. Biochem.* 329, 73–91. doi: 10.1007/s11010-009-0111-8

Arai, Y., Shibata, T., Matsuoka, S., Sato, M. J., Yanagida, T., and Ueda, M. (2010). Self-organization of the phosphatidylinositol lipids signaling system for random cell migration. *Proc. Natl. Acad. Sci. U. S. A.* 107, 12399–12404. doi: 10.1073/pnas.0908278107

Arrieumerlou, C., and Meyer, T. (2005). A local coupling model and compass parameter for eukaryotic chemotaxis. *Dev. Cell* 8, 215–227. doi: 10.1016/j.devcel.2004.12.007

Artemenko, Y., Axiotakis, L., Borleis, J., Iglesias, P. A., and Devreotes, P. N. (2016). Chemical and mechanical stimuli act on common signal transduction and cytoskeletal networks. *Proc. Natl. Acad. Sci. U. S. A.* 113, E7500–E7509. doi: 10.1073/pnas.1608767113

Artemenko, Y., Lampert, T. J., and Devreotes, P. N. (2014). Moving towards a paradigm: common mechanisms of chemotactic signaling in Dictyostelium and mammalian leukocytes. *Cell. Mol. Life Sci.* 71, 3711–3747. doi: 10.1007/s00018-014-1638-8

Benard, V., Bohl, B. P., and Bokoch, G. M. (1999). Characterization of Rac and Cdc42 activation in chemoattractant- stimulated human neutrophils using a novel assay for active GTPases. *J. Biol. Chem.* 274, 13198–13204. doi: 10.1074/jbc.274.19.13198

Bivona, T. G., Wiener, H. H., Ahearn, I. M., Silletti, J., Chiu, V. K., and Philips, M. R. (2004). Rap1 up-regulation and activation on plasma membrane regulates T cell adhesion. *J. Cell Biol.* 164, 461–470. doi: 10.1083/JCB.200311093

Bloomfield, G., Traynor, D., Sander, S. P., Veltman, D. M., Pachebat, J. A., and Kay, R. R. (2015). Neurofibromin controls macropinocytosis and phagocytosis in Dictyostelium. *Elife* 4:e04940. doi: 10.7554/eLife.04940

Bolourani, P., Spiegelman, G. B., and Weeks, G. (2006). Delineation of the roles played by RasG and RasC in cAMP-dependent signal transduction during the early development of Dictyostelium discoideum. *Mol. Biol. Cell* 17, 4543–4550. doi: 10.1091/mbc.E05-11-1019

Bretschneider, T., Diez, S., Anderson, K., Heuser, J., Clarke, M., Müller-Taubenberger, A., et al. (2004). Dynamic Actin Patterns and Arp2/3 Assembly at the Substrate-Attached Surface of Motile Cells. *Curr. Biol.* 14, 1–10. doi: 10.1016/J.CUB.2003.12.005

Cai, H., Das, S., Kamimura, Y., Long, Y., Parent, C. A., and Devreotes, P. N. (2010). Ras-mediated activation of the TORC2-PKB pathway is critical for chemotaxis. *J. Cell Biol.* 190, 233–245. doi: 10.1083/jcb.201001129

Cha, I., and Jeon, T. J. (2011). Dynamic localization of the actin-bundling protein cortexillin i during cell migration. *Mol. Cells* 32, 281–287. doi: 10.1007/s10059-011-0072-0

Chiu, V. K., Bivona, T., Hach, A., Sajous, J. B., Silletti, J., Wiener, H., et al. (2002). Ras signalling on the endoplasmic reticulum and the Golgi. *Nat. Cell Biol.* 4, 343–350.

Chung, C. Y., and Firtel, R. A. (1999). PAKa, a putative PAK family member, is required for cytokinesis and the regulation of the cytoskeleton in Dictyostelium discoideum cells during chemotaxis. *J. Cell Biol.* 147, 559–575. doi: 10.1083/jcb.147.3.559

Décave, E., Rieu, D., Dalous, J., Fache, S., Brechet, Y., Fourcade, B., et al. (2003). Shear flow-induced motility of Dictyostelium discoideum cells on solid substrate. *J. Cell Sci.* 116, 4331–4343. doi: 10.1242/jcs.00726

Derose, R., Miyamoto, T., and Inoue, T. (2013). Manipulating signaling at will: chemically-inducible dimerization (CID) techniques resolve problems in cell biology. *Pflugers Arch.* 465, 409–417. doi: 10.1007/s00424-012-1208-6

Devreotes, P. N., Bhattacharya, S., Edwards, M., Iglesias, P. A., Lampert, T., and Miao, Y. (2017). Excitable Signal Transduction Networks in Directed Cell Migration. *Annu. Rev. Cell Dev. Biol.* 33, 103–125. doi: 10.1146/annurev-cellbio-100616-060739

Dormann, D., Weijer, G., Parent, C. A., Devreotes, P. N., and Weijer, C. J. (2002). Visualizing PI3 kinase-mediated cell-cell signaling during Dictyostelium development. *Curr. Biol.* 12, 1178–1188. doi: 10.1016/S0960-9822(02)00950-8

Dunn, J. D., Bosmani, C., Barisch, C., Raykov, L., Lefrançois, L. H., Cardenal-Muñoz, E., et al. (2018). Eat prey, live: dictyostelium discoideum as a model for cell-autonomous defenses. *Front. Immunol.* 8:1906. doi: 10.3389/fimmu.2017.01906

Edwards, M., Cai, H., Abubaker-Sharif, B., Long, Y., Lampert, T. J., and Devreotes, P. N. (2018). Insight from the maximal activation of the signal transduction excitable network in Dictyostelium discoideum. *Proc. Natl. Acad. Sci. U. S. A.* 115, E3722–E3730. doi: 10.1073/pnas.1710480115

Emami, N., Sedaei, Z., and Ferdousi, R. (2021). Computerized cell tracking: current methods, tools and challenges. *Vis. Informatics* 5, 1–13. doi: 10.1016/j.visinf.2020.11.003

Fegan, A., White, B., Carlson, J. C. T., and Wagner, C. R. (2010). Chemically controlled protein assembly: techniques and applications. *Chem. Rev.* 110, 3315–3336. doi: 10.1021/cr8002888

Fritz-Laylin, L. K., Riel-Mehan, M., Chen, B. C., Lord, S. J., Goddard, T. D., Ferrin, T. E., et al. (2017). Actin-Based protrusions of migrating neutrophils are intrinsically lamellar and facilitate direction changes. *Elife* 6:e26990. doi: 10.7554/eLife.26990

Gamarra, M., Zurek, E., Escalante, H. J., Hurtado, L., and San-Juan-Vergara, H. (2019). Split and merge watershed: a two-step method for cell segmentation in fluorescence microscopy images. *Biomed. Signal Process. Control* 53:101575. doi: 10.1016/j.bspc.2019.101575

Gao, L., Shao, L., Higgins, C. D., Poulton, J. S., Peifer, M., Davidson, M. W., et al. (2012). Noninvasive imaging beyond the diffraction limit of 3D dynamics in thickly fluorescent specimens. *Cell* 151, 1370–1385. doi: 10.1016/j.cell.2012.10.008

Gebbie, L., Benghezal, M., Cornillon, S., Froquet, R., Cherix, N., Malbouyres, M., et al. (2004). Phg2, a Kinase Involved in Adhesion and Focal Site Modeling in Dictyostelium. *Mol. Biol. Cell* 15, 3915–3925. doi: 10.1091/MBC.E03-12-0908

Gerhardt, M., Ecke, M., Walz, M., Stengl, A., Beta, C., and Gerisch, G. (2014). Actin and PIP3 waves in giant cells reveal the inherent length scale of an excited state. *J. Cell Sci.* 127, 4507–4517. doi: 10.1242/jcs.156000

Gerisch, G., Bretschneider, T., Müller-Taubenberger, A., Simmeth, E., Ecke, M., Diez, S., et al. (2004). Mobile actin clusters and traveling waves in cells recovering from actin depolymerization. *Biophys. J.* 87, 3493–3503. doi: 10.1529/biophysj.104.047589

Gerisch, G., Ecke, M., Neujahr, R., Prassler, J., Stengl, A., Hoffmann, M., et al. (2013). Membrane and actin reorganization in electropulseinduced cell fusion. *J. Cell Sci.* 126, 2069–2078. doi: 10.1242/jcs.124073

Gerisch, G., Ecke, M., Wischnewski, D., and Schroth-Diez, B. (2011). Different modes of state transitions determine pattern in the Phosphatidylinositide-Actin system. *BMC Cell Biol.* 12:42. doi: 10.1186/1471-2121-12-42

Gerisch, G., Schroth-Diez, B., Müller-Taubenberger, A., and Ecke, M. (2012). PIP3 waves and PTEN dynamics in the emergence of cell polarity. *Biophys. J.* 103, 1170–1178. doi: 10.1016/j.bpj.2012.08.004

Guntas, G., Hallett, R. A., Zimmerman, S. P., Williams, T., Yumerefendi, H., Bear, J. E., et al. (2015). Engineering an improved light-induced dimer (iLID) for controlling the localization and activity of signaling proteins. *Proc. Natl. Acad. Sci. U. S. A.* 112, 112–117. doi: 10.1073/pnas.1417910112

Hecht, I., Kessler, D. A., and Levine, H. (2010). Transient localized patterns in noise-driven reaction-diffusion systems. *Phys. Rev. Lett.* 104:158301. doi: 10.1103/physrevlett.104.158301

Huang, C. H., Tang, M., Shi, C., Iglesias, P. A., and Devreotes, P. N. (2013). An excitable signal integrator couples to an idling cytoskeletal oscillator to drive cell migration. *Nat. Cell Biol.* 15, 1307–1316. doi: 10.1038/ncb2859

Huang, Y. E., Iijima, M., Parent, C. A., Funamoto, S., Firtel, R. A., and Devreotes, P. (2003). Receptor-mediated regulation of PI3Ks confines PI(3,4,5)P3 to the leading edge of chemotaxing cells. *Mol. Biol. Cell* 14, 1913–1922. doi: 10.1091/mbc.E02-10-0703

Iijima, M., and Devreotes, P. (2002). Tumor suppressor PTEN mediates sensing of chemoattractant gradients. *Cell* 109, 599–610. doi: 10.1016/S0092-8674(02)00745-6

Janetopoulos, C., Ma, L., Devreotes, P. N., and Iglesias, P. A. (2004). Chemoattractant-induced phosphatidylinositol 3,4,5-trisphosphate accumulation is spatially amplified and adapts, independent of the actin cytoskeleton. *Proc. Natl. Acad. Sci. U. S. A.* 101, 8951–8956. doi: 10.1073/pnas.0402152101

Kae, H., Lim, C. J., Spiegelman, G. B., and Weeks, G. (2004). Chemoattractant-induced Ras activation during Dictyostelium aggregation. *EMBO Rep.* 5, 602–606. doi: 10.1038/sj.embor.7400151

Kennedy, M. J., Hughes, R. M., Peteya, L. A., Schwartz, J. W., Ehlers, M. D., and Tucker, C. L. (2010). Rapid blue-light-mediated induction of protein interactions in living cells. *Nat. Methods* 7, 973–975. doi: 10.1038/nmeth.1524

Kortholt, A., Kataria, R., Keizer-Gunnink, I., Van Egmond, W. N., Khanna, A., and Van Haastert, P. J. M. (2011). Dictyostelium chemotaxis: essential Ras activation and accessory signalling pathways for amplification. *EMBO Rep.* 12, 1273–1279. doi: 10.1038/embor.2011.210

Kortholt, A., Keizer-Gunnink, I., Kataria, R., and Haastert, P. J. M. V. (2013). Ras activation and symmetry breaking during dictyostelium chemotaxis. *J. Cell Sci.* 126, 4502–4513. doi: 10.1242/jcs.132340

Kriebel, P. W., Barr, V. A., and Parent, C. A. (2003). Adenylyl cyclase localization regulates streaming during chemotaxis. *Cell* 112, 549–560. doi: 10.1016/S0092-8674(03)00081-3

Levine, H., Kessler, D. A., and Rappel, W. J. (2006). Directional sensing in eukaryotic chemotaxis: a balanced inactivation model. *Proc. Natl. Acad. Sci. U. S. A.* 103, 9761–9766. doi: 10.1073/pnas.0601302103

Li, X., Miao, Y., Pal, D. S., and Devreotes, P. N. (2020). Excitable networks controlling cell migration during development and disease. *Semin. Cell Dev. Biol.* 100, 133–142. doi: 10.1016/j.semcdb.2019.11.001

Liu, Y., and Robinson, D. (2018). Recent advances in cytokinesis: understanding the molecular underpinnings [version 1; referees: 2 approved]. *F1000Res.* 7:1849. doi: 10.12688/f1000research.16502.1

Loovers, H. M., Postma, M., Keizer-Gunnink, I., Huang, Y. E., Devreotes, P. N., and Van Haastert, P. J. M. (2006). Distinct roles of PI(3,4,5)P3 during chemoattractant signaling in Dictyostelium: a quantitative in vivo analysis by inhibition of PI3-kinase. *Mol. Biol. Cell* 17, 1503–1513. doi: 10.1091/mbc.E05-09-0825

Mato, J. M., Losada, A., Nanjundiah, V., and Konijn, T. M. (1975). Signal input for a chemotactic response in the cellular slime mold Dictyostelium discoideum. *Proc. Natl. Acad. Sci. U. S. A.* 72, 4991–4993. doi: 10.1073/pnas.72.12.4991

Meili, R., Ellsworth, C., and Firtel, R. A. (2000). A novel Akt/PKB-related kinase is essential for morphogenesis in Dictyostelium. *Curr. Biol.* 10, 708–717. doi: 10.1016/S0960-9822(00)00536-4

Meili, R., Ellsworth, C., Lee, S., Reddy, T. B. K., Ma, H., and Firtel, R. A. (1999). Chemoattractant-mediated transient activation and membrane localization of Akt/PKB is required for efficient chemotaxis to cAMP in Dictyostelium. *EMBO J.* 18, 2092–2105. doi: 10.1093/EMBOJ/18.8.2092

Meinhardt, H. (1999). Orientation of chemotactic cells and growth cones: models and mechanisms. *J. Cell Sci.* 112, 2867–2874. doi: 10.1242/jcs.112.17.2867

Meinhardt, H., and Gierer, A. (2000). Pattern formation by local self-activation and lateral inhibition. *Bioessays* 22, 753–760. doi: 10.1002/1521-1878

Miao, Y., Bhattacharya, S., Banerjee, T., Abubaker-Sharif, B., Long, Y., Inoue, T., et al. (2019). Wave patterns organize cellular protrusions and control cortical dynamics. *Mol. Syst. Biol.* 15:e8585. doi: 10.15252/msb.20188585

Miao, Y., Bhattacharya, S., Edwards, M., Cai, H., Inoue, T., Iglesias, P. A., et al. (2017). Altering the threshold of an excitable signal transduction network changes cell migratory modes. *Nat. Cell Biol.* 19, 329–340. doi: 10.1038/ncb3495

Neilson, M. P., Veltman, D. M., van Haastert, P. J. M., Webb, S. D., Mackenzie, J. A., and Insall, R. H. (2011). Chemotaxis: a feedback-based computational model robustly predicts multiple aspects of real cell behaviour. *PLoS Biol.* 9:e1000618. doi: 10.1371/journal.pbio.1000618

Nichols, J. M. E., Veltman, D., and Kay, R. R. (2015). Chemotaxis of a model organism: progress with Dictyostelium. *Curr. Opin. Cell Biol.* 36, 7–12. doi: 10.1016/j.ceb.2015.06.005

Nishikawa, M., Hörning, M., Ueda, M., and Shibata, T. (2014). Excitable signal transduction induces both spontaneous and directional cell asymmetries in the phosphatidylinositol lipid signaling system for eukaryotic chemotaxis. *Biophys. J.* 106, 723–734. doi: 10.1016/j.bpj.2013.12.023

Okumoto, S., Jones, A., and Frommer, W. B. (2012). Quantitative imaging with fluorescent biosensors. *Annu. Rev. Plant Biol.* 63, 663–706. doi: 10.1146/annurev-arplant-042110-103745

Papakonstanti, E. A., Ridley, A. J., and Vanhaesebroeck, B. (2007). The p110δ isoform of PI 3-kinase negatively controls RhoA and PTEN. *EMBO J.* 26, 3050–3061. doi: 10.1038/sj.emboj.7601763

Parent, C. A., Blacklock, B. J., Froehlich, W. M., Murphy, D. B., and Devreotes, P. N. (1998). G protein signaling events are activated at the leading edge of chemotactic cells. *Cell* 95, 81–91. doi: 10.1016/S0092-8674(00)81784-5

Park, J., Holmes, W. R., Lee, S. H., Kim, H. N., Kim, D. H., Kwak, M. K., et al. (2017). Mechanochemical feedback underlies coexistence of qualitatively distinct Cell polarity patterns within diverse cell populations. *Proc. Natl. Acad. Sci. U. S. A.* 114, E5750–E5759. doi: 10.1073/pnas.1700054114

Park, K. C., Rivero, F., Meili, R., Lee, S., Apone, F., and Firtel, R. A. (2004). Rac regulation of chemotaxis and morphogenesis in Dictyostelium. *EMBO J.* 23, 4177–4189. doi: 10.1038/SJ.EMBOJ.7600368

Reversat, A., Gaertner, F., Merrin, J., Stopp, J., Tasciyan, S., Aguilera, J., et al. (2020). Cellular locomotion using environmental topography. *Nature* 582, 582–585. doi: 10.1038/s41586-020-2283-z

Riedl, J., Crevenna, A. H., Kessenbrock, K., Yu, J. H., Neukirchen, D., Bista, M., et al. (2008). Lifeact: a versatile marker to visualize F-actin. *Nat. Methods* 5, 605–607. doi: 10.1038/nmeth.1220

Sasaki, A. T., Chun, C., Takeda, K., and Firtel, R. A. (2004). Localized Ras signaling at the leading edge regulates PI3K, cell polarity, and directional cell movement. *J. Cell Biol.* 167, 505–518. doi: 10.1083/jcb.200406177

Schindelin, J., Arganda-Carreras, I., Frise, E., Kaynig, V., Longair, M., Pietzsch, T., et al. (2012). Fiji: an open-source platform for biological-image analysis. *Nat. Methods* 9, 676–682. doi: 10.1038/nmeth.2019

Schroth-Diez, B., Gerwig, S., Ecke, M., Heger, R., Diez, S., and Gerisch, G. (2009). Propagating waves separate two states of actin organization in living cells. *HFSP J.* 3, 412–427. doi: 10.2976/1.3239407

Shibata, T., Nishikawa, M., Matsuoka, S., and Ueda, M. (2012). Modeling the self-organized phosphatidylinositol lipid signaling system in chemotactic cells using quantitative image analysis. *J. Cell Sci.* 125, 5138–5150. doi: 10.1242/jcs.108373

Shu, S., Liu, X., and Korn, E. D. (2005). Blebbistatin and blebbistatin-inactivated myosin II inhibit myosin II-independent processes in Dictyostelium. *Proc. Natl. Acad. Sci. U. S. A.* 102, 1472–1477. doi: 10.1073/pnas.0409528102

Song, L., Nadkarni, S. M., Bödeker, H. U., Beta, C., Bae, A., Franck, C., et al. (2006). Dictyostelium discoideum chemotaxis: threshold for directed motion. *Eur. J. Cell Biol.* 85, 981–989. doi: 10.1016/j.ejcb.2006.01.012

Strickland, D., Lin, Y., Wagner, E., Hope, C. M., Zayner, J., Antoniou, C., et al. (2012). TULIPs: tunable, light-controlled interacting protein tags for cell biology. *Nat. Methods* 9, 379–384. doi: 10.1038/nmeth.1904

Swaminathan, K., Müller-Taubenberger, A., Faix, J., Rivero, F., and Noegel, A. A. (2014). A Cdc42- and Rac-interactive binding (CRIB) domain mediates functions of coronin. *Proc. Natl. Acad. Sci. U. S. A.* 111, E25–E33. doi: 10.1073/pnas.1315368111

Swaney, K. F., Borleis, J., Iglesias, P. A., and Devreotes, P. N. (2015). Novel protein Callipygian defines the back of migrating cells. *Proc. Natl. Acad. Sci. U. S. A.* 112, E3845–E3854. doi: 10.1073/pnas.1509098112

Swaney, K. F., Huang, C. H., and Devreotes, P. N. (2010). Eukaryotic chemotaxis: a network of signaling pathways controls motility, directional sensing, and polarity. *Annu. Rev. Biophys.* 39, 265–289. doi: 10.1146/annurev.biophys.093008.131228

Takeda, K. (2012). Incoherent feedforward control governs adaptation of activated ras in a eukaryotic chemotaxis pathway. *Sci. Signal.* 5:ra2. doi: 10.1126/scisignal.2002413

Tang, L., Franca-Koh, J., Xiong, Y., Chen, M. Y., Long, Y., Bickford, R. M., et al. (2008). tsunami, the Dictyostelium homolog of the Fused kinase, is required for polarization and chemotaxis. *Genes Dev.* 22, 2278–2290. doi: 10.1101/gad.1694508

Tang, M., Wang, M., Shi, C., Iglesias, P. A., Devreotes, P. N., and Huang, C. H. (2014). Evolutionarily conserved coupling of adaptive and excitable networks mediates eukaryotic chemotaxis. *Nat. Commun.* 5, 1–13. doi: 10.1038/ncomms6175

Taniguchi, D., Ishihara, S., Oonuki, T., Honda-Kitahara, M., Kaneko, K., and Sawai, S. (2013). Phase geometries of two-dimensional excitable waves govern self-organized morphodynamics of amoeboid cells. *Proc. Natl. Acad. Sci. U. S. A.* 110, 5016–5021. doi: 10.1073/pnas.1218025110

Taylor, S. J., Resnick, R. J., and Shalloway, D. (2001). Nonradioactive determination of Ras-GTP levels using activated Ras interaction assay. *Methods Enzymol.* 333, 333–342. doi: 10.1016/S0076-6879(01)33067-7

Thomas, M. A., Kleist, A. B., and Volkman, B. F. (2018). Decoding the chemotactic signal. *J. Leukoc. Biol.* 104, 359–374. doi: 10.1002/JLB.1MR0218-044

Thomas Lampert, J., Kamprad, N., Edwards, M., Borleis, J., Watson, A. J., and Tarantola, M. (2017). Shear force-based genetic screen reveals negative regulators of cell adhesion and protrusive activity. *Proc. Natl. Acad. Sci. U. S. A.* 114, E7727–E7736. doi: 10.1073/pnas.1616600114

Toettcher, J. E., Voigt, C. A., Weiner, O. D., and Lim, W. A. (2011). The promise of optogenetics in cell biology: interrogating molecular circuits in space and time. *Nat. Methods* 8, 35–38. doi: 10.1038/nmeth.f.326

Tranquillo, R. T., Lauffenburger, D. A., and Zigmond, S. H. (1988). A stochastic model for leukocyte random motility and chemotaxis based on receptor binding fluctuations. *J. Cell Biol.* 106, 303–309. doi: 10.1083/jcb.106.2.303

Van Haastert, P. J. M., and Devreotes, P. N. (2004). Chemotaxis: signalling the way forward. *Nat. Rev. Mol. Cell Biol.* 5, 626–634. doi: 10.1038/nrm1435

Van Haastert, P. J. M., Keizer-Gunnink, I., and Kortholt, A. (2017). Coupled excitable Ras and F-actin activation mediates spontaneous pseudopod formation and directed cell movement. *Mol. Biol. Cell* 28, 922–934. doi: 10.1091/mbc.E16-10-0733

Van Haren, J., Charafeddine, R. A., Ettinger, A., Wang, H., Hahn, K. M., and Wittmann, T. (2018). Local control of intracellular microtubule dynamics by EB1 photodissociation. *Nat. Cell Biol.* 20, 252–261. doi: 10.1038/s41556-017-0028-5

Vicker, M. G. (2002). F-actin assembly in Dictyostelium cell locomotion and shape oscillations propagates as a self-organized reaction-diffusion wave. *FEBS Lett.* 510, 5–9. doi: 10.1016/S0014-5793(01)03207-0

Vogel, G., Thilo, L., Schwarz, H., and Steinhart, R. (1980). Mechanism of phagocytosis in dictyostelium discoideum: phagocytosis is mediated by different recognition sites as disclosed by mutants with altered phagocytotic properties. *J. Cell Biol.* 86, 456–465. doi: 10.1083/jcb.86.2.456

Wang, H., Vilela, M., Winkler, A., Tarnawski, M., Schlichting, I., Yumerefendi, H., et al. (2016). LOVTRAP: an optogenetic system for photoinduced protein dissociation. *Nat. Methods* 13, 755–758. doi: 10.1038/nmeth.3926

Wang, M.-J., Iglesias, P. A., and Devreotes Correspondence, P. N. (2014). The Directional Response of Chemotactic Cells Depends on a Balance between Cytoskeletal Architecture and the External Gradient Overall directional response depends on gradient and internal polarity. *Cell Rep.* 9, 1110–1121. doi: 10.1016/j.celrep.2014.09.047

Weiner, O. D., Neilsen, P. O., Prestwich, G. D., Kirschner, M. W., Cantley, L. C., and Bourne, H. R. (2002). A PtdInsP3- and Rho GTPase-mediated positive feedback loop regulates neutrophil polarity. *Nat. Cell Biol.* 4, 509–512. doi: 10.1038/ncb811

Williams, J. G. (2010). Dictyostelium finds new roles to model. *Genetics* 185, 717–726. doi: 10.1534/genetics.110.119297

Wills, R. C., Goulden, B. D., and Hammond, G. R. V. (2018). Genetically encoded lipid biosensors. *Mol. Biol. Cell* 29, 1526–1532. doi: 10.1091/mbc.E17-12-0738

Wong, R., Hadjiyanni, I., Wei, H. C., Polevoy, G., McBride, R., Sem, K. P., et al. (2005). PIP2 hydrolysis and calcium release are required for cytokinesis in Drosophila spermatocytes. *Curr. Biol.* 15, 1401–1406. doi: 10.1016/j.cub.2005.06.060

Xiong, D., Xiao, S., Guo, S., Lin, Q., Nakatsu, F., and Wu, M. (2016). Frequency and amplitude control of cortical oscillations by phosphoinositide waves. *Nat. Chem. Biol.* 12, 159–166. doi: 10.1038/nchembio.2000

Xiong, Y., Huang, C. H., Iglesias, P. A., and Devreotes, P. N. (2010). Cells navigate with a local-excitation, global-inhibition-biased excitable network. *Proc. Natl. Acad. Sci. U. S. A.* 107, 17079–17086. doi: 10.1073/pnas.1011271107

Yamada, K. M., and Cukierman, E. (2007). Modeling tissue morphogenesis and cancer in 3D. *Cell* 130, 601–610.

Yamada, K. M., and Sixt, M. (2019). Mechanisms of 3D cell migration. *Nat. Rev. Mol. Cell Biol.* 20, 738–752. doi: 10.1038/s41580-019-0172-9

Zhan, H., Bhattacharya, S., Cai, H., Iglesias, P. A., Huang, C. H., and Devreotes, P. N. (2020). An Excitable Ras/PI3K/ERK Signaling Network Controls Migration and Oncogenic Transformation in Epithelial Cells. *Dev. Cell* 54, 608–623.e5. doi: 10.1016/j.devcel.2020.08.001

Zhao, M., Jin, T., McCaig, C. D., Forrester, J. V., and Devreotes, P. N. (2002). Genetic analysis of the role of G protein-coupled receptor signaling in electrotaxis. *J. Cell Biol.* 157, 921–927. doi: 10.1083/jcb.200112070

Zigmond, S. (1974). Mechanisms of sensing chemical gradients by polymorphonuclear leukocytes. *Nature* 249, 450–452. doi: 10.1038/249450a0

Conflict of Interest: The authors declare that the research was conducted in the absence of any commercial or financial relationships that could be construed as a potential conflict of interest.

Publisher's Note: All claims expressed in this article are solely those of the authors and do not necessarily represent those of their affiliated organizations, or those of the publisher, the editors and the reviewers. Any product that may be evaluated in this article, or claim that may be made by its manufacturer, is not guaranteed or endorsed by the publisher.

Copyright © 2021 Kuhn, Lin and Devreotes. This is an open-access article distributed under the terms of the Creative Commons Attribution License (CC BY). The use, distribution or reproduction in other forums is permitted, provided the original author(s) and the copyright owner(s) are credited and that the original publication in this journal is cited, in accordance with accepted academic practice. No use, distribution or reproduction is permitted which does not comply with these terms.

frontiers in Cell and Developmental Biology

REVIEW
published: 07 October 2021
doi: 10.3389/fcell.2021.752175

Dictyostelium discoideum as a Model to Assess Genome Stability Through DNA Repair

Catherine J. Pears, Julien Brustel and Nicholas D. Lakin*

Department of Biochemistry, University of Oxford, Oxford, United Kingdom

Preserving genome integrity through repair of DNA damage is critical for human health and defects in these pathways lead to a variety of pathologies, most notably cancer. The social amoeba *Dictyostelium discoideum* is remarkably resistant to DNA damaging agents and genome analysis reveals it contains orthologs of several DNA repair pathway components otherwise limited to vertebrates. These include the Fanconi Anemia DNA inter-strand crosslink and DNA strand break repair pathways. Loss of function of these not only results in malignancy, but also neurodegeneration, immune-deficiencies and congenital abnormalities. Additionally, *D. discoideum* displays remarkable conservations of DNA repair factors that are targets in cancer and other therapies, including poly(ADP-ribose) polymerases that are targeted to treat breast and ovarian cancers. This, taken together with the genetic tractability of *D. discoideum*, make it an attractive model to assess the mechanistic basis of DNA repair to provide novel insights into how these pathways can be targeted to treat a variety of pathologies. Here we describe progress in understanding the mechanisms of DNA repair in *D. discoideum*, and how these impact on genome stability with implications for understanding development of malignancy.

Keywords: *Dictyostelium*, genome stability, DNA repair, cancer, Fanconi Anemia, interstrand crosslink, PARP (poly(ADP-ribose) polymerase, *D. discoideum*

OPEN ACCESS

Edited by:
Robin S. B. Williams, University of London, United Kingdom

Reviewed by:
Thomas Winckler, Friedrich Schiller University Jena, Germany
Cynthia Damer, Central Michigan University, United States
Tetsuya Muramoto, Toho University, Japan

****Correspondence:***
Catherine J. Pears
catherine.pears@bioch.ox.ac.uk

Specialty section:
This article was submitted to Molecular and Cellular Pathology, a section of the journal Frontiers in Cell and Developmental Biology

Received: *02 August 2021*
Accepted: *20 September 2021*
Published: *07 October 2021*

Citation:
Pears CJ, Brustel J and Lakin ND (2021) Dictyostelium discoideum as a Model to Assess Genome Stability Through DNA Repair. Front. Cell Dev. Biol. 9:752175. doi: 10.3389/fcell.2021.752175

INTRODUCTION

Maintaining genome integrity through DNA repair is critical for human health. DNA is continually being exposed to a variety of agents that induce DNA damage. This includes exogenous agents such as ultraviolet light, ionizing radiation and mutagenic chemicals, in addition to those generated during cellular metabolic processes such as reactive oxygen species or formaldehyde. These insults can lead to a wide variety of changes in DNA structure, including loss or chemical alteration of bases, chemical crosslinks (between or within a strand) and cleavage of the phosphodiester backbone to generate single (SSB) or double strand (DSB) DNA breaks. These chemically distinct lesions require a set of pathways known as the DNA damage response (DDR) to detect the different types of DNA damage and regulate mechanisms for their repair, as well as activating checkpoints to inhibit cell cycle progression. A failure of these pathways can lead to accumulation of mutations and chromosome instability that can manifest itself in a variety of pathologies, including neuro-degeneration, congenital abnormalities, immune deficiencies, and malignancy. Therefore,

understanding the mechanistic basis of these DNA repair pathways provides insights into the causes of these conditions and, importantly, strategies for their treatment.

Study of DNA repair pathways by genetic approaches in a number of model organisms, most notably *Saccharomyces cerevisiae* and *Schizosaccharomyces pombe*, has been instrumental in unraveling the complexity of the DDR, identifying pathways and molecules, which are highly conserved in vertebrates. However, some of the pathways known to be critical to maintain genome stability in human cells are absent in the most commonly used models to study DNA repair. Instead, work from several laboratories over a number of years has pointed to the social amoeba *Dictyostelium discoideum* (Kessin, 2001; Pears and Gross, 2021) as an alternative model to study DNA repair mechanisms where these show limited conservation, or are difficult to study in other models (Hudson et al., 2005; Zhang et al., 2009; Couto et al., 2013b; Pears and Lakin, 2014). Intriguingly, the genome sequence of *D. discoideum* (Eichinger et al., 2005) revealed that it contains genes encoding a number of DNA repair proteins involved in resolving different types of damage that were previously believed to be restricted to vertebrates. This list includes proteins involved in repair of DNA DSBs by non-homologous end joining (NHEJ) such as DNA-PKcs and artemis (Dclre1; Block and Lees-Miller, 2005; Hudson et al., 2005; Hsu et al., 2011), in addition to XRCC1 and DNA ligase III that are involved in base excision (BER) and SSB repair (SSBR; Pears et al., 2012). In addition, *D. discoideum* has a small genome size to facilitate genetic screens and the genome often contains a limited number of orthologs of proteins, reducing the complexity caused by redundancy in mammalian systems. This is especially relevant for studying the role of histones and how their post-translational modification at the site of DNA damage regulate DNA repair. *D. discoideum* contains single copies of genes encoding the majority of histone variants (Stevense et al., 2011; Hsu et al., 2012), allowing their disruption or mutation by gene replacement or genome editing by CRISPR/Cas9 (Muramoto et al., 2010; Hsu et al., 2012; Sekine et al., 2018; Iriki et al., 2019; Asano et al., 2021). In recent years a range of methods have been developed with which to study mutation rates (Saxer et al., 2012; Pontel et al., 2016) and specific repair pathways, including NHEJ, homologous recombination (HR; Hudson et al., 2005; Couto et al., 2011, 2013a) and the post-translational modifications that regulate these pathways, such as ADP-ribosylation (ADPr; Couto et al., 2011; Kolb et al., 2018).

The presence of a wide range of repair proteins and pathways, as well as the high level of tolerance of this organism to a range of DNA damaging agents, make *D. discoideum* an attractive model to study the molecular basis of the DDR. In particular, understanding the mechanistic basis of *D. discoideum*'s resistance to DNA damage will shed light on mechanisms of intrinsic and acquired resistance of tumors to chemotherapeutic drugs that induce DNA damage. This review discusses advances made in our understanding of repair of both interstrand cross-links and DNA strand breaks in *D. discoideum* and how the study of these pathways is providing novel insights into repair mechanisms in humans. The conservation of DNA damage-induced ADPr in *D. discoideum* is then used to illustrate how *D. discoideum* can provide insights into downstream DDR mechanisms, as well as the mechanistic action of agents that target this post translational modification in treatment of cancer.

GENOME STABILITY AND RESISTANCE TO DNA DAMAGING AGENTS

The haploid 34 Mb genome of *D. discoideum* contains around 12,000 genes arranged on 6 chromosomes along with an extrachromosomal palindrome containing the rRNA genes (Eichinger et al., 2005). The genome is AT-rich, containing 77.6% AT overall and 72% AT in coding regions. Simple sequence repeats make up an unusually high percentage (14.3%) of the *D. discoideum* genome. These are biased toward repeats of 3 and 6 nucleotides that are found in over 2000 coding regions (Eichinger et al., 2005) leading to long strings of single amino acids such as polyglutamine, that are tolerated in proteins. Genome analysis of wild *D. discoideum* populations reveal a low level of genetic variation, consistent with low mutation rates (Flowers et al., 2010), a conclusion reinforced by whole genome sequence analysis of mutation accumulation (MA) lines (McConnell et al., 2007; Saxer et al., 2012; Kucukyildirim et al., 2020). These are lines bred from a single common ancestor in which mutations generated during cell growth and division are fixed by random selection of single clonal progeny. Initial analysis of microsatellite repeats in 90 MA lines revealed low rates of mutation (McConnell et al., 2007). This was subsequently reinforced by whole genome sequence analysis of 3 and then 37 MA lines (Saxer et al., 2012; Kucukyildirim et al., 2020), revealing a mutation rate of around 2.5×10^{-11} base substitutions per site per generation in nuclear DNA. This is 10-100-fold lower than the majority of eukaryotic (Denver et al., 2004; Farlow et al., 2015; Long et al., 2016a; Krasovec M. et al., 2017) and prokaryotic organisms (Lee et al., 2012; Krasovec R. et al., 2017), but similar to that described in ciliates such as *Tetrahymena thermophila* (Long et al., 2016b). The GC to AT mutation rate is approximately 10-fold higher than that observed for AT to GC, which might contribute to the high AT bias in the genome. There is a two-fold higher frequency of small insertions or deletions of 1–30 bp (5×10^{-11} per nucleotide per generation), with the majority being small deletions (Kucukyildirim et al., 2020), compared to base substitutions. These low mutation rates are consistent with highly efficient DNA repair. However, the number of simple sequence repeats has been shown to be highly variable, both within and outside coding regions (Scala et al., 2012) consistent with a higher rate of slippage mutations (Kucukyildirim et al., 2020) and duplications of regions larger than 15 kb have been identified (Bloomfield et al., 2008).

Consistent with the low mutation rates of *D. discoideum*, vegetatively growing amoebae have long been known to be extremely resistant to a range of DNA damaging agents (Freim and Deering, 1970; Deering, 1994; Yu et al., 1998; Zhang et al., 2009), showing one of the highest levels of resistance known to ionizing radiation, which induces a variety of damage types, most notably DNA strand breaks (Deering, 1968). This high efficiency of DNA repair has been postulated to be required to counteract the damage caused on phagocytic ingestion of soil

bacteria used as a food source by the amoebae (Deering, 1994). In this regard, *D. discoideum* cells disrupted in the gene encoding the DNA nuclease Xpf, which is involved in several DNA repair pathways, show a growth defect on bacteria not apparent in axenic media (Zhang et al., 2009; Pontel et al., 2016). Growth of *xpf*$^{-}$ *D. discoideum* cells on bacteria (live or heat inactivated) led to an increased rate of mutation relative to wild type cells and to *xpf*$^{-}$ cells grown in axenic media, as measured by accumulation of inactivating mutations in the *catA* gene, loss of which results in resistance to methanol. The mutagenic effect of phagocytosis could be due to factors generated by the bacteria, although these factors need to survive heat inactivation, or by agents generated by the *D. discoideum* amoebae to kill the ingested bacteria, such as reactive oxygen species that are known to be highly mutagenic. Interestingly, similar mechanisms are used by professional phagocytes such as neutrophils in mammals to kill ingested bacteria using a respiratory burst (Chen et al., 2007; Dunn et al., 2017). Therefore, understanding different sensitivities to growth inhibition by different bacteria in *D. discoideum* could shed light on distinct mechanisms of bacterial killing by phagocytes in the mammalian immune system.

DNA DOUBLE STRAND BREAK REPAIR AND REPAIR PATHWAY CHOICE

The appreciation of the tolerance of amoebae to DNA damaging agents and the publication of the genome sequence triggered a resurgence in studying the mechanistic basis of the DDR in *D. discoideum*. The value of studying DSB repair in this organism (reviewed in, Pears and Lakin, 2014) was reinforced by identification of genes encoding DSB repair pathway components (**Table 1**) that were previously thought to be confined to vertebrates, such as DNAPKcs (Block and Lees-Miller, 2005; Hudson et al., 2005; Hsu et al., 2011). DNA DSBs are a particularly toxic form of DNA damage and cells possess a number of pathways for their repair. These include pathways based on HR in which a second copy of the DNA is used as a template for accurate repair, and pathways based on NHEJ with processing of the ends and subsequent ligation. As NHEJ can be mutagenic (for example by loss or addition of DNA during end-processing), the choice of pathway plays an important role in overall genome stability. In *D. discoideum* loss of NHEJ proteins such as Ku70/80 have a minor impact during growth on tolerance to agents that induce DSBs, presumably as HR can be employed to repair DNA damage (Hudson et al., 2005; Hsu et al., 2011). It has not been possible to generate cells deficient in core HR components, consistent with a major role for HR in genome stability in *D. discoideum*. However, disruption of the gene encoding the nuclease Exo1 leads to a decrease in HR efficiency and sensitivity to DNA DSBs during growth (Hsu et al., 2011). Exo1 is one of a number of nucleases acting in resection of the DNA DSB, a key event in HR that provides a 3′ overhang that is required for strand invasion and sequence homology searching during HR. However, further investigation revealed that, as in mammalian cells, NHEJ is active in vegetative amoebae, as evidenced by the efficiency of a plasmid insertion assay which is specific for NHEJ (Hsu et al., 2011). The delayed kinetics of DSB repair in the absence of NHEJ factors such as Dclre1 suggest that this pathway is attempted initially, but if unsuccessful then HR is employed (Hsu et al., 2011). Interestingly, *D. discoideum* undergoes a developmental life cycle in response to starvation in which it forms a multicellular structure with spores supported on a column of stalk cells. Hatching spores showed an increased dependence on NHEJ for tolerance to DSBs, suggesting that the choice to repair DSBs by NHEJ or HR may alter in some differentiated cells (Hudson et al., 2005).

So what factors regulate the choice between the NHEJ and HR pathways? An early step in NHEJ is the binding of the Ku70/80 heterodimer to DNA DSBs to initiate the pathway. Whilst disruption of the gene encoding the Ku80 subunit supresses NHEJ in vegetative *D. discoideum*, it promotes HR, indicating the binding of Ku to DSBs is a key determinant of *D. discoideum* DSB repair pathway choice (Hsu et al., 2011). This observation is consistent with the more rapid kinetics of recruitment of Ku to DSBs than HR components in mammalian cells (Kim et al., 2005) and protection of DNA ends from resection to suppress HR (Pierce et al., 2001). Indeed, it has subsequently been established that protection of DNA ends by 53BP1 and the Shieldin complex is a key regulator in promoting NHEJ at the expense of HR in human cells (Findlay et al., 2018; Gupta et al., 2018; Noordermeer et al., 2018; Setiaputra and Durocher, 2019). Whether similar mechanisms exist in *D. discoideum* remains to be tested.

DNA INTERSTRAND CROSSLINK REPAIR

Interstrand crosslinks (ICLs) are a toxic form of DNA damage as they prevent separation of the two strands of DNA during transcription and DNA replication. Rapidly dividing cells are therefore particularly vulnerable to ICLs. This has led to a number of drugs that induce ICLs such as platinum, cisplatin and mitomycin C, being used in chemotherapy to target a range of tumors. Therefore, a mechanistic understanding of the repair pathways used to combat ICLs will facilitate identification of genetic vulnerabilities that render tumors sensitive to these agents, and also methods to combat acquired resistance to these treatments. As well as exogenous cross-linking agents, endogenous sources of ICLs include naturally generated metabolites such as formaldehyde (Langevin et al., 2011; Nakamura and Nakamura, 2020). Vertebrates express a number of pathways to repair ICLs, including those involving the translesion DNA polymerases REV1 and REV3, and nucleases such as XPF (McHugh, 2020). The importance of ICL repair is illustrated by the developmental and health consequences of mutations in the Fanconi Anemia (FA) pathway (Duxin and Walter, 2015). FA is an inherited syndrome, with at least 22 complementation groups, that leads to progressive bone marrow failure and increased risk of various malignancies, particularly leukemia and solid tumors, as well as growth and developmental defects, including skeletal abnormalities and short stature. Cells from FA patients show increased sensitivity to ICL-inducing agents such as cisplatin and FA proteins are involved in repair

TABLE 1 | DNA repair factors experimentally verified to have a role in repair of interstrand cross links, double and single strand DNA breaks in *D. discoideum*.

DNA damage repair pathway	Protein	Gene id	Putative function	References
ICL repair	FancE	DDB_G0279669	Bridge between core complex and FancD2	Zhang et al., 2009
	FancM	DDB_G0274841	DNA-dependent helicase	
	Ube2T	DDB_G0291199	Ubiquitin ligase in core complex	
	FancL	DDB_G0292744		
	FancD2	DDB_G0268216	Mono-ubiquitinylated following damage, associate	
	FancI	DDB_G0293476	with damage site to recruit repair factors	
	FancJ	DDB_G0286621	DNA helicase	
	Xpf/FancQ	DDB_G0284419	Endonuclease	
	Mus81	DDB_G0276519	Nuclease	
	Rev3/DNApol Zeta	DDB_G0271608	Translesion DNA synthesis	
	Adprt2	DDB_G0292820	ADPr transferase	Gunn et al., 2016
	APL	DDB_G0293866	PAR-binding protein	
DSB repair by classical NHEJ	Adprt1a	DDB_G0278741	ADPr transferase	Couto et al., 2011
	Ku70	DDB_G0286069	DNA DSB end binding	Hudson et al., 2005
	Ku80	DDB_G0286303	DNA DSB end binding	
	DNAPKcs	DDB_G0281167	Protein kinase forming complex with Ku78/80 heterodimer	
	Dclre1	DDB_G0277755	Nuclease	Hsu et al., 2011
DSB repair by Alt-NHEJ	PolQ	DDB_G0277749	DNA polymerase	Kolb et al., 2017
	DNA Ligase III	DDB_G0283857	DNA ligase	
DSB repair by HR	Exo1	DDB_G0291570	Exonuclease	Hsu et al., 2011
	Xpf1	DDB_G0284419	Endonuclease	Zhang et al., 2009
	Rad51	DDB_G0273139	DNA binding and promotion of strand exchange	Kolb et al., 2017
SSB repair	Adprt2	DDB_G0292820	ADPr transferase	Couto et al., 2011
	Adprt1b	DDB_G0279195	ADPr transferase	

The protein name, the gene id on dictybase (dictybase.org) and the reference demonstrating function are shown.

of ICLs, particularly when replication forks encounter these lesions during S-phase. The identification of formaldehydes as the predominant source of damage repaired by the FA pathway also raises the possibility that it is of particular importance for the type of cross-links induced by this agent, including cross-linking DNA to protein (Langevin et al., 2011). In the vertebrate FA pathway, a large core complex of 11 or more proteins associates with chromatin upon DNA damage in which the catalytic subunit FANCL functions as an E3 ubiquitin ligase to mono-ubiquitinylate both FANCI and FANCD2. These form a heterodimeric complex, and their ubiquitylation is required for tolerance to ICL by integrating nucleotide excision repair (NER), a pathway also used to remove UV-induced thymidine dimers, with translesion DNA polymerases and HR to restore genome integrity (Garcia-de-Teresa et al., 2020).

The number of pathways to repair ICLs has expanded with organism complexity. In *S. cerevisiae* repair of ICLs is mainly due to NER (Lehoczky et al., 2007). Whilst the majority of proteins associated with FA are not conserved in yeast, the *D. discoideum* genome contains an expanded repertoire of FA proteins similar to those observed in humans (Zhang et al., 2009). This includes orthologs of genes encoding the heterodimer FANCI/D2 and the E2 (Ube2T) and E3 (FANCL) ubiquitin ligases required for their modification (**Table 1**). However, the majority of core complex components are not apparent by sequence homology, suggesting a simplified version of the pathway may operate. *D. discoideum* strains deficient in the *fanc* genes such as *fancD2* or *fancL* indeed show mildly increased sensitivity to cisplatin, as do strains deficient in the translesion DNA polymerase *rev3*. However, the majority of *D. discoideum*'s tolerance to cisplatin requires the nuclease Xpf, as *xpf*$^{-}$ cells show 50–100 fold greater sensitivity to cisplatin than cells disrupted in *fancD2* or *rev3*. Double mutants, such as *xpf*$^{-}$*fancD2*$^{-}$ strains, do not show additive sensitivity. This suggests that Xpf does function in the *D. discoideum* FA pathway, but that its major role in tolerance to cisplatin is independent of this pathway. This alternate role for Xpf is not in NER as disruption of another component of this pathway does not sensitize *D. discoideum* cells to cisplatin, but could be related to a role in HR. Subsequently, mutations in *xpf* have been found in FA patients (Bogliolo et al., 2013; Kashiyama et al., 2013) and studies in mice and human cells demonstrate that the role for XPF in tolerance to ICL involves a pathway other than its known roles in excision repair (Mulderrig and Garaycoechea, 2020).

Dictyostelium discoideum offers an easily tractable system to unravel the complex interactions between repair pathways which may depend on the exact nature of the ICL, and phase of the cell cycle. In this respect it is noteworthy that *D. discoideum* amoebae are predominantly in G2 phase of the cell cycle, with a very short or undetectable G1 phase (Durston et al., 1984; Weijer et al., 1984), offering one potential explanation for the minimal requirement of the FA pathway for tolerance to cisplatin. In addition, cisplatin favors GC crosslinks and it will also be of interest to compare the involvement of different pathways using agents that induce other forms of cross-link that may be more abundant in the AT-rich *D. discoideum* genome. In particular the developmental defects in FA patients are believed to be due to

endogenous metabolites that are able to form crosslinks such as formaldehyde (Langevin et al., 2011). However, the sensitivity of *D. discoideum* cells deficient in different pathway components to such agents is not known.

In a parallel approach, identification of mutant *D. discoideum* strains that are resistant to cisplatin has revealed sphingolipid metabolism as a regulator of tolerance to this chemotherapeutic drug (Min et al., 2004, 2005a; Alexander et al., 2006). For example, overexpression of sphingosine-1-phosphate lyase or loss of sphingosine kinase, both of which lead to a reduction in levels of sphingosine-1-phosphate, results in increased sensitivity to cisplatin (Min et al., 2004). This was subsequently shown to also be true in human cells, providing pharmacological targets for increasing tumor sensitivity to cisplatin (Min et al., 2005b). Gene expression studies revealed genes with expression levels altered on cisplatin treatment. Many of these changes were altered in resistant mutants and subsequent disruption of five of these also altered cisplatin sensitivity, revealing novel tolerance pathways (Van Driessche et al., 2007).

STRAND BREAK REPAIR AND ADP-RIBOSYLATION

One family of DNA repair enzymes that are found in *D. discoideum* that are absent or show limited conservation in other non-vertebrates are ADP-ribosyl transferases (ARTs), a family of proteins that catalyze the addition of single or poly-ADP-ribose moieties onto target proteins using NAD^+ as substrate (Gibson and Kraus, 2012; Vyas et al., 2014; Martin-Hernandez et al., 2017). In humans, 17 genes containing predicted ART domains have been identified (Hottiger et al., 2010). ADPr has been implicated in a wide variety of processes, including cell growth and differentiation, transcriptional regulation and programmed cell death (Gibson and Kraus, 2012) and in a number of diseases, including cancer, neurological disorders, and cardiovascular disease (Palazzo et al., 2019). However, the best-defined role of these enzymes, which are also known as poly ADPr-polymerases (PARP)s, is in regulating DNA repair, particularly of DNA strand breaks (**Figure 1**; Caldecott, 2014; Azarm and Smith, 2020). PARP1, the founder member of the PARP family in mammalian cells, recognizes SSBs generated directly or as a consequence of base excision repair (BER), and becomes activated to ADPr substrates at the break site. This promotes accumulation of the XRCC1 scaffolding protein at DNA damage sites that subsequently leads to assembly of repair factors at the lesion that resolve the damage (Caldecott, 2014). Small molecule inhibitors of PARPs are in use in the clinic to treat cancers which are deficient in HR, most notably those with mutations in *BRCA1* and *BRCA2*. Loss of function of these genes predisposes individuals to developing breast and ovarian cancers (Bryant et al., 2005; Farmer et al., 2005; Slade, 2020). Therefore, understanding the mechanistic basis of how PARPs regulate repair of different DNA lesions and how redundancy between these pathways allows cells to tolerate DNA damage will facilitate identification of cancers responding to PARP inhibition and suggest mechanisms to overcome acquired resistance to these agents.

Poly ADPr-polymerase activity was identified in *D. discoideum* many years ago (Rickwood and Osman, 1979; Kofler et al., 1993; Rajawat et al., 2007; Mir et al., 2015) and a cDNA sequence revealed considerable homology to mammalian PARPs (Auer et al., 1995). The completed genome sequence of *D. discoideum* (Eichinger et al., 2005) revealed 15 genes encoding proteins with putative ART catalytic domains. Four of these proteins also contain other domains found in human PARPs that respond to DNA damage, including protein-protein interaction domains such as BRCT domains, and nucleic acid binding WGR and zinc fingers domains (**Figure 2A**; Otto et al., 2005; Citarelli et al., 2010; Couto et al., 2011; Pears et al., 2012). As in humans, two PARPs (Adprt1b and 2) play a role in SSBR/BER as their loss leads to sensitivity to hydrogen peroxide and methanesulphonate (MMS), agents that induce damage that requires these pathways for repair (Couto et al., 2011). However, a third ART, Adprt1a, that is not required for tolerance to DNA SSBs, plays a role in DNA DSB repair (Couto et al., 2011). Importantly, disruption of the *adprt1a* gene results in a reduced ability to retain Ku70 at DSBs, with a consequent reduction in NHEJ efficiency (**Figure 2B**; Couto et al., 2011). Studies carried out at a similar time also revealed a role for a third ART, PARP3, in promoting NHEJ in human cells (Boehler et al., 2011; Rulten et al., 2011; Beck et al., 2014), confirming the value of the *D. discoideum* model.

In a pre-genome editing era, an important strength of the *D. discoideum* model was the ability to disrupt multiple genes in combination to assess genetic interactions and redundancies within biological pathways. This approach highlighted novel compensatory repair mechanisms that are employed upon inactivation of PARPs, particularly with reference to *D. discoideum* cells lacking Adprt2, the major ART required for tolerance to DNA SSBs (**Figure 2C**). Intriguingly, *adprt2*$^-$ cells still show robust ADPr of proteins following treatment with MMS which induces DNA base alkylation that is subsequently converted to SSBs during BER. However, this is lost on further deletion of the gene encoding the DSB-responsive ART, Adprt1a (Couto et al., 2013b) and *adprt1a*$^-$ *adprt2*$^-$ double mutant cells show increased sensitivity to MMS relative to cells with disruption of the *adprt2* gene alone. The known role for Adprt1a in NHEJ suggested that in the absence of effective repair, SSBs are converted to DSBs that are subsequently repaired by NHEJ. Consistent with this hypothesis, *adprt2*$^-$ cells show increased recruitment of Ku80 to chromatin following MMS treatment that is dependent on the presence of Adprt1a. Moreover, disruption of NHEJ pathway components in *adprt2*$^-$ cells increases the sensitivity of these cells to MMS. Together, this analysis reveals the importance for NHEJ in the absence of effective SSB repair. Therefore redundancy between PARP-dependent repair mechanisms is not only due to multiple PARPs regulating the same repair mechanism, but also disruption of one specific PARP-dependent repair pathway channeling DNA damage through alternate repair routes that are dependent on another PARP. Importantly, these studies prompted analysis of similar functional overlap of human PARPs in regulating DNA repair. It has been known for some time that both PARP1

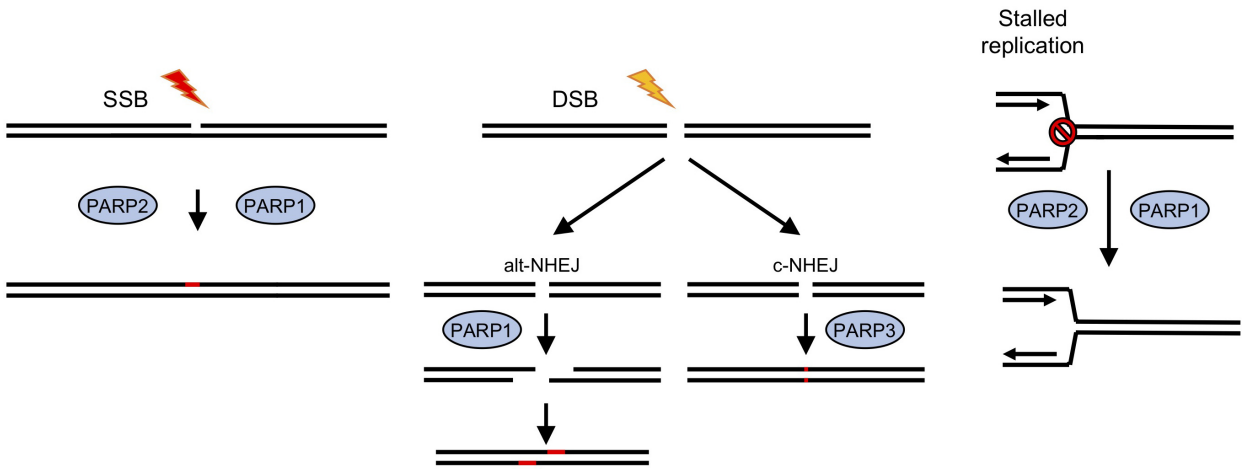

FIGURE 1 | Roles for ADP-ribosyl transferases in strand break repair in human cells. In human cells PARPS have a well-established role in DNA repair (Caldecott, 2014; Azarm and Smith, 2020). PARPs 1 and 2 have been implicated in repair of single strand breaks (SSB), which are induced either directly by exogenous or endogenous damaging agents, or as a result of base excision repair (BER) pathways following base damage. Recruitment of PARPs1/2 to the break site and subsequent ADP-ribosylation of proteins, including histones at the damage site, lead to recruitment or stabilization of repair factors and subsequent damage resolution. DNA double strand break (DSB) repair by classical non-homologous end joining (c-NHEJ) involves a third PARP, PARP3, whereas an alternative version (alt-NHEJ) is dependent on PARP1. Stalled replication forks can lead to fork collapse and restart is also thought to be PARP-dependent.

and PARP2 function in repair of DNA SSBs (Schreiber et al., 2002; Menissier de Murcia et al., 2003; Hanzlikova et al., 2017). However, more recently it has also become apparent that, similar to *D. discoideum*, disruption of SSB repair can channel DNA damage through alternate repair mechanisms that employ other PARPs (Ronson et al., 2018). This redundancy has implications for use of inhibitors specific for individual PARPs, suggesting that inhibitors targeting several PARPs involved in distinct DNA repair pathways may be required for complete loss of repair functions in chemotherapy. Understanding these relationships in organisms such as *D. discoideum* will provide important information about redundant PARP-dependent repair mechanisms in human cells and potential clinical applications.

IDENTIFYING ADP-RIBOSYLATION BINDING MOTIFS IN *D. discoideum* TO EXPAND THE ROLE FOR ADP-RIBOSYLATION – A NOVEL ROLE FOR ADP-RIBOSYLATION IN REPAIR OF INTERSTRAND CROSSLINKS

Once activated, ARTs catalyze ADPr of proteins at sites of DNA damage leading in turn to recruitment of DNA repair and chromatin remodeling factors to aid resolution of the damage. This is achieved by interaction between proteins containing PAR-binding motifs with mono- or poly-ADP-ribosylated proteins. A number of these PAR binding motifs (PBM) have been identified, including a 20 amino-acid PBM, PAR-binding zinc finger (PBZ), WWE, and macro-domains (Gibson and Kraus, 2012). Bioinformatic identification of proteins containing these motifs is an invaluable tool to identify downstream response systems. Three PBZ domain containing proteins have been identified in vertebrates, CHFR, APLF, and APL (Ahel et al., 2008). All of these proteins have been implicated in the DDR, and the PBZ domains of APLF and CHFR are required for association of these proteins with sites of DNA damage. *D. discoideum* contains an expanded family of seven PBZ-domain containing proteins (Ahel et al., 2008), implicating ARTs in the regulation of these proteins, and the pathways in which they function. For example, *D. discoideum* Ku70 contains a PBZ domain which is required for efficient enrichment of the Ku70/Ku80 complex on chromatin in response to DSBs and efficient NHEJ (Couto et al., 2011). Interestingly, vertebrate Ku70 does not contain a PBZ domain, although NHEJ is dependent on PARP activity in these organisms (Boehler et al., 2011; Rulten et al., 2011; Beck et al., 2014). This suggests that different mechanisms for recruitment of NHEJ proteins may have arisen during evolution, and that the expanded number of ADPr-binding domains in *D. discoideum* may provide a novel approach to identify response systems downstream of ADPr.

Macrodomains are more diverse, binding a range of motifs such as MAR, PAR and O-acetyl ADP-ribose and a number have been characterized as domains that catalyze the metabolism of ADPr such as PAR and MAR hydrolysis to remove these modifications (Rack et al., 2016, 2020). Again in vertebrates a number of proteins with a role in the DDR (Jankevicius et al., 2013; Rosenthal et al., 2013; Barkauskaite et al., 2015) contain macro domains which are required for their recruitment to site of damage, including ALC1 and the histone variant macroH2A1.1 (Ahel et al., 2009; Gottschalk et al., 2009; Timinszky et al., 2009). Bioinformatic analysis identified six *D. discoideum* proteins containing macrodomains (Gunn et al., 2016). As proof of concept, this list contained DNA ligase III, a DNA repair protein that does not contain a macrodomain in vertebrates. A novel

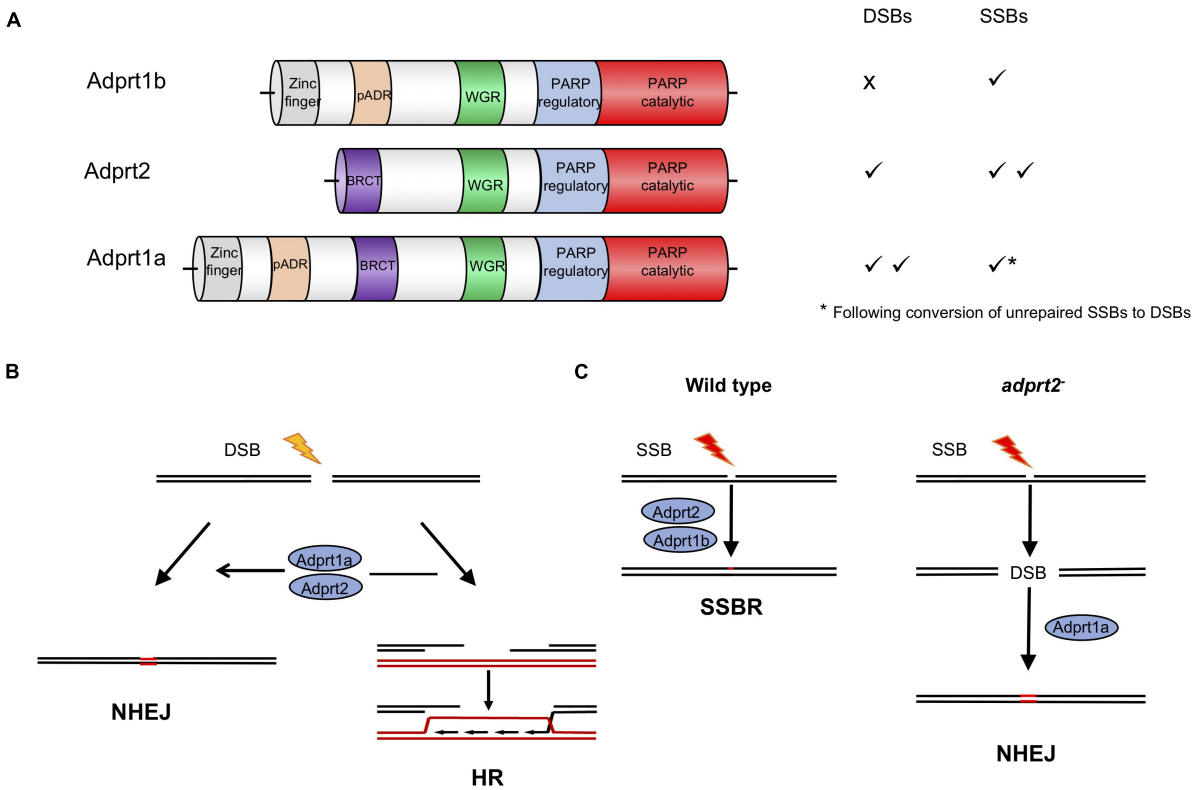

FIGURE 2 | Roles for ADP-ribosyl transferases in strand break repair in *D. discoideum* cells. **(A)** Three *D. discoideum* ARTS have been demonstrated to have a role in DNA repair of strand breaks. As well as a catalytic domain at the C terminus, all three contain N terminal motifs associated with DNA repair proteins in mammals, including BRCT, WGR and zinc finger domains (Otto et al., 2005; Citarelli et al., 2010; Pears et al., 2012). **(B)** Adprt1a and, in its absence Adprt2, regulate choice between repair of DSBs by NHEJ or HR. Their action favors NHEJ by stabilizing recruitment of the Ku70/80 heterodimer to the ends, protecting them from end resection by nucleases, the initial step in the HR pathway. In *D. discoideum* Ku70 contains a PBZ domain, an ADPR-binding motif, required to stabilize its association with damaged chromatin (Couto et al., 2011; Hsu et al., 2011). **(C)** In wild type cells Adprt2 and Adprt1b are required for tolerance to SSBs. In *adprt2*$^{-}$ cells, unrepaired SSBs can be converted to DSBs and repair is then dependent on Adprt1a and subsequent Ku70/80 recruitment to promote NHEJ (Couto et al., 2011, 2013b).

protein identified in this approach, APL, contains an unusual macrodomain with a circular permutation which interacts with PAR in an *in vitro* binding assay. Interestingly, APL also contains a PBZ domain with PAR binding activity. One interpretation of this is that these two domains may act in tandem to increase binding affinity to a PAR chain, or that APL may bridge ADPr proteins to generate a complex. The presence of another protein-protein interaction FHA domain and the lack of any domain containing recognized enzymatic activity would be consistent with a scaffolding role for APL.

The identification of APL in *D. discoideum* revealed a novel role for ADPr in tolerance to cisplatin (**Table 1**). APL enrichment to chromatin was only detectable following treatment with cisplatin, and not with agents inducing predominantly SSBs or DSBs, the classical pathways that depend on ADPr (Gunn et al., 2016). Deletion of the macrodomain alone severely abrogated APL recruitment to chromatin following induction of ICLs, despite the presence of the intact PBZ and FHA domains, and this event was largely dependent on Adprt2, an enzyme previously implicated in *D. discoideum* SSB repair. A role for ADPr in ICL repair has subsequently been demonstrated in human cells (Li et al., 2020). ADPr by PARP1 is required to recruit the NEIL3 DNA glycosylase to ICLs and loss of either NEIL3 or inhibition of ADPr leads to increased sensitivity to ICLs, in a pathway distinct from the FA pathway. This example demonstrates the power of using the presence of ADPr-binding domains as surrogate markers for novel PARP-dependent pathways and highlights the importance of characterizing other *D. discoideum* proteins containing PBZ and macro domains in the future (Ahel et al., 2008; Gunn et al., 2016).

TARGETING OF ADP-RIBOSYL TRANSFERASES IN CANCER

Redundancy between repair pathways in tolerance of DNA damage has been exploited in a synthetic lethal strategy to selectively kill cancer cells which are deficient in repair pathways. This deficiency likely promotes the accumulation of mutations driving tumor formation, but can also provide an Achille's heel to target in treatments (Bryant et al., 2005; Farmer et al., 2005; Slade, 2020). PARP inhibitors function by trapping PARPs at

DNA SSBs, leading to a block in DNA replication and fork collapse (Rouleau et al., 2010). This generates DNA DSBs that under normal circumstances can be repaired by HR in a pathway that is dependent on BRCA1/2. Therefore, in the absence of these, or other HR factors, PARP inhibitor-induced DSBs are repaired by mutagenic DNA repair pathways (both classical c-NHEJ and atypical alt-NHEJ) that results in genome instability and cell death (**Figure 3**). Therefore, PARP inhibitors are selectively toxic to HR-deficient tumor cells while HR proficient non-tumor cells remain viable. PARP inhibitors such as Olaparib are in use in the clinic to treat breast and ovarian cancers that are deficient in BRCA1 or BRCA2, encoded by genes associated with inherited susceptibility to breast cancer (Slade, 2020).

Treatment of *D. discoideum* with the PARP inhibitor NU1025 leads to chromatin recruitment of the HR protein Rad51, indicating that, similar to humans, DNA damage induced by PARP inhibitors is repaired by HR. Consistent with this model, strains lacking the nuclease Exo1 that are defective in HR, show synthetic lethality with PARP inhibitors (Kolb et al., 2017). The conservation of this phenomenon with humans makes *D. discoideum* an attractive system to identify mutations which lead to resistance of HR-deficient strains to PARP inhibitors and therefore potentially cause resistance of tumors to PARP inhibitor treatment. In human cells two pathways have been proposed to compete with HR to repair DNA damage: c-NHEJ and alt-NHEJ (Ceccaldi et al., 2015; Mateos-Gomez et al., 2015). Disruption the NHEJ gene *dnapkcs*, supresses sensitivity of *D. discoideum exo1*$^{-}$ cells to PARP inhibitors. This is consistent with mutagenic c-NHEJ becoming the predominant pathway to repair PARP inhibitor-induced DNA damage and driving inhibitor toxicity when HR is absent. In contrast, disruption of genes encoding DNA ligase III and DNA polymerase theta, components of alt-NHEJ (McVey and Lee, 2008), does not impact on tolerance to PARP inhibitors either in the presence or absence of Exo1. This could reflect the dependence of alt-NHEJ on PARP. The specificity of involvement of distinct ARTs in different pathways highlights the desirability of unraveling their specific roles and pathway interactions, and for developing PARP inhibitors that are specific for different ARTs in the clinical setting. Currently, clinically approved PARP inhibitors such as Olaparib are broad spectrum inhibitors with activity toward all known ARTs involved in DNA repair, but inhibitors specific for individual ARTs are under development (Slade, 2020).

Understanding the interplay between PARP-dependent and -independent repair mechanisms will aid identification of tumors that are likely to respond to PARP inhibitors either alone, or in combination therapies, in addition to mechanisms by which tumors become resistant to these agents. For example, reactivation of HR in mammalian cells by loss of the DNA end resection inhibiting factor 53BP1 can cause resistance to PARP inhibitors (Cao et al., 2009) and has been reported in BRCA-deficient breast cancers (Bouwman et al., 2010). Screens to identify 53BP1 effectors identified 53BP1-interacting proteins as components of the shieldin complex (Findlay et al., 2018; Gupta et al., 2018; Noordermeer et al., 2018), which acts to protect DNA ends from end resection (Setiaputra and Durocher,

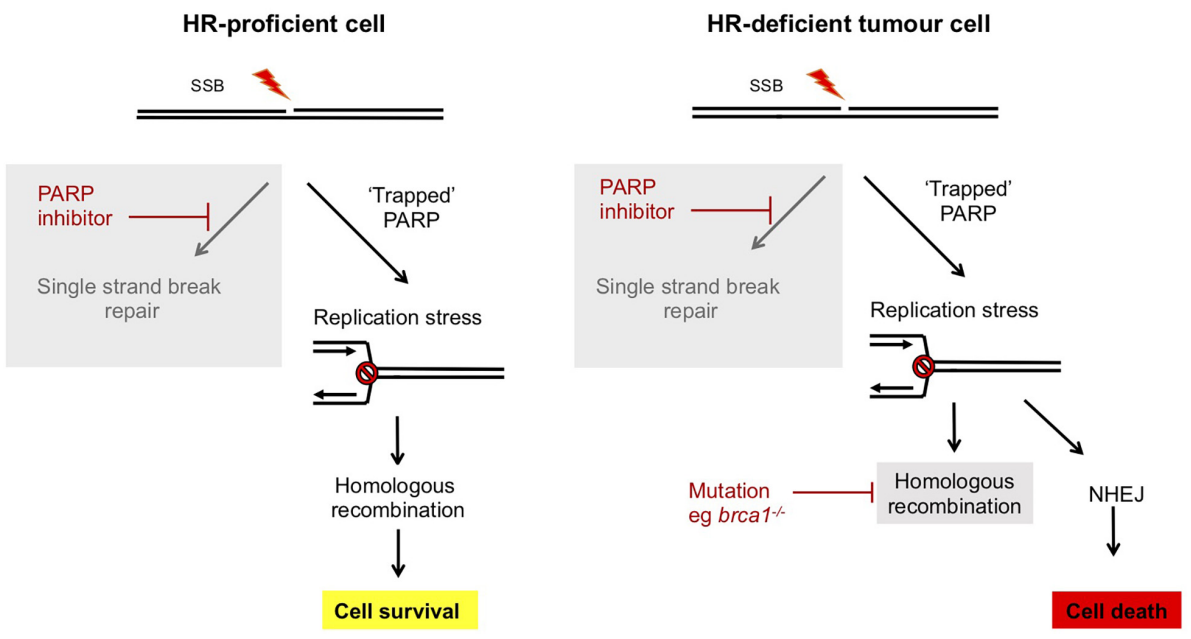

FIGURE 3 | Synthetic lethality of PARP inhibitors in treatment of breast and ovarian cancers deficient in BRCA1/2. In normal human cells, single strand breaks are repaired by PARP-dependent SSBR. In the presence of ART inhibitors PARP is trapped at the lesion and this impedes DNA replication. However, this replication stress can be repaired by an HR dependent mechanism and cells survive. However, in tumor cells which are deficient in components of HR, such as *brca1/2*$^{-/-}$ breast or ovarian cancers, HR-dependent resolution of replication stress is not possible and instead mutagenic NHEJ pathways prevail. This results in selective killing of tumor cells by PARP inhibitors (Bryant et al., 2005; Farmer et al., 2005; Slade, 2020).

2019). The ability to rapidly generate strains with multiple gene disruptions in *D. discoideum* facilitates analysis of this druggable pathway as resistance can be easily investigated following blocking combinations of pathways in the presence or absence of inhibitors. For example, this approach demonstrated that resistance to PARP inhibitors observed by disrupting NHEJ in an *exo1*$^{-}$ background (*dnapkcs*$^{-}$*exo1*$^{-}$ cells) is mediated by promoting end-resection to reactivate HR. Small molecule inhibitors of Mre11, a second nuclease involved in strand resection during HR, restores sensitivity of *dnapkcs*$^{-}$*exo1*$^{-}$ cells to PARP inhibitors (Kolb et al., 2017). This highlights redundancy between the nucleases Exo1 and Mre11 in HR and suggests combination approaches to avoid resistance in cells deficient in one nuclease.

The importance of understanding the role for ADPr in interplay between repair pathways in cancer therapy is also apparent when considering repair of ICLs by drugs such as cisplatin, which are used to treat a number of cancers. Studies in *D. discoideum* first revealed a role for ADPr in tolerance to cisplatin and, as initially demonstrated for SSBR, inhibition of one ART leads to channeling the damage to a second ART-dependent repair pathway (Gunn et al., 2016) reminiscent of the interplay identified for SSB repair (Couto et al., 2013b). *D. discoideum* cells lacking Adprt2 (the major ART required for SSB repair) show increased sensitivity to cisplatin. However, in the absence of Adprt2, the damage is channeled into an Adprt1a-dependent pathway, which is most likely NHEJ. In human cells, a PARP-dependent pathway has been recently identified as playing an important role in repair of ICL (Li et al., 2020). The consequence of disrupting genes encoding NHEJ proteins in cells deficient in ICLs repair, such as FA cells, has been found to lead to either increased or decreased tolerance to cisplatin (Houghtaling et al., 2005; Adamo et al., 2010; Pace et al., 2010; Bunting et al., 2012). This difference may reflect the cell cycle profile of the cells. *D. discoideum* cells are predominantly in G2 phase (Weijer et al., 1984) and these may utilize NHEJ effectively whereas NHEJ is particularly toxic when used during S phase (Rothkamm et al., 2003). Overall understanding the interplay between ARTs in repair of different types of DNA damage and the generation of inhibitors specific for particular ARTs will allow for improved treatment strategies.

FUTURE DIRECTIONS

Dictyostelium discoideum clearly has much to offer in terms of a system to study the DDR both to delineate pathway mechanisms and investigate the interplay between pathways that play a vital role in genome stability. Initial interest focused on genetic analysis of strains disrupted in pathway components shared with mammalian cells, though the development of genome editing techniques means this analysis, in addition to genome-wide genetic screens, is now feasible in human cells. However, *D. discoideum* still has an important role to play in this regard, for example in instances where human cells contain multiple copies of genes encoding enzymes with overlapping activities. An important example of this is probing modification of histone proteins as the *D. discoideum* genome has mostly single copy genes encoding a range of histone variants (Stevense et al., 2011; Hsu et al., 2012). Introduction of mutations into endogenous single copy histone genes has been used to demonstrate a role for these in transcriptional memory, interplay between histone modifications, and in tolerance of cells to agents that target histone deacetylases used in cancer treatments (Muramoto et al., 2010; Hsu et al., 2012; Huang et al., 2021). It has long been apparent that histones are a major substrate for ADPr following DNA damage, and this is also true in *D. discoideum* (Rickwood and Osman, 1979; Rajawat et al., 2007; Couto et al., 2011; Rakhimova et al., 2017). Advances in mass spectrometry have recently revealed the major sites on histones that are ADPr in response to DNA damage (Jungmichel et al., 2013; Hottiger, 2015; Leidecker et al., 2016; Palazzo et al., 2018; Chen et al., 2021). The ability to manipulate multiple genes simultaneously and, in particular, to introduce mutations into endogenous histone proteins both singly and in combination (Rakhimova et al., 2017; Asano et al., 2021), offers a unique opportunity to study the role of these modifications in orchestrating DNA repair pathways.

Whilst screens of mutations introduced by CRISPR/Cas9 are now possible in human cells, the mutations are loss of function and the large number of genes, often with redundant functions, make these screens time consuming and expensive. The small genome size of *D. discoideum* facilitates saturation screens following treatment with DNA damaging agents and their subsequent identification by whole genome sequencing. Importantly, this approach has been shown to identify dominant, gain of function, as well as recessive mutations (Li et al., 2016). Therefore, *D. discoideum* has important potential in screens for example for tolerance to DNA damaging agents used in chemotherapy or mutations that drive resistance to these and other agents, for example PARP inhibitors. The ability to specifically manipulate genes offers the further possibility to perform these experiments in a variety of genetic backgrounds such as those containing mutations found in human cancer predispositions. In an alternative approach, genes encoding a small number of proteins implicated in DNA repair pathways in other eukaryotes are not apparent in the *D. discoideum* genome including ATM (Block and Lees-Miller, 2005; Hudson et al., 2005), a damage-activated protein kinase whose mutation in humans leads to Ataxia Telangiectasia. Similarly, *D. discoideum* undergoes a sexual life cycle with evidence for high levels of meiotic recombination but is missing an ortholog of Spo11, an enzyme required to initiate crossover during meiosis in other eukaryotes (Bloomfield, 2019; Bloomfield et al., 2019). Characterizing the molecular mechanisms which replace these "missing" components will reveal alternative pathways that might be exploited to ameliorate human diseases caused by their loss.

The majority of investigations into the mammalian DDR take place in proliferating cultured cells, which precludes an understanding of the effect of DNA damage and repair in a developmental context. Although unicellular when feeding, on starvation *D. discoideum* amoebae aggregate to form a multicellular structure which undergoes a rapid developmental process to generate a fruiting body with spores supported

by a stalk comprised of dead, vacuolated cells (Kessin, 2001; Pears and Gross, 2021). This unusual developmental life cycle provides a tractable system in which to investigate any changes in repair activity during multicellular development and in differentiated cells (Kadam et al., 2021). It also facilitates analysis of the developmental consequences for cells accumulating DNA damage, as single cells can be fluorescently labeled and imaged throughout the process. Single cell transcriptomics has revealed a population of growing *D. discoideum* cells with high levels of spontaneous DNA damage, identified by expression of high levels of transcripts encoding the *D. discoideum* ortholog of Rad51, a repair protein involved in HR (Miermont et al., 2019). Interestingly cells expressing high levels of Rad51 are able to enter development but are frequently lost from the multicellular structure and excluded from entering the spore differentiation pathway. Prespore cells undergo a round of division during mid development (Muramoto and Chubb, 2008), so this might be explained by a block or delay in cell cycle progression caused by DNA damage inducing arrest at a cell cycle checkpoint. Spores are very resistant to DNA damage and loss of a prespore-specific catalase gene leads to sensitivity to hydrogen peroxide, an agent that induces predominantly single strand breaks (Garcia et al., 2003). Germinating spores have been shown to have an increased dependency on NHEJ to repair DNA DSBs as opposed to growing cells, which preferentially use accurate HR repair (Hudson et al., 2005). Understanding the interplay between development and DNA repair as well as the consequences of accumulation of mutations in differentiated tissue, will inform on the developmental consequences of inherited mutations in repair pathways, as seen in FA patients or neurological defects associated with genome instability syndromes such as Ataxia Telangiectasia or Nijmegen breakage syndrome.

CONCLUSION

Preserving genome integrity through repair of DNA damage is critical for human health. Defects in repair pathways lead to a variety of diseases such as neurodegeneration, immune-deficiencies, congenital abnormalities and malignancy. The presence of repair pathways and components in *D. discoideum* lacking in other model organisms has been instrumental in revealing interplay between repair pathways with implications for targeting these in treatment of these, notably in cancer. The integration of traditional genetic and biochemical approaches along with next generation sequencing of both genomes and RNA in single cells, along with the ease of investigating the developmental program, will facilitate future discoveries.

AUTHOR CONTRIBUTIONS

CP wrote the manuscript. NL and JB revised and edited the manuscript. All authors contributed to manuscript revision, read, and approved the submitted version.

FUNDING

Research in CP lab was funded by National Centre for the Replacement Refinement and Reduction of Animals in Research (NC3Rs) grant numbers NC/M000834/1 and NCK500355/1 and CrackIt Solutions Funding. Research in NL lab was funded by the MRC (MR/P028284/1 and MR/P018963/1). JB was funded by the EPA Cephalosporin Fund, award number CF 345.

REFERENCES

Adamo, A., Collis, S. J., Adelman, C. A., Silva, N., Horejsi, Z., Ward, J. D., et al. (2010). Preventing nonhomologous end joining suppresses DNA repair defects of Fanconi anemia. *Mol. Cell* 39, 25–35. doi: 10.1016/j.molcel.2010.06.026

Ahel, D., Horejsi, Z., Wiechens, N., Polo, S. E., Garcia-Wilson, E., Ahel, I., et al. (2009). Poly(ADP-ribose)-dependent regulation of DNA repair by the chromatin remodeling enzyme ALC1. *Science* 325, 1240–1243. doi: 10.1126/science.1177321

Ahel, I., Ahel, D., Matsusaka, T., Clark, A. J., Pines, J., Boulton, S. J., et al. (2008). Poly(ADP-ribose)-binding zinc finger motifs in DNA repair/checkpoint proteins. *Nature* 451, 81–85. doi: 10.1038/nature06420

Alexander, S., Min, J., and Alexander, H. (2006). *Dictyostelium discoideum* to human cells: pharmacogenetic studies demonstrate a role for sphingolipids in chemoresistance. *Biochim. Biophys. Acta* 1760, 301–309. doi: 10.1016/j.bbagen.2005.11.015

Asano, Y., Yamashita, K., Hasegawa, A., Ogasawara, T., Iriki, H., and Muramoto, T. (2021). Knock-in and precise nucleotide substitution using near-PAMless engineered Cas9 variants in *Dictyostelium discoideum*. *Sci. Rep.* 11:11163. doi: 10.1038/s41598-021-89546-0

Auer, B., Flick, K., Wang, Z. Q., Haidacher, D., Jager, S., Berghammer, H., et al. (1995). On the biological role of the nuclear polymerizing NAD+: protein(ADP-ribosyl) transferase (ADPRT): ADPRT from *Dictyostelium discoideum* and inactivation of the ADPRT gene in the mouse. *Biochimie* 77, 444–449. doi: 10.1016/0300-9084(96)88158-2

Azarm, K., and Smith, S. (2020). Nuclear PARPs and genome integrity. *Genes Dev.* 34, 285–301. doi: 10.1101/gad.334730.119

Barkauskaite, E., Jankevicius, G., and Ahel, I. (2015). Structures and mechanisms of enzymes employed in the synthesis and degradation of PARP-dependent protein ADP-ribosylation. *Mol. Cell* 58, 935–946. doi: 10.1016/j.molcel.2015.05.007

Beck, C., Boehler, C., Guirouilh Barbat, J., Bonnet, M. E., Illuzzi, G., Ronde, P., et al. (2014). PARP3 affects the relative contribution of homologous recombination and nonhomologous end-joining pathways. *Nucleic Acids Res.* 42, 5616–5632. doi: 10.1093/nar/gku174

Block, W. D., and Lees-Miller, S. P. (2005). Putative homologues of the DNA-dependent protein kinase catalytic subunit (DNA-PKcs) and other components of the non-homologous end joining machinery in *Dictyostelium discoideum*. *DNA Repair* 4, 1061–1065. doi: 10.1016/j.dnarep.2005.06.008

Bloomfield, G. (2019). Sex and macrocyst formation in *Dictyostelium*. *Int. J. Dev. Biol.* 63, 439–446. doi: 10.1387/ijdb.190183gb

Bloomfield, G., Paschke, P., Okamoto, M., Stevens, T. J., and Urushihara, H. (2019). Triparental inheritance in *Dictyostelium*. *Proc. Natl. Acad. Sci. U.S.A.* 116, 2187–2192. doi: 10.1073/pnas.1814425116

Bloomfield, G., Tanaka, Y., Skelton, J., Ivens, A., and Kay, R. R. (2008). Widespread duplications in the genomes of laboratory stocks of *Dictyostelium discoideum*. *Genome Biol.* 9:R75. doi: 10.1186/gb-2008-9-4-r75

Boehler, C., Gauthier, L. R., Mortusewicz, O., Biard, D. S., Saliou, J. M., Bresson, A., et al. (2011). Poly(ADP-ribose) polymerase 3 (PARP3), a newcomer in cellular response to DNA damage and mitotic progression. *Proc. Natl. Acad. Sci. U.S.A.* 108, 2783–2788. doi: 10.1073/pnas.1016574108

Bogliolo, M., Schuster, B., Stoepker, C., Derkunt, B., Su, Y., Raams, A., et al. (2013). Mutations in ERCC4, encoding the DNA-repair endonuclease XPF,

cause Fanconi anemia. *Am. J. Hum. Genet.* 92, 800–806. doi: 10.1016/j.ajhg.2013.04.002

Bouwman, P., Aly, A., Escandell, J. M., Pieterse, M., Bartkova, J., van der Gulden, H., et al. (2010). 53BP1 loss rescues BRCA1 deficiency and is associated with triple-negative and BRCA-mutated breast cancers. *Nat. Struct. Mol. Biol.* 17, 688–695. doi: 10.1038/nsmb.1831

Bryant, H. E., Schultz, N., Thomas, H. D., Parker, K. M., Flower, D., Lopez, E., et al. (2005). Specific killing of BRCA2-deficient tumours with inhibitors of poly(ADP-ribose) polymerase. *Nature* 434, 913–917. doi: 10.1038/nature03443

Bunting, S. F., Callen, E., Kozak, M. L., Kim, J. M., Wong, N., Lopez-Contreras, A. J., et al. (2012). BRCA1 functions independently of homologous recombination in DNA interstrand crosslink repair. *Mol. Cell* 46, 125–135. doi: 10.1016/j.molcel.2012.02.015

Caldecott, K. W. (2014). Protein ADP-ribosylation and the cellular response to DNA strand breaks. *DNA Repair* 19, 108–113. doi: 10.1016/j.dnarep.2014.03.021

Cao, L., Xu, X., Bunting, S. F., Liu, J., Wang, R. H., Cao, L. L., et al. (2009). A selective requirement for 53BP1 in the biological response to genomic instability induced by Brca1 deficiency. *Mol. Cell* 35, 534–541. doi: 10.1016/j.molcel.2009.06.037

Ceccaldi, R., Liu, J. C., Amunugama, R., Hajdu, I., Primack, B., Petalcorin, M. I., et al. (2015). Homologous-recombination-deficient tumours are dependent on Poltheta-mediated repair. *Nature* 518, 258–262. doi: 10.1038/nature14184

Chen, G., Zhuchenko, O., and Kuspa, A. (2007). Immune-like phagocyte activity in the social amoeba. *Science* 317, 678–681. doi: 10.1126/science.1143991

Chen, Q., Bian, C., Wang, X., Liu, X., Ahmad Kassab, M., Yu, Y., et al. (2021). ADP-ribosylation of histone variant H2AX promotes base excision repair. *EMBO J.* 40:e104542. doi: 10.15252/embj.2020104542

Citarelli, M., Teotia, S., and Lamb, R. S. (2010). Evolutionary history of the poly(ADP-ribose) polymerase gene family in eukaryotes. *BMC Evol. Biol.* 10:308. doi: 10.1186/1471-2148-10-308

Couto, C. A., Hsu, D. W., Teo, R., Rakhimova, A., Lempidaki, S., Pears, C. J., et al. (2013b). Nonhomologous end-joining promotes resistance to DNA damage in the absence of an ADP-ribosyltransferase that signals DNA single strand breaks. *J. Cell Sci.* 126(Pt 15), 3452–3461. doi: 10.1242/jcs.128769

Couto, A. M., Lakin, N. D., and Pears, C. J. (2013a). Investigation of DNA repair pathway activity. *Methods Mol. Biol.* 983, 295–310. doi: 10.1007/978-1-62703-302-2_16

Couto, C. A., Wang, H. Y., Green, J. C., Kiely, R., Siddaway, R., Borer, C., et al. (2011). PARP regulates nonhomologous end joining through retention of Ku at double-strand breaks. *J. Cell Biol.* 194, 367–375. doi: 10.1083/jcb.201012132

Deering, R. A. (1968). *Dictyostelium discoideum*: a gamma-ray resistant organism. *Science* 162, 1289–1290. doi: 10.1126/science.162.3859.1289

Deering, R. A. (1994). *Dictyostelium discoideum*, a lower eukaryote model for the study of DNA repair: implications for the role of DNA-damaging chemicals in the evolution of repair proficient cells. *Adv. Space Res.* 14, 389–393. doi: 10.1016/0273-1177(94)90492-8

Denver, D. R., Morris, K., Lynch, M., and Thomas, W. K. (2004). High mutation rate and predominance of insertions in the *Caenorhabditis elegans* nuclear genome. *Nature* 430, 679–682. doi: 10.1038/nature02697

Dunn, J. D., Bosmani, C., Barisch, C., Raykov, L., Lefrancois, L. H., Cardenal-Munoz, E., et al. (2017). Eat prey, live: *Dictyostelium discoideum* as a model for cell-autonomous defenses. *Front. Immunol.* 8:1906. doi: 10.3389/fimmu.2017.01906

Durston, A. J., Weijer, C. J., Jongkind, J. F., Verkerk, A., Timmermans, A., and Te Kulve, W. (1984). A flow fluorimetric analysis of the cell cycle during growth and differentiation in *Dictyostelium discoideum*. *Wilehm Roux. Arch. Dev. Biol.* 194, 18–24. doi: 10.1007/BF00848949

Duxin, J. P., and Walter, J. C. (2015). What is the DNA repair defect underlying Fanconi anemia? *Curr. Opin. Cell Biol.* 37, 49–60. doi: 10.1016/j.ceb.2015.09.002

Eichinger, L., Pachebat, J. A., Glockner, G., Rajandream, M. A., Sucgang, R., Berriman, M., et al. (2005). The genome of the social amoeba *Dictyostelium discoideum*. *Nature* 435, 43–57. doi: 10.1038/nature03481

Farlow, A., Long, H., Arnoux, S., Sung, W., Doak, T. G., Nordborg, M., et al. (2015). The spontaneous mutation rate in the fission yeast *Schizosaccharomyces pombe*. *Genetics* 201, 737–744. doi: 10.1534/genetics.115.177329

Farmer, H., McCabe, N., Lord, C. J., Tutt, A. N., Johnson, D. A., Richardson, T. B., et al. (2005). Targeting the DNA repair defect in BRCA mutant cells as a therapeutic strategy. *Nature* 434, 917–921. doi: 10.1038/nature03445

Findlay, S., Heath, J., Luo, V. M., Malina, A., Morin, T., Coulombe, Y., et al. (2018). SHLD2/FAM35A co-operates with REV7 to coordinate DNA double-strand break repair pathway choice. *EMBO J.* 37:e100158. doi: 10.15252/embj.2018100158

Flowers, J. M., Li, S. I., Stathos, A., Saxer, G., Ostrowski, E. A., Queller, D. C., et al. (2010). Variation, sex, and social cooperation: molecular population genetics of the social amoeba *Dictyostelium discoideum*. *PLoS Genet.* 6:e1001013. doi: 10.1371/journal.pgen.1001013

Freim, J. O. Jr., and Deering, R. A. (1970). Ultraviolet irradiation of the vegetative cells of *Dictyostelium discoideum*. *J. Bacteriol.* 102, 36–42. doi: 10.1128/JB.102.1.36-42.1970

Garcia, M. X., Alexander, H., Mahadeo, D., Cotter, D. A., and Alexander, S. (2003). The *Dictyostelium discoideum* prespore-specific catalase B functions to control late development and to protect spore viability. *Biochim. Biophys. Acta* 1641, 55–64. doi: 10.1016/s0167-4889(03)00064-8

Garcia-de-Teresa, B., Rodriguez, A., and Frias, S. (2020). Chromosome instability in Fanconi anemia: from breaks to phenotypic consequences. *Genes* 11:1528. doi: 10.3390/genes11121528

Gibson, B. A., and Kraus, W. L. (2012). New insights into the molecular and cellular functions of poly(ADP-ribose) and PARPs. *Nat. Rev. Mol. Cell Biol.* 13, 411–424. doi: 10.1038/nrm3376

Gottschalk, A. J., Timinszky, G., Kong, S. E., Jin, J., Cai, Y., Swanson, S. K., et al. (2009). Poly(ADP-ribosyl)ation directs recruitment and activation of an ATP-dependent chromatin remodeler. *Proc. Natl. Acad. Sci. U.S.A.* 106, 13770–13774. doi: 10.1073/pnas.0906920106

Gunn, A. R., Banos-Pinero, B., Paschke, P., Sanchez-Pulido, L., Ariza, A., Day, J., et al. (2016). The role of ADP-ribosylation in regulating DNA interstrand crosslink repair. *J. Cell Sci.* 129, 3845–3858. doi: 10.1242/jcs.193375

Gupta, R., Somyajit, K., Narita, T., Maskey, E., Stanlie, A., Kremer, M., et al. (2018). DNA repair network analysis reveals shieldin as a key regulator of NHEJ and PARP inhibitor sensitivity. *Cell* 173, 972–988.e23. doi: 10.1016/j.cell.2018.03.050

Hanzlikova, H., Gittens, W., Krejcikova, K., Zeng, Z., and Caldecott, K. W. (2017). Overlapping roles for PARP1 and PARP2 in the recruitment of endogenous XRCC1 and PNKP into oxidized chromatin. *Nucleic Acids Res.* 45, 2546–2557. doi: 10.1093/nar/gkw1246

Hottiger, M. O. (2015). Nuclear ADP-ribosylation and its role in chromatin plasticity, cell differentiation, and epigenetics. *Annu. Rev. Biochem.* 84, 227–263. doi: 10.1146/annurev-biochem-060614-034506

Hottiger, M. O., Hassa, P. O., Luscher, B., Schuler, H., and Koch-Nolte, F. (2010). Toward a unified nomenclature for mammalian ADP-ribosyltransferases. *Trends Biochem. Sci.* 35, 208–219. doi: 10.1016/j.tibs.2009.12.003

Houghtaling, S., Newell, A., Akkari, Y., Taniguchi, T., Olson, S., and Grompe, M. (2005). Fancd2 functions in a double strand break repair pathway that is distinct from non-homologous end joining. *Hum. Mol. Genet.* 14, 3027–3033. doi: 10.1093/hmg/ddi334

Hsu, D. W., Chubb, J. R., Muramoto, T., Pears, C. J., and Mahadevan, L. C. (2012). Dynamic acetylation of lysine-4-trimethylated histone H3 and H3 variant biology in a simple multicellular eukaryote. *Nucleic Acids Res.* 40, 7247–7256. doi: 10.1093/nar/gks367

Hsu, D. W., Kiely, R., Couto, C. A., Wang, H. Y., Hudson, J. J., Borer, C., et al. (2011). DNA double-strand break repair pathway choice in *Dictyostelium*. *J. Cell Sci.* 124(Pt 10), 1655–1663. doi: 10.1242/jcs.081471

Huang, L. Y., Hsu, D. W., and Pears, C. J. (2021). Methylation-directed acetylation of histone H3 regulates developmental sensitivity to histone deacetylase inhibition. *Nucleic Acids Res.* 49, 3781–3795. doi: 10.1093/nar/gkab154

Hudson, J. J., Hsu, D. W., Guo, K., Zhukovskaya, N., Liu, P. H., Williams, J. G., et al. (2005). DNA-PKcs-dependent signaling of DNA damage in *Dictyostelium discoideum*. *Curr. Biol.* 15, 1880–1885. doi: 10.1016/j.cub.2005.09.039

Iriki, H., Kawata, T., and Muramoto, T. (2019). Generation of deletions and precise point mutations in *Dictyostelium discoideum* using the CRISPR nickase. *PLoS One* 14:e0224128. doi: 10.1371/journal.pone.0224128

Jankevicius, G., Hassler, M., Golia, B., Rybin, V., Zacharias, M., Timinszky, G., et al. (2013). A family of macrodomain proteins reverses cellular mono-ADP-ribosylation. *Nat. Struct. Mol. Biol.* 20, 508–514. doi: 10.1038/nsmb.2523

Jungmichel, S., Rosenthal, F., Altmeyer, M., Lukas, J., Hottiger, M. O., and Nielsen, M. L. (2013). Proteome-wide identification of poly(ADP-Ribosyl)ation targets in different genotoxic stress responses. *Mol. Cell* 52, 272–285. doi: 10.1016/j.molcel.2013.08.026

Kadam, A., Abuthakir, M. H. S., Jubin, T., Vaishnav, J., Garg, A., Balaji, C., et al. (2021). Identification and characterization of Poly(ADP-ribose) polymerase-1 interacting proteins during development of *Dictyostelium discoideum*. *Protein Expr. Purif.* 186:105923. doi: 10.1016/j.pep.2021.105923

Kashiyama, K., Nakazawa, Y., Pilz, D. T., Guo, C., Shimada, M., Sasaki, K., et al. (2013). Malfunction of nuclease ERCC1-XPF results in diverse clinical manifestations and causes Cockayne syndrome, xeroderma pigmentosum, and Fanconi anemia. *Am. J. Hum. Genet.* 92, 807–819. doi: 10.1016/j.ajhg.2013.04.007

Kessin, R. H. (2001). *Dictyostelium: Evolution, Cell Biology, and the Development of Multicellularity*. Cambridge: Cambridge University Press.

Kim, J. S., Krasieva, T. B., Kurumizaka, H., Chen, D. J., Taylor, A. M., and Yokomori, K. (2005). Independent and sequential recruitment of NHEJ and HR factors to DNA damage sites in mammalian cells. *J. Cell Biol.* 170, 341–347. doi: 10.1083/jcb.200411083

Kofler, B., Wallraff, E., Herzog, H., Schneider, R., Auer, B., and Schweiger, M. (1993). Purification and characterization of NAD+:ADP-ribosyltransferase (polymerizing) from *Dictyostelium discoideum*. *Biochem. J.* 293(Pt 1), 275–281. doi: 10.1042/bj2930275

Kolb, A. L., Gunn, A. R., and Lakin, N. D. (2017). Redundancy between nucleases required for homologous recombination promotes PARP inhibitor resistance in the eukaryotic model organism *Dictyostelium*. *Nucleic Acids Res.* 45, 10056–10067. doi: 10.1093/nar/gkx639

Kolb, A. L., Hsu, D. W., Wallis, A. B. A., Ura, S., Rakhimova, A., Pears, C. J., et al. (2018). Dictyostelium as a model to assess site-specific ADP-ribosylation events. *Methods Mol. Biol.* 1813, 125–148. doi: 10.1007/978-1-4939-8588-3_9

Krasovec, M., Eyre-Walker, A., Sanchez-Ferandin, S., and Piganeau, G. (2017). Spontaneous mutation rate in the smallest photosynthetic eukaryotes. *Mol. Biol. Evol.* 34, 1770–1779. doi: 10.1093/molbev/msx119

Krasovec, R., Richards, H., Gifford, D. R., Hatcher, C., Faulkner, K. J., Belavkin, R. V., et al. (2017). Spontaneous mutation rate is a plastic trait associated with population density across domains of life. *PLoS Biol.* 15:e2002731. doi: 10.1371/journal.pbio.2002731

Kucukyildirim, S., Behringer, M., Sung, W., Brock, D. A., Doak, T. G., Mergen, H., et al. (2020). Low base-substitution mutation rate but high rate of slippage mutations in the sequence repeat-rich genome of *Dictyostelium discoideum*. *G3* 10, 3445–3452. doi: 10.1534/g3.120.401578

Langevin, F., Crossan, G. P., Rosado, I. V., Arends, M. J., and Patel, K. J. (2011). Fancd2 counteracts the toxic effects of naturally produced aldehydes in mice. *Nature* 475, 53–58. doi: 10.1038/nature10192

Lee, H., Popodi, E., Tang, H., and Foster, P. L. (2012). Rate and molecular spectrum of spontaneous mutations in the bacterium *Escherichia coli* as determined by whole-genome sequencing. *Proc. Natl. Acad. Sci. U.S.A.* 109, E2774–E2783. doi: 10.1073/pnas.1210309109

Lehoczky, P., McHugh, P. J., and Chovanec, M. (2007). DNA interstrand crosslink repair in *Saccharomyces cerevisiae*. *FEMS Microbiol. Rev.* 31, 109–133. doi: 10.1111/j.1574-6976.2006.00046.x

Leidecker, O., Bonfiglio, J. J., Colby, T., Zhang, Q., Atanassov, I., Zaja, R., et al. (2016). Serine is a new target residue for endogenous ADP-ribosylation on histones. *Nat. Chem. Biol.* 12, 998–1000. doi: 10.1038/nchembio.2180

Li, C. L., Santhanam, B., Webb, A. N., Zupan, B., and Shaulsky, G. (2016). Gene discovery by chemical mutagenesis and whole-genome sequencing in *Dictyostelium*. *Genome Res.* 26, 1268–1276. doi: 10.1101/gr.205682.116

Li, N., Wang, J., Wallace, S. S., Chen, J., Zhou, J., and D'Andrea, A. D. (2020). Cooperation of the NEIL3 and Fanconi anemia/BRCA pathways in interstrand crosslink repair. *Nucleic Acids Res.* 48, 3014–3028. doi: 10.1093/nar/gkaa038

Long, H., Behringer, M. G., Williams, E., Te, R., and Lynch, M. (2016a). Similar mutation rates but highly diverse mutation spectra in ascomycete and basidiomycete yeasts. *Genome Biol. Evol.* 8, 3815–3821. doi: 10.1093/gbe/evw286

Long, H., Winter, D. J., Chang, A. Y., Sung, W., Wu, S. H., Balboa, M., et al. (2016b). Low base-substitution mutation rate in the germline genome of the ciliate *Tetrahymena thermophil*. *Genome Biol. Evol.* 8, 3629–3639. doi: 10.1093/gbe/evw223

Martin-Hernandez, K., Rodriguez-Vargas, J. M., Schreiber, V., and Dantzer, F. (2017). Expanding functions of ADP-ribosylation in the maintenance of genome integrity. *Semin. Cell Dev. Biol.* 63, 92–101. doi: 10.1016/j.semcdb.2016.09.009

Mateos-Gomez, P. A., Gong, F., Nair, N., Miller, K. M., Lazzerini-Denchi, E., and Sfeir, A. (2015). Mammalian polymerase theta promotes alternative NHEJ and suppresses recombination. *Nature* 518, 254–257. doi: 10.1038/nature14157

McConnell, R., Middlemist, S., Scala, C., Strassmann, J. E., and Queller, D. C. (2007). An unusually low microsatellite mutation rate in *Dictyostelium discoideum*, an organism with unusually abundant microsatellites. *Genetics* 177, 1499–1507. doi: 10.1534/genetics.107.076067

McHugh, P. J. (2020). XPF-ERCC1: linchpin of DNA crosslink repair. *PLoS Genet.* 16:e1008616. doi: 10.1371/journal.pgen.1008616

McVey, M., and Lee, S. E. (2008). MMEJ repair of double-strand breaks (director's cut): deleted sequences and alternative endings. *Trends Genet.* 24, 529–538. doi: 10.1016/j.tig.2008.08.007

Menissier de Murcia, J., Ricoul, M., Tartier, L., Niedergang, C., Huber, A., Dantzer, F., et al. (2003). Functional interaction between PARP-1 and PARP-2 in chromosome stability and embryonic development in mouse. *EMBO J.* 22, 2255–2263. doi: 10.1093/emboj/cdg206

Miermont, A., Antolovic, V., Lenn, T., Nichols, J. M. E., Millward, L. J., and Chubb, J. R. (2019). The fate of cells undergoing spontaneous DNA damage during development. *Development* 146:dev174268. doi: 10.1242/dev.174268

Min, J., Stegner, A. L., Alexander, H., and Alexander, S. (2004). Overexpression of sphingosine-1-phosphate lyase or inhibition of sphingosine kinase in *Dictyostelium discoideum* results in a selective increase in sensitivity to platinum-based chemotherapy drugs. *Eukaryot. Cell* 3, 795–805. doi: 10.1128/EC.3.3.795-805.2004

Min, J., Traynor, D., Stegner, A. L., Zhang, L., Hanigan, M. H., Alexander, H., et al. (2005a). Sphingosine kinase regulates the sensitivity of *Dictyostelium discoideum* cells to the anticancer drug cisplatin. *Eukaryot. Cell* 4, 178–189. doi: 10.1128/EC.4.1.178-189.2005

Min, J., Van Veldhoven, P. P., Zhang, L., Hanigan, M. H., Alexander, H., and Alexander, S. (2005b). Sphingosine-1-phosphate lyase regulates sensitivity of human cells to select chemotherapy drugs in a p38-dependent manner. *Mol. Cancer Res.* 3, 287–296. doi: 10.1158/1541-7786.MCR-04-0197

Mir, H., Alex, T., Rajawat, J., Kadam, A., and Begum, R. (2015). Response of *Dictyostelium discoideum* to UV-C and involvement of poly (ADP-ribose) polymerase. *Cell Prolif.* 48, 363–374. doi: 10.1111/cpr.12182

Mulderrig, L., and Garaycoechea, J. I. (2020). XPF-ERCC1 protects liver, kidney and blood homeostasis outside the canonical excision repair pathways. *PLoS Genet.* 16:e1008555. doi: 10.1371/journal.pgen.1008555

Muramoto, T., and Chubb, J. R. (2008). Live imaging of the *Dictyostelium* cell cycle reveals widespread S phase during development, a G2 bias in spore differentiation and a premitotic checkpoint. *Development* 135, 1647–1657. doi: 10.1242/dev.020115

Muramoto, T., Muller, I., Thomas, G., Melvin, A., and Chubb, J. R. (2010). Methylation of H3K4 Is required for inheritance of active transcriptional states. *Curr. Biol.* 20, 397–406. doi: 10.1016/j.cub.2010.01.017

Nakamura, J., and Nakamura, M. (2020). DNA-protein crosslink formation by endogenous aldehydes and AP sites. *DNA Repair* 88:102806. doi: 10.1016/j.dnarep.2020.102806

Noordermeer, S. M., Adam, S., Setiaputra, D., Barazas, M., Pettitt, S. J., Ling, A. K., et al. (2018). The shieldin complex mediates 53BP1-dependent DNA repair. *Nature* 560, 117–121. doi: 10.1038/s41586-018-0340-7

Otto, H., Reche, P. A., Bazan, F., Dittmar, K., Haag, F., and Koch-Nolte, F. (2005). In silico characterization of the family of PARP-like poly(ADP-ribosyl)transferases (pARTs). *BMC Genomics* 6:139. doi: 10.1186/1471-2164-6-139

Pace, P., Mosedale, G., Hodskinson, M. R., Rosado, I. V., Sivasubramaniam, M., and Patel, K. J. (2010). Ku70 corrupts DNA repair in the absence of the Fanconi anemia pathway. *Science* 329, 219–223. doi: 10.1126/science.1192277

Palazzo, L., Leidecker, O., Prokhorova, E., Dauben, H., Matic, I., and Ahel, I. (2018). Serine is the major residue for ADP-ribosylation upon DNA damage. *Elife* 7:e34334. doi: 10.7554/eLife.34334

Palazzo, L., Mikolcevic, P., Mikoc, A., and Ahel, I. (2019). ADP-ribosylation signalling and human disease. *Open Biol.* 9:190041. doi: 10.1098/rsob.190041

Pears, C. J., Couto, C. A., Wang, H. Y., Borer, C., Kiely, R., and Lakin, N. D. (2012). The role of ADP-ribosylation in regulating DNA double-strand break repair. *Cell Cycle* 11, 48–56. doi: 10.4161/cc.11.1.18793

Pears, C. J., and Gross, J. D. (2021). Microbe profile: *Dictyostelium discoideum*: model system for development, chemotaxis and biomedical research. *Microbiology* 167. doi: 10.1099/mic.0.001040 [Epub ahead of print].

Pears, C. J., and Lakin, N. D. (2014). Emerging models for DNA repair: *Dictyostelium discoideum* as a model for nonhomologous end-joining. *DNA Repair* 17, 121–131. doi: 10.1016/j.dnarep.2014.01.008

Pierce, A. J., Hu, P., Han, M., Ellis, N., and Jasin, M. (2001). Ku DNA end-binding protein modulates homologous repair of double-strand breaks in mammalian cells. *Genes Dev.* 15, 3237–3242. doi: 10.1101/gad.946401

Pontel, L. B., Langenick, J., Rosado, I. V., Zhang, X. Y., Traynor, D., Kay, R. R., et al. (2016). Xpf suppresses the mutagenic consequences of phagocytosis in *Dictyostelium*. *J. Cell Sci.* 129, 4449–4454. doi: 10.1242/jcs.196337

Rack, J. G., Perina, D., and Ahel, I. (2016). Macrodomains: structure, function, evolution, and catalytic activities. *Annu. Rev. Biochem.* 85, 431–454. doi: 10.1146/annurev-biochem-060815-014935

Rack, J. G. M., Palazzo, L., and Ahel, I. (2020). (ADP-ribosyl)hydrolases: structure, function, and biology. *Genes Dev.* 34, 263–284. doi: 10.1101/gad.334631.119

Rajawat, J., Vohra, I., Mir, H. A., Gohel, D., and Begum, R. (2007). Effect of oxidative stress and involvement of poly(ADP-ribose) polymerase (PARP) in *Dictyostelium discoideum* development. *FEBS J.* 274, 5611–5618. doi: 10.1111/j.1742-4658.2007.06083.x

Rakhimova, A., Ura, S., Hsu, D. W., Wang, H. Y., Pears, C. J., and Lakin, N. D. (2017). Site-specific ADP-ribosylation of histone H2B in response to DNA double strand breaks. *Sci. Rep.* 7:43750. doi: 10.1038/srep43750

Rickwood, D., and Osman, M. S. (1979). Characterisation of poly(ADP-Rib) polymerase activity in nuclei from the slime mould *Dictyostelium discoideum*. *Mol. Cell. Biochem.* 27, 79–84. doi: 10.1007/BF00218351

Ronson, G. E., Piberger, A. L., Higgs, M. R., Olsen, A. L., Stewart, G. S., McHugh, P. J., et al. (2018). PARP1 and PARP2 stabilise replication forks at base excision repair intermediates through Fbh1-dependent Rad51 regulation. *Nat. Commun.* 9:746. doi: 10.1038/s41467-018-03159-2

Rosenthal, F., Feijs, K. L., Frugier, E., Bonalli, M., Forst, A. H., Imhof, R., et al. (2013). Macrodomain-containing proteins are new mono-ADP-ribosylhydrolases. *Nat. Struct. Mol. Biol.* 20, 502–507. doi: 10.1038/nsmb.2521

Rothkamm, K., Kruger, I., Thompson, L. H., and Lobrich, M. (2003). Pathways of DNA double-strand break repair during the mammalian cell cycle. *Mol. Cell. Biol.* 23, 5706–5715. doi: 10.1128/MCB.23.16.5706-5715.2003

Rouleau, M., Patel, A., Hendzel, M. J., Kaufmann, S. H., and Poirier, G. G. (2010). PARP inhibition: PARP1 and beyond. *Nat. Rev. Cancer* 10, 293–301. doi: 10.1038/nrc2812

Rulten, S. L., Fisher, A. E., Robert, I., Zuma, M. C., Rouleau, M., Ju, L., et al. (2011). PARP-3 and APLF function together to accelerate nonhomologous end-joining. *Mol. Cell* 41, 33–45. doi: 10.1016/j.molcel.2010.12.006

Saxer, G., Havlak, P., Fox, S. A., Quance, M. A., Gupta, S., Fofanov, Y., et al. (2012). Whole genome sequencing of mutation accumulation lines reveals a low mutation rate in the social amoeba *Dictyostelium discoideum*. *PLoS One* 7:e46759. doi: 10.1371/journal.pone.0046759

Scala, C., Tian, X., Mehdiabadi, N. J., Smith, M. H., Saxer, G., Stephens, K., et al. (2012). Amino acid repeats cause extraordinary coding sequence variation in the social amoeba *Dictyostelium discoideum*. *PLoS One* 7:e46150. doi: 10.1371/journal.pone.0046150

Schreiber, V., Ame, J. C., Dolle, P., Schultz, I., Rinaldi, B., Fraulob, V., et al. (2002). Poly(ADP-ribose) polymerase-2 (PARP-2) is required for efficient base excision DNA repair in association with PARP-1 and XRCC1. *J. Biol. Chem.* 277, 23028–23036. doi: 10.1074/jbc.M202390200

Sekine, R., Kawata, T., and Muramoto, T. (2018). CRISPR/Cas9 mediated targeting of multiple genes in *Dictyostelium*. *Sci. Rep.* 8:8471. doi: 10.1038/s41598-018-26756-z

Setiaputra, D., and Durocher, D. (2019). Shieldin – the protector of DNA ends. *EMBO Rep.* 20:e47560. doi: 10.15252/embr.201847560

Slade, D. (2020). PARP and PARG inhibitors in cancer treatment. *Genes Dev.* 34, 360–394. doi: 10.1101/gad.334516.119

Stevense, M., Chubb, J. R., and Muramoto, T. (2011). Nuclear organization and transcriptional dynamics in *Dictyostelium*. *Dev. Growth Differ.* 53, 576–586. doi: 10.1111/j.1440-169X.2011.01271.x

Timinszky, G., Till, S., Hassa, P. O., Hothorn, M., Kustatscher, G., Nijmeijer, B., et al. (2009). A macrodomain-containing histone rearranges chromatin upon sensing PARP1 activation. *Nat. Struct. Mol. Biol.* 16, 923–929. doi: 10.1038/nsmb.1664

Van Driessche, N., Alexander, H., Min, J., Kuspa, A., Alexander, S., and Shaulsky, G. (2007). Global transcriptional responses to cisplatin in *Dictyostelium discoideum* identify potential drug targets. *Proc. Natl. Acad. Sci. U.S.A.* 104, 15406–15411. doi: 10.1073/pnas.0705996104

Vyas, S., Matic, I., Uchima, L., Rood, J., Zaja, R., Hay, R. T., et al. (2014). Family-wide analysis of poly(ADP-ribose) polymerase activity. *Nat. Commun.* 5:4426. doi: 10.1038/ncomms5426

Weijer, C. J., Duschl, G., and David, C. N. (1984). A revision of the *Dictyostelium discoideum* cell cycle. *J. Cell Sci.* 70, 111–131.

Yu, S. L., Lee, S. K., Alexander, H., and Alexander, S. (1998). Rapid changes of nucleotide excision repair gene expression following UV-irradiation and cisplatin treatment of *Dictyostelium discoideum*. *Nucleic Acids Res.* 26, 3397–3403. doi: 10.1093/nar/26.14.3397

Zhang, X. Y., Langenick, J., Traynor, D., Babu, M. M., Kay, R. R., and Patel, K. J. (2009). Xpf and not the Fanconi anaemia proteins or Rev3 accounts for the extreme resistance to cisplatin in *Dictyostelium discoideum*. *PLoS Genet.* 5:e1000645. doi: 10.1371/journal.pgen.1000645

Conflict of Interest: The authors declare that the research was conducted in the absence of any commercial or financial relationships that could be construed as a potential conflict of interest.

Publisher's Note: All claims expressed in this article are solely those of the authors and do not necessarily represent those of their affiliated organizations, or those of the publisher, the editors and the reviewers. Any product that may be evaluated in this article, or claim that may be made by its manufacturer, is not guaranteed or endorsed by the publisher.

Copyright © 2021 Pears, Brustel and Lakin. This is an open-access article distributed under the terms of the Creative Commons Attribution License (CC BY). The use, distribution or reproduction in other forums is permitted, provided the original author(s) and the copyright owner(s) are credited and that the original publication in this journal is cited, in accordance with accepted academic practice. No use, distribution or reproduction is permitted which does not comply with these terms.

frontiers in Cell and Developmental Biology

REVIEW
published: 13 October 2021
doi: 10.3389/fcell.2021.731964

Dictyostelium Dynamin Superfamily GTPases Implicated in Vesicle Trafficking and Host-Pathogen Interactions

Ana Katic[1†], Dario Hüsler[1†], François Letourneur[2] and Hubert Hilbi[1*]*

[1] *Institute of Medical Microbiology, University of Zürich, Zurich, Switzerland,* [2] *Laboratory of Pathogen Host Interactions, Université de Montpellier, CNRS, INSERM, Montpellier, France*

OPEN ACCESS

Edited by:
Annette Müller-Taubenberger, Ludwig Maximilian University of Munich, Germany

Reviewed by:
Monica Hagedorn, Jacobs University Bremen, Germany
James Alan Marrs, Indiana University, Purdue University Indianapolis, United States
Shigehiko Yumura, Yamaguchi University, Japan

****Correspondence:***
François Letourneur
francois.letourneur@umontpellier.fr
Hubert Hilbi
hilbi@imm.uzh.ch

† These authors have contributed equally to this work

Specialty section:
This article was submitted to Molecular and Cellular Pathology, a section of the journal Frontiers in Cell and Developmental Biology

Received: *28 June 2021*
Accepted: *14 September 2021*
Published: *13 October 2021*

Citation:
Katic A, Hüsler D, Letourneur F and Hilbi H (2021) Dictyostelium Dynamin Superfamily GTPases Implicated in Vesicle Trafficking and Host-Pathogen Interactions. Front. Cell Dev. Biol. 9:731964. doi: 10.3389/fcell.2021.731964

The haploid social amoeba *Dictyostelium discoideum* is a powerful model organism to study vesicle trafficking, motility and migration, cell division, developmental processes, and host cell-pathogen interactions. Dynamin superfamily proteins (DSPs) are large GTPases, which promote membrane fission and fusion, as well as membrane-independent cellular processes. Accordingly, DSPs play crucial roles for vesicle biogenesis and transport, organelle homeostasis, cytokinesis and cell-autonomous immunity. Major progress has been made over the last years in elucidating the function and structure of mammalian DSPs. *D. discoideum* produces at least eight DSPs, which are involved in membrane dynamics and other processes. The function and structure of these large GTPases has not been fully explored, despite the elaborate genetic and cell biological tools available for *D. discoideum*. In this review, we focus on the current knowledge about mammalian and *D. discoideum* DSPs, and we advocate the use of the genetically tractable amoeba to further study the role of DSPs in cell and infection biology. Particular emphasis is put on the virulence mechanisms of the facultative intracellular bacterium *Legionella pneumophila*.

Keywords: amoebae, *Dictyostelium discoideum*, effector protein, large GTPase, host-pathogen interaction, *Legionella*, *Mycobacterium*, vesicle trafficking

DICTYOSTELIUM DISCOIDEUM AS A MODEL TO STUDY MEMBRANE DYNAMICS AND HOST-PATHOGEN INTERACTIONS

The social soil amoeba *Dictyostelium discoideum* is a primordial phagocyte in its unicellular form and has been used as a model organism to analyze developmental processes, cytokinesis, vesicle trafficking, cell motility and migration, as well as host cell-pathogen interactions. In some instances, *D. discoideum* represents a valid model for human diseases, because the amoeba harbor a number of genes, which are implicated (in mutant form) in human diseases (Müller-Taubenberger et al., 2013). The haploid genome of *D. discoideum* is approximately 34 Mb large, comprises six chromosomes

Abbreviations: GPCR, G protein coupled receptor; Icm/Dot, intracellular multiplication/defective organelle trafficking; LCV, *Legionella*-containing vacuole; PI, phosphoinositide; PtdIns, phosphatidylinositol; T4SS, type IV secretion system.

and encodes approximately 12,500 predicted proteins, including a large number of mammalian orthologs (Eichinger et al., 2005). A large *D. discoideum* mutant collection is available from the *Dictyostelium* stock center[1] (Gaudet et al., 2011), and the amoeba can be genetically manipulated rather easily, using a remarkable repertoire of molecular genetic tools. Non-essential genes can be disrupted or replaced by homologous recombination, RNA interference has been described, and ectopic expression of endogenous or foreign genes is straightforward (Kuspa and Loomis, 1992; Faix et al., 2004; Kuhlmann et al., 2006; Paschke et al., 2018). In fact, recent cell biological and infection studies using dually labeled *D. discoideum* strains and confocal laser scanning microscopy or imaging flow cytometry revealed intriguing mechanistic insights into the virulence of the facultative intracellular bacterium *Legionella pneumophila* (Weber et al., 2014, 2018; Bärlocher et al., 2017a; Steiner et al., 2017; Welin et al., 2018; Hüsler et al., 2021).

Membrane dynamics, vesicle trafficking and organelle identity are controlled by a class of compartment-specific phospholipids termed phosphoinositide (PI) lipids (Payrastre et al., 2001; Di Paolo and De Camilli, 2006; Michell, 2008; Balla, 2013). The headgroup phosphatidylinositol (PtdIns) is reversibly mono- or polyphosphorylated by PI kinases and phosphatases at the 3′, 4′, and/or 5′ positions of the inositol ring. *D. discoideum* defined deletion mutants have been instrumental to elucidate the role of PI-metabolizing enzymes for membrane dynamics and vesicle trafficking, or cell motility and chemotaxis. Representative examples include PI 3-kinases (PI3Ks) and the PI 3-phosphatase PTEN (phosphatase and tensin homolog), which spatially and temporally regulate chemotaxis (Funamoto et al., 2002; Kölsch et al., 2008). The PI 5-phosphatase Dd5P4, a homolog of the mammalian enzyme OCRL (oculocerebrorenal syndrome of Lowe), acts on PtdIns(4,5)P_2 and PtdIns(3,4,5)P_3 and is implicated in phagocytosis (Loovers et al., 2007). The PI 5-kinase PIKfyve phosphorylates PtdIns(3)*P* during endocytosis (Buckley et al., 2019). Finally, RpkA (receptor phosphatidylinositol kinase A), a seven-helix transmembrane protein with a GPCR (G protein coupled receptor) signature and a predicted PtdIns(4)*P* 5-kinase domain is also implicated in phagocytosis and endocytosis (Riyahi et al., 2011).

In addition to the analysis of cell biological processes, *D. discoideum* has also been used as a model to study cellular host-pathogen interactions. In particular, the virulence of amoeba-resistant bacterial pathogens, such as *L. pneumophila* (Hoffmann et al., 2014b; Swart et al., 2018) or *Mycobacterium marinum* (Cardenal-Muñoz et al., 2017) can be assessed in *D. discoideum* at high spatial resolution and by live-cell microscopy. A drawback of using *D. discoideum* as an infection model for *L. pneumophila* is that the amoebae grow optimally at 23°C and die off beyond 26°C, while the pathogen has a growth optimum of 37°C and grows considerably slower at an infection temperature of 25°C. However, since many basic cell biological pathways are conserved in *D. discoideum* and mammalian cells, the amoebae are a powerful and versatile model to study the pathogenesis of *L. pneumophila* despite this limitation.

[1]http://dictybase.org/

The Gram-negative environmental bacterium *L. pneumophila* is the causative agent of a life-threatening pneumonia termed Legionnaires' disease (Newton et al., 2010). The main virulence factor of *L. pneumophila* is the Icm/Dot type IV secretion system (T4SS), which translocates more than 300 different "effector" proteins into host cells, where they subvert pivotal processes (Finsel and Hilbi, 2015; Qiu and Luo, 2017; Swart et al., 2020a). The opportunistic pathogen replicates intracellularly within a unique compartment, the *Legionella*-containing vacuole (LCV), in free-living amoebae as well as in macrophages (Hoffmann et al., 2014b; Boamah et al., 2017; Swart et al., 2018). This compartment restricts fusion with lysosomes, but communicates with the endosomal, secretory and retrograde vesicle trafficking pathways (Isberg et al., 2009; Hubber and Roy, 2010; Asrat et al., 2014; Personnic et al., 2016; Bärlocher et al., 2017b; Swart and Hilbi, 2020; **Figure 1**).

D. discoideum mutants were used to investigate the role of PI-metabolizing enzymes for intracellular growth of *L. pneumophila*. *D. discoideum* strains lacking PI3Ks (Weber et al., 2006; Peracino et al., 2010), PIKfyve (Buckley et al., 2019), Dd5P4/OCRL (Weber et al., 2009) or RpkA (Riyahi et al., 2011) are more permissive for *L. pneumophila* growth. In contrast, the deletion of PTEN does not affect intracellular growth, but reduces the uptake of *L. pneumophila* (Peracino et al., 2010), while PI3Ks are largely dispensable for bacterial uptake (Weber et al., 2006).

Decisive steps in the maturation of the LCV are a PI lipid conversion from the endosomal PtdIns(3)*P* to the secretory PtdIns(4)*P* (Weber et al., 2006, 2014; Steiner et al., 2018a; Swart and Hilbi, 2020), covalent and non-covalent subversion of small GTPases of the Arf, Rab, Ran, and Rap families (Rothmeier et al., 2013; Sherwood and Roy, 2013; Schmölders et al., 2017; Swart et al., 2020b), modulation of other trafficking factors such as the retromer coat complex (Finsel et al., 2013; Bärlocher et al., 2017a; Romano-Moreno et al., 2017; Yao et al., 2018), as well as the recruitment of tubular endoplasmic reticulum (ER) in *D. discoideum* and *A. castellanii* amoebae (Abu Kwaik, 1996; Lu and Clarke, 2005; Weber et al., 2014) and macrophages (Swanson and Isberg, 1995; Tilney et al., 2001; **Figure 1**). Proteomics of LCVs purified from infected *D. discoideum* revealed the presence of some of these factors on the pathogen vacuole (Urwyler et al., 2009; Hoffmann et al., 2014a; Schmölders et al., 2017). Interestingly, among the plethora of LCV host factors, we also identified dynamin superfamily proteins (DSPs), such as the fusion DSP Sey1/Atl3 and the scaffold DSP Gnbp (see below).

DYNAMIN SUPERFAMILY PROTEINS: MEDIATORS OF MEMBRANE FISSION AND FUSION

Cellular membranes are highly dynamic lipid bilayer structures that undergo constant remodeling. Among the numerous actors involved in the mechanisms underlying membrane remodeling, DSPs are well-studied large GTPases, which catalyze membrane fission and fusion events, and thus play key roles in endomembrane transport, vesicle biogenesis, organelle homeostasis, and cell division (Ramachandran and Schmid, 2018;

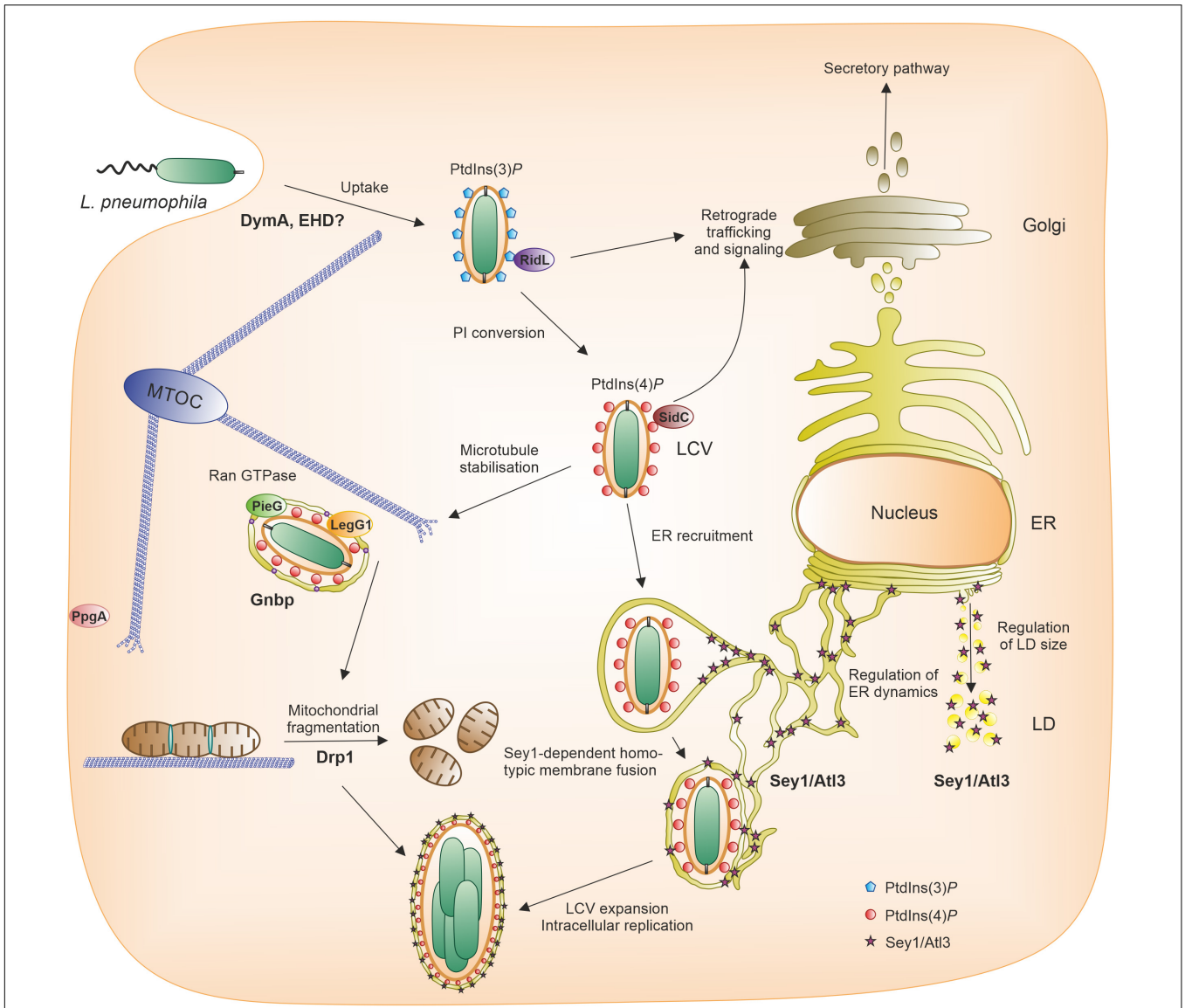

FIGURE 1 | Pathogen vacuole formation and intracellular replication of *L. pneumophila*. Following uptake of *L. pneumophila* by the host cell, a unique pathogen vacuole forms, the *Legionella*-containing vacuole (LCV). The LCV restricts interactions with lysosomes, but communicates with the endosomal, secretory and retrograde trafficking pathways and finally intimately associates with the ER. A hallmark of LCV maturation is the phosphoinositide (PI) lipid conversion from the endosomal PtdIns(3)*P* to the secretory PtdIns(4)*P*, both of which serve as membrane anchors of distinct *L. pneumophila* effector proteins (e.g., RidL, SidC). The RCC1 repeat domain effectors LegG1/MitF, PieG or PpgA localize to the LCV or the plasma membrane, respectively, and activate the small GTPase Ran to stabilize microtubules. In the course of LCV maturation, large GTPases also play a role. The dynamin superfamily protein (DSP) Sey1/Atl3 catalyzes pathogen vacuole expansion, the fission DSP Drp1 promotes intracellular bacterial replication by modulating mitochondrial fusion/fission dynamics, and the scaffold DSP Gnbp localizes to the pathogen vacuole. The *D. discoideum* DSP DymA and EHD possibly play a role for bacterial uptake. Accordingly, different DSPs play a role in LCV formation either *in cis* (on the LCV) or *in trans* (in a distance from the LCV). ER, endoplasmic reticulum; LCV, *Legionella*-containing vacuole; LD, lipid droplet; MTOC, microtubule organizing center; PI, phosphoinositide.

Jimah and Hinshaw, 2019). In addition, DSPs play important roles in cell-autonomous immunity to fight pathogens, as well as in the organization and regulation of microtubules and the actin cytoskeleton (Shpetner and Vallee, 1989; Palmer et al., 2015; Zhang et al., 2020). DSPs are present in all eukaryotic cells, and even bacteria display dynamin-like proteins with functions in cytokinesis, toxin secretion and drug resistance (Bramkamp, 2012; Liu et al., 2018; Wang et al., 2019; **Table 1**).

The phylogenetic tree of eukaryotic DSPs reveals a number of interesting facts (**Figure 2**). The human dynamins (Dnm1–3) form a separate cluster and are related to *D. discoideum* DymA and DymB. Interestingly, these *D. discoideum* DSPs are even more closely related to human dynamin-related protein 1 (Drp1) and yeast (*S. cerevisiae*) vacuolar protein sorting-associated protein 1 (Vps1). The *D. discoideum* dynamin-like proteins (DlpA-C) form a separate cluster within the fission

TABLE 1 | Eukaryotic dynamin superfamily proteins.

Protein family	Representative DSP member	*D. discoideum* ortholog	Function in *D. discoideum*
Fission DSP Dynamins	*H. sapiens* Dynamin-1 (Dnm1)	Not identified	Unknown
Fission DSP Dynamin-like	*H. sapiens* Dynamin-related protein-1 (Drp1)	Dynamin A (DymA) DDB_G0277849	Phagocytosis, cytokinesis
	S. cerevisiae Vacuolar protein sorting-associated protein-1 (Vps1)	Dynamin B (DymB) DDB_G0277851	Peroxisome scission
	Plant and algae Dynamin-related protein-5A (DRP5A)	Dynamin-like protein A, DlpA, DDB_G0268592	Cytokinesis, phagocytosis?
		Dynamin-like protein B, DlpB, DDB_G0285931	Cytokinesis
		Dynamin-like protein C, DlpC, DDB_G0271628	Cytokinesis?
Fusion DSP Atlastins	*H. sapiens* Atlastin-1-3 (Atl1-3)	Sey1/Atl3 DDB_G0279823	ER tubule fusion, exocytosis
Fusion DSP Mitofusin-like	*S. cerevisiae* Mitofusin-1 (Fzo1)	Similar to Fzo-1 DDB_G0287331	Unknown
Membrane-independent scaffold DSP Guanylate-binding proteins	*H. sapiens* GBP1-5	Gnbp DDB_G0281639	Unknown
Membrane-independent scaffold DSP Myxovirus resistance proteins	*H. sapiens* MxA-B	Not identified	Unknown

DSPs. Among the fusion DSPs, the human atlastins (Atl1-3) form a cluster, which is separated from *D. discoideum* and *S. cerevisiae* Sey1 (Atl3).

Several recent comprehensive reviews have covered DSP members, as well as the structural bases for their respective functions (Ramachandran and Schmid, 2018; Ford and Chappie, 2019; Jimah and Hinshaw, 2019; Kalia and Frost, 2019). Some general features common to all DSPs have emerged that we briefly present here. The main scope of this review is to focus on DSP members identified so far in *D. discoideum* and highlight their importance for cellular membrane dynamics and host-pathogen interactions.

STRUCTURAL AND FUNCTIONAL CHARACTERISTICS OF DYNAMIN SUPERFAMILY PROTEINS

Dynamin was initially identified as a mechano-chemical GTPase, which bundles microtubules and catalyzes the constriction and scission of budding vesicles on the plasma membrane during clathrin-mediated endocytosis (Shpetner and Vallee, 1989; Ramachandran and Schmid, 2018; Jimah and Hinshaw, 2019). The signature structural feature of dynamin comprises a large GTPase (G) domain (∼280 amino acids) adjacent to a helical bundle stalk, which was subsequently identified in numerous proteins now regrouped under the generic name dynamin superfamily proteins (DSPs) (Ramachandran and Schmid, 2018; Jimah and Hinshaw, 2019; **Figure 3A** and **Table 1**). Some DSPs also contain supplementary domains providing diverse properties (e.g., protein/lipid interactions) (Ford and Chappie, 2019). Another common trait of DSPs is that these large GTPases are not regulated by guanine nucleotide exchange factors (GEFs) or GTPase-activating proteins (GAPs) (Binns et al., 2000; Narayanan et al., 2005), and their activity is greatly enhanced by nucleotide-induced dimerization (Praefcke and McMahon, 2004). Notably, the first identified dynamin and its homologs are now referred to as classical/modern dynamins, while other DSP members with diverse structural determinants (and functions) are collectively named dynamin-like or dynamin-related proteins, and most of them are regarded as ancestors of the modern DSP branch. DSPs can be functionally grouped in three main types, referred to as fission, fusion and membrane-independent scaffold DSPs (Ramachandran and Schmid, 2018).

Fission DSPs are cytosolic proteins that share among them a similar domain organization. Archetypes of this family include classical dynamins and some dynamin-like proteins (Ramachandran and Schmid, 2018; **Table 1**). Three isoforms of classical dynamin exist in vertebrates. While dynamin-1 (Dnm1) is exclusively present in neurons, dynamin-2 (Dnm2) is ubiquitously produced, and dynamin-3 (Dnm3) is mainly present in neurons and testes. These dynamins harbor five domains: a catalytic N-terminal G domain, a bundle signaling element (BSE), a four alpha-helix stalk, a phospholipid-interacting pleckstrin homology (PH) domain, and a C-terminal proline/arginine-rich domain (PRD) that interacts with SH3 domain-containing proteins (**Figure 3A**).

Extensive structural studies have elucidated the overall architecture of dynamin in solution and bound to membranes, providing insights into the mechanism of membrane scission

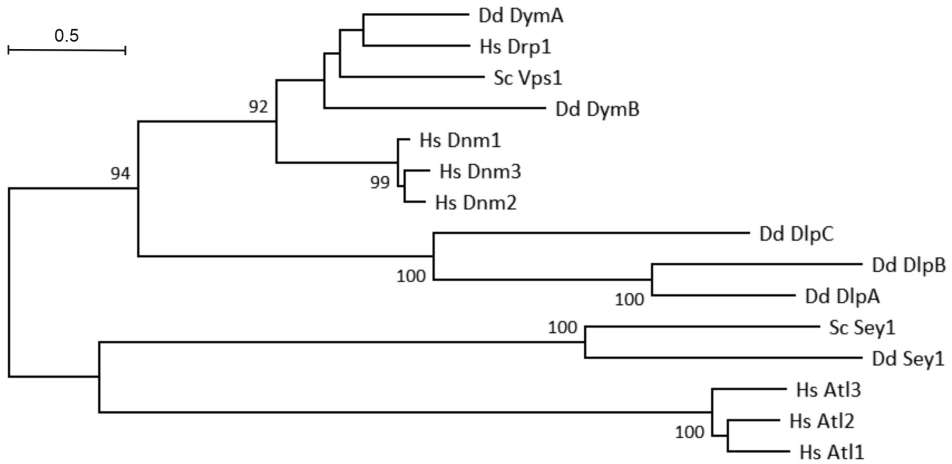

FIGURE 2 | Phylogenetic tree of eukaryotic dynamin superfamily proteins. Evolutionary analyses were conducted using the MUSCLE algorithm for sequence alignment in the Molecular Evolutionary Genetics Analysis (MEGA) X software package (Kumar et al., 2018); the phylogenetic tree was built using the Maximum Likelihood method and Le-Gascuel model (Le and Gascuel, 2008). The tree is drawn to scale, with branch lengths corresponding to the number of substitutions per site. Numbers on the branches indicate bootstrap support for nodes from 500 bootstrap replicates (only values above 75% are shown). The scale bar represents the estimated evolutionary distance (number of amino acid substitutions per site).

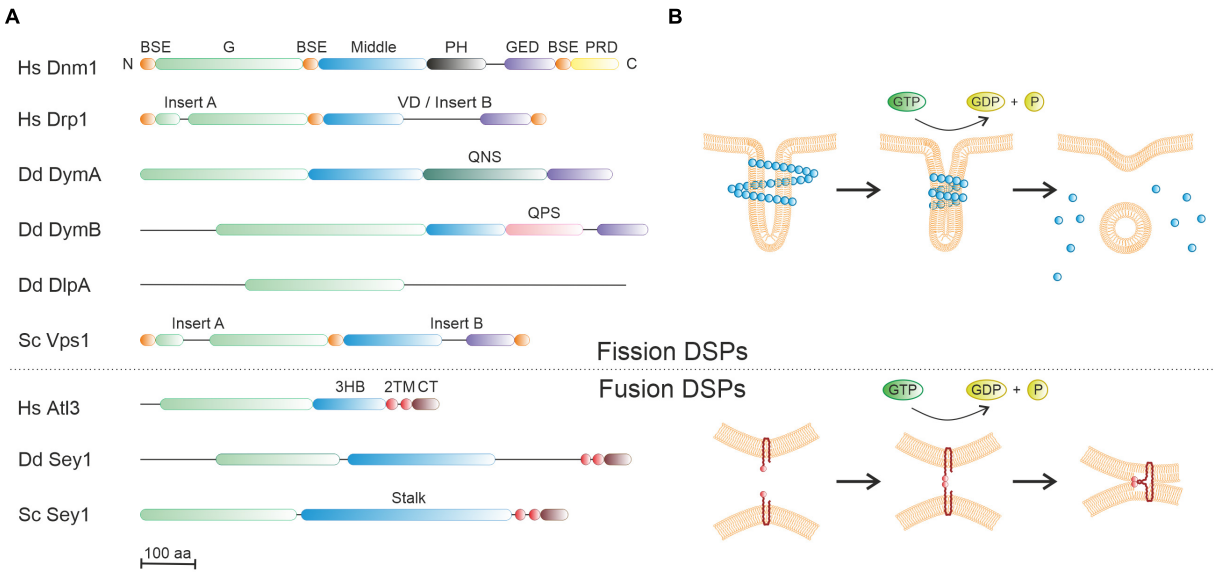

FIGURE 3 | Molecular architecture and mode of action of dynamin superfamily proteins. **(A)** Domain organization of representative members of dynamin superfamily proteins (DSPs) from human, *D. discoideum* or *S. cerevisiae*. The large GTPase domain (green) is conserved, and the "stalk/middle" domains (blue) along with the BSE (orange) fold into a four- or three-helix bundle. BSE, bundle signaling element; G, GTPase domain; GED, GTPase effector domain; PH, pleckstrin homology domain; PRD, proline rich domain; 3HB, three-helix bundle; VD, variable domain; TM, transmembrane domain; CT, cytosolic domain; QNS, glutamine-asparagine-serine-rich domain; QPS, glutamine-proline-serine-rich domain. **(B)** The putative mode of action of fission DSPs (upper panel) and fusion DSPs (lower panel). The basic unit of fission and fusion DSPs is a dimer or a monomer, respectively. Fission DSPs (e.g., dynamin) are dimeric cytosolic proteins, which assemble into helical polymers around tubular target membranes. The assembly-stimulated GTPase activity likely promotes membrane constriction by shear forces, followed by DSP disassembly. In contrast, fusion DSPs (e.g., Sey1/atlastin) are monomeric membrane-anchored proteins, which dimerize only upon GTP binding, thus presumably tethering opposing membranes. GTPase activity triggers bending of the DSPs, which likely compresses the adjacent membrane lattices.

(Chappie et al., 2011; Faelber et al., 2011; Ford et al., 2011; **Figure 3B**, upper panel). Accordingly, dynamins are obligate homodimers, wherein the stalk of each monomer interacts in a criss-cross fashion. This dimeric building block can similarly assemble via two additional stalk interfaces into a tetramer. Further assembly is prevented by a regulatory interaction between the PH domain and the stalk domains. Upon recognition of the membrane PI lipid phosphatidylinositol 4,5-diphosphate (PtdIns(4,5)P_2) by the PH domain, this inhibition is removed, and dynamin switches from a closed to an open

conformation. The structural change enables the self-assembly into helical polymers on target membranes and stimulates the GTPase activity. This will eventually drive membrane fission and subsequent disassembly of helical polymers (**Figure 3B**, upper panel), though the actual fission mechanism is still controversial (Ford and Chappie, 2019). Remarkably, a newly developed single-particle orientation and rotational tracking technique has recently revealed that dynamin drives a strong rotational twist of clathrin-coated vesicles, which might assist the vesicle scission step (Cheng et al., 2021).

A representative fission DSP that belongs to the dynamin-like group is mammalian Drp1, which is a major mitochondrial fission GTPase and also contributes to peroxisome division (Kraus et al., 2021; **Figure 3A**). In Drp1, the PH and PRD domains of classical dynamins are replaced by an unstructured region known as the variable domain (VD), which is responsible for the recruitment to the mitochondrial outer membrane, but can also inhibit Drp1 self-assembly in the absence of membrane interactions. In a GTP-dependent manner, Drp1 forms helical oligomers bound to the outer mitochondrial membrane inducing membrane constriction and severing (Kraus and Ryan, 2017). Drp1 also promotes the intracellular replication of *L. pneumophila* in LCVs, likely due to its role in catalyzing microtubule-dependent mitochondrial fission and its role in cellular bioenergetics (Escoll et al., 2017).

Besides their membrane fission activity, dynamin and the dynamin-like group of DSPs exert additional functions. Notably, classical dynamins interact with microtubules and the actin cytoskeleton and regulate the formation and the function of these cytoskeletal structures (Menon and Schafer, 2013). In addition to its actin-binding capacities (Ji et al., 2015), mammalian Drp1 also physically interacts with specific mitochondrial membrane adaptors. In turn, the adaptors affect the remodeling of the inner mitochondrial membrane mediated by the DSP Opa1, leading to the release of cytochrome c during intrinsic apoptosis (Otera et al., 2016).

Vps1 is a conserved fungal DSP, which shares many structural features with Dnm1, such as the G, BSE, middle and GED domains (Varlakhanova et al., 2018; **Figure 3A** and **Table 1**). In addition, Vps1 contains two inserts, Insert A and Insert B, the function of which is unknown. Vps1 has been implicated in both membrane fission and fusion processes (Peters et al., 2004), as well as in peroxisome homeostasis, endocytosis (Smaczynska-De Rooji et al., 2010; Varlakhanova et al., 2018), and retrograde trafficking originating from endosomes or the vacuole (Chi et al., 2014; Arlt et al., 2015; **Figure 4**).

Fusion DSPs are preferentially inserted into or anchored to membranes and exist as monomers. Atlastins and mitofusins are typical members of this DSP class, which share a similar domain organization and fusogenic mechanism (Moon and Jun, 2020), and are involved in homotypic ER tubule fusion or mitochondrial outer membrane fusion, respectively (**Table 1**). Moreover, atlastins also promote lipid droplet biogenesis and size regulation (Klemm et al., 2013) (**Figure 4**). Atlastins are found in all eukaryotic cells and composed of a cytosolic N-terminal G domain, a three-helix bundle (3HB) region (analogous to the middle/stalk/BSE domains of other DSPs), two transmembrane (TM) segments (forming intramembrane hairpin loops) (Betancourt-Solis et al., 2018) and a C-terminal tail (**Figure 3A**). GTP binding induces atlastin homodimerization either on the same (*cis*) or opposing membranes (*trans*), whereas GTP hydrolysis seems to promote the disassembly into monomers (**Figure 3B**, lower panel). The TM domains are required for fusion while the cytoplasmic tail mediates membrane tethering. In addition to their ER fusogenic function, atlastins are involved in an impressive number of processes including vesicle packaging, endocytic trafficking, lipid droplet biogenesis, ER-phagy, microtubule dynamics, calcium signaling and protein homeostasis (Lü et al., 2020), as well as bacterial infection (see below).

Mitofusins in mammals (Fzo1 in yeast) contain an N-terminal G domain, a heptad repeat region (HR1), two TM regions, and a second heptad repeat region (HR2). Upon GTP hydrolysis, mitofusins from two different membranes dimerize via their G domain, subsequently inducing conformation changes that bring the membranes closer together and enable their fusion. Whereas the HR2 domains contribute to dimerization of mitofusins on opposing membranes by forming antiparallel dimers, the HR1 domain facilitates membrane fusion by perturbing local membrane structures in its vicinity (Gao and Hu, 2021).

Membrane-independent scaffold DSPs comprise two main representative members, guanylate-binding proteins (GBPs) and Myxovirus resistance (Mx) proteins, the closest DSP homologs of which are atlastins (**Table 1**). GBPs are induced by interferon-γ (IFN-γ) as immunity-related GTPases in vertebrates and are involved in the cellular immune responses against bacterial, viral, and protozoan pathogens (Ngo and Man, 2017; Tretina et al., 2019; **Figure 4**). These DSPs also display antitumor and antiproliferative properties, as well as actin remodeling activities. The architecture of GBPs consists of an N-terminal G domain followed by an extended C-terminal helical domain. Three of the seven human GBP (GBP1, –2, –5) possess a CaaX box at the C-terminus required for post-translational isoprenylation, which promotes the association with membranes and/or pathogens. GTP binding promotes the self-assembly of GBPs into homodimers but also into supramolecular structures (several thousand monomers). These nanostructures can deposit on pathogen-associated membranes and serve as mechano-enzymes fatally disrupting membranes from pathogens and/or vacuoles containing pathogens in host cells. The nanostructures can also function as cellular sensory platforms for the detection of pathogens and the subsequent induction of several defense mechanisms, including inflammasome-driven responses (Tretina et al., 2019).

The production of Mx proteins also strictly depends on interferon signaling and contributes to the innate immunity against diverse RNA viruses (Haller et al., 2015; **Figure 4**). Two Mx proteins exist in humans. Mx1 (MxA) shows a wide antiviral activity against RNA and DNA viruses. In contrast, Mx2 (MxB) activity is restricted to only a few viruses including HIV-1. Similarly to classical dynamin, Mx proteins harbor G, BSE and stalk domains, but the PH and PRD domains are missing.

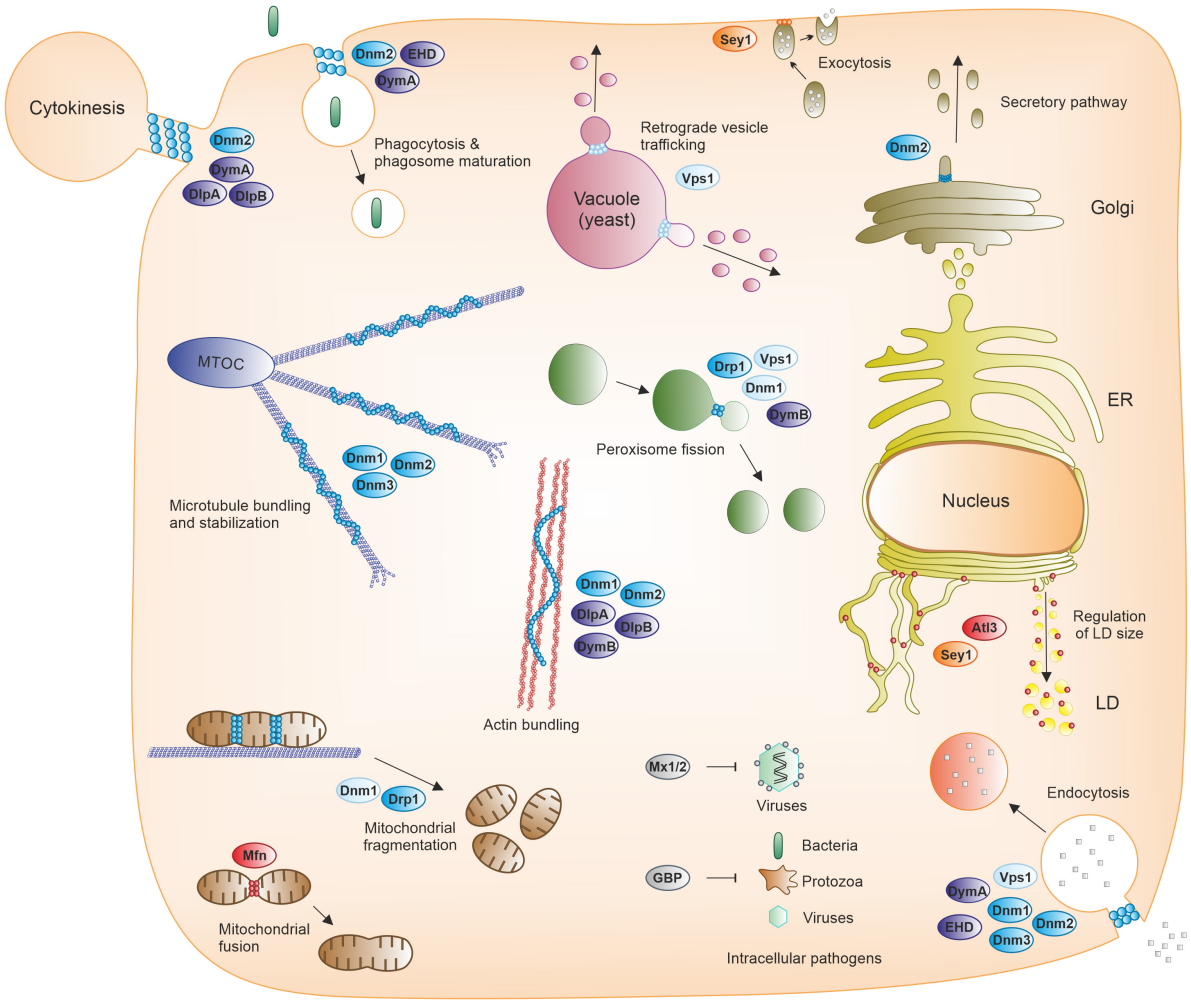

FIGURE 4 | Cellular processes mediated by dynamin superfamily proteins. Fission, fusion, and membrane-independent scaffold DSPs participate in various cellular processes, including endomembrane transport (such as phagocytosis, macropinocytosis, endocytosis, secretory and retrograde trafficking, or autophagy), organelle and cytoskeleton homeostasis, cytokinesis, and immunity against viral, bacterial and protozoan pathogens. ER, endoplasmic reticulum; GBP, guanylate-binding protein; LD, lipid droplet; MTOC, microtubule-organizing center; Mx1/2, Myxovirus resistance protein 1/2.

Instead, a 40 amino acid loop (L4 loop) replaces the PH domain and mediates membrane lipid and viral target interactions. The antiviral activity depends on the GTP-dependent multimeric assembly of the Mx proteins. Mx oligomers form ring-like structures with the G domains directed to the outer side and the stalks located on the opposite inner side. These Mx rings might inhibit different steps of viral replication cycles occurring in the cytosol and the nucleus, although the actual antiviral mechanism is still not clearly established.

Taken together, DSPs participate in various cellular processes, including endomembrane transport (such as phagocytosis, macropinocytosis, endocytosis, secretory pathway, retrograde trafficking, autophagy), organelle and cytoskeleton homeostasis, cytokinesis, and immunity against viral, bacterial and protozoan pathogens (**Figure 4**).

DYNAMIN SUPERFAMILY PROTEINS IN *D. DISCOIDEUM*

In *D. discoideum* five dynamin-like proteins, DymA (gene ID: DDB_G0277849), DymB (DDB_G0277851), DlpA (DDB_G0268592), DlpB (DDB_G0285931) and DlpC (DDB_G0271628), as well as the fusion DSP Sey1/Atl3 (DDB_G0279823) have been described (**Figure 3A** and **Table 1**). Moreover, BLAST searches have revealed putative orthologs of a mammalian GBP (DDB_G0281639) and a yeast Fzo1/mitofusin-like DSP (DDB_G0287331). Since there are only few DSPs in *D. discoideum* compared to vertebrates, we discuss here each individual member, rather than adopting a classification based on their functions (e.g., phagocytosis, organelle morphogenesis, cytokinesis) (**Figure 4**).

DYNAMIN A PROMOTES ENDOCYTOSIS AND PHAGOSOME MATURATION

Dynamin A (DymA) is most similar to the mammalian fission dynamin-1-like protein (Drp1) and is classified as a dynamin-related protein (DRP) or ancient DSP. The 3D structure of its G domain was the first to be solved among DSPs (Niemann et al., 2001). One characteristic feature is the replacement of the PH and PRD domains found in classical dynamin by a segment, which is rich in asparagine, glutamine and serine residues, inserted between the middle domain (also known as three-helix bundle domain) and the C-terminal GED (**Figure 3A**). This domain might contribute to the reported interaction of DymA with membrane lipids (Klockow et al., 2002) or the regulation of G domain dimerization.

DymA was first identified on post-lysosomes, mitochondria and Golgi compartments (Wienke et al., 1999). Later studies have additionally revealed its recruitment to phagosomes containing latex beads during the early phase of the phagocytic process but also to some extent at late/final stages (Gopaldass et al., 2012; **Figure 4**). DymA was also shown to localize to the furrow of dividing cells during the entire cytokinesis process (Masud Rana et al., 2013; **Figure 4**). However, recent live cell imaging has revealed a more specific localization restricted to the intercellular bridge only during the final separation phase of dividing cells (Fujimoto et al., 2019).

As implied by these numerous cellular localizations, deletion of DymA results in pleiotropic effects comprising alterations in mitochondrial morphology and functions, impairment of cytokinesis and endosomal morphology (accumulation of membrane tubules in proximity to nuclei and plasma membrane), as well as a defect in fluid-phase uptake and increased phagocytic rates (Wienke et al., 1999). Whether these multiple defects reflect direct DymA functions or are indirect consequences of the DymA deletion remains unclear. For instance, the defective mitochondrial morphology in *dymA* null cells is not associated with any mitochondrial dynamics and fission/fusion defects (Schimmel et al., 2012), but instead is likely due to other impaired DymA-dependent cellular processes. Moreover, *dymA* null cells show an aberrant localization of myosin II and disorganized actin filaments at the furrow of dividing cells (Masud Rana et al., 2013). DymA was also shown to interact with the actin-binding protein Abp1 (Dieckmann et al., 2010) and could thus regulate actin assembly at the furrow rather than or in addition to exhibiting membrane fission activity at this site. Instead, the latter function might rely on DlpA and DlpB, two other DSP more abundantly present at the cleavage furrow (Fujimoto et al., 2019) (see below).

Phagosomes are well described to undergo several maturation steps involving membrane vesicle fusion and fission events (Kinchen and Ravichandran, 2008). In the absence of DymA, phagosome acidification is impaired, a clear indication of its direct role in the phagosomal maturation process (Gopaldass et al., 2012). F-actin binding to early phagosomes is also compromised in *dymA* null cells, in agreement with functions of DymA independent of vesicle scission. Accordingly, DymA also interacts with the C-terminal Eps15-homology-domain (EHD) protein (Gueho et al., 2016), which seems to further extend the functional spectrum of DymA. EHDs are ATPase mechano-enzymes related to the dynamin superfamily, implicated in membrane scission and the regulation of endocytic events (Naslavsky and Caplan, 2011). In addition to membrane remodeling functions, *D. discoideum* EHD interacts with other binding partners (Gueho et al., 2016), and thus, EHD might adopt scaffolding functions together with DymA.

Moreover, a possible interplay between DymA and other DSP members cannot be excluded. DSPs can form hetero-multimers with other DSP members such as DlpA (see below), and these cooperative arrangements might support new functions. Hence, DlpA (independently of DlpB) was shown to accumulate at the phagocytic cups and on nascent phagosomes containing bacteria (Fujimoto et al., 2019). Hypothetically, DlpA might transiently form heterodimers with DymA and/or EHD on newly formed phagosomes, and these complexes might contribute to the phagosomal maturation process (Dieckmann et al., 2010; Gueho et al., 2016).

DYNAMIN B REGULATES MEMBRANE FISSION AND ACTIN DYNAMICS

Dynamin B (DymB) is classified as a dynamin-like protein and shares the same domain organization as DymA, including the substitution of the PH and PRD domains by an unstructured domain rich in glutamine, proline, and serine residues (Rai et al., 2011; **Figure 3A**). In addition, DymB possess a particular N-terminal sequence (136 amino acids) responsible for its localization to mitochondria (Rai et al., 2013). Such an N-terminal mitochondrial targeting sequence (MTS) is notably also observed in the human dynamin-like GTPase Opa1 implicated in mitochondrial fusion. However, a phylogenetic analysis indicates that DymB is more closely related to yeast Vps1, a dynamin-like protein involved in endocytosis, vacuolar trafficking and peroxisomal division (Miyagishima et al., 2008; **Figure 2**). After cleavage of the N-terminal peptide by mitochondrial proteases, the mature DymB protein still localizes to the outside of the outer mitochondrial membrane, in contrast to Opa1, which associates with the outer surface of the inner mitochondrial membrane.

DymB localization was initially determined in DymB-GFP expressing cells, revealing a predominant distribution to mitochondria and a minor presence on other organelles and the plasma membrane (Rai et al., 2011). However, endogenous DymB detected with a specific antibody appears to localize mainly to the cytosol (Masud Rana et al., 2013). Thus, DymB might be weakly or transiently associated with mitochondria, and might also function in various other cellular compartments (**Figure 4**). Accordingly, DymB-depleted cells do not present any mitochondrial morphological and functional defects and are fully competent for mitochondrial fission (Rai et al., 2011; Schimmel et al., 2012). Instead, the absence of DymB results in multiple defects including increased peroxisome size and impaired peroxisome function, increased tubulation of the contractile vacuole system and decreased

contractile activity of large cisternae, as well as dysregulation of F-actin formation and distribution (Rai et al., 2011). In conclusion, DymB adopts membrane scission functions at various cell locations and regulates actin assembly as well as actin-dependent processes. It is unknown whether the transient localization of DymB to mitochondria contributes to the regulation of the amount of cytosolic enzyme by controlling the rate limiting proteolysis step. Alternatively, mitochondria, through their frequent interactions with other organelles at membrane contact sites (MCS), might support DymB delivery to specific sites.

THE DYNAMIN-LIKE PROTEINS DLPA, DLPB AND DLPC REGULATE CYTOKINESIS

In addition to DymA and DymB, *D. discoideum* produces three dynamin-like proteins (DlpA, DlpB, and DlpC), which harbor only a DSP-characteristic G domain near their N-terminus without any other known domains (InterProScan and Prosite analyses) (**Figure 3A**). Their primary sequences are quite similar (sequence identity between DlpA and DlpB > 36%; DlpA or DlpB and DlpC > 27%). Phylogenetic analyses indicate that these DSPs belong to the monophyly comprising plant and algae DRP5A proteins involved in cytokinesis, and they display a distant relationship with chloroplast division DRP5B proteins (Miyagishima et al., 2008).

A seminal study first revealed the implication of DlpA, DlpB, and DlpC in cytokinesis, as individual gene deletions resulted in multinucleated enlarged cells, and DlpA was present on the cleavage furrow (Miyagishima et al., 2008). This observation was partially confirmed for DlpA and DlpB, but not for DlpC, whose inactivation had no impact on cytokinesis (Masud Rana et al., 2013). To clarify this discrepancy, the function of DlpC in cytokinesis needs to be readdressed with an independently generated *dlpC* knockout strain. Indeed, genetic compensation in response to gene knockout is a widespread phenomenon that could explain such phenotypic differences (El-Brolosy and Stainier, 2017). For instance, upregulation of DlpA and DlpB in the existing *dlpC* mutant might compensate the cytokinesis defect in this case.

Interestingly, DlpA and DlpB have to form hetero-oligomers to be recruited to the cleavage furrow (Fujimoto et al., 2019). As described for *dymA* null cells, deletion of either DlpA or DlpB induced the disorganization of the actomyosin cytoskeleton at the furrow region (Masud Rana et al., 2013; Fujimoto et al., 2019). Both proteins were shown to associate with the actin cytoskeleton and stabilize actin filaments. In the current working model, DlpA, DlpB, and DymA are proposed to cooperate in the cytokinesis process. Accordingly, DlpA and DlpB would stabilize the actin filament in the contracting ring, whereas DymA would be recruited to the intercellular bridge only during the final separation step and scission of the dividing cells (Fujimoto et al., 2019).

A puzzling observation is the accumulation of DlpA without DlpB at the phagocytic cup formed during uptake of bacteria (Fujimoto et al., 2019). The molecular basis for this transient and selective DlpA recruitment to phagosomal membranes is unknown. DlpA recruitment might involve the putative participation of DlpA-binding partners specifically associated with nascent phagosomes and/or the possible cooperation with other DSP members. Moreover, the function of DlpA on the phagosomal cup has yet to be assessed. Similarly to its role in cytokinesis, DlpA might presumably regulate the actin cytoskeleton dynamics during phagocytic cup formation, although a membrane scission function cannot be excluded. Notably, such a dynamin-actin cross-talk has been described for Dnm2 in macrophages during both phagosome formation and closure, preceding the function of Dnm2 in phagosome scission (Marie-Anais et al., 2016). Further detailed analysis of phagocytosis in *dlpA* null cells should reveal new insights into DlpA functions.

D. DISCOIDEUM SEY1 PROMOTES ENDOPLASMIC RETICULUM DYNAMICS AND *LEGIONELLA* GROWTH

Sey1/Atl3 is the only atlastin ortholog present in *D. discoideum,* and it shares the same domain organization as the mammalian atlastins described above (Steiner et al., 2017; **Figure 3A**). Sey1 localizes to interconnected ER membranes and ER tubules as well as to perinuclear ER membranes. To determine its function, we have recently generated and characterized a *sey1* deletion mutant strain (Δ*sey1*) (Hüsler et al., 2021). Cells lacking Sey1 show pleiotropic defects, including aberrant ER morphology and ER tubules dynamics, defective lysosomal enzymes exocytosis and intracellular proteolysis, impaired cell motility, and inability to cope with prolonged ER stress. Remarkably, all these defects were complemented by plasmid-borne wild-type Sey1, but not by a catalytically-inactive Sey1 variant (Sey1_K154A), indicating that Sey1 GTPase-dependent functions are important for the normal course of these cellular processes.

It is unclear at present whether the defects observed in Δ*sey1* cells are a direct consequence of the absence of Sey1 GTPase-dependent function(s), or whether these defects are due to the altered ER morphology in the mutant cells. For instance, the tubular ER network forms abundant MCS with organelles and the plasma membrane to support exchanges between organelles (e.g., lipids, Ca^{2+}), and it participates in various other cellular processes (Phillips and Voeltz, 2016). Hence, the altered ER network in Δ*sey1* cells might impede the formation, location or function of these ER-MCS, and consequently this would result in the dysfunction of multiple MCS-dependent cellular processes. Further studies will be required to explore this hypothesis and the role of Sey1 in different functions reported for atlastins in other organisms (e.g., ER-phagy, lipid droplet biogenesis).

Intriguingly, the intracellular replication of *L. pneumophila* has recently been shown to be regulated by Sey1/Atl3 (Steiner et al., 2017, 2018b; **Figure 1**). Sey1 was found to localize to early LCVs, and over production of the DSP promoted intracellular growth of *L. pneumophila*. Production of a

catalytically inactive, dominant-negative Sey1_K154A mutant protein, or Atl3 depletion, restricted pathogen replication and impaired LCV maturation. An ultrastructural analysis by electron microscopy confirmed that dominant-negative Sey1 compromises ER accumulation on LCVs. Of note, Sey1 was not required for the formation of the PtdIns(4)*P*-positive LCVs and initial ER recruitment, but for the DSP-catalyzed pathogen vacuole expansion. Moreover, *D. discoideum* lacking the *sey1* gene was found to be less permissive for intracellular *L. pneumophila* replication (Hüsler et al., 2021). LCV formation was impaired in this mutant strain, since the ER was less efficiently recruited to the pathogen vacuole, and LCV expansion was retarded at early stages of infection. Taken together, the DSP Sey1/Atl3 controls circumferential ER remodeling during LCV maturation and intracellular replication of *L. pneumophila*. The molecular mechanism of how Sey1/Atl3 promotes LCV expansion and *L. pneumophila* growth has not been elucidated, but might involve a more efficient delivery of ER to LCV-ER contact sites and lipid exchange among the compartments.

THE GUANYLATE-BINDING PROTEIN GNBP IS POSSIBLY IMPLICATED IN PATHOGEN-HOST CELL INTERACTIONS

As mentioned above, mammalian GBPs are DSPs regulating inflammasome-dependent responses to bacterial infection (Tretina et al., 2019). *D. discoideum* harbors a single GBP homolog encoded by the *gnbp* gene (Dunn et al., 2017), which might adopt similar immune functions in the amoeba (**Figure 4**). Protein domain prediction (InterProScan, TMHMM Server v. 2.0) revealed the presence of an N-terminal signal peptide, a conserved G domain, and a C-terminal TM domain. The helical part of human GBP following the G domain is replaced by a long protein sequence in *D. discoideum* with no predicted structural motif. This predicted domain organization suggests that *D. discoideum* GBP might be constantly inserted into membranes independently of GTP binding, as observed in atlastins and in contrast to GBPs in other species. Similarly to atlastin, *D. discoideum* GBP might thus display membrane tethering and/or fusion properties. Interestingly, tethering functions have been previously described for Gbp1 (Shydlovskyi et al., 2017). In addition, *D. discoideum* GBP has been described as a putative binding partner of Sec7, a GEF specific for the small GTPase ARF (ADP-ribosylation factor), implicated in vesicular trafficking (Müller et al., 2013). *D. discoideum* GBP is also present in the proteome of macropinosomes, and therefore, this protein is likely to be involved in vesicular trafficking along the endocytic pathway (Journet et al., 2012). Whether *D. discoideum* GBP also plays a role in cell-autonomous immunity similarly to other GBPs is unknown.

Intriguingly, Gnbp was also identified in the proteome of LCVs purified from *L. pneumophila*-infected *D. discoideum* (Hoffmann et al., 2014a; **Figure 1**). This finding is in agreement with the notion that the *D. discoideum* GBP is implicated in the recognition of and/or defense against intracellular pathogens. However, the function of this scaffold DSP on the LCV or in the context of an *L. pneumophila* infection remains to be elucidated.

CONCLUSION AND OUTLOOK

The soil amoeba *D. discoideum* is a versatile model organism to study vesicle trafficking, motility and migration, cell division, as well as host cell-pathogen interactions. Large GTPases of the dynamin superfamily play crucial roles for membrane dynamics, vesicle trafficking, organelle homeostasis, cytokinesis and cell-autonomous immunity. Insights into the cellular localization, function and structure of DSPs have soared over the last years. *D. discoideum* produces at least eight DSPs, which are involved in membrane fission and fusion events, as well as possibly in cell-autonomous immunity. Moreover, the amoebae produce one ortholog of mammalian atlastins, Sey1, which is implicated in ER dynamics and intracellular growth of the opportunistic pathogen *L. pneumophila*. Amoebae deleted for Sey1 show pleiotropic defects, including aberrant ER morphology and dynamics, as well as impaired pathogen vacuole formation and replication of *L. pneumophila*. We propose to harness the wide array of biochemical, genetic and cell biological tools available for *D. discoideum* to further exploit the functions of DSPs in cellular processes and upon infection with pathogens.

AUTHOR CONTRIBUTIONS

FL and HH wrote the manuscript. AK and DH prepared the figures and edited the manuscript. All authors contributed to the article and approved the submitted version.

FUNDING

Research in the laboratory of HH was supported by the Swiss National Science Foundation (SNF; 31003A_175557, 310030_200706). FL was supported by the CNRS and the University of Montpellier.

REFERENCES

Abu Kwaik, Y. (1996). The phagosome containing *Legionella pneumophila* within the protozoan *Hartmannella vermiformis* is surrounded by the rough endoplasmic reticulum. *Appl. Environ. Microbiol.* 62, 2022–2028. doi: 10.1128/aem.62.6.2022-2028.1996

Arlt, H., Reggiori, F., and Ungermann, C. (2015). Retromer and the dynamin Vps1 cooperate in the retrieval of transmembrane proteins from vacuoles. *J. Cell Sci.* 128, 645–655.

Asrat, S., De Jesus, D. A., Hempstead, A. D., Ramabhadran, V., and Isberg, R. R. (2014). Bacterial pathogen manipulation of host membrane trafficking. *Annu. Rev. Cell Dev. Biol.* 30, 79–109. doi: 10.1146/annurev-cellbio-100913-013439

Balla, T. (2013). Phosphoinositides: tiny lipids with giant impact on cell regulation. *Physiol. Rev.* 93, 1019–1137. doi: 10.1152/physrev.00028.2012

Bärlocher, K., Hutter, C. A. J., Swart, A. L., Steiner, B., Welin, A., Hohl, M., et al. (2017a). Structural insights into *Legionella* RidL-Vps29 retromer subunit interaction reveal displacement of the regulator TBC1D5. *Nat. Commun.* 8:1543.

Bärlocher, K., Welin, A., and Hilbi, H. (2017b). Formation of the *Legionella* replicative compartment at the crossroads of retrograde trafficking. *Front. Cell. Infect. Microbiol.* 7:482. doi: 10.3389/fcimb.2017.00482

Betancourt-Solis, M. A., Desai, T., and Mcnew, J. A. (2018). The atlastin membrane anchor forms an intramembrane hairpin that does not span the phospholipid bilayer. *J. Biol. Chem.* 293, 18514–18524. doi: 10.1074/jbc.ra118.003812

Binns, D. D., Helms, M. K., Barylko, B., Davis, C. T., Jameson, D. M., Albanesi, J. P., et al. (2000). The mechanism of GTP hydrolysis by dynamin II: a transient kinetic study. *Biochemistry* 39, 7188–7196. doi: 10.1021/bi000033r

Boamah, D. K., Zhou, G., Ensminger, A. W., and O'Connor, T. J. (2017). From many hosts, one accidental pathogen: the diverse protozoan hosts of *Legionella*. *Front. Cell. Infect. Microbiol.* 7:477. doi: 10.3389/fcimb.2017.00477

Bramkamp, M. (2012). Structure and function of bacterial dynamin-like proteins. *Biol. Chem.* 393, 1203–1214. doi: 10.1515/hsz-2012-0185

Buckley, C. M., Heath, V. L., Gueho, A., Bosmani, C., Knobloch, P., Sikakana, P., et al. (2019). PIKfyve/Fab1 is required for efficient V-ATPase and hydrolase delivery to phagosomes, phagosomal killing, and restriction of *Legionella* infection. *PLoS Pathog.* 15:e1007551. doi: 10.1371/journal.ppat.1007551

Cardenal-Muñoz, E., Barisch, C., Lefrancois, L. H., López-Jiménez, A. T., and Soldati, T. (2017). When dicty met myco, a (not so) romantic story about one amoeba and its intracellular pathogen. *Front. Cell. Infect. Microbiol.* 7:529. doi: 10.3389/fcimb.2017.00529

Chappie, J. S., Mears, J. A., Fang, S., Leonard, M., Schmid, S. L., Milligan, R. A., et al. (2011). A pseudoatomic model of the dynamin polymer identifies a hydrolysis-dependent powerstroke. *Cell* 147, 209–222. doi: 10.1016/j.cell.2011.09.003

Cheng, X., Chen, K., Dong, B., Yang, M., Filbrun, S. L., Myoung, Y., et al. (2021). Dynamin-dependent vesicle twist at the final stage of clathrin-mediated endocytosis. *Nat. Cell Biol.* 23, 859–869. doi: 10.1038/s41556-021-00713-x

Chi, R. J., Liu, J., West, M., Wang, J., Odorizzi, G., and Burd, C. G. (2014). Fission of SNX-BAR-coated endosomal retrograde transport carriers is promoted by the dynamin-related protein Vps1. *J. Cell Biol.* 204, 793–806. doi: 10.1083/jcb.201309084

Di Paolo, G., and De Camilli, P. (2006). Phosphoinositides in cell regulation and membrane dynamics. *Nature* 443, 651–657. doi: 10.1038/nature05185

Dieckmann, R., Von Heyden, Y., Kistler, C., Gopaldass, N., Hausherr, S., Crawley, S. W., et al. (2010). A myosin IK-Abp1-PakB circuit acts as a switch to regulate phagocytosis efficiency. *Mol. Biol. Cell* 21, 1505–1518. doi: 10.1091/mbc.e09-06-0485

Dunn, J. D., Bosmani, C., Barisch, C., Raykov, L., Lefrancois, L. H., Cardenal-Muñoz, E., et al. (2017). Eat prey, live: *Dictyostelium discoideum* as a model for cell-autonomous defenses. *Front. Immunol.* 8:1906. doi: 10.3389/fimmu.2017.01906

Eichinger, L., Pachebat, J. A., Glöckner, G., Rajandream, M. A., Sucgang, R., Berriman, M., et al. (2005). The genome of the social amoeba *Dictyostelium discoideum*. *Nature* 435, 43–57.

El-Brolosy, M. A., and Stainier, D. Y. R. (2017). Genetic compensation: a phenomenon in search of mechanisms. *PLoS Genet.* 13:e1006780. doi: 10.1371/journal.pgen.1006780

Escoll, P., Song, O. R., Viana, F., Steiner, B., Lagache, T., Olivo-Marin, J. C., et al. (2017). *Legionella pneumophila* modulates mitochondrial dynamics to trigger metabolic repurposing of infected macrophages. *Cell Host Microbe* 22, 302–316.e7.

Faelber, K., Posor, Y., Gao, S., Held, M., Roske, Y., Schulze, D., et al. (2011). Crystal structure of nucleotide-free dynamin. *Nature* 477, 556–560. doi: 10.1038/nature10369

Faix, J., Kreppel, L., Shaulsky, G., Schleicher, M., and Kimmel, A. R. (2004). A rapid and efficient method to generate multiple gene disruptions in *Dictyostelium discoideum* using a single selectable marker and the Cre-loxP system. *Nucleic Acids Res.* 32:e143. doi: 10.1093/nar/gnh136

Finsel, I., and Hilbi, H. (2015). Formation of a pathogen vacuole according to *Legionella pneumophila*: how to kill one bird with many stones. *Cell. Microbiol.* 17, 935–950. doi: 10.1111/cmi.12450

Finsel, I., Ragaz, C., Hoffmann, C., Harrison, C. F., Weber, S., Van Rahden, V. A., et al. (2013). The *Legionella* effector RidL inhibits retrograde trafficking to promote intracellular replication. *Cell Host Microbe* 14, 38–50. doi: 10.1016/j.chom.2013.06.001

Ford, M. G. J., and Chappie, J. S. (2019). The structural biology of the dynamin-related proteins: new insights into a diverse, multitalented family. *Traffic* 20, 717–740. doi: 10.1111/tra.12676

Ford, M. G., Jenni, S., and Nunnari, J. (2011). The crystal structure of dynamin. *Nature* 477, 561–566.

Fujimoto, K., Tanaka, M., Rana, A., Jahan, M. G. S., Itoh, G., Tsujioka, M., et al. (2019). Dynamin-like protein B of *Dictyostelium* contributes to cytokinesis cooperatively with other dynamins. *Cells* 8:781. doi: 10.3390/cells8080781

Funamoto, S., Meili, R., Lee, S., Parry, L., and Firtel, R. A. (2002). Spatial and temporal regulation of 3-phosphoinositides by PI 3-kinase and PTEN mediates chemotaxis. *Cell* 109, 611–623. doi: 10.1016/s0092-8674(02)00755-9

Gao, S., and Hu, J. (2021). Mitochondrial fusion: the machineries in and out. *Trends Cell Biol.* 31, 62–74. doi: 10.1016/j.tcb.2020.09.008

Gaudet, P., Fey, P., Basu, S., Bushmanova, Y. A., Dodson, R., Sheppard, K. A., et al. (2011). dictyBase update 2011: web 2.0 functionality and the initial steps towards a genome portal for the *Amoebozoa*. *Nucleic Acids Res.* 39, D620–D624.

Gopaldass, N., Patel, D., Kratzke, R., Dieckmann, R., Hausherr, S., Hagedorn, M., et al. (2012). Dynamin A, myosin IB and Abp1 couple phagosome maturation to F-actin binding. *Traffic* 13, 120–130. doi: 10.1111/j.1600-0854.2011.01296.x

Gueho, A., Bosmani, C., Gopaldass, N., Molle, V., Soldati, T., and Letourneur, F. (2016). *Dictyostelium* EHD associates with dynamin and participates in phagosome maturation. *J. Cell Sci.* 129, 2354–2367.

Haller, O., Staeheli, P., Schwemmle, M., and Kochs, G. (2015). Mx GTPases: dynamin-like antiviral machines of innate immunity. *Trends Microbiol.* 23, 154–163. doi: 10.1016/j.tim.2014.12.003

Hoffmann, C., Harrison, C. F., and Hilbi, H. (2014b). The natural alternative: protozoa as cellular models for *Legionella* infection. *Cell. Microbiol.* 16, 15–26. doi: 10.1111/cmi.12235

Hoffmann, C., Finsel, I., Otto, A., Pfaffinger, G., Rothmeier, E., Hecker, M., et al. (2014a). Functional analysis of novel Rab GTPases identified in the proteome of purified *Legionella*-containing vacuoles from macrophages. *Cell. Microbiol.* 16, 1034–1052.

Hubber, A., and Roy, C. R. (2010). Modulation of host cell function by *Legionella pneumophila* type IV effectors. *Annu. Rev. Cell Dev. Biol.* 26, 261–283. doi: 10.1146/annurev-cellbio-100109-104034

Hüsler, D., Steiner, B., Welin, A., Striednig, B., Swart, A. L., Molle, V., et al. (2021). *Dictyostelium* lacking the single atlastin homolog Sey1 shows aberrant ER architecture, proteolytic processes and expansion of the *Legionella*-containing vacuole. *Cell. Microbiol.* 23:e13318.

Isberg, R. R., O'connor, T. J., and Heidtman, M. (2009). The *Legionella pneumophila* replication vacuole: making a cosy niche inside host cells. *Nat. Rev. Microbiol.* 7, 13–24. doi: 10.1038/nrmicro1967

Ji, W. K., Hatch, A. L., Merrill, R. A., Strack, S., and Higgs, H. N. (2015). Actin filaments target the oligomeric maturation of the dynamin GTPase Drp1 to mitochondrial fission sites. *eLife* 4:e11553.

Jimah, J. R., and Hinshaw, J. E. (2019). Structural insights into the mechanism of dynamin superfamily proteins. *Trends Cell Biol.* 29, 257–273. doi: 10.1016/j.tcb.2018.11.003

Journet, A., Klein, G., Brugiere, S., Vandenbrouck, Y., Chapel, A., Kieffer, S., et al. (2012). Investigating the macropinocytic proteome of *Dictyostelium* amoebae by high-resolution mass spectrometry. *Proteomics* 12, 241–245. doi: 10.1002/pmic.201100313

Kalia, R., and Frost, A. (2019). Open and cut: allosteric motion and membrane fission by dynamin superfamily proteins. *Mol. Biol. Cell* 30, 2097–2104. doi: 10.1091/mbc.e16-10-0709

Kinchen, J. M., and Ravichandran, K. S. (2008). Phagosome maturation: going through the acid test. *Nat. Rev. Mol. Cell Biol.* 9, 781–795. doi: 10.1038/nrm2515

Klemm, R. W., Norton, J. P., Cole, R. A., Li, C. S., Park, S. H., Crane, M. M., et al. (2013). A conserved role for atlastin GTPases in regulating lipid droplet size. *Cell Rep.* 3, 1465–1475. doi: 10.1016/j.celrep.2013.04.015

Klockow, B., Tichelaar, W., Madden, D. R., Niemann, H. H., Akiba, T., Hirose, K., et al. (2002). The dynamin A ring complex: molecular organization and nucleotide-dependent conformational changes. *EMBO J.* 21, 240–250. doi: 10.1093/emboj/21.3.240

Kölsch, V., Charest, P. G., and Firtel, R. A. (2008). The regulation of cell motility and chemotaxis by phospholipid signaling. *J. Cell Sci.* 121, 551–559. doi: 10.1242/jcs.023333

Kraus, F., and Ryan, M. T. (2017). The constriction and scission machineries involved in mitochondrial fission. *J. Cell Sci.* 130, 2953–2960.

Kraus, F., Roy, K., Pucadyil, T. J., and Ryan, M. T. (2021). Function and regulation of the divisome for mitochondrial fission. *Nature* 590, 57–66. doi: 10.1038/s41586-021-03214-x

Kuhlmann, M., Popova, B., and Nellen, W. (2006). RNA interference and antisense-mediated gene silencing in *Dictyostelium*. *Methods Mol. Biol.* 346, 211–226. doi: 10.1385/1-59745-144-4:211

Kumar, S., Stecher, G., Li, M., Knyaz, C., and Tamura, K. (2018). MEGA X: molecular evolutionary genetics analysis across computing platforms. *Mol. Biol. Evol.* 35, 1547–1549. doi: 10.1093/molbev/msy096

Kuspa, A., and Loomis, W. F. (1992). Tagging developmental genes in *Dictyostelium* by restriction enzyme-mediated integration of plasmid DNA. *Proc. Natl. Acad. Sci. U.S.A.* 89, 8803–8807. doi: 10.1073/pnas.89.18.8803

Le, S. Q., and Gascuel, O. (2008). An improved general amino acid replacement matrix. *Mol. Biol. Evol.* 25, 1307–1320. doi: 10.1093/molbev/msn067

Liu, J., Noel, J. K., and Low, H. H. (2018). Structural basis for membrane tethering by a bacterial dynamin-like pair. *Nat. Commun.* 9:3345.

Loovers, H. M., Kortholt, A., De Groote, H., Whitty, L., Nussbaum, R. L., and Van Haastert, P. J. (2007). Regulation of phagocytosis in *Dictyostelium* by the inositol 5-phosphatase OCRL homolog Dd5P4. *Traffic* 8, 618–628. doi: 10.1111/j.1600-0854.2007.00546.x

Lu, H., and Clarke, M. (2005). Dynamic properties of *Legionella*-containing phagosomes in *Dictyostelium* amoebae. *Cell. Microbiol.* 7, 995–1007. doi: 10.1111/j.1462-5822.2005.00528.x

Lü, L., Niu, L., and Hu, J. (2020). "At last in" the physiological roles of the tubular ER network. *Biophys. Rep.* 6, 105–114. doi: 10.1007/s41048-020-00113-y

Marie-Anais, F., Mazzolini, J., Herit, F., and Niedergang, F. (2016). Dynamin-actin cross talk contributes to phagosome formation and closure. *Traffic* 17, 487–499. doi: 10.1111/tra.12386

Masud Rana, A. Y., Tsujioka, M., Miyagishima, S., Ueda, M., and Yumura, S. (2013). Dynamin contributes to cytokinesis by stabilizing actin filaments in the contractile ring. *Genes Cells* 18, 621–635. doi: 10.1111/gtc.12060

Menon, M., and Schafer, D. A. (2013). Dynamin: expanding its scope to the cytoskeleton. *Int. Rev. Cell Mol. Biol.* 302, 187–219.

Michell, R. H. (2008). Inositol derivatives: evolution and functions. *Nat. Rev. Mol. Cell Biol.* 9, 151–161. doi: 10.1038/nrm2334

Miyagishima, S. Y., Kuwayama, H., Urushihara, H., and Nakanishi, H. (2008). Evolutionary linkage between eukaryotic cytokinesis and chloroplast division by dynamin proteins. *Proc. Natl. Acad. Sci. U.S.A.* 105, 15202–15207. doi: 10.1073/pnas.0802412105

Moon, Y., and Jun, Y. (2020). The effects of regulatory lipids on intracellular membrane fusion mediated by dynamin-like GTPases. *Front. Cell Dev. Biol.* 8:518. doi: 10.3389/fcell.2020.00518

Müller, R., Herr, C., Sukumaran, S. K., Omosigho, N. N., Plomann, M., Riyahi, T. Y., et al. (2013). The cytohesin paralog Sec7 of *Dictyostelium discoideum* is required for phagocytosis and cell motility. *Cell Commun. Signal.* 11:54.

Müller-Taubenberger, A., Kortholt, A., and Eichinger, L. (2013). Simple system–substantial share: the use of *Dictyostelium* in cell biology and molecular medicine. *Eur. J. Cell Biol.* 92, 45–53. doi: 10.1016/j.ejcb.2012.10.003

Narayanan, R., Leonard, M., Song, B. D., Schmid, S. L., and Ramaswami, M. (2005). An internal GAP domain negatively regulates presynaptic dynamin in vivo: a two-step model for dynamin function. *J. Cell Biol.* 169, 117–126. doi: 10.1083/jcb.200502042

Naslavsky, N., and Caplan, S. (2011). EHD proteins: key conductors of endocytic transport. *Trends Cell Biol.* 21, 122–131. doi: 10.1016/j.tcb.2010.10.003

Newton, H. J., Ang, D. K., Van Driel, I. R., and Hartland, E. L. (2010). Molecular pathogenesis of infections caused by *Legionella pneumophila*. *Clin. Microbiol. Rev.* 23, 274–298. doi: 10.1128/cmr.00052-09

Ngo, C. C., and Man, S. M. (2017). Mechanisms and functions of guanylate-binding proteins and related interferon-inducible GTPases: roles in intracellular lysis of pathogens. *Cell. Microbiol.* 19:e12791. doi: 10.1111/cmi.12791

Niemann, H. H., Knetsch, M. L., Scherer, A., Manstein, D. J., and Kull, F. J. (2001). Crystal structure of a dynamin GTPase domain in both nucleotide-free and GDP-bound forms. *EMBO J.* 20, 5813–5821. doi: 10.1093/emboj/20.21.5813

Otera, H., Miyata, N., Kuge, O., and Mihara, K. (2016). Drp1-dependent mitochondrial fission via MiD49/51 is essential for apoptotic cristae remodeling. *J. Cell Biol.* 212, 531–544. doi: 10.1083/jcb.201508099

Palmer, S. E., Smaczynska-De Rooji, I. I., Marklew, C. J., Allwood, E. G., Mishra, R., Johnson, S., et al. (2015). A dynamin-actin interaction is required for vesicle scission during endocytosis in yeast. *Curr. Biol.* 25, 868–878. doi: 10.1016/j.cub.2015.01.061

Paschke, P., Knecht, D. A., Silale, A., Traynor, D., Williams, T. D., Thomason, P. A., et al. (2018). Rapid and efficient genetic engineering of both wild type and axenic strains of *Dictyostelium discoideum*. *PLoS One* 13:e0196809. doi: 10.1371/journal.pone.0196809

Payrastre, B., Missy, K., Giuriato, S., Bodin, S., Plantavid, M., and Gratacap, M. (2001). Phosphoinositides: key players in cell signalling, in time and space. *Cell. Signal.* 13, 377–387. doi: 10.1016/s0898-6568(01)00158-9

Peracino, B., Balest, A., and Bozzaro, S. (2010). Phosphoinositides differentially regulate bacterial uptake and Nramp1-induced resistance to *Legionella* infection in *Dictyostelium*. *J. Cell Sci.* 123, 4039–4051. doi: 10.1242/jcs.072124

Personnic, N., Bärlocher, K., Finsel, I., and Hilbi, H. (2016). Subversion of retrograde trafficking by translocated pathogen effectors. *Trends Microbiol.* 24, 450–462. doi: 10.1016/j.tim.2016.02.003

Peters, C., Baars, T. L., Buhler, S., and Mayer, A. (2004). Mutual control of membrane fission and fusion proteins. *Cell* 119, 667–678. doi: 10.1016/j.cell.2004.11.023

Phillips, M. J., and Voeltz, G. K. (2016). Structure and function of ER membrane contact sites with other organelles. *Nat. Rev. Mol. Cell Biol.* 17, 69–82. doi: 10.1038/nrm.2015.8

Praefcke, G. J., and McMahon, H. T. (2004). The dynamin superfamily: universal membrane tubulation and fission molecules? *Nat. Rev. Mol. Cell Biol.* 5, 133–147. doi: 10.1038/nrm1313

Qiu, J., and Luo, Z. Q. (2017). *Legionella* and *Coxiella* effectors: strength in diversity and activity. *Nat. Rev. Microbiol.* 15, 591–605. doi: 10.1038/nrmicro.2017.67

Rai, A., Nothe, H., Tzvetkov, N., Korenbaum, E., and Manstein, D. J. (2011). *Dictyostelium* dynamin B modulates cytoskeletal structures and membranous organelles. *Cell. Mol. Life Sci.* 68, 2751–2767. doi: 10.1007/s00018-010-0590-5

Rai, A., Tzvetkov, N., and Manstein, D. J. (2013). Functional dissection of the *Dictyostelium discoideum* dynamin B mitochondrial targeting sequence. *PLoS One* 8:e56975. doi: 10.1371/journal.pone.0056975

Ramachandran, R., and Schmid, S. L. (2018). The dynamin superfamily. *Curr. Biol.* 28, R411–R416.

Riyahi, T. Y., Frese, F., Steinert, M., Omosigho, N. N., Glöckner, G., Eichinger, L., et al. (2011). RpkA, a highly conserved GPCR with a lipid kinase domain, has a role in phagocytosis and anti-bacterial defense. *PLoS One* 6:e27311. doi: 10.1371/journal.pone.0027311

Romano-Moreno, M., Rojas, A. L., Williamson, C. D., Gershlick, D. C., Lucas, M., Isupov, M. N., et al. (2017). Molecular mechanism for the subversion of the retromer coat by the *Legionella* effector RidL. *Proc. Natl. Acad. Sci. U.S.A.* 114, E11151–E11160.

Rothmeier, E., Pfaffinger, G., Hoffmann, C., Harrison, C. F., Grabmayr, H., Repnik, U., et al. (2013). Activation of Ran GTPase by a *Legionella* effector promotes microtubule polymerization, pathogen vacuole motility and infection. *PLoS Pathog.* 9:e1003598. doi: 10.1371/journal.ppat.1003598

Schimmel, B. G., Berbusse, G. W., and Naylor, K. (2012). Mitochondrial fission and fusion in *Dictyostelium discoideum*: a search for proteins involved in membrane dynamics. *BMC Res. Notes* 5:505. doi: 10.1186/1756-0500-5-505

Schmölders, J., Manske, C., Otto, A., Hoffmann, C., Steiner, B., Welin, A., et al. (2017). Comparative proteomics of purified pathogen vacuoles correlates intracellular replication of *Legionella pneumophila* with the small GTPase Ras-related protein 1 (Rap1). *Mol. Cell Proteomics* 16, 622–641. doi: 10.1074/mcp.m116.063453

Sherwood, R. K., and Roy, C. R. (2013). A Rab-centric perspective of bacterial pathogen-occupied vacuoles. *Cell Host Microbe* 14, 256–268. doi: 10.1016/j.chom.2013.08.010

Shpetner, H. S., and Vallee, R. B. (1989). Identification of dynamin, a novel mechanochemical enzyme that mediates interactions between microtubules. *Cell* 59, 421–432. doi: 10.1016/0092-8674(89)90027-5

Shydlovskyi, S., Zienert, A. Y., Ince, S., Dovengerds, C., Hohendahl, A., Dargazanli, J. M., et al. (2017). Nucleotide-dependent farnesyl switch orchestrates polymerization and membrane binding of human guanylate-binding protein 1. *Proc. Natl. Acad. Sci. U.S.A.* 114, E5559–E5568.

Smaczynska-De Rooji, I. I., Allwood, E. G., Aghamohammadzadeh, S., Hettema, E. H., Goldberg, M. W., and Ayscough, K. R. (2010). A role for the dynamin-like protein Vps1 during endocytosis in yeast. *J. Cell Sci.* 123(Pt 20), 3496–3506. doi: 10.1242/jcs.070508

Steiner, B., Swart, A. L., Welin, A., Weber, S., Personnic, N., Kaech, A., et al. (2017). ER remodeling by the large GTPase atlastin promotes vacuolar growth of *Legionella pneumophila*. *EMBO Rep.* 18, 1817–1836. doi: 10.15252/embr.201743903

Steiner, B., Weber, S., and Hilbi, H. (2018a). Formation of the *Legionella*-containing vacuole: phosphoinositide conversion, GTPase modulation and ER dynamics. *Int. J. Med. Microbiol.* 308, 49–57. doi: 10.1016/j.ijmm.2017.08.004

Steiner, B., Weber, S., Kaech, A., Ziegler, U., and Hilbi, H. (2018b). The large GTPase atlastin controls ER remodeling around a pathogen vacuole. *Commun. Integr. Biol.* 11, 1–5. doi: 10.1080/19420889.2018.1440880

Swanson, M. S., and Isberg, R. R. (1995). Association of *Legionella pneumophila* with the macrophage endoplasmic reticulum. *Infect. Immun.* 63, 3609–3620. doi: 10.1128/iai.63.9.3609-3620.1995

Swart, A. L., and Hilbi, H. (2020). Phosphoinositides and the fate of *Legionella* in phagocytes. *Front. Immunol.* 11:25. doi: 10.3389/fimmu.2020.00025

Swart, A. L., Harrison, C. F., Eichinger, L., Steinert, M., and Hilbi, H. (2018). *Acanthamoeba* and *Dictyostelium* as cellular models for *Legionella* infection. *Front. Cell. Infect. Microbiol.* 8:61. doi: 10.3389/fcimb.2018.00061

Swart, A. L., Gomez-Valero, L., Buchrieser, C., and Hilbi, H. (2020a). Evolution and function of bacterial RCC1 repeat effectors. *Cell. Microbiol.* 22:e13246.

Swart, A. L., Steiner, B., Gomez-Valero, L., Schütz, S., Hannemann, M., Janning, P., et al. (2020b). Divergent evolution of *Legionella* RCC1 repeat effectors defines the range of Ran GTPase cycle targets. *mBio* 11:e00405-20.

Tilney, L. G., Harb, O. S., Connelly, P. S., Robinson, C. G., and Roy, C. R. (2001). How the parasitic bacterium *Legionella pneumophila* modifies its phagosome and transforms it into rough ER: implications for conversion of plasma membrane to the ER membrane. *J. Cell Sci.* 114, 4637–4650. doi: 10.1242/jcs.114.24.4637

Tretina, K., Park, E. S., Maminska, A., and Macmicking, J. D. (2019). Interferon-induced guanylate-binding proteins: guardians of host defense in health and disease. *J. Exp. Med.* 216, 482–500. doi: 10.1084/jem.20182031

Urwyler, S., Nyfeler, Y., Ragaz, C., Lee, H., Mueller, L. N., Aebersold, R., et al. (2009). Proteome analysis of *Legionella* vacuoles purified by magnetic immunoseparation reveals secretory and endosomal GTPases. *Traffic* 10, 76–87. doi: 10.1111/j.1600-0854.2008.00851.x

Varlakhanova, N. V., Alvarez, F. J. D., Brady, T. M., Tornabene, B. A., Hosford, C. J., Chappie, J. S., et al. (2018). Structures of the fungal dynamin-related protein Vps1 reveal a unique, open helical architecture. *J. Cell Biol.* 217, 3608–3624. doi: 10.1083/jcb.201712021

Wang, M., Guo, X., Yang, X., Zhang, B., Ren, J., Liu, A., et al. (2019). Mycobacterial dynamin-like protein IniA mediates membrane fission. *Nat. Commun.* 10:3906.

Weber, S. S., Ragaz, C., and Hilbi, H. (2009). The inositol polyphosphate 5-phosphatase OCRL1 restricts intracellular growth of *Legionella*, localizes to the replicative vacuole and binds to the bacterial effector LpnE. *Cell. Microbiol.* 11, 442–460. doi: 10.1111/j.1462-5822.2008.01266.x

Weber, S. S., Ragaz, C., Reus, K., Nyfeler, Y., and Hilbi, H. (2006). *Legionella pneumophila* exploits PI(4)*P* to anchor secreted effector proteins to the replicative vacuole. *PLoS Pathog.* 2:e46. doi: 10.1371/journal.ppat.0020046

Weber, S., Steiner, B., Welin, A., and Hilbi, H. (2018). *Legionella*-containing vacuoles capture PtdIns(4)*P*-rich vesicles derived from the Golgi apparatus. *mBio* 9:e02420-18.

Weber, S., Wagner, M., and Hilbi, H. (2014). Live-cell imaging of phosphoinositide dynamics and membrane architecture during *Legionella* infection. *mBio* 5:e00839-13.

Welin, A., Weber, S., and Hilbi, H. (2018). Quantitative imaging flow cytometry of *Legionella*-infected *Dictyostelium* amoebae reveals the impact of retrograde trafficking on pathogen vacuole composition. *Appl. Environ. Microbiol.* 84:e00158-18.

Wienke, D. C., Knetsch, M. L., Neuhaus, E. M., Reedy, M. C., and Manstein, D. J. (1999). Disruption of a dynamin homologue affects endocytosis, organelle morphology, and cytokinesis in *Dictyostelium discoideum*. *Mol. Biol. Cell* 10, 225–243. doi: 10.1091/mbc.10.1.225

Yao, J., Yang, F., Sun, X., Wang, S., Gan, N., Liu, Q., et al. (2018). Mechanism of inhibition of retromer transport by the bacterial effector RidL. *Proc. Natl. Acad. Sci. U.S.A.* 115, E1446–E1454.

Zhang, R., Lee, D. M., Jimah, J. R., Gerassimov, N., Yang, C., Kim, S., et al. (2020). Dynamin regulates the dynamics and mechanical strength of the actin cytoskeleton as a multifilament actin-bundling protein. *Nat. Cell Biol.* 22, 674–688. doi: 10.1038/s41556-020-0519-7

Conflict of Interest: The authors declare that the research was conducted in the absence of any commercial or financial relationships that could be construed as a potential conflict of interest.

Publisher's Note: All claims expressed in this article are solely those of the authors and do not necessarily represent those of their affiliated organizations, or those of the publisher, the editors and the reviewers. Any product that may be evaluated in this article, or claim that may be made by its manufacturer, is not guaranteed or endorsed by the publisher.

Copyright © 2021 Katic, Hüsler, Letourneur and Hilbi. This is an open-access article distributed under the terms of the Creative Commons Attribution License (CC BY). The use, distribution or reproduction in other forums is permitted, provided the original author(s) and the copyright owner(s) are credited and that the original publication in this journal is cited, in accordance with accepted academic practice. No use, distribution or reproduction is permitted which does not comply with these terms.

frontiers in Cell and Developmental Biology

HYPOTHESIS AND THEORY
published: 08 November 2021
doi: 10.3389/fcell.2021.758317

Possible Involvement of the Nutrient and Energy Sensors mTORC1 and AMPK in Cell Fate Diversification in a Non-Metazoan Organism

Julian D. Gross and Catherine J. Pears*

Department of Biochemistry, University of Oxford, Oxford, United Kingdom

mTORC1 and AMPK are mutually antagonistic sensors of nutrient and energy status that have been implicated in many human diseases including cancer, Alzheimer's disease, obesity and type 2 diabetes. Starved cells of the social amoeba *Dictyostelium discoideum* aggregate and eventually form fruiting bodies consisting of stalk cells and spores. We focus on how this bifurcation of cell fate is achieved. During growth mTORC1 is highly active and AMPK relatively inactive. Upon starvation, AMPK is activated and mTORC1 inhibited; cell division is arrested and autophagy induced. After aggregation, a minority of the cells (prestalk cells) continue to express much the same set of developmental genes as during aggregation, but the majority (prespore cells) switch to the prespore program. We describe evidence suggesting that overexpressing AMPK increases the proportion of prestalk cells, as does inhibiting mTORC1. Furthermore, stimulating the acidification of intracellular acidic compartments likewise increases the proportion of prestalk cells, while inhibiting acidification favors the spore pathway. We conclude that the choice between the prestalk and the prespore pathways of cell differentiation may depend on the relative strength of the activities of AMPK and mTORC1, and that these may be controlled by the acidity of intracellular acidic compartments/lysosomes (pHv), cells with low pHv compartments having high AMPK activity/low mTORC1 activity, and those with high pHv compartments having high mTORC1/low AMPK activity. Increased insight into the regulation and downstream consequences of this switch should increase our understanding of its potential role in human diseases, and indicate possible therapeutic interventions.

Keywords: *Dictyostelium discoideum*, cell fate decision, AMP-dependent protein kinase (AMPK), mechanistic target of rapamycin complex 1 (mTORC1), ammonia, acidic vesicles, DIF-1

OPEN ACCESS

Edited by:
Robert J. Huber,
Trent University, Canada

Reviewed by:
Sarah Jane Annesley,
La Trobe University, Australia
Robin S. B. Williams,
University of London, United Kingdom

****Correspondence:***
Julian D. Gross
juliandavid910@outlook.com

Specialty section:
This article was submitted to Molecular and Cellular Pathology, a section of the journal Frontiers in Cell and Developmental Biology

Received: *13 August 2021*
Accepted: *19 October 2021*
Published: *08 November 2021*

Citation:
Gross JD and Pears CJ (2021) Possible Involvement of the Nutrient and Energy Sensors mTORC1 and AMPK in Cell Fate Diversification in a Non-Metazoan Organism. Front. Cell Dev. Biol. 9:758317. doi: 10.3389/fcell.2021.758317

INTRODUCTION

Individual starved amoebae of *D. discoideum* aggregate to form loose mounds, which are transformed into "tight aggregates", in which the amoebae are closely associated via lateral and polar contacts and become surrounded by a complex extracellular matrix of protein and cellulose to create, in effect, a multicellular organism (Kessin, 2001; Pears and Gross, 2021). Once within the mounds, the cells become divided into two cell types, prestalk and prespore cells, defined by myriad differences in gene expression. The two types of cell are initially distributed in a salt and pepper

manner within mounds (Thompson et al., 2004) but soon separate, with the prestalk cells moving first to the periphery of the mound and then to its apex; the aggregate then elongates to form a "first finger" or "standing slug" divided into a leading zone made up of prestalk (pst) cells, and a posterior zone of prespore (psp) cells. This standing structure can fall over onto the substratum and migrate for a period as a migratory slug or proceed immediately to form a fruiting body consisting of mature spores held up by a cellular stalk made up of stalk cells.

Early attempts to answer the question of how the divergence of cell type is achieved focused on the stalk cell-inducing factor DIF-1 (Town et al., 1976; Kay and Jermyn, 1983). DIF-1 is a low molecular weight chlorinated alkyl phenone that was purified from the conditioned medium of developing amoebae and induces isolated amoebae to differentiate into vacuolated stalk cells following pre-treatment with a high concentration of extracellular cyclic AMP (cAMP). A number of different models have been proposed in which DIF-1 plays a central role in controlling cell type divergence (Gross et al., 1981; Meinhardt, 1983; Gruenheit et al., 2018). Factors such as the glycogen content of amoebae grown in high glucose and the cell cycle phase at the onset of starvation are known to influence cell fate preference (McDonald and Durston, 1984; Weijer et al., 1984; Gomer and Firtel, 1987; Araki et al., 1994; Thompson and Kay, 2000a). These have been proposed to lead to differential sensitivity to DIF-1 induction of prestalk gene expression (Thompson and Kay, 2000a; Gruenheit et al., 2018). However, although mutants unable to synthesise or respond to DIF-1 display a number of developmental defects, in particular lacking one subtype of prestalk cell, they are able to form normal developmental structures such as first fingers, slugs and fruiting bodies with a roughly normal pattern of prestalk and prespore cells (Thompson and Kay, 2000b; Saito et al., 2008; Murata et al., 2016). Therefore, differential ability of cells to respond to DIF-1 cannot explain cell type divergence.

Roles of AMPK and mTORC1 in Cell Fate Choice

The proposal we wish to make is based on the behavior of the nutrient and energy sensors mTORC1 (mechanistic target of rapamycin complex 1) and AMPK (AMP-activated protein kinase), and on the fact that *Dictyostelium* development takes place during starvation. The universal serine/threonine protein kinases mTORC1 and AMPK (Hardie, 2007; Saxton and Sabatini, 2017) have emerged as major nutrient sensors that control the responses to changes in nutrient and energy levels by activating complex downstream networks of signaling proteins such as other protein kinases and transcription factors. When eukaryotic cells are incubated in the presence of adequate concentrations of amino acids and glucose, mTORC1 is activated and AMPK activity is inhibited; cells multiply and autophagy is reduced. In response to starvation, mTORC1 activity declines and AMPK activity increases, resulting in arrest of cell division in G1 (Rattan et al., 2005) and the induction of autophagy which has the effect of conserving energy and obtaining a minimal level of nutrients from catabolism (Hardie, 2007; Jung et al., 2010; Saxton and Sabatini, 2017).

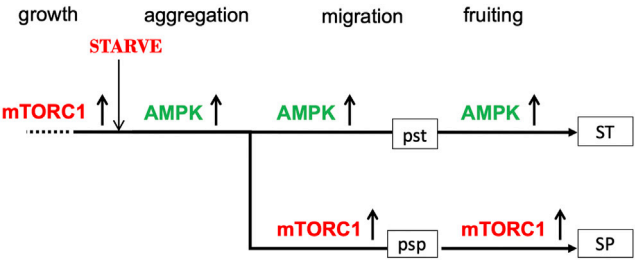

FIGURE 1 | Suggested roles of AMPK and mTORC1 activities in the prestalk (pst) and prespore (psp) pathways. During growth, mTORC1 is active (upward arrow) and AMPK activity is low (not shown). Upon nutrient withdrawal, mTORC1 activity is rapidly switched off and AMPK activity upregulated (upward arrow); as a result, aggregative stage gene expression is turned on, growth is arrested and autophagy activated. At the mound stage, mTORC1 is re-activated in some 80% of the amoebae (and AMPK downregulated) and expression of the prespore transcriptome is initiated; AMPK continues to be highly active in the remaining 20% of amoebae, which eventually form vacuolated stalk cells. The prestalk pathway is represented by a continuous straight line with the prespore pathway diverging from it to emphasise the asymmetry of the proposed bifurcation process. Only the member of the AMPK/mTORC1 pair that is highly active at any one time is shown.

This response is conserved when amoebae of *D. discoideum* are starved: mTORC1 activity is rapidly down-regulated and AMPK activity increases (Rosel et al., 2012; Jaiswal and Kimmel, 2019); cell division and DNA replication soon cease, autophagosomes appear in increased numbers (Zimmerman and Weijer, 1993; King et al., 2011) and autophagy genes are upregulated (Jaiswal et al., 2019). At the same time, development is initiated and transcription switches from the growth transcriptome to the early aggregative transcriptome (Jaiswal and Kimmel, 2019). However, while cell division ceases at the onset of development, it recommences post aggregation in the posterior region of slugs containing the prespore cells [(Zimmerman and Weijer, 1993; Muramoto and Chubb, 2008) and references therein]. At the same time autophagic activity declines, but does not altogether cease, in the prespore population.

It occurred to us that this reversal of activities in the prespore cells could be the consequence of a reversal of the relative activities of AMPK and mTORC1 in these cells; in other words, that prespore gene expression might be initiated in the future prespore cells when AMPK activity was down-regulated and mTORC1 activity restored. It has already been proposed that the mutual inhibition between mTORC1 and AMPK constitutes a regulatory switch responsible for initiating development (Jaiswal and Kimmel, 2019), and our suggestion is just an extension of this idea to account for the bifurcation of cell fates. The most straightforward test of our proposal would be to follow the phosphorylation activities of AMPK and mTORC1 during early development to determine if AMPK activity declines and mTORC1 activity increases prior to the appearance of prespore cell-specific markers.

This hypothesis for the relationship between the pst and psp pathways envisages the stalk cell pathway as a continuous pathway starting from starvation and the onset of development and proceeding all the way through aggregation to the formation of vacuolated stalk cells (**Figure 1**). The spore pathway, on the other hand, is seen as *deviating from* the prestalk pathway. This asymmetry is consistent with the observation that many "prestalk-specific" genes are first expressed during the aggregation stage (Jermyn et al., 1987; Tsujioka et al., 2001) whereas prespore-specific genes tend to be first expressed after aggregation, at around 8–10 h into development (Iranfar et al., 2001). We refer to the point at which this deviation occurs as the bifurcation point. The spore pathway can include novel products not present during growth, such as the spore coat proteins, since cells entering the spore pathway contain transcriptional machinery made during the aggregation stage.

Evidence for Stalk Pathway Control by AMPK

In vivo Stalk Cell Formation

If the choice of the prestalk pathway is controlled by the activation of AMPK we might expect that overexpressing AMPK would increase the ratio of prestalk: prespore cells, and an effect of this kind has been observed by several workers. AMPK, as its full name of 5′AMP-activated protein kinase indicates, is activated by an increase in the AMP:ATP ratio. Mutants lacking AMP deaminase cannot deaminate AMP (adenosine 5′-monophosphate) to IMP (inosine 5-monophosphate) and as a result accumulate abnormally high levels of AMP (Chae et al., 2002). These strains form fruiting bodies with short, thick stalks and fewer than 5% of the usual number of spores; levels of prestalk-specific mRNAs are more than two-fold higher than those in wild-type strains and prespore-specific mRNAs are reduced. Slugs formed by the mutant strain have twice the normal number of prestalk cells, and enlarged prestalk zones. Similarly, expression of a truncated (and hence deregulated) form of the *Dictyostelium* AMPK catalytic subunit to increase AMPK activity led to the same kind of "stalky" phenotype as over-expression of AMPK (Bokko et al., 2007). Similar developmental effects have been observed in strains with defective mitochondrial function, which is thought to lead to reduced ATP synthesis and an elevated AMP/ATP ratio, and so to hyper-activation of AMPK. However, we note that, in contradiction to the above findings, fruiting bodies from cells lacking the catalytic subunit of AMPK have been reported to have increased prestalk zones (Maurya et al., 2017). However, late developmental phenotypes were not complemented by re-expression of the relevant subunit. Also AMPK transcripts were found to be restricted to the pst cells of slugs (Maurya et al., 2017), supporting the idea that AMPK activity is downregulated in the prespore "compartment".

In vitro Stalk Cell Formation in Response to DIF-1

As mentioned, DIF-1 does not seem to play a decisive role in the initial cell fate choice in normal development and yet it dramatically stimulates stalk cell formation when cells are starved in monolayers in the presence of cAMP (Town et al., 1976). If AMPK controls the stalk pathway *in vivo* as we propose, we would expect it also to play a role in DIF-induced stalk cell formation. In agreement with this suggestion, exposure of *Dictyostelium* amoebae to DIF-1 leads to extensive changes in protein phosphorylation at sites many of which fit the AMPK consensus motif (Sugden et al., 2015), and DIF-1 activates AMPK in mouse 3T3-L1 fibroblasts (Kubohara et al., 2021). Also there is substantial evidence that DIF-1 acts by increasing cytosolic Ca^{2+}, which is known in other systems to activate AMPK via the Ca^{2+}/calmodulin-dependent protein kinase, CaMKK2 (Hurley et al., 2005) (**Figure 2**). Addition of DIF-1 has been shown to induce a rapid increase of intracellular Ca^{2+} (Azhar et al., 1997; Traynor and Kay, 2017), as well as a gradual and sustained rise in cytosolic Ca^{2+} (Schaap et al., 1996), and the stalk-cell inducing activity of DIF-1 is mimicked by the Ca^{2+}-ATPase inhibitors BHQ and thapsigargin, which raise cytosolic Ca^{2+} by inhibiting sequestration of Ca^{2+} into intracellular stores (Schaap et al., 1996; Kubohara et al., 2007; Kubohara et al., 2021). Moreover DIF-1 fails to induce a rise in cytosolic Ca^{2+} in mutants lacking IplA, the putative endoplasmic reticulum IP3 receptor (Traynor and Kay, 2017), and also fails to induce stalk cells in these mutants (Lam et al., 2008).

Evidence for Control of the Spore Pathway by mTORC1

Prespore-specific gene expression requires exposure to extracellular cAMP, which acts on cell surface receptors (cARs) [see (Yamada and Schaap, 2019)]. A provisional prespore pathway (Grimson et al., 2000) derived from the work of several groups and based on mutants with reduced proportions of prespore cells is:

cAMP receptor → Zak1 → GskA--→ Aar (a β-catenin homolog)→ psp gene expression.

For reasons that are not understood, mutations affecting this pathway have very variable effects on the extent of prespore and spore cell formation [see for example (Schilde et al., 2004)]. On the other hand, strains with disruption of the genes encoding any of these proteins that have been tested have the same effect in the monolayer differentiation system: they render stalk cell induction by DIF-1 insensitive to inhibition by the presence of cAMP (Harwood et al., 1995), because of partial or complete elimination of the psp pathway as a competitor to the stalk pathway (Early and Williams, 1988; Berks and Kay, 1990). A corollary of this is that stalk cell induction in these mutants is hypersensitive to DIF-1 (needs lower concentrations of DIF-1) when the assay is performed with cAMP present along with the DIF-1.

Until recently there was no evidence connecting the spore pathway with mTORC1. Any effect of mTORC1 could involve a parallel pathway or mTORC1 could influence the activity of the above pathway. There is clearly a complex interaction between mTORC1 and Gsk3 activity in humans which is not fully understood (Sun, 2021) and has been implicated in tumour resistance to mTORC1 inhibition. Recently a *Dictyostelium* mutant has been described in which the gene encoding

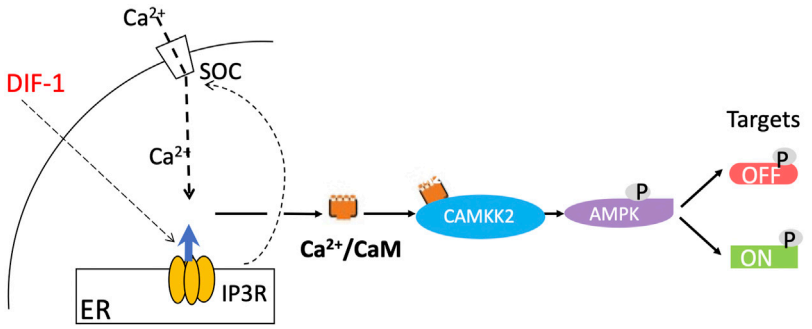

FIGURE 2 | Proposed pathway of stalk cell induction by DIF-1. DIF-1 triggers an increase in cytosolic Ca^{2+}, a process dependent on IplA, a protein related to the mammalian IP_3 receptor, which triggers Ca^{2+} release from the endoplasmic reticulum (Traynor and Kay, 2017) and may also induce Ca^{2+} entry into the cell via a store-operated calcium channel. The concentration of Ca^{2+}/calmodulin in turn increases, binding to and activating the calmodulin-dependent protein kinase CaMKK2. This then phosphorylates and activates AMPK, which phosphorylates various target proteins, activating some (including calcineurin and inhibiting others (Sugden et al., 2015) and initiating the prestalk/stalk (ST) pathway.

1-phosphatidylinositol-3-phosphate 5-kinase (PIKfyve) has been disrupted (Yamada et al., 2021), and properties of the mutant strain point to involvement of mTORC1 in the psp/spore pathway. PIKfyve converts PtdIns3P to PtdIns3,5P_2 (PIP_2), and there is strong evidence that PIP_2 is located on the vacuole membrane of yeast and on acidic vesicle/endosomal membranes in mammalian cells and act as an anchor to associate mTORC1 to these membranes (Bridges et al., 2012), a precondition for its activation. The mutant has enlarged lower stalks; spore coat protein synthesis is initiated in Golgi-derived prespore vesicles as in the wild type, but mature spore formation is highly defective. Most importantly, *in vitro* observations show that the mutant is clearly DIF-1 hypersensitive, as defined above. Since this seems to be a characteristic of all mutants blocked in the spore pathway, it is consistent with the inference that PIKfyve, and, by extension, mTORC1, is a key player in that pathway. This conclusion could be tested by measuring mTORC1 activity in the mutant; also by seeing whether mTORC1 inhibitors render stalk cell induction in cell monolayers hypersensitive to DIF-1 in the presence of cAMP and block *in vitro* psp/spore formation in response to cAMP (in the absence of DIF-1).

In humans, the central roles of PIKfyve in endosomal trafficking and autophagy make it an attractive candidate for treatment of a number of diseases, using PIKfyve inhibitors such as apilimod. These diseases include cancer and neurodegenerative conditions as well as viral infections including those due to coronaviruses (Ikonomov et al., 2019; Huang et al., 2021). Understanding its interplay with the mTORC1 and AMPK pathways in *Dictyostelium* will have a bearing on the development of such inhibitor treatments.

pHv and Symmetry Breaking

If we accept that the prespore pathway is initiated when AMPK is downregulated, and mTORC1 upregulated, in some 80% of the aggregated cells, what might be responsible for this switch? During growth and early in development, the acidic intracellular compartments of amoebae [although these are of various kinds, we will refer to them throughout as acidic vesicles (AVs)] are highly acidic and are stained by the weak base, neutral red, whereas at the first finger and slug stage of development, the AVs of prespore cells have lost their acidity and are unstained (Bonner, 1952). We suggest that this change in acidic vesicle pH (pHv) is responsible for downregulating AMPK and upregulating mTORC1 in these cells, although we cannot exclude the possibility that it is simply a consequence of their differences in gene expression. Support for the former possibility is based primarily on the finding that exposure of developing amoebae *in vitro* to weak bases switches them from the stalk to the spore pathway, whereas weak acids have the opposite effect (Gross et al., 1983; Kubohara and Okamoto, 1994) while at the same time altering the pH of their AVs (Yamamoto and Takeuchi, 1983; Marchetti et al., 2009). Although the differential neutral red staining pattern is sometimes not evident until slugs have migrated for some time, it is revealed within minutes by covering the slugs with mineral oil, which provides an impermeable barrier to the diffusion of ammonia (Feit et al., 1990). This effect can be explained if there is already a substantial difference in pHv between the cell types at the beginning of the experiment, but that for loss of neutral red staining of the prespore cells to occur, ammonia must accumulate in the AV's of these cells to a level at which their pHv is above the pKa (pH6.7) of neutral red.

In contrast to the marked difference between prestalk and prespore cells in terms of pHv, their cytosolic pH values are either not different (Kay et al., 1986; Town et al., 1987) or differ by at most 0.2 pH units (Inouye, 1988), so the effects of pH on cell type choice are unlikely to depend on a difference in cytosolic pH. Exposure to 50 mM ammonia lowered the acidity of AVs by at least two orders of magnitude but had no detectable effect on cytosolic pH (Davies et al., 1993), thus identifying AVs as the likely target of weak base action. These effects are seen at the level of prestalk versus prespore gene expression, as well as in terms of the final mature cell types (Bradbury and Gross, 1989), and are most easily accounted for if vesicle pH controls the pathway of gene expression.

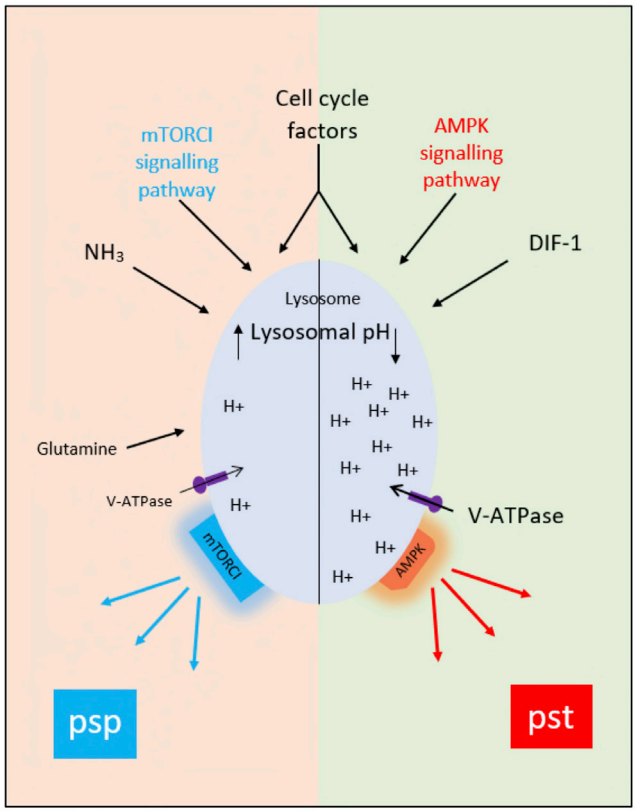

FIGURE 3 | The proposed role of acidic vesicle pH (pHv) in control of the prestalk and prespore pathways at the mound stage of development. Multiple factors including AMPK and mTORC1, cell cycle stage at the time of starvation, glycogen content, V-ATPase activities, cell adhesion and cell movement probably contribute to the division of a population of aggregated amoebae into those with acidified acidic vesicles (right-hand side of diagram). and those with neutralised acidic vesicles (left-hand side of diagram). We suggest that AMPK remains activated in the former group of cells, leading to continued prestalk gene expression, whereas it is downregulated in the latter group of cells and mTORC1 activated, initiating prespore gene expression.

Further evidence that pHv influences cell fate choice comes from the remarkable 1-dimensional differentiation system devised by Bonner (Bonner et al., 1995). In this system an extracellular pH gradient is generated by spontaneous ammonia production (Sawai et al., 2002), and cells expressing a prespore gene appear at the alkaline end of the pH gradient while those expressing prestalk genes are found at the more acidic end (Sawai et al., 2002) where AV's have been shown to be acidic (Azhar et al., 1996).

The idea that AV acidification status influences cell fate choice is not as strange as it might once have seemed since, in addition to their well-known activities in degradation and recycling, lysosomes are now seen to be organizing hubs regulating such processes as signaling, nutrient sensing, metabolic adaptation, organellar interactions and aging (Savini et al., 2019). Moreover, both AMPK and mTORC1 are thought to be present on lysosomes, and to be physically associated with the lysosomal V-ATPase responsible for acidifying the lysosomal lumen (Zhang et al., 2014) (**Figure 3**), potentially via PIP_2 (Ho et al., 2012; Jin et al., 2014). In many cases activation of mTORC1 appears to require lysosomal acidification and/or V-ATPase activity (Laplante and Sabatini, 2012). In the case of *Dictyostelium*, the proposed association between loss of acidity and initiation of the prespore pathway at the bifurcation point would require that it is AMPK activity that is dependent on vesicle acidification. If that is the case, we would expect that reduced vesicle acidification at the point when amoebae are starved to initiate development would interfere with the activation of AMPK and the corresponding downregulation of mTORC1 activity. In agreement with this expectation, the loss of mTORC1 activity upon starvation is delayed in a *Dictyostelium* mutant defective in acidifying AVs (Chang et al., 2020). Interestingly, loss of presenilin genes in *Dictyostelium* has been shown to block development by reducing vesicular acidification (Sharma et al., 2019). Mutations in presenilins in humans associated with Alzheimer's disease also result in elevated lysosomal pH and defects in autophagy (Lee et al., 2010). Other neurodegenerative disorders such as Parkinson's disease also show alterations in this pathway (Nixon, 2013). Thus, understanding the mechanisms and consequences of alterations in pHv in *Dictyostelium* will have an impact on our understanding of Alzheimer's disease and other neurogenerative diseases and on the eventual development of treatments.

An alternative interpretation of the mode of action of ammonia has been proposed to explain its well-known inhibitory effect on cAMP levels (Singleton et al., 1998), in which ammonia transporters act as ammonia sensors activating or inhibiting the hybrid histidine kinase DhkC in response to the local ammonia level; the level of DhkC activation would then be relayed to the RegA cAMP phosphodiesterase which would in turn be activated or inhibited. The authors discount a role for vacuolar pH in this process. While a role for DhkC in the cAMP response to ammonia levels has been established, it seems unlikely that the ammonia transporters are acting directly as sensors, since many other weak bases affect cAMP levels in the same way as ammonia and are not substrates of the ammonia transporters. Moreover, mutants in the V-ATPase itself cause the same developmental defects as exposure to weak bases (including prolonged slugging) (Davies et al., 1996), which would not be the case if these defects were due to ammonia transport activity. Instead, we suggest that defects in vesical acidification have two, probably independent, consequences: on the one hand they result in activation of the DhkC phosphorelay and breakdown of cAMP, on the other they inhibit AMPK activation (and/or promote mTORC1 activation).

The question remains of how the cells of aggregates become split into those with acidified vesicles and those with neutralized vesicles. One mechanism for creating such a division would be a process of local self-activation and lateral inhibition (Meinhardt, 1983), with ammonia as inhibitor, taking place within small random groups of cells in cell aggregates. However, the sorting behavior of mutants defective in vesicle acidification casts doubt on this idea. We would expect that on a lateral diffusion model, cells defective in acidification would sort preferentially to the prespore region in mixtures with wild type cells, since that is the

region occupied by cells with neutralized AVs; instead, they show a remarkable preferential localization in the anterior, acidified, compartment (Kirsten et al., 2008; Sharma et al., 2019). This indicates that pHv influences cell fate choice in *some* way, perhaps associated with the cell cycle, since cell fate is also strongly influenced by the stage of the division cycle at which cells are starved (McDonald and Durston, 1984; Araki et al., 1994; Huang et al., 1997; Jang and Gomer, 2011; Gruenheit et al., 2018) and other factors (**Figure 3**). Thus, the mechanism controlling differences in pHv appears to be complex and is elusive.

DISCUSSION

Gene expression in response to cAMP signaling in *Dictyostelium* is thought to involve two processes: firstly activation of poorly understood intracellular pathways by extracellular cAMP signals acting on cell surface G protein-coupled cAMP receptors, and secondly activation of cAMP-dependent protein kinase by cAMP synthesized within the cell by the actions of three distinct adenylate cyclases. According to our proposal, cell-type specialization, with its accompanying differential gene expression, is controlled by the opposing actions of mTORC1 and AMPK acting on this background of cAMP signaling. mTORC1 and AMPK, are often viewed as predominantly controlling responses to variations in food and energy supplies by phosphorylating cytoplasmic factors such as p70S6K and 4E-BP1. If those were their only targets it would be hard to see how they could control differential gene transcription on the two differentiation pathways. However, both agents are now known to also have profound effects on cell type-specific gene transcription in mammalian cells (Laplante and Sabatini, 2012; Sukumaran et al., 2020). The genome of *D. discoideum* contains at least 245 genes predicted to encode transcription factors, more than half of which are restricted to either prestalk or prespore cells (Forbes et al., 2019). Of these 245 transcription factors, just 34 have been examined in gene disruption or knockdown experiments, and nine of them caused defects in one specific cell type. There would therefore be ample opportunity for phosphorylation by mTORC1 and AMPK to control the differential production and/or activities of particular transcription factors and thus differential gene transcription in the two pathways. Interestingly, in the similar system involving the choice between adipocyte and osteocyte differentiation in human mesenchymal stem cells, which is controlled by mTORC1 and AMPK (Chen et al., 2017), recent work has revealed a network of transcription factors and enhancers that control adipogenesis (Rauch et al., 2019).

As well as this choice between the osteoblast and adipocyte fates of mesenchymal stem cells (Chen et al., 2017), many other cell fate choices in metazoans are also controlled by the mutually antagonistic effects of mTORC1 and AMPK. This applies for example to alternative T cell differentiation pathways in response to antigen (Chi, 2012), and the control of ageing in both yeast and higher organisms (Hindupur et al., 2015). Similarly, the inflammatory cells activated by pathogens and tissue damage are mTOR-dependent while anti-inflammatory cells are AMPK-dependent (O'Neill and Hardie, 2013). However, although the bifurcation of cell fates in *Dictyostelium* as we envisage it would reflect the same mutual antagonism between AMPK and mTORC1, it is unlike those situations in that it takes place under starvation where mTORC1 is not normally activated. In fact, according to our suggestion, prespore/spore pathway cells would resemble more closely tumour cells since in both mTORC1 activation is uncoupled from normal regulatory nutrient signals.

There is another possible parallel between tumour cells and prespore pathway cells. Paradoxically, many tumours, though fundamentally mTORC1-dependent and not dependent on extensive autophagic activity nevertheless rely on a low level of autophagy for their growth and spread, and hence on residual AMPK activity (given that autophagy depends on AMPK activity) (Kimmelman and White, 2017). Autophagy is thought to supply nutrients to these tumours and confer resistance to stressors such as starvation, anti-cancer drugs etc, and clinical trials are currently underway to test inhibition of autophagy as an anticancer strategy (Perez-Hernandez et al., 2019). Interestingly, a strikingly similar observation to the situation in those tumours is found in the case of the *Dictyostelium* prespore pathway (Yamada and Schaap, 2019); mutations such as *atg7* that reduce the efficiency of autophagy virtually eliminate prespore gene expression while not affecting prestalk gene expression. This can be understood in terms of our basic proposal if we suppose that autophagy, while an essential component of the prestalk pathway, is also needed at a low level in the prespore pathway; it should therefore be fully activated by AMPK in the pst pathway but substantially downregulated by mTORC1 in the prespore pathway. Consequently, if the efficiency of autophagy is reduced by a mutation such as *atg7* this will virtually eliminate autophagy in the prespore pathway and block prespore gene expression, while leaving the prestalk pathway almost intact.

Understanding the mechanisms and consequences of mTORC1 regulation in *Dictyostelium* has implications for treatment of a range of human diseases. For example, ketogenic diets, which involve intake of high levels of fat and low levels of carbohydrate, were developed to mimic starvation (Augustin et al., 2018). Such diets are used to treat seizures although recently it has been suggested that their mode of action is not due to the diet itself but to a direct effect of medium chain fatty acids such as decanoic acid, a major dietary breakdown product of diglycerides (Chang et al., 2013; Warren et al., 2018). Studies in *Dictyostelium* have demonstrated that decanoic acid inhibits mTORC1 activity, independently of glucose and insulin signaling (Warren et al., 2020). This work has identified a novel pathway to regulate mTORC1 activity. Decanoic acid inhibits mTORC1 activity in mammalian cells including astrocytes from tuberous sclerosis complex (TSC) patients. This syndrome is caused by mutations in TSC1 or TSC2, resulting in epilepsy, cognitive disfunction and behavioral abnormalities. Individuals with this neurodevelopmental disorder have hyperactive mTORC1. This work in *Dictyostelium* therefore points to decanoic acid as a promising therapy. Conversely cannabidiol (CBD), a major component of cannabis oil, enhances mTORC1 activity in *Dictyostelium* in a mechanism dependent on inositol polyphosphate multikinase (Damstra-Oddy et al., 2021). This pathway has been verified in

mammalian cells and shown to increase mTORC1 activity in primary peripheral blood mononuclear cells from patients suffering from multiple sclerosis. This work initiated in *Dictyostelium* identifies CBD as a potential therapy for multiple sclerosis through increased mTORC1 activity. DIF-1 inhibits the growth of a range of different cancer cells (Takahashi-Yanaga et al., 2014; Kubohara et al., 2015; Arioka et al., 2017). The mechanisms of action is as yet ill-defined although there is a recent report that it supresses the growth of triple negative breast cancer cells by a mechanism involving AMPK-dependent inhibition of mTORC1 activity (Seto-Tetsuo et al., 2021) in a pathway reminiscent of the cell fate decision pathway we are proposing in *Dictyostelium*. It will be of interest to define the role of the pH of acidic vesicles in the effect of DIF-1 on growth of these cancer cells as alteration of this may offer an alternative therapy route.

In conclusion, *Dictyostelium* may provide a tractable non-metazoan model for examining in detail how the two ancient sensor molecules, mTORC1 and AMPK, control the differential gene expression underlying a cell fate choice.

DATA AVAILABILITY STATEMENT

The original contributions presented in the study are included in the article/Supplementary Material, further inquiries can be directed to the corresponding author.

AUTHOR CONTRIBUTIONS

JG wrote the manuscript. CP revised, commented and edited the manuscript.

FUNDING

Work in CJP lab is funded by National Centre for the Replacement Refinement and Reduction of Animals in Research (NC3Rs) grant numbers NC/M000834/1 and NC/K500355/1 and CrackIt Solutions Funding.

REFERENCES

Araki, T., Nakao, H., Takeuchi, I., and Maeda, Y. (1994). Cell-cycle-dependent Sorting in the Development of Dictyostelium Cells. *Dev. Biol.* 162 (1), 221–228. doi:10.1006/dbio.1994.1080

Arioka, M., Takahashi-Yanaga, F., Kubo, M., Igawa, K., Tomooka, K., and Sasaguri, T. (2017). Anti-tumor Effects of Differentiation-Inducing Factor-1 in Malignant Melanoma: GSK-3-Mediated Inhibition of Cell Proliferation and GSK-3-independent Suppression of Cell Migration and Invasion. *Biochem. Pharmacol.* 138, 31–48. doi:10.1016/j.bcp.2017.05.004

Augustin, K., Khabbush, A., Williams, S., Eaton, S., Orford, M., Cross, J. H., et al. (2018). Mechanisms of Action for the Medium-Chain Triglyceride Ketogenic Diet in Neurological and Metabolic Disorders. *Lancet Neurol.* 17 (1), 84–93. doi:10.1016/S1474-4422(17)30408-8

Azhar, M., Kennady, P. K., Pande, G., and Nanjundiah, V. (1997). Stimulation by DIF Causes an Increase of Intracellular Ca^{2+} in *Dictyostelium discoideum*. *Exp. Cel Res.* 230 (2), 403–406. doi:10.1006/excr.1996.3420

Azhar, M., Manogaran, P. S., Kennady, P. K., Pande, G., and Nanjundiah, V. (1996). A Ca2+-dependent Early Functional Heterogeneity in Amoebae of *Dictyostelium discoideum* Revealed by Flow Cytometry. *Exp. Cel Res.* 227 (2), 344–351. doi:10.1006/excr.1996.0283

Berks, M., and Kay, R. R. (1990). Combinatorial Control of Cell Differentiation by cAMP and DIF-1 during Development of *Dictyostelium discoideum*. *Development* 110 (3), 977–984. doi:10.1242/dev.110.3.977

Bokko, P. B., Francione, L., Bandala-Sanchez, E., Ahmed, A. U., Annesley, S. J., Huang, X., et al. (2007). Diverse Cytopathologies in Mitochondrial Disease Are Caused by AMP-Activated Protein Kinase Signaling. *MBoC* 18 (5), 1874–1886. doi:10.1091/mbc.e06-09-0881

Bonner, J. T. (1952). The Pattern of Differentiation in Amoeboid Slime Molds. *The Am. Naturalist* 86, 69–89. doi:10.1086/281707

Bonner, J. T., Compton, K. B., Cox, E. C., Fey, P., and Gregg, K. Y. (1995). Development in One Dimension: the Rapid Differentiation of *Dictyostelium discoideum* in Glass Capillaries. *Proc. Natl. Acad. Sci.* 92 (18), 8249–8253. doi:10.1073/pnas.92.18.8249

Bradbury, J. M., and Gross, J. D. (1989). The Effect of Ammonia on Cell-type-specific Enzyme Accumulation in *Dictyostelium discoideum*. *Cel Differ. Dev.* 27 (2), 121–128. doi:10.1016/0922-3371(89)90741-7

Bridges, D., Ma, J.-T., Park, S., Inoki, K., Weisman, L. S., and Saltiel, A. R. (2012). Phosphatidylinositol 3,5-bisphosphate Plays a Role in the Activation and Subcellular Localization of Mechanistic Target of Rapamycin 1. *MBoC* 23 (15), 2955–2962. doi:10.1091/mbc.E11-12-103

Chae, S.-C., Fuller, D., and Loomis, W. F. (2002). Altered Cell-type Proportioning in Dictyostelium Lacking Adenosine Monophosphate Deaminase. *Dev. Biol.* 241 (1), 183–194. doi:10.1006/dbio.2001.0491

Chang, F.-S., Wang, Y., Dmitriev, P., Gross, J., Galione, A., and Pears, C. (2020). A Two-Pore Channel Protein Required for Regulating mTORC1 Activity on Starvation. *BMC Biol.* 18 (1), 8. doi:10.1186/s12915-019-0735-4

Chang, P., Terbach, N., Plant, N., Chen, P. E., Walker, M. C., and Williams, R. S. B. (2013). Seizure Control by Ketogenic Diet-Associated Medium Chain Fatty Acids. *Neuropharmacology* 69, 105–114. doi:10.1016/j.neuropharm.2012.11.004

Chen, S. C., Brooks, R., Houskeeper, J., Bremner, S. K., Dunlop, J., Viollet, B., et al. (2017). Metformin Suppresses Adipogenesis through Both AMP-Activated Protein Kinase (AMPK)-dependent and AMPK-independent Mechanisms. *Mol. Cell Endocrinol.* 440, 57–68. doi:10.1016/j.mce.2016.11.011

Chi, H. (2012). Regulation and Function of mTOR Signalling in T Cell Fate Decisions. *Nat. Rev. Immunol.* 12 (5), 325–338. doi:10.1038/nri3198

Damstra-Oddy, J. L., Warren, E. C., Perry, C. J., Desfougères, Y., Fitzpatrick, J. M. K., Schaf, J., et al. (2021). Phytocannabinoid-dependent mTORC1 Regulation Is Dependent upon Inositol Polyphosphate Multikinase Activity. *Br. J. Pharmacol.* 178 (5), 1149–1163. doi:10.1111/bph.15351

Davies, L., Farrar, N. A., Satre, M., Dottin, R. P., and Gross, J. D. (1996). Vacuolar H+-ATPase and Weak Base Action in Dictyostelium. *Mol. Microbiol.* 22 (1), 119–126. doi:10.1111/j.1365-2958.1996.tb02661.x

Davies, L., Satre, M., Martin, J.-B., and Gross, J. D. (1993). The Target of Ammonia Action in Dictyostelium. *Cell* 75 (2), 321–327. doi:10.1016/0092-8674(93)80073-n

Early, A. E., and Williams, J. G. (1988). A Dictyostelium Prespore-specific Gene Is Transcriptionally Repressed by DIF *In Vitro*. *Development* 103 (3), 519–524. doi:10.1242/dev.103.3.519

Forbes, G., Chen, Z.-h., Kin, K., Lawal, H. M., Schilde, C., Yamada, Y., et al. (2019). Phylogeny-wide Conservation and Change in Developmental Expression, Cell-type Specificity and Functional Domains of the Transcriptional Regulators of Social Amoebas. *BMC Genomics* 20 (1), 890. doi:10.1186/s12864-019-6239-3

Gomer, R., and Firtel, R. (1987). Cell-autonomous Determination of Cell-type Choice in Dictyostelium Development by Cell-Cycle Phase. *Science* 237 (4816), 758–762. doi:10.1126/science.3039657

Grimson, M. J., Coates, J. C., Reynolds, J. P., Shipman, M., Blanton, R. L., and Harwood, A. J. (2000). Adherens Junctions and β-catenin-mediated Cell Signalling in a Non-metazoan Organism. *Nature* 408 (6813), 727–731. doi:10.1038/35047099

Gross, J. D., Town, C. D., Brookman, J. J., Jermyn, K. A., Peacey, M. J., and Kay, R. R. (1981). Cell Patterning in Dictyostelium. *Phil. Trans. R. Soc. Lond. B* 295 (1078), 497–508. doi:10.1098/rstb.1981.0156

Gross, J. D., Bradbury, J., Kay, R. R., and Peacey, M. J. (1983). Intracellular pH and the Control of Cell Differentiation in *Dictyostelium discoideum*. *Nature* 303 (5914), 244–245. doi:10.1038/303244a0

Gruenheit, N., Parkinson, K., Brimson, C. A., Kuwana, S., Johnson, E. J., Nagayama, K., et al. (2018). Cell Cycle Heterogeneity Can Generate Robust Cell Type Proportioning. *Dev. Cel* 47 (4), 494–508. doi:10.1016/j.devcel.2018.09.023

Hardie, D. G. (2007). AMP-activated/SNF1 Protein Kinases: Conserved Guardians of Cellular Energy. *Nat. Rev. Mol. Cel Biol* 8 (10), 774–785. doi:10.1038/nrm2249

Harwood, A. J., Plyte, S. E., Woodgett, J., Strutt, H., and Kay, R. R. (1995). Glycogen Synthase Kinase 3 Regulates Cell Fate in Dictyostelium. *Cell* 80 (1), 139–148. doi:10.1016/0092-8674(95)90458-1

Hindupur, S. K., González, A., and Hall, M. N. (2015). The Opposing Actions of Target of Rapamycin and AMP-Activated Protein Kinase in Cell Growth Control. *Cold Spring Harb Perspect. Biol.* 7 (8), a019141. doi:10.1101/cshperspect.a019141

Ho, C. Y., Alghamdi, T. A., and Botelho, R. J. (2012). Phosphatidylinositol-3,5-bisphosphate: No Longer the Poor PIP2. *Traffic* 13 (1), 1–8. doi:10.1111/j.1600-0854.2011.01246.x

Huang, H.-J., Takagawa, D., Weeks, G., and Pears, C. (1997). Cells at the Center ofDictyosteliumAggregates Become Spores. *Dev. Biol.* 192 (2), 564–571. doi:10.1006/dbio.1997.8769

Huang, P.-T., Einav, S., and Asquith, C. R. M. (2021). PIKfyve: a Lipid Kinase Target for COVID-19, Cancer and Neurodegenerative Disorders. *Nat. Rev. Drug Discov.* 20 (10), 730. doi:10.1038/d41573-021-00158-9

Hurley, R. L., Anderson, K. A., Franzone, J. M., Kemp, B. E., Means, A. R., and Witters, L. A. (2005). The Ca2+/calmodulin-dependent Protein Kinase Kinases Are AMP-Activated Protein Kinase Kinases. *J. Biol. Chem.* 280 (32), 29060–29066. doi:10.1074/jbc.M503824200

Ikonomov, O. C., Sbrissa, D., and Shisheva, A. (2019). Small Molecule PIKfyve Inhibitors as Cancer Therapeutics: Translational Promises and Limitations. *Toxicol. Appl. Pharmacol.* 383, 114771. doi:10.1016/j.taap.2019.114771

Inouye, K. (1988). Differences in Cytoplasmic pH and the Sensitivity to Acid Load between Prespore Cells and Prestalk Cells of Dictyostelium. *J. Cel Sci.* 91, 109–115. doi:10.1242/jcs.91.1.109

Iranfar, N., Fuller, D., Sasik, R., Hwa, T., Laub, M., and Loomis, W. F. (2001). Expression Patterns of Cell-type-specific Genes inDictyostelium. *MBoC* 12 (9), 2590–2600. doi:10.1091/mbc.12.9.2590

Jaiswal, P., and Kimmel, A. R. (2019). mTORC1/AMPK Responses Define a Core Gene Set for Developmental Cell Fate Switching. *BMC Biol.* 17 (1), 58. doi:10.1186/s12915-019-0673-1

Jaiswal, P., Majithia, A. R., Rosel, D., Liao, X.-H., Khurana, T., and Kimmel, A. R. (2019). Integrated Actions of mTOR Complexes 1 and 2 for Growth and Development of Dictyostelium. *Int. J. Dev. Biol.* 63 (8-9-10), 521–527. doi:10.1387/ijdb.190245ak

Jang, W., and Gomer, R. H. (2011). Initial Cell Type Choice in Dictyostelium. *Eukaryot. Cel* 10 (2), 150–155. doi:10.1128/EC.00219-10

Jermyn, K. A., Berks, M., Kay, R. R., and Williams, J. G. (1987). Two Distinct Classes of Prestalk-Enriched mRNA Sequences in *Dictyostelium discoideum*. *Development* 100 (4), 745–755. doi:10.1242/dev.100.4.745

Jin, S. Y., Lee, H. S., Kim, E. K., Ha, J. M., Kim, Y. W., and Bae, S. (2014). Reactive Oxygen Species and PI3K/Akt Signaling in Cancer. *Free Radic. Biol. Med.* 75 (Suppl. 1), S34–S35. doi:10.1016/j.freeradbiomed.2014.10.773

Jung, C. H., Ro, S.-H., Cao, J., Otto, N. M., and Kim, D.-H. (2010). mTOR Regulation of Autophagy. *FEBS Lett.* 584 (7), 1287–1295. doi:10.1016/j.febslet.2010.01.017

Kay, R. R., Gadian, D. G., and Williams, S. R. (1986). Intracellular pH in Dictyostelium: a 31P Nuclear Magnetic Resonance Study of its Regulation and Possible Role in Controlling Cell Differentiation. *J. Cel Sci* 83, 165–179. doi:10.1242/jcs.83.1.165

Kay, R. R., and Jermyn, K. A. (1983). A Possible Morphogen Controlling Differentiation in Dictyostelium. *Nature* 303 (5914), 242–244. doi:10.1038/303242a0

Kessin, R. H. (2001). *Dictyostelium: Evolution, Cell Biology, and the Development of Multicellularity*. Cambridge: Cambridge University Press.

Kimmelman, A. C., and White, E. (2017). Autophagy and Tumor Metabolism. *Cel Metab.* 25 (5), 1037–1043. doi:10.1016/j.cmet.2017.04.004

King, J. S., Veltman, D. M., and Insall, R. H. (2011). The Induction of Autophagy by Mechanical Stress. *Autophagy* 7 (12), 1490–1499. doi:10.4161/auto.7.12.17924

Kirsten, J. H., Xiong, Y., Davis, C. T., and Singleton, C. K. (2008). Subcellular Localization of Ammonium Transporters in *Dictyostelium discoideum*. *BMC Cel Biol* 9, 71. doi:10.1186/1471-2121-9-71

Kubohara, Y., Arai, A., Gokan, N., and Hosaka, K. (2007). Pharmacological Evidence that Stalk Cell Differentiation Involves Increases in the Intracellular Ca2+ and H+ Concentrations in *Dictyostelium discoideum*. *Dev. Growth Differ.* 49 (3), 253–264. doi:10.1111/j.1440-169X.2007.00920.x

Kubohara, Y., Homma, Y., Shibata, H., Oshima, Y., and Kikuchi, H. (2021). Dictyostelium Differentiation-Inducing Factor-1 Promotes Glucose Uptake, at Least in Part, via an AMPK-dependent Pathway in Mouse 3T3-L1 Cells. *Ijms* 22 (5), 2293. doi:10.3390/ijms22052293

Kubohara, Y., Komachi, M., Homma, Y., Kikuchi, H., and Oshima, Y. (2015). Derivatives of Dictyostelium Differentiation-Inducing Factors Inhibit Lysophosphatidic Acid-Stimulated Migration of Murine Osteosarcoma LM8 Cells. *Biochem. Biophysical Res. Commun.* 463 (4), 800–805. doi:10.1016/j.bbrc.2015.06.016

Kubohara, Y., and Okamoto, K. (1994). Cytoplasmic Ca^{2+} and H^{+} Concentrations Determine Cell Fate in *Dictyostelium discoideum*. *FASEB j.* 8 (11), 869–874. doi:10.1096/fasebj.8.11.8070636

Lam, D., Kosta, A., Luciani, M.-F., and Golstein, P. (2008). The Inositol 1,4,5-trisphosphate Receptor Is Required to Signal Autophagic Cell Death. *MBoC* 19 (2), 691–700. doi:10.1091/mbc.e07-08-0823

Laplante, M., and Sabatini, D. M. (2012). mTOR Signaling in Growth Control and Disease. *Cell* 149 (2), 274–293. doi:10.1016/j.cell.2012.03.017

Lee, J.-H., Yu, W. H., Kumar, A., Lee, S., Mohan, P. S., Peterhoff, C. M., et al. (2010). Lysosomal Proteolysis and Autophagy Require Presenilin 1 and Are Disrupted by Alzheimer-Related PS1 Mutations. *Cell* 141 (7), 1146–1158. doi:10.1016/j.cell.2010.05.008

Marchetti, A., Lelong, E., and Cosson, P. (2009). A Measure of Endosomal pH by Flow Cytometry in Dictyostelium. *BMC Res. Notes* 2, 7. doi:10.1186/1756-0500-2-7

Maurya, R., Kumar, R., and Saran, S. (2017). Dictyostelium AMPKα Regulates Aggregate Size and Cell-type Patterning. *Open Biol.* 7 (7), 170055. doi:10.1098/rsob.170055

McDonald, S. A., and Durston, A. J. (1984). The Cell Cycle and Sorting Behaviour in *Dictyostelium discoideum*. *J. Cel Sci* 66, 195–204. doi:10.1242/jcs.66.1.195

Meinhardt, H. (1983). A Model for the Prestalk/prespore Patterning in the Slug of the Slime Mold *Dictyostelium discoideum*. *Differentiation* 24 (3), 191–202. doi:10.1111/j.1432-0436.1983.tb01319.x

Muramoto, T., and Chubb, J. R. (2008). Live Imaging of the Dictyostelium Cell Cycle Reveals Widespread S Phase during Development, a G2 Bias in Spore Differentiation and a Premitotic Checkpoint. *Development* 135 (9), 1647–1657. doi:10.1242/dev.020115

Murata, C., Ogura, T., Narita, S., Kondo, A. P., Iwasaki, N., Saito, T., et al. (2016). Synthesis and SAR of 4-Methyl-5-Pentylbenzene-1,3-Diol (MPBD), Produced by *Dictyostelium discoideum*. *Bioorg. Med. Chem. Lett.* 26 (5), 1428–1433. doi:10.1016/j.bmcl.2016.01.067

Nathan Feit, I., Bonner, J. T., and Suthers, H. B. (1990). Regulation of the Anterior-like Cell State by Ammonia in *Dictyostelium discoideum*. *Dev. Genet.* 11 (5-6), 442–446. doi:10.1002/dvg.1020110519

Nixon, R. A. (2013). The Role of Autophagy in Neurodegenerative Disease. *Nat. Med.* 19 (8), 983–997. doi:10.1038/nm.3232

O'Neill, L. A. J., and Hardie, D. G. (2013). Metabolism of Inflammation Limited by AMPK and Pseudo-starvation. *Nature* 493 (7432), 346–355. doi:10.1038/nature11862

Pears, C. J., and Gross, J. D. (2021). Microbe Profile: *Dictyostelium discoideum*: Model System for Development, Chemotaxis and Biomedical Research. *Microbiology (Reading)* 167 (3). doi:10.1099/mic.0.001040

Pérez-Hernández, M., Arias, A., Martínez-García, D., Pérez-Tomás, R., Quesada, R., and Soto-Cerrato, V. (2019). Targeting Autophagy for Cancer Treatment and Tumor Chemosensitization. *Cancers* 11 (10), 1599. doi:10.3390/cancers11101599

Rattan, R., Giri, S., Singh, A. K., and Singh, I. (2005). 5-Aminoimidazole-4-carboxamide-1-β-D-ribofuranoside Inhibits Cancer Cell Proliferation *In Vitro* and *In Vivo* via AMP-Activated Protein Kinase. *J. Biol. Chem.* 280 (47), 39582–39593. doi:10.1074/jbc.M507443200

Rauch, A., Haakonsson, A. K., Madsen, J. G. S., Larsen, M., Forss, I., Madsen, M. R., et al. (2019). Osteogenesis Depends on Commissioning of a Network of Stem Cell Transcription Factors that Act as Repressors of Adipogenesis. *Nat. Genet.* 51 (4), 716–727. doi:10.1038/s41588-019-0359-1

Rosel, D., Khurana, T., Majithia, A., Huang, X., Bhandari, R., and Kimmel, A. R. (2012). TOR Complex 2 (TORC2) in Dictyostelium Suppresses Phagocytic Nutrient Capture Independently of TORC1-Mediated Nutrient Sensing. *J. Cel Sci* 125 (Pt 1), 37–48. doi:10.1242/jcs.077040

Saito, T., Kato, A., and Kay, R. R. (2008). DIF-1 Induces the Basal Disc of the Dictyostelium Fruiting Body. *Dev. Biol.* 317 (2), 444–453. doi:10.1016/j.ydbio.2008.02.036

Savini, M., Zhao, Q., and Wang, M. C. (2019). Lysosomes: Signaling Hubs for Metabolic Sensing and Longevity. *Trends Cel Biol.* 29 (11), 876–887. doi:10.1016/j.tcb.2019.08.008

Sawai, S., Hirano, T., Maeda, Y., and Sawada, Y. (2002). Rapid Patterning and Zonal Differentiation in a Two-Dimensional Dictyostelium Cell Mass: the Role of pH and Ammonia. *J. Exp. Biol.* 205 (Pt 17), 2583–2590. doi:10.1242/jeb.205.17.2583

Saxton, R. A., and Sabatini, D. M. (2017). mTOR Signaling in Growth, Metabolism, and Disease. *Cell* 168 (6), 960–976. doi:10.1016/j.cell.2017.02.004

Schaap, P., Nebl, T., and Fisher, P. R. (1996). A Slow Sustained Increase in Cytosolic Ca2+ Levels Mediates Stalk Gene Induction by Differentiation Inducing Factor in Dictyostelium. *EMBO J.* 15 (19), 5177–5183. doi:10.1002/j.1460-2075.1996.tb00902.x

Schilde, C., Araki, T., Williams, H., Harwood, A., and Williams, J. G. (2004). GSK3 Is a Multifunctional Regulator of Dictyostelium Development. *Development* 131 (18), 4555–4565. doi:10.1242/dev.01330

Seto-Tetsuo, F., Arioka, M., Miura, K., Inoue, T., Igawa, K., Tomooka, K., et al. (2021). DIF-1 Inhibits Growth and Metastasis of Triple-Negative Breast Cancer through AMPK-Mediated Inhibition of the mTORC1-S6k Signaling Pathway. *Oncogene* 40 (37), 5579–5589. doi:10.1038/s41388-021-01958-4

Sharma, D., Otto, G., Warren, E. C., Beesley, P., King, J. S., and Williams, R. S. B. (2019). Gamma Secretase Orthologs Are Required for Lysosomal Activity and Autophagic Degradation in *Dictyostelium discoideum*, Independent of PSEN (Presenilin) Proteolytic Function. *Autophagy* 15 (8), 1407–1418. doi:10.1080/15548627.2019.1586245

Singleton, C. K., Zinda, M. J., Mykytka, B., and Yang, P. (1998). The Histidine Kinase DhkC Regulates the Choice between Migrating Slugs and Terminal Differentiation in *Dictyostelium discoideum*. *Dev. Biol.* 203 (2), 345–357. doi:10.1006/dbio.1998.9049

Sugden, C., Urbaniak, M. D., Araki, T., and Williams, J. G. (2015). The Dictyostelium Prestalk Inducer Differentiation-Inducing Factor-1 (DIF-1) Triggers Unexpectedly Complex Global Phosphorylation Changes. *MBoC* 26 (4), 805–820. doi:10.1091/mbc.E14-08-1319

Sukumaran, A., Choi, K., and Dasgupta, B. (2020). Insight on Transcriptional Regulation of the Energy Sensing AMPK and Biosynthetic mTOR Pathway Genes. *Front. Cel Dev. Biol.* 8, 671. doi:10.3389/fcell.2020.00671

Sun, S.-Y. (2021). mTOR-Targeted Cancer Therapy: Great Target but Disappointing Clinical Outcomes, Why. *Front. Med.* 15 (2), 221–231. doi:10.1007/s11684-020-0812-7

Takahashi-Yanaga, F., Yoshihara, T., Jingushi, K., Igawa, K., Tomooka, K., Watanabe, Y., et al. (2014). DIF-1 Inhibits Tumor Growth *In Vivo* Reducing Phosphorylation of GSK-3β and Expressions of Cyclin D1 and TCF7L2 in Cancer Model Mice. *Biochem. Pharmacol.* 89 (3), 340–348. doi:10.1016/j.bcp.2014.03.006

Thompson, C. R. L., and Kay, R. R. (2000a). Cell-fate Choice in Dictyostelium: Intrinsic Biases Modulate Sensitivity to DIF Signaling. *Dev. Biol.* 227 (1), 56–64. doi:10.1006/dbio.2000.9877

Thompson, C. R. L., and Kay, R. R. (2000b). The Role of DIF-1 Signaling in Dictyostelium Development. *Mol. Cel* 6 (6), 1509–1514. doi:10.1016/s1097-2765(00)00147-7

Thompson, C. R. L., Reichelt, S., and Kay, R. R. (2004). A Demonstration of Pattern Formation without Positional Information in Dictyostelium. *Dev. Growth Differ.* 46 (4), 363–369. doi:10.1111/j.1440-169x.2004.00753.x

Town, C. D., Dominov, J. A., Karpinski, B. A., and Jentoft, J. E. (1987). Relationships between Extracellular pH, Intracellular pH, and Gene Expression in *Dictyostelium discoideum*. *Dev. Biol.* 122 (2), 354–362. doi:10.1016/0012-1606(87)90300-9

Town, C. D., Gross, J. D., and Kay, R. R. (1976). Cell Differentiation without Morphogenesis in *Dictyostelium discoideum*. *Nature* 262 (5570), 717–719. doi:10.1038/262717a0

Traynor, D., and Kay, R. R. (2017). A Polycycstin-type Transient Receptor Potential (Trp) Channel that Is Activated by ATP. *Biol. Open* 6 (2), 200–209. doi:10.1242/bio.020685

Tsujioka, M., Yokoyama, M., Nishio, K., Kuwayama, H., Morio, T., Katoh, M., et al. (2001). Spatial Expression Patterns of Genes Involved in Cyclic AMP Responses in *Dictyostelium discoideum* Development. *Dev. Growth Differ.* 43 (3), 275–283. doi:10.1046/j.1440-169x.2001.00572.x

Warren, E. C., Dooves, S., Lugarà, E., Damstra-Oddy, J., Schaf, J., Heine, V. M., et al. (2020). Decanoic Acid Inhibits mTORC1 Activity Independent of Glucose and Insulin Signaling. *Proc. Natl. Acad. Sci. USA* 117 (38), 23617–23625. doi:10.1073/pnas.2008980117

Warren, E. C., Walker, M. C., and Williams, R. S. B. (2018). All You Need Is Fats-For Seizure Control: Using Amoeba to Advance Epilepsy Research. *Front. Cel. Neurosci.* 12, 199. doi:10.3389/fncel.2018.00199

Weijer, C. J., Duschl, G., and David, C. N. (1984). Dependence of Cell-type Proportioning and Sorting on Cell Cycle Phase in *Dictyostelium discoideum*. *J. Cel Sci* 70, 133–145. doi:10.1242/jcs.70.1.133

Yamada, Y., Forbes, G., Du, Q., Kawata, T., and Schaap, P. (2021). Loss of PIKfyve Causes Transdifferentiation of Dictyostelium Spores into Basal Disc Cells. *Front. Cel Dev. Biol.* 9, 692473. doi:10.3389/fcell.2021.692473

Yamada, Y., and Schaap, P. (2019). Cyclic AMP Induction of Dictyostelium Prespore Gene Expression Requires Autophagy. *Dev. Biol.* 452 (2), 114–126. doi:10.1016/j.ydbio.2019.04.017

Yamamoto, A., and Takeuchi, I. (1983). Vital Staining of Autophagic Vacuoles in Differentiating Cells of *Dictyostelium discoideum*. *DIfferentiation* 24, 83–87. doi:10.1111/j.1432-0436.1983.tb01307.x

Zhang, C.-S., Jiang, B., Li, M., Zhu, M., Peng, Y., Zhang, Y.-L., et al. (2014). The Lysosomal V-ATPase-Ragulator Complex Is a Common Activator for AMPK and mTORC1, Acting as a Switch between Catabolism and Anabolism. *Cel Metab.* 20 (3), 526–540. doi:10.1016/j.cmet.2014.06.014

Zimmerman, W., and Weijer, C. J. (1993). Analysis of Cell Cycle Progression during the Development of Dictyostelium and its Relationship to Differentiation. *Dev. Biol.* 160 (1), 178–185. doi:10.1006/dbio.1993.1296

Conflict of Interest: The authors declare that the research was conducted in the absence of any commercial or financial relationships that could be construed as a potential conflict of interest.

Publisher's Note: All claims expressed in this article are solely those of the authors and do not necessarily represent those of their affiliated organizations, or those of the publisher, the editors and the reviewers. Any product that may be evaluated in this article, or claim that may be made by its manufacturer, is not guaranteed or endorsed by the publisher.

Copyright © 2021 Gross and Pears. This is an open-access article distributed under the terms of the Creative Commons Attribution License (CC BY). The use, distribution or reproduction in other forums is permitted, provided the original author(s) and the copyright owner(s) are credited and that the original publication in this journal is cited, in accordance with accepted academic practice. No use, distribution or reproduction is permitted which does not comply with these terms.

frontiers in Cell and Developmental Biology

ORIGINAL RESEARCH
published: 17 November 2021
doi: 10.3389/fcell.2021.742310

Formation of Cytoplasmic Actin-Cofilin Rods is Triggered by Metabolic Stress and Changes in Cellular pH

Hellen C. Ishikawa-Ankerhold[1,2], *Sophie Kurzbach*[3†], *Arzu S. Kinali*[2] *and Annette Müller-Taubenberger*[3*]

[1]Department of Internal Medicine I, University Hospital, LMU Munich, Munich, Germany, [2]Walter Brendel Centre of Experimental Medicine, University Hospital, LMU Munich, Munich, Germany, [3]Department of Cell Biology (Anatomy III), Biomedical Center (BMC), LMU Munich, Munich, Germany

OPEN ACCESS

Edited by:
Claudia Fiorillo, University of Florence, Italy

Reviewed by:
Jung A (Alexa) Woo, Case Western Reserve University, United States
Raymond A. Swanson, University of California, San Francisco, United States

***Correspondence:**
Annette Müller-Taubenberger
amueller@bmc.med.lmu.de

†Present address:
Sophie Kurzbach, Center for Protein Assemblies and Lehrstuhl für Biophysik (E27), Physics Department, Technical University Munich (TUM), Garching, Germany

Specialty section:
This article was submitted to Molecular and Cellular Pathology, a section of the journal Frontiers in Cell and Developmental Biology

Received: *16 July 2021*
Accepted: *27 October 2021*
Published: *17 November 2021*

Citation:
Ishikawa-Ankerhold HC, Kurzbach S, Kinali AS and Müller-Taubenberger A (2021) Formation of Cytoplasmic Actin-Cofilin Rods is Triggered by Metabolic Stress and Changes in Cellular pH. Front. Cell Dev. Biol. 9:742310. doi: 10.3389/fcell.2021.742310

Actin dynamics plays a crucial role in regulating essential cell functions and thereby is largely responsible to a considerable extent for cellular energy consumption. Certain pathological conditions in humans, like neurological disorders such as Alzheimer's disease or amyotrophic lateral sclerosis (ALS) as well as variants of nemaline myopathy are associated with cytoskeletal abnormalities, so-called actin-cofilin rods. Actin-cofilin rods are aggregates consisting mainly of actin and cofilin, which are formed as a result of cellular stress and thereby help to ensure the survival of cells under unfavorable conditions. We have used *Dictyostelium discoideum*, an established model system for cytoskeletal research to study formation and principles of cytoplasmic actin rod assembly in response to energy depletion. Experimentally, depletion of ATP was provoked by addition of either sodium azide, dinitrophenol, or 2-deoxy-glucose, and the formation of rod assembly was recorded by live-cell imaging. Furthermore, we show that hyperosmotic shock induces actin-cofilin rods, and that a drop in the intracellular pH accompanies this condition. Our data reveal that acidification of the cytoplasm can induce the formation of actin-cofilin rods to varying degrees and suggest that a local reduction in cellular pH may be a cause for the formation of cytoplasmic rods. We hypothesize that local phase separation mechanistically triggers the assembly of actin-cofilin rods and thereby influences the material properties of actin structures.

Keywords: actin, cofilin, cytoskeleton, cytoplasmic rod, *Dictyostelium discoideum*, intracellular pH, metabolic stress, neurodegenerative disease

INTRODUCTION

Actin is among the most abundant and most highly conserved proteins in eukaryotic cells, and as such essential for many processes including cell growth, differentiation, cell division, motility, intracellular movement, and mechanic stability. To fulfil these different functions, actin assemblies form a variety of dynamically regulated membrane-associated or intracellular structures (Chhabra and Higgs, 2007), and after long debates on the existence of actin in the nucleus, the specific roles have been elucidated in recent years (Kelpsch and Tootle, 2018; Caridi et al., 2019; Hyrskyluoto and Vartiainen, 2020).

Actin serves as both a structural and a force-generating protein. Inside cells, there is a dynamic equilibrium of monomeric actin (G-actin) sequestered by monomer-binding proteins like profilin, and filamentous actin (F-actin). Monomeric actin contains one nucleotide and can exist either in the ATP, ADP-Pi or ADP form. The assembly and disassembly of actin filaments is principally dependent upon the concentrations of actin monomers, and the critical concentrations for actin assembly vary as actin filaments themselves show a polarity and have different critical concentrations for polymerization on either end. The assembly of monomeric actin into filaments and the disassembly of filamentous actin involves a whole arsenal of actin-binding proteins that regulate actin functions including nucleation, sequestering, and crosslinking, and the highly energy-dependent dynamic turnover has been described as "actin-treadmilling" (Pollard and Borisy, 2003).

Among the proteins crucial for the dynamic turnover of actin filaments *in vivo* are those of the actin-depolymerizing factor (ADF)/cofilin family. Members of the cofilin family are highly conserved and functionally related proteins (Bernstein and Bamburg, 2010; Kanellos and Frame, 2016). Cofilin severs actin filaments at low cofilin/actin ratios and stabilizes filaments at high ratios. The activity of cofilin is enhanced by coronin 1A (Cai et al., 2007), which helps in recruiting cofilin, and actin-interacting protein 1 (Aip1), which enhances the severing function of cofilin (Pollard and Borisy, 2003; Kanellos and Frame, 2016). In contrast to mammalian cells, in *Dictyostelium*, cofilin activity is not regulated by phosphorylation (Aizawa et al., 1995). LIMK1/2 (or TESK1/2) and slingshot (SSH1L) phosphatase are not present. The absence of this regulation in *Dictyostelium* simplifies the approach to investigate the general principles of cofilin functions on actin organization under different conditions.

Several disease pathologies are characterized by the polymerization of actin into stable filament bundles called actin-cofilin rods. Actin-cofilin rods consist of equimolar ratios of actin and cofilin (Nishida et al., 1987; Minamide et al., 2010). Rods can be formed either inside the nucleus or the cytoplasm. Cytoplasmic rods are associated with several neurodegenerative diseases like Alzheimer's and Parkinson's disease, variants of amyotrophic lateral sclerosis (ALS) (Bamburg and Wiggan, 2002; Bamburg and Bernstein, 2010; Schonhofen et al., 2014; Bamburg and Bernstein, 2016; Wang et al., 2020), and spinal muscular atrophy (SMA) (Walter et al., 2021). Intranuclear actin-cofilin rods were identified as hallmarks in muscle cells of patients with intranuclear rod myopathy (IRM), a specific form of nemaline myopathy (Goebel and Warlo, 1997; Sparrow et al., 2003; Ilkovski et al., 2004; Domazetovska et al., 2007a; Domazetovska et al., 2007), and Huntington's disease (HD) (Munsie et al., 2011). However, our understanding of the specific mechanisms that cause actin-cofilin rod formation in either the cytoplasm or the nucleus, and how rod formation is modulated by physiological parameters is still incomplete.

The *Dictyostelium discoideum* system has many technical advantages in comparison to mammalian models and pioneered a variety of scientific approaches to study basic cellular functions relevant for disease-related states (Müller-Taubenberger et al., 2013). In fact, before their description in neuronal cells, nuclear actin-cofilin rods were discovered in *Dictyostelium* amoebae and in HeLa cells after treatment with high concentrations of dimethyl sulfoxide (Fukui, 1978; Fukui and Katsumaru, 1979, 1980; Sanger et al., 1980). Previous work from our lab focused on the analysis and characterization of nuclear rods in *Dictyostelium* (Ishikawa-Ankerhold et al., 2017). Thereby, we examined the stages of assembly, the composition, stability, and dismantling of nuclear rods.

The present work investigates the formation of cytoplasmic actin-cofilin rods as a result of experimental treatments that simulate transient stress states that can still be reversed to normal physiological states. Several other studies already reported that actin-cofilin rods are formed in result of either ATP depletion or other stress conditions (Yahara et al., 1996; Minamide et al., 2000; Ashworth et al., 2003; Bernstein and Bamburg, 2003; Huang et al., 2008; Bernstein et al., 2012; Won et al., 2018). Here, we took advantage of *Dictyostelium*, an established model for cytoskeletal research, and have analyzed the composition and dynamics of cytoplasmic actin-cofilin rods and followed their formation after application of different stressors by live-cell imaging. Our data provide evidence that cytoplasmic actin-cofilin rods are formed not only in response to energy depletion, but also show that acidification of the cytoplasm is an important factor that can trigger the formation of actin-cofilin assemblies.

MATERIALS AND METHODS

Strains and Cell Culture

All *Dictyostelium discoideum* strains used in this study derived from the axenic strain AX2-214 (considered as wild type), and were cultivated in Petri dishes in HL5 medium (Formedium) at 22C. *Dictyostelium* cells expressing GFP-cofilin or mCherry-cofilin, or the mutant strain lacking Aip1 (Konzok et al., 1999) and expressing GFP-cofilin were described earlier (Ishikawa-Ankerhold et al., 2017).

Energy Depletion, Hyperosmotic Shock, pH Adjustment and Drug Treatment

For all experiments, *Dictyostelium* cells were cultivated in HL5 medium at 22°C. For the specific treatments, the medium was replaced by HL5 medium supplemented with the respective agent.

Sodium azide (NaN_3): 10 mM in HL5 medium. To test the stability of rods when the stress stimulus is removed, cells treated with 10 mM sodium azide for 60 min were washed and incubated in HL5 medium for recovery.

2, 4-Dinitrophenol (DNP): 200 µM in HL5 medium.

Hyperosmotic shock (SOR): 200 and 400 mM D-sorbitol (Sigma-Aldrich) in HL5 medium.

Sorbic acid (SA) and propionic acid (PA): the respective pH values of the HL5 medium were adjusted with stock solutions of 14 mM sorbic acid or 134 mM propionic acid.

2-deoxy-glucose (2-DG): HL5 medium without glucose (Formedium HLB0102) supplemented with 10 g/L 2-deoxy-D-glucose (Roth)

Cytochalasin D (CytD) and Latrunculin A (LatA) (both Sigma-Aldrich): final concentrations of 1, 2, 4, 6, 8, 10, and 20 μM, or 1, 5, and 10 μM, respectively, in HL5 medium were tested. *Dictyostelium* cells expressing GFP-cofilin were plated on 12-mm cover glasses placed in 24-well plates and treated with cytochalasin D or latrunculin A for 60 min before induction of rod assembly with 10 mM sodium azide for 60 min. Then, cells were fixed with methanol at −20°C for 15 min and stained for actin.

The experiments were repeated at least 3 times for each treatment. For quantification, cells with cytoplasmic rods were counted from at least 10 different fields of view (image size of 512 × 512 μm).

For quantification of cells with cytoplasmic rods, Zen blue software was used (Carl Zeiss Microscopy).

Vector for Ratiometric pH Measurements

For cytosolic pH measurements, the ratiometric fluorescent protein pHluorin2 (Mahon 2011) was cloned via *Hin*dIII and *Cla*I into a pDEX-based *Dictyostelium* vector enabling expression under control of an actin-15 promoter and conferring resistance to blasticidin (Müller-Taubenberger, 2006). The pEntry-mCherry-pHluorin2 vector (GFP-RFPpHluorin; plasmid Y872) was a kind gift of Prof. Simon Alberti (Dresden), and was used as template for amplification in combination with the primers 5′-gtg aag ctt aaa atg cca act ttg tac aaa aaa gca gg-3′ and 5′-gtg atc gat tta ttt gta tag ttc atc cat gcc atg tg-3′.

AX2 cells were transfected by electroporation using a gene pulser (Bio-Rad Laboratories) at 0.8–0.9 kV and 3 μF in 4-mm cuvettes. Transformants were selected and cultivated in the presence of 10 μg/ml blasticidin-S (ICN Biomedicals Inc.).

Immunocytochemistry and Antibodies

Cells were plated on round 12-mm glass cover glasses coated with poly-lysine (Merck) and placed in 24-well plates, and after 1 h were subjected to the specified treatment. Thereafter, cells were fixed in methanol at −20°C for 15 min and labeled as described (Ishikawa-Ankerhold et al., 2017). After fixation, cells were washed three times with PBS, and then incubated in blocking buffer (PBS plus 2% bovine serum albumin) for 1 h at room temperature (RT). After blocking, the cells were washed three times with PBS and immunolabeled with the primary antibodies. Secondary antibodies were added for 1 h at RT. Then, samples were washed and mounted using Gelvatol or Dako. Primary antibodies used were specific for: actin (mAb Act1) (Simpson et al., 1984), Aip1 (mAb 246-153-2 and 246-404-2) (Konzok et al., 1999), coronin (mAb 176-3-6) (de Hostos et al., 1991), cofilin (pAb 496) (Ishikawa-Ankerhold et al., 2017), and isotype IgG (Molecular Probes). Secondary antibodies used in the study were Cy3, Alexa Fluor-488, -563, or -594 goat anti-mouse or anti-rabbit IgG (Molecular Probes). For some experiments, Atto 550-phalloidin (Molecular Probes, Sigma-Aldrich), and DAPI (1:1,000) were added together with the secondary antibodies.

Confocal Microscopy

A confocal LSM 880 microscope (Carl Zeiss Microscopy) equipped with an Airyscan module and Plan-Apo 20x/NA 0.8 and Plan-Apo 63x/NA 1.46 oil immersion objectives, or a confocal LSM 510 microscope (Carl Zeiss Microscopy) equipped with a 63x Neofluar 1.4 oil immersion objective were used for image acquisition.

For live-cell microscopy, *Dictyostelium* cells expressing GFP-cofilin were plated into an open chamber or into 35-mm glass-bottom dishes (ibidi, μ-Dish 35 mm, high glass bottom), and incubated and recorded in medium or in medium adapted to the respective treatment conditions.

FRAP (fluorescence recovery after photobleaching) measurements were performed as described previously for nuclear rods (Ishikawa-Ankerhold et al., 2017). In short, living cells with cytoplasmic GFP-cofilin rods were photobleached using a LSM 510 Meta laser scanning confocal microscope with a 488-nm laser line at 100% intensity for 20 interactions as described in the detailed protocol (Müller-Taubenberger and Ishikawa-Ankerhold, 2013).

For the actin-cofilin rod disassembly experiments, the GFP-cofilin cells were plated on coverslips coated with poly-lysine, and treated with 10 mM sodium azide for 1 h at RT to induce the assembly of cytoplasmic actin-cofilin rods. After rod induction, the cells were washed to remove the chemical stimulus and incubated with medium for recovery. After 0, 5, 10, 15, 20 and 30 min under medium conditions, the cells were fixed with cold methanol (−20°C) for 15 min, washed and mounted for image acquisition.

Ratiometric Measurements

For ratiometric pH measurements, *Dictyostelium* cells expressing GFP-mRFP-pHluorin2 were seeded at 1×10^4 per ml into 35-mm glass-bottomed dishes (ibidi, μ-Dish 35 mm, high glass bottom), before imaging. The images were acquired using a LSM 880 confocal microscope with an Airyscan module (Carl Zeiss Microscopy). All imaging parameters for excitation, detection and all software settings were kept identical for the different sample acquisitions [laser intensity 488 nm (2%) and 561 nm (2%), image size (212 × 212 μm), Z-stack (30 μm), objective Plan-Apochromat ×20/0.8, pixel time (0.77 s), frame time (943.72 s)].

The images were analyzed with the ZEN software using the plugin (Histo), where a defined ROI of 4 μm^2 was applied to the selected cells to obtain the mean fluorescence intensity from each channel (green and red). The ratios of green/red channels were plotted as median with interquartile range to represent the pH fluorescence changes inside the cells. pHluorin2 allowed us to monitor decreases of the intracellular pH after acidification of the extracellular medium, which was identified by an increase in the ratio of pH-sensitive GFP versus pH-insensitive mCherry fluorescence. In measurements where we tested the application of HL5 medium adjusted to pH values below 5.5 (pH 5.25 and 5.0), we did not detect a linear increase of the GFP fluorescence anymore, and therefore show only the measurements for pH 5.75 and 5.5.

Statistics

Statistical analyses were calculated and graphically plotted with GraphPad Prism 9 (GraphPad Software, La Jolla, CA,

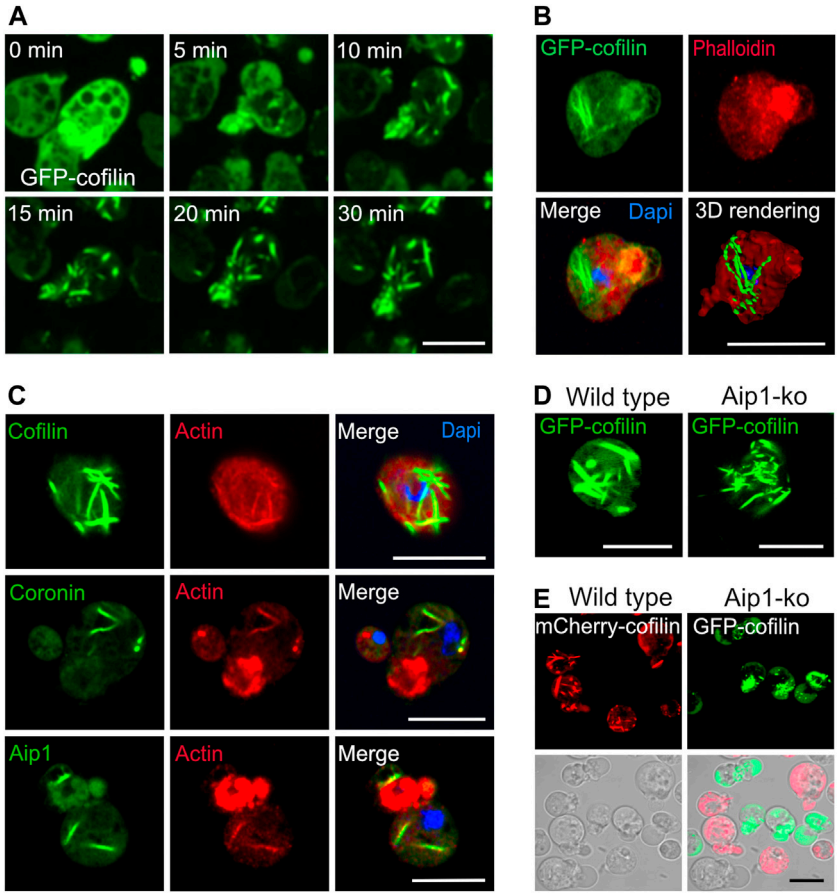

FIGURE 1 | Cytoplasmic actin-cofilin rods induced by sodium azide. **(A)** Time series of confocal images of rod formation induced by 10 mM sodium azide. *Dictyostelium* cells expressing GFP-cofilin (green) were exposed to medium containing 10 mM sodium azide, and recorded by live-cell microscopy for 30 min. The time series show that already after 5 min of treatment, GFP-cofilin starts to redistribute from cortical areas into bundles of increasing size inside the cytoplasm. See also **Supplementary Video S1** for the complete time series showing an overview of several cells. **(B)** Cytoplasmic actin-cofilin rods do not bind phalloidin. *Dictyostelium* cells expressing GFP-cofilin were fixed after 60 min of sodium azide treatment. GFP-cofilin (green) visualizes the cytoplasmic rods, phalloidin (red) is not co-localizing with GFP-cofilin rods. Dapi was used to label the nucleus. 3D rendering of the Z-stack projection was reconstructed using Imaris software. **(C)** Immunofluorescence labeling of cytoplasmic rods for the main constituents, actin and cofilin, as well as Aip1 and coronin after induction by sodium azide treatment in *Dictyostelium* wild-type cells. Cofilin, Aip1 and coronin were immunolabeled with the respective primary antibodies (green) and co-immunolabeled by an anti-actin antibody (red). Dapi was used to mark the nucleus (blue). Isotype controls are shown in **Supplementary Figure S1A**. **(D)** Rod formation after sodium azide treatment in *Dictyostelium* wild-type and Aip1-knockout (ko) cells expressing GFP-cofilin. **(E)** *Dictyostelium* cells expressing mCherry-cofilin and GFP-cofilin expressed in wild-type (red) or in Aip1-ko (green) cells were platted together and treated with sodium azide for 60 min. In the absence of Aip1, GFP-cofilin rods are not compacted into thicker bundles and remain more dispersed in comparison to wild-type cells. All scale bars, 10 µm.

United States). Data are means ± standard deviation of the mean (SD). Statistical analyses were conducted as described in the figure legends. Findings were considered statistically significant at $p < 0.05$.

RESULTS

Characterization of Cytoplasmic Actin-Cofilin Rods Induced by ATP-Depletion

Earlier work conducted in our laboratory and data from other studies suggested that cytoplasmic actin-cofilin rods are induced by treatments that cause depletion of ATP (Ashworth et al., 2003; Bernstein and Bamburg, 2003; Bernstein et al., 2006; Huang et al., 2008). The current investigations aimed to identify similarities and differences between nuclear and cytoplasmic rods in *Dictyostelium* cells, and to analyze the formation of cytoplasmic rods under different stress conditions by live-cell imaging.

In first experiments, ATP-depletion was provoked experimentally by addition of sodium azide (Ishikawa-Ankerhold et al., 2017), which acts by uncoupling the respiratory chain. Sodium azide induces cytoplasmic actin-cofilin rods both in wild-type as well as in GFP-cofilin expressing cells to a very similar extent (**Supplementary Figure S1**), and in order to follow formation of actin-cofilin

rods by live-cell imaging, most experiments were performed with GFP-cofilin expressing cells. Addition of sodium azide to the cells causes within minutes a rapid shape change and reorganization of the actin cytoskeleton (**Figure 1A** and **Supplementary Video S1**). First actin-cofilin rods become visible within 10 min of sodium azide treatment, and after 1 h, all cells are rounded up, and rods are detected in about 80% of cells. Image reconstruction using 3D rendering confirmed the cytoplasmic localization of actin-cofilin rods (**Figure 1B** and **Supplementary Video S2**).

Our earlier studies on nuclear rods showed that these contain in addition to actin and cofilin a distinct set of other proteins comprising actin-interacting protein 1 (Aip1), coronin (CorA), filactin (Fia), and the 34-kDa actin-bundling protein B (AbpB), and we found a finely tuned spatial-temporal pattern of protein recruitment during formation of rods inside the nuclei (Ishikawa-Ankerhold et al., 2017). For cytoplasmic rods, we confirmed actin and cofilin as the main constituents (**Figure 1C**, **Supplementary Figure S1C**, and **Supplementary Video S3**), and by immunofluorescence labeling we identified in addition Aip1 and coronin (**Figure 1C**), but did not detect, in contrast to nuclear rods, a sequential recruitment.

Like for nuclear rods, the compaction of cytoplasmic rods requires Aip1, a protein that induces the disassembly of actin filaments in conjunction with cofilin (Nadkarni and Brieher, 2014). Induction of cytoplasmic rods by sodium azide in a mutant lacking Aip1 (Konzok et al., 1999) revealed that rods are less compacted (**Figures 1D,E**), a result suggesting that the turnover of actin is a critical determinant for unimpeded rod formation.

This assumption is further supported by the application of drugs that interfere with actin polymerization. We have used cytochalasin D (CytD) that by binding to the high affinity growing ends prevents the elongation of actin nuclei and filaments (Casella et al., 1981), and latrunculin A (LatA), a drug that binds actin monomers and thus prevents polymerization of actin (Morton et al., 2000). The formation of cytoplasmic rods was increasingly inhibited with rising concentrations of CytD (**Supplementary Figure S2A**). Similarly, LatA inhibited the emergence of rods in a dose-dependent manner (**Supplementary Figure S2B**). These results indicate that under conditions of low ATP, the turnover of actin and the availability of actin monomers are crucial and limiting for the formation of cytoplasmic rods. In contrast to intranuclear rods, cytoplasmic actin-cofilin rods are not stainable with phalloidin (**Figure 1B** and **Supplementary Video S2**), which indicates that these assemblies are structurally different to cortical actin and intranuclear rods, a finding that has been described already earlier (Nishida et al., 1987; Ishikawa-Ankerhold et al., 2017).

In order to address the change in the dynamics of cytoplasmic actin-cofilin rods over time (i.e., newly assembled versus "aged" rods), we analyzed the exchange between the assembled and diffuse pool of GFP-cofilin by FRAP (fluorescence recovery after photobleaching). For this, GFP-labeled rods were bleached using high laser power (100%), and fluorescence recovery was monitored over time (**Figures 2A–C** and **Supplementary Video S4**). The mobile fraction represented by the fluorescence recovery of GFP-cofilin rods after photobleaching was about 20%, meaning that cytoplasmic rods are rather stable structures with low protein exchange.

The formation of actin-cofilin rods is rapidly reversible when the stress stimulus is removed (**Figures 2D,E**). After induction of cytoplasmic rods by addition of 10 mM sodium azide, the percentage of cells with cytoplasmic rods decreased rapidly when the sodium azide was washed out and replaced by standard HL5 medium. 5 min after replacement of sodium azide by medium, cytoplasmic rods started to disassemble, recognizable as shortening cofilin bundles. In the subsequent recovery phase, the bundles were shortened further and appeared as punctuated small cofilin aggregates, which continued to disintegrate.

Another drug that causes energy depletion is 2,4-dinitrophenol (DNP). DNP acts as protonophore and causes uncoupling of respiratory chain oxidative phosphorylation thereby inhibiting ATP production. Previous work by Gerisch and colleagues (Jungbluth et al., 1994) showed that addition of 50 μM DNP causes the reversible compartmentalization of the actin cytoskeleton. However, the available microscopical techniques were limited at that time, and did not allow a detailed resolution of cytoskeletal structures.

We have visualized the formation of cytoplasmic actin-cofilin rods in GFP-cofilin expressing cells after addition of DNP (**Figure 3A**). Live-cell microscopy revealed a rapid reorganization of the actin cytoskeleton after addition of DNP, and rods became visible within 10–15 min (**Supplementary Figure S3A**). After 2 h with DNP, 50% of cells showed cytoplasmic rods. Rod formation was fully reversible after an incubation time of 3 h by replacing the DNP medium with standard medium similar to the recovery after sodium azide treatment.

Formation of Cytoplasmic Actin-Cofilin Rods Under Hyperosmotic Conditions

Next, we tested hyperosmotic stress as another condition that we assumed to potentially induce cytoplasmic actin-cofilin rods. Hyperosmotic stress was induced by addition of 200 and 400 mM sorbitol (**Figure 3B**). It was reported earlier that in consequence of hyperosmotic conditions, *Dictyostelium* cells rearrange their cytoskeleton. This transition was postulated to constitute the major osmoprotective mechanism in *Dictyostelium* accompanied by a rapid acidification of the cytosol (Ott et al., 2000; Pintsch et al., 2001), but the cytoskeletal changes were not investigated in greater detail. In addition, it was found that vesicle mobility and membrane flow were downregulated under hyperosmotic conditions (Pintsch et al., 2001) a notion supported in studies of fluid- to solid-like state transitions more recently (Munder et al., 2016). We found that hyperosmotic conditions caused a rapid formation of cytoplasmic actin-cofilin rods (**Figure 3B**). After 2 h of incubation with 200 mM sorbitol, about one third of the cells showed cytoplasmic rods, with 400 mM sorbitol about 50% (**Figure 3C**).

Since hyperosmotic conditions were described to be accompanied by a rapid drop in intracellular pH, we next set

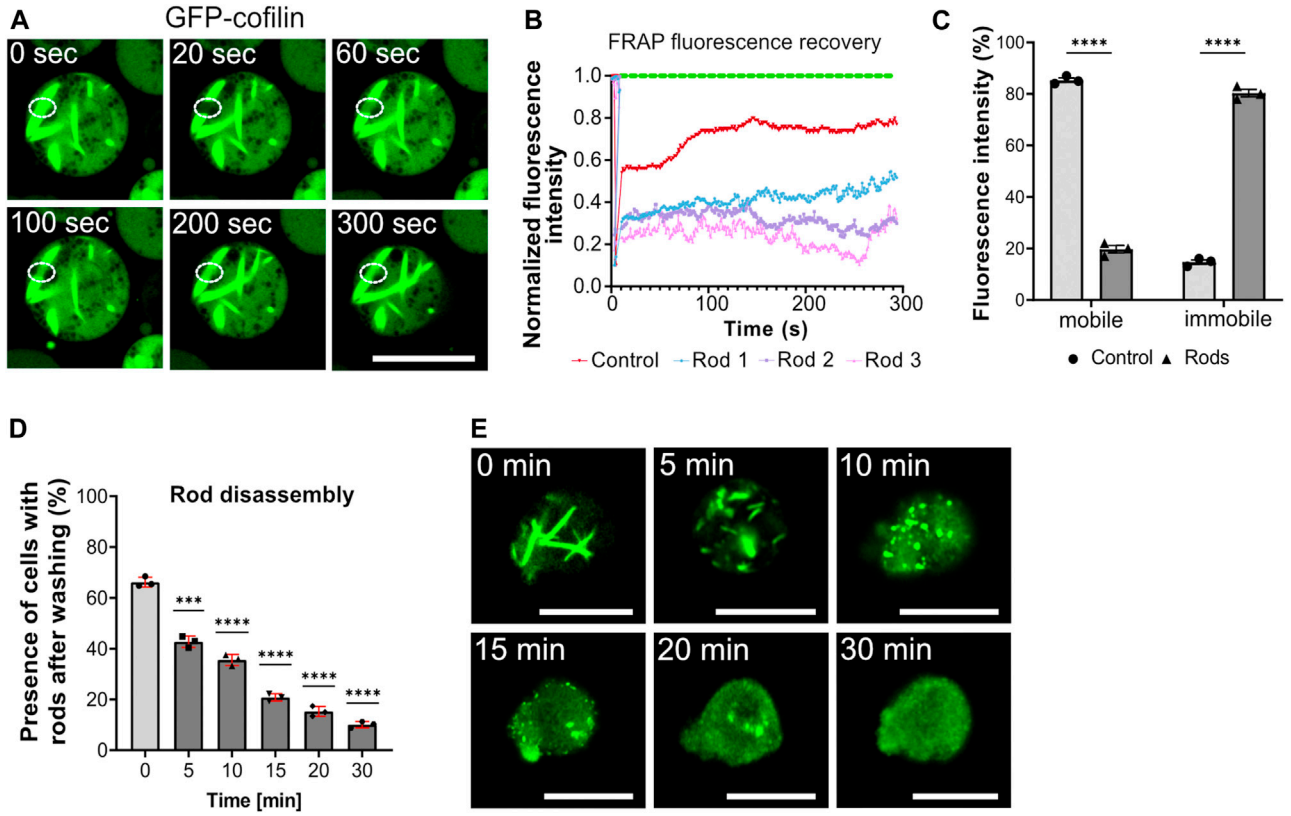

FIGURE 2 | Cytoplasmic actin-cofilin rod assembly/disassembly dynamics. **(A)** Fluorescence recovery after photobleaching (FRAP) of cytoplasmic rods. Formation of cytoplasmic rods was induced by addition of 10 mM sodium azide for 60 min. Rods were selectively photobleached by drawing a ROI to apply high laser power for 10 s to bleach the GFP. The GFP diffusion into the ROI area (fluorescence recovery) was recorded for 300 s. See also **Supplementary Video S4**. Scale bar, 10 µm. **(B)** Fluorescence recovery of photobleached rods. Bleaching curves of three different cytoplasmic rods of sodium azide-treated cells (blue, pink, purple lines) and the untreated control cell are plotted (red). **(C)** The histogram depicts the relative proportions of mobile and immobile fractions of cells without rods (control) and with cytoplasmic rods. The average of fluorescence recovery was about 20%, indicating that rods are rather stable structures with low exchange inside the rod bundles. **(D)** Actin-cofilin rods are rapidly disintegrating structures. After induction of cytoplasmic rods by addition of 10 mM sodium azide, the percentage of cells with cytoplasmic rods decreases rapidly when the sodium azide is washed out and replaced by standard medium. Three experiments were performed and for each experiment at least 50 cells were evaluated. Data are presented as mean ± SD (red bars). Statistical significance was calculated by unpaired Welch´s t-test. $p \leq 0.05$ was considered significant and (***$p < 0.0001$). **(E)** Visualization of actin-cofilin rod disassembly stages. Within 30 min after wash-out of the sodium azide, actin-cofilin rods are almost completely disintegrated. The disassembly takes place via shorter bundles and punctiform actin-cofilin aggregates. Scale bars, 10 µm.

out to determine changes in the intracellular pH of *Dictyostelium* cells. Previous studies using ^{31}P-NMR (nuclear magnetic resonance) showed that the intracellular pH of growth-phase *Dictyostelium* cells is around pH 7.3 (Kay et al., 1986). To directly monitor changes of the intracellular pH, we initially tested established intracellular pH indicators used for pH determination in other eukaryotic cell lines. Under our experimental conditions, BCECF (Invitrogen) and pHrodo (Life technologies) were not usable because they were rapidly sequestered into the endosomal compartment of *Dictyostelium* cells. We therefore generated a vector for expression of the ratiometric pH sensor pHluorin2 (Mahon, 2011), and examined pHluorin2 expressing *Dictyostelium* cells in live-cell measurements in order to monitor changes in the intracellular pH after reduction of the pH of the extracellular medium to 5.75 and 5.5. While DNP had no effect on the intracellular pH of *Dictyostelium* cells, application of 400 mM sorbitol caused a reduction of the cytoplasmic pH (**Figure 3D**) consistent with earlier results (Pintsch et al., 2001).

Reduction of Cellular pH Induces the Formation of Cytoplasmic Actin-Cofilin Rods

In order to investigate whether an acidification of the cytosol itself could trigger the formation of cytoplasmic actin-cofilin rods, we systematically examined the formation of rods by increasingly lowering the pH of the extracellular medium by the addition of weak acids. Under standard laboratory conditions, axenically growing *Dictyostelium* cells are cultivated in medium with a pH of 6.4. By addition of weak membrane-permeable acids, sorbic or propionic acid, we reduced the pH of the growth medium (5.75, 5.5, 5.25, 5.0) and followed the formation of cytoplasmic actin-cofilin rods either in fixed cells (**Figure 4A**) or by live-cell microscopy

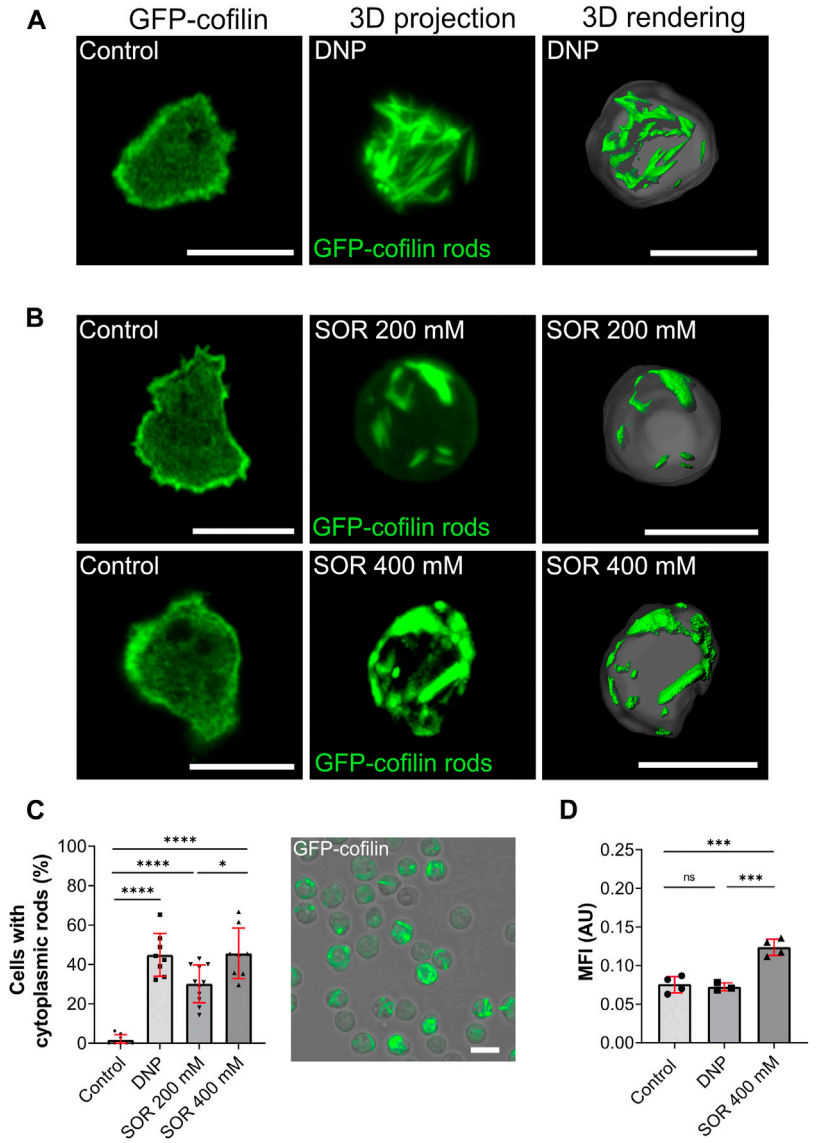

FIGURE 3 | Cytoplasmic actin-cofilin rods induced by DNP or hyperosmotic shock. **(A)** Non-treated cells (vehicle control), 3D projection and image rendering of rods formed by GFP-cofilin expressing cells treated with 200 µM DNP for 2 h. Scale bar, 10 µm. **(B)** Fluorescent images of non-treated GFP-cofilin expressing cells (vehicle control) and cytoplasmic actin-cofilin rods induced by treatment with 200 or 400 mM sorbitol (SOR). Scale bar, 10 µm. **(C)** Percentage of cells with rods after treatment with DNP or sorbitol for 2 h. Fluorescence image on the right shows a representative overview used for quantification (212 × 212 µm). For each experiment (n > 6), 10x overview images were quantified. Scale bar, 10 µm. **(D)** Ratiometric fluorescence measurements show a drop in the intracellular pH after treatment with 400 mM sorbitol for 2 h. Histograms depict median fluorescence intensity (MFI). More acidic values result in higher MFI. Error bars are median with interquartile range (red). Samples were considered significant when $p \leq 0.05$. Welch´s t-test was applied. n = 3-4 experiments; more than 20 cells were analyzed per experiment, and the average of fluorescence intensity was determined.

(**Figure 4B**). All pH conditions tested provoked the formation of cytoplasmic actin-cofilin rods. The rods varied from bar-shaped at low extracellular pH (pH 5.75 and 5.5) to more needle-like condensates at very low extracellular pH conditions (pH 5.25 and 5.0) (**Figures 4A,B** and **Supplementary Figure S3B**). With sorbic acid buffered medium, the percentage of cells with rods was highest with the slightest pH-shift (pH 5.75), and then decreased at lower values (**Figure 4C**). With propionic acid buffered medium, about 60% of cells formed cytoplasmic rods at pH 5.25, but rods were also detected at a considerable extent at the other pH values tested (**Figure 4D**). Ratiometric measurements of cells in sorbic and propionic acid containing medium confirmed the reduction of the intracellular pH compared to control cells (**Figure 4E**).

Starvation by Glucose Deprivation Induces Development and is Accompanied by a Transient Appearance of Cytoplasmic Rods

The life cycle of *Dictyostelium* cells is characterized by two main phases, the growth stage, in which the cells multiply by mitotic

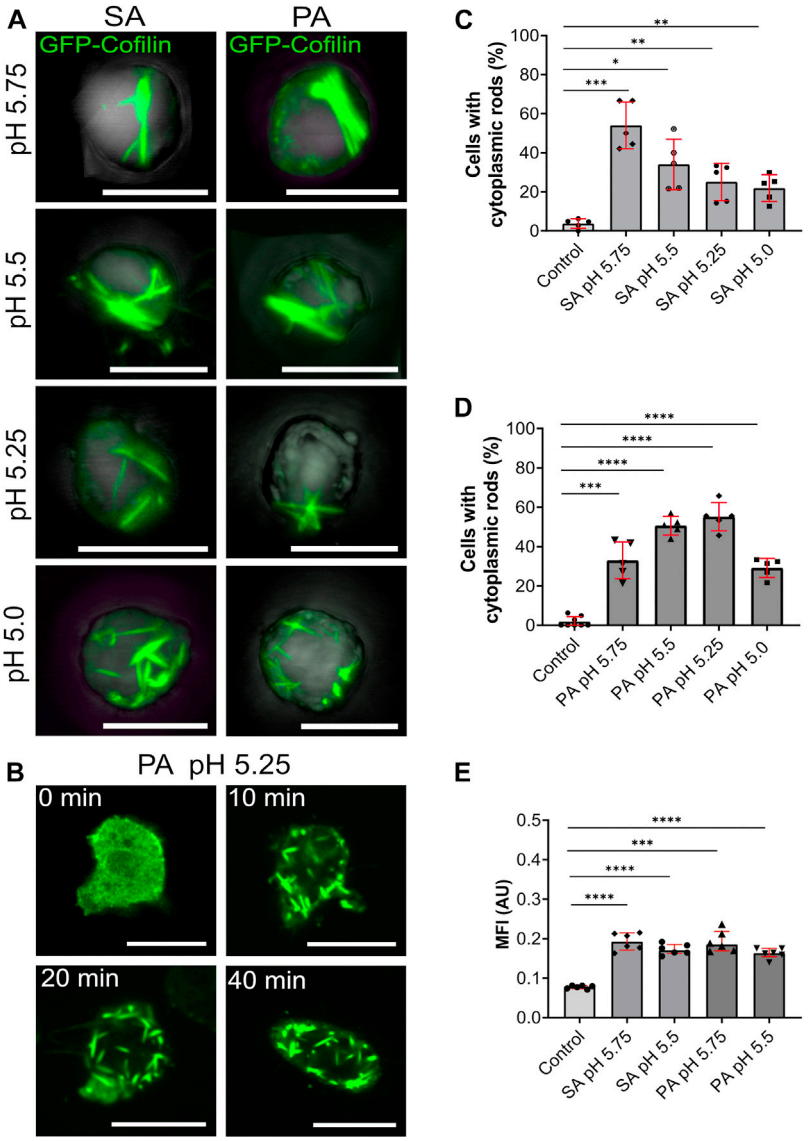

FIGURE 4 | Cytoplasmic actin-cofilin rods are induced by lowering the intracellular pH. **(A)** 3D projection images of GFP-cofilin rods (green) formed by GFP-cofilin expressing cells cultivated for 2 h in medium adjusted to lower pH values with sorbic acid (SA) or propionic acid (PA) (pH 5.75, 5.5, 5.25 and 5.0). Scale bars are 10 µm. **(B)** Time lapse images of GFP-cofilin expressing cells placed in medium adjusted to pH 5.25 with PA. After 10 min, GFP-cofilin rods (green) start to assemble in the cytoplasm. Scale bars, 10 µm. **(C,D)** Percentage of cells with GFP-cofilin rods in medium adjusted with SA **(C)** or PA **(D)** to the indicated pH values. $n = 5$ experiments. **(E)** Ratiometric pH measurements to determine acidification of the intracellular pH. *Dictyostelium* cells expressing pHluorin2 cells were incubated with medium adjusted with either SA or PA to pH 5.75 and 5.5. An increase of MFI indicates the lowering of the intracellular pH. $n = 6$ experiments per treatment. More than 20 cells were analyzed for each experiment and treatment. Error bars are median with interquartile range (red). Samples were considered significant when $p \leq 0.05$. Welch´s t-test was applied.

divisions, and a developmental stage, in which the cells aggregate to form a multicellular slug and finally fruiting bodies. The transition from growth to development is induced by starvation.

In the course of experiments where we tested energy depletion, we cultivated *Dictyostelium* cells in glucose-free medium containing 2-deoxyglucose (2-DG). In contrast to mammalian cells, application of 2-DG did not result in the same effect as ATP depletion with sodium azide or DNP. Instead, we observed that after 5–6 h a low percentage of cells (<5%) were characterized by the appearance of rods. After 18 h, about 20% of cells showed cytoplasmic rods (**Figures 5A,C**). Ratiometric measurements of pHluorin-cells after application of 2-DG medium revealed a significant drop in the intracellular pH after 18 h (**Figure 5D**). After 24 h, rods were not detectable anymore, but most cells were characterized by an elongated shape typical for *Dictyostelium* cells of the aggregation stage (**Figure 5B**).

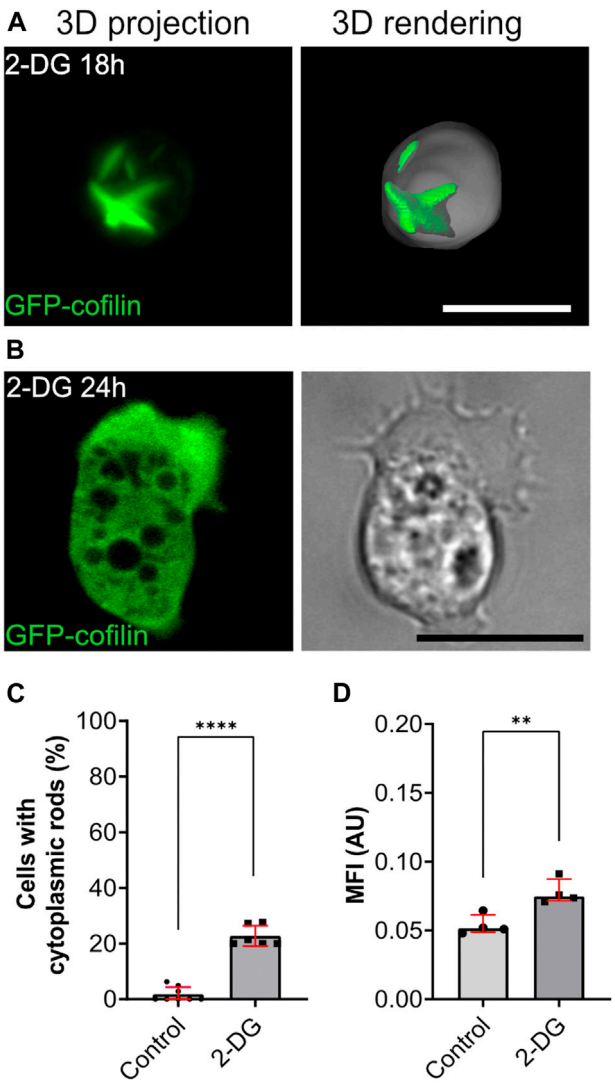

FIGURE 5 | Starvation induced by glucose-deprivation (2-DG) causes transient formation of cytoplasmic actin-cofilin rods. **(A)** 3D projection and rendering of GFP-cofilin expressing cells treated with 2-DG for 18 h, or **(B)** 24 h. Scale bars, 10 µm. **(C)** Percentage of cells with cytoplasmic rods after 18 h of glucose deprivation. For each experiment, 10x images (212 × 212 µm) were used for quantification (n = 6). **(D)** Ratiometric pH measurements 18 h after incubation of cells in 2-DG-containing medium. For each experiment, 10x images (212 × 212 µm) with a total of more than 20 cells per experiment were analyzed to determine the mean of fluorescence intensity (n = 4). Error bars are median with interquartile range (red). Samples were considered significant when $p \leq 0.05$. Welch's t-test was applied.

DISCUSSION

A series of studies suggested that under conditions that cause cellular stress, complexes of actin and cofilin, so-called actin-cofilin rods, are formed and interfere with essential cell functions, and consequently were held responsible for causing the disease states (Bamburg and Wiggan, 2002; Maloney and Bamburg, 2007; Bamburg et al., 2010; Munsie et al., 2011; Hoffmann et al., 2019; Wang et al., 2020). Experimental work also showed that formation of actin-cofilin rods can be provoked by various types of stressors either inside the nucleus or in the cytoplasm. However, despite the finding that the appearance of actin-cofilin rods is linked to several diseases, fundamentally important questions remained unanswered. For instance, it is unknown whether these structures are related, similar in their composition, or serve a specific function to maintain the cellular equilibrium. Similarly, the functional differences of nuclear and cytoplasmic rods are unclear. The current picture is that the formation of actin-cofilin rods is much more complex and may be triggered by different causes.

Even though the exact role of actin-cofilin rods still needs to be elucidated in more detail, the general assumption is that the formation of rods constitutes a strategy for the cell to reduce energy consumption due to a shut-off of actin-treadmilling. The constant turnover of actin is a highly energy-dependent process, which consumes up to 50% of the cellular ATP (Daniel et al., 1986; Bernstein and Bamburg, 2003). Thus, actin-cofilin rod formation may provide a protective mechanism for cells under stress conditions. This notion is supported by the assumption that cellular metabolism and actin remodeling are coupled processes (DeWane et al., 2021).

In the present study we have used the *Dictyostelium* model system to explore the characteristics and principles of cytoplasmic actin-cofilin rod formation. Like nuclear rods, cytoplasmic rods consist of actin and cofilin and contain coronin and Aip1 as associated proteins. However, we do not find the finely tuned spatial-temporal pattern of protein recruitment that we found for nuclear rod assembly (Ishikawa-Ankerhold et al., 2017). Conditions that cause depletion of ATP, like blockage of the respiratory chain, induce the formation of cytoplasmic actin-cofilin rods. Limiting ATP production is accompanied by the production of reactive oxygen species (ROS), and several studies indicated that ROS induce the formation of actin-cofilin rods (reviewed by Bamburg and Bernstein, 2016). Though we were not able to distinguish whether ATP depletion or ROS formation is decisive for the formation of cytoplasmic rods, in our initial experiments we have applied sodium azide known to block the mitochondrial respiratory chain, and followed and visualized rod formation by live-cell imaging.

In contrast to nuclear rods, cytoplasmic rods are not stainable by phalloidin suggesting a variant arrangement of filamentous actin in the rods (Nishida et al., 1987; Aizawa et al., 1999; Ishikawa-Ankerhold et al., 2017). Similar to nuclear rods, Aip1 is a crucial factor for the compaction of cytoplasmic rods. Mutant cells lacking Aip1 are characterized by less compacted and more needle-like cytoplasmic rods. Aip1, as well as coronin, have been shown to cooperate with cofilin to enhance depolymerization of filamentous actin (Ono, 2003; Kueh et al., 2008; Ishikawa-Ankerhold et al., 2010; Nadkarni and Brieher, 2014; Mikati et al., 2015).

Application of cytochalasin D, a drug blocking the fast-growing ends of actin filaments, inhibits the assembly of cytoplasmic actin-cofilin rods already at low doses. Similarly, LatA inhibits cytoplasmic rod formation to a considerable extent. These results suggest that the availability of actin monomers as

well as free barbed end are important for the formation of cytoplasmic actin-cofilin assemblies. It is likely that cofilin and cytochalasin D interfere at barbed ends, an assumption that is fostered by recent *in-vitro* data showing cofilin accelerates actin dynamics at both ends (Wioland et al., 2017; Romet-Lemonne and Jegou, 2021). From this it can be concluded that in addition to regulatory proteins such as Aip1 and coronin, the complex regulation of cofilin itself is one of the decisive factors for the formation of cytoplasmic actin-cofilin rods.

In the current study, we show that a reduction of the intracellular pH induces the assembly of actin-cofilin rods in the cytoplasm. The application of the weak acids sorbic (SA) and propionic acid (PA) to the extracellular medium, shows slight differences which may be attributed to differences in the efficiency of their membrane permeability. However, our results using the pHluorin2 as reporter show that cultivation of *Dictyostelium* cells in medium adjusted to lower pH values by either sorbic or propionic acid reduces the intracellular pH to a considerable extent. Our data are also consistent with earlier NMR-measurements that showed a reduction of intracellular pH by the addition of propionic acid (Satre et al., 1989).

We conclude that a decrease in cellular pH is a critical determinant of cytoplasmic actin-cofilin rod formation. This assumption is strengthened by the finding that hyperosmotic conditions, accompanied by a drop in cellular pH, induce the formation of cytoplasmic actin-cofilin rods. Moreover, it has been shown that in *Dictyostelium* the switch between growth and development, which is induced by starvation of the cells is accompanied by a transient drop in the intracellular pH (Aerts et al., 1987). This may explain the temporary appearance of rods in our experiments employing 2-DG to simulate glucose deprivation. These results suggest that acidification or even a locally limited drop in the intracellular pH can cause the formation of actin-cofilin rod structures, and it is obvious to speculate that local changes in intracellular pH are also important determinants for the transient formation of rods in other cell types and in particular neuronal cells.

Protein aggregates and macromolecular assemblies have been shown to play a role in the development of a number of degenerative diseases, for instance neurofibrillary tangles typically associated with Alzheimer's disease or aberrant RNP granules with ALS or FTD (frontotemporal dementia). Recent work suggested that impairments in the control of phase separation are causative for at least some neurological disease pathologies (Alberti and Hyman, 2016; Hofweber et al., 2018; Alberti and Hyman, 2021). Phase separation describes the separation of a homogenous mix of proteins into two coexisting phases, a more liquid phase that is enriched for these molecules and a phase that is depleted, and thereby enables the formation of membrane-less cellular compartments with different physical properties by the condensation of macromolecules (Alberti, 2017). How phase transitions organize cellular condensates is currently a matter of intense research (Boeynaems et al., 2018).

A current working concept is that protein phase separation may be used by cells to regulate protein synthesis and to ensure adaptation to a broad range of stress situations (Kroschwald and Alberti, 2017). De-mixing and the formation of protein assemblies may provide an evolutionarily conserved mechanism for cells to adapt to and to survive extreme situations. Our results showing that the intracellular pH could be a critical determinator for actin-cofilin rod formation fits into the recent concept that pH could be a regulator of phase separation (Kroschwald and Alberti, 2017). Whether these considerations play a role for the pathological states of neuronal cells through the formation of actin-cofilin rods needs to be examined more closely.

DATA AVAILABILITY STATEMENT

The raw data supporting the conclusion of this article will be made available by the authors, without undue reservation.

AUTHOR CONTRIBUTIONS

HI-A, SK, AK, and AM-T performed experiments, HI-A and AM-T analyzed data and wrote the manuscript, AM-T designed and supervised the project. All authors reviewed and agreed to the manuscript.

FUNDING

This work was supported by the grants from the Deutsche Forschungsgemeinschaft (SFB 914, projects Z01 (HI-A) and A07E (AM-T)).

ACKNOWLEDGMENTS

We thank Dominic van den Heuvel and Daniel Setzensack (Department of Internal Medicine I and Walter Brendel Centre of Experimental Medicine, LMU Munich), as well as Daniela Rieger and Gudrun Trommler (Biomedical Center, LMU Munich) for technical assistance.

SUPPLEMENTARY MATERIAL

The Supplementary Material for this article can be found online at: https://www.frontiersin.org/articles/10.3389/fcell.2021.742310/full#supplementary-material

REFERENCES

Aerts, R. J., Durston, A. J., and Konijn, T. M. (1987). Cytoplasmic pH at the Onset of Development in Dictyostelium. *J. Cel. Sci.* 87 (Pt 3) (Pt 3), 423–430. doi:10.1242/jcs.87.3.423

Aizawa, H., Katadae, M., Maruya, M., Sameshima, M., Murakami-Murofushi, K., and Yahara, I. (1999). Hyperosmotic Stress-Induced Reorganization of Actin Bundles inDictyosteliumcells Over-expressing Cofilin. *Genes to Cells* 4 (6), 311–324. doi:10.1046/j.1365-2443.1999.00262.x

Aizawa, H., Sutoh, K., Tsubuki, S., Kawashima, S., Ishii, A., and Yahara, I. (1995). Identification, Characterization, and Intracellular Distribution of Cofilin in *Dictyostelium discoideum*. *J. Biol. Chem.* 270 (18), 10923–10932. doi:10.1074/jbc.270.18.10923

Alberti, S., and Hyman, A. A. (2016). Are Aberrant Phase Transitions a Driver of Cellular Aging? *Bioessays* 38 (10), 959–968. doi:10.1002/bies.201600042

Alberti, S., and Hyman, A. A. (2021). Biomolecular Condensates at the Nexus of Cellular Stress, Protein Aggregation Disease and Ageing. *Nat. Rev. Mol. Cel. Biol.* 22 (3), 196–213. doi:10.1038/s41580-020-00326-6

Alberti, S. (2017). The Wisdom of Crowds: Regulating Cell Function through Condensed States of Living Matter. *J. Cel. Sci.* 130 (17), 2789–2796. doi:10.1242/jcs.200295

Ashworth, S. L., Southgate, E. L., Sandoval, R. M., Meberg, P. J., Bamburg, J. R., and Molitoris, B. A. (2003). ADF/cofilin Mediates Actin Cytoskeletal Alterations in LLC-PK Cells during ATP Depletion. *Am. J. Physiology-Renal Physiol.* 284 (4), F852–F862. doi:10.1152/ajprenal.00210.2002

Bamburg, J. R., and Bernstein, B. W. (2016). Actin Dynamics and Cofilin-Actin Rods in Alzheimer Disease. *Cytoskeleton* 73 (9), 477–497. doi:10.1002/cm.21282

Bamburg, J. R., Bernstein, B. W., Davis, R. C., Flynn, K. C., Goldsbury, C., Jensen, J. R., et al. (2010). ADF/Cofilin-actin Rods in Neurodegenerative Diseases. *Car* 7 (3), 241–250. doi:10.2174/156720510791050902

Bamburg, J. R., and Bernstein, B. W. (2010). Roles of ADF/cofilin in Actin Polymerization and beyond. *F1000 Biol. Rep.* 2, 62. doi:10.3410/B2-62

Bamburg, J. R., and Wiggan, O. N. P. (2002). ADF/cofilin and Actin Dynamics in Disease. *Trends Cel Biol.* 12 (12), 598–605. doi:10.1016/s0962-8924(02)02404-2

Bernstein, B. W., and Bamburg, J. R. (2003). Actin-ATP Hydrolysis Is a Major Energy drain for Neurons. *J. Neurosci.* 23 (1), 1–6. doi:10.1523/jneurosci.23-01-00002.2003

Bernstein, B. W., and Bamburg, J. R. (2010). ADF/cofilin: a Functional Node in Cell Biology. *Trends Cel. Biol.* 20 (4), 187–195. doi:10.1016/j.tcb.2010.01.001

Bernstein, B. W., Chen, H., Boyle, J. A., and Bamburg, J. R. (2006). Formation of Actin-ADF/cofilin Rods Transiently Retards Decline of Mitochondrial Potential and ATP in Stressed Neurons. *Am. J. Physiology-Cell Physiol.* 291 (5), C828–C839. doi:10.1152/ajpcell.00066.2006

Bernstein, B. W., Shaw, A. E., Minamide, L. S., Pak, C. W., and Bamburg, J. R. (2012). Incorporation of Cofilin into Rods Depends on Disulfide Intermolecular Bonds: Implications for Actin Regulation and Neurodegenerative Disease. *J. Neurosci.* 32 (19), 6670–6681. doi:10.1523/JNEUROSCI.6020-11.2012

Boeynaems, S., Alberti, S., Fawzi, N. L., Mittag, T., Polymenidou, M., Rousseau, F., et al. (2018). Protein Phase Separation: A New Phase in Cell Biology. *Trends Cel. Biol.* 28 (6), 420–435. doi:10.1016/j.tcb.2018.02.004

Cai, L., Marshall, T. W., Uetrecht, A. C., Schafer, D. A., and Bear, J. E. (2007). Coronin 1B Coordinates Arp2/3 Complex and Cofilin Activities at the Leading Edge. *Cell* 128 (5), 915–929. doi:10.1016/j.cell.2007.01.031

Caridi, C. P., Plessner, M., Grosse, R., and Chiolo, I. (2019). Nuclear Actin Filaments in DNA Repair Dynamics. *Nat. Cel. Biol.* 21 (9), 1068–1077. doi:10.1038/s41556-019-0379-1

Casella, J. F., Flanagan, M. D., and Lin, S. (1981). Cytochalasin D Inhibits Actin Polymerization and Induces Depolymerization of Actin Filaments Formed during Platelet Shape Change. *Nature* 293 (5830), 302–305. doi:10.1038/293302a0

Chhabra, E. S., and Higgs, H. N. (2007). The many Faces of Actin: Matching Assembly Factors with Cellular Structures. *Nat. Cel. Biol.* 9 (10), 1110–1121. doi:10.1038/ncb1007-1110

Daniel, J. L., Molish, I. R., Robkin, L., and Holmsen, H. (1986). Nucleotide Exchange between Cytosolic ATP and F-Actin-Bound ADP May Be a Major Energy-Utilizing Process in Unstimulated Platelets. *Eur. J. Biochem.* 156 (3), 677–683. doi:10.1111/j.1432-1033.1986.tb09631.x

de Hostos, E. L., Bradtke, B., Lottspeich, F., Guggenheim, R., and Gerisch, G. (1991). Coronin, an Actin Binding Protein of *Dictyostelium discoideum* Localized to Cell Surface Projections, Has Sequence Similarities to G Protein Beta Subunits. *EMBO J.* 10 (13), 4097–4104. doi:10.1002/j.1460-2075.1991.tb04986.x

DeWane, G., Salvi, A. M., and DeMali, K. A. (2021). Fueling the Cytoskeleton - Links between Cell Metabolism and Actin Remodeling. *J. Cel. Sci.* 134 (3), 1. doi:10.1242/jcs.248385

Domazetovska, A., Ilkovski, B., Cooper, S. T., Ghoddusi, M., Hardeman, E. C., Minamide, L. S., et al. (2007a). Mechanisms Underlying Intranuclear Rod Formation. *Brain* 130 (Pt 12), 3275–3284. doi:10.1093/brain/awm247

Domazetovska, A., Ilkovski, B., Kumar, V., Valova, V. A., Vandebrouck, A., Hutchinson, D. O., et al. (2007). Intranuclear Rod Myopathy: Molecular Pathogenesis and Mechanisms of Weakness. *Ann. Neurol.* 62 (6), 597–608. doi:10.1002/ana.21200

Fukui, Y. (1978). Intranuclear Actin Bundles Induced by Dimethyl Sulfoxide in Interphase Nucleus of Dictyostelium. *J. Cel. Biol.* 76 (1), 146–157. doi:10.1083/jcb.76.1.146

Fukui, Y., and Katsumaru, H. (1980). Dynamics of Nuclear Actin Bundle Induction by Dimethyl Sulfoxide and Factors Affecting its Development. *J. Cel. Biol.* 84 (1), 131–140. doi:10.1083/jcb.84.1.131

Fukui, Y., and Katsumaru, H. (1979). Nuclear Actin Bundles in Amoeba, Dictyostelium and Human HeLa Cells Induced by Dimethyl Sulfoxide. *Exp. Cel. Res.* 120 (2), 451–455. doi:10.1016/0014-4827(79)90412-9

Goebel, H. H., and Warlo, I. (1997). Nemaline Myopathy with Intranuclear Rods-Intranuclear Rod Myopathy. *Neuromuscul. Disord.* 7 (1), 13–19. doi:10.1016/s0960-8966(96)00404-x

Hoffmann, L., Rust, M. B., and Culmsee, C. (2019). Actin(g) on Mitochondria - a Role for Cofilin1 in Neuronal Cell Death Pathways. *Biol. Chem.* 400 (9), 1089–1097. doi:10.1515/hsz-2019-0120

Hofweber, M., Hutten, S., Bourgeois, B., Spreitzer, E., Niedner-Boblenz, A., Schifferer, M., et al. (2018). Phase Separation of FUS Is Suppressed by its Nuclear Import Receptor and Arginine Methylation. *Cell* 173 (3), 706–719. e713. doi:10.1016/j.cell.2018.03.004

Huang, T. Y., Minamide, L. S., Bamburg, J. R., and Bokoch, G. M. (2008). Chronophin Mediates an ATP-Sensing Mechanism for Cofilin Dephosphorylation and Neuronal Cofilin-Actin Rod Formation. *Dev. Cel.* 15 (5), 691–703. doi:10.1016/j.devcel.2008.09.017

Hyrskyluoto, A., and Vartiainen, M. K. (2020). Regulation of Nuclear Actin Dynamics in Development and Disease. *Curr. Opin. Cel. Biol.* 64, 18–24. doi:10.1016/j.ceb.2020.01.012

Ilkovski, B., Nowak, K. J., Domazetovska, A., Maxwell, A. L., Clement, S., Davies, K. E., et al. (2004). Evidence for a Dominant-Negative Effect in ACTA1 Nemaline Myopathy Caused by Abnormal Folding, Aggregation and Altered Polymerization of Mutant Actin Isoforms. *Hum. Mol. Genet.* 13 (16), 1727–1743. doi:10.1093/hmg/ddh185

Ishikawa-Ankerhold, H. C., Daszkiewicz, W., Schleicher, M., and Müller-Taubenberger, A. (2017). Actin-Interacting Protein 1 Contributes to Intranuclear Rod Assembly in *Dictyostelium discoideum*. *Sci. Rep.* 7, 40310. doi:10.1038/srep40310

Ishikawa-Ankerhold, H. C., Gerisch, G., and Müller-Taubenberger, A. (2010). Genetic Evidence for Concerted Control of Actin Dynamics in Cytokinesis, Endocytic Traffic, and Cell Motility by Coronin and Aip1. *Cytoskeleton* 67 (7), 442–455. doi:10.1002/cm.20456

Jungbluth, A., von Arnim, V., Biegelmann, E., Humbel, B., Schweiger, A., and Gerisch, G. (1994). Strong Increase in the Tyrosine Phosphorylation of Actin upon Inhibition of Oxidative Phosphorylation: Correlation with Reversible Rearrangements in the Actin Skeleton of Dictyostelium Cells. *J. Cel. Sci.* 107 (Pt 1), 117–125. doi:10.1242/jcs.107.1.117

Kanellos, G., and Frame, M. C. (2016). Cellular Functions of the ADF/cofilin Family at a Glance. *J. Cel. Sci.* 129 (17), 3211–3218. doi:10.1242/jcs.187849

Kay, R. R., Gadian, D. G., and Williams, S. R. (1986). Intracellular pH in Dictyostelium: a 31P Nuclear Magnetic Resonance Study of its Regulation and Possible Role in Controlling Cell Differentiation. *J. Cel. Sci.* 83, 165–179. doi:10.1242/jcs.83.1.165

Kelpsch, D. J., and Tootle, T. L. (2018). Nuclear Actin: From Discovery to Function. *Anat. Rec.* 301 (12), 1999–2013. doi:10.1002/ar.23959

Konzok, A., Weber, I., Simmeth, E., Hacker, U., Maniak, M., and Müller-Taubenberger, A. (1999). DAip1, a Dictyostelium Homologue of the Yeast Actin-Interacting Protein 1, Is Involved in Endocytosis, Cytokinesis, and Motility. *J. Cel. Biol.* 146 (2), 453–464. doi:10.1083/jcb.146.2.453

Kroschwald, S., and Alberti, S. (2017). Gel or Die: Phase Separation as a Survival Strategy. *Cell* 168 (6), 947–948. doi:10.1016/j.cell.2017.02.029

Kueh, H. Y., Charras, G. T., Mitchison, T. J., and Brieher, W. M. (2008). Actin Disassembly by Cofilin, Coronin, and Aip1 Occurs in Bursts and Is Inhibited by Barbed-End Cappers. *J. Cel. Biol.* 182 (2), 341–353. doi:10.1083/jcb.200801027

Mahon, M. J. (2011). pHluorin2: an Enhanced, Ratiometric, pH-Sensitive green Florescent Protein. *Abb* 02 (3), 132–137. doi:10.4236/abb.2011.23021

Maloney, M. T., and Bamburg, J. R. (2007). Cofilin-mediated Neurodegeneration in Alzheimer's Disease and Other Amyloidopathies. *Mol. Neurobiol.* 35 (1), 21–43. doi:10.1007/bf02700622

Mikati, M. A., Breitsprecher, D., Jansen, S., Reisler, E., and Goode, B. L. (2015). Coronin Enhances Actin Filament Severing by Recruiting Cofilin to Filament Sides and Altering F-Actin Conformation. *J. Mol. Biol.* 427 (19), 3137–3147. doi:10.1016/j.jmb.2015.08.011

Minamide, L. S., Maiti, S., Boyle, J. A., Davis, R. C., Coppinger, J. A., Bao, Y., et al. (2010). Isolation and Characterization of Cytoplasmic Cofilin-Actin Rods. *J. Biol. Chem.* 285 (8), 5450–5460. doi:10.1074/jbc.m109.063768

Minamide, L. S., Striegl, A. M., Boyle, J. A., Meberg, P. J., and Bamburg, J. R. (2000). Neurodegenerative Stimuli Induce Persistent ADF/cofilin-actin Rods that Disrupt Distal Neurite Function. *Nat. Cel. Biol.* 2 (9), 628–636. doi:10.1038/35023579

Morton, W. M., Ayscough, K. R., and McLaughlin, P. J. (2000). Latrunculin Alters the Actin-Monomer Subunit Interface to Prevent Polymerization. *Nat. Cel. Biol.* 2 (6), 376–378. doi:10.1038/35014075

Müller-Taubenberger, A. (2006). Application of Fluorescent Protein Tags as Reporters in Live-Cell Imaging Studies. *Methods Mol. Biol.* 346, 229–246. doi:10.1385/1-59745-144-4:229

Müller-Taubenberger, A., and Ishikawa-Ankerhold, H. C. (2013). Fluorescent Reporters and Methods to Analyze Fluorescent Signals. *Methods Mol. Biol.* 983, 93–112. doi:10.1007/978-1-62703-302-2_5

Müller-Taubenberger, A., Kortholt, A., and Eichinger, L. (2013). Simple System - Substantial Share: the Use of Dictyostelium in Cell Biology and Molecular Medicine. *Eur. J. Cel. Biol.* 92 (2), 45–53. doi:10.1016/j.ejcb.2012.10.003

Munder, M. C., Midtvedt, D., Franzmann, T., Nüske, E., Otto, O., Herbig, M., et al. (2016). A pH-Driven Transition of the Cytoplasm from a Fluid- to a Solid-like State Promotes Entry into Dormancy. *Elife* 5, 1. doi:10.7554/eLife.09347

Munsie, L., Caron, N., Atwal, R. S., Marsden, I., Wild, E. J., Bamburg, J. R., et al. (2011). Mutant Huntingtin Causes Defective Actin Remodeling during Stress: Defining a New Role for Transglutaminase 2 in Neurodegenerative Disease. *Hum. Mol. Genet.* 20 (10), 1937–1951. doi:10.1093/hmg/ddr075

Nadkarni, A. V., and Brieher, W. M. (2014). Aip1 Destabilizes Cofilin-Saturated Actin Filaments by Severing and Accelerating Monomer Dissociation from Ends. *Curr. Biol.* 24 (23), 2749–2757. doi:10.1016/j.cub.2014.09.048

Nishida, E., Iida, K., Yonezawa, N., Koyasu, S., Yahara, I., and Sakai, H. (1987). Cofilin Is a Component of Intranuclear and Cytoplasmic Actin Rods Induced in Cultured Cells. *Proc. Natl. Acad. Sci.* 84 (15), 5262–5266. doi:10.1073/pnas.84.15.5262

Ono, S. (2003). Regulation of Actin Filament Dynamics by Actin Depolymerizing Factor/cofilin and Actin-Interacting Protein 1: New Blades for Twisted Filaments. *Biochemistry* 42 (46), 13363–13370. doi:10.1021/bi034600x

Ott, A., Oehme, F., Keller, H., and Schuster, S. C. (2000). Osmotic Stress Response in Dictyostelium Is Mediated by cAMP. *EMBO J.* 19 (21), 5782–5792. doi:10.1093/emboj/19.21.5782

Pintsch, T., Satre, M., Klein, G., Martin, J.-B., and Schuster, S. C. (2001). Cytosolic Acidification as a Signal Mediating Hyperosmotic Stress Responses in *Dictyostelium discoideum*. *BMC Cel. Biol.* 2, 9. doi:10.1186/1471-2121-2-9

Pollard, T. D., and Borisy, G. G. (2003). Cellular Motility Driven by Assembly and Disassembly of Actin Filaments. *Cell* 112 (4), 453–465. doi:10.1016/s0092-8674(03)00120-x

Romet-Lemonne, G., and Jégou, A. (2021). The Dynamic Instability of Actin Filament Barbed Ends. *J. Cel. Biol.* 220 (4), 1. doi:10.1083/jcb.202102020

Sanger, J. W., Sanger, J. M., Kreis, T. E., and Jockusch, B. M. (1980). Reversible Translocation of Cytoplasmic Actin into the Nucleus Caused by Dimethyl Sulfoxide. *Proc. Natl. Acad. Sci.* 77 (9), 5268–5272. doi:10.1073/pnas.77.9.5268

Satre, M., Martin, J.-B., and Klein, G. (1989). Methyl Phosphonate as a 31P-NMR Probe for Intracellular pH Measurements in Dictyostelium Amoebae. *Biochimie* 71 (8), 941–948. doi:10.1016/0300-9084(89)90076-x

Schonhofen, P., Medeiros, L. M., Chatain, C., Bristot, I., and Klamt, F. (2014). Cofilin/actin Rod Formation by Dysregulation of Cofilin-1 Activity as a central Initial Step in Neurodegeneration. *Mrmc* 14 (5), 393–400. doi:10.2174/1389557514666140506161458

Simpson, P. A., Spudich, J. A., and Parham, P. (1984). Monoclonal Antibodies Prepared against Dictyostelium Actin: Characterization and Interactions with Actin. *J. Cel. Biol.* 99 (1 Pt 1), 287–295. doi:10.1083/jcb.99.1.287

Sparrow, J. C., Nowak, K. J., Durling, H. J., Beggs, A. H., Wallgren-Pettersson, C., Romero, N., et al. (2003). Muscle Disease Caused by Mutations in the Skeletal Muscle Alpha-Actin Gene (ACTA1). *Neuromuscul. Disord.* 13 (7-8), 519–531. doi:10.1016/s0960-8966(03)00101-9

Walter, L. M., Rademacher, S., Pich, A., and Claus, P. (2021). Profilin2 Regulates Actin Rod Assembly in Neuronal Cells. *Sci. Rep.* 11 (1), 10287. doi:10.1038/s41598-021-89397-9

Wang, Q., Yuan, W., Yang, X., Wang, Y., Li, Y., and Qiao, H. (2020). Role of Cofilin in Alzheimer's Disease. *Front. Cel. Dev. Biol.* 8, 584898. doi:10.3389/fcell.2020.584898

Wioland, H., Guichard, B., Senju, Y., Myram, S., Lappalainen, P., Jégou, A., et al. (2017). ADF/Cofilin Accelerates Actin Dynamics by Severing Filaments and Promoting Their Depolymerization at Both Ends. *Curr. Biol.* 27 (13), 1956–1967. doi:10.1016/j.cub.2017.05.048

Won, S. J., Minnella, A. M., Wu, L., Eun, C. H., Rome, E., Herson, P. S., et al. (2018). Cofilin-actin Rod Formation in Neuronal Processes after Brain Ischemia. *PLoS One* 13 (10), e0198709. doi:10.1371/journal.pone.0198709

Yahara, I., Aizawa, H., Moriyama, K., Iida, K., Yonezawa, N., Nishida, E., et al. (1996). A Role of Cofilin/destrin in Reorganization of Actin Cytoskeleton in Response to Stresses and Cell Stimuli. *Cell Struct. Funct.* 21 (5), 421–424. doi:10.1247/csf.21.421

Conflict of Interest: The authors declare that the research was conducted in the absence of any commercial or financial relationships that could be construed as a potential conflict of interest.

Publisher's Note: All claims expressed in this article are solely those of the authors and do not necessarily represent those of their affiliated organizations, or those of the publisher, the editors and the reviewers. Any product that may be evaluated in this article, or claim that may be made by its manufacturer, is not guaranteed or endorsed by the publisher.

Copyright © 2021 Ishikawa-Ankerhold, Kurzbach, Kinali and Müller-Taubenberger. This is an open-access article distributed under the terms of the Creative Commons Attribution License (CC BY). The use, distribution or reproduction in other forums is permitted, provided the original author(s) and the copyright owner(s) are credited and that the original publication in this journal is cited, in accordance with accepted academic practice. No use, distribution or reproduction is permitted which does not comply with these terms.

frontiers in Cell and Developmental Biology

ORIGINAL RESEARCH
published: 23 November 2021
doi: 10.3389/fcell.2021.720623

The Dynamics of Aerotaxis in a Simple Eukaryotic Model

Marta Biondo[1], Cristina Panuzzo[2], Shahzad M. Ali[2], Salvatore Bozzaro[2], Matteo Osella[1], Enrico Bracco[3†] and Barbara Pergolizzi[2†]*

[1] Department of Physics, INFN, University of Turin, Turin, Italy, [2] Department of Clinical and Biological Science, University of Turin, Turin, Italy, [3] Department of Oncology, University of Turin, Turin, Italy

In aerobic organisms, oxygen is essential for efficient energy production, and it acts as the last acceptor of the mitochondrial electron transport chain and as regulator of gene expression. However, excessive oxygen can lead to production of deleterious reactive oxygen species. Therefore, the directed migration of single cells or cell clumps from hypoxic areas toward a region of optimal oxygen concentration, named aerotaxis, can be considered an adaptive mechanism that plays a major role in biological and pathological processes. One relevant example is the development of O_2 gradients when tumors grow beyond their vascular supply, leading frequently to metastasis. In higher eukaryotic organisms, aerotaxis has only recently begun to be explored, but genetically amenable model organisms suitable to dissect this process remain an unmet need. In this regard, we sought to assess whether *Dictyostelium* cells, which are an established model for chemotaxis and other motility processes, could sense oxygen gradients and move directionally in their response. By assessing different physical parameters, our findings indicate that both growing and starving *Dictyostelium* cells under hypoxic conditions migrate directionally toward regions of higher O_2 concentration. This migration is characterized by a specific pattern of cell arrangement. A thickened circular front of high cell density (*corona*) forms in the cell cluster and persistently moves following the oxygen gradient. Cells in the colony center, where hypoxia is more severe, are less motile and display a rounded shape. Aggregation-competent cells forming streams by chemotaxis, when confined under hypoxic conditions, undergo stream or aggregate fragmentation, giving rise to multiple small loose aggregates that coordinately move toward regions of higher O_2 concentration. By testing a panel of mutants defective in chemotactic signaling, and a catalase-deficient strain, we found that the latter and the pkbR1^{null} exhibited altered migration patterns. Our results suggest that in Dictyostelium, like in mammalian cells, an intracellular accumulation of hydrogen peroxide favors the migration toward optimal oxygen concentration. Furthermore, differently from chemotaxis, this oxygen-driven migration is a G protein-independent process.

Keywords: aerotaxis, oxidative stress, hydrogen peroxide, collective cell migration, *Dictyostelium*, G-protein, catalase

OPEN ACCESS

Edited by:
Robin S. B. Williams, University of London, United Kingdom

Reviewed by:
Igor Weber, Rudjer Boskovic Institute, Croatia
Paul Robert Fisher, La Trobe University, Australia

***Correspondence:**
Barbara Pergolizzi
barbara.pergolizzi@unito.it

† These authors have contributed equally to this work and share last authorship

Specialty section:
This article was submitted to Molecular and Cellular Pathology, a section of the journal Frontiers in Cell and Developmental Biology

Received: *04 June 2021*
Accepted: *13 October 2021*
Published: *23 November 2021*

Citation:
Biondo M, Panuzzo C, Ali SM, Bozzaro S, Osella M, Bracco E and Pergolizzi B (2021) The Dynamics of Aerotaxis in a Simple Eukaryotic Model. Front. Cell Dev. Biol. 9:720623. doi: 10.3389/fcell.2021.720623

INTRODUCTION

Oxygen (O_2) is required for cell survival, oxidative metabolism, and synthesis of adenosine 5′-triphosphate (ATP), being the final electron acceptor in oxidative phosphorylation (Wilson, 2017). Moreover, advances in the understanding of the physiology of O_2 have shown that it is also important as a signaling molecule. Indeed, in multicellular organisms, it is an essential micro-environmental factor controlling developmental processes (Dunwoodie, 2009).

Maintenance of cellular O_2 level, supply, and consumption are precisely regulated, as oxygen imbalance could increase reactive oxygen species (ROS) production. To maintain oxygen homeostasis, metazoan organisms use the hypoxic signaling pathway to facilitate O_2 delivery and cellular adaptation to oxygen deprivation (Claesson-Welsh, 2020). Mammalian cells under hypoxic conditions adapt rather quickly by inhibiting proliferation and relying on glycolysis rather than oxidative phosphorylation for energy production, thus preventing further O_2 consumption. As a consequence, all these processes increase the production of angiogenic factors that can drive vascular remodeling and eventually improve tissue perfusion and O_2 delivery (Rey and Semenza, 2010).

The relationship between O_2 depletion and cancer is a common feature among most solid tumors. The hypoxic core microenvironment provides an aggressive ecological selective pressure for resilient stem-like cancerous cells. Furthermore, hypoxic environmental conditions may induce advanced and dysfunctional vascularization and promote epithelial-to-mesenchymal transition, resulting in high cell mobility and a high risk of developing metastasis (Muz et al., 2015). In this regard, O_2 gradients are crucial in early stages of sarcoma development, where cells respond to the hypoxic gradient by aggressively invading the matrix, and subsequently show fast and long-distance migration (Lewis et al., 2016). Furthermore, immortalized mammary epithelial cells, residing within deep hypoxia, migrate directionally toward oxygen by the process named aerotaxis, through an ROS-dependent enhanced epidermal growth factor receptor (EGFR) activation (Deygas et al., 2018).

Although the reports described above suggest that O_2 acts as a chemoattractant for cancer cells to the neighboring blood vessels, the molecular players and signaling pathways triggering this process remain understudied. Aerotaxis has been long studied in prokaryotes (Taylor et al., 1999; Sporer et al., 2017), whereas in eukaryotes it started to be investigated in *Caenorhabditis elegans* (Gray et al., 2004; Chang et al., 2006; Demir et al., 2020), the choanoflagellate *Salpingoeca rosetta* (Kirkegaard et al., 2016), and more recently in mammalian cells (Deygas et al., 2018). In all these cases, cells can first sense and navigate toward oxygen and then react appropriately by eventually organizing a coordinated and directional movement. Nonetheless, the molecular players remain largely unknown.

A relevant part of current knowledge of the mechanisms regulating oriented cell migration, in response to various stimuli, has been obtained in the social amoeba *Dictyostelium discoideum*, which has proven to be an excellent model system to study almost every kind of random and directional cell motility, including chemo-, electro-, and rheo-taxis (Bozzaro, 2013; Lima et al., 2014; Devreotes and Horwitz, 2015; Jeon et al., 2019; Guido et al., 2020). Cell motility is very similar in *Dictyostelium* and neutrophils, and the molecular components involved in cell migration are remarkably conserved between *Dictyostelium* and mammalian cells (Stuelten et al., 2018; Bozzaro, 2019; Pal et al., 2019).

Based on this large plethora of studies and the availability of well-defined mutants in genes regulating cell motility and signal transduction (Fey et al., 2019), we thought that *Dictyostelium* could be a very suitable model for studying aerotaxis. In this report, we analyzed aerotactic migration parameters in *Dictyostelium* wild-type cells and a panel of mutants defective in chemotaxis and/or electrotaxis. In agreement with previous findings in mammals, the oxygen sensing of *Dictyostelium* cells seems very likely associated with high cytoplasmic levels of hydrogen peroxidase. Furthermore, the observed "aerotaxis" does not share the signaling pathways regulating chemotaxis and electrotaxis.

MATERIALS AND METHODS

Dictyostelium discoideum Cell Culture and Development

The parental wild-type (WT) AX2 and mutant strains were cultured in an axenic medium (Ashworth and Watts, 1970) at 23°C under shaking at 150 rpm as previously described (Pergolizzi et al., 2017b). The mutant strains were obtained from the Dicty Stock Center[1], except for mutant HSB1, available in the laboratory, generated by chemical mutagenesis as described (Bozzaro et al., 1987), and previously characterized as temperature-sensitive for the piaA gene (Pergolizzi et al., 2002).

Aerotaxis Assay

The aerotaxis assay was modified from Deygas et al. (2018). Basically, growing *Dictyostelium* cells were seeded at a density of approximately 10,000 cells/mm^2 as a 10-µl drop containing 50,000 cells in the center of a 24-well culture plate. After cell attachment to the substratum, 400 µl of the axenic medium was added, and two 14 mm-diameter glass coverslips were placed on top to cover and confine the cell cluster. As a control in the not-confined (NC) system condition, cells were simply seeded without coverslips.

To assay the ability of aggregation competent cells to sense oxygen gradients, axenically growing AX2 cells were washed twice in a Soerensen phosphate buffer and resuspended at 5×10^6 cells/ml. Afterward, a 10-µl drop containing 50,000

[1]www.dictybase.org

cells was spotted in the center of the 24-well culture plate and let adhere for 10 min, before covering with 400 μl of buffer. The cells were then confined immediately (t0) or after 7 h (t7) when the aggregates were well-formed. No confinement (NC) conditions were used as a control of the experiment.

Time lapse movies of cell migration under confinement (C) or no confinement (NC) were recorded with times up to 24 h using a Lumenera Infinity 3 camera coupled to a Zeiss Axiovert 200 microscope, with a 5 × objective. Photograms were taken at intervals varying between 20 and 360 s (Pergolizzi et al., 2017b).

Quantification of Cell Arrangement During Migration

In our experimental setting, the circular 10-μl *Dictyostelium* cell layer was approximated to a bidimensional system of cells adhering to the substrate.

Therefore, the cell density (i.e., number of cells per unit area) represents a convenient parameter to characterize and define the arrangement of cells within the cluster. To quantitatively measure the density of cells, bright field images were split into portions of a defined and regular area, and the number of cells was determined using the Python package Trackpy (Allan et al., 2021).

Alternatively, in case of high cellular density, a much simpler indirect cell density measurement approach was undertaken represented by the relative number of cells expressed as percentage (%). Briefly, the bright field images were binarized through an adaptive threshold using the Python library OpenCV (Bradski, 2000). As a result, the cells appeared as white shapes on a black background in the binarized images. Brightness, i.e., the fraction of white pixels, can be used to detect changes in cell density as a first approximation. By partitioning the binarized images in circular areas, this method has been used to draw the cell density heat maps and radial profiles of the relative number of cells at different times. The latter were then analyzed to measure the displacement of its peak, which identifies the *corona*.

To investigate the role of cell duplication during collective migration, we instead considered a circular sector of the cell cluster and we segmented single cells using Trackpy (Allan et al., 2021). The increase in the number of cells counted in this specific area can only be attributed to cell duplication, since for symmetry reasons we do not expect on average any net flux of cells through the sector.

Analysis of the "*Corona*" Features

The most visually striking peculiarity of the migration pattern of the confined *Dictyostelium* cells consisted in the formation of a ring of high cell density, which we named *corona*, that moves away from the hypoxic region.

To characterize the kinetics and pattern features of this process, we first measured the formation time of the *corona* (T*), defined as the time required to detect a local maximum in the cell distribution profile at the periphery of the cell cluster.

Measuring the distance between the peak of cellular density and the center of the colony identified the position of the ring. Next, we determined the kinetics of the ring displacement $\Delta R(t)$ (R = radius; t = time) by assessing either its average velocity during the first 2 h after its formation (v_i) or for longer time points (v_f) (i.e., 10–24 h). T*, v_i, and the propagation of the ring have been quantified in at least three experiments for each cellular strain.

The features of the ring dynamics (i.e., width and density in time) were assessed in three independent experiments in the period 10–24 h by setting a minimum threshold value for the cell density. We acquired one measurement every 6 min and performed data binning to group five measurements per data point (data point ± vertical bar = mean value ± standard deviation).

Estimation of the Expansion Velocity of the Non-confined Cell Cluster

To describe the spreading of the cell cluster in the absence of cell confinement, we analyzed the first 5 h of independent experiments in the non-confined conditions. For each experiment (exp), we located the border of the cluster setting a minimum threshold value (th) for the density profiles; we assessed the displacement of the cluster border to measure the instantaneous expansion velocity of the cluster over 1-min time-lapse [$^{exp}v_{th}(t)$], and we then averaged these values to determine the spreading velocity $^{exp}v_{th}$. Since the choice of the cell density threshold was arbitrary, we considered a range of possible values, obtaining a set of $^{exp}v_{th}$ that was averaged to estimate the expansion velocity of the cluster (^{exp}v). We repeated this evaluation process for three independent experiments, and we measured $v_{NC} = 0.8 \pm 0.3$ μm/min (mean value ± standard deviation) that can be used as reference value for further comparisons with the cell dynamics in confined conditions.

Single Cell Tracking

Employing the Trackpy package, we determined the aerotactic pattern of *Dictyostelium* cells from the point of view of single cells: for both the confined and not confined conditions, we analyzed a video lasting 30 min with a resolution of three frames per minute providing the tracking software with the parameters "typical size" and "maximum speed" of the cells (10 μm and 10 μm/min, respectively). Given the symmetry of the colony, single-cell trajectories were described using polar coordinates (R,θ). The instantaneous speed [$|v|(t_i,R)$], radial component of the velocity [$v_r(t_i,R)$], and ratio between them [$v_r/|v|(t_i,R)$] were measured over time periods of 1 min for each detected cell. These measurements were grouped according to their distance from the center of the colony (R) using the sliding window method (150 μm interval) to describe the average motility of cells in a given position [$<|v|>(R)$, $<v_r>(R)$, and $<v_r/|v|>(R)$].

Cell tracking was also performed on videos of cells uniformly distributed over a plate to quantify their spontaneous motility in the absence of any hypoxia condition or oxygen gradient.

Oxygen Level Measurement

Oxygen concentration was determined over time using the VisiSens detector unit DUO1 coupled to the oxygen sensor foil SF-RPSu4. Data were analyzed with the AnalytiCal1 software

(PreSens, Germany). Under our experimental conditions, the time lapse of cell displacement and oxygen level detection were two mutually exclusive measurements.

RESULTS

Dictyostelium Cells Migrate and Regularly Deploy in Response to an Oxygen Gradient

We sought to assess whether *Dictyostelium* cells were able to sense an oxygen gradient and to move directionally toward the oxygen source. To generate an O_2 gradient, we took benefit of the method previously developed by Deygas et al. (2018) and modified it as indicated in the section "Materials and Methods." The oxygen gradient was induced by confining (C) the cells under coverslips. As a control, not confined (NC) cells were used. Oxygen levels were directly visualized by dynamic measurements with the VisiSens detector unit, confirming the different hypoxic profiles between the two conditions (**Supplementary Figure 1**).

A detailed analysis revealed that growing *Dictyostelium* cells moved with a peculiar pattern toward the higher oxygen concentration when subjected to confinement conditions. After approximately 1 h, a fraction of confined cells began to move coordinately, assuming an arrangement characterized by a thickened front, the *corona,* that once shaped, persistently moved toward the oxygen source (**Figure 1A** and **Supplementary Movie 1**). Interestingly, underneath the *corona*, the cells lined up in two further regimes that were easily recognized because of their differential cell density (**Figure 1B**). At the center of the colony, where oxygen concentration was lowest (**Supplementary Figure 1**), the cells were rather rounded, and their density was highest, although on average it decreases by 35% in the time-range 10–24 h. This stratification of the cluster in three density regimes was found to be fairly constant over time. The central area abutted with a wide region with lowest cellular density, in which the cells displayed an elongated shape (**Figure 1B**). While the size of the central high-density region was approximately constant, the lowest density sector expanded as the ring moved away from the center. Interestingly, the cells that trigger the formation of the *corona* were not the outermost ones (**Supplementary Figure 2** and **Supplementary Movies 1, 2**).

The shape of the cell clusters in C or NC was very similar at the beginning of the experiment (**Figure 2A**), displaying a circular geometry with the cell density decreasing as it approached the periphery (**Figure 2B**). Noticeably, in the NC system, cell distribution was maintained throughout the time. The only difference detected was the progressive spreading of the cell cluster with typical velocity of the cluster expansion $v_{NC} = 0.8 \pm 0.3$ μm/min, presumably by virtue of random cell motility and cell duplication, as the cells are incubated in a nutrient-rich growth medium.

On the contrary, under confined (C) conditions, we noticed that the pattern of cell arrangement was considerably dynamic over time. When compared with the onset condition, a thickened circular front, the *corona*, featured by a relatively high cell density, emerged, and persistently moved radially following the same direction of the oxygen gradient (**Figure 2B**).

To exclude that what we observed was the outcome of the pressure caused by the glass coverslips, we also performed the NC experiment by adding an amount of the axenic medium corresponding to the weight of the glass coverslips (0.1 g). Even under such conditions, the cells displayed a behavior identical to that of the NC counterpart (data not shown), indicating that the outcome observed under confinement was tightly associated with hypoxic stress.

Assessment of the Dynamic Physical Properties of the *corona* Structure

We then examined the peculiar biological process by which the vegetative *Dictyostelium* cell cluster reacted to the confined system within 24 h. Using density profiles, we determined the time required for the *corona* formation under confinement (T^*), which turned out to be nearly 60 ± 20 min for the parental strain AX2 (**Supplementary Table 1**). Concerning the dynamics of the *corona*, besides experimental variability, we found that after a transient period of a few hours, the initial velocity (v_i) of the *corona* propagation decreased until it reached a constant value (v_f), after approximately 10 h (**Figure 3A**). The initial velocity (v_i) of the *corona*, measured within the first 140 min, was equal to 2.2 μm/min (**Figure 3B**), but then it fell sharply to approximately 30% of v_i (v_f = 0.67 μm/min) and remained constant for the rest of the experiment, i.e., in the time range 10–24 h (**Figure 3C**). The decline in the *corona* speed is not sudden but rather smooth. This non-linear velocity trend could simply reflect continuous changes in microenvironmental conditions (e.g., variations of the oxygen profile in the radial direction). Our experimental settings (i.e., cells in the axenic medium and a 24-h time window) are, in principle, compatible with cell proliferation. Indeed, our estimates of cell duplication (**Supplementary Figure 3** for details) revealed that, under confinement, the cells were growing within the first few hours, but that after 10 h the number of cells in the colony was essentially constant (**Figure 3D**). At least within the 10–24 h period, cell growth can be regarded as a negligible effect and, thus, scarcely impacts the *corona* dynamics.

We then assessed the *corona* cell density in the time range 10–24 h. Despite experimental fluctuations, our measurements indicate that, on average, after 10 h, the *corona* cell density reached a steady state (**Figure 3E**).

If the number of cells that compose the *corona* and coordinately migrate is constant, as suggested by the fact that cell duplication is negligible, in order to maintain the same cell density, the width of the *corona* has to decrease. These simple geometric arguments provide an analytic prediction given the circular shape of the *corona* and the empirical linear growth in time of the *corona* radius $R(t) = R0 + \Delta R(t)$. If a *corona* of width L(t) and radius R(t) has to conserve the total area of the ring, its width will decrease as $L(t + \Delta t) = L(t)R(t)/R(t + \Delta t)$. The parameters of this model are the average number of cells [N(t)], the cell density within the *corona,* and its area. For each

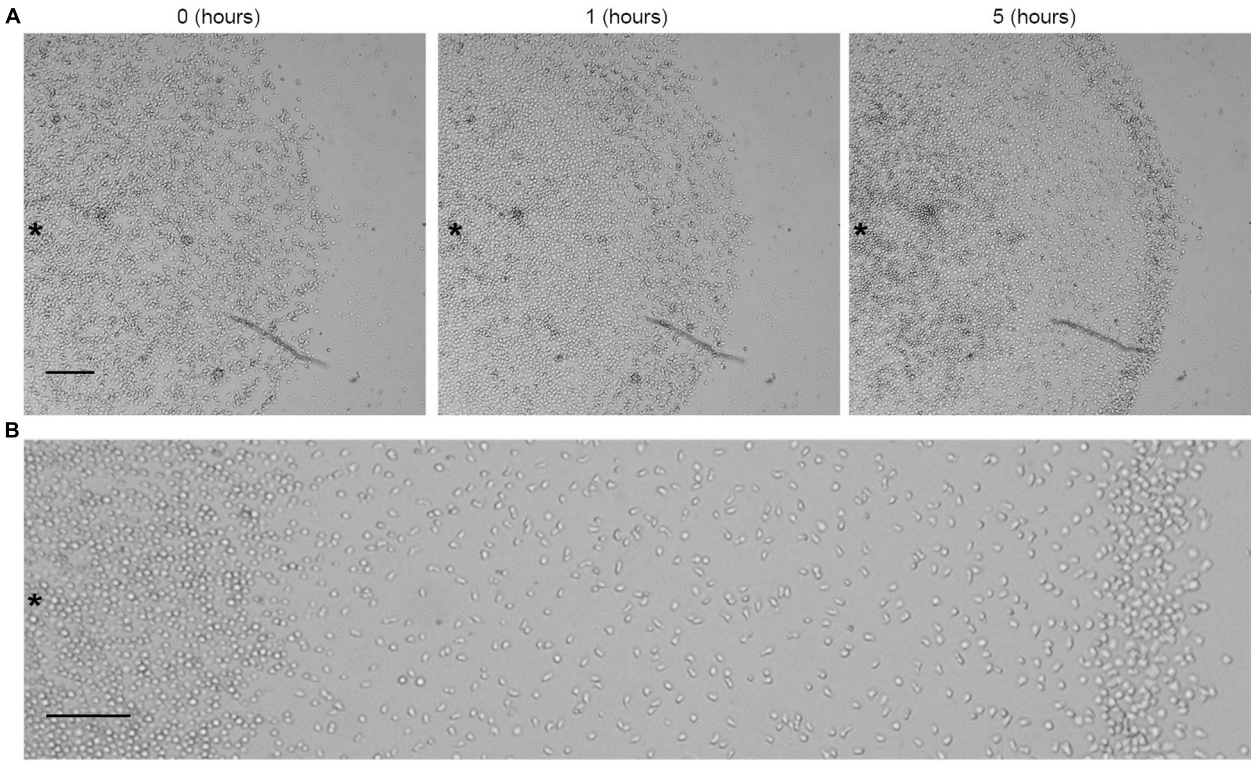

FIGURE 1 | Aerotactic migration of growing AX2 cells. **(A)** Time lapse images of live-cell migration toward a region of higher oxygen concentration (on the right of the image). Time (h) refers to the time that elapsed under confinement. **(B)** Magnification of the image after 5 h of confinement. Scale bar = 200 μm. Asterisks indicate approximately the center of the cell cluster.

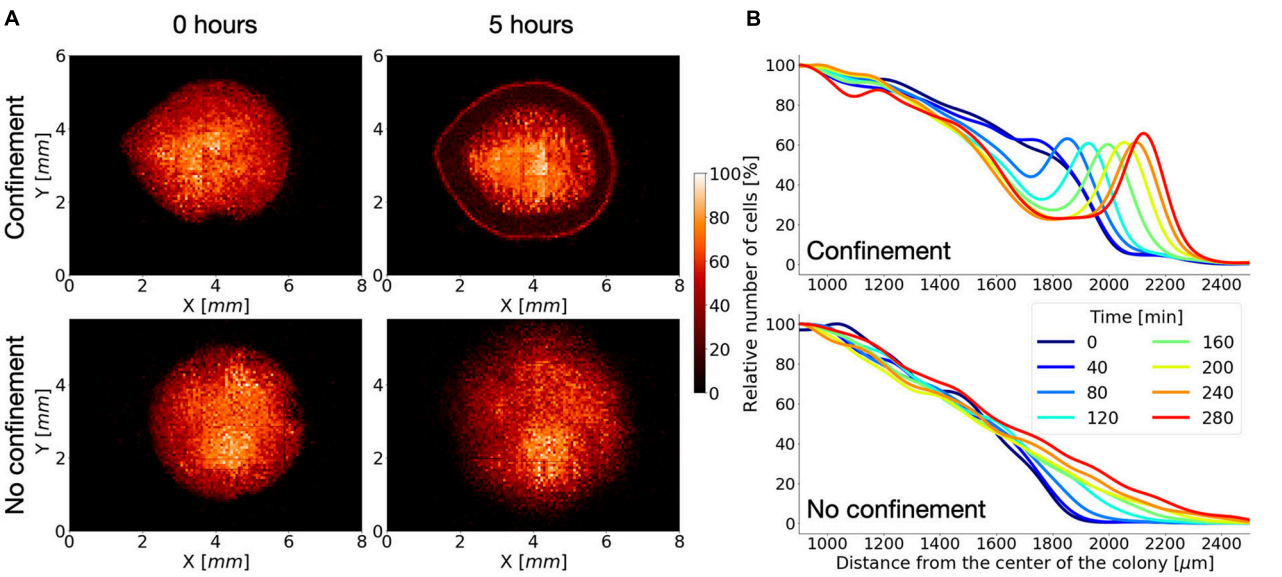

FIGURE 2 | Growing *Dictyostelium* wild-type cells react to the oxygen gradient. **(A)** Distribution of cells at the beginning of the experiment and after 5 h under confined (top) or not confined (bottom) conditions. **(B)** Corresponding cell density profiles (estimated as explained in the section "Materials and Methods") along the radial direction at different times are shown.

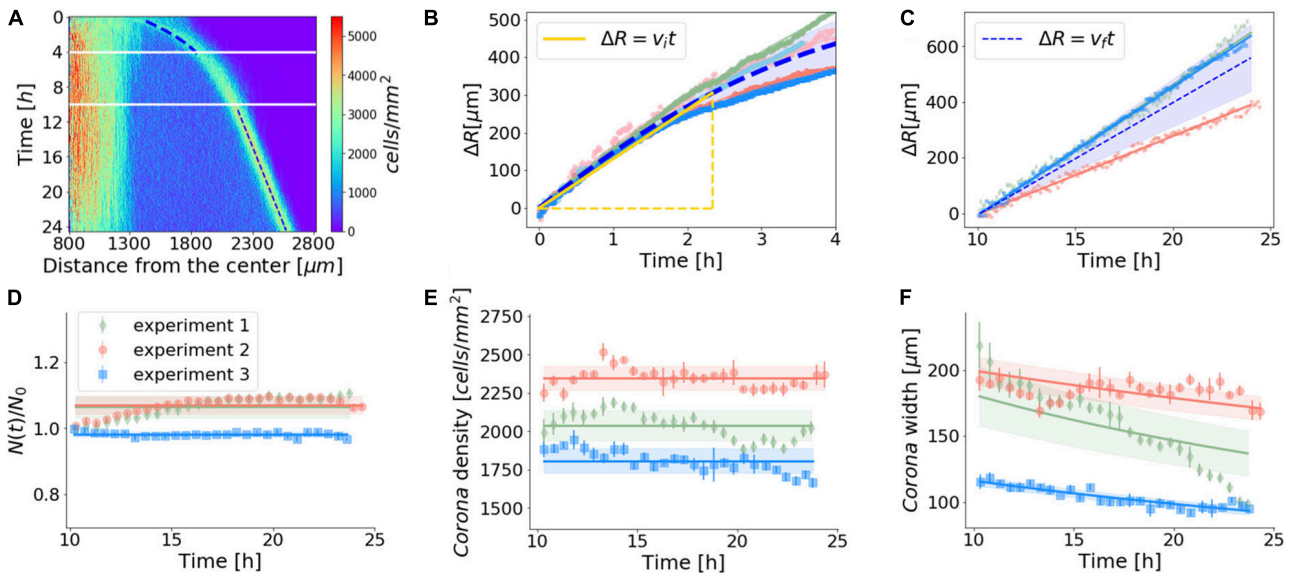

FIGURE 3 | Quantitative description of the aerotactic pattern of growing *Dictyostelium* wild-type cells. **(A)** Cell density for the confined system over 24 h as a function of radial distance and time; blue dashed lines highlight the dynamics of the front in the two time windows that were then studied in detail. Heatmap revealed that over a 24-h time period the very inner core of the cell cluster and the area between the latter and the *corona* maintained two distinct but unaltered density profiles. **(B,C)** Time evolution of *corona* displacement: blue dashed lines represent the average trends [ΔR(t)], computed *via* the mean value of the *corona* displacement measured in different experiments (corresponding to different colors); at any time, the variability of ΔR among the experiments was quantified by the standard deviation, represented by the blue shaded regions. **(B)** Early hours after corona formation: the yellow line shows the time range used to define the initial speed of the front, $\langle v_i \rangle = 2.2 \pm 0.2$ μm/min (mean value ± standard deviation, measured over five independent experiments). **(C)** Ten hours after confinement, the displacement of the ring grew linearly with time, i.e., with constant velocity v_f. This value displayed large statistical variability among three different experiments, $\langle v_f \rangle = 0.67 \pm 0.14$ μm/min. In panels **(D–F)**, the continuous lines and the shaded regions correspond to the model of a circular ring of cells that enlarges in radius while keeping the cell density constant without any cell duplication. **(D)** Number of cells over time (estimated as described in **Supplementary Figure 3**) indicated that cell duplication played a minor role when the ring propagated at constant velocity. Ratio between the number of cells N(t) and the one measured 10 h after the confinement of the colony [$N_0 = N(t = 10\ h)$] was approximately constant. **(E)** Cell density of the *corona* remained constant as the *corona* moves radially. Its value was comparable to the cell density detected in the inner region of the center of the colony. **(F)** Width of the front decreases as it escapes hypoxia.

experiment (represented in **Figures 3C–F** by different colors), we independently estimated the best values of these parameters and their error (mean ± standard deviation), and used them to produce respectively the continuous lines and the shaded regions in **Figures 3D–F**, which can explain reasonably well the empirical trends that we observed. To further exclude a role of cell duplication in the formation and progression of the *corona*, we assayed aerotaxis in starving WT cells, which are unable to duplicate. Even under these conditions, the cellular behavior was indistinguishable from that of growing cells (**Figure 4** and **Supplementary Movie 3**). As expected, under starvation, the cells lying within the *corona* reached the aggregation competence with timing comparable with that of the unconfined cells. Indeed, a *corona*-like front emerges within 2 h and persists for up to 4–5 h. By this time, the starving cells become aggregation-competent and start aggregating by chemotaxis driven by self-generated cAMP. This leads to fragmentation of the *corona* in streaming aggregates. These results confirm that cell division plays a negligible role in the formation of the *corona*. In addition, this assay proves that the exhaustion of nutrients does not represent a key event in triggering the movement toward the oxygen source, because otherwise the *corona* formation of starving cells would be faster than the response of growing cells. Ultimately, these findings also suggest that the *corona* structure represents a barrier to the oxygen to flow in the inner core of the cluster and when fragmented, because cells aggregate, and the oxygen gradient becomes discontinuous, thus inhibiting the formation of a new *corona*.

Different Motility Features Are Associated With the Cluster Density Profiles

We examined single-cell tracks of the confined cluster to ascertain cell motility features, such as average directionality, speed, and their association with the distance from the center. A survey was carried out in three different regions, namely, the center of the cell cluster, the *corona,* and the region in between (**Figure 5A**). The analysis was performed over 30 min in the time frame between 270 and 300 min, which was a convenient time scale to track thousands of cells per frame without significant changes in the cell cluster density profile and in the *corona* displacement (**Figure 5B**). To quantify the single cell motility, we measured the average instantaneous speed $[\langle |v| \rangle_C]$, at different distances from the cluster center. Conversely, the cell directionality was examined, by determining the average ratio between the radial component of the instantaneous velocity and the instantaneous

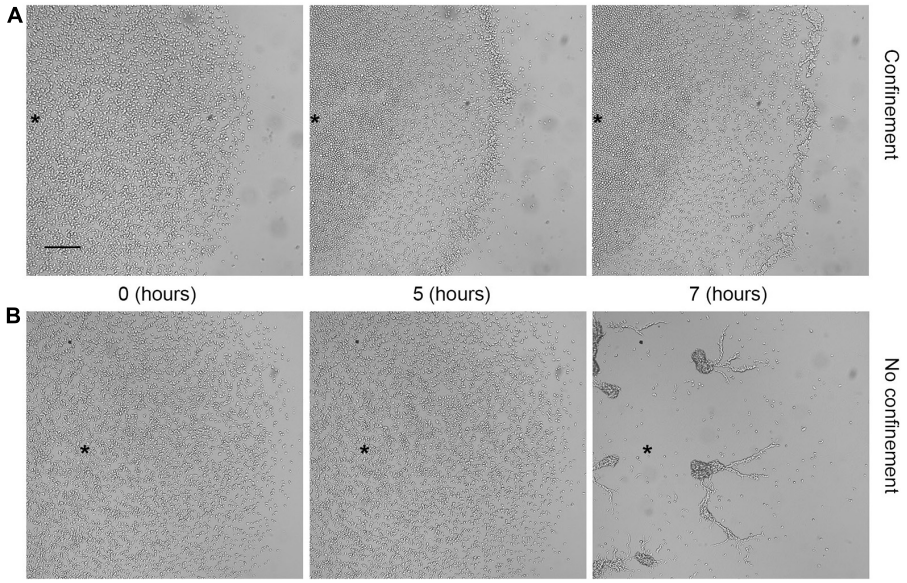

FIGURE 4 | Aerotactic migration occurred independently from cell proliferation. *Dictyostelium* starving cells under **(A)** confinement or **(B)** no confinement conditions. Photograms taken at different times (0, 1, and 5 h) using Zeiss Axiovert 200 microscope, with a magnification of 5×. Scale bar = 200 μm. Asterisks indicate approximately the center of the cell cluster.

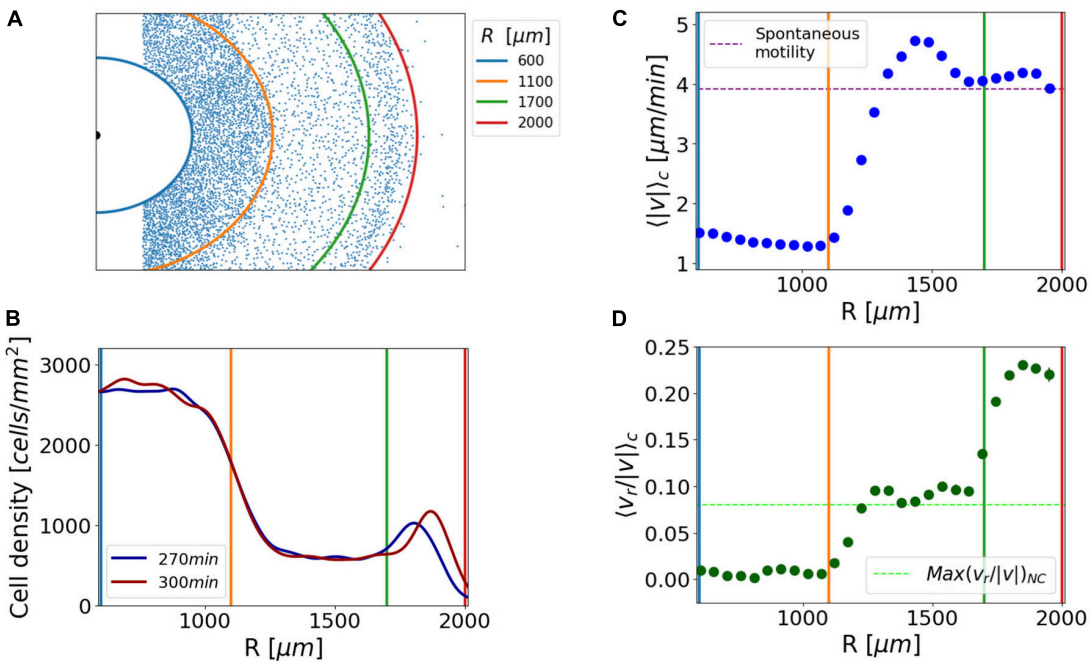

FIGURE 5 | Confined growing *Dictyostelium* cells displayed different motility profiles associated with areas of different cell densities. **(A)** Distribution of the tracked cells; continuous lines delimit three cell density regimes and serve as references for the plots that follow. **(B)** Cell density profiles did not change significantly in the observation time of 30 min, during which we performed cell tracking. **(C)** Cell average instantaneous speed $<|v|>_C$ as a function of their radial position R; the purple dashed line corresponds to the average speed measured for the WT spontaneous motility assay. **(D)** Average cosine of directions relative to the oxygen gradient direction $<v_r/|v|>_C$ as a function of their radial position; as a benchmark for the directionality of the cells, we plot the maximum directionality measured in the not-confined cell cluster [Max($<v_r/|v|>_{NC}$) = 0.08], (green dashed line).

speed [$<v_r/|v|>_C$]. To assess the average directionality of cells in the absence of a substantial oxygen gradient, we tracked the cells of the not confined system during the same timeframe.

Our analysis identified three different motility profiles, strictly associated with the three regions of different cellular density previously described. On average, cells lying in the center of the cluster (600 μm < R < 1,100 μm) displayed a rather stationary behavior with minor or no displacement (**Figure 5C**). Notably, those fewer cells showing displacement did not exhibit any preferential direction with respect to the geometry of the system [$<v_r/|v|>_C = 0$].

The cells embedded in the *corona* (R > 1,700 μm) displayed an average instantaneous speed comparable with that of cellular random motility (3.9 μm/min, **Figure 5C**). For the sake of clarity, we refer to random motility as that recorded for growing cells seeded under no confinement and incubated in the axenic medium. The comparison between the average $<v_r/|v|>_C$ of the cells belonging to the *corona* and the directionality measured in the non-confined cell cluster $<v_r/|v|>_{NC}$ allowed us to conclude that the former exhibited evident directionality toward regions of higher oxygen concentration. As a matter of fact, the value of $<v_r/|v|>_{NC}$ calculated as a function of the distance from the center had a maximum value of 0.08 in the outer colony region. On the other hand, $<v_r/|v|>_C$ is 0.24 if evaluated in the *corona* returned to 0.08 in the low-density region (**Figure 5D**). In order to support this result, we performed a Von Mises fit of cell angular displacement distributions to estimate the mean direction (μ) and the accuracy of the orientation (k) of the cells of the *corona* (Fisher and Annesley, 2006). Given the initial cell distribution within the cluster and the circular symmetry of the system, it was not surprising that the mean direction of cells was the radial one. However, we next imposed μ = 0, and assessed the accuracy of the orientation (k). The directionality of the cells belonging to the *corona* was higher than the one measured for the confined cells in the intermediate region and for cells in the not confined cluster (**Supplementary Figure 4A**).

When compared with the very inner region of the cell cluster, cells in the intermediate low-density region, (1,100 μm < R < 1,700 μm) showed higher speed with a velocity peak immediately behind the *corona* (**Figure 5C**).

In conclusion, cells in the intermediate region displayed an appreciable movement directionality toward the oxygen source $<v_r/|v|>_C > 0$ (**Figure 5D**), but compatible with the random spreading of *Dictyostelium* from a high cell density region as measured in the not-confined system [$<v_r/|v|>_C \approx \mathrm{Max}(<v_r/|v|>_{NC})$]. Similarly, the average radial velocity of the cells in the low-density region was compatible with the rate of expansion of the non-confined cluster $<v_r>_C \approx v_{NC}$ (**Supplementary Figures 4B,C**) suggesting again that the migration in this area could not be driven by the oxygen gradient.

The reduced directionality of the cells of the intermediate region with respect to those belonging to the *corona* implies that it is unlikely that cells of the intermediate region can supply the *corona*. Therefore, it is likely that the cells that migrate coordinately in the *corona* are always the same (i.e., their number is conserved).

Hypoxia Selectively Blocks *Dictyostelium* Cell Aggregation and Triggers Oxygen-Dependent Collective Migration

When starved under normoxic conditions (18–21% O_2), *Dictyostelium* cells aggregate, generate migratory slugs, and ultimately culminate to form fruiting bodies. Oxygen concentration regulates the aggregate size and the orientation of the prestalk-prespore pattern (Sternfeld and Bonner, 1977; Sternfeld and David, 1981), while below 10%, oxygen hinders culmination (Sandonà et al., 1995). To test the ability of aggregation-competent cells to react to hypoxia, we assessed aerotaxis in cells starved for 7 h. Briefly, aggregates formed under submerged conditions were confined and then assayed. Within the first few minutes, the aggregates suffered profound rearrangements, getting looser and partially disaggregating. Eventually, within the next 30–40 min, the loose aggregates directionally moved following the oxygen gradient (**Supplementary Movie 4**). Single cells still exhibited their elongated shape and arranged themselves in streaming-like structures (**Figure 6A**) that eventually moved toward the oxygen source displaying collective cell migration. Under such conditions, the absence of a clear-cut corona can be a consequence that the aggregates give rise to a discontinuous hypoxic gradient all over the cell cluster.

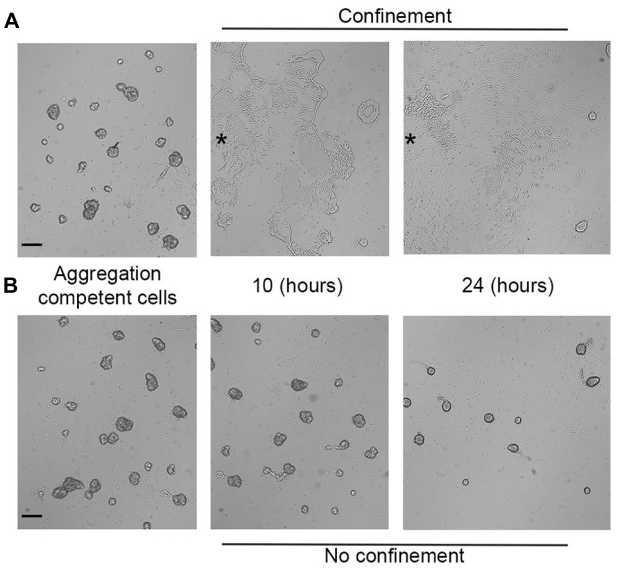

FIGURE 6 | Aerotactic migration of aggregation-competent cells. Photograms taken at different times (7, 10, and 24 h) using a Zeiss Axiovert 200 microscope, with a magnification of 5×. Aggregates under **(A)** confinement or **(B)** no confinement. Scale bar = 200 μm. Asterisks indicate approximately the center of the cell cluster.

In the NC control, the aggregates became more compact as time progressed (**Figure 6B**).

Dictyostelium Aerotactic Migration Relies on Impaired Intracellular Hydrogen Peroxide Degradation but Not on Chemotaxis Signaling Pathways

In mammalian cells migration toward an oxygen gradient is associated with a significant accumulation of H_2O_2 at the border of the cell cluster. This represents the most prominent event coinciding with the onset of directional motility (Deygas et al., 2018).

Based on this finding, we sought to assess the aerotaxis process in a *Dictyostelium* mutant defective in catalase activity (Garcia et al., 2002). This enzyme catalyzes the decomposition of H_2O_2 into H_2O and O_2. As a consequence, mutants with no catalase activity are hypersensitive to oxidative stress from hydrogen peroxide. Indeed, $catA^{null}$ cells display a severely impaired response to hydrogen peroxide even at a very low concentration (**Supplementary Figure 5**).

The aerotactic migration of the $catA^{null}$ mutant was assayed and compared with that of the WT. With regard to the cell density profiles, they were indistinguishable. On the contrary, the kinetics of the process highlighted that the time required to organize the *corona* (T^*) was shortened for $catA^{null}$ when compared with that of the WT cells (**Figure 7A**). The $catA^{null}$ showed a decline of T^* of approximately 50% (28 ± 2) (**Figure 7D** and **Supplementary Table 1**). In contrast, the initial velocity (v_i) of the *corona* propagation of $catA^{null}$ cells exhibited only a moderate increase when compared with that of the WT (**Figure 7E** and **Supplementary Table 1**). Therefore, although evolutionarily distant, both *Dictyostelium* and mammalian cells utilize intracellular H_2O_2 as an activator or enhancer of aerotactic migration.

We also tested a panel of mutants defective in chemotaxis and/or electrotaxis to assess whether they displayed altered aerotaxis, suggesting potential links between these motility processes. As summarized in **Supplementary Table 2**, the mutants either fail to aggregate at all or display impaired aggregation because of defects in the signaling pathways. A preliminary qualitative analysis of all the mutants showed that none of the strains displayed major defects in aerotaxis.

Quantitative analysis was restricted to three mutants: the $G\beta^{null}$ mutant, which lacks the beta subunit of the G protein and is, thus, essential for transducing GPCR chemotactic signals (Lilly et al., 1993; Pergolizzi et al., 2017a); the HSB1 mutant, harboring the *pianissimo* gene mutation pia^{G917D}, required for adenylyl cyclase activation (Pergolizzi et al., 2002); and $pkbR1^{null}$ (Meili et al., 2000), defective in the PKB/AKT related kinase. Under confinement, all the mutants behave as the WT cells (**Figures 7B,C** and **Supplementary Figure 6**). With the only exception of the $pkbR1^{null}$ strain, in which a moderate decline in the time required for *corona* formation (T^*) was observed, for the other mutants, no significant differences were detected (**Figure 7D** and **Supplementary Table 1**). However, the $pkbR1^{null}$ and, to a much lesser extent, $G\beta^{null}$ strains exhibited higher initial propagation speed of the *corona*, and the latter similar to $catA^{null}$ (**Figure 7E** and **Supplementary Table 1**). These results suggest that signals transduced *via* G-protein coupled receptor(s) and PKBR1 serve to restrain or inhibit the sensitivity of the cells to O_2 gradients in aerotaxis. Conversely, such differences were abolished when considering the time scale of within 10–24 h (**Supplementary Figure 7**). To rule out that the prominent initial speed detected in $pkbR1^{null}$ cells was the outcome of increased single cell motility, we also measured its spontaneous motility and compared it with that of the WT. We found that the random movement of $pkbR1^{null}$cells displayed an average speed basically indistinguishable from that of the WT strain AX2 (**Figure 7F**).

DISCUSSION

Mild to severe O_2 deprivation (hypoxia) due to high tumor cell metabolic rate and aberrant vascularization is associated with altered cellular metabolism as well as resistance to chemotherapy and radiotherapy (Horsman and Overgaard, 2016; Parks et al., 2017). Furthermore, hypoxia regulates cell proliferation and supports apoptosis evasion by tumor cells. On the whole, hypoxia exerts a selection pressure that leads to the survival of subpopulations of viable cells with the genetic machinery for malignant progression. Indeed, hypoxia has been associated with metastasis, which usually leads to a very poor prognostic outcome (Rankin and Giaccia, 2016). Although metastasis accounts for the great majority of cancer-associated deaths, this complex process still remains the least understood aspect of cancer biology (Lambert et al., 2017). In this regard the prerequisites for the migration of tumor cells from a primary site to a secondary/metastatic site include weakening of the cell-to-cell adhesion and capability to directionally move away from the tumor mass toward an oxygenated blood vessel (Seyfried and Huysentruyt, 2013). While the molecular mechanisms responsible for the lessening of the intercellular cell adhesion have been largely ascertained, those enabling the directional "navigation" away from the mass have, only recently, started to be explored.

Besides bacteria (Taylor et al., 1999; Sporer et al., 2017), response to O_2 gradient has started only lately to be assessed in simple eukaryotic model systems (Gray et al., 2004; Chang et al., 2006; Kirkegaard et al., 2016; Demir et al., 2020) and more recently in mammalian cells (Deygas et al., 2018).

Early studies on *Dictyostelium* demonstrated that the cells responded by moving up the oxygen gradient, while late in development, the prestalk-prespore pattern can be oriented by the gradient (Sternfeld and Bonner, 1977; Sternfeld and David, 1981). Hence, we have attempted to quantitatively assess whether *Dictyostelium* cells can escape hypoxia moving along an oxygen gradient. Our findings indicate that, as in other organisms, *Dictyostelium* cells react to hypoxia in a time scale of 30-60 min. This implies the presence of a very efficient detection mechanism. Our current results do not allow to distinguish between positive (aero)taxis or negative chemotaxis because of accumulation of repellent/s. However, depletion of key nutrients can be excluded, as starving cells showed the

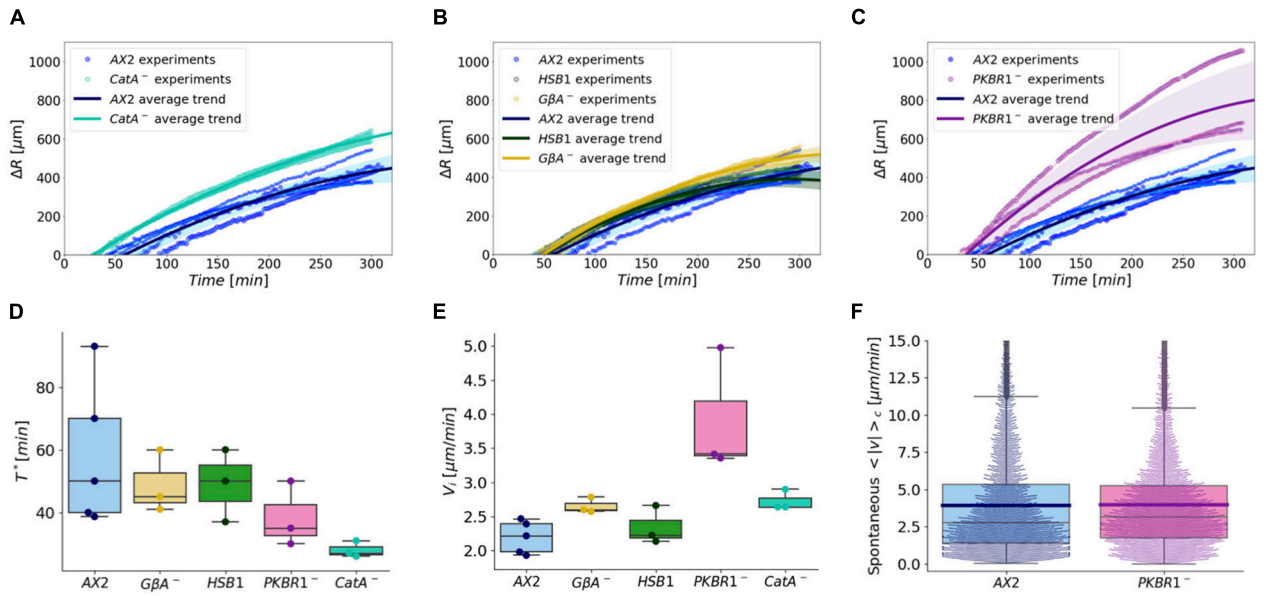

FIGURE 7 | Comparison between the migration of wild-type cells and various chemotaxis deficient mutants under growing conditions. **(A–C)** We report the time evolution of the corona displacement of independent experiments (colored bullets): different colors represent different *Dictyostelium* strains, whereas the size of the markers corresponds to distinct experiments. To group the corona displacement trends of the same genotype, we represented the mean value of all the experiments (continuous colored lines) and their standard deviation (colored shaded regions). Comparison of the ring dynamics **(A)** between WT and *catA*^{null} mutants; **(B)** among WT, *HSB1,* and *Gβ*^{null} mutants; **(C)** between WT and *pkbR1*^{null} mutant. Boxplots in panels **(D,E)** summarize, respectively, the estimated ring formation time T* (measured over at least three experiments for each cell type) and the ring initial propagation speed v_i. **(F)** The spontaneous motility (measured as the average instantaneous speed) under not confined conditions for single cells of the WT and *pkbR1*^{null} strains (mean values are represented by the blue and purple horizontal lines).

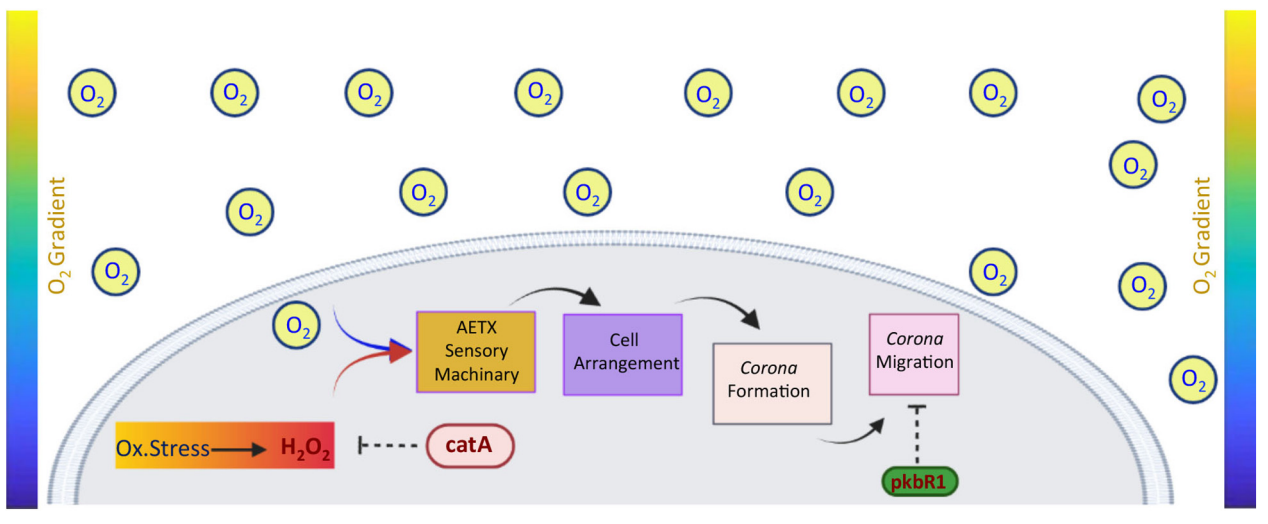

FIGURE 8 | Model of sensing and oriented migration of *Dictyostelium* cells under oxygen gradient. Under oxidative stress conditions, cells accumulate hydrogen peroxide up to a critical threshold (dark red in the rectangle). Once the latter is reached, the cells react and coordinately arrange themselves to give rise to a *corona*. These early events are regulated by unknown aerotaxis (AETX) sensory machinery/ies by which catalase A might represent either a regulatory component or a direct player. Afterward, the *corona* moves toward the higher concentration of oxygen, and its speed is negatively controlled by the PKBR1 protein.

same behavior as growing cells. In this context, however, we can maintain that migration is the result of oxygen gradient as a phenomenon, without implying a mechanistic cause-effect.

The cells migrate following the gradient by adopting a peculiar arrangement, consisting of a peripheral structure (*corona*) characterized by contiguous cells exhibiting high speed and significant directionality toward a region of suitable oxygen level.

Interestingly, the cells that converge to form the *corona* are not the most external ones, which would be those closer to the region with high oxygen concentration. Instead, the local density maximum, which identifies the *corona*, forms within the colony radius. If the *corona* formation was simply caused by a critical hypoxic level, the migration would, in principle, start from the center of the colony, and all cells would move to escape the region of hypoxia, as long as the critical value does not lead to rounding of the cells. On the other hand, if the trigger was only the presence of an oxygen gradient, the migration would start earlier at the border of the colony, where we measured a slight oxygen gradient already 5 min after the confinement. A minimal model of this phenomenon (excluding intercellular communication) could consider as possible cause of the observed migration a critical hypoxic level in the presence of an oxygen gradient.

In contrast to *Dictyostelium* clusters, mammalian cell clusters under hypoxic conditions do not arrange so neatly, although a sort of "inner-core," characterized by almost stationary cells, is common to both cell types (Deygas et al., 2018). The mechanism leading to this singular arrangement assumed by *Dictyostelium* cells remains currently unknown. Nevertheless, a detailed analysis of the dynamics of aerotaxis in *Dictyostelium* suggests that such arrangement is not random but that it is dictated by dynamic microenvironmental conditions. Behind the *corona*, displaying a rather high cellular density, we identified a wider region with lower density, in which the cells are appreciably elongated. Remarkably, the cells immediately behind the *corona* showed the highest speed, although their directionality was lower than that of the *corona*. We also noticed that, even if *Dictyostelium* WT cells are incubated in the axenic medium, after approximately 10–15 h, cell duplication is largely inhibited.

While drafting this manuscript, the team of Rieu reported results that mostly overlapped with ours (Cochet-Escartin et al., 2021). However, the experimental settings are quite different, and there are some contrasting results. For example, they suggest that, in growing cells, cell division plays an important role during aerotactic migration, while in our case, if any, this is restricted exclusively to the early-mid events. Noteworthy, our findings achieved by starving cells strengthen the hypothesis that, at least under our experimental settings, the role played by cell division is negligible for reacting to an oxygen gradient and for the *corona* formation and propagation.

Such discrepancy might be due to the different number of cells used for the spot assay to induce the oxygen gradient, giving rise to different microenvironmental conditions. Similarly, their experiments do not show radial motion of the cells outside the *corona*.

Overall, our analysis indicates that the aerotaxis migration differs from all the other *Dictyostelium* taxis (i.e., chemo-, electro- and rheo-taxis) so far described in the social ameba (Zhao et al., 2002; Decave et al., 2003; Lima et al., 2014; Devreotes and Horwitz, 2015; Gao et al., 2015). We also assessed the migration behavior of developing cellular aggregates under confined conditions. Diversely from vegetative cells, aggregating cells have acquired different properties, such as the ability to produce and secrete the chemoattractant cAMP and to tightly adhere to each other by virtue of the adhesion molecule gp80/csA (Noegel et al., 1985). Accordingly, *Dictyostelium* cell aggregates have recently been regarded as a potential and challenging model to investigate solid tumor mass (Trigos et al., 2018; Mathavarajah et al., 2021). Under hypoxic conditions, the aggregates became loose and portions of them detached within minutes. This finding suggests weakening of cell-cell adhesion. Even if different time scales and distinct molecular players are involved, such behavior recalls the epithelial-mesenchymal transition that is pivotal in favoring the metastasis process (Pastushenko and Blanpain, 2019). Our data indicate that, because of the short time window, the reduced cell-cell adhesion is independent from a transcriptional event, suggesting rapid regulation, internalization, or post-translational modification of the adhesion molecules. Furthermore, these findings definitely indicate that hypoxia-sensing mechanisms are present at both the vegetative and aggregation stages, suggesting a common sensor that is retained throughout *Dictyostelium* life cycle. This would be consistent with early reports that an oxygen gradient regulates aggregate size, migration, and pattern formation (Sternfeld and Bonner, 1977; Sternfeld and David, 1981) as well as gene expression (Schiavo and Bisson, 1989; Sandonà et al., 1995).

In animals, a crucial oxygen sensor is the transcription factor HIF1α that under normoxic conditions has a very short half-life, while its degradation is retarded under decreasing oxygen concentration conditions. The more stable HIF1α further translocates to the nucleus, where it dimerizes with HIF1β, and the dimer eventually regulates gene transcription (Semenza, 2012). However, very recent data with animal cells (Kirkegaard et al., 2016; Deygas et al., 2018) indicate that HIF1α does not act as a sensor for aerotaxis. The *Dictyostelium* genome does not encode for the putative HIF1α. Interestingly, in mammalian cells incubated under hypoxic conditions, the driving event triggering the cell movement toward an oxygen source is intracellular accumulation, restricted to the very peripheral cells of the cluster, of hydrogen peroxide (Deygas et al., 2018). Hydrogen peroxide is a rather unstable molecule. However, it is more stable and less noxious than other reactive oxygen species (ROS), but interconvertible with other forms such as hydroxyl radicals and singlet oxygen by iron-catalyzed Haber-Weiss reactions. Like other cells, *Dictyostelium* amebae dispose hydrogen peroxide with the enzyme catalase, degrading it to $H_2O + O_2$ (Parish, 1975; Hayashi and Suga, 1978; Sepasi Tehrani and Moosavi-Movahedi, 2018). The *Dictyostelium* genome harbors two catalase-encoding genes, *catA* and *catB*. Whereas the latter is prespore-specific, the former shows a fairly constant gene expression level at all stages of growth and development (Garcia et al., 2000; Garcia et al., 2002). Hence, we analyzed the aerotactic behavior of the *Dictyostelium catA*/null strain that, although aggregating and developing normally, reacted to oxygen deprivation faster than the WT strain. How can the suppression of catalase A affect cell migration? Hypoxia has been shown to favor the synthesis of plasmalogens, which occurs in peroxisomes (Jain et al., 2020). Their synthesis will increase the ratio of unsaturated vs. saturated phospholipids in the membrane, favoring membrane fluidity (Nagura et al., 2004; Dean and Lodhi, 2018), which in turn could result in increased cell motility (Taraboletti et al., 1989; Edmond et al., 2015; Zhao et al., 2016; Angelucci et al., 2018).

We speculate that ROS accumulation, resulting from hypoxia, stimulates plasmalogen synthesis, a process further enhanced by catalase A inactivation. It is worth mentioning, in this context, that the plasmalogen form of phosphatidylethanolamine is the major phospholipid constituent of *Dictyostelium* cell membrane (Weeks and Herring, 1980). In addition, hydrogen peroxide is also a crucial regulator of the cytoskeleton dynamics on the leading edge of migrating cells and thus controlling cell polarity (Hurd et al., 2012; Emre et al., 2021).

Overall, these results let hypothesize that catalase, by regulating intracellular hydrogen peroxide pool, represents a component or regulator of a putative sensor machinery plausibly conserved throughout different kingdoms.

In an attempt to identify other possible players regulating aerotaxis, we tested a panel of mutants defective in chemotaxis. In terms of signal transduction mechanisms, *Dictyostelium* chemotaxis and electrotaxis diverge relatively little (e.g., G-protein and PKBR-1), while most of the players appear to be shared (pianissimo, rip3, and PTEN, etc.). Because we were unable to examine the whole collection of chemo- and electrotaxis mutants, we chose several archetypal strains and analyzed their behavior. *Dictyostelium* cells possess only one Gβ subunit, which is essential for all G protein-dependent signal transduction pathways. Unlike chemotaxis, but more similar to electrotaxis, the G protein appears to be a secondary regulator constraining the bias shown by our survey carried out with the $G\beta^{null}$ mutant. Likewise, our findings indicate that *Dictyostelium* hypoxia-driven migration is a process independent from mTORC2 that is, on the contrary, an essential regulator for both chemo- and electro-taxis (Chen et al., 1997; Pergolizzi et al., 2002; Lee et al., 2005; Gao et al., 2015). Lastly, our evidence suggests that, different from electrotaxis, PKBR-1 acts as a negative regulator during the aerotactic *corona* migration. The different aerotaxis behavior between the $pkbR1^{null}$ and mTORC2-deficient mutants is puzzling. Besides its mTORC2 independent activation, the molecular mechanisms by which PKBR-1 negatively regulates the *corona* speed remain currently unknown. PKB activation is rather complex, and its full activation is achieved only when both the activation loop (AL) and hydrophobic motif (HM) are phosphorylated (Pearce et al., 2010). However, partial PKB activation can be attained in an mTORC2-independent way through sole AL phosphorylation (Guertin et al., 2006). Strikingly, the role of PKBR-1 seems to be strictly restricted in controlling the velocity of *corona* migration.

Although the signaling that finely tunes the response to oxygen deprivation in *Dictyostelium* remains mostly unknown, based on our discoveries, we can speculate on a possible model that could be tested in future experiments l (**Figure 8**). In analogy with mammalian cells, this model proposes that a *Dictyostelium* cell cluster responds to oxygen depletion through a peripheral cell sub-population. This very early event is most likely triggered by an intracellular accumulation of H_2O_2 without the involvement of substantial transcriptional events. Afterward, the cell cluster arranges with a peripheral ring structure, the *corona*, that moves outward and whose speed is negatively regulated by PKBR-1.

In conclusion *Dictyostelium*, represents a novel alternative and genetically amenable model that can be widely exploited to unravel some basic cell biology aspects of directional migration toward oxygen.

DATA AVAILABILITY STATEMENT

The original contributions presented in the study are included in the article/**Supplementary Material**, further inquiries can be directed to the corresponding author.

AUTHOR CONTRIBUTIONS

BP, EB, MO, and MB contributed to the conception and design of the study. BP, EB, CP, and SA conducted the experiments. MB and MO developed the analytic tools and analyzed the data. BP, EB, MO, and MB wrote the first draft of the manuscript. SB revised the manuscript and contributed to the discussion. All authors contributed to manuscript revision, and read and approved the submitted version.

FUNDING

This study was supported by a grant of AIRBB to BP and the "Departments of Excellence" grant of the MIUR (L. 232/2016) to MO and MB.

ACKNOWLEDGMENTS

We thank Guido Serini for the helpful discussions.

SUPPLEMENTARY MATERIAL

The Supplementary Material for this article can be found online at: https://www.frontiersin.org/articles/10.3389/fcell.2021.720623/full#supplementary-material

REFERENCES

Allan, D. B., Caswell, T., Keim, N. C., van der Wel, C. M., and Verweij, R. W. (2021). *soft-matter/trackpy: Trackpy v0.5.0*. Genève: Zenodo.

Angelucci, C., D'Alessio, A., Iacopino, F., Proietti, G., Di Leone, A., Masetti, R., et al. (2018). Pivotal role of human stearoyl-CoA desaturases (SCD1 and 5) in breast cancer progression: oleic acid-based effect of SCD1 on cell migration and a novel pro-cell survival role for SCD5. *Oncotarget* 9, 24364–24380. doi: 10.18632/oncotarget.25273

Ashworth, J. M., and Watts, D. J. (1970). Metabolism of the cellular slime mould Dictyostelium discoideum grown in axenic culture. *Biochem. J.* 119, 175–182. doi: 10.1042/bj1190175

Bozzaro, S. (2013). The model organism dictyostelium discoideum. *Methods Mol. Biol.* 983, 17–37. doi: 10.1007/978-1-62703-302-2_2

Bozzaro, S. (2019). The past, present and future of Dictyostelium as a model system. *Int. J. Dev. Biol.* 63, 321–331. doi: 10.1387/ijdb.190128sb

Bozzaro, S., Hagmann, J., Noegel, A., Westphal, M., Calautti, E., and Bogliolo, E. (1987). Cell differentiation in the absence of intracellular and extracellular

cyclic AMP pulses in Dictyostelium discoideum. *Dev. Biol.* 123, 540–548. doi: 10.1016/0012-1606(87)90412-x

Bradski, G. (2000). The Opencv library. *Dr. Dobb's J. Software Tools* 120, 122–125. doi: 10.1109/MRA.2009.933612

Chang, A. J., Chronis, N., Karow, D. S., Marletta, M. A., and Bargmann, C. I. (2006). A distributed chemosensory circuit for oxygen preference in *C. elegans*. *PLoS Biol.* 4:e274. doi: 10.1371/journal.pbio.0040274

Chen, M. Y., Long, Y., and Devreotes, P. N. (1997). A novel cytosolic regulator, Pianissimo, is required for chemoattractant receptor and G protein-mediated activation of the 12 transmembrane domain adenylyl cyclase in Dictyostelium. *Genes Dev.* 11, 3218–3231. doi: 10.1101/gad.11.23.3218

Claesson-Welsh, L. (2020) Oxygen sensing; a stunningly elegant molecular machinery highjacked in cancer. *Ups J Med Sci.* 125, 205–210. doi: 10.1080/03009734.2020.1769231

Cochet-Escartin, O., Mete, D., Satomi, H., Blandine, A., Philippe, G., Mikaelian, I., et al. (2021). Hypoxia triggers collective aerotactic migration in Dictyostelium discoideum. *eLife* 10:e64731. doi: 10.7554/eLife.64731

Dean, J. M., and Lodhi, I. J. (2018). Structural and functional roles of ether lipids. *Protein Cell* 9, 196–206. doi: 10.1007/s13238-017-0423-425

Decave, E., Rieu, D., Dalous, J., Fache, S., Brechet, Y., Fourcade, B., et al. (2003). Shear flow-induced motility of Dictyostelium discoideum cells on solid substrate. *J. Cell Sci.* 116, 4331–4343. doi: 10.1242/jcs.00726

Demir, E., Yaman, Y. I., Basaran, M., and Kocabas, A. (2020). Dynamics of pattern formation and emergence of swarming in Caenorhabditis elegans. *eLife* 9:e52781. doi: 10.7554/eLife.52781

Devreotes, P., and Horwitz, A. R. (2015). Signaling networks that regulate cell migration. *Cold Spring Harb. Perspect. Biol.* 7:a005959. doi: 10.1101/cshperspect.a005959

Deygas, M., Gadet, R., Gillet, G., Rimokh, R., Gonzalo, P., and Mikaelian, I. (2018). Redox regulation of EGFR steers migration of hypoxic mammary cells towards oxygen. *Nat. Commun.* 9:4545. doi: 10.1038/s41467-018-06988-6983

Dunwoodie, S. L. (2009). The role of hypoxia in development of the Mammalian embryo. *Dev. Cell* 17, 755–773. doi: 10.1016/j.devcel.2009.11.008

Edmond, V., Dufour, F., Poiroux, G., Shoji, K., Malleter, M., Fouqué, A., et al. (2015). Downregulation of ceramide synthase-6 during epithelial-to-mesenchymal transition reduces plasma membrane fluidity and cancer cell motility. *Oncogene* 34, 996–1005. doi: 10.1038/onc.2014.55

Emre, B., Johanna, K., and Yvonne, S. (2021). Redox Regulation of the actin cytoskeleton in cell migration and adhesion: on the way to a spatiotemporal view. *Front Cell Dev. Biol.* 8. doi: 10.3389/fcell.2020.618261

Fey, P., Dodson, R. J., Basu, S., Hartline, E. C., and Chisholm, R. L. (2019). dictyBase and the Dicty Stock Center (version 2.0) - a progress report. *Int. J. Dev. Biol.* 63, 563–572. doi: 10.1387/ijdb.190226pf

Fisher, P. R., and Annesley, S. J. (2006). Slug phototaxis, thermotaxis, and spontaneous turning behavior. *Meth. Mol. Biol.* 346, 137–170.

Gao, R., Zhao, S., Jiang, X., Sun, Y., Zhao, S., Gao, J., et al. (2015). A large-scale screen reveals genes that mediate electrotaxis in Dictyostelium discoideum. *Sci. Signal.* 8:ra50. doi: 10.1126/scisignal.aab0562

Garcia, M. X. U., Foote, C., van Es, S., Devreotes, P. N., Alexander, S., and Alexander, H. (2000). Differential developmental expression and cell type specificity of Dictyostelium catalases and their response to oxidative stress and UV-light. *Biochim. Biophys. Acta* 1492, 295–310. doi: 10.1016/s0167-4781(00)00063-4

Garcia, M. X. U., Roberts, C., Alexander, H., Stewart, A. M., Harwood, A., Alexander, S., et al. (2002). Methanol and acriflavine resistance in Dictyostelium are caused by loss of catalase. *Microbiology* 148, 333–340. doi: 10.1099/00221287-148-1-333

Gray, J. M., Karow, D. S., Lu, H., Chang, A. J., Chang, J. S., Ellis, R. E., et al. (2004). Oxygen sensation and social feeding mediated by a *C. elegans* guanylate cyclase homologue. *Nature* 430, 317–322. doi: 10.1038/nature02714

Guertin, D. A., Stevens, D. M., Thoreen, C. C., Burds, A. A., Kalaany, N. Y., Moffat, J., et al. (2006). Ablation in mice of the mTORC components raptor, rictor, or mLST8 reveals that mTORC2 is required for signaling to Akt-FOXO and PKCalpha, but not S6K1. *Dev. Cell* 11, 859–871. doi: 10.1016/j.devcel.2006.10.007

Guido, I., Diehl, D., Olszok, N. A., and Bodenschatz, E. (2020). Cellular velocity, electrical persistence and sensing in developed and vegetative cells during electrotaxis. *PLoS One* 15:e0239379. doi: 10.1371/journal.pone.0239379

Hayashi, H., and Suga, T. (1978). Some characteristics of peroxisomes in the slime mold, Dictyostelium discoideum. *J. Biochem.* 84, 513–520. doi: 10.1093/oxfordjournals.jbchem.a132155

Horsman, M. R., and Overgaard, J. (2016). The impact of hypoxia and its modification of the outcome of radiotherapy. *J. Radiat. Res.* 57, 90–98. doi: 10.1093/jrr/rrw007

Hurd, T. R., DeGennaro, M., and Lehmann, R. (2012). Redox regulation of cell migration and adhesion. *Trends Cell Biol.* 22, 107–115. doi: 10.1016/j.tcb.2011.11.002

Jain, I. H., Calvo, S. E., Markhard, A. L., Skinner, O. S., To, T. L., Ast, T., et al. (2020). Genetic screen for cell fitness in high or low oxygen highlights mitochondrial and lipid metabolism. *Cell* 181, 716–727.e11. doi: 10.1016/j.cell.2020.03.029

Jeon, T. J., Gao, R., Kim, H., Lee, A., Jeon, P., Devreotes, P. N., et al. (2019). Cell migration directionality and speed are independently regulated by RasG and Gβ in Dictyostelium cells in electrotaxis. *Biol. Open* 8:bio042457. doi: 10.1242/bio.042457

Kirkegaard, J. B., Bouillant, A., Marron, A. O., Leptos, K. C., and Goldstein, R. E. (2016). Aerotaxis in the closest relatives of animals. *eLife* 5:e18109. doi: 10.7554/eLife.18109

Lambert, A. W., Pattabiraman, D. R., and Weinberg, R. A. (2017). Emerging biological principles of metastasis. *Cell* 168, 670–691. doi: 10.1016/j.cell.2016.11.037

Lee, S., Comer, F. I., Sasaki, A., McLeod, I. X., Duong, Y., Okumura, K., et al. (2005). TOR complex 2 integrates cell movement during chemotaxis and signal relay in Dictyostelium. *Mol. Biol. Cell* 16, 4572–4583. doi: 10.1091/mbc.e05-04-0342

Lewis, D. M., Park, K. M., Tang, V., Xu, Y., Pak, K., and Eisinger-Mathason, T. S. E. A. (2016). Intratumoral oxygen gradients mediate sarcoma cell invasion. *Proc. Natl. Acad. Sci. U S A.* 113, 9292–9297. doi: 10.1073/pnas.1605317113

Lilly, P., Wu, L. J., Welker, D. L., and Devreotes, P. N. (1993). A G-protein beta-subunit is essential for Dictyostelium development. *Genes Dev.* 7, 986–995. doi: 10.1101/gad.7.6.986

Lima, W. C., Vinet, A., Pieters, J., and Cosson, P. (2014). Role of PKD2 in rheotaxis in Dictyostelium. *PLoS One* 9:e88682. doi: 10.1371/journal.pone.0088682

Mathavarajah, S., VanIderstine, C., Dellaire, G., and Huber, R. J. (2021). Cancer and the breakdown of multicellularity: what Dictyostelium discoideum, a social amoeba, can teach us. *Bioessays* 43:e2000156. doi: 10.1002/bies.202000156

Meili, R., Ellsworth, C., and Firtel, R. A. (2000). A novel Akt/PKB-related kinase is essential for morphogenesis in Dictyostelium. *Curr. Biol.* 10, 708–717. doi: 10.1016/s0960-9822(00)00536-4

Muz, B., de la Puente, P., Azab, F., and Azab, A. K. (2015). The role of hypoxia in cancer progression, angiogenesis, metastasis, and resistance to therapy. *Hypoxia (Auckl)* 3, 83–92. doi: 10.2147/hp.s93413

Nagura, M., Saito, M., Iwamori, M., Sakakihara, Y., and Igarashi, T. (2004). Alterations of fatty acid metabolism and membrane fluidity in peroxisome-defective mutant ZP102 cells. *Lipids* 39, 43–50. doi: 10.1007/s11745-004-1200-z

Noegel, A., Harloff, C., Hirth, P., Merkl, R., Modersitzki, M., Stadler, J., et al. (1985). Probing an adhesion mutant of Dictyostelium discoideum with cDNA clones and monoclonal antibodies indicates a specific defect in the contact site A glycoprotein. *EMBO J.* 4, 3805–3810

Pal, D. S., Li, X., Banerjee, T., Miao, Y., and Devreotes, P. N. (2019). The excitable signal transduction networks: movers and shapers of eukaryotic cell migration. *Int. J. Dev. Biol.* 63, 407–416. doi: 10.1387/ijdb.190265pd

Parish, R. W. (1975). Mitochondria and peroxisomes from the cellular slime mould Dictyostelium discoideum. Isolation techniques and urate oxidase association with peroxisomes. *Eur. J. Biochem.* 58, 523–531. doi: 10.1111/j.1432-1033.1975.tb02401.x

Parks, S. K., Cormerais, Y., and Pouysségur, J. (2017). Hypoxia and cellular metabolism in tumour pathophysiology. *J. Physiol.* 595, 2439–2450. doi: 10.1113/jp273309

Pastushenko, I., and Blanpain, C. (2019). EMT transition states during tumor progression and metastasis. *Trends Cell Biol.* 29, 212–226. doi: 10.1016/j.tcb.2018.12.001

Pearce, L. R., Komander, D., and Alessi, D. R. (2010). The nuts and bolts of AGC protein kinases. *Nat. Rev. Mol. Cell Biol.* 11, 9–22. doi: 10.1038/nrm2822

Pergolizzi, B., Bozzaro, S., and Bracco, E. (2017a). G-Protein dependent signal transduction and ubiquitination in Dictyostelium. *Int. J. Mol. Sci.* 18:2180. doi: 10.3390/ijms18102180

Pergolizzi, B., Bracco, E., and Bozzaro, S. (2017b). A new HECT ubiquitin ligase regulating chemotaxis and development in Dictyostelium discoideum. *J. Cell Sci.* 130, 551–562. doi: 10.1242/jcs.194225

Pergolizzi, B., Peracino, B., Silverman, J., Ceccarelli, A., Noegel, A., Devreotes, P., et al. (2002). Temperature-sensitive inhibition of development in Dictyostelium due to a point mutation in the piaA gene. *Dev. Biol.* 251, 18–26. doi: 10.1006/dbio.2002.0809

Rankin, E. B., and Giaccia, A. J. (2016). Hypoxic control of metastasis. *Science* 352, 175–180. doi: 10.1126/science.aaf4405

Rey, S., and Semenza, G. L. (2010). Hypoxia-inducible factor-1-dependent mechanisms of vascularization and vascular remodelling. *Cardiovasc. Res.* 1, 236–242. doi: 10.1093/cvr/cvq045

Sandonà, D., Gastaldello, S., Rizzuto, R., and Bisson, R. (1995). Expression of cytochrome c oxidase during growth and development of Dictyostelium. *J. Biol. Chem.* 270, 5587–5593. doi: 10.1074/jbc.270.10.5587

Schiavo, G., and Bisson, R. (1989). Oxygen influences the subunit structure of cytochrome c oxidase in the slime mold Dictyostelium discoideum. *J. Biol. Chem.* 264, 7129–7134. doi: 10.1016/s0021-9258(18)83211-2

Semenza, G. L. (2012). Hypoxia-inducible factors in physiology and medicine. *Cell* 148, 399–408. doi: 10.1016/j.cell.2012.01.021

Sepasi Tehrani, H., and Moosavi-Movahedi, A. A. (2018). Catalase and its mysteries. *Prog. Biophys. Mol. Biol.* 140, 5–12. doi: 10.1016/j.pbiomolbio.2018.03.001

Seyfried, T. N., and Huysentruyt, L. C. (2013). On the origin of cancer metastasis. *Crit. Rev. Oncog.* 18, 43–73. doi: 10.1615/critrevoncog.v18.i1-2.40

Sporer, A. J., Kahl, L. J., Price-Whelan, A., and Dietrich, L. E. P. (2017). Redox-Based regulation of bacterial development and behavior. *Annu. Rev. Biochem.* 86, 777–797. doi: 10.1146/annurev-biochem-061516-44453

Sternfeld, J., and Bonner, J. T. (1977). Cell differentiation in Dictyostelium under submerged conditions. *Proc. Natl. Acad. Sci. U S A.* 74, 268–271. doi: 10.1073/pnas.74.1.268

Sternfeld, J., and David, C. N. (1981). Oxygen gradients cause pattern orientation in Dictyostelium cell clumps. *J. Cell Sci.* 50, 9–17.

Stuelten, C. H., Parent, C. A., and Montell, D. J. (2018). Cell motility in cancer invasion and metastasis: insights from simple model organisms. *Nat. Rev. Cancer* 18, 296–312. doi: 10.1038/nrc.2018.15

Taraboletti, G., Perin, L., Bottazzi, B., Mantovani, A., Giavazzi, R., and Salmona, M. (1989). Membrane fluidity affects tumor-cell motility, invasion and lung-colonizing potential. *Int. J. Cancer* 44, 707–713. doi: 10.1002/ijc.2910440426

Taylor, B. L., Zhulin, I. B., and Johnson, M. S. (1999). Aerotaxis and other energy-sensing behavior in bacteria. *Annu. Rev. Microbiol.* 53, 103–128. doi: 10.1146/annurev.micro.53.1.103

Trigos, A. S., Pearson, R. B., Papenfuss, A. T., and Goode, D. L. (2018). How the evolution of multicellularity set the stage for cancer. *Br. J. Cancer* 118, 145–152. doi: 10.1038/bjc.2017.398

Weeks, G., and Herring, F. G. (1980). The lipid composition and membrane fluidity of Dictyostelium discoideum plasma membranes at various stages during differentiation. *J. Lipid. Res.* 21, 681–686.

Wilson, D. F. (2017). Oxidative phosphorylation: regulation and role in cellular and tissue metabolism. *J. Physiol.* 595, 7023–7038. doi: 10.1113/jp273839

Zhao, M., Jin, T., McCaig, C. D., Forrester, J. V., and Devreotes, P. N. (2002). Genetic analysis of the role of G protein-coupled receptor signaling in electrotaxis. *J. Cell Biol.* 157, 921–927. doi: 10.1083/jcb.200112070

Zhao, W., Prijic, S., Urban, B. C., Tisza, M. J., Zuo, Y., Li, L., et al. (2016). Candidate antimetastasis drugs suppress the metastatic capacity of breast cancer cells by reducing membrane fluidity. *Cancer Res.* 76, 2037–2049. doi: 10.1158/0008-5472.can-15-1970

Conflict of Interest: The authors declare that the research was conducted in the absence of any commercial or financial relationships that could be construed as a potential conflict of interest.

Publisher's Note: All claims expressed in this article are solely those of the authors and do not necessarily represent those of their affiliated organizations, or those of the publisher, the editors and the reviewers. Any product that may be evaluated in this article, or claim that may be made by its manufacturer, is not guaranteed or endorsed by the publisher.

Copyright © 2021 Biondo, Panuzzo, Ali, Bozzaro, Osella, Bracco and Pergolizzi. This is an open-access article distributed under the terms of the Creative Commons Attribution License (CC BY). The use, distribution or reproduction in other forums is permitted, provided the original author(s) and the copyright owner(s) are credited and that the original publication in this journal is cited, in accordance with accepted academic practice. No use, distribution or reproduction is permitted which does not comply with these terms.

frontiers | Frontiers in Cell and Developmental Biology

ORIGINAL RESEARCH
published: 13 April 2022
doi: 10.3389/fcell.2022.741967

The *Dictyostelium* Model for Mucolipidosis Type IV

*Claire Y. Allan and Paul R. Fisher**

Department of Physiology, Anatomy and Microbiology, La Trobe University, Melbourne, VIC, Australia

Mucolipidosis type IV, a devastating neurological lysosomal disease linked to mutations in the transient receptor potential channel mucolipin 1, TRPML1, a calcium permeable channel in the membranes of vesicles in endolysosomal system. TRPML1 function is still being elucidated and a better understanding of the molecular pathogenesis of Mucolipidosis type IV, may facilitate development of potential treatments. We have created a model to study mucolipin function in the eukaryotic slime mould *Dictyostelium discoideum* by altering expression of its single mucolipin homologue, *mcln*. We show that in *Dictyostelium* mucolipin overexpression contributes significantly to global chemotactic calcium responses in vegetative and differentiated cells. Knockdown of mucolipin also enhances calcium responses in vegetative cells but does not affect responses in 6–7 h developed cells, suggesting that in developed cells mucolipin may help regulate local calcium signals rather than global calcium waves. We found that both knocking down and overexpressing mucolipin often, but not always, presented the same phenotypes. Altering mucolipin expression levels caused an accumulation or increased acidification of Lysosensor Blue stained vesicles in vegetative cells. Nutrient uptake by phagocytosis and macropinocytosis were increased but growth rates were not, suggesting defects in catabolism. Both increasing and decreasing mucolipin expression caused the formation of smaller slugs and larger numbers of fruiting bodies during multicellular development, suggesting that mucolipin is involved in initiation of aggregation centers. The fruiting bodies that formed from these smaller aggregates had proportionately larger basal discs and thickened stalks, consistent with a regulatory role for mucolipin-dependent Ca^{2+} signalling in the autophagic cell death pathways involved in stalk and basal disk differentiation in *Dictyostelium*. Thus, we have provided evidence that mucolipin contributes to chemotactic calcium signalling and that *Dictyostelium* is a useful model to study the molecular mechanisms involved in the cytopathogenesis of Mucolipidosis type IV.

Keywords: mucolipidosis IV, calcium signalling, acidic vesicles, lysosomes, endocytosis, plasma membrane, aggregation, growth

OPEN ACCESS

Edited by:
Robert J. Huber,
Trent University, Canada

Reviewed by:
Stephane Lefrancois,
Université du Québec, Canada
Sabateeshan Mathavarajah,
Dalhousie University, Canada
Pierre Cosson,
Université de Genève, Switzerland

***Correspondence:**
Paul R. Fisher
p.fisher@latrobe.edu.au

Specialty section:
This article was submitted to Molecular and Cellular Pathology, a section of the journal Frontiers in Cell and Developmental Biology

Received: *15 July 2021*
Accepted: *21 March 2022*
Published: *13 April 2022*

Citation:
Allan CY and Fisher PR (2022) The Dictyostelium Model for Mucolipidosis Type IV. Front. Cell Dev. Biol. 10:741967. doi: 10.3389/fcell.2022.741967

1 INTRODUCTION

Transient receptor potential mucolipins (TRPML) belong to a conserved family of ion channels (Dong et al., 2010), which localize to the membranes of components of the endocytic pathway. The three mammalian mucolipin homologues, TRPML1, TRPML2 and TRPML3, are encoded by the genes *MCOLN 1–3* (Cheng et al., 2010; Grimm et al., 2012). TRPML channels are non-selective

cation channels permeable to a range of cations. Alongside two pore channels (TPC), TRPML channels are believed to facilitate endolysosomal Ca^{2+} signalling which regulates trafficking and sorting of the membranes of endocytic vesicles (Cheng et al., 2010), organelle homeostasis, compartmental acidification (Gerasimenko et al., 1998; Dong et al., 2010; Morgan et al., 2011) and homotypic and heterotypic vesicle fusion and reformation (Pryor et al., 2000; Hay, 2007; Luzio et al., 2007; Brailoiu and Brailoiu, 2016; Cao et al., 2017). Additionally, TRPML1 is implicated in regulation of autophagy, mechanistic target of rapamycin (mTOR) and transcription factor EB (TFEB) signalling (Sun et al., 2018; Boudewyn and Walkley, 2019). Loss of function mutations in TRPML1, causes the neurological disease Mucolipidosis Type IV (MLIV) (Sun et al., 2000), and TRPML-associated dysfunction in the endolysosomal system is implicated in other neurodegenerative diseases (Santoni et al., 2020; Lee et al., 2021). Therefore, TRPMLs may underpin the pathophysiology of neurodegenerative disease more generally and are suggested to be a therapeutic target.

It is not well understood how loss TRPML1 function causes lysosomal storage and neuronal dysfunction, but it is believed that Ca^{2+} signalling plays a central role. The vesicles of the endolysosomal system are essential to maintenance of cellular homeostasis through macromolecule recycling and are important Ca^{2+} storage organelles which are integral to cellular Ca^{2+} signalling (Patel and Docampo, 2010; Patel and Cai, 2015) and can help regulate ER calcium signals by sequestering calcium (López-Sanjurjo et al., 2013; López-Sanjurjo et al., 2014). Ca^{2+}-dependent signalling is thought to regulate the soluble N-ethylmaleimide-sensitive-factor attachment protein receptors (SNARE) complex proteins, which are proteins involved in the fusion of vesicle membranes (Bharat et al., 2014; Han et al., 2017). Alongside SNAREs, the protein early endosome antigen-1 (EEA1) is necessary for vesicle tethering prior to fusion, and is regulated by Ca^{2+}/calmodulin dependent signalling through its IQ domain (Mills et al., 1998; Christoforidis et al., 1999; Lawe et al., 2003). TRPML specific perilysosomal calcium signals have been notoriously difficult to measure due to the localised nature of the signals which are often clouded by larger global calcium signals. In an attempt to resolve the local calcium signals genetically encoded calcium sensors directly tagged to TRPML1 have been used to measure local calcium transients (Shen et al., 2012; Cao et al., 2015; Medina et al., 2015). The TRPML agonist ML-SA1 stimulates calcium release into the cytoplasm (Shen et al., 2012), which in some cell types is independent of extracellular and ER calcium pools (Gómez et al., 2018). However, some evidence shows that TRPML channels can affect ER calcium release and activate influx of calcium across the plasma membrane to contribute to global calcium signals (Kilpatrick et al., 2016), and small calcium release from the acidic stores can prime and amplify calcium release from the ER (Ronco et al., 2015).

A variety of model organisms have been used to study TRPML proteins including the mouse (Kim et al., 2007; Micsenyi et al., 2009; Curcio-Morelli et al., 2010), zebrafish (Benini et al., 2013), *Drosophila* (Venkatachalam et al., 2008; Wong et al., 2012; Feng et al., 2014), *C. elegans* (Fares and Greenwald, 2001; Treusch et al., 2004) and yeast (Denis and Cyert, 2002). One important cellular model, the eukaryotic social amoeba, *Dictyostelium*, encodes a single mucolipin homologue, *mcln* (Wilczynska et al., 2005; Lima et al., 2012) which has been the subject of only a limited number of studies. *Dictyostelium* is a well-established model to study neurodegenerative and lysosomal disease (Annesley and Fisher 2009; Maniak, 2011; Annesley et al., 2014; Martín-González et al., 2021). This model organism has been extensively employed to study neuronal ceroid lipofuscinosis (NCL) (Huber, 2020), a group of lysosomal diseases linked to mutations in the genes, *CLN1–CLN8* and *CLN10–CLN14* (Yap et al., 2021). Therefore, *Dictyostelium* is an ideal model to study lysosomal disorders and mucolipin function. In other work, expression of FLAG-tagged mucolipin was used to show that the protein localizes predominately to post-lysosomes, but may also be present in other endocytic compartments (Lima et al., 2012), and accordingly controls lysosome exocytosis. Evidence suggests that mucolipin is involved in Ca^{2+} homeostasis and signalling because knockout cells had reduced Ca^{2+} concentrations in secretory lysosomes (Lima et al., 2012) and are also defective in rheotaxis, a calcium-regulated mechanosensing mechanism (Lima et al., 2014). The role of this putative channel in Ca^{2+} signalling has not been studied, so it was of particular interest to investigate the role of mucolipin in chemotactic calcium signalling in *Dictyostelium*.

Dictyostelium is a well-established model to study calcium signalling, and cells experience cytosolic calcium transients when stimulated with various extracellular stimuli including the chemoattractants cAMP and folic acid (Nebl and Fisher, 1997; Traynor et al., 2000; Nebl et al., 2002; Schaloske et al., 2005; Fisher and Wilczynska, 2006; Malchow et al., 2008). These Ca^{2+} signals originate from the extracellular environment, the endoplasmic reticulum (ER) (Wilczynska et al., 2005) and the contractile vacuole (CV) (Malchow et al., 2006; Gross, 2009). Other intracellular Ca^{2+} stores including mitochondria, acidocalcisomes and vesicles of the endocytic pathway are likely to also contribute to the calcium responses. Given the localisation of mucolipin at the post-lysosomes and potentially other vesicles of the endocytic pathway, we decided to determine if mucolipin and these endocytic vesicles are involved in cytosolic Ca^{2+} responses to chemoattractants.

To achieve this, we created mucolipin overexpression and knockdown strains which coexpress the calcium-sensitive luminescent protein apoaequorin which allowed us to analyze real-time chemotactic induced cytoplasmic Ca^{2+} responses (Nebl and Fisher, 1997). Our experiments revealed that when overexpressed, mucolipin is involved in chemoattractant-elicited Ca^{2+} responses because overexpression strains had enhanced responses to both cAMP and folic acid. Surprisingly, chemoattractant Ca^{2+} responses in knockdown strains were also enhanced, but only in vegetative cells. Responses in aggregation-competent cells were not affected in the knockdown strains, suggesting that, unless overexpressed, mucolipin is not a major contributor to cAMP-mediated calcium responses. However, it may be involved in local Ca^{2+} signalling associated with changes in the vesicle trafficking pathways throughout the developmental cycle, in particular aggregation center formation and autophagic

cell death. In other work, the cellular phenotypes of growth, endocytosis and multicellular development were found to be unaffected in mucolipin knockout cells created from the parental strain DH1-10 (Lima et al., 2012). Therefore, we decided to analyze these phenotypes in our strains which were created from the parental strain AX2. We discovered that mucolipin expression did affect growth rates and nutrient uptake via macropinocytosis and phagocytosis in AX2. Surprisingly however, the phenotypes were not linear in that both increasing and decreasing expression of mucolipin often, but not always, resulted in the same phenotypic outcome. Both overexpression and knockdown strains had increased fluorescence in cells stained with Lysosensor blue, indicating either increased acidification of the vesicles or increased abundance of the vesicles. Phagocytosis and pinocytosis rates were upregulated, but this did not correlate with an increase in growth rates, which suggests defects in catabolism, in endocytic vesicle trafficking or in endolysosomal breakdown of macromolecular contents. Mucolipin is involved in the regulation of aggregation as both overexpression and knockdown strains formed smaller, more numerous slugs and fruiting bodies than AX2, a phenotype that is also present in other *Dictyostelium* lysosomal disease models of NCL (Huber et al., 2014; Huber et al., 2017; Smith et al., 2019; McLaren et al., 2021). Increased numbers of cells entering the autophagic cell death pathway were also evident in mucolipin mutants because they had thickened stalks compared to AX2. Our results suggest that normal growth and development of *Dictyostelium* is sensitive to mucolipin expression, and our strains show similar phenotypes to other *Dictyostelium* lysosomal disease models further affirming that *Dictyostelium* is an ideal model to study lysosomal disease.

2 MATERIALS AND METHODS

2.1 Gene Cloning and Sequence Analysis

To create a mucolipin overexpression construct, the 2,599 bp *mcln* genomic DNA (DictyBase gene no. DDB_G0291275) was amplified in two sections from parental strain AX2 genomic DNA using the primers MUF (CGCGGATCCATCGAT*ATG*ACATCT TTTAAAGGTGACAG) and MuMR (AACTAAC**GGT ACC**AGGTACTTC) for the 5′ fragment, and MuMF (GAA GTACCT**GGTACC**GTTAGTTC) and MUR2 (CGCGGA TCCCTCGAGCATCATATC TCAATACCTGAATC) for the 3′ fragment. A three fragment ligation allowed the full length genomic DNA to be cloned into the bacterial vector pZErO™-2(Invitrogen, Carlsbad, CA, United States) with the restriction enzyme *Bam*HI (underlined). To join the 5′ and 3′ fragments of the gene together, the primers used in amplification of the two fragments spanned a region of the gene that encodes the restriction site *Kpn*I (bold) this allowed seamless ligation of the two gene fragments. The full-length gene was then subcloned for overexpression into the *Dictyostelium* vector pA15GFP using the restriction cut sites *Cla*I and *Xho*I, this plasmid was named pPROF638. To create the *mcln* antisense RNA inhibition plasmid (pPROF650) a fragment encoding 1411bp of the gene from position 1365bp to position 3776bp in the gDNA sequence was amplified via PCR with the primers MuMF (GAAGTACCT**GGTACC**GTTAGTTC) and MUR2 (CGCGGATCCCTCGAGCATCATATC TCAATACCTGAATC) from genomic DNA extracted from vegetative AX2 cells using DNAzol® (Invitrogen). The products were then cloned into pZErO™-2 using *Bam*H1 and *Kpn*1 and subcloned into the *Dictyostelium* expression vector pDNeo2 (Witke et al., 1987) with *Bam*H1 and *Kpn*1. Clones were verified by restriction digestion as well as sequencing at the Australian Genome Research Facility, Brisbane, Australia. Sequence analyses, alignments, and database searches were conducted using Web-based software through DictyBase.org (Fey et al., 2009), ExPASy and the Australian Genome Research Facility.

2.2 Strains and Culture Conditions

All experiments were conducted with *Dictyostelium* parental strain AX2, and transformants derived from it (names beginning with HPF). Each transformant strain carried multiple copies of the constructs: 1) pPROF120 (apoaequorin expression plasmid) and pPROF650 (antisense strains: HPF812-818, HPF640); 2) pPROF120 and pPROF652 (sense strains: HFP819 and HPF861) and 3) pPROF120 and pPROF638 (overexpression strains: HPF820-829, HFP654-656). The $Ca(PO_4)_2$/DNA coprecipitation method was used to isolate all transformants, by cotransformation with both plasmids (Nellen et al., 1984). Transformants were selected as isolated colonies on lawns of *Micrococcus luteus* (Wilczynska and Fisher, 1994) on standard medium agar [(SM) 1.0% (w/v) Oxoid agar; 1.0% (w/v) Oxoid bacteriological peptone; 1.0% (w/v) glucose; 0.1% (w/v) Oxoid yeast extract; 4.1 mM $MgSO_4{\cdot}7H_2O$; 16.2 mM KH_2PO_4; 5.8 mM K_2HPO_4 supplemented with 20 μg ml^{-1} Geneticin (G-418) (Promega Corporation, Madison, WI, United States)]. *D. discoideum* cells were grown on lawns of *Enterobacter aerogenes* as a food source on SM (Standard Medium) nutrient agar and incubated at 21°C for 3–4 days and subcultured as required from a single colony. To prepare liquid cultures, 5–10 spores were inoculated into a well of a 24-well Costar plate containing 1.5 ml HL5 axenic medium (1% (w/v) Bacto™ proteose peptone; 0.5% (w/v) Bacto™ yeast extract; 2.8 mM $Na_2HPO_4{\cdot}2H_2O$; 2.6 mM KH_2PO_4; 1% (w/v) glucose pH 6.4) supplemented with geneticin (20 μg ml^{-1}), ampicillin (100 μg ml^{-1}), streptomycin (500 μg ml^{-1}) and tetracycline (100 μg ml^{-1}), and incubated at 21°C to allow spores to germinate and form amoebae. Once confluence was reached 1 ml of culture was inoculated into 10 ml HL5 in T25 flask (Falcon) and cells were grown to the density of 1–2 × 10^6 cells ml^{-1} shaking at 150 rpm and 21°C. Strains were then subcultured at least once into HL5 without antibiotics and grown for 24–48 h prior to use in phenotypic assays to remove possible effects of the antibiotics on phenotypic readouts. Unless otherwise stated, cells were harvested by centrifugation at 500 ×*g* for 5 min.

2.3 Estimation of Plasmid Copy Number

Genomic DNA was extracted from transformants using DNAzol® (Invitrogen). Quantitative Southern blot was used to estimate

plasmid copy number of *mcln* overexpression strains (Fernando et al., 2020). DNA loaded gels were stained with SYBR® Green I nucleic acid gel stain (Sigma-Aldrich®) and DNA was quantified using the Storm 860 Fluroimager (GE Healthcare, United Kingdom) in fluorescence mode. Southern blots of the same DNA samples were quantitated using fluorescein-labelled DNA probes, in conjunction with anti-fluorescein alkaline peroxidase conjugate antibody, and enhanced with the chemi-fluorescein substrate (GE Healthcare, United Kingdom). The Storm 860 Fluroimager fluorescence mode was used to quantitate Southern blots.

Quantitative real time PCR was used to estimate plasmid copy number in *mcln* antisense RNA strains (Fernando et al., 2020). SYBR® Green (BioRad, Hercules, CA, United States) was used for amplicon detection of a 135 bp fragment of *mcln* with the primers (500 nM final concentration) MF1.1 (5-GATTGGTCTTGGTAC TTTGTTA-3) and MR1.2 (5-GGGAGACTTCCAGCCGAG-3), within the genomic DNA extracts, and to construct a standard curve, over a range of DNA concentrations using purified pPROF650 as a template. To quantify genomic DNA extracts a 100 bp filamin amplicon was amplified with the primers FIL1588F (5-CCCTCAATGATGAAGCC-3) and FIL1688R (5-CCATCTAAACCTGGACC-3) in genomic DNA from all strains, and the concentrations calculated from a standard curve. The PCR amplification used 35 cycles of denaturation at 95°C for 30 s, annealing at 58°C for 30 s and extension and data collection at 72°C for 1 min.

2.4 Expression Analysis

Quantitative real time RT-PCR was used to quantitate expression levels of *mcln* messenger RNA. RNA was collected from 10^7 vegetative cells or developing cells harvested from water agar at the time points indicated over the course of development, and extracted using TRIzol® (Invitrogen). The iScript™ One-Step RT-PCR Kit with SYBR® Green (BioRad, Hercules, CA, United States) was used for amplicon detection of a 135 bp fragment of *mcln* with the primers MF1.1 and MR1.2, and a 100 bp amplicon of the constitutively expressed protein filamin, with the primers FIL1588F and FIL1688R. A total RNA template of 50–100 ng was added to the total reaction mixture of 50 µl; cDNA synthesis was performed at 50°C for 10 min, and the PCR amplification used 35 cycles of denaturation at 95°C for 30 s, annealing at 58°C for 30 s and extension and data collection at 72°C for 1 min. Expression levels were normalised against the filamin levels to adjust for loading and then measured relative to AX2 controls.

2.5 Protein Techniques

2.5.1 Antibody Production

A polyclonal antibody called anti-MUECD directed against the *Dictyostelium* mucolipin was used in the study. A 200aa His-tagged portion of mucolipin (aa101–aa301) was expressed in *E. coli* and purified by Genscript®. Polyclonal antibodies directed against MUECD were raised in a rabbit by the Institute of Medical and Veterinary Science (Adelaide, SA, Australia), and affinity purified as described previously (Smith and Fisher, 1984).

2.5.2 Western Blot

Cells were grown in HL5 medium and 1×10^6 cells harvested and lysed in 100 µl 1 × Bolt LDS sample buffer (Thermo Fisher Scientific) with a protease inhibitor 1 cocktail (Complete-EDTA free, Roche) on ice from 30 min then centrifuged at 1,200 rpm for 2 min. 10 µl of lysate was mixed with 1% Bolt sample reducing agent (Thermo Fisher Scientific) was incubated at 70°C for 10 min then loaded onto a Bolt™ 4–12%, Bis-Tris-Plus, 1.0 mm, Protein Gel, 12-well (Invitrogen) with the Broad Multi Color Pre-Stained Protein Standard (Genscript) and subject to electrophoresis. To visualise the protein bands, protein was transferred to PVDF membrane (Amersham Hybond™-P, GE Healthcare) for 1 h at 100 V at 4°C. Protein was visualised on the membrane by staining with No Stain Protein Labelling Reagent (Invitrogen) as per the manufactures instructions, and visualised on a Bio Rad Chemidoc MP imaging system. Membraned we then blocked with 1% casein in 1 × TBS for 3 h RT and probed with polyclonal rabbit anti-MUECD 1:500 in 1% casein in 1 × TBS with 0.1% Tween-20 for 2 h RT. The SNAP i.d.® 2.0 Protein Detection System was used for application of anti-rabbit HRP conjugate (Life technologies) 1: 10,000 in TBS-T as per manufacturer's instructions. Bands were detected with Clarity Western ECL substrate (Bio Rad), with chemiluminescence imaged on Amersham Imager 600 (GE Healthcare Life Sciences). The intensities of the total loaded protein in each lane and specific antigen bands were quantified digitally using the Image Quant TL 1D v 8.1 software 19 (GE Healthcare Life Sciences).

2.6 Determination of Growth Rates

2.6.1 Growth on Bacterial Lawns

Growth rates of *Dictyostelium* on lawns of bacteria were measured as previously described (Bokko et al., 2007). Lawns of *E. coli* B2 were prepared on normal agar [20 g L^{-1} agar (Difco, Detroit, MI, United States); 1 g L^{-1} peptone (Oxoid, Basingstoke, United Kingdom), 1.1 g L^{-1} anhydrous glucose, 1.9972 g L^{-1} KH_2PO_4, and 0.356 g L^{-1} $Na_2HPO_4{\cdot}2H_2O$, pH 6.0]. An aliquot of 20 µl of *Dictyostelium* culture at a density of 1×10^6 cells ml^{-1}, was inoculated onto the center of each lawn and incubated at 21°C for 100 h, during which time the plaque diameter (mm) was measured at intervals of 8–12 h. The recorded values were analyzed by linear regression using the "R" environment for statistical computing and graphics (http://www.R-project.org) to determine the plaque expansion rate (mm/h).

2.6.2 Growth Rates of Axenically Growing Cultures

Generation times of axenically growing *Dictyostelium* cultures was measured as previously described (Bokko et al., 2007). Cultures of *Dictyostelium* were grown to exponential phase in HL5 medium to a density of ~1–2 × 10^6 cells ml^{-1} and were used to inoculate 50 ml of fresh HL5 medium (no antibiotics) to an initial density of 1×10^4 cells ml^{-1}. Cultures were incubated at 21°C on an orbital shaker at 150 rpm for 100 h, during which time cell densities were determined at 8–12 h intervals, by counting 10 µl aliquots using a hemocytometer. The cell densities were then analyzed by log-linear regression using the "R"

programming environment computer software to determine the generation time from the exponential growth curve.

2.7 Measurements of Macropinocytosis Rates

Measurements of macropinocytosis rates as previously described (Bokko et al., 2007), were performed using fluorescein isothiocyanate (FITC)-dextran (Sigma-Aldrich; average mol. mass, 70 kDa; working concentration, 2 mg ml^{-1} in HL5 growth medium). Cultures of axenically growing *Dictyostelium* cells were harvested, and resuspended in fresh HL5 medium and shaken at 150 rpm for 30 min at 21°C, and after the addition of FITC-dextran, duplicate aliquots at time points 0 and 70 min were lysed in 0.25% (vol/vol) Triton X-100 in 100 mM Na_2HPO_4, pH 9.2 and the fluorescence of the lysate was measured in a Modulus fluorometer (Turner BioSystems) using the (Green Module 525 nm excitation and 580–640 nm emission). The cell density, increase in fluorescence over 70 min, and a separate calibration curve relating fluorescence signal to the volume of fluorescent medium, were used to calculate the hourly rate of uptake of medium.

2.8 Measurements of Phagocytosis Rates

The rate of uptake of *E. coli* expressing the fluorescent protein DsRed (Maselli et al., 2002) was used to measure phagocytosis rates in *Dictyostelium* strains. DsRed-expressing *E. coli* (DsRed-Ec) cells were harvested from NB cultures (containing 75 μg ml^{-1} ampicillin and 1 mM IPTG), grown at 37°C shaking for 24 h and resuspended to a density of 2–4 × 10^{10} bacteria ml^{-1} in 20 mM Sorenson's buffer (2.353 mM $Na_2HPO_42H_2O$ and 17.65 mM KH_2PO_4, pH 6.3). The density and fluorescence of the bacterial culture in a given experiment, were used to determine the fluorescence signal per million bacteria. A separate calibration curve was used to determine the relationship between OD600 and the density of the bacterial suspension.

Cultures of *Dictyostelium* were harvested, washed, and resuspended in Sorenson's buffer at 1 × 10^6 cells ml^{-1} and starved for 30 min at 21°C shaking. Following the 30 min incubation 1 ml of the prepared DsRed-Ec suspension was added to the *Dictyostelium* cultures and immediately duplicate ^{0}T aliquots were removed and added to preprepared ice cold 20 mM Sorenson's buffer containing 5 mM sodium azide. The remaining amoebae were allowed to uptake DsRed-Ec for 30 min with shaking. During this time amoebae in the ^{0}T samples were collected by centrifugation at 1, 000 × g for 30 s and cells washed with 20 mM Sorenson's buffer containing 5 mM sodium azide, resuspended in 3 ml of 20 mM Sorenson's buffer and counted using a hemocytometer. After 30 min of uptake duplicate T30 aliquots of the amoebae/DsRed-Ec suspension we removed and added to preprepared ice cold 20 mM Sorenson's buffer containing 5 mM sodium azide and the amoebae washed free of bacteria. A Modulus fluorometer 9200-003 (Turner Bio-Systems, Sunnyvale, CA, United States) fitted with a specially constructed module designed for DsRed-Ec (530-nm excitation and 580-nm emission) was used to measure fluorescence in samples that had been lysed by the addition of 0.25% (v/v) Triton X-100 in Na_2HPO_4. Increase in fluorescence over 30 min was used to calculate ingestion of DsRed-Ec cells per hour by a single amoeba.

ΔF (bacteria ml^{-1}) = difference in fluorescence over the course of the assay (fluorescence at T30–T0).

Uptake (bacteria $amoeba^{-1}$ h^{-1}) = ΔF × 10^6/total cell count (amoebae ml^{-1})/time (h).

2.9 Quantification of Aggregate Size

Quantification of aggregate size was achieved by determining the number of cells in individual slugs. Strains were grown to exponential phase in HL5 medium and 1 × 10^7 cells were harvested, washed 2 × in PBS and resuspended in 1 ml 1 × PBS. The suspension was then inoculated onto a water agar plate (10 g agar/1 L dH_2O) in a 1 cm × 5 cm line, to give a density of 2 × 10^6 cells/cm^2 and allowed to dry. The plate was placed in a dark container with a single point of light source and incubated at 21°C until slugs had formed and migrated away from the point of inoculation (typically ~12–16 h). Individual slugs were then isolated using a sterile needle and resuspended in 100 μl of saline and dissociated by repeat pipetting. The number of cells per slug was then calculated after counting the number of cells in duplicate 10 μl suspensions using a hemocytometer in 30 individual slugs for each strain.

2.10 Morphology, Quantification of Number of Fruiting Bodies and Quantification of Sorus Area

Mature fruiting body morphology was observed, after multicellular development on lawns of *Enterobacter* as described previously (Kotsifas et al., 2002). Images were taken after 24 h of development. Photographs were taken using from above or from the side on an excised piece of agar using a Moticam 2300 camera attached to an Olympus SZ61 stereomicroscope. To quantify the number of fruiting bodies images were taken from above at the same magnification for all strains. The number of fruiting bodies in the same area of photograph were counted and the means calculated. Sorus area was quantified from the same photographs of fruiting bodies from above using the ImageJ measurement tool. The area was then converted to volume on the assumption that the sorus is approximately spherical using equation [V = 4/3 * A/sqrt (A/pi)] (A = area) and presented as mm^3.

2.11 Quantification of LysoSensor™ Blue DND-167 Staining in Cells

Dictyostelium cells were grown in HL5 medium to a density of 1–3 × 10^6 cells ml^{-1}1 × 10^7 cells were harvested (1,500 ×*g* for 2 min) and diluted 1:10 in Lo-Flo HL5 either with or without 500 nM LysoSensor™ Blue DND-167 (Invitrogen) and incubated covered in foil at 21°C shaking for 30 min. Cells were washed twice with 1 × PBS and resuspended to a density of 0.5 × 10^6 cells ml^{-1} in PBS and the fluorescence of a 2 ml sample measured in a Modulus™ 9200-003 fluorometer (Turner

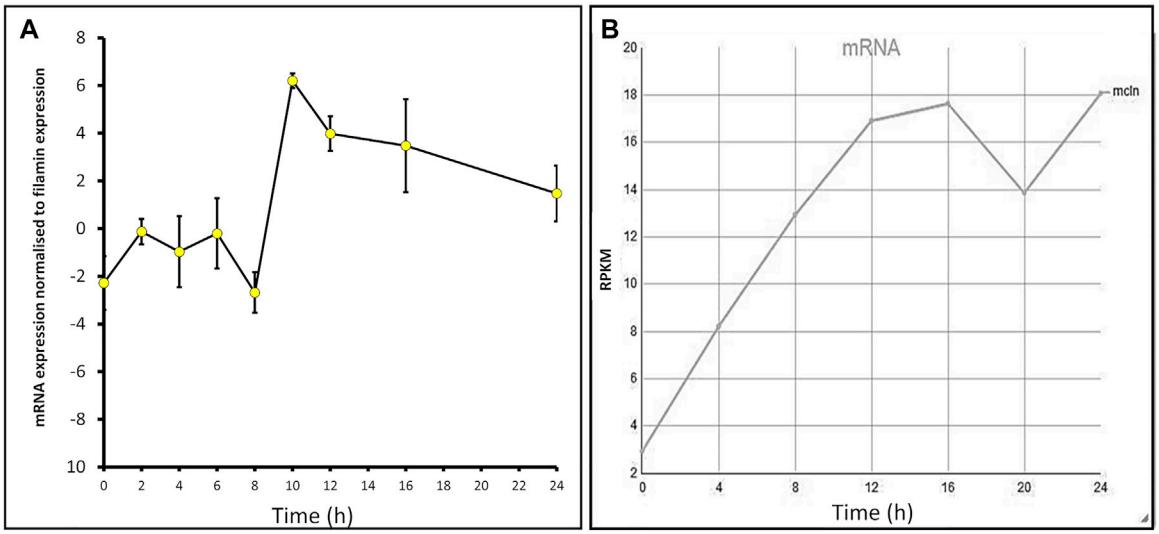

FIGURE 1 | *mcln* mRNA expression increases throughout development in *Dictyostelium* AX2 and AX4. **(A)** Semiquantitative RT-PCR was used to determine the *mcln* expression in AX2 throughout development presented normalised to filamin expression. RNA was extracted from cells developing on water agar every 2 h for 24 h in two separate experiments. Error bars are standard errors of the mean. **(B)** Developmental timing of expression of *mcln* in AX4 as measured by RNA-Seq. Reads per kilobase per million (RPKM) over 24 h. Published on DictyBase (Parikh et al., 2010; Stajdohar et al., 2017).

BioSystems, Sunnyvale, CA, United States) using the UV module kit 9200-041 (Ex. 365 nm, Em. 410–460 nm). The background fluorescence of the cells that had not been dyed was subtracted from the fluorescence recorded from the Lysosensor Blue stained cells.

2.12 LysoSensor Blue DND-167 Imaging of Live Cells

Cells were grown in HL5 medium to a density of 1–3 × 10^6 cells ml^{-1}. An aliquot containing 10^6 cells were harvested (1,500 ×*g* for 2 min) and resuspended in Lo-Flo HL5 containing 500 nM LysoSensor Blue DND-167 (Invitrogen) and incubated at 21˚C shaking for 30 min. Cells were washed 2 times in 1 × PBS, resuspended to a density of 1 × 10^6 cells ml^{-1} and 10 µl of suspension mounted onto microscope slides. Live cells were viewed through the DAPI filter with an Olympus BX61 fluorescent microscope.

2.13 Measurement of Cellular Autofluorescence

Cells were harvested and processed in the same manner as **Section 2.11**, however omitting the treatment with LysoSensor ™ Blue DND-167. Fluorescent readings of 1 × 10^6 cells were recorded immediately after two washes in 1 × PBS with the UV module kit 9200-041 (Ex. 365 nm, Em. 410–460 nm).

2.14 Calcium Experiments

2.14.1 *Dictyostelium* Culture and Development

Expression of the Ca^{2+} sensitive luminescent protein aequorin, in each *Dictyostelium*, strain was used to measure cytosolic Ca^{2+} concentration. *Dictyostelium* cultures were grown and allowed to develop as described previously (Nebl and Fisher, 1997). Axenic cultures in HL5 medium were grown to a density of 1–2 × 10^6 cells ml^{-1}, and 1 × 10^8 cells were harvested, washed twice in 20 ml of MES-DB [(MES development buffer) (10 mM MES/NaOH, pH 6.2, 10 mM KCl, 0.25 mM $CaCl_2$)], resuspended in MES-DB or HL5 to a final density of 2 × 10^7 cells ml^{-1} and loaded with 5 µM Coelenterazine-h (Invitrogen). Cultures were incubated at 21˚C shaking at 150 rpm for 4 h (vegetative cells) or 7 h (aggregation competent cells).

2.14.2 Aequorin Consumption and *In Vivo* Ca^{2+} Measurements

Aequorin consumption was carried out as previously described (Nebl and Fisher 1997). All measurements were taken inside a Lumitran® model L-3000 photometer (New Brunswick Scientific). During measurements, the cells were stirred at 100 rpm in 20 ml sample vessels and placed in front of a photomultiplier. Luminescence signals were recorded from 5 ml cell suspensions stimulated with 1 µm chemoattractant, either cAMP or folic acid. The signal was captured by a model PCI-20428 multifunction I/O data acquisition board (Intelligent Instruments Pty. Ltd.). The signal was then converted into values of cytosolic calcium concentration on a PC using in-house purpose-designed software (Prof. P. R. Fisher).

2.15 Statistical Analysis

Data was analysed in Excel. Means were compared using independent t-tests or One-Way ANOVA, with pairwise comparisons made by the Least Squares Difference method. Significant correlations were determined by Pearson product-

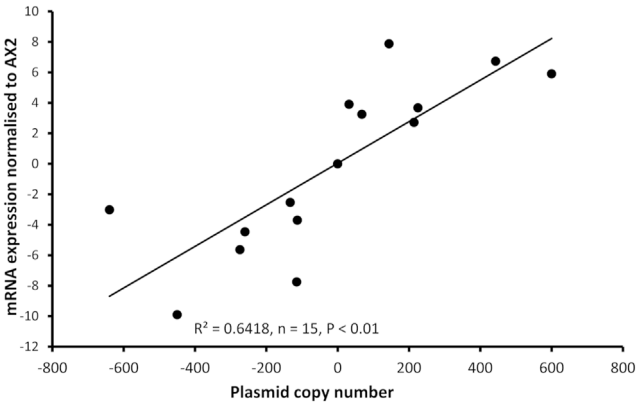

FIGURE 2 | Plasmid copy number of mucolipin strains was correlated with mRNA expression levels in the transformants. Semiquantitative RT-PCR was performed to determine mRNA expression levels in each strain. Copy numbers of overexpressing strains were determined by quantitative Southern blotting, and copy numbers of antisense strains were determined by quantitative real time PCR. Expression levels were normalised against the filamin mRNA to adjust for loading and then measured relative to AX2 expression. Expression correlates with plasmid copy number showing that the antisense RNA construct decreases *mcln* expression and the overexpression increases it. The correlation was highly significant, $p = 2.36 \times 10^{-5}$ (Pearson product-moment correlation coefficient, ρ) and similar results were also obtained using non-parametric methods (Spearman's rank $p = 1.195 \times 10^{-5}$ and Kendall's rank $p = 9.995 \times 10^{-5}$). Each point represents mean data for a single strain for three experiments. Negative values refer to copy numbers of antisense constructs and positive values to copy numbers of overexpression constructs, AX2 has a copy number of 0 as contains neither construct.

moment, Spearman's rank and Kendall's rank correlation coefficients.

3 RESULTS

3.1 Developmental Expression of *mcln* Over 24 h

The expression profiles of many *Dictyostelium* genes change throughout development. To determine the *mcln* mRNA expression levels throughout development, AX2 cells were developed on water agar plates for 24 h, and RNA extracts were taken at 2-h intervals. Semiquantitative RT-PCR was used to assess the relative expression of *mcln* in cells at these time points. Expression changed throughout development, rising slightly during early differentiation in response to the onset of starvation, falling to a trough at 8 h, but then increasing rapidly to a maximum at 10 h during aggregation. Expression remained at high levels during subsequent multicellular development (**Figure 1A**). The measured developmental expression profile is similar to the RNA-Seq expression profile of *D. discoideum* AX4 published on DictyBase (Parikh et al., 2010; Stajdohar et al., 2017), which shows increased *mcln* expression over the course of development (**Figure 1B**). Subtle differences in the patterns of expression in our experiments compared to those published on DictyBase (Parikh et al., 2010) could arise from differences in the parental strain used (AX2 in our experiments and AX4 for DictyBase) and also from the fact that in our experiments the cells were developed on water agar, as opposed to filters. This expression pattern suggests important roles for mucolipin-dependent calcium signalling in early starvation-induced differentiation, in chemotactic aggregation and subsequently during the multicellular stages of the life cycle.

3.2 Genetic Alteration of *Dictyostelium* Changes *mcln* mRNA Expression

Dictyostelium strains were created by transformation with expression constructs to either knockdown expression via antisense mRNA inhibition or overexpress the protein. Integration of the plasmid construct occurs randomly in the genome by recombination and rolling circle replication, therefore each strain contains different numbers of the plasmid constructs thus different levels of expression (Barth et al., 1998). For this reason, the copy number of the plasmid in each strain was determined, as was the mRNA expression level. As expected, antisense inhibition caused a measurable decrease in mRNA transcripts and overexpression caused an increase in mRNA transcripts. The relative mRNA expression was correlated with the copy number of the plasmid construct in the strains (**Figure 2**).

3.3 Overexpressed Mucolipin Can Be Detected in Western Blot

We created a polyclonal antibody directed against a 200aa portion of *Dictyostelium* mucolipin, anti-MUECD. In a western blot this antibody detected multiple bands so was not suitable to be used for localisation studies. To determine if any of these bands did represent mucolipin, we tested the antibody the against mucolipin knockout cell lysate (Lima et al., 2012) and ran these proteins alongside protein extracted from DH1-10 (the parental strain for the knockout cell line), AX2 and our mucolipin overexpression and knockdown strains. Indeed, there were two bands absent in the mucolipin knockout lysate but present in the mucolipin overexpression strains which ran at approximately 95 and 120 kDa. The 120 kDa band was also detected in DH1-10 (**Figures 3A,B**). It was not observed in the knockout strain derived from DH1-10, despite a similar protein loading in the gel. These bands were not detected in AX2 or our mucolipin antisense strains, presumably because the wild type and knockdown expression levels for mucolipin were insufficient for detection by our antibody. Mass spectrometry analysis of bands excised from a Coomassie Blue-stained Bis-Tris-Plus gel (**Supplementary Figure S1** and **Supplementary Method 1**) confirmed the presence of mucolipin in these two bands (indicated by the red stars in **Figure 3B**), but not the smaller molecular weight bands. We thus confirmed that there are two genuine mucolipin bands—one at the predicted MW position ~95 kDa and one running at ~120 kDa. There are two possible explanations for the presence of two bands. Firstly, the upper band could be a posttranslationally modified (glycosylated) form of the protein as is reported for

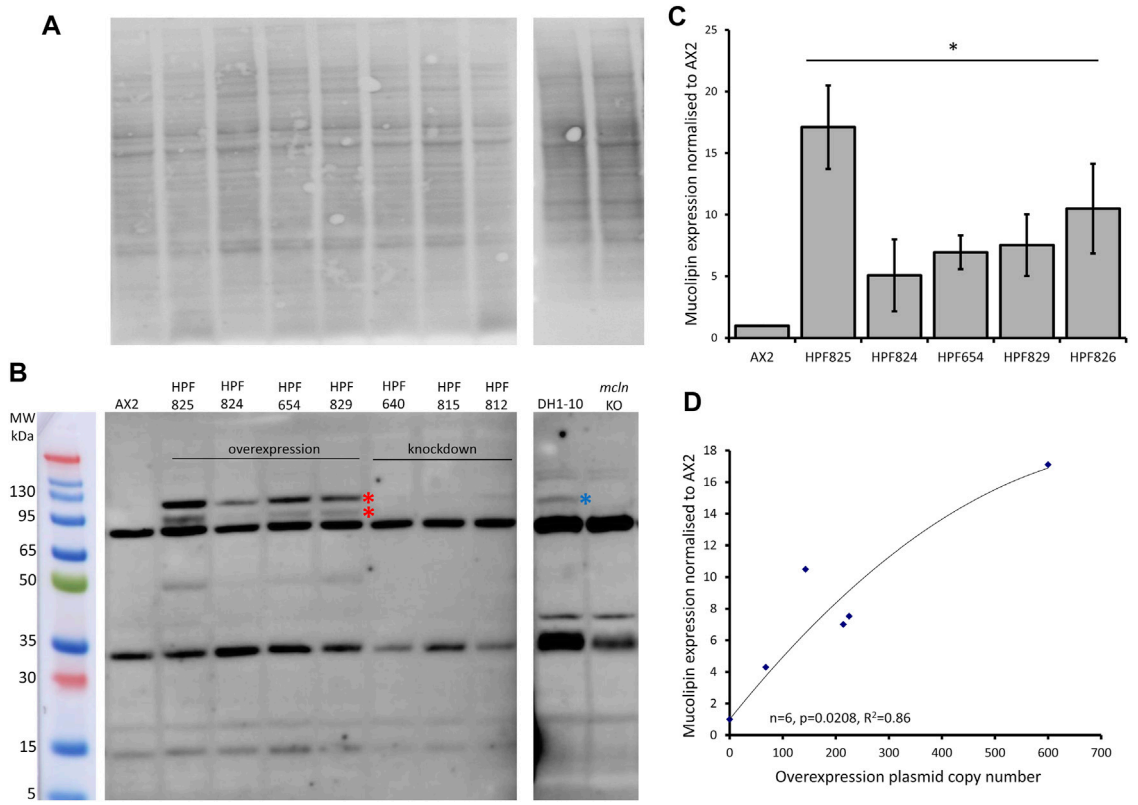

FIGURE 3 | Mucolipin can be detected in protein extracted from overexpression strains. **(A)** Total protein extracted from AX2, four representative mucolipin overexpression strains, three representative mucolipin knockdown strains, DH1-10 and mucolipin knockout, were separated by on a Bis-Tris-Plus gel by electrophoresis, transferred to PVDF membrane and stained with No Stain Protein Labelling Reagent (Invitrogen). Protein lysate for DH1-10 and *mcln* KO were kindly provided by Professor Pierre Cosson (Lima et al., 2012). **(B)** Western blot of the same membrane, the anti-MUECD antibody detects multiple bands. Markers were the Broad Multi Color Pre-Stained Protein Standard (Genscript). Two bands of ~95 and ~120 kDa were absent in the mucolipin knockout cells but present in the mucolipin overexpression strains (Red stars) and the higher MW band also detected in DH1-10 (blue star). **(C)** Quantification of mucolipin expression in overexpression strains. To quantify mucolipin expression the combined intensity of the 120 and 95 kDa bands was measured in Image Lab™ and normalised to the intensity of the total protein loaded in each lane **(A)**. Expression in each strain was then and normalised to AX2 expression. As no bands were visualised for AX2 at these sizes, AX2 expression was determined by measuring the intensity of a similar sized area on the blot where the bands would be located. Each strain was tested 2–4 times and data was pooled from each experiment and the means calculated (error bars are standard errors of the mean). Expression is relative to AX2 and is increased in overexpression strains (* = <0.05, One-Way ANOVA, with pairwise comparisons made by the Least Squares Difference method, AX2 vs. strain). **(D)** Protein expression in overexpression strains correlates with overexpression construct copy number. AX2 had a construct copy number of 0 as does not contain an overexpression construct. The correlation was highly significant (Spearman's rank p = 0.0208 and Kendall's rank p = 0.0194).

human TRPML1 (Miedel et al., 2006), and the lower band could be the native nonglycosylated protein. Secondly, the upper band could be the native, full-length protein running a little more slowly than expected, and the lower band could be a cleavage product. The human TRPML1 has a proteolytic cleavage site in the intralumenal loop between transmembrane domains 1 and 2, and this cleavage is believed to be involved in regulation of channel activity (Kiselyov et al., 2005). Since we confirmed that these bands represented mucolipin, we were able to confirm by quantification that mucolipin expression is increased in our overexpression strains (**Figure 3C**), and the protein expression was significantly correlated with copy number of the overexpression plasmid construct (**Figure 3D**).

3.4 Mucolipin Contributes to Chemotactic Calcium Signals in *Dictyostelium*

TRPMLs are thought to be important for Ca^{2+} signalling events associated with Ca^{2+}-dependent fusion/fission events of membranes along the late endocytic pathway (LaPlante et al., 2004; Luzio et al., 2007; Brailoiu and Brailoiu 2016). In *Dictyostelium* DH1-10 cells, knockout of mucolipin reduces Ca^{2+} concentrations in secretory post-lysosomes, measured using dextran-coupled fluorophores (Lima et al., 2012) suggesting a role in regulation of calcium homeostasis/signalling. To further investigate the role of mucolipin in Ca^{2+} signalling, and the possible contribution of the acidic stores to chemotactic Ca^{2+} responses, we measured the cytosolic Ca^{2+} transients in

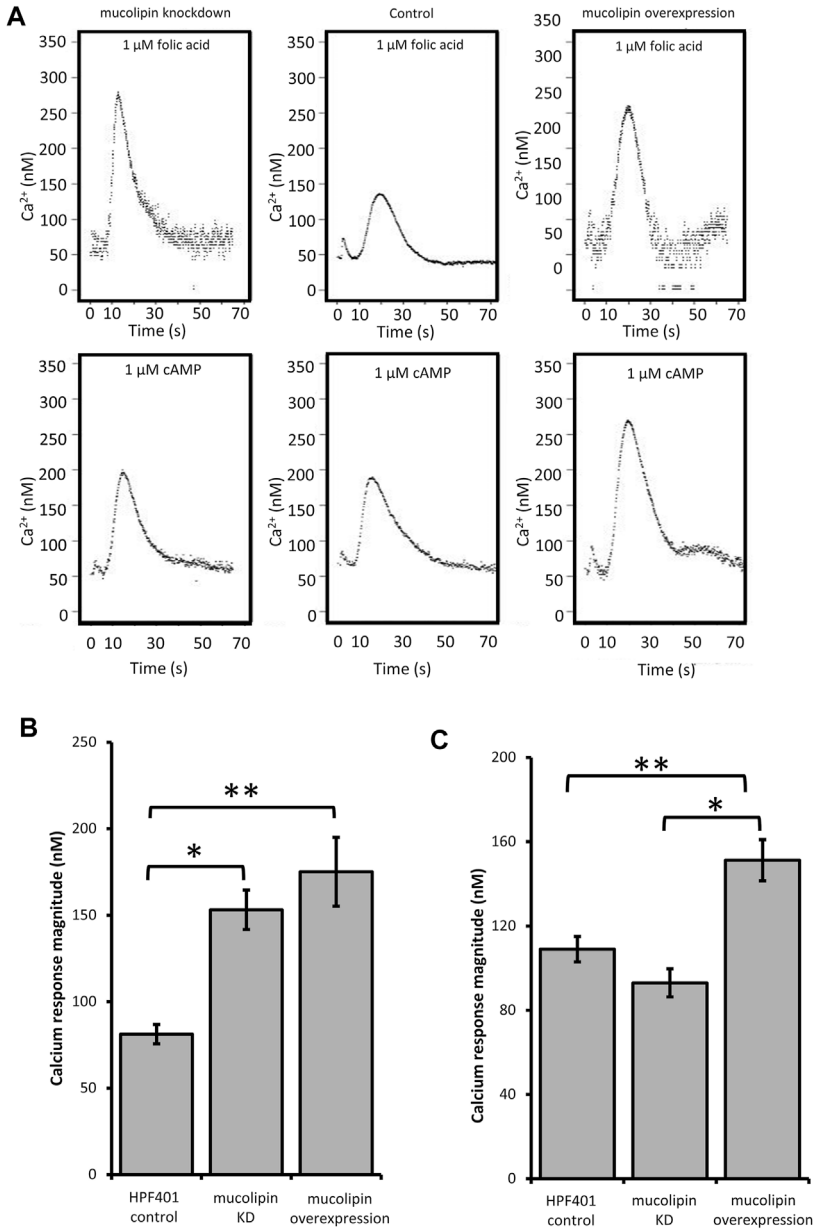

FIGURE 4 | Cytosolic calcium responses to cAMP and folic acid stimulation. **(A)** Representative real time recordings of cytoplasmic Ca^{2+} responses to chemoattractants. Upper panel: Real time recordings of Ca^{2+} responses to 1 μM folate in vegetative cells. Left to right: mucolipin KD (knockdown), HPF401 control strain and mucolipin overexpression. Lower panel: Real time recordings of Ca^{2+} responses to 1 μM cAMP in cells at 7 h development. Left to right: as above. Recordings began at 0 s and the stimulus was injected immediately after. The small peak preceding the Ca^{2+} response is due to a Ca^{2+} response to the mechanical stimulus of chemoattractant injection, which has no effect on the chemoattractant responses (Nebl and Fisher, 1997). **(B)** Mean calcium response magnitudes in vegetative cells stimulation with 1 μM folic acid. Ca^{2+} response magnitudes (Ca^{2+} nM) were measured in mucolipin KD, mucolipin overexpression and control strain HPF401. There was no correlation with copy number so data from strain groups was pooled and the means compared. Both knockdown and overexpression of mucolipin significantly enhances the magnitude of the response compared to the control strain HPF401 ($^{*}p = 3.15 \times 10^{-5}$, $^{**}p = 4.7 \times 10^{-4}$). Means were compared using an independent one-tailed *t*-test. Errors are standard errors of the mean. Individual strains were tested in 3–9 independent experiments in five mucolipin overexpression ($n = 13$), six mucolipin knockdown strains ($n = 30$) and control strain HPF401 ($n = 12$), and all experiments from each strain group were pooled to determine the mean. **(C)** Mean calcium response magnitudes (Ca^{2+} nM) in developed cells stimulated with 1 μM cAMP. Ca^{2+} response magnitudes were measured in overexpression, knockdown and control strain HPF401. Cells were developed to 7 h in MED-DB. Overexpression of mucolipin increases the response magnitude significantly compared to both control HPF401 and knockdown strains ($^{*}p = 1.33 \times 10^{-6}$, $^{**}p = 5{,}928 \times 10^{-4}$). knockdown of mucolipin has no effect on response magnitude in developed cells when compared to wildtype ($p = 0.083$). Means were compared using an independent one-tailed *t*-test. Errors are standard errors of the mean. Individual strains were tested in 2–9 independent experiments and all experiments were pooled to determine the mean. Mucolipin overexpression eight strains ($n = 37$), mucolipin knockdown seven strains ($n = 33$), control HPF401 ($n = 12$).

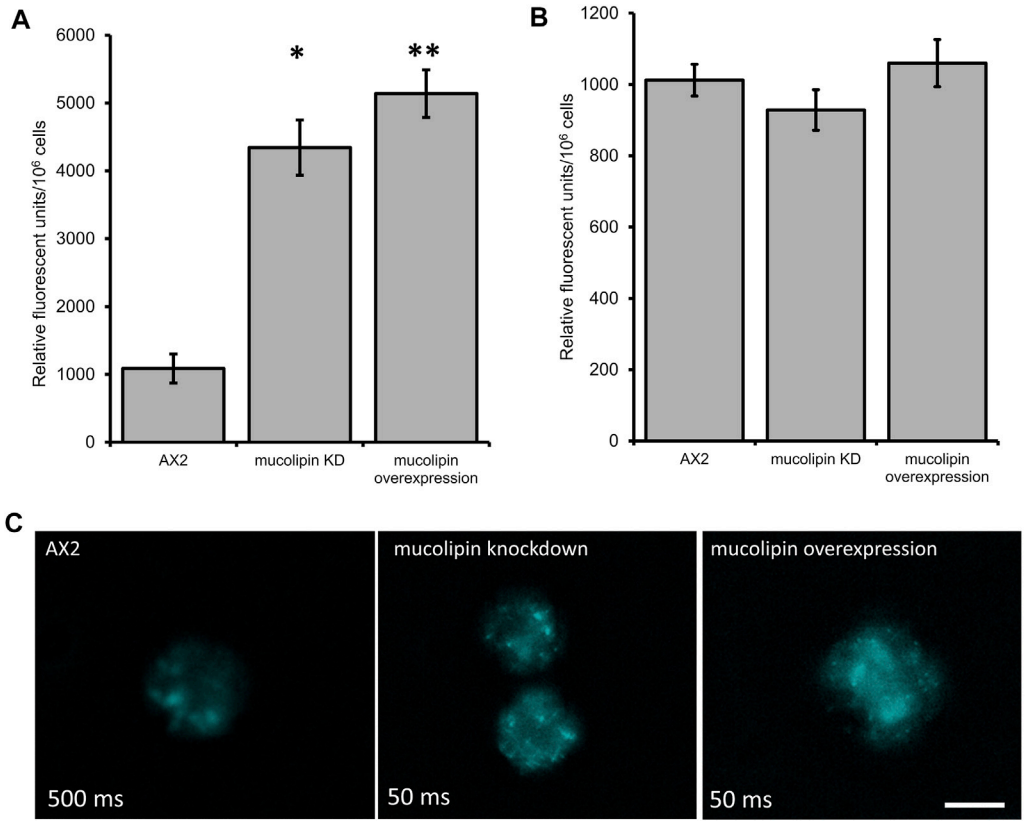

FIGURE 5 | Altering mucolipin expression causes accumulation or increased acidification of vesicles stained with LysoSensor™ Blue DND-167 but does not cause autofluorescence. **(A)** Quantification of LysoSensor™ Blue DND-167 was performed by measuring the increase in fluorescence in 1×10^6 vegetative cells after incubation with 500 nM LysoSensor™ Blue DND-167. Data was collected from seven knockdown strains and six overexpression strains in three individual experiments and the mean calculated, error bars are standard errors of the mean. There was no correlation with copy number of the plasmid constructs, therefore data for strain groups was pooled. The mean fluorescence of AX2 ($n = 3$) was significantly different to the means of either knockdown ($n = 21$) or overexpression strains ($n = 18$) (Pairwise comparisons, Independent *t*-test, $^*p = 0.00067$, $^{**}p = 0.01107312$). **(B)** Fluorescence measured in *Dictyostelium* strains harvested from low fluorescence medium. The level of fluorescence in knockdown and overexpression strains was measured in 1×10^6 cells. Autofluorescence was measured in a fluorometer (Modulus 9200-003 Turner Bio systems) using the UV module (excitation 365 nm, emission 410–460 nm). Fluorescence displayed in relative fluorescent units, was measured in two independent experiments for AX2 ($n = 2$), six knockdown strains ($n = 12$) and six overexpression strains ($n = 12$) and the mean within each group calculated. Error bars are standard errors of the mean. There was no significant difference ($p > 0.05$, One-Way ANOVA, multiple comparisons made by the Least Squares Difference method). **(C)** Representative live cells stained with LysoSensor™ Blue DND-167. *Dictyostelium* AX2, mucolipin knockdown (copy number 274) and overexpression (copy number 443) were incubated in the presence of 500 nM LysoSensor™ Blue DND-167 for 1 h and observed under fluorescence microscopy (Excitation- 373 nm, Emission- 425 nm). The AX2 image was taken at 500 ms exposure, the knockdown and overexpression cells were overexposed at this exposure so were taken at 50 ms. Scale bar = 5 μm.

vegetative cells (folic acid responses), and in aggregation competent cells (cAMP responses) in mucolipin knockdown and overexpressing strains. All strains also ectopically expressed a recombinant Ca^{2+}-sensitive luminescent protein, apoaequorin, to allow real time recordings of cytosolic Ca^{2+} responses. These chemotactic Ca^{2+} responses have been well characterized in wild type cells expressing apoaequorin (HPF401) (Nebl and Fisher, 1997). In this work we compared the mutants' Ca^{2+} responses with wild type responses to gain insight into the molecular mechanisms involved. Representative real-time recordings of cytosolic calcium concentration in wild type aequorin-expressing strain (HPF401), mucolipin knockdown strain (HPF812) and mucolipin overexpression strain (HPF825) when stimulated with 1 μM chemoattractant are shown in **Figure 4A**.

3.4.1 Overexpression of Mucolipin Enhances the Ca^{2+} Responses to cAMP and Folic Acid

Real time recordings of the Ca^{2+} responses for control, knockdown and overexpression strains to both cAMP and folic acid were recorded over multiple experiments and analysed. As there was no correlation between the various parameters and plasmid copy number, data was pooled for all transformants within each group for combined analysis. Overexpression of mucolipin significantly enhanced Ca^{2+} response magnitudes to both folic acid (vegetative cells) and cAMP (aggregation competent cells) compared to the control (**Figures 4B,C**). The response magnitudes were increased

compared to the control by an average of 46.4% and 28.0% for the folic acid responses and cAMP responses respectively. This result suggests, mucolipin is involved in Ca^{2+} chemotactic calcium responses and because the channel localises to post-lysosomes and possibly other endocytic compartments (Lima et al., 2012), the results suggest that these vesicles are also involved in the calcium response.

3.4.2 Knockdown of Mucolipin Increases Ca^{2+} Response Magnitudes in Vegetative Cells, but Not in Aggregation Competent Cells

Given that overexpression of mucolipin enhances the responses to folic acid and cAMP, it was expected that knockdown of mucolipin would reduce the magnitude of calcium responses. Surprisingly, the magnitude of the Ca^{2+} responses to 1 μM folic acid was significantly increased in knockdown strains compared to the control (**Figure 4B**). Contrary to the folate responses, the magnitude of the cAMP Ca^{2+} responses in aggregation competent cells were slightly reduced in mucolipin knockdown strains compared to the control (**Figure 4C**), but the difference did not reach statistical significance ($p = 0.083$).

3.5 The Role of Mucolipin in the Endocytic Pathway

Dictyostelium mucolipin overexpression and knockdown strains both exhibit increased Ca^{2+} signalling in vegetative cells. As Ca^{2+} plays an important role in the endocytic pathways it was of interest to assess the role of mucolipin in these processes.

3.5.1 Overexpression and Knockdown of Mucolipin Increases Fluorescence of Cells Stained With LysoSensor™ Blue DND-167

One of the hallmarks of MLIV cells is an accumulation of hybrid late endosome-lysosome compartments (LELs) with defective exit of lipids from LELs to the trans-Golgi network (Chen et al., 1998; LaPlante et al., 2004). The connection between Ca^{2+} release via TRPMLs and build-up of hybrid LELs is somewhat undecided. To assess this phenotype in AX2 *Dictyostelium* cells, we stained vegetative mucolipin knockdown and overexpressing cells with LysoSensor™ Blue DND-167 which has a pK_a of is ~5.1 and accumulates in acidic vesicles. There was a significant increase in fluorescence in the mutants compared to AX2 (**Figure 5A**) representative images of live stained cells are presented in **Figure 5C**. This could reflect an increase in lysosomal mass, or because the fluorescence of LysoSensor™ Blue DND-167 increases as the pH decreases, our results could reflect increased acidification of the lysosomes.

3.5.2 Altering Mucolipin Expression Does Not Cause Autofluorescence

Accumulation of autofluorescent material has been observed in MLIV cell lines and is thought to be related to specific compounds stored in the lysosomes (Goldin et al., 1995). Autofluorescence is also a hallmark of NCL (Dowson et al., 1982), and has been detected in some *Dictyostelium* NCL models. In the cln3 model, *cln3*$^{-}$ cells do not accumulate autofluorescent material during the growth stage (Huber et al., 2014), however in starved *cln3*$^{-}$ cells autofluorescent material was detected (Huber and Mathavarajah, 2019). In the cln2 lysosomal disease model, mutants with knockdown and knockout of the *tpp1/cln2* gene, which encodes the lysosomal protein tripeptidyl peptidase I (TPP-I), a soluble lysosomal aminopeptidase, accumulate cellular autofluorescent material (Phillips and Gomer, 2015; Smith et al., 2019). Therefore, we

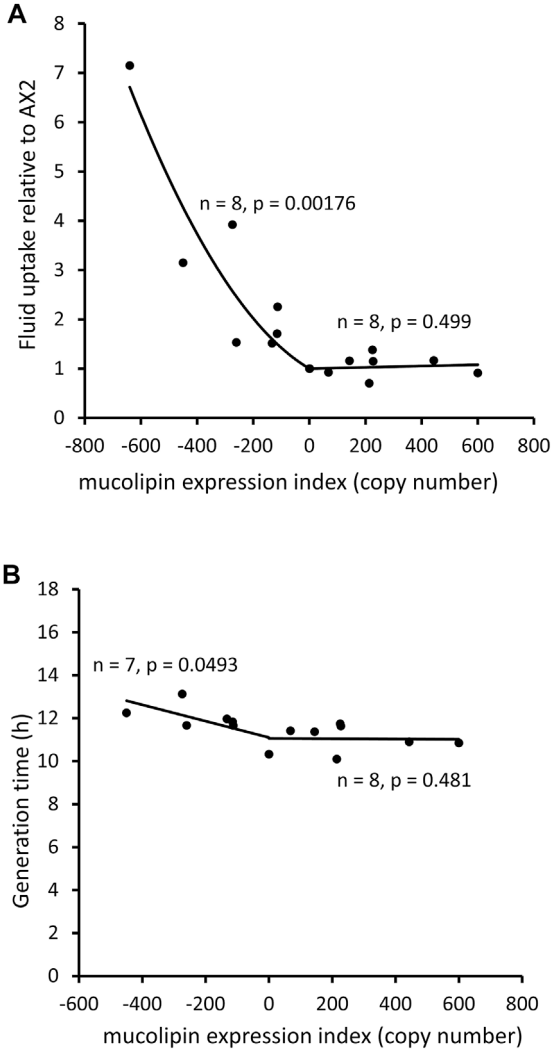

FIGURE 6 | Mucolipin knockdown affects macropinocytic uptake and growth rates of cells in HL5 medium. **(A)** Consumption of HL-5 medium containing FITC dextran via macropinocytosis in knockdown strains (negative copy numbers), overexpression strains (positive copy numbers) and wild type normalised to AX2. In the antisense strains fluid uptake normalized to AX2 was increased and correlates with mucolipin expression index (Pearson correlation coefficient, $p = 0.00176$), however there was no correlation in the overexpression strains (Pearson correlation coefficient, $p = 0.499$). Each point represents the mean uptake from a single strain. Duplicate samples were assayed for each strain in two to six separate experiments and data was normalised within each experiment to AX2. **(B)** Generation times (h) of mucolipin strains and AX2 grown in HL5 medium. In the antisense strains generation time was increased and correlates with mucolipin expression index (Pearson correlation coefficient, $p = 0.0493$), however there was no correlation in the overexpression strains (Pearson correlation coefficient, $p = 0.481$). AX2 has a copy number of 0.

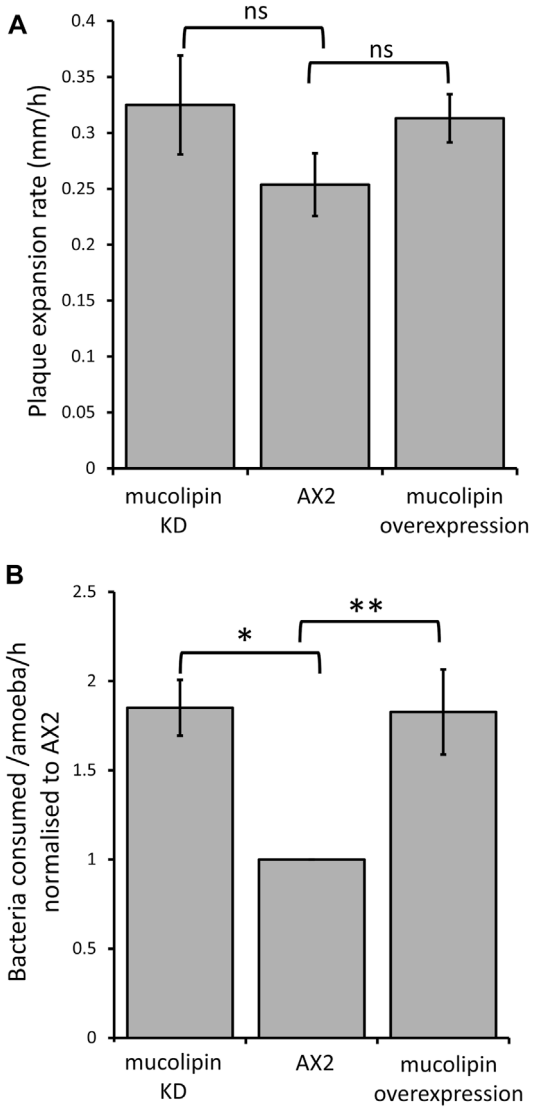

FIGURE 7 | Mucolipin expression did not affect plaque expansion rates but increased phagocytosis rates. **(A)** Plaque expansion rates (growth velocity) were measured from linear regressions of plaque diameters vs. time during growth at 21°C on an *E. coli* B lawn. Growth velocity was not significantly altered in mucolipin knockdown compared to AX2 ($p = 0.278$) or overexpression compared to AX2 ($p = 0.133$) (One-Way ANOVA, with pairwise comparisons made by the Least Squares Difference method). Analysis revealed that all there was no correlation between construct copy number and growth velocity of the mucolipin overexpressing strains therefore, the growth velocities for different strains in each of the two sets of transformants were pooled to calculate the means for comparison with AX2. Individual strains were each tested in 2–4 independent experiments and the data pooled to calculate the mean. Eight overexpression strains ($n = 33$), seven knockdown strains ($n = 20$) and the control strain ($n = 4$) were tested (n = total number of experiments in each strain group). Errors are standard errors of the mean. **(B)** Uptake of *E. coli* cells expressing the fluorescent red protein Ds-Red via phagocytosis was significantly increased in both knockdown and overexpression mucolipin transformants when compared to AX2 (*$p = 3.35 \times 10^{-5}$, **$p = 0.002$, One-Way ANOVA, with pairwise comparisons made by the Least Squares Difference method). All of the mucolipin overexpressing strains exhibited similarly elevated phagocytosis rates so that there was no correlation (*Continued*)

FIGURE 7 | amongst them between construct copy number and phagocytosis rates (Pearson product-moment correlation coefficient, ρ, overexpression $p = 0.15$). The same was true of the mucolipin knockdown strains (Pearson product-moment correlation coefficient, ρ, $p = 0.48$). Accordingly, the uptake rates obtained from different strains within each group were pooled and the means calculated. Individual strains were tested in 2–4 independent experiments. Seven overexpression ($n = 24$), seven knockdown strains ($n = 19$) and the control strain ($n = 4$) were tested (n = total number of experiments). Errors are standard errors of the mean.

measured autofluorescence in *Dictyostelium* mucolipin knockdown and overexpression strains under UV light. No increase of autofluorescence was detected in any of our mucolipin mutants (**Figure 5B**). This phenotype in *Dictyostelium* lysosomal disease models seems to be specific to the particular disease gene in question.

3.5.3 Knockdown of Mucolipin Increases Macropinocytic Uptake, but Decreases Growth Rates of Cells in Liquid Medium, While Overexpression Does Not Affect Growth or Macropinocytosis

An analysis of uptake of medium as compared to growth rates can indicate whether ingested nutrients are efficiently catabolised. The rate of fluid uptake by macropinocytosis was increased in mucolipin knockdown strains and correlated with plasmid copy number, however overexpression had no affect (**Figure 6A**). Surprisingly the growth rates of mucolipin knockdown strains were slower than AX2 (longer generation times) and similarly correlated with plasmid copy number, while overexpression had no affect (**Figure 6B**).

3.5.4 Mucolipin Knockdown and Overexpression Increase Phagocytosis, but Do Not Affect Growth Rates on Lawns of Bacteria

Dictyostelium consume bacteria by phagocytosis in their natural environment and can be cultured on lawns of bacteria where they grow as plaques which gradually expand as the amoebae consume bacteria. The plaque expansion rates (growth velocity) of mucolipin transformants were slightly but not significantly elevated compared to AX2 (**Figure 7A**). The rates of phagocytosis in mucolipin transformants and AX2 control were assayed by measuring the uptake of fluorescently labelled live *E. coli* cells. Surprisingly, unlike the plaque expansion rates on bacterial lawns, both overexpression and knockdown of mucolipin significantly increased the rates of phagocytosis of *E.coli* (**Figure 7B**). These results indicate although these transformants are engulfing bacteria at a faster rate than AX2, this does not significantly increase the growth rates.

3.6 Mucolipin Expression Affects *Dictyostelium* Multicellular Development

Multicellular development in *Dictyostelium* is initiated by starvation upon which the cells undergo a developmental program leading to multicellular morphogenesis and culmination into mature fruiting bodies consisting of a spore

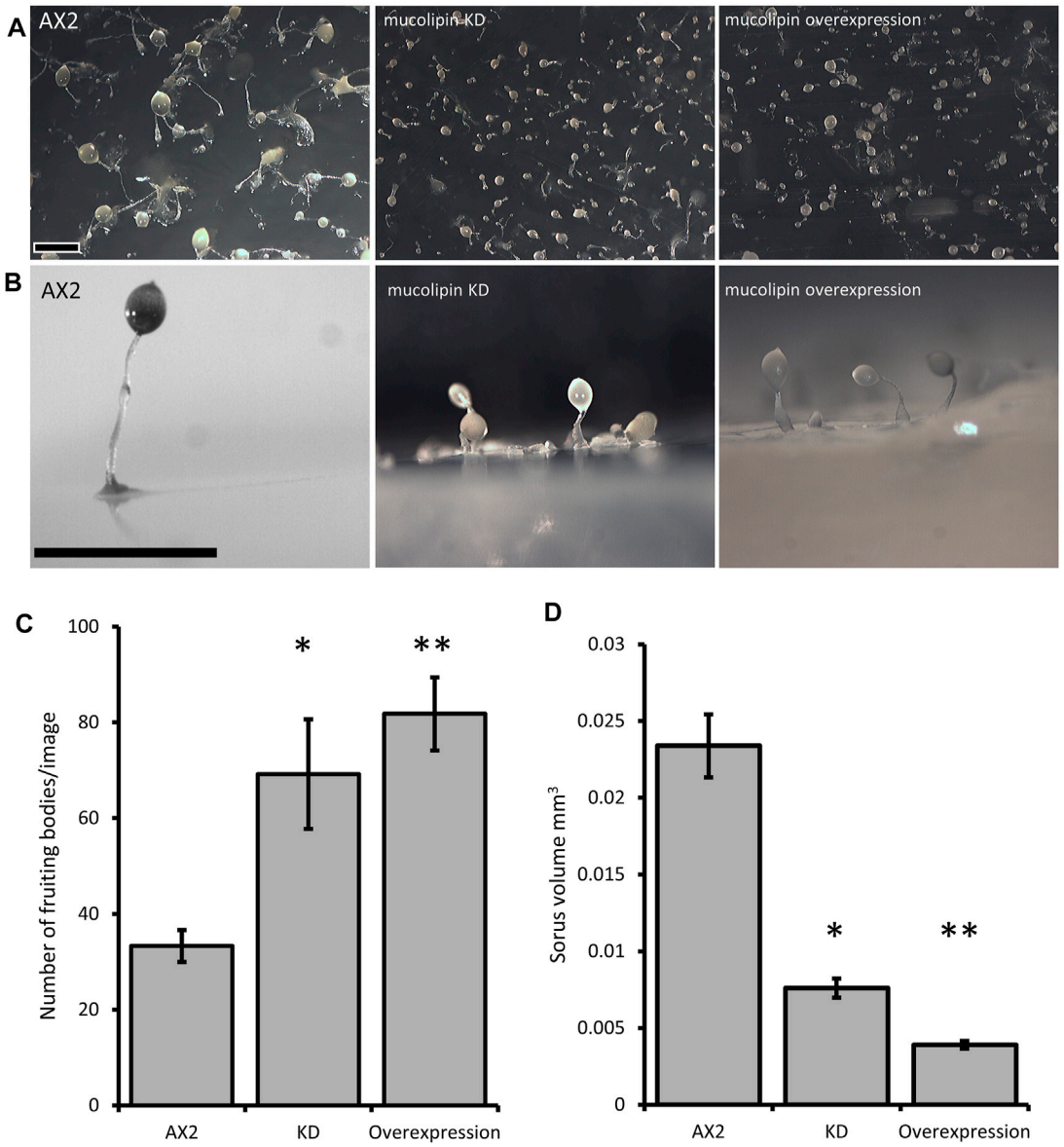

FIGURE 8 | Mucolipin knockdown and overexpression strains form smaller more numerous fruiting bodies. **(A)** AX2 wild type, mucolipin KD (knockdown) strain HPF817 (copy number 450) and mucolipin overexpression strain HPF825 (copy number 600). Cells grown on lawns of *E. aerogenes* at 21°C for ~24 h until fruiting bodies had formed which were photographed from above. **(B)** The same strains photographed from the side. Both increasing and decreasing mucolipin expression results in very small fruiting bodies compared to that of AX2. In high copy number strains the stalks and basal disks are thickened and enlarged. Scale bar = 1 mm. **(C)** The number of fruiting bodies were significantly increased in mucolipin knockdown and overexpression strains. Images were taken from above at the same magnification for all strains and the number of fruiting bodies in the same area of photograph were counted and the means calculated. (AX2: $n = 3$; KD: $n = 5$, overexpression: $n = 5$) (independent t-test $^{*}p = 0.0470$ vs. AX2, $^{**}p = 0.00303$ vs. AX2). **(D)** Sorus volume was smaller in the knockdown and overexpression strains than AX2. Sorus area was quantified from photographs of fruiting bodies from above using the ImageJ measurement tool and then converted to volume on the assumption that the sorus is approximately spherical using equation (V = 4/3*A/sqrt (A/pi) (A = area) and presented as mm^3. For each strain 30–111 sori were measured. The sorus size was significantly reduced in knockdown ($p = 2.402 \times 10^{-20}$ vs. AX2) and overexpression strains ($^{**}p = 1.8998 \times 10^{-56}$ vs. AX2). Sample sizes: AX2—N = 3 images, $n = 97$ sori; KD—N = 5 strains, $n = 349$ sori; overexpression—N = 5 strains, $n = 298$ sori) (independent t-test).

droplet (sorus), stalk and basal disc. The stalk cells undergo autophagic cell death and so are nonviable. The developmental timing of expression of mucolipin suggests it is involved in chemotactic aggregation and progression through multicellular morphogenesis, likely through mucolipin-dependent calcium signalling, and its effects on the endocytic system. Calcium signalling plays an important role during development, from chemotactic aggregation to cell type differentiation. To investigate how expression levels of mucolipin affect multicellular morphogenesis in *Dictyostelium*, knockdown and overexpression strains were observed at the slug and fruiting body stage. Both knockdown and overexpression strains formed

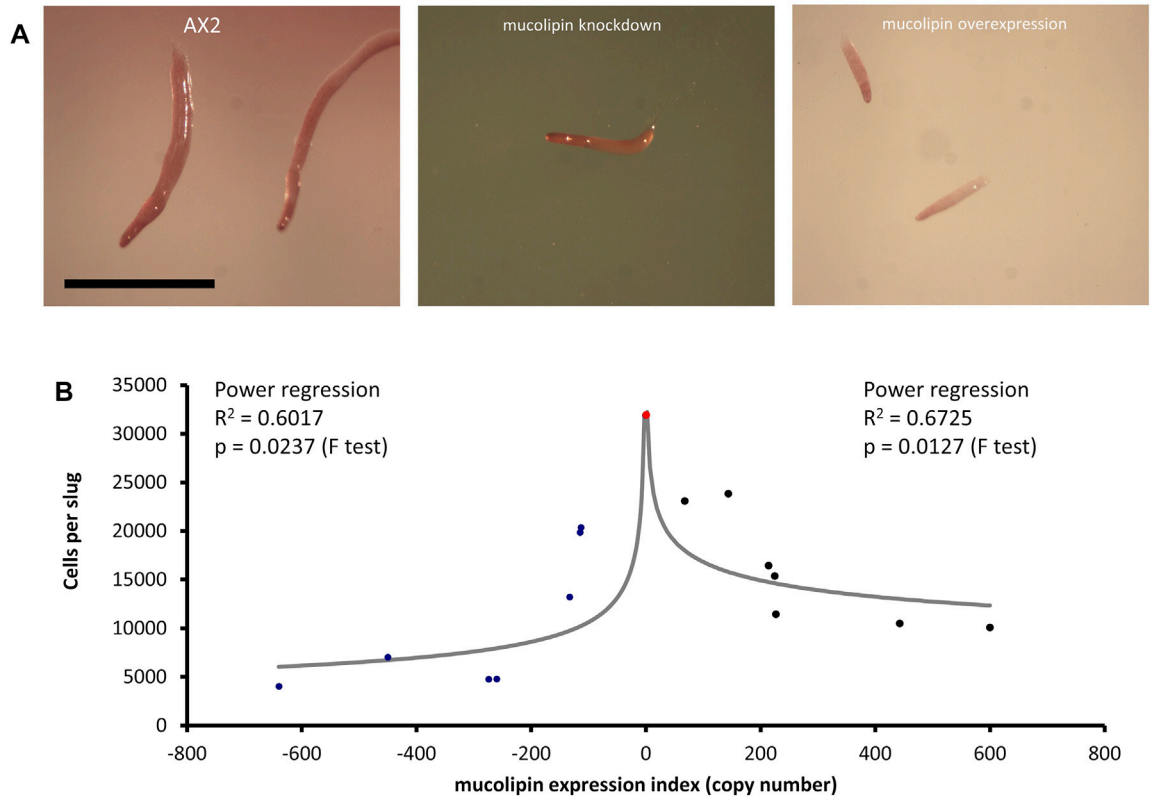

FIGURE 9 | Slug sizes are smaller in mucolipin knockdown and overexpression strains and is copy number dependent. **(A)** Slugs formed after ~16 h of development on water agar. Mutants formed smaller slugs than AX2 Scale bars = 1 mm. **(B)** Both increasing and decreasing mucolipin expression reduces aggregate size. The aggregate size of overexpression and knockdown strains was quantified by determining the number of cells per slug. The mean aggregate size for each transformant was determined by isolating single slugs and counting the number of cells in each slug using a haemocytometer (n = 30). The mean aggregate size was reduced in a copy number dependent manner, the regressions were significant indicated by the p values. Positive copy numbers represent overexpression strains and negative numbers knockdown strains, AX2 had a copy number of 0 as it contains neither plasmid (indicated as red circle).

smaller fruiting bodies than AX2. In high copy number strains, the stalks and basal disks of the fruiting bodies appear thickened indicating increased stalk cell differentiation (**Figures 8A,B**), fruiting bodies were more numerous (**Figures 8C**) and formed smaller sori (**Figures 8D**). We then determined if the smaller fruiting bodies were the result of small aggregate and slug formation in the mutants. Indeed, both knockdown and overexpression strains developed into smaller slugs containing fewer cells compared to AX2 (**Figure 9A**). The aggregate size was quantified by determining the number of cells per slug, revealing a dramatic copy number-dependent reduction in slug size in both overexpression and knockdown strains (**Figure 9B**). This phenotype is also present in *cln2* knockdown mutants (Smith et al., 2019), and similarly *cln3*$^{-}$ and *cln5*$^{-}$ mutants have increased numbers of tipped mounds, fingers, slugs and fruiting bodies for the same density of cells (Huber et al., 2014; Huber et al., 2017; McLaren et al., 2021).

4 DISCUSSION

In this study we have used the model organism *Dictyostelium* to investigate if mucolipin expression can affect global calcium signals during chemotactic calcium responses. Gross (2009) suggested that the *Dictyostelium* acidic stores, which includes the endolysosomal vesicles, the contractile vacuole system and the acidocalcisomes, can release Ca^{2+} and increase cytosolic Ca^{2+} during chemotaxis. A selection of calcium channels have been identified to be associated with the acidic stores including the P2X receptors of the contractile vacuole (Fountain et al., 2007), the two pore channel (TPC) (Wilczynska et al., 2005; Chang et al., 2020), and mucolipin. Given that mucolipin resides in late endosomes and other endocytic vesicles (Lima et al., 2012), we hypothesized that mucolipin could contribute to calcium release from these stores. We measured cytosolic Ca^{2+} responses to chemoattractants in mucolipin knockdown and overexpression transformants using the luminescence of the Ca^{2+}-sensitive luminescent protein, apoaequorin, which we ectopically expressed in the same cells (Nebl and Fisher 1997). We found that overexpression of mucolipin significantly increased the magnitudes of the cytosolic Ca^{2+} responses to folic acid and cAMP. While we cannot determine if the increased calcium influx into the cytosol is the result of direct release of calcium from the endocytic compartments through mucolipin itself, our results do implicate mucolipin in cytosolic calcium signalling. Lima et al.

(2012) provided evidence of mucolipin involvement in calcium homeostasis because knockout cells grew faster in calcium-depleted medium and had reduced lumenal calcium concentrations in the post-lysosomes, below 0.2 μM, much lower than the 1–3 μM of the wild type control. In other cell types TRPML1 has been shown to affect lysosomal pH (Soyombo et al., 2006; Miedel et al., 2008), therefore, knocking out mucolipin in *Dictyostelium* could affect the proton/Ca^{2+} exchange between the vesicle lumen and cytoplasm, thereby reducing steady state Ca^{2+} levels in the lumen as has been reported (Lima et al., 2012). This could in turn mean that overexpressing mucolipin may result in elevated resting lumenal Ca^{2+}, again because of the disturbed pH gradient across the vesicle membrane. This, and the greater number of available channels could then facilitate the larger responses in our overexpressing strains. Lima et al. (2012) hypothesized that mucolipin may be responsible for transfer of calcium from the cytosol to the lumen where the vesicles meet high local cytosolic calcium concentrations. Our results suggest that, at least when overexpressed, mucolipin significantly contributes to cytosolic signals, thus could function as a calcium release channel. It is possible that the channel could work both ways depending on the particular cellular requirements.

As stated previously, in other cell types TRPML channels are known to regulate localised calcium signals, as well as global calcium waves via activation of ER and plasma membrane calcium flux (Kilpatrick et al., 2016). The same may be true in *Dictyostelium*—if mucolipin is capable of activating calcium release from ER and across the plasma membrane, then overexpressing the channel would enhance the cytosolic calcium responses as we observed in our experiments. It is also possible that overexpression of mucolipin results in expression at the plasma membrane, as this has been reported for TRPML1 expression in HEK293 cells (Kiselyov et al., 2005), or it may be translocated there during exocytosis as TRPML1 is in *Xenopus* oocytes (LaPlante et al., 2002). The *Dictyostelium* channels responsible for plasma membrane and ER calcium release are still not confirmed. Contenders are IplA, a channel related to the mammalian ER IP_3 receptors (Taylor et al., 1999; Lusche et al., 2012) and pkd2 the *Dictyostelium* polycystin-2, another member of the TRP superfamily (Lima et al., 2014; Traynor and Kay, 2017). Both IplA and pkd2 have been localised to the plasma membrane (Lusche et al., 2012; Lima et al., 2014). However, IplA localises primarily to unidentified cytoplasmic inclusions, and it has not been determined whether this includes the ER (Lusche et al., 2012). Some studies have found that knockout of IplA abolishes calcium responses to chemoattractants (Traynor et al., 2000; Traynor and Kay, 2017), however another reported that the Ca^{2+}response to high concentrations of cAMP is maintained but smaller (Schaloske et al., 2005). Calcium responses to cAMP and folic acid are retained in pkd2 knockout cells (Traynor and Kay, 2017). Therefore, clarification of which channels involved in ER and plasma membrane calcium signalling is still necessary. Future work to investigate if mucolipin contributes to calcium influx across the plasma membrane and release from the ER calcium could include measurement of the uptake of $^{45}Ca^{2+}$ from the extracellular milieu, treatment of overexpression cells with thapsigargin to reduce ER calcium content (Lytton et al., 1991), and with EGTA to chelate extracellular calcium.

We also analysed cytosolic calcium signals in mucolipin knockdown strains, and were surprised to find that reducing mucolipin expression resulted in larger, rather than smaller Ca^{2+} responses. However, this occurred only in vegetative cells, the magnitudes of the calcium responses in differentiated cells stimulated with cAMP were not significantly different from controls (**Figure 4**). The enhanced Ca^{2+} responses observed in our vegetative mucolipin knockdown strains might be caused by a decrease in Ca^{2+} buffering capacity by the acidic stores. Lysosomes can shape calcium signals by tempering cytosolic calcium released from the ER (López-Sanjurjo et al., 2013). It has been reported that the ability of lysosomes to buffer Ca^{2+} in lysosomally diseased cells is greatly reduced, possibly because of the accumulation of undigested lysosomal cargo (Lloyd-Evans et al., 2008). Furthermore, buffering of cytosolic calcium by the mitochondria is defective in MLIV cells (Jennings et al., 2006). As calcium buffering is a mechanism involved in tempering calcium responses, loss of buffering capacity could actually result in enhanced global calcium signals. A similar mechanism has been demonstrated in *Dictyostelium* cells lacking the ER calcium binding proteins calnexin and calreticulin, as these strains had much larger calcium responses to chemoattractants than control cells (Wilczynska et al., 2005).

Since our mucolipin knockdown strains exhibited increased, as opposed to decreased, cytosolic Ca^{2+} signals during the vegetative phase of the lifecycle, it was surprising to find that when these strains were allowed to differentiate to aggregation-competence, their Ca^{2+} responses to cAMP were unaffected. Similarly, Chang et al. (2020) reported that in *Dictyostelium* TPC-null cells the magnitude of cAMP-mediated Ca^{2+} responses was comparable to that in wild type AX2 cells. Together these results suggest that mucolipin-dependent calcium signalling is not a major contributor to cytosolic calcium responses at this stage of development. Instead the role of mucolipin in the differentiated cells may be restricted to regulating local calcium signalling. Accordingly, the cAMP responses in the TPC null cells were slightly delayed in the time of onset, and this may be related to local calcium release from the acidic stores in "priming" ER calcium release (Chang et al., 2020), but this will require further investigation.

In previous work, the cellular phenotypes of growth, endocytosis and multicellular development were unaffected in mucolipin knockout cells created from the parental strain DH1-10 (Lima et al., 2012). Since our strains were made in the parental strain AX2, we wanted to also characterise these phenotypes in our strains. We found that surprisingly our strains did have abnormal phenotypes and many, but not all of these, presented similarly in the knockdown cells as overexpression cells. Furthermore, some of the phenotypes in our strains were similar to those reported in *Dictyostelium* NCL models.

Phagocytosis rates were increased in both mucolipin knockdown and overexpression cells. This may be directly related to the increased calcium signalling in these strains as evidence suggests that calcium is involved in phagocytosis (Muller-Taubenberger et al., 2001; Yuan et al., 2001; Fajardo et al., 2004; Pikzack et al., 2005). Pinocytosis rates were increased in knockdown strains, but

unaffected in overexpression strains which suggests the defect is not directly caused by the abnormal calcium signalling. The involvement of Ca^{2+} in macropinocytosis is unclear. Extracellular Ca^{2+} is not essential (Williams and Kay, 2018), but both liberation of intracellular Ca^{2+} by caffeine treatment and inhibition of Ca^{2+} transport by La^{3+} treatment reduces macropinocytosis (Gonzalez et al., 1990). However, both caffeine and La^{2+} can affect other processes. Our results suggest different roles for mucolipin function in macropinocytosis and phagocytosis.

When measuring growth rates, we expected that the increase in phagocytosis rates would correlate with an increase in growth rates on bacterial lawns, however both knockdown and overexpression strains grew normally on *E. coli*. Furthermore, axenic growth rates were slightly reduced in knockdown strains, so again did not correlate with the increase in pinocytic uptake. This phenotype was also present in *cln2* knockdown mutants (Smith et al., 2019) and together these results may represent the presence of compensatory feedback pathways that upregulate rates of endocytosis as a response to nutrient deprivation caused by defective endolysosomal trafficking. This kind of reverse coupling of growth and endocytosis rates has also been observed in relation to other *Dictyostelium* lysosomal proteins. A *Dictyostelium* knockout of *alyA* (encoding the major lysozyme isoform) has 40% reduction in total lysozyme activity, exhibits slow growth on bacterial lawns but increased phagocytosis of fluorescently labelled yeast cells due to a compensatory pathway (Müller et al., 2005). Knocking down expression of lysosomal Tpp1 (tripeptidyl peptidase I encoded by *cln2/tpp1*) caused reductions in the growth rate in liquid medium, slower plaque expansion rates on bacterial lawns, but elevated rates of phagocytosis (Smith et al., 2019). These effects were mediated by reduced activity of the *Dictyostelium* TORC1 (homologue of the human mechanistic Target of Rapamycin Complex I) signalling pathway, being mimicked by rapamycin treatment (inhibitor of TORC1) and Rheb knockdown (upstream activator of TORC1), and rescued by Rheb overexpression (Smith et al., 2019). Other *Dictyostelium* NCL models have shown varying phenotypes in their growth and nutrient uptake phenotypes. Mutants lacking *cln3* and *cln5* displayed enhanced proliferation in HL5 medium, however pinocytic uptake was not significantly different from AX3, and the *cln3*$^-$ phenotype was rescued by overexpression of GFP-cln3 (Huber et al., 2014; McLaren et al., 2021). Combined these results indicate abnormalities in nutrient uptake and growth and the pathways that connect them in the different lysosomal disease models.

The defects in catabolism that we observed in our strains could also be caused by disruptions in mucolipin-mediated Ca^{2+}-dependent vesicle fragmentation/fusion which is characteristic of MLIV and other MLIV models (Berman et al., 1974; Bargal and Bach, 1997; Lubensky et al., 1999). We observed that mucolipin knockdown and overexpression strains had increased fluorescence when stained with Lysosensor Blue. This may be linked to accumulation of Lysosensor Blue-stained vesicles as a result of Ca^{2+}-dependent increases in homotypic or heterotypic vesicle fusion during the endosomal mixing stage and subsequent failure to progress through to exocytosis. Studies in other models reported that the defective membrane trafficking can be caused by both knockout and overexpression of TRPMLs causing accumulation of large hybrid late endosome-lysosomal compartments (Berman et al., 1974; Lubensky et al., 1999) as well as enlargement and clustering of endosomes (Fares and Greenwald, 2001; Kim et al., 2007; Martina et al., 2009; Vergarajauregui et al., 2009). In *Dictyostelium* DH1-10 mucolipin knockout cells, a significant increase in generation of post-lysosomes was reported, however as this was coupled with enhanced rate of post-lysosome fusion with the plasma membrane, and subsequent exocytosis, so that there was no measurable build-up of vesicles (Lima et al., 2012). We did not measure exocytosis rates in our strains, so further experiments could determine if exocytosis is blocked in our strains and account for the accumulation.

Alternatively, because Lysosensor Blue fluorescence increases as the pH becomes more acidic, the increased fluorescence in our knockdown and overexpression strains could also be caused by a decrease in the pH of the vesicles. Dysregulated lysosomal pH is common to lysosomal storage disease cells, however this is generally linked to increased pH as reported in MLIV fibroblasts type (Bach et al., 1999) and most NCLs (Holopainen et al., 2001). However, decreased lysosomal pH has been described in some MLIV fibroblasts (Soyombo et al., 2006). It is important to note that *Dictyostelium* cells lacking mucolipin exhibited no change in the pH of endosomal compartments (Lima et al., 2012).

A further consequence of dysfunctional catabolism, retention of unprocessed nutrients and decreased release of amino acids from the vesicles, could be that the cells are in a state of partial starvation and this would favour the initiation of aggregation. In support of this, both mucolipin knockdown and overexpression strains exhibited increased numbers of aggregation centers and accordingly formed slugs and fruiting bodies significantly smaller than those of AX2. This implicates mucolipin in activation of aggregation center formation and could be linked to calcium-dependent regulation of developmental processes (Sakamoto et al., 2003; Poloz and O'Day, 2012). The same phenotype is present in *IplA*$^-$ cells which form smaller mounds and fruiting bodies due to fragmented aggregation streams (Traynor et al., 2000; Schaloske et al., 2005). Similar phenotypes are also present in other *Dictyostelium* lysosomal disease models. Mutants with knocked down *cln2/tpp1* form smaller aggregates and fruiting bodies (also mediated by reduced TORC1 signalling, Smith et al., 2019), and *cln2/tpp1*$^-$ mutants progress faster through development (Phillips and Gomer, 2015). Cells lacking *cln3* and *cln5* exhibit precocious development, increased numbers of tipped mounds, fingers and slugs, similar to our mucolipin strains (Huber et al., 2014; Huber et al., 2017; McLaren et al., 2021). Interestingly, the precocious development in *cln3*$^-$ cells was rescued by chelation of calcium with EGTA. This implicates Cln3 in calcium regulation, likely due to its localisation at the contractile vacuole, a major calcium regulatory organelle (Malchow et al., 2006; Huber et al., 2014), and suggests calcium dysregulation may be common to lysosomal disease cells.

In addition to the increased numbers of aggregates formed in our knockdown and overexpression mutants, an increased proportion of the cells in the aggregates appear to be entering the autophagic cell death pathway. This was suggested by the proportionately thicker stalks and enlarged basal disks, a phenotype associated with increased autophagic cell death (Bokko et al., 2007). This is another phenotype common among *Dictyostelium* lysosomal disease mutants. It is also present in *tpp1* knockdown cells where it is mediated by reduced

TORC1 signalling (Smith et al., 2019). Furthermore, enhanced autophagy has been reported in *tpp1* knockout cells (Phillips and Gomer, 2015) and *cln5*$^{-}$ cells display aberrant autophagy (McLaren et al., 2021). TPC knockout cells also accumulate autophagosomes (Chang et al., 2020) which further implicates calcium signalling through the acidic stores in autophagic processes. As autophagic cell death occurs late in the developmental cycle during stalk formation, it is possible that during autophagy, mucolipin together with other calcium channels in that location (TPC in particular) could play similar roles in generating a local Ca^{2+} cloud to facilitate fusion of the autophagosome and lysosome during formation of the stalk cell vacuole. Schaap et al. (1996) showed that a sustained elevation of resting cytoplasmic Ca^{2+} levels mediates late stalk gene (*ecmB*) induction by the morphogen DIF (Differentiation Inducing Factor) in *Dictyostelium*. Mucolipin could play a role in this process. In that case, as we have seen in the endolysosomal pathway, mucolipin overexpression and knockdown would both cause increased Ca^{2+} signals and subsequent disturbances in autophagolysosome formation, possibly explaining the stalk phenotype. An increase in cellular autophagic vacuoles is a characteristic associated with MLIV (Vergarajauregui et al., 2008) is observed both in mouse models (Curcio-Morelli et al., 2010), and *Drosophila* mucolipin knockout flies (Wong et al., 2012). The underlying nature of the autophagic defect may be related to disruption in signalling by the nutrient stress sensor mTORC1, a key regulator of autophagy. One study has shown that mTORC1 can directly phosphorylate TRPML1 to negatively regulate channel activity and decrease autophagy (Onyenwoke et al., 2015). To add further complexity, recent evidence has revealed that TRPML1 Ca^{2+} release can regulate mTORC1 autophagic pathways through a nutrient-sensitive negative feedback loop (Sun et al., 2018). Furthermore, TRPML1 is directly involved in the Ca^{2+}/calmodulin dependent protein kinase β (CaMKKβ) activation of AMP-activated protein kinase (AMPK) (Scotto-Rosato et al., 2019). AMPK in turn inhibits TORC1 and thereby activates autophagy.

The nature of these complex signalling pathways still needs to be unravelled, therefore our study supports the view that *Dictyostelium* offers a tractable, simple model for MLIV cytopathology. The results suggest it would be valuable in future experiments to investigate further the signalling pathways involved in mucolipin Ca^{2+} signalling-dependent regulation of cellular growth and autophagy through *Dictyostelium* TORC1. This is of particular interest because the role of Ca^{2+} signalling in regulation of mTORC1 autophagy pathways is evident, but details are still unclear (Decuypere et al., 2011), as are mTORC1-TRPML signalling pathways. Therefore, it would be relevant to explore whether the growth and developmental defects can be rescued by genetically altering *Dictyostelium* TORC1 and *Dictyostelium* AMPK expression in mucolipin knockdown and overexpression backgrounds.

The results we have presented here highlight common phenotypes amongst *Dictyostelium* lysosomal disease models suggesting they may share common pathologies. We have also shown that both increasing and decreasing mucolipin expression levels can cause the same phenotypic outcome. Our results are similar to other studies where reports of both increased and decreased expression of mucolipin proteins can cause problems along the endocytic pathways. For example, when TRPML3 is knocked down there are defects in endosomal acidification and also increased homotypic endosomal fusion (Lelouvier and Puertollano, 2011), while when TRPML3 is overexpressed, endosomes become enlarged (Martina et al., 2009; Lelouvier and Puertollano, 2011). In *C. elegans*, both mucolipin knockout and some overexpression coelomocytes, exhibited the formation of large vacuoles (Fares and Geenwald, 2001). Similarly, overexpression of TRPML1 results in accumulation of enlarged endosomes containing both early (Hrs) and late (CD63) endocytic markers (Vergarajauregui et al., 2009) and induces an aberrant distribution of these compartments within the cell (Manzoni et al., 2004). These combined reports show that the endocytic pathway is clearly impacted by disturbances in both directions in the expression levels or activities of mucolipin proteins and the resultant alterations in Ca^{2+} signalling.

DATA AVAILABILITY STATEMENT

Raw data will be made available by contacting the corresponding authors, without reservation.

AUTHOR CONTRIBUTIONS

CA performed the experiments, curated the data and wrote the manuscript. PF conceptualized the project, supervised. CA, helped analyse data, reviewed and helped write the manuscript.

FUNDING

This work was funded by Australian Research Council Discovery Project Grant DP140104276.

ACKNOWLEDGMENTS

We are grateful to Professor Pierre Cosson for kindly providing us with nitrocellulose membranes and cell lysate from DH1-10 and mucolipin knockout cells and Anna Dardel for carefully preparing and sending the materials to us. We are grateful to Dr. Sarah Annesley who provided advice on some of the techniques and critiqued the manuscript for us.

SUPPLEMENTARY MATERIAL

The Supplementary Material for this article can be found online at: https://www.frontiersin.org/articles/10.3389/fcell.2022.741967/full#supplementary-material

REFERENCES

Annesley, S. J., Chen, S., Francione, L. M., Sanislav, O., Chavan, A. J., and Farah, C. (2014). *Dictyostelium*, a Microbial Model for Brain Disease. *Biochim. Biophys. Acta* 1840, 1413–1432. doi:10.1016/j.bbagen.2013.10.019

Annesley, S. J., and Fisher, P. R. (2009). *Dictyostelium discoideum*-a Model for many Reasons. *Mol. Cel Biochem.* 329, 73–91. doi:10.1007/s11010-009-0111-8

Bach, G., Chen, C. S., and Pagano, R. E. (1999). Elevated Lysosomal pH in Mucolipidosis Type IV Cells. *Clin. Chim. Acta* 280 (1-2), 173–179. doi:10.1016/s0009-8981(98)00183-1

Bargal, R., and Bach, G. (1997). Mucolipidosis Type IV: Abnormal Transport of Lipids to Lysosomes. *J. Inherit. Metab. Dis.* 20, 625–632. doi:10.1023/a:1005362123443

Barth, C., Fraser, D. J., and Fisher, P. R. (1998). Co-insertional Replication Is Responsible for Tandem Multimer Formation during Plasmid Integration into the *Dictyostelium* Genome. *Plasmid* 39, 141–153. doi:10.1006/plas.1997.1326

Benini, A., Bozzato, A., Mantovanelli, S., Calvarini, L., Giacopuzzi, E., Bresciani, R., et al. (2013). Characterization and Expression Analysis of mcoln1.1 and mcoln1.2, the Putative Zebrafish Co-orthologs of the Gene Responsible for Human Mucolipidosis Type IV. *Int. J. Dev. Biol.* 57 (1), 85–93. doi:10.1387/ijdb.120033gb

Berman, E. R., Livni, N., Shapira, E., Merin, S., and Levij, I. S. (1974). Congenital Corneal Clouding with Abnormal Systemic Storage Bodies: a New Variant of Mucolipidosis. *J. Pediatr.* 84 (4), 519–526. doi:10.1016/s0022-3476(74)80671-2

Bharat, T. A., Malsam, J., Hagen, W. J., Scheutzow, A., Söllner, T. H., and Briggs, J. A. G. (2014). SNARE and Regulatory Proteins Induce Local Membrane Protrusions to Prime Docked Vesicles for Fast Calcium-Triggered Fusion. *EMBO Rep.* 15, 308–314. doi:10.1002/embr.201337807

Bokko, P. B., Francione, L., Bandala-Sanchez, E., Ahmed, A. U., Annesley, S. J., Huang, X., et al. (2007). Diverse Cytopathologies in Mitochondrial Disease Are Caused by AMP-Activated Protein Kinase Signalling. *Mol. Biol. Cel.* 18, 1874–1886. doi:10.1091/mbc.E06-09-0881

Boudewyn, L. C., and Walkley, S. U. (2019). Current Concepts in the Neuropathogenesis of Mucolipidosis Type IV. *J. Neurochem.* 148, 669–689. doi:10.1111/jnc.14462

Brailoiu, G. C., and Brailoiu, E. (2016). Modulation of Calcium Entry by the Endo-Lysosomal System. *Adv. Exp. Med. Biol.* 898, 423–447. doi:10.1007/978-3-319-26974-0_18

Cao, Q., Yang, Y., Zhong, X. Z., and Dong, X. P. (2017). The Lysosomal Ca^{2+} Release Channel TRPML1 Regulates Lysosome Size by Activating Calmodulin. *J. Biol. Chem.* 292, 8424–8435. doi:10.1074/jbc.M116.772160

Cao, Q., Zhong, X. Z., Zou, Y., Zhang, Z., Toro, L., and Dong, X. P. (2015). BK Channels Alleviate Lysosomal Storage Diseases by Providing Positive Feedback Regulation of Lysosomal Ca^{2+} Release. *Dev. Cel* 33 (4), 427–441. doi:10.1016/j.devcel.2015.04.010

Chang, F. S., Wang, Y., Dmitriev, P., Gross, J., Galione, A., and Pears, C. (2020). A Two-Pore Channel Protein Required for Regulating mTORC1 Activity on Starvation. *BMC Biol.* 18 (1), 8. doi:10.1186/s12915-019-0735-4

Chen, C. S., Bach, G., and Pagano, R. E. (1998). Abnormal Transport along the Lysosomal Pathway in Mucolipidosis, Type IV Disease. *PNAS USA* 95, 6373–6378. doi:10.1073/pnas.95.11.6373

Cheng, X., Shen, D., Samie, M., and Xu, H. (2010). Mucolipins: Intracellular TRPML1-3 Channels. *FEBS Lett.* 584, 2013–2021. doi:10.1016/j.febslet.2009.12.056

Christoforidis, S., McBride, H. M., Burgoyne, R. D., and Zerial, M. (1999). The Rab5 Effector EEA1 Is a Core Component of Endosome Docking. *Nature* 397, 621–625. doi:10.1038/17618

Curcio-Morelli, C., Charles, F. A., Micsenyi, M. C., Cao, Y., Venugopal, B., Browning, M. F., et al. (2010). Macroautophagy Is Defective in Mucolipin-1-Deficient Mouse Neurons. *Neurobiol. Dis.* 40, 370–377. doi:10.1016/j.nbd.2010.06.010

Decuypere, J. P., Bultynck, G., and Parys, J. B. (2011). A Dual Role for Ca^{2+} in Autophagy Regulation. *Cell Calcium* 50, 242–250. doi:10.1016/j.ceca.2011.04.001

Denis, V., and Cyert, M. S. (2002). Internal Ca^{2+} Release in Yeast Is Triggered by Hypertonic Shock and Mediated by a TRP Channel Homologue. *J. Cel. Biol.* 156, 29–34. doi:10.1083/jcb.200111004

Dong, X. P., Wang, X., and Xu, H. (2010). TRP Channels of Intracellular Membranes. *J. Neurochem.* 113, 313–328. doi:10.1111/j.1471-4159.2010.06626.x

Dowson, J. H., Armstrong, D., Koppang, N., Lake, B. D., and Jolly, R. D. (1982). Autofluorescence Emission Spectra of Neuronal Lipopigment in Animal and Human Ceroidoses (Ceroid-lipofuscinoses). *Acta Neuropathol.* 58, 152–156. doi:10.1007/BF00691656

Fajardo, M., Schleicher, M., Noegel, A., Bozzaro, S., Killinger, S., Heuner, K., et al. (2004). Calnexin, Calreticulin and Cytoskeleton-Associated Proteins Modulate Uptake and Growth of *Legionella pneumophila* in *Dictyostelium discoideum*. *Microbiology* 150, 2825–2835. doi:10.1099/mic.0.27111-0

Fares, H., and Greenwald, I. (2001). Regulation of Endocytosis by CUP-5, the *Caenorhabditis elegans* Mucolipin-1 Homolog. *Nat. Genet.* 28, 64–68. doi:10.1038/88281

Feng, X., Huang, Y., Lu, Y., Xiong, J., Wong, C. O., Yang, P., et al. (2014). *Drosophila* TRPML Forms PI(3,5)P2-activated Cation Channels in Both Endolysosomes and Plasma Membrane. *J. Biol. Chem.* 289, 4262–4272. doi:10.1074/jbc.M113.506501

Fernando, S., Allan, C. Y., Mroczek, K., Pearce, X., Sanislav, O., Fisher, P. R., et al. (2020). Cytotoxicity and Mitochondrial Dysregulation Caused by α-Synuclein in. *Dictyostelium discoideum. Cell* 9 (10), 2289. doi:10.3390/cells9102289

Fey, P., Gaudet, P., Curk, T., Zupan, B., Just, E. M., Basu, S., et al. (2009). dictyBase-a *Dictyostelium* Bioinformatics Resource Update. *Nucleic Acids Res. (Database Issue)*, D515–D519. doi:10.1093/nar/gkn844

Fisher, R., and Wilczynska, Z. (2006). Contribution of Endoplasmic Reticulum to Ca^{2+} Signals in *Dictyostelium* Depends on Extracellular Ca^{2+}. *FEMS Microbiol. Lett.* 257, 268–277. doi:10.1111/j.1574-6968.2006.00180.x

Fountain, S. J., Parkinson, K., Young, M. T., Cao, L., Thompson, C. R. L., and North, R. A. (2007). An Intracellular P2X Receptor Required for Osmoregulation in *Dictyostelium discoideum*. *Nature* 448 (7150), 200–203. doi:10.1038/nature05926

Gerasimenko, J. V., Tepikin, A. V., Petersen, O. H., and Gerasimenko, O. V. (1998). Calcium Uptake via Endocytosis with Rapid Release from Acidifying Endosomes. *Curr. Biol.* 8, 1335–1338. doi:10.1016/S0960-9822(07)00565-9

Goldin, E., Blanchette-Mackie, E. J., Dwyer, N. K., Pentchev, P. G., and Brady, R. O. (1995). Cultured Skin Fibroblasts Derived from Patients with Mucolipidosis 4 Are Auto-Fluorescent. *Pediatr. Res.* 37, 687–692. doi:10.1203/00006450-199506000-00003

Gómez, N. M., Lu, W., Lim, J. C., Kiselyov, K., Campagno, K. E., Grishchuk, Y., et al. (2018). Robust Lysosomal Calcium Signaling through Channel TRPML1 Is Impaired by Lysosomal Lipid Accumulation. *FASEB J.* 32 (2), 782–794. doi:10.1096/fj.201700220RR

Gonzalez, C., Klein, G., and Satre, M. (1990). Caffeine, an Inhibitor of Endocytosis in *Dictyostelium discoideum* Amoebae. *J. Cel Physiol.* 144, 408–415. doi:10.1002/jcp.1041440307

Grimm, C., Jörs, S., Guo, Z., Obukhov, A. G., and Heller, S. (2012). Constitutive Activity of TRPML2 and TRPML3 Channels versus Activation by Low Extracellular Sodium and Small Molecules. *J. Biol. Chem.* 287 (27), 22701–22708. doi:10.1074/jbc.M112.369876

Gross, J. D. (2009). Acidic Ca^{2+} Stores, Excitability, and Cell Patterning in *Dictyostelium discoideum*. *Eukaryot. Cel* 8 (5), 696–702. doi:10.1128/ec.00360-08

Han, J., Pluhackova, K., and Böckmann, R. A. (2017). The Multifaceted Role of SNARE Proteins in Membrane Fusion. *Front. Physiol.* 8, 5. doi:10.3389/fphys.2017.00005

Hay, J. C. (2007). Calcium, a Fundamental Regulator of Membrane Fusion? *EMBO Rep.* 8 (3), 236–240. doi:10.1038/sj.embor.7400921

Holopainen, J. M., Saarikoski, J., Kinnunen, P. K. J., and Jarvela, I. (2001). Elevated Lysosomal pH in Neuronal Ceroid Lipofuscinoses (NCLs). *Eur. J. Biochem.* 268, 5851–5856. doi:10.1046/j.0014-2956.2001.02530.x

Huber, R. J., and Mathavarajah, S. (2019). Comparative Transcriptomics Reveals Mechanisms Underlying Cln3-Deficiency Phenotypes in *Dictyostelium*. *Cell Signal* 58, 79–90. doi:10.1016/j.cellsig.2019.02.004

Huber, R. J. (2020). Molecular Networking in the Neuronal Ceroid Lipofuscinoses: Insights from Mammalian Models and the Social Amoeba *Dictyostelium discoideum*. *J. Biomed. Sci.* 27 (1), 64. doi:10.1186/s12929-020-00653-y

Huber, R. J., Myre, M. A., and Cotman, S. L. (2017). Aberrant Adhesion Impacts Early Development in a *Dictyostelium* Model for Juvenile Neuronal Ceroid

Lipofuscinosis. *Cell Adh Migr* 11 (4), 399–418. doi:10.1080/19336918.2016.1236179

Huber, R. J., Myre, M. A., and Cotman, S. L. (2014). Loss of Cln3 Function in the Social Amoeba *Dictyostelium discoideum* Causes Pleiotropic Effects that Are Rescued by Human CLN3. *PLoS ONE* 9 (10), e110544. doi:10.1371/journal.pone.0110544

Jennings, J. J., Jr, Zhu, J. H., Rbaibi, Y., Luo, X., Chu, C. T., and Kiselyov, K. (2006). Mitochondrial Aberrations in Mucolipidosis Type IV. *J. Biol. Chem.* 281 (51), 39041–39050. doi:10.1074/jbc.M607982200

Kilpatrick, B. S., Yates, E., Grimm, C., Schapira, A. H., and Patel, S. (2016). Endo-lysosomal TRP Mucolipin-1 Channels Trigger Global ER Ca^{2+} Release and Ca^{2+} Influx. *J. Cel Sci.* 129 (20), 3859–3867. doi:10.1242/jcs.190322

Kim, H. J., Li, Q., Tjon-Kon-Sang, S., So, I., Kiselyov, K., and Muallem, S. (2007). Gain-of-function Mutation in TRPML3 Causes the Mouse Varitint-Waddler Phenotype. *J. Biol. Chem.* 282, 36138–36142. doi:10.1074/jbc.C700190200

Kiselyov, K., Chen, J., Rbaibi, Y., Oberdick, D., Tjon-Kon-Sang, S., Shcheynikov, N., et al. (2005). TRP-ML1 Is a Lysosomal Monovalent Cation Channel that Undergoes Proteolytic Cleavage. *J. Biol. Chem.* 280, 43218–43223. doi:10.1074/jbc.M508210200

Kotsifas, M., Barth, C., Lay, S. T., Lozanne, A., and Fisher, P. R. (2002). Chaperonin 60 and Mitochondrial Disease in *Dictyostelium*. *J. Muscle Res. Cel Motil* 23, 839–852. doi:10.1023/A:1024444215766

LaPlante, J. M., Falardeau, J., Sun, M., Kanazirska, M., Brown, E. M., Slaugenhaupt, S. A., et al. (2002). Identification and Characterization of the Single Channel Function of Human Mucolipin-1 Implicated in Mucolipidosis Type IV, a Disorder Affecting the Lysosomal Pathway. *FEBS Lett.* 532, 183–187. doi:10.1016/S0014-5793(02)03670-0

LaPlante, J. M., Ye, C. P., Quinn, S. J., Goldin, E., Brown, E. M., Slaugenhaupt, S. A., et al. (2004). Functional Links between Mucolipin-1 and Ca^{2+}-dependent Membrane Tracking in Mucolipidosis IV. *Biochem. Biophys. Res. Commun.* 322, 1384–1391. doi:10.1016/j.bbrc.2004.08.045

Lawe, D. C., Sitouah, N., Hayes, S., Chawla, A., Virbasius, J. V., Tuft, R., et al. (2003). Essential Role of Ca^{2+}/Calmodulin in Early Endosome Antigen-1 Localization. *Mol. Biol. Cel* 14 (7), 2935–2945. doi:10.1091/mbc.e02-09-0591

Lee, K., Jo, Y. Y., Chung, G., Jung, J. H., Kim, Y. H., and Park, C. K. (2021). Functional Importance of Transient Receptor Potential (TRP) Channels in Neurological Disorders. *Front. Cel. Dev. Biol.* 9, 611773. doi:10.3389/fcell.2021.611773

Lelouvier, B., and Puertollano, R. (2011). Mucolipin-3 Regulates Lumenal Calcium, Acidification, and Membrane Fusion in the Endosomal Pathway. *J. Biol. Chem.* 286, 9826–9832. doi:10.1074/jbc.M110.169185

Lima, W. C., Leuba, F., Soldati, T., and Cosson, P. (2012). Mucolipin Controls Lysosome Exocytosis in *Dictyostelium*. *J. Cel Sci.* 125, 2315–2322. doi:10.1242/jcs.100362

Lima, W. C., Vinet, A., Pieters, J., and Cosson, P. (2014). Role of PKD2 in Rheotaxis in *Dictyostelium*. *PLoS ONE* 9 (2), e88682. doi:10.1371/journal.pone.0088682

Lloyd-Evans, E., Morgan, A., He, X., Smith, D. A., Elliot-Smith, E., Sillence, D. J., et al. (2008). Niemann-Pick Disease Type C1 Is a Sphingosine Storage Disease that Causes Deregulation of Lysosomal Calcium. *Nat. Med.* 14, 1247–1255. doi:10.1038/nm.1876

López-Sanjurjo, C. I., Tovey, S. C., Prole, D. L., and Taylor, C. W. (2013). Lysosomes Shape Ins(1,4,5)P3-Evoked Ca^{2+} Signals by Selectively Sequestering Ca^{2+} Released from the Endoplasmic Reticulum. *J. Cel Sci.* 126 (1), 289–300. doi:10.1242/jcs.116103

López-Sanjurjo, C. I., Tovey, S. C., and Taylor, C. W. (2014). Rapid Recycling of Ca^{2+} between IP3-Sensitive Stores and Lysosomes. *PLoS One* 9 (10), e111275. doi:10.1371/journal.pone.0111275

Lubensky, I. A., Schiffmann, R., Goldin, E., and Tsokos, M. (1999). Lysosomal Inclusions in Gastric Parietal Cells in Mucolipidosis Type IV: a Novel Cause of Achlorhydria and Hypergastrinemia. *Am. J. Surg. Pathol.* 23, 1527–1531.

Lusche, D. F., Wessels, D., Scherer, A., Daniels, K., Kuhl, S., and Sol, l. D. R. (2012). The IplA Ca^{2+} Channel of *Dictyostelium discoideum* Is Necessary for Ca^{2+}, but Not cAMP Chemotaxis, and Plays a Fundamental Role in Natural Aggregation. *J. Cel Sci.* 125 (7), 1770–1783.

Luzio, J. P., Bright, N. A., and Pryor, P. R. (2007). The Role of Calcium and Other Ions in Sorting and Delivery in the Late Endocytic Pathway. *Biochem. Soc. Trans.* 35, 1088–1091. doi:10.1042/BST0351088

Lytton, J., Westlin, M., and Hanley, M. R. (1991). Thapsigargin Inhibits the Sarcoplasmic or Endoplasmic Reticulum Ca^{2+}-ATPase Family of Calcium Pumps. *J. Biol. Chem.* 266, 17067–17071.

Malchow, D., Lusche, D. F., De Lozanne, A., and Schlatterer, C. (2008). A Fast Ca^{2+}-Induced Ca^{2+}-Release Mechanism in *Dictyostelium discoideum*. *Cell Calcium* 43 (6), 521–530. doi:10.1016/j.ceca.2007.08.002

Malchow, D., Lusche, D. F., Schlatterer, C., De Lozanne, A., and Müller-Taubenberger, A. (2006). The Contractile Vacuole in Ca^{2+}-Regulation in *Dictyostelium*: its Essential Function for cAMP-Induced Ca^{2+}-Influx. *BMC Dev. Biol.* 6, 31. doi:10.1186/1471-213X-6-31

Maniak, M. (2011). *Dictyostelium* as a Model for Human Lysosomal and Trafficking Diseases. *Semin. Cel Dev Biol* 22 (1), 114–119. doi:10.1016/j.semcdb.2010.11.001

Manzoni, M., Monti, E., Bresciani, R., Bozzato, A., Barlati, S., Bassi, M. T., et al. (2004). Overexpression of Wild-type and Mutant Mucolipin Proteins in Mammalian Cells: Effects on the Late Endocytic Compartment Organization. *FEBS Lett.* 567, 219–224. doi:10.1016/j.febslet.2004.04.080

Martín-González, J., Montero-Bullón, J. F., and Lacal, J. (2021). *Dictyostelium discoideum* as a Non-mammalian Biomedical Model. *Microb. Biotechnol.* 14 (1), 111–125. doi:10.1111/1751-7915.13692

Martina, J. A., Lelouvier, B., and Puertollano, R. (2009). The Calcium Channel Mucolipin-3 Is a Novel Regulator of Trafcking along the Endosomal Pathway. *Traffic* 10, 1143–1156. doi:10.1111/j.1600-0854.2009.00935.x

Maselli, A., Laevsky, G., and Knecht, D. A. (2002). Kinetics of Binding, Uptake and Degradation of Live Fluorescent (DsRed) Bacteria by *Dictyostelium discoideum*. *Microbiology (Reading)* 148, 413–420. doi:10.1099/00221287-148-2-413

McLaren, M. D., Mathavarajah, S., Kim, W. D., Yap, S. Q., and Huber, R. J. (2021). Aberrant Autophagy Impacts Growth and Multicellular Development in a *Dictyostelium* KO Model of CLN5 Disease. *Front. Cell Dev. Biol.* 9, 657406. doi:10.3389/fcell.2021.657406

Medina, D. L., Di Paola, S., Peluso, I., Armani, A., De Stefani, D., Venditti, R., et al. (2015). Lysosomal Calcium Signalling Regulates Autophagy through Calcineurin and TFEB. *Nat. Cel Biol* 17 (3), 288–299. doi:10.1038/ncb3114

Micsenyi, M. C., Dobrenis, K., Stephney, G., Pickel, J., Vanier, M. T., Slaugenhaupt, S. A., et al. (2009). Neuropathology of the Mcoln1(-/-) KO Mouse Model of mucolipidosis type IV. *J. Neuropathol. Exp. Neurol.* 68, 125–135. doi:10.1097/NEN.0b013e3181942cf0

Miedel, M. T., Rbaibi, Y., Guerriero, C. J., Colletti, G., Weixel, K. M., Weisz, O. A., et al. (2008). Membrane Traffic and Turnover in TRP-ML1-Deficient Cells: a Revised Model for Mucolipidosis Type IV Pathogenesis. *J. Exp. Med.* 205 (6), 1477–1490. doi:10.1084/jem.20072194

Miedel, M. T., Weixel, K. M., Bruns, J. R., Traub, L. M., and Weisz, O. A. (2006). Posttranslational Cleavage and Adaptor Protein Complex-dependent Trafficking of Mucolipin-1. *J. Biol. Chem.* 281 (18), 12751–12759. doi:10.1074/jbc.M511104200

Mills, I. G., Jones, A. T., and Clague, M. J. (1998). Involvement of the Endosomal Autoantigen EEA1 in Homotypic Fusion of Early Endosomes. *Curr. Biol.* 8, 881–884. doi:10.1016/s0960-9822(07)00351-x

Müller, I., Šubert, N., Otto, H., Herbst, R., Rühling, H., Maniak, M., et al. (2005). A *Dictyostelium* Mutant with Reduced Lysozyme Levels Compensates by Increased Phagocytic Activity. *J. Biol. Chem.* 280, 10435–10443. doi:10.1074/jbc.M411445200

Müller-Taubenberger, A., Lupas, A. N., Li, H., Ecke, M., Simmeth, E., and Gerisch, G. (2001). Calreticulin and Calnexin in the Endoplasmic Reticulum Are Important for Phagocytosis. *EMBO J.* 20 (23), 6772–6782. doi:10.1093/emboj/20.23.6772

Morgan, A. J., Platt, F. M., Lloyd-Evans, E., and Galione, A. (2011). Molecular Mechanisms of Endolysosomal Ca^{2+} Signalling in Health and Disease. *Biochem. J.* 439 (3), 349–374.

Nebl, T., and Fisher, P. R. (1997). Intracellular Ca^{2+} Responses by *Dictyostelium* Amoebae to Nanomolar Chemoattractant Stimuli Are Mediated Exclusively by Ca^{2+} Influx. *J. Cel Sci.* 110, 2845–2853.

Nebl, T., Kotsifas, M., Schaap, P., and Fisher, P. R. (2002). Multiple Pathways Connect Chemoattractant Receptors and Ca^{2+} Channels in *Dictyostelium*. *J. Muscle Res. Cel Motil* 23, 853–865. dio: doi:10.1023/a:1024496232604

Nellen, W., Silan, C., and Firtel, R. A. (1984). DNA-mediated Transformation in *Dictyostelium discoideum*: Regulated Expression of an Actin Gene Fusion. *Mol. Cel. Biol.* 4, 2890–2898. doi:10.1128/mcb.4.12.2890-2898.1984

Onyenwoke, R. U., Sexton, J. Z., Yan, F., Díaz, M. C. H., Forsberg, L. J., Major, M. B., et al. (2015). The Mucolipidosis IV Ca^{2+} Channel TRPML1 (MCOLN1) Is Regulated by the TOR Kinase. *Biochem. J.* 470, 331–342. doi:10.1042/BJ20150219

Parikh, A., Miranda, E. R., Katoh-Kurasawa, M., Fuller, D., Rot, G., Zagar, L., et al. (2010). Conserved Developmental Transcriptomes in Evolutionarily Divergent Species. *Genome Biol.* 11 (3), R35. doi:10.1186/gb-2010-11-3-r35

Patel, S., and Cai, X. (2015). Evolution of Acidic Ca^{2+} Stores and Their Resident Ca2+-Permeable Channels. *Cell Calcium* 57 (3), 222–230. doi:10.1016/j.ceca.2014.12.005

Patel, S., and Docampo, R. (2010). Acidic Calcium Stores Open for Business: Expanding the Potential for Intracellular Ca^{2+} Signaling. *Trends Cel Biol* 20 (5), 277–286. doi:10.1016/j.tcb.2010.02.003

Phillips, J. E., and Gomer, R. H. (2015). Partial Genetic Suppression of a Loss-Of-Function Mutant of the Neuronal Ceroid Lipofuscinosis-Associated Protease TPP1 in *Dictyostelium discoideum*. *Dis. Model. Mech.* 8, 147–156. doi:10.1242/dmm.018820

Pikzack, C., Prassler, J., Furukawa, R., Fechheimer, M., and Rivero, F. (2005). Role of Calcium-dependent Actin-Bundling Proteins: Characterization of *Dictyostelium* Mutants Lacking Fimbrin and the 34-kilodalton Protein. *Cell Motil. Cytoskeleton* 62, 210–231. doi:10.1002/cm.20098

Poloz, Y., and O'Day, D. H. (2012). Colchicine Affects Cell Motility, Pattern Formation and Stalk Cell Differentiation in *Dictyostelium* by Altering Calcium Signaling. *Differentiation* 83, 185–199. doi:10.1016/j.diff.2011.12.006

Pryor, P. R., Mullock, B. M., Bright, N. A., Gray, S. R., and Luzio, J. P. (2000). The Role of Intraorganellar Ca^{2+} in Late Endosome-Lysosome Heterotypic Fusion and in the Reformation of Lysosomes from Hybrid Organelles. *J. Cel Biol.* 149 (5), 1053–1062. doi:10.1083/jcb.149.5.1053

Ronco, V., Potenza, D. M., Denti, F., Vullo, S., Gagliano, G., Tognolina, M., et al. (2015). A Novel Ca^{2+}-Mediated Cross-Talk between Endoplasmic Reticulum and Acidic Organelles: Implications for NAADP-dependent Ca^{2+} Signalling. *Cell Calcium* 57 (2), 89–100. doi:10.1016/j.ceca.2015.01.001

Sakamoto, H., Nishio, K., Tomisako, M., Kuwayama, H., Tanaka, Y., et al. (2003). Identification and Characterization of Novel Calcium-Binding Proteins of *Dictyostelium* and Their Spatial Expression Patterns during Development. *Dev. Growth Differ.* 45, 507–514. doi:10.1111/j.1440-169X.2003.00718.x

Santoni, G., Maggi, F., Amantini, C., Marinelli, O., Nabissi, M., and Morelli, M. B. (2020). Pathophysiological Role of Transient Receptor Potential Mucolipin Channel 1 in Calcium-Mediated Stress-Induced Neurodegenerative Diseases. *Front. Physiol.* 11, 251. doi:10.3389/fphys.2020.00251

Schaap, P., Nebl, T., and Fisher, P. R. (1996). A Slow Sustained Increase in Cytosolic Ca^{2+} Levels Mediates Stalk Gene Induction by Differentiation Inducing Factor in *Dictyostelium*. *EMBO J.* 15 (19), 5177–5183. doi:10.1002/j.1460-2075.1996.tb00902.x

Schaloske, H., Lusche, F., Bezares-Roder, K., Happle, K., Malchow, D., and Schlatterer, C. (2005). Ca^{2+} Regulation in the Absence of the iplA Gene Product in *Dictyostelium discoideum*. *BMC Cel Biol* 6 (1), 13. doi:10.1186/1471-2121-6-13

Scotto-Rosato, A., Montefusco, S., Soldati, C., Di Paola, S., Capuozzo, A., Monfregola, J., et al. (2019). TRPML1 Links Lysosomal Calcium to Autophagosome Biogenesis through the Activation of the CaMKKβ/VPS34 Pathway. *Nat. Commun.* 10 (1), 5630. doi:10.1038/s41467-019-13572-w

Shen, D., Wang, X., Li, X., Zhang, X., Yao, Z., Dibble, S., et al. (2012). Lipid Storage Disorders Block Lysosomal Trafficking by Inhibiting a TRP Channel and Lysosomal Calcium Release. *Nat. Commun.* 3, 731. doi:10.1038/ncomms1735

Smith, D. E., and Fisher, P. A. (1984). Identification, Developmental Regulation, and Response to Heat Shock of Two Antigenically Related Forms of a Major Nuclear Envelope Protein in *Drosophila* Embryos: Application of an Improved Method for Affinity Purification of Antibodies Using Polypeptides Immobilized on Nitrocellulose Blots. *J. Cel. Biol.* 99, 20–28. doi:10.1083/jcb.99.1.20

Smith, P. K., Sen, M. G., Fisher, P. R., and Annesley, S. J. (2019). Modelling of Neuronal Ceroid Lipofuscinosis Type 2 in *Dictyostelium discoideum* Suggests that Cytopathological Outcomes Result from Altered TOR Signalling. *Cells* 8 (5), 469. doi:10.3390/cells8050469

Soyombo, A. A., Tjon-Kon-Sang, S., Rbaibi, Y., Bashllari, E., Bisceglia, J., Muallem, S., et al. (2006). TRP-ML1 Regulates Lysosomal pH and Acidic Lysosomal Lipid Hydrolytic Activity. *J. Biol. Chem.* 281 (11), 7294–7301. doi:10.1074/jbc.M508211200

Stajdohar, M., Rosengarten, R. D., Kokosar, J., Jeran, L., Blenkus, D., Shaulsky, G., et al. (2017). dictyExpress: a Web-Based Platform for Sequence Data Management and Analytics in *Dictyostelium* and beyond. *BMC Bioinformatics* 18 (1), 291. doi:10.1186/s12859-017-1706-9

Sun, M., Goldin, E., Stahl, S., Falardeau, J. L., Kennedy, J. C., Acierno, J. S., Jr., et al. (2000). Mucolipidosis Type IV Is Caused by Mutations in a Gene Encoding a Novel Transient Receptor Potential Channel. *Hum. Mol. Genet.* 9 (17), 2471–2478. doi:10.1093/hmg/9.17.2471

Sun, X., Yang, Y., Zhong, X. Z., Cao, Q., Zhu, X.-H., Zhu, X., et al. (2018). A Negative Feedback Regulation of MTORC1 Activity by the Lysosomal Ca^{2+} Channel MCOLN1 (Mucolipin 1) Using a CALM (Calmodulin)-dependent Mechanism. *Autophagy* 14, 1–15. doi:10.1080/15548627.2017.1389822

Taylor, C. W., Genazzani, A. A., and Morris, S. A. (1999). Expression of Inositol Trisphosphate Receptors. *Cell Calcium* 26, 237–251. doi:10.1054/ceca.1999.0090

Traynor, D., and Kay, R. R. (2017). A Polycystin-type Transient Receptor Potential (Trp) Channel that Is Activated by ATP. *Biol. Open* 6, 200–209. doi:10.1242/bio.020685

Traynor, D., Milne, J. L., Insall, R. H., and Kay, R. R. (2000). Ca^{2+} Signalling Is Not Required for Chemotaxis in *Dictyostelium*. *EMBO J.* 19 (17), 4846–4854. doi:10.1093/emboj/19.17.4846

Treusch, S., Knuth, S., Slaugenhaupt, S. A., Goldin, E., Grant, B. D., and Fares, H. (2004). *Caenorhabditis elegans* Functional Orthologue of Human Protein H-Mucolipin-1 Is Required for Lysosome Biogenesis. *PNAS USA* 101, 4483–4488. doi:10.1073/pnas.0400709101

Venkatachalam, K., Long, A. A., Elsaesser, R., Nikolaeva, D., Broadie, K., and Montell, C. (2008). Motor Decit in a Drosophila Model of Mucolipidosis Type IV Due to Defective Clearance of Apoptotic Cells. *Cell* 135, 838–851. doi:10.1016/j.cell.2008.09.041

Vergarajauregui, S., Connelly, P. S., Daniels, M. P., and Puertollano, R. (2008). Autophagic Dysfunction in Mucolipidosis Type IV Patients. *Hum. Mol. Genet.* 17, 2723–2737. doi:10.1093/hmg/ddn174

Vergarajauregui, S., Martina, J. A., and Puertollano, R. (2009). Identification of the Penta-EF-Hand Protein ALG-2 as a Ca^{2+}-dependent Interactor of Mucolipin-1. *J. Biol. Chem.* 284, 36357–36366. doi:10.1074/jbc.M109.047241

Wilczynska, Z., and Fisher, P. R. (1994). Analysis of a Complex Plasmid Insertion in a Phototaxis-Deficient Transformant of *Dictyostelium discoideum* Selected on a *Micrococcus Luteus* Lawn. *Plasmid* 32, 182–194. doi:10.1006/plas.1994.1054

Wilczynska, Z., Happle, K., Müller-Taubenberger, A., Schlatterer, C., Malchow, D., and Fisher, P. R. (2005). Release of Ca^{2+} from the Endoplasmic Reticulum Contributes to Ca^{2+} Signalling in *Dictyostelium*. *Eukaryot. Cel* 4 (9), 1513–1525. doi:10.1128/EC.4.9.1513-1525.2005

Williams, T. D., and Kay, R. R. (2018). The Physiological Regulation of Macropinocytosis during *Dictyostelium* Growth and Development. *J. Cel Sci.* 131, jcs–213736. doi:10.1242/jcs.213736

Witke, W., Nellen, W., and Noegel, A. (1987). Homologous Recombination in the *Dictyostelium* Alpha-Actinin Gene Leads to an Altered mRNA and Lack of the Protein. *EMBO J.* 6, 4143–4148.

Wong, C. O., MontellLi, R. C., and Venkatachalam, K. (2012). Drosophila TRPML Is Required for TORC1 Activation. *Curr. Biol.* 22, 1616–1621. doi:10.1016/j.cub.2012.06.055

Yap, S. Q., Mathavarajah, S., and Huber, R. J. (2021). The Converging Roles of Batten Disease Proteins in Neurodegeneration and Cancer. *iScience* 24 (4), 102337. doi:10.1016/j.isci.2021.102337

Yuan, A., Siu, C.-H., and Chia, C. P. (2001). Calcium Requirement for Efficient Phagocytosis by *Dictyostelium discoideum*. *Cell Calcium* 29, 229–238. doi:10.1054/ceca.2000.0184

Conflict of Interest: The authors declare that the research was conducted in the absence of any commercial or financial relationships that could be construed as a potential conflict of interest.

Publisher's Note: All claims expressed in this article are solely those of the authors and do not necessarily represent those of their affiliated organizations, or those of the publisher, the editors and the reviewers. Any product that may be evaluated in this article, or claim that may be made by its manufacturer, is not guaranteed or endorsed by the publisher.

Copyright © 2022 Allan and Fisher. This is an open-access article distributed under the terms of the Creative Commons Attribution License (CC BY). The use, distribution or reproduction in other forums is permitted, provided the original author(s) and the copyright owner(s) are credited and that the original publication in this journal is cited, in accordance with accepted academic practice. No use, distribution or reproduction is permitted which does not comply with these terms.

frontiers | Frontiers in Cell and Developmental Biology

REVIEW
published: 19 July 2022
doi: 10.3389/fcell.2021.765316

The Polarized Redistribution of the Contractile Vacuole to the Rear of the Cell is Critical for Streaming and is Regulated by PI(4,5)P2-Mediated Exocytosis

Sana A. Fadil[1,2] *and Chris Janetopoulos*[1,3,4]*

[1]Department of Biological Sciences, University of the Sciences in Philadelphia, Philadelphia, PA, United States, [2]Department of Natural product, Faculty of Pharmacy, King Abdulaziz University, Saudia Arabia, [3]The Science Research Institute, Albright College, Reading, PA, United States, [4]The Department of Cell Biology at Johns Hopkins University School of Medicine, Baltimore, MD, United States

OPEN ACCESS

Edited by:
Robin S. B. Williams,
University of London, United Kingdom

Reviewed by:
Richard McCann,
Mercer University School of Medicine, United States
Hua Su,
Huazhong University of Science and Technology, China

***Correspondence:**
Chris Janetopoulos
cjanetopoulos@albright.edu

Specialty section:
This article was submitted to Molecular and Cellular Pathology, a section of the journal Frontiers in Cell and Developmental Biology

Received: 26 August 2021
Accepted: 20 October 2021
Published: 19 July 2022

Citation:
Fadil SA and Janetopoulos C (2022) The Polarized Redistribution of the Contractile Vacuole to the Rear of the Cell is Critical for Streaming and is Regulated by PI(4,5)P2-Mediated Exocytosis. Front. Cell Dev. Biol. 9:765316. doi: 10.3389/fcell.2021.765316

Dictyostelium discoideum amoebae align in a head to tail manner during the process of streaming during fruiting body formation. The chemoattractant cAMP is the chemoattractant regulating cell migration during this process and is released from the rear of cells. The process by which this cAMP release occurs has eluded investigators for many decades, but new findings suggest that this release can occur through expulsion during contractile vacuole (CV) ejection. The CV is an organelle that performs several functions inside the cell including the regulation of osmolarity, and discharges its content via exocytosis. The CV localizes to the rear of the cell and appears to be part of the polarity network, with the localization under the influence of the plasma membrane (PM) lipids, including the phosphoinositides (PIs), among those is PI(4,5)P2, the most abundant PI on the PM. Research on *D. discoideum* and neutrophils have shown that PI(4,5)P2 is enriched at the rear of migrating cells. In several systems, it has been shown that the essential regulator of exocytosis is through the exocyst complex, mediated in part by PI(4,5)P2-binding. This review features the role of the CV complex in *D. discoideum* signaling with a focus on the role of PI(4,5)P2 in regulating CV exocytosis and localization. Many of the regulators of these processes are conserved during evolution, so the mechanisms controlling exocytosis and membrane trafficking in *D. discoideum* and mammalian cells will be discussed, highlighting their important functions in membrane trafficking and signaling in health and disease.

Keywords: contractile vacuole, polarity, phosphoinositide (4, 5)-bisphosphate, signal relay, chemotaxis

INTRODUCTION

Chemotaxis is a form of migration where cells migrate directionally, typically towards a gradient of chemicals known as chemoattractants. During this process, cells often have asymmetric responses and develop a polarized morphology, where they have a distinct front and rear (Devreotes and Janetopoulos, 2003). In the model organism *Dictyostelium discoideum,* a soil-living amoeba, cells move towards one another in a head-to-tail fashion and align in streams (Kriebel et al., 2008). The

cyclic adenosine monophosphate (cAMP) is the chemoattractant that leads to aggregation of the amoebas into multicellular structures during starvation conditions (Konijn et al., 1969; Goldbeter, 1975; Goldbeter, 2006). Although many researchers have studied intracellular signaling in *D. discoideum*, the mechanism by which cAMP release occurs, setting up a gradient at the rear of individual cells, has remained elusive. How does signal relay produce an effective, localized chemotactic response from the rear of a cell? The enzyme that synthesizes cAMP, adenylyl cyclase (ACA), has been reported to be in a gradient along the periphery of the cell, with more accumulated in the rear (Kriebel et al., 2008). ACA also appears to be enriched in intracellular vesicles within the cell and multivesicular bodies left behind migrating cells. In this same study, Kriebel et al. suggested that cAMP is released from the rear of migrating cells *via* these extracellular vesicles (Kriebel et al., 2018).

The main regulator of ACA, known as the Cytosolic Regulator of Adenylyl Cyclase (CRAC), contains a pleckstrin homology (PH) domain which regulates the translocation to the leading edge of the cell during each transient activation of ACA (Insall et al 1994; Lilly and Devreotes 1994; Parent et al., 1998; Ruchira et al., 2004). This PH domain of CRAC binds to PI(3,4)P2 and PI(3,4,5)P3, with these two PIs being synthesized at the very front of the cell. This PH domain is required for ACA function, suggesting that the membrane localization of CRAC brings the regulator in close proximity to ACA for activation (Ruchira et al., 2004). It is unclear how or if CRAC at the leading edge of the cell activates the ACA at the trailing edge. If it somehow leads to ACA activity at the rear, the cAMP will still need to be somehow released from the cell.

Interestingly, another potential regulator of cAMP signaling from the rear of the cell has emerged. Fadil et al. (2022) discovered that the CV is redistributed to the rear of migrating cells and regulates cell streaming and cAMP secretion. In this mechanism, CRAC recruitment and ACA activity at the leading edge can synthesize cAMP, which then would diffuse through the cytosol and be pumped into the CV network. The mechanism controlling the CV redistribution is still under investigation, however evidence is emerging that higher levels of PI(4,5)P2 and potentially other charged lipids may play a role in the CV localization. The CV appears to be part of the overall polarity network, localizing to areas of actomyosin contraction.

In addition to being targeted to particular regions of the periphery of the cell, once there, the CV regulates the discharge of water by a kiss-and-run exocytic event (Essid et al., 2012). Exocytosis is an essential membrane trafficking process that can discharge soluble and insoluble intracellular protein contents including neurotransmitters, hormones, and cytokines, as well as many other small molecules and metabolites into the extracellular space (Voets, 2000; Rettig and Neher, 2002; Sudhof, 2013; Imig et al., 2014). As described here, PI(4,5)P2, plays a role in many of the PM-related cellular activities, including regulated vesicle exocytosis (Wenk et al., 2001). PI(4,5)P2 has been found to be critical for exocytosis in several mammalian cell types and is involved in neuronal function and disrupted in several human diseases (Stokes et al., 1978; Cremona et al., 1999; Nandez et al., 2014; Li et al., 2020). This review describes the importance of the polarity network regulating CV localization and highlights the important role PI(4,5)P2 plays in mediating vesicle fusion and CV-PM interactions.

CONTRACTILE VACUOLES AND EXOCYTOSIS IN *DICTYOSTELIUM DISCOIDEUM*

Freshwater protists like the amoeba, Heliozoans, and many Ciliates regulate water's penetration by a complex organelle responsible for their osmoregulation. This organelle is known as the contractile vacuole (Schneider, 1960; De Chastellier et al., 1978; Patterson, 1980; Hausmann and Patterson, 1984; Allen, 2000; Frankel, 2000). In *D. discoideum,* the CV organelle is composed of an extensive network of tubules and bladders linked to the PM. This is critical when the cell encounters hypotonic environments where maintaining osmoregulation is critical (Gerisch et al., 2002). The excess water accumulates in the tubules, filling the vacuoles, which then fuse with the PM to expel the water into the extracellular medium (Heuser et al., 1993). After ejection of water through the vacuole, the tubules elongate again and collect water for resuming the cycle. Late in the cycle, the CV ejects its content in a focal kiss-and-run exocytic event where the CV and PM transiently interconnect (Allen, 2000; Allen and Naitoh, 2002; Frankel, 2000; Essid et al., 2012; McKanna, 1973, 1976).

There are several critical proteins that control CV function, including calmodulin (Moniakis et al., 1995). In fact, antibodies against calmodulin were one of the first markers used to identify the CV in fixed cells (Gerisch et al., 2002; Zhu and Clarke, 1992). LvsA (large volume sphere), a protein that binds to calmodulin, has been shown to localize to the CV and is required for osmoregulation (Gerald et al., 2001; Malchow et al., 2006). Mutant cells missing the LvsA protein are osmo-sensitive and impaired in the vacuole discharge (Gerald et al., 2001). Another protein, Disgorgin, which is a GAP for Rab8a is also required for CV discharge mediated by fusion with the PM (Du et al., 2008). Disgorgin and LvsA, together with GTP hydrolysis by Rab8a, are also essential for the CV detachment from the PM after discharging its contents (Essid et al., 2012) while Rab2 and RabS have also been shown to be localize to the CV and be important for osmoregulation (Maringer et al., 2016). The distribution of adaptor proteins AP 1 (Lefkir et al., 2003) or AP 180 (Stavrou and O'Halloran, 2006) each caused disruption in osmoregulation. Proteins that govern this specialized organelle's activities in *D. discoideum* have been conserved throughout evolution and many of their orthologs have been shown to regulate mammalian membrane trafficking (Duhon and Cardelli, 2002; Neuhaus et al., 2002).

The connections between the CV and the PM are regulated by the exocyst complex, and contain Rab GTPases localized to the CV, which assist in regulating fusion with the PM (Yeaman et al., 2001; Essid et al., 2012; He and Guo, 2009; Maringer et al., 2016). Exocytosis and vesicular transport are known to be regulated by PIs (Paolo et al., 2004). In particular, PI(4,5)P2 is involved in the priming of the vesicle to the targeted membrane and fusion step

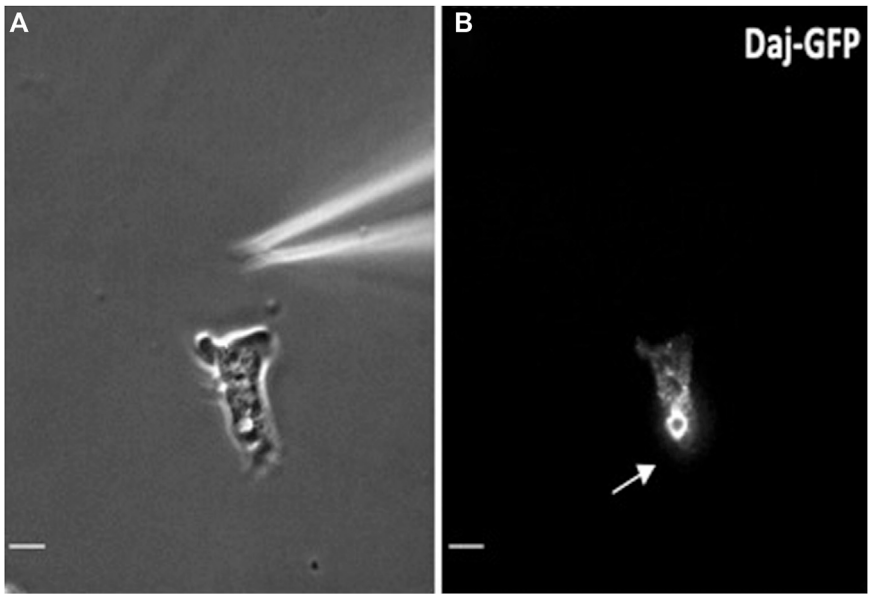

FIGURE 1 | The CV is localized at the rear of migrating cells. **(A)** Phase contrast image of the CV at the rear of the polarized migrating cell. **(B)** The same cell as in 1C expressing Dajumin-GFP moving toward a micropipette filled with chemoattractant cAMP. Arrow indicates the localization of the CV. Courtesy of Fadil et al., 2022.

(Cremona et al., 1999; Paolo et al., 2004; Holz et al., 2000; James et al., 2008; Milosevic et al., 2005; Martin, 2001; Wenk et al., 2001). The exocyst complex is an octameric complex of the subunits Sec3, Sec5, Sec6, Sec8, Sec10, Sec15, Exo70, and Exo84 and contains other components, including the SNARE (soluble N-ethylmaleimide-sensitive factor (NSF) attachment protein receptors)- associated protein SecA that have also been shown to be required for the CV discharge function (Sriskanthadevan et al., 2009; Zanchi et al., 2010; Essid et al., 2012). Among different Rab GTPase proteins, RabD (Knetsch et al., 2001; Harris and Cardelli, 2002), Rab4 (Bush et al., 1994, 1996), Rab8a (Essid et al., 2012), and Rab11 (Harris et al., 2002) are identified as regulators for discharge function.

The Role of Rear Contractile Vacuole in cAMP Secretion

During the process of polarization, the CV redistributes to the rear of *D. discoideum* cells and is critical for the streaming phenomena mediated by the chemoattractant cAMP (**Figure 1**) (Fadil et al., 2022). The cAMP binds to the serpentine cAMP receptors, triggering heterotrimeric G signaling with the cell. Downstream responses include the activation of PI3 Kinase, which leads to the recruitment of the CRAC protein, triggering the synthesis of cAMP from ATP by ACA. In this new model, cAMP diffuses within the cytosol and is pumped into the CV network by the AbcC8 transporter (Fadil et al., 2022). The cell then discharges cAMP, likely along with Ca^{+2} (Fadil et al., 2022; Parkinson et al., 2014) from the cell's rear through the CV vacuole tethered to PM. This provides the localized cAMP release from the back of the cells and supports the head to tail streaming characterized during early aggregation. The Dajumin-GFP (Gerisch et al., 2002) labeled the CV vacuoles and tubules and was localized to the rear of migrating cells (**Figure 1**). The cAMP transporter AbcC8 has recently been identified as the main cAMP transporter (Kriebel et al., 2018), and when fluorescently tagged, its localization mirrored that of Dajumin, localizing throughout the CV and tubules (Fadil et al., 2022). Thus, the presence of the AbcC8 transporter within the CV network provides a mechanism for cAMP to enter the CV tubules, with cAMP being released from the rear of the cell during the ejection phase of the CV cycle.

To confirm the importance of a functional CV in cell streaming, two different mutant cell lines were tested that have major defects in assembling a functional CV, Huntingtin null and LvsA null cells. The exact function of both proteins is not known, with evidence suggesting they are involved in membrane trafficking. In mammals, the huntingtin protein is critical for neuronal function, but like its ortholog, the role of this protein is not clear. While still having the ability to chemotax, both *D. discoideum* cell lines displayed decreased stability of head-to-tail cell contacts and lacked the normal streaming behavior seen in wild-type cells. Additionally, the periodic cAMP waves seen during early aggregation were disrupted, as was visualized using the cytosolic cAMP indicator, Flamindo2 (Fadil et al., 2022; Hashimura et al., 2019). Thus, the ability of the cells to perform signal relay was dramatically inhibited in cells with defective CV function.

Involvement of PI(4,5)P2 in Polarity Network and Contractile Vacuole Localization

PI(4,5)P2 has been suggested to be elevated at the cell's trailing edge in *D. discoideum* and in neutrophils (Janetopoulos et al., 2005; Hind

et al., 2016; Iijima et al., 2004). PIs are regulated by different phosphatases and kinases localized at distinct areas in the cell (Balla, 2013; Choi et al., 2016). Phosphoinositide 3-kinases (PI3Ks) are the enzymes that convert PI(4)P and PI(4,5)P2 into PI(3,4)P2 and PI(3,4,5)P3, respectively. PI3Ks localize to the leading edge of migrating cells, while the phosphatase and tensin homolog (PTEN), the phosphatase that utilizes PI(3,4,5)P3 has a substrate, and synthesizes PI(4,5)P2, localizes to the rear of migrating cells (Devreotes and Janetopoulos, 2003; Funamoto et al., 2002; Kriebel et al., 2003; Luo et al., 2003). PTEN activity and the sharp localization at the rear of the polarized cell is, in part, regulated by PI(4,5)P2 binding motif at the N terminus of PTEN (Iijima et al., 2004; Nguyen et al., 2014). Similar morphology has been shown in cells during cytokinesis and in polarized neutrophils (Janetopoulos et al., 2005; Lacalle et al., 2007; Lokuta et al., 2007). The net charge of PI(4,5)P2 is -4, which enables this lipid to contribute to the localization and the activity of various proteins by interacting with their polybasic clusters (Ellenbroek et al., 2011). During the process of aggregation, it is possible that SNARE proteins or other proteins with polybasic motifs, link the CV to the plasma membrane, as discussed below, and contribute to the rearward distribution of the CV to the back of *D. discoideum* cells (Fadil et al., 2022) (**Figure 1**). Interestingly, this polarized localization can occur in drug treated cells lacking an actin cytoskeleton or functional microtubule network, suggesting that the direct interaction with the PM is responsible for CV localization. CVs were still able to accumulate towards the low side of the chemoattractant gradient, when cells were in the presence of drugs that disrupted the actin cytoskeleton, similar to the movements that can be seen with the reciprocal regulation of PI3K and PTEN (Janetopoulos et al., 2004). The CV and PI(4,5)P2 are elevated in areas of the cell where there are not membrane protrusions (Fadil et al., 2022), which suggests a key role for this lipid in regulating the CV organelle's localization. The CV disassembles at metaphase, when PI(4,5)P2 levels reach an intermediate level across the entire periphery of the cell, and then begin to reassemble in the furrow during telophase and the initiation of cytokinesis, as PI(4,5)P2 levels elevate (Janetopoulos et al., 2005). The CVs regenerate during the final stages of cytokinesis, with primordial CVs often formed on the trailing edge of the two daughter cells. In budding yeast, the exocyst components, specifically Sec3 and Exo70 (see below) have also been shown to localize to the cleavage furrow throughout cytokinesis (Wu and Guo 2015). Interestingly, in mammalian cells, the exocyst is also enriched at the cleavage furrow and is under the control of Rab11 and RalA (Fielding et al., 2005; Chen et al., 2006; Neto et al., 2013). The amplification of PI(4,5)P2 in the back of the cell during migration and in the cleavage furrow during cytokinesis likely contributes to the CV localization and could provide the proper targeting of proteins needed for regulating exocytosis. This may also assist in the targeted release of smaller vesicles, sometimes termed exosomes, that have also have been postulated to play a role in the release of cAMP at the rear of the cell (Kriebel, et al., 2018). Therefore, in addition to helping position the CV within the cell, elevated levels of PI(4,5)P2 appear to regulate CV fusion with the PM during vegetative growth and at the rear of migrating cells.

Involvement of PI(4,5)P2 in Contractile Vacuole Exocytosis

PI(4,5)P2, which is the most abundant negatively charged PI on the PM, has multiple roles within a cell, coordinating actin dynamics, contributing to cell polarity and appears to be critical in exocytosis (Di Paolo and De Camilli 2006; Holz et al., 2000; Martin, 2001; Martin, 2015). PI(4,5)P2 interacts with various positively charged proteins in the exocyst complex, suggesting a major role for this PI in regulating the CV organelle's exocytosis (Essid et al., 2012). This binding of exocyst subunits to the PM delivers the vesicles to the targeted PI(4,5)P2 within the PM for the tethering step. It has been demonstrated that the exocyst subunits Sec3 and Exo70 bind to PI(4,5)P2 at the PM (He et al., 2007; Liu et al., 2007; Zhang et al., 2008; Shewan et al., 2011; Pleskot et al., 2015). Furthermore, it is well-established that polarized exocytosis, which is a multistep vesicular trafficking process, transfers signals and proteins to specific PM sites, and is mediated by PI(4,5)P2 (He and Guo, 2009). SecA, a *D. discoideum* homolog of the yeast Sec1p and the mammalian Munc18 protein, localizes to the CV. Cells with a defect in SecA cannot regulate their osmotic pressure and have a defect in CV discharge (Zanchi et al., 2010). Sec1p and Munc18 proteins are essential for different exocytosis steps as they interact with exocytic SNARE proteins during vesicle docking and fusion, also mediated by PI(4,5)P2 (see below) (Carr et al., 1999; Grote et al., 2000; Shen et al., 2007; Sudhof and Rothman, 2009). SecA is therefore necessary for CV fusion to the PM and water discharge. A recent study suggested that PI(4,5)P2 regulates the trafficking of the CV to the fusion site and cells with a defect in Dd5P4, the enzyme which uses the 5-phosphates of PI(4,5)P2 as substrate, displayed inefficient CV fusion (Luscher et al., 2019).

Exocytosis associated with CV function is regulated by SNARE proteins. There are four homologs of mammalian SNAREs present in *D. discoideum*: vesicle-associated membrane protein 7 (v-SNARE VAMP7), and three t-SNAREs, syntaxin 7, syntaxin 8 and Vti1(Bogdanovic et al., 2000, 2002). It has been reported that VAMP7 and syntaxin 7 are present in the bladder of the CV. The other two SNARE proteins, syntaxin 8 and Vti1 have been seen in both the CV's bladders and tubular networks (Bennett et al., 2008). Some of the SNARE proteins have also been identified as interactors with PI(4,5)P2 (Murray and Tamm 2009). Clathrin assembly proteins, such as AP180 and AP1, are also related to CV activity. AP180 null cells show unusual large CVs and are osmo-sensitive (Stavrou and O'Halloran, 2006). Moreover, AP180 has been reported to interact with another SNARE, Vamp7B (Wen et al., 2009). AP180 also binds to PI(4,5)P2, through the NH2-terminal homology domain known as ANTH (AP180 N-terminal homology) and assists in clathrin assembly on lipid monolayers (Ford et al., 2001). The ANTH domain is conserved among all members of the AP180 family (Norris et al., 1995; Ye et al., 1995; Hao et al., 1997; Ford et al., 2001; Mao et al., 2001; Stavrou and O'Halloran, 2006). Thus, PI(4,5)P2 has been shown to be a critical regulator of exocytic events in both *D. discoideum* and many eukaryotes, including mammals.

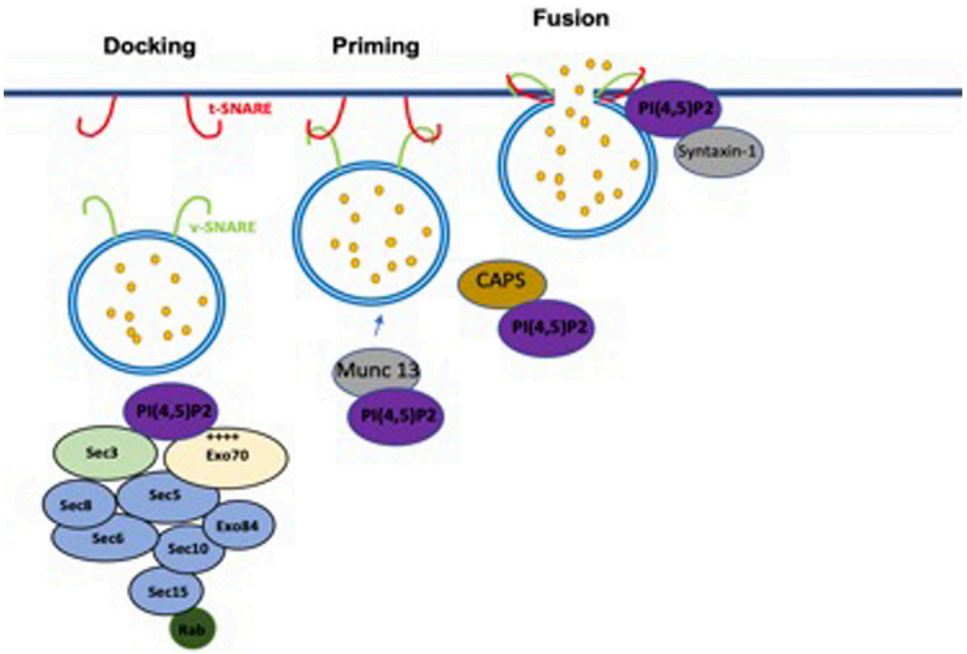

FIGURE 2 | Involvement of PI(4,5)P2 in the exocytosis steps. PI(4,5)P2 is required for mediating tethering of vesicles to the PM. In the priming step, PI(4,5)P2 modulates the vesicles priming by interacting with Munc13 and CAPS. PI(4,5)P2 controls vesicles fusion by interacting with SNARE complex.

THE GENERAL ROLE OF PI(4,5)P2 IN EUKARYOTIC EXOCYTOSIS

In addition to exocytosis being a critical component of CV dynamics, it is also essential for vesicles to eject their contents in metazoans. Exocytosis is a membrane trafficking process that can discharge soluble and insoluble protein contents including neurotransmitters, hormones, and cytokines, as well as many other small molecules and metabolites to the extracellular space. In eukaryotes, this process also mediates the polarized delivery of vesicular trafficking proteins and lipids to specific PM domains. As has been mentioned, several studies show that PI(4,5)P2 and its effectors play critical roles in all steps of exocytosis (**Figure 2**) (Cremona et al., 1999; Paolo et al., 2004; Holz et al., 2000; James et al., 2008; Milosevic et al., 2005; Martin, 2001; Wenk et al., 2001). To perform this function, secretory vesicles undergo three defined trafficking steps during exocytosis (**Figure 2**): the docking process for recruiting vesicles to the PM, the priming process for maturing the vesicles, the fusion process to fuse with the PM, and the release of vesicle contents (Voets, 2000; Rettig and Neher, 2002; Sudhof, 2013; Imig et al., 2014). PI(4,5)P2 is capable of engaging in a multitude of cellular functions that are temporally and spatially controlled by the localized distribution of PI(4,5)P2 along the PM (Bai et al., 2004). PI(4,5)P2 has been shown to be enriched in domains at the PM and at the vesicle exocytosis sites (Trexler et al., 2016). Furthermore, the recruitment of enzymes that hydrolyze PI(4,5)P2 at the docking sites results in inefficient docking of the vesicles to the PM (Cremona et al., 1999; Honigmann et al., 2013). This initial priming step of exocytosis is controlled by different proteins and their effectors such as the Ca^{2+}-dependent activator protein for secretion (CAPS) and Munc13 (Shin et al., 2010; Kabachinski et al., 2014; Martin, 2015). These proteins are also regulated by PI(4,5P)2, with the PH domain of CAPS binding to PI(4,5)P2 for activation (Grishanin et al., 2004; Kabachinski et al., 2014; Martin, 2015). SNAREs also interact with PI(4,5)P2 for vesicle fusion (Martin, 2001; James et al., 2008).

Involvement of PI(4,5)P2 With the Exocyst Complex

The exocyst complex has been involved in various cellular processes including exocytosis, cell growth, cytokinesis, cell migration, primary ciliogenesis and tumorigenesis. Furthermore, the exocyst protein complex has a crucial role in polarized membrane protein trafficking (He and Guo, 2009). The exocyst complex (**Figure 2**) consists of eight subunits (Sec3, Sec5, Sec6, Sec8, Sec10, Sec15, Exo70, and Exo84) that mediate the vesicles' tethering to the PM and is conserved among the eukaryotic kingdom (He and Guo, 2009; Yeaman et al., 2001). Exocyst subunits interact with each other in pairs: such as Sec3–Sec5, Sec6–Sec8, and Sec10–Sec15 (Guo et al., 2000; Katoh et al., 2015; Heider et al., 2016; Matern et al., 2001; Munson and Novick 2006; Vega and Hsu 2001). The exocyst complex mediates localization and tethering of vesicles to targeted membranes and enables the assembly of SNARE

complexes before the fusion step (Pfeffer, 1999; Guo et al., 2000; Waters and Hughson., 2000; Whyte and Munro, 2002). Exo70 is localized near cell-cell contacts on the PM, meaning that Exo70 can mediate PM interaction in these cells independently of the remaining exocyst components (Matern et al., 2001). Indeed, the exocyst needs to interact with the target membrane to achieve tethering function after the delivery of the vesicles. This process appears to be mediated by direct binding of Sec3 and Exo70 subunits with PI(4,5)P2 enriched at the inner leaflet of the PM (He et al., 2007; Liu et al., 2007; Zhang et al., 2008; Shewan et al., 2011; Pleskot et al., 2015). Exo70 exhibits a positively charged surface domain at its C-terminus in mammalian cells which mediates the binding to PI(4,5)P2. Interestingly, the C-terminal sequence of Exo70 is the most evolutionarily conserved region of the protein, suggesting this PI(4,5)P2 is critical for many organisms. The same study has also revealed that Exo70 can recruit the other exocyst components to the PM (Liu et al., 2007). Furthermore, studies on yeast have shown that Exo70 is an effecter of the GTPase Rho3, which plays regulatory roles in actin organization and exocytosis (Adamo et al., 1999; Robinson et al., 1999). The disruption of the Exo70–lipid interaction resulted in exocyst mis-localization and ablation of the enzyme secretion responsible for yeast cell growth. On the other hand, disruption of Exo70–Rho3 interaction did not show any noticeable defects (He et al., 2007). The binding affinity of Exo70 for PI(4,5)P2 is higher than PI(3,5)P2, PI(3)P or PI(4)P (He et al., 2007). The other component that mediates the delivery of the vesicles to the targeted membrane is Sec3. The association between the amino-terminal PH domain of Sec3 and PI(4,5)P2 mediates Sec3's localization to the PM (Luo et al., 2014). It has been reported that the PH domain of Sec3 also interacts with small GTPases such as Cdc42 and Rho1 (Guo et al., 2000; Zhang et al., 2001; Zhang et al., 2008). Small GTPases and PI(4,5)P2 can synergistically influence the exocyst complex's position and function at the PM. When both Exo70 and Sec3 are impaired, it is no longer possible to anchor the exocyst complex to the targeted membrane (He et al., 2007). Thus, Exo70 and Sec3 bind to PI(4,5)P2 and function in concert to mediate the association of the exocyst complex with the PM.

PI(4,5)P2 is the Binding Site for CAPS and Munc-13

CAPS and Munc-13 are major contributors to the priming step in exocytosis of synaptic vesicles and dense-core vesicles (**Figure 2**) (Wojcik and Brose, 2007; Stevens and Rettig, 2009; James and Martin, 2013). These synaptic vesicles and dense core vesicles play an essential role in neuronal communication and brain development (Rettig and Neher, 2002; Sudhof and Rizo, 2011). It has been reported that Munc-13 is critical for synaptic vesicle exocytosis, while CAPS plays a central role in dense-core vesicles (Augustin et al., 1999; Varoqueaux et al., 2002; Grishanin et al., 2004; Speese et al., 2007; Liu et al., 2008). Moreover, CAPS and Munc-13 have been shown to regulate SNARE assembly with the vesicles and are crucial for exocytosis (Basu et al., 2005; James et al., 2009; Daily et al., 2010; Khodthong et al., 2011; Ma et al., 2011; Wang et al., 2017). CAPS and Munc13 proteins have interconnected C-terminal SNARE protein–binding domains (Koch et al., 2000; Guan et al., 2008; Pei et al., 2009). Deleterious mutations in the PH domain of CAPS result in controlled exocytosis failure (Grishanin et al., 2002). Also, CAPS interacts with syntaxin-1 near its PI(4,5)P2 binding site, indicating that PI(4,5)P2 is an essential co-factor for activating CAPS via binding to its PH domain. On the other hand, Munc13 binds to PI(4,5)P2 in a Ca^{2+}-dependent manner through its C2B domain (James et al., 2010; Shin et al., 2010). Moreover, a study on neuroendocrine cells has shown that Munc-13 is cytoplasmic and translocates to PI(4,5)P2-rich PM domains in response to Ca^{2+} influx (Kabachinski et al., 2014; Martin, 2015). In line with this, Munc13-1-GFP translocation to microdomains was blocked by overexpression of the high-affinity PI(4,5)P2-binding PH domain of PLCδ1, demonstrating their affinity for the same PM site (Kabachinski et al., 2014). Indeed, both CAPS and Munc13 can promote the recruitment of vesicles to PI(4,5)P2-rich membranes in a Ca2+-dependent manner (Junge et al., 2004; Zikich et al., 2008; Kabachinski et al., 2016; Kreutzberger et al., 2017).

PI(4,5)P2 interacts With SNARE Complex

SNARE proteins are the central components of the fusion step, the final process in exocytosis vesicle trafficking (**Figure 2**). All SNARE family members have a distinctive preserved homolog stretch of 60–70 amino acids, known as the SNARE motif (Barg et al., 2010). Among a large number of SNARE proteins, three complexes were carefully studied and identified. These complexes are Syntaxin-1, synaptosome-associated protein (SNAP-25), and synaptobrevin2/vesicle-associated membrane protein 2 (VAMP2) (Barg et al., 2010; Rickman et al., 2010; Bar-On et al., 2012; Ji et al., 2015). It has been reported that PI(4,5)P2 activates syntaxin-1 promoting assembly with SNAP-25 (Murray and Tamm 2009). Furthermore, syntaxin interactions with PI(4,5)P2 play a positive role in vesicle fusion with the membrane by localizing the protein on the membrane or promoting SNAP-25 interactions (Van den Bogaart et al., 2011). Fusion-competent vesicles in PC12 have been suggested to localize preferentially to PM sites that contain either PI(4,5)P2 domains or PI(4,5)P2 domains co-localized with syntaxin-1 clusters (Van den Bogaart et al., 2011). Other studies demonstrated that a subset of docked vesicles are actually present in PI(4,5)P2-enriched areas where exocytosis occurs under optimal Ca^{2+} influx conditions (Ji et al., 2015; Ji and Lou, 2016). Syntaxin-1 interacts with PIs through a membrane-proximal sequence of basic residues which includes K^{260}ARRKK^{265}. Importantly, syntaxin-1 clusters were eliminated by treatment of PC12 cells with the 5-phosphatase synaptojanin-1. Synaptotagmin1, another calcium sensor for exocytosis, is anchored to the membrane of secretory organelles which is mediated by PI(4,5)P2 clusters in plasma domains (Aoyagi et al., 2005; Gandasi and Barg, 2014; Murray and Tamm, 2009). Moreover, the interaction between PI(4,5)P2 and Synaptotagmin increases the excitation-secretion in response to Ca^{2+} (Bai et al., 2004). SNARE proteins therefore play a critical role in the fusion step and are regulated by local PI(4,5)P2 levels as they modulate vesicle exocytosis.

DISCUSSION

The contractile vacuole is part of the polarity circuit and is enriched at the rear of migrating cells, with this localization being critical for cAMP secretion. PI(4,5)P2 is the most abundant PIs in the PM and has been shown to be elevated at the rear of the cell and in areas reciprocally regulated with PI(3,4,5)P3 and membrane protrusions. PI(4,5)P2 has multiple roles in the cell, and is intimately involved in membrane trafficking, endocytosis and exocytosis. The regulatory factors governing exocytosis are highly conserved across species and as highlighted in this review are relevant to many mammalian cell trafficking pathways. The rear CV enrichment and exocytosis described here may be related to this migracytosis mechanism recently described which has been implicated in cell-cell communication in mammalian cells. Migrasomes exist in many cell types such as normal rat kidney cells, macrophages, primary neurons, human breast cancer cells, and embryonic stem cells (Ma et al., 2015). Migracytosis is a cell migration-dependent mechanism for releasing cellular contents by migrasome organelles which localize at the rear of the cell and play a potential role in cell-cell communication.

PI(4,5)P2 pathway dysregulation and failure of proper exocytosis has been identified in many different diseases such as Lowe syndrome, neuronal disorders and various forms of cancer (Dannemann et al., 2012; Kim et al., 2017; Prosseda et al., 2017; Raghu et al., 2019). Lowe oculocerebrorenal syndrome, a congenital disease characterized by low IQ, and defective kidney proximal tubule resorption, is caused by a defect in the OCRL gene. OCRL is an inositol polyphosphate 5-phosphatase that hydrolyzes the 5-phosphate of PI(4,5)P2 into PI4P (Prosseda et al., 2017). Interestingly, a recent study in *D. discoideum* has shown that OCRL-like protein of *D. discoideum*, Dd5P4, is recruited to the CV membrane upon the kiss-and-run exocytic event (Luscher et al., 2019). Therefore, it is possible that the exocytic function of ORCL contributes to the pathological process of Lowe syndrome. Chediak-Higashi syndrome (CHS) is an autosomal human disorder characterized by immunodeficiency and the formation of giant lysosomes or lysosome-related organelles. In *D. discoideum,* the homolog to one of the Chediak-Higashi syndrome (CHS) proteins is LvsA, which interestingly enough labels the CV bladder and remains associated throughout the discharge phase until fusion with the PM (Gerald et al., 2002). In addition, it also seems plausible that the localized fusion that occurs with CV discharge is correlated with the small extracellular vesicles documented during *D. discoideum* streaming (Kreibel, et al., 2018). Extracellular vesicles are critical for many aspects in tumor progression (Xavier et al., 2020), so studying these processes is of utmost importance. Given that PI(4,5)P2 levels are critical to so many processes in the cell, there are certain to many critical roles and potential therapeutic interventions that can be performed by regulating PI(4,5)P2 levels. Understanding the basic function of PI(4,5)P2 in CV ejection or neurotransmitter release may even help with diseases of the brain. PI(4,5)P2 levels are decreased in the brain of Alzheimer's patients, for instance, although the exact role in Alzheimer's disease has yet to be elucidated (Stokes et al., 1978; Arancio., 2008). There are many steps in CV localization and function where PI(4,5)P2 seems to be required, so understanding the basic functions to their targeting and function should enhance our understating of exocytosis-related diseases.

AUTHOR CONTRIBUTIONS

SF wrote the majority of the manuscript with editorial assistance from CJ. SF designed and made the figures.

REFERENCES

Adamo, J. E., Rossi, G., and Brennwald, P. (1999). The Rho GTPase Rho3 Has a Direct Role in Exocytosis that Is Distinct from its Role in Actin Polarity. *MBoC.* 10 (12), 4121–4133. doi:10.1091/mbc.10.12.4121

Allen, R. D. (2000). The Contractile Vacuole and its Membrane Dynamics. *Bioessays.* 22 (11), 1035–1042. doi:10.1002/1521-1878(200011)22::11<1035: aid-bies10>3.0.co;2-a

Allen, R. D., and Naitoh, Y. (2002). Osmoregulation and Contractile Vacuoles of Protozoa. *Int. Rev. Cytol.* 215, 351–394. doi:10.1016/s0074-7696(02)15015-7

Aoyagi, K., Sugaya, T., Umeda, M., Yamamoto, S., Terakawa, S., and Takahashi, M. (2005). The activation of exocytotic sites by the formation of phosphatidylinositol 4,5-bisphosphate microdomains at syntaxin clusters. *Journal of Biological Chemestry* 280, 17346–17352. doi:10.1074/jbc.M413307200

Arancio, O. (2008). PIP2: a New Key Player in Alzheimer's Disease. *Cellscience.* 5 (1), 44–47.

Augustin, I., Rosenmund, C., Südhof, T. C., and Brose, N. (1999). Munc13-1 Is Essential for Fusion Competence of Glutamatergic Synaptic Vesicles. *Nature.* 400 (6743), 457–461. doi:10.1038/22768

Bai, J., Tucker, W. C., and Chapman, E. R. (2004). PIP2 Increases the Speed of Response of Synaptotagmin and Steers its Membrane-Penetration Activity Toward the Plasma Membrane. *Nat. Struct. Mol. Biol.* 11 (1), 36–44. doi:10.1038/nsmb709

Balla, T. (2013). Phosphoinositides: Tiny Lipids With Giant Impact on Cell Regulation. *Physiol. Rev.* 93 (3), 1019–1137. doi:10.1152/physrev.00028.2012

Bar-On, D., Wolter, S., Van De Linde, S., Heilemann, M., Nudelman, G., Nachliel, E., et al. (2012). Super-Resolution Imaging Reveals the Internal Architecture of Nano-Sized Syntaxin Clusters. *J. Biol. Chem.* 287 (32), 27158–27167. doi:10.1074/jbc.m112.353250

Barg, S., Knowles, M. K., Chen, X., Midorikawa, M., and Almers, W. (2010). Syntaxin Clusters Assemble Reversibly at Sites of Secretory Granules in Live Cells. *Proc. Natl. Acad. Sci.* 107 (48), 20804–20809. doi:10.1073/pnas.1014823107

Basu, J., Shen, N., Dulubova, I., Lu, J., Guan, R., Guryev, O., et al. (2005). A Minimal Domain Responsible for Munc13 Activity. *Nat. Struct. Mol. Biol.* 12 (11), 1017–1018. doi:10.1038/nsmb1001

Bennett, N., Letourneur, F., Ragno, M., and Louwagie, M. (2008). Sorting of the v-SNARE VAMP7 in Dictyostelium discoideum: a role for more than one Adaptor Protein (AP) complex. *Experimental cell research* 314 (15), 2822–2833. doi:10.1016/j.yexcr.2008.06.019

Bogdanovic, A., Bennett, N., Kieffer, S., Louwagie, M., Morio, T., Garin, J., et al. (2002). Syntaxin 7, Syntaxin 8, Vti1 and VAMP7 (Vesicle-Associated Membrane Protein 7) Form an Active SNARE Complex for Early

Macropinocytic Compartment Fusion in *Dictyostelium discoideum*. *Biochem. J.* 368 (1), 29–39. doi:10.1042/bj20020845

Bogdanovic, A., Bruckert, F., Morio, T., and Satre, M. (2000). A Syntaxin 7 Homologue Is Present in *Dictyostelium discoideum* Endosomes and Controls Their Homotypic Fusion. *J. Biol. Chem.* 275 (47), 36691–36697. doi:10.1074/jbc.m006710200

Bush, J., Nolta, K., Rodriguez-Paris, J., Kaufmann, N., O'Halloran, T., Ruscetti, T., et al. (1994). A Rab4-Like GTPase in *Dictyostelium discoideum* Colocalizes With V-H(+)-ATPases in Reticular Membranes of the Contractile Vacuole Complex and in Lysosomes. *J. Cell. Sci.* 107 (10), 2801–2812. doi:10.1242/jcs.107.10.2801

Bush, J., Temesvari, L., Rodriguez-Paris, J., Buczynski, G., and Cardelli, J. (1996). A Role for a Rab4-Like GTPase in Endocytosis and in Regulation of Contractile Vacuole Structure and Function in *Dictyostelium discoideum*. *MBoC.* 7 (10), 1623–1638. doi:10.1091/mbc.7.10.1623

Carr, C. M., Grote, E., Munson, M., Hughson, F. M., and Novick, P. J. (1999). Sec1p Binds to SNARE Complexes and Concentrates at Sites of Secretion. *J. Cell. Biol.* 146 (2), 333–344. doi:10.1083/jcb.146.2.333

Chen, X.-W., Inoue, M., Hsu, S. C., and Saltiel, A. R. (2006). RalA-Exocyst-Dependent Recycling Endosome Trafficking Is Required for the Completion of Cytokinesis. *J. Biol. Chem.* 281 (50), 38609–38616. doi:10.1074/jbc.m512847200

Choi, S., Hedman, A. C., Sayedyahossein, S., Thapa, N., Sacks, D. B., and Anderson, R. A. (2016). Agonist-stimulated Phosphatidylinositol-3,4,5-Trisphosphate Generation by Scaffolded Phosphoinositide Kinases. *Nat. Cell. Biol.* 18 (12), 1324–1335. doi:10.1038/ncb3441

Cremona, O., Di Paolo, G., Wenk, M. R., Lüthi, A., Kim, W. T., Takei, K., et al. (1999). Essential Role of Phosphoinositide Metabolism in Synaptic Vesicle Recycling. *Cell.* 99, 179–188. doi:10.1016/s0092-8674(00)81649-9

Daily, N. J., Boswell, K. L., James, D. J., and Martin, T. F. J. (2010). Novel Interactions of CAPS (Ca2+-Dependent Activator Protein for Secretion) with the Three Neuronal SNARE Proteins Required for Vesicle Fusion. *J. Biol. Chem.* 285 (46), 35320–35329. doi:10.1074/jbc.m110.145169

Dannemann, N., Hart, J. R., Ueno, L., and Vogt, P. K. (2012). Phosphatidylinositol 4, 5-Bisphosphate (PIP2)-specific AKT1 Is Oncogenic.(Vol 127, Pg 239, 2010). *Int. J. Cancer.* 130 (12), E3. doi:10.1002/ijc.25012

de Chastellier, C., Quiviger, B., and Ryter, A. (1978). Observations on the Functioning of the Contractile Vacuole of *Dictyostelium discoideum* With the Electron Microscope. *J. Ultrastruct. Res.* 62 (3), 220–227. doi:10.1016/s0022-5320(78)80019-7

Devreotes, P., and Janetopoulos, C. (2003). Eukaryotic Chemotaxis: Distinctions Between Directional Sensing and Polarization. *J. Biol. Chem.* 278, 20445–20448. doi:10.1074/jbc.r300010200

Di Paolo, G., and De Camilli, P. (2006). Phosphoinositides in Cell Regulation and Membrane Dynamics. *Nature.* 443, 651–657. doi:10.1038/nature05185

Du, F., Edwards, K., Shen, Z., Sun, B., De Lozanne, A., Briggs, S., et al. (2008). Regulation of Contractile Vacuole Formation and Activity in Dictyostelium. *Embo J.* 27 (15), 2064–2076. doi:10.1038/emboj.2008.131

Duhon, D., and Cardelli, J. (2002). The Regulation of Phagosome Maturation in Dictyostelium. *J. Muscle Res. Cell. Motil.* 23 (7), 803–808. doi:10.1023/a:1024435913949

Ellenbroek, W. G., Wang, Y.-H., Christian, D. A., Discher, D. E., Janmey, P. A., and Liu, A. J. (2011). Divalent Cation-Dependent Formation of Electrostatic PIP2 Clusters in Lipid Monolayers. *Biophysical J.* 101 (9), 2178–2184. doi:10.1016/j.bpj.2011.09.039

Essid, M., Gopaldass, N., Yoshida, K., Merrifield, C., and Soldati, T. (2012). Rab8a Regulates the Exocyst-Mediated Kiss-And-Run Discharge of the Dictyostelium Contractile Vacuole. *MBoC.* 23 (7), 1267–1282. doi:10.1091/mbc.e11-06-0576

Fadil, S. A., Ring, A., Jowhar, D., Smith, K., Lord, W., Jensen, D., et al. (2022). Retrograde Localization of the CV Is Critical for Signal Relay and Cellular Streaming in Dictyostelium Discoideum. *Nat. Comm Bio.*

Fielding, A. B., Schonteich, E., Matheson, J., Wilson, G., Yu, X., Hickson, G. R. X., et al. (2005). Rab11-FIP3 and FIP4 Interact With Arf6 and the Exocyst to Control Membrane Traffic in Cytokinesis. *Embo J.* 24 (19), 3389–3399. doi:10.1038/sj.emboj.7600803

Ford, M. G. J., Pearse, B. M. F., Higgins, M. K., Vallis, Y., Owen, D. J., Gibson, A., et al. (2001). Simultaneous Binding of PtdIns(4,5)P 2 and Clathrin by AP180 in the Nucleation of Clathrin Lattices on Membranes. *Science.* 291 (5506), 1051–1055. doi:10.1126/science.291.5506.1051

Frankel, J. (1999). Chapter 2 Cell Biology of Tetrahymena Thermophila. *Methods Cell. Biol.* 62, 27–125. doi:10.1016/s0091-679x(08)61528-9

Funamoto, S., Meili, R., Lee, S., Parry, L., and Firtel, R. A. (2002). Spatial and Temporal Regulation of 3-Phosphoinositides by PI 3-Kinase and PTEN Mediates Chemotaxis. *Cell.* 109 (5), 611–623. doi:10.1016/s0092-8674(02)00755-9

Gerald, N. J., Siano, M., and De Lozanne, A. (2002). The Dictyostelium LvsA Protein Is Localized on the Contractile Vacuole and Is Required for Osmoregulation. *Traffic.* 3 (1), 50–60. doi:10.1034/j.1600-0854.2002.30107.x

Gerisch, G., Heuser, J., and Clarke, M. (2002). Tubular-vesicular transformation in the contractile vacuole system of Dictyostelium. *Cell Biol Int* 26, 845–852. doi:10.1006/cbir.2002.0938

Goldbeter, A. (1975). Mechanism for Oscillatory Synthesis of Cyclic AMP in *Dictyostelium Discoideum*. *Nature.* 253 (5492), 540–542. doi:10.1038/253540a0

Goldbeter, A. (2006). Oscillations and Waves of Cyclic AMP in Dictyostelium: A Prototype for Spatio-Temporal Organization and Pulsatile Intercellular Communication. *Bull. Math. Biol.* 68, 1095–1109. doi:10.1007/s11538-006-9090-z

Grishanin, R. N., Klenchin, V. A., Loyet, K. M., Kowalchyk, J. A., Ann, K., and Martin, T. F. J. (2002). Membrane Association Domains in Ca2+-Dependent Activator Protein for Secretion Mediate Plasma Membrane and Dense-Core Vesicle Binding Required for Ca2+-Dependent Exocytosis. *J. Biol. Chem.* 277 (24), 22025–22034. doi:10.1074/jbc.m201614200

Grishanin, R. N., Kowalchyk, J. A., Klenchin, V. A., Ann, K., Earles, C. A., Chapman, E. R., et al. (2004). CAPS Acts at a Prefusion Step in Dense-Core Vesicle Exocytosis as a PIP2 Binding Protein. *Neuron.* 43, 551–562. doi:10.1016/j.neuron.2004.07.028

Grote, E., Carr, C. M., and Novick, P. J. (2000). Ordering the Final Events in Yeast Exocytosis. *J. Cell. Biol.* 151 (2), 439–452. doi:10.1083/jcb.151.2.439

Guan, R., Dai, H., and Rizo, J. (2008). Binding of the Munc13-1 MUN Domain to Membrane-Anchored SNARE Complexes. *Biochemistry.* 47, 1474–1481. doi:10.1021/bi702345m

Guo, W., Sacher, M., Barrowman, J., Ferro-Novick, S., and Novick, P. (2000). Protein Complexes in Transport Vesicle Targeting. *Trends Cell. Biol.* 10 (6), 251–255. doi:10.1016/s0962-8924(00)01754-2

Hao, W., Tan, Z., Prasad, K., Reddy, K. K., Chen, J., Prestwich, G. D., et al. (1997). Regulation of AP-3 Function by Inositides. *J. Biol. Chem.* 272 (10), 6393–6398. doi:10.1074/jbc.272.10.6393

Harris, E., and Cardelli, J. (2002). RabD, aDictyosteliumRab14-Related GTPase, Regulates Phagocytosis and Homotypic Phagosome and Lysosome Fusion. *J. Cell. Sci.* 115 (18), 3703–3713. doi:10.1242/jcs.00050

Harris, E., Wang, N., Wu, W.-I., Weatherford, A., De Lozanne, A., and Cardelli, J. (2002). DictyosteliumLvsB Mutants Model the Lysosomal Defects Associated With Chediak-Higashi Syndrome. *MBoC* 13 (2), 656–669.

Hashimura, H., Morimoto, Y. V., Yasui, M., and Ueda, M. (2019). Collective cell migration of Dictyostelium without cAMP oscillations at multicellular stages. *Communications biology* 2 (1), 1–15. doi:10.1038/s42003-018-0273-6

Hausmann, K., and Patterson, D. J. (1984). "Contractile Vacuole Complexes in Algae," in *Compartments in Algal Cells and Their Interaction* (Berlin, Heidelberg: Springer), 139–146. doi:10.1007/978-3-642-69686-2_15

He, B., Xi, F., Zhang, X., Zhang, J., and Guo, W. (2007). Exo70 Interacts with Phospholipids and Mediates the Targeting of the Exocyst to the Plasma Membrane. *Embo J.* 26 (18), 4053–4065. doi:10.1038/sj.emboj.7601834

He, B., and Guo, W. (2007). The exocyst complex in polarized exocytosis. *Current opinion in cell biology* 21 (4), 537–542. doi:10.1016/j.ceb.2009.04.007

Heider, M. R., Gu, M., Duffy, C. M., Mirza, A. M., Marcotte, L. L., Walls, A. C., et al. (2016). Subunit connectivity, assembly determinants and architecture of the yeast exocyst complex. *Nature structural and molecular biology* 23 (1), 56–99. doi:10.1038/nsmb.3146

Heuser, J., Zhu, Q., and Clarke, M. (1993). Proton Pumps Populate the Contractile Vacuoles of Dictyostelium Amoebae. *J. Cell. Biol.* 121, 1311–1327. doi:10.1083/jcb.121.6.1311

Hind, L. E., Vincent, W. J. B., and Huttenlocher, A. (2016). Leading From the Back: The Role of the Uropod in Neutrophil Polarization and Migration. *Developmental Cell.* 38, 161–169. doi:10.1016/j.devcel.2016.06.031

Holz, R. W., Hlubek, M. D., Sorensen, S. D., Fisher, S. K., Balla, T., Ozaki, S., et al. (2000). A Pleckstrin Homology Domain Specific for Phosphatidylinositol 4,5-

Bisphosphate (PtdIns-4,5-P2) and Fused to Green Fluorescent Protein Identifies Plasma Membrane PtdIns-4,5-P2 as Being Important in Exocytosis. *J. Biol. Chem.* 275 (23), 17878–17885. doi:10.1074/jbc.m000925200

Honigmann, A., Van Den Bogaart, G., Iraheta, E., Risselada, H. J., Milovanovic, D., Mueller, V., et al. (2013). Phosphatidylinositol 4,5-Bisphosphate Clusters Act as Molecular Beacons for Vesicle Recruitment. *Nat. Struct. Mol. Biol.* 20 (6), 679–686. doi:10.1038/nsmb.2570

Iijima, M., Huang, Y. E., Luo, H. R., Vazquez, F., and Devreotes, P. N. (2004). Novel Mechanism of PTEN Regulation by its Phosphatidylinositol 4,5-Bisphosphate Binding Motif Is Critical for Chemotaxis. *J. Biol. Chem.* 279 (16), 16606–16613. doi:10.1074/jbc.m312098200

Imig, C., Min, S.-W., Krinner, S., Arancillo, M., Rosenmund, C., Südhof, T. C., et al. (2014). The Morphological and Molecular Nature of Synaptic Vesicle Priming at Presynaptic Active Zones. *Neuron.* 84, 416–431. doi:10.1016/j.neuron.2014.10.009

Insall, R., Kuspa, A., Lilly, P. J., Shaulsky, G., Levin, L. R., Loomis, W. F., et al. (1994). CRAC, a Cytosolic Protein Containing a Pleckstrin Homology Domain, Is Required for Receptor and G Protein-Mediated Activation of Adenylyl Cyclase in Dictyostelium. *J. Cell. Biol.* 126, 1537–1545. doi:10.1083/jcb.126.6.1537

James, D. J., Khodthong, C., Kowalchyk, J. A., and Martin, T. F. J. (2008). Phosphatidylinositol 4,5-Bisphosphate Regulates SNARE-Dependent Membrane Fusion. *J. Cell. Biol.* 182 (2), 355–366. doi:10.1083/jcb.200801056

James, D. J., Khodthong, C., Kowalchyk, J. A., and Martin, T. F. J. (2010). Phosphatidylinositol 4,5-Bisphosphate Regulation of SNARE Function in Membrane Fusion Mediated by CAPS. *Adv. Enzyme Regul.* 50 (1), 62–70. doi:10.1016/j.advenzreg.2009.10.012

James, D. J., Kowalchyk, J., Daily, N., Petrie, M., and Martin, T. F. J. (2009). CAPS Drives Trans-SNARE Complex Formation and Membrane Fusion through Syntaxin Interactions. *Proc. Natl. Acad. Sci.* 106 (41), 17308–17313. doi:10.1073/pnas.0900755106

James, D. J., and Martin, T. F. J. (2013). CAPS and Munc13: CATCHRs that SNARE Vesicles. *Front. Endocrinol.* 4, 187. doi:10.3389/fendo.2013.00187

Janetopoulos, C., Borleis, J., Vazquez, F., Iijima, M., and Devreotes, P. (2005). Temporal and Spatial Regulation of Phosphoinositide Signaling Mediates Cytokinesis. *Developmental Cell.* 8, 467–477. doi:10.1016/j.devcel.2005.02.010

Janetopoulos, C., Ma, L., Devreotes, P. N., and Iglesias, P. A. (2004). Chemoattractant-induced Phosphatidylinositol 3,4,5-Trisphosphate Accumulation Is Spatially Amplified and Adapts, Independent of the Actin Cytoskeleton. *Proc. Natl. Acad. Sci.* 101 (24), 8951–8956. doi:10.1073/pnas.0402152101

Ji, C., and Lou, X. (2016). Single-molecule Super-resolution Imaging of Phosphatidylinositol 4,5-bisphosphate in the Plasma Membrane With Novel Fluorescent Probes. *J. Vis. Exp.* (116), e54466. doi:10.3791/54466

Ji, C., Zhang, Y., Xu, P., Xu, T., and Lou, X. (2015). Nanoscale Landscape of Phosphoinositides Revealed by Specific Pleckstrin Homology (PH) Domains Using Single-Molecule Superresolution Imaging in the Plasma Membrane. *J. Biol. Chem.* 290 (45), 26978–26993. doi:10.1074/jbc.m115.663013

Junge, H. J., Rhee, J.-S., Jahn, O., Varoqueaux, F., Spiess, J., Waxham, M. N., et al. (2004). Calmodulin and Munc13 Form a Ca2+ Sensor/effector Complex that Controls Short-Term Synaptic Plasticity. *Cell.* 118, 389–401. doi:10.1016/j.cell.2004.06.029

Kabachinski, G., Kielar-Grevstad, D. M., Zhang, X., James, D. J., and Martin, T. F. J. (2016). Resident CAPS on Dense-Core Vesicles Docks and Primes Vesicles for Fusion. *MBoC.* 27 (4), 654–668. doi:10.1091/mbc.e15-07-0509

Kabachinski, G., Yamaga, M., Kielar-Grevstad, D. M., Bruinsma, S., and Martin, T. F. J. (2014). CAPS and Munc13 Utilize Distinct PIP2-Linked Mechanisms to Promote Vesicle Exocytosis. *MBoC.* 25 (4), 508–521. doi:10.1091/mbc.e12-11-0829

Katoh, Y., Nozaki, S., Hartanto, D., Miyano, R., and Nakayama, K. (2015). Architectures of multisubunit complexes revealed by a visible immunoprecipitation assay using fluorescent fusion proteins. *Journal of cell science* 128 (12), 2351–2362. doi:10.1242/jcs.168740

Khodthong, C., Kabachinski, G., James, D. J., and Martin, T. F. J. (2011). Munc13 Homology Domain-1 in CAPS/UNC31 Mediates SNARE Binding Required for Priming Vesicle Exocytosis. *Cel Metab.* 14 (2), 254–263. doi:10.1016/j.cmet.2011.07.002

Kim, S. J., Jeong, M. J., Jo, H. J., Jung, J. H., Kaang, B. K., Choi, Y. B., et al. (2017). Identification of Postsynaptic Phosphatidylinositol-4,5-Bisphosphate (PIP2) Roles for Synaptic Plasticity Using Chemically Induced Dimerization. *Sci. Rep.* 7 (1), 3351–3412. doi:10.1038/s41598-017-03520-3

Knetsch, M. L. W., Schafers, N., Horstmann, H., and Manstein, D. J. (2001). The Dictyostelium Bcr/Abr-Related Protein DRG Regulates Both Rac- and Rab-dependent Pathways. *EMBO J.* 20, 1620–1629. doi:10.1093/emboj/20.7.1620

Koch, H., Hofmann, K., and Brose, N. (2000). Definition of Munc13-Homology-Domains and Characterization of a Novel Ubiquitously Expressed Munc13 Isoform. *Biochem. J.* 349 (1), 247–253. doi:10.1042/bj3490247

Konijn, T. M., Chang, Y.-Y., and Bonner, J. T. (1969). Synthesis of Cyclic AMP in *Dictyostelium discoideum* and *Polysphondylium pallidum*. *Nature.* 224 (5225), 1211–1212. doi:10.1038/2241211a0

Kreutzberger, A. J. B., Kiessling, V., Liang, B., Seelheim, P., Jakhanwal, S., Jahn, R., et al. (2017). Reconstitution of Calcium-Mediated Exocytosis of Dense-Core Vesicles. *Sci. Adv.* 3 (7), e1603208. doi:10.1126/sciadv.1603208

Kriebel, P. W., Barr, V. A., and Parent, C. A. (2003). Adenylyl Cyclase Localization Regulates Streaming During Chemotaxis. *Cell.* 112, 549–560. doi:10.1016/s0092-8674(03)00081-3

Kriebel, P. W., Barr, V. A., Rericha, E. C., Zhang, G., and Parent, C. A. (2008). Collective Cell Migration Requires Vesicular Trafficking for Chemoattractant Delivery at the Trailing Edge. *J. Cell. Biol.* 183, 949–961. doi:10.1083/jcb.200808105

Kriebel, P. W., Majumdar, R., Jenkins, L. M., Senoo, H., Wang, W., Ammu, S., et al. (2018). Extracellular Vesicles Direct Migration by Synthesizing and Releasing Chemotactic Signals. *J. Cell. Biol.* 217 (8), 2891–2910. doi:10.1083/jcb.201710170

Lacalle, R. A., Peregil, R. M., Albar, J. P., Merino, E., Marti´nez-A, C., Me´rida, I., et al. (2007). Type I Phosphatidylinositol 4-Phosphate 5-kinase Controls Neutrophil Polarity and Directional Movement. *J. Cell. Biol.* 179 (7), 1539–1553. doi:10.1083/jcb.200705044

Lefkir, Y., de Chassey, B., Dubois, A., Bogdanovic, A., Brady, R. J., Destaing, O., et al. (2003). The AP-1 Clathrin-Adaptor Is Required for Lysosomal Enzymes Sorting and Biogenesis of the Contractile Vacuole Complex inDictyosteliumCells. *MBoC.* 14 (5), 1835–1851. doi:10.1091/mbc.e02-10-0627

Li, S., Ghosh, C., Xing, Y., and Sun, Y. (2020). Phosphatidylinositol 4,5-bisphosphate in the Control of Membrane Trafficking. *Int. J. Biol. Sci.* 16 (15), 2761–2774. doi:10.7150/ijbs.49665

Lilly, P. J., and Devreotes, P. N. (1994). Identification of CRAC, a Cytosolic Regulator Required for Guanine Nucleotide Stimulation of Adenylyl Cyclase in Dictyostelium. *J. Biol. Chem.* 269, 14123–14129. doi:10.1016/s0021-9258(17)36763-7

Liu, J., Zuo, X., Yue, P., and Guo, W. (2007). Phosphatidylinositol 4,5-Bisphosphate Mediates the Targeting of the Exocyst to the Plasma Membrane for Exocytosis in Mammalian Cells. *MBoC.* 18 (11), 4483–4492. doi:10.1091/mbc.e07-05-0461

Liu, Y., Schirra, C., Stevens, D. R., Matti, U., Speidel, D., Hof, D., et al. (2008). CAPS Facilitates Filling of the Rapidly Releasable Pool of Large Dense-Core Vesicles. *J. Neurosci.* 28 (21), 5594–5601. doi:10.1523/jneurosci.5672-07.2008

Lokuta, M. A., Senetar, M. A., Bennin, D. A., Nuzzi, P. A., Chan, K. T., Ott, V. L., et al. (2007). Type Iγ PIP Kinase Is a Novel Uropod Component that Regulates Rear Retraction During Neutrophil Chemotaxis. *MBoC.* 18 (12), 5069–5080. doi:10.1091/mbc.e07-05-0428

Luo, G., Zhang, J., and Guo, W. (2014). The Role of Sec3p in Secretory Vesicle Targeting and Exocyst Complex Assembly. *MBoC.* 25 (23), 3813–3822. doi:10.1091/mbc.e14-04-0907

Luo, H. R., Huang, Y. E., Chen, J. C., Saiardi, A., Iijima, M., Ye, K., et al. (2003). Inositol Pyrophosphates Mediate Chemotaxis in Dictyostelium via Pleckstrin Homology Domain-PtdIns(3,4,5)P3 Interactions. *Cell.* 114 (5), 559–572. doi:10.1016/s0092-8674(03)00640-8

Luscher, A., Fröhlich, F., Barisch, C., Littlewood, C., Metcalfe, J., Leuba, F., et al. (2019). Lowe Syndrome-Linked Endocytic Adaptors Direct Membrane Cycling Kinetics with OCRL in *Dictyostelium discoideum*. *MBoC.* 30 (17), 2268–2282. doi:10.1091/mbc.e18-08-0510

Ma, C., Li, W., Xu, Y., and Rizo, J. (2011). Munc13 Mediates the Transition From the Closed Syntaxin-Munc18 Complex to the SNARE Complex. *Nat. Struct. Mol. Biol.* 18 (5), 542–549. doi:10.1038/nsmb.2047

Ma, L., Li, Y., Peng, J., Wu, D., Zhao, X., Cui, Y., et al. (2015). Discovery of the Migrasome, an Organelle Mediating Release of Cytoplasmic Contents During Cell Migration. *Cell Res* 25 (1), 24–38. doi:10.1038/cr.2014.135

Malchow, D., Lusche, D. F., Schlatterer, C., De Lozanne, A., and Müller-Taubenberger, A. (2006). The Contractile Vacuole in Ca2+-Regulation in Dictyostelium: its Essential Function for cAMP-Induced Ca2+-Influx. *BMC Dev. Biol.* 6 (1), 31–38. doi:10.1186/1471-213X-6-31

Mao, Y., Chen, J., Maynard, J. A., Zhang, B., and Quiocho, F. A. (2001). A Novel All helix Fold of the AP180 Amino-Terminal Domain for Phosphoinositide Binding and Clathrin Assembly in Synaptic Vesicle Endocytosis. *Cell.* 104, 433–440. doi:10.1016/s0092-8674(01)00230-6

Maringer, K., Yarbrough, A., Sims-Lucas, S., Saheb, E., Jawed, S., and Bush, J. (2016). *Dictyostelium discoideum* RabS and Rab2 Colocalize with the Golgi and Contractile Vacuole System and Regulate Osmoregulation. *J. Biosci.* 41, 205–217. doi:10.1007/s12038-016-9610-4

Martin, T. F. J. (2001). PI(4,5)P2 Regulation of Surface Membrane Traffic. *Curr. Opin. Cel Biol.* 13, 493–499. doi:10.1016/s0955-0674(00)00241-6

Martin, T. F. J. (2015). PI(4,5)P2-Binding Effector Proteins for Vesicle Exocytosis. *Biochim. Biophys. Acta (Bba) - Mol. Cel Biol. Lipids.* 1851 (6), 785–793. doi:10.1016/j.bbalip.2014.09.017

Matern, H. T., Yeaman, C., Nelson, W. J., and Scheller, R. H. (2001). The Sec6/8 Complex in Mammalian Cells: Characterization of Mammalian Sec3, Subunit Interactions, and Expression of Subunits in Polarized Cells. *Proc. Natl. Acad. Sci.* 98 (17), 9648–9653. doi:10.1073/pnas.171317898

McKAN, J. A. (1973). Fine Structure of the Contractile Vacuole Pore inParamecium*. *The J. Protozoology.* 20 (5), 631–638. doi:10.1111/j.1550-7408.1973.tb03587.x

McKanna, J. A. (1976). Fine Structure of Fluid Segregation Organelles of Paramecium Contractile Vacuoles. *J. Ultrastruct. Res.* 54 (1), 1–10. doi:10.1016/s0022-5320(76)80002-0

Milosevic, I., Sørensen, J. B., Lang, T., Krauss, M., Nagy, G., Haucke, V., et al. (2005). Plasmalemmal phosphatidylinositol-4, 5-bisphosphate level regulates the releasable vesicle pool size in chromaffin cells. *Journal of Neuroscience* 25 (10), 2557–2565. doi:10.1523/JNEUROSCI.3761-04.2005

Moniakis, J., Coukell, M. B., and Forer, A. (1995). Molecular Cloning of an Intracellular P-type ATPase from Dictyostelium that Is Up-Regulated in Calcium-Adapted Cells. *J. Biol. Chem.* 270 (47), 28276–28281. doi:10.1074/jbc.270.47.28276

Munson, M., and Novick, P. (2006). The exocyst defrocked, a framework of rods revealed. *Nature structural and molecular biology* 13 (7), 577–581. doi:10.1038/nsmb1097

Murray, D. H., and Tamm, L. K. (2009). Clustering of syntaxin-1A in Model Membranes Is Modulated by Phosphatidylinositol 4,5-bisphosphate and Cholesterol. *Biochemistry.* 48, 4617–4625. doi:10.1021/bi9003217

Nández, R., Balkin, D. M., Messa, M., Liang, L., Paradise, S., Czapla, H., et al. (2014). A Role of OCRL in Clathrin-Coated Pit Dynamics and Uncoating Revealed by Studies of Lowe Syndrome Cells. *Elife.* 3, e02975. doi:10.7554/eLife.02975

Neto, H., Kaupisch, A., Collins, L. L., and Gould, G. W. (2013). Syntaxin 16 Is a Master Recruitment Factor for Cytokinesis. *MBoC.* 24 (23), 3663–3674. doi:10.1091/mbc.e13-06-0302

Neuhaus, E. M., Almers, W., and Soldati, T. (2002). Morphology and Dynamics of the Endocytic Pathway inDictyostelium Discoideum. *MBoC.* 13 (4), 1390–1407. doi:10.1091/mbc.01-08-0392

Nguyen, H.-N., Yang, J.-M., Afkari, Y., Park, B. H., Sesaki, H., Devreotes, P. N., et al. (2014). Engineering ePTEN, an Enhanced PTEN with Increased Tumor Suppressor Activities. *Proc. Natl. Acad. Sci. USA.* 111 (26), E2684–E2693. doi:10.1073/pnas.1409433111

Norris, F. A., Ungewickell, E., and Majerus, P. W. (1995). Inositol Hexakisphosphate Binds to Clathrin Assembly Protein 3 (AP-3/AP180) and Inhibits Clathrin Cage Assembly *In Vitro*. *J. Biol. Chem.* 270 (1), 214–217. doi:10.1074/jbc.270.1.214

Paolo, G. D., Moskowitz, H. S., Gipson, K., Wenk, M. R., Voronov, S., Obayashi, M., et al. (2004). Impaired PtdIns(4,5)P2 Synthesis in Nerve Terminals Produces Defects in Synaptic Vesicle Trafficking. *Nature* 431, 415–422. doi:10.1038/nature02896

Parent, C. A., Blacklock, B. J., Froehlich, W. M., Murphy, D. B., and Devreotes, P. N. (1998). G Protein Signaling Events Are Activated at the Leading Edge of Chemotactic Cells. *Cell.* 95, 81–91. doi:10.1016/s0092-8674(00)81784-5

Parkinson, K., Baines, A. E., Keller, T., Gruenheit, N., Bragg, L., North, R. A., et al. (2014). Calcium-Dependent Regulation of Rab Activation and Vesicle Fusion by an Intracellular P2X Ion Channel. *Nat. Cel Biol.* 16 (1), 87–98. doi:10.1038/ncb2887

Patterson, D. J. (1980). Contractile Vacuoles and Associated Structures: Their Organization and Function. *Biol. Rev.* 55 (1), 1–46. doi:10.1111/j.1469-185x.1980.tb00686.x

Pei, J., Ma, C., Rizo, J., and Grishin, N. V. (2009). Remote Homology Between Munc13 MUN Domain and Vesicle Tethering Complexes. *J. Mol. Biol.* 391 (3), 509–517. doi:10.1016/j.jmb.2009.06.054

Pfeffer, S. R. (1999). Transport-vesicle Targeting: Tethers before SNAREs. *Nat. Cell. Biol.* 1 (1), E17–E22. doi:10.1038/8967

Pleskot, R., Cwiklik, L., Jungwirth, P., Žárský, V., and Potocký, M. (2015). Membrane Targeting of the Yeast Exocyst Complex. *Biochim. Biophys. Acta (Bba) - Biomembranes.* 1848 (7), 1481–1489. doi:10.1016/j.bbamem.2015.03.026

Prosseda, P. P., Luo, N., Wang, B., Alvarado, J. A., Hu, Y., and Sun, Y. (2017). Loss of OCRL Increases Ciliary PI(4,5)P2 in Lowe Oculocerebrorenal Syndrome. *J. Cell. Sci* 130 (20), 3447–3454. doi:10.1242/jcs.200857

Raghu, P., Joseph, A., Krishnan, H., Singh, P., and Saha, S. (2019). Phosphoinositides: Regulators of Nervous System Function in Health and Disease. *Front. Mol. Neurosci.* 12, 208. doi:10.3389/fnmol.2019.00208

Rettig, J., and Neher, E. (2002). Emerging Roles of Presynaptic Proteins in Ca ++ -Triggered Exocytosis. *Science.* 298, 781–785. doi:10.1126/science.1075375

Rickman, C., Medine, C. N., Dun, A. R., Moulton, D. J., Mandula, O., Halemani, N. D., et al. (2010). t-SNARE Protein Conformations Patterned by the Lipid Microenvironment. *J. Biol. Chem.* 285 (18), 13535–13541. doi:10.1074/jbc.m109.091058

Robinson, N. G. G., Guo, L., Imai, J., Toh-e, A., Matsui, Y., and Tamanoi, F. (1999). Rho3 of *Saccharomyces cerevisiae* , Which Regulates the Actin Cytoskeleton and Exocytosis, Is a GTPase Which Interacts with Myo2 and Exo70. *Mol. Cell. Biol.* 19 (5), 3580–3587. doi:10.1128/mcb.19.5.3580

Ruchira, Hink, M. A., Bosgraaf, L., van Haastert, P. J. M., and Visser, A. J. W. G. (2004). Pleckstrin Homology Domain Diffusion in Dictyostelium Cytoplasm Studied Using Fluorescence Correlation Spectroscopy. *J. Biol. Chem.* 279, 10013–10019. doi:10.1074/jbc.m310039200

Schneider, L. (1960). Elektronenmikroskopische Untersuchungen über das Nephridialsystem vonParamaecium. *J. Protozoology.* 7 (1), 75–90. doi:10.1111/j.1550-7408.1960.tb00712.x

Shen, J., Tareste, D. C., Paumet, F., Rothman, J. E., and Melia, T. J. (2007). Selective Activation of Cognate SNAREpins by Sec1/Munc18 Proteins. *Cell.* 128, 183–195. doi:10.1016/j.cell.2006.12.016

Shewan, A., Eastburn, D. J., and Mostov, K. (2011). Phosphoinositides in Cell Architecture. *Cold Spring Harbor Perspect. Biol.* 3 (8), a004796. doi:10.1101/cshperspect.a004796

Shin, O.-H., Lu, J., Rhee, J.-S., Tomchick, D. R., Pang, Z. P., Wojcik, S. M., et al. (2010). Munc13 C2B Domain Is an Activity-Dependent Ca2+ Regulator of Synaptic Exocytosis. *Nat. Struct. Mol. Biol.* 17 (3), 280–288. doi:10.1038/nsmb.1758

Speese, S., Petrie, M., Schuske, K., Ailion, M., Ann, K., Iwasaki, K., et al. (2007). UNC-31 (CAPS) Is Required for Dense-Core Vesicle but Not Synaptic Vesicle Exocytosis in *Caenorhabditis elegans*. *J. Neurosci.* 27 (23), 6150–6162. doi:10.1523/jneurosci.1466-07.2007

Sriskanthadevan, S., Lee, T., Lin, Z., Yang, D., and Siu, C.-H. (2009). Cell Adhesion Molecule DdCAD-1 Is Imported into Contractile Vacuoles by Membrane Invagination in a Ca2+- and Conformation-Dependent Manner. *J. Biol. Chem.* 284 (52), 36377–36386. doi:10.1074/jbc.m109.057257

Stavrou, I., and O'Halloran, T. J. (2006). The Monomeric Clathrin Assembly Protein, AP180, Regulates Contractile Vacuole Size inDictyostelium Discoideum. *MBoC.* 17 (12), 5381–5389. doi:10.1091/mbc.e06-06-0531

Stevens, D. R., and Rettig, J. (2009). The Ca2+-Dependent Activator Protein for Secretion CAPS: Do I Dock or Do I Prime? *Mol. Neurobiol.* 39 (1), 62–72. doi:10.1007/s12035-009-8052-5

Stokes, C. E., and Hawthorne, J. N. (1987). Reduced Phosphoinositide Concentrations in Anterior Temporal Cortex of Alzheimer-Diseased Brains. *J. Neurochem.* 48 (4), 1018–1021. doi:10.1111/j.1471-4159.1987.tb05619.x

Südhof, T. C., and Rothman, J. E. (2009). Membrane Fusion: Grappling With SNARE and SM Proteins. *Science.* 323, 474–477. doi:10.1126/science.1161748

Südhof, T. C. (2013). Neurotransmitter Release: the Last Millisecond in the Life of a Synaptic Vesicle. *Neuron.* 80, 675–690. doi:10.1016/j.neuron.2013.10.022

Südhof, T. C., and Rizo, J. (2011). Synaptic Vesicle Exocytosis. *Cold Spring Harbor Perspect. Biol.* 3 (12), a005637. doi:10.1101/cshperspect.a005637

Trexler, A. J., Sochacki, K. A., and Taraska, J. W. (2016). Imaging the Recruitment and Loss of Proteins and Lipids at Single Sites of Calcium-Triggered Exocytosis. *MBoC.* 27 (15), 2423–2434. doi:10.1091/mbc.e16-01-0057

Van den Bogaart, G., Meyenberg, K., Risselada, H. J., Amin, H., Willig, K. I., Hubrich, B. E., et al. (2011). Membrane Protein Sequestering by Ionic Protein-Lipid Interactions. *Nature.* 479, 552–555. doi:10.1038/nature10545

Varoqueaux, F., Sigler, A., Rhee, J.-S., Brose, N., Enk, C., Reim, K., et al. (2002). Total Arrest of Spontaneous and Evoked Synaptic Transmission but normal Synaptogenesis in the Absence of Munc13-Mediated Vesicle Priming. *Proc. Natl. Acad. Sci.* 99 (13), 9037–9042. doi:10.1073/pnas.122623799

Vega, I. E., and Hsu, S. C. (2001). The exocyst complex associates with microtubules to mediate vesicle targeting and neurite outgrowth. *Journal of Neuroscience* 21 (11), 3839–3848. doi:10.1523/JNEUROSCI.21-11-03839.2001

Voets, T. (2000). Dissection of Three Ca 2+ -Dependent Steps Leading to Secretion in Chromaffin Cells from Mouse Adrenal Slices. *Neuron.* 28, 537–545. doi:10.1016/s0896-6273(00)00131-8

Wang, S., Choi, U. B., Gong, J., Yang, X., Li, Y., Wang, A. L., et al. (2017). Conformational Change of Syntaxin Linker Region Induced by Munc13s Initiates SNARE Complex Formation in Synaptic Exocytosis. *EMBO J.* 36, 816–829. doi:10.15252/embj.201695775

Waters, M. G., and Hughson, F. M. (2000). Membrane Tethering and Fusion in the Secretory and Endocytic Pathways. *Traffic.* 1 (8), 588–597. doi:10.1034/j.1600-0854.2000.010802.x

Wen, Y., Stavrou, I., Bersuker, K., Brady, R. J., De Lozanne, A., and O'Halloran, T. J. (2009). AP180-Mediated Trafficking of Vamp7B Limits Homotypic Fusion ofDictyosteliumContractile Vacuoles. *MBoC.* 20 (20), 4278–4288. doi:10.1091/mbc.e09-03-0243

Wenk, M. R., Pellegrini, L., Klenchin, V. A., Di Paolo, G., Chang, S., Daniell, L., et al. (2001). PIP Kinase Iγ Is the Major PI(4,5)P2 Synthesizing Enzyme at the Synapse. *Neuron.* 32, 79–88. doi:10.1016/s0896-6273(01)00456-1

Whyte, J. R. C., and Munro, S. (2002). Vesicle Tethering Complexes in Membrane Traffic. *J. Cell. Sci.* 115 (13), 2627–2637. doi:10.1242/jcs.115.13.2627

Wojcik, S. M., and Brose, N. (2007). Regulation of Membrane Fusion in Synaptic Excitation-Secretion Coupling: Speed and Accuracy Matter. *Neuron.* 55, 11–24. doi:10.1016/j.neuron.2007.06.013

Wu, X., and Guo, W. (2015). Mutagen Sensitivity. *J. Cell. Sci.* 128 (16), 2957–2961. doi:10.1007/978-3-662-46875-3_3908

Xavier, C. P. R., Caires, H. R., Barbosa, M. A. G., Bergantim, R., Guimarães, J. E., and Vasconcelos, M. H. (2020). The Role of Extracellular Vesicles in the Hallmarks of Cancer and Drug Resistance. *Cells.* 9 (5), 1141. doi:10.3390/cells9051141

Ye, W., Ali, N., Bembenek, M. E., Shears, S. B., and Lafer, E. M. (1995). Inhibition of Clathrin Assembly by High Affinity Binding of Specific Inositol Polyphosphates to the Synapse-Specific Clathrin Assembly Protein AP-3. *J. Biol. Chem.* 270 (4), 1564–1568. doi:10.1074/jbc.270.4.1564

Yeaman, C., Grindstaff, K. K., Wright, J. R., and Nelson, W. J. (2001). Sec6/8 Complexes on Trans-golgi Network and Plasma Membrane Regulate Late Stages of Exocytosis in Mammalian Cells. *J. Cell. Biol.* 155 (4), 593–604. doi:10.1083/jcb.200107088

Zanchi, R., Howard, G., Bretscher, M. S., and Kay, R. R. (2010). The Exocytic Gene secA Is Required for Dictyostelium Cell Motility and Osmoregulation. *J. Cell. Sci.* 123 (19), 3226–3234. doi:10.1242/jcs.072876

Zhang, X., Bi, E., Novick, P., Du, L., Kozminski, K. G., Lipschutz, J. H., et al. (2001). Cdc42 Interacts With the Exocyst and Regulates Polarized Secretion. *J. Biol. Chem.* 276 (50), 46745–46750. doi:10.1074/jbc.m107464200

Zhang, X., Orlando, K., He, B., Xi, F., Zhang, J., Zajac, A., et al. (2008). Membrane Association and Functional Regulation of Sec3 by Phospholipids and Cdc42. *J. Cell. Biol.* 180 (1), 145–158. doi:10.1083/jcb.200704128

Zhu, Q., and Clarke, M. (1992). Association of Calmodulin and an Unconventional Myosin with the Contractile Vacuole Complex of *Dictyostelium discoideum*. *J. Cell. Biol.* 118 (2), 347–358. doi:10.1083/jcb.118.2.347

Zikich, D., Mezer, A., Varoqueaux, F., Sheinin, A., Junge, H. J., Nachliel, E., et al. (2008). Vesicle Priming and Recruitment by ubMunc13-2 Are Differentially Regulated by Calcium and Calmodulin. *J. Neurosci.* 28 (8), 1949–1960. doi:10.1523/jneurosci.5096-07.2008

Conflict of Interest: The authors declare that the research was conducted in the absence of any commercial or financial relationships that could be construed as a potential conflict of interest.

Publisher's Note: All claims expressed in this article are solely those of the authors and do not necessarily represent those of their affiliated organizations, or those of the publisher, the editors and the reviewers. Any product that may be evaluated in this article, or claim that may be made by its manufacturer, is not guaranteed or endorsed by the publisher.

Copyright © 2022 Fadil and Janetopoulos. This is an open-access article distributed under the terms of the Creative Commons Attribution License (CC BY). The use, distribution or reproduction in other forums is permitted, provided the original author(s) and the copyright owner(s) are credited and that the original publication in this journal is cited, in accordance with accepted academic practice. No use, distribution or reproduction is permitted which does not comply with these terms.

Advantages of publishing in Frontiers

OPEN ACCESS
Articles are free to read for greatest visibility and readership

FAST PUBLICATION
Around 90 days from submission to decision

HIGH QUALITY PEER-REVIEW
Rigorous, collaborative, and constructive peer-review

TRANSPARENT PEER-REVIEW
Editors and reviewers acknowledged by name on published articles

Frontiers
Avenue du Tribunal-Fédéral 34
1005 Lausanne | Switzerland

Visit us: www.frontiersin.org
Contact us: frontiersin.org/about/contact

REPRODUCIBILITY OF RESEARCH
Support open data and methods to enhance research reproducibility

DIGITAL PUBLISHING
Articles designed for optimal readership across devices

FOLLOW US
@frontiersin

IMPACT METRICS
Advanced article metrics track visibility across digital media

EXTENSIVE PROMOTION
Marketing and promotion of impactful research

LOOP RESEARCH NETWORK
Our network increases your article's readership